



Universitat Autònoma de Barcelona

ADVERTIMENT. L'accés als continguts d'aquesta tesi queda condicionat a l'acceptació de les condicions d'ús establertes per la següent llicència Creative Commons:  http://cat.creativecommons.org/?page_id=184

ADVERTENCIA. El acceso a los contenidos de esta tesis queda condicionado a la aceptación de las condiciones de uso establecidas por la siguiente licencia Creative Commons:  <http://es.creativecommons.org/blog/licencias/>

WARNING. The access to the contents of this doctoral thesis it is limited to the acceptance of the use conditions set by the following Creative Commons license:  <https://creativecommons.org/licenses/?lang=en>

**Hydrolysis of the Trifluoromethyl Group in
Triarylphosphines: Scope of the Reaction in the Preparation
of Carboxylic-Trifluoromethylated Phosphines and their
Applications**

Daniel Herrera Miranda

Tesi Doctoral

Programa de Doctorat en Química

Prof. Joan Carles Bayón Rueda

Departament de Química

Facultat de Ciències

2018

Memòria presentada per aspirar al Grau de Doctor per Daniel Herrera Miranda

Daniel Herrera Miranda

Vist i plau

Prof. Joan Carles Bayón Rueda

Departament de Química

Facultat de Ciències

Universitat Autònoma de Barcelona

Bellaterra, 19 de juliol de 2018

Aknowledgement

Si bien es cierto que, al final del día, esta tesis doctoral lleva el nombre de un único autor, sería completamente injusto atribuir el mérito de ésta a un único individuo. Como en la vida, cada persona con la que me he cruzado en estos últimos años ha determinado en mayor o menor medida el resultado de este trabajo, el resultado de la persona que soy hoy. Espero no olvidarme de nadie.

Quiero empezar dando las gracias a mi director de tesis. Gracias, Joan Carles, por haber confiado en mí desde el primer momento y, sobretodo, por no haber dejado de hacerlo nunca. Hay personas que enseñan a base de explicar sus conocimientos y otras que lo hacen siendo ellas mismas el ejemplo a seguir. No sabría en qué grupo clasificarte (quizás tampoco es necesario). Rara vez te ha faltado una explicación que dar a cualquier pregunta o duda que te haya podido plantear. Pero, al mismo tiempo, ha sido impresionante observar la dedicación, rigor y pasión que pones en tú día a día y el grado de implicación con el que acompañas a tus alumnos en su proceso (sean del nivel que sean). No diré aquel tópico de que “siempre has tenido la puerta del despacho abierta” porque todo el mundo sabe que 3 de cada 4 veces que llamas a la puerta de Joan Carles ya hay alguien dentro. Pero sí que diré que siempre has buscado un momento para atenderme aunque eso implicase alargar tu jornada diaria.

No me gustaría dejar de mencionar a los otros “jefes” del grupo, Juli Real y Teresa Flor. Aunque en el trabajo de la tesis hemos tenido la oportunidad de coincidir poco, ha sido un placer aprender de vosotros en los laboratorios de docencia. En este mismo aspecto, quiero acordarme también de los demás de profesores de la planta.

I would like also to thank to Prof. Dieter Vogt for kindly accepting me in his group in Edinburgh and for all the fruitful discussions about catalysis.

A la Universitat Autònoma de Barcelona per la beca PIF, sense la qual la realització d'aquest treball hagués sigut molt difícil, així com també la beca d'estades a l'estranger que em va permetre treballar a la Universitat d'Edimburg durant tres mesos. També agraeixo al Servei de llengües de la UAB per la beca per a la redacció de tesis en anglès.

Mención especial merece todo el equipo de mantenimiento y limpieza de la Facultat de Ciències de la UAB así como el equipo administrativo y de servicios técnicos por el

gran trabajo diario que realizan. En este aspecto quisiera destacar a Dolores Mesa, Neli carmona, Núria Alsina y Elena Jiménez de la secretaría del departamento así como la de las doctoras Alba Eustaquio y María Jesús Ibarz del *SAQ* y al Dr Pau Nolis del *Servei de Ressonància* de la UAB.

Quiero agradecer al Dr Ángel Álvarez del *Servei de Diffracció* de la UAB por la asistencia con las estructuras cristalinas y, en especial, por haber tenido la paciencia suficiente de enseñarme a lidiar con el desorden de los CF_3 y responder a mis dudas sobre difracción.

Es el turno ahora para los compañeros de fatigas y demás especies de laboratorio.

Empezando por el grupo Bayón-C7/315. A Mercedes “Maricheli” Cerdón. Por ser la compañera ideal: siempre alegre, dispuesta a hablar, dispuesta a escuchar, dispuesta a ayudar y con algo de picar siempre en el cajón (que de alguna que otra me ha salvado). Porque vales más de lo que crees y eres capaz de mucho más de lo que te piensas. Gracias de corazón. A João Balbino por ser la positividad hecha persona, por los dulces brasileiros y por tu valentía al dejar tu hogar y emprender una nueva aventura (dos veces). Me quedo tu frase: “no hay colores de chicos ni de chicas, sólo prejuicios”. A Jose “Joselito” Pérez, cultivador de rosas, autodestructor de documentos y bailongo empedernido. Por hacer más ameno el día a día siendo simplemente tú. A los compañeros del Bayón-C7/321. A Miriam por lidiar como nadie con la “basura” de papel (lo tenía que decir), a Dani “tercero” García, a Héctor (sí, te considero del otro lab. Tú sabrás) y a Sònia. Aunque con vosotros he compartido menos ratos, me llevo muy buenos recuerdos. Y no me quiero olvidar de Adu “Señorito” Njie y M^a Ángeles que ya partieron con su título de doctor bajo el brazo. Otro que ya partió y que merece una mención especial por mi parte es Dani Peral. Gracias por todo lo que me enseñaste en aquellos ahora lejanos días de Máster. Sin todos esos conocimientos esta tesis habría sido algo muy diferente. Gracias por estar siempre ahí tanto dentro como fuera del laboratorio.

Gracias también a los compañeros de los demás grupos de la planta. Joan Aguiló, Jonathan, Rosa, Hai-jie, Marcos, Jordi Creus, Jordi Borràs, Nacho, Jordi Martínez, Natalia, Alba, Katia, Selene, Quim,...

I would like also to mention all the people from the Vogt's group in Edinburgh. Viktor, Laura, Anna, George, Lewis, Veronica, Eszter and Bachir. Thanks so much for making me feel like home. Quiero tener una mención especial para María por abrirme las puertas de tu casa (y la de Dani) durante aquel genial mes de Abril.

Y si bien el entorno académico es importante, no lo son menos aquellas personas que me han acompañado fuera del laboratorio. Gracias por entender las veces en que no os he podido dedicar tiempo porque tenía una tesis que acabar. A los *Against the Inspiration*, (Adri, Adrio, Carlos) por toda la paciencia que tuvisteis conmigo. A Carlos por estar ahí siempre, por enseñarme la importancia del diseño en cualquier aspecto de la vida y por mostrarme putos de vista muy alejados de mi lógica "científica". Edu, por el currazo *in extremis* que te has pegado con la portada y por demostrarme que puedo contar contigo cuando lo necesite. A Dani "pelirojodemierda" Barros, porque te quiero y punto. Y a toda la familia Bunkay, en especial al *Shihan* Juan por darme unos valores que me han sido imprescindibles para llegar a donde estoy hoy. Al *Sensei* Óscar por construir una pala diminuta con maquinaria industrial y a Niceto, Miguel, David, Carlos, Alejandro y todos los demás por los buenos ratos en el dojo (y en Panticosa!).

A mi familia. A mi madre por ser la persona más trabajadora y más fuerte que conozco. Por todos esos años de sacrificio que ni mi hermano ni yo te podremos pagar nunca. Por ser el mejor ejemplo a seguir. A Raúl, por esa magia de entendernos sin hablar. Simplemente por el increíble regalo de tener un hermano como tú a mi lado.

A mi familia política, Carmen, Yassen y Omar, por estar ahí siempre.

Y finalmente, a Sandra. Por tu apoyo incondicional en todo momento. Por entender todas las horas de más que le he dedicado a esto. Por poner color a mi día a día. Por ser, en definitiva, mi compañera de viaje ideal.

Daniel

The work developed in this doctoral thesis has been financially supported by Lubrizol Advanced Materials.

A mi madre y a mi hermano

Glossary of terms and abbreviations

1. General

acac	acetylacetonate
ATR-FTIR	Attenuated total reflectance-Fourier transform infrared
DCC	<i>N,N'</i> -Dicyclohexylcarbodiimide
DMF	<i>N,N</i> -Dimethylformamide
EA	Elemental analysis
ESI	Electrospray ionisation
GC	Gas chromatography
GP	Protecting group
HP	High pressure
HR-MS	High resolution mass spectroscopy
IR	Infrared
L	Ligand
NMR	Nuclear magnetic resonance
BuLi	Butyllithium
NBS	<i>N</i> -Bromosuccinimide
NIS	<i>N</i> -Iodosuccinimide
TBAOH	Tetrabutylammonium hydroxide
TfOH	trifluoromethanesulfonic acid, triflic acid
THF	Tetrahydrofurane
TLC	Thin layer chromatography
TOF	Turnover frequency
VT	Variable Temperature
XRD	X-ray diffraction

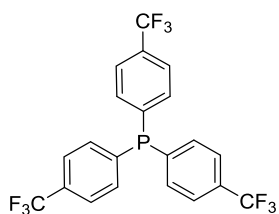
2. Ligands

DPPBA	diphenylphosphinobenzoic acid
dppbz	1,2-Bis(diphenylphosphino)benzene
BIPHEP	2,2'-Bis(diphenylphosphino)biphenyl
BISBI	2,2'-Bis(diphenylphosphinomethyl)-1,1'-biphenyl
TPP	Triphenylphosphine
Xantphos	4,5-Bis(diphenylphosphino)-9,9-dimethylxantene

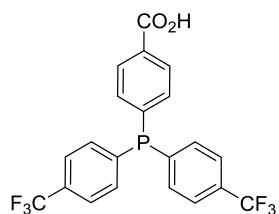
3. NMR-related

δ	chemical shift
<i>b</i>	broad signal
dec	decaplet
d	doublet
dd	doublet of doublets
ddd	double doublet of doublets
dq	doublet of quartets
dt	doublet of triplets
${}^nJ_{AB}$	n-bond coupling constant between nuclei A and B
m	multiplet
q	quartet
qd	quartet of doublets
quint	quintet
sept	septet
s	singlet
t	triplet
td	triplet of doublets

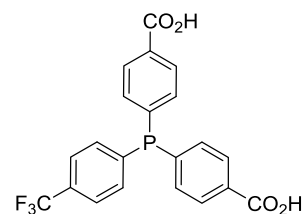
Index of selected phosphines and related compounds



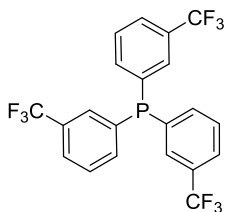
p-trisCF₃ (1)



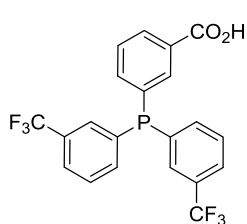
p-Miranphos (2)



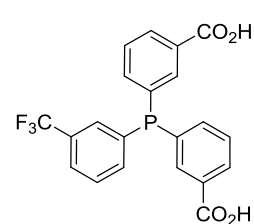
p-Miran2phos (3)



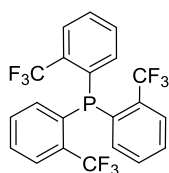
m-trisCF₃ (5)



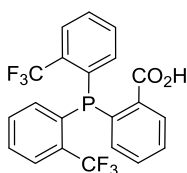
m-Miranphos (6)



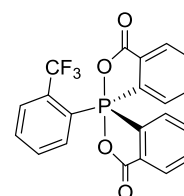
m-Miran2phos (7)



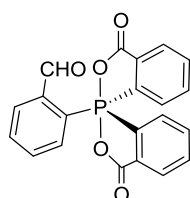
o-trisCF₃ (9)



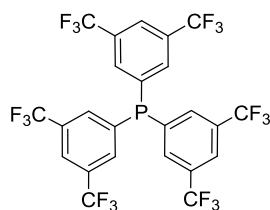
o-Miranphos (10)



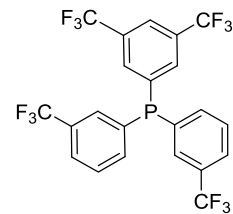
(12)



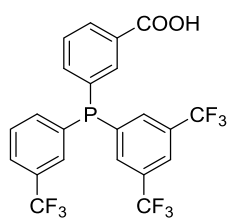
(13)



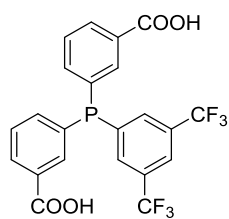
3,5-trisCF₃ (14)



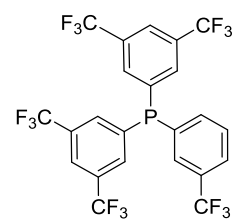
3,5-1 *m*-2 (15)



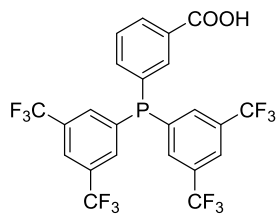
3,5-1 *m*-Miranphos (16)



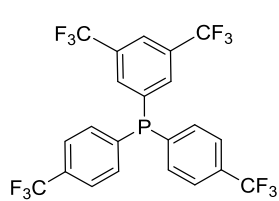
3,5-1 *m*-Miran2phos (17)



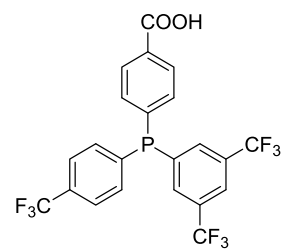
3,5-2 *m*-1 (18)



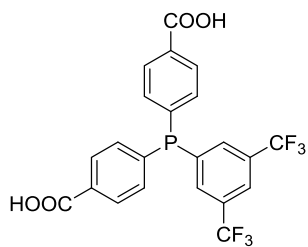
3,5-2 *m*-Miranphos (19)



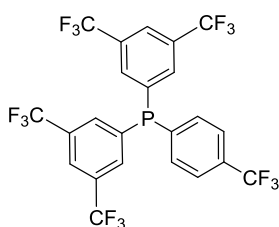
3,5-1 *p*-2 (20)



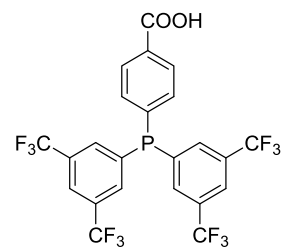
(21)



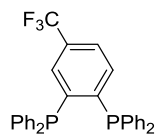
(22)



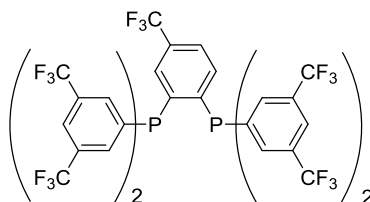
3,5-2 *p*-1 (23)



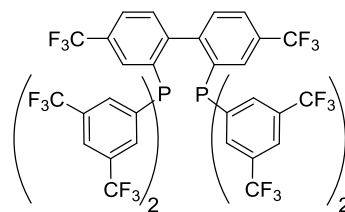
(24)



(30)



(31)



(32)

Table of contents

Chapter 1	General Introduction	1
1.1.	Phosphines	3
1.1.1.	Phosphines as ligands	3
1.1.2.	Carboxylic phosphines	5
1.1.2.1.	Synthesis of carboxylic phosphines	15
1.2.	Hydrolysis of the trifluoromethyl group	17
1.2.1.	Hydrolysis of the trifluoromethyl group in phosphines. Precedents	20
1.3.	³¹ P and ¹⁹ F Nuclear Magnetic Resonance (NMR)	22
1.3.1.	³¹ P NMR	22
1.3.2.	¹⁹ F NMR	26
Chapter 2	Objectives	31
Chapter 3	Hydrolysis of the Trifluoromethyl Group in Triarylphosphines	35
3.1.	Synthesis of trifluoromethylated triarylphosphines	37
3.1.1.	Homoleptic trifluoromethylated triarylphosphines	37
3.1.2.	Heteroleptic trifluoromethylated triarylphosphines	40
3.2.	Study of the electronic properties of the trifluoromethylated phosphines	45
3.2.1.	Vaska-type Ir (I) complexes	45
3.2.2.	Phosphine selenides and phosphonium ions	47
3.3.	Hydrolysis of the trifluoromethyl group	52
3.3.1.	Hydrolysis of the trifluoromethyl in the homoleptic phosphines	54
3.3.1.1.	Hydrolysis of the trifluoromethyl group in phosphines 1 and 5	54
3.3.1.2.	Hydrolysis of the trifluoromethyl group in phosphine 9	69
3.3.1.2.1.	<i>o</i> -Miranphos phosphine (10): structural study	77
3.3.1.3.	Hydrolysis of the trifluoromethyl group in phosphine 14	83
3.3.2.	Hydrolysis of the trifluoromethyl in the heteroleptic phosphines	84
3.3.2.1.	Reaction of hydrolysis of the trifluoromethyl group in <i>meta</i> -substituted heteroleptic triarylphosphines 15 and 18	85
3.3.2.1.1.	Reaction of hydrolysis in phosphine 15	87

3.3.2.1.2. Reaction of hydrolysis in phosphine 18	90
3.3.2.2. Reaction of hydrolysis of the trifluoromethyl group in <i>para</i> -substituted heteroleptic triarylphosphines 20 and 23	92
3.4. Study of the σ -basicity of the Miranphos and Miran2phos ligands. Synthesis of the phosphine selenides	98
3.5. Summary and concluding remarks	100
Chapter 4 Insights into the Hydrolysis of the Trifluoromethyl Group	101
4.1. Introduction	103
4.2. Role of boric acid in the reaction of hydrolysis of the trifluoromethyl group	103
4.2.1. Chemistry of superacids	103
4.2.2. Boric acid and the hydrolysis of the CF ₃	105
4.3. Reaction mechanism	112
4.3.1. Relation between the rate of hydrolysis of the CF ₃ and the pattern of substitution in the phosphines	116
4.4. <i>Ortho</i> -carboxylic phosphine and pentacoordinate species. Mechanism of formation	118
4.5. Summary and concluding remarks	129
Chapter 5 Hydrolysis of the Trifluoromethyl Group in Diphosphines	131
5.1. Introduction	133
5.2. Design and synthesis of the trifluoromethylated diphosphines	134
5.2.1. Synthesis of diphosphine 31	134
5.2.2. Synthesis of diphosphine 32	148
5.3. Reaction of hydrolysis of the trifluoromethyl group in diphosphines	151
5.3.1. Hydrolysis of the trifluoromethyl in diphosphine 31	151
5.3.2. Hydrolysis of the trifluoromethyl in diphosphine 32	158
5.4. Electronic properties of the trifluoromethylated aryl diphosphines: preparation of the selenide derivatives	163
5.5. Summary and concluding remarks	168

Chapter 6	Failed Synthetic Procedures in the Preparation of the Trifluoromethylated Diphosphines	169
6.1.	Introduction	171
6.2.	Failed procedures in the synthesis of diphosphine 31	171
6.3.	Failed procedures in the synthesis of diphosphine 32	176
Chapter 7	Applications of the Miranphos and Miran2phos Ligands	183
7.1.	Chelating diphosphines supported on latex particles	185
7.1.1.	Introduction and objectives	185
7.1.2.	Design and synthesis of the chelating ligands	187
7.1.3.	Rh-catalysed hydroformylation of 1-octene	195
7.1.3.1.	Introduction to the reaction of hydroformylation	195
7.1.3.2.	Catalytic experiments	201
7.1.3.3.	Experiments at high pressure	210
7.1.3.4.	Molecular Mechanics calculations	217
7.1.4.	Catalytic reactions with the latex-supported ligands	219
7.2.	Miranphos and Miran2phos <i>trans</i> -[PdCl ₂ L ₂] complexes: Synthesis and structural determination	220
7.3.	Summary and concluding remarks	225
Chapter 8	General Conclusions	227
Chapter 9	Experimental Procedures	233
9.1.	General procedures and instrumentation	235
9.1.1.	Nuclear Magnetic Resonance	235
9.1.2.	High Resolution Mass Spectrometry (HR-MS)	236
9.1.3.	Elemental Analysis (EA)	237
9.1.4.	Gas Chromatography (GC)	237
9.1.5.	Infrared Spectroscopy (IR)	237
9.1.6.	X-ray diffraction (XRD)	238
9.2.	Catalytic experiments: Rh-catalysed hydroformylation of 1-octene	238
9.2.1.	Conversion, chemoselectivity, regioselectivity and TOF	238

9.2.2. Description of the autoclave and gas line system	239
9.2.3. General experimental procedure	242
9.3. <i>In situ</i> experiments: High Pressure NMR and High Pressure IR	244
9.3.1. HP-NMR	244
9.3.2. HP-IR	244
9.4. Computational calculations and simulations	245
9.4.1. Variable Temperature (VT) NMR	245
9.4.2. Molecular Mechanics: determination of the chelating mode of P-bz and M-bz	247
9.5. Synthetic procedures	252
9.5.1. Trifluoromethylated homoleptic phosphines and oxides	252
9.5.2. Trifluoromethylated heteroleptic phosphines	256
9.5.3. Iridium complexes	265
9.5.4. Carboxylic-trifluoromethylated phosphines and spirocyclic oxyphosphoranes	268
9.5.5. Trifluoromethylated diphosphines and intermediate compounds	280
9.5.5.1. Diphosphines 30 and 31 , and intermediate compounds	280
9.5.5.2. Diphosphine 32 and intermediate compounds	287
9.5.6. Miranphos derivatives: Chelating diphosphine-diamides and intermediate compounds	294
9.5.7. Palladium complexes of Miranphos and Miran2phos ligands. <i>trans</i> -[PdCl ₂ L ₂]	303

Chapter 1

General Introduction

1.1. Phosphines

Phosphines and phosphanes are the names by which the organophosphorus compounds derived from the phosphine (PH_3) are known. Their general structure is PR_3 , where R can vary between H, alkyl groups, aryl groups and halides.¹ They can be divided into three groups:² homoleptic, when the three substituents on the P atom are identical, heteroleptic, when they have two different substituents ($\text{R}_2\text{PR}'$) and asymmetric phosphines, when the three substituents are different.

The stereoelectronic properties of phosphines can be easily tuned by using different substituents on the phosphorus atom, which make them highly versatile ligands. As a consequence of this versatility, phosphines have become one of the most important ligands in coordination chemistry and, in particular, in homogenous catalysis.

Importantly, the strong affinity between phosphorus and oxygen is responsible for the air instability of phosphines. However, the oxidation of phosphines, as well as their behaviour as ligands, is highly dependent on the stereoelectronic properties. As a general trend, phosphines substituted with electron-withdrawing or bulky substituents are more stable towards oxidation since the lone pair on the phosphorus atom will be less available to react with oxygen. On the contrary, phosphines substituted with electron-donating groups behave as stronger bases and are more prone to react with oxygen.

1.1.1. Phosphines as ligands

Two contributors are normally considered when referring to the electronic properties of phosphines as ligands: σ -donor (σ -basicity) and π -acceptor (π -acidity) abilities. The σ -donation of a phosphine is related to its capability to donate the lone pair of the P atom to, for instance, coordinate a metal atom or to bond a heteroatom, such as oxygen or selenium. Phosphines substituted with electron-donating groups (*i.e.* alkylphosphines) behave as strong bases and thus have a stronger σ -donating behaviour.

¹ Hartley, F. R. Chapter 1: Introduction. In *The Chemistry of Organophosphorus Compounds: Primary, secondary and tertiary phosphines, polyphosphines and heterocyclic organophosphorus(III) compounds*; Frank R. Hartley, Ed.; John Wiley & Sons, Inc.: Hoboken, NJ, USA, **1990**; pp 1–8.

² Kendall, A. J.; Tyler, D. R. *Dalt. Trans.* **2015**, *44* (28), 12473–12483.

The same reasoning applies to phosphines substituted with electron-withdrawing groups, which are weaker σ -donating ligands. On the other hand, in coordination chemistry, π -acidity is related to the ability of the phosphine ligand to accept electron density from the metal atom. Although still a matter of research,³ it has been generally accepted that such electron-back donation takes place from the d -orbitals of the metal centre to the empty σ^* -orbitals of the phosphorus ligand (antibonding P-C centred, in the case of phosphines),⁴ **Figure 1.1**. In the literature, a wide variety of methods have been reported to evaluate the σ -donor and π -acceptor ability of phosphines.⁵

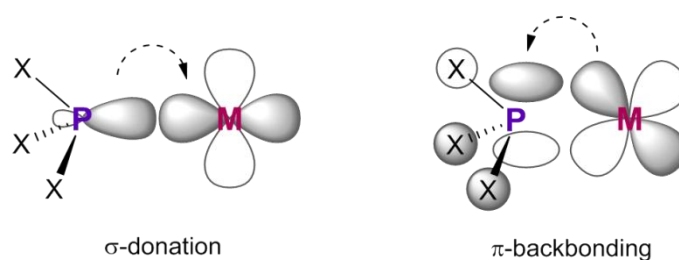


Figure 1.1. Representation of the σ -donation between phosphorus lone-pair and an empty metal d -orbital and the π -back donation from the occupied d -orbital of the metal centre to the antibonding P-X σ^* orbital of the phosphorus ligand. When X = carbon atom, the ligand is a phosphine.

Therefore it is possible to prepare phosphines with different σ -donor and π -acceptor abilities thus modulating the electron density of the metal centre.

The behaviour of phosphines as ligands does not only depend on the electronic properties of the phosphorus atom but also depends on the steric properties conferred by the substituents. The most accepted parameter to express the steric bulk component of phosphine ligands is Tolman's cone angle (θ), **Figure 1.2**. In 1977 Tolman reported a study to provide an explanation of the effect produced by a ligand from the point of view of its steric demand.⁵ The cone angle (θ) was initially calculated with CPK (Corey, Pauling, Koltum) molecular models and was defined as the angle of the cone centred at

³ a) Leysens, T.; Peeters, D.; Orpen, A. G.; Harvey, J. N. *New J. Chem.* **2005**, 29 (11), 1424–1430.

b) Leysens, T.; Peeters, D.; Orpen, A. G.; Harvey, J. N. *Organometallics* **2007**, 26 (10), 2637–2645.

c) Fey, N.; Orpen, A. G.; Harvey, J. N. *Coord. Chem. Rev.* **2009**, 253 (5–6), 704–722.

⁴ a) Xiao, S. X.; Trogler, W. C.; Ellis, D. E.; Berkovitch-Yellin, Z. *J. Am. Chem. Soc.* **1983**, 105 (24), 7033–7037. b) Marynick, D. S. *J. Am. Chem. Soc.* **1984**, 106 (14), 4064–4065. c) Orpen, A. G.; Connelly, N. G. *J. Chem. Soc. Chem. Commun.* **1985**, 1310–1311. d) Tossell, J. A.; Moore, J. H.; Giordan, J. C. *Inorg. Chem.* **1985**, 24 (7), 1100–1103. e) Orpen, A. G.; Connelly, N. G. *Organometallics* **1990**, 9, 1206–1210.

⁵ Tolman, C. A. *Chem. Rev.* **1977**, 77 (3), 313–348.

a metal located at 2.28 Å from the P atom (typical P-Ni bond distance) that embraces all the atoms of the ligand. Before the publication of Tolman's cone angle, the effect produced by a ligand was only explained in terms of electronic effects.⁶

For bidentate diphosphine ligands, Casey and co-workers introduced the concept of the natural bite angle (β).⁷ This parameter is defined as the preferred angle adopted by a chelating ligand when coordinated to a *dummy* metal centre at a distance of 2.315 Å, **Figure 1.2.** The *dummy* metal ensures that the angle obtained is only defined by the ligand backbone constrains and not by the metal valence angles. The natural bite angle is determined by molecular mechanics calculations (MM) in which the P-M-P bending force constant is set to zero during the optimisation. Therefore, the bite angle will only depend on the preferred conformation of the ligand. Natural bite angle has been correlated with both the activity and selectivity of catalytic reactions hence becoming an important factor when studying diphosphine chelating ligands.⁸

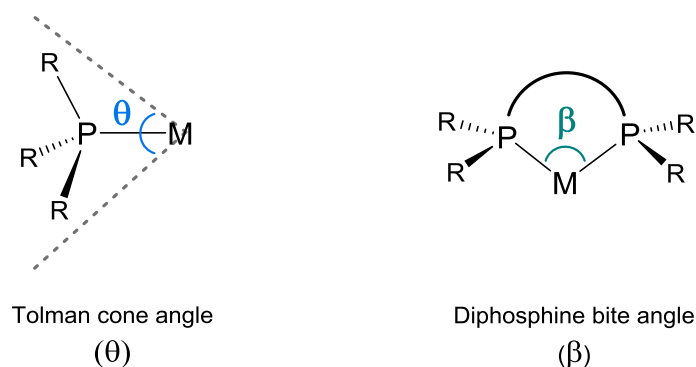


Figure 1.2. Tolman's cone angle parameter (θ) for mono phosphines and bite angle parameter (β) for diphosphines.

1.1.2. Carboxylic phosphines

Phosphines containing carboxylic groups have been widely reported in the literature. Although, as will be described in the next lines, the most extended use of these organophosphorus compounds is in coordination chemistry and as ligands in transition

⁶ Tolman, C. A. *J. Am. Chem. Soc.* **1970**, *92* (10), 2953–2956.

⁷ Casey, C. P.; Whiteker, G. T. *Isr. J. Chem.* **1990**, *30* (4), 299–304.

⁸ a) Dierkes, P.; van Leeuwen, P. W. N. M. *J. Chem. Soc. Dalton Trans.* **1999**, No. 10, 1519–1530. b) van Leeuwen, P. W. N. M.; Kamer, P. C. J.; Reek, J. N. H. *Pure Appl. Chem.* **1999**, *71* (8), 1443–1452. c) Freixa, Z.; van Leeuwen, P. W. N. M. *Dalton Trans.* **2003**, No. 10, 1890–1901. d) Birkholz, M. N.; Freixa, Z.; van Leeuwen, P. W. N. M. *Chem. Soc. Rev.* **2009**, 1099–1118.

metal-based catalytic processes, it is also possible to find other uses beyond these fields. Following carboxylic phosphines will be divided into two main groups depending on whether the carboxylic function is found in an alkylic chain or in an aromatic ring.

Alkyl-carboxylic phosphines

Within this group, the most referred phosphine by far is the tris(2-carboxyethyl)phosphine (TCEP), **Chart 1.1**. Surprisingly for the organometallic chemist, the most extended application of TCEP is as reducing agent of disulfide bonds.⁹ Its high water solubility together with its stability within a broad range of pH values make this phosphine an ideal reagent for biological applications in the cleavage of disulfide bonds in proteins and peptides,¹⁰ showing some advantages over other sulfuryl reductant agents classically used.¹¹ These reducing properties of TCEP have also been used for the controlled drug release in shell cross-linked micelles¹² or in phosphatase-based immunosensor.¹³ Moreover, it has been described its use to regenerate ascorbic acid from dehydroascorbic acid in the process of water reduction catalysis.¹⁴

It is also possible to find applications of TCEP in the area of coordination chemistry. Bal's group studied the coordination of both TCEP and its oxide with Ni, Zn, Pb and Cd.¹⁵ More recently, Pruchnik *et al.* described the complex *cis*-[PtCl₂{TCEP}₂] as new potential anticancer drug candidate analogous to cisplatin.¹⁶ In the field of transition metal-based catalysis, TCEP has been essayed as ligand in the Rh-catalysed

⁹ Burns, J. A.; Butler, J. C.; Moran, J.; Whitesides, G. M. *J. Org. Chem.* **1991**, *56* (8), 2648–2650.

¹⁰ a) Doucette, P. A.; Whitson, L. J.; Cao, X.; Schirf, V.; Demeler, B.; Valentine, J. S.; Hansen, J. C.; Hart, P. J. *J. Biol. Chem.* **2004**, *279* (52), 54558–54566. b) Cline, D. J.; Redding, S. E.; Brohawn, S. G.; Psathas, J. N.; Schneider, J. P.; Thorpe, C. *Biochemistry* **2004**, *43* (48), 15195–15203. c) Lai, Y. J.; Tseng, W. L. *Talanta* **2012**, *91*, 103–109.

¹¹ Getz, E. B.; Xiao, M.; Chakrabarty, T.; Cooke, R.; Selvin, P. R. *Anal. Biochem.* **1999**, *273* (1), 73–80.

¹² Li, Y.; Lokitz, B. S.; Armes, S. P.; McCormick, C. L. *Macromolecules* **2006**, *39* (8), 2726–2728.

¹³ Akanda, M. R.; Aziz, M. A.; Jo, K.; Tamilavan, V.; Hyun, M. H.; Kim, S.; Yang, H. *Anal. Chem.* **2011**, *83* (10), 3926–3933

¹⁴ Bachmann, C.; Probst, B.; Guttentag, M.; Alberto, R. *Chem. Commun.* **2014**, *50* (51), 6737–6739.

¹⁵ Krężel, A.; Latajka, R.; Bujacz, G. D.; Bal, W. *Inorg. Chem.* **2003**, *42* (6), 1994–2003.

¹⁶ Pruchnik, H.; Kral, T.; Hof, M. *J. Membr. Biol.* **2017**, *250* (5), 461–470.

hydroformylation of alkenes in both biphasic aqueous media and alcoholic aqueous media¹⁷ and in the Pd-catalysed Sonogashira coupling in aqueous media.¹⁸

Another alkyl-carboxylic phosphine worth to mention is the diphenylphosphinoacetic acid, **Chart 1.1**. Besides its important application as *P,O*-chelating ligand for the Ni-catalysed Shell Higher Olefin Process (SHOP),¹⁹ this ligand was also used in a wide variety of transition metal complexes, with metals such as Rh, Ir, Pd, Pt²⁰ and Ru^{20c,21} with different catalytic applications such as ring closing metathesis²¹ and in the Suzuki coupling.^{20e}

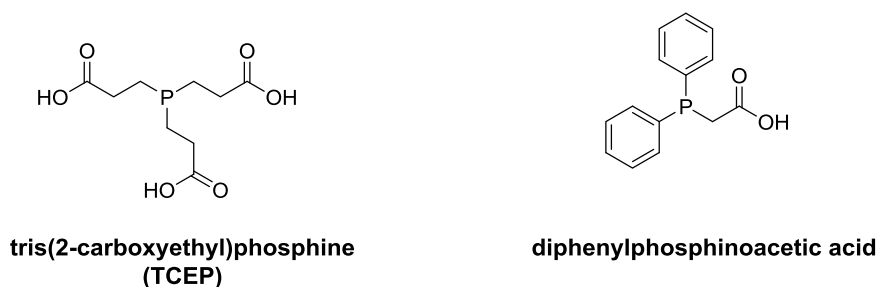


Chart 1.1. tris(2-carboxyethyl)phosphine (TCEP) and diphenylphosphine acetic acid

Diphenylphosphino alkyl-carboxylic phosphines with different chain lengths, **Chart 1.2**, have also been described in the literature. The Rh complexes of the phosphines with alkyl chains of 6 and 8 carbon atoms, diphenylphosphino sodium hexanoate and diphenylphosphino sodium octanoate, respectively, were found to be active in the hydrogenation of olefins in water.²² Other related carboxylic phosphines included in this section are those incorporating a cyclohexyl moiety, such as

¹⁷ a) Vasam, C. S.; Modem, S.; Kankala, S.; Budige, G.; Vadde, R. *Appl. Organomet. Chem.* **2009**, *23* (11), 460–466. b) Vasam, C. S.; Modem, S.; Kankala, S.; Kanne, S.; Budige, G.; Vadde, R. *Cent. Eur. J. Chem.* **2010**, *8* (1), 77–86.

¹⁸ López-Deber, M. P.; Castedo, L.; Granja, J. R. *Org. Lett.* **2001**, *3* (18), 2823–2826.

¹⁹ Peuckertt, M.; Keim, W. *Organometallics* **1983**, *2* (5), 594–597.

²⁰ a) Jegorov, A.; Kratochvil, B.; Langer, V.; Podlahova, J. *Inorg. Chem.* **1984**, *23* (25), 4288–4291. b) Braunstein, P.; Matt, D.; Nobel, D.; Bouaoud, S.-E.; Grandjean, D. *J. Organomet. Chem.* **1986**, *301* (3), 401–410. c) Taqui Khan, M. M.; Nazeeruddin, M. K.; Bajaj, H. C. *Inorg. Chim. Acta* **1988**, *143* (2), 177–184. d) Mecking, S.; Keim, W. *Organometallics* **1996**, *15* (11), 2650–2656. e) Guo, M.; Jian, F.; He, R. *J. Fluor. Chem.* **2006**, *127* (2), 177–181.

²¹ Zhang, W.; Liu, P.; Jin, K.; He, R. *J. Mol. Catal. A Chem.* **2007**, *275* (1–2), 194–199.

²² Mudalige, D. C.; Rempel, G. L. *J. Mol. Catal. A Chem.* **1997**, *116* (1–2), 309–316.

1-(diphenylphosphanyl)cyclohexane-2-carboxylic acid²³ and the *N*-substituted diphenylphosphanylglycines,²⁴ **Chart 1.2**.

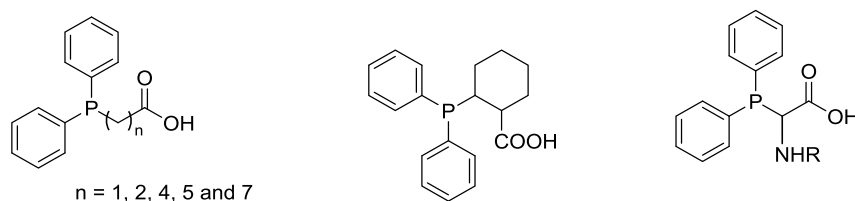


Chart 1.2. Other alkyl-carboxylic diphenylphosphines

Aryl-carboxylic phosphines

The carboxylated derivatives of the triphenylphosphine, diphenylphosphinobenzoic acids (DPPBA), **Chart 1.3**, have been used as ligands in a wide array of transition metal-based catalytic reactions, it being those using Rh, Pd and Ru the most extended processes.

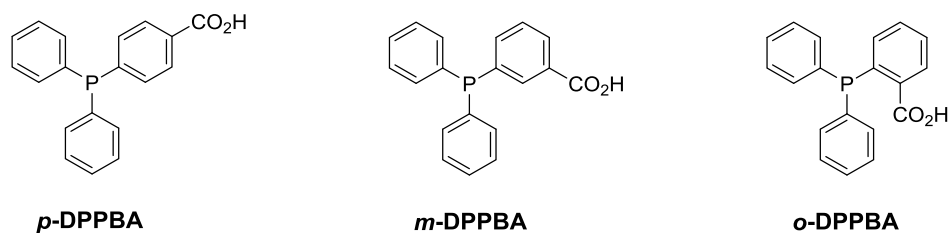


Chart 1.3. *o*, *m* and *p*-(diphenylphosphino)benzoic acids (DPPBA)

Rhodium complexes of DPPBA ligands have been essayed as catalysts in the hydroformylation of alkenes, either in aqueous-biphasic media or in single phase,^{17b,22,25} as well as in the hydrogenation of nitrocompounds in DMF-water media.²⁶ Remarkably, Chang *et al.* reported up to 7 recycling cycles in the organic-organic biphasic Rh-catalysed hydroacylation of olefins with primary alcohols using *p*-DPPBA as ligand.²⁷

²³ Brauer, D. J.; Kottsieper, K. W.; Nickel, T.; Stelzer, O.; Sheldrick, W. S. *Eur. J. Inorg. Chem.* **2001**, No. 5, 1251–1259.

²⁴ Lach, J.; Peulecke, N.; Kindermann, M. K.; Palm, G. J.; Köckerling, M.; Heinicke, J. W. *Tetrahedron* **2015**, *71* (30), 4933–4945.

²⁵ a) Buhling, A.; Kamer, P. C. J.; van Leeuwen, P. W. N. M. *J. Mol. Catal. A Chem.* **1995**, *98* (2), 69–80.
b) Buhling, A.; Kamer, P. C. J.; van Leeuwen, P. W. N. M.; Elgersma, J. W. *J. Mol. Catal. A Chem.* **1997**, *116* (1–2), 297–308.

²⁶ Usha Rani, P.; Muralidhar Reddy, P.; Shanker, K.; Ravinder, V. *Transition. Met. Chem.* **2008**, *33* (2), 153–160.

²⁷ Chang, D. H.; Lee, D. Y.; Hong, B. S.; Choi, J. H.; Jun, C. H. *J. Am. Chem. Soc.* **2004**, *126* (2), 424–425.

Palladium complexes of these monocarboxylic ligands have been reported to catalyse the Suzuki polycondensation reaction²⁸ or the allylic alkylation in which high control of regio- and diastereoselectivity has been achieved for the *o*-DPPBA.²⁹ This isomer (*ortho*) is the one which has been used most often in Ru chemistry in reactions such as ring-closing metathesis^{21,30} or allylic amination.³¹ Just to mention other transition metals, Ringenberg *et al.* reported the preparation of Fe and Ni complexes with *o*-DPPBA acting as *P,O*-chelating ligand.³² Finally, the sodium salt of *p*-DPPBA, as well as some amide derivatives, were used in the synthesis of gold complexes as cathepsin inhibitor.³³

While diphenylphosphinobenzoic acids have been used in different applications in coordination chemistry, the versatility of the carboxylic acid has given rise to a greater number of reports in which derivatives of these ligands are used, mostly amides and esters. In this regard, amongst the three isomers, a larger number of publications deal with the *ortho*-isomer. The relative disposition of the P atom and the carbonyl group makes this organophosphorus compound and its derivatives especially interesting as chelating ligands. In this respect, it is worth highlighting the Trost chiral diphosphines,³⁴ and the related ligands published more recently based in other amines or alcohols³⁵ or based in sugar backbones³⁶ (**Chart 1.4**). All these ligands have been extensively studied in the Pd-catalysed asymmetric allylic alkylation.^{34,35,36,37}

²⁸ Li, J.; Fu, H.; Hu, P.; Zhang, Z.; Li, X.; Cheng, Y. *Chem. Eur. J.* **2012**, *18* (44), 13941–13944.

²⁹ Kawatsura, M.; Ikeda, D.; Komatsu, Y.; Mitani, K.; Tanaka, T.; Uenishi, J. *Tetrahedron* **2007**, *63* (36), 8815–8824.

³⁰ Samec, J. S. M.; Grubbs, R. H. *Chem. Eur. J.* **2008**, *14* (9), 2686–2692.

³¹ Kawatsura, M.; Ata, F.; Hirakawa, T.; Hayase, S.; Itoh, T. *Tetrahedron Lett.* **2008**, *49* (33), 4873–4875.

³² Ringenberg, M. R.; Gray, D. L.; Rauchfuss, T. B. *Organometallics* **2011**, *30* (10), 2885–2888.

³³ Gunatilleke, S. S.; Barrios, A. M. *J. Inorg. Biochem.* **2008**, *102* (3), 555–563.

³⁴ Trost, B. M.; Van Vranken, D. L.; Bingel, C. *J. Am. Chem. Soc.* **1992**, *114* (24), 9327–9343.

³⁵ Mahadik, G. S.; Knott, S. A.; Szczipura, L. F.; Hitchcock, S. R. *Tetrahedron: Asymmetry* **2009**, *20* (10), 1132–1137.

³⁶ Del Litto, R.; De Roma, A.; Ruffo, F. *Inorg. Chem. Commun.* **2007**, *10* (5), 618–622.

³⁷ a) Trost, B. M.; Crawley, M. L. *Chem. Rev.* **2003**, *103* (8), 2921–2943. b) Trost, B. M.; Machacek, M. R.; Aponick, A. *Acc. Chem. Res.* **2006**, *39* (10), 747–760.

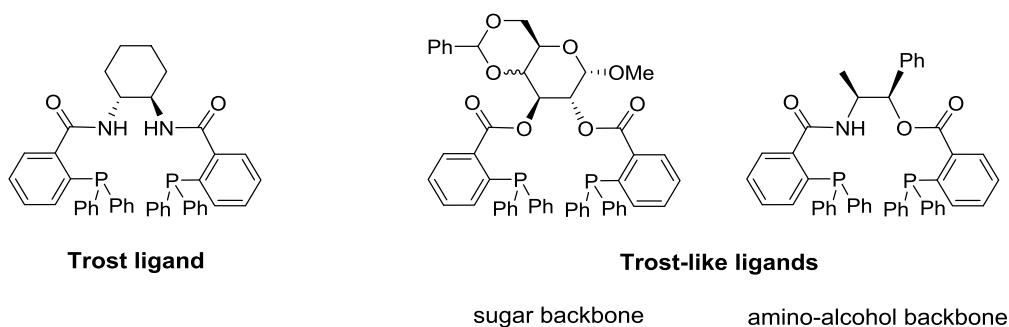


Chart 1.4. Trost diphosphine ligand and analogues

Apart from the Trost and Trost-like ligands, a large collection of other bisphosphine compounds prepared by derivatisation of the carboxylic functions of the DPPBA are found in the literature. Guisado-Barrios *et al.* published a series of diphosphines prepared by reaction of the DPPBA (*ortho*, *meta*, and *para*-isomers) with the amine function of a cyclic decapeptide (gramicidin S) for the Rh-catalysed asymmetric hydrogenation of functionalised alkenes and the Pd-catalysed asymmetric allylic alkylation of 1,3-diphenyl acetate.³⁸ Van Leeuwen and co-workers reported the preparation of assembled diphosphines through interaction of the carboxylic function of DPPBA with the central atom of tin porphyrins³⁹ or with the zinc atom in Robson macrocycles.⁴⁰ Although the assembled molecules resulted in active systems in the Rh-catalysed hydroformylation of 1-octene, the regioselectivities obtained indicate no chelating coordination of the phosphines. Reek's group reported the synthesis of chelating diphosphines (DIMPhos ligands) containing an anion receptor backbone (DIM pocket), **Chart 1.5**. The supramolecular interactions of the anion receptor resulted in improved selectivities in the Rh-catalysed hydroformylation of functionalised alkenes, due to substrate preorganisation.⁴¹

³⁸ Guisado-Barrios, G.; Muñoz, B. K.; Kamer, P. C. J.; Lastdrager, B.; Van der Marel, G.; Overhand, M.; Vega-Vázquez, M.; Martín-Pastor, M. *J. Chem. Soc. Dalton Trans.* **2013**, 42 (2), 1973–1978.

³⁹ Slagt, V. F.; Van Leeuwen, P. W. N. M.; Reek, J. N. H. *J. Chem. Soc. Dalton Trans.* **2007**, No. 22, 2302–2310.

⁴⁰ Ponsico, S.; Gulyas, H.; Martínez-Belmonte, M.; Escudero-Adán, E. C.; Freixa, Z.; van Leeuwen, P. W. N. M. *Dalton Trans.* **2011**, 40 (40), 10686–10697.

⁴¹ a) Dydio, P.; Dzik, W. I.; Lutz, M.; De-Bruin, B.; Reek, J. N. H. *Angew. Chemie - Int. Ed.* **2011**, 50 (2), 396–400. b) Dydio, P.; Detz, R. J.; Reek, J. N. H. *J. Am. Chem. Soc.* **2013**, 135 (29), 10817–10828. c) Dydio, P.; Detz, R. J.; De Bruin, B.; Reek, J. N. H. *J. Am. Chem. Soc.* **2014**, 136 (23), 8418–8429.

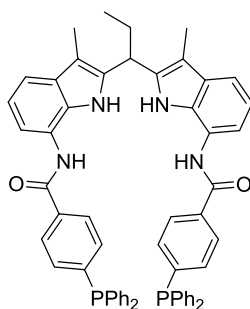


Chart 1.5. Reek's group DIMPhos

Besides the preparation of diphosphine ligands, a wide variety of monophosphines derived from DPPBA and their use as ligands have also been reported. Friederici and *et al.* described a thiol-modified ester derivative of the *p*-DPPBA for surface functionalisation of Au-nanoparticles.⁴² Moreover, Friesen *et al.* reported a perfluoropolyalkylether derivative of the *p*-DPPBA which allows the Rh-catalysed hydrogenation reaction in biphasic fluoruous media with recycling of the catalyst up to 6 times.⁴³

Interestingly, the diphenylphosphinobenzoic acids have been derivatised with different and diverse biocompounds such as peptides,⁴⁴ glucosamines,⁴⁵ guanidine,⁴⁶ oligonucleotides⁴⁷ and cinchona alkaloids⁴⁸ with different applications in transition metal-based catalysis including the Pd-catalysed allylic alkylation,^{45c,d} the Suzuki cross-coupling reaction in water,^{45a,b} the Rh-catalysed hydrogenation^{44,49} and in the Rh-catalysed hydroformylation reaction making use of supramolecular interactions of the ligand to obtain more selective systems.^{46,49}

⁴² Friederici, M.; Angurell, I.; Seco, M.; Rossell, O.; Llorca, J. *Dalton Trans.* **2011**, 40 (31), 7934–7940.

⁴³ Friesen, C. M.; Montgomery, C. D.; Temple, S. A. J. U. *J. Fluor. Chem.* **2012**, 144, 24–32.

⁴⁴ a) Laan, W.; Muñoz, B. K.; Den Heeten, R.; Kamer, P. C. J. *ChemBioChem* **2010**, 11 (9), 1236–1239. b) Laungani, A. C.; Breit, B. *Chem. Commun.* **2008**, No. 7, 844–846.

⁴⁵ a) Parisot, S.; Kolodziuk, R.; Goux-Henry, C.; Iourtchenko, A.; Sinou, D. *Tetrahedron Lett.* **2002**, 43 (41), 7397–7400. b) Kolodziuk, R.; Penciu, A.; Tollabi, M.; Framery, E.; Goux-Henry, C.; Iourtchenko, A.; Sinou, D. *J. Organomet. Chem.* **2003**, 687 (2), 384–391. c) Johannesen, S. A.; Glegoła, K.; Sinou, D.; Framery, E.; Skrydstrup, T. *Tetrahedron Lett.* **2007**, 48 (20), 3569–3573. d) Benessere, V.; Ruffo, F. *Tetrahedron: Assymetry* **2010**, 21 (2), 171–176.

⁴⁶ Šmejkal, T.; Gribkov, D.; Geier, J.; Keller, M.; Breit, B. *Chem. Eur. J.* **2010**, 16 (8), 2470–2478.

⁴⁷ Nuzzolo, M.; Grabulosa, A.; Slawin, A. M. Z.; Meeuwenoord, N. J.; van Der Marel, G. A.; Kamer, P. C. J. *Eur. J. Org. Chem.* **2010**, No. 17, 3229–3236.

⁴⁸ Sladojevich, F.; Trabocchi, A.; Guarna, A.; Dixon, D. J. *J. Am. Chem. Soc.* **2011**, 133 (6), 1710–1713.

⁴⁹ Laungani, A. C.; Slattery, J. M.; Krossing, I.; Breit, B. *Chem. Eur. J.* **2008**, 14 (15), 4488–4502.

The anchoring of the *p*-DPPBA on different surfaces, using the carboxylic group, has been extensively reported. These surfaces include inorganic solids such as silica⁵⁰ and magnetic nanoparticles,⁵¹ as well as polymeric materials such as polystyrene,⁵² polyethylene glycol-polystyrene,⁵³ and amphiphilic polymers⁵⁴, all of them with applications in transition metal-catalytic processes. In this sense, it should be mentioned the use of *p*-DPPBA in the chemistry of dendrimers with the goal of preparing gold complexes⁵⁵ or in the Pd-catalysed Heck reaction.⁵⁶

Beyond the application of the derivatives of DPPBA as ligands for catalytic processes, it is worth mentioning other interesting uses of these organophosphorus compounds. Zhang *et al.* reported a thioester derivative of *o*-DPPBA for the reductive disulfide formation of *S*-nitrosothiols.⁵⁷ Dubikovskaya *et al.* investigated the use of the luciferine-derived amide of *o*-DPPBA for real-time bioluminescence imaging of glycans.⁵⁸ Interestingly, *o*-DPPBA has also been used as directing group in the allylic substitution with organocopper reagents⁵⁹ and in the copper-mediated S_N2' reaction.⁶⁰ On the other hand, the amide-derivatives of *p*-DPPBA were used as phosphonium ylides

⁵⁰ Chen, C.; Shao, X.; Yao, K.; Yuan, J.; Shangguan, W.; Kawaguchi, T.; Shimazu, K. *Langmuir* **2011**, *27* (19), 11958–11965.

⁵¹ a) Shylesh, S.; Wang, L.; Thiel, W. R. *Adv. Synth. Catal.* **2010**, *352* (2–3), 425–432. b) Shylesh, S.; Wang, L.; Demeshko, S.; Thiel, W. R. *ChemCatChem* **2010**, *2* (12), 1543–1547.

⁵² Bergbreiter, D. E.; Li, C. *Org. Lett.* **2003**, *5* (14), 2445–2447.

⁵³ Uozumi, Y.; Danjo, H.; Hayashi, T. *Tetrahedron Lett.* **1997**, *38* (20), 3557–3560.

⁵⁴ Bortenschlager, M.; Schöllhorn, N.; Wittmann, A.; Weberskirch, R. *Chem. Eur. J.* **2007**, *13* (2), 520–528.

⁵⁵ a) Lange, P.; Schier, A.; Schmidbaur, H. *Inorg. Chim. Acta* **1995**, *235* (1–2), 263–272. b) Friggeri, A.; Van Manen, H. J.; Auletta, T.; Li, X. M.; Zapotoczny, S.; Schönherr, H.; Vancso, G. J.; Huskens, J.; Van Veggel, F. C. J. M.; Reinhoudt, D. N. *J. Am. Chem. Soc.* **2001**, *123* (26), 6388–6395.

⁵⁶ a) Dahan, A.; Portnoy, M. *Org. Lett.* **2003**, *5* (8), 1197–1200. b) Dahan, A.; Portnoy, M. *J. Am. Chem. Soc.* **2007**, *129* (18), 5860–5869.

⁵⁷ Zhang, J.; Li, S.; Zhang, D.; Wang, H.; Whorton, A. R.; Xian, M. *Org. Lett.* **2010**, *12* (18), 4208–4211.

⁵⁸ Dubikovskaya, E. a; Cohen, A. S.; Bertozzi, C. R. *J. Am. Chem. Soc.* **2010**, *132* (25), 8563–8565.

⁵⁹ a) Breit, B.; Schmidt, Y. Directed Reactions of Organocopper Reagents. *Chemical Reviews*. 2008, 2928–2951. b) Schmidt, Y.; Breit, B. *Chem. Eur. J.* **2011**, *17* (42), 11780–11788.

⁶⁰ Spangenberg, T.; Schoenfelder, A.; Breit, B.; Mann, A. *Eur. J. Org. Chem.* **2010**, No. 31, 6005–6018.

for the controlled DNA-templated synthesis of oligomers⁶¹ and in the preparation of heterobimetallic complexes and their study as anticancer agents.⁶²

Aryl polycarboxylic phosphines have also been described in the literature although in a lesser extent than the monocarboxylic ones. The dicarboxylic derivatives of the triphenylphosphine⁶³ (**Chart 1.6**), and their Rh²⁶ and Pt complexes⁶⁴ have been reported. Also, the oxide of the *p*-isomer, 4,4'-(phenylphosphanediyl)dibenzoic acid, has been used as flame retardant additive in polymers.⁶⁵

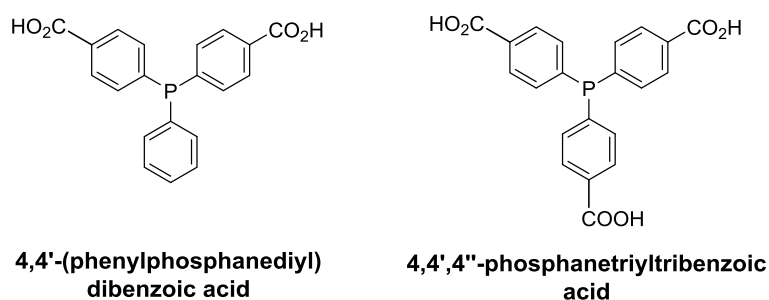


Chart 1.6. Examples of di- and tricarboxylic phosphines. 4,4'-(phenylphosphanediyl)dibenzoic acid and phosphanetriyltribenzoic acid

The *meta* and *para*-isomers of the tricarboxylic derivative of the triphenylphosphine have shown different applications depending on the disposition of the carboxylic group. While the *meta*-isomer, 3,3',3''-phosphanetriyltribenzoic acid has been used as ligand in different reactions, such as the Pd-catalysed Heck reaction,⁶⁶ the Rh-catalysed hydroformylation in aqueous biphasic media with cyclodextrines⁶⁷ and the Pd-catalysed Sonogashira coupling in aqueous biphasic media, allowing the recycling of the

⁶¹ McKee, M. L.; Milnes, P. J.; Bath, J.; Stulz, E.; O'Reilly, R. K.; Turberfield, A. J. *J. Am. Chem. Soc.* **2012**, *134* (3), 1446–1449.

⁶² Wenzel, M.; Bigaeva, E.; Richard, P.; Le Gendre, P.; Picquet, M.; Casini, A.; Bodio, E. *J. Inorg. Biochem.* **2014**, *141*, 10–16.

⁶³ a) Herd, O.; Heßler, A.; Hingst, M.; Tepper, M.; Stelzer, O. *J. Organomet. Chem.* **1996**, *522* (1), 69–76. b) Hingst, M.; Tepper, M.; Stelzer, O. *Eur. J. Inorg. Chem.* **1998**, No. 1, 73–82.

⁶⁴ Ravindar, V.; Schumann, H.; Hemling, H.; Blum, J. *Inorg. Chim. Acta* **1995**, *240* (1–2), 145–152.

⁶⁵ a) Wang, L. S.; Wang, X. L.; Yan, G. L. *Polym. Degrad. Stab.* **2000**, *69* (1), 127–130. b) Wang, L. S.; Kang, H. B.; Wang, S. B.; Liu, Y.; Wang, R. *Fluid Ph. Equilibria* **2007**, *258* (2), 99–107.

⁶⁶ a) Amengual, R.; Genin, E.; Michelet, V.; Savignac, M.; Genêt, J. P. *Adv. Synth. Catal.* **2002**, *344* (3–4), 393–398.

⁶⁷ Tilloy, S.; Genin, E.; Hapiot, F.; Landy, D.; Fourmentin, S.; Genêt, J. P.; Michelet, V.; Monflier, E. *Adv. Synth. Catal.* **2006**, *348* (12–13), 1547–1552.

catalyst,⁶⁸ the applications of the *para*-isomer, 4,4',4''-phosphanetriyltribenzoic acid (**Chart 1.6**), have been focused in the preparation of porous coordination materials (metal-organic frameworks) using this ligand as tritopic linker.⁶⁹ Additionally, the synthesis of carboxylated triarylphosphines containing more than one carboxylic group in the same ring or with combination of carboxylic acids and alcohols or sulfonic acids have also been reported.^{63b,70}

A few examples of carboxylic diphosphines are also found in the literature, **Chart 1.7**. Lesseurre *et al.* reported the synthesis of carboxylic analogues of MeOBIPHEP ligand and their application in the Ru-catalysed hydrogenation of different functionalised alkenes in water.⁷¹ The tetra-carboxylated analogue of 1,2-bis(diphenylphosphino)benzene (dppbz) was reported by Bohnsack *et al.* and was used as tetratopic building block in the synthesis of porous metal-organic frameworks.⁷²

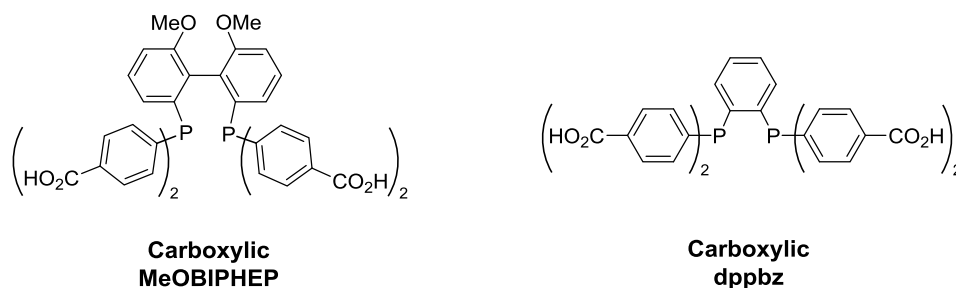


Chart 1.7. Carboxylic diphosphines. MeOBIPHEP and dppbz carboxylic analogues

As final examples of aryl carboxylated phosphines, it is worth mentioning the ferrocene derivatives reported by Štěpnička and Císařová,⁷³ **Chart 1.8**, and the preparation of the Pd complexes of these ligands.

⁶⁸ Genin, E.; Amengual, R.; Michelet, V.; Savignac, M.; Jutand, A.; Neuville, L.; Genêt, J. P. *Adv. Synth. Catal.* **2004**, *346* (13–15), 1733–1741.

⁶⁹ a) Nuñez, A. J.; Shear, L. N.; Dahal, N.; Ibarra, I. A.; Yoon, J.; Hwang, Y. K.; Chang, J. S.; Humphrey, S. M. *Chem. Commun.* **2011**, *47* (43), 11855–11857. b) Nuñez, A. J.; Chang, M. S.; Ibarra, I. A.; Humphrey, S. M. *Inorg. Chem.* **2014**, *53* (1), 282–288. c) Václavík, J.; Servalli, M.; Lothschütz, C.; Szlachetko, J.; Ranocchiari, M.; van Bokhoven, J. A. *ChemCatChem* **2013**, *5* (3), 692–696. d) Bezrukov, A. A.; Törnroos, K. W.; Dietzel, P. D. C. *Cryst. Growth Des.* **2017**, *17* (6), 3257–3266.

⁷⁰ Brauer, D. J.; Hingst, M.; Kottsieper, K. W.; Liek, C.; Nickel, T.; Tepper, M.; Stelzer, O.; Sheldrick, W. S. *J. Organomet. Chem.* **2002**, *645* (1–2), 14–26.

⁷¹ Lesseurre, L.; Püntener, K.; Genêt, J. P.; Scalone, M.; Michelet, V. *Adv. Synth. Catal.* **2011**, *353* (18), 3269–3277.

⁷² Bohnsack, A. M.; Ibarra, I. A.; Bakhmutov, V. I.; Lynch, V. M.; Humphrey, S. M. *J. Am. Chem. Soc.* **2013**, *135* (43), 16038–16041.

⁷³ Štěpnička, P.; Císařová, I. *Organometallics* **2003**, *22* (8), 1728–1740.

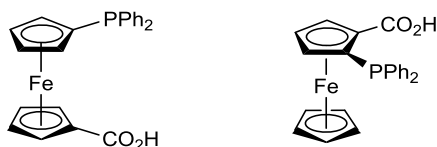
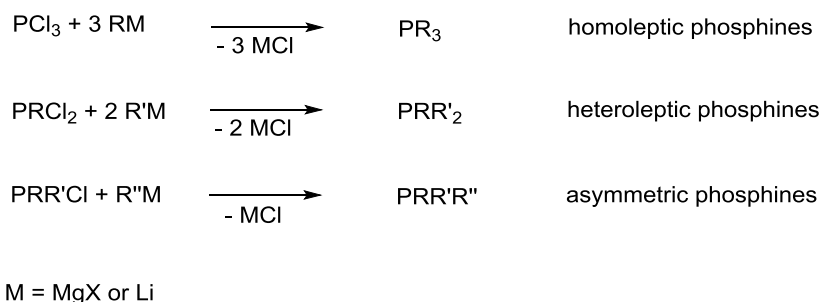


Chart 1.8. Ferrocene carboxylic phosphines

1.1.2.1. Synthesis of carboxylic phosphines

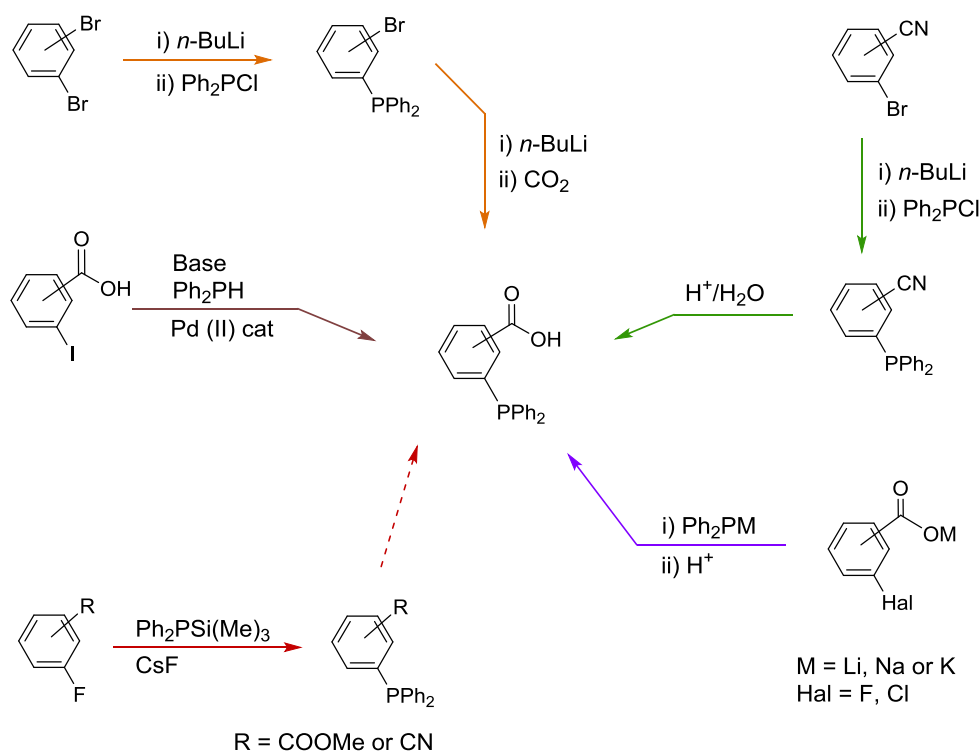
The most extended and simple methods of synthesis of tertiary phosphines consist in the formation of carbon-phosphorus bonds by reaction of chlorophosphines with organometallic reagents, mainly Grignard compounds or organolithium derivatives. This methodology affords the formation of homoleptic, heteroleptic and asymmetric phosphines by using different chlorophosphines,⁷⁴ **Scheme 1.1.**



Scheme 1.1. General schematics of the synthesis of tertiary phosphines by reaction of chlorophosphines with organometallic compounds (Grignard or organolithium)

Given the reactivity of organometallic compounds with acidic protons, the approach described above is not suitable for the preparation of carboxylic phosphines and consequently alternative procedures have to be applied. **Scheme 1.2,** provides a general vision of the most reported procedures for the synthesis of carboxylic triarylphosphines.

⁷⁴ Gilheany, D. G.; Mitchell, C. M. Chapter 7: Preparation of Phosphines. In *The Chemistry of Organophosphorus Compounds*; Frank R. Hartley, Ed.; John Wiley & Sons, Inc.: Hoboken, NJ, USA, 1990; pp 151–162.



Scheme 1.2. General procedures reported for the synthesis of carboxylic phosphines

Organolithium derivatives of bromophosphines have been reported to undergo carbonation by reaction with CO_2 to yield carboxylic phosphines.⁷⁵ Although this reaction affords the preparation of the mono-carboxylic phosphines (*o*-, *m*- and *p*-isomers), do not allow the synthesis of the di- and tricarboxylic phosphines successfully due to the notable presence of ketone products. The hydrolysis of nitrile groups afforded an alternative methodology to prepare mono-, di- and tricarboxylic phosphines of the *meta*- and *para*-isomers in good yields.^{75a} This approach has also been used to prepare the alkylic phosphine TCEP, both in basic⁷⁶ and acid media.⁹ The nucleophilic reaction between arylphosphides and halogen derivatives, another common procedure in the synthesis of phosphines,⁷⁷ have been used to prepare a variety of aryl-carboxylic phosphines^{25a,63b,78} and is not limited to benzoic acids but has also been applied to the preparation of alkylic-carboxylic phosphines such as diphenylphosphino acetic acid and

⁷⁵ a) Ravindar, V.; Hemling, H.; Schumann, H.; Blum, J. *Synth. Commun.* **1992**, 22 (6), 841–851. b) Ravindar, V.; Hemling, H.; Schumann, H.; Blum, J. *Synth. Commun.* **1992**, 22 (10), 1453–1459.

⁷⁶ Rauhut, M. M.; Hechenbleikner, I.; Currier, H. A.; Schaefer, F. C.; Wystrach, V. P. *J. Am. Chem. Soc.* **1959**, 81 (5), 1103–1107.

⁷⁷ Gilheany, D. G.; Mitchell, C. M. Chapter 7: Preparation of Phosphines. In *The Chemistry of Organophosphorus Compounds*; Frank R. Hartley, Ed.; John Wiley & Sons, Inc.: Hoboken, NJ, USA, **1990**; pp 163-167.

⁷⁸ Hoots, J. E.; Rauchfuss, T. B.; Wroblewski, D. A.; Knachel, H. C. *Inorg. Synth.* **1982**, 175–179.

analogues.^{25b} It is worth noticing that, in this approach, the incompatibility between the highly basic phosphides and carboxylic acids is overcome by using the corresponding carboxylic salts or strong basic conditions. Pd(II)-catalysed P-C coupling has also been essayed in the synthesis of this kind of phosphines.^{63a} Moreover, the fluoride-catalysed P-C coupling between silylated phosphines and arylfluoride derivatives has been reported to prepare methyl ester and nitrile triarylphosphine derivatives.⁷⁹ These compounds could be potentially used to prepare carboxylic phosphines by reaction of saponification or hydrolysis, respectively.

1.2. Hydrolysis of the trifluoromethyl group

Carbon-fluorine bond is the strongest single bond in organic molecules (105 kcal/mol).⁸⁰ Nevertheless, under certain conditions this bond can be cleaved with the generation of other chemical bonds as a result. Since the formation of the C-F bond is a rather tough process,⁸¹ the activation of this bond has little interest from a synthetic point of view. However, nowadays fluorocarbon compounds are extensively used in applications such as refrigeration systems (halofluorocarbons), polymers (Teflon), pesticides (*Trifluralin*, herbicide), liquid crystals, drugs (*Efavirenz*, anti-viral) and fluorinated pharmaceuticals (medicinal imaging processes) amongst others.⁸² Because of the high stability of organofluorines, methods for the treatment of these substances become necessary to reduce their accumulation in the environment. Amongst these methodologies, hydrodefluorination, consisting in the transformation of the C-F bonds into C-H bonds, is one of the most extended procedures. Metal complexes⁸³ as well as different Lewis acid species⁸⁴ have been reported as efficient catalysts for the

⁷⁹ Reis, A.; Dehe, D.; Farsadpour, S.; Munstein, I.; Sun, Y.; Thiel, W. R. *New J. Chem.* **2011**, 35 (11), 2488–2495.

⁸⁰ O'Hagan, D. *Chem. Soc. Rev.* **2008**, 37 (2), 308–319.

⁸¹ Krespan, C. G.; Petrov, V. A. *Chem. Rev.* **1996**, 96 (8), 3269–3301.

⁸² Kirsch, P. Chapter 1: Introduction. In *Modern Fluoroorganic Chemistry: Synthesis, Reactivity and Applications*; Wiley-VCH Verlag GmbH & Co. KGaA: Weinheim, Germany, **2013**; pp 1–24.

⁸³ a) Kiplinger, J. L.; Richmond, T. G.; Osterberg, C. E. *Chem. Rev.* **1994**, 94, 373–431. b) Kraft, B. M.; Lachicotte, R. J.; Jones, W. D. *J. Am. Chem. Soc.* **2001**, 123 (44), 10973–10979. c) Kuehnel, M. F.; Lentz, D.; Braun, T. *Angew. Chem. Int. Ed.* **2013**, 52 (12), 3328–3348.

⁸⁴ a) Meier, G.; Braun, T. *Angew. Chem. Int. Ed.* **2009**, 48 (9), 1546–1548. b) Stahl, T.; Klare, H. F. T.; Oestreich, M. *ACS Catal.* **2013**, 3 (7), 1578–1587.

hydrodefluorination. Other forms of C-F activation are currently being under development including C-C bond formation or other derivatives.⁸⁵

The strength of the carbon-fluorine bond confers to the trifluoromethyl group (CF₃) high stability under a wide range of conditions. However, this group is not exempt from C-F activation by the methods explained before⁸⁶ or others such as the activation using phosphonium cations,⁸⁷ or the defluorinative triallylation reaction catalysed by Nb(V).⁸⁸

Interestingly, carbonyl compounds can be prepared from the CF₃ group. In 1949, Le Fave reported the formation of benzoic acids from the hydrolysis of the trifluoromethyl group in trifluoromethylbenzene and derivatives, using concentrated sulfuric acid followed by the treatment of the mixture with water,⁸⁹ **Scheme 1.3**. One year later, Le Fave and Scheurer proved that benzoic esters could be obtained when treating the reaction mixtures with alcohols instead of water.⁹⁰ These authors also reported the preparation of phthalic acids by hydrolysis of the corresponding bis(trifluoromethyl)benzenes in an equimolar mixture of sulfuric acid and chlorosulfuric acid.⁹¹ Although it is true that Le Fave was pioneer in the extensive study of the hydrolysis of the CF₃ in a range of different trifluoromethylbenzene derivatives, as far as we are concern, a few other publications mentioned the reaction previously. In 1943, Simmons and Edwards⁹² and Gilman and Blume⁹³ reported the hydrolysis of the trifluoromethyl group, using sulfuric acid, as methodology to establish the structure of different derivatives of trifluoromethylbenzene. Moreover, in 1947, Jones published the hydrolysis of *o*-trifluoromethylphenol in concentrated NaOH to yield, after acidic treatment, salicylic acid.⁹⁴

⁸⁵ for recent review on the topic see: Shen, Q.; Huang, Y. G.; Liu, C.; Xiao, J. C.; Chen, Q. Y.; Guo, Y. *J. Fluor. Chem.* **2015**, *179*, 14–22.

⁸⁶ in addition to the previous references cited in the text see: Fuchibe, K.; Hatta, H.; Oh, K.; Oki, R.; Ichikawa, J. *Angew. Chem. Int. Ed.* **2017**, *56* (21), 5890–5893.

⁸⁷ Mallov, I.; Johnstone, T. C.; Burns, D. C.; Stephan, D. W. *Chem. Commun.* **2017**, *53* (54), 7529–7532.

⁸⁸ Saito, K.; Umi, T.; Yamada, T.; Suga, T.; Akiyama, T. *Org. Biomol. Chem.* **2017**, *15* (8), 1767–1770.

⁸⁹ Le Fave, G. M. *J. Am. Chem. Soc.* **1949**, *71* (12), 4148–4149.

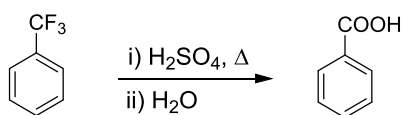
⁹⁰ Le Fave, G. M.; Scheurer, P. G. *J. Am. Chem. Soc.* **1950**, *72* (6), 2464–2465.

⁹¹ Scheurer, P. G.; Le Fave, G. M. *J. Am. Chem. Soc.* **1950**, *72* (7), 3308–3309.

⁹² Simons, J. H.; Ramler, E. O. *J. Am. Chem. Soc.* **1943**, *65* (3), 389–392.

⁹³ Gilman, H.; Blume, D. *J. Am. Chem. Soc.* **1943**, *65* (12), 2467–2468.

⁹⁴ Jones, R. G. *J. Am. Chem. Soc.* **1947**, *69* (10), 2346–2350.



Scheme 1.3. Hydrolysis of the CF₃ in trifluoromethylbenzene according to Le Fave⁸⁹

In spite of these early publications, the reaction of hydrolysis of the CF₃ has not attracted much interest and only a few more examples have been reported after the studies of Le Fave. Wen and co-workers applied the reaction of hydrolysis, using fuming sulfuric acid, in the preparation of cholesteryl *p*-perfluoroalkyl benzoates.⁹⁵ Platonov and co-workers showed the formation of perfluorobenzoic acids from the reaction of the corresponding perfluorotoluene derivative with CF₃COOH/SbF₅ and the subsequent aqueous treatment.⁹⁶ Kethe *et al.* studied the hydrolysis of one CF₃ group in 1,3,5-tris(trifluoromethyl)benzene with either triflic acid (CF₃SO₃H) or fluorosulfuric acid (HSO₃F).⁹⁷

It is worth noting that the reaction is not limited to the use of superacid systems or Lewis acids but also, although rather scarce, examples in basic media can be found such as the basic hydrolysis of the CF₃ in trifluoromethyl imidazoles⁹⁸ or in trifluoromethylated indoles.⁹⁹ More recently, Suzuki *et al.* observed the solvolysis of the CF₃ group of Zn-porphyrins in MeOH to yield the methyl ester derivative.¹⁰⁰

Under similar Brønsted superacid conditions, as shown for the formation of carboxylic acids from trifluoromethyl groups, diaryl ketones were prepared by reaction of trifluoromethylbenzene with triflic acid in the presence of benzene in a Friedel-Craft-like manner, suggesting the formation of carbocation intermediates.^{97,101} Aluminium oxide also has been proven to catalyse the formation of diarylketones with the observation of carboxylic acids as side products.¹⁰² Moreover, Bell and co-workers

⁹⁵ Wang, K.; Li, H.; Wen, J. *J. Fluor. Chem.* **2001**, *109*, 205–208.

⁹⁶ Zonov, Y. V.; Karpov, V. M.; Platonov, V. E. *J. Fluor. Chem.* **2007**, *128* (9), 1058–1064.

⁹⁷ Kethe, A.; Tracy, A. F.; Klumpp, D. A. *Org. Biomol. Chem.* **2011**, *9*, 4545–4549.

⁹⁸ a) Hayakawa, Y.; Kimoto, H.; Cohen, L. A.; Kirk, K. L. *J. Org. Chem.* **1998**, *63* (25), 9448–9454. b) Collman, J. P.; Boulatov, R.; Sunderland, C. J.; Zhong, M. *J. Fluor. Chem.* **2000**, *106*, 189–197.

⁹⁹ Bornstein, J.; Leone, S. A.; Sullivan, W. F.; Benett, O. F. *J. Am. Chem. Soc.* **1957**, *79* (7), 1745–1748.

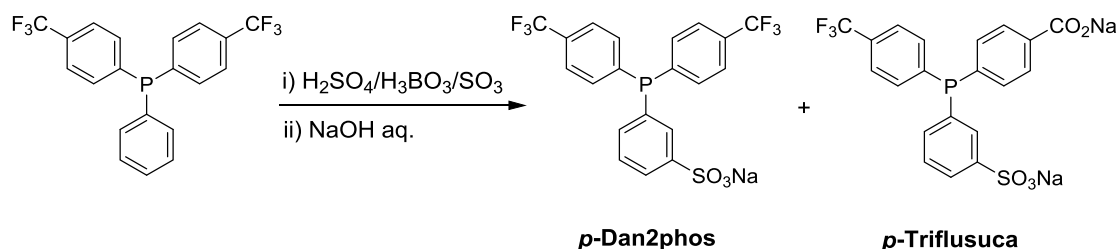
¹⁰⁰ Suzuki, M.; Neya, S.; Nishigaichi, Y. *Molecules* **2016**, *21* (3), 252.

¹⁰¹ Wang, F.; Hu, J. *Chinese J. Chem.* **2009**, *27* (1), 93–98.

¹⁰² Papanian, O.; Amsharov, K. Y. *Chem. Commun.* **2016**, *52* (7), 1505–1508.

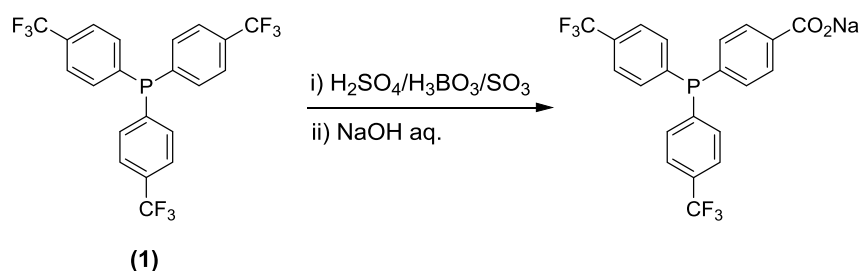
showed the formation of benzoylfluoride from trifluoromethylbenzene in the presence of trifluoroacetic acid and niobium oxide as catalyst.¹⁰³

1.2.1. Hydrolysis of the trifluoromethyl group in phosphines. Precedents



Scheme 1.4. Reaction of sulfonation of phenylbis(4-trifluoromethyl)phenyl)phosphine with the formation of *p*-Dan2phos and the carboxylic phosphine, *p*-triflusuca

In spite of the above mentioned applications of the hydrolysis of the trifluoromethyl group and related reactions, no precedents were known of the use of these reactions in the synthesis of phosphine compounds. In this regard, it is worth mentioning that in our group, during the development of the Ph.D. thesis of Daniel Peral,¹⁰⁴ it was observed that the reaction of sulfonation of phenylbis(4-trifluoromethyl)phenyl)phosphine using fuming sulfuric acid and boric acid gave rise to the product of hydrolysis of the trifluoromethyl group, *p*-triflusuca, in addition to the sulfonated compound, *p*-Dan2phos, **Scheme 1.4**. The reaction was also applied to tris(4-trifluoromethyl)phenyl)phosphine **1**, showing that the hydrolysis of the trifluoromethyl was also possible regardless of the presence of the sulfonic groups in the phosphine, **Scheme 1.5**.



Scheme 1.5. Reaction of hydrolysis of the trifluoromethyl group in the trifluoromethylated phosphine **1**

¹⁰³ Zakzeski, J.; Fan, I. S.; Bell, A. T. *Appl. Catal. A Gen.* **2009**, *360* (1), 33–37.

¹⁰⁴ Peral Crespo, D. *Triarilfosfines Sulfonades Trifluorometilades. Aplicacions en Processos Catalitics*. Ph.D. Thesis. Universitat Autònoma de Barcelona, **2013**.

This reaction offers a new synthetic procedure to obtain carboxylic phosphines with a relatively simple procedure. Not only this, but it also opens the possibility to prepare a new family of phosphines containing both carboxylic and trifluoromethyl groups. On the one hand, the carboxylic group confers chemical versatility to the phosphines. As commented before, the number of derivatives that can be prepared with carboxylic phosphines is huge and covers a wide variety of applications, including those derived from the amphiphilic character of the carboxylic group. On the other hand, the trifluoromethyl group confers to the phosphines greater π -acidity, which turns into a higher stability towards oxidation. Phosphines with π -acidic character have proven to increase the activity of certain transition metal-catalysed reactions such as some C-C couplings¹⁰⁵ and reactions of carbonylation.¹⁰⁶

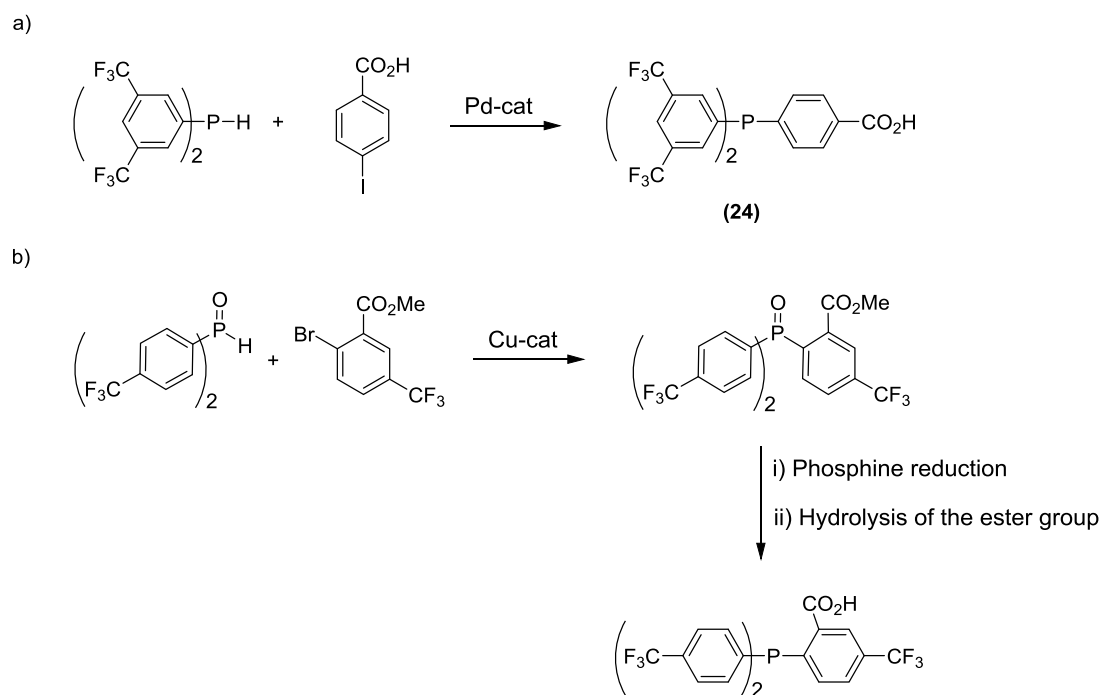
The difficulties that arise from the preparation of carboxylic phosphines due to incompatibility of carboxylic acids with the reagents commonly used in the preparation of phosphines were exposed before. Therefore, with this new approach, the trifluoromethyl group will be used as a masked carboxylic acid, thus overcoming these synthetic issues.

To the best of our knowledge, before the beginning of the present work no other carboxylic and trifluoromethylated arylphosphines had been described in the literature. Two examples, though, were reported during the development of the present dissertation. Reek's group reported the synthesis of **24** through Pd catalysed P-C coupling (**Scheme 1.6-a**).^{41b} In the following chapters, this synthetic methodology will be compared to the one developed in this work. More recently, Starkov *et al.* described the synthesis of an *ortho*-carboxylic trifluoromethylated phosphine by several-steps reaction in which the P-C bond is constructed through a Cu-mediated coupling with the carboxylic group protected as methyl ester (**Scheme 1.6-b**).¹⁰⁷

¹⁰⁵ a) Itami, K.; Kamei, T.; Yoshida, J. I. *J. Am. Chem. Soc.* **2001**, *123* (36), 8773–8779. b) Vogler, T.; Studer, A. *Org. Lett.* **2008**, *10* (1), 129–131. c) Hirata, Y.; Yukawa, T.; Kashihara, N.; Nakao, Y.; Hiyama, T. *J. Am. Chem. Soc.* **2009**, *131* (31), 10964–10973.

¹⁰⁶ a) Palo, D. R.; Erkey, C. *Organometallics* **2000**, *19* (1), 81–86. b) Fujita, S. I.; Fujisawa, S.; Bhanage, B. M.; Arai, M. *Tetrahedron Lett.* **2004**, *45* (6), 1307–1310. c) Koeken, A. C. J.; van Vliet, M. C. A.; van den Broeke, L. J. P.; Deelman, B.-J.; Keurentjes, J. T. F. *Adv. Synth. Catal.* **2008**, *350* (1), 179–188. d) Peral, D.; Herrera, D.; Real, J.; Flor, T.; Bayón, J. C. *Catal. Sci. Technol.* **2016**, *6* (3), 800–808.

¹⁰⁷ Starkov, P.; Moore, J. T.; Duquette, D. C.; Stoltz, B. M.; Marek, I. *J. Am. Chem. Soc.* **2017**, *139* (28), 9615–9620.



Scheme 1.6. Trifluoromethylated and carboxylated phosphines

1.3. ^{31}P and ^{19}F Nuclear Magnetic Resonance (NMR)

1.3.1. ^{31}P NMR

Natural phosphorus consists in a single isotope, ^{31}P . This nucleus is dipolar ($I = 1/2$) and thus it is not only active in NMR spectroscopy but also, as any other dipolar nucleus, give strong and sharp signals due to the spherical charge distribution of these nuclei. ^{31}P NMR is, consequently, a powerful tool when studying phosphorus compounds.¹⁰⁸

Like any other active nucleus in NMR, chemical shifts (δ) of phosphorus compounds are influenced by the environment of the P atom. In this sense, three main factors might be considered to explain upfield and downfield chemical shifts:

- i) the degree of *s*-character of the bonds formed by phosphorus. This contribution is directly related to the bond angles (*i.e.* Tolman cone angle in the case of phosphines)

¹⁰⁸ Kühl, O. *Phosphorus-31 NMR Spectroscopy: A Concise Introduction for the Synthetic Organic and Organometallic Chemist*; Springer Berlin Heidelberg, 2009.

- ii) the electron density on the P atom. This factor depends on the electronegativity of the substituents bond to the phosphorus atom
- iii) the shielding cones of unsaturated systems. This factor is related to the π -bonding character of the substituents.

Figure 1.3 shows the δ of selected phosphorus compounds, with special focus on P(III) species, and will be used to illustrate the factors affecting the chemical shift.

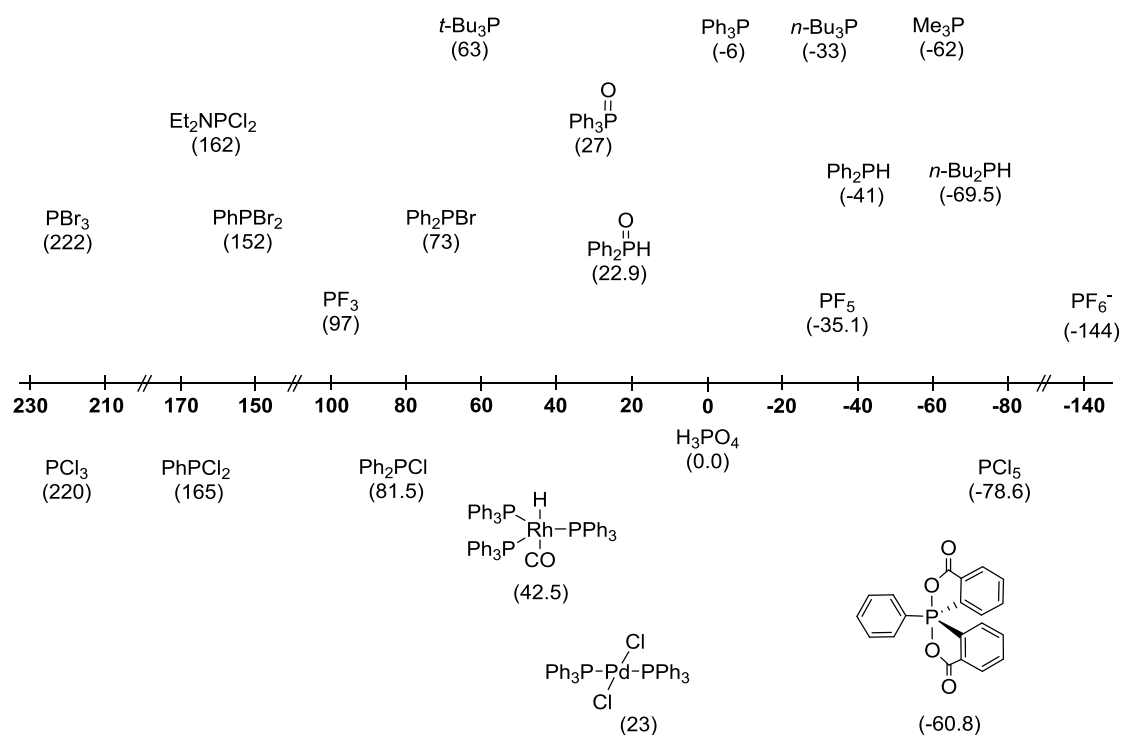


Figure 1.3. General view of ^{31}P NMR. δ (ppm) of representative phosphorus species. Values extracted from the literature^{108,109}

Notice that chemical shifts are referred to an aqueous solution of 85 % H_3PO_4 (0.0 ppm), with positive values being considered when downfield shifted from the reference. Triarylphosphines are found in the range of -3 to -15 ppm in the ^{31}P NMR spectrum, while trialkylphosphines cover a wider range of values, generally upfield shifted. Exception to this rule is found in $\text{P}(t\text{-Bu})_3$ in which the steric hindrance of the *tert*-butyl groups has a large influence in the Tolman cone angle. In these P(III) compounds, when

¹⁰⁹ a) Moedritzer, K.; Maier, L.; Groenweghe, L. C. D. *J. Chem. Eng. Data* **1962**, 7 (2), 307–310. b) Mark, V.; Dugan, C.; Crutchfield, M.; van Wazer, J. *Compilation of P31 NMR Data. Topics in Phosphorus Chemistry* **1967**, 5, 227–457. c) Segall, Y.; Granoth, I. *J. Am. Chem. Soc.* **1978**, 100 (16), 5130–5134. d) Brown, J. M.; Canning, L. R.; Kent, A. G.; Sidebottom, P. J. *J. Chem. Soc. Chem. Commun.* **1982**, No. 13, 721–723.

a carbon atom bonded to the phosphorus is replaced with a less electronegative atom, such as hydrogen, the chemical shift is displaced upfield (see PPh_3 vs HPPH_2 and $\text{P}(n\text{-Bu})_3$ vs $\text{HP}(n\text{-Bu})_2$). On the contrary, when the carbon atom is replaced with a more electronegative atom, such Cl or Br, the signal is downfield shifted as a result of a decreased electron density on the P atom. This displacement downfield is more pronounced the higher the electronegativity of the atom is, with the exception of PF_3 given the backbonding ability of fluorine atoms. Increasing the number of halogen atoms attached to the phosphorus results in downfield displacement of the signals (see the series PPh_3 , Ph_2PX , PhPX_2 and PX_3 , with $\text{X} = \text{Cl}$ or Br). Similarly, the oxidation of the phosphines causes the electron density on the P atom to decrease with the subsequent downfield displacement of the chemical shift (see PPh_3 vs OPPh_3 and HPPH_2 vs H(O)PPH_2). This effect is also observed in the formation of metal complexes. Coordination of the phosphine to a metal centre decreases the electron density on the phosphorus since the lone pair of the phosphine is used in the formation of the P-metal bond.

Pentacoordinated PCl_5 is found 297 ppm upfield shifted from PCl_3 . This subtle sharp change in δ is attributed not only to the oxidation state of the phosphorus atom (from +5 to +3), but also to the different molecular geometry (from trigonal bipyramidal in PCl_5 to trigonal pyramidal in PCl_3). Same behaviour is observed with PF_3 , PF_5 and PF_6^- . Other pentacoordinate compounds such as spirocyclic oxyphosphoranes (-60.8 ppm) are found in the negative region of the spectrum.

Broadly speaking, coupling constants (J) in ^{31}P NMR are larger than those we normally find in ^1H and ^{13}C NMR. **Table 1.1** shows general trends in the coupling constants of phosphorus compounds and metal complexes.

Coupling to proton, $^n\text{J}_{\text{HP}}$, tends to decrease with n. Although commonly proton-decoupled ^{31}P NMR ($^{31}\text{P}\{^1\text{H}\}$) are registered, and thus $^n\text{J}_{\text{HP}}$ are not observed in the spectra, these coupling constants are of great importance in the ^1H NMR spectra. One-bond coupling, $^1\text{J}_{\text{HP}}$, is probably the most interesting coupling to be observed in the phosphorus spectra. Their values oscillate between 100 and 600 Hz depending on the electron density on the P atom, as well as on the steric bulk of the substituents. As general trend, increasing either the electronegativity or the steric bulk of the substituents on the P atom causes $^1\text{J}_{\text{HP}}$ to increase. The magnitude of $^2\text{J}_{\text{HP}}$ and $^3\text{J}_{\text{HP}}$ are sensitive to

structural factors such as the dihedral angle similarly to what happens in J_{HH} , and range between 10 to 30 Hz. ${}^4J_{\text{HP}}$ is normally small and hardly observed.

Table 1.1. Examples of coupling constants in ${}^{31}\text{P}$ NMR of phosphorus compounds (in Hz)^a

${}^1J_{\text{HP}}$	190	214	225
${}^1J_{\text{CP}}$	12.5	104.4	
${}^2J_{\text{CP}}$	19.6	9.8	
${}^3J_{\text{CP}}$	6.8	12.1	
${}^4J_{\text{CP}}$	0.3	2.8	
${}^1J_{\text{PP}}$	364		
${}^1J_{\text{MP}}$	155	$P_z = 151.1$ $P_x = 127.9^b$	3606
${}^2J_{\text{PP}}$	-	119.1	-
${}^2J_{\text{HP}}$	14	12.2 and 18.2	-

^a Values in Hz. ^b Values for Xanphos as chelating ligand. Data from the literature^{108,109b,110}

In the case of coupling of ${}^{31}\text{P}$ to ${}^{13}\text{C}$, the magnitude of ${}^nJ_{\text{CP}}$ depends on different factors such as the oxidation state of the phosphorus atom, the value of n , the stereochemical conformation and the electronegativity of the substituents on the phosphorus. With respect to the dependence of ${}^nJ_{\text{CP}}$ with n , it is worth mentioning that it does not necessarily depend linearly with n . For instance, in the case of triarylphosphines, although not a general trend, frequently the ${}^2J_{\text{CP}}$ (*ortho*-carbon) is greater than coupling to *ipso*-carbon (${}^1J_{\text{CP}}$), followed by ${}^3J_{\text{CP}}$ and ${}^4J_{\text{CP}}$. When the phosphorus atom loses the lone pair, for instance in phosphine oxides, ${}^1J_{\text{CP}}$ becomes much larger than in the corresponding phosphines. Increasing the steric bulk of the substituents also causes ${}^1J_{\text{CP}}$

¹¹⁰ a) Brown, J. M.; Canning, L. R.; Kent, A. G.; Sidebottom, P. J. *J. Chem. Soc. Chem. Commun.* **1982**, No. 13, 721–723. b) Casey, C. P.; Lin Paulsen, E.; Beuttenmueller, E. W.; Proft, B. R.; Petrovich, L. M.; Matter, B. A.; Powell, D. R. *J. Am. Chem. Soc.* **1997**, *119* (49), 11817–11825. c) McFarlane, H. C. E.; McFarlane, W. *Polyhedron* **1999**, *18* (16), 2117–2127.

to increase in tetrahedral compounds. In pentacoordinate geometries $^1J_{CP}$ is smaller with the axial C atoms, although normally due to the fast axial-equatorial exchange (pseudorotation) an average value is observed.

Coupling between different phosphorus atoms, either in the same molecule or as different coordinating ligands in metal complexes, is frequently observed in ^{31}P NMR. In the last case, *trans*- $^2J_{PP}$ is normally larger than *cis*- $^2J_{PP}$. In this regard, also coupling to metals, especially dipolar nuclei such as ^{103}Rh and ^{195}Pt , are observed. $^1J_{PM}$ in metal complexes increase when decreasing the *s*-character of the M-P bond. For trigonal bipyramidal geometries, $^1J_{PM}$ is larger in equatorial ligands than in axial position. Interestingly, in chelating phosphines, the size of the metallacycle significantly influences the coupling constant J_{M-P} .¹¹¹

1.3.2. ^{19}F NMR

The other NMR active nucleus of especial interest of the present dissertation is fluorine. ^{19}F has spin 1/2 with 100% of natural abundance.

Chemical shifts in organofluorinated compounds lie in a range of about 500 ppm. Positive and negative values are assigned using CFCl_3 as reference at 0.0 ppm. The vast number of the existent fluorinated compounds makes it impossible to be summarised in a few lines.¹¹² Instead, we will move shallowly on the general description of the chemical shifts of some fluorine compounds with special mention to the most relevant fluorine species in this dissertation, **Figure 1.4**.

Organofluorine compounds are mainly found in the negative range of the spectrum (upfield from CFCl_3), with the exception of a few compounds such as acyl fluoride and benzyl fluoride. The δ of these compounds depends, as usual, on the substituents attached close to the fluorine (shielding or deshielding effects) as well as on the degree of fluorination of the carbon atom. In this way, significant differences are found between CF , CF_2 and CF_3 groups. $^nJ_{CF}$ values decrease with *n* and has common values of 160 Hz for *n* = 1, 20 Hz for *n* = 2 and between 3 and 6 Hz for *n* = 3 and 4. In

¹¹¹ Garrou, P. E. *Chem. Rev.* **1981**, *81* (3), 229–266.

¹¹² for recent reviews on the topic see: a) Dolbier, W. R. *Guide to Fluorine NMR for Organic Chemists*; John Wiley and Sons, 2008. b) Espinet, P.; Albéniz, A. C.; Casares, J. A.; Martínez-Ilarduya, J. M. *Coord. Chem. Rev.* **2008**, *252* (21–22), 2180–2208.

trifluoromethylated compounds, though, $^1J_{CF}$ and $^2J_{CF}$ are much larger, with values between 275-285 Hz and 25-35 Hz, respectively.

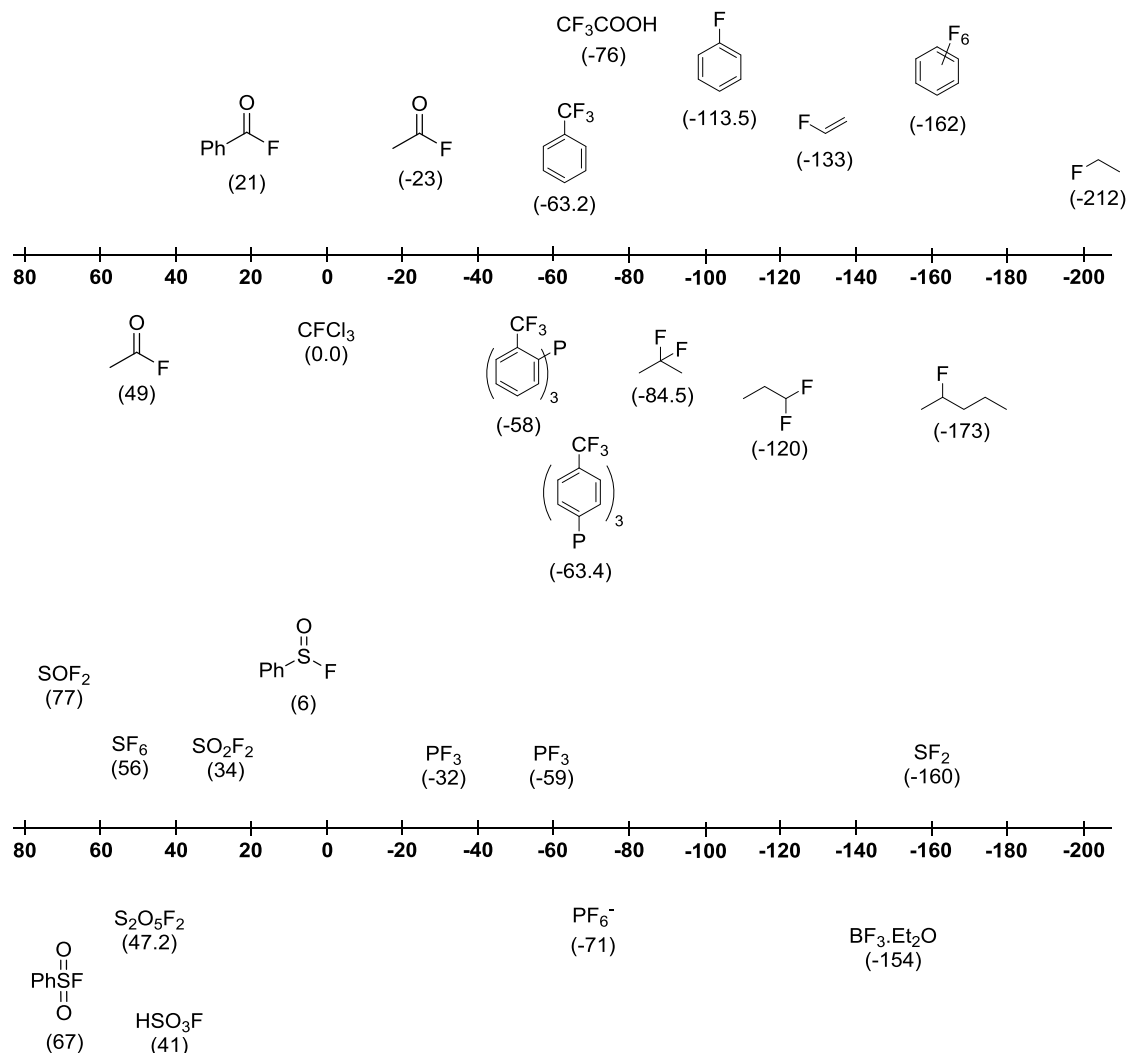


Figure 1.4. General view of ^{19}F NMR chemical shifts (ppm) of representative fluorine species. **Top:** carbon-fluorine bonds. **Bottom:** heteroatom-fluorine bonds. Values from the literature.^{112a,113,114,115,116}

Chemical shift of trifluoromethylbenzene is -63.2 ppm and the same value is observed in trifluoromethylated triarylphosphines with the CF_3 group at *meta* or *para*-position with respect to the P atom. However, when the trifluoromethyl group is located at the

¹¹³ Miller, G. R.; Yankowsky, A. W.; Grim, S. O. *J. Chem. Phys.* **1969**, *51* (8), 3185–3190.

¹¹⁴ Eapen, K. C.; Tamborski, C. *J. Fluor. Chem.* **1980**, *15* (3), 239–243.

¹¹⁵ Krespan, C. G.; England, D. C. *J. Org. Chem.* **1975**, *40* (20), 2937–2940.

¹¹⁶ a) Cicha, W. V.; Herring, F. G.; Aubke, F. *Can. J. Chem.* **1990**, *68* (1), 102–108. b) Kühn-velten, J.; Bodenbinder, M.; Bröchler, R.; Hägele, G.; Aubke, F. *Can. J. Chem.* **2002**, *80*, 1265–1277.

ortho-position, δ is shifted downfield to values around -58 ppm in both the phosphine and its oxide.^{113,114} Coupling between ^{31}P and ^{19}F in trifluoromethylated phosphines are only observed in the *ortho*-substituted ones with values of *ca.* 55 Hz and it is assumed to take place in a *through-space* mechanism as it will be commented in more detail later on. Similar chemical shifts for the CF_3 group than those of *o*-substituted phosphines are observed in bisarylated Pd complexes with 2,4,6-tris(trifluoromethyl)phenyl groups.¹¹⁷

Unlike organofluorines, fluorine atoms attached to heteroatoms cover a wider range of the ^{19}F NMR spectrum. Species such as PF_3 , PF_5 and PF_6^- show chemical shifts upfield from CFCl_3 . Chemical shifts of these compounds as well as the coupling constants, J_{PF} , decrease when increasing the number of F groups, although geometric factors must be also taken into consideration. The values found in these species are -32 ppm and 1141 Hz, -59 ppm and 938 Hz and -71 ppm and 707 Hz, respectively. S-F species cover negative and positive values of δ , depending on the oxidation state and the coordination geometries of the sulfur atoms. For example, SF_2 has a shift of -160 ppm while SF_6 has a value of 56 ppm. Oxyfluoride compounds are mainly found in the range of 77 to 30 ppm, such as $\text{S}_2\text{O}_5\text{F}_2$ at 47.2 ppm¹¹⁵ or fluorosulfuric acid at 41 ppm.¹¹⁶

Through-space coupling

Coupling between non-covalently bonded nuclei can take place in a *through-space* mechanism and requires the overlap of lone pair orbitals in close proximity atoms.¹¹⁸ Although *through-space* coupling is not exclusive of fluorinated molecules, it has been studied in more detail in F-containing compounds, with especial focus on the *through-space* ^{19}F - ^{19}F coupling ($^{\text{TS}}J_{\text{FF}}$) of these compounds.¹¹⁹ Coupling between ^{19}F and other nuclei has also been studied such as $^{\text{TS}}J_{\text{NF}}$ in fluorinated oximes¹²⁰ or $^{\text{TS}}J_{\text{PF}}$ in fluorinated phosphines.^{113,119b,121} It is worth noting that the value of $^{\text{TS}}J$ is sensitive to the distance

¹¹⁷ Bartolomé, C.; Espinet, P.; Martín-Álvarez, J. M.; Villafañe, F. *Eur. J. Inorg. Chem.* **2004**, No. 11, 2326–2337.

¹¹⁸ for recent review on the topic see: a) Mallory, F. B.; Mallory, C. W. *Coupling Through Space in Organic Chemistry*. In *eMagRes*; Grant, D. M., Harris, R. K., Eds.; John Wiley & Sons, Ltd: Chichester, UK, **1996**; pp 1491–1501. Online **2007** John Wiley & Sons, Ltd. b) Hiero, J. C. *Chem. Rev.* **2014**, *114* (9), 4838–4867.

¹¹⁹ a) Chambers, R. D.; Sutcliffe, L. H.; Tiddy, G. J. T. *Trans. Faraday Soc.* **1970**, *66*, 1025–1038. b) Mallory, F. B.; Mallory, C. W.; Butler, K. E.; Lewis, M. B.; Xia, A. Q.; Luzik, E. D.; Fredenburgh, L. E.; Ramanjulu, M. M.; Van, Q. N.; Francl, M. M.; et al. *J. Am. Chem. Soc.* **2000**, *122* (17), 4108–4116.

¹²⁰ Mallory, F. B.; Luzik, E. D.; Mallory, C. W.; Carroll, P. J. *J. Org. Chem.* **1992**, *57* (1), 366–370.

¹²¹ Bonnafoux, L.; Ernst, L.; Leroux, F. R.; Colobert, F. *Eur. J. Inorg. Chem.* **2011**, No. 22, 3387–3397.

between the two nuclei and to the degree of overlap between the lone pairs.^{118a} Miller *et al.* reported a value of ${}^{4\text{TS}}J_{\text{PF}}$ of 55 Hz in the *o*-trifluoromethylated phosphine **9**, while the *meta* and *para*-derivatives (**5** and **1**, respectively) did not show P-F coupling, **Chart 1.9**. Importantly, the oxide derivative of the *o*-substituted phosphine (**ox-9**) did not show coupling either,¹¹⁴ which illustrates the fact that lone pair orbital interaction is required in *through-space* coupling. Bonnafoux and co-workers also reported this effect in the ${}^{\text{TS}}J_{\text{PP}}$ in biaryldiphosphines and the corresponding oxides and selenides.¹²¹

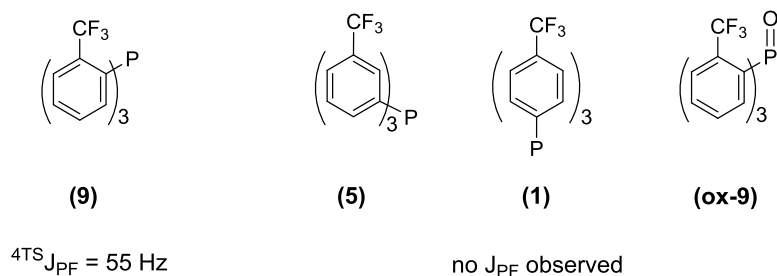


Chart 1.9. J_{PF} in trifluoromethylated phosphines

Chapter 2

Objectives

The reaction of hydrolysis of the trifluoromethyl group in trifluoromethylated triarylphosphines using fuming sulfuric acid opens a new and alternative synthetic route in the preparation of carboxylic phosphines. With this in mind, the main objective of the present work is the exploration of the scope and applicability of the reaction of hydrolysis in trifluoromethylated phosphines. Such broad study implies the following specific objectives:

1. Preparation of trifluoromethylated triarylphosphines with different pattern of substitution including both homoleptic and heteroleptic phosphines. The reaction of hydrolysis of the trifluoromethyl group in these phosphines will be explored. Optimisation of the process and development of a methodology of separation and purification of the carboxylic phosphines is also included in this first specific objective.

2. Development of the synthetic procedure for the preparation of trifluoromethylated diphosphines, which will be used to expand the study of the applicability of the reaction of hydrolysis, eventually leading to carboxylated diphosphines.

3. The reaction of hydrolysis of the trifluoromethyl will be studied in detail. This third specific objective, is aimed to investigate the role of the reagents participating in the reaction as well as to establish and propose a reaction mechanism. All in all, this third objective is meant to clear the unknowns around the reaction.

4. The fourth specific objective is centred on the exploration of the applications of the carboxylic phosphines synthesised in this work as building blocks to construct more elaborated ligands. Special interest will be focused in the design and synthesis of chelating diphosphines by using bridging diamines as ligand backbone and their application in catalytic processes.

Chapter 3

Hydrolysis of the Trifluoromethyl Group in Triarylphosphines

3.1. Synthesis of trifluoromethylated triarylphosphines

In order to explore the scope of the reaction of hydrolysis of the trifluoromethyl group in triarylphosphines, several of these compounds were prepared to cover a range of trifluoromethylated phosphines as wide as possible. In this regard, two groups of triarylphosphines were synthesised: homoleptic trifluoromethylated phosphines, which have three identical substituents on the phosphorus atom (PR_3), and heteroleptic trifluoromethylated phosphines, including those phosphines that have two distinct substituents on the phosphorus atom ($\text{R}_2\text{PR}'$).

3.1.1. Homoleptic trifluoromethylated triarylphosphines

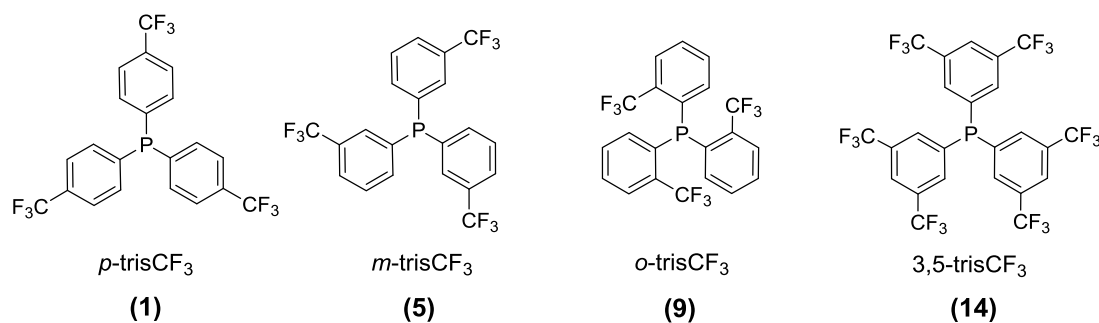


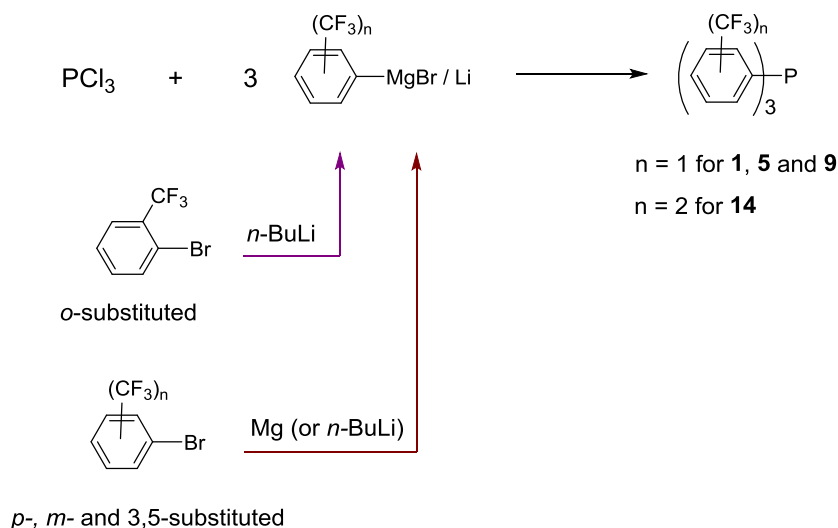
Chart 3.1. Homoleptic trifluoromethylated phosphines used in this work

Homoleptic triarylphosphines are generally synthesised by a straightforward method consisting in the reaction between phosphorus trichloride and the corresponding Grignard reagent or organolithium derivative.¹ Using this methodology, the trifluoromethylated homoleptic phosphines tris(4-trifluoromethylphenyl)phosphine (*p*-trisCF₃, **1**), tris(3-trifluoromethylphenyl)phosphine (*m*-trisCF₃, **5**), tris(2-trifluoromethylphenyl)phosphine (*o*-trisCF₃, **9**) and tris(3,5-bis(trifluoromethyl)phenyl)phosphine (3,5-trisCF₃, **14**), **Chart 3.1**, can be prepared as already reported in the literature.² The Grignard reagent or the organolithium derivative, prepared from the reaction of the corresponding bromo-aryl derivative with Mg or *n*-BuLi, respectively, is added to a solution of PCl_3 in ethereal solvent (normally diethyl ether) to yield the

¹ Gilheany, D. G.; Mitchell, C. M. Chapter 7: Preparation of Phosphines. In *The Chemistry of Organophosphorus Compounds*; Frank R. Hartley, Ed.; John Wiley & Sons, Inc.: Hoboken, NJ, USA, **1990**; pp 154–158.

² a) Miller, G. R.; Yankowsky, A. W.; Grim, S. O. *J. Chem. Phys.* **1969**, *51* (8), 3185–3190. b) Eapen, K. C.; Tamborski, C. *J. Fluor. Chem.* **1980**, *15* (3), 239–243. c) Jeschke, J.; Korb, M.; Ruffer, T.; Gäbler, C.; Lang, H. *Adv. Synth. Catal.* **2015**, *357* (18), 4069–4081.

corresponding homoleptic triarylphosphine, **Scheme 3.1**. It is important to mention that, while the Grignard reagent is normally chosen to prepare these phosphines, this reagent cannot be applied to the bulkier *ortho*-substituted one. In this case, the phosphine is efficiently prepared through the organolithium derivative. Either way, the simplicity of the reaction allows the preparation of these ligands in multigram scale.



Scheme 3.1. General synthesis of the trifluoromethylated homoleptic phosphines

In the present work, phosphines **1**, **5** and **9** have been synthesised and completely characterised by multinuclear NMR (^1H , ^{13}C , ^{19}F and ^{31}P). 3,5-substituted phosphine **14**, although used in the experiments of the hydrolysis of the trifluoromethyl group, was taken from a batch synthesised in our group in a previous work.³

With respect to the characterisation of these ligands, we will highlight a few features of the different spectra. The $^{31}\text{P}\{^1\text{H}\}$ NMR spectra of these phosphines are singlets in all cases except for the *o*-substituted phosphine **9**, which shows a characteristic decaplet due to P-F coupling with $^{4\text{TS}}J_{\text{PF}} = 55.5$ Hz. This multiplicity will be relevant in the monitoring of the reaction of hydrolysis of the CF_3 with this phosphine. In the same manner, $^{19}\text{F}\{^1\text{H}\}$ NMR spectra of **9** shows a doublet, contrary to the singlet observed with the other homoleptic phosphines. **Figure 3.1** shows the $^{31}\text{P}\{^1\text{H}\}$ and $^{19}\text{F}\{^1\text{H}\}$ NMR spectra of **9** compared to the *para*-substituted phosphine **1**, as an example.

³ Peral Crespo, D. *Triarilfosfines Sulfonades Trifluorometilades. Aplicacions en Processos Catalitics*. Ph.D. Thesis. Universitat Autònoma de Barcelona, **2013**.

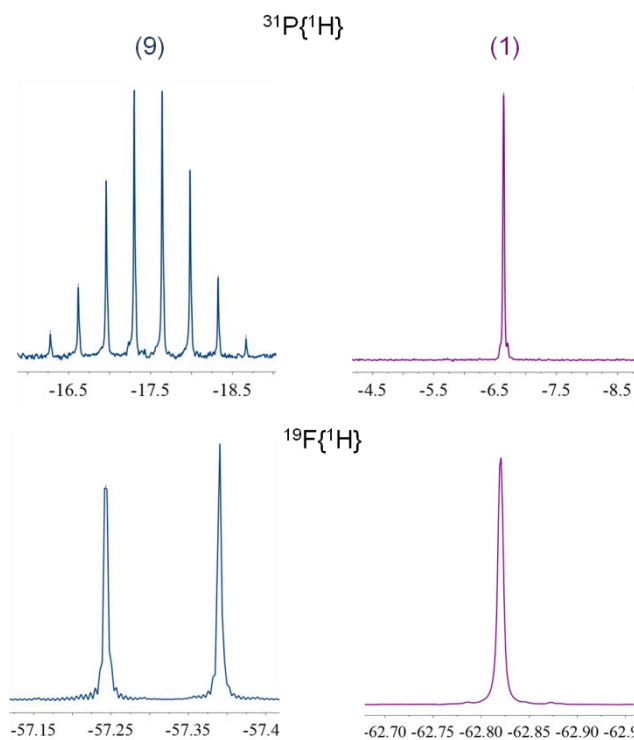


Figure 3.1. $^{31}\text{P}\{^1\text{H}\}$ (161.98 MHz) and $^{19}\text{F}\{^1\text{H}\}$ (376.50 MHz) of homoleptic trifluoromethylated phosphines **9** and **1**. Solvent: CDCl_3 . δ in ppm

^1H NMR spectra of these phosphines present a wider variety of patterns. From the simple spectra of **14** showing a singlet at 7.99 ppm and a doublet at 7.75 ppm with $^3J_{\text{HP}} = 7.0$ Hz, to the more complex spectra of the less symmetric *meta* and *ortho*-substituted phosphines, **5** and **9**, respectively (**Figure 3.2**). Assignment of the signals was made with the help of bidimensional COSY and, in a few instances, with $^1\text{H}\{^{31}\text{P}\}$ NMR experiments.

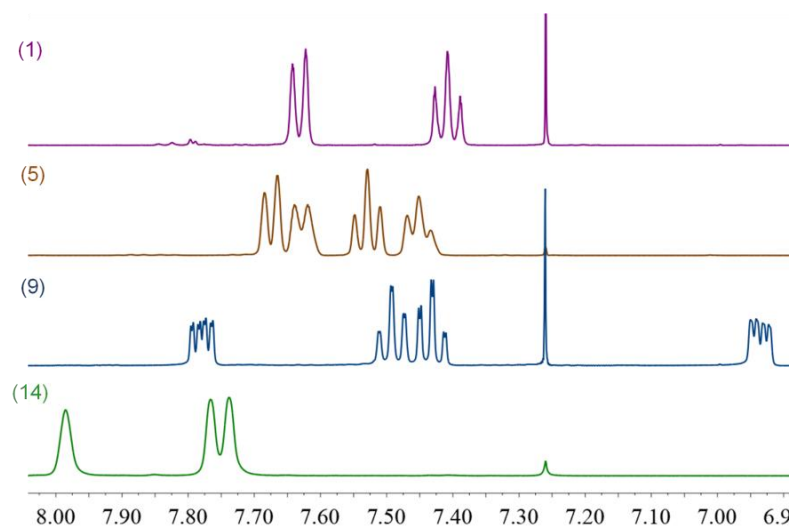


Figure 3.2 ^1H NMR spectra of the homoleptic phosphines **1**, **5**, **9** and **14**. Solvent: CDCl_3 . δ in ppm

With respect to $^{13}\text{C}\{^1\text{H}\}$ NMR, the chemical shifts observed are found within the values expected for aromatic carbon atoms (140-120 ppm). The presence of phosphorus and fluorine atoms in these compounds gives rise to a set of different multiplets in the spectra covering a wide variety of J_{CP} and J_{CF} couplings. **Figure 3.3** shows the $^{13}\text{C}\{^1\text{H}\}$ NMR spectra of tris-(3-trifluoromethylphenyl)phosphine (**5**), as example.

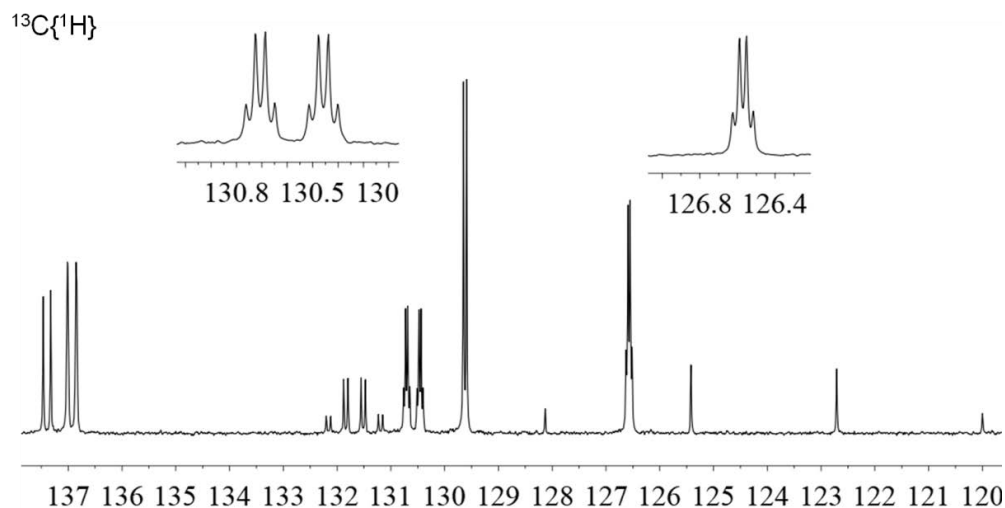


Figure 3.3. $^{13}\text{C}\{^1\text{H}\}$ NMR spectra (100.6 MHz) of phosphine **5**. Solvent: CDCl_3 . δ in ppm

3.1.2. Heteroleptic trifluoromethylated triarylphosphines

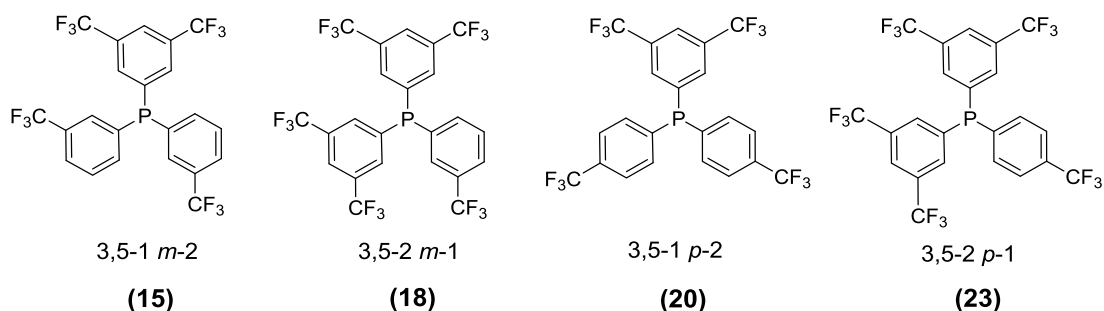


Chart 3.2. Heteroleptic trifluoromethylated phosphines used in this work

The heteroleptic phosphines used in this work were designed with the intention of having two different types of trifluoromethyl groups in each phosphine. As it will be shown later on in this chapter, the reactivity of the trifluoromethyls towards hydrolysis depends on their relative position with respect to the phosphorus atom. Moreover, although 3,5-trifluoromethyl groups are located in *meta*-position, their reactivity differ from those groups located at “single” *meta*-positions (**5** vs **14**, for instance). With this in

mind, two sets of heteroleptic trifluoromethylated phosphines combining either *meta*- or *para*-substituents with 3,5-CF₃ groups were synthesised, **Chart 3.2**.

The preparation of heteroleptic phosphines is more complex than that of the homoleptic ones. Generally speaking, the different methodologies described in the synthesis of these compounds can be classified into two groups, depending on the oxidation state of the phosphorus atom.⁴ On the one hand, we find those synthetic procedures which make use of trivalent phosphorus compounds. Chlorophosphines and metal phosphides are normally used as precursors in this synthesis. Given the air-sensitive nature of these phosphorus compounds towards oxidation and hydrolysis (P-O formation), these methodologies require of rigorous oxygen- and water-free experimental conditions and the strict use of Schlenk techniques. In this sense, one might bear in mind that the stability towards oxidation can be reduced by the presence of electron-withdrawing groups bonded to the phosphorus atom. The main advantage of these procedures, though, is that once all the P-C bonds are formed the phosphorus compound is already a phosphine and thus no further step of P-O reduction is required. The second approach for the synthesis of heteroleptic triarylphosphines implies the use of tetrahedral P=O species, including phosphonates, phosphinates or secondary phosphine oxide amongst others.⁵ These phosphorus species are stable towards oxidation and hydrolysis thus overcoming the main issues encountered with those phosphorus species with lower oxidation states. Since the phosphorus atom needs to be reduced at the end of the reaction, simple bench-top chemistry is allowed in most of the reaction steps. One of the difficulties of the synthesis of heteroleptic phosphines with P=O species is the reduction of the phosphine oxide in a selective manner. In view of the advantages of these methodologies, a new interest has arisen in the recent years to improve the existing methodologies.^{4,5,6} So far, however, it seems that the most efficient processes are limited to alkyl-containing phosphines.

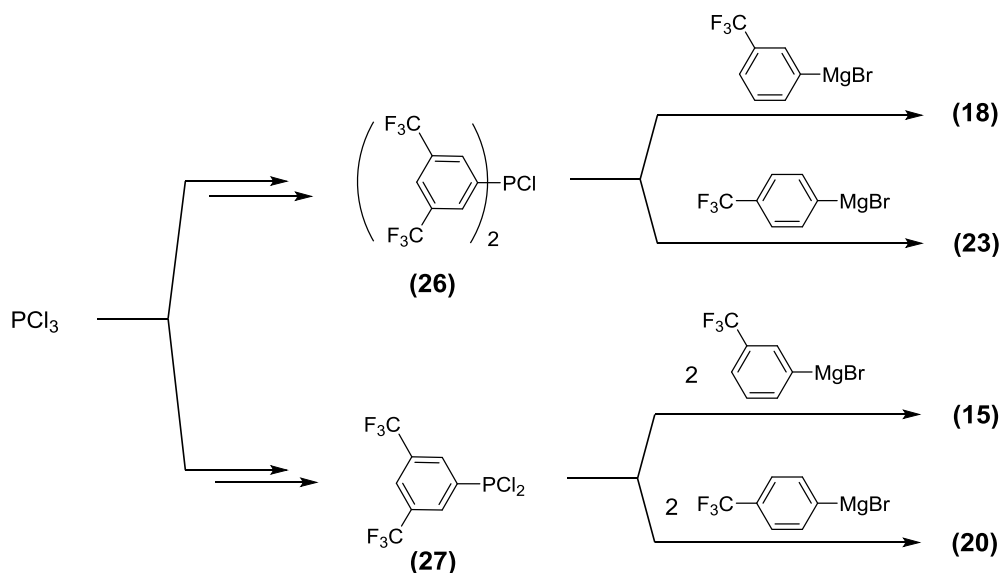
Given our experience in the synthesis of phosphines, we decided to prepare the heteroleptic phosphines in analogy with the procedure of synthesis of the homoleptic ones. That is using PCl₃ as trivalent phosphorus precursor, and the corresponding

⁴ Kendall, A. J.; Tyler, D. R. *Dalton Trans.* **2015**, 44 (28), 12473–12483.

⁵ a) Kendall, A. J.; Seidenkranz, D. T.; Tyler, D. R. *Organometallics* **2017**, 36 (13), 2412–2417. b) Rinehart, N. I.; Kendall, A. J.; Tyler, D. R. *Organometallics* **2018**, 37 (2), 182–190.

⁶ Kendall, A. J.; Salazar, C. A.; Martino, P. F.; Tyler, D. R. *Organometallics* **2014**, 33 (21), 6171–6178.

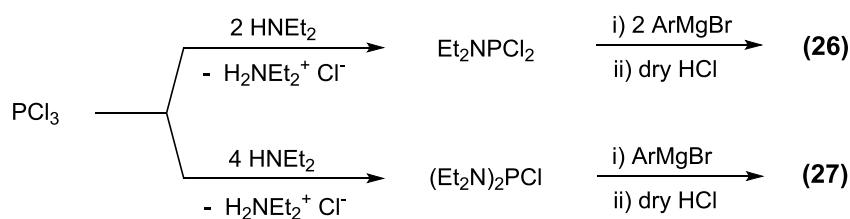
Grignard reagents in a sequential way. Two chlorophosphines are therefore necessary to prepare the four heteroleptic phosphines: bis(3,5-bis(trifluoromethyl)phenyl)chlorophosphine (**26**) and (3,5-bis(trifluoromethyl)phenyl)dichlorophosphine (**27**), **Scheme 3.2**.



Scheme 3.2. Formation of heteroleptic phosphines **18**, **23**, **15**, and **20** from PCl_3

The high reactivity of PCl_3 makes it necessary the protection of chlorine groups as *N,N*-diethylphosphoramidous dichloride, Et_2NPCl_2 , and *N,N,N',N'*-tetraethylphosphorodiamidous chloride, $(\text{Et}_2\text{N})_2\text{PCl}$. This compounds will be used to selectively form the chlorophosphines **26** and **27** after reaction with the corresponding Grignard reagent followed by P-N cleavage with HCl gas, **Scheme 3.3**.⁷ In this respect, HCl gas can be generated *in situ* by slow addition of 35 % aqueous HCl over concentrated sulfuric acid. The gas generated is then bubbled into the corresponding solution containing the trifluoromethylated aryl phosphoramidous compounds. Alternatively, HCl gas was bubbled into dry Et_2O to generate an ethereal solution of dry HCl, with concentration up to 2 M, which was stable at 7 °C for at least a month. This solution can afterwards be added when needed as a more controlled source of dry HCl.

⁷ a) Casalnuovo, A. L.; RajanBaby, T. V.; Ayers, T. A.; Warren, T. H. *J. Am. Chem. Soc.* **1994**, *116* (22), 9869–9882. b) Whitaker, C. M.; Kott, K. L.; McMahon, R. J. *J. Org. Chem.* **1995**, *60* (11), 3499–3508. c) Klaehn, J. R.; Peterman, D. R.; Harrup, M. K.; Tillotson, R. D.; Luther, T. A.; Law, J. D.; Daniels, L. M. *Inorg. Chim. Acta* **2008**, *361* (8), 2522–2532. d) Holstein, P. M.; Vogler, M.; Larini, P.; Pilet, G.; Clot, E.; Baudoin, O. *ACS Catal.* **2015**, *5* (7), 4300–4308.



Scheme 3.3. Reaction of formation of heteroleptic phosphines **18**, **21**, **15**, and **20**. ArMgBr = (3,5-bis(trifluoromethyl)phenyl)magnesium bromide

Chlorophosphines **26** and **27** are more prone to undergo P-Cl hydrolysis than the non-trifluoromethylated equivalents chlorodiphenylphosphine and dichlorophenylphosphine, respectively. The trifluoromethylated aryl groups at **26** and **27**, as electron-withdrawing groups, increase the electrophilicity of the phosphorus atom, thus facilitating the reaction with water. In this regard, it is recommended to prepare the chlorophosphines **26** and **27** and use them within a period of time no longer than two weeks. When stored for larger periods of time, even at 7 °C and under N₂ atmosphere in a Schlenk tube, the formation of precipitate together with yellow colouring of the solution, indicating degradation of the chlorophosphine, was observed.

With this procedure, the heteroleptic phosphines (3,5-bis(trifluoromethyl)phenyl)bis(3-(trifluoromethyl)phenyl)phosphine (3,5-1 *m*-2, **15**), bis(3,5-bis(trifluoromethyl)phenyl)(3-(trifluoromethyl)phenyl)phosphine (3,5-2 *m*-1, **18**), (3,5-bis(trifluoromethyl)phenyl)bis(4-(trifluoromethyl)phenyl)phosphine (3,5-1 *p*-2, **20**) and bis(3,5-bis(trifluoromethyl)phenyl)(4-(trifluoromethyl)phenyl)phosphine (3,5-2 *p*-1, **23**) were prepared in acceptable overall yields. As far as we are concerned, these heteroleptic phosphines had not been described in the literature before.

The characterisation of the heteroleptic phosphines was done by multinuclear NMR spectroscopy (¹H, ¹³C, ¹⁹F and ³¹P), High Resolution Mass Spectrometry (HR-MS) and Elemental Analysis (C and H). ¹³C{¹H} and ¹⁹F{¹H} NMR spectra of the phosphines show in all cases the two distinct CF₃ groups, *meta* and 3,5 in the case of **15** and **18**, and *para* and 3,5 in the case of **20** and **23**. As a matter of example, the ¹³C{¹H} and ¹⁹F{¹H} NMR spectra of **15** are shown in **Figure 3.4**. Moreover, ¹H NMR spectra show the pattern of substitution of each of the aryl groups in each phosphine, **Figure 3.5**.

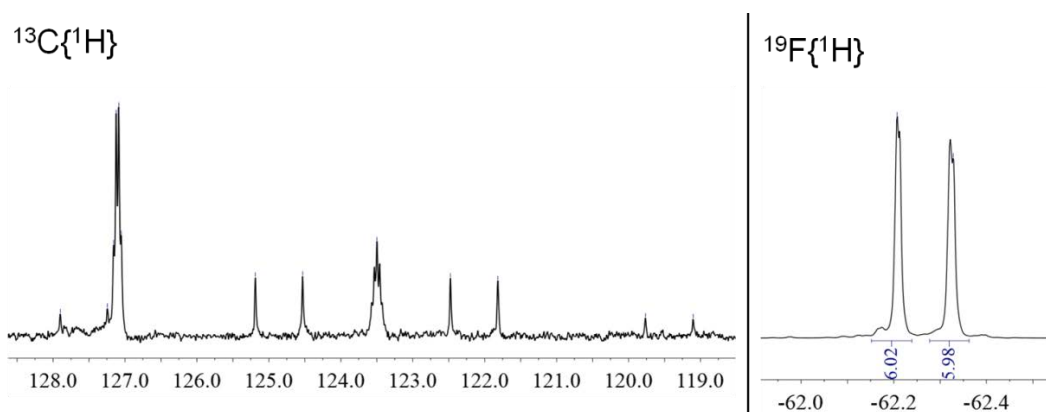


Figure 3.4. $^{13}\text{C}\{^1\text{H}\}$ (100.6 MHz), only region of the CF_3 group is shown, and $^{19}\text{F}\{^1\text{H}\}$ (376.5 MHz) NMR spectra of the heteroleptic phosphine **15**. Solvent: CDCl_3 . δ in ppm

Furthermore, crystals of good quality for single-crystal X-ray diffraction of phosphine 3,5-1 *p*-2, **20** were obtained by slow precipitation in CH_2Cl_2 . ORTEP diagram and some selected distances and angles are shown in **Figure 3.6**. Helix-like arrangement of the phosphine is observed in **20**, as expected for a triarylphosphine. Values of P-C distances and C-P-C angles were also found within the expected magnitudes.

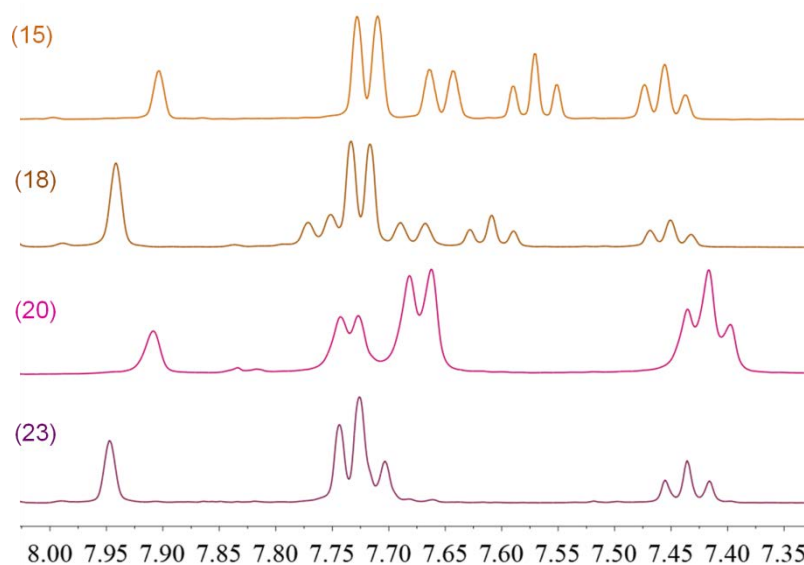


Figure 3.5. ^1H NMR spectra (400.13 MHz) of the heteroleptic phosphines **15**, **18**, **20** and **23**. Solvent: CDCl_3 . δ in ppm

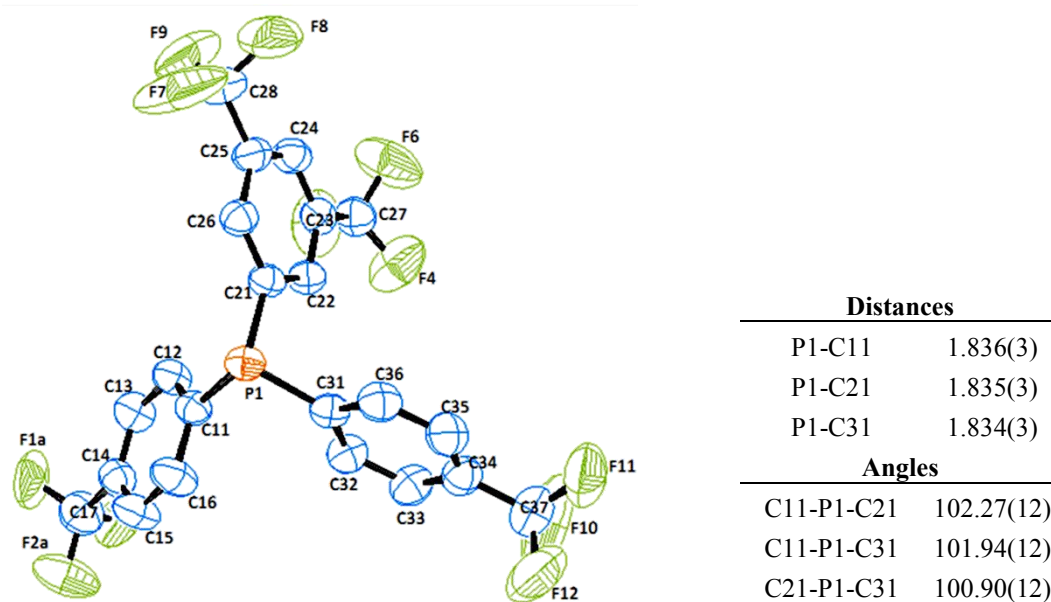


Figure 3.6. ORTEP plot (ellipsoid at 50% probability) of **20** and selected distances (Å) and angles (°). Only one orientation of the disordered CF₃ group is drawn. Aromatic H atoms omitted for clarity

3.2. Study of the electronic properties of the trifluoromethylated phosphines

The electronic properties of the trifluoromethylated phosphines presented above were evaluated by the preparation of different derivatives: Vaska-type Ir(I) complexes, phosphine selenides and by protonation of the phosphorus atom (phosphonium ions).

3.2.1. Vaska-type Ir (I) complexes

Stretching frequencies of coordinated CO ligand in metal complexes is a common and simple resource to study the σ/π -bonding behaviour of phosphines. Tolman studied the electron donor-acceptor properties of different phosphorus ligands measuring the carbonyl A₁ stretching frequency of Ni(CO)₃L complexes in CH₂Cl₂.⁸ The increased π -acidity of phosphorus ligands substituted with more electron-withdrawing groups is clearly observed by displacement of the CO frequency to higher values (cm⁻¹). Electron-back donation from the metal centre to these acidic phosphorus ligands is increased as a result of their π -acceptor ability. This effect reduces the electron density on the metal centre and, as consequence, decreases the back donation to the CO ligand, resulting in a shorter (stronger) C-O distance, and hence in higher carbonyl frequencies (**Figure 3.7**).

⁸ Tolman, C. A. *J. Am. Chem. Soc.* **1970**, *92* (10), 2953–2956.

The opposite effect is therefore observed with those phosphorus ligands which have higher σ -donor and lower π -acceptor character.

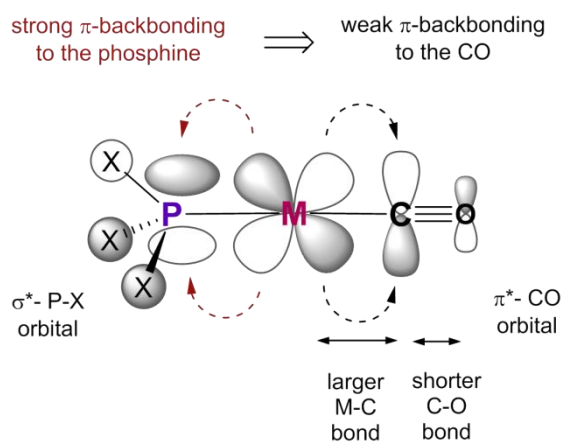


Figure 3.7. Representation of the effect of strong π -acidic phosphorus ligands in the C-O distance

In analogy with the Ni-carbonyl complexes of Tolman, Vaska-type complexes can also be used to determine the σ/π -bonding characteristics of phosphines.⁹ Vaska's compound is the name given to *trans*-carbonylchlorobis(triphenylphosphine)iridium(I) (*trans*-[Ir(CO)Cl(PPh₃)₂]). Although it was firstly reported by Angoletta,¹⁰ its composition was correctly elucidated by Vaska and DiLuzio two years later.¹¹ Nowadays, Vaska-type complexes are considered those with the general formula *trans*-[M(CO)X(L)₂], where M can be either Rh or Ir, X is an halogen or pseudohalogen and L refers to a neutral ligand.^{9a}

Vaska's analogue complexes of the formula *trans*-[Ir(CO)Cl(L)₂] with the homoleptic and heteroleptic trifluoromethylated phosphines were prepared. Following the synthetic procedure previously described in our group,³ [Ir(COD)Cl]₂ was mixed with the corresponding phosphine (4 mol of phosphine per mol of Ir precursor dimer) and the resulting orange solution was bubbled with CO until the formation of a yellow solution. The Vaska-type complex was finally isolated by precipitation in diethylether and characterised by NMR spectroscopy (³¹P, ¹⁹F and ¹H) and HR-MS. Also the Vaska's compound, (*trans*-[Ir(CO)Cl(PPh₃)₂]) was prepared for comparison purposes.

⁹ a) Roodt, A.; Otto, S.; Steyl, G. *Coord. Chem. Rev.* **2003**, 245 (1–2), 121–137. b) Otto, S.; Roodt, A. *Inorg. Chim. Acta* **2004**, 357 (1), 1–10.

¹⁰ Angoletta, M. *Gazz. Chim. Ital.* **1959**, 89, 2359.

¹¹ a) Vaska, L.; DiLuzio, J. W. *J. Am. Chem. Soc.* 1961, 2784–2785. b) Kirss, R. U. *Bull. Hist. Chem.* **2013**, 38 (1), 52–60.

Vaska-type complexes of all the trifluoromethylated phosphines were successfully prepared with exception of the *ortho*-substituted phosphine (**9**) which did not coordinate the metal and the heteroleptic phosphine (**15**) which could not be purified by precipitation in diethyl ether, *n*-hexane or several other solvents or combinations of them including water and methanol.

The IR spectra of the complexes was registered as solid (ATR-FTIR) and in CH₂Cl₂ solution. **Table 3.1** shows the CO frequency of the complexes. The values of CO vibration in solution observed in the Vaska-type complexes showed good correlation between the CO frequencies and the number of CF₃ groups in the phosphines. As expected, when the number of trifluoromethyl groups in the phosphines is increased, the CO frequencies are shifted to higher wavenumbers as a result of a lower σ -donor ability and greater π -acidic character of the phosphine ligand. No significant differences were found between the *para* and the *meta*-isomers. However, it can be observed that values of frequencies in solid (ATR-FTIR) do not follow the same tendency as observed in solution. These observations might be tentatively attributed to interactions in the solid structures of the complexes.

Table 3.1. Carbonyl stretching IR frequencies (cm⁻¹) of the Vaska-type complexes *trans*-[Ir(CO)Cl(L)₂]

Ligand (L)	CH ₂ Cl ₂ ^a	Solid (ATR-FTIR) ^b
TPP ^c	1964	1949
<i>p</i> -trisCF ₃ (1)	1975 ^d	1974 ^d
3,5-1 <i>p</i> -2 (20)	1979	1972
3,5-2 <i>p</i> -1 (23)	1983	1973
<i>m</i> -trisCF ₃ (5)	1976	1982
3,5-1 <i>m</i> -2 (15)	-	-
3,5-2 <i>m</i> -1 (18)	1983	1988
3,5-trisCF ₃ (14)	1986 ^d	1979 ^d
<i>o</i> -trisCF ₃ (9)	-	-

^a IR spectra registered in solution in CH₂Cl₂. ^b IR spectra registered as solid compound.

^c Triphenylphosphine. ^d Value from previous work in our group³

3.2.2. Phosphine selenides and phosphonium ions

The σ -donation ability of the phosphines have been evaluated by measuring the ¹J_{PSe} coupling in the Se⁷⁷ (s=1/2, 7.63 % natural abundance) isotopomer of the corresponding phosphine selenides. Given that the P-Se bond character is mainly simple-bond and has

little double-bond contribution,¹² it can be considered that the phosphine selenide coupling constant is directly related to the σ -donor ability of the ligand, in contrast to the carbonyl IR frequency of metal-carbonyl complexes shown above, the value of which accounts for both σ -donor and π -acceptor properties. Direct spin-spin coupling constant in organophosphorus selenides has been reported as a simple and straightforward manner to evaluate the σ -donation ability of phosphorus ligands.¹³ Allen and Taylor^{13a,b} observed that the value of the $^1J_{\text{PSe}}$ in phosphine selenides increased when introducing electro-withdrawing groups bonded to the phosphorus atom. These observations were attributed to an increase in the s character of the phosphorus lone pair in agreement with Bent's rule.¹⁴ The opposite effect was reported with electro-donating or bulky substituents. X-ray diffraction structures of some phosphine selenides have shown shorter P-Se distances in trifluoromethylated triarylphosphines with respect to triphenylphosphine.¹⁵ Moreover, Malito *et al.* proved good correlation between P-Se distance and the $^1J_{\text{PSe}}$ in phosphine selenides.^{13c} Also good correlation between the Brønsted basicity of phosphines (measured as $\text{p}K_{\text{a}}$ or $\text{p}K_{\text{b}}$) and the $^1J_{\text{PSe}}$ of the corresponding selenides has been reported^{13c,d,15}, showing larger values of $^1J_{\text{PSe}}$ when reducing the basicity of the phosphines. Deviation of this trend, though, was observed in phosphines containing bulky substituents.

Therefore the selenide derivatives of homoleptic phosphines **1**, **5** and **14** and the heteroleptic phosphines **15**, **18**, **20** and **23** were prepared. The standard procedure consisted in the preparation of a 0.01 M solution of the corresponding phosphine in degassed CDCl_3 to which 1.5 equivalents of Se black was added. The mixture was then stirred overnight under inert atmosphere at room temperature to obtain the corresponding phosphine selenide. Alternatively, for the less basic phosphines, stirring at 50 °C was preferred to obtain the selenide quantitatively. Excess selenium was then filtered through a celite pad previous to the NMR analysis. **Figure 3.8** shows the

¹² a) McFarlane, W.; Rycroft, D. S. *J. Chem. Soc. Dalton Trans.* **1973**, No. 20, 2162–2166. b) Grim, S. O.; Walton, E. D. *Inorg. Chem.* **1980**, *19* (7), 1982–1987.

¹³ a) Allen, D. W.; Taylor, B. F. *J. Chem. Soc. Dalton Trans.* **1982**, No. 1, 51–54. b) Allen, D. W.; March, L. A.; Nowell, I. W. *J. Chem. Soc. Dalton Trans.* **1984**, No. 3, 483–485. c) Malito, J.; Alyeat, E. C. *Phosphorus. Sulfur. Silicon Relat. Elem.* **1990**, *54* (1–4), 95–99. d) Beckmann, U.; Süslüyan, D.; Kunz, P. C. *Phosphorus. Sulfur. Silicon Relat. Elem.* **2011**, *186* (10), 2061–2070.

¹⁴ Bent, H. A. *Chem. Rev.* **1961**, *61* (3), 275–311.

¹⁵ Howell, J. A. S.; Fey, N.; Lovatt, J. D.; Yates, P. C.; McArdle, P.; Cunningham, D.; Sadeh, E.; Gottlieb, H. E.; Goldschmidt, Z.; Hursthouse, M. B.; Light, M. B. *J. Chem. Soc. Dalton Trans.* **1999**, No. 17, 3015–3028.

$^{31}\text{P}\{^1\text{H}\}$ NMR spectra of the selenides of the homoleptic phosphines **1**, **5** and **14**, as representative examples.

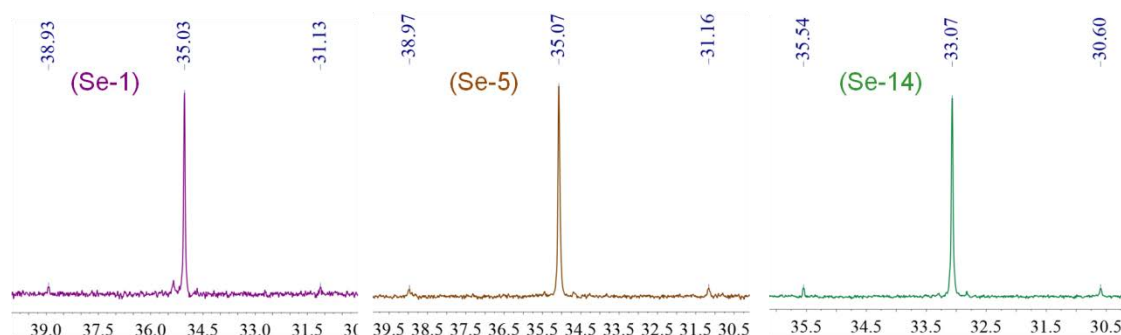


Figure 3.8. $^{31}\text{P}\{^1\text{H}\}$ (161.98 MHz) NMR spectra of the selenides of phosphines **1**, **5** and **14** (**Se-1**, **Se-5** and **Se-14**, respectively). Solvent: CDCl_3 . δ in ppm

The *o*-substituted phosphine **9** did not afford the corresponding selenide under these conditions. Attempts to obtain the corresponding selenide by refluxing the reaction mixture for three days also resulted unsuccessful. Steric hindrance around the P atom produced by the trifluoromethyl groups is thought to be responsible for the inertness of this phosphine towards the formation of the selenide. With this in mind, and knowing that coordination to metal failed as well, we tried an alternative methodology to measure the basicity of this phosphine. It has been shown that the magnitude of the one-bond H-P coupling constant ($^1J_{\text{HP}}$) increases with decreasing the basicity of protonated phosphorus ligands (phosphines and phosphites).¹⁶ We thought therefore that hydrogen, it being a considerably smaller atom than selenium, would be able to bond the sterically hindered phosphorus atom of the *ortho*-substituted phosphine **9**, thus providing information about the basicity of this ligand. A 0.05 M solution of **9** was prepared by dissolving the phosphine in concentrated sulfuric acid and was analysed by ^{31}P and $^{31}\text{P}\{^1\text{H}\}$ NMR, **Figure 3.9**. Comparison of both spectra shows clear protonation of the phosphine with $^1J_{\text{HP}} = 500$ Hz. Due to the broadness of the signal in the ^{31}P NMR produced by the coupling to the proton and the fluorine atoms, fine measurement of the coupling constant was done with the ^1H NMR spectrum. In this respect, $^{31}\text{P}\{^1\text{H}\}$ NMR showed a decaplet, as expected, but with a P-F coupling 5-fold smaller than that of the non-protonated phosphine (11 Hz vs 55 Hz). This is a nice example of the *through-*

¹⁶ a) Olah, G. A.; McFarland, C. W. *J. Org. Chem.* **1969**, *34* (6), 1832–1834. b) McFarlane, W.; White, R. F. M. *J. Chem. Soc. D.* **1969**, No. 13, 744. c) Allman, T.; Goel, R. G. *Can. J. Chem.* **1982**, *60* (6), 716–722.

space coupling between P and F. While in phosphine **9** the lone pair of the phosphorus atom is free to interact with fluorine atoms in *ortho*, in the protonated form this interaction is no longer possible and, as a consequence, no *through-space* coupling is possible.

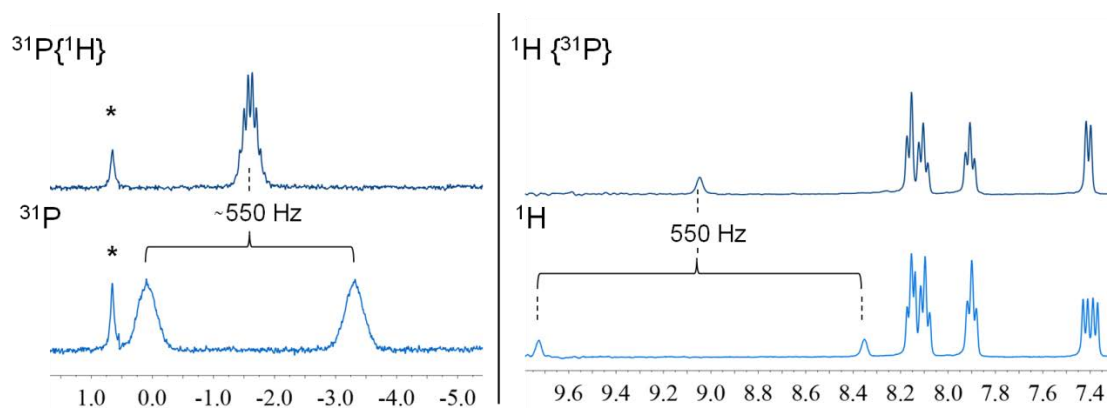


Figure 3.9. **Left-** ^{31}P and $^{31}\text{P}\{^1\text{H}\}$ (161.98 MHz) NMR spectra of phosphine **9** in concentrated sulfuric acid (0.05 M). Signals relative to a solution of NH_4PF_6 (0.08 g/ml in D_2O) used as internal standard. Singlet indicated as * correspond to the partial degradation of the internal standard. **Right-** ^1H and $^1\text{H}\{^{31}\text{P}\}$ (400.13 Hz) NMR spectra of **9** under the same conditions as in **Left**. Only aromatic region is shown. δ in ppm

The same procedure was performed with the full set of trifluoromethylated phosphines studied in this section to obtain the protonated phosphines. The key point of these experiments is that quantitative protonation of the phosphines is needed. Otherwise, an average value between the protonated form and the phosphine would be obtained. In this sense, Pestovsky *et al.*¹⁷ reported full protonation of arylphosphines in 1.5 M solutions of $\text{CF}_3\text{SO}_3\text{H}$ in $\text{H}_2\text{O}/\text{CH}_3\text{CN}$. We assumed then, that concentrated sulfuric acid would yield quantitative protonation of the trifluoromethylated phosphines. In fact, complete protonation of phosphines in this acid as well as HSO_3F or trifluoroacetic has also been reported with similar values of $^1J_{\text{PH}}$ for triphenylphosphine.¹⁶

For a better comparison, values of $^1J_{\text{HP}}$ of the phosphoniums together with the $^1J_{\text{PSe}}$ of the selenides are shown in **Table 3.2**.

¹⁷ Pestovsky, O.; Shuff, A.; Bakac, A. *Organometallics* **2006**, 25 (11), 2894–2898.

Table 3.2. Values of $^1J_{\text{PSe}}$ and $^1J_{\text{HP}}$ for the corresponding selenides and phosphonium ions, respectively, with the trifluoromethylated triarylphosphines

Ligand	Selenide $^1J_{\text{PSe}}^{\text{a}}$	Protonated phosphonium $^1J_{\text{HP}}^{\text{b}}$
TPP ^c	731	503
<i>p</i> -trisCF ₃ (1)	766	527
3,5-1 <i>p</i> -2 (20)	779	536
3,5-2 <i>p</i> -1 (23)	790	546
<i>m</i> -trisCF ₃ (5)	767	528
3,5-1 <i>m</i> -2 (15)	780	538
3,5-2 <i>m</i> -1 (18)	791	545
3,5-trisCF ₃ (14)	800	555
<i>o</i> -trisCF ₃ (9)	-	550 ^d

^a Values obtained from the $^{31}\text{P}\{^1\text{H}\}$ in CDCl_3 . See text for more details. ^b Values obtained from the ^{31}P NMR in conc. H_2SO_4 . See text for more details. ^c Triphenylphosphine. ^d From ^1H NMR.

Both $^1J_{\text{HP}}$ and $^1J_{\text{PSe}}$ follow the same trend and higher values were observed when increasing the number of trifluoromethyl groups in the phosphines. As observed by Howell *et al.* in the selenides of phosphines **1**, **5** and **14**,¹⁵ it was found that the values of $^1J_{\text{PSe}}$ are cumulative in the whole series of the trifluoromethylated phosphines studied. In this way, the addition of three CF₃ groups in the aromatic rings produces an increase in the $^1J_{\text{PSe}}$ of about 35 Hz (TPP vs **1** or **5**, and **14** vs **1** or **5**). If this trend were true, the effect of adding one trifluoromethyl would be of *ca.* 11-12 Hz, which is what was observed in the series **1** - **20** - **23** - **14** and **5** - **15** - **18** - **14**. Interestingly, the same behaviour was found in the protonated phosphines. In this case, each trifluoromethyl accounts for an increase of 9-10 Hz in the $^1J_{\text{HP}}$. The *ortho*-trifluoromethylated phosphine was found to be the exception to the rule, most likely due to strong inductive effects of the trifluoromethyls groups, although steric factors might not be completely discarded.

Finally, excellent correlation was found between the magnitude of the $^1J_{\text{PSe}}$ in the selenide and the $^1J_{\text{HP}}$ of the corresponding phosphonium ions, **Figure 3.10**.

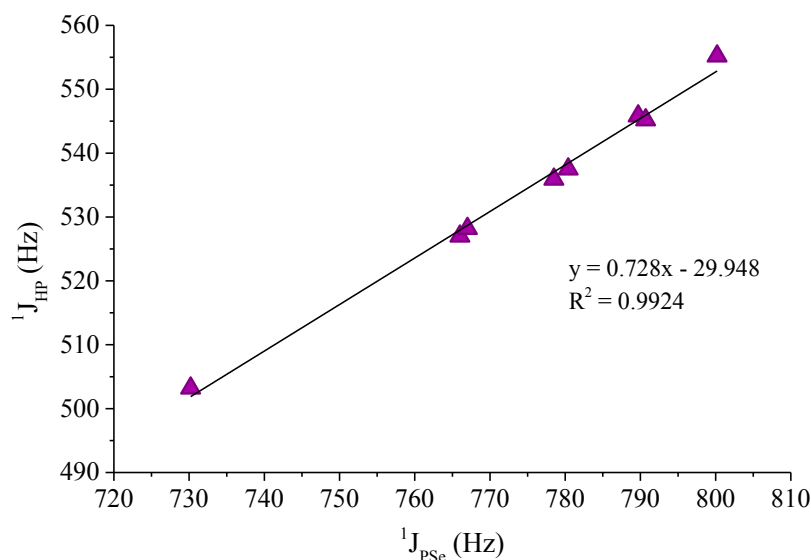


Figure 3.10. Correlation between $^1J_{\text{PSe}}$ and $^1J_{\text{HP}}$ of the trifluoromethylated phosphines

3.3. Hydrolysis of the trifluoromethyl group

As previously mentioned in the introduction, the hydrolysis of the trifluoromethyl group in arylphosphines, using fuming sulfuric acid and boric acid, was firstly observed during the sulfonation of bis(4-trifluoromethylphenyl)phenylphosphine and subsequently in the tris(4-trifluoromethylphenyl)phosphine **1**.³ In this approach, once the reaction was finished and, after hydrolysing the sulfuric solution containing SO_3 , H_3BO_3 and the phosphine, the mixture was neutralised with NaOH. The main drawback of this procedure, however, was the large amount of Na_2SO_4 generated, even larger than the quantity of phosphine synthesised, found also as a sodium salt and which should be separated from the sulfate. A second disadvantage of this procedure is the fact that the neutralization of the sulfuric solution is an exothermic process which favours the oxidation of the phosphines, thus reducing the yield of the reaction.

As an alternative method, the carboxylic phosphines were extracted from the sulfuric mixture using CH_2Cl_2 , thus avoiding the neutralisation. Extraction experiments were performed using phosphine **1** as model molecule. The phosphine was dissolved in a mixture of concentrated sulfuric acid and boric acid before the addition of SO_3 as oleum, with final concentrations of phosphine, boric acid and sulfur trioxide of 0.15 M, 0.6 M and 10.7 M, respectively, in similar conditions to those used in our group previously. Aliquots of the reaction mixture were hydrolysed at different reaction times

and extracted with CH_2Cl_2 . After solvent evaporation the samples were analysed by $^{31}\text{P}\{^1\text{H}\}$ NMR. It was observed that, at short reaction times, all the phosphorus products were extracted into the organic phase. However at longer reaction times (around 48 h), the addition of CH_2Cl_2 produced the formation of an insoluble gel-like substance. $^{31}\text{P}\{^1\text{H}\}$ NMR showed that the gel-like phase was composed of phosphine oxides, proven by their typical signal at about 26 ppm, but also a small fraction of non oxidised phosphines were detected in this phase. In order to solve this issue, diethyl ether was used instead of CH_2Cl_2 . By using this solvent all the phosphorus products were extracted into the organic phase, proven by the absence of phosphorus compounds in the $^{31}\text{P}\{^1\text{H}\}$ NMR analysis of the aqueous phase. Therefore CH_2Cl_2 was discarded as the extracting solvent and diethyl ether was used in all the synthetic procedures described in this work. It is worth mentioning that, compared to the previous procedure which involved the neutralisation with NaOH, the extraction with the organic solvent offers an improvement in terms of time (the neutralisation should be carried out slowly to avoid the phosphine oxidation) as well as in terms of the simplicity of purification of the final product.

Once the general synthetic procedure was improved and, in order to determine the scope of the reaction of hydrolysis of the trifluoromethyl group, the reaction was applied to the two different sets of trifluoromethylated triarylphosphines: homoleptic (phosphines **1**, **5**, **9**, and **14**) and heteroleptic (phosphines **15**, **18**, **20**, and **23**).

Initial remarks

Since the amount of SO_3 can differ with factors such as the number of times the bottle of oleum has been opened as well as the atmospheric humidity, slightly different results can be obtained using the same reaction conditions. For this reason, every time we intended to compare results with different conditions, the whole set of reactions have been performed either simultaneously or in consecutive days under the same atmospheric conditions. Same reaction volumes were also used to this intention. Whenever the reactions are performed with synthetic purpose, control of the reaction evolution with time is absolutely necessary.

Although initially, the reaction conditions were described as equivalents of SO₃ and H₃BO₃,^{3,18} it was later acknowledged that this terminology had been misused. Instead, concentration of each component of the reaction was used. The term “equivalent” generally refers to the stoichiometric relation between the components of a given reaction. However, this term was used to refer to the molar ratio between the phosphine and sulfur trioxide and boric acid. We later saw that the stoichiometry of these reactants in the reaction was different from 1:1:1 (see chapter 4). Regardless of this rather puristic point of view, the use of concentrations was of greater utility than merely referring to molar ratios. As a matter of fact, the later includes the former, and not the other way around.

3.3.1. Hydrolysis of the trifluoromethyl in the homoleptic phosphines

In addition to the before mentioned tris(4-trifluoromethylphenyl)phosphine (**1**), tris(3-trifluoromethylphenyl)phosphine (**5**), tris-(2-trifluoromethylphenyl)phosphine (**9**) and tris(3,5-bis(trifluoromethyl)phenyl)phosphine (**14**) were used in this study.

Preliminary results on the reaction of hydrolysis of the trifluoromethyl group in the *para* and *meta*-substituted phosphines, **1** and **5**, were investigated by the author in his Master's thesis.¹⁸ Nonetheless, it was decided to include them here for a better understanding of the reaction.

3.3.1.1. Hydrolysis of the trifluoromethyl group in phosphines **1** and **5**

The reaction of hydrolysis of the trifluoromethyl group in both *para* and *meta*-substituted phosphines, **1** and **5** respectively, will be discussed together in this section because, as it will be shown, the behaviour of these phosphines in the reaction of study is comparable between them and, to some extent, different to the other two phosphines, **9** and **14**.

¹⁸ Herrera Miranda, D. *Síntesis de Nuevas Triarilfosfinas Carboxiladas Mediante Hidrólisis del Grupo Trifluorometilo. Aplicaciones en Catálisis de Intercambio de Fase y Anclaje Sobre Silica*. Master's Thesis. Universitat Autònoma de Barcelona, **2012**.

Para-substituted phosphine 1

In the first instance an experiment was performed to evaluate the evolution of the reaction with time. The chosen conditions were the same as D. Peral had used when observed the reaction by the first time, that is to say, dissolving the phosphine in a solution of concentrated H_2SO_4 (2.3 mL per mmol of phosphine) with 4 moles of H_3BO_3 per mol of phosphine and with the addition of 70 moles of SO_3 per mol of phosphine as fuming sulfuric acid (65% w/w SO_3). The concentrations of phosphine, boric acid and sulfur trioxide in the reaction mixture were 0.15 M, 0.6 M and 10.5 M, respectively. The reaction evolution was monitored by $^{31}\text{P}\{^1\text{H}\}$ NMR. Each sample was obtained by adding an aliquot of the reaction mixture into a vial containing frozen water. Then it was extracted twice with diethyl ether and the organic fractions were evaporated. Afterwards, the obtained residue was analysed by $^{31}\text{P}\{^1\text{H}\}$ NMR, **Figure 3.11**.

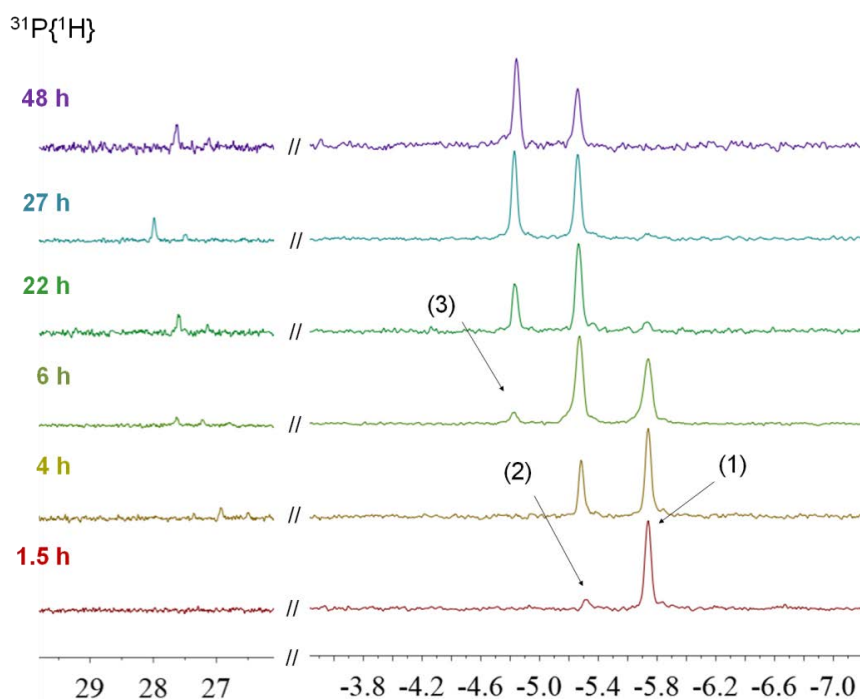
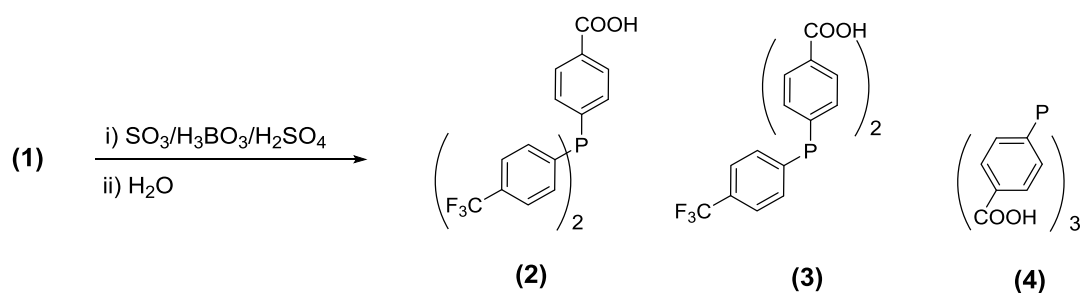


Figure 3.11. Evolution of the reaction of hydrolysis of the phosphine **1** with time. Products extracted with Et_2O from the aqueous phase after quenching in water. Analysis in $\text{CDCl}_3/\text{MeOH}$ (4:1). δ in ppm. Reaction conditions: $[\text{Phosphine}] = 0.15 \text{ M}$, $[\text{H}_3\text{BO}_3] = 0.6 \text{ M}$, $[\text{SO}_3] = 10.5 \text{ M}$. See text for further details

One hour and a half after the addition of oleum, a new signal was observed in the NMR spectrum at 0.5 ppm with respect to the starting phosphine **1**. The intensity of this new signal increased at the same time as the signal of phosphine **1** decreased in intensity and

corresponds to the product of the hydrolysis of one trifluoromethyl group, 4-(bis(4-(trifluoromethyl)phenyl)phosphanyl)benzoic (**2**), **Scheme 3.4**. Six hours after the addition of oleum, a second new signal was observed in the $^{31}\text{P}\{^1\text{H}\}$ NMR, shifted 0.4 ppm with respect to the compound **2** and which corresponds to the product of hydrolysis of a second trifluoromethyl group, 4,4'-((4-(trifluoromethyl)phenyl)phosphanediyl)-dibenzoic acid (**3**) (**Scheme 3.4**). After 27 hours of reaction, no signal for the starting phosphine **1** was observed and only carboxylated products **2** and **3** remained in the reaction mixture.



Scheme 3.4. Products of the hydrolysis of **1**

From **Figure 3.11** it can be observed that the hydrolysis reaction is not completely sequential. In other words, the formation of the dicarboxylated product **3** begins before the starting phosphine **1** has been completely consumed. Most probably the reaction rate for the hydrolysis of the second trifluoromethyl group is similar to that of the first one regardless of whether the other aromatic rings contain a trifluoromethyl group or not. Therefore the distribution of the reaction products resembles a statistic distribution. It is worth noticing that, under the conditions described, the formation of the tricarboxylated phosphine was not observed.

In order to obtain more information about what happens with the fluorine atoms of the trifluoromethyl group during the reaction, a set of experiments were carried out. After quenching an aliquot of the sulfuric reaction mixture with water and extracting with diethyl ether, both aqueous and organic phase were analysed by means of $^{19}\text{F}\{^1\text{H}\}$ NMR. While the organic phase showed only signals corresponding to trifluoromethyl groups (around -63 ppm), the aqueous phase showed a single signal around -156 ppm which could correspond to aqueous HF. After adding few droplets of a solution of NaOH to the aqueous phase it was observed that the signal at -156 ppm decreased while a new signal appeared at around -126 ppm, typical of aqueous fluoride.

Since, during the hydrolysis of the trifluoromethyl group, the reaction media does not contain water as such, other species in between the trifluoromethyl and the carboxylic groups should exist. In an attempt to obtain more information about fluorine products formed, the crude reaction media was monitored by $^{19}\text{F}\{^1\text{H}\}$ NMR. To that end, a sample of the reaction mixture was introduced into an NMR tube containing a capillary tube of a solution of NH_4PF_6 in D_2O as internal reference and lock, respectively. A new signal at 42.6 ppm in the $^{19}\text{F}\{^1\text{H}\}$ NMR was observed which increased in intensity at the same time as the reaction of hydrolysis progressed. This signal had not been observed before either in the organic or the aqueous phase after quenching the reaction mixture with water and extracting with organic solvent. It is important to note the fact that this signal has been observed in all the reactions involving the hydrolysis of the trifluoromethyl group in the present work and can be attributed to HSO_3F . Its identification and origin will be described in detail the next chapter.

The evolution of the products in the sulfuric media was also monitored by $^{31}\text{P}\{^1\text{H}\}$ NMR of the crude reaction (**Figure 3.12**). This procedure should minimise the possible phosphine oxidation produced during the quenching and extraction methodology. Although ideally, the determination of the actual concentration of phosphine oxides in the mixture must be possible by the direct analysis of the crude reaction, signals corresponding to phosphine oxides are broader in the sulfuric medium, which adds difficulty to their determination. As in the case of $^{19}\text{F}\{^1\text{H}\}$, a capillary tube with a solution of NH_4PF_6 in D_2O was used.

It should be emphasized that signals corresponding to phosphines and to phosphine oxides are shifted downfield than compared to the signals after the quenching with water. Two reasons can explain this variation in the chemical shifts. The first one is that at the pH of the reaction both phosphines and phosphines oxides can be protonated,¹⁹ **Scheme 3.5**. The second one is that, unlike what happens in the samples after treating the reaction with water, in the sulfuric media the products observed are not carboxylic acids but intermediates between this group and the trifluoromethyl group, which would influence the chemical shifts as well.

¹⁹ a) Haake, P.; Cook, R. D.; Hurst, G. H. *J. Am. Chem. Soc.* **1967**, *89* (11), 2650–2654. b) Furin, G. G.; Krupoder, S. A.; Rezvukhin, A. I.; Kilina, T. M.; Yakobson, G. G. *J. Fluor. Chem.* **1983**, *22* (4), 345–375. c) Tolstikova, L. L.; Bel'skikh, A. V.; Shainyan, B. A. *Russ. J. Gen. Chem.* **2011**, *81* (3), 474–480.

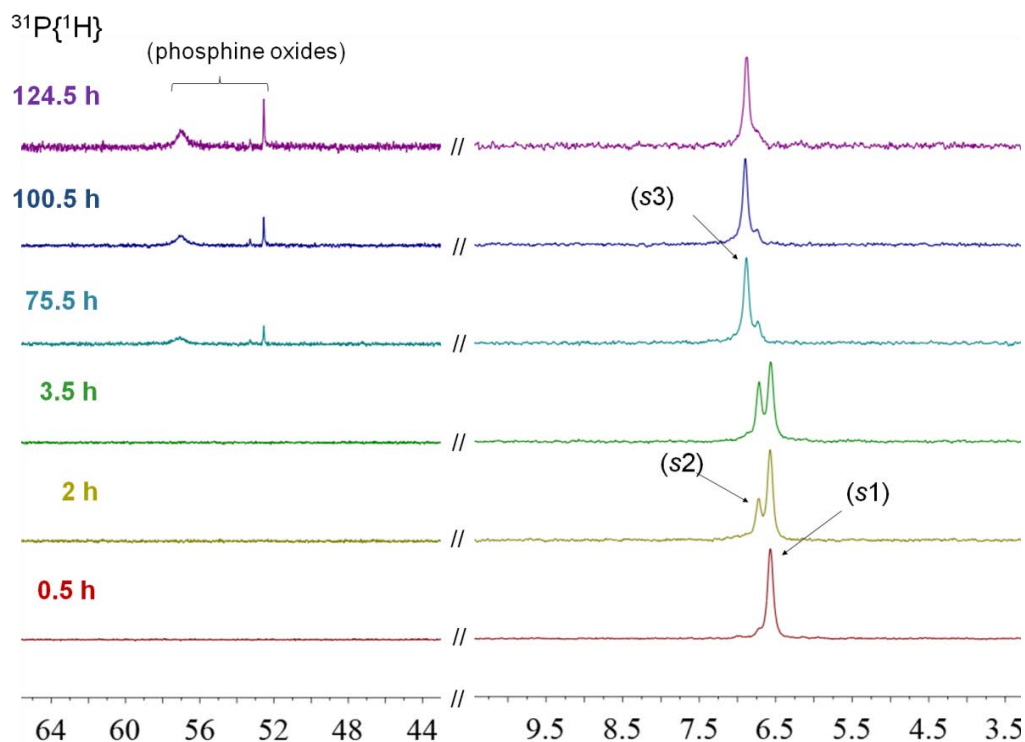
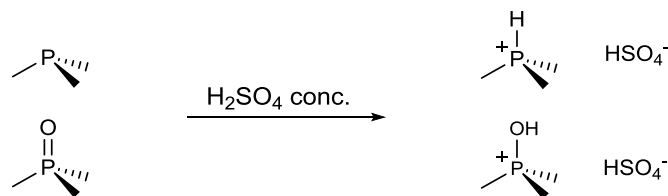


Figure 3.12. Evolution of the reaction of hydrolysis of phosphine **1** with time. $^{31}\text{P}\{^1\text{H}\}$ NMR (101.27 MHz) analysis of the crude reaction. Signals (intensity and position) relative to NH_4PF_6 used as internal standard. δ in ppm. **s1**, **s2** and **s3** refer to compounds **1**, **2**, and **3** in sulfuric medium, respectively. Reaction conditions: $[\text{Phosphine}] = 0.15 \text{ M}$, $[\text{H}_3\text{BO}_3] = 0.6 \text{ M}$, $[\text{SO}_3] = 10.5 \text{ M}$



Scheme 3.5. Schematic representation of the protonation of phosphines and phosphine oxides in acidic media

The reaction was explored in a series of experiments with the aim of studying the effect produced by different concentrations of reactants. The reactions were monitored using the quenching and extractions procedure followed by the analysis of the products by $^{31}\text{P}\{^1\text{H}\}$ NMR in a mixture of $\text{CDCl}_3/\text{MeOH}$ (4:1). The percentage of the products was determined using the integration of the signals in the NMR spectra. The evolution of the experiments is graphically shown in **Figure 3.13**.

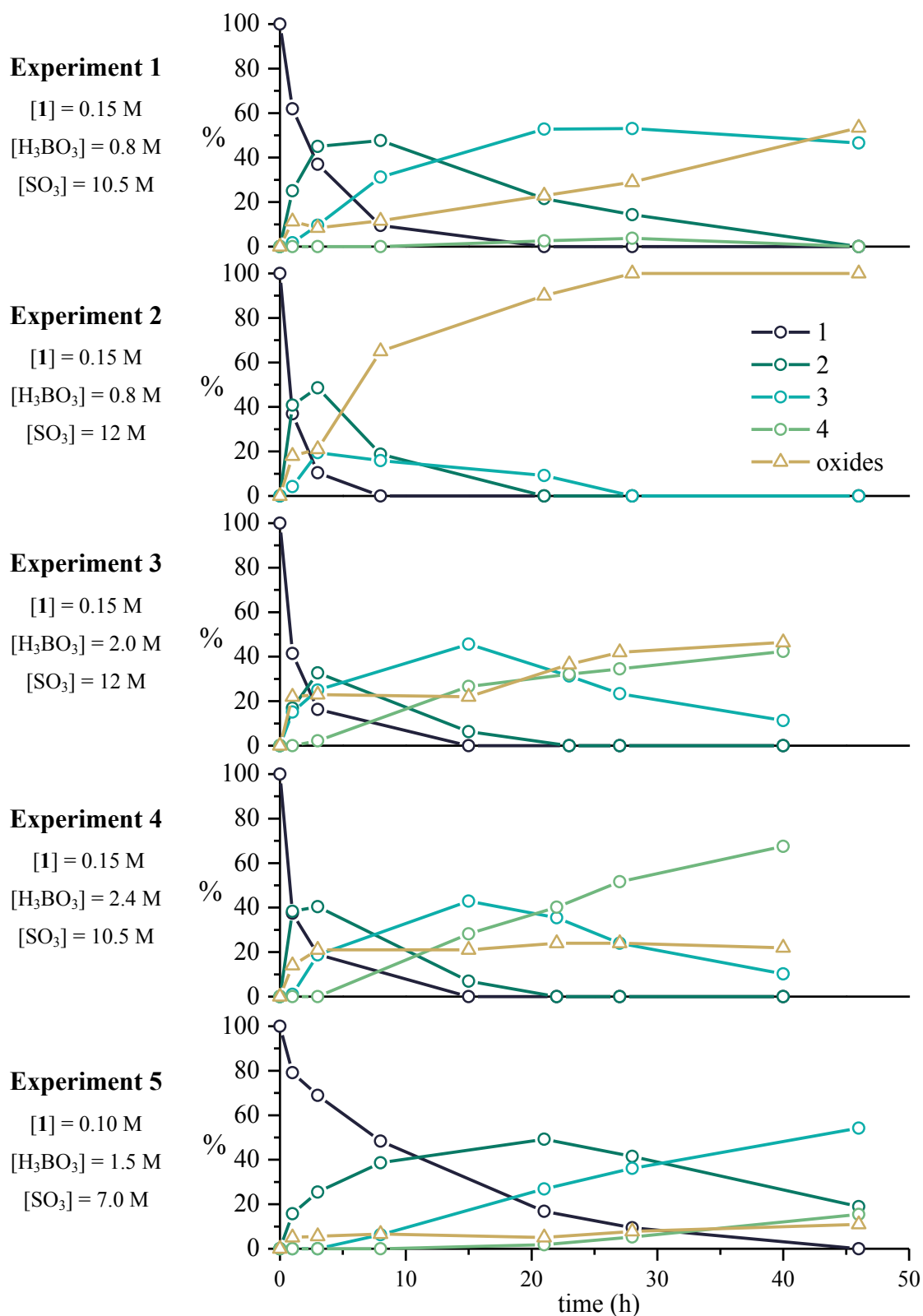


Figure 3.13. Evolution with time of the reaction of hydrolysis in phosphine **1** at different reaction conditions. Products extracted with Et₂O from the aqueous phase after quenching in water. % of compounds correspond to the integration of the phosphorus products in ³¹P{¹H} NMR. 0.6 mmol of phosphine

In *experiment 1*, the same concentration of phosphine and sulfur trioxide as in the preliminary studies were used and the concentration of boric acid was increased from 0.6 to 0.8 M. Slightly higher reaction rates were observed in *experiment 1* compared to the preliminary reaction, showing a composition of **1**, **2** and **3** of *ca.* 35, 45 and 10 %, respectively, in only 3 h of reaction. In the preliminary experiment, when 0.6 M of boric acid was used, similar composition of phosphorus compounds was obtained after 6 h of reaction. Moreover, *experiment 1* the product of the complete hydrolysis of the trifluoromethyl groups, **4**, was observed although in hardly 4 %. Since this phosphine does not contain any trifluoromethyl group it is expected to be more sensitive towards oxidation than the trifluoromethylated equivalent phosphines. Phosphine **4** is therefore likely to be formed in the reaction and rapidly oxidised which would explain why it had not been observed before.

When the concentration of SO₃ was increased to 12 M (*experiment 2*) the rate of phosphine oxidation also increased dramatically, proving the oxidising power of this reagent. The rate of the hydrolysis did also increase and, in only 1 h of reaction, phosphine **1**, **2** and **3** were found in *ca.* 35, 40 and 5 %, respectively. Importantly, when under this high concentration of SO₃ the concentration of boric acid was also increased (*experiment 3*), the oxidation rate of the phosphines was noticeably lowered while keeping similar reaction rates. The amount of phosphine oxides initially oxidised accounted for 20 % and kept constant during 15 h. Under these conditions, phosphine **4** was observed in larger amount than in the previous reactions.

In the next experiment, *experiment 4*, instead of increasing the concentration of SO₃ with respect to *experiment 1*, only the concentration of boric acid was increased to 2.4 M. Interestingly, the same rate of hydrolysis as in *experiment 2*, was observed but with much lower oxidation of the phosphine products. In this case, phosphine **4** was found in high percentage, it being the major product after 40 h of reaction. As in the case of *experiment 3*, an initial oxidation of 20 % was found and, this time, it kept constant over the course of the reaction. In both *experiment 3* and *4*, the reaction mixture previous to the addition of oleum was not a completely clear solution but a white viscous suspension was formed instead, contrary to what was observed with lower concentrations of boric acid (preliminary experiments and *experiment 1*) in which a slightly pink clear solution was obtained. This observation suggests that in *experiments 3* and *4*, phosphine **1** was not completely dissolved in the volume of H₂SO₄ used. This

fact is supported taking into account that in both experiments the same percentage of initial phosphine oxide was obtained. It is known that the protection of the phosphines against oxidation is achieved by quarterisation of the phosphorus atom in the highly acidic media.²⁰ Therefore under these reaction conditions, 20 % of phosphine **1** could remain undissolved and undergo oxidation rapidly after the addition of SO₃. Once this amount of undissolved phosphine (and thus unprotected) is oxidised, the rest of phosphine remains protected for a long period of time. Same behaviour was lately observed for the heteroleptic phosphines and will be studied in the next section.

Experiment 5 supports the idea of the initial oxidation due to the solubility stated before. Same molar ratios of phosphine, boric acid and sulfur trioxide than used in *experiment 4* were used, but with the difference that the volume of sulfuric acid used to dissolve the phosphine and the boric acid, previous to the addition of oleum, was increased 1.5 times. In this way, complete solution of phosphine and boric acid was obtained and the initial oxidation was reduced to less than 5 %.

It is important to highlight the fact that in the previous experiments of optimisation an important proportion of the oxidation that phosphines undergo during the reaction is due to the process of sampling. Although Schlenk techniques have been used during the study, the reaction mixture is highly sensitive to air. It is only necessary to compare the results measuring the evolution in a NMR tube (**Figure 3.12**) to those obtained with the process of extraction (*experiment 1*) to see this effect. While, after 28h of reaction, the NMR tube showed no significant oxidation, around 25 % of oxidation was observed in *experiment 1*. Moreover, when the reactions were performed in high scale, this process of oxidation with time was also reduced.

Besides from the process of phosphine oxidation, important differences were observed in the evolution of the products of trifluoromethyl hydrolysis depending on the concentration of SO₃ and H₃BO₃. The most surprising fact from those experiments was that, in contrast to what was observed for the reactions of sulfonation,^{3,21} H₃BO₃ seems to have an important role in the reaction beyond its effect in the reduction of the oxidation of phosphines. This effect will be studied in detail in the next chapter.

²⁰ Herrmann, W. A.; Albanese, G. P.; Manetsberger, R. B.; Lappe, P.; Bahrmann, H. *Angew. Chem. Int. Ed. Engl.* **1995**, *34* (7), 811–813.

²¹ Peral, D.; Herrera, D.; Real, J.; Flor, T.; Bayón, J. C. *Catal. Sci. Technol.* **2016**, *6* (3), 800–808.

Another important point to note is that, according to **Figure 3.13**, in all cases the reaction of the first trifluoromethyl group is faster than the hydrolysis of the second one, which in turn, is faster than the hydrolysis of the third one.

From all previous experiments, it can be concluded that the best conditions to prepare phosphines **2** and **3** are the ones from *experiment 1*. These conditions allow the obtention of the phosphines in relatively short time (around 18 h for a 50 % mixture of each phosphine) and with low amounts of undesired products, such as phosphine oxides or phosphine **4**. Moreover, by controlling the reaction times it is possible to control the composition of products at the end of the reaction. For instance, if the goal is the preparation of preparing the monocarboxylic phosphine **2**, time could be shortened to get a *ca.* 50 % of this phosphine together with the unreacted phosphine **1**, which could be reused in a new reaction, after separation. On the other hand, phosphine **4** can also be prepared using conditions in *experiment 4*. This opens a new alternative process to those already known procedures for the synthesis of this tricarboxylic phosphine, although such conditions need fairly long reaction times.

Meta*-substituted phosphine **5*

Once the reaction with the *para*-substituted phosphine **1** was explored, it was studied with phosphine **5**, in which the trifluoromethyl substituent is located at *meta*-position with respect to the phosphorus atom. In this study the optimised conditions obtained with the *para*-substituted phosphine have been used, which correspond to the *experiment 1*.

Firstly, the reaction was monitored directly in an NMR tube, without quenching and extracting with ether. As in the case of phosphine **1**, also in with of phosphine **5** the signal at 41.6 ppm in $^{19}\text{F}\{^1\text{H}\}$ NMR was observed. The reaction was then scaled up with the same conditions and was monitored by aliquoting with time. Each one of the aliquots was then quenched with water and extracted with diethyl ether before being analysed by $^{31}\text{P}\{^1\text{H}\}$ NMR, just as has been described for phosphine **1**. The results are shown in **Figure 3.14**.

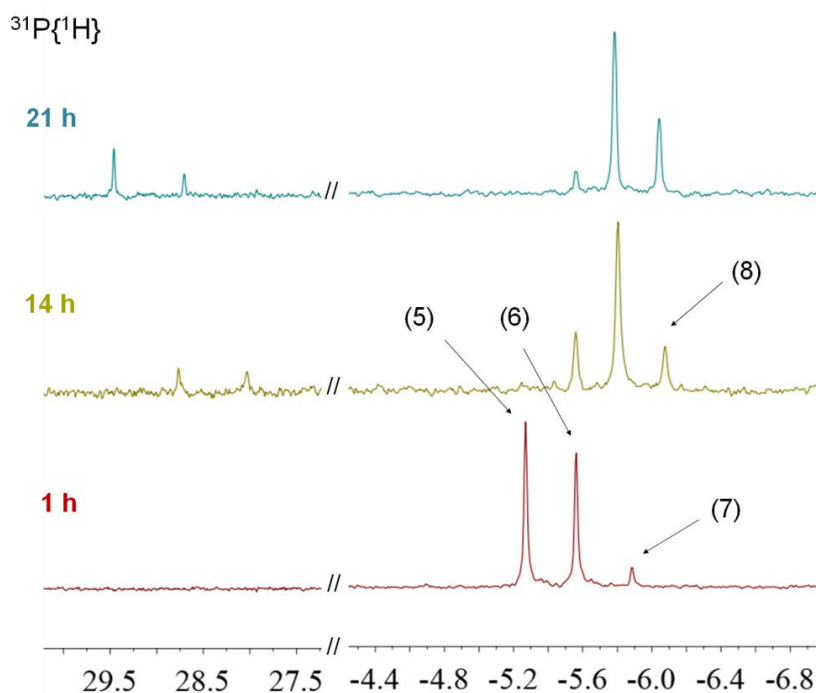
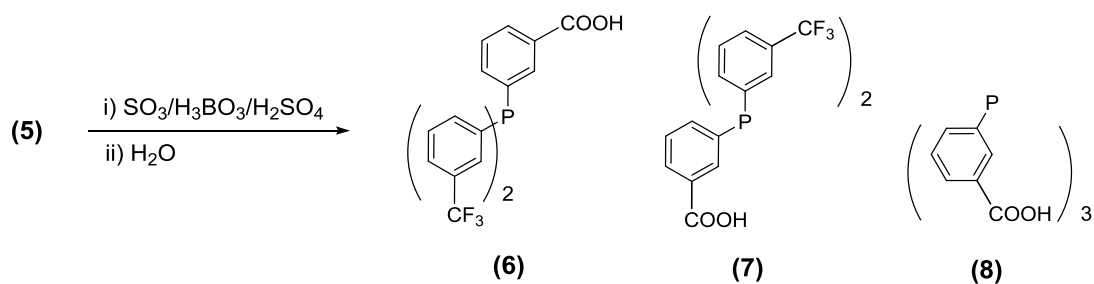


Figure 3.14. Evolution of the reaction of hydrolysis of the phosphine **5** with time. Products extracted with Et₂O from the aqueous phase after quenching in water. Analysis in CDCl₃/MeOH (4:1). Only phosphine region of the NMR spectra is shown. δ in ppm. Reaction conditions: [Phosphine] = 0.15 M, [H₃BO₃] = 0.8 M, [SO₃] = 10.5 M

As what happened with phosphine **1**, it was also possible to observe the products of hydrolysis with phosphine **5**, 3-(bis(3-(trifluoromethyl)phenyl)phosphanyl)benzoic acid (**6**), 3,3'-(3-(trifluoromethyl)phenyl)phosphanediyl)dibenzoic acid (**7**) and 3,3',3''-phosphanetriyltribenzoic acid (**8**), **Scheme 3.6**.



Scheme 3.6. Products of the hydrolysis of **5**

Compared to the reaction using **1**, in this case the signal in $^{31}\text{P}\{^1\text{H}\}$ NMR for the monocarboxylated phosphine **6** appears at -0.4 ppm with respect to the starting phosphine **5**. Signals corresponding to di- and tricarboxylated phosphines, **7** and **8** respectively, follow the same trend; the higher the number of hydrolysed trifluoromethyl groups the more negative the chemical shift is. Moreover, it can be stated that under the same conditions, the reaction of the trifluoromethyl group in *meta*

is much faster than that of the trifluoromethyl groups in *para*. The reaction with phosphine **5** shows 40 % of the hydrolysed product, phosphine **6**, in only 1 h, while phosphine **1** needs about 4 h to obtain a similar amount of monocarboxylated phosphine **2**. Furthermore, contrary to what was observed for *para*-substituted phosphine **1**, the reaction with the *meta*-substituted one yields a significant amount of the tricarboxylated product **8** in less than 24 h of reaction.

Summarising the observations of the reaction with phosphine **5**, it can be concluded that not only does the reaction of hydrolysis of the trifluoromethyl group work in the *meta*-substituted phosphine **5**, as happened with the *para*-substituted phosphine, but also the reaction is faster in the case of the former.

Separation and purification of the reaction products

Once the reaction of hydrolysis of trifluoromethyl had been studied for phosphines **1** and **5** it was essential to find an effective way to separate and purify the reaction products. The separation was aimed at based on the fact that the solubility of carboxylic acids changes as a function of pH. While at acidic pH values carboxylic acids exist as such, at basic values of pH they are deprotonated thus favouring their solubility in aqueous media. Phosphine **5** was used as model to optimise the process of separation and purification of the reaction products, and lately the system was proven to be equally effective for the separation and purification of phosphine **1** and its reaction products. In this way, and with the interest of covering all the possible phosphine products which can be obtained by hydrolysis of the trifluoromethyl groups, a reaction of carboxylation with phosphine **5** at optimum conditions was performed and stopped after 20 h. Thus a mixture of **6**, **7** and **8** in *ca.* 7, 68 and 24 %, respectively, was obtained. Phosphine **5**, which does not has pH-dependent solubility, was added as internal standard. This blend containing the four different phosphine products of the *meta*-series was used to optimise the conditions of the separation. To this mixture of phosphines, which was dissolved in diethyl ether, water was added to yield a biphasic organic-aqueous system. Next a solution of 10 % aqueous NaOH was added progressively to basify the mixture and form the sodium salts of the carboxylic phosphines. After each addition of base, the mixture was vigorously stirred for a few seconds. Then the two phases were allowed to separate before measuring the pH of the aqueous solution and, at the desired pH, an

aliquot of the organic phase was taken for its analysis by NMR. The $^{31}\text{P}\{^1\text{H}\}$ NMR spectra of each sample is shown in **Figure 3.15**.

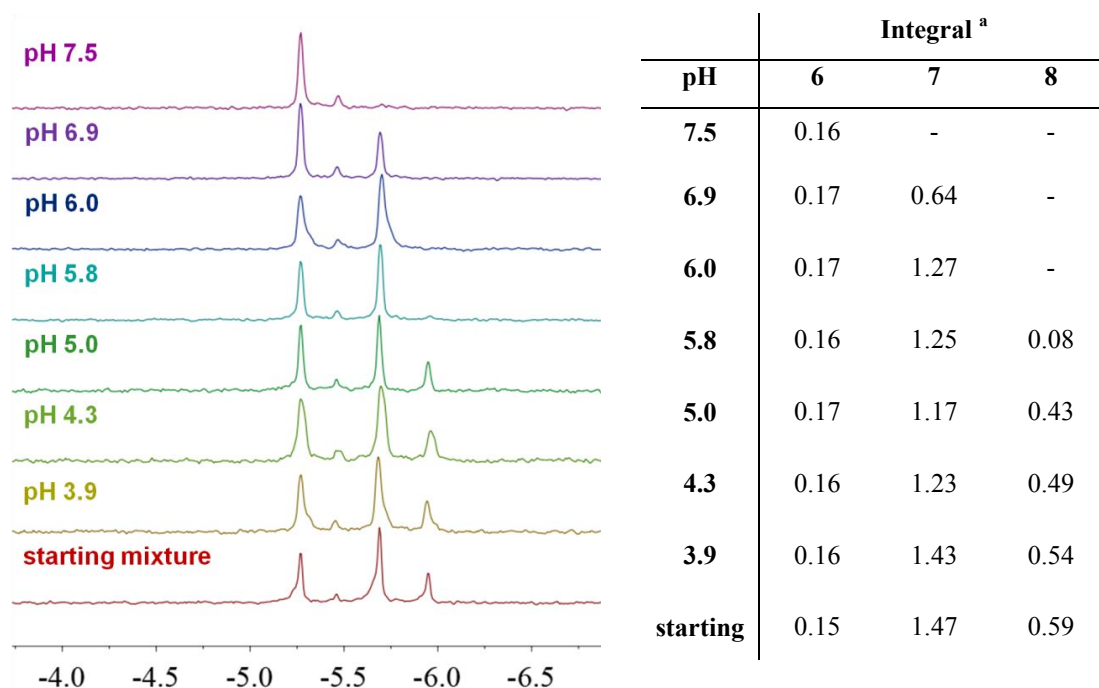


Figure 3.15 $^{31}\text{P}\{^1\text{H}\}$ NMR (101.27 MHz) analysis of the organic phase during the biphasic extraction at different pH with the *meta*-substituted phosphines. NMR performed in $\text{CDCl}_3:\text{MeOH}$ (4:1). δ in ppm.

^a Table shows the values of integrals with respect to phosphine **5**

The experiment showed the feasibility of the separation system for the di- and tricarboxylic compounds. While at pH 6.0, the tricarboxylated phosphine **8** was completely extracted into the aqueous phase, the dicarboxylic phosphine **7** was extracted at pH between 6.0 and 7.5, both as sodium salts. Although one would also expect the extraction of phosphine **6** into the aqueous phase, the fact is that values of pH above 7.5 did not allow its separation, and emulsified systems were observed, which were especially evident in the case of the *para*-substituted phosphines. Therefore, with this procedure, phosphines **7** and **8** were efficiently separated to the aqueous phase at different values of pH. Next, the acidification of each one of these aqueous phases to pH 2 allowed the re-extraction of the phosphines in the acidic form of the carboxylic acid using diethyl ether.

Interestingly, a second set of experiments did show that phosphine oxides can also be selectively extracted into the aqueous phase. A sample composed of **5**, **6**, **7** and the corresponding oxides, **ox-5**, **ox-6** and **ox-7**, respectively, was subjected to biphasic extraction at different pH, as explained above, **Figure 3.16**.

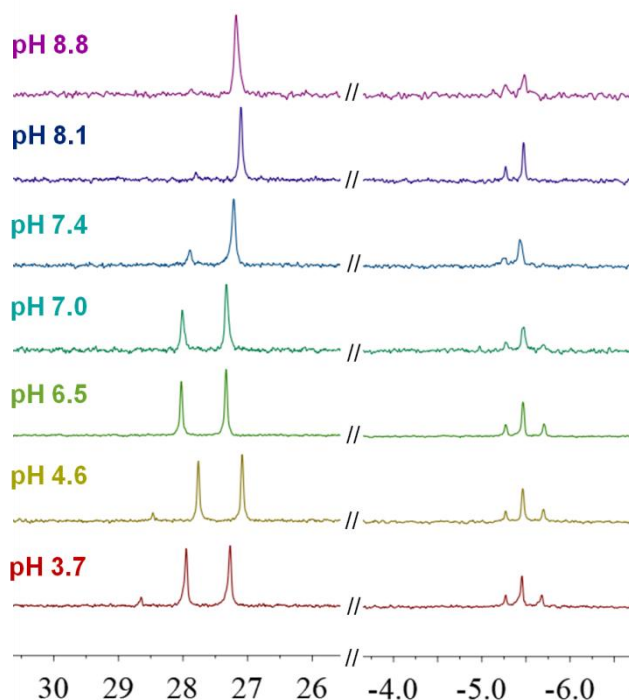


Figure 3.16. $^{31}\text{P}\{^1\text{H}\}$ NMR (101.27 MHz) analysis of the organic phase during the biphasic extraction at different pH with the *meta*-substituted phosphines **5**, **6**, **7** and the corresponding phosphine oxides, **ox-5**, **ox-6** and **ox-7**. NMR performed in $\text{CDCl}_3:\text{MeOH}$ (4:1). δ in ppm

According to the observations, the dicarboxylic phosphine oxide **ox-7** is extracted into the aqueous phase between pH values of 4.6 and 6.5 and the monocarboxylic one, **ox-6**, is extracted at pH between 6.5 and 8.8. As expected, the oxide of the starting phosphine **5**, **ox-5**, did not show pH dependent solubility.

It is worth noticing that the pH region of extraction of **ox-6** (from 6.5 to 8.8) overlaps that of the phosphine **7** (from 6.0 to 7.5) and separation of these compounds is not possible using this methodology. Fortunately, in practice, the reaction of hydrolysis of the trifluoromethyl group under optimised conditions hardly gives reaction mixtures containing phosphine **7** and significant amounts of **ox-6**. It seems somehow that the reaction of hydrolysis is faster in the phosphine oxides than it is in the phosphines. Therefore, at reaction times at which the dicarboxylic phosphine **7** is the main compound, the oxides present in the mixture are generally **ox-7** and **ox-8**. The same observations are extensive to the other phosphines, **5** and **6**. Special care must be therefore taken during the process of separation in order to minimise the formation of oxides.

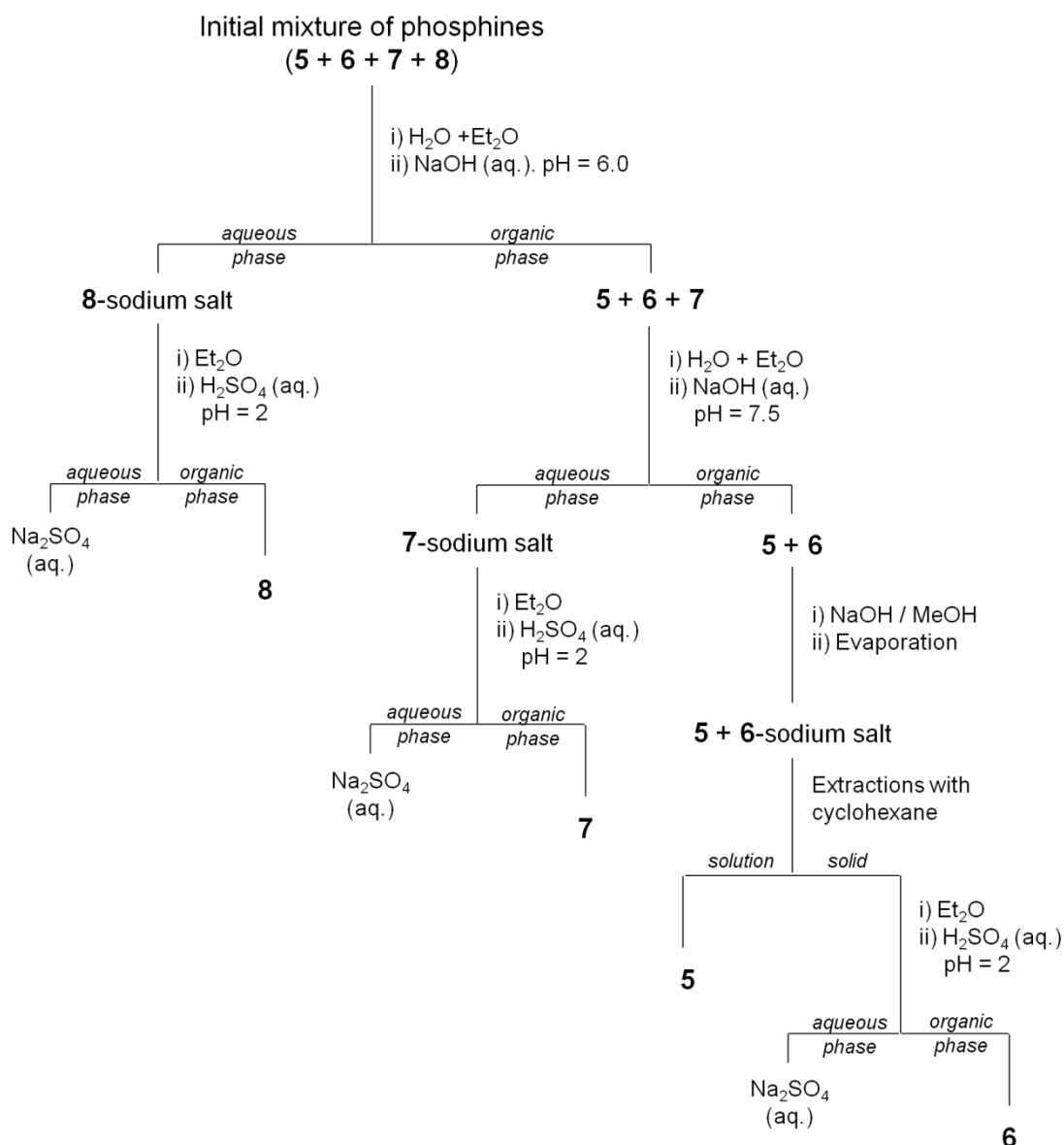
Given that the separation of the non-water soluble phosphines **5** and **6** was not possible by using extractions at different pH, an alternative strategy was established. After the

separation of phosphines **7** and **8**, the organic phase containing **5** and **6** was vacuum evaporated. To the solid residue, a solution of 10 % NaOH in MeOH was added dropwise until complete deprotonation of the carboxylic group of **6**. This process can be simply monitored by TLC in diethyl ether:ethyl acetate (8:2). Next, the solution obtained was dry evaporated to give a solid residue which was washed with cyclohexane to remove **5** and any possible oxide of this phosphine. Other solvents like diethyl ether, dichloromethane and *n*-hexane were also tested for this purpose showing poor results. While Et₂O and CH₂Cl₂ partially solubilised the sodium salt of **6**, *n*-hexane was excessively apolar to provide complete separation of **5** within a reasonable number of extractions. Moreover, phosphine oxide **ox-5** was not soluble in this last solvent. Finally, after washing with cyclohexane, phosphine **6** was recovered again as carboxylic acid by acidification to pH 2 followed by extraction in diethyl ether.

This procedure of isolation of the different phosphine compounds obtained after the hydrolysis of the CF₃ group of the *meta*-substituted phosphine **5** has been proven to be equally effective in the separation of the products of the hydrolysis in the *para*-substituted phosphine **1**. **Scheme 3.7** summarises the whole process of separation described in this section.

All in all, with this procedure, it was possible to prepare a new family of mono- and dicarboxylic trifluoromethylated triarylphosphines, the Miranphos and Miran2phos phosphines, respectively, in both the *para*- and *meta*-isomers, **Chart 3.3**. These compounds were covered under patent²² and are currently part of the catalogue of Strem Chemicals company, sold under license from the UAB for research purposes only.

²² Herrera Miranda, D.; Peral Crespo, D.; Bayon Rueda, J. C. *Trifenilfosfinas Carboxilicas*. ES2459790 (B1), **2012**. Universitat Autònoma de Barcelona



Scheme 3.7. Separation of the phosphines products of the reaction of hydrolysis of the trifluoromethyl group in phosphine **5**

The Miranphos and Miran2phos ligands were fully characterised by NMR spectroscopy (^1H , ^{13}C , ^{19}F and ^{31}P), HR-MS and Elemental Analysis. As in the case of trifluoromethylated phosphines **1** and **5**, the $^{19}\text{F}\{^1\text{H}\}$ NMR spectra of these carboxylic ligands show a singlet around -63 ppm, characteristic of aryl CF_3 groups. A singlet is also observed in the $^{31}\text{P}\{^1\text{H}\}$ NMR in the region of triarylphosphines. In the $^{13}\text{C}\{^1\text{H}\}$ the signals previously observed in the trifluoromethylated phosphines are also observed together with a new set of aromatic signals corresponding to the carboxylic ring and a singlet at *ca.* 170 ppm corresponding to the carboxylic carbon atom.

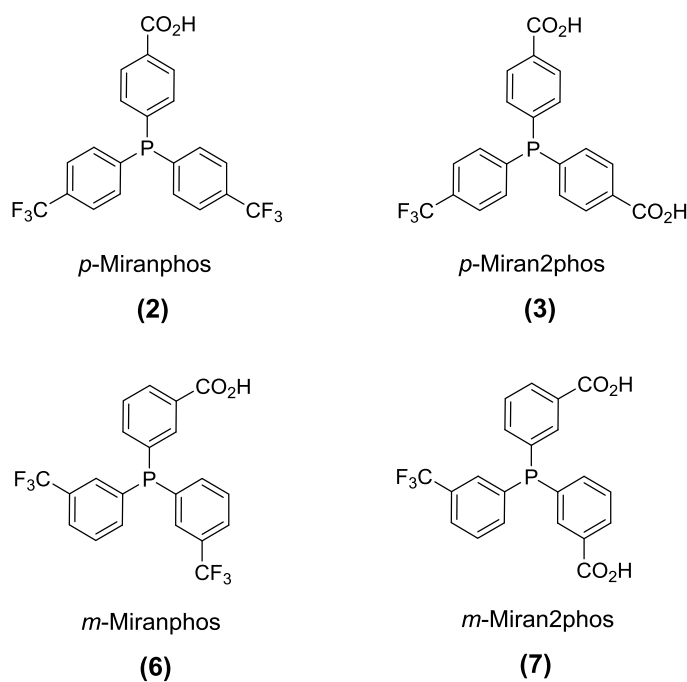


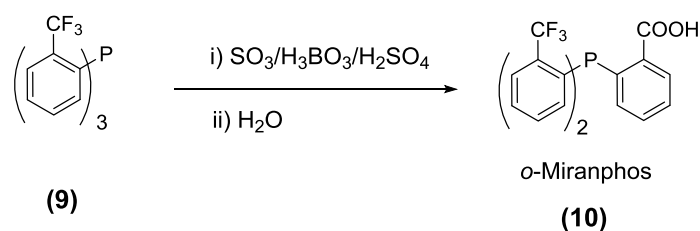
Chart 3.3. Miranphos and Miran2phos phosphines

These new family of phosphines were a proof concept of the application of the hydrolysis of the trifluoromethyl group in trifluoromethylated arylphosphines using sulfuric fuming acid and boric acid, and opened a new synthetic route in the synthesis of these sort of compounds. In continuation with the study, the reaction was next applied to other trifluoromethylated phosphines.

3.3.1.2. Hydrolysis of the trifluoromethyl group in phosphine **9**

The reaction of hydrolysis of the trifluoromethyl groups in the *ortho*-substituted triarylphosphine **9** was firstly essayed using the standard conditions previously applied in the reactions with the *para* and *meta*-isomers ($[\text{phosphine}] = 0.15\text{M}$, $[\text{SO}_3] = 10.5\text{ M}$, $[\text{H}_3\text{BO}_3] = 0.8\text{ M}$). Following the procedure described in the previous section, aliquots of the reaction mixture were quenched in frozen water, followed by extractions with diethyl ether and the analysis of the organic fractions by $^{31}\text{P}\{^1\text{H}\}$ NMR. Under these conditions, the reaction was observed to be much slower than the *para* and *meta*-isomers, showing the formation of a new low intensity signal, shifted 6 ppm downfield with respect to **9**, after more than 120 h of reaction. The multiplicity of the signal, a septuplet with $J_{\text{P-F}} = 56.5\text{ Hz}$, confirmed the hydrolysis of one trifluoromethyl group with the formation of monocarboxylic phosphine *o*-Miranphos (**10**), **Scheme 3.8**.

Direct analysis of the crude reaction mixture by $^{19}\text{F}\{^1\text{H}\}$ NMR showed the singlet at 42.6 ppm, further supporting the reaction of hydrolysis of the trifluoromethyl in **9**.



Scheme 3.8. Hydrolysis of the trifluoromethyl group of the *ortho*-substituted phosphine **9**

After 200 h of reaction only a slight increase in the concentration of **10** was observed, with no formation of the dicarboxylated product or other phosphorus compounds, such as phosphine oxides. In view of the slow rate of the reaction of hydrolysis in the *ortho*-substituted phosphine **9**, a new reaction was performed using the same conditions as previously, but increasing the temperature up to 55°C in order to accelerate the rate of hydrolysis. Although this option would be unthinkable with the *para* and *meta*-substituted phosphines, **1** and **4**, it was foreseen that the enhanced resistance towards oxidation of phosphine **9** would allow the use of more drastic reaction conditions. After 20 h, the $^{31}\text{P}\{^1\text{H}\}$ NMR analysis of the reaction mixture, by quenching in water, showed a single signal at -56 ppm. This is an unusual chemical shift for triarylphosphines. $^{19}\text{F}\{^1\text{H}\}$ NMR analysis of the product did not show the presence of fluorine. On the other hand, ^1H NMR showed different aromatic signals of non-defined multiplicity, typical of *ortho*-substituted phosphines. Furthermore, the $^{13}\text{C}\{^1\text{H}\}$ NMR analysis showed the presence of 2 different carbonyl atoms, with $^3J_{\text{CP}} = 1.8$ Hz, together with a complex set of aromatic carbon atoms, **Figure 3.17**.

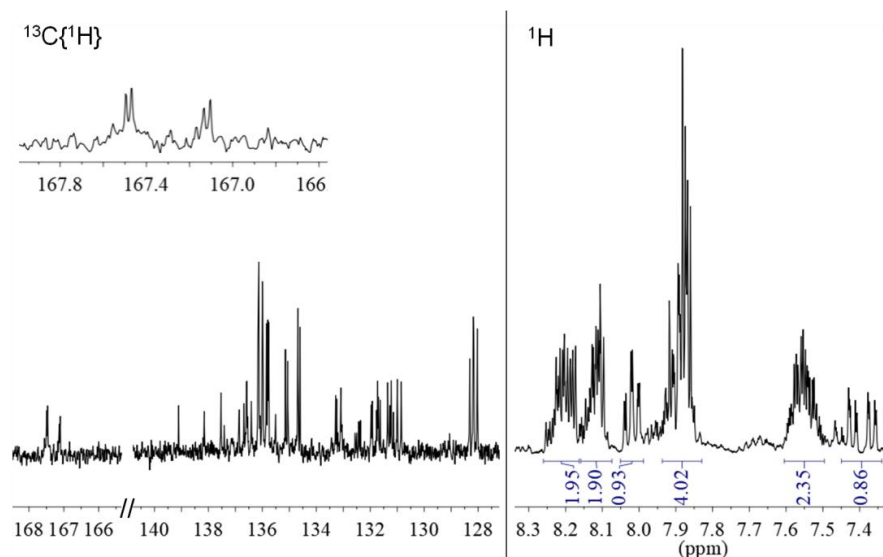


Figure 3.17. $^{13}\text{C}\{^1\text{H}\}$ (100.61 MHz) and ^1H (400.13) of compound **11**. Solvent: MeOH-D4

Finally, the HR-MS analysis of the product resulted in an elemental composition of $\text{PC}_{21}\text{H}_{13}\text{O}_6$ (m/z : 391.0376, expected for M-H: 391.0377). All in all these results were in agreement with those reported for the spirocyclic compound **11** (Chart 3.4).²³

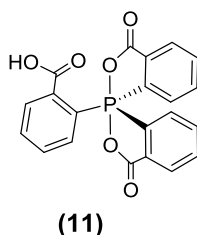


Chart 3.4. Structure of spirocyclic oxyphosphorane **11**

The high temperature used in the last experiment did not allow the observation of any intermediates between phosphine **9** and the spiro **11**. Consequently, and with the objective of studying the intermediate products in the formation of the spiro carboxylated compound **11**, the strategy was modified. Instead of increasing the temperature, the reaction was carried out at higher concentrations of boric acid and sulfur trioxide ($[\text{P}] = 0.07\text{M}$, $[\text{B}] = 1.9\text{M}$ and $[\text{SO}_3] = 14.0\text{M}$), while keeping the temperature at *ca.* 25 °C. The reaction was monitored by $^{31}\text{P}\{^1\text{H}\}$ and ^1H NMR by quenching aliquots of the reaction mixture as usual, **Figure 3.18**. As expected, the monocarboxylic phosphine **10** was formed faster than when standard conditions were used, it being detected at 27 hours after the addition of oleum. After 75 h of reaction, two new signals in the ^{31}P NMR were observed in the region of the spirocyclic

²³ Chandrasekaran, A.; Day, R. O.; Holmes, R. R. *Inorg. Chem.* **2001**, *40* (24), 6229–6238.

oxyphosphoranes, at *ca.* -54.5 and -57.5 ppm corresponding to the trifluoromethylated spirocyclic compound **12** and the aldehydic spirocompound **13**, respectively (**Chart 3.5**). While the concentration of **12** did not seem to change with time, the signal corresponding to product **13** increased as the monocarboxylated phosphine **10** was being consumed. The ^1H NMR showed the progressive formation of a singlet in the aldehydic region of the spectrum at the same time as the concentration of **13** in $^{31}\text{P}\{^1\text{H}\}$ NMR increased. After 1156 h only product **13** was observed as main compound, which did not further evolve after heating up the reaction mixture at 50 °C for more than 5 h. The resolution of the $^{31}\text{P}\{^1\text{H}\}$ NMR spectra was not enough to distinguish between the signals of **12** and **11**.

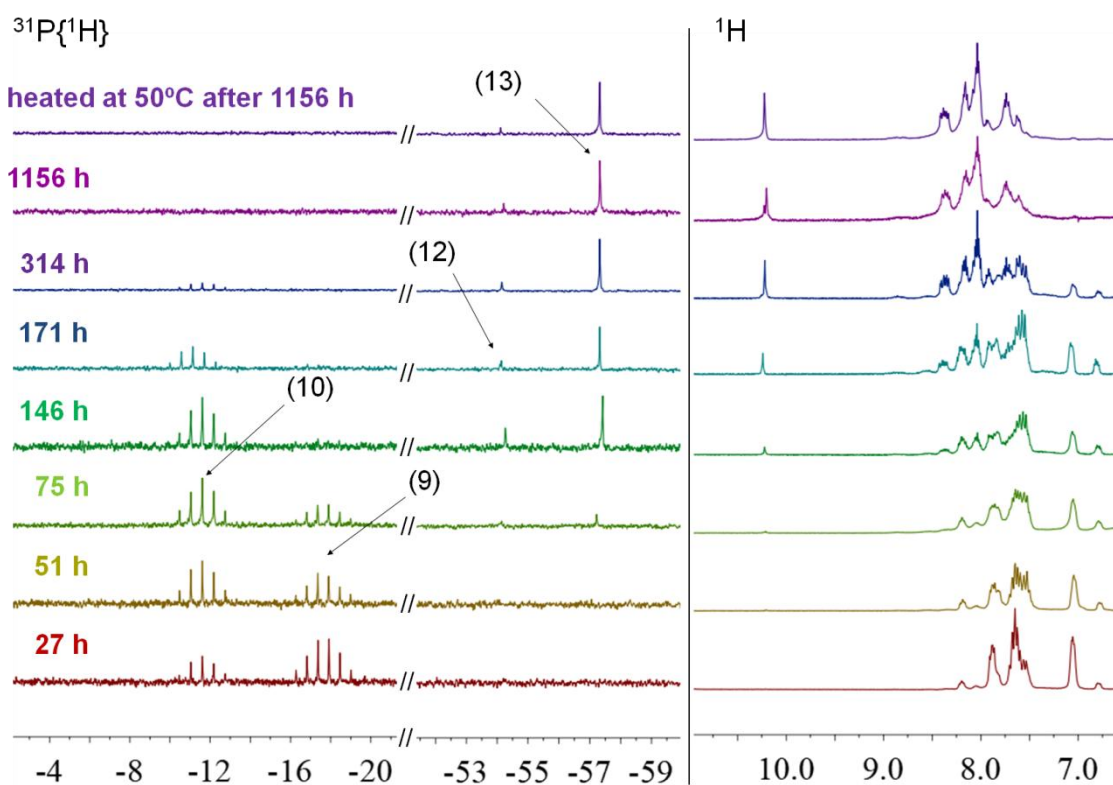


Figure 3.18. Evolution of the reaction of hydrolysis of phosphine **9** with time. Products extracted with Et_2O from the aqueous phase after quenching in water. NMR analysis in acetone- D_6 . δ in ppm. Only aromatic and aldehydic protons shown in the ^1H NMR spectra (250.16 MHz). In the $^{31}\text{P}\{^1\text{H}\}$ NMR spectra (101.27 MHz), only phosphine and spiro oxyphosphorane regions are shown. No other phosphorus products than those shown in the figure were observed. Reaction conditions: 0.6 mmol of phosphine. $[\text{Phosphine}] = 0.07 \text{ M}$, $[\text{H}_3\text{BO}_3] = 1.9 \text{ M}$, $[\text{SO}_3] = 14.0 \text{ M}$

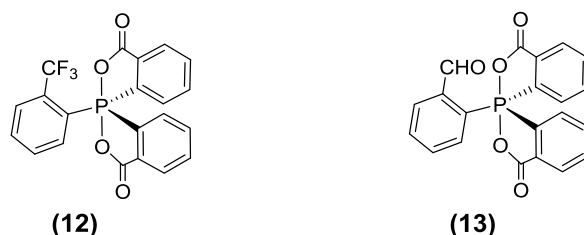
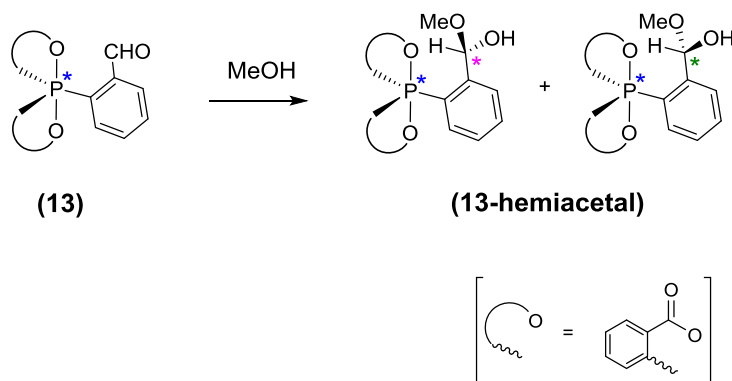


Chart 3.5. Structure of the spirocyclic oxyphosphorane **12** and **13**

Although in **Figure 3.18** the NMR spectra were collected in acetone-D₆ as solvent, we normally used a mixture of CDCl₃:MeOH (4:1) as standard solvent for these reactions. Interestingly, when CDCl₃:MeOH was applied, the formation of the hemiacetal of the aldehydic spiro oxyphosphorane **13** was observed. Given the chiral nature of **13** (with a stereogenic P atom), and the prochiral nature of the aldehyde group, the reaction with MeOH generates a second stereogenic group resulting in the formation of two diastereomeric molecules (**Scheme 3.9**), observed as two singlets at -33 and -36 ppm in the ³¹P{¹H} NMR. As a matter of example, in **Figure 3.19** the ³¹P{¹H} and ¹H NMR spectra of a sample extracted at 170 h analysed in CDCl₃:MeOH (4:1) are shown. Therefore, acetone-D₆ was only used to prove the behaviour observed in the CDCl₃:MeOH mixture.



Scheme 3.9. Schematic formation of two different hemiacetal diastereomers from the reaction between **13** and methanol. For simplicity, only one of the enantiomers of **13** is depicted.

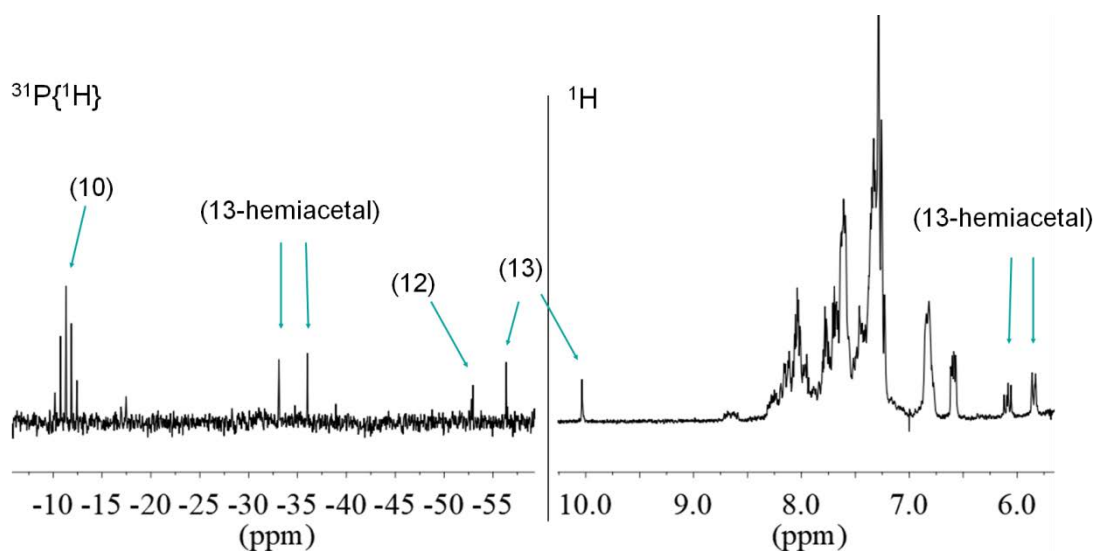


Figure 3.19. Reaction of hydrolysis of the trifluoromethyl group in phosphine **9**. Sample extracted at 170 h. Solvent $\text{CDCl}_3:\text{MeOH}$ (4:1). $^{31}\text{P}\{^1\text{H}\}$ NMR (101.27 MHz) and ^1H NMR (250.16 MHz) Reaction conditions: 0.6 mmol of phosphine. $[\text{Phosphine}] = 0.07 \text{ M}$, $[\text{H}_3\text{BO}_3] = 1.9 \text{ M}$, $[\text{SO}_3] = 14.0 \text{ M}$

Separation, purification and structure determination of the products in the reaction of hydrolysis of phosphine **9**

With the object of developing a method of separation, a new reaction was carried out under the same conditions described in the previous experiment. It should be borne in mind that the product of interest in this synthetic procedure is the *o*-Miranphos phosphine (**10**) and thus the reaction conditions and the process of separation were optimised with the purpose of maximising the yield of such compound. The reaction was stopped at 90h giving a mixture formed by the starting trifluoromethylated phosphine **9**, the monocarboxylated phosphine **10** and the spiro oxyphosphoranes **11**, **12** and **13**, in *ca.* 22, 54, 5, 4 and 10 %, respectively, together with 5 % of phosphine oxide. In this way, we can obtain a relatively high concentration of **10** with minimum amounts of the spirocyclic side-products.

The process of separation essayed was based on biphasic extractions in water/ Et_2O at different pH values, in analogy to that used for the *para* and *meta*-trifluoromethylated phosphines **1** and **5**. The $^{31}\text{P}\{^1\text{H}\}$ NMR analysis of the organic phase during the process of extraction at different pH is shown in **Figure 3.20**.

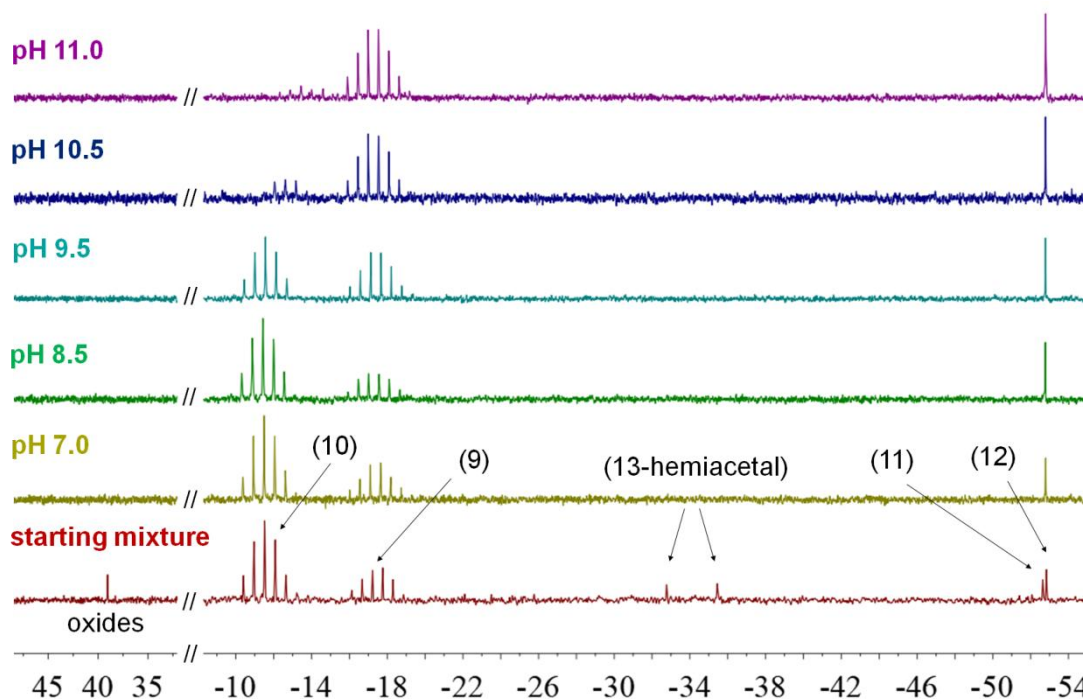


Figure 3.20. $^{31}\text{P}\{^1\text{H}\}$ NMR (101.27 MHz) analysis of the organic phase during the biphasic extraction at different pH. NMR performed in $\text{CDCl}_3:\text{MeOH}$ (4:1). δ in ppm

At pH 7.0 the spiro aldehyde **13**, the carboxylic spiro **11** and the possible traces of phosphine oxides were extracted in the aqueous phase. Whereas the spiro compounds **13** and **11** can be quantitatively brought again to Et_2O by performing several extractions, the oxides remained mainly dissolved in the aqueous phase or in the form of an insoluble interface. Further purification of **13** through silica column in ethyl acetate: CH_2Cl_2 (5:5) was necessary to eliminate the carboxylic spiro oxyphosphorane **11**. In this way the aldehydic spiro oxyphosphorane **13** was isolated and fully characterised by the common techniques. Furthermore, the structure was finally confirmed by single-crystal XRD. The crystals obtained were racemic mixtures of **13**. The geometry of the phosphorus atom in **13** is a trigonal bipyramid with two oxygen atom occupying axial positions and the P-C bonds in the equatorial plane. Contrary to the reported structures of other similar compounds,²³ the carbonyl oxygen atom of the aldehyde group does not interact with the phosphorus atom. In fact, the oxygen atom is pointing in opposite direction to the phosphorus thus preventing any intramolecular P-O coordination (acid-base Lewis interaction). ORTEP diagram of the single-crystal X-ray structure of **13** and some selected distances and angles are shown in, **Figure 3.21**.

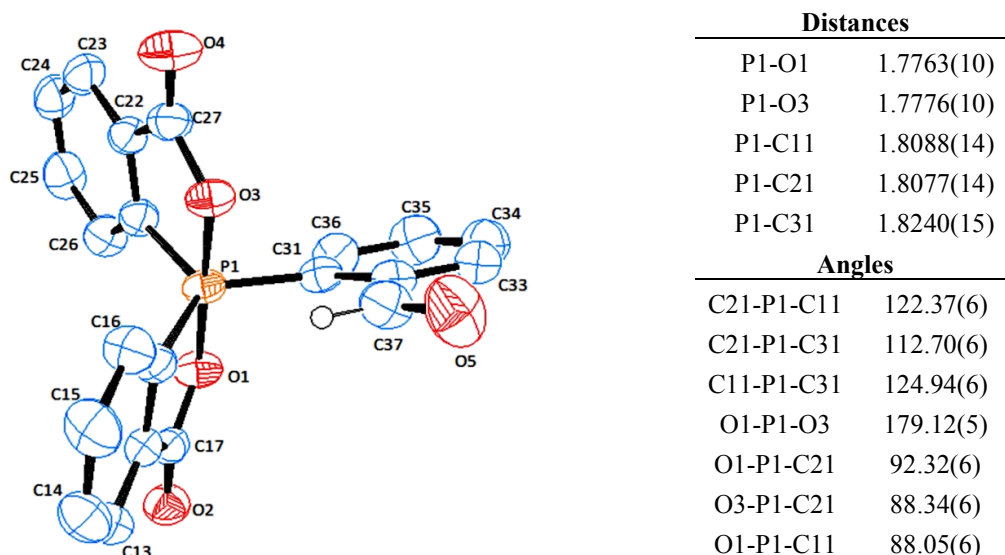


Figure 3.21. ORTEP plot (ellipsoid at 50% probability) of **13** and selected distances (Å) and angles (°). Only one enantiomer is shown. Aromatic hydrogens omitted for clarity

Following with the separation process, after having removed the spiro **11** and **13** and the oxides from the reaction mixture, the organic phase containing **9**, **10** and **12** was extracted again while increasing the pH. Only the monocarboxylic phosphine **10** was extracted into the aqueous phase in the form of sodium salt at pH between 9.5 and 11. This observation was somehow surprising since the *para* and *meta*-isomers (**2** and **6**) were not extracted in water even at high values of pH due to the formation of emulsions. One can understand that the dipolar moment of *o*-Miranphos (**10**) is lower than that of *p*-Miranphos (**2**) and *m*-Miranphos (**6**) and thus its behaviour as surfactant is less pronounced. After acidifying the aqueous solution, phosphine **10** was again extracted into fresh Et₂O and was fully characterised by the common techniques. The next section will be devoted to comment on some interesting structural features of this compound.

Since the two products remaining in the original organic mixture, *o*-tris(trifluoromethylphenyl)phosphine (**9**) and the trifluoromethylated spiro oxyphosphorane (**12**) did not show pH-based solubility, the products were successfully separated by silica column in Et₂O. Before the separation, though, we took advantage of the mixture to determine the number of CF₃ groups in the spiro compound. Using the ratio of signals between the spiro **12** and the phosphine **9** in ³¹P{¹H} NMR (1:5.5) and in ¹⁹F{¹H} NMR (1:15.1), and assuming that both compounds have one phosphorus atom, it was possible to confirm that compound **12** contained one trifluoromethyl group.

Finally, after its isolation, **12** was characterised by the common techniques confirming the proposed structure.

Even though other reaction conditions were tested to optimise the synthesis of the carboxylic phosphine **10** by changing the concentrations of phosphine, boric acid and sulfur trioxide at room temperature, the variation in the observed reaction rates was not significant. It is important to take into account that low concentrations of boric acid and sulfur trioxide give rise to low reaction rates and using higher concentrations of these reagents than those already used in the last synthesis, shown above, is not feasible given the nature of the system (*i.e.* the SO₃ concentration in 65% SO₃ oleum lies around 16 M, and a minimum volume of sulfuric acid is necessary in the previous solution of the phosphine). Either way, whenever the monocarboxylic phosphine **10** is the product of interest, it is preferred to stop the reaction before the formation of the spiro compounds. In this manner, the separation and purification is simplified and the main by-product present in the mixture, the starting trifluoromethylated phosphine **9**, can be recycled in a new reaction.

3.3.1.2.1. *o*-Miranphos phosphine (10): structural study

With respect to the characterisation of the monocarboxylated *ortho*-substituted phosphine (**10**), *o*-Miranphos, it was observed that, whereas ³¹P{¹H}, ¹³C{¹H} and ¹H NMR matched the expected results, the signal found in ¹⁹F{¹H} NMR was completely unexpected, showing two broad signals in the region of the *o*-CF₃, at 25 °C.

Variable temperature NMR (VT-NMR) experiments showed the dynamic behaviour of the system, **Figure 3.22**. It is noteworthy the fact that a single suitable solvent which allowed solubility of the phosphine within the temperature range of VT-NMR was not found and therefore acetone-D₆ was used at low temperatures while DMSO-D₆ was used at higher temperatures. While at 270 K two doublets of equal intensity are observed with ⁴TS_{J_{P-F} = 57 Hz, only one doublet with the same coupling constant was observed above 340 K. At temperatures in between those values an average of the two situations was observed in the shape of wide signals. ³¹P{¹H} NMR spectra was also acquired but did not change with the temperature.}

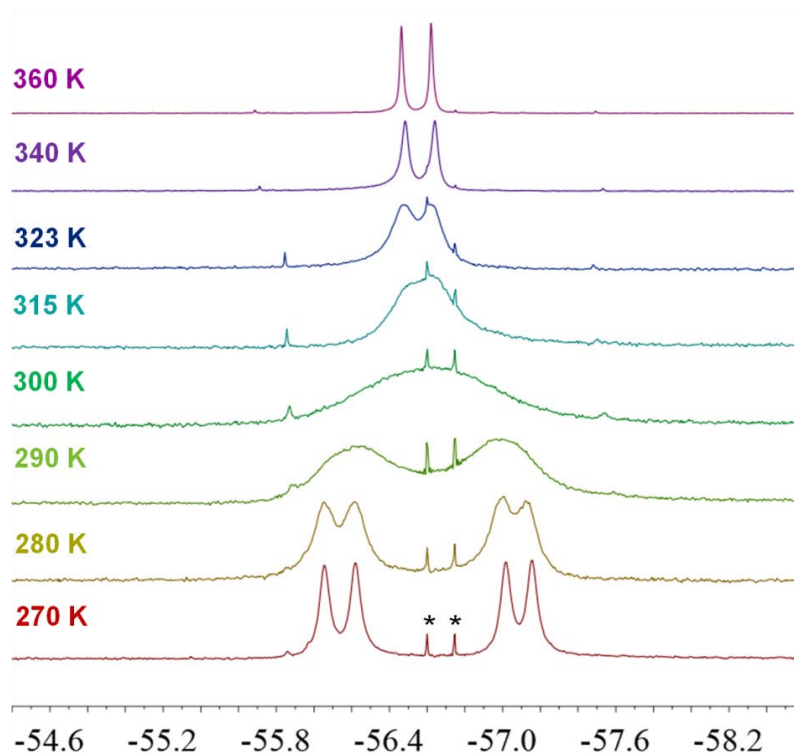


Figure 3.22. $^{19}\text{F}\{^1\text{H}\}$ NMR (376.50 MHz) of *o*-Miranphos (**10**) at different temperatures. From 270 K to 323 K, acetone- D_6 was used as solvent. Experiments at 340 K and 360 K were performed in DMSO- D_6 . δ in ppm. Spectra were calibrated using the signal of phosphine **9** (-56.67 ppm, labelled as *), which was present as impurity in 1.4 %

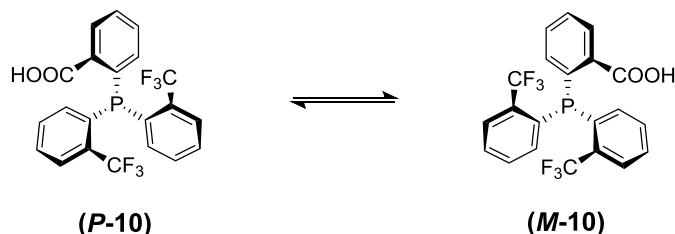
The results obtained in the VT-NMR experiments are in agreement with non-equivalent trifluoromethyl groups in fast exchange above 340 K. It is known that triarylphosphines are helically chiral molecules due to their propeller-shaped conformation (axial chirality). Accordingly, and in analogy to *delta* and *lambda* enantiomers in octahedral complexes, two enantiomeric forms of these compounds can be differentiated, *P* (clockwise) and *M* (counter clockwise), respectively, **Scheme 3.10**.²⁴ Nevertheless triarylphosphines are normally considered achiral molecules due to fast helicity interconversion at room temperature.²⁵ This helicity inversion though can be lowered by the presence of bulky substituents.^{25a,26} In our case, above 340 K, rapid helicity exchange results in an average situation between conformations *P*-**10** and *M*-**10**. The trifluoromethyl groups in this average conformation are then enantiotopic, showing a

²⁴ a) Mislow, K. *Acc. Chem. Res.* **1976**, *9* (1), 26–33. b) Laleu, B.; Bernardinelli, G.; Chauvin, R.; Lacour, J. *J. Org. Chem.* **2006**, *71* (19), 7412–7416.

²⁵ a) Whitnall, M. R.; Hii, K. K. M.; Thornton-Pett, M.; Kee, T. P. *J. Organomet. Chem.* **1997**, *529* (1–2), 35–50. b) Wyatt, P.; Eley, H.; Charmant, J.; Daniel, B. J.; Kantacha, A. *Eur. J. Org. Chem.* **2003**, *2003* (21), 4216–4226.

²⁶ Boeré, R. T.; Zhang, Y. *J. Organomet. Chem.* **2005**, *690* (10), 2651–2657.

single signal in the $^{19}\text{F}\{^1\text{H}\}$ NMR spectra. However, below 280 K, slow rotation of the aryl groups on the NMR time scale would virtually freeze the exchange between the two enantiomeric forms. As a result, the two trifluoromethyls of each conformation (**P-10** and **M-10**) become diastereotopic, thus showing two different signals in the $^{19}\text{F}\{^1\text{H}\}$ NMR. At temperatures close to 298 K coalescence was observed.



Scheme 3.10. Enantiomeric forms of *o*-Miranphos (**10**)

The exchange barrier between **P-10** and **M-10** was determined using the VT-NMR experiments.^{25a,27} The rate constant at each temperature was calculated using the IvorySoft gNMR software. In order to avoid issues due to different solvents, only values measured in acetone were used in the simulations. The spectra were therefore carefully recorded from 270 K to 323 K and simulations were performed to determine the interconversion rates at each temperature. **Figure 3.23** shows the experimental and simulated spectra of selected calculations, including the interconversion rates obtained the simulation.

Using the values of the exchange rate calculated at each temperature, the activation energy (E_a), and the enthalpy and entropy of activation (ΔH^\ddagger and ΔS^\ddagger , respectively) associated to the helicity interconversion in **10** were graphically determined, **Figure 3.24**. Arrhenius equation was applied to calculate the E_a (13.4 kcal/mol) and the average of ΔH^\ddagger (12.8 kcal/mol) within the studied temperatures, according to $\Delta H^\ddagger = E_a - RT$. Eyring equation was used for graphically determining ΔH^\ddagger (12.8 kcal/mol) and ΔS^\ddagger (-2.17 cal/K·mol). Also Gibbs energy of activation (ΔG^\ddagger) at each temperature was calculated from ΔH^\ddagger and ΔS^\ddagger . Given the small value of ΔS^\ddagger , ΔG^\ddagger was almost constant within the range of temperatures studied (13.49 kcal/mol). Further experimental details are provided in the experimental part.

²⁷ Zimmer, K. D.; Shoemaker, R.; Ruminski, R. R. *Inorg. Chim. Acta* **2006**, 359 (5), 1478–1484.

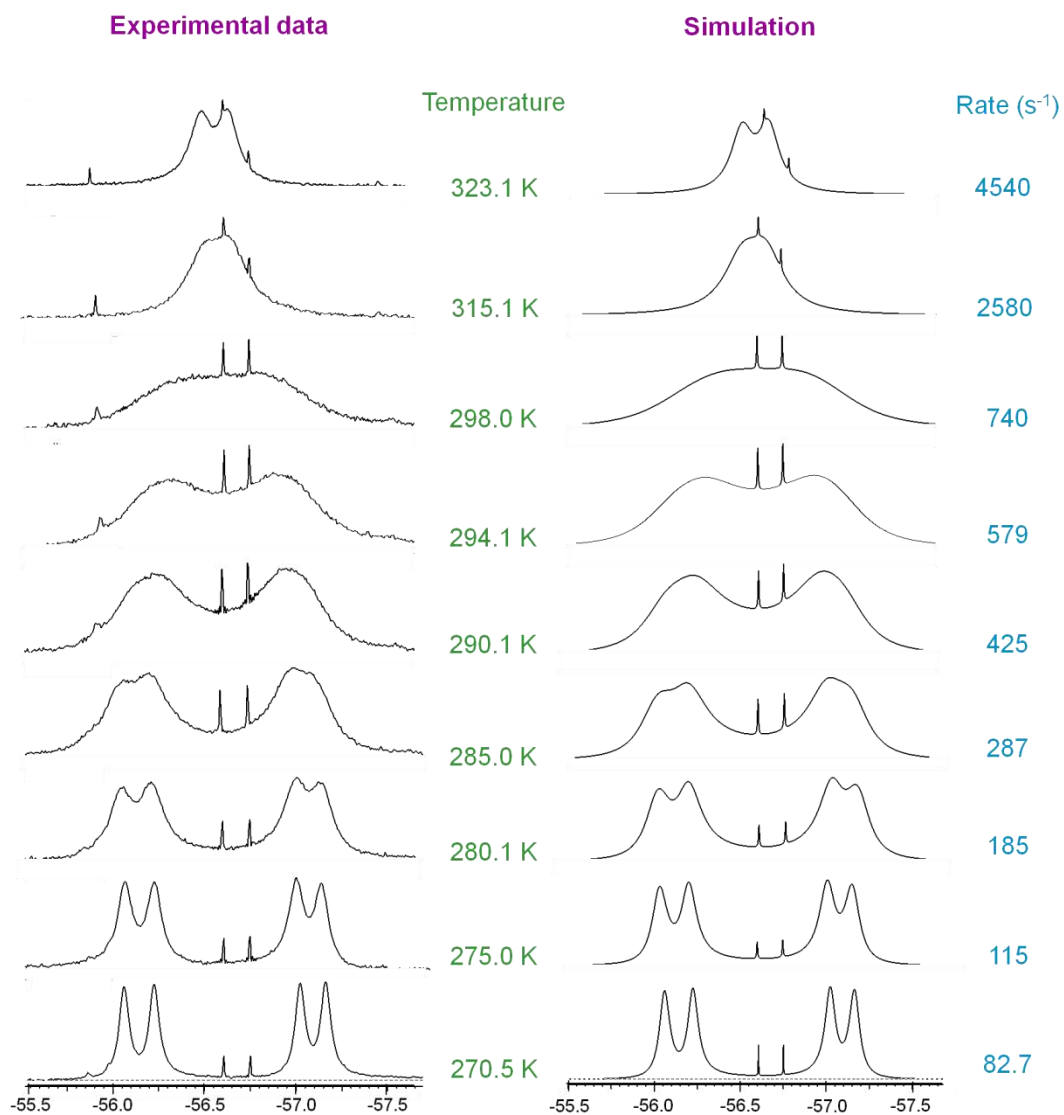


Figure 3.23. Selected experimental (**left**) and simulated (**right**) spectra and the calculated rates at different temperatures. $^{19}\text{F}\{^1\text{H}\}$ NMR (376.50 MHz), acetone-D₆. δ in ppm

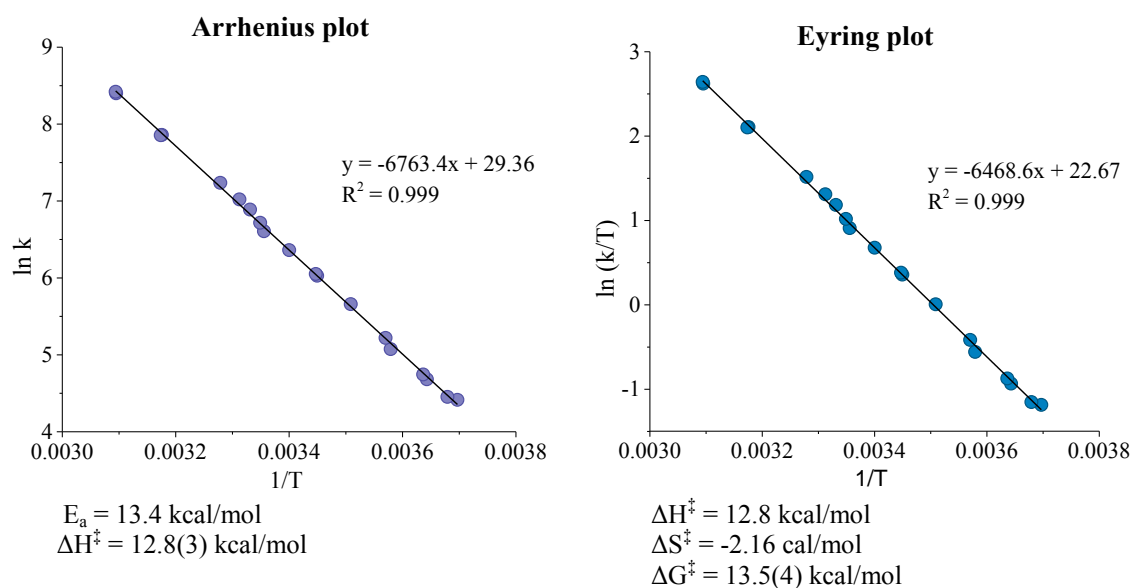
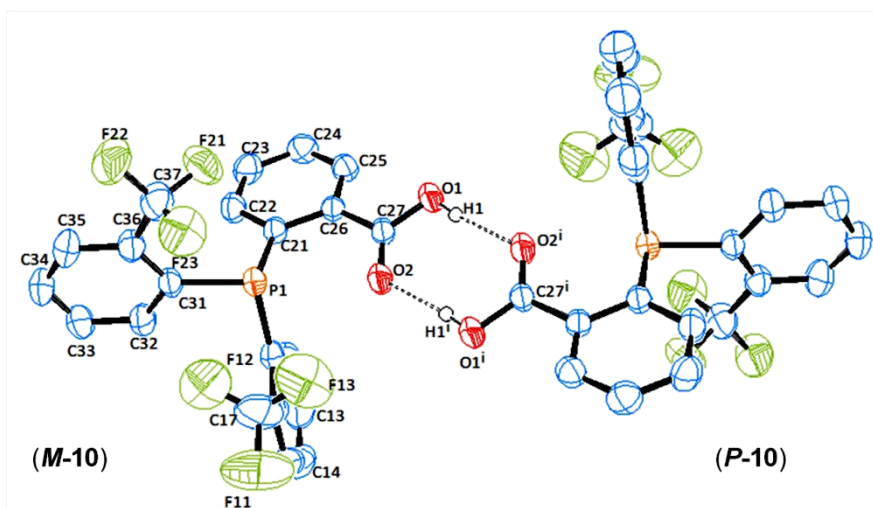


Figure 3.24. Arrhenius and Eyring plots for the calculations of the activation energies associated to the exchange between the two enantiomeric forms of *o*-Miranphos (**10**), **P-10** and **M-10**. Parameters derived from each one of the plots are indicated below the corresponding plot.

For each enantiomer, the different chemical shifts of the two trifluoromethyls at low temperature, -56.15 and -57.08 ppm, could be attributed to an anisotropic effect produced by the different proximities of the CF₃ to the CO₂H group. This statement was supported by the XRD structure. Crystals of *o*-Miranphos (**10**) of suitable quality for XRD were obtained from slow precipitation in acetone. *o*-Miranphos crystallised as a dimeric structure in which one molecule the enantiomer **P-10** is linked to a molecule of the other enantiomer, **M-10**, by means H-bonding through the carboxylic groups (**Figure 3.25**). The helix-like conformation is clearly seen in the crystal structure. Top view of **M-10** (**Figure 3.26**) emphasises the helical arrangement of the aromatic rings. Closer proximity of one of the trifluoromethyl groups (C17, F11, F12, F13) to the carboxylic acid can also be observed, which is in agreement with the anisotropic effect observed in the ¹⁹F{¹H} NMR spectra at low temperature, as stated before.



Distances		Angles	
P1-C11	1.8464(18)	C11-P1-C21	102.06(8)
P1-C21	1.8487(17)	C11-P1-C31	99.90(7)
P1-C31	1.8568(16)	C21-P1-C31	100.84(7)
C27-O1	1.3194(19)	O2-C27-O1	123.35(15)
C27-O2	1.218(2)	O2-C27-C26	122.70(14)
		O1-C27-C26	113.94(15)

Hydrogen bonding interactions

D-H...A	d(D-H)	d(H...A)	d(D...A)	angle (D-H-A)
O1-H1...O2	0.78(2)	1.91(3)	2.6864(18)	173(3)

(-x+1, -y+1, -z+1). D = hydrogen atom donor and A = hydrogen atom acceptor

Figure 3.25. ORTEP plot (ellipsoid at 50% probability) of 10 showing the hydrogen bonding between the two enantiomers, *P*-10 and *M*-10. Selected distances (Å) and angles (°). Aromatic hydrogen atoms omitted for clarity

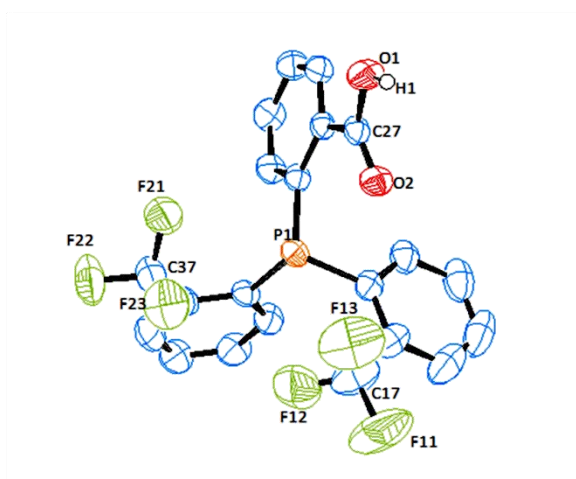


Figure 3.26. ORTEP plot (ellipsoid at 50% probability) top view of 10 to emphasise the helical structure and the anisotropic effect of the carboxylic acid on the CF₃ (C17). For clarity, only isomer *M*-10 is shown. Aromatic hydrogen atoms were omitted

3.3.1.3. Hydrolysis of the trifluoromethyl group in phosphine 14

Having explored the reaction of hydrolysis in the homoleptic phosphines containing one trifluoromethyl group on each ring, it was decided to test the reaction with a homoleptic triarylphosphine containing more trifluoromethyls per ring. In this case the doubly *meta*-substituted phosphine tris[3,5-bis(trifluoromethyl)phenyl]phosphine (**14**) was chosen, **Chart 3.6**.

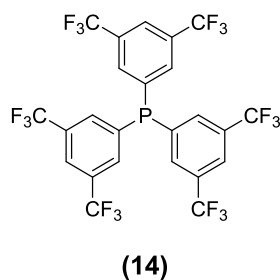


Chart 3.6. tris[3,5-bis(trifluoromethyl)phenyl]phosphine

Phosphine **14** was studied under the same reaction conditions as used for the *meta*-substituted phosphine **5**, that is, [phosphine] = 0.15 M, [SO₃] = 10.5 M, [H₃BO₃] = 0.8 M, showing unexpectedly slow reaction rates. This resulted in a competition between the reaction of hydrolysis of the trifluoromethyl and the oxidation of the phosphine, yielding phosphine oxides as main products. HR-MS analysis of the reaction mixture showed the monocarboxylic phosphine (m/z: 645.0115, expected for C₂₄H₉F₁₅PO₂⁺: 645.0101) and the monocarboxylic and dicarboxylic phosphine oxides of **14** (m/z: 661.0090, expected for C₂₄H₉F₁₅PO₃⁺: 661.0050 and m/z: 637.0097, expected for C₂₄H₁₀F₁₂PO₅⁺: 637.0074, respectively). However the pattern of carboxylation in the sicarboxylic compound (same or different ring) could not be determined. Similar results were observed when the concentration of boric acid was increased, **Figure 3.27**. Heating up the reaction did only increase the oxidation rate.

Unexpectedly, the reaction of hydrolysis using the doubly *meta*-substituted phosphine **14** was much slower than when the “single” substituted one **5** was used. Even though the products of hydrolysis were detected, the slow reaction rate produced the complete oxidation of the phosphines.

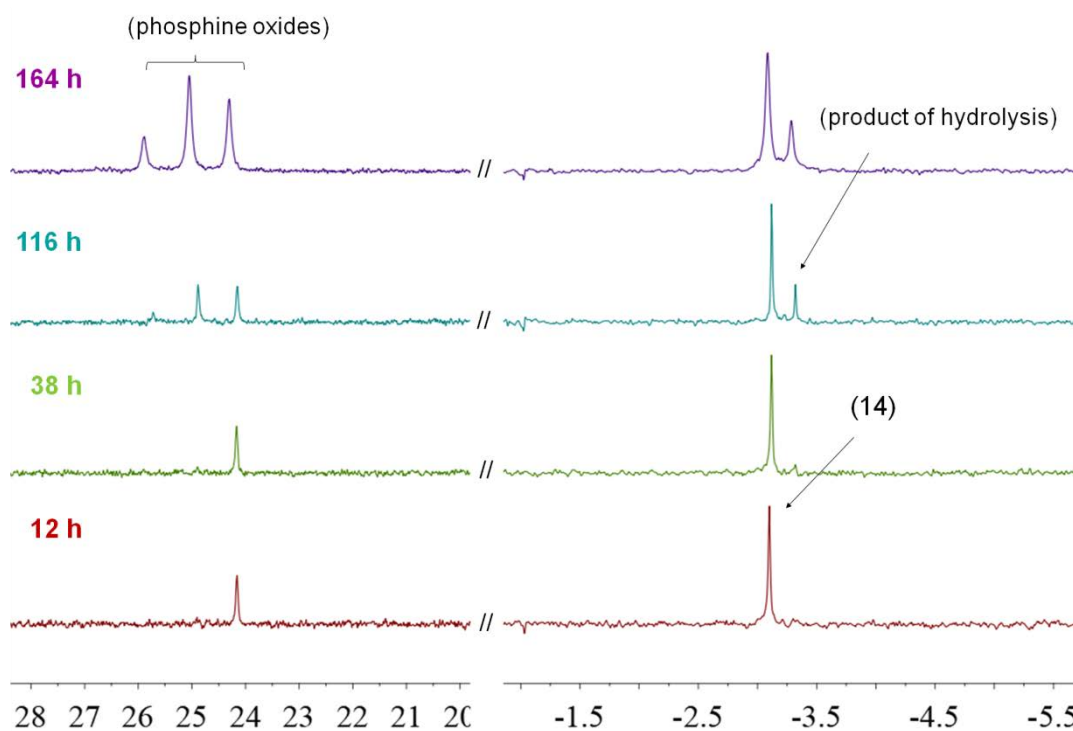


Figure 3.27. Evolution of the reaction of hydrolysis of phosphine **14** with time. Products extracted with Et₂O from the aqueous phase after quenching in water. NMR analysis in CDCl₃:MeOH (4:1), δ in ppm. ³¹P{¹H} NMR spectra (101.27 MHz). No other phosphorus products than those shown in the figure were observed. Reaction conditions: 0.75 mmol of phosphine. [Phosphine] = 0.09 M, [H₃BO₃] = 1.6 M, [SO₃] = 6.4 M

3.3.2. Reaction of hydrolysis of the trifluoromethyl group in the heteroleptic triarylphosphines

Up to this point, the reaction of hydrolysis of the trifluoromethyl group in different trisubstituted homoleptic phosphines was described. Given that the reaction in the *para* (**1**) and *meta*-substituted (**5**) phosphines worked reasonably well, while the reaction with the 3,5 substituted one (**14**) did not proceed under the essayed conditions, it was of appealing interest to study the reaction in heteroleptic phosphines containing both patterns of substitution, **15**, **18**, **20** and **23**. It was also of interest to study the influence of different trifluoromethyl groups on the hydrolysis of those groups located on other rings, something that was not possible to study in the homoleptic phosphines.

In view that the rate of the reaction of hydrolysis in the *meta*-substituted phosphine **5** was faster than in the *para*-substituted one (**1**), as shown in the previous sections of this chapter, the study of the hydrolysis in the heteroleptic phosphines was divided into two sections: heteroleptic *meta*-substituted phosphines, **15** and **18**, and heteroleptic *para*-substituted phosphines, **20** and **23**.

3.3.2.1. Reaction of hydrolysis of the trifluoromethyl group in *meta*-substituted heteroleptic triarylphosphines **15** and **18**

In a first screening, the reaction was essayed using the same synthetic conditions as used before in the reaction with the homoleptic *m*-substituted phosphine **5** ([phosphine] = 0.15 M, [SO₃] = 11.0 M, [H₃BO₃] = 0.8 M). Contrary to phosphine **5**, heteroleptic phosphines **15** and **18** were not completely dissolved in the mixture with boric acid and sulfuric acid previous to the addition of oleum, it being the one with more CF₃ groups, phosphine **18**, the phosphine with the lowest solubility. Therefore we were forced to increase the amount of sulfuric acid to achieve the apparent complete dissolution of the phosphines, reaching final concentrations of [phosphine] = 0.1 M, [SO₃] = 6.7 M and [H₃BO₃] = 0.5 M. Under these conditions also the homoleptic *meta*-substituted phosphine **5** was tested in order to compare the whole set of *meta*-substituted phosphines. The reactions were monitored by sampling with time and quenching in water and, as usual, analysing by ³¹P{¹H} NMR. **Figure 3.28** shows the evolution of the reaction products with time.

Interestingly, as observed for the *m*-homoleptic phosphine **5**, the NMR signals corresponding to the products of hydrolysis of phosphines **15** and **18** are also shifted upfield (see, for instance, **Figure 3.30**). As expected, no hydrolysis of the trifluoromethyls at 3,5-positions was observed in the reaction with neither phosphine **15** nor with phosphine **18**, and only those groups in “pure” *meta* position (different from 3,5-position) underwent hydrolysed. Therefore, phosphine **15** yielded two different carboxylic phosphines by hydrolysis of one or two *m*-CF₃, **16** or **17**, respectively, and only one carboxylic phosphine was observed in the reaction with phosphine **18**, **19** (**Scheme 3.11**). It was observed that the reaction rate becomes slower when increasing the number of trifluoromethyl groups. For instance, after *ca.* 30 h, the reaction with **18** showed only about 10 % of the carboxylic phosphine **19**, while the reaction with **15**, showed around 40 % of the monocarboxylic product **16** and 5 % of the dicarboxylic one, **17**. In contrast, after the same reaction time, the homoleptic phosphine **5** showed the monocarboxylated and dicarboxylated products, **6** and **7**, in about 30 % and 50 % respectively. Interestingly, this behaviour shows how the hydrolysis of a trifluoromethyl group is affected by the electronic properties of the aromatic rings to which such trifluoromethyl is not attached.

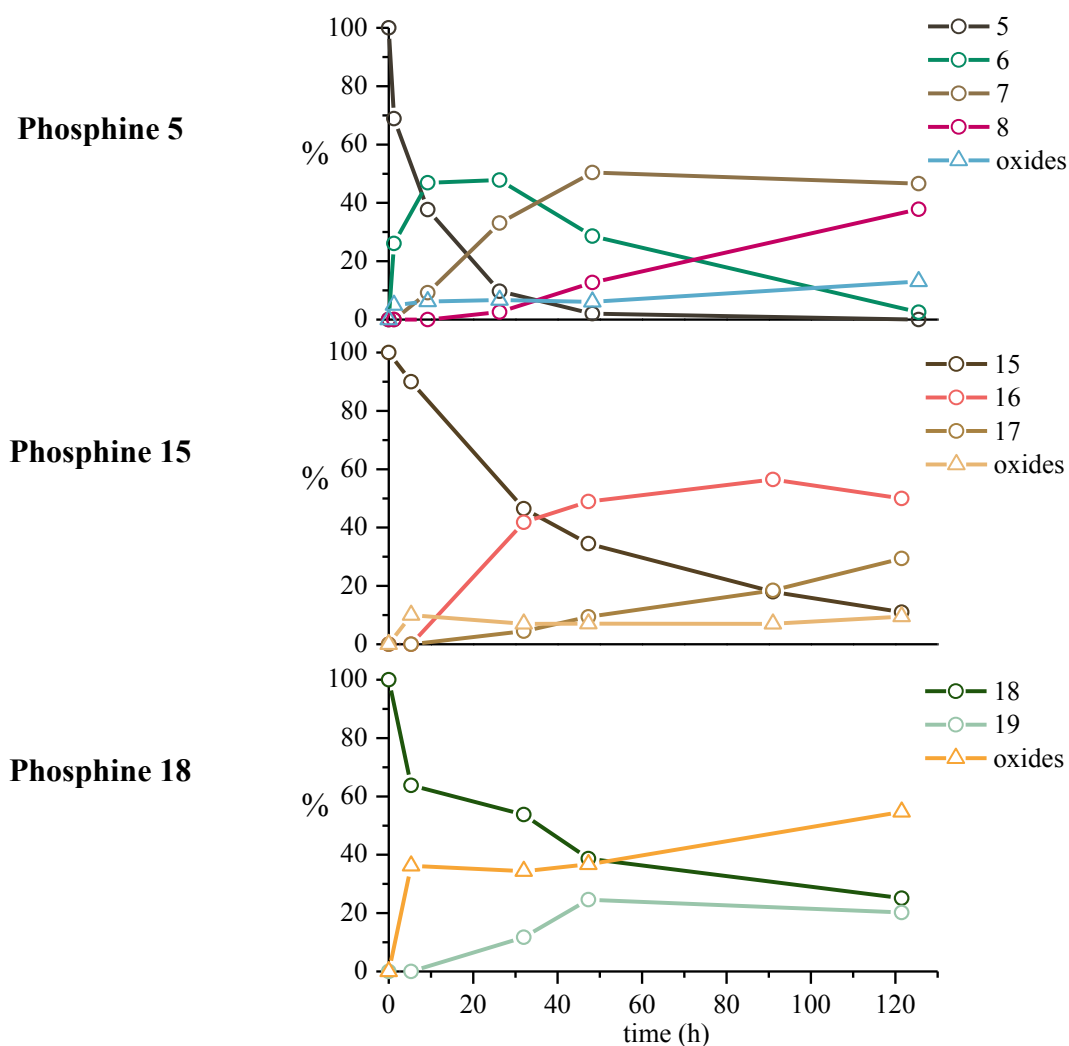
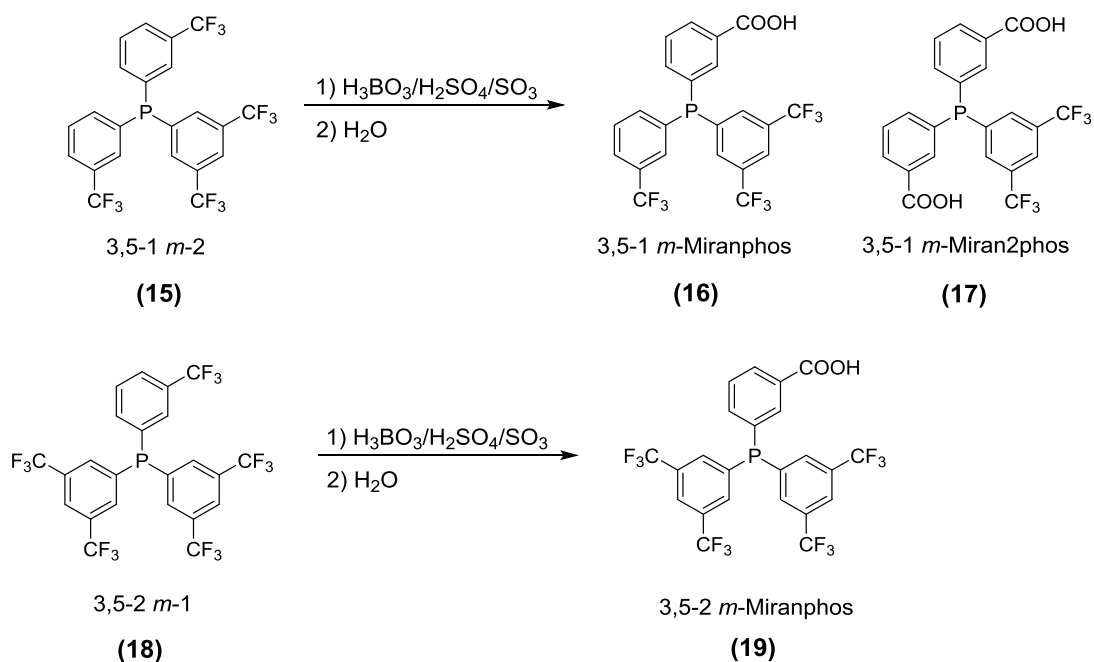


Figure 3.28. Evolution of the reaction of hydrolysis in phosphines **5**, **15** and **18** with time. Products extracted with Et₂O from the aqueous phase after quenching in water. % of compounds correspond to the integration of the phosphorus products in ³¹P{¹H} NMR. Reaction conditions: 0.6 mmol of phosphine. [Phosphine] = 0.1 M, [H₃BO₃] = 0.5 M, [SO₃] = 6.7 M.

On the other hand, the rate of the hydrolysis of the trifluoromethyl groups follows the opposite trend than that of the phosphine oxidation, specially the initial oxidation. As stated before and as will be discussed in the next chapter, the protection of the phosphines in these reactions is based on the protonation of the phosphorus atom.²⁰ The non-dissolved fraction of phosphine before the addition of oleum would not be protonated and hence not protected. Although the protonation of a phosphine is related to its basicity, we can assume that in this high acidic media the fraction of dissolved phosphines will be completely protonated. Concerning the solubility, phosphines with a high number of CF₃ groups are likely to be less soluble in polar media such as sulfuric acid. Consequently, these trifluoromethylated phosphines would have a higher fraction

of the non-protonated form which will be immediately oxidized in contact to oleum than those phosphines with a lower number of trifluoromethyl groups.



Scheme 3.11. Reaction of hydrolysis in the heteroleptic *meta*-trifluoromethylated phosphines

After this first screening and comparison of the reaction rates in the *meta*-substituted phosphines **5**, **15** and **18**, the reaction was studied individually for the two heteroleptic phosphines in more detail.

3.3.2.1.1. Reaction of hydrolysis in phosphine **15**

It has been shown that phosphine **15** gives two carboxylic products, **16** and **17**, depending on the number of *m*-trifluoromethyl groups hydrolysed. It was also observed that, under the essayed conditions, the reaction was slow and thus the formation of phosphine oxides represented an important percentage of the reaction products at high reaction times.

With the aim of increasing the rate of the hydrolysis while decreasing the formation of phosphine oxides, 3 new reaction conditions were explored (**Figure 3.29**). As usual, the reaction was followed by $^{31}\text{P}\{^1\text{H}\}$ NMR analysis of the quenched samples after extraction in Et_2O . It was decided to reduce the phosphine concentration to 0.07 M in all the reactions with the objective of ensuring its complete dissolution.

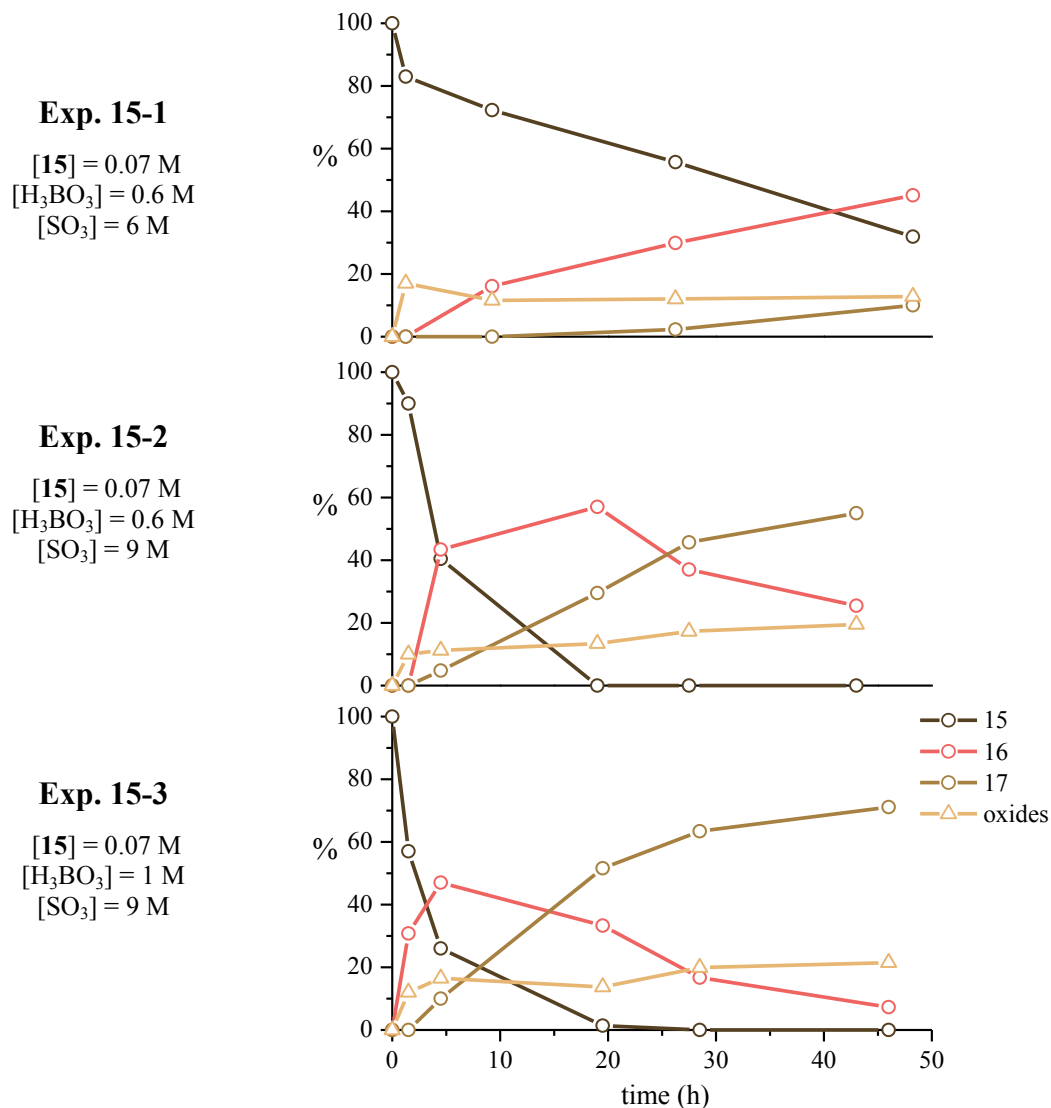


Figure 3.29. Evolution of the reaction of hydrolysis in phosphine **15** under different reaction conditions. Products extracted with Et₂O from the aqueous phase after quenching in water. % of compounds correspond to the integration of the phosphorus products in ³¹P{¹H} NMR

Experiment 15-1, set at the lowest concentration of sulfur trioxide (6 M), showed also the lowest reaction rate of the 3 experiments. The percentage of the phosphine oxides was constant during the reaction time, accounting for about 15 % after more than 50 h. At this time the amount of phosphine products were around 30 % for the starting phosphine **15** and 45 and 10 % for the mono- and dicarboxylic products, **16** and **17**, respectively. When the concentration of SO₃ was increased to 9 M, *experiment 15-2*, the rate of hydrolysis was also substantially increased giving *ca.* 60 % of monocarboxylic compound **16** and 30 % of the dicarboxylic **17**, after 20 h, with phosphine oxides around 15-20 %. At this point, trying to accelerate the reaction of hydrolysis by increasing the concentration of SO₃ above 9 M would, most probably,

give a higher oxidation rate, as observed previously for the *p*-substituted phosphine **1**. It was therefore decided to increase the concentration of boric acid instead. When boric acid was increased to 1 M, *experiment 15-3*, the rate of hydrolysis did also increase, showing in 10 h reaction similar composition than that observed in *experiment 15-2* after more than 20 h. Again, the amount of phosphine oxides was not significantly increased. None of those experiments showed hydrolysis of the trifluoromethyl group at 3,5-position.

In view of the results obtained from this set of experiments, the reaction was scaled up using conditions in-between *experiments 15-2* and *15-3*. Thus, for 2.5 g of phosphine **15**, with concentrations of phosphine, boric acid and sulfur trioxide to 0.07 M, 0.8 M and 9 M, respectively, and after 18 h reaction, the mixture showed a composition of *ca.* 11 % of **15**, 53 % of **16** and 36 % of **17** (**Figure 3.30**). Low signal-to-noise ratio did not allow the determination of the % of oxides.

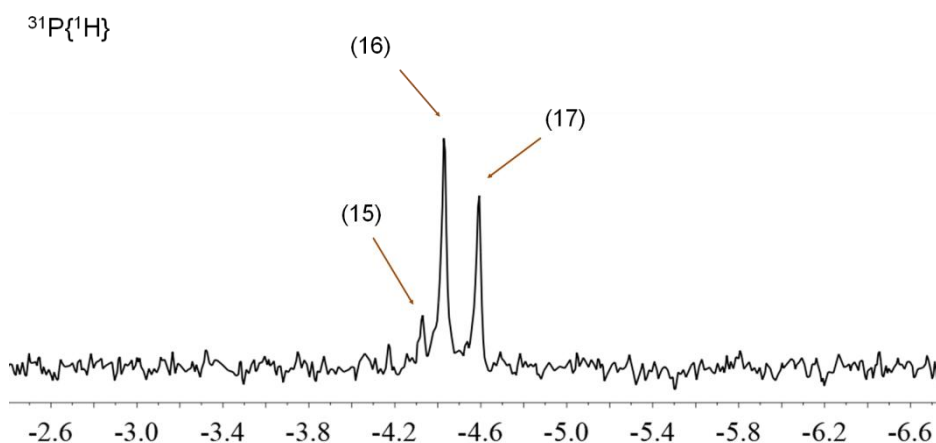


Figure 3.30. Reaction of hydrolysis of the trifluoromethyl group in phosphine **15**. Sample extracted at 18 h. Solvent CDCl₃:MeOH (4:1). ³¹P{¹H} NMR (101.27 MHz). δ in ppm. Reaction conditions: 4.7 mmol of phosphine. [Phosphine] = 0.07 M, [H₃BO₃] = 0.8 M, [SO₃] = 9 M.

Mono- and dicarboxylic phosphines, **16** and **17**, were successfully separated and purified following the pH-based procedure described for phosphines **1** and **5**. In this case, the pH of extraction in the aqueous phase were 6.7 for the oxides and 8.5 for the dicarboxylic product **17**. Unreacted phosphine **15** was separated from the monocarboxylic phosphine **16** by forming its sodium salt and extracting with cyclohexane. Later acidification of the sodium salt afforded **16**. The products were fully characterised as usually.

3.3.2.1.2. Reaction of hydrolysis in phosphine **18**

We have shown previously that the reaction of hydrolysis of the trifluoromethyl group can be applied to phosphine **18** showing one single product of reaction, which corresponds to the hydrolysis of the CF₃ located in *meta* (and different from those located in 3,5 position), **19**. Nevertheless the reaction, under the essayed conditions, was slow and most importantly, with an initial formation of phosphine oxides of about 40 %.

A set of 3 reactions were performed following the similar approach described above for **15**. Thus the concentration of phosphine was reduced to 0.08 M to ensure its complete dissolution, while varying the concentrations of SO₃ and H₃BO₃ (**Figure 3.31**). When concentrations of 8 M of SO₃ and 0.4 M of H₃BO₃ were used, *experiment 18-1*, an initial phosphine oxidation of around 15 % was observed, which increased slowly along the reaction until reaching a value close to 25 % at 100 h. Regarding the reaction of hydrolysis, low reaction rates were observed, showing a maximum percentage of carboxylated phosphine **19** of 60 % after 100 h of reaction together with 15 % of remaining unreacted phosphine **18**. Surprisingly, when the boric acid was reduced to 0.2 M, *experiment 18-2*, phosphine oxides were only detected after 24 h of reaction. However, after this point their concentration increases relatively fast with time showing 35 % at 100 h. This reaction was performed twice, observing the very same reaction profile in both cases. Interestingly, the rate of the reaction of hydrolysis was not significantly different from the observed in *experiment 18-1*. A last experiment was performed, *experiment 18-3*, in which the concentration of SO₃ was increased to 9 M with the intention of speeding up the reaction rate, while H₃BO₃ was set at 0.4 M in order to keep constant the oxidation of phosphines with time. An increase in the hydrolysis rate was observed with respect to previous experiments, reaching complete hydrolysis of the starting material after 50 h of reaction together with an amount of phosphine oxides below 30 %, which was constant over the time. It seems that somehow the concentration of boric acid influences both the initial oxidation as well as the oxidation produced with time. This same behaviour was found in the *para*-heteroleptic phosphines **20** and **23**, as will be shown in next section of the present chapter.

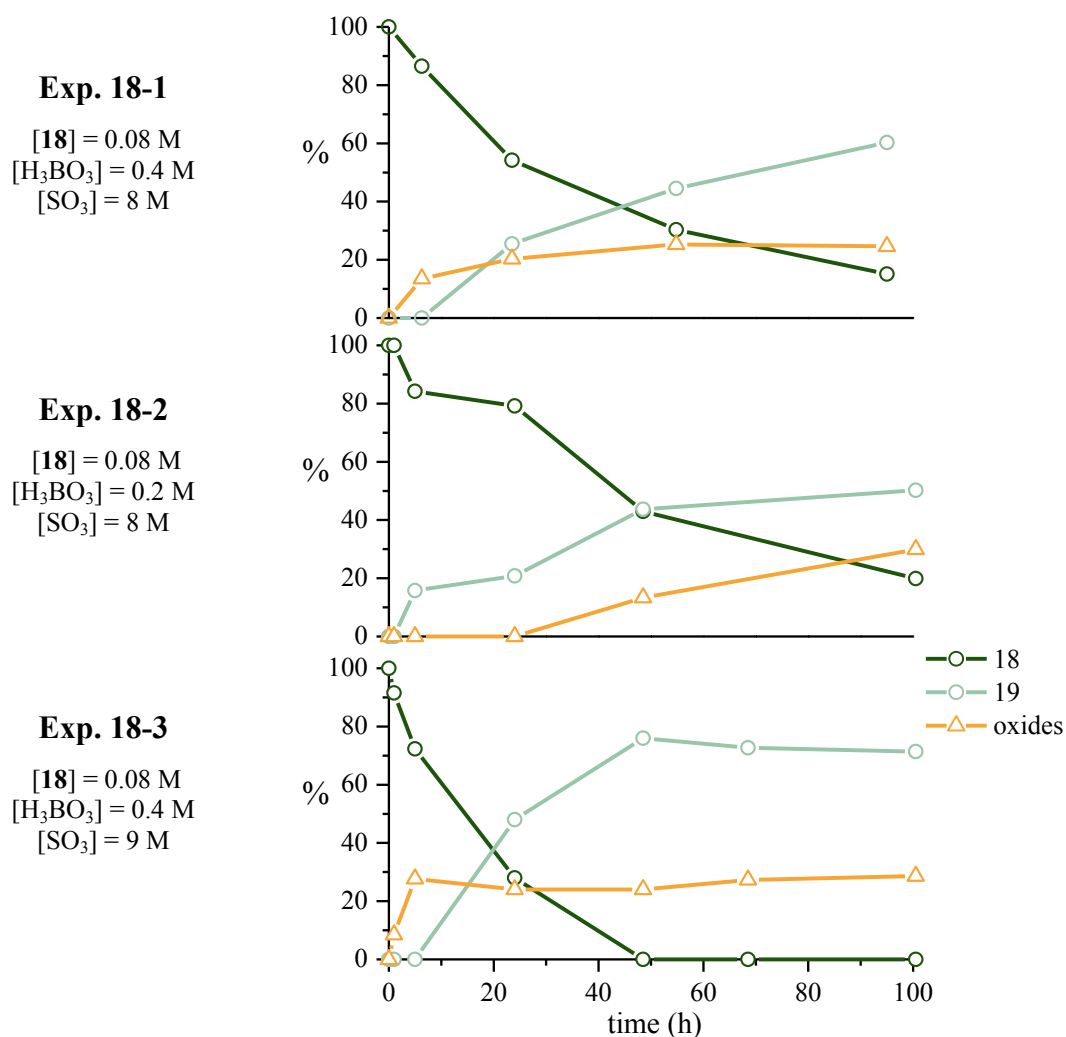


Figure 3.31. Evolution of the reaction of hydrolysis in phosphine **18** under different reaction conditions. Products extracted with Et₂O from the aqueous phase after quenching in water. % of compounds correspond to the integration of the phosphorus products in ³¹P{¹H} NMR

All in all, conditions of *experiment 18-3* were chosen as the most suitable conditions between all the essayed ones. Although under these conditions the reaction produced about 30 % of phosphine oxides, it is true that it was the only side-product observed, meaning that carboxylated phosphine **19** can be virtually obtained in 70 % yield in a relative short period of time. The purification of the reaction product was performed by column chromatography to eliminate the oxides. In cases where the starting phosphine was still present as impurity, it was efficiently separated by firstly neutralising the carboxylated phosphine and then using extractions with cyclohexane, as described before for other phosphines.

It is worth mentioning that in reactions performed during long times as those showed in this section, there is always an intrinsic oxidation due to the sampling methodology,

especially in the cases with low concentrations of boric acid. Although special care is taken and sampling is always performed under positive pressure of nitrogen, the highly oxidative media makes it difficult to reduce this side reaction.

3.3.2.2. Reaction of hydrolysis of the trifluoromethyl group in the heteroleptic triarylphosphines **20** and **23**

Once the reaction had been studied for the *meta*-substituted heteroleptic phosphines and the carboxylated products had been isolated, it was decided to test the reaction with the *para*-heteroleptic homologues. In this case, and as observed for the *meta*-heteroleptic phosphines, the reaction rates decreased when increasing the number of 3,5-substituted rings. In the same way as described for the homoleptic phosphines **5** and **1**, the reaction in the *para*-heteroleptic phosphines **20** and **23** was slower than in the *meta* homologues **15** and **18**, adding an additional degree of difficulty to the process. Because of this fact, the reactions of hydrolysis with phosphines **20** and **23** were found to be challenging in terms of reaction rates and phosphine oxidation. Next the results obtained will be presented.

As a first screening, both phosphine **20** and phosphine **23** were tested using molar concentrations of SO₃, H₃BO₃ and phosphine of 9, 1 and 0.07, respectively, **Figure 3.32**, as previously used with phosphine **15**. While phosphine **20** showed an initial oxidation of 20 %, *experiment 20-1*, with phosphine **23** this oxidation represented about 60 % of the composition of the phosphines in the mixture, *experiment 23-1*. We related this effect, again, to a problem of solubility. Although phosphine concentration was diluted to 0.07 M, the mixture of phosphine **23** in sulfuric acid and boric acid previous to the addition of oleum was turbid, contrary to the phosphine **20** which was dissolved, according to the visual inspection. Comparing the behaviour of the two phosphines under these conditions, it should be mentioned that, as observed for the homoleptic *para*-substituted phosphine **1**, the signals in ³¹P{¹H} NMR of the carboxylic products are shifted downfield, **Figure 3.33**.

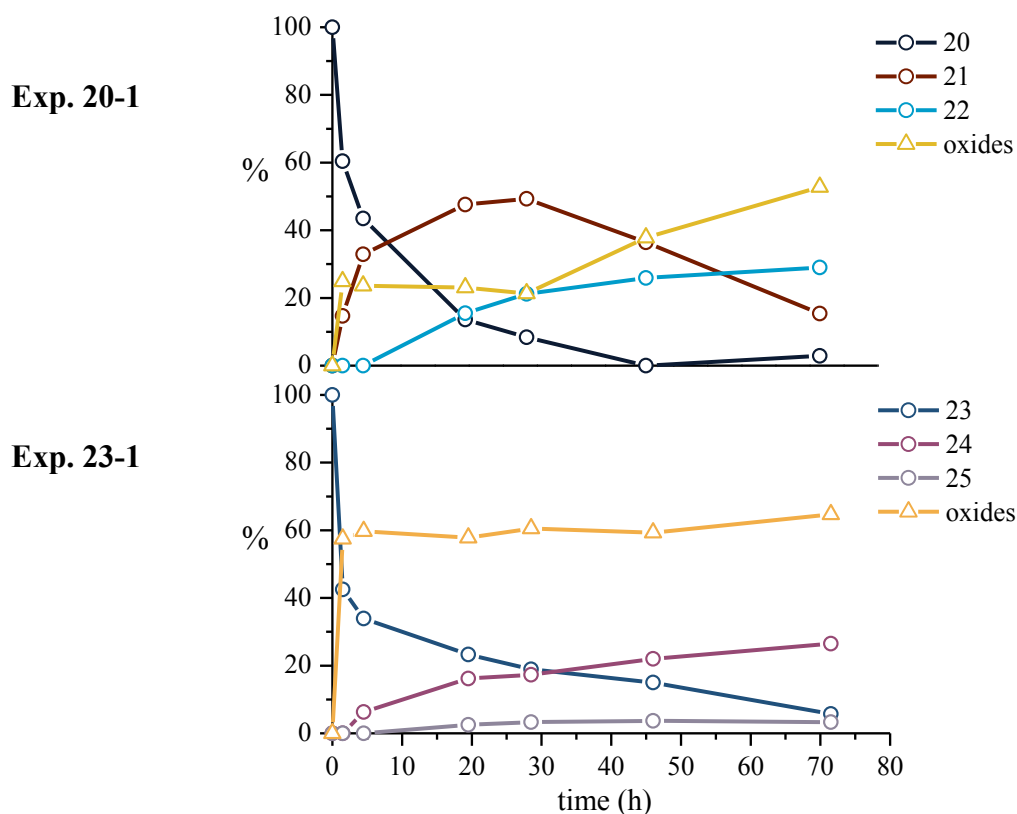


Figure 3.32. Evolution of the reaction of hydrolysis in phosphines **20** and **23**. Products extracted with Et₂O from the aqueous phase after quenching in water. % of compounds correspond to the integration of the phosphorus products in ³¹P{¹H} NMR. Reaction conditions: [SO₃] = 9 M, [H₃BO₃] = 1 M, [P] = 0.07 M.

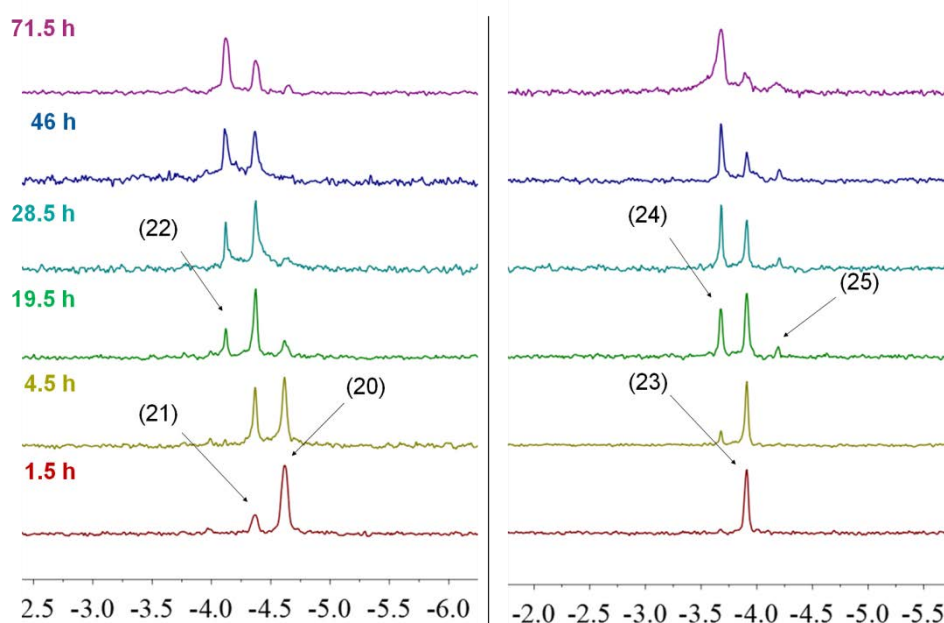
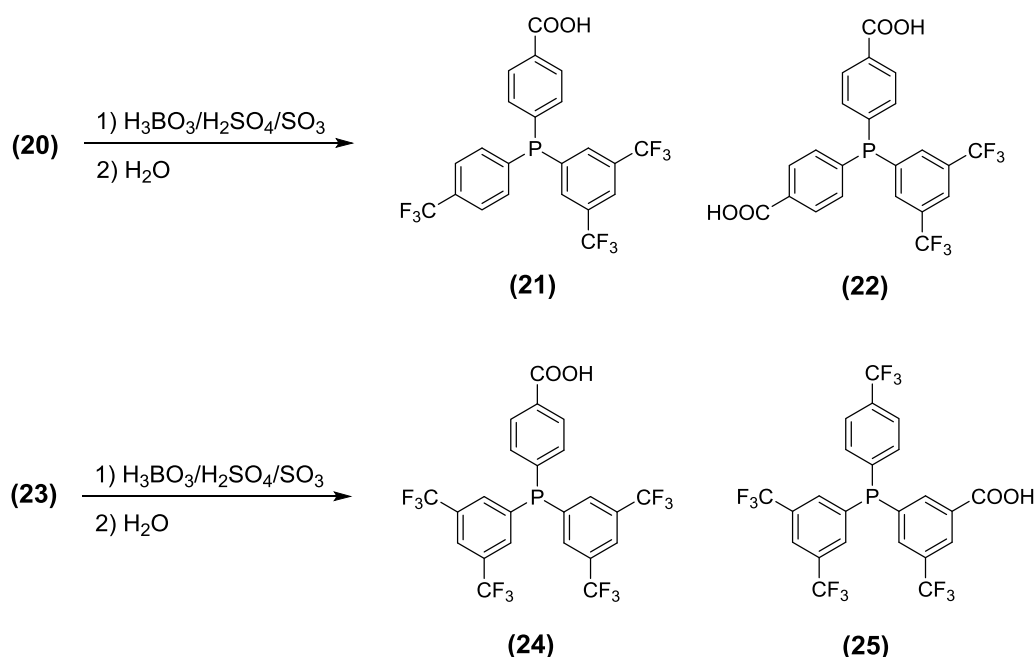


Figure 3.33. ³¹P{¹H} NMR (101.27 MHz) spectra of the evolution of the reaction of hydrolysis of the trifluoromethyl group in phosphines **20** (left) and **23** (right). Solvent CDCl₃:MeOH (4:1). δ in ppm. These spectra correspond to the *experiments 20-1* and *23-1*. Only phosphine region of the spectra is shown. See footnotes in **Figure 3.32** for further experimental details.

In the reaction with phosphine **20** the formation of two new products were observed. The displacement of their chemical shifts in $^{31}\text{P}\{^1\text{H}\}$ NMR towards more positive values indicates the hydrolysis of those trifluoromethyl groups at *para*-position, with the formation of the mono carboxylated **21** and dicarboxylated **22** phosphines, **Scheme 3.12**. However, the formation of the dicarboxylic **22** was overshadowed by the large amount of phosphine oxides present at long reaction times. On the other hand, the same criterion was used to assign the structure of the signals observed in NMR spectra. Downfield displacement of the signal with respect to the initial phosphine **23** indicates the reaction the hydrolysis of the *para*-located CF_3 , **24**. Moreover, another signal shifted upfield, **25**, which could be attributed to the hydrolysis of a 3,5-group, was also observed (**Scheme 3.12**). The small percentage of this compound found in the mixture (below 5 %) illustrates the difficulty associated to the hydrolysis of the 3,5- CF_3 groups. High percent of phosphine oxides (60 %) were observed from the very beginning of the reaction



Scheme 3.12. Reaction of hydrolysis in the heteroleptic *para*-trifluoromethylated phosphines

The behaviour of phosphine **23**, under three new different conditions, was next studied (**Figure 3.34**).

As mentioned before, in the hydrolysis of the *meta*-heteroleptic phosphine **18**, the concentration of boric acid may play a role in the initial oxidation of the phosphines. This effect is clearly shown when comparing *experiments 23-1*, *23-2* and *23-3* in which

different concentrations of boric acid were used while keeping the same concentrations of phosphine and sulfur trioxide. When no boric acid was used (*experiment 23-2*) the initial oxidation accounted for a roughly 10 %, while when this reagent was used in a 0.14 M concentration (*experiment 23-3*) this oxidation accounted for around 20 %. Both *experiment 23-2* and *23-3* produced clear solutions previous to the addition of oleum. *Experiment 23-1* exemplified the most extreme case of this behaviour with 60 % of oxide. Moreover, under these same conditions, but diluting the phosphine concentration to 0.03 M, *experiment 23-4*, although no complete dissolution of the phosphine was achieved, the initial oxidation was reduced to a 40 %, thus demonstrating that this phenomenon is closely related to the solubility of the phosphine. It is also possible to observe from these experiments that, in spite of increasing the initial oxidation, boric acid also increases the reaction rate.

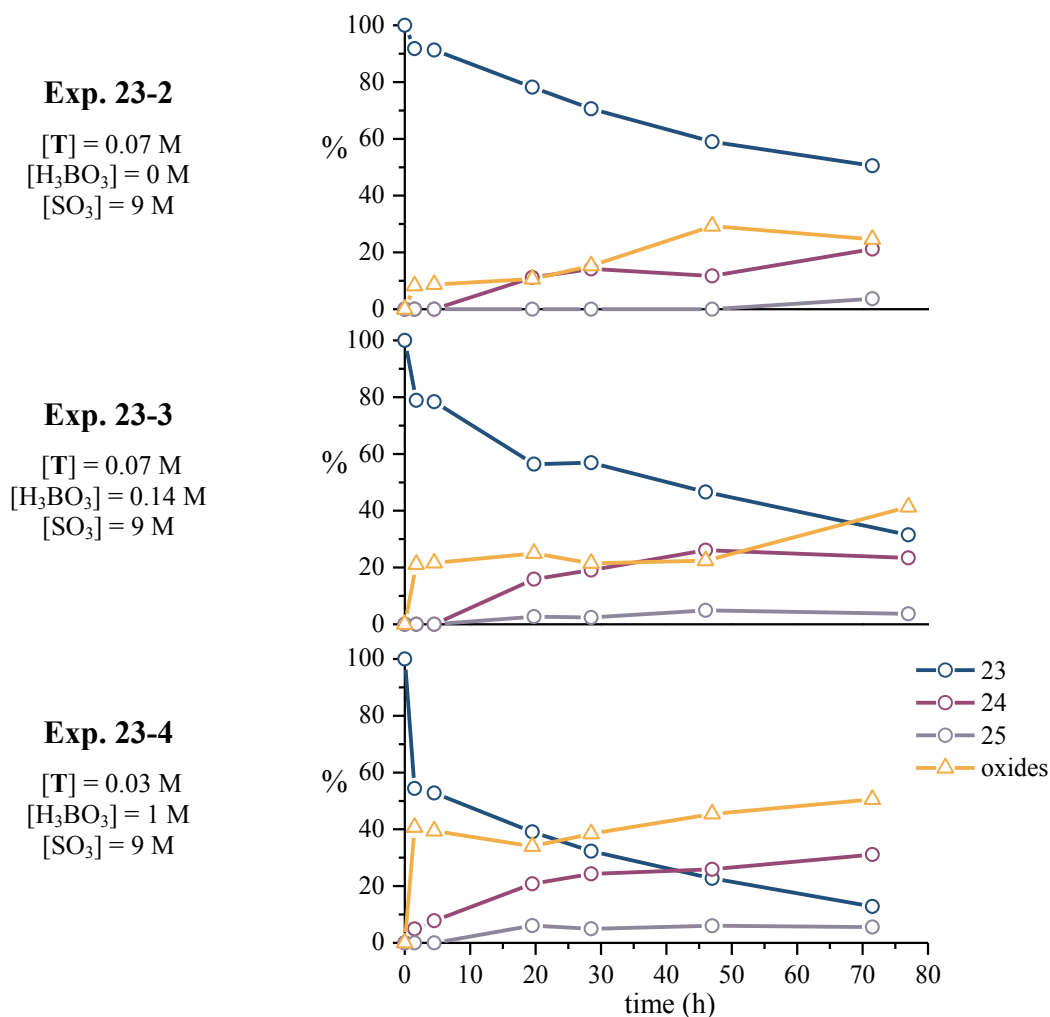


Figure 3.34. Evolution of the reaction of hydrolysis in phosphine **23** under different reaction conditions. Products extracted with Et₂O from the aqueous phase after quenching in water. % of

compounds correspond to the integration of the phosphorus products in $^{31}\text{P}\{^1\text{H}\}$ NMR

To explain how the initial oxidation is related to the concentration of boric acid and, at the same time, how this reagent affects the solubility of the phosphines one could take into consideration the reaction that takes place between boric and sulfuric acid. Although it will be explained in more detail in the next chapter, generally speaking the reaction between these two compounds consumes three mols of sulfuric acid per mol of boric acid and generates boron tri(hydrogensulfate) together with three mols of water, eq. **3.1**. This water generated would, on the one hand, change the polarity of the media, thus affecting the solubility of the phosphines, especially to the more apolar highly trifluoromethylated phosphines, such as **23**. On the other hand, water would dilute the acidic media which would affect to the degree of protonation of the phosphines, being those phosphines with higher number of trifluoromethyls, and thus more acidic, the most affected by this change in the media (compare *experiments 20-1* and *23-1*). To prove this hypothesis, 2 new reaction conditions were tested, *experiments 23-5* and *23-6*, **Figure 3.35**.



Both *experiment 23-5* and *23-6* emulates conditions of *experiment 23-1*. In *experiment 23-5*, boric acid was dissolved in oleum previous to the addition of the resulting mixture onto a solution of the phosphine in sulfuric acid. Sulfur trioxide present in oleum consumes the water molecules generated in the reaction with boric acid, and shifts eq. **3.1** to the formation of the superacid species tetra(hydrogensulfato)boric acid, $\text{HB}(\text{HSO}_4)_4$, eq. **3.2** (this reaction will be studied in detail in the next chapter). With this methodology, the initial oxidation was reduced to 25 %, although no higher reaction rates were obtained. *Experiment 23-6* was based in changing the order of addition of the reactants. Thus, oleum was added onto a solution of the phosphine in sulfuric acid previous to the addition of boric acid. Given that we knew that boric acid helps reduce the oxidation, a small amount of it (4 % of the total amount of boric acid) was added to the solution of phosphine. The rest of the boric acid was added just after the addition of oleum. With this approach the initial oxidation was reduced to *ca.*10 %, although the reaction rate was still slow. These results were in agreement with the assumption that the initial oxidation of the phosphines is due to a change in the reaction media previous to the addition of oleum. Such change could be attributed to either a reduced acidity or a

change in the polarity of the reaction media. Either way, both are produced by the formation of water in the reaction between boric and sulfuric acid.

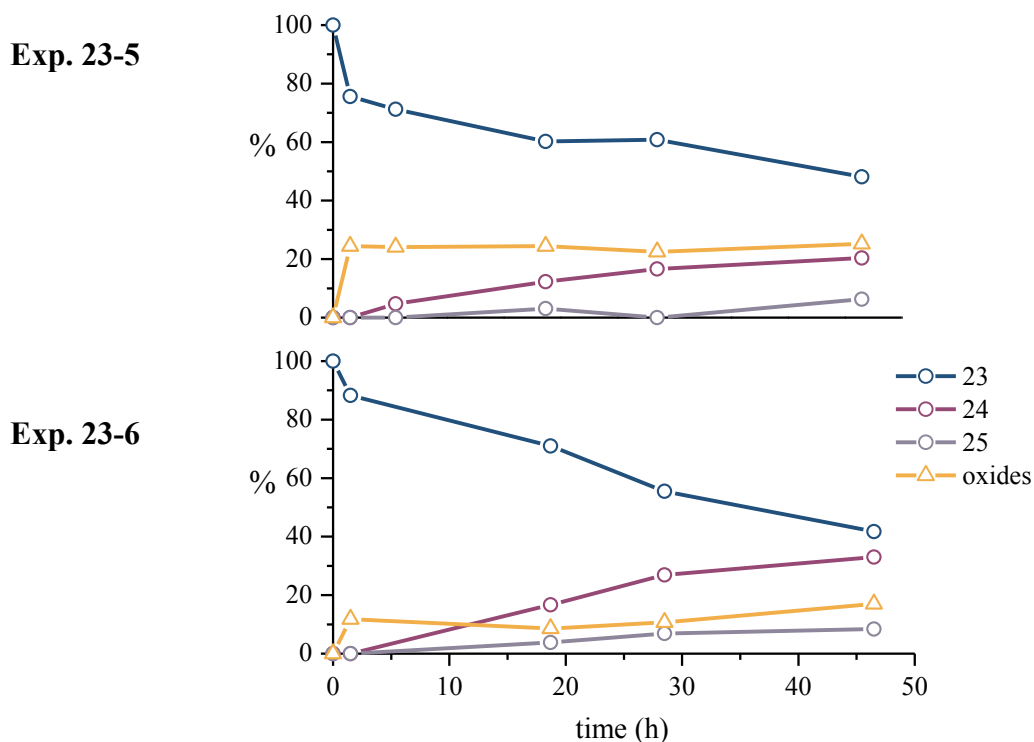
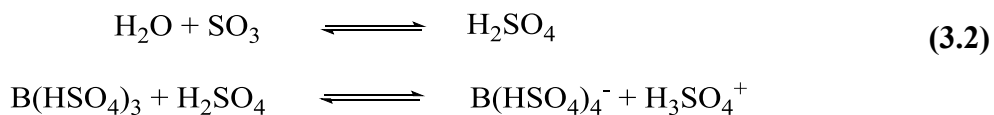


Figure 3.35. Evolution of the reaction of hydrolysis in phosphine **23** under different reaction conditions. Products extracted with Et₂O from the aqueous phase after quenching in water. % of compounds correspond to the integration of the phosphorus products in ³¹P{¹H} NMR. Reaction conditions: [Phosphine] = 0.07 M, [H₃BO₃] = 1.0 M, [SO₃] = 9.0 M.



As a general rule, it has been demonstrated that the reactions of hydrolysis of the trifluoromethyl groups in heteroleptic phosphines **20** and **23** are slow and that are competing with the oxidation of the phosphine. Moreover, the impact of boric acid in the initial oxidation added a degree of difficulty to the process. At this point, it is worth evaluating this synthetic route in the preparation of the carboxylic phosphines **21**, **22** and **24**. In contrast to the trifluoromethylated homoleptic phosphines, the synthesis of the trifluoromethylated heteroleptic phosphines is not so straightforward and implies, as previously described in this chapter, the preparation and purification of several intermediates most of which are air and moisture sensitive compounds. If we add the conditions needed to produce the carboxylated products, there is little doubt that this

strategy is more tedious and less efficient than the traditional syntheses of this sort of compounds.²⁸ It must be noticed, however, that the objective behind the interest in the trifluoromethylated heteroleptic phosphines was no other than providing deeper knowledge to the reaction of hydrolysis of the trifluoromethyl group in triarylphosphines. In this sense, this study has been absolutely fruitful since it provided us with more information with respect to the reaction of hydrolysis. In fact, as stated in the introduction, the synthesis phosphine **24** through the Pd-cat C-P coupling has been published during the development of the present work^{28d} which, in view of the above described results, is probably a most efficient synthetic approach to this phosphine.

3.4. Study of the σ -basicity of the Miranphos and Miran2phos ligands. Synthesis of the phosphine selenides

Selenide derivatives of the carboxylic and trifluoromethylated phosphines were prepared to study the σ -basicity of these ligands, in analogy to the trifluoromethylated ones described in the previous sections of this chapter.

The synthesis of the selenides was carried out as previously shown. 0.01 M solution of the corresponding phosphine was stirred overnight at 40 °C under nitrogen atmosphere with 1.5 equivalents of Se black. Since the solubility in chloroform of some of the carboxylic phosphines was found to be moderate, especially of those containing two carboxylic acid groups (Miran2phos ligands), the reactions were performed in acetone. However, considering that coupling constants can vary with the solvent,^{13d,29} once the selenide was formed and the excess selenium had been removed, the resulting solution was evaporated and the NMR analysis was performed in chloroform. This way, the values of $^1J_{\text{PSe}}$ of the selenides of all the phosphines described in this chapter were comparable, **Table 3.3**. The selenide derivative of the *ortho*-substituted phosphine *o*-Miranphos could not be obtained even refluxing it in chloroform for 5 days.

²⁸ a) Ravindar, V.; Hemling, H.; Schumann, H.; Blum, J. *Synth. Commun.* **1992**, *22* (6), 841–851.
b) Ravindar, V.; Hemling, H.; Schumann, H.; Blum, J. *Synth. Commun.* **1992**, *22* (10), 1453–1459.
c) Herd, O.; Heßler, A.; Hingst, M.; Tepper, M.; Stelzer, O. *J. Organomet. Chem.* **1996**, *522* (1), 69–76.
d) Dydio, P.; Detz, R. J.; Reek, J. N. H. *J. Am. Chem. Soc.* **2013**, *135* (29), 10817–10828. e) Starkov, P.; Moore, J. T.; Duquette, D. C.; Stoltz, B. M.; Marek, I. *J. Am. Chem. Soc.* **2017**, *139* (28), 9615–9620.

²⁹ Barfield, M.; Johnston, M. D. *Chem. Rev.* **1973**, *73* (1), 53–73.

Table 3.3. Values of $^1J_{\text{PSe}}$ for the selenide derivatives of the carboxylic and trifluoromethylated triarylphosphines (Miranphos and Miran2phos family) and selected values from **Table 3.2**

Ligand	$^1J_{\text{PSe}}^{\text{a}}$	$^1J_{\text{PSe}}^{\text{calculated b}}$
TPP	731	-
<i>p</i> -DPPBA ^c	740	740
<i>p</i> -trisCF ₃ (1)	766	765.5
<i>p</i> -Miranphos (2)	764	763
<i>p</i> -Miran2phos (3)	761	760.5
<i>m</i> -trisCF ₃ (5)	767	765.5
<i>m</i> -Miranphos (6)	764	763
<i>m</i> -Miran2phos (7)	761	760.5
3,5-trisCF ₃ (14)	800	800
3,5-2 <i>m</i> -1 (18)	791	788.5
3,5-2 <i>m</i> -Miranphos (19)	786	786
3,5-1 <i>m</i> -2 (15)	780	777
3,5-1 <i>m</i> -Miranphos (16)	776	774.5
3,5-1 <i>m</i> -Miran2phos (17)	773	772
<i>o</i> -Miranphos (10)	-	765.5

^a Values obtained from the $^3\text{P}\{^1\text{H}\}$ in CDCl_3 . See text for more details ^b Values estimated from equation **3.3**. ^c *p*-(diphenylphosphino)benzoic acid.

The table shows that, in the phosphines studied, the hydrolysis of each trifluoromethyl group causes a moderate decrease, between 2 and 5 Hz, in the $^1J_{\text{PSe}}$ of the phosphine selenides. Given that carboxylic acids are electron-withdrawing groups, but weaker than trifluoromethyls, the results are within what one could expect. Interestingly, it can be observed that the addition of one carboxylic acid to triphenylphosphine (*p*-DPPBA) increases 9 Hz the coupling constant. We showed before that the introduction of a trifluoromethyl group was cumulative and resulted in the increase of 11-12 Hz in the $^1J_{\text{PSe}}$. Assuming that the introduction of carboxylic moieties is also cumulative, we established the following equation (**eq. 3.3**) to roughly estimate the magnitude of the $^1J_{\text{PSe}}$ in trifluoromethylated and/or carboxylic triarylphosphines.

$$^1J_{\text{PSe}} = 731 + 11.5 \cdot CF_3 + 9 \cdot CO_2H \quad (3.3)$$

where CF_3 and CO_2H are the number of trifluoromethyl and carboxylic groups in the phosphine, respectively. This equation describes the $^1J_{\text{PSe}}$ of the selenide derivatives of the whole set of phosphines studied in this chapter within a difference below 3 Hz.

3.5. Summary and concluding remarks

Trifluoromethylated triarylphosphines, including a set of four new heteroleptic phosphines, were successfully synthesised in this chapter. The reaction of hydrolysis of the trifluoromethyl group using fuming sulfuric acid and boric acid was then applied to these compounds.

Different reactivity was observed depending on the position of the CF₃ group in the aromatic ring. In the series of homoleptic phosphines, the fastest reaction rate was observed in the *meta*-substituted phosphine **5**, followed by the *para*-substituted one **1**. Much slower reaction rates were observed in the 3,5-substituted phosphine **14** and in the *ortho*-substituted one **9**. While in **14** the slow rate of hydrolysis of the trifluoromethyl group favoured the oxidation of the phosphines, the enhanced protection towards oxidation provided by the *ortho*-CF₃ groups in **9** afforded the preparation of the monocarboxylic compound **10**. However spirocyclic oxyphosphoranes compounds were formed at longer reaction times.

Same behaviour was observed in the heteroleptic phosphines; trifluoromethyls at *meta* undergo hydrolysis in faster rate than those at *para* positions. Moreover, negative effect in the hydrolysis of the CF₃ groups was observed when increasing the number of 3,5-trifluoromethyls located at different rings of the phosphine.

The methodology of separation and purification developed in this work afforded the preparation of 8 new trifluoromethylated and carboxylated phosphines. The whole procedure has been covered under patent and four of these compounds are commercially available through the Strem Chemicals company.

Chapter 4

Insights into the Reaction of Hydrolysis of the Trifluoromethyl Group

4.1. Introduction

Understanding how a chemical reaction works is always an issue of interest to the synthetic chemist, not only from an intellectual point of view, but also from a more practical perspective. Knowing the details of a given reaction makes it possible to address synthetic procedures in a more efficient way.

At this point, it is probably not necessary to mention that the reaction of hydrolysis of the trifluoromethyl group comprises a substantial part of the present work. During the study of this reaction in trifluoromethylated triarylphosphines several questions arose that, had them been answered in the previous chapter, would have led to a more complex text. Therefore, before continuing with further exploration of the reaction of hydrolysis, the present chapter will be addressed to give a more detailed picture of the reaction mechanism in an attempt to justify the different products and reactivity observed.

Three main blocks will be presented herein covering the primary concerns about the reaction of hydrolysis of the trifluoromethyl group under the essayed conditions. The first one will be focused on the role of boric acid, together with the boron species found in the reaction mixture. Then, the reaction mechanism that takes place during the conversion of trifluoromethyl groups into carboxylic acids in aryl phosphines will be studied. Finally, the formation of the spiro oxyphosphoranes during the reaction with the 2-tris(trifluoromethylphenyl)phosphine (**9**) will be analysed, in order to propose a mechanism consistent with the observed results.

4.2. Role of boric acid in the reaction of hydrolysis of the trifluoromethyl group

4.2.1. Chemistry of superacids¹

The term *superacid* refers to those acid systems stronger than 100 % sulfuric acid. This definition was proposed by Gillespie and has been accepted since then.² More

¹ for an extensive review on the topic, see: Olah, G. A.; Prakash, G. K. S.; Molnar, Á.; Sommar, J. *Superacid Chemistry*; John Wiley & Sons, Inc.: Hoboken, NJ, USA, 2009. 2nd Ed

specifically, this definition corresponds to that of Brønsted superacids. For Lewis superacids, the reference compound is anhydrous aluminium trichloride. However, in this section the term *superacid* will refer exclusively to Brønsted superacids. Because these species only exist in non-aqueous solvents, the measurement of the acidity of superacids cannot be expressed in the pH scale. Instead, the degree of protonation of a weak base is used, expressed as Hammett acidity function (H_0),³ equation 4.1,

$$H_0 = \text{p}K_{\text{BH}^+} - \log \frac{[\text{BH}^+]}{[\text{B}]} \quad (4.1)$$

where K_{BH^+} is the dissociation constant of the conjugate acid of a weak base B (equation 4.2) and $[\text{BH}^+]/[\text{B}]$ is the ionisation ratio, which is normally determined spectroscopically. In this scale, 100 % sulfuric acid has a value of H_0 of -11.9.



Superacid species can be divided into different categories. Primary superacids are single-component Brønsted superacids such as perchloric acid ($H_0 = -13$), fluorosulfuric acid ($H_0 = -15.1$), triflic acid ($H_0 = -14.1$) and anhydrous hydrogen fluoride ($H_0 = -15.1$). Moreover, the acidity of primary superacids can be enhanced by combination with other Brønsted superacids or, more interestingly, with Lewis superacids. These are the so-called binary superacids. As a matter of example, the acidity of sulfuric acid reaches a value of Hammett constant of -14.4 in combination with 50 mol% of SO_3 .⁴ Probably the most famous and extensively studied binary superacid is the combination of fluorosulfuric acid with antimony pentafluoride, $\text{HSO}_3\text{F-SbF}_5$, also known as *Magic Acid*. Values of H_0 of about -21 have been reported for a mixture of $\text{HSO}_3\text{F-SbF}_5$ with 25 mol% of SbF_5 .⁵ Furthermore, a few ternary superacids such as $\text{HSO}_3\text{F-SbF}_5\text{-SO}_3$ have been reported in the literature.⁶

² a) Gillespie, R. J.; Peel, T. E. *Adv. Phys. Org. Chem.* **1971**, 9 (C), 1–24. b) Olah, G. A.; Prakash, G. K.; Sommer, J. *Science* **1979**, 206 (4414), 13–20.

³ Hammett, L. P.; Deyrup, A. J. *J. Am. Chem. Soc.* **1932**, 54 (7), 2721–2739.

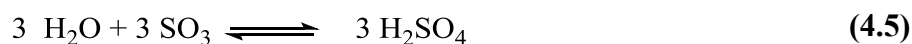
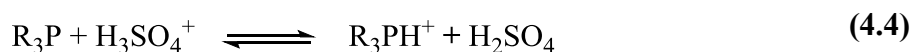
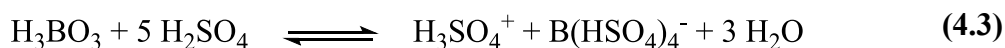
⁴ Gillespie, R. J.; Peel, T. E.; Robinson, E. A. *J. Am. Chem. Soc.* **1971**, 93 (20), 5083–5087.

⁵ Touiti, D.; Jost, R.; Sommer, J. *J. Chem. Soc. Perkin Trans. 2* **1986**, (11), 1793.

⁶ Thompson, R. C.; Barr, J.; Gillespie, R. J.; Milne, J. B.; Rothenbury, R. A. *Inorg. Chem.* **1965**, 4 (11), 1641–1649.

4.2.2. Boric acid and the hydrolysis of the CF₃

Although the reaction of hydrolysis of the trifluoromethyl group can be carried out under different conditions (see chapter 1), in this work a superacid system made of SO₃-H₂SO₄-H₃BO₃ was used. This same system, although with much lower concentrations of SO₃, was described by Hermann's group in the sulfonation of aromatic phosphines.⁷ According to the authors, the addition of boric acid in the sulfonating mixture minimises the phosphine oxidation by the generation of the superacid species tetra(hydrogensulfato)boric acid, HB(HSO₄)₄, which is known to ionise in sulfuric acid to form a superacid system⁸ in accordance with eq. 4.3. This superacid media would act as sulfonating agent and, at the same time, would ensure the protection of the phosphines by quantitative protonation of the phosphorus atom, eq. 4.4. In the reported reaction by Herrmann, sulfur trioxide is used to quantitatively remove water from the reaction medium, eq. 4.5, shifting the equilibrium towards the formation of the superacid species.



In fact, previous to the addition of SO₃, the boron species present in the reaction medium are a mixture of the tricoordinate species boron tri(hydrogensulfate) and the tetracoordinate species tetra(hydrogensulfato)boric anion in equilibrium, equation 4.6. After the addition of SO₃, the equilibrium is completely shifted towards the tetracoordinate species. Herrmann's group showed this behaviour by ¹¹B NMR and was also supported by the previous observations of Olah *et al.* in the B(SO₃CF₃)₃-B(SO₃CF₃)₄⁻ system in trifluoromethanesulfonic acid.⁹ We proved that these assumptions and observations were also valid for our trifluoromethylated

⁷ Herrmann, W. A.; Albanese, G. P.; Manetsberger, R. B.; Lappe, P.; Bahrmann, H. *Angew. Chem. Int. Ed. Engl.* **1995**, *34* (7), 811–813.

⁸ a) Bass, S. J.; Flowers, R. H.; Gillespie, R. J.; Robinson, E. A.; Solomons, C. *J. Chem. Soc.* **1960**, 4315–4320. b) Barr, J.; Gillespie, R. J.; Robinson, E. A. *Can. J. Chem.* **1961**, *39* (6), 1266–1273.

⁹ Olah, G. A.; Laali, K.; Farooq, O. *J. Org. Chem.* **1984**, *49* (24), 4591–4594.

phosphines. Therefore *p*-tris(trifluoromethylphenyl)phosphine (**1**) was dissolved in a solution of boric acid in sulfuric acid, emulating the conditions used in a standard reaction. The resulting solution was then analysed by ^{31}P and $^{31}\text{P}\{^1\text{H}\}$, confirming the quaternisation of the phosphine as phosphonium with $^1J_{\text{HP}} = 524.5$ Hz, **Figure 4.1**. The solution was also analyzed by $^{11}\text{B}\{^1\text{H}\}$ NMR before and after the addition of oleum to the solution, **Figure 4.2**. Since ^{11}B is a quadrupolar nucleus ($I = 3/2$), the shape of the signals in the NMR spectra is affected by the geometry of the molecule and thus by the charge distribution. As a consequence, tetrahedral boron species (high symmetry environment) give sharper signals than the corresponding trigonal species (low symmetry environment). In our experiments with $^{11}\text{B}\{^1\text{H}\}$ NMR we observed a sharp signal at -3.85 ppm corresponding to the highly symmetrical tetracoordinate species, $\text{B}(\text{HSO}_4)_4^-$, together with a broader signal at 0.90 ppm, corresponding to the tricoordinate species, $\text{B}(\text{HSO}_4)_3$, which disappears upon addition of oleum. These observations were in agreement with those described by Herrmann.

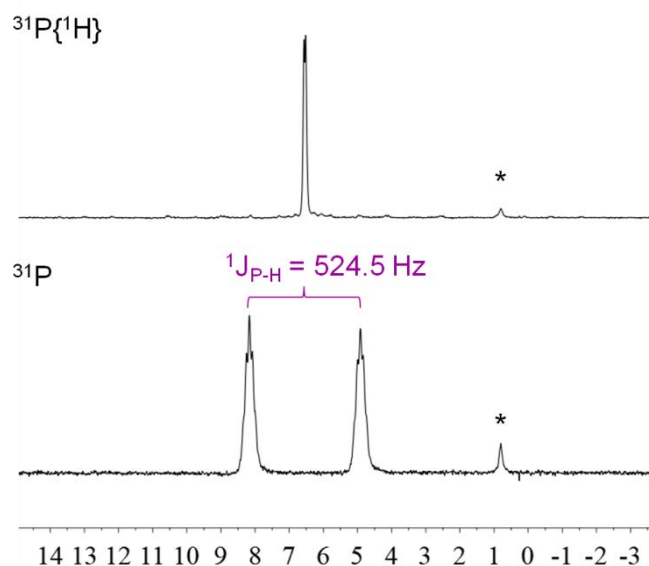


Figure 4.1. Protonation of phosphine **1** in a solution of boric acid in sulfuric acid. $^{31}\text{P}\{^1\text{H}\}$ and ^{31}P NMR (161.98MHz). δ in ppm. Signals relative to NH_4PF_6 (internal standard, -144.45 ppm). Signal of partly hydrolysed NH_4PF_6 denoted as *

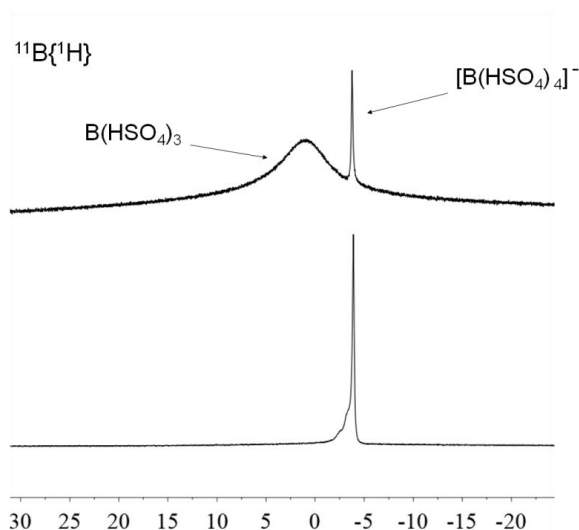


Figure 4.2. $^{11}\text{B}\{^1\text{H}\}$ NMR (128.38 MHz) of a solution of boric acid in sulfuric acid before (**top**) and after (**bottom**) the addition of oleum. δ in ppm. Signals relative to $\text{BF}_3 \cdot \text{Et}_2\text{O}$ (0.0 ppm) used as external standard)

The amount of SO_3 used in Hermann's approach is only the required to titrate the water formed in the reaction between boric and sulfuric acid. The superacid system in that reaction media can therefore be considered the binary Brønsted super acid $\text{HB}(\text{HSO}_4)_4\text{-H}_2\text{SO}_4$. In this sense, Hermann and co-workers attributed the protection of the phosphine to both the quaternisation of the phosphorus atom and the substitution of sulfur trioxide for other less oxidative sulfonating species. However, because of the large excess of SO_3 used in the present research, no such assumptions should be done. Previous work in our group, focussed in the sulfonation of trifluoromethylated phosphines, showed that this reaction can also be performed under excess of SO_3 , with minimum phosphine oxidation when boric acid is also used.¹⁰ This would indicate that the phosphine protection is not only due to a reduction in the concentration of sulfur trioxide in the reaction medium, but there might be an increase in the acidity of the medium, ensuring the protonation of the phosphine. A ternary super acid $\text{HB}(\text{HSO}_4)_4\text{-SO}_3\text{-H}_2\text{SO}_4$ is then proposed as the super acid existing under the reaction conditions used for the hydrolysis of the trifluoromethyl groups in arylphosphines. The next part of this section will be devoted to prove the hypothesis that ternary superacid mixture $\text{HB}(\text{SO}_4)_4\text{-SO}_3\text{-H}_2\text{SO}_4$ is a stronger superacid than the binary $\text{HB}(\text{SO}_4)_4\text{-H}_2\text{SO}_4$.

Although the binary super acid mixtures $\text{SO}_3\text{-H}_2\text{SO}_4$ (oleum) and $\text{HB}(\text{HSO}_4)_4\text{-H}_2\text{SO}_4$ were extensively studied by Gillespie and co-workers during the sixties and

¹⁰ Peral Crespo, D. *Triarilfosfines Sulfonades Trifluorometilades. Aplicacions en Processos Catalitics*. Ph.D. Thesis. Universitat Autònoma de Barcelona, **2013**.

seventies,^{4,8,11} to the best of our knowledge, the ternary $\text{HB}(\text{HSO}_4)_4\text{-SO}_3\text{-H}_2\text{SO}_4$ mixture has not been studied. Therefore, the first attempt to understand this ternary superacid was based on the comparison of the behaviour of the two binary superacid mixtures, $\text{SO}_3\text{-H}_2\text{SO}_4$ and $\text{HB}(\text{HSO}_4)_4\text{-H}_2\text{SO}_4$ according to the literature. Gillespie and co-workers showed that higher acidities can be reached with the $\text{SO}_3\text{-H}_2\text{SO}_4$ superacid mixture than with the $\text{HB}(\text{SO}_4)_4\text{-H}_2\text{SO}_4$ system,⁴ **Figure 4.3**. Although the initial increase in $-H_0$ is greater in $\text{HB}(\text{SO}_4)_4\text{-H}_2\text{SO}_4$, only a maximum $-H_0$ value of 13.6 was observed. This effect was attributed to the formation of polymeric boron sulfates which precipitate from the solution at concentrations above 32 mol% of $\text{HB}(\text{SO}_4)_4$. In contrast, the $-H_0$ value for 65 wt% SO_3 fuming sulfuric acid (69.5 mol% SO_3) is as high as 14.9. This result is appealing, since it would indicate that there is no need to use boric acid (*i.e.* to form $\text{HB}(\text{HSO}_4)_4\text{-H}_2\text{SO}_4$) to protect phosphines by protonation, because the oleum itself can reach higher values of $-H_0$. Nevertheless, as stated before, it was observed a positive effect inhibiting the phosphine oxidation when using oleum combined with boric acid in the sulfonation of arylphosphines.^{7,10} Also positive effects in both oxidation and in the rate of hydrolysis of the CF_3 was shown in the previous chapter.

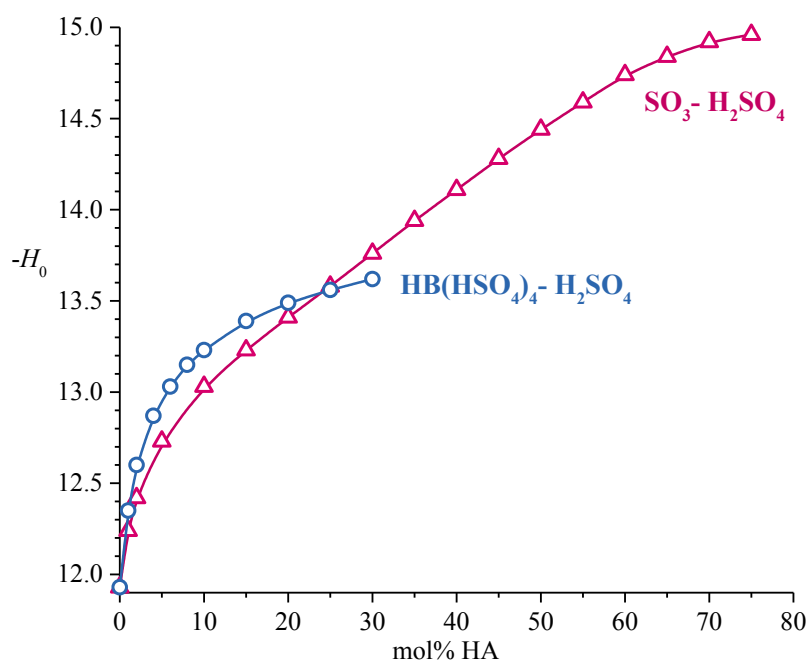
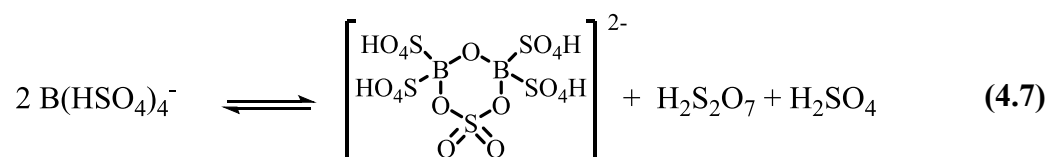


Figure 4.3. $-H_0$ values for the $\text{HB}(\text{HSO}_4)_4\text{-H}_2\text{SO}_4$ and the $\text{SO}_3\text{-H}_2\text{SO}_4$ systems. mol% of HA refers to the amount of either $\text{HB}(\text{HSO}_4)_4$ or SO_3 in the binary system. Adapted from⁴

¹¹ Robinson, E. A.; Gillespie, R. J. *Can. J. Chem.* **1962**, *40* (4), 658–674.

To shed light on this apparently contradictory evidence, the pioneering studies of Gillespie and Robison on the behaviour of tetra(hydrogensulfato)boric acid in sulfuric acid¹² were analysed. By means of Raman spectroscopy, the authors showed the formation of disulfuric (“pyrosulfuric”) acid (H₂S₂O₇) in concentrated solutions of HB(HSO₄)₄. This observation was best justified by a process of condensation of B(SO₄)₄⁻ with the subsequent formation of polymeric boron sulfates and the elimination of disulfuric acid, according to equation 4.7. Cryoscopic and conductometric experiments indicated that the most plausible composition of the polyborates is a mixture of the six-membered ring compound showed in equation 4.7 and oligomeric forms derived of it. Therefore, and regardless of the structure of the polyborates, it could be accepted that the addition of oleum would shift the equilibrium towards the left thus dissolving the polyborates. Rise in the acidity of the media would then be produced due to the increasing concentration of H₃SO₄⁺ B(HSO₄)₄⁻.



At this point, an attempt to estimate the acidity of the ternary HB(SO₄)₄–SO₃–H₂SO₄ superacid was essayed. Exact measure of super acids requires certain degree of expertise and would be outside the scope of the present work. However, one could compare the acidity of two media by comparison of the evolution of an acid-dependent reaction in these two different media. Fortunately, the main reaction studied in the present work, the hydrolysis of the trifluoromethyl in triarylphosphines, depends on the acidity of the medium. As will be shown in detail in the next section of this chapter, the C-F cleavage is acid promoted, it being faster under more acidic condition. Moreover it has been proven in the previous chapter that the reaction evolution can be easily monitored by ³¹P{¹H} NMR.

With this in mind, the reaction of hydrolysis of the *m*-tris(trifluoromethylphenyl)phosphine (**5**) was performed under two reaction conditions. In *reaction A*, the phosphine was dissolved in sulfuric acid before the addition of oleum, therefore the superacid system used in this reaction would be the

¹² a) Gillespie, R. J.; Robinson, E. A. *Can. J. Chem.* **1962**, *40* (4), 784–787. b) Gillespie, R. J.; Robinson, E. A. *Can. J. Chem.* **1962**, *40* (4), 1009–1017.

binary $\text{SO}_3\text{-H}_2\text{SO}_4$. In *reaction B*, the standard conditions of hydrolysis tested for the *meta*-substituted phosphine in the previous chapter were used. That is, the phosphine was dissolved in a solution of boric acid in sulfuric acid before oleum was added, thus the ternary $\text{HB}(\text{SO}_4)_4\text{-SO}_3\text{-H}_2\text{SO}_4$ would be the superacid used in this reaction. Same amounts of phosphine, oleum and sulfuric acid were used in both reactions and were performed simultaneously. Aliquots of the reaction mixtures were taken and quenched with water. Then the aqueous phase was extracted with Et_2O and the organic phase was analysed by $^{31}\text{P}\{^1\text{H}\}$ NMR, as usual. The *meta*-substituted phosphine **5** was chosen in this experiment because, it being the phosphine that showed faster reaction rates, would allow to carry out the study within a short period of time thus minimising the contribution of the oxidation to the reaction mixture. **Figure 4.4** shows the evolution of the reaction products with time.

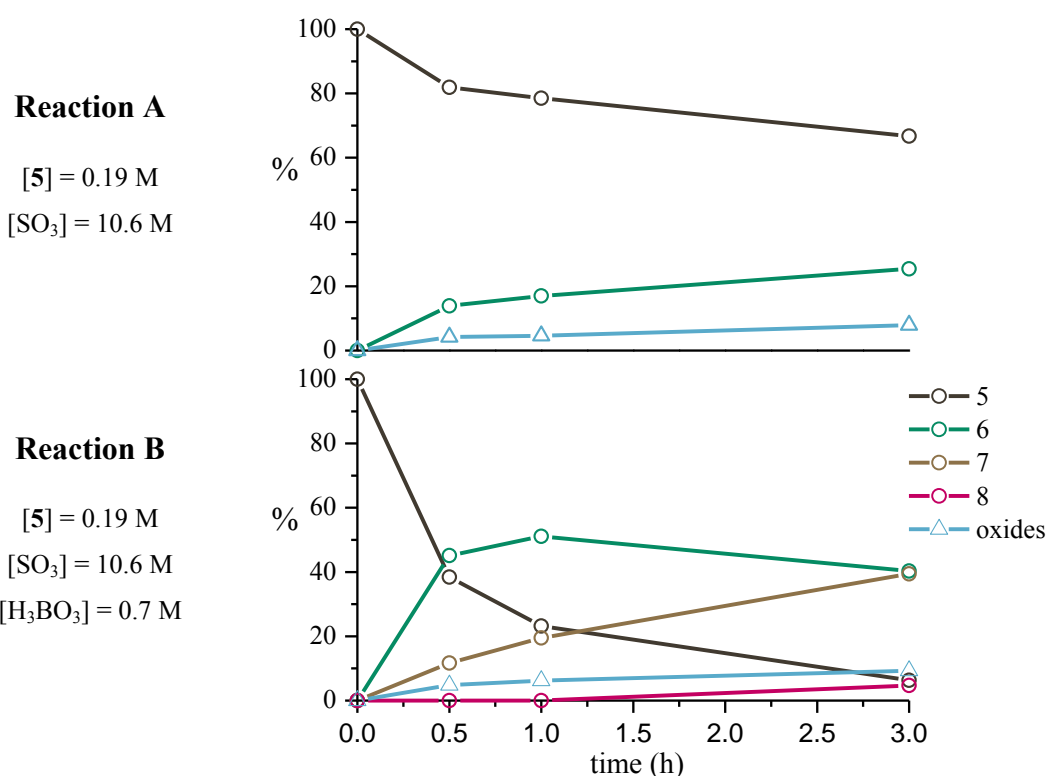


Figure 4.4. Evolution of the reaction of hydrolysis of the trifluoromethyl group in *m*-substituted homoleptic phosphine **5**. % of product composition according to $^{31}\text{P}\{^1\text{H}\}$ NMR.
 Reaction **A**: $\text{SO}_3\text{-H}_2\text{SO}_4$ system: 0.5 mmol of phosphine **5**, 0.8 ml of H_2SO_4 , 1.85 ml of oleum (65 wt% SO_3).
 Reaction **B**: $\text{HB}(\text{HSO}_4)_4\text{-SO}_3\text{-H}_2\text{SO}_4$ system: 0.5 mmol of phosphine **5**, 1.9 mmol of H_3BO_3 , 0.8 ml of H_2SO_4 , 1.85 ml of oleum (65 wt% SO_3)

At first sight it can be observed that the reaction rate was remarkably higher when boric acid was used. While at 30 min, *reaction A* only showed about 15 % of the

monocarboxylated product **6**, *reaction B* showed almost 45 % of this compound, together with 12 % of the dicarboxylic phosphine **7**. After 3 h of reaction the differences in the mixture composition became even more evident. Under reaction conditions *A*, 25 % of monocarboxylic phosphine **6** was observed as the only product of hydrolysis, while in *reaction B* the consumption of the starting phosphine was almost complete and the product of hydrolysis of all the trifluoromethyls, **8**, was also detected.

Consequently, it has been proven that the reaction of hydrolysis is much faster when boric acid is loaded in the reaction mixture thus indicating a stronger acidity of the ternary $\text{HB}(\text{HSO}_4)_4\text{-SO}_3\text{-H}_2\text{SO}_4$ than the binary $\text{SO}_3\text{-H}_2\text{SO}_4$. Under the essayed conditions, the binary mixture (*reaction A*) accounts for a 50.9 mol% SO_3 which, according to **Figure 4.3**, would correspond to a $-H_0$ of about 14.4. Making use of equations **4.3** and **4.5**, one could also estimate the composition of the ternary mixture (*reaction B*) it being of 46.9 mol% of SO_3 and 4.1 mol% of $\text{HB}(\text{HSO}_4)_4$. This very same percentage of $\text{HB}(\text{HSO}_4)_4$ would correspond to a $-H_0$ of 12.9 in the binary $\text{HB}(\text{HSO}_4)_4\text{-H}_2\text{SO}_4$ mixture. It is worth noting that the ternary $\text{HB}(\text{HSO}_4)_4\text{-SO}_3\text{-H}_2\text{SO}_4$ mixture used in the reaction is more acidic despite having reduced the mol% of SO_3 with respect to the binary $\text{SO}_3\text{-H}_2\text{SO}_4$.

As final remark of this evaluation, it can be concluded that the ternary $\text{HB}(\text{HSO}_4)_4\text{-SO}_3\text{-H}_2\text{SO}_4$ superacid used in the reactions of hydrolysis has a $-H_0$ greater than 14.4. This value is higher than the maximum $-H_0$ observed in the binary $\text{HB}(\text{HSO}_4)_4\text{-H}_2\text{SO}_4$ super acid by Gillespie, which was of 13.6. These observations could be explained by the dissolution of the polymeric boron species, according to eq. **4.7** and are in agreement with the hypothesis that ternary super acid mixture $\text{HB}(\text{HSO}_4)_4\text{-SO}_3\text{-H}_2\text{SO}_4$ is a stronger superacid than the binary $\text{HB}(\text{HSO}_4)_4\text{-H}_2\text{SO}_4$. Another example of a binary system the acidity of which can be increased by addition of SO_3 is $\text{HSO}_3\text{F-SbF}_5$ (*Magic Acid*). The addition of up to 3 mols of SO_3 to a solution of SbF_5 in HSO_3F produces a stronger acid than *Magic Acid*.⁶ In this case the increased acidity was attributed to the formation of the species $\text{H}[\text{SbF}_3(\text{SO}_3\text{F})_3]$ and $\text{H}[\text{SbF}_2(\text{SO}_3\text{F})_4]$.

4.3. Reaction mechanism

The previous study provided specific information about the reaction medium used in the hydrolysis of the trifluoromethyl group in triarylphosphines. Following this line, we found it appropriate to study the mechanism of this reaction, which eventually will be useful to give an explanation to the different reaction rates observed depending on the relative position of the CF_3 with respect to the phosphorus atom.

As stated in the general introduction, there are different possibilities in the activation of C-F bonds. According to the previous section, under the essayed conditions, the hydrolysis of the trifluoromethyl group in triarylphosphines would take place in a ternary $\text{HB}(\text{HSO}_4)_4\text{-SO}_3\text{-H}_2\text{SO}_4$ superacid mixture. In the first instance, Lewis acid activation was considered in view of the known reactivity of SO_3 towards insertion into C-F bonds.¹³ However, it was rejected, at least as a large contribution in the reaction output, given that this insertion normally requires pure SO_3 at high temperatures or used together with a stronger Lewis acid. Moreover, the fact that an increased reaction rate was observed when using boric acid, which actually consumes SO_3 to generate the Brønsted super acid $\text{H}_3\text{SO}_4^+ \text{B}(\text{HSO}_4)_4^-$, according to eq. 4.3 and 4.5, supports the idea of a Brønsted acid-activated reaction. As further supporting evidence, it is known that sulfur trioxide, when dissolved in H_2SO_4 , is mainly found as disulfuric acid, $\text{H}_2\text{S}_2\text{O}_7$, which is a weakest Lewis acid than sulfur trioxide. Therefore, it seems reasonable to state that under the ternary super acid mixture $\text{HB}(\text{HSO}_4)_4\text{-SO}_3\text{-H}_2\text{SO}_4$ the reaction of hydrolysis of the trifluoromethyl is Brønsted acid-activated.

The nature of the medium makes it difficult to study the reaction mechanism. In this respect, NMR is certainly the most useful tool to be used, specially $^{19}\text{F}\{^1\text{H}\}$ NMR due to the sensitivity of this nuclei and the high percentage of fluorine in the trifluoromethylated phosphines. As a matter of example, **Figure 4.5** shows the evolution of the reaction of the hydrolysis of the trifluoromethyl group in the *p*-tris(trifluoromethylphenyl)phosphine (**1**). The reaction was monitored inside a sealed NMR tube using a capillary tube with a solution of NH_4PF_6 in D_2O as ^{19}F and ^{31}P reference and lock. It can be observed that, at the same time as the phosphorus products evolve due to the formation of the carbonylic phosphines, the signals of the CF_3 groups

¹³ a) Krespan, C. G.; Petrov, V. A. *Chem. Rev.* **1996**, 96 (8), 3269–3301. b) Petrov, V. A. *J. Org. Chem.* **1998**, 63, 2988–2992.

(ca. -63 ppm) also change. Importantly a singlet in $^{19}\text{F}\{^1\text{H}\}$ at 42.6 ppm, corresponding to the $-\text{OSO}_2\text{F}$ moiety¹⁴ was detected, the intensity of which increased with time. Because of the low sensitivity of ^{13}C NMR it has been impossible to use this technique to monitor the reaction. The high concentration of phosphines required to observe the ^{13}C signals within a reasonable time could not be applied. ^1H NMR was also attempted, failing in providing any additional information.

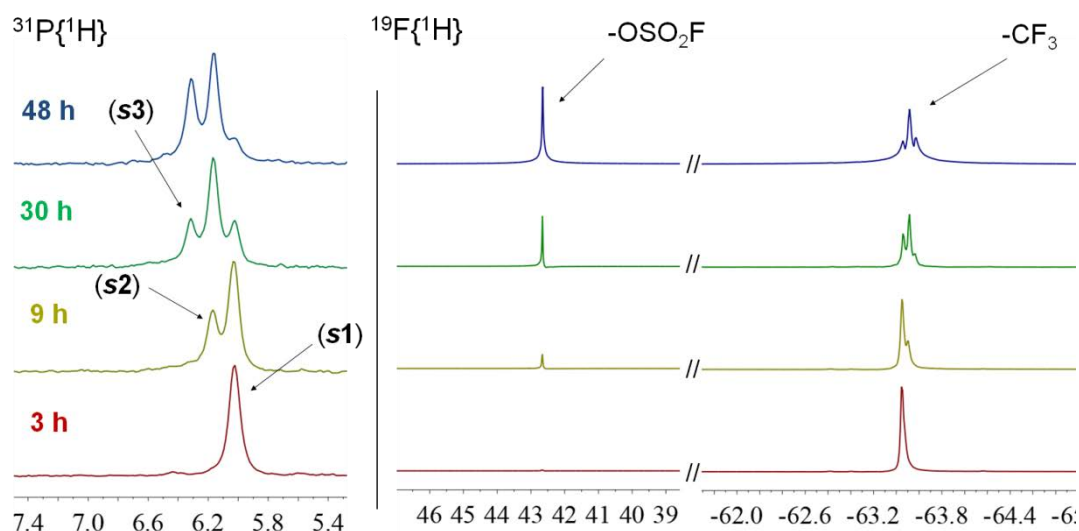


Figure 4.5. Evolution of the reaction of hydrolysis in phosphine **1**. Analysis of the crude reaction by $^{31}\text{P}\{^1\text{H}\}$ (101.27 MHz) (**left**) and $^{19}\text{F}\{^1\text{H}\}$ NMR (235.4 MHz) (**right**). Signals (intensity and position) relative to NH_4PF_6 used as internal standard (-144.45 ppm and -72.65 ppm, respectively). δ in ppm. In $^{31}\text{P}\{^1\text{H}\}$ NMR, only phosphine region is shown. **s1**, **s2** and **s3** refer to compounds **1**, **2**, and **3** in sulfuric medium. In $^{19}\text{F}\{^1\text{H}\}$, no other signals than those shown in the image were observed (excluding those signals for the internal standard). Reaction conditions: [Phosphine] = 0.16 M, $[\text{H}_3\text{BO}_3]$ = 0.8 M, $[\text{SO}_3]$ = 11.5 M

Although C-F bond activation using strong protic acids is widely known, the chemistry of this reaction has not raised much attention.¹⁵ With regard to the reaction mechanism in trifluoromethylbenzenes, both experimental and theoretical studies suggested that the first reaction step is the protonation of a F atom followed by the loss of a molecule of HF.¹⁶ Klumpp and co-workers studied the reaction of hydrolysis in the 1,3,5-tris(trifluoromethyl)benzene using fluorosulfuric acid, HSO_3F .¹⁷ The authors proposed a reaction mechanism based on previous works on the topic and their observations by

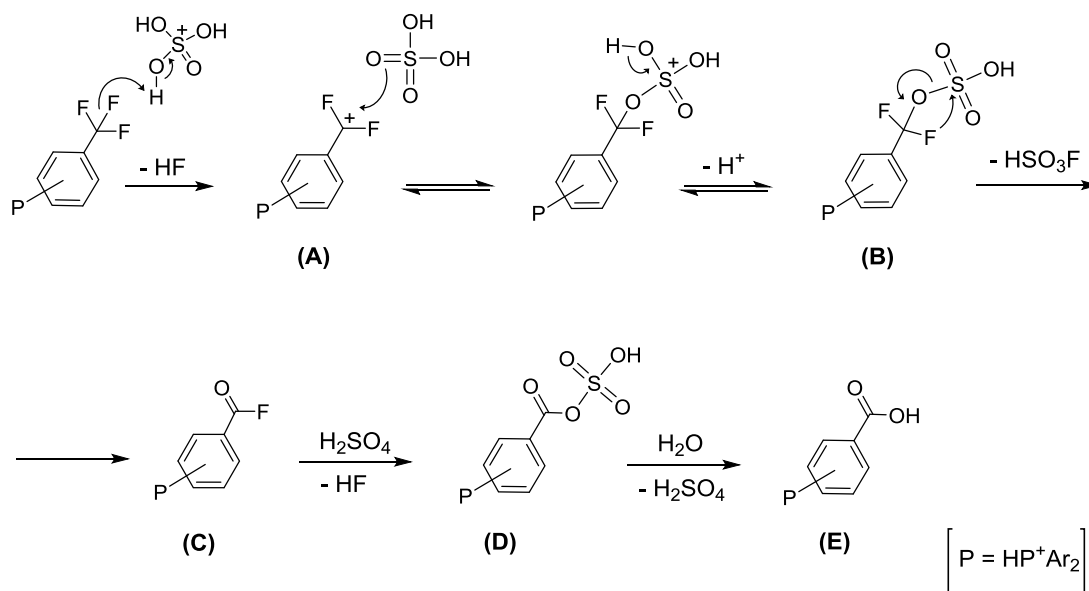
¹⁴ Krespan, C. G.; England, D. C. *J. Org. Chem.* **1975**, *40* (20), 2937–2940.

¹⁵ a) Amii, H.; Uneyama, K. *Chem. Rev.* **2009**, *109* (5), 2119–2183. b) Shen, Q.; Huang, Y. G.; Liu, C.; Xiao, J. C.; Chen, Q. Y.; Guo, Y. *J. Fluor. Chem.* **2015**, *179*, 14–22.

¹⁶ a) Aschi, M.; Chiavarino, B.; Crestoni, M. E.; Fornarini, S. *J. Phys. Chem.* **1996**, *100* (51), 19859–19863. b) Zakzeski, J.; Fan, I. S.; Bell, A. T. *Appl. Catal. A Gen.* **2009**, *360* (1), 33–37. c) Wang, F.; Hu, J. *Chinese J. Chem.* **2009**, *27* (1), 93–98.

¹⁷ Kethe, A.; Tracy, A. F.; Klumpp, D. A. *Org. Biomol. Chem.* **2011**, *9*, 4545–4549.

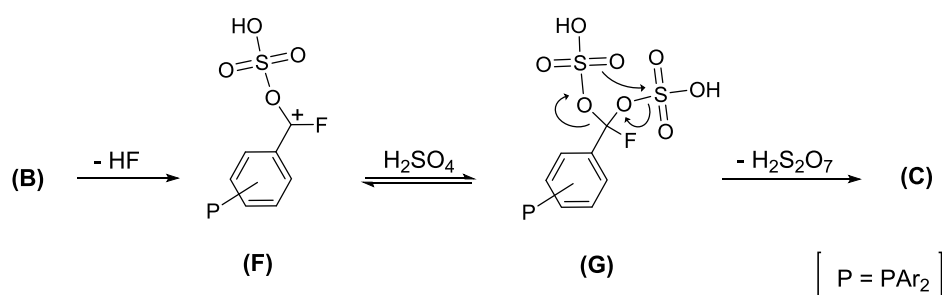
$^{13}\text{C}\{^1\text{H}\}$. The reaction mechanism shown hereafter (**Scheme 4.1**) is a modification of the one reported by Klumpp's group in which H_2SO_4 or $\text{H}_2\text{S}_2\text{O}_7$ is used instead of HSO_3F . In order to simplify the mechanism and its explanation, only H_2SO_4 will be considered, although $\text{H}_2\text{S}_2\text{O}_7$ could be used similarly. We will further support this mechanism with the information obtained from our $^{19}\text{F}\{^1\text{H}\}$ NMR experiments.



Scheme 4.1. Proposed reaction mechanism of the hydrolysis of the trifluoromethyl group in the ternary superacid $\text{HB}(\text{HSO}_4)_4\text{-SO}_3\text{-H}_2\text{SO}_4$

In a first step, strong interaction between acidic proton of the superacid and fluorine (H bond) promotes the C-F bond cleavage with the loss of a HF molecule and the generation of the difluorobenzyl carbocation (**A**). Next, the nucleophilic attack of a molecule of H_2SO_4 on the carbocation **A** yields the formation of the sulfuric ester **B**. Although H_2SO_4 is not a strong nucleophile, the reaction may be favoured by the highly electrophilic fluorinated carbocation. Regarding the next reaction step, the formation of the carbonyl fluoride (**C**), Klumpp and co-workers proposed two different possibilities. The first one, as indicated in **Scheme 4.1**, consists in the concerted elimination of HSO_3F to give the corresponding acyl fluoride (**C**). This is the same mechanism as proposed by Bell and co-workers in the preparation of benzyl fluoride from trifluoromethylbenzene.^{16b} In the second proposed possibility, **Scheme 4.2**, the sulfuric ester **B** would react with the superacid with the elimination of HF, in the same way as in the first step, to form the carbocation **F**, which would again react with a second molecule of sulfuric acid to give the double sulfuric ester **G**. Elimination of disulfuric acid in **G** would further yield acyl fluoride **C**. No evidence was found to distinguish

which of the two routes is giving rise to the formation of the acyl fluoride. While the first option directly generates HSO_3F , the signal of which in $^{19}\text{F}\{^1\text{H}\}$ NMR has been described at 40–41 ppm¹⁸ and matches the observed one in the hydrolysis of the trifluoromethyl group in trifluoromethylated triarylphosphines, both reactions generate HF which reacts with SO_3 to form HSO_3F (no free HF has been detected before the reaction was quenched with water). On the whole, three molecules of HSO_3F are formed in both reaction pathways. Regardless of the mechanism of formation of the acyl fluoride (**C**), once it is formed, it reacts with H_2SO_4 to yield the mixed sulfonic-carboxylic anhydride (**D**), similarly to what was reported for acyl chlorides.¹⁹ Although the formation of mixed anhydrides by addition of SO_3 to acyl fluorides has been reported in the literature,¹⁴ this option was discarded considering that such reaction requires the use of pure SO_3 . Moreover, the signal for the corresponding fluorinated mixed anhydride in $^{19}\text{F}\{^1\text{H}\}$ NMR (above 45 ppm) was not detected. After quenching the reaction in water, **D** is hydrolysed to form the carboxylic acid (**E**).



Scheme 4.2. Alternative reaction of formation of the acyl fluoride (**C**)

It is worth mentioning that neither signal for the fluorinated carbocation (**A**) (*ca.* 23 ppm)²⁰ nor the corresponding to the acyl fluoride (**C**) (*ca.* 17.7 ppm)²¹ or any other intermediates were detected in our $^{19}\text{F}\{^1\text{H}\}$ NMR experiments, thus indicating that the elimination of HF to form the carbocation (**A**) is likely to be the rate determining reaction step.

¹⁸ a) Cicha, W. V.; Herring, F. G.; Aubke, F. *Can. J. Chem.* **1990**, *68* (1), 102–108. b) Kühn-velten, J.; Bodenbinder, M.; Bröchler, R.; Hägele, G.; Aubke, F. *Can. J. Chem.* **2002**, *80*, 1265–1277.

¹⁹ Karger, M. H.; Maztjr, Y. *J. Org. Chem.* **1971**, *36* (4), 528–531.

²⁰ Petrov, V. A.; Marchione, A.; Marshall, W. *J. Fluor. Chem.* **2008**, *129*, 1011–1017.

²¹ Bhadury, P. S.; Pandey, M.; Jaiswal, D. K. *J. Fluor. Chem.* **1995**, *73* (2), 185–187

4.3.1. Relation between the rate of hydrolysis of the CF₃ and the pattern of substitution in the phosphines

During the study of the reaction of hydrolysis of the trifluoromethyl group in the trifluoromethylated triarylphosphines, different reaction rates were observed depending on the relative position of the CF₃ with respect to the phosphorus atom. For the homoleptic phosphines, the reaction rate observed follows the next order: *meta* > *para* > *ortho*, 3,5, **Figure 4.6-a**. Also, the rate in the heteroleptic phosphines decreases when the number of trifluoromethyl groups increases. For instance, in the *meta*-series the observed rates follows the next trend: *tris-meta* > 3,5-1 *meta*-2 > 3,5-2 *meta*-1, **Figure 4.6-b**.

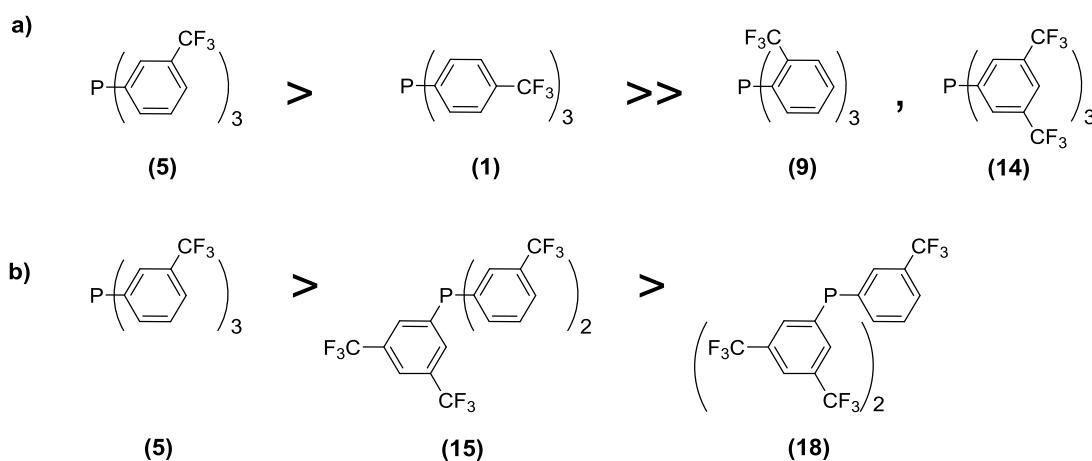
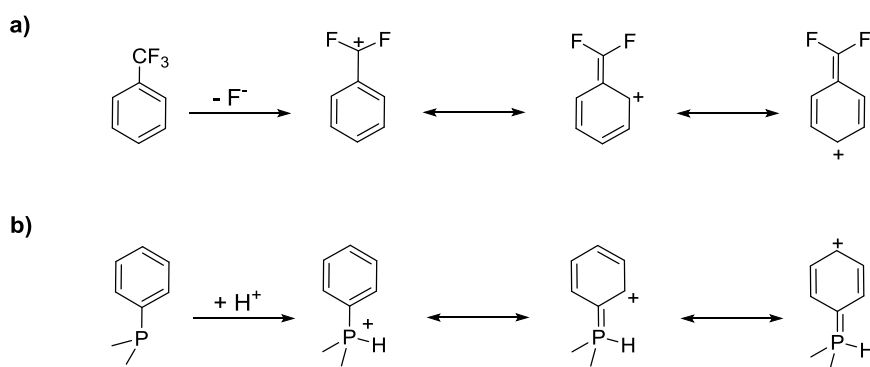


Figure 4.6. Schematic representation of the reaction rates in a) homoleptic triarylphosphines and b) heteroleptic triarylphosphines

Whereas in the heteroleptic phosphines the trend in the reaction rate is clearly ruled by the electronic effect produced by the increasing number of trifluoromethyl groups, the pattern is not that clear in the case of the homoleptic phosphines. The key point to explain the different reaction rates is based in the fact that, under the reaction conditions, phosphines are protonated. Consequently, the formation of the difluorobenzyl cation (**A**), which is thought to be the rate determining step, implies the generation of a second positive charge on the molecule. Using resonance structures one can see that the positive charge on the carbocation is delocalised through the aromatic ring in *para* and *ortho*-positions. In fact the same delocalisation can be done with the positive charge on the phosphorus atom giving the same pattern of delocalisation in *para* and *ortho*-positions with respect to the phosphorus atom, **Scheme 4.3**.



Scheme 4.3. a) delocalisation of carbocationic positive charge. b) delocalisation of the phosphonium positive charge

In this way, in *para* and *ortho*-substituted phosphines the positive charges of the carbocation and the phosphonium are delocalised at adjacent atoms while in *meta*-substituted phosphines these charges of the same sign are never localised on adjacent atoms. Therefore, the formation of the difluorobenzylic carbocation is more favourable when the CF_3 group is in *meta*-position than when located in *para* or *ortho*-position. The difference in reaction rates between these two last positions can be explained by the proximity of the trifluoromethyl to the phosphorus atom. Both steric hindrance as well as inductive effects would be responsible for the low reaction rates found in the *ortho*-substituted phosphine. Similarly, inductive effects also play an important role in the 3,5-substitution pattern since, in spite of formally having trifluoromethyls in *meta*-position with respect to the phosphorus, the presence of another electron withdrawing CF_3 group in the same ring destabilizes the formation of the carbocation. **Figure 4.7** summarises these effects.

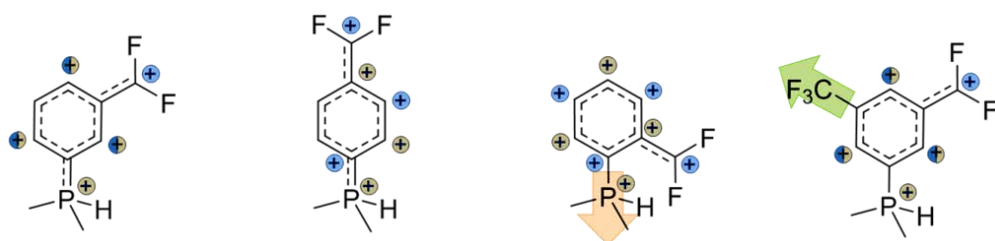


Figure 4.7. Schematic representation of effects in the stabilisation of the carbocation: charges delocalisation (blue for the carbocation and brown for the phosphonium) and inductive effects (orange arrow for the phosphine and green arrow for the trifluoromethyl group)

According to this reasoning, the hydrolysis in a non-protonated phosphine would be faster than with the protonated form of the same phosphine. This assumption was proven by performing the reaction with the oxide of the *ortho*-substituted phosphine (**9**).

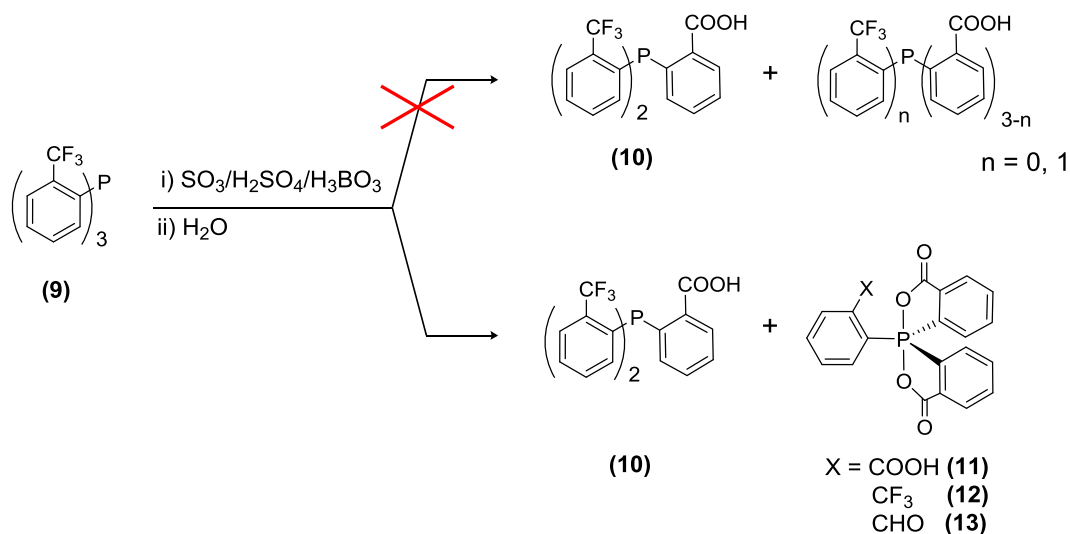
This experiment was designed within the study of the formation of the spiro oxyphosphoranes, as will be shown in the next section, and further supported the role of phosphonium in the formation of the carbocation.

With respect to the heteroleptic phosphines investigated, the inductive effect produced by the 3,5-substituted rings may be responsible for the decreased reaction rate when increasing the number of these groups due to a lower stabilisation of the carbocation.

4.4. *Ortho*-carboxylic phosphine and pentacoordinate species.

Mechanism of formation

As described in the previous chapter (chapter 3), and contrary to what was observed with the homologues *para* and *meta*-substituted phosphines, in the reaction of hydrolysis with the *ortho*-tris(trifluoromethylphenyl)phosphine (**9**) neither dicarboxylic nor tricarboxylic phosphines were detected. Instead, spirocyclic oxyphosphoranes were observed, **Scheme 4.4**.



Scheme 4.4. Observed reaction products in the hydrolysis of the *ortho*-substituted phosphine **9**

An important observation regarding the hydrolysis of the CF₃ in phosphine **9** is its behaviour depending on the reaction temperature. As described in chapter 3, when the reaction was performed at 55 °C only the carboxylic spiro species **11** was observed as reaction product. On the contrary, when the reaction was performed at room temperature, the main product obtained was the aldehydic spiro **13** together with a small percentage of the trifluoromethylated spiro **12**. No carboxylic spiro **11** was detected

under these conditions, **Figure 4.8**. Moreover when, after 314 h, the reaction mixture containing only **13** and **12** was heated at 55 °C, the aldehydic spiro **13** was observed as single product which did not further evolved. This reaction was monitored simultaneously by the quenching procedure and the direct measure of the crude reaction mixture (**Figure 4.8**).

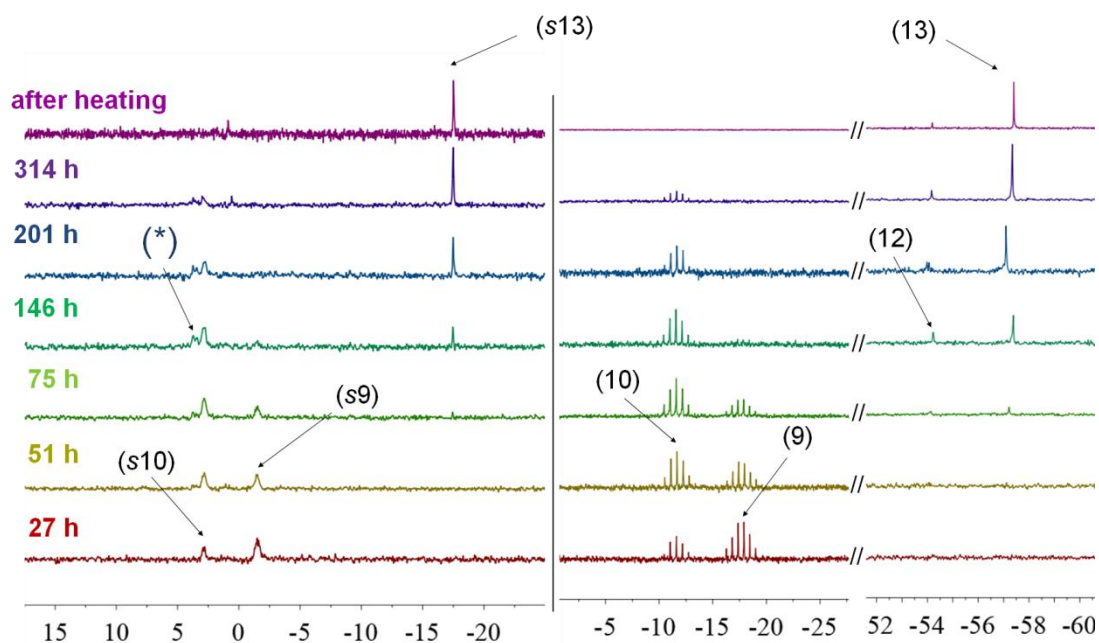


Figure 4.8. Reaction of hydrolysis of the *ortho*-substituted phosphine **9** monitored by $^{31}\text{P}\{^1\text{H}\}$ NMR (101.2 MHz). $[\text{P}] = 0.07 \text{ M}$, $[\text{H}_3\text{BO}_3] = 1.9 \text{ M}$, $[\text{SO}_3] = 14.0 \text{ M}$. No other signals than those showed in the image were observed (excluding the internal standard). δ in ppm. **Left**- Crude reaction. Signals (intensity and position) relative to NH_4PF_6 used as internal standard (-144.45 ppm). **s9**, **s10** and **s13** refer to compounds **9**, **10**, and **13** in sulfuric medium, respectively. Signal referred as (*) is related to compound **12** in sulfuric medium (see text). **Right**- Sample aliquots quenched in water. Solvent: acetone- d_6 . Signals calibrated using the value of **10** (at -11.6 ppm with respect to 85% H_3PO_4)

Interestingly, the chemical shift of the signal corresponding to the aldehydic spirocyclic oxyphosphorane **13** in the crude reaction (**s13** in **Figure 4.8**) is quantitatively different to that after quenching in water and analysed in acetone- D_6 (-17.5 ppm and -57.4 ppm, respectively). Correct attribution of this signal to **13** was confirmed by dissolving the isolated spiro aldehyde in concentrated sulfuric acid. $^{31}\text{P}\{^1\text{H}\}$ NMR analysis of this mixture showed a singlet at -13.9 ppm. The reversibility of the process was proven by adding this sulfuric solution in water and extracting with Et_2O . The $^{31}\text{P}\{^1\text{H}\}$ NMR analysis showed a signal at -57.4 ppm together with two new minor signals close to that position. ^1H NMR showed partial decrease of the aldehydic proton with respect to the aromatic signal, thus indicating possible oxidation of the aldehyde group. The same simple experiment was performed with the trifluoromethylated spiro **12**, showing a

singlet at -11.0 ppm in the $^{31}\text{P}\{^1\text{H}\}$ NMR of the sulfuric acid solution. In this case the process is also completely reversible and no other compounds in the $^{31}\text{P}\{^1\text{H}\}$ and ^1H NMR analyses were detected after quenching in water and extracting with Et_2O . Moreover, it is known that carbonylic compounds can be protonated in acidic media.²² Such protonation of the carboxyl oxygen could be responsible for the high change in the chemical shifts. This difference in the δ is similar to that observed in the hemiacetalic forms of the aldehydic spiro **13** (-33 and -36 ppm). Another experimental observation worth mentioning is that, unlike phosphine **9** and the carboxylic phosphine **10**, the phosphorus atom in the spiro compounds, or the derived species found in the sulfuric mixture, were not protonated in the reaction medium.

Although the signal corresponding to the trifluoromethylated spirocyclic **12** was not observed in the $^{31}\text{P}\{^1\text{H}\}$ NMR experiments of the crude reaction, a closer look to the spectra (**Figure 4.9**) showed a small and broad peak at 3.6 ppm, shifted 0.8 ppm from the monocarboxylic phosphine **10**. The relative intensity of this peak in the reaction mixture is comparable to that of the spiro CF_3 after quenching in water.

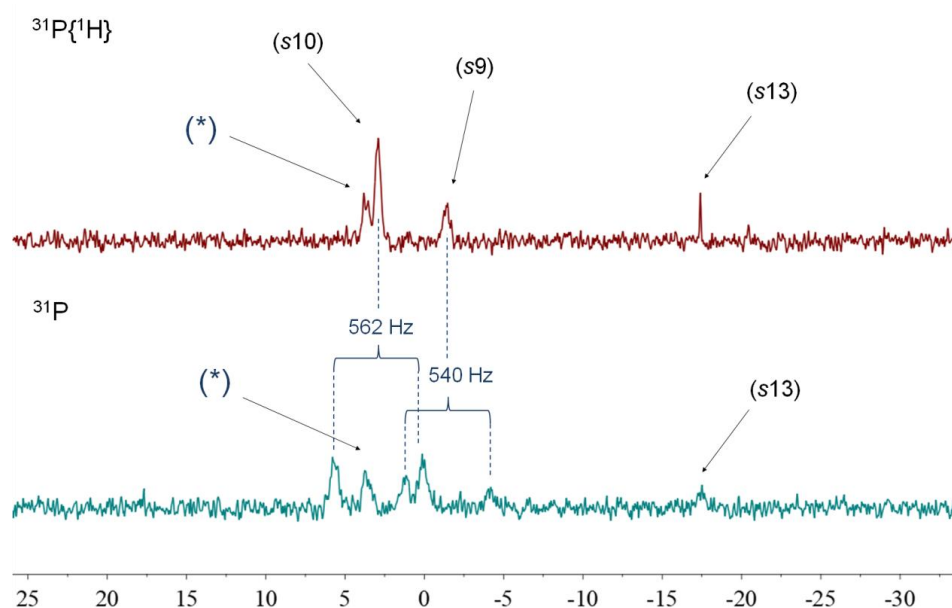
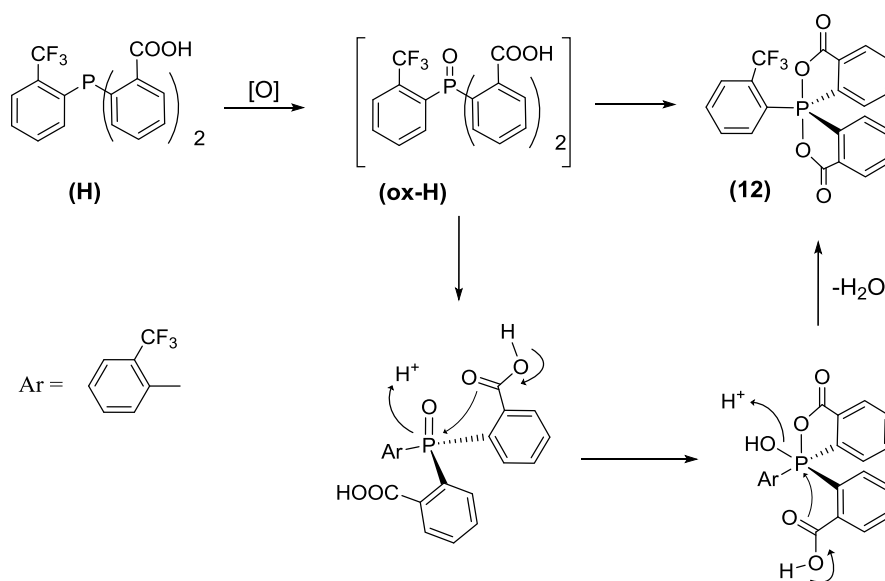


Figure 4.9. $^{31}\text{P}\{^1\text{H}\}$ NMR (**top**) and ^{31}P NMR (**bottom**) (101.2 MHz) of the crude reaction of the hydrolysis of phosphine **9** at 105 h. $[\text{P}] = 0.07 \text{ M}$, $[\text{H}_3\text{BO}_3] = 1.9 \text{ M}$, $[\text{SO}_3] = 14.0 \text{ M}$. Signals (intensity and position) relative to NH_4PF_6 used as internal standard. δ in ppm. **s9**, **s10**, **s13** refer to compounds **9**, **10**, and **13** in sulfuric medium, respectively. Signal referred as (*) is related to compound **12** in sulfuric medium (see text)

²² a) Jost, R.; Rimmelin, P.; Sommer, J. M. *J. Chem. Soc. D.* **1971**, (15), 879-881. b) Sommer, J.; Rimmelin, P.; Drakenberg, T. *J. Am. Chem. Soc.* **1976**, 98 (9), 2671.

In a first instance, these observations would be consistent with the presence of the dicarboxylated phosphine **H** (Scheme 4.5). Oxidation of **H** would promote cyclisation in an acid-catalysed process, as reported in other cyclic oxyphosphoranes²³ to form the trifluoromethylated spirocycle **12**. Nevertheless, if this assumption were true, the phosphorus atom in **H** should be protonated in the reaction media, just as observed for **9** and **10**. The lack of protonation of this signal at 3.6 ppm in the ³¹P NMR analysis of the crude reaction allows to discard this hypothesis. The attribution of the signal at 3.6 to the phosphine oxide of **H** (**ox-H**) was also discarded taking into account the high reactivity of the non-trifluoromethylated equivalent phosphine oxide to form the spirocycle, reported by Segall and Granoth.^{23,24} Actually, as reported by these authors, the cyclisation is so fast that the *o*-dicarboxylic triphenylphosphine oxide could not be isolated. Thus presumably, the observed signal at 3.6 ppm corresponds to an intermediate between the phosphine oxide **ox-H** and the spirocyclic compound **12**.



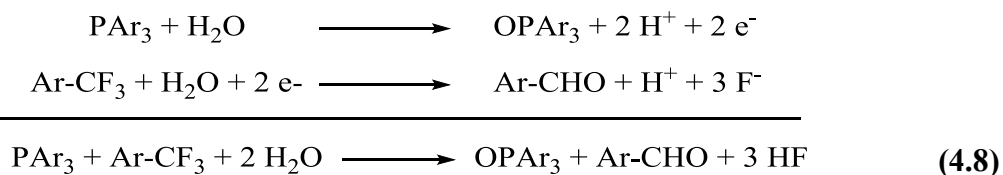
Scheme 4.5. Mechanism of formation of spiro oxyphosphoranes from dicarboxylic phosphine based on the work of Segall and Granoth²³

Nevertheless, we must not lose sight of the fact that **12** is a minor product of the reaction only detected in small amounts. Surprisingly, the main product observed, the aldehydic spiro **13**, is completely anomalous given that its formation implies, on the one hand, the oxidation of the phosphine in a medium in which it should be protected and, on the other hand, it involves the formation of an aldehyde, which unavoidably means

²³ Segall, Y.; Granoth, I. *J. Am. Chem. Soc.* **1978**, *100* (16), 5130–5134.

²⁴ Segall, Y.; Granoth, I.; Kalir, A.; Bergmann, E. D. *J. Chem. Soc. Chem. Commun.* **1975**, No. 10, 399.

the reduction of a carbon atom (from CF₃ to CHO) in such an oxidative medium. On this basis, the reaction can hardly be explained as two separate reactions. However, the equation makes sense when considered as dependent reactions (equation 4.8).



In fact, given that the reaction takes place in oleum, without the presence of water, the equation must be more properly written as follows (eq. 4.9).



It seems thus reasonable to consider that the reduction of the carbon is associated to the oxidation of the phosphorus atom, since there are not other species in the reaction medium able to be oxidised rather than the phosphine. To have a better understanding of how this redox reaction takes place, the source of the aldehydic proton was firstly studied. The crude reaction was also monitored by ¹H NMR allowing to observe a singlet at *ca.* 9.6 ppm, the intensity of which increased at the same time as did the intensity of the signal of the aldehyde proton in the spirocyclic **13** after quenching with water, **Figure 4.10**. The chemical shift of this signal is in agreement with the reported value for the aldehydic proton of protonated benzaldehyde.^{22a} Although the signal of the protonated carbonyl group (*ca.* 13 ppm for protonated benzaldehyde) could not be observed due to the intensity of the signal of the acidic reaction media, all signs indicate the formation of the C-H aldehyde bond before the mixture is treated with water. Moreover, in order to ensure that water was not the source of this hydrogen atom, the reaction mixture at 201 h was quenched using H₂O and D₂O in parallel samples. The ratio between the aldehydic H and the aromatic ones was the same in both cases, thus proving that the source of the aldehydic proton is not water and also supporting the redox reaction in sulfuric acid.

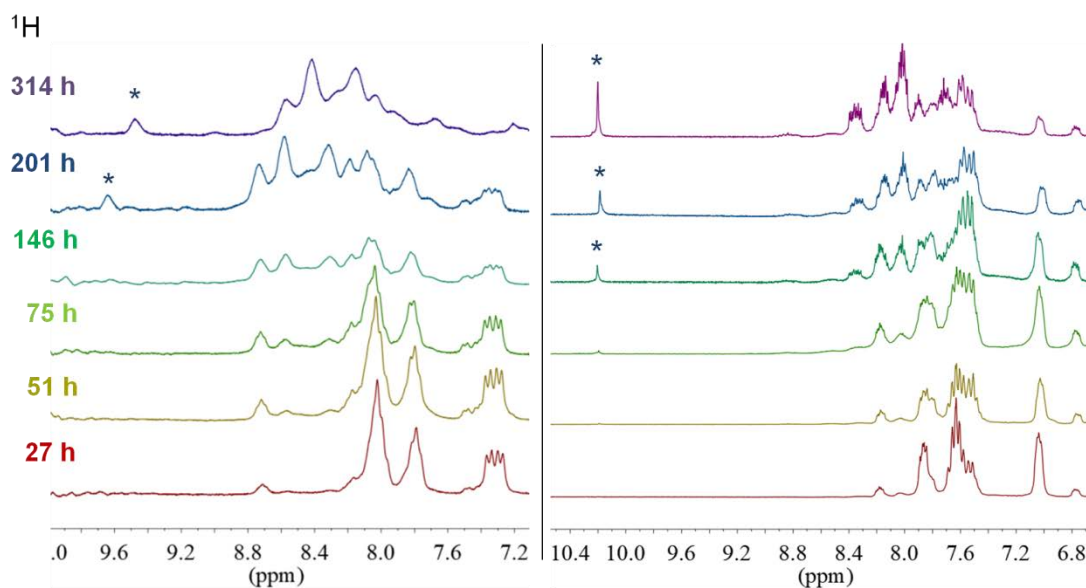


Figure 4.10. Reaction of hydrolysis of the *ortho*-substituted phosphine (**9**) monitored by ^1H NMR (250.16 MHz). $[\text{P}] = 0.07 \text{ M}$, $[\text{H}_3\text{BO}_3] = 1.9 \text{ M}$, $[\text{SO}_3] = 14.0 \text{ M}$. Only aromatic and aldehydic protons (referred as *) shown. **left**- Crude reaction. **right**- Sample aliquots quenched in water. Solvent: acetone- D_6 . Signals calibrated using the value of the solvent (2.05 ppm)

All these observations clearly suggest that the formation of the C-H aldehyde bond takes place in the sulfuric reaction medium. However, because of the nature of such a bond it should be assumed to be formed by some sort of hydride transfer. Free hydrides are not expected to be found in highly acidic media, thus another source of them had to be visualised. The X-ray diffraction structure of the aldehydic spiro oxyphosphorane **13** (see chapter 3) allowed to speculate about the origin of the C-H bond. As it was shown, the H of the aldehyde group is pointing towards the phosphorus atom, **Figure 4.11**. This conformation is anomalous given the Lewis acid character of the P atom in this sort of compounds. In fact one should expect to find the carbonyl oxygen atom coordinating to phosphorus in distorted trigonal bipyramidal geometry as reported by Holmes' group not only for carbonylic spirocyclic oxyphosphoranes, but also for carbonylic triarylphosphines and phosphine oxides.²⁵

²⁵ a) Chandrasekaran, A.; Day, R. O.; Holmes, R. R. *Inorg. Chem.* **2001**, *40* (24), 6229–6238. b) Chandrasekaran, A.; Day, R. O.; Holmes, R. R. *Inorg. Chem.* **2002**, *41* (6), 1645–1651. c) Chandrasekaran, A.; Timosheva, N. V.; Day, R. O.; Holmes, R. R. *Inorg. Chem.* **2003**, *42* (10), 3285–3292.

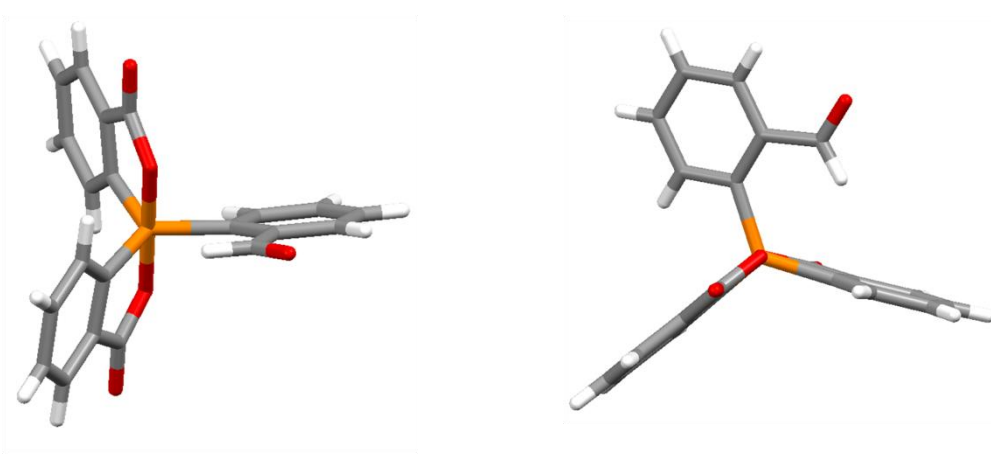


Figure 4.11. Stick representation of the X-ray structure of **13**. Side view (**left**) and top view (**right**)

The unexpected conformation of the aldehyde found in the X-ray structure of **13** led us to suggest that the H atom initially located on the protonated phosphine is somehow transferred to the trifluoromethyl carbon atom, which eventually becomes the aldehyde carbon. To show evidence supporting this hypothesis, the reaction was performed using the *o*-tris(trifluoromethylphenyl)phosphine oxide (**ox-9**) as starting material to hamper the protonation of the phosphorus atom. The reaction was followed by NMR analysis of both the crude reaction and samples quenched in water and extracted in Et₂O, **Figure 4.12**. In this second case, the samples were analysed in deuterated acetone and, additionally, in a mixture of CDCl₃:MeOH (4:1) in order to detect any traces of **13** as hemiacetal in the ³¹P{¹H}. It can be observed a higher reaction rate compared to the non oxidised phosphine under the same conditions. This is in agreement with the proposed reasoning for the different reaction rates in the hydrolysis of the trifluoromethyl group depending on the relative position of the P atom with respect to the CF₃ (previous section of this chapter). Analysis of the mixture composition at 3 h of reaction showed the starting phosphine oxide and the trifluoromethylated spiro oxyphosphorane **12** as the main components. No signal for the aldehydic spirocyclic **13** was observed. Surprisingly, the monocarboxylated phosphine oxide was hardly observed, which can be explained by assuming the fact that the second hydrolysis is faster than the first one, most likely driven by the immediate formation of the spirocycle. Apparently, the trifluoromethylated spirocyclic oxyphosphorane evolves to a third product (*ca.* 35 ppm in oleum and -53 ppm in acetone) which is likely to be the carboxylated compound **11**. ¹⁹F{¹H} NMR analysis of the crude reaction showed the signal at -42.6 ppm, confirming the hydrolysis of the trifluoromethyl groups. Moreover, the ¹H NMR analysis of the quenched samples (**Figure 4.13**), did not show the presence of aldehyde protons, in

agreement to the observations in the $^{31}\text{P}\{^1\text{H}\}$ NMR. All in all, no aldehyde was observed either in ^1H or $^{31}\text{P}\{^1\text{H}\}$ NMR, which is consistent with the theory that the aldehyde is formed by hydrogen transfer from the phosphonium fragment.

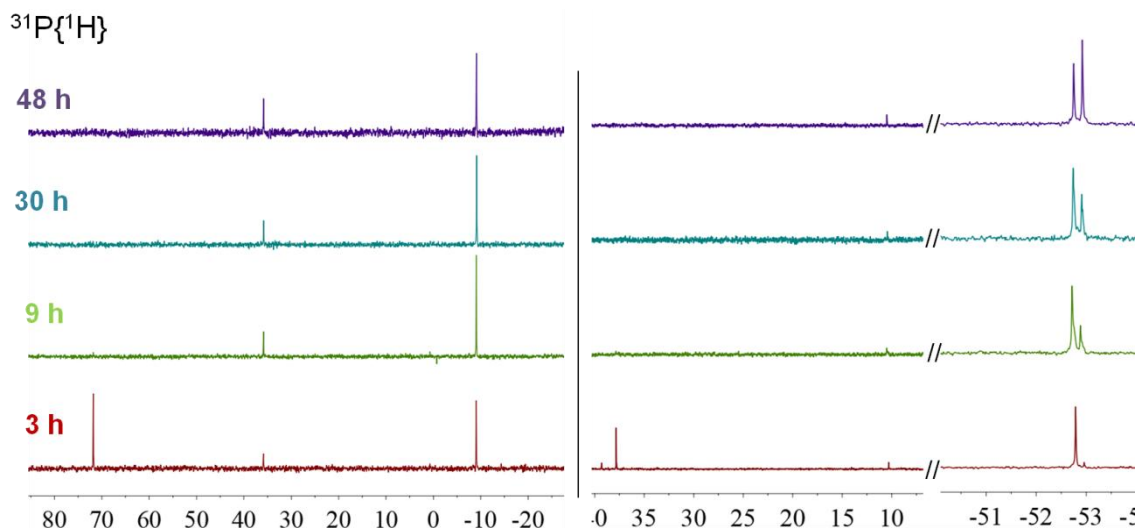


Figure 4.12. Reaction of hydrolysis of the *ortho*-substituted phosphine oxide (**ox-9**) monitored by $^{31}\text{P}\{^1\text{H}\}$ NMR (101.2 MHz). δ in ppm. No other signals than those shown in the image were observed (excluding the internal standard). Reaction conditions: $[\text{P}] = 0.07 \text{ M}$, $[\text{H}_3\text{BO}_3] = 1.9 \text{ M}$, $[\text{SO}_3] = 14.0 \text{ M}$.

left- Crude reaction. Signals (intensity and position) relative to NH_4PF_6 used as internal standard.
right- Sample aliquots quenched in water. Solvent: acetone- D_6

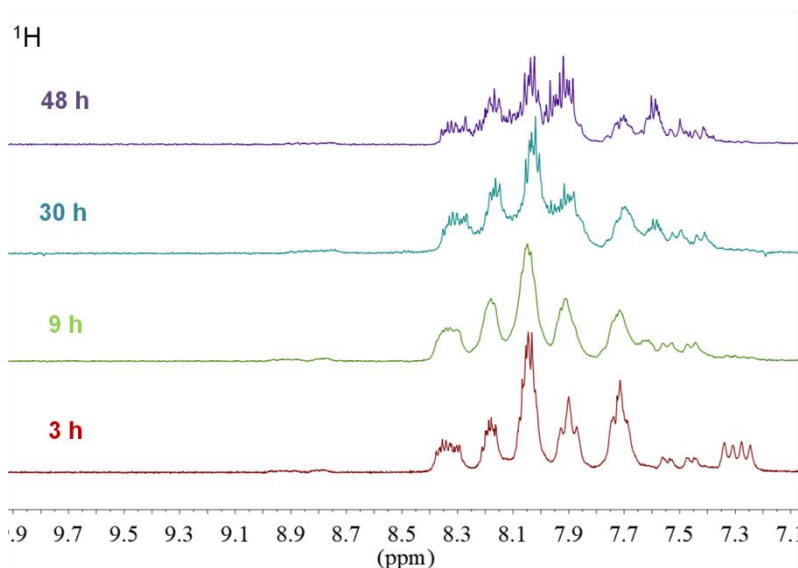
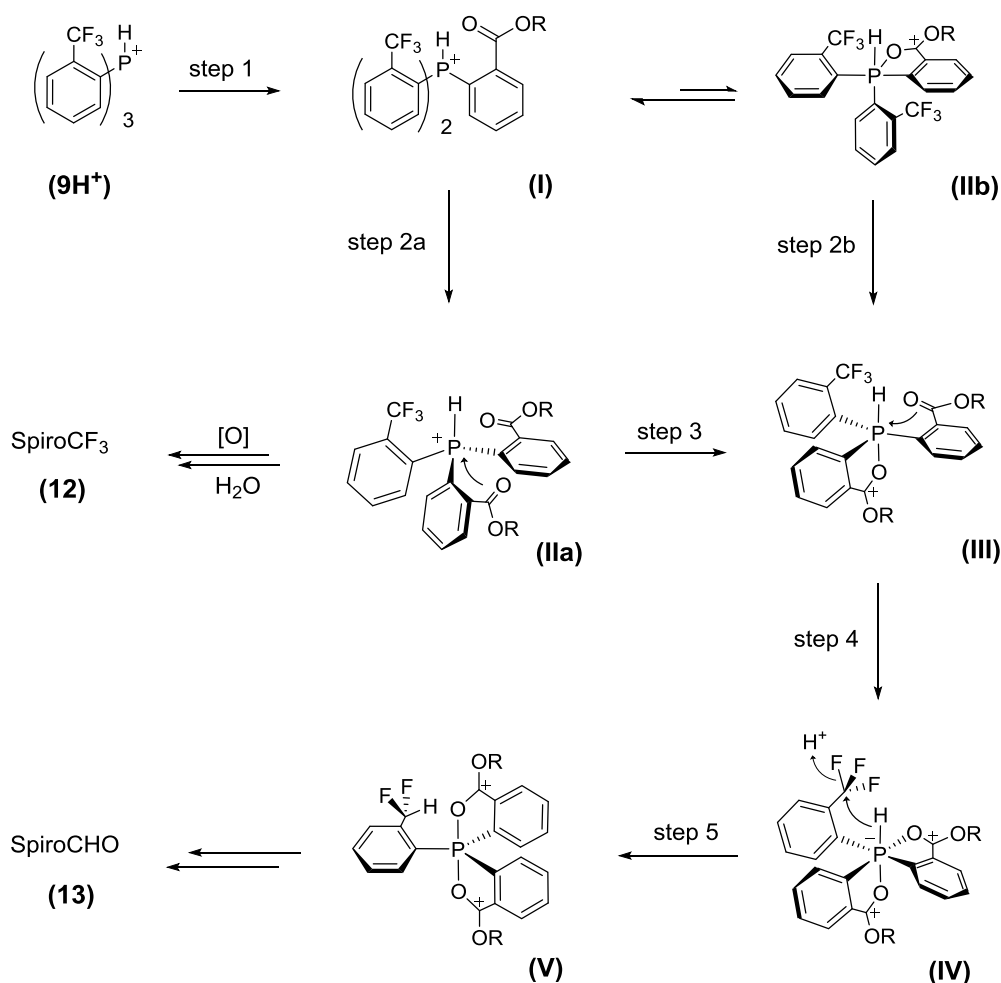


Figure 4.13. Reaction of hydrolysis of the *ortho*-substituted phosphine oxide (**ox-9**) monitored by $^{31}\text{P}\{^1\text{H}\}$ NMR (101.2 MHz). Sample aliquots quenched in water. Solvent: acetone- D_6 . Signals calibrated using the value of the solvent (2.05 ppm). Reaction conditions: $[\text{P}] = 0.07 \text{ M}$, $[\text{H}_3\text{BO}_3] = 1.9 \text{ M}$, $[\text{SO}_3] = 14.0 \text{ M}$.

Considering all the findings and observations explained so far, a mechanism for the formation of the aldehydic spirocyclic **13** can be proposed, **Scheme 4.6**. The protonated *ortho* tris-trifluoromethylated phosphine **9H⁺** reacts in the superacidic medium to give **I** (step 1) through the C-F bond cleavage mechanism previously introduced in this chapter. The reaction of a second CF₃ group would be slow enough to allow the observation of **I** in NMR and also its isolation as *o*-Miranphos (**10**) after aqueous treatment. However, once the second CF₃ group has reacted (step 2a), compound **IIa**, which contain the two carbonyl group necessary to form the spirocyclic structure, would undergo intramolecular nucleophilic attack of the carbonylic oxygen atoms to the phosphorus atom giving rise to the formation of the hexacoordinated phosphorus compound **IV** (steps 3 and 4). The negative formal charge on the P atom in **IV** would increase the hydride character of the H atom bonded to it thus facilitating the hydride transfer from the phosphorus atom to the trifluoromethyl carbon atom, with the formation of a difluoromethyl group (step 5). Recently, Wang *et al.* showed the formation of benzaldehyde from difluoromethylbenzene with sulfuric acid.²⁶ According to this, compound **V** will further undergo C-F cleavage to finally yield the aldehydic spiro oxyphosphorane **13**. It is worth mentioning that, although the nucleophilic reaction can be envisaged in compound **I** to alternatively form the pentacoordinate compound **IIb**, no evidence for the formation of this compound has been found in the NMR of the crude reaction, indicating either reversibility of the addition, with the equilibrium shifted towards **I**, or fast conversion of the trifluoromethyl group in compound **IIb** to yield **III**.

²⁶ Wang, L.; Wei, J.; Wu, R.; Cheng, G.; Li, X.; Hu, J.; Hu, Y.; Sheng, R. *Org. Chem. Front.* **2017**, *4* (2), 214–223.

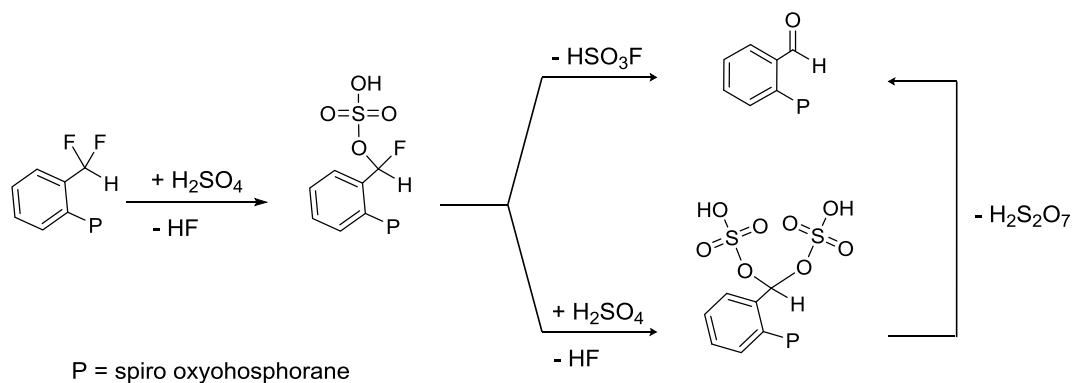


Scheme 4.6. Proposed mechanism of formation of the aldehydic spirocyclic oxyphosphorane from the *ortho*-substituted trifluoromethylated phosphine (**9**) in the ternary superacid $HB(HSO_4)_4-SO_3-H_2SO_4$. $R = SO_3H$

Concerning the hydride migration (step 5), we proposed the formation of the C-H bond at the same time as the C-F bond is cleaved in an S_N2 -like manner, with the loss of HF. Alternatively, and in agreement with the mechanism of hydrolysis of the CF_3 , one could think of the hydride transfer taking place after the formation of the difluorobenzyl carbocation. Although the formal positive charge on the carbon would facilitate the hydride migration, the 3D model of this intermediate shows that this reaction would be geometrically impossible. Coplanarity between the carbocation and the aromatic ring together with the C-P-H angle at 90° would hamper the hydride migration from the P-H bond. On the contrary, the tetrahedral conformation of the CF_3 easily allows an S_N2 -like reaction.

After the formation of **(V)**, the rotation of the CHF_2 group could be hindered due to the bulky oxyphosphorane in *ortho* and probably also due to H bond formation between the

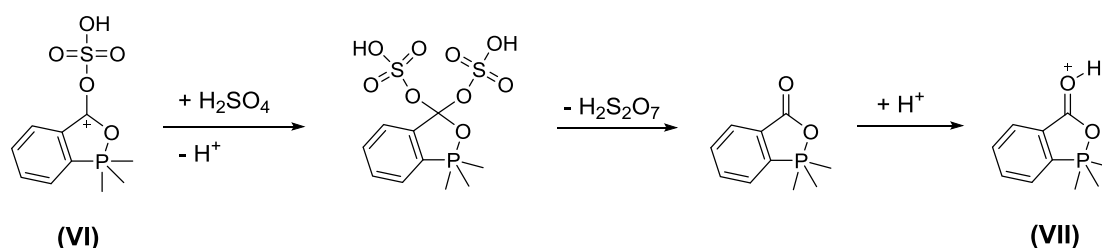
H of this group and the oxygen in the oxyphosphorane. Therefore, the H would remain in the same conformation during the further C-F cleavage in the formation of the aldehyde group. Most likely, this reaction proceeds through the same mechanism as proposed for the formation of the mixed anhydride in the hydrolysis of the trifluoromethyl group, **Scheme 4.7**.



Scheme 4.7. Proposed formation of the aldehyde group in the spiro oxyphosphorane **13**

Since none of the proposed intermediates between (**I**) and the spirocyclic **13** have been observed in the NMR analysis of the crude reaction, it can be assumed that once the dicarbonylic phosphine (**IIa**) is formed, the reaction rapidly evolves to the formation of the spiro aldehyde **13**, driven by the simultaneous oxidation of the phosphorus atom, the reduction of the trifluoromethyl carbon atom and the formation of the spirocyclic structure.

A last remark concerning the proposed reaction mechanism refers to the nature of the carbonyl groups after the nucleophilic attack, in the reaction medium. Although they have been depicted as carbocationic structures in which one of the oxygen atoms is attached to the phosphorus atom and the other one is involved in the formation of the O-SO₃H bond (**Scheme 4.6**, species **IIb**, **III**, **IV** and **V**), they could be also described as either neutral structures or, because of the highly acidic medium, as protonated carbonyls, **Scheme 4.8**. The formation of the protonated carbonyl **VII** from the carbocationic structure **VI** would simply imply the addition of a molecule of H₂SO₄ followed by the loss of a molecule of H₂S₂O₇.



Scheme 4.8. Formation of the protonated carbonyl group in the spirocyclic oxyphosphoranes. For simplicity, only one of the carbonyl atoms is shown.

The mechanism herein proposed is in agreement with the experimental evidences observed and explains the unusual conformation of the aldehyde observed in the X-ray diffraction structure of the spirocyclic oxyphosphorane **13**. Although the energy of the internal phenyl-CO rotation in benzaldehyde is close to 8 kcal/mol,²⁷ it can reach values of 16 kcal/mol in *ortho*-Br substituted benzaldehydes. Similar values have also been reported in the protonated benzaldehyde.^{22a} This would explain why, after the formation of the aldehyde in **13**, the orientation of the aldehydic proton does not change.

Regarding the formation of the carboxylic spirocyclic compound **11**, only observed when the reaction was performed at 55 °C from the very beginning, it can be attributed to the oxidation of the phosphine by the reaction media. The formation of the aldehyde would then be prevented, since no H transfer would be possible and the reaction would only be able proceed to the cyclisation and further hydrolysis of the last CF₃. Whether the oxidation takes place before, after or even at the same time as the hydrolysis of the two first CF₃ groups could not be determined.

4.5. Summary and concluding remarks

Insights about the reaction of hydrolysis of the trifluoromethyl group in trifluoromethylated phosphines have been obtained through the study of three main blocks.

In a first block, it has been shown that in the reaction media phosphines are protected against oxidation by quaternisation of the phosphorous atom in the shape of protonated phosphonium ions. The ternary superacid mixture HB(SO₄)₄-SO₃-H₂SO₄ is assumed to be the superacid responsible of the protonation of the phosphines in the reaction

²⁷ Godunov, I. A.; Bataev, V. A.; Abramnikov, A. V.; Pupyshev, V. I. *J. Phys. Chem. A* **2014**, *118* (44), 10159–10165.

conditions used in this work. At the same time this ternary mixture provides a strong acidic media which accelerates the reaction of hydrolysis of the CF_3 group. The higher acidity of the $\text{HB}(\text{SO}_4)_4\text{-SO}_3\text{-H}_2\text{SO}_4$ system compared to the binary $\text{SO}_3\text{-H}_2\text{SO}_4$ superacid has been estimated. This increase in the acidity has been tentatively attributed to the dissolution of the polymeric boron sulfates after the addition of oleum.

In a second block, the mechanism of the reaction of hydrolysis in the superacid mixture used in the present work has been proposed in accordance to the reported mechanism in CF_3SO_3 or HSO_3F in the literature. This reaction mechanism has been further supported by $^{19}\text{F}\{^1\text{H}\}$ NMR experiments. C-F bond cleavage to generate a difluorocarocation seems to be the rate limiting reaction step. This assumption, together with the fact that, under the reaction conditions, phosphines are protonated has been used to explain the different reaction rates of hydrolysis with dependence of the position of the trifluoromethyl group in the aromatic ring.

In the third block, the formation of the spiro compounds during the hydrolysis of the trifluoromethyl in the *ortho*-substituted phosphine **9** has been studied. The mechanism of formation of these compounds has been proposed. The experimental observations seem to indicate that phosphine oxidation is required to form the spirocyclic structure. The aldehydic spiro oxyphosphorane **13** would be formed by simultaneous oxidation of the P atom and the reduction of the C atom of the CF_3 group, involving the transference of the proton on the phosphorus atom to the carbon atom.

Chapter 5

Hydrolysis of the Trifluoromethyl Group in Diphosphines

5. 1. Introduction

After having explored the reaction of hydrolysis of the trifluoromethyl group in triarylmonophosphines, it was decided to essay this reaction in tryfluoromethylated aryldiphosphines. The previous results with monophosphines showed that the reaction rate is highly dependent on the relative position of the trifluoromethyl group with respect to the phosphorus atom, it being faster in *meta* than it is in *para*-position and, at the same time, much faster than the trifluoromethyl groups located in *ortho* or 3,5-position. This fact was borne in mind in order to synthesise the new trifluoromethylated diphosphines, **31** and **32**, **Chart 5.1**.

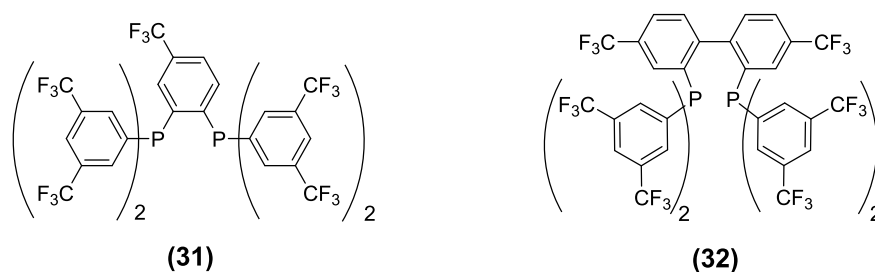


Chart 5.1. Trifluoromethylated diphosphines

Diphosphines **31** and **32** are similar in terms of the number and distribution of the trifluoromethyl groups. Two different types of these groups can be distinguished in both diphosphines: hydrolysable trifluoromethyl groups and non-hydrolysable trifluoromethyl groups. Such classification was made according to the reaction rate of hydrolysis observed during the study with monophosphines. The first group includes those trifluoromethyl located at *meta* and *para* position with respect to the phosphorus atom, meaning those with a relative fast hydrolysis rate. In contrast, the second group comprises those trifluoromethyls whose hydrolysis is far too slow to be actually considered hydrolysable. In this way, we could ideally control the positions where the carboxylic acid will be located and thus control the properties and possible applications of the final diphosphines. Another common feature of diphosphines **31** and **32** is the fact that all the aromatic rings are substituted with at least one trifluoromethyl group. In this way the sulfonation of the aromatic rings, a reaction that is not desired in this case, is prevented.

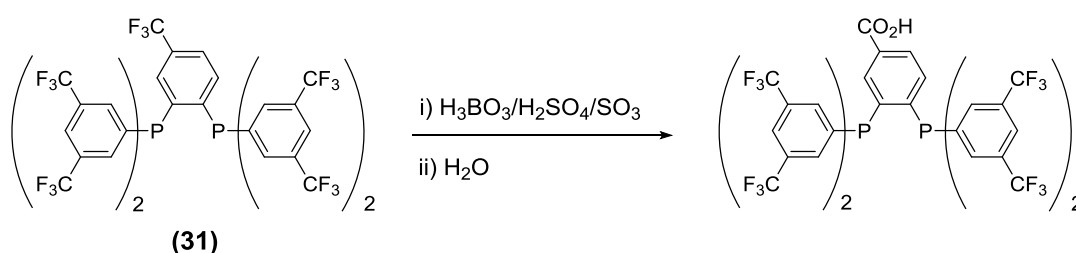
Concerning the differences between **31** and **32**, it is worth noticing the way the two phosphorus atoms are connected in the molecule. While in ligand **31** the phosphorus

atoms are attached to the same ring, in ligand **32** they are located at different aromatic moieties. According to the previous experiments with the heteroleptic trifluoromethylated monophosphines, the presence of 3,5-trifluoromethyl groups has an important influence on the hydrolysis of the trifluoromethyl groups located at other rings. These two ligands were therefore designed so that the effect of 3,5-trifluoromethyl groups located at different phosphorus atoms could also be studied. Furthermore, it should be emphasised that, taking into account the large amount of 3,5-trifluoromethyl groups on both diphosphines, a very slow reaction rate in the hydrolysis of the trifluoromethyl groups was initially expected.

5. 2. Design and synthesis of the trifluoromethylated diphosphines

5.2.1. Synthesis of diphosphine **31**

Diphosphine **31** is a trifluoromethylated derivative of the 1,2-bis(diphenylphosphino)benzene (dppbz). Its structure contains eight 3,5-trifluoromethyl groups in addition to one single trifluoromethyl group located at *meta* and *para* with respect to each of the phosphorus atoms. This trifluoromethyl group was the only one to be expected to undergo hydrolysis. The idea was therefore to obtain a highly trifluoromethylated diphosphine with a single carboxylic group, after performing the reaction with oleum and boric acid, **Scheme 5.1**. Such a group could later on be used for different applications such as anchoring the ligand on a solid support as previously done for *p*-Miranphos ligand.¹

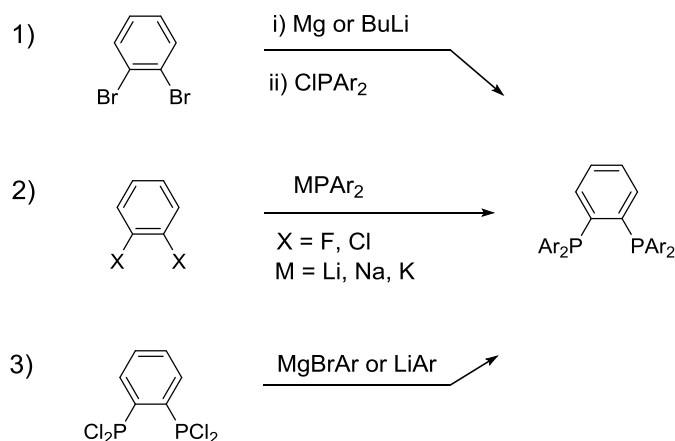


Scheme 5.1. Expected hydrolysis of the trifluoromethyl group in diphosphine **31**

The synthesis of dppbz and derivatives has been widely reported in the literature. Among the different synthetic procedures that can be found, three main approaches are

¹ Herrera Miranda, D. *Síntesis de Nuevas Triarilfosfinas Carboxiladas Mediante Hidrólisis del Grupo Trifluorometilo. Aplicaciones en Catálisis de Intercambio de Fase y Anclaje Sobre Silica*. Master's Thesis. Universitat Autònoma de Barcelona, **2012**.

predominant (**Scheme 5.2**): 1) the reaction between the Grignard or the lithium derivative of 1,2-dibromobenzene and a chlorodiarylphosphine.² 2) the nucleophilic attack of diphenylphosphide to a 1,2-dihalobenzene.³ And 3) the reaction between 1,2-bis(dichlorophosphino)benzene and aryl-Grignard or aryl-lithium reagents.⁴



Scheme 5.2. Different synthetic procedures to prepare dppbz and derivatives

The synthetic procedure 3) was discarded since the preparation of the trifluoromethylated derivative of 1,2-bis(dichlorophosphino)benzene would require the synthesis of several intermediates involving many reaction steps,⁵ similarly to the synthesis of the heteroleptic monophosphines presented in chapter 3. Therefore procedures 1) and 2) were tested, it being the first approach the one that afforded diphosphine **31** successfully. In order to keep the current section as simple as possible, only the procedure 1) will be described herein. However since we strongly believe in the fact that not only successful results should be published, but also those that do not yield to the desired result can be of the interest to the researchers, details of procedure 2) will be found in chapter 6.

An important remark about the synthesis of **31** is that the experiments performed in the optimisation of the synthetic procedure of this phosphine were firstly carried out using

² Tunney, S. E.; Stille, J. K. *J. Org. Chem.* **1987**, *52* (5), 748–753.

³ a) McFarlane, H. C. E.; McFarlane, W. *Polyhedron* **1988**, *7* (19–20), 1875–1879. b) Baker, B. A.; Bošković, Ž. V.; Lipshutz, B. H. *Org. Lett.* **2008**, *10* (2), 289–292.

⁴ a) Kaufhold, O.; Stasch, A.; Edwards, P. G.; Hahn, F. E. *Chem. Commun.* **2007**, No. 18, 1822–1824. b) Igawa, S.; Hashimoto, M.; Kawata, I.; Yashima, M.; Hoshino, M.; Osawa, M. *J. Mater. Chem. C* **2013**, *1* (3), 542–551.

⁵ a) Zhao, B.; Peng, X.; Wang, Z.; Xia, C.; Ding, K. *Chem. Eur. J.* **2008**, *14* (26), 7847–7857. b) Zuidema, E.; Elsbeth Goudriaan, P.; Swennenhuis, B. H. G.; Kamer, P. C. J.; Van Leeuwen, P. W. N. M.; Lutz, M.; Spek, A. L. *Organometallics* **2010**, *29* (5), 1210–1221.

the equivalent diphosphine **30** as model molecule, **Chart 5.2**. In contrast to ligand **31**, the starting phosphorus sources necessary for the preparation of **30**, such as chlorodiphenylphosphine and potassium diphenylphosphine, are commercially available.

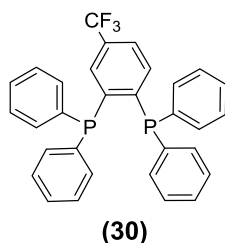


Chart 5.2. Structure of diphosphine **30**

Even though the synthetic procedure proposed for phosphines **30** and **31** was based on previously reported syntheses for similar phosphine ligands, it is important to stress that some of those synthetic steps from the literature were found to be difficult to apply in the synthesis of **30** and **31**. For this reason, it was of great importance to study and understand step-by-step how the reactions of formation of the diphosphine work.

Synthesis of 1,2-di-Grignard and 1,2-dilithium aryl compounds: general view

The above mentioned strategy 1) for the synthesis of ligand **31** is based on the reaction between a Grignard or organolithium reagent with a chlorodiarylphosphine, a reaction widely used in the general synthesis of phosphines. Aryl bromides are commonly used in the synthesis of Grignard and organolithium aryl compounds since the reactivity of these compounds in the synthesis of organometallic derivatives, as well as the price, falls in between that of the less reactive and more affordable chloroaryls and the more reactive, but less affordable, iodoaryls.

The synthesis of 1,2-bis(bromomagnesio)benzene by direct reaction of 1,2-dibromobenzene with magnesium has been reported in low yields, it being benzyne the main product of this reaction.⁶ Probably the most successful way to obtain 1,2-bis(bromomagnesio)benzene is by a transmetallation reaction using *ortho*-dilithiobenzene, with *ortho*-phenylenemercury as intermediate.⁷ Moreover similar behaviour was found with 1,2-dilithium aryl reagents. *Ortho*-dilithiobenzene was firstly

⁶ Hart, F. A.; Mann, F. G. *J. Chem. Soc.* **1957**, 3939.

⁷ Wittig, G.; Bickelhaupt, F. *Chem. Ber.* **1958**, 91 (4), 883–894.

reported by Wittig's group by means of reductive cleavage of *ortho*-phenylenemercury trimer with lithium metal.⁸ As in the case of 1,2-bis(bromomagnesium)benzene, the direct synthesis of 1,2-dilithiobenzene from 1,2-dibromobenzene shows some difficulties. The direct reaction of with either *n*-BuLi⁹ or *t*-BuLi¹⁰ in THF:Et₂O (1:1) requires temperatures below -90 °C in order to avoid lithium bromide elimination in the 1,2-lithiobromobenzene intermediate. Such low temperatures seem to deactivate the second bromine-lithium exchange to form 1,2-dilithiobenzene. Increasing the reaction temperatures does not proceed to the formation of the *o*-dilithiobenzene, but biphenyl products are formed instead through the aryne mechanism.^{9,10,11} An exception to this general path is found with the perfluorinated bromobenzene in which higher temperatures can be used to obtain the *o*-dilithiated product. Tamborski and Soloski reported the synthesis of 1,2-dilithiotetrafluorobenzene at -70 °C using 20 % excess of *n*-BuLi and 1,2-dibromotetrafluorobenzene.¹² This reaction has been later used in the synthesis of perfluoroaryl boranes¹³ in good yields. Recently, Durka *et al.*¹⁴ have reported the synthesis of phthalic acid in moderate yields from the dilithiation of 1,2-diiodobenzene in excess of *t*-BuLi and the following reaction with CO₂. Summary of the most relevant reactions of formation of the di-Grignard and dilithio organometallic compounds from 1,2-dibromobenzene is shown in **Scheme 5.3**.¹⁵

⁸ a) Wittig, G.; Bickelhaupt, F. *Angew. Chemie* **1957**, *69* (3), 93–93. b) Wittig, G. *Angew. Chemie* **1957**, *69* (8), 245–251.

⁹ Chen, L. S.; Chen, G. J.; Tamborski, C. *J. Organomet. Chem.* **1980**, *193* (3), 283–292.

¹⁰ Bettinger, H. F.; Filthaus, M. *J. Org. Chem.* **2007**, *25* (17), 9750–9752.

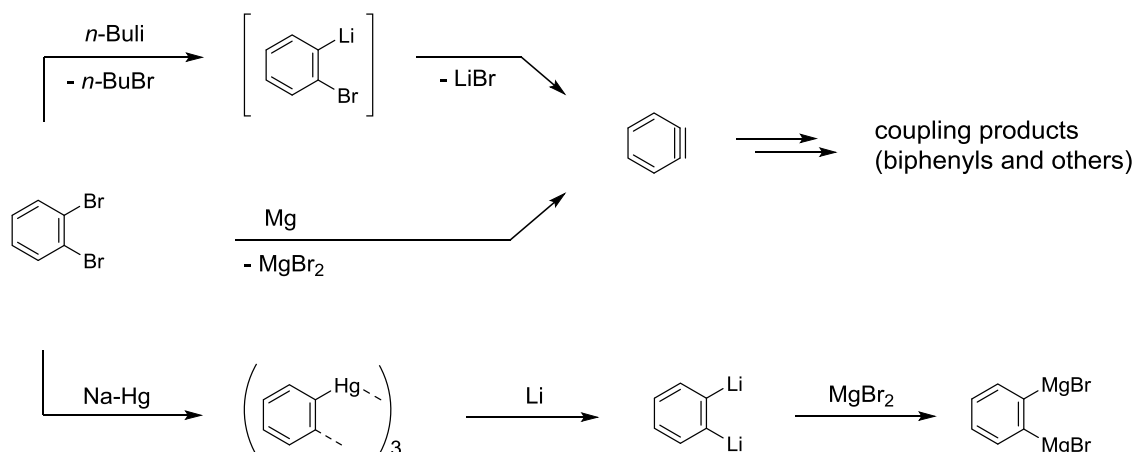
¹¹ a) Leroux, F.; Schlosser, M. *Angew. Chem. Int. Ed.* **2002**, *41* (22), 4272–4274. b) Eda, S.; Hamura, T. *Molecules* **2015**, *20* (10), 19449–19462.

¹² Tamborski, C.; Soloski, E. *J. Organomet. Chem.* **1969**, *20* (1), 245–250.

¹³ Chase, P. A.; Henderson, L. D.; Piers, W. E.; Parvez, M.; Clegg, W.; Elsegood, M. R. *J. Organometallics* **2006**, *25* (2), 349–357.

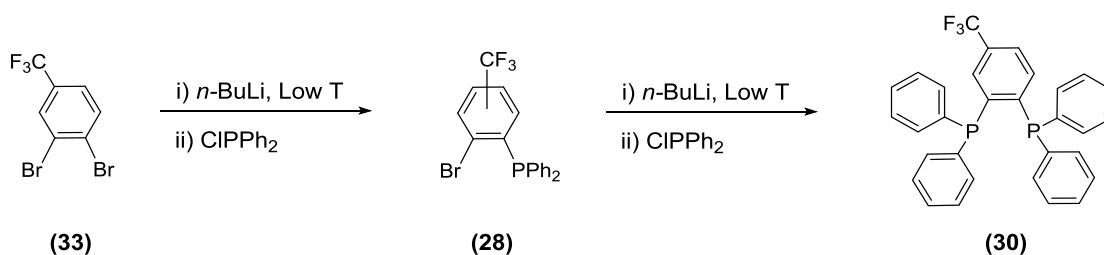
¹⁴ Durka, J.; Lujski, J.; Amborski, M.; Serwatowski, J. *Eur. J. Org. Chem.* **2014**, 4562–4570.

¹⁵ for general reviews on the topic see: a) Bickelhaupt, F. *Pure Appl. Chem.* **1986**, *58* (4), 537–542. b) Bickelhaupt, F. *J. Organomet. Chem.* **1994**, *475*, 1–14. c) Bickelhaupt, F. *Chem. Soc. Rev.* **1999**, *28* (1), 17–23.



Scheme 5.3. Summary of relevant reactions of formation of di-Grignard and dilithio organometallic compounds from 1,2-dibromobenzene

Consequently, since the direct synthesis of 1,2-di-Grignard reagents from the corresponding 1,2-dihalide is specially difficult, it was decided to synthesise diphosphine **30** sequentially, **Scheme 5.4**. That is, preparing the *o*-bromolithium derivative at low temperature and, after reacting with the chlorophosphine to form the *o*-halophosphine (**28**), repeating the process to obtain the final product.^{2,5a,16}



Scheme 5.4. Sequential synthesis of **30** from **33**

Synthesis of 1,2-dibromo-4-(trifluoromethyl)benzene (**33**)

Although 1,2-dichloro-4-(trifluoromethyl)benzene was much more affordable than the brominated equivalent compound, 1,2-dibromo-4-(trifluoromethyl)benzene (**33**), halogen-metal exchange is more favourable when using arylbromides than arylchlorides. Higher temperatures are generally required when using arylchlorides. The synthesis of aromatic organolithium compounds from chloroaryls has been described at *ca.* 0 °C by either

¹⁶ a) Reetz, M. T.; Gosberg, A. *Tetrahedron: Asymmetry* **1999**, *10* (11), 2129–2137. b) Luo, X.; Zhang, H.; Duan, H.; Liu, Q.; Zhu, L.; Zhang, T.; Lei, A. *Org. Lett.* **2007**, *9* (22), 4571–4574.

using lithium metal¹⁷ or Na enriched lithium,¹⁸ or at -78 °C with lithium metal and a catalytic amount of naphthalene.¹⁹ It is of great importance to bear in mind the fact that the stability of the 1,2-halolithioaryl intermediate requires low temperatures to avoid decomposition. As reported by Gilman and Gorsich,²⁰ while temperatures as low as -90°C allow the preparation of *o*-chlorophenyllithium using *n*-Buli and *o*-chlorobromobenzene, the same reaction performed at -65 °C produces only 2-chloro-2'-lithiobiphenyl and 2-(*o*-chlorophenyl)-2'-lithiobiphenyl, due to the decomposition of *o*-chlorobromobenzene.

In view of these precedents, it was decided to use 1,2-dibromo-4-(trifluoromethyl)benzene (**33**). Nevertheless, and motivated by the high commercial price of this dibrominated reagent (about 300 €/g, vs 0.2 €/g for the chlorinated compound from the same supplier), it was decided to synthesise the dibromoaryl compound in the laboratory.

Electrophilic bromination of arenes has been widely reported. While electron-rich aromatics, such as amines or phenols, undergo bromination using diluted Br₂ at room temperature, less activated arenes require Lewis acid catalysts.²¹ The difficulty arises when dealing with deactivated aromatics. In that sense the combination of *N*-halosuccinimide with a superacid has been successfully applied in the halogenation of electron-poor aromatics. Olah and co-workers reported the electrophilic iodination of deactivated arenes in high yields with *N*-iodosuccinimide (NIS) in trifluoromethanesulfonic acid (NIS/triflic acid system).²² More recently, they have extended the reaction to chlorination, bromination and iodination using *N*-halosuccinimide/BF₃·H₂O system.²³ However this last approach requires higher temperatures for the chlorination and bromination of trifluoromethylbenzene which, according to the authors, yields the hydrolysis of CF₃.

¹⁷ Screttas, C. G.; Steele, B. R.; Micha-Screttas, M.; Heropoulos, G. A. *Org. Lett.* **2012**, *14* (22), 5680–5683.

¹⁸ De Crisci, A. G.; Lough, A. J.; Multani, K.; Fekl, U. *Organometallics* **2008**, *27* (8), 1765–1779.

¹⁹ Huerta, F. F.; Gómez, C.; Yus, M. *Tetrahedron* **1999**, *55* (13), 4043–4050.

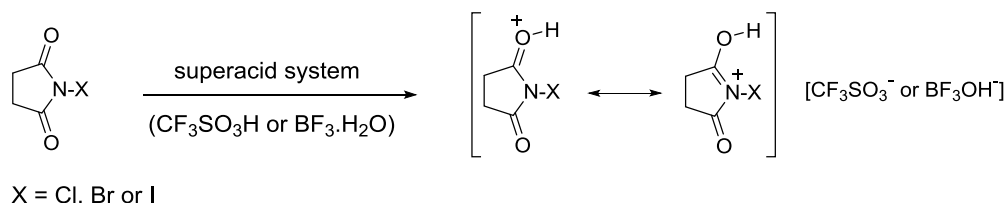
²⁰ Gilman, H.; Gorsich, R. D. *J. Am. Chem. Soc.* **1956**, *78* (10), 2217–2222.

²¹ Smith, M.; March, J. Chapter 11: Aromatic Substitution, Electrophilic. In *March's Advanced Organic Chemistry: Reactions, Mechanisms, and Structure*; John Wiley & Sons, Inc.: Hoboken, NJ, USA, **2007**; 6th Edition. pp 698-699.

²² Olah, G. A.; Wang, Q.; Sandford, G.; Prakash, G. K. S. *J. Org. Chem.* **1993**, *58*, 3194–3195.

²³ Prakash, G. K. S.; Mathew, T.; Hoole, D.; Esteves, P. M.; Wang, Q.; Rasul, G.; Olah, G. A. *J. Am. Chem. Soc.* **2004**, *126* (48), 15770–15776.

The halogenation of deactivated arenes is possible using triflic acid and $\text{BF}_3 \cdot \text{H}_2\text{O}$ given that, according to NMR experiments, these superacids would protonate the NXS (where $\text{X} = \text{Cl}, \text{Br}$ or I) thus forming a superelectrophilic reagent (**Scheme 5.5**). That is to say that the protonation of the NXS increases the electrophilicity of the X^+ .



Scheme 5.5 Protonation of *N*-halosuccinimide to form the halogenating species, according to the reported procedures^{22,23}

In order to prepare 1,2-dibromo-4-(trifluoromethyl)benzene, *N*-bromosuccinimide and trifluoromethanesulfonic acid were used in similar manner to that reported for the NIS/triflic acid system.²⁴ Although, both CF_3 and Br are deactivating groups in the electrophilic aromatic substitution, CF_3 is a *meta*-directing group whereas Br , as any halogen atom, behaves as *ortho* and *para*-directing group. Therefore the bromination of 4-(trifluoromethyl)bromobenzene should afford **33** as single product (**Figure 5.1**).

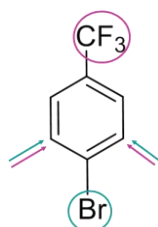


Figure 5.1. Directing effect of the trifluoromethyl group and the bromine atom in the electrophilic aromatic substitution of 4-(trifluoromethyl)bromobenzene

The reaction was successfully performed in multigram scale using a 1:1:2.5 ratio (arene:NBS:Triflic acid) obtaining the dibromoderivative in good yield and with purity above 99 %, according to GC. With this procedure, the cost of 1,2-dibromo-4-(trifluoromethyl)benzene (**33**), according to the price of the chemicals used, was of about 3 €/g.

²⁴ Blurton, P.; Burkamp, F.; Churcher, I.; Harrison, T.; Joseph, N. *Arylacetic acids and related compounds for treatment of alzheimer's disease*. WO2006008558 (A1). **2006**.

Lithiation and phosphorylation of 33

Once the dibromo-derivative had been successfully obtained, it was tested in the reaction with BuLi and the chlorophosphine to obtain the diphosphine ligand **30**. The first step of the reaction, the formation of the *o*-bromophosphines **28** (**Scheme 5.4**) is probably the most important one due to the thermal instability of the 1,2-bromolithium-intermediate, as previously mentioned.

The reaction conditions were explored by using different solvents, temperatures, concentrations and reaction times. Regarding the reaction media, ethereal solvents like THF or Et₂O are normally used for the preparation of organolithium compounds although a mixture of both THF:Et₂O (50:50) has been generally reported as solvent for this reaction. It is well known that the solvent influences the aggregation state of organolithium compounds²⁵ and thus, varies their reactivity. For instance, whereas *n*-butyllithium is hexameric in hydrocarbons,²⁶ it forms tetrameric species in Et₂O²⁷ and is found as a tetramer-dimer mixture in THF.²⁸ For this reason, apart from using THF:Et₂O (50:50) mixture, we have studied the reaction in other solvents. Concerning the reaction temperature, although a range of -110 to -130 °C has normally been reported, we have essayed the reaction at -95 °C, which is the reported temperature at which the *o*-bromobenzene begins to decompose through the aryne mechanism.⁹ As reported for fluorine-substituted dibromobenzene¹² and diiodobenzene¹⁴ it seems that fluorine confers a higher stability to the organolithium arene compared to the non-fluorinated arene. In our case, the CF₃ group could also enhance the stability of the organolithium derivative thus allowing working at higher temperatures.

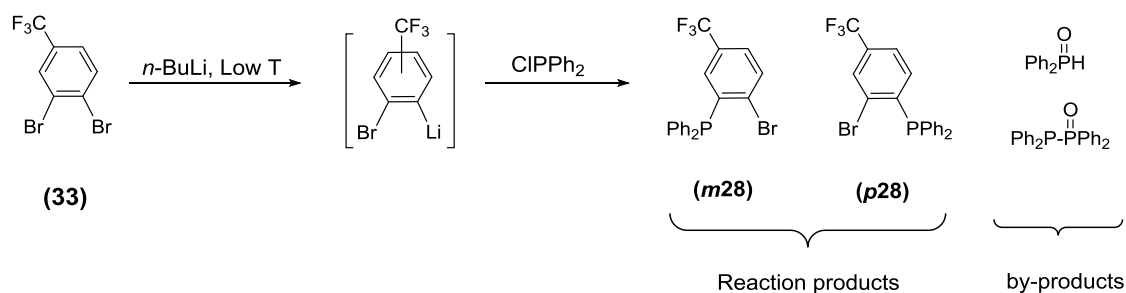
The evaluation of the reaction was carried out taking into account the different phosphorus-containing compounds formed after the addition of the chlorophosphine to the organolithium compound, **Scheme 5.6**. The composition of each reaction was analysed by ³¹P{¹H} NMR after treatment with water and extractions of the reaction compounds in Et₂O.

²⁵ a) Elschenbroich, C. Chapter 5: Organometallic Chemistry of Alkali Metals. In *Organometallics.*; Wiley-VCH Verlag GmbH & Co. KGaA: Weinheim, **2006**. 3rd Edition. pp 34-37. b) Reich, H. J. *Chem. Rev.* **2013**, *113* (9), 7130–7178.

²⁶ Thomas, R. D.; Jensen, R. M.; Young, T. C. *Organometallics* **1987**, *6* (3), 565–571.

²⁷ Lewis, H. L.; Brown, T. L. *J. Am. Chem. Soc.* **1970**, *92* (15), 4664–4670.

²⁸ McGarrity, J. F.; Ogle, C. A.; Brich, Z.; Loosli, H. R. *J. Am. Chem. Soc.* **1985**, *107* (7), 1810–1815.



Scheme 5.6. Different compounds observed in the lithiation/phosphorylation of **33**

The experimental results are summarised in **Table 5.1**. In order to simplify the analysis only *meta* (**m28**) and *para*-substituted (**p28**) *o*-bromophosphines, and diphenylphosphine oxide (**DPPO**) were shown in the table. While bromophosphines are an indication of the success of the reaction, diphenylphosphine oxide (*ca.* 22.3 ppm), indicates the unreacted chlorophosphine and, indirectly, how the previous formation of the bromolithioarene worked. Other phosphorus compounds such as diphenylbutylphosphine (*ca.* 0 ppm) and tetraphenyldiphosphine monoxide (two doublets at *ca.* 38 and -21 ppm with $^1J_{\text{PP}} = 234$ Hz) were also detected as minor impurities. In a few instances, a quartet at 11.5 ppm with $^4J_{\text{PF}} = 66$ Hz has also been observed in amounts lower than 5%. This coupling pattern indicates a phosphorus atom at *ortho*-position with respect to the trifluoromethyl group, which would be formed by H-Li exchange of a proton of high acidity in *ortho*-position to the CF_3 . However, the structure of this compound could not be determined.

As expected, the best results were obtained using an equal amount of THF and diethyl ether as solvent. By comparing entries 1 and 2, it is possible to observe that increasing the reaction time produces a decrease in the amount of bromophosphines. This fact may be attributed to the decomposition of the *o*-bromolithium derivative most probably through the aryne mechanism. Entries 2 and 3 indicate that higher dilution of **33** seems to improve the results, even when the reaction time was increased with respect to entry 1. With this in mind, experiment 6 was essayed. A higher dilution and the same reaction time were used in this one compared to entry 1. However, whereas increasing the dilution should reduce the formation of biphenyl products, it might also decrease the reaction rate between *n*-BuLi and the dibromoderivative. With the aim of increasing the rate while maintaining the reaction time short, the temperature was increased to -95 °C. Under these conditions the best result was obtained which has been consistently reproduced 3 times, showing the same results.

Table 5.1. Study of the reaction of formation of *ortho*-bromophosphines

Entry	Solvent	Conc. of 33 ^a	Reaction time ^b (min)	Temp. (°C)	28 ^c (%) (<i>m28</i> : <i>p28</i>)	DPPO ^c (%)
1	THF:Et ₂ O (1:1)	0.10	30	-120	61.7 (2.3:1)	17.5
2	THF:Et ₂ O (1:1)	0.10	60	-120	26.1 (2.5:1)	69.6
3	THF:Et ₂ O (1:1)	0.05	100	-120	45.6 (2.2:1)	41.5
4	Hexanes: Et ₂ O (3:1)	0.05	100	-120	30.9 (2.9:1)	69.1
5	Hexanes	0.05	60	-120	8.9 (1.2:1)	67.1
6	THF:Et ₂ O (1:1)	0.03	30	-95	88.2 (2.5:1)	7.80
7	THF:Et ₂ O (1:1)	neat ^d	30	-95	47.5 (3.8:1)	29.3

General procedure: 1 g of 1,2-dibromo-4-(trifluoromethyl)benzene (**33**) was mixed with the solvent and cooled down to the reaction temperature using a cooling bath with liquid N₂ and the corresponding organic solvent (EtOH for -120 °C or Toluene for -95 °C). Then, *n*-BuLi (2.5 M in hexanes) was added dropwise for 10 minutes and the mixture was stirred at the reaction temperature for a variable time. Afterwards, ClPPh₂ was added dropwise during 5 minutes before allowing the bath to warm up to room temperature slowly.

^a Concentration of **33** in the solution previous to the addition of *n*-BuLi. In g/ml.

^b Reaction time between 3,4-dibromobenzotrifluoride and *n*-BuLi.

^c Percentage with respect to all the phosphorus compounds in the reaction mixture. Measured by integration of the ³¹P{¹H} NMR. In parenthesis, *m28* to *p28* ratio.

^d *n*-BuLi mixed with the solvent and cooled down before the addition of neat 1,2-dibromo-4-(trifluoromethyl)benzene (**33**). Solvent volume equivalent to entry 6.

According to entry 7, the percentage of *o*-bromophosphines was lower when the addition order was reversed. It is important to highlight that under these conditions a product of Li-H exchange in *ortho* with respect to the CF₃ was observed in the NMR (quadruplet, ⁴J_{P-F} = 66 Hz) in *ca.* 16 %. Regarding the use of other solvents, either mixture of hexanes:Et₂O (3:1) or 100 % hexanes did not show any improvements in the reaction. Another interesting remark is the fact that the *m28* : *p28* ratio differs depending on the solvent used. While in THF:Et₂O the ratio is around 2.5:1, with exception of the reversed order in which a 3.75:1 ratio was obtained, in hexanes:Et₂O it was 2.9:1 and using only hexanes as reaction media this ratio was lowered to 1.2:1. Either way, *m28*, the product of the reaction of the bromine located in *meta* with respect to the CF₃, was always the major one. This can be explained due to the inductive effect of the CF₃ group which stabilises the negative charge on the organolithium compound. This effect is greater the closer to the carbon atom is the CF₃ group.

A close look at the $^{31}\text{P}\{^1\text{H}\}$ NMR of **m28** and **p28**, **Figure 5.2**, reveals that the signal corresponding to the *para*-isomer is a broad quartet ($J = 1.6$ Hz). This coupling pattern can only be explained due to the coupling between the phosphorus atom and the CF_3 group. Interestingly, such a long range P-F coupling has not been observed in the equivalent non-brominated phosphines, **1** and **5**, nor in the *meta* isomer **m28** in spite of the fact that in this isomer the distance between the phosphorus and the fluorine atoms is smaller than in the *para*-isomer **p28**. Unfortunately, little has been reported regarding long range P-F coupling and the effect of halogen atoms on such coupling. Therefore, in order to give an explanation to the observed effect, a systematic comparison in similar environments has been carried out.

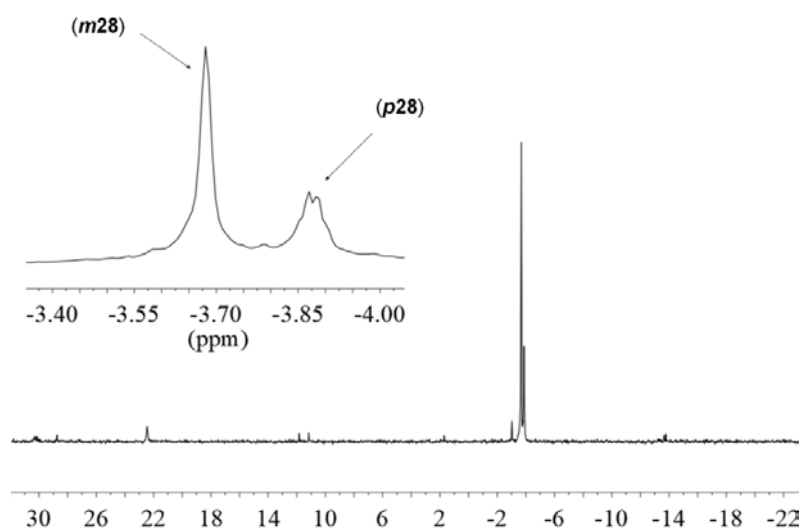
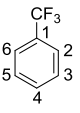


Figure 5.2. $^{31}\text{P}\{^1\text{H}\}$ NMR (101.2 MHz) of reaction mixture corresponding to entry 6 in **Table 5.1**.

Firstly we took into account the reported $J_{\text{C-F}}$ in halo-substituted trifluoromethylbenzenes²⁹ (**Table 5.2**). It is observed that regardless the position of the halogen atom, the coupling constants follow the same trend: $^1J_{\text{C-F}} > ^2J_{\text{C-F}} > ^3J_{\text{C-F}} > ^5J_{\text{C-F}} > ^4J_{\text{C-F}}$. Actually, the trend is observed also with other substituents, such as $-\text{CO}_2\text{H}$, $-\text{CN}$, $-\text{NH}_2$ and $-\text{OH}$ or even without any substituent. As consequence, although in this series of trifluoromethylbenzenes the substituent do not seem to change the value of the C-F coupling constant, it is interesting to observe how the coupling is larger in *para* than it is in *meta*-positions, as observed in the $J_{\text{P-F}}$ in the bromophosphines **m28** and **p28**.

²⁹ Newmark, R. A.; Hill, J. R. *Org. Magn. Reson.* **1977**, 9 (10), 589–592.

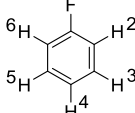
Table 5.2. C-F coupling in chloro- and bromo-substituted trifluoromethylbenzenes²⁹

	pattern of substitution					
	none	2-Br	2-Cl	3-Br	4-Br	4-Cl
CF ₃ (¹ J _{C-F})	271.5	273.1	272.6	272.6	272.0	271.1
1 (² J _{C-F})	32.2	31.2	31.3	33.0	32.9	33.0
2 (³ J _{C-F})	3.9	2.0	2.0	3.9	3.8	3.8
3 (⁴ J _{C-F})	- ^a	- ^a	- ^a	- ^a	- ^a	- ^a
4 (⁵ J _{C-F})	1.4	1.1	1.1	1.2	1.6	1.6
5 (⁴ J _{C-F})		- ^a	- ^a	- ^a		
6 (³ J _{C-F})		5.5	5.3	3.8		

J_{C-F} in Hz. ^a Not resolved. According to the authors this coupling must be less than the observed line-width of the *meta* carbon, 0.4Hz

More information can be obtained from studying the J_{H-F} in fluorobenzenes,³⁰ **Table 5.3.** In this case, the effect of the halogen atom (Cl or Br) on the coupling constant is more pronounced and it is different depending on the pattern of substitution. The authors described the same behaviour when using F or NO₂ and a linear correlation with the electronegativity of the substituents.

Table 5.3. C-F coupling in chloro and bromo-substituted fluorobenzenes³⁰

	pattern of substitution						
	none	2-Br	2-Cl	3-Br	3-Cl	4-Br	4-Cl
2 (³ J _{H-F})	9.31	-	-	8.69	8.63	8.62	8.48
3 (⁴ J _{H-F})	5.79	7.10	7.62	-	-	4.90	4.79
4 (⁵ J _{H-F})	0.34	-0.52	-0.85	-0.63	-0.47	-	-
5 (⁴ J _{H-F})	5.79	4.97	5.01	6.45	6.30	4.90	4.79
6 (³ J _{H-F})	9.31	9.10	9.64	8.61	9.02	8.62	8.48

J_{C-F} in Hz. Solvent acetone-D6.

As shown in **Table 5.3**, the authors reported J_{H-F} up to 5 bonds distance. Interestingly ⁶J_{H-F} in *p*-fluorotoluene has also been observed by Schaefer *et al.*³¹ having a value of 1.12 Hz. All in all, what probably is more interesting of these data is the fact that, unlike H-H coupling, long-range C-F and H-F coupling constants in aromatics are commonly

³⁰ Loemker, J. E.; Pryse, K. M.; Read Jr., J. M.; Goldstein, J. H. *Can. J. Chem.* **1969**, *47* (2), 209–213.

³¹ Schaefer, T.; Danchura, W.; Niemczura, W.; Peeling, J. *Can. J. Chem.* **1978**, *56* (18), 2442–2446.

observed and their value do not necessarily decrease with the distance. Also the effect of electronegative atoms in the aromatic ring should be mentioned. As stated by Fraser in the study of coupling constant in benzenes,³² changes in coupling constants can be attributed to changes in π -electron distribution. Due to the lack of information about long-range J_{P-F} we are just tempted to extrapolate the reported data for C-F and H-H couplings in order to rationalise the observed coupling in the *para*-isomer of the brominated phosphines.

Turning to the issue of the synthesis of the phosphines, although there was no need to separate the *meta* and the *para*-bromophosphine isomers for the next step in the synthesis of phosphine **30**, a small amount of the bromophosphine **p28** was isolated by subsequent recrystallizations in MeOH (this isomer is less soluble than the *meta* one). Suitable crystals for X-ray diffraction were then obtained by slow crystallization in $\text{CH}_2\text{Cl}_2/n$ -hexane. ORTEP diagram of the X-ray structure and some selected distances and angles are shown in **Figure 5.3**.

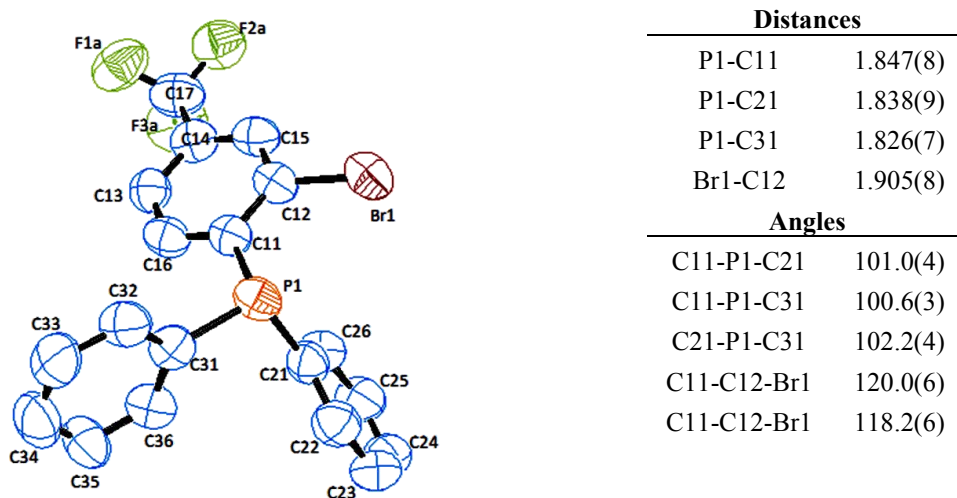
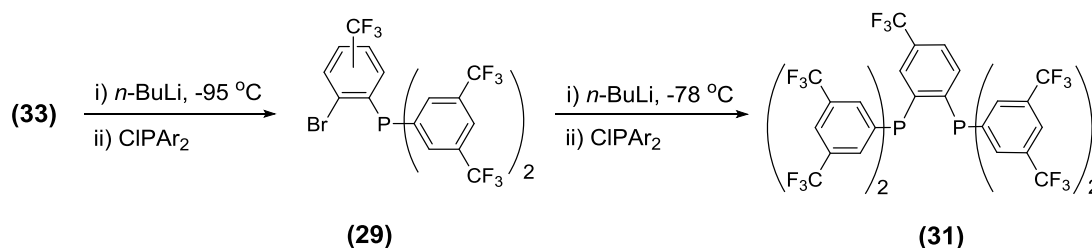


Figure 5.3. ORTEP plot (ellipsoid at 50% probability) of **p28** and selected distances (Å) and angles (°). Only one orientation of the disordered CF_3 group is drawn. Aromatic H atoms omitted for clarity

Once the most suitable conditions for the synthesis of the *ortho*-bromophosphines **28** had been successfully obtained, the second phosphorylation was easily achieved by following a modification of reported methods.^{2,16a} Thus bromine-lithium exchange was performed at low temperature and, followed by the addition of chlorodiphenylphosphine, the final diphosphine **30** was afforded.

³² Fraser, R. R. *Can. J. Chem.* **1966**, *44* (22), 2737–2741.

Finally, the methodology developed in the synthesis of diphosphine **30** was successfully applied to the synthesis of diphosphine **31**. The same reaction conditions used in ligand **30** were used for the synthesis of the highly trifluoromethylated ligand **31** obtaining similar results, **Scheme 5.7**.



Scheme 5.7. Synthesis of ligand **31**

In the first step, *m29* and *p29* were obtained in 3.2:1 ratio. Again, the signal observed for the *para*-isomer in $^{31}\text{P}\{^1\text{H}\}$ was a broad quartet ($J = 1.0\text{ Hz}$), **Figure 5.4**. Finally, the **29** mixture was subjected to a reaction of lithiation/phosphorylation to afford the diphosphine **31**.

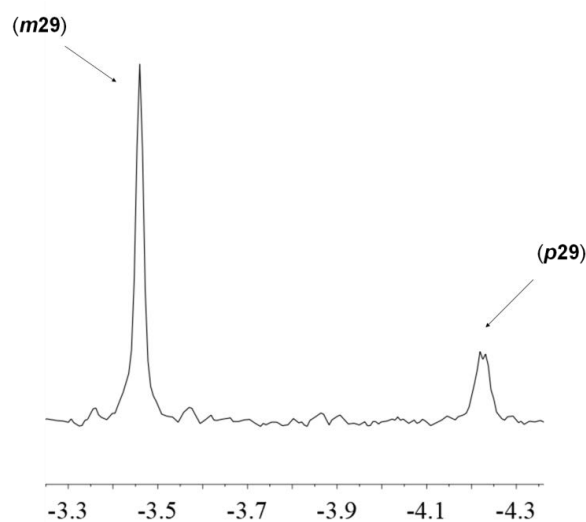


Figure 5.4. $^{31}\text{P}\{^1\text{H}\}$ NMR (101.2 MHz). δ in ppm. Mixture of *m29* and *p29* phosphines

Slow crystallization of **31** in $\text{CH}_2\text{Cl}_2/n\text{-hexane}$ yielded crystals of good quality. The X-ray diffraction structure of diphosphine **31** was then obtained (**Figure 5.5**).

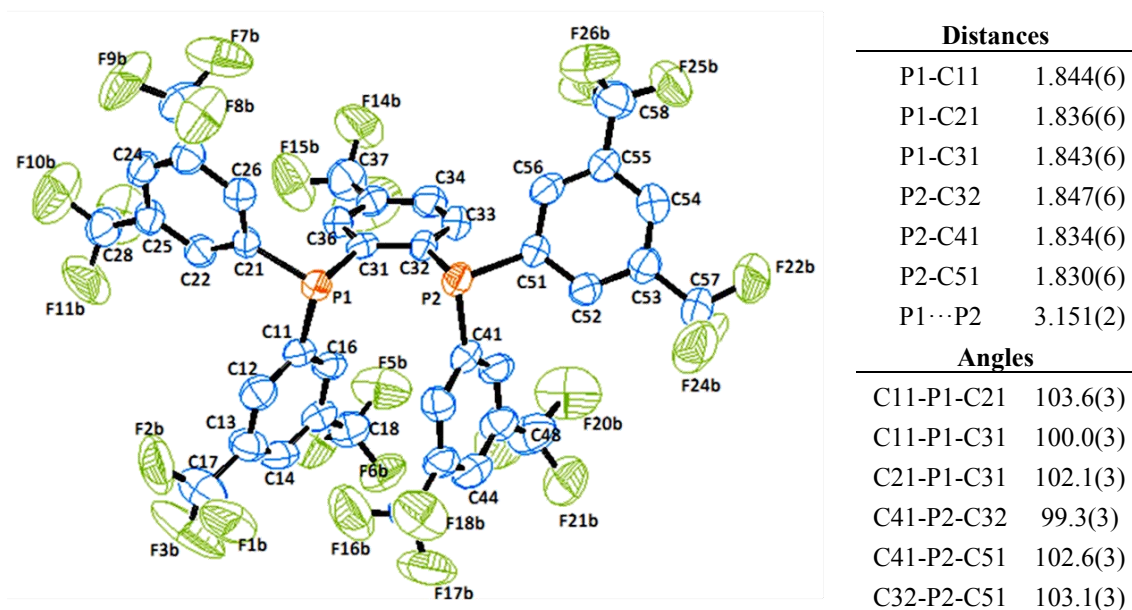
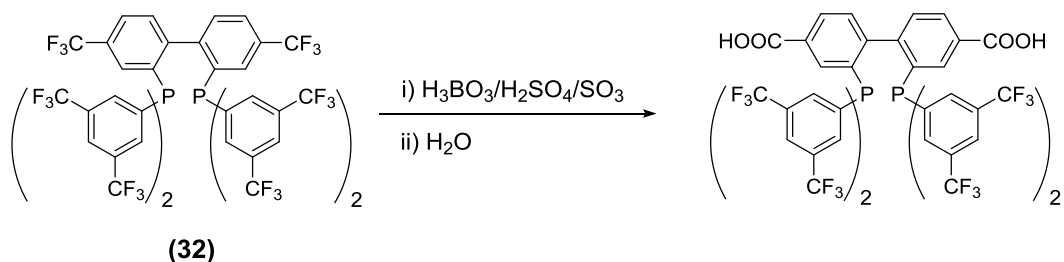


Figure 5.5. ORTEP plot (ellipsoid at 50% probability) of **31** and selected distances (Å) and angles (°). Only one orientation of each of the disordered CF₃ group is drawn. Aromatic hydrogen atoms omitted for clarity

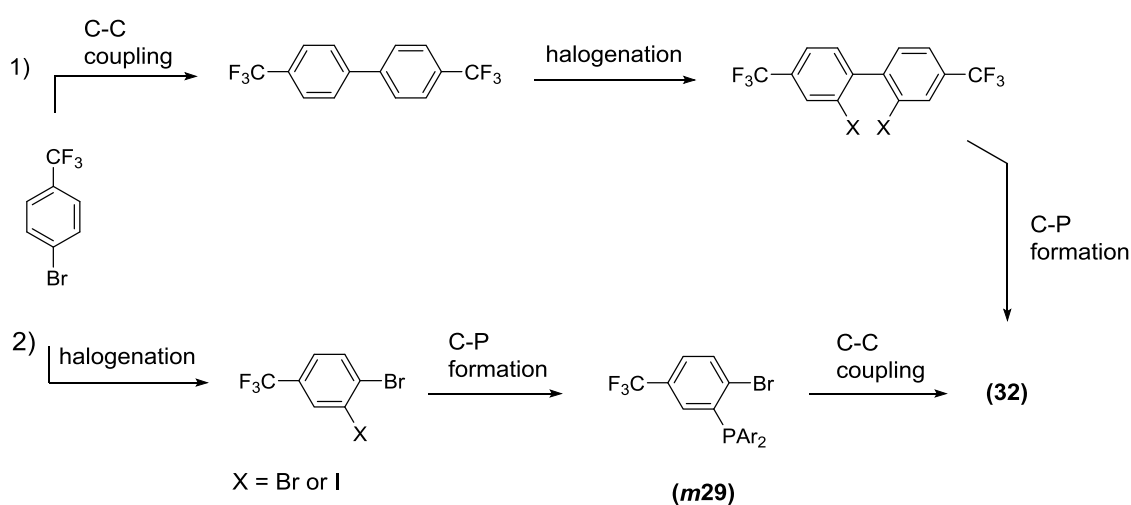
5.2.2. Synthesis of diphosphine **32**

Diphosphine **32** belongs to the family of 2,2'-bis(diphenylphosphino)-1,1'-biphenyl (BIPHEP) ligands. As in the case of diphosphine **31**, its structure contains both hydrolysable and non hydrolysable CF₃ groups, with the difference that while the former only contained one potentially non-hydrolysable group, diphosphine **32** contains two of them, which are both in *meta*-position with respect to the phosphorus atom. Ideally, these two CF₃ groups would hydrolyse yielding a dicarboxylated ligand, **Scheme 5.8**. The position of these carboxylic groups in the backbone of the diphosphines would allow the synthesis of polyesters or polyamides, incorporating the diphosphine functionality, by reaction of the dicarboxylic diphosphines with diols or diamines, respectively, as an example of application.



Scheme 5.8. Expected hydrolysis of the trifluoromethyl group in diphosphine **32**

Two different synthetic routes were proposed for **32** based on the reported syntheses for BIPHEP and derivatives,³³ **Scheme 5.9**. Essentially, both routes are based on the same chemical transformations, but differ in the order in which these transformations are applied. Ideally, by performing a series of C-C coupling, halogenation and C-P bond formation on 4-bromobenzotrifluoride, it would be possible to prepare diphosphine **32**. Although both procedures were tested, only with route 2) was possible to obtain **32**. As stated before for diphosphine **31**, only the route by which the preparation of the diphosphine was possible will be explained in this chapter, although complete detailed description of route 1) will be found in chapter 6.



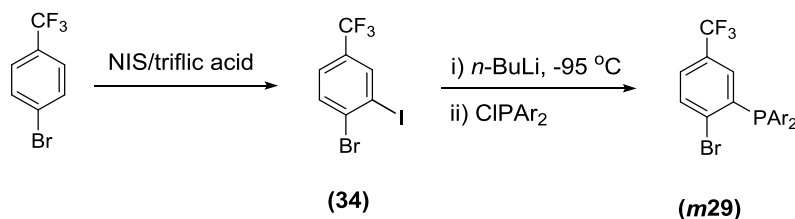
Scheme 5.9. Proposed syntheses for diphosphine **32**. Ar = 3,5-bis(trifluoromethyl)benzene

Synthesis of 1-bromo-2-iodo-4-(trifluoromethyl)benzene (**34**) and phosphine **m29**

The proposed synthesis for diphosphine **32** implies the use of **m29**. This compound was prepared, in a mixture of isomers **m29** and **p29**, during the synthesis of **31** described above. However this time it was necessary to prepare **m29** as a pure isomer. Making use of the reaction of bromination explored before for 4-(trifluoromethyl)bromobenzene, this compound was selectively iodinated using NIS/triflic. In this way, 1-bromo-2-iodo-4-(trifluoromethyl)benzene (**34**) was obtained in excellent yield and purity. Next, and

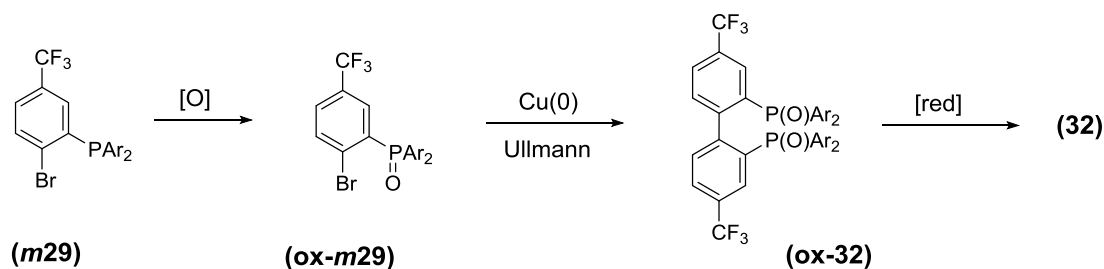
³³ a) Desponds, O.; Schlosser, M. *J. Organomet. Chem.* **1996**, 507 (1–2), 257–261. b) Ogasawara, M.; Yoshida, K.; Hayashi, T. *Organometallics* **2000**, 19 (8), 1567–1571. c) Jeulin, S.; De Paule, S. D.; Ratovelomanana-Vidal, V.; Genêt, J. P.; Champion, N.; Dellis, P. *Angew. Chem. Int. Ed.* **2004**, 43 (3), 320–325. d) Liu, L.; Wu, H. C.; Yu, J. Q. *Chem. Eur. J.* **2011**, 17 (39), 10828–10831. e) Bonnafoux, L.; Gramage-Doria, R.; Colobert, F.; Leroux, F. R. *Chem. Eur. J.* **2011**, 17 (39), 11008–11016. f) Aikawa, K.; Miyazaki, Y.; Mikami, K. *Bull. Chem. Soc. Jpn.* **2012**, 85 (2), 201–208.

taking advantage of the higher reactivity of iodine compared to bromine in the halogen-lithium exchange, **34** was treated with *n*-BuLi at -95 °C and subsequently phosphorylated to obtain **m29**, using the optimum conditions described in the previous section, **Scheme 5.10**.



Scheme 5.10. Synthesis of **m29**. Ar = 3,5-bis(trifluoromethyl)benzene

The next step, the C-C coupling to obtain the diphosphine **32**, was afterwards essayed using the classic Ullmann coupling with Cu. This reaction has been widely used in the synthesis of BIPHEP derivatives.^{33a,b,34} The process implies the use of an *ortho*-halophosphine oxide (normally Br or I) and excess of copper metal, **Scheme 5.11**.



Scheme 5.11. Synthesis of **32** via Ullmann coupling. Ar = 3,5-bis(trifluoromethyl)benzene

Bromophosphine **m-29** was oxidized using H₂O₂ previous to performing the coupling reaction using excess of activated Cu powder in DMF at 140 °C. The reaction worked, as expected, furnishing the diphosphine dioxide (**ox-32**) in good yield. Reduction of **ox-32** to afford the final diphosphine **32** was carried out using HSiCl₃ and NEt₃ in dry toluene. The reaction evolution could be easily monitored by GC. It is worth mentioning that the reaction did not take place at reflux after 24 h. However it was successfully performed using the same reactants, but under two different conditions. In a first approach, the reaction was performed under microwave radiation in closed vessels (150°C, 300W, 100psi. Discover Focused Microwave Synthesis System 908005) and the reduction took place in about 1.5 h. However, the small size of the vessels (*ca.* 10

³⁴ a) Dziuba, K.; Flis, A.; Szmigielska, A.; Pietrusiewicz, K. M. *Tetrahedron: Assymetry* **2010**, *21* (11–12), 1401–1405. b) Xu, W.; Zou, J. P.; Zhang, W. *Tetrahedron Lett.* **2010**, *51* (19), 2639–2643.

ml) made it difficult to scale the reaction up. Most probably, what made this reaction possible was the fact that temperature was increased to 150 °C and that the closed vessel avoids the evaporation of the volatile compounds (HSiCl₃ and NEt₃), rather than the use of microwaves. Having this in mind, we changed the system and the reaction was successfully performed in a larger scale in a stainless steel autoclave at 180 °C, without using microwave radiation. Higher temperatures were required in this case most probably due to the higher reaction volume used compared to the MW vessel. In both cases, surprisingly the reduction of the second phosphine oxide was much slower than the reduction of the first one. All in all, diphosphine **32** was obtained in moderate yields.

5.3. Reaction of hydrolysis of the trifluoromethyl group in diphosphines

Once the two diphosphines **31** and **32** had been prepared the next step was to study the behaviour of these phosphines in the reaction with oleum and boric acid.

5.3.1. Hydrolysis of the trifluoromethyl in diphosphine 31

The previous experiments in the hydrolysis of the trifluoromethyl group with the heteroleptic trifluoromethylated monophosphines showed that the reaction rate was highly dependent on the number of CF₃ groups in 3,5-position. Being aware of this fact, we expected slow hydrolysis rates with diphosphine **31**. A first reaction was performed using concentrations of diphosphine, sulfur trioxide and boric acid of 0.07, 6.2 and 0.03 M, respectively. To our surprise the NMR analysis of the sample, after quenching an aliquot of the reaction mixture with water and extracting with diethyl ether, showed only two doublets in ³¹P{¹H} at *ca.* 28.3 ppm (³J_{PP} = 7.2 Hz). These values of chemical shift and coupling constants are in agreement with the dioxidised form of diphosphine **31**, as reported for similar compounds.³⁵ The ¹⁹F{¹H} analysis showed two signals in the CF₃ region in 8:1 ratio, corresponding to the two different CF₃ groups in the molecule, thus indicating that no carboxylation had taken place, **Figure 5.6**. The subsequent addition of extra oleum and boric acid until reaching concentrations of SO₃

³⁵ McFarlane, H. C. E.; McFarlane, W. *Polyhedron* **1999**, *18* (16), 2117–2127.

of 10.5 M and boric acid of 2.1 M, did not afford the product of hydrolysis after more than 15 days of reaction.

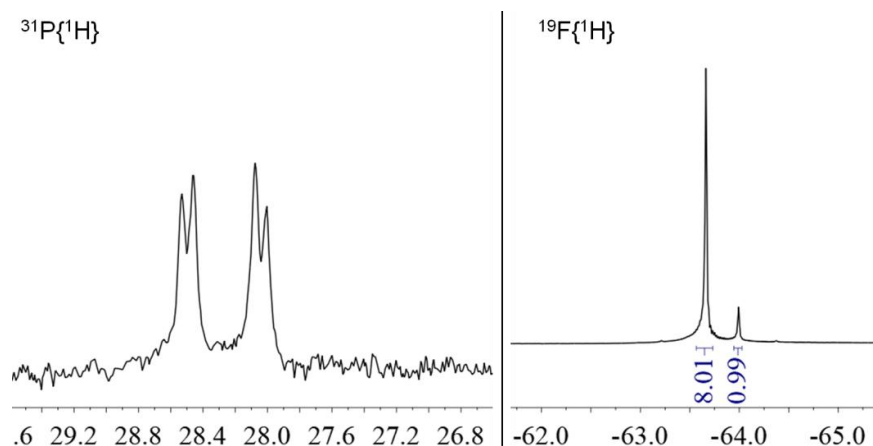


Figure 5.6. $^{31}\text{P}\{^1\text{H}\}$ (101.2 MHz) and $^{19}\text{F}\{^1\text{H}\}$ (235.2 MHz) NMR spectra of an aliquot of the reaction of **31** with oleum and boric acid. Solvent: CDCl_3 . δ in ppm. No other signals than those shown in the figure were observed.

Amongst all the trifluoromethylated phosphines that have been tested in the hydrolysis of the CF_3 so far, the diphosphine **31** is the one that contained the highest number of CF_3 groups. It is known that the robustness towards oxidation of the phosphines, as well as the π -acidity, increases with the number of trifluoromethyls in the aryl substituents.³⁶ Therefore it was not expected to find the oxidation of **31** under similar conditions in which the monophosphines were stable. A possible explanation of this fact is that the high number of trifluoromethyl groups on diphosphine **31** can decrease the basicity of the phosphorus atoms to the point that they cannot be protonated by the superacid system. As mentioned in the previous chapter, the protection of the phosphine takes place by protonation. This way the phosphine lone pair is no longer available to bond to oxygen. Other less plausible explanation for the oxidation of diphosphine **31** could be that the molecule geometry does not allow the protonation of the two phosphorus atoms due to steric hindrance.

A simple protonation study consisting of comparing diphosphine **31** to its non-trifluoromethylated equivalent, diphosphine **30**, was carried out. Two different samples of each ligand were prepared by dissolving 0.02 mmol of the phosphine in 0.4 ml of concentrated sulfuric acid. 0.2 mmol of boric acid was added to one of the samples of

³⁶ a) Peral Crespo, D. *Triarilfosfines Sulfonades Trifluorometilades. Aplicacions en Processos Catalitics*. Ph.D. Thesis. Universitat Autònoma de Barcelona, **2013**. b) Peral, D.; Herrera, D.; Real, J.; Flor, T.; Bayón, J. C. *Catal. Sci. Technol.* **2016**, 6 (3), 800–808.

each ligand. The mixtures were introduced into NMR tubes and analysed by ^{31}P and $^{31}\text{P}\{^1\text{H}\}$ NMR, **Figure 5.7** and **Figure 5.8**.

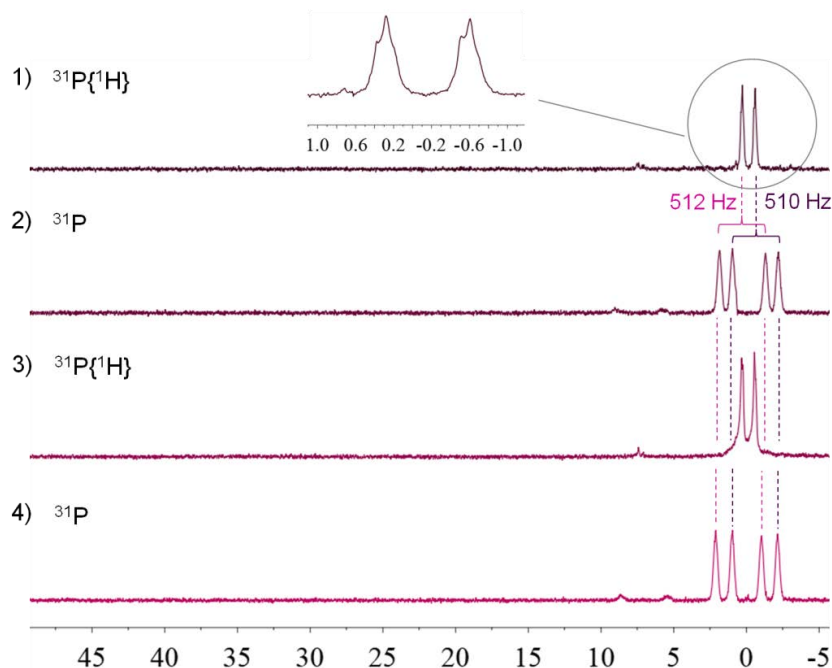


Figure 5.7. ^{31}P and $^{31}\text{P}\{^1\text{H}\}$ NMR spectra (161.98 MHz) of diphosphine **30** in sulfuric acid without boric acid (spectra -1- and -2-) and with boric acid (spectra -3- and -4-). Signals relative to NH_4PF_6 (-144.45 ppm) used as internal standard. δ in ppm. No other signals than those shown in the image were observed (excluding those of the internal standard). See text for detailed experimental conditions

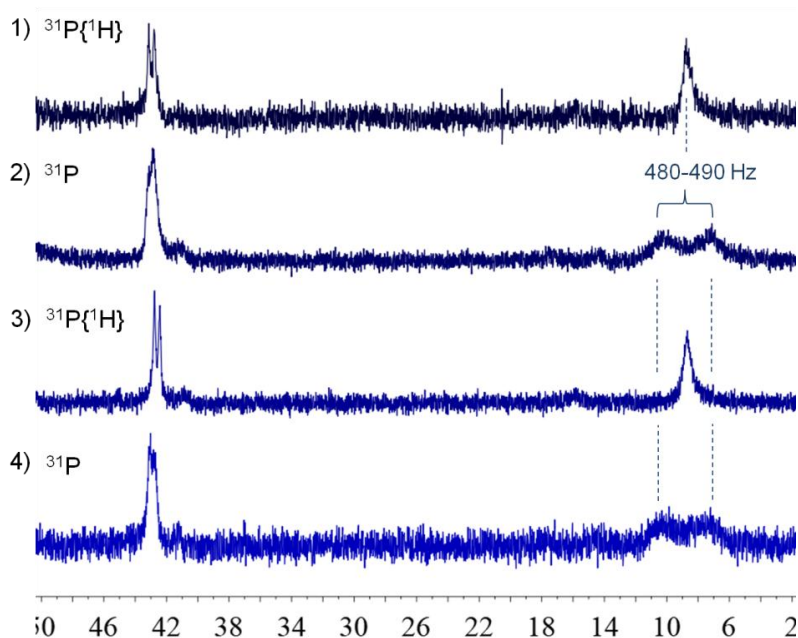
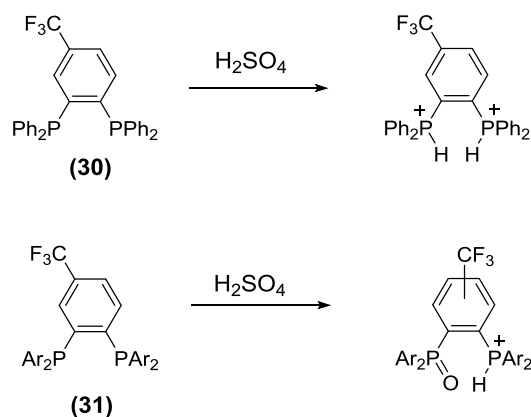


Figure 5.8. ^{31}P and $^{31}\text{P}\{^1\text{H}\}$ NMR spectra (161.98 MHz) of diphosphine **31** in sulfuric acid without boric acid (spectra -1- and -2-) and with boric acid (spectra -3- and -4-). Signals relative to NH_4PF_6 (-144.45 ppm) used as internal standard. δ in ppm. No other signals than those shown in the image were observed (excluding those of the internal standard). See text for detailed experimental conditions

As common trend in both ligands, no differences were observed when boric acid was used either in terms of protonation or oxidation of the phosphorus atoms. However, while diphosphine **30** (**Figure 5.7**) was completely protonated, showing signals only in the region of protonated phosphines ($^1J_{\text{HP1}} = 512 \text{ Hz}$, $^1J_{\text{HP2}} = 510 \text{ Hz}$, $^3J_{\text{P1P2}} = 14 \text{ Hz}$), the highly trifluoromethylated diphosphine **31** (**Figure 5.8**) showed one signal in the region of the phosphine oxides and another one in the region of protonated phosphines ($^1J_{\text{H-P}} = 480\text{-}490 \text{ Hz}$) in 1:1 ratio. The broadness of the signals did not allow measuring the coupling constant with precision.

These observations suggested that diphosphine **30** is completely protonated in a sulfuric medium. On the contrary, when **31** is dissolved in sulfuric acid, the species formed is a half-protonated and half-oxidised phosphine (**Scheme 5.12**). The inability of the highly trifluoromethylated diphosphine **31** to be fully protonated, and thus to be protected, explains why this diphosphine was completely oxidised in contact with sulfuric fuming acid. Moreover, the fact that diphosphine **30** was diprotonated in sulfuric acid excludes steric hindrance as the reason why **31** was not protonated, and further supports low basicity of the phosphorus atoms as the main reason of this effect.



Scheme 5.12. Reaction of diphosphine **30** and **31** in sulfuric acid. Ar = 3,5-bis(trifluoromethyl)benzene

According to the NMR experiments, the highly trifluoromethylated diphosphine **31** can only be protonated when one of the phosphorus atoms is oxidised. Hydrogen bonding between the oxygen atom in the oxidised phosphine and the acidic proton on the other phosphorus would stabilise the half-protonated species observed in the NMR. To proof this idea, the previous NMR experiments were reproduced replacing sulfuric acid to triflic acid, which in addition to be more acidic ($-H_0 = 14.6$ vs 11.9 for sulfuric), is less oxidant than sulfuric acid. The NMR spectra (**Figure 5.9**) confirmed our hypothesis.

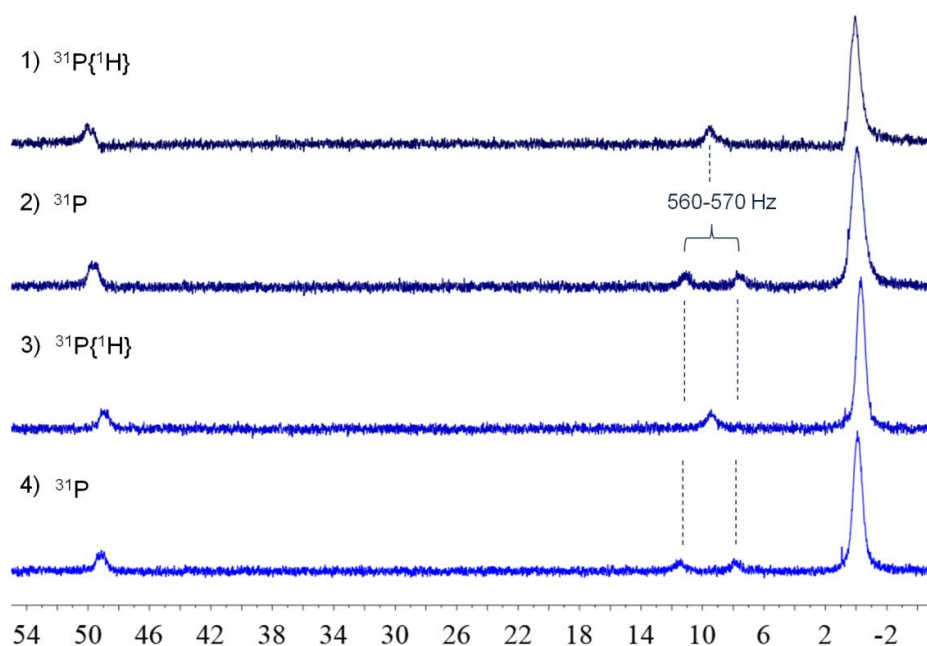


Figure 5.9 ^{31}P and $^{31}\text{P}\{^1\text{H}\}$ NMR spectra (161.98 MHz) of diphosphine **31** in triflic acid without boric acid (spectra -1- and -2-) and with boric acid (spectra -3- and -4-). Signals relative to NH_4PF_6 (-144.45 ppm) used as internal standard. δ in ppm. No other signals than those shown in the image were observed (excluding those signals for the internal standard). See text for detailed experimental conditions

The main phosphorus product observed in the NMR spectra was the non-protonated phosphine (*ca.* 0.1 ppm). Unlike the previous experiments in sulfuric acid, in triflic acid only a small fraction of the diphosphine was found as protonated phosphine ($^1J_{\text{HP}} = 560\text{-}570$ Hz). The ratio between the protonated phosphine and the oxide was again 1:1, pointing to the formation of the monoprotated-monoxidated species. In spite of the fact that triflic acid is more acidic than sulfuric acid, the amount of protonated phosphine found in the experiment was much lower than that found in the previous experiment with sulfuric acid. Therefore it seems quite reasonable to consider that the protonation of the phosphine is driven by the previous oxidation of one of the phosphorus atoms. With respect to boric acid, as observed in the experiments in sulfuric acid, it did not appear to have an important effect under the experimental conditions assayed. The ^{11}B NMR analysis of the sample containing diphosphine **31**, triflic acid and boric acid showed the formation of two boron species (**Figure 5.10**).

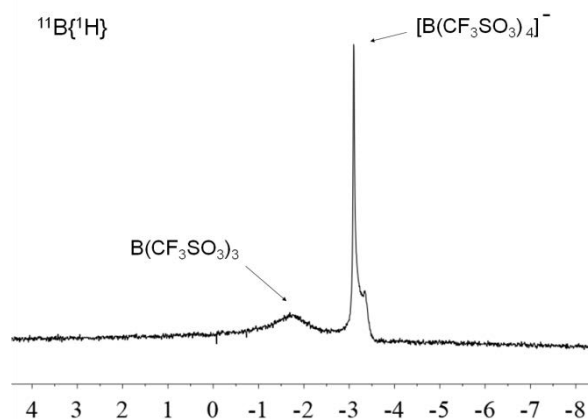
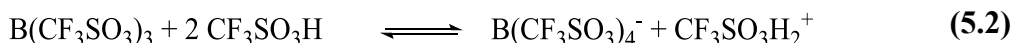


Figure 5.10. $^{11}\text{B}\{^1\text{H}\}$ NMR spectrum (128.38 MHz) of the mixture composed by triflic acid, boric acid and diphosphine **31** (corresponding to spectra **-3-** and **-4-** in **Figure 5.9**). δ in ppm. Signals relative to $\text{BF}_3 \cdot \text{Et}_2\text{O}$ (0.0 ppm) used as external standard

In analogy to sulfuric acid, triflic acid reacts with boric acid to form boron tris(triflate), $\text{B}(\text{CF}_3\text{SO}_3)_3$, and tetrakis(triflate)boron acid, $\text{HB}(\text{CF}_3\text{SO}_3)_4$, equation **5.1**. In an excess of triflic acid, this species is able to protonate the acid with the formation of the superacid species $\text{CF}_3\text{SO}_3\text{H}_2^+ \text{-B}(\text{OSO}_2\text{CF}_3)_4^-$, equation **5.2**. Therefore, in the $^{11}\text{B}\{^1\text{H}\}$ NMR spectra, the broad signal at -1.7 ppm corresponds to the less symmetric species boron, $\text{B}(\text{CF}_3\text{SO}_3)_3$, and the sharp singlet at -3.1 ppm corresponds to the more symmetric, $\text{CF}_3\text{SO}_3\text{H}_2^+ \text{-B}(\text{OSO}_2\text{CF}_3)_4^-$.³⁷ In the same manner as the acidity of sulfuric acid is increased with the addition of boron tri(hydrogensulfate), the acidity of triflic acid can be increased by addition boron tris(triflate).³⁸ The presence of water due to the formation of the boron triflates by reaction with boric acid was likely to lower the acidity of the superacid system. By removing the water, we should be able to shift the equilibrium to the formation of $\text{HB}(\text{CF}_3\text{SO}_3)_4$.



In our efforts to protonate diphosphine **31**, dry $\text{B}(\text{OSO}_2\text{CF}_3)_3$ was synthesised by reacting boron trichloride with triflic acid following the reported procedure.³⁷ Next, 2 equivalents of triflic acid were added to form the derivative conjugate superacid $\text{CF}_3\text{SO}_3\text{H}_2^+ \text{-B}(\text{OSO}_2\text{CF}_3)_4^-$. This product was characterised by ^{11}B NMR showing a

³⁷ Olah, G. A.; Laali, K.; Farooq, O. *J. Org. Chem.* **1984**, *49* (24), 4591–4594.

³⁸ Olah, G. A.; Prakash, G. K. S.; Molnar, Á.; Sommar, J. *Superacid Chemistry*; John Wiley & Sons, Inc.: Hoboken, NJ, USA, **2009**. 2nd Ed

sharp singlet at -3.1 ppm, which matches the value reported in the literature³⁷ **Figure 5.11**).

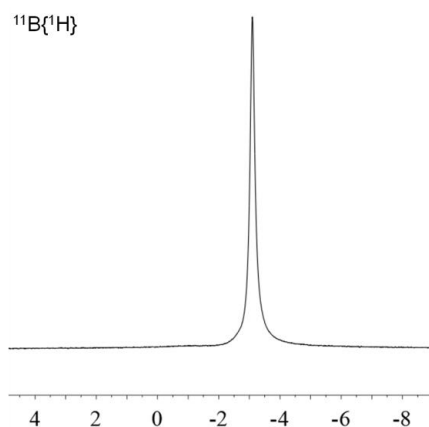


Figure 5.11. $^{11}\text{B}\{^1\text{H}\}$ NMR spectrum (128.38 MHz) of $\text{CF}_3\text{SO}_3\text{H}_2^+\text{-B}(\text{OSO}_2\text{CF}_3)_4^-$. δ in ppm. Signal relative to $\text{BF}_3\cdot\text{Et}_2\text{O}$ (0.0 ppm) used as external standard

According to the literature, a mixture of triflic acid with 22 mol% of boron tris(triflate) has a value of $-H_0$ of 18.5. Actually this is the highest value that could be measured for this system, although it is thought that, by extrapolation, a 40 mol% mixture would lead to a value of $-H_0$ of 20.³⁸ In that way, the $-H_0$ of the mixture we prepared in this experiment, which contain around 33 mol% of boron tris(triflate), should lie between 18.5 and 20.

The protonation of **31** was then attempted using the super acid mixture. About 0.03 g of the ligand was dissolved in 1 ml of the superacid and the resulted solution was analysed by ^{31}P NMR, **Figure 5.12**. Although the protonation of the phosphine was fully accomplished ($^1J_{\text{HP}} = 530$ Hz), no reaction of hydrolysis was observed. The NMR tube containing the crude reaction was analysed again after 4 days, showing no phosphorus signal at all. When the tube was opened, colourless bubbles came out from the reaction mixture, which could indicate complete degradation of the phosphine.

All in all, the results indicate that the protonation of diphos **31** requires extreme acidic conditions, which in turn would produce the decomposition of the phosphine.

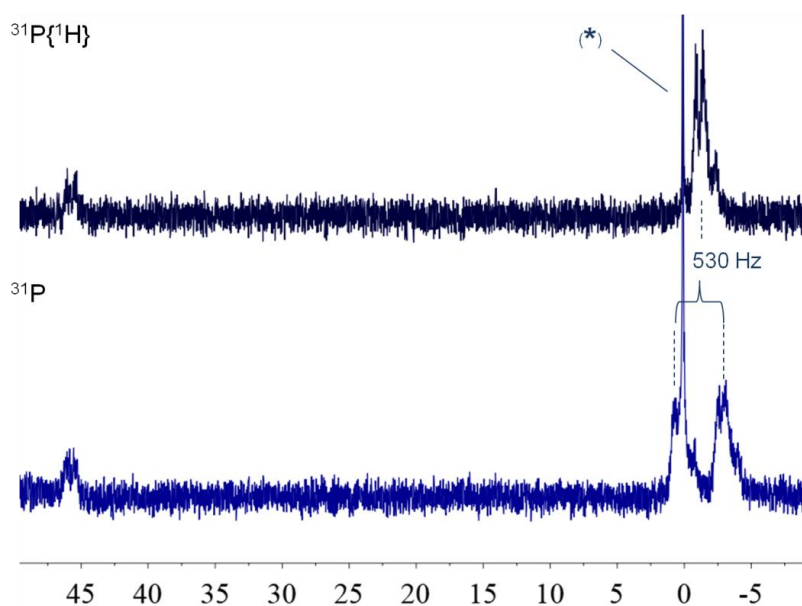


Figure 5.12. ^{31}P and $^{31}\text{P}\{^1\text{H}\}$ NMR spectra (161.98 MHz) of diphosphine **31** in the super acid $\text{CF}_3\text{SO}_3\text{H}_2^+ \text{B}(\text{OSO}_2\text{CF}_3)_4^-$. Signals relative to NH_4PF_6 (-144.45 ppm) used as internal standard. δ in ppm. No other signals than those shown in the image were observed (excluding those signals for the internal standard). (*) indicates the signal of phosphoric acid, produced by partial hydrolysis of the NH_4PF_6 .

5.3.2. Hydrolysis in of the trifluoromethyl group in diphosphine **32**

The trifluoromethylated diphosphine **32** was the last ligand used within the study of the scope of the reaction of hydrolysis of the trifluoromethyl group in arylphosphines.

In view of the previous experience with diphosphine **31**, first the protonation of **32** prior to the addition of oleum was studied. Therefore, the diphosphine was dissolved in concentrated sulfuric acid. The resulting mixture was then analysed by ^{31}P and $^{31}\text{P}\{^1\text{H}\}$ NMR, **Figure 5.13**. In the NMR spectra, two signals can be observed at 48.7 and 1.80 ppm, corresponding to an oxidised phosphorus atom and a protonated one ($^1J_{\text{HP}} = 547$ Hz), respectively, in 1:1 ratio. The effect of boric acid was also studied, in 0.3 M concentration, showing the same results. The ratio between the phosphine oxide and the protonated one, together with the absence of other signals, pointed to the formation of the monoxidated-monoprotonated species, as previously observed with diphosphine **31**.

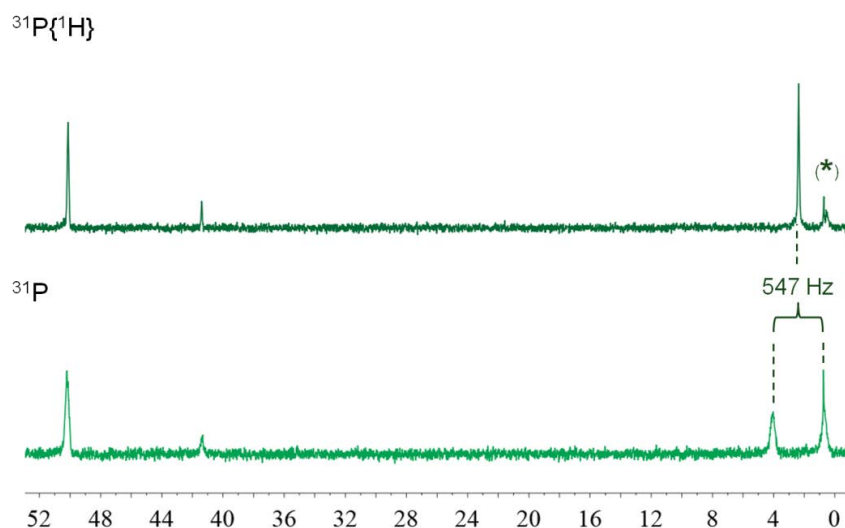


Figure 5.13. ^{31}P and $^{31}\text{P}\{^1\text{H}\}$ NMR spectra (161.98 MHz) of diphosphine **32** in sulfuric acid. Signals relative to NH_4PF_6 (-144.45 ppm) used as internal standard. δ in ppm. No other signals than those shown in the image were observed (excluding those signals for the internal standard). (*) indicates the signal of phosphoric acid, produced by partial hydrolysis of the NH_4PF_6 . [diphosphine] = 0.03 M.

Oleum (65 wt % SO_3) was then added to the solution of **32** in sulfuric acid and, after 2 h, the crude reaction mixture was analysed. Three different signals were observed in the NMR spectra at 75.6, 60.0 and 0.8 ppm, corresponding to the dioxide **ox-32**, and the monoxidised-monoprotonated species, **Figure 5.14**. This assignment was performed according to the NMR analysis of one aliquot of the reaction mixture quenched with water and extracted with Et_2O , which showed a mixture of **ox-32** and the monoxide derivative of **32**. The $^{19}\text{F}\{^1\text{H}\}$ NMR analysis of the crude reaction showed no hydrolysis of the trifluoromethyl group. When the mixture was analysed after 20 h from the addition of oleum, complete oxidation of the diphosphine was observed and only the dioxidised species was detected (75.6 ppm). $^{19}\text{F}\{^1\text{H}\}$ NMR did not show hydrolysis of the trifluoromethyl group. Analysis of the reaction mixture at 124 h showed no differences with respect to the observations at 20 h.

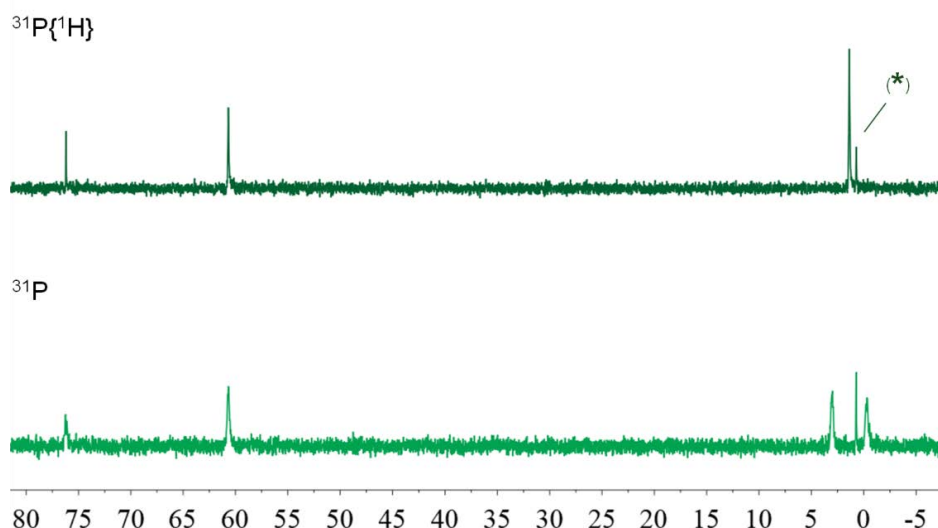


Figure 5.14. ^{31}P and $^{31}\text{P}\{^1\text{H}\}$ NMR spectra (161.98 MHz) of the reaction mixture in the hydrolysis of the CF_3 group in diphosphine **32** at 2 h of reaction. Signals relative to NH_4PF_6 (-144.45 ppm) used as internal standard. δ in ppm. No other signals than those shown in the image were observed (excluding those signals for the internal standard). (*) indicates the signal of phosphoric acid, produced by partial hydrolysis of the NH_4PF_6 . [diphosphine] = 0.01 M. $[\text{SO}_3]$ = 6.5 M.

Next, the protonation of the diphosphine was studied in $\text{CF}_3\text{SO}_3\text{H}$. In this case the ^{31}P and $^{31}\text{P}\{^1\text{H}\}$ NMR analysis of the solution did not show the presence of phosphine oxide, but only a signal corresponding to protonated phosphine was detected ($^1J_{\text{HP}} = 530$ Hz), **Figure 5.15**.

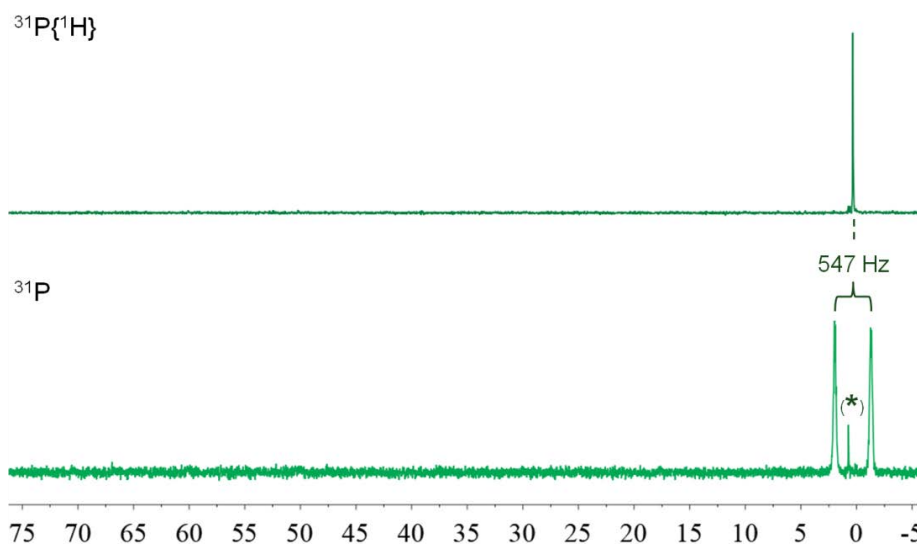


Figure 5.15. ^{31}P and $^{31}\text{P}\{^1\text{H}\}$ NMR spectra (161.98 MHz) of diphosphine **32** in triflic acid. Signals relative to NH_4PF_6 (-144.45 ppm) used as internal standard. δ in ppm. No other signals than those shown in the image were observed (excluding those signals for the internal standard). (*) indicates the signal of phosphoric acid, produced by partial hydrolysis of the NH_4PF_6 . [diphosphine] = 0.03 M.

Following the procedure performed above in sulfuric acid, oleum was added to the solution of diphosphine **32** in triflic acid. Generation of bubbles in the reaction mixture

was observed with time. When the mixture was analysed 1 h after the addition of oleum, only the dioxidised species was observed, **Figure 5.16**. The reaction was analysed again at 20 h and 124 h showing no differences in the $^{31}\text{P}\{^1\text{H}\}$ NMR spectra.

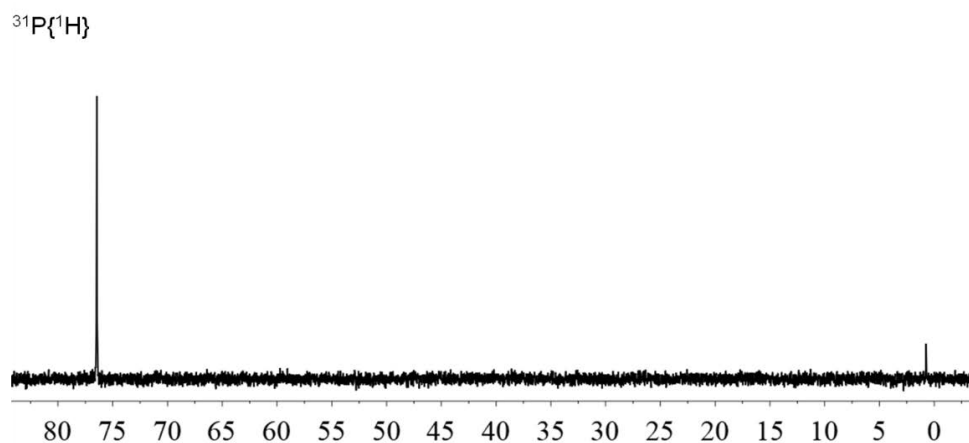


Figure 5.16. ^{31}P and $^{31}\text{P}\{^1\text{H}\}$ NMR spectra (161.98 MHz) of diphosphine **32** in triflic acid 1 h after the addition of oleum. Signals relative to NH_4PF_6 (-144.45 ppm) used as internal standard. δ in ppm. No other signals than those shown in the image were observed (excluding those signals for the internal standard). [diphosphine] = 0.01 M. $[\text{SO}_3] = 8.1$ M.

More information could be extracted from the $^{19}\text{F}\{^1\text{H}\}$ NMR, **Figure 5.17**. A singlet at 41 ppm, attributable to HSO_3F , is observed at 20 h, the intensity of which increases with time. This could indicate the hydrolysis of the CF_3 in the phosphine. However, a set of other signals the intensity of which also varies with time was observed (*ca.* -20, -54 and -57 and -73 ppm). Even though none of these additional signals could be certainly assigned, signal at -20 ppm can be tentatively attributed to acyl fluoride species in agreement to some heteroatom-substituted acyl fluoride derivatives reported in the literature such as carbonisocyanatidic fluoride ($\text{FC}(\text{O})\text{NCO}$) at -23.5 ppm,³⁹ fluorocarbonyl trifluoromethanesulfonate ($\text{FC}(\text{O})\text{OSO}_2\text{CF}_3$) at -13.6 ppm⁴⁰ and carbonyl fluoride ($\text{FC}(\text{O})\text{F}$) at -23 ppm.⁴¹ It is important to notice that the signals corresponding to the trifluoromethyl groups of the diphosphine oxide (*ca.* -65) did not evolve with time. Additionally, a blank experiment was performed by mixing the same volume of oleum and triflic acid, without diphosphine. In this experiment also bubbling was observed. Interestingly, similar pattern of signals was observed in the $^{19}\text{F}\{^1\text{H}\}$ NMR spectra regardless of the presence of the phosphine (*blank* in **Figure 5.17**). Therefore, in

³⁹ Haas, A.; Reinke, H. *Angew. Chem. Int. Ed.* **1967**, 6 (8), 705.

⁴⁰ Della Védova, C. O.; Downs, A. J.; Novikov, V. P.; Oberhammer, H.; Parsons, S.; Romano, R. M.; Zawadski, A. *Inorg. Chem.* **2004**, 43 (13), 4064–4071.

⁴¹ Dolbier, W. R. *Guide to Fluorine NMR for Organic Chemists*; John Wiley and Sons, 2008.

view of the results, it seems that triflic acid, in contact to oleum, would decompose with the generation of fluorosulfuric acid and acyl fluoride derivatives, amongst other fluorine species. In this process, the phosphine is oxidised and, in spite of the highly acidic conditions, no hydrolysis of the trifluoromethyl group of the diphosphine was observed.

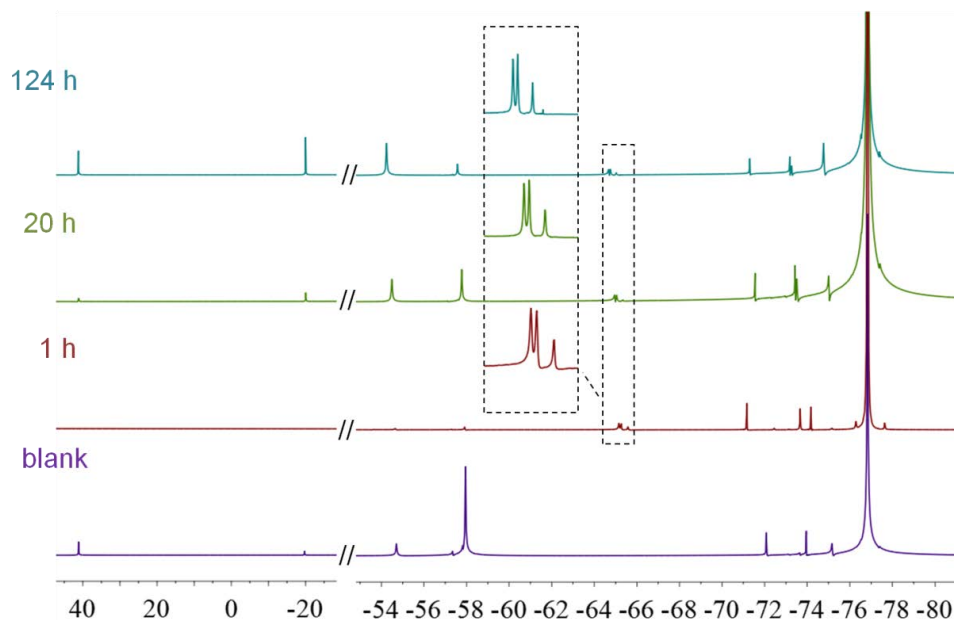


Figure 5.17. $^{19}\text{F}\{^1\text{H}\}$ NMR spectra. Evolution of the crude reaction with diphosphine **32** in a mixture of triflic acid and oleum at 1, 20 and 124 h and blank reaction (mixture of triflic acid and oleum). Signals relative to NH_4PF_6 (-72.65 ppm) used as internal standard. δ in ppm. No other signals than those shown in the image were observed (excluding those signals for the internal standard).
[diphosphine] = 0.01 M. $[\text{SO}_3] = 8.1$ M.

Summing up, sulfuric acid might not be acidic enough to protonate both phosphorus atoms in diphosphine **32**, with the consequent oxidation of the non-protonated phosphorus atom. Unlike diphosphine **31**, our observations seem to indicate that protonation of **32** does not require the previous oxidation of one phosphorus atom, but it simply would require stronger acidic conditions. This is supported by the complete protonation of the ligand in triflic acid. Nevertheless, this acid was neither able to protect the diphosphine from oxidation when oleum was added and the dioxidated form of diphosphine **32** was immediately obtained. Oxidation upon addition of oleum to the solution of **32** in sulfuric acid was found to be slower than in triflic acid, most probably due to an added stabilisation of the monoxide-monoprotonated-diphosphine. In either way, the hydrolysis of the trifluoromethyl group did not proceed substantially. In view of these observations and the previous results obtained with diphos **31**, the reaction of

hydrolysis of the trifluoromethyl group in the diphosphine **32** was not further investigated.

5.4. Electronic properties of the trifluoromethylated aryl diphosphines: preparation of the selenide derivatives

In analogy with the trifluoromethylated and the carboxylic monophosphines, the basicity of the trifluoromethylated diphosphines **31** and **32** was studied through the preparation of the corresponding selenides. Additionally, the selenides of dppbz and diphosphine **30** were also prepared.

With the non-trifluoromethylated dppbz and the monotrifluoromethylated diphosphine **30** the reaction of formation of the selenides proceeded without difficulties. 0.01 M solution of the corresponding diphosphine was stirred at 40 °C for 20 h with different amounts of selenium metal. While 1 mol of Se per mol of diphosphine provided mixtures composed of the monoselenide as major compound with variable amounts of unreacted diphosphine, the reaction using 3 mol of Se yielded the diselenide derivatives as main compound with variable quantities of monoselenide. **Figure 5.18** and **Figure 5.19** show the $^{31}\text{P}\{^1\text{H}\}$ NMR spectra of the corresponding mono and diselenides of **30**, respectively. As expected, a mixture of the two possible isomers of the monoselenide was observed. Also, signals of two non-equivalent phosphorus atoms are observed in the diselenide.

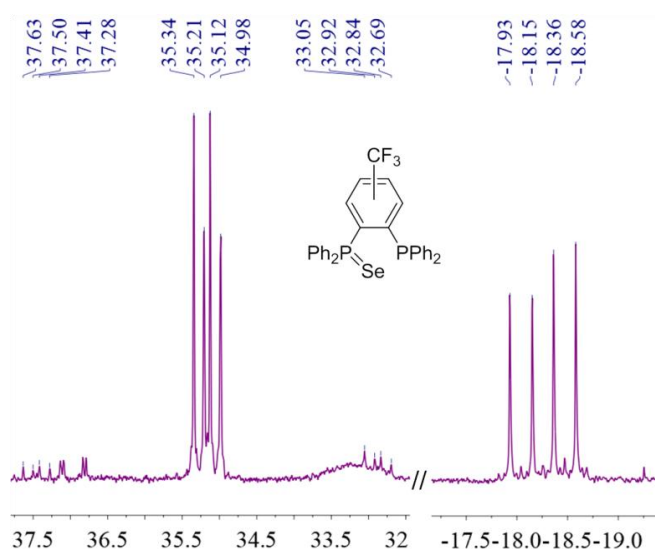


Figure 5.18. Signals of the monoselenides of diphosphine **30** in the $^{31}\text{P}\{^1\text{H}\}$ NMR spectra (161.98 MHz). δ in ppm. solvent CCl_3

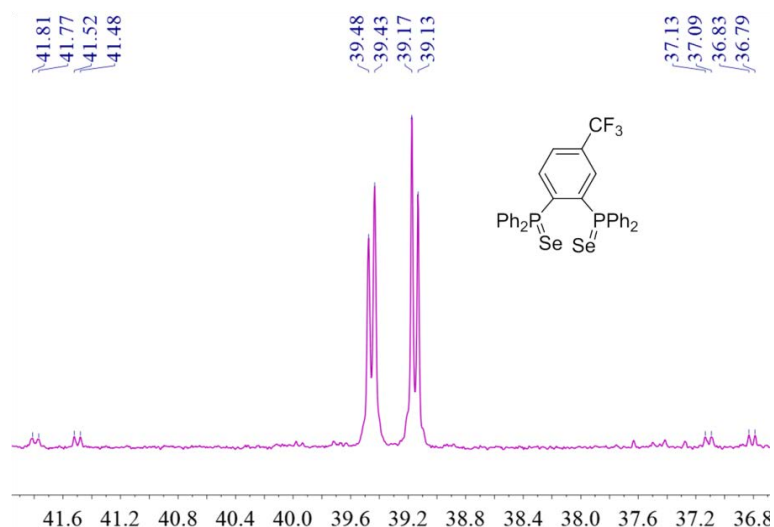


Figure 5.19. Signals of the diselenide of diphosphine **30** in the $^{31}\text{P}\{^1\text{H}\}$ NMR spectra (161.98 MHz). δ in ppm. Solvent CDCl_3

The preparation of the selenide derivatives of the trifluoromethylated diphosphines **31** and **32** required more drastic conditions. The use of stoichiometric amounts of selenium did not afford the monoselenides. In the case of the biphenylic diphosphine **32**, 0.01 M solution of the phosphine in chloroform was stirred at reflux with excess Se metal for 4 days to obtain a mixture of diselenide and monoselenide derivatives together with some unreacted phosphine. After 6 days under these conditions, the diselenide derivative was obtained as major compound, **Figure 5.20** and **Figure 5.21**, respectively.

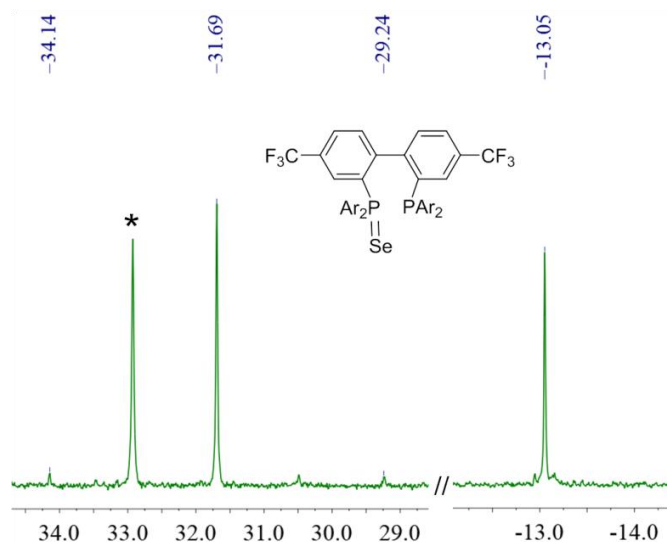


Figure 5.20. Signals of the monoselenide of diphosphine **32** in the $^{31}\text{P}\{^1\text{H}\}$ NMR spectra (161.98 MHz). δ in ppm. Solvent CDCl_3 . Signal marked with * in the spectrum corresponds to the diselenide. Ar = 3,5-bis(trifluoromethyl)benzene

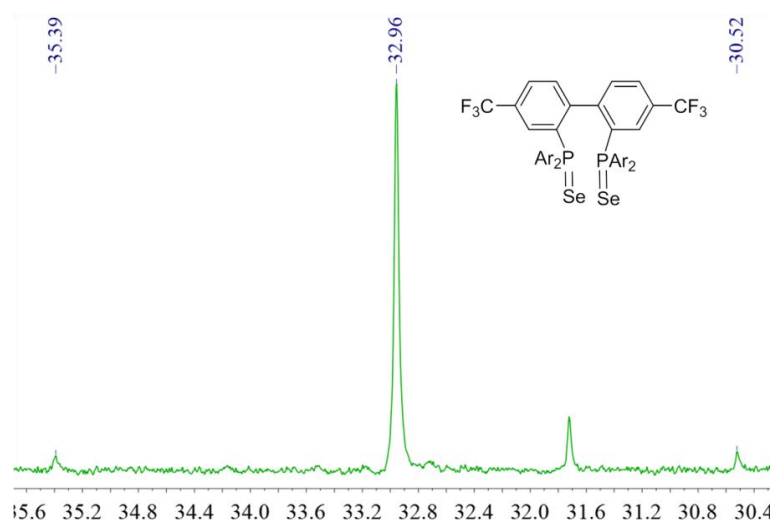


Figure 5.21. Signals of the diselenide of diphosphine **32** in the $^{31}\text{P}\{^1\text{H}\}$ NMR spectra (161.98 MHz). δ in ppm. Solvent CDCl_3 . Ar = 3,5-bis(trifluoromethyl)benzene

Under the same conditions (0.01 M, reflux in chloroform, excess Se), the formation of the monoselenide derivative of diphosphine **31** was observed after 4 days, **Figure 5.22**.

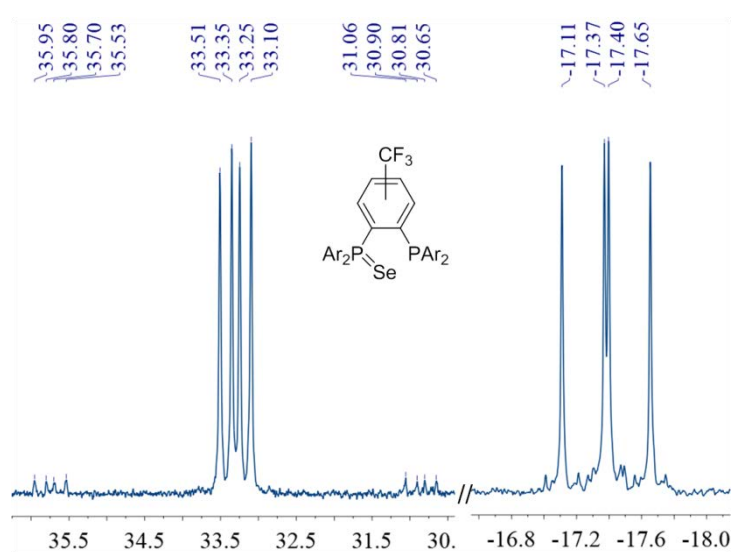
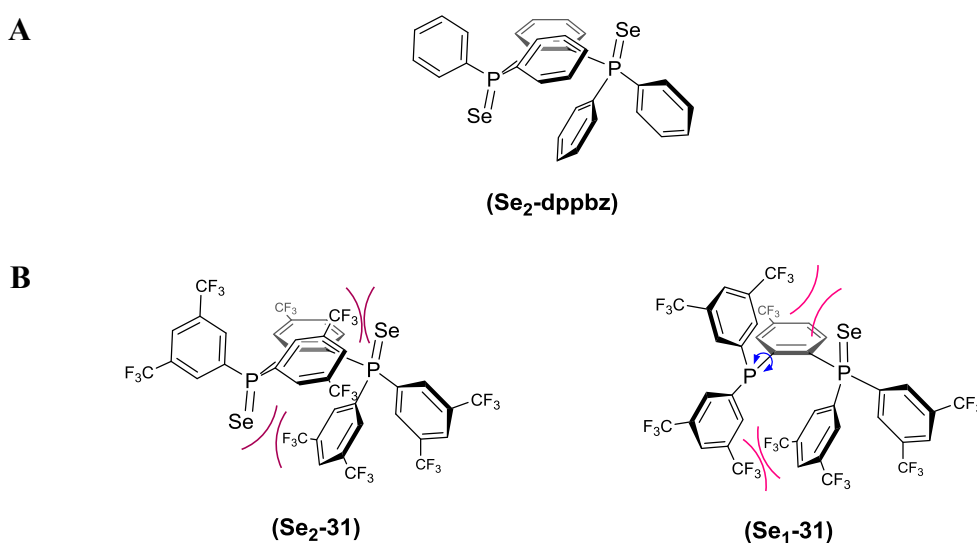


Figure 5.22. Signals of the monoselenide of diphosphine **31** in the $^{31}\text{P}\{^1\text{H}\}$ NMR spectra (161.98 MHz). δ in ppm. Solvent CDCl_3 . Ar = 3,5-bis(trifluoromethyl)benzene

Contrary to the other diphosphines, the diselenide derivative of **31** could not be obtained even after 1 week of reaction. Other solvents as acetone or methanol were tested with the same results. Suárez and Pizzano reported the formation of the diselenide derivative of phosphine-phosphite ligands of related structure,⁴² having $^1J_{\text{PSe}}$ of 1053-1061 Hz for the phosphite. Therefore, the σ -donor ability of diphosphine **31** might not be the main responsible for the apparently low reactivity of the ligand to form the diselenide and

⁴² Suárez, A.; Méndez-Rojas, M. A.; Pizzano, A. *Organometallics* **2002**, *21* (22), 4611–4621.

consequently sterics should be taken into account. Given the big radius of selenium, alternate configuration of dppbz diselenide ($\text{Se}_2\text{-dppbz}$) has been observed crystallographically, **Scheme 5.13-A**.⁴³ Molecular models show that such conformation of the diselenide derivative of **31** ($\text{Se}_2\text{-31}$) would be highly sterically constrained due to the interactions between the CF_3 groups and the selenium atoms, **Scheme 5.13-B**. Moreover, the structural conformation of the monoselenide ($\text{Se}_1\text{-31}$) itself would have restricted flexibility providing a sterically demanding environment for the phosphorus atom not attached to selenium. C-P bond rotation required to orientate the lone pair of the phosphorus atom to bond selenium would therefore be impeded.



Scheme 5.13. **A)** Representation of the conformation of the diselenide derivative of dppbz according to the X-ray structure.⁴³ **B)** Description of the steric interactions between the selenide atoms and the trifluoromethyl groups in the di- and monoselenide derivatives of **31**

As general trend, and as previously shown for trifluoromethylated monophosphines, the magnitude of the P-Se coupling constants in the selenides ($^1J_{\text{PSe}}$) increased with the number of trifluoromethyl groups (**Table 5.4**). The value for dppbz is in good agreement with literature.³⁵ Introducing one trifluoromethyl group in the dppbz structure (diphosphine **30**) results in an increase of 9 Hz in both the monoselenide and the diselenide. When comparing dppbz with the highly trifluoromethylated diphosphine **31**, a value of $^1J_{\text{PSe}}$ 61 Hz greater was observed in the monoselenides. The values of 3-bond P-P coupling ($^3J_{\text{PP}}$) are within the expected numbers for dppbz-related compounds.³⁵ The BIPHEP-derived phosphine **32** showed $^1J_{\text{PSe}}$ coupling constants similar to that of **31**. When compared to the structurally-related diphosphines, BINAP

⁴³ Tiedemann, M. A.; Mandell, C. L.; Chan, B. C.; Nataro, C. *Inorg. Chim. Acta* **2014**, *422*, 193–201.

and BIPHEP-derived compounds (**Scheme 5.14**), it was observed that the couplings follow the expected trend and greater values were obtained for the trifluoromethylated diphosphine **32**. Unfortunately no data for the monoselenides of these or other related diphosphines were found in the literature.

Table 5.4. ^{31}P - ^{77}Se coupling constant ($^1J_{\text{PSe}}$) and 3-bond P-P coupling constants in trifluoromethylated diphosphine selenides ^a

diphosphine	$^1J_{\text{PSe}}(\text{Se}_1)$ ^b	$^1J_{\text{PSe}}(\text{Se}_2)$ ^c	$^3J_{\text{PP}}$
dppbz	732	749	36.5 (Se ₁) / 7.3 (Se ₂)
30	741	758	35.5 (Se ₁) / 7.1 (Se ₂)
31	793	-	42.2
32	796	789	-
BINAP ^d	-	738	-
MeOBIPHEP ^e	-	743	-
3,5-(CF ₃) ₂ MeOBIPHEP ^e	-	782	-

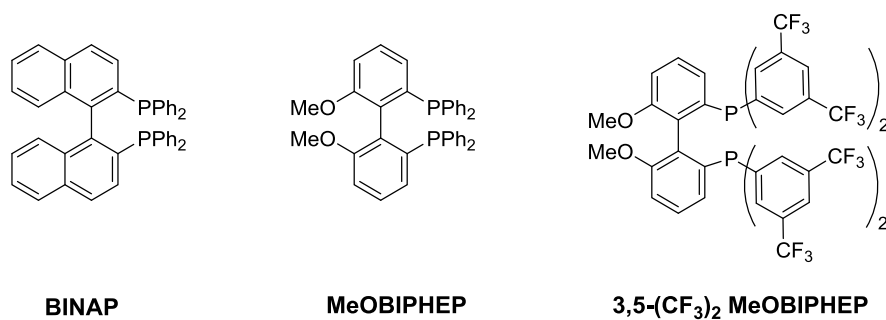
^a J in Hz. All coupling constants measured from $^{31}\text{P}\{^1\text{H}\}$ (161.98 MHz) in CDCl₃. ^b monoselenide.

^c diselenide. ^d Value from the literature.^{33c} ^e Value from the literature⁴⁴

Interestingly, differences in the values of mono- and diselenides were observed. Dependence of $^1J_{\text{PSe}}$ upon the degree of selenation could be an indicative of steric interactions due to repulsion between the P=Se groups. As stated by Beckmann *et al.*⁴⁵ these values of $^1J_{\text{PSe}}$ should be carefully used to measure the basicity of diphosphines. McFarlane's group reported variations of the $^1J_{\text{PSe}}$ in *polykis*(diphenylphosphino)benzenes depending on proximity of the phosphine groups.³⁵ In any case, a clear increase in $^1J_{\text{PSe}}$ was observed with increasing the number of trifluoromethyl groups in the diphosphines.

⁴⁴ Le Boucher, F.; Herouvi, F.; Mi, A.; Caon, M.; Michelet, V. *J. Org. Chem.* **2011**, 76 (16), 6925–6930.

⁴⁵ Beckmann, U.; Süslüyan, D.; Kunz, P. C. *Phosphorus. Sulfur. Silicon Relat. Elem.* **2011**, 186 (10), 2061–2070.



Scheme 5.14. BINAP and BIPHEP-derived diphosphines

5.5. Summary and concluding remarks

Two new trifluoromethylated diphosphines have been designed and successfully synthesised. In spite of the efforts invested in their preparation, the reaction of hydrolysis of the trifluoromethyl groups, under the essayed conditions, did not work on these diphosphines and partial or complete oxidation of the phosphines was observed instead. The hydrolysis of the CF₃ groups in the dppbz-derived phosphine **31** was essayed in the superacid CF₃SO₃H₂⁺-B(OSO₂CF₃)₄⁻ and, although protonation of the phosphine was achieved, the extreme acidic conditions produced the degradation of the phosphine. Additionally the π-acidity of the diphosphines was studied by means of the selenide derivatives.

The results obtained in this chapter, far from discourage us, were found to be of great importance to better understand how the reaction of hydrolysis of the trifluoromethyl group works in phosphines.

Chapter 6

Failed Synthetic Procedures in the Preparation of the Trifluoromethylated Diphosphines

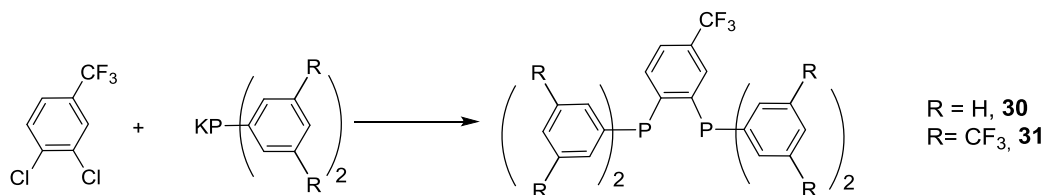
6.1. Introduction

During the synthesis of the trifluoromethylated diphosphines **31** and **32** described in the previous chapter, some of the synthetic approaches essayed did not yield the desired compounds. However, these reactions still provided valuable information about the reactivity of some synthetic intermediates. Moreover, in a few instances, these unsuccessful synthetic routes afforded the preparation of new chemicals. Therefore, these mistakenly called “negative results” might be indeed considered useful pieces of information for future researchers in the area.

Obviously, negative results can sometimes be attributed to experimental mistakes. In this sense, this chapter will only cover those experiments that, although not giving the expected results, were reproducible.

6.2. Failed procedures in the synthesis of diphosphine **31**

The synthesis of diphosphine **31** was unsuccessfully attempted by means of a nucleophilic aromatic substitution (S_NAr). This synthetic procedure was firstly applied to the preparation of diphosphine **30**, **Scheme 6.1**, which was used as a cheap model before the application of the procedure for **31**. In this way, the reaction between the inexpensive and commercially available 3,4-dichlorobenzotrifluoride and potassium diphenylphosphide afforded **30**. However, the preparation of diphosphine **31** by the same route was hampered by difficulties arising from the synthesis of the trifluoromethylated phosphide.



Scheme 6.1. S_NAr between potassium diphenylphosphides and 3,4-dichlorobenzotrifluoride

For this first trial in the synthesis of **30**, 3,4-dichlorobenzotrifluoride was used as precursor of the phosphine backbone. Even though fluoro-derivatives are generally

more reactive and they are normally preferred for the S_NAr ,¹ in this case, the chlorinated derivative was more available and still reactive enough in front of a good nucleophile as diphenylphosphide. Following a modification of the reported procedure used in our group in the synthesis of *P,N*-donor ligands,² two equivalents of potassium diphenylphosphide in THF were added dropwise to a solution of 3,4-dichlorobenzotrifluoride in diethyl ether at -84 °C. Once the addition had finished, the reaction mixture was allowed to warm up to room temperature before being refluxed overnight. $^{31}P\{^1H\}$ NMR analysis of the crude reaction mixture showed the formation of the desired product **30** (-13.5 ppm) as the major phosphorus compound in the mixture. The second most intense signal, found at -9.9 ppm, was attributed to the monosubstituted phosphine in *para* with respect to the trifluoromethyl group. Such assignation was made according to the previous observations with the brominated equivalent compounds, **p28** and **p29**. The remaining signals in the NMR spectrum corresponded to tetradiphenyldiphosphine monoxide ($Ph_2P-P(O)PPh_2$) (two doublets at -22.0 and 36.5 ppm, $^1J_{PP} = 228$ Hz)³ and diphenylphosphine ($HPPH_2$) (-40.0 ppm) that were detected as minor impurities, **Figure 6.1**.

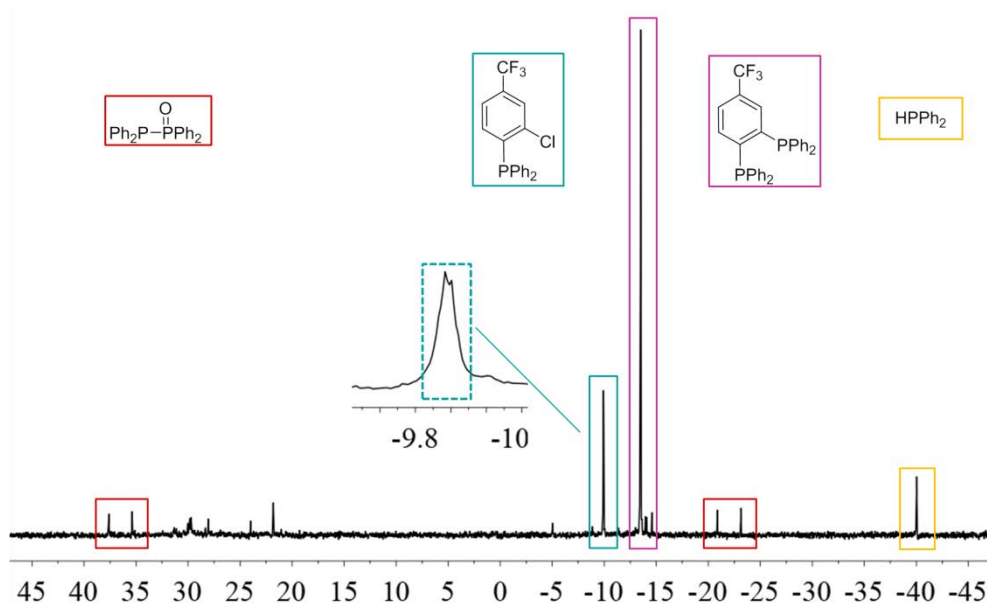


Figure 6.1. $^{31}P\{^1H\}$ NMR spectrum (101.2 MHz) of the crude reaction between 3,4-dichlorobenzotrifluoride and diphenylphosphide. Solvent: $CDCl_3$. δ in ppm

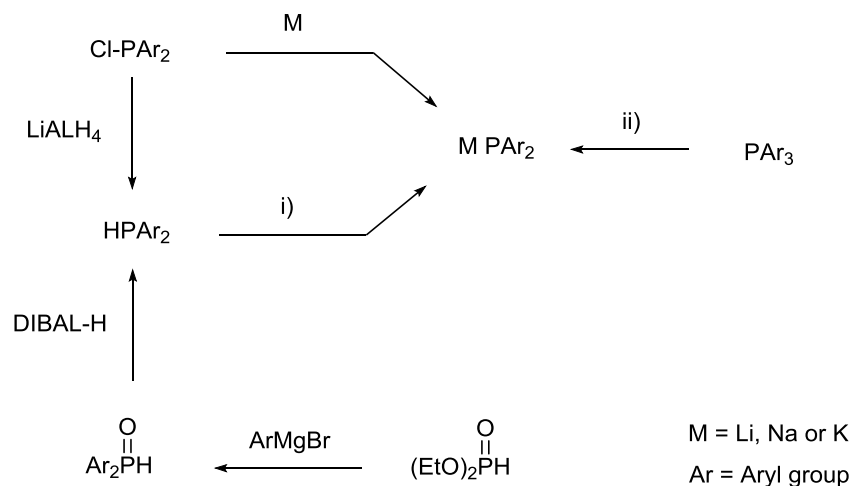
¹ Carey, F. A.; Sundberg, R. J. Chapter 9: Aromatic Substitution. In *Advanced Organic Chemistry. Part A: Structure and Mechanisms*; Springer, Boston, MA, **2007**. 5th ed. pp 817-819

² Aguirre, P. A.; Lagos, C. A.; Moya, S. A.; Zúñiga, C.; Vera-Oyarce, C.; Sola, E.; Peris, G.; Bayón, J. C. *Dalton Trans.* **2007**, No. 46, 5419–5426.

³ Ding, M.; Stille, J. K. *Macromolecules* **1983**, *16* (6), 839–843.

Once the reaction was proven to be suitable to obtain the diphosphine **30**, the procedure was attempted in the preparation of diphosphine **31**.

Direct methods for the synthesis of diarylphosphides, including the direct reaction between the chlorodiarylphosphine and an alkali metal, have been described in the literature, **Scheme 6.2**.



Scheme 6.2. General synthesis of alkali diarylphosphides.

i) Different reagents: alkali metal (Li, Na or K); *n*-BuLi; *t*-BuOK; LDA; KH

ii) Different conditions: Li/THF; Na/THF; Na/NH₃(l)

The reaction of a diarylphosphine with either an alkali metal⁴ or a strong base such as *n*-Buli and *t*-BuOK,^{4a} lithium diisopropylamide (LDA)⁵ or KH⁶ has been widely used to prepare alkali diphenylphosphides as well as the trifluoromethylated equivalent. This method, though, needs the previous preparation of the diarylphosphine, which can be synthesised from the reduction of a chlorodiarylphosphine with lithium aluminium hydride⁶ or by reduction of a diarylphosphine oxide using diisobutylaluminium hydride (DIBAL-H).⁷ At the same time, diarylphosphine oxide can be prepared from diethyl phosphite and a Grignard reagent.⁸ Alternatively, diarylphosphides can be prepared by

⁴ a) Ashby, E. C.; Gurumurthy, R.; Riddlehuber, R. W. *J. Org. Chem.* **1993**, *58* (21), 5832–5837. b) Brusentsev, Y.; Eklund, P. *Catal. Today* **2015**, *241*, 260–263. c) Yu, I.; Wallis, C. J.; Patrick, B. O.; Mehrkhodavandi, P. *Organometallics* **2009**, *28* (21), 6370–6373.

⁵ Mustafa, S.; Venanzi, L. M.; Gerfin, T.; Gramlich, V. *Inorg. Chim. Acta* **1998**, *270* (1–2), 499–510.

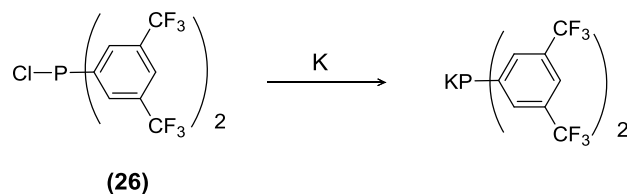
⁶ Casey, C. P.; Lin Paulsen, E.; Beuttenmueller, E. W.; Proft, B. R.; Petrovich, L. M.; Matter, B. A.; Powell, D. R. *J. Am. Chem. Soc.* **1997**, *119* (49), 11817–11825.

⁷ Busacca, C. A.; Lorenz, J. C.; Grinberg, N.; Haddad, N.; Hrapchak, M.; Latli, B.; Lee, H.; Sabila, P.; Saha, A.; Sarvestani, M.; Shen, S.; Varsolona, R.; Wei, X.; Senanayake, C. H. *Org. Lett.* **2005**, *7* (19), 4277–4280.

⁸ Busacca, C. A.; Lorenz, J. C.; Sabila, P.; Haddad, N.; Senanayake, C. H. *Org. Synth.* **2007**, *84*, 242–261.

reductive cleavage of the C-P bond in triarylphosphines using an alkali metal. This procedure has been reported using different reducing agents such as Na/NH₃, Li/THF⁹ and Na/THF.¹⁰ Although successfully applied to triphenylphosphine and other substituted triarylphosphines, the reaction does not work when applied to the trifluoromethylated triarylphosphines, namely 4-tris(trifluoromethylphenyl)phosphine (**1**) and 3-tris(trifluoromethylphenyl)-phosphine (**5**).^{9a} The authors correlated the calculated LUMO energies and coefficients to the experimental results, concluding that triarylphosphines substituted with electron-withdrawing groups cannot undergo P-C bond cleavage. This result was corroborated in our group.¹¹ Reaction of Li/THF with 2-tris(trifluoromethylphenyl)phosphine (**9**) or 3,5-tris(trifluoromethylphenyl)phosphine (**14**) did not yield the corresponding diarylphosphides, but the starting triarylphosphines were recovered.

Although the direct synthesis of alkali diphenylphosphides by reaction of chlorodiphenylphosphine with lithium,¹² sodium¹³ or potassium¹⁴ has been reported, as far as we concern, no references for the synthesis of alkali trifluoromethylated diarylphosphides using this reaction has been described. In spite of the lack of precedents, it was decided to test the reaction given its simplicity in performance (**Scheme 6.3**).



Scheme 6.3. Reaction of formation of the trifluoromethylated phosphide from **26** and K metal

⁹ a) Budzelaar, P. H. M.; van Doorn, J. A.; Meijboom, N. *Recl. Trav. Chim. Pays-Bas* **1991**, *110* (10), 420–432. b) van Doorn, J. A.; Meijboom, N. *Recl. Trav. Chim. Pays-Bas* **1992**, *111* (4), 170–177.

¹⁰ Kang, L.; Chen, J.; Teng, T.; Chen, X.-L.; Yu, R.; Lu, C.-Z. *Dalt. Trans.* **2015**, *44* (25), 11649–11659.

¹¹ Peral Crespo, D. *Triarilfosfines Sulfonades Trifluorometilades. Aplicacions en Processos Catalitics*. Ph.D. Thesis. Universitat Autònoma de Barcelona, **2013**.

¹² a) Leone-Bay, A. *J. Org. Chem.* **1986**, *51* (12), 2378–2379. b) Stepanova, V. A.; Dunina, V. V.; Smoliakova, I. P. *Organometallics* **2009**, *28* (22), 6546–6558.

¹³ a) Ashby, E. C.; Deshpande, A. K. *J. Org. Chem.* **1995**, *60* (22), 7117–7124. b) Cao, K.; Tsang, B.; Liu, Y.; Chelladural, D.; Power, W. P.; Wang, X. *Organometallics* **2014**, *33* (2), 531–539.

¹⁴ Baker, B. A.; Bošković, Ž. V.; Lipshutz, B. H. *Org. Lett.* **2008**, *10* (2), 289–292.

According to the reported synthesis of potassium diphenylphosphide,¹⁴ the trifluoromethylated chlorophosphine **26** was added dropwise to a suspension of K, previously cut into small pieces, in dry THF at room temperature. It was necessary to reflux the mixture to start observing a red colouring on the K surface, indicating the formation of the phosphide. After two hours, an orange-red solution was obtained together with the formation of a green-greying precipitate. A reaction sample was quenched with water and extracted three times with diethyl ether. The organic phase was then analysed by ^{31}P and $^{31}\text{P}\{^1\text{H}\}$ NMR showing a complex mixture of phosphorous compounds, **Figure 6.2**.

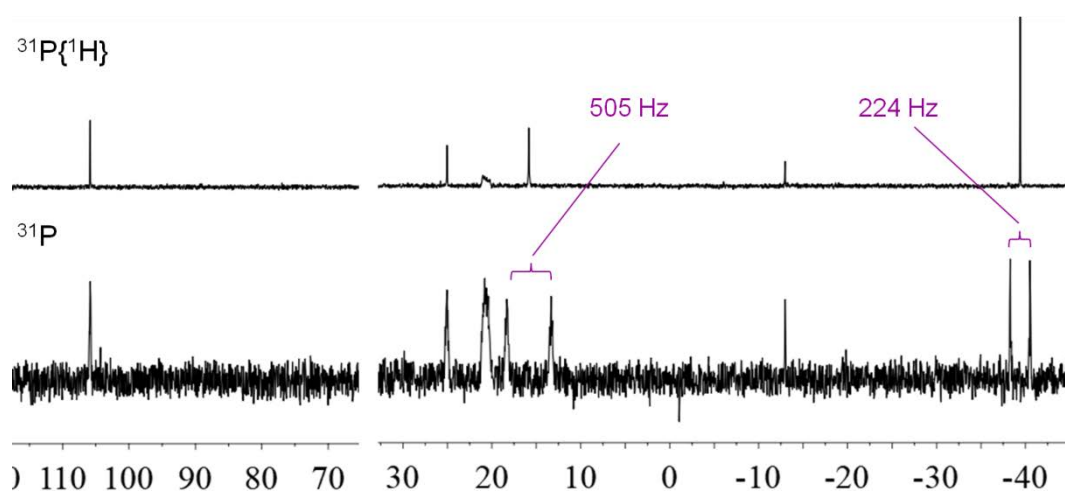
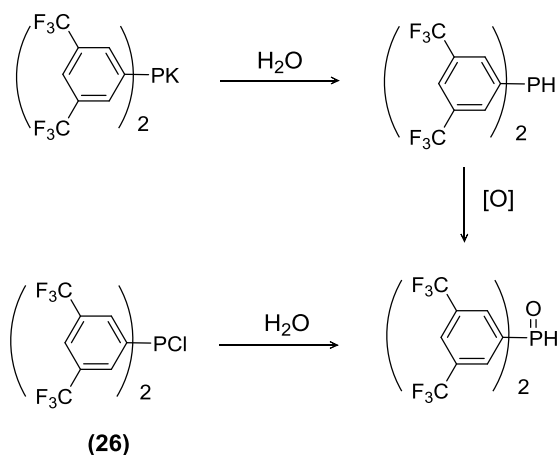


Figure 6.2. $^{31}\text{P}\{^1\text{H}\}$ (top) and ^{31}P NMR (bottom) spectra (101.2 MHz) of the reaction between potassium and the trifluoromethylated chlorophosphine **26**. Sample quenched with water and extracted with Et_2O previous to the NMR analysis of the organic phase. Solvent: CDCl_3 . δ in ppm

Although up to six different signals were observed in the NMR spectrum, only two of them were identified according to their chemical shifts and the $^1J_{\text{HP}}$: bis(3,5-bis(trifluoromethyl)phenyl)phosphine and its oxide (*ca.* -40 and -15 ppm, respectively). While the former is unambiguously produced by reaction of the phosphide with water, the latter can be obtained by either oxidation of the diarylphosphine or by the reaction of the chlorophosphine **26** with water, **Scheme 6.4**. Refluxing for longer time did not produce any change in the composition of the reaction mixture products. Neither the addition of 3,4-dichlorobenzotrifluoride afforded **31**. The reaction was essayed twice obtaining the same results in both experiments.

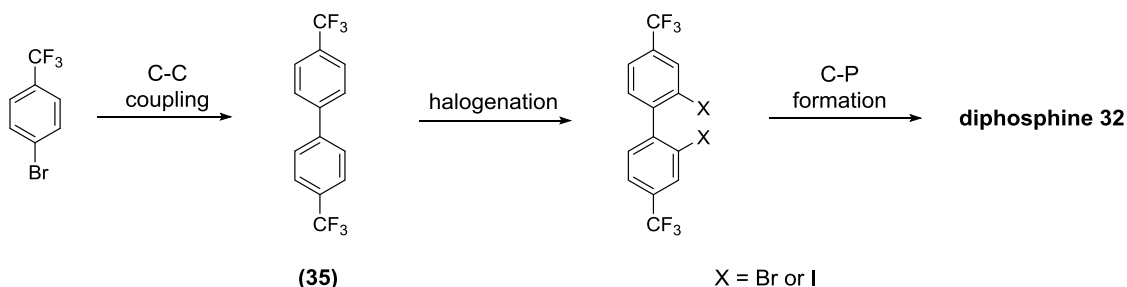


Scheme 6.4. Reaction of formation of the trifluoromethylated diarylphosphine and its oxide

In spite of the wide variety of methodologies reported for the synthesis of diarylphosphides, these syntheses require greater number of reaction steps than the direct reaction between an alkali metal and the corresponding chlorophosphine and thus lower global yields are expected. Consequently, this strategy aside was left aside. The alternative approach described in the previous chapter, which finally afforded the diphosphines **30** and **31**, was then tested.

6.3. Failed procedures in the synthesis of diphosphine **32**

As previously introduced in chapter 5, diphosphine **32** was satisfactorily prepared starting by 4-(trifluoromethyl)bromobenzene by means of a first reaction of halogenation followed by C-P formation reaction and a final C-C coupling reaction. However, the preparation of **32** was also attempted by applying the same chemical transformation, but in a different sequence order, **Scheme 6.5**.



Scheme 6.5. Proposed synthesis of diphosphine **32**

According to the title of this chapter, the ending of this synthetic procedure can be foreseen. In the following lines the different steps of this synthesis will be described,

explaining which of them could be implemented and understanding where this procedure failed.

The first step is the synthesis of the trifluoromethylated biphenyl, 4,4'-bis(trifluoromethyl)biphenyl (**35**), starting from 4-(trifluoromethyl)bromobenzene. Different approaches have been described in the literature for the C-C homocoupling of haloarenes. Amongst them, one interesting methodology consists on the formation of a Grignard derivative followed by the reaction with a transition metal chloride and the subsequent oxidation to obtain the coupled product,¹⁵ **Scheme 6.6**.



Scheme 6.6. General reaction of homocoupling of arylmagnesium halides (Grignard) with transition metal halides

Although the homocoupling of arylmagnesium halides in the presence of transition metal halides, which serve at the same time as catalyst precursor and oxidant, was firstly reported in 1939,¹⁶ currently it is possible to find more efficient applications of the reaction using different transition metal halides and oxidants such as CuBr/dinitroarenes,¹⁷ CoCl₂/dry air,¹⁸ MnCl₂/1,2-dichloroethane¹⁹ or FeCl₃/dry air.²⁰ It was this last methodology that called our attention due to its relative simplicity and the use of iron as convenient, cheap and environmentally friendly catalyst. Therefore, following the reported synthesis with the FeCl₃/dry air system,²⁰ **35** was prepared from 4-(trifluoromethyl)bromobenzene, **Scheme 6.7**. After the preparation of the Grignard derivative in THF, anhydrous FeCl₃ (5 mol%) was added resulting in the rapid formation of a black gel mixture. Then dry air was bubbled through the solution. After 1 hour the reaction was quenched with 10 % aqueous HCl and extracted with ethyl

¹⁵ Seyferth, D. The Grignard Reagents. *Organometallics*. 2009, pp 1598–1605.

¹⁶ Gilman, H.; Lichtenwaltr, M. *J. Am. Chem. Soc.* **1939**, *61* (4), 957–959.

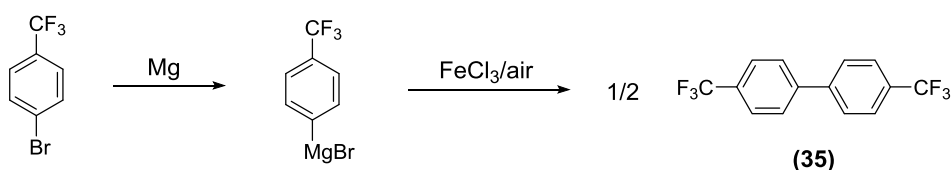
¹⁷ Surry, D. S.; Su, X.; Fox, D. J.; Franckevicius, V.; Macdonald, S. J. F.; Spring, D. R. *Angew. Chem. Int. Ed.* **2005**, *44* (12), 1870–1873.

¹⁸ Chen, S. Y.; Zhang, J.; Li, Y. H.; Wen, J.; Bian, S. Q.; Yu, X. Q. *Tetrahedron Lett.* **2009**, *50* (49), 6795–6797.

¹⁹ Zhou, Z.; Xue, W. *J. Organomet. Chem.* **2009**, *694* (5), 599–603.

²⁰ Cahiez, G.; Moyeux, A.; Buendia, J.; Duplais, C. *J. Am. Chem. Soc.* **2007**, *129* (45), 13788–13789.

acetate, washed with brine and dried with MgSO_4 obtaining a red powder suspension. The filtration of this suspension was found to be rather challenging. Sintered-glass filter, or this filter with either a layer of silica gel or Celite, rapidly clogged because of the red powder. Filter paper seemed to give better results, although it had to be replaced several times during the process. All in all, resulted in hardly 10 % isolated yield, compared to the 70 % of conversion according to the GC-FID analysis of the reaction mixture previous to the purification. This was the reason why another procedure was tested.

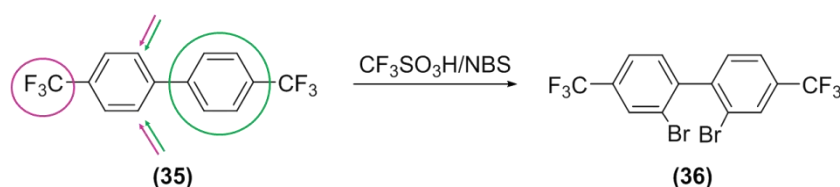


Scheme 6.7. Reaction of homocoupling with FeCl_3/air to prepare **35**

In conjunction with the use of more environmentally friendly procedures, the C-C coupling was essayed using *in situ* formed Pd-nanoparticles in water with glucose as reducing agent, as reported by Monopoli *et.al.*²¹ Due to the immiscibility of the aryl derivative in water, this Ullmann-type homocoupling reaction requires tetrabutylammonium hydroxide as phase-transfer agent and as base. In comparison with the previous trial using FeCl_3 , this synthesis utilises a more expensive catalyst, such as $\text{Pd}(\text{AcO})_2$. Nevertheless, several advantages might be noted. Since no Grignard compound has to be synthesised, there is no need to work under strict water free conditions. In fact water is used as reaction mixture which, together with the use of glucose as reducing agent, makes the reaction greener. In summary, the process became simpler and easier in terms of product purification. Although the synthesis was originally reported using 3 mol% Pd catalyst and temperatures between 40 and 60 °C for 6 h, it was found that the catalyst amount could be reduced to 1.2 mol% while increasing the reaction temperature and time to 115 °C and 40 h, respectively. Under these conditions it was possible to scale the reaction using up to 49.8 mmol of 4-bromobenzotrifluoride and affording **35** in 61 % isolated yield.

²¹ Monopoli, A.; Calò, V.; Ciminale, F.; Cotugno, P.; Angelici, C.; Cioffi, N.; Nacci, A. *J. Org. Chem.* **2010**, 75 (11), 3908–3911.

Once the biaryl backbone of the diphosphine **32** was obtained, the next step to follow in the synthetic route was the bromination of **35**. Given that aryl groups behave as *ortho* and *para*-directing groups and trifluoromethyls are *meta*-directing, the electrophilic aromatic substitution of this biphenyl derivative using triflic acid ($\text{CF}_3\text{SO}_3\text{H}$)/*N*-bromosuccinimide (NBS), as used previously in the bromination of 4-(trifluoromethyl)bromobenzene, should yield the brominated biphenyl with the expected pattern of substitution, **Scheme 6.8**.



Scheme 6.8. Bromination of **35**. Coloured arrows indicate the directing effect of the CF_3 and the aryl group in the electrophilic aromatic substitution

The evolution of the reaction between **35** and $\text{CF}_3\text{SO}_3\text{H}/\text{NBS}$ was monitored by GC. It is worth mentioning that the slow addition of NBS to the reaction mixture was found to be of great importance in order to reduce the amount of tribromination. Slow addition of NBS and in small portions together with the use of high dilution was helpful to obtain **36** with only 6 % of tribrominated product according to GC (**Figure 6.3**). Separation of the two brominated compounds was performed by distillation.

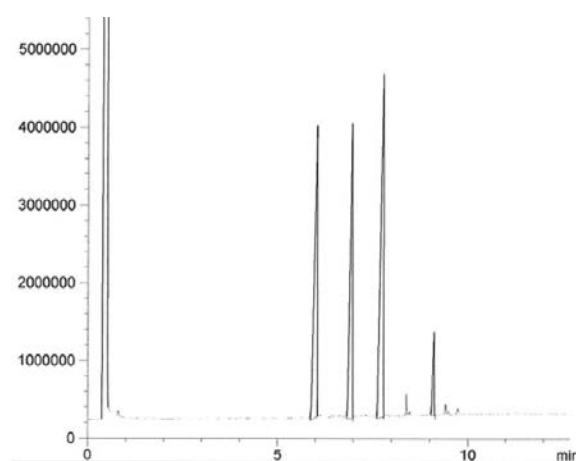


Figure 6.3. GC-FID analysis of the bromination of **35**. Example containing the 3 brominated compounds together with the starting material. Peaks at 6.031, 6.959, 7.768 and 9.108 min corresponding to **35**, monobrominated product, **36** and tribrominated product, respectively. Peak assignment was made according to GC-MS

At this point, the Li/Br exchange reaction between the dibrominated biaryl **35** and *n*-BuLi was performed. Complete formation of the dilithio derivative was obtained after addition of 2 equivalents of *n*-BuLi to a solution of **36** in THF at -84 °C, according to the GC-FID chromatogram of a sample quenched with water (only trifluoromethylbenzene was detected). Following, the addition of two equivalents of the trifluoromethylated chlorodiarylphosphine (**26**), would have been the most simple and straightforward way to prepare diphosphine **32**. However, this reaction did not yield pure **32**. Instead, a complex mixture of phosphorus compounds was obtained, **Figure 6.4**.

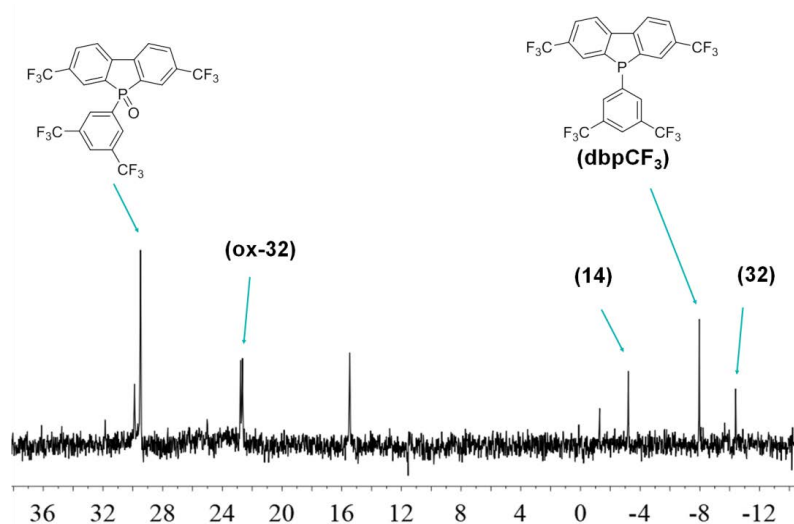
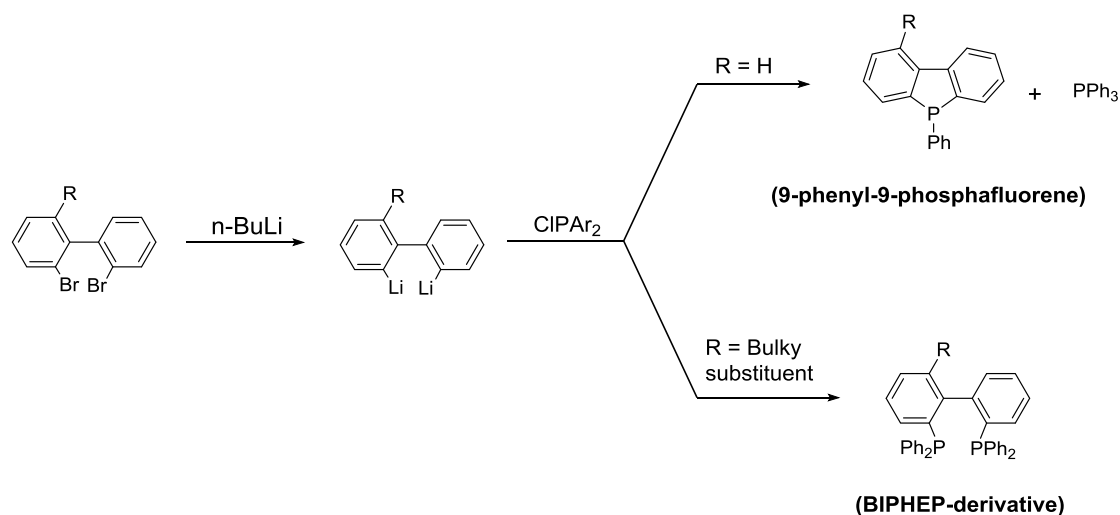


Figure 6.4. $^{31}\text{P}\{^1\text{H}\}$ NMR spectra (101.2 MHz) of the reaction between the product of Br/Li exchange in **36** and the trifluoromethylated chlorophosphine **26**. δ in ppm. Solvent: CDCl_3 . No other signals were detected

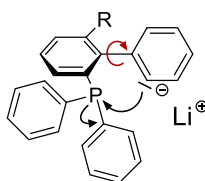
Among this blend of compounds, diphosphine **32** and its oxide (**ox-32**) were identified, together with the 3,5- CF_3 -homoleptic phosphine (**14**). Signals at -8.0 ppm and 29.5 ppm were tentatively attributed to the trifluoromethylated dibenzophosphole (**dbpCF₃**) and its oxide, respectively, according the literature.²² Other signals in the NMR spectrum could not be identified. It is worth noticing that neither unreacted chlorophosphine (**26**) nor its product of hydrolysis were observed.

²² van Kalker, H. A.; Leenders, S. H. A. M.; Hommersom, C. R. A.; Rutjes, F. P. J. T.; Van Delft, F. L. *Chem. Eur. J.* **2011**, *17* (40), 11290–11295.



Scheme 6.9. Reaction products formed by reaction of 2,2'-biphenyldilithium derivatives and chlorophosphines

It has been reported that the reaction between 2,2'-dilithiobiphenyls and chlorodiarylphosphines to form bis(diphenylphosphino)-biphenyls works only when the biphenyl rotation is blocked, **Scheme 6.9**. On the contrary, the reaction between chlorodiphenylphosphine and 2,2'-biphenyldilithium gives an equimolar amount of 9-phenyl-9-phosphafluorene and triphenylphosphine instead of BIPHEP ligand.²³ Furthermore, the yield towards the diphosphine increases when bulky substituents in 6-position are used²⁴ or using less bulky substituents in 6,6'-positions.²³ Otherwise, the small torsion angle of the biphenyl favours the intramolecular nucleophilic substitution at the phosphorus atom of the monophosphorylated intermediate giving rise to the elimination of phenyl lithium, **Scheme 6.10**.^{23,25} Unfortunately, the trifluoromethylated biphenyl **35** was not an exception of the rule.



Scheme 6.10. Formation of a dibenzophosphole by intramolecular substitution of the monophosphorylated intermediate, according to the literature.²³ The reaction can be suppressed by including a bulky R group in the biphenyl structure

²³ Desponds, O.; Schlosser, M. *J. Organomet. Chem.* **1996**, 507 (1–2), 257–261.

²⁴ Bonnafoux, L.; Gramage-Doria, R.; Colobert, F.; Leroux, F. R. *Chem. Eur. J.* **2011**, 17 (39), 11008–11016.

²⁵ Leroux, F. R.; Mettler, H. *Adv. Synth. Catal.* **2007**, 349 (3), 323–336.

In view of these results, the efforts were focused on finding an alternative synthetic procedure to prepare the diphosphine **32**, as it is described in the previous chapter.

Chapter 7

Applications of the Miranphos and Miran2phos Ligands

7.1. Chelating diphosphines supported on latex particles

Previous considerations

This part of the work was carried out in collaboration with the group of Prof. Dieter Vogt in the University of Edinburgh. While the synthesis and characterization of the ligands, which will be shown in this chapter, was mainly performed in Barcelona, most of the catalytic experiments and all of the *in situ* studies using these ligands were performed in the facilities of the University of Edinburgh. Computational studies of the bite angle were also performed in Barcelona. All of these experiments were carried out by the author of the present work.

The preparation of the latex particles were gently performed by Dr. Daniel Peral at the Technische Universität Berlin.

7.1.1. Introduction and objectives

As it is well known, one of the most important drawbacks of homogeneous catalysis is the final separation of the reaction products from the catalyst. Different approaches have been used to solve this problem, such as biphasic catalytic systems¹ or the anchoring of molecular catalyst to solid supports.² Nevertheless, both strategies show some drawbacks. For instance, biphasic systems are not efficient when the substrate is not soluble enough in the phase which contains the catalyst, whereas solid supported catalysts often show problems related to substrate diffusion into the solid phase and leaching of the catalyst. Other methodologies, which can be described as half way between the mentioned strategies, have been essayed. For instance, in the so-called SAPC (Supported Aqueous Phase Catalyst), developed by Davis' group,³ the water-soluble catalyst is dissolved in a film of water which is supported on the surface of a hydrophilic solid.

¹ Adams, D. J.; Dyson, P. J.; Tavener, S. J.; Chapter 2: Multiphasic Solvent System. In *Chemistry in Alternative Reaction Media*; John Wiley & Sons, Ltd: Chichester, UK, **2005**; pp 33–56.

² a) Sandee, A. J.; van Der Veen, L. A.; Reek, J. N. H.; Kamer, P. C. J.; Lutz, M.; Spek, A. L.; van Leeuwen, P. W. N. M. *Angew. Chem. Int. Ed.* **1999**, *38* (21), 3231–3235. b) Li, C.; Wang, W.; Yan, L.; Ding, Y. *Front. Chem. Sci. Eng.* **2018**, *12* (1), 113–123.

³ Arhancet, J. P.; Davis, M. E.; Merola, J. S.; Hanson, B. E. *Nature* **1989**, *339*, 454–455.

More recently, great efforts have been focused towards the research of greener and more environmentally friendly catalytic processes involving water as the only solvent in the reactions.⁴ In this sense, different approaches have been developed to overcome mass transfer limitations of those poorly water-soluble substrates. Amongst others,⁵ water-dispersible polystyrene-based lattices have been proven to be suitable platforms not only as phase-transfer agents, increasing the interface between aqueous media and the organic substrates, but also as catalyst support allowing the recovering and recycling of the rather expensive catalysts.⁶ The features of the Miranphos ligands previously studied in the present work make them particularly good candidates for this kind of applications. On the one hand, trifluoromethyl groups confer to the phosphines a higher resistance towards the oxidation,⁷ an important feature when catalyst recycling is considered. On the other, the carboxylic functionality is chemically versatile, it being easy to convert this group into a derivative such as an ester or an amide functionality, which is a useful tool when supporting molecules to different solid matrices such as silica⁸ or, as in our case, to a latex surface. Furthermore, it is important to bear in mind that trifluoromethyl-containing phosphines have also been proved to enhance the activity of some transition metal-based catalytic processes.^{7,9,10}

⁴ Dixneuf, P. H.; Cadierno, V; *Metal-Catalyzed Reactions in Water*; Wiley-VCH Verlag GmbH & Co. KGaA: Weinheim, Germany, **2013**.

⁵ for general review about the state of the art in the hydroformylation of alkenes, see: a) Obrecht, L.; Kamer, P. C. J.; Laan, W. *Catal. Sci. Technol.* **2013**, *3*, 541–551. b) Sharma, S. K.; Jasra, R. V. *Catal. Today* **2015**, *247*, 70–81.

⁶ a) Kunna, K.; Müller, C.; Loos, J.; Vogt, D. *Angew. Chem. Int. Ed.* **2006**, *45*, 7289–7292. b) Nowothnick, H.; Rost, A.; Hamerla, T.; Schomäcker, R.; Müller, C.; Vogt, D. *Catal. Sci. Technol.* **2013**, *3*, 600–605. c) Cardozo, A. F.; Julcour, C.; Barthe, L.; Blanco, J.-F.; Chen, S.; Gayet, F.; Manoury, E.; Zhang, X.; Lansalot, M.; Charleux, B.; D'Agosto, F.; Poli, R.; Delmas, H. *J. Catal.* **2015**, *324*, 1–8. d) Lobry, E.; Cardozo, A. F.; Barthe, L.; Blanco, J. F.; Delmas, H.; Chen, S.; Gayet, F.; Zhang, X.; Lansalot, M.; D'Agosto, F.; Poli, R.; Manoury, E.; Julcour, C. *J. Catal.* **2016**, *342*, 164–172.

⁷ Peral, D.; Herrera, D.; Real, J.; Flor, T.; Bayón, J. C. *Catal. Sci. Technol.* **2016**, *6* (3), 800–808.

⁸ Chen, C.; Shao, X.; Yao, K.; Yuan, J.; Shangguan, W.; Kawaguchi, T.; Shimazu, K. *Langmuir* **2011**, *27* (19), 11958–11965.

⁹ a) Palo, D. R.; Erkey, C. *Organometallics* **2000**, *19* (1), 81–86. b) Koeken, A. C. J.; van Vliet, M. C. A.; van den Broeke, L. J. P.; Deelman, B.-J.; Keurentjes, J. T. F. *Adv. Synth. Catal.* **2008**, *350* (1), 179–188.

¹⁰ Peral Crespo, D. *Triarilfosfines Sulfonades Trifluorometilades. Aplicacions en Processos Catalitics*. Ph.D. Thesis. Universitat Autònoma de Barcelona, **2013**.

7.1.2. Design and synthesis of the chelating ligands

Synthetically speaking, the anchoring of the Miranphos ligands to the latex surface cannot be performed directly. It is first necessary the derivatisation of the ligand to include the proper chemical moiety previous to being anchored. If it is true that interaction between the ligand and the latex particles can be of electrostatic nature, such as sulfonated phosphines with ammonium-modified surfaces,^{6a} covalent bounding of the ligands has also been successfully reported.^{6c,11} Given the structure of the Miranphos ligands and our previous experience on the functionalisation of silica particles with amide derivatives of these ligands,¹² we decided to use the covalent approach.

Latex particles are generally formed by radical polymerization of alkenes such as isoprene or styrene. It is also common to add a small percentage of dienes, such as 1,4-divinylbenzene, as cross-linker during the synthesis of the rubbers. Therefore, including a styrene moiety in the phosphine structure seemed the most reasoning way as anchoring point which would eventually react together with the latex monomers to form the final functionalised latex.

At this point, two different approaches to prepare the Miranphos-modified latex were considered: monophosphine or diphosphine approach, **Figure 7.1**. The first one consists on the direct anchoring of the Miranphos ligand without any other modification than the introduction of the styrene moiety. In contrast, the second option consists on going a step further and firstly prepare a chelating diphosphine from the Miranphos ligands which will eventually be supported on the polymer surface. Whether to use a monophosphine or a diphosphine was decided on the assumption that a supported system resembles a high dilution situation in which the ligands will be ideally highly dispersed over the latex surface. With monophosphines the coordination of more than one ligand to a metal centre is unlikely to happen thus providing different coordination environments in the reaction media. However, the chelating diphosphine system will ideally provide a single coordination environment and, at the same time, a more robust metal coordination compared to the monophosphine, thus reducing the metal leaching,

¹¹ Shibahara, F.; Nozaki, K.; Matsuo, T.; Hiyama, T. *Bioorganic Med. Chem. Lett.* **2002**, *12* (14), 1825–1827.

¹² Herrera Miranda, D. *Síntesis de Nuevas Triarilfosfinas Carboxiladas Mediante Hidrólisis del Grupo Trifluorometilo. Aplicaciones en Catálisis de Intercambio de Fase y Anclaje Sobre Silica*. Master's Thesis. Universitat Autònoma de Barcelona, **2012**.

an important factor when catalyst recycling is concerned. Furthermore, the coordination and catalytic performance of the diphosphines could be studied in a homogeneous system by preparing the equivalent ligand without the anchoring point. Therefore, despite being a more elaborate approach from the synthetic point of view, the diphosphine route was proposed to covalently anchor the Miranphos ligands to latex particles due to its coordination and stability advantages.

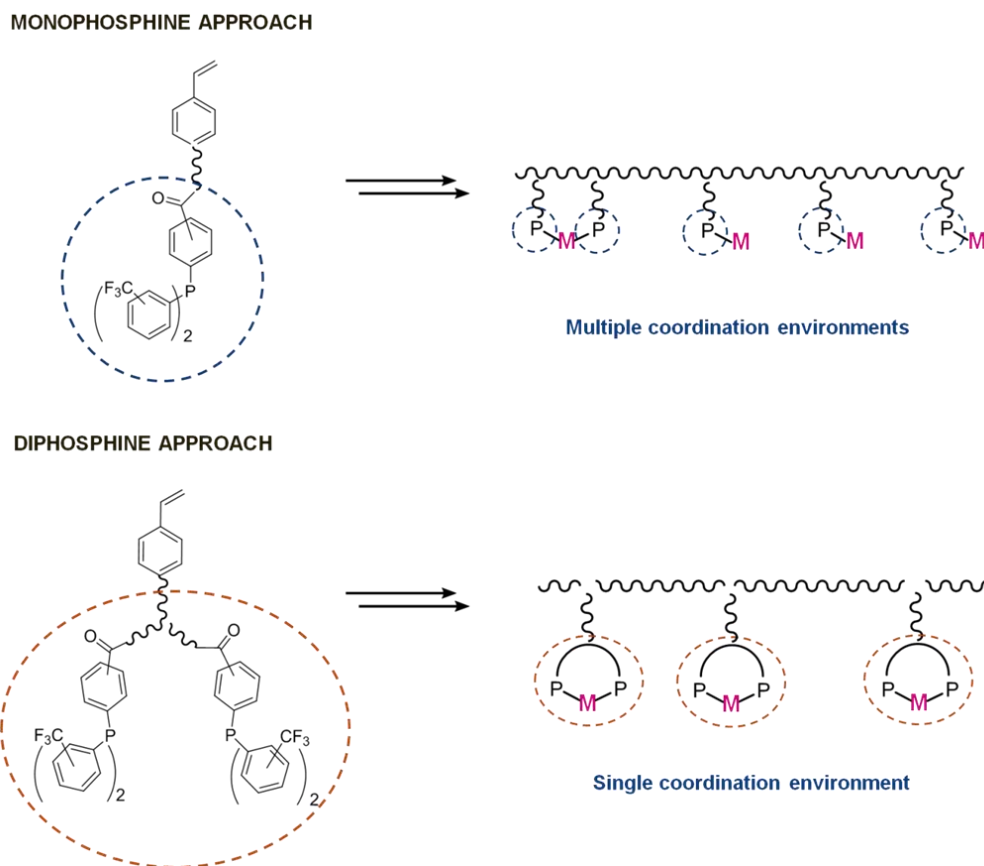


Figure 7.1. Schematic representation of the monophosphine approach vs the diphosphine approach in the latex-supported phosphines

The general structure of the Miranphos-derived diphosphines is depicted in **Chart 7.1**. As ligand backbone, diethylenetriamine (**37**) was chosen. Apart from being a non-expensive and commercially available compound, this amine shows several advantages. First of all, the phosphines are linked by means of the formation of amide bonds, which are robust chemical bonds and inert under a wide range of conditions. Secondly, the different chemical reactivity of the primary and secondary amine allows, after a set of protection and deprotection reactions, to build up the final structure of the diphosphine. While the two primary amine groups serve as linking point for the phosphines, the secondary amine is the point at which the styrene-like moiety is introduced. Moreover,

the distance between the phosphorus atoms is an important factor as well. While a long chain backbone will produce overly flexible molecules which would possibly behave as non-chelating ligands, excessively short backbone would yield rather rigid and non-chelating diphosphine ligands as well. On a first sight, the chain length of diethylenetriamine, although apparently being quite flexible, could be long enough to provide a suitable chelating diphosphine. Preliminary Molecular Mechanics experiments were in agreement with the previous statement.

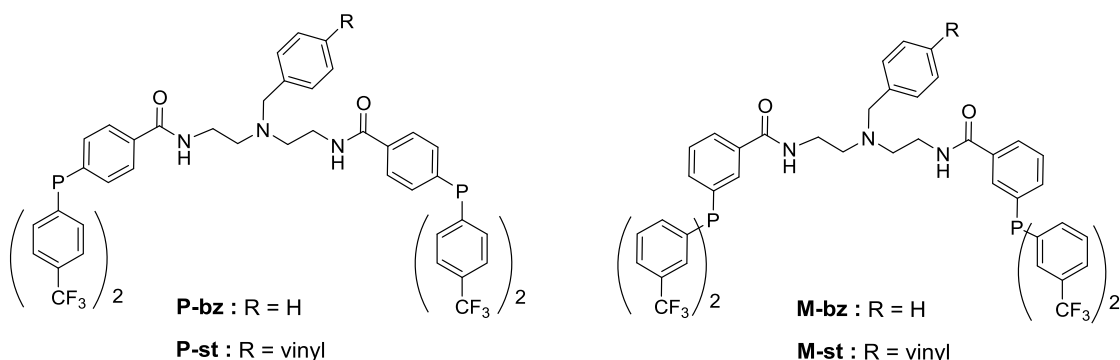
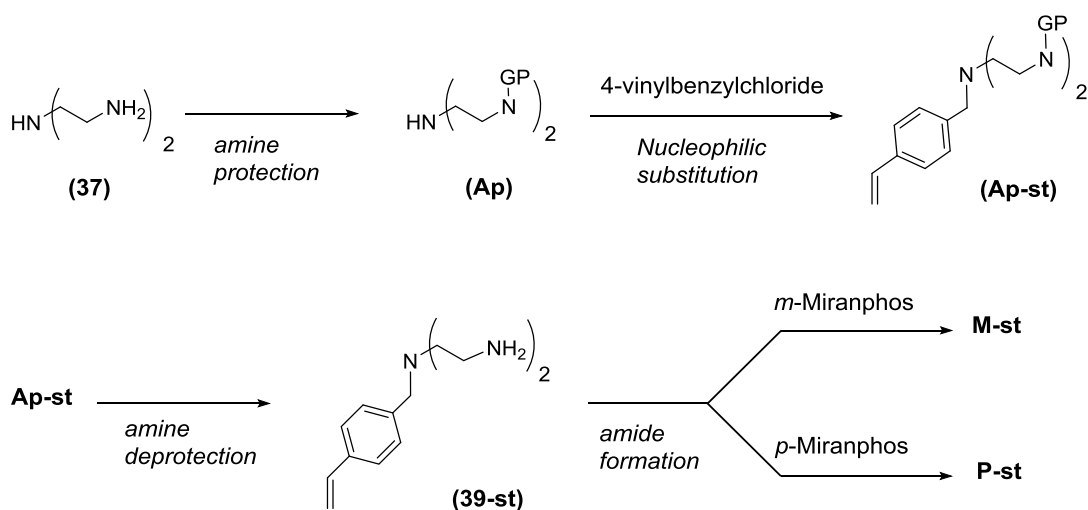


Chart 7.1. General structure for the Miranphos-derived diphosphines

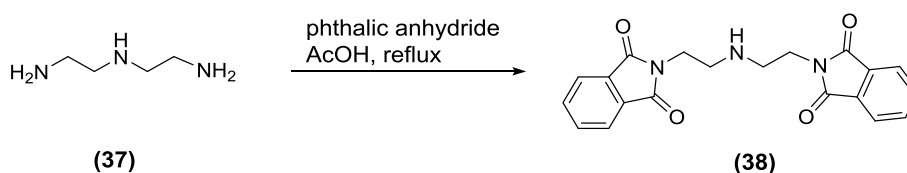
The general reaction procedure for the synthesis of the diphosphines is shown in **Scheme 7.1**. The first step of the synthesis of the ligands consists in the protection of the primary amine groups in the diethylenetriamine (**37**). Afterwards, the protected amine (**Ap**) will be reacted with 4-vinylbenzyl chloride through a nucleophilic substitution. Then, after the deprotection of **Ap-st**, the reaction between the benzylic amine (**39-st**) and the Miranphos ligand will yield final diphosphines, **P-st** and **M-st**.



Scheme 7.1. General reaction scheme proposed to synthesise the diamide-diphosphines

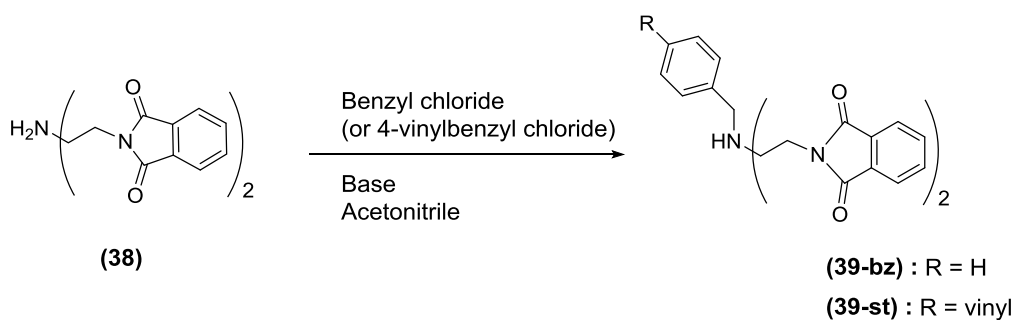
In order to optimize the process, the non-vinyl derivative, benzyl chloride, was used since it is much cheaper and easier to handle than the vinyl derivative. Moreover the non-vinyl phosphines, **P-bz**, and **M-bz**, will be used to study the properties of the ligand in homogeneous conditions.

Firstly, the triamine was protected by reaction of the primary amine groups with phthalic anhydride in glacial acetic acid (**Scheme 7.2**). The phthalimide protected amine, **38**, was obtained as white powder.



Scheme 7.2. Reaction of protection of the primary amine groups of **37**

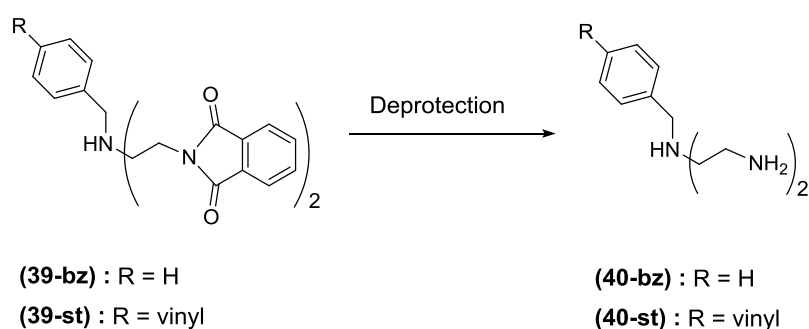
The nucleophilic attack of the secondary amine to benzyl chloride in acetonitrile afforded the benzylamine **39-bz** (**Scheme 7.3**). Two different bases, triethylamine and potassium carbonate, were essayed in this reaction, as well as the use of NaI as catalyst to activate the electrophile. It was observed that while the reaction using potassium carbonate as base yielded almost quantitatively the final product in less than 17 h, the reaction using triethylamine resulted in only 36 % conversion according to the ^1H NMR analysis after the same reaction time. It was also observed that sodium iodide had not an important role in accelerating the reaction. The reaction was also successfully applied with 4-vinylbenzyl chloride to yield **39-st**.



Scheme 7.3. Nucleophilic substitution between benzyl chloride and the protected amine **38**

The next step in the synthesis was the deprotection to obtain the diamine **40-bz**, **Scheme 7.4**. In a first attempt, the hydrolysis of the phthalimide-protected amine **39-bz** was essayed using concentrated solution of hydrochloric acid, as previously reported in the

literature.¹³ After stirring **39-bz** in concentrated hydrochloric acid at 65 °C for 16 h, the reaction mixture was treated with NaOH to pH 7 and then extracted with ethyl acetate and evaporated before being analysed by ¹H NMR. No deprotection was observed through this method. Before changing the reaction conditions, a simple experiment was performed to study the compatibility between hydrochloric acid and the vinyl group. 4-vinylbenzyl chloride was stirred at 65 °C in concentrated hydrochloric acid for 17 h. The analysis of the reaction mixture showed the product of the HCl addition to the vinyl group in agreement with Markovnikov's rule, thus indicating a different deprotecting method had to be used.



Scheme 7.4. Deprotection of the phthalimide-protected amine

One should bear in mind that the reaction will be eventually used to prepare the styrene derivative compound. Since these compounds tend to polymerise if not handled carefully our efforts were focused on finding procedures which imply rather soft conditions and simple and straightforward purification steps. In this sense the reaction was carried out following a modification of the procedure described in the literature.¹⁴ The protected amine was stirred at reflux in a mixture of EtOH (96 %) and CHCl₃ before the addition of hydrazine. The precipitated phthalhydrazide was filtered off and the solution was vacuum evaporated. Complete removal of phthalhydrazide was achieved by re-suspension in pure chloroform and subsequent filtration. The deprotected amine **40-bz** was obtained as yellow oil.

¹³ Ambrosi, G.; Formica, M.; Fusi, V.; Giorgi, L.; Guerri, A.; Micheloni, M.; Paoli, P.; Pontellini, R.; Rossi, P. *Inorg. Chem.* **2007**, *46* (11), 4737–4748.

¹⁴ a) Striegler, S. *Tetrahedron* **2001**, *57* (12), 2349–2354. b) Arbuse, A.; Font, M.; Martínez, M. A.; Fontrodona, X.; Prieto, M. J.; Moreno, V.; Sala, X.; Llobet, A. *Inorg. Chem.* **2009**, *48* (23), 11098–11107. b) Arbuse, A.; Mandal, S.; Maji, S.; Martínez, M. A.; Fontrodona, X.; Utz, D.; Heinemann, F. W.; Kisslinger, S.; Schindler, S.; Sala, X.; Llobet, A. *Inorg. Chem.* **2011**, *50* (15), 6878–6889.

Once the procedure to deprotect the non-vinyl amine had been optimized, the reaction was applied to the deprotection of the amine that contains the styrene moiety, **39-st**. In this regard, the most important problem that we encountered was the fact that the deprotected product **40-st** is highly unstable towards polymerization. After evaporation of the solvent in the last step of the reaction, an oily product was obtained which, in a matter of minutes at room temperature, became an insoluble rubber-like substance. Most probably this polymerisation is promoted by the radical decomposition of chloroform. The presence of ethanol during the reaction with hydrazine at reflux would avoid the decomposition of chloroform (in fact, ethanol is a common stabiliser for chloroform). The evaporation of the solvent and the addition of fresh chloroform to promote the precipitation of phthalhydrazide would favour the decomposition of this solvent with the generation of radical species which, after concentration by evaporation, would promote the radical polymerisation of **40-st**. Since light accelerates the decomposition of chloroform, this undesired polymerization of **40-st** was successfully prevented by minimising contact to light during the whole reaction process. Nevertheless the ^1H NMR analysis of **40-st** showed the presence of the product of reduction of the double bond, **40-red**, as an impurity (**Figure 7.2**).

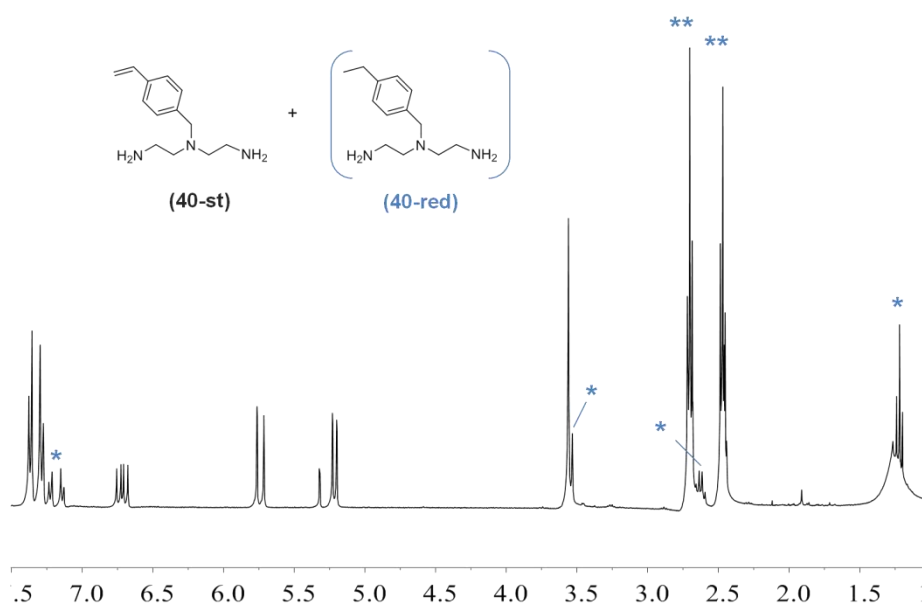


Figure 7.2. ^1H NMR spectrum of **40-st** with **40-red** as minor impurity. 360.13 MHz. CD_2Cl_2 . δ in ppm

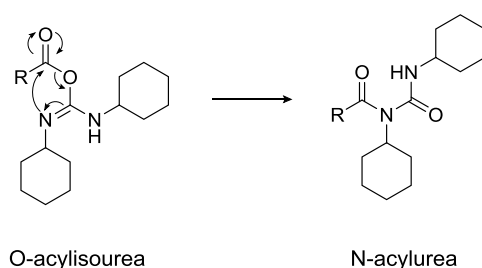
* : signals of **40-red**.

** : signals of **40-red** overlapped with signals of **40-st**.

With the aim of lessening the amount of the reduced by-product, **40-red**, the reaction with hydrazine was carried out at room temperature for 24 h instead of refluxing for 1.5

h. After that time, the reaction mixture was filtered off to remove the phthalhydrazide and the solvent was vacuum evaporated. The remaining phthalhydrazide was then precipitated by stirring with CHCl_3 for only 1.5 h before filtering off again. The solvent was vacuum evaporated yielding the final product as pale yellow oil which was immediately stored at $-34\text{ }^\circ\text{C}$ to minimize the polymerization. The product was stable at this temperature for less than two weeks. Again, it was important to avoid contact to light as much as possible and, at the same time, to work under oxygen free atmosphere during all the synthetic procedure.

At this point, the last step to be studied in the reaction of formation of the diamide-diphosphine ligands was the final reaction, in which the deprotected amine is reacted with the carboxylic acid group in the phosphine. As in the previous steps, the reaction was essayed and optimised for the benzylic molecule. As a first trial, dicyclohexylcarbodiimide (DCC), which is a very common reagent in the synthesis of esters and amides, was used. Normally this reagent is used together with 4-*N,N*-dimethylaminopyridine (DMAP) as catalyst, especially in the synthesis of esters. However, since nitrogen is a better nucleophile than oxygen and in order to simplify the final purification of the product, we decided to test the reaction without using DMAP. Unfortunately, the reaction afforded a mixture of different products, neither of which seemed to be the diamide-diphosphine ligand. According to the literature,¹⁵ in the absence of DMAP, the reaction is usually too slow to give the ester or amide and the *O*-acylisourea intermediate leads to the formation of an *N*-acylurea instead through a rearrangement (**Scheme 7.5**).



Scheme 7.5. Reaction of formation of an *N*-acylurea through the rearrangement of an *O*-acylisourea

It was also observed that the reaction between the carboxylic phosphine and the DCC is very slow without the presence of the catalyst. The $^{31}\text{P}\{^1\text{H}\}$ NMR spectrum of a mixture

¹⁵ a) Neises, B.; Steglich, W. *Angew. Chem. Int. Ed. Engl.* **1978**, *17* (7), 522–524. b) Hegarty, A. F.; McCormack, M. T.; Brady, K.; Ferguson, G.; Roberts, P. J. *J. Chem. Soc. Perkin Trans. 2* **1980**, (6), 867.

of *p*-Miranphos and DCC showed only one signal corresponding to the unreacted phosphine. However, when this mixture was in contact with a solution of the deprotected amine **40-bz**, it yielded two different signals. According to these observations, the amine itself would act as catalyst in the formation of the *O*-acylisourea the rearrangement of which would compete with the nucleophilic attack of the amine to form the amide. On the contrary, when a solution of DCC was added to a mixture of the carboxylic acid with the amine and DMAP in dry dichloromethane, the desired diamide was formed as the major product. After purifying through silica column (ethyl acetate:hexanes, 8:1) the diamide-diphosphine could be obtained in moderate yields. Even though the diamide-diphosphine **P-bz** was obtained with this method, some impurities were also observed even after the silica column purification. Therefore a cleaner reaction was explored.

In this case, the preparation of **P-bz** was essayed by means of the preparation of the acyl chloride of the *p*-Miranphos ligand followed by the reaction with the diamide **40-bz**. Such a reaction had been previously explored in our group¹² and has been slightly modified during the current synthesis. As far as we are concern, this has been the first time such methodology has been used in the synthesis of the acyl chloride of a phosphine without the generation of the phosphine oxide as side-product. Therefore, the carboxylic phosphine was solved in dry dichloromethane and a catalytic amount of *N,N*-dimethylformamide was added followed by the addition of oxalyl chloride (Vilsmeier-Haack reagent).¹⁶ This procedure generates the acid chloride of the carboxylic phosphine and CO, CO₂ and HCl as by-products. Addition of triethylamine followed by the addition of the diamine **40-bz** and subsequent purification by column chromatography in silica afforded the final product successfully.

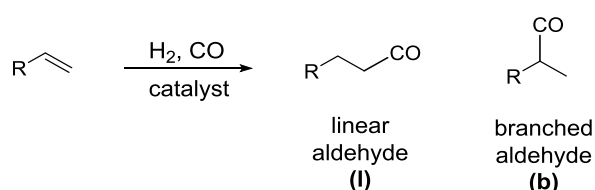
This approach being clean and easy was the chosen one to the preparation of the diphosphines and was successfully applied to the synthesis of the *meta*-isomer, **M-bz**, and to the styrene modified diphosphines, **P-st** and **M-st**.

¹⁶ Su, W.; Weng, Y.; Jiang, L.; Yang, Y.; Zhao, L.; Chen, Z.; Li, Z.; Li, J. *Org. Prep. Proced. Int.* **2010**, *42* (6), 503–555.

7.1.3. Rh-catalysed hydroformylation of 1-octene

7.1.3.1. Introduction to the reaction of hydroformylation

Formally, the reaction of hydroformylation consists in the addition of equimolar amounts of H₂ and CO (syngas) to olefins with the formation of an aldehyde group. Therefore, for terminal alkenes, two possible aldehyde products, branched and linear, can be formed, **Scheme 7.6**.



Scheme 7.6. Formation of linear (l) and branched (b) aldehydes from terminal alkenes

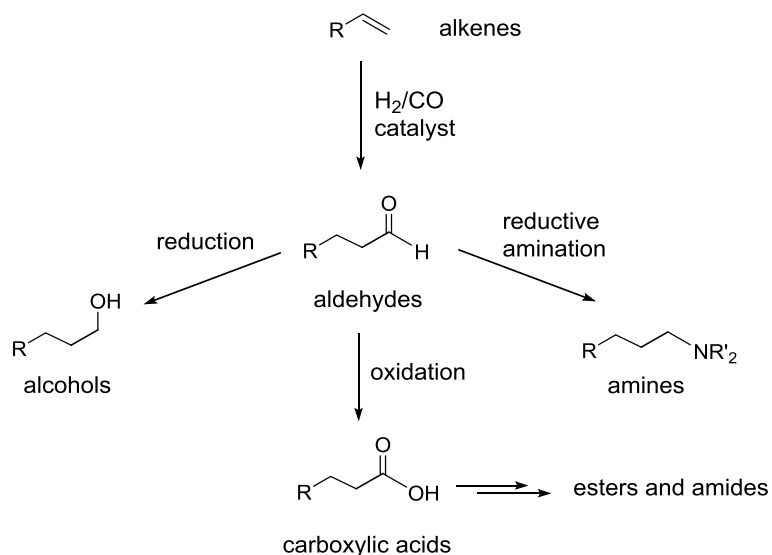
The discovery of the reaction is attributed to Otto Roelen which, during the study of the Fisher-Tropsch process with a cobalt catalyst, observed the formation of oxygenated products.¹⁷ Due to the nature of the compounds observed in the reaction, it was firstly called *oxo* process, and it was not until a few years later that Adkins used the term *hydroformylation*.¹⁸ The importance of the reaction of hydroformylation is based on the addition of one extra carbon atom (homologation) together with the formation of an aldehyde group, a valuable intermediate in the synthesis of bulk chemicals such as alcohols, carboxylic acids and their derivatives (esters, amides) and amines (**Scheme 7.7**).

Currently, more than 10 million metric tons of aliphatic aldehydes are industrially produced per year by hydroformylation around the world,¹⁹ which make hydroformylation the most important industrial process using homogeneous catalysts.

¹⁷ Roelen, O. Deutsches Patent schrift 849.548, 1938/1952; US Pat. 2.327.066, 1943

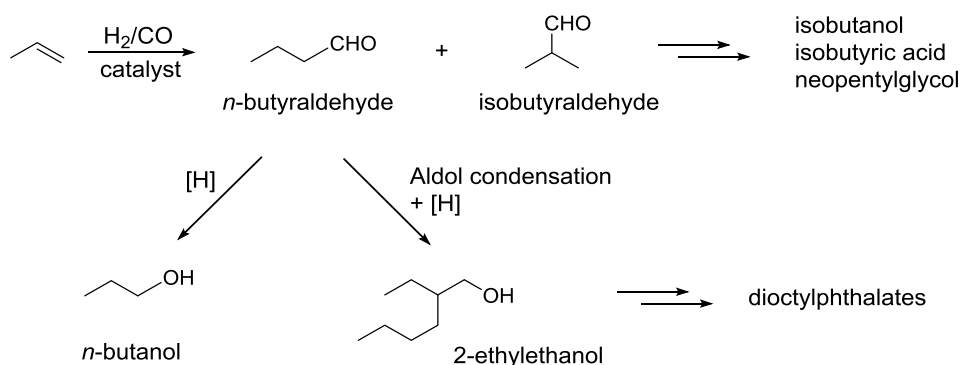
¹⁸ Adkins, H.; Krsek, G. *J. Am. Chem. Soc.* **1949**, *71* (9), 3051–3055.

¹⁹ a) Franke, R.; Selent, D.; Börner, A. *Chem. Rev.* **2012**, *112* (11), 5675–5732. b) Börner, A.; Franke, R. Chapter 1: Introduction. In *Hydroformylations: Fundamentals, Processes and Applications in Organic Synthesis*; Wiley-VCH Verlag GmbH & Co. KGaA: Weinheim, Germany, **2016**; Vol. 1–2. p 1



Scheme 7.7. Formation of different functional groups from alkenes by the generation of aldehydes intermediates through hydroformylation

Amongst the chemicals produced by the oxo process, *n*-butyraldehyde and isobutyraldehyde, both produced by hydroformylation of propene, are by far the most important products. As a matter of fact, in 2014 75 % of world consumption of oxo products corresponded to these two compounds,²⁰ it being the linear aldehyde the most important of the two isomers. *n*-Butyraldehyde is mainly consumed in the preparation of 2-ethylethanol via aldol condensation and hydrogenation, which is further used in the production of dioctylphthalates as plasticizer for PVC. *n*-Butanol can also be produced by reduction of *n*-butyraldehyde. On the other side, the branched aldehyde, isobutyraldehyde, is used in the production of isobutanol, isobutyric acid and neopentylglycol, **Scheme 7.8**.



Scheme 7.8. Hydroformylation of propene and derivatives of their products

²⁰ IHS Markit. Oxo Chemicals. 2018. <https://ihsmarkit.com/products/oxo-chemicals-economics-landbook.html>.

Although initially the oxo process made use of the so-called unmodified cobalt catalyst ($\text{HCo}(\text{CO})_4$), early studies of Wilkinson's group using phosphine-modified Rh-catalyst²¹ gave rise to, probably, the most important change in the world of hydroformylation. Since then, ligand-modified rhodium compounds have replaced cobalt catalysts in most industrial processes given their much higher activities and selectivities.²² Milder reaction conditions can therefore be used with Rh-organophosphine compounds. Nevertheless Rh-complexes suffer from thermal decomposition which hampers catalyst recycling. Because of this reason, Co catalyst is still industrially applied in the hydroformylation of higher alkenes, such as those of the SHOP process.

Trivalent phosphorus compounds are, by far, the most used ligands in the Rh-catalysed hydroformylation. A variety of phosphorus ligands have been described in the literature ranging from phosphines to phosphites, either monodentate or chelating.^{19a,23}

The most accepted reaction mechanism with phosphine ligands is the so-called dissociative mechanism described by Wilkinson for the phosphine-substituted species $\text{HRh}(\text{PPh}_3)_3\text{CO}$ (**A**) as starting complex,^{21,24} **Scheme 7.9**. In fact, this mechanism is a modification of the proposed mechanism for the Co-catalysed reaction published by Heck and Breslow.²⁵

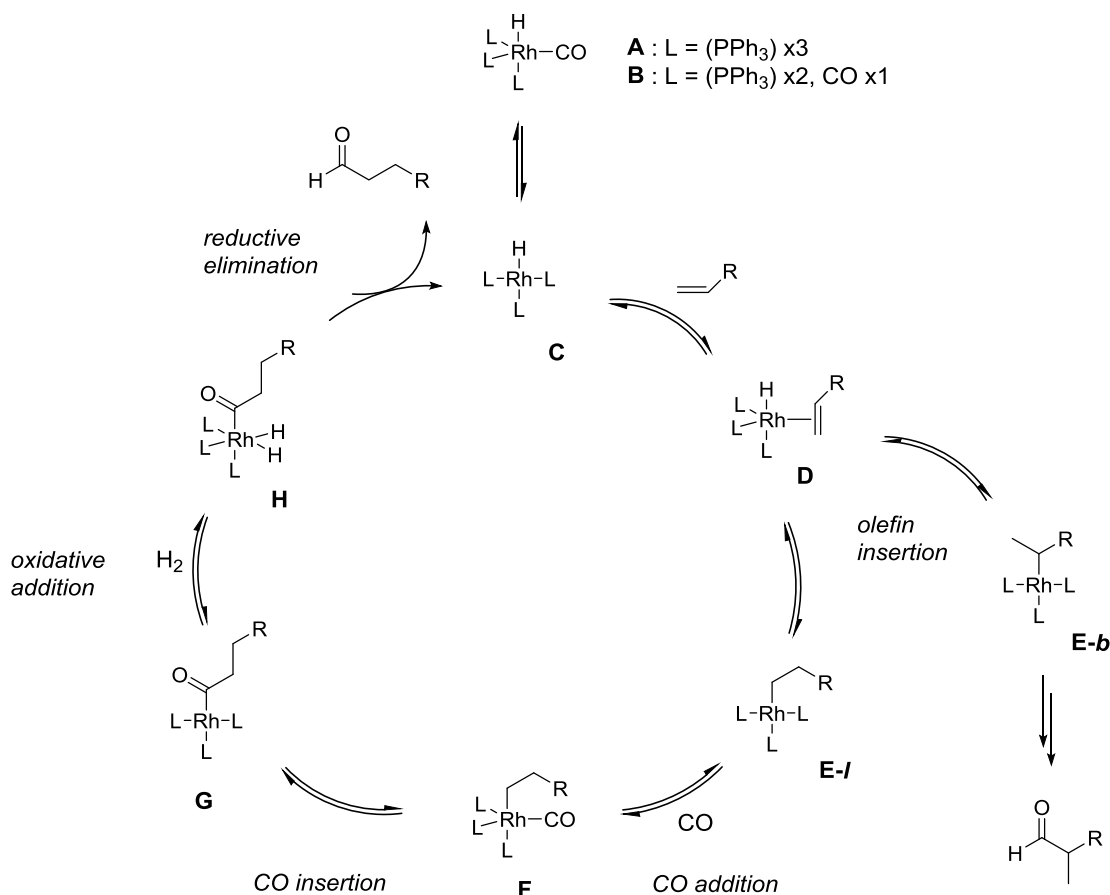
²¹ Evans, D.; Osborn, J. A.; Wilkinson, G. *J. Chem. Soc. A Inorganic, Phys. Theor.* **1968**, 3133.

²² Bayón, J.C. Chapter 6: Carbonilación. In *Fundamentos y aplicaciones de la catálisis homogénea*. Oro, L. A.; Sola, E.; Eds; Zaragoza. **2000**. 2nd Edition. pp 75-76

²³ a) *Rhodium Catalyzed Hydroformylation*; van Leeuwen, P. W. N. M., Claver, C., Eds.; Kluwer Academic Publishers, Dordrecht, **2000**. b) van Leeuwen, P. W. N. M.; Freixa, Z. 7.03- Application of Rhodium Complexes in Homogeneous Catalysis with Carbon Monoxide. In *Comprehensive Organometallic Chemistry III. From Fundamentals to Applications*; Mingos, D. Mi. P., Cabtree, R. H., Eds.; Elsevier Ltd, **2007**; pp 237–265.

²⁴ a) Yagupsky, M.; Brown, C. K.; Yagupsky, G.; Wilkinson, G. *J. Chem. Soc. A Inorganic, Phys. Theor. Chem.* **1970**, 0, 937–941. b) Yagupsky, M.; Wilkinson, G. *J. Chem. Soc. A Inorganic, Phys. Theor. Chem.* **1970**, 941–944.

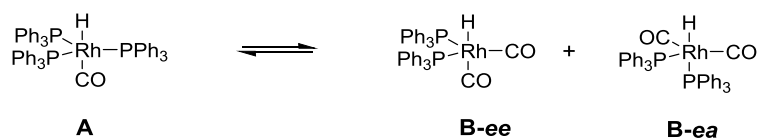
²⁵ Heck, R. F.; Breslow, D. S. *J. Am. Chem. Soc.* **1961**, 83 (19), 4023–4027.



Scheme 7.9. Mechanism of the Rh-catalysed hydroformylation of alkenes according to the literature.^{21,24}
L = PPh₃ or CO

Under hydroformylation conditions, displacement of one phosphine ligands occurs with the formation of an isomeric mixture of species **B**, in which phosphine ligands occupy either bis-equatorial coordination positions (**B-ee**) or equatorial-apical (**B-ea**) positions, **Scheme 7.10**. For PPh₃, Brown and Kent showed an *ee:ea* ratio of 85:15.²⁶ Square planar 16 electron species **C** are formed by dissociation of L (CO or phosphine) followed by the coordination of the olefin to form pentacoordinated species **D**. The migratory insertion of the olefin into the Rh-H bond to form square planar alkyl species **E** will define the regioselectivity of the reaction by the formation of the linear alkyl complex, **E-I**, or the branched isomer, **E-b**. Next, coordination of a CO ligand (**F**) followed by the CO insertion into the Rh-alkyl bond give rise to the acyl complex **G**, which further undergoes oxidative addition of H₂ and reductive elimination of the aldehyde to close the cycle with the regeneration of **C**.

²⁶ Brown, J. M.; Kent, A. G. *J. Chem. Soc. Perkin Trans. 2* **1987**, No. 11, 1597–1607.



Scheme 7.10. Pentacoordinated Rh-CO-phosphine species under hydroformylation conditions

As stated before, the regioselectivity of the reaction is determined in the step at which the alkene complex **D** is transformed into the four-coordinate alkyl complexes **E**. The preferred coordination of the phosphorus ligands in the **B** species has been related to the regioselectivity of the reaction. In this sense, Brown and Kent showed that **B-ee** species lead to the formation of the linear aldehyde preferentially. The concentration of the phosphorus ligand, as well as its electronic and steric properties, also influences the *ee-ea* equilibrium and thus the regioselectivities. In this respect, *ee-ea* equilibrium can be modulated by using diphosphine ligands with different bite angles. As in the case of monophosphines, diphosphines show dynamic equilibrium between bis-equatorial and equatorial-axial species.²⁷ Casey and Whiteker found good correlation between the bite angle and the selectivity in the reaction of Rh-catalysed hydroformylation.²⁸ It was believed that diphosphines with bite angles close to 120° would preferentially coordinated in an *ee* fashion while diphosphines with bites close to 90° would act as *ea* chelating ligands. Later on, the studies of van Leeuwen's group corroborated the relationship between the bite angle and the regioselectivity although also proved that the *ee-ea* equilibrium was not the factor governing the regioselectivities within a small range of bite angles.^{27b,29} Steric effects have also been considered to be responsible of the bite angle effect in the regioselectivities.³⁰

As part of the study of the diphosphine-diamide ligands, previous to the anchoring to the latex surface, the non-vinyllic ligands, *p*-diphosdiam (**P-bz**) and *m*-diphosdiam

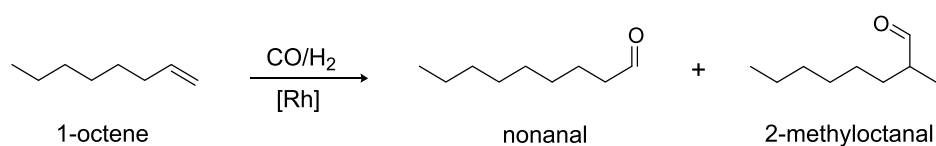
²⁷ a) Casey, C. P.; Lin Paulsen, E.; Beuttenmueller, E. W.; Proft, B. R.; Petrovich, L. M.; Matter, B. A.; Powell, D. R. *J. Am. Chem. Soc.* **1997**, *119* (49), 11817–11825. b) van Der Veen, L. A.; Boele, M. D. K.; Bregman, F. R.; Kamer, P. C. J.; van Leeuwen, P. W. N. M.; Goubitz, K.; Fraanje, J.; Schenk, H.; Bo, C. *J. Am. Chem. Soc.* **1998**, *120* (45), 11616–11626.

²⁸ Casey, C. P.; Whiteker, G. T.; Melville, M. G.; Petrovich, L. M.; Gavney, J. A.; Powell, D. R. *J. Am. Chem. Soc.* **1992**, *114* (14), 5535–5543.

²⁹ a) van Der Veen, L. A.; Kamer, P. C. J.; van Leeuwen, P. W. N. M. *Organometallics* **1999**, *18* (23), 4765–4777. b) vanderVeen, L. a; Keeven, P. H.; Schoemaker, G. C.; Reek, J. N. H.; Kamer, P. C. J.; van Leeuwen, P.; Lutz, M.; Spek, a L. *Organometallics* **2000**, *19* (5), 872–883.

³⁰ for a review on this topic, see: Freixa, Z.; van Leeuwen, P. W. N. M. *Dalton Trans.* **2003**, No. 10, 1890–1901.

(**M-bz**), were applied in the homogeneous Rh-catalysed hydroformylation of 1-octene, **Scheme 7.11**.



Scheme 7.11. Rhodium-catalysed hydroformylation of 1-octene

Previous considerations

The catalytic experiments included in this chapter have been performed in two different facilities: in the University of Edinburgh (System ED) and in the Universitat Autònoma de Barcelona (System BCN). In both systems the reactions have been carried out in a mechanically stirred reactor containing a gas-entrainment impeller. However, while in the System ED the gas consumption during the catalytic reaction was monitored using a Mass-flow controller, in the System BCN the gas consumption was monitored using a pressure transducer connected to a gas reservoir from which the reactor was constantly fed during the reaction. These inputs allow us to follow the reaction with time and, once the conversion is determined by GC analysis, to calculate the values of TOF at 50 % conversion.

Great efforts were focused in the modification of the system used in Barcelona in order to reproduce the values of the System ED. In this sense, the reactor was intensively improved, including the installation of a dropping funnel, which allows the addition of the substrate under gas pressure, and the design and construction of a home-made gas-entrainment impeller. In this regard, more details can be found in the experimental section (chapter 9).

Values of conversion, regioselectivity and chemoselectivities (isomerisation and hydrogenation) have been perfectly reproduced in both systems. However, in spite of our efforts, values of TOF could not be reproduced. Given the different procedures for monitoring the gas consumption used in the two systems, significant differences were obtained. Mass-flow controller provides a more sensitive system than when using the pressure transducer. As a matter of example, in a reaction using 75 mmol of 1-octene, the Mass-flow controller would measure the flow of about 3000 mL of gas at the end of the reaction, with a precision of 10⁻⁵ mL (System ED). The same reaction when

monitored with the pressure transducer would register a pressure difference of about 11 bar with 0.1 bar of precision (System BCN). Moreover, in this second system, the reactor is fed through a pressure regulator which is manually set at the chosen working pressure. We have observed a sort of dynamic behaviour by which, once the reaction has started, it is necessary a certain pressure drop in the reactor (usually around 0.5 bar) for the regulator to start feeding the reactor again, and thus to start observing a pressure difference in the gas reservoir cylinder. Although this behaviour has little or none effect in the rate and selectivities of the reaction, it is of greater significance to the TOF calculations. Because of this, in the following catalytic results, only values of TOF of reactions performed in the same reactor system will be compared. All other parameters have been found to be perfectly reproducible and comparable.

7.1.3.2. Catalytic experiments

First screening with the diphosphine ligands **P-bz** and **M-bz** was focused on the effect produced in the selectivity and activity at different ligand-to-rhodium ratios, **Table 7.1**.

Table 7.1. Hydroformylation of 1-octene with ligands **P-bz** and **M-bz** at different L:Rh ratios^a

Ligand	Entry	[L]/[Rh]	Conv. ^b (%)	l/b ^c (%)	<i>n</i> -aldehyde ^d (%)	2-octenes ^e (%)	octane ^f (%)	TOF 50 % ^g (min ⁻¹)
<i>m</i> -diphosdiam (M-bz)	1	10	97.1	92.8	88.9	3.7	0.5	51.4
	2	5	98.6	91.7	86.6	5.1	0.5	47.5
	3	2	98.8	91.9	88.1	3.6	0.4	47.1
	4	1.3	97.6	78.7	70.1	8.3	1.0	42.1
	5	1	97.1	75.6	67.0	10.3	1.1	31.7
<i>p</i> -diphosdiam (P-bz)	6	8	97.9	95.5	85.8	9.0	1.1	53.7
	7	5	97.9	95.2	86.0	8.5	1.3	58.1
	8	2	98.2	95.7	88.2	6.1	1.7	61.5
	9	1.3	96.6	82.4	72.8	9.4	2.2	47.2
none	10	-	52.0	71.8	43.9	37.5	1.4	n.d.

^a Conditions: 20 bar CO:H₂ (1:1); 80 °C; 3 h of reaction; 1-octene/Rh = 5000; [Rh] = 0.65 mM in toluene; *n*-decane 0.3 mM as internal standard; Stirring rate 700 rpm. (Catalyst preformation: 16 bar CO:H₂ (1:1); 80°C, 1.5h)

^b Conversion of 1-octene: (mmol of converted substrate/mmol of starting substrate) x 100

^c Regioselectivity: (mmol of linear aldehyde/mmol of aldehydes) x 100

^d Overall catalyst selectivity: (mmol of linear aldehyde/mmol of converted substrate) x 100

^e Isomerisation: (mmol of 2-octenes/mmol of converted substrate) x 100

^f Hydrogenation: (mmol of octane/mmol of converted substrate) x 100

^g TOF at 50 % of conversion

High conversions were obtained after 3 h of reaction for both ligands regardless of the ligand-to-rhodium ratio used. In terms of regioselectivity and reaction rate, optimum L:Rh value of 2 was observed for both ligands. The use of higher ratios did not show any differences. However when values of L:Rh < 2 were used, a substantial decrease in the regioselectivity towards linear aldehyde as well as in the TOF was observed. This effect has been reported for other chelating diphosphines. Although it was firstly attributed to the formation of more selective species containing 3 coordinating phosphorus atoms at ligand-to-rhodium ratios greater than 2, as observed by NMR analysis,³¹ (Chart 7.2) later it was shown that the formation of tris-phosphine species is favoured at the high concentrations required for the NMR studies. Under catalytic concentrations only HRh(P-P)(CO)₂ species have been observed.³² Therefore, under our catalytic conditions, a ligand-to-rhodium ratio of 2 would be necessary to ensure complete formation of the active HRh(P-P)(CO)₂ species. Similar behaviour has been reported for other chelating ligands.³³



Chart 7.2. Tris-phosphine carbonyl rhodium-hydrido species with diphosphines

With the *meta*-isomer diphosphine, ligand **M-bz**, the % of hydrogenation and, specially, the % of isomerisation clearly increased when decreasing the ligand-to-rhodium ratio below 2 (entries 4 and 5). This effect could be related to the formation of less selective rhodium species with lower number of coordinating phosphorus atoms such as HRh(CO)₄ or HRhP(CO)₃ (with *P* being a ligand coordinated by a single phosphorus atom), which would be formed at low phosphine concentrations. The use of no ligand (entry 10) gives support to the increased isomerisation observed at low phosphine concentrations. In the case of ligand **P-bz**, this trend was not clearly observed.

³¹ a) Hughes, O. R.; Young, D. A. *J. Am. Chem. Soc.* **1981**, *103* (22), 6636–6642. b) Unruh, J.; Christenson, J. R. *J. Mol. Catal.* **1982**, *14*, 19–34.

³² Nettekoven, U.; Kamer, P. C. J.; Wildhalm, M.; van Leeuwen, P. W. N. M. *Organometallics* **2000**, *19* (22), 4596–4607.

³³ a) Kranenburg, M.; van der Burgt, Y. E. M.; Kamer, P. C. J.; van Leeuwen, P. W. N. M.; Goubitz, K.; Fraanje, J. *Organometallics* **1995**, *14* (6), 3081–3089. b) van der Slot, S. C.; Duran, J.; Luten, J.; Kamer, P. C. J.; van Leeuwen, P. W. N. M. *Organometallics* **2002**, *21* (19), 3873–3883.

At $L:Rh \geq 2$, the activity of both ligands, **M-bz** and **P-bz**, was similar with values of TOF at 50 % of conversion around 50 min^{-1} for the former and slightly higher for the later. Although the observed aldehyde l/b ratios were moderately greater for the *para*-isomer, **P-bz**, also higher activity towards isomerisation was observed for this ligand, thus resulting in virtually the same overall catalyst yield towards *n*-aldehyde, between 86 and 89 %, for both ligands **M-bz** and **P-bz**. The formation of 2-octene has been recognised as an “escape” route for the branched alkyl-rhodium intermediate, especially for less basic diphosphines.^{27b}

Values of l/b obtained using the diphosphine-diamide ligands **P-bz** and **M-bz** are comparable to those of more rigid ligands under similar conditions such as phosxantphos, although are far from those obtained for Xantphos and BISBI.^{29b} It is noteworthy, however, that the values of TOF obtained with our diphosphines are higher than those reported for the mentioned ligands, and similar to those reported for the more active pyrrolyl analogues of Xantphos.³⁴

The isomerisation of the catalytic reactions at $L:Rh = 2$ and 20 bar of syngas was monitored by sampling the reaction mixtures with time. The aldehyde l/b ratio was plotted against the conversion of 1-octene (**Figure 7.3**). Similar results were obtained for both ligands. Even though little variation of the regioselectivity (l/b) was observed during most of the reaction, a sudden decrease above 80 % of 1-octene conversion, with ligand **M-bz**, and above 90 % of conversion, with ligand **P-bz**, was observed. This trend is attributed to the fact that, once most of the linear alkene is consumed, the internal alkenes, which are far less reactive towards hydrofomylation, would start reacting giving rise to an increase of the amount of branched aldehyde. This sudden drop of the l/b ratio is more marked with the *meta*-isomer (**M-bz**) and would explain the lower % of 2-octenes at the end of the reaction obtained with this ligand with respect to the *para*-isomer (**P-bz**).

³⁴ Diebolt, O.; Tricas, H.; Freixa, Z.; van Leeuwen, P. W. N. M. *ACS Catal.* **2013**, 3 (2), 128–137.

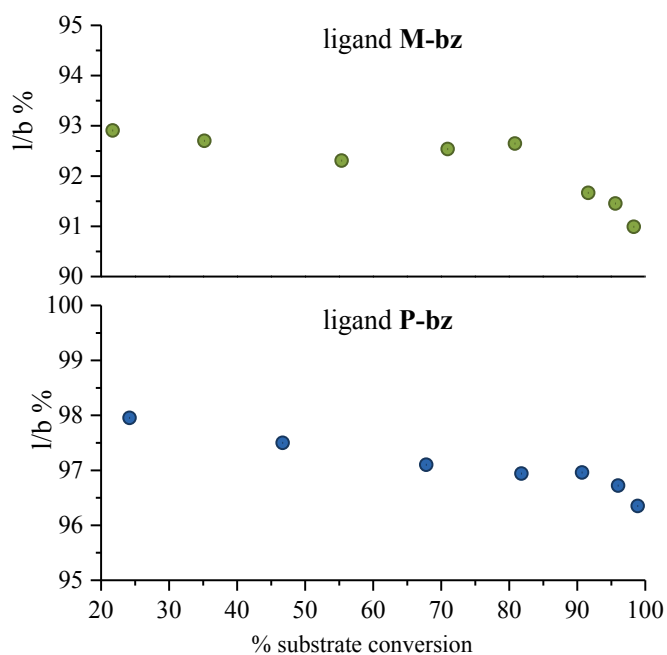


Figure 7.3. Plot of the l/b ratios vs % substrate conversion in the Rh-catalysed hydroformylation of 1-octene with diphosphines **P-bz** and **M-bz**. Same reaction conditions as in entries 3 and 8 (see footnote in **Table 7.1**)

Next, a new set of catalytic experiments was performed in order to evaluate the effect of the syngas pressure, with a ligand-to-rhodium ratio of 2, **Table 7.2**. As general trend with both ligands, the regioselectivity towards the linear aldehyde, as well as the isomerisation, decreased when increasing the syngas pressure, without affecting to the hydrogenation. At high CO pressure, the process of β -hydride elimination in the branched rhodium alkyl complex is reduced by promoting the migratory insertion into the Rh-CO bond to form the *iso*-aldehyde, **Scheme 7.12**. In the same way, the β -hydride elimination in the linear rhodium alkyl complex is also suppressed, however this process has no influence in the isomerisation since β -elimination of the linear rhodium alkyl re-forms the linear alkene.³⁵ Moreover, under high CO pressures, carbon monoxide would compete with phosphine ligand thus favouring partial dissociation of the diphosphine ligand (**Scheme 7.13**) and giving rise to reduced l/b ratios. This effect has been reported with bulky diphosphite ligands.³⁶ The same reasoning applies to the observed increase in the isomerisation under lower syngas pressures.

³⁵ Kamer, P.C.J.; Reek, J.; van Leeuwen, P. W. N. M. Chapter 3: Rhodium Phosphite catalysts. In *Rhodium Catalyzed Hydroformylation*; van Leeuwen, P. W. N. M., Claver, C., Eds.; Kluwer Academic Publishers, Dordrecht, 2000. pp 41-42

³⁶ van Rooy, A.; Kamer, P. C. J.; van Leeuwen, P. W. N. M.; Goubitz, K.; Fraanje, J.; Veldman, N.; Spek, A. L. *Organometallics* **1996**, *15* (2), 835-847.

Table 7.2. Hydroformylation of 1-octene with ligands P-bz and M-bz at different syngas pressure and selected entries from **Table 7.1**.^a

Ligand	Entry	Syngas Pressure (bar)	Conv. ^b (%)	l/b ^c (%)	<i>n</i> -aldehyde ^d (%)	2-octenes ^e (%)	octane ^f (%)
<i>m</i> -diphosdiam (M-bz)	11	40	99.0	88.2	85.9	2.1	0.5
	3	20	98.8	91.9	88.1	3.6	0.4
	12	10	98.0	94.0	87.8	6.1	0.5
	13	5	97.5	95.7	87.9	7.9	0.3
<i>p</i> -diphosdiam (P-bz)	14	40	97.7	93.1	90.7	1.8	0.8
	8	20	98.2	95.7	88.2	6.1	1.7
	15	10	98.4	96.2	88.9	6.9	0.7
	16	5	98.4	97.3	88.2	8.7	0.7

^a Conditions: 20 bar CO:H₂ (1:1); 80 °C; 3 h of reaction; 1-octene/Rh = 5000; L/Rh = 2; [Rh] = 0.65 mM in toluene; *n*-decane 0.3 mM as internal standard; Stirring rate 700 rpm. (Catalyst preformation: 16 bar CO:H₂ (1:1); 80 °C, 1.5h). In reactions with pressure lower than 20 bar, the reactor was depressurised to the reaction pressure after the preformation.

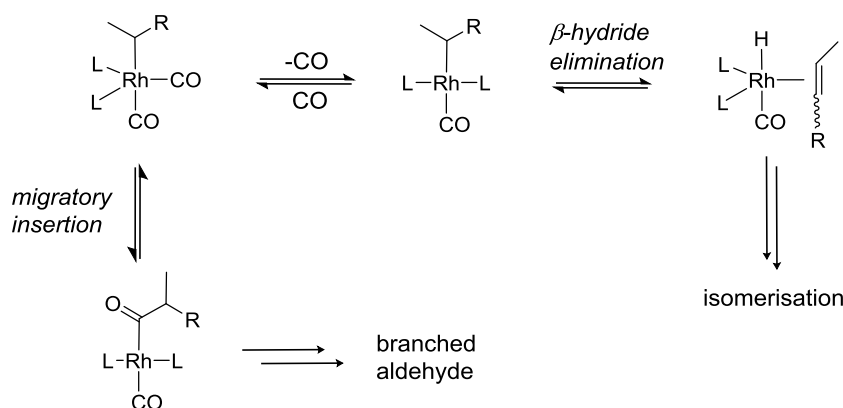
^b Conversion of 1-octene: (mmol of converted substrate/mmol of starting substrate) x 100

^c Regioselectivity: (mmol of linear aldehyde/mmol of aldehydes) x 100

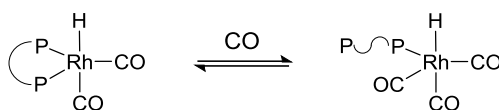
^d Overall catalyst selectivity: (mmol of linear aldehyde/mmol of converted substrate) x 100

^e Isomerisation: (mmol of 2-octenes/mmol of converted substrate) x 100

^f Hydrogenation: (mmol of octane/mmol of converted substrate) x 100

**Scheme 7.12.** Isomerisation pathways in the Rh-catalysed hydroformylation

Most significantly, when ligand **P-bz** was used under 5 bar of syngas, values of regioselectivity as high as 97.3 % was obtained, with still high conversion after 3 h of reaction. Values of the overall selectivity in linear aldehyde, however, were not appreciably greater than those observed at higher syngas pressure.

**Scheme 7.13.** Partial dissociation of diphosphine-rhodium complex at high P_{CO}.

The influence of the temperature was also studied for ligand **M-bz** at 10 bar of syngas. The reaction of hydroformylation of 1-octene was performed at 90 and 70 °C and the results were compared with the standard temperature of 80 °C, **Table 7.3**. At 70 °C, conversions higher than 92 % were roughly obtained, showing also a marked decrease in the TOF at 50 % of conversion. No differences were observed in the values of regioselectivities, isomerisation and hydrogenation. On the contrary, increasing the reaction temperature to 90 °C did not result in higher reaction rates than compared to the results obtained at 80 °C. Importantly, regioselectivity towards linear aldehyde considerably decreased at 90 °C to 86.8 %, as also did the overall catalyst selectivity towards linear aldehyde to 78.9 %. **Figure 7.4** shows the evolution of the 1-octene conversion, calculated from gas uptake during the reaction, at 70, 80 and 90 °C.

Table 7.3. Evaluation of the temperature in the hydroformylation of 1-octene with ligand **M-bz**.^a

Entry	Temperature (°C)	Conv. ^b (%)	l/b ^c (%)	<i>n</i> -aldehyde ^d (%)	2-octenes ^e (%)	octane ^f (%)	TOF 50 % ^g (min ⁻¹)
17	90	98.7	86.8	78.9	7.6	1.4	82.1
18	80	97.9	93.9	87.2	6.7	0.5	83.2
19	70	92.4	92.9	87.1	5.8	0.4	26.2

^a Conditions: 10 bar CO:H₂ (1:1); 3 h of reaction; 1-octene/Rh = 5000; L/Rh = 2; [Rh] = 0.65 mM in toluene; *n*-decane 0.3 mM as internal standard; Stirring rate 700 rpm. (Catalyst preformation: 16 bar CO:H₂ (1:1); 80 °C, 1.5h)

^b Conversion of 1-octene: (mmol of converted substrate/mmol of starting substrate) x 100

^c Regioselectivity: (mmol of linear aldehyde/mmol of aldehydes) x 100

^d Overall catalyst selectivity: (mmol of linear aldehyde/mmol of converted substrate) x 100

^e Isomerisation: (mmol of 2-octenes/mmol of converted substrate) x 100

^f Hydrogenation: (mmol of octane/mmol of converted substrate) x 100

^g TOF at 50 % of conversion

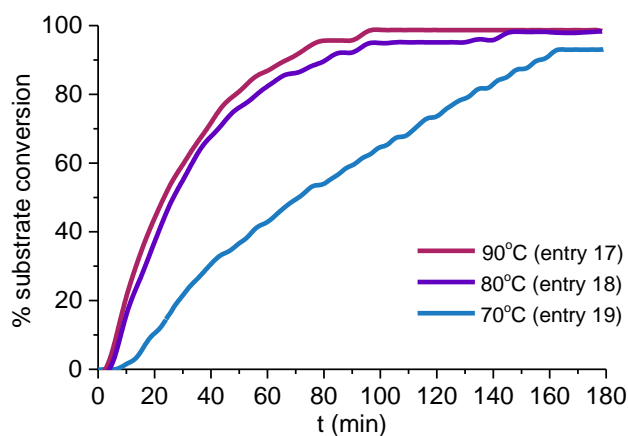


Figure 7.4. % substrate conversion with time in the Rh-catalysed HF of 1-octene (see **Table 7.3**)

Finally, the hydroformylation of 1-octene was performed using the monophosphines *m*-Miranphos and *p*-Miranphos as ligands, **Table 7.4**. The electronic properties of these monophosphines would resemble those of the diphosphines thus allowing the evaluation of the chelating effect of **P-bz** and **M-bz**. The less acidic triphenylphosphine (TPP) was also included in the series. Clearly, the values of regioselectivity obtained with the monophosphines were considerably lower than when the diphosphine-diamide ligands were used, even when increasing the L:Rh ratio to 10. This is a strong indicative of the chelating behaviour of the diphosphines **P-bz** and **M-bz**. Values of TOF at 50 % of conversion observed with *m*-Miranphos were similar to those obtained with the diphosphines.

Table 7.4. Hydroformylation of 1-octene with monophosphine ligands^a

Ligand	Entry	[L]/[Rh]	Conv. ^b (%)	l/b ^c (%)	n-aldehyde ^d (%)	2-octenes ^e (%)	octane ^f (%)	TOF 50 % ^g (min ⁻¹)
TPP	20	6	97.7	71.4	70.0	1.5	0.5	35.7
	21	10	96.7	71.5	69.9	1.6	0.6	40.1
<i>m</i> -Miranphos	22	6	98.9	73.0	71.8	1.2	0.4	50.6
	23	10	97.9	73.7	71.8	2	0.6	50.7
	24^h	6	98.8	73.0	71.4	1.7	0.5	81.9
<i>p</i> -Miranphos	25	6	72.8	75.6	75.6	n.d.	n.d.	13
	26^h	6	98.9	75.6	74.1	1.6	0.4	45.8

^a Conditions: 20 bar CO:H₂ (1:1); 80 °C; 3 h of reaction; 1-octene/Rh = 5000; [Rh] = 0.65 mM in toluene; n-decane 0.3 mM as internal standard; Stirring rate 700 rpm. (Catalyst preformation: 16 bar CO:H₂ (1:1); 80 °C, 1.5 h).

^b Conversion of 1-octene: (mmol of converted substrate/mmol of starting substrate) x 100

^c Regioselectivity: (mmol of linear aldehyde/mmol of aldehydes) x 100

^d Overall catalyst selectivity: (mmol of linear aldehyde/mmol of converted substrate) x 100

^e Isomerisation: (mmol of 2-octenes/mmol of converted substrate) x 100

^f Hydrogenation: (mmol of octane/mmol of converted substrate) x 100

^g TOF at 50 % of conversion

^h Solvent mixture of toluene:methanol (93:7)

Brief report about the reactions with the *Miranphos* ligands

The influence of the electron withdrawing ligands was evidenced when comparing TPP with *m*-Miranphos. As expected, higher l/b ratios and rates were obtained with the later. It is known that electron poor phosphorus ligands give rise to more active systems in the rhodium-catalysed hydroformylation of alkenes.³⁷ The positive effect of using

³⁷ a) van Leeuwen, P. W. N. M.; Roobeek, C. F. *J. Organomet. Chem.* **1983**, 258 (3), 343–350. b) Moser, W. R.; Papile, C. J.; Brannon, D. A.; Duwell, R. A.; Weininger, S. J. *J. Mol. Catal.* **1987**, 41 (3), 271–292.

triarylphosphines containing electron-withdrawing groups, such as trifluoromethyls, has been widely acknowledged for monophosphines^{7,38} as well as for diphosphines.^{27b,31b,32} Although the rate-determining step in the rhodium-phosphine-catalysed hydroformylation strongly depends on the reaction conditions, it has been generally accepted that under standard conditions the rate of the reaction is determined in the first stages of the catalytic cycle. This includes the dissociation of CO, the complexation of alkene and the migratory insertion of the olefin into the Rh-H bond.³⁹ Different computational studies have been reported pointing to the alkene coordination/insertion as rate-determining steps when using phosphines as ligands.⁴⁰ Recent DFT calculations on the full catalytic cycle with triphenylphosphine indicate that the rate of the reaction is determined by the olefin migratory insertion into the rhodium-hydride bond.⁴¹ Importantly, kinetic isotope effects together with DFT calculations on Xantphos-rhodium catalysed hydroformylation of 1-octene showed that the rate-determining step is more properly described as a set of reactions, including CO dissociation and alkene coordination, which end in the hydride migration as most important contributor to the overall rate.⁴² Gleich and Hutter showed that the olefin coordination becomes thermodynamically more favourable when decreasing the basicity of the phosphine ligand,^{40a} which would explain the enhanced performance of the hydroformylation with the electron poor trifluoromethylated phosphines. The π -accepting features of these ligands would also decrease the back-donation of the rhodium to CO ligand thus weakening the Rh-CO bond and facilitating the CO dissociation.

Coming back to the experimental reactions with the monophosphines, interestingly the hydroformylation of 1-octene in toluene using *p*-Miranphos ligand did show much lower conversion and activity than when TPP or *m*-Miranphos were used. A slightly turbid yellow solution was formed when *p*-Miranphos and Rh(acac)(CO)₂ were mixed

³⁸ Chan, A. S.; *Improved hydroformylation process to prepare glycol aldehydes*. EP0102341 (B1). **1984**. Monsanto Co.

³⁹ van Leeuwen, P. W. N. M.; Casey, C. P.; Whiteker, G.T. Chapter 4: Phosphines as ligands. In *Rhodium Catalyzed Hydroformylation*; van Leeuwen, P. W. N. M., Claver, C., Eds.; Kluwer Academic Publishers, Dordrecht, 2000. pp 69-72

⁴⁰ a) Gleich, D.; Hutter, J. *Chem. Eur. J.* **2004**, *10*, 2435–2444. b) Sparta, M.; Børve, K. J.; Jensen, V. R. *J. Am. Chem. Soc.* **2007**, *129* (27), 8487–8499. c) Aguado-Ullate, S.; Baker, J. A.; González-González, V.; Müller, C.; Hirst, J. D.; Carbó, J. J. *Catal. Sci. Technol.* **2014**, *4*, 979–987.

⁴¹ Jacobs, I.; De Bruin, B.; Reek, J. N. H. *ChemCatChem* **2015**, *7*, 1708–1718.

⁴² Zuidema, E.; Escorihuela, L.; Eichelsheim, T.; Carbó, J. J.; Bo, C.; Kamer, P. C. J.; van Leeuwen, P. W. N. M. *Chem. Eur. J.* **2008**, *14*, 1843–1853.

in toluene, previous to the catalyst preformation. After the 3 h of reaction, the solution obtained was almost colourless and showed a yellow precipitate, the composition of which could not be determined. These very same observations were reported by Buhling *et.al.* in the Rh-catalysed hydroformylation of 1-octene using the equivalent non-trifluoromethylated carboxylic phosphine, *p*-DPPBA.⁴³ The authors attributed the low activity to the formation of polymeric rhodium structures in which both phosphorus and carboxylic group would coordinate the metal. To overcome this solubility issue, we decided to perform the catalytic reaction in toluene:methanol (93:7) as solvent mixture. Under these conditions the system was found to be completely homogeneous, giving rise to a higher rate and almost full conversion. No other by-products were detected. An unexpected improvement of the rate was also obtained when this solvent mixture was tested in the reaction with *m*-Miranphos ligand. Unlike the *p*-Miranphos-Rh system in toluene, with *m*-Miranphos no precipitate was observed either before or after the catalytic reaction. The positive effect of methanol is most likely due to the solvation of the carboxylic groups thus minimizing any possible coordination to Rh. The inhibitory effect produced by the presence of carboxylic acids has been reported in the hydroformylation of 1-hexene⁴⁴ and 1-octene.⁴³ However solubility effects should not be completely excluded in this case. In fact, the reaction curve in toluene shows a slight increase in the rate above 60-70 % of substrate conversion (the slope is more pronounced), which might be a result of a higher solubility of the catalytic species as 1-octene is being replaced to the more polar aldehydes (this curve has been reproduced at least twice). **Figure 7.5** compares the substrate conversion of the Rh-catalysed hydroformylation of 1-octene using the *p*-Miranphos and *m*-Miranphos ligands in the two different solvent systems.

⁴³ Buhling, A.; Kamer, P. C. J.; van Leeuwen, P. W. N. M. *J. Mol. Catal. A Chem.* **1995**, *98* (2), 69–80.

⁴⁴ Mieczynska, E.; Trzeciak, A. M.; Ziolkowski, J. J. *J. Mol. Catal.* **1993**, *80* (2), 189–200.

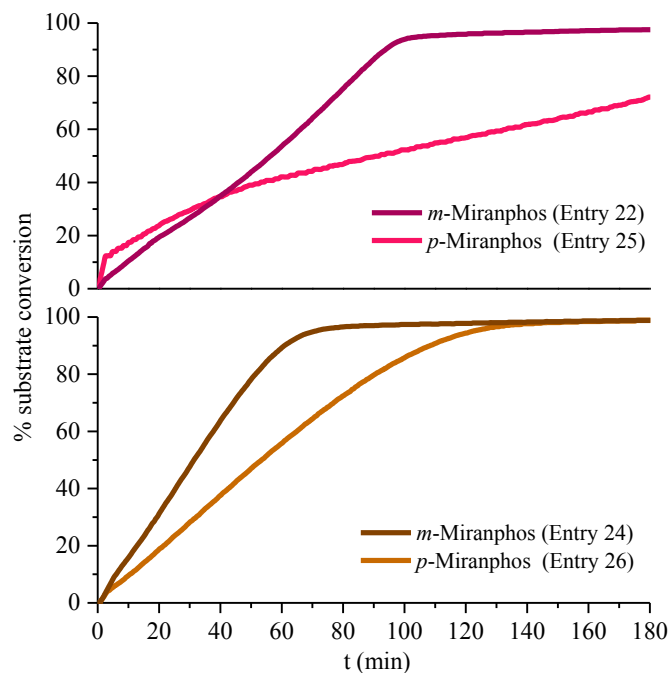


Figure 7.5 Hydroformylation of 1-octene with *m*-Miranphos and *p*-Miranphos. **Top:** reaction performed in toluene. **Bottom:** reaction performed in Toluene:MeOH (93:7). See footnotes in **Table 7.4** for experimental conditions.

7.1.3.3 Experiments at high pressure

The preferred coordination mode of the diphosphines **P-bz** and **M-bz** as well as the complexes formed under hydroformylation conditions have been studied by means of high pressure (HP) NMR and HP IR spectroscopy.

High-Pressure NMR measurements

HP NMR experiments were performed in toluene- D_8 at 20 bar and 20 °C after a period of 1.5 h at 80 °C, emulating the catalyst preformation time used in the catalytic experiments. Due to the small thickness of the sapphire tube used in these experiments, concentrations of Rh of 0.032 M were necessary to obtain satisfactory signal-to-noise response. The L:Rh ratios studied were 1.3, 2 and 5 (**Figure 7.6**).

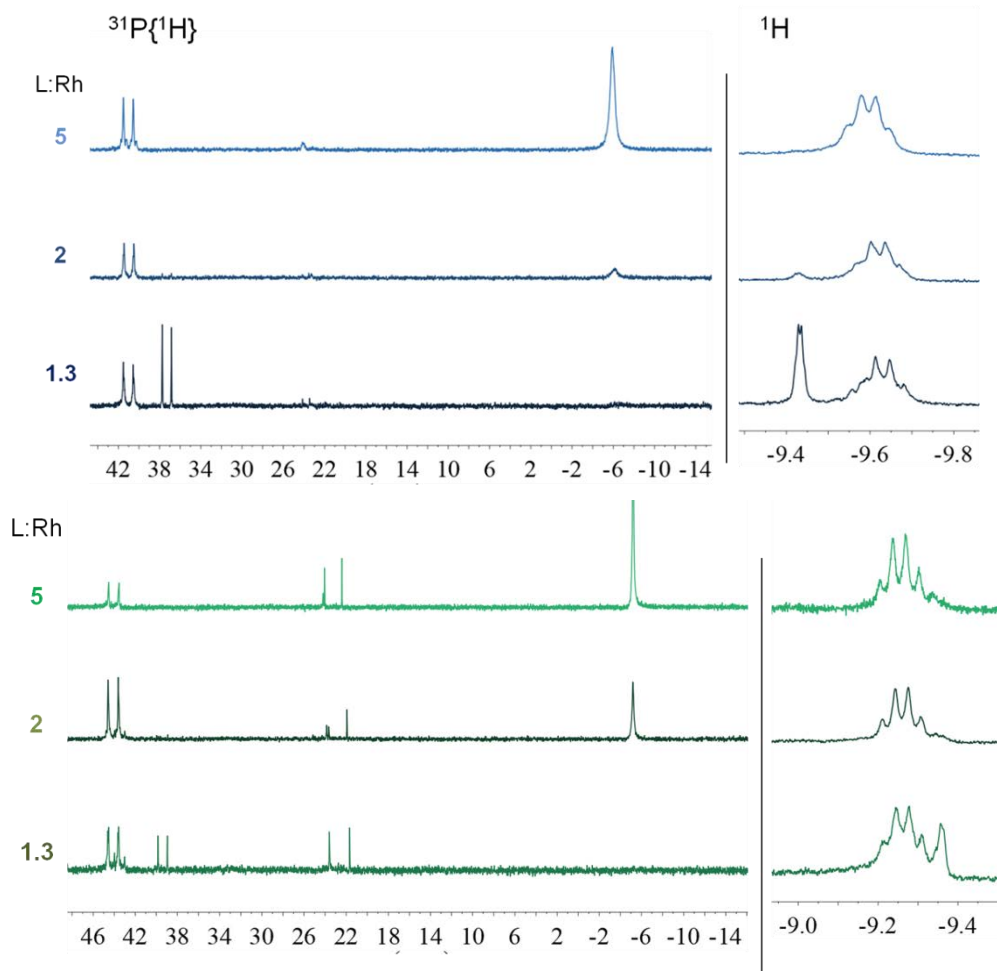


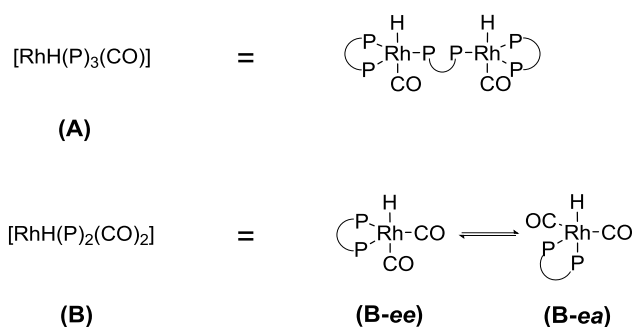
Figure 7.6. $^{31}\text{P}\{^1\text{H}\}$ (161.98 MHz) (left) and ^1H (hydride region) (400.13 MHz) (right) NMR spectra. δ in ppm. **Top** (blue): **P-bz**. **Bottom** (green): **M-bz**.

Similar behaviour was observed with both ligands, **P-bz** and **M-bz**. As a matter of example, using the *para*-isomer (**P-bz**) at ligand-to-rhodium ratio of 1.3, the $^{31}\text{P}\{^1\text{H}\}$ NMR spectrum showed two doublets at 41.0 and 37.3 ppm, with $^1J_{\text{Rh-P}} = 154$ and 144 ppm, respectively. The hydride region of the ^1H NMR showed two quartets at -9.4 and -9.6 ppm, with coupling constants of 2.5 and 13.3 Hz, respectively. When the L:Rh ratio was increased, the signal at 37.3 ppm in $^{31}\text{P}\{^1\text{H}\}$ NMR disappeared together with the hydride at -9.4 ppm. A new singlet at -6 ppm in the $^{31}\text{P}\{^1\text{H}\}$ appeared, corresponding to non-coordinating phosphorus atom. This pattern of signals is in agreement with the presence of tris- and bis-coordinated rhodium hydrido species, $[\text{RhH}(\text{P})_3(\text{CO})_2]$ (**A**) and $[\text{RhH}(\text{P})_2(\text{CO})_2]$ (**B**), respectively, where *P* refers to one coordinated phosphorus atom. This assignment was made on the basis of previous reported HP-NMR studies with triphenylphosphine,^{26,45} triphenylphosphine derivatives⁴⁶ and with other chelating

⁴⁵ Brown, J. M.; Canning, L. R.; Kent, A. G.; Sidebottom, P. J. *J. Chem. Soc. Chem. Commun.* **1982**, No. 13, 721–723.

diphosphines.^{27b,47} Furthermore, the relative integration of the signals of species **A** and **B** in the $^{31}\text{P}\{^1\text{H}\}$ spectrum correlates with the relative integration of the hydride signals in the ^1H spectrum thus further supporting the structure of the species detected in the high pressure NMR experiments.

Tris-phosphine coordinated species **A** generally display chemical shifts in the $^{31}\text{P}\{^1\text{H}\}$ at about 40 ppm with $^1J_{\text{Rh-P}}$ around 154 Hz. $^2J_{\text{H-P}}$ couplings of 14 Hz are characteristic of this species and $^1J_{\text{Rh-H}}$, when observable, are normally smaller than 2-3 Hz. Tentatively, we can propose a structure for these tris-coordinated rhodium hydrido species with our diphosphines in which one of the ligands would be acting as a chelating diphosphine, with both phosphorus atoms coordinated to the same metal centre, while the second ligand would bridge two different Rh atoms, as depicted in **Scheme 7.14**. The large number of atoms between each one of the phosphorus in the diphosphine would make all the coordinated phosphorus atoms indistinguishable showing a single chemical shift in the $^{31}\text{P}\{^1\text{H}\}$ spectrum and the same $^1J_{\text{H-P}}$, thus explaining the quartet observed for the hydride signal. Another conformation in which the second ligand would coordinate by a single phosphorus atom, as previously described in **Chart 7.2**, could not be completely discarded, especially at higher ligand concentrations.



Scheme 7.14. Proposed structures for Rh-Diphosphine complexes **A** and **B** under CO/H₂ pressure

Regarding the bis-coordinated species **B**, the values of chemical shift in the $^{31}\text{P}\{^1\text{H}\}$ NMR reported in the literature are normally a few ppm smaller than the equivalent tris-coordinated species **A**. Also values of $^1J_{\text{Rh-P}}$ are usually smaller and fall around 140 Hz. Most importantly, fast exchange between bis-equatorial (**B-ee**) and equatorial-apical (**B-ea**) isomers, (**Scheme 7.14**) is normally found on the NMR time scale at room

⁴⁶ Aghmiz, A.; Claver, C.; Masdeu-Bultó, A. M.; Maillard, D.; Sinou, D. *J. Mol. Catal. A Chem.* **2004**, *208* (1–2), 97–101.

⁴⁷ Dydio, P.; Detz, R. J.; De Bruin, B.; Reek, J. N. H. *J. Am. Chem. Soc.* **2014**, *136* (23), 8418–8429.

temperature.²⁷ The observed $^2J_{\text{H-P}}$ is, therefore, an average of those of the conformational isomers and has been used to estimate the mixture composition in chelating diphosphines, assuming *cis*- $^2J_{\text{H-P}}$ of around 2 Hz and *trans*- $^2J_{\text{H-P}}$ of around 100 Hz.^{27b} The small values of $^2J_{\text{H-P}}$ found for both ligands **P-bz** and **M-bz** are good indicative of preferential *ee* coordination.

As stated before, the behaviour observed when the *meta*-isomer diphosphine (**M-bz**) was used was mainly the same as for the *para*-isomer (**P-bz**). Nevertheless, apart from the signals of species **A** and **B**, the $^{31}\text{P}\{^1\text{H}\}$ NMR of the Rh-(**M-bz**) mixture under 20 bar of syngas showed two singlets of variable intensity between 20 and 25 ppm. In this region of the spectrum triarylphosphine oxides as well as dimeric Rh(0) species can be found.⁴⁸ However, the later species can be excluded since no P-Rh coupling was observed.

It is important to bear in mind that, because of the high concentrations required in the NMR experiments, the species found may be different from those actually present under the catalytic conditions. In this sense, HP IR experiments will help to shed more light on the actual composition of Rh-phosphine species at actual catalytic concentrations.

High-Pressure IR measurements

Compared to NMR, IR spectroscopy is a faster and a more sensitive technique. Due to the strong CO stretching absorptions of the Rh-carbonyl complexes, real catalytic conditions can be used.

Rh(acac)(CO)₂ and the corresponding diphosphine, in 1:2 ratio, were dissolved in CH₂Cl₂, in identical concentrations as in the catalytic experiments. The solution was then pressurised to 20 bar of syngas and heated up to 40 °C while being monitored with time by IR spectroscopy. Experiments using both ligands, **P-bz** and **M-bz**, (**Figure 7.7**) showed the presence of the CO bands corresponding to the species **B-ee** and **B-ea**, it being the bis-equatorial isomer the major one.^{27b,49} This preferential formation of the bis-equatorial species was expected for these electro-withdrawing ligands as reported for the Xantphos family^{27b} and the DIMphos-derived ligands.⁴⁷ Unambiguous

⁴⁸ Bianchini, C.; Lee, H. M.; Meli, A.; Vizza, F. *Organometallics* **2000**, *19* (5), 849–853.

⁴⁹ Kamer, P. C. J.; van Rooy, A.; Schoemaker, G. C.; van Leeuwen, P. W. N. M. *Coord. Chem. Rev.* **2004**, *248* (21–24), 2409–2424.

assignment of the bands was performed using D₂ instead of H₂. Due to the *trans* relationship between the hydride and the carbonyl in the trigonal bipyramid Rh complex, the H/D exchange only affects the **B-*ee*** isomer, shifting the bands to lower wavenumbers. The complete formation of these bis-coordinated rhodium hydrido species (**B**) took place in less than 60 min, under the essayed conditions. No signals for other Rh-carbonyl species were observed.

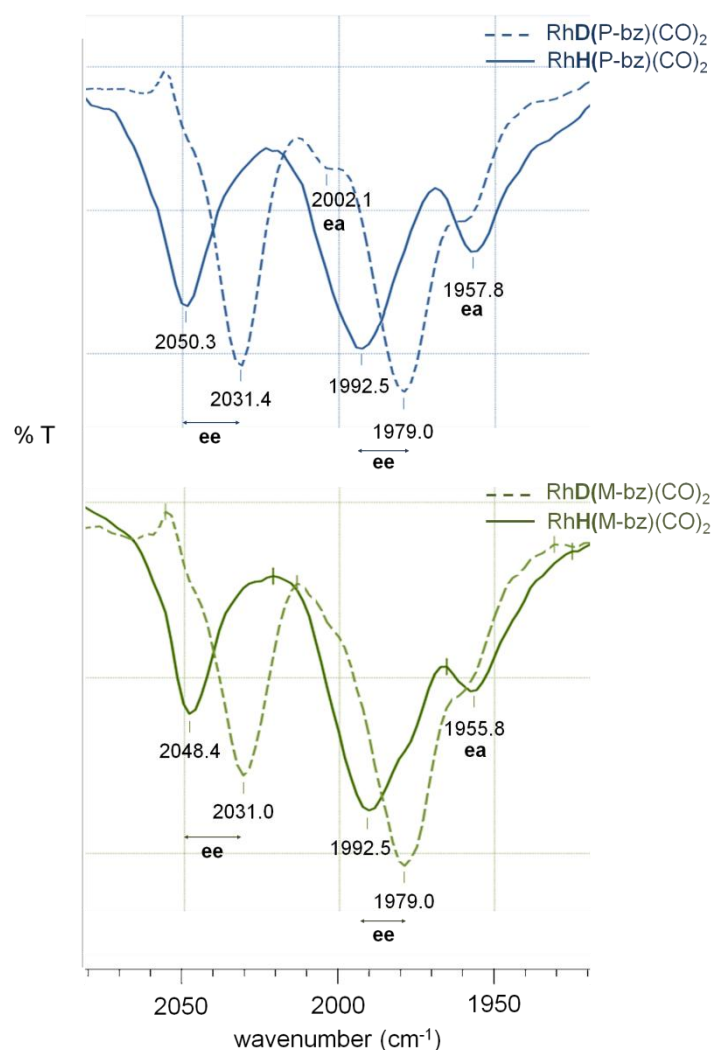


Figure 7.7. High pressure IR spectra (wavenumber cm⁻¹) of [RhH(L)(CO)₂] (solid line) and [RhD(L)(CO)₂] (dashed line) under 20 bar of syngas (CO/H₂ and CO/D₂, respectively) at 40 °C in CH₂Cl₂. -**Top**, *p*-diphosdiam (**P-bz**). -**Bottom**: *m*-diphosdiam (**M-bz**).

In other to determine the catalyst resting state, after the formation of the bis-coordinated rhodium hydrido species (**B**), 1-octene was added to the reactor and the reaction was monitored by IR at 40°C, **Figure 7.8**. The fast formation of the aldehyde product was evidenced by the CO band at 1722 cm⁻¹ which increased in intensity during the reaction. According to the IR spectra, the catalytic species did not change during the reaction, thus proving the bis-coordinated rhodium hydrido species (**B**) as the catalytic resting

species. This is in agreement with previous reported studies on the Rh-phosphine catalysed hydroformylation of alkenes.^{27b,47,50}

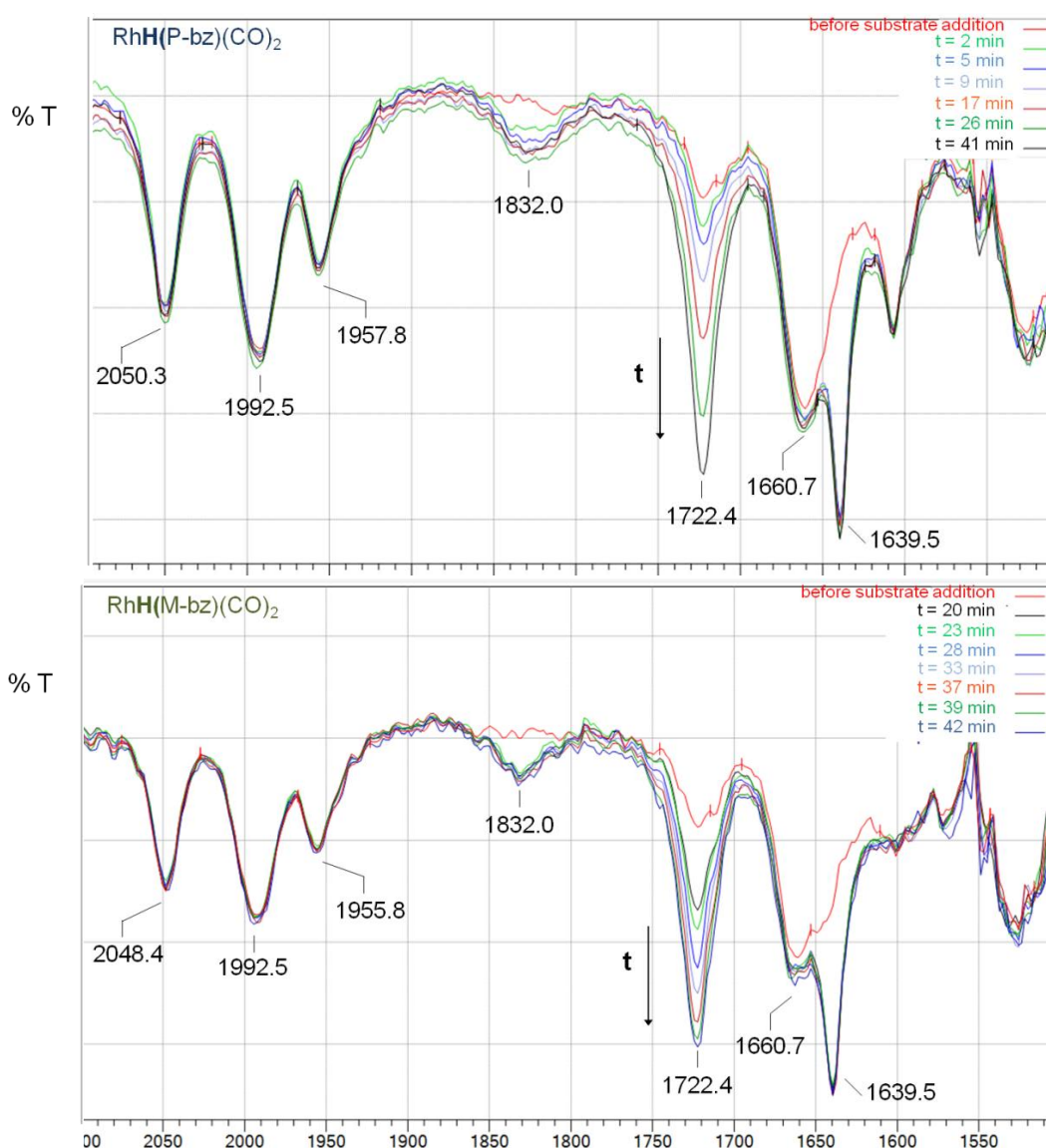


Figure 7.8. High pressure IR spectra (wavenumber cm^{-1}) of $[\text{RhH}(\text{L})(\text{CO})_2]$ after addition of 1-octene. Conditions: 20 bar $\text{CO}:\text{H}_2$ (1:1); 40 °C; 1-octene/Rh = 250; L/Rh = 2; $[\text{Rh}] = 1.4 \text{ mM}$ in CH_2Cl_2 ; Stirring rate 1400 rpm. -**Top:** *p*-diphosdiam ligand (**P-bz**). -**Bottom:** *m*-diphosdiam ligand (**M-bz**). Signals: between 2050 and 1960 cm^{-1} , $[\text{RhH}(\text{L})(\text{CO})_2]$; 1832.0 and 1639.5 cm^{-1} , 1-octene; 1722.4 cm^{-1} , aldehyde; 1660.7 cm^{-1} , amide (of the diphosphine backbone).

Although toluene was also tested as solvent for these experiments, it was rejected due to the absorption bands of this solvent in the Rh-CO region. Alternatively cyclohexene was also tested but the Rh complexes were found to be insoluble in this solvent.

⁵⁰ a) Diéguez, M.; Claver, C.; Masdeu-Bultó, A. M.; Ruiz, A.; van Leeuwen, P. W. N. M.; Schoemaker, G. C. *Organometallics* **1999**, 18 (11), 2107–2115. b) Dydio, P.; Dzik, W. I.; Lutz, M.; De-Bruin, B.; Reek, J. N. H. *Angew. Chem. Int. Ed.* **2011**, 50 (2), 396–400.

Additionally full catalytic experiments with the diphosphine ligands, **P-bz** and **M-bz**, in CH₂Cl₂ at 40 °C were performed (**Table 7.5**) showing similar results in terms of selectivity than those obtained with toluene. These results support the idea of the presence of the same catalytic species in both solvents. The low temperature used in the experiments with dichloromethane had an obvious effect in lowering the reaction rate.

Table 7.5. Hydroformylation of 1-octene with ligands (**M-bz**) and (**P-bz**) in CH₂Cl₂^a

Ligand	Entry	Conv. ^b (%)	l/b ^c (%)	n-aldehyde ^d (%)	2-octenes ^e (%)	octane ^f (%)
<i>m</i> -diphosdiam (M-bz)	27	34.4	90.0	89.6	0.4	0.1
<i>p</i> -diphosdiam (P-bz)	28	49.5	95.3	92.2	2.8	0.5

^a Conditions: 10 bar CO:H₂ (1:1); 40 °C; 24 h of reaction; 1-octene/Rh = 5000; L/Rh = 2; [Rh] = 0.65 mM in CH₂Cl₂; n-decane 0.3 mM as internal standard; Stirring rate 700 rpm. (Catalyst preformation: 16 bar CO:H₂ (1:1); 40 °C, 1.5 h).

^b Conversion of 1-octene: (mmol of converted substrate/mmol of starting substrate) x 100

^c Regioselectivity: (mmol of linear aldehyde/mmol of aldehydes) x 100

^d Overall catalyst selectivity: (mmol of linear aldehyde/mmol of converted substrate) x 100

^e Isomerisation: (mmol of 2-octenes/mmol of converted substrate) x 100

^f Hydrogenation: (mmol of octane/mmol of converted substrate) x 100

As concluding remark of this section, **Table 7.6** shows a summary of the spectroscopic data obtained under high pressure conditions. Some of these data are compared to the reported values for the triphenylphosphine-Rh complexes as model molecules, although several other phosphines or diphosphines of those references cited in this section could have been used indistinctively.

Table 7.6. Spectroscopic data for Rh-diphosphine species in HP-NMR and HP-IR experiments compared to reported results for TPP^a

Rhodium species	Ligand	δ_P (ppm)	δ_H (ppm)	$^1J_{Rh-P}$ (Hz)	$^2J_{H-P}$ (Hz)	$^1J_{Rh-H}$ (Hz)	ν (CO) (cm ⁻¹)
[RhH(P) ₃ (CO) ₂]	P-bz	41.0	-9.6	154.0	13.3	≤ 3	-
(A)	M-bz	44.0	-9.3	154.5	12.9	≤ 3	-
	TPP ^b	42.5	-9.3	155	14	≤ 1	-
[RhH(P) ₂ (CO) ₂]	P-bz	37.3	-9.4	144.0	2.5	2.5	2050.3, 1992.5, 1957.8
(B)	M-bz	39.4	-9.4	143.9	≤ 3	≤ 3	2048.4, 1992.5, 1955.8
	TPP ^b	39.9	-8.9*	138	n.d.*	3.8*	2042, 1992, 1981, 1947
[RhD(P) ₂ (CO) ₂]	P-bz	-	-	-	-	-	2031.0, 2002.1, 1979.0, 1961.6
	M-bz	-	-	-	-	-	2031.0, 1979.0, 1960.6

^a HP-NMR in toluene-D8 at 20° C and 20 bar CO/H₂ (1:1). HP-IR in CH₂Cl₂ at 40 °C and 20 bar CO/H₂ (1:1). See text for further details.

^b Triphenylphosphine. For this ligand, all the NMR values were extracted from Brown *et al.*⁴⁵ except for those marked with a star (*) which were extracted from Segarra.⁵¹ The IR values were extracted from Diéguez *et al.*^{50a}

7.1.3.4. Molecular Mechanics calculations

In addition to the *in situ* experiments described so far, the coordination mode of the bis-chelating phosphines, **P-bz** and **M-bz**, has been further studied by means of molecular mechanics (MM) calculations. In analogy to the reported methodology by Casey and Whiteker,⁵² the natural bite angle and the flexibility range of **P-bz** and **M-bz** were determined. Moreover, according to a previous reported procedure in our group,⁵³ the so-called *dynamic bite angle* was also determined for these diphosphines. This parameter is an average value of the P-Rh-P angle adopted by the ligand at 400 K, and thus gives a more realistic description of the flexibility. A detailed description of the parameters and methodology used in the calculations is provided in the experimental

⁵¹ Segarra Masset, M. D. *Switchable and tunable ligands for homogeneous catalysis*, Universitat Rovira i Virgili, **2010**.

⁵² a) Casey, C. P.; Whiteker, G. T. *Isr. J. Chem.* **1990**, *30* (4), 299–304. b) Casey, C. P.; Whiteker, G. T.; Melville, M. G.; Petrovich, L. M.; Gavney, J. A.; Powell, D. R. *J. Am. Chem. Soc.* **1992**, *114* (14), 5535–5543.

⁵³ Freixa, Z.; Pereira, M. M.; Pais, A. A. C. C.; Bayón, J. C. *J. Chem. Soc. Dalton Trans.* **1999**, No. 18, 3245–3251.

part (Chapter 9). The results obtained for the two ligands, **P-bz** and **M-bz**, are shown in **Table 7.7**.

Table 7.7. Calculated Natural and Dynamic bite angles and flexibility range for ligands **P-bz** and **M-bz**

Ligand	Bite Angle (°)		Flexibility range (°)
	Natural	Dynamic	
<i>m</i> -diphosdiam (M-bz)	102.8	120.2 (9.7) ^a	85-127
<i>p</i> -diphosdiam (P-bz)	108.3	125.7 (10.7) ^a	88-138

^a Standard deviation

See experimental section for detailed procedure.

The natural and dynamic bite angles obtained for **M-bz** were 102.8° and 120.2°, respectively. Both parameters were found to be 5.5° higher for the *para*-isomer **P-bz** (108.3° and 125.7°, respectively). However the biggest differences were found in the flexibility range, defined as the accessible range of P-Rh-P angles within 3 kcal/mol of strain energy from the calculated natural bite angle. While **P-bz** allows bite angles between 88° and 138°, ligand **M-bz** was found to accommodate angles between 85° and 127° within 3 kcal/mol of excess energy strain. These differences are clearly observed in the graphical representation of the flexibility range (**Figure 7.9**).

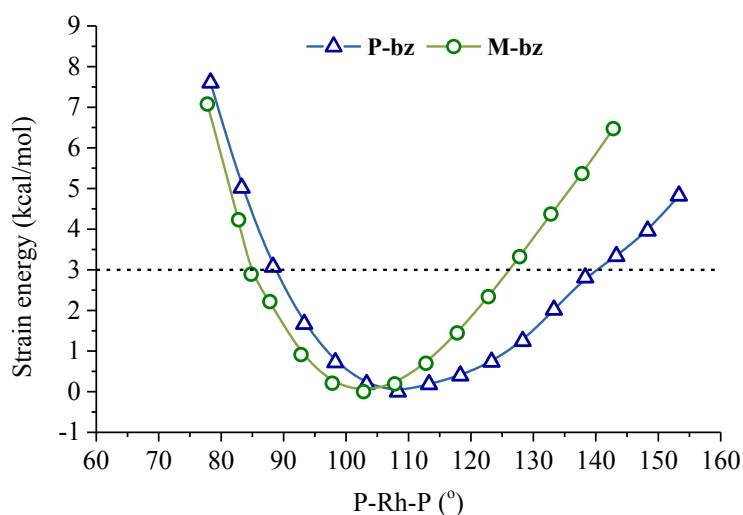


Figure 7.9. Calculated excess strain energy of rhodium chelates of ligands **P-bz** and **M-bz** as a function of the P-Rh-P bite angle. The horizontal dotted line indicates a value of 3 kcal/mol above the energy minimum

The correlation between the diphosphine bite angle and the regioselectivity in the Rh-catalysed hydroformylation of 1-alkenes has been widely acknowledged, it being generally more selective towards the formation of the linear aldehyde when enlarging

the bite angle of the ligand.^{29b,33a,52b,54} It would be easy to think that, when bipyramidal complexes are considered, such as the bis-coordinated rhodium hydrido species (**B**), ligands with bite angles close to 90° would preferentially coordinate in equatorial-axial fashions and, in same the manner, bis-chelating ligands with bites close to 120° would tend to coordinate in bis-equatorial disposition. However attempts to correlate the chelation mode of the bisphosphine ligands and the regioselectivity showed that the equilibrium between **B-ee** and **B-ea** species (the resting states of the reaction) is not the key parameter controlling the regioselectivity.^{27b,30,54} The effect of the bite angle on the selectivity towards linear aldehyde was attributed to the four-coordinate intermediate species (diphosphine)Rh(CO)H. The increased steric congestion produced by ligands with wider bite angles would favour the subsequent formation of the less sterically hindered linear alkyl rhodium complexes.

Either way, the calculated bite angles for ligands **P-bz** and **M-bz** were in agreement with the catalytic observed catalytic results. **P-bz**, having wider natural bite angle and flexibility range compared to the *meta*-isomer **M-bz**, would produce a greater steric congestion around the metal centre thus enhancing the formation of the linear aldehyde.

7.1.4. Catalytic reactions with the latex-supported ligands

After the complete study of the diphosphine-diamide ligands in homogeneous conditions, the preparation of latex-supported diphosphines was undertaken.

The preparation of phosphine-functionalised latex particles was attempted by a free radical co-polymerisation process in water, following a modification of a reported procedure.⁵⁵ Therefore, the water soluble monomers (*p*-vinylbenzyl)trimethylammonium tetrafluoroborate (20 mol%) and *p*-(vinylbenzyl)poly(ethyleneglycol)-2000 (4 mol%) were dissolved in water at 80 °C previous to the addition of styrene (73 mol%), *p*-divinylbenzene (3 mol%) and the corresponding diphosphine (0.18 mol%) followed by 2,2'-azobis[2-methyl-*N*-(2-hydroxyethyl)propionate] as radical initiator (1 mol%). After 4 hours at 80°C, the obtained emulsion was cooled down to room temperature and dialysed for 5 days with a 14000 Da molecular weight cutoff cellulose membrane. Latex

⁵⁴ van Leeuwen, P. W. N. M.; Kamer, P. C. J.; Reek, J. N. H.; Dierkes, P. *Chem. Rev.* **2000**, *100* (8), 2741–2769.

⁵⁵ Peral, D.; Stehl, D.; Bibouche, B.; Yu, H.; Mardoukh, J.; Schomäcker, R.; Klitzing, R. von; Vogt, D. *J. Colloid Interface Sci.* **2018**, *513*, 638–646.

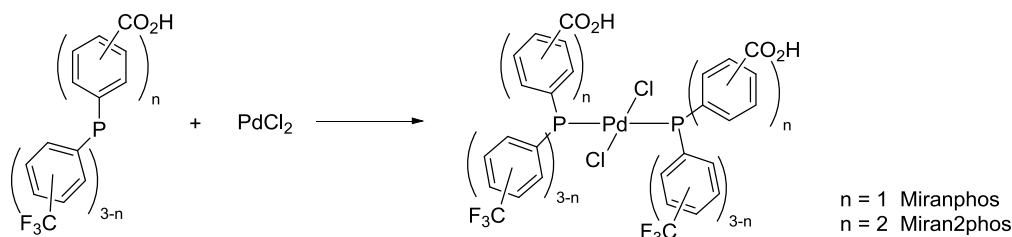
particles were therefore obtained as water stable suspensions. Due to time and sample limitations, only one test with each of the diphosphines could be performed, using 60 mg of the ligands. The solid residue of each of the latex-suspensions, which serves as estimation of the degree of polymerisation of the monomers, was quantified after elimination of the water of 2 ml samples by a freeze-drying process. The solid residue of the latex obtained using phosphine **M-st** was 13 mg/ml, a value too low to be accepted and, consequently, had to be discarded. On the other hand, when using **P-st**, the solid residue obtained was 52 mg/ml. Moreover, the content of phosphorus of this latex was determined by ICP-MS analysis of the solid residue. The expected value for the P content was about 0.5 mg of P per gram of solid residue, knowing that the total amount of monomers was of 6.67 g and assuming the same degree of polymerisation of all the monomers. The content of P according to the ICP-MS analysis was below 0.05 mg of P per gram of solid residue which is, at best, 10 times smaller than expected. In spite of the low content of phosphorus in the latex, the particles were tested in the Rh-catalysed hydroformylation of 1-octene, under similar conditions to those reported above for the homogeneous reactions. Conversion of 1-octene below 16 %, both at 10 and 30 bar of syngas, after 15 h of reaction were observed. No recycling experiments were performed.

The results obtained in both the synthesis of the phosphine-modified latex particles and their application in catalytic experiments are far from what one would expect. However it is important to notice that these were preliminary experiments and much further work is necessary before drawing conclusions on this respect.

7.2. Miranphos and Miran2phos *trans*-[PdCl₂L₂] complexes: Synthesis and structural determination

Miranphos and Miran2phos ligands (*meta* and *para*-isomers) were used to prepare the *trans*-[PdCl₂L₂] complexes, **Scheme 7.15**. The corresponding phosphine was dissolved in CH₂Cl₂ previous to the addition of a solution of palladium (II) chloride in CH₃CN. The resulting orange solution evolves to a yellow suspension indicating the formation of the complexes, with the exemption of *trans*-[PdCl₂(*m*-Miranphos)₂] which was found to be soluble. Filtration of the yellow precipitate afforded the corresponding Pd-complexes in good yields. However, given the high solubility of the *m*-Miranphos complex not

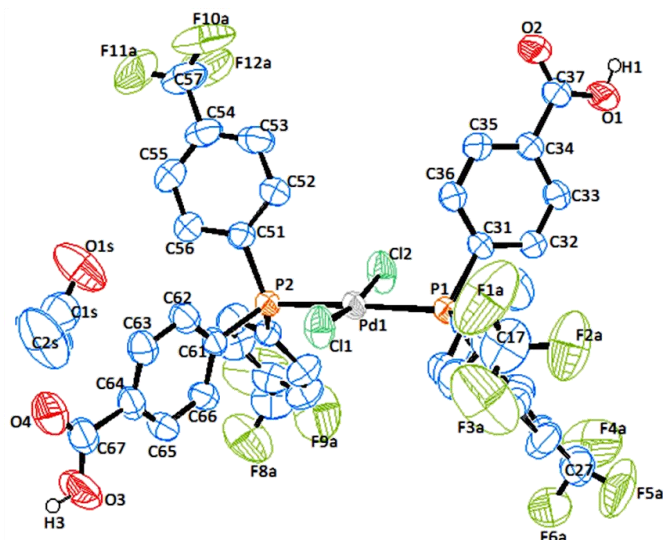
only in the reaction media, but also in a variety of solvents including CH₂Cl₂, Et₂O, acetone, CH₃CN and ethyl acetate, the complex was isolated by evaporation of the solvent followed by recrystallisation in CH₂Cl₂/cyclohexane.



Scheme 7.15. Synthesis of *trans*-[PdCl₂L₂] complexes of Miranphos and Miran2phos ligands

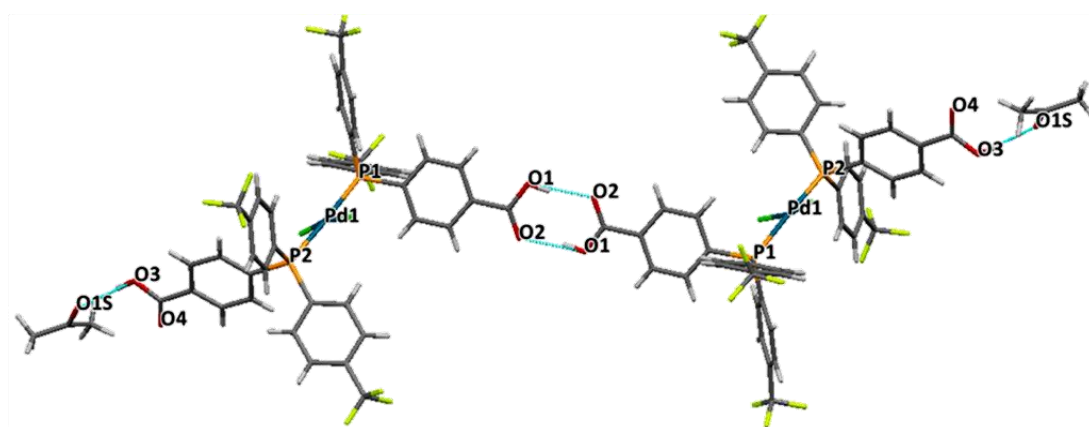
All the *trans*-[PdCl₂L₂] complexes were found to be highly soluble in acetone and were characterised by NMR (¹H, ³¹P{¹H} and ¹⁹F{¹H}). Moreover, efforts were focused in the preparation of crystals for the structural determination of the complexes. Crystals of suitable quality for XRD were obtained but only with the *p*-Miranphos and *m*-Miranphos complexes. Crystals of *trans*-[PdCl₂(*p*-Miranphos)₂] were obtained by slow evaporation of a saturated solution of the complex in a mixture of acetone/*n*-hexane. *Trans*-[PdCl₂(*m*-Miranphos)₂] was crystallised by slow diffusion of *n*-hexane into a solution of the complex in CH₂Cl₂. In spite of the different methods attempted, the palladium complexes with the Miran2phos ligands only precipitated in the form of powder solids.

The *trans*-[PdCl₂(*p*-Miranphos)₂] complex crystallised as mono-acetone solvate. The structure obtained by single-crystal X-ray diffraction confirmed the *trans*-coordination of the ligands, as expected, showing a slightly distorted square-planar geometry. **Figure 7.10** shows the structure together with the most relevant distances and angles for *trans*-[PdCl₂(*p*-Miranphos)₂].acetone complex. More interestingly, it was observed the formation of dimeric structures by bridging between the carboxylic groups of one of the *p*-Miranphos ligands of each monomer. The carboxylic acid group of the other coordinated phosphine is interacting through H-bonding with a molecule of acetone, **Figure 7.11**.



Distances				Angles			
Pd1-Cl1	2.2723(8)	P2-C41	1.824(3)	P1-Pd1-Cl1	93.98(3)	C21-P1-C31	104.16(13)
Pd1-Cl2	2.3044(8)	P2-C51	1.823(3)	P1-Pd1-Cl2	88.85(3)	C41-P2-C51	107.32(13)
Pd1-P1	2.3194(8)	P2-C61	1.822(3)	P2-Pd1-Cl1	89.87(3)	C41-P2-C61	103.62(13)
Pd1-P2	2.3419(8)	O1-C37	1.277(4)	P2-Pd1-Cl2	87.76(3)	C51-P2-C61	104.81(13)
P1-C11	1.819(3)	O2-C37	1.234(4)	Cl1-Pd1-Cl2	171.34(4)	O1-C37-O2	124.2(3)
P1-C21	1.833(3)	O3-C67	1.292(5)	P1-Pd1-P2	175.18(3)	O1-C37-C34	116.1(3)
P1-C31	1.819(3)	O4-C67	1.204(5)	C11-P1-C21	105.68(15)	O3-C67-O4	123.5(3)
				C11-P1-C31	103.72(14)	O3-C67-C64	114.8(4)

Figure 7.10. ORTEP plot (ellipsoid at 50% probability) of *trans*-[PdCl₂(*p*-Miranphos)₂].acetone. Selected distances (Å) and angles (°). Aromatic hydrogen atoms omitted for clarity. Only one conformation of the disordered CF₃ is shown.



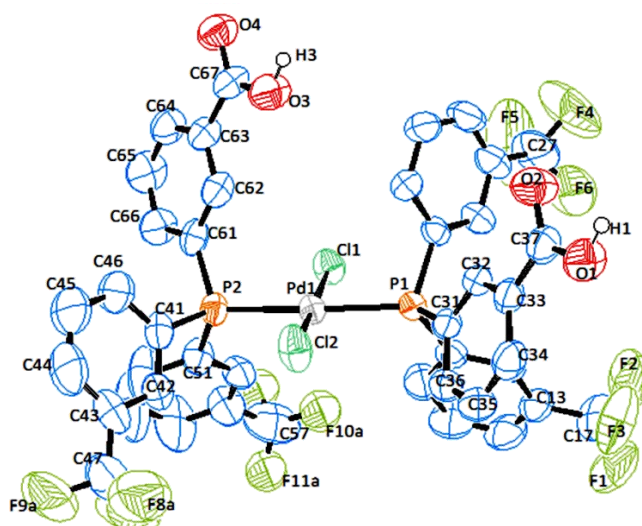
Hydrogen bonding interactions

D-H...A	d(D-H)	d(H...A)	d(D...A)	angle (D-H-A)
O1-H1...O2 ^a	0.82	1.82	2.615(3)	163.6
O3-H3...O1S ^b	0.82	1.90	2.697(5)	164.6

^a (-x+1, -y+1, -z). ^b (-x, y+1/2, -z+1/2). D = hydrogen atom donor and A = hydrogen atom acceptor

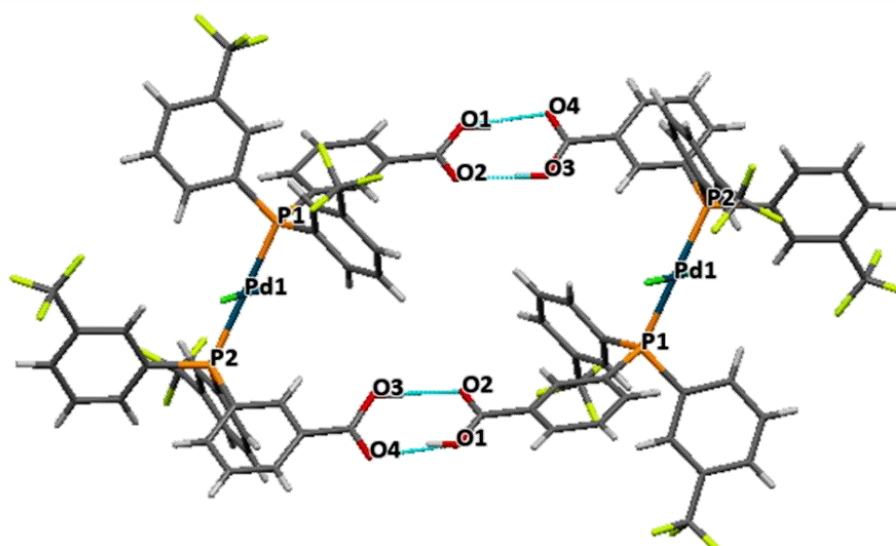
Figure 7.11. Stick representation of the dimeric structure of the complex of *trans*-[PdCl₂(*p*-Miranphos)₂].acetone. Only one conformation of the disordered CF₃ is shown. H-bond interactions distances (Å) and angles (°)

Similarly, the structure of *trans*-[PdCl₂(*m*-Miranphos)₂] shows the *trans*-coordination of the ligands in a square planar geometry, **Figure 7.12**. Also a dimeric structure is observed in this complex although, unlike to what was observed in the previous structure, in the *m*-isomer both coordinating phosphines participate in the H-bond interactions with the carboxylic groups of the phosphines of the other complex, **Figure 7.13**.



Distances				Angles			
Pd1-Cl1	2.314(2)	P2-C41	1.821(8)	P1-Pd1-Cl1	86.93(7)	C41-P2-C51	102.1(4)
Pd1-Cl2	2.261(2)	P2-C51	1.837(8)	P1-Pd1-Cl2	92.18(7)	C41-P2-C61	104.8(4)
Pd1-P1	2.3164(19)	P2-C61	1.804(8)	P2-Pd1-Cl1	89.07(7)	C51-P2-C61	108.3(4)
Pd1-P2	2.3212(19)	O1-C37	1.292(9)	P2-Pd1-Cl2	91.78(8)	O1-C37-O2	121.9(8)
P1-C11	1.812(7)	O2-C37	1.264(9)	Cl1-Pd1-Cl2	175.98(7)	O1-C37-C33	119.7(7)
P1-C21	1.815(7)	O3-C67	1.288(9)	P1-Pd1-P2	175.92(9)	O2-C37-C33	118.4(7)
P1-C31	1.821(7)	O4-C67	1.242(9)	C11-P1-C21	109.1(4)	O3-C67-O4	122.0(8)
				C11-P1-C31	101.0(4)	O3-C67-C63	117.1(7)
				C21-P1-C31	103.6(3)	O4-C67-C63	121.6(4)

Figure 7.12. ORTEP plot (ellipsoid at 50% probability) of *trans*-[PdCl₂(*m*-Miranphos)₂]. Selected distances (Å) and angles (°). Aromatic hydrogen atoms omitted for clarity. Only one conformation of the disordered CF₃ is shown.

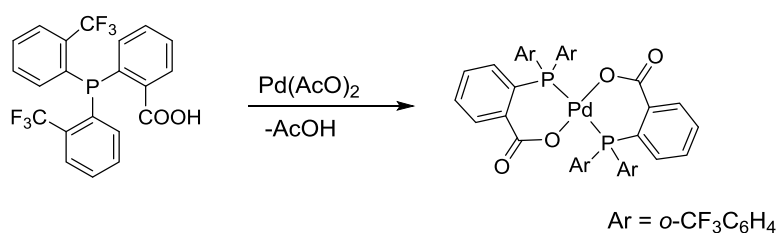


Hydrogen bonding interactions				
D-H...A	d(D-H)	d(H...A)	d(D...A)	angle (D-H-A)
O1-H1...O4	0.82	1.87	2.673(9)	167.3
O3-H3...O2	0.82	1.80	2.609(8)	168.2

(-x+2, -y+1, -z). D = hydrogen atom donor and A = hydrogen atom acceptor

Figure 7.13. Stick representation of the dimeric structure of the complex of *trans*-[PdCl₂(*m*-Miranphos)₂]. Only one conformation of the disordered CF₃ is shown. H-bond interactions distances (Å) and angles (°)

Besides these two complexes, the Pd(II)-complex of the *o*-Miranphos was studied in our group.⁵⁶ The reaction between Pd(AcO)₂ and two moles of *o*-Miranphos afforded the bis-chelate complex *trans*-bis[(bis(*o*-trifluoromethyl phenyl)phosphino- κP -*o*-benzoato- κO)]palladium(II), **Scheme 7.16**, proving the chelating behaviour of the phosphine.



Scheme 7.16. Synthesis of *trans*-bis[(bis(*o*-trifluoromethyl phenyl)phosphino- κP -*o*-benzoato- κO)]palladium(II) complexes

⁵⁶ Daniel Garcia Martos. *Sulfonated trifluoromethylated arylphosphines for the Heck reaction: an aqueous biphasic approach*. Undergraduate Thesis. Universitat Autònoma de Barcelona. **2016**

7.3. Summary and concluding remarks

The *p*-Miranphos and *m*-Miranphos phosphines have been used to prepare new chelating diphosphines using a diamine as linker between the ligands. With the intention of supporting the ligands on the surface of latex particles, a vinyl moiety was included in their structures.

The non-vinyllic analogous of the diphosphines were synthesised as model molecules to study the properties of the ligands in the Rh-catalysed hydroformylation of 1-octene. Slightly higher values of regioselectivities were obtained when the *p*-isomer phosphine, **P-bz**, was used as ligand although it was also more active in the isomerisation showing the same overall catalyst selectivity than the *meta*-isomer, **M-bz**. High pressure studies showed that, under catalytic conditions, the bis-coordinated hydrido species (**B**) are the resting state in the reactions, with preferential coordination of the ligands in bis-equatorial fashion. Under higher concentrations, the NMR experiments showed also the formation of the tris-phosphine coordinated species (**A**). The molecular mechanics calculations showed a slightly greater bite angle for the **P-bz** ligand with also a wider flexibility range compared to **M-bz**.

The *p*-Miranphos and *m*-Miranphos ligands were also tested in the Rh-catalysed hydroformylation of 1-octene, resulting in more active systems compared to the triphenylphosphine. Solubility issues were observed, especially for the *para*-isomer ligand.

Finally, the palladium complexes, *trans*-[PdCl₂L₂], of the Miranphos and Miran2phos ligands were prepared. The single-crystal X-ray diffractions of the complexes with the Miranphos ligands were obtained.

Chapter 8

General Conclusions

In this work, the reaction of hydrolysis of the trifluoromethyl group in arylphosphines using sulfuric fuming acid and boric acid, to generate carboxylic acids, has been studied in detail. In order to evaluate the scope of the applicability of the reaction, four new heteroleptic trifluoromethylated phosphines and two diphosphines were synthesised. In total, the reaction of hydrolysis was investigated in a set of eight monophosphines, of which four were homoleptic and the other four were heteroleptic. Two diphosphines were also essayed in this reaction.

The following conclusions can be extracted, according to the objectives of this dissertation and the experimental work carried out:

The reactions with the trifluoromethylated phosphines showed that the rate of the hydrolysis of the trifluoromethyl depends on the relative position of this group with respect to the phosphorus atom. The *meta*-CF₃ groups show faster rates than those in *para*-position. At the same time, much slower rates were found in those CF₃ groups in *ortho*- and 3,5-positions than in *meta* and *para*. The generation of a carbocation seems to be the rate-limiting step of the reaction and its relative stability has been used as main factor to justify the different reaction rates observed between the *meta*- and *para*-CF₃. Additional destabilisation of the carbocation in *ortho*-position produced by both steric and inductive effects of the phosphorus atom will be responsible of the slow rate observed for the hydrolysis of the trifluoromethyl group in *ortho*-position. Inductive effects produced by the 3,5-groups have been related to the slow reaction rates observed when 3,5-trifluoromethyls were present in phosphines in either the homoleptic phosphine or the heteroleptic ones. With this procedure, eight new carboxylic-trifluoromethylated phosphines were synthesised. These compounds are covered under patent and four of them, *para*- and *meta*-Miranphos and *para*- and *meta*-Miran2phos, are available at the catalogue of Strem Chemicals under a license of the Universitat Autònoma de Barcelona.

Special behaviour was observed in the hydrolysis reaction of the tris(*o*-(trifluoromethyl)phenyl)phosphine. Although the monocarboxylic phosphine was obtained, the dicarboxylic compound was never detected. Instead, a set of spirocyclic compounds were observed. In this regard, two new spirocyclic oxyphosphoranes were isolated and characterised. The formation of these compounds was studied and a

mechanism of formation was proposed in which the oxidation of the phosphorus atom is required to form the spirocyclic structure.

Concerning the insights into the reaction of hydrolysis, it was concluded that the superacid mixture involved in the hydrolysis of the trifluoromethyl group, under the conditions used in this work, was the ternary superacid mixture $\text{HB}(\text{SO}_4)_4\text{-SO}_3\text{-H}_2\text{SO}_4$. The acidity of this system was estimated to be higher than the binary mixtures $\text{SO}_3\text{-H}_2\text{SO}_4$ and $\text{HB}(\text{SO}_4)_4\text{-H}_2\text{SO}_4$. As previously reported by other authors, the superacid would promote the cleavage of the C-F bond driven by the protonation of a fluorine atom with the subsequent formation of HF and a difluorocarocation. Moreover, it was also concluded that the protection of the phosphines against oxidation takes place by protonation of the phosphorus atom.

With the trifluoromethylated diphosphines the reaction conditions were found to be unsuitable to promote the hydrolysis of the CF_3 group. The high number of CF_3 groups in this diphosphines would be responsible of this lack of reactivity. When sulfuric acid was tested, partial or complete oxidation of the phosphorus atoms was observed and protonation of the P atom was only observed in the form of half-oxidised half-protonated species. The less oxidative acid $\text{CF}_3\text{SO}_3\text{H}$ allowed the complete protonation of the BIPHEP-derived diphosphine. For the dppbz-derived diphosphine, only when using the stronger superacid $\text{CF}_3\text{SO}_3\text{H}_2^+\text{-B}(\text{OSO}_2\text{CF}_3)_4^-$ was the diprotonated species observed. However, this high acidic condition yielded the decomposition of the diphosphine.

The carboxylic phosphines *p*-Miranphos and *m*-Miranphos were used to prepare chelating diphosphines, by reaction with a diamine leading to amide linkages. Vinyl moiety was included in the structure of the diamine in order to eventually form a polymer-supported diphosphine by co-polymerisation with latex particles. The non-vinyl diphosphines were also prepared as model molecules to study the performance of these ligands in the Rh-catalysed hydroformylation of 1-octene in homogeneous conditions. The results showed the chelating behaviour of the ligands with regioselectivities up to 97 %, expressed as the percentage of linear aldehyde relative to total aldehydes obtained. Preliminary experiments on the preparation of the ligand-supported latex particles did not afford the expected results. Further experiment might be required.

Finally, *p*-Miranphos and *m*-Miranphos phosphines were tested as monodentate ligands in the Rh-catalysed hydroformylation of 1-octene, showing higher TOF than triphenylphosphine. Moreover, these carboxylic ligands together with the *p*-Miran2phos and *m*-Miran2phos, were used to prepare the *trans*-[PdCl₂L₂] complexes, where L is a carboxylic phosphine acting exclusively as P-donor ligand. The complexes show appealing supramolecular structures due to intermolecular H-bonding formation.

Chapter 9

Experimental Procedures

9.1. General procedures and instrumentation

Unless otherwise mentioned, all the synthetic manipulations were performed under nitrogen atmosphere using standard Schlenk techniques.¹ Solvents and liquid reagents were deoxygenated by bubbling nitrogen for 10-15 minutes. General chemical reagents and solvents were purchased from commercial suppliers which include Sigma-Aldrich, Scharlab and Acros Organics. Trifluoromethylated compounds were purchased from Cymmit. 65 % fuming sulfuric acid was exclusively purchased from VWR and transition metal compounds were mainly purchased from Alfa Aesar. Except where otherwise specified, these chemicals were used without further purification.

Anhydrous solvents and reagents were used when required. The elimination of water was carried out by using different standard procedures.² Non-protic solvents, including toluene, hexanes, THF and Et₂O, were distilled over Na/benzophenone. Additional distillation over LiAlH₄ was performed when severe dry conditions were required. CH₂Cl₂ was distilled over CaH₂ and methanol was distilled over Mg/I₂. Amines were distilled over KOH. Once distilled, all solvents were stored with 3 Å molecular sieves under inert atmosphere for a period no longer than 2 days.

Spare parts for the high pressure autoclaves were purchased from Swagelok.

9.1.1. Nuclear Magnetic Resonance

The signals in the NMR spectra of the synthesised compounds have been assigned using bidimensional experiments (COSY, HSQC, HMBC) and some specific monodimensional experiments such as ¹H{³¹P} and DEPT.

The NMR spectra, including ¹H, ¹H{³¹P}, ¹³C{¹H}, ³¹P{¹H}, ³¹P, ¹⁹F{¹H}, ¹¹B{¹H} and the bidimensional experiments COSY, HSQC and HMBC, were recorded at the Servei de Resonància Magnètica Nuclear at the UAB on three different NMR spectrometers:

Bruker Avance 250 (250.16 MHz for ¹H, 62.90 MHz for ¹³C, 235.2 MHz for ¹⁹F and 101.27 MHz for ³¹P)

¹ Shriver, D. A.; Drezdon, M. A. *The Manipulation of Air-Sensitive Compounds*. 2nd Ed. Wiley-Interscience, New York. **1986**.

² Armarego, W. L. F.; Chai, C. *Purification of Laboratory Chemicals*., 6th ed.; Elsevier Science, **2009**.

Bruker Avance DPX 360 (360.13 MHz for ^1H and 90.56 MHz for ^{13}C)

Bruker Avance III 400 (400.13 MHz for ^1H , 100.61 MHz for ^{13}C , 376.50 MHz for ^{19}F , 161.98 MHz for ^{31}P and 128.38 MHz for ^{11}B).

In a few instances Bruker Avance III 500 NMR spectrometer (500.13 MHz for ^1H , 125.80 MHz for ^{13}C and 202.46 MHz for ^{31}P) was used at the NMR lab of the School of Chemistry at the University of Edinburgh.

Chemical shifts in ^1H and ^{13}C NMR, and the bidimensional experiments with these nuclei, are relative to the signal of the solvent.³ In ^{31}P NMR chemical shifts are relative to 85 % H_3PO_4 (0.0 ppm), used as external standard. For ^{19}F NMR and ^{11}B NMR experiments the signals are relative to fluorene (-113.15 ppm with respect to CFCl_3) and $\text{BF}_3 \cdot \text{Et}_2\text{O}$ (0.0 ppm), respectively.

In ^{31}P NMR experiments, whenever two different phosphorus atoms were present in the samples (*i.e.* a phosphine and a phosphine oxide), accurate determination of the values of integrals was performed by increasing the relaxation delay to 10 seconds. This procedure is necessary since the relaxation time of nuclei is strongly dependent on the environment.

Unless otherwise stated, all the NMR experiments were performed at 298 K.

9.1.2. High Resolution Mass Spectrometry (HR-MS)

HR-MS analyses were performed by the *Servei d'Anàlisi Química* at UAB in a Bruker microTOF spectrometer coupled to an Apollo II electrospray source (ESI).

Some of the phosphine products have been detected as the corresponding phosphine oxides, especially those phosphines with a high acidic character. The reason behind this phenomenon is related to the degree of ionisation of the compounds. Unlike the phosphine oxides, highly acidic phosphines are hardly ionized. Thus, traces of oxide present in the sample (or formed during the analysis) are the main compounds detected. In some instances this issue has been solved by adding 0.2 % formic acid in the solution of the phosphines before the injection in the spectrometer.

³ Fulmer, G. R.; Miller, A. J. M.; Sherden, N. H.; Gottlieb, H. E.; Nudelman, A.; Stoltz, B. M.; Bercaw, J. E.; Goldberg, K. I. *Organometallics* **2010**, 29 (9), 2176–2179.

9.1.3. Elemental Analysis (EA)

Elemental analyses (C, H and N) were performed by the *Servei d'Anàlisi Química* at UAB in a Thermo Fisher Scientific Flash EA 2000 CHNS.

9.1.4. Gas Chromatography (GC)

The evolution of synthetic reactions was carried out in a Hewlett Packard HP5890 gas chromatograph equipped with a FID detector and an Agilent HP5 column (30 m long, 0.32 mm ID and 0.25 μm film thickness).

Conversions and selectivities of the Rh-catalysed hydroformylation of 1-octene were obtained with an Agilent Technologies 6850 equipped with a FID detector and an Agilent 7683B Series injector and with a Shimadzu GC-2010 FID, equipped with a AOC-20i autoinjector. The columns used were Agilent HP5 and Agilent J&W Ultra 2 (25 m long, 0.20 mm ID and 0.33 μm film thickness), respectively.

For compound identification, both in synthetic and catalytic experiments, an Agilent Technologies 6850 equipped with an Agilent Technologies 5975C VL MSD mass spectrometer detector and an Agilent HP5-MS column (30 m long, 0.32 mm ID and 0.5 μm film thickness) were employed. The Wiley7N library was used for the identification according to the fragmentation of the compounds.

9.1.5. Infrared Spectroscopy (IR)

IR spectra recorded in solution were performed in a Perkin Elmer 2000 IR-FT spectrometer. Solid ATR-FTIR spectra were recorded in a Bruker IR Tensor 27 spectrometer equipped with an ATR Specac Golden Gate single reflexion diamond ATR system.

High Pressure IR (HP-IR) experiments were carried out in a Shimadzu IRTracer-100 spectrophotometer.

9.1.6. X-ray diffraction (XRD)

Unless otherwise stated, single-crystal XRD data were collected on a Bruker SMART-APEX diffractometer using Mo K α radiation at the *Servei de Difracció de Raigs X* at the UAB. An empirical absorption correction was applied to the gathered data (SADABS).⁴ The structure was solved by either direct methods or Patterson (SHELXLS-86) and refined by full-matrix least-squares methods on F^2 using SHELXL-2013.⁵ Plot of the structures was obtained either with ORTEP or MERCURY software included in the WINGX package.⁶ Refinement of the structures was performed by the author of the present dissertation with the kind assistance of Dr. Ángel Álvarez. Disordered CF₃ groups were refined according to the methodologies described in the literature.⁷ Detailed information about refinement (isotropic/anisotropic atoms, disordered groups, etc) of each of the structures is provided in the experimental description of each one of these compounds.

9.2. Catalytic experiments: Rh-catalysed hydroformylation of 1-octene

9.2.1. Conversion, chemoselectivity, regioselectivity and TOF

A few important terms used in the comparison of the different catalytic reactions will be explained in the following lines.

Conversion is defined as the quantity of substrate consumed during the catalytic reaction. It can be calculated by determination of remaining amount of substrate at the end of the reaction and comparing it to the initial amount.

Whenever different functional groups can be obtained in a catalytic reaction, the *chemoselectivity* refers to the ability of the catalytic system to yield the product with the aimed functional group. It is expressed as the ratio between the amount of the aimed products and the total amount of reaction products.

⁴ Bruker, SADABS, Bruker Analytical X-Ray Division, Madison **2001**

⁵ Sheldrick, G. M.; *Acta Crystallogr. Sect. A Found. Crystallogr.* **2008**, *64* (1), 112–122.

⁶ Farrugia, L. J.; *J. Appl. Crystallogr.* **1999**, *32* (4), 837–838.

⁷ a) Muller, P. *Crystallogr. Rev.* **2009**, *15* (1), 57–83. b) Ng, S. W. *Chinese J. Struct. Chem* **2005**, *24* (12), 1425–1439.

The term *regioselectivity* applies when different isomers can be obtained in a given reaction. It is calculated as the ratio between the major isomer and the sum of all the isomers.

9.2.2. Description of the autoclaves and gas line system

University of Edinburgh

Catalytic experiments performed at the University of Edinburgh were carried out in 100 ml mechanically stirred stainless steel autoclaves with gas entrainment impeller. Addition of the substrate was done through a dropping funnel. The autoclaves were equipped with heating jacket, temperature sensor (thermocouple) and pressure sensor. Moreover, a mass-flow controller (Brooks Instruments) was used to feed the autoclave with gas in order to keep the pressure constant inside the reactor. All of these devices were coupled to data-logging system for data collection via PC. **Figure 9.1** shows a picture of the before described autoclave together with the schematics.

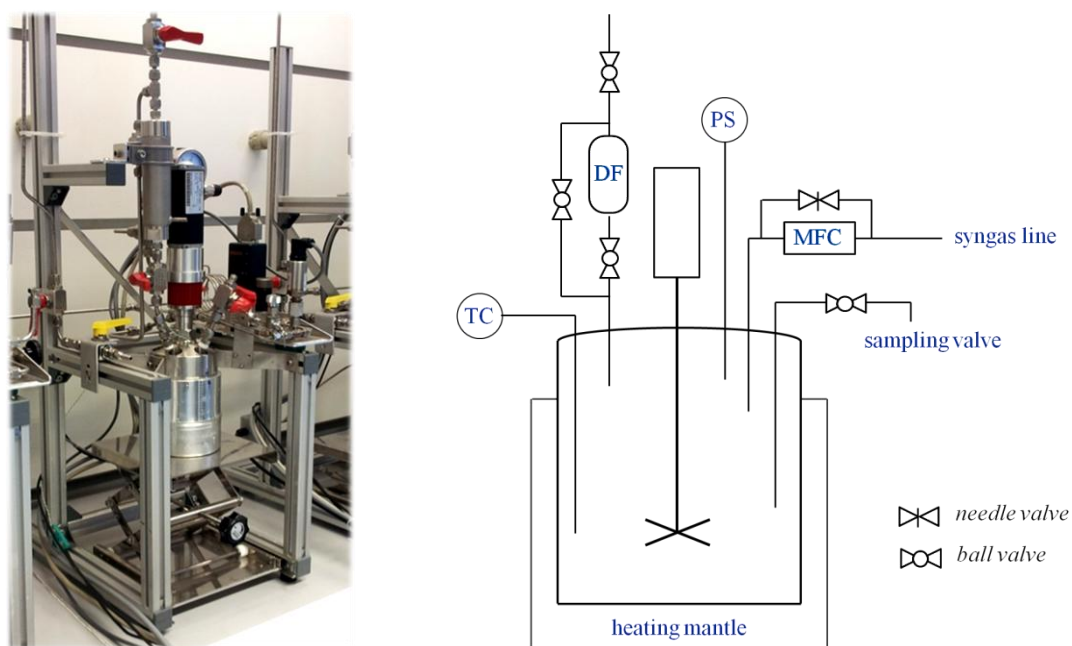


Figure 9.1. left- image of the reactor used in the catalytic reactions in Edinburgh and right- schematics of the reactor. TC = thermocouple, DF = dropping funnel, PS = pressure sensor/transducer, MFC = mass-flow controller.

Univerisitat Autònoma de Barcelona

The final setup used in the reactions of hydroformylation in Barcelona was based in the modification of the mechanically stirred autoclave of a *Parr 4598 Micro Bench Top*

Reactor, with the aim of obtaining a system which could reproduce the results obtained in Edinburgh. Such modification consisted, in first place, in adapting an addition funnel which allowed the catalyst preformation followed by the addition of the substrate without the need of depressurising the autoclave. Also, a gas entrainment impeller was designed and included in the modification of the reactor. **Figure 9.2** shows the picture of the reactor and the corresponding schematics.

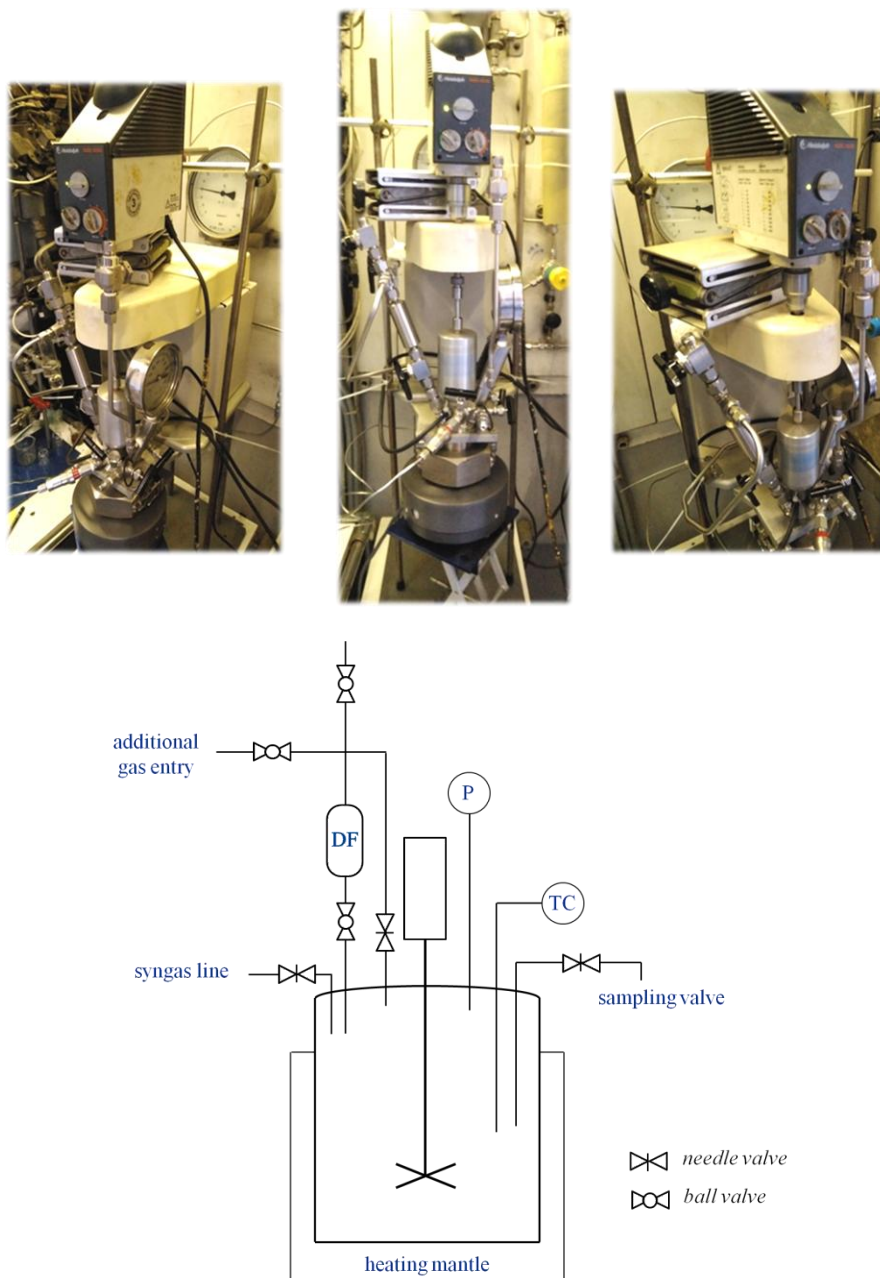


Figure 9.2. top- lateral and front images of the reactor used in the catalytic reactions in Barcelona. bottom- schematics of the autoclave. DF = dropping funnel, P = manometer, TC = thermocouple

The final setup consisted in a 25 ml autoclave equipped with a gas entrainment impeller and a dropping funnel. Heating was provided with a heating jacket. Syngas mixture (H_2 + CO) was prepared in a gas cylinder (reservoir) which constantly fed the reactor through a gas regulator set at the selected reaction pressure. Temperature was controlled with a thermocouple and pressure drop during the reaction was monitored with a pressure transducer connected to the feeding gas cylinder, **Figure 9.3**. Control unit allowed the adjustment of temperature and stirring rates. The motor of the mechanic stirrer included in the system provides stirring rates up to 700 rpm. Alternatively, if higher rates were required, an overhead stirrer (*Heidolph RZR 2020*) could be coupled after disassembling the drive belt of the motor of the reactor stirrer (as shown in **Figure 9.2**). Data during the reactions (temperature and pressure) was collected via PC connected to the control unit. During the reactions, the feeding gas cylinder was thermally isolated to keep the temperature approximately constant along the process.

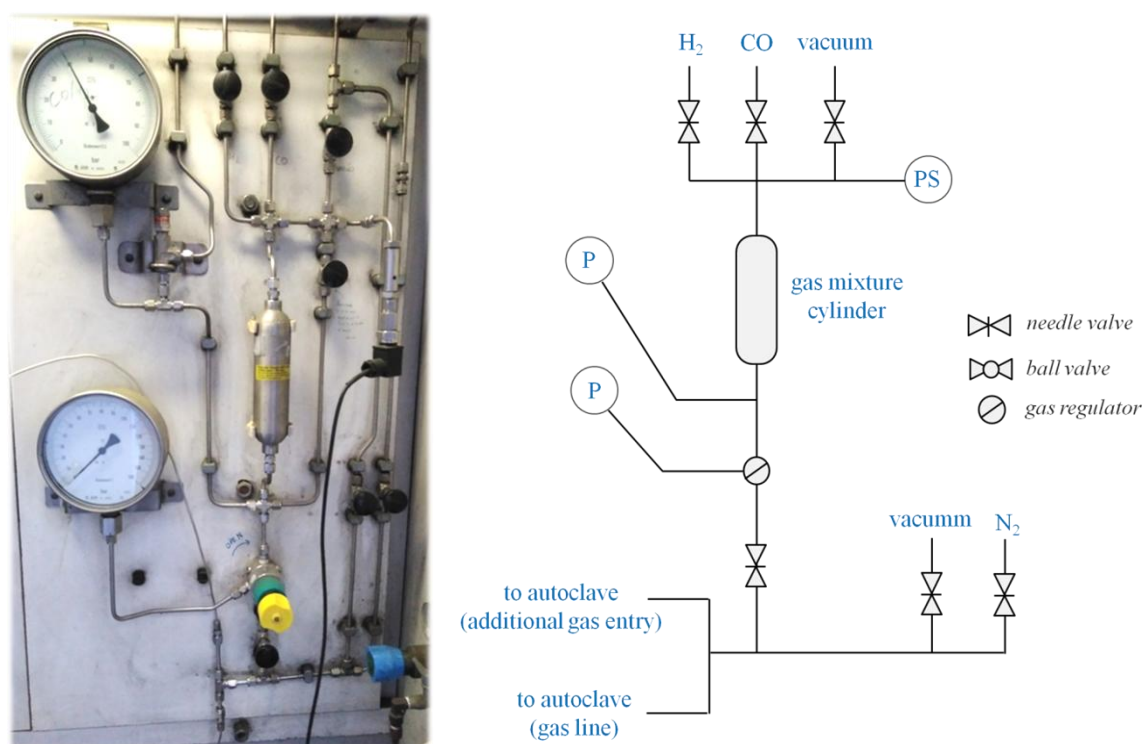


Figure 9.3. left- image of the gas line and right- schematics of the gas line.
PS = pressure sensor/transducer, P = manometer, R = reducer

As commented above, the stirrer of the original autoclave was replaced to a gas-entrainment impeller. This impeller was designed by the author of this work and was kindly constructed by Mr Óscar Sánchez from Tallers Caballé S.L. The design was

based on the impeller used in the autoclave from Edinburgh and the commercial models of impellers available for this reactor, with some modifications.⁸

Detailed explanation on the principle of work of this kind of impellers can be found in the literature.⁹ The impeller consists in three different parts (**Figure 9.4**): one solid shaft (1) which is connected to the head stirrer and to a hollow shaft (2) which, at the same time, is connected to the hollow blades (3) of the stirrer. Since three different vessels can be used in this autoclave (25, 50 and 100 ml), three different hollow shafts were designed and constructed.



Figure 9.4. Picture of the gas entrainment impeller in its three different parts

9.2.3. General experimental procedure

In a typical experiment, under argon atmosphere, the autoclave was loaded with a solution of 3.8 mg of $\text{Rh}(\text{acac})_2\text{CO}$ ($15 \cdot 10^{-3}$ mmol) and the corresponding amount of ligand in 5 ml of toluene. Five further millilitres of toluene were used to ensure quantitative addition of the mixture into the autoclave. Then the addition funnel was loaded with 11.7 ml of 1-octene (75 mmol), previously filtered through activated alumina, and 1.5 ml of *n*-decane (7.5 mmol) as standard. (An aliquot of this mixture was used as “t = 0” conversion for the analysis of the reaction conversion via GC-FID) Following, the reactor was pressurised at 16 bar with syngas ($\text{CO}:\text{H}_2$, 1:1) and the autoclave was stirred at 700 rpm and 80 °C for 1.5 h (catalyst preformation). The system was then pressurised at 20 bar, the data logging was started and the contents of the addition funnel were added to the autoclave. The mixture was allowed to react for 3 h. After this time, data logging and stirring were stopped, the autoclave was cooled down and depressurised. An aliquot of the reaction mixture was filtered through a silica pad and analysed via GC-FID. Comparison of the ratio of areas between the substrate and

⁸ Parr Instrument Company. Gas Entrainment Impellers. 2018. <https://www.parrinst.com/products/stirred-reactors/options-accessories/gas-entrainment-impellers/>

⁹ Ye, Q.; Li, Z.; Wu, H. Principle and Performance of Gas Self-Inducing Reactors and Applications to Biotechnology. In *Bioreactor Engineering Research and Industrial Applications II*; Bao, J., Ye, Q., Zhong, J.-J., Eds.; Springer Heidelberg: New York, Dodrecht, London, 2015; pp 1–33.

the standard before and after the catalytic reaction was used to determine the reaction conversion.

Graphical representation of mmol of substrate consumed with time (**Figure 9.5**) can then be obtained from the gas consumption curve. When mass-flow controller was used to acquire the data (Edinburgh), the input information was expressed in ml of gas per unit of time. When the pressure transducer was used (Barcelona), the input information was expressed in bar per unit of time. In either case, the input values together with the reaction conversion were used to obtain the representation of consumed mol of substrate with time.

From this representation, TOF at 50 % of conversion was graphically determined by plotting the line within 45 and 55 % of substrate conversion (black line in **Figure 9.5**). The slope of this line represents the average value of converted substrate at 50 % of conversion.

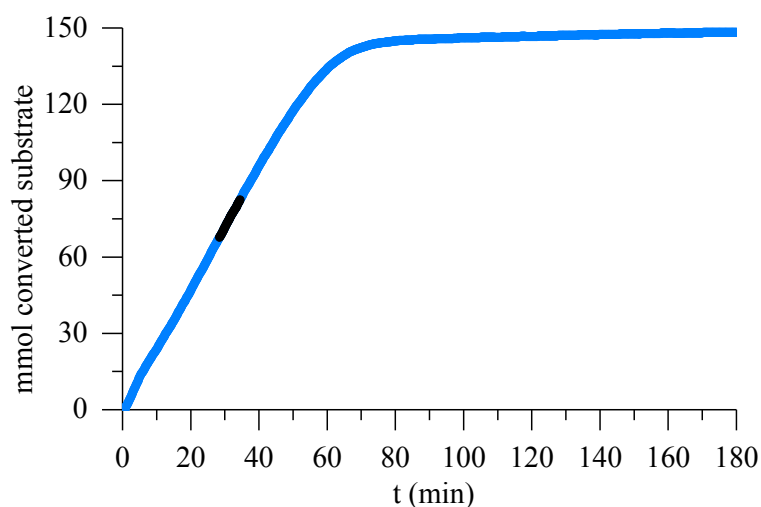


Figure 9.5. Graphical representation of mmol of substrate converted (consumed) during the catalytic reaction (blue curve). In black, the line included between 45 and 55 % conversion which is used to calculate the TOF at 50 % of conversion

Graphical representation of % substrate converted with time was used to compare reactions in which different amount of substrate were used.

9.3. *In situ* experiments: High Pressure NMR and High Pressure IR

9.3.1. HP-NMR

High Pressure NMR experiments were carried out in a 4 mm OD sapphire NMR tube with stainless steel cap. Data acquisition was performed in a Bruker Avance III 400 spectrometer.

In a typical experiment, 2.5 mg of Rh(acac)(CO)₂ ($9.7 \cdot 10^{-3}$ mmol) and the corresponding amount of ligand were mixed in 0.3 ml of toluene-D8 in a 3 ml vial under Ar atmosphere. The vial was then transferred into an stainless steel autoclave and, after purging 3 times with 10 bar of syngas, the solution was stirred under 16 bar of syngas at 80 °C for 1.5 h, emulating the conditions of preformation of the catalyst. After that time, the reactor was cooled down and depressurised and the solution was immediately transferred into the HP NMR tube. The tube was then purged three times with 10 bar of syngas and was finally pressurised at 20 bar for, at least, 30 minutes before collecting the NMR spectra. Longer times did not show any difference in the spectra.

9.3.2. HP IR

High Pressure IR experiments were performed in a 50 ml stainless steel autoclave equipped with Cleartran™ windows (ZnS, transparent up to 700 cm^{-1}). Stirring of the solution was provided by a six-blade impeller which allowed fast recirculation through the windows compartment. Heater was provided by means of electrical heaters. Temperature and pressure were monitored with thermocouple and pressure transducer, respectively. More details on the schematics of the IR autoclave can be found in the literature.¹⁰ IR data was recorded with a Shimadzu IR Tracer-100 spectrometer.

In a typical experiment, under Ar atmosphere, the autoclave was charged with a solution of 3.8 mg of Rh(acac)₂CO ($15 \cdot 10^{-3}$ mmol) and the corresponding amount of ligand in 10 ml of CH₂Cl₂. The autoclave was then stirred at 1400 rpm, heated at 40 °C, and charged with 20 bar of syngas. Either rapid scan mode or Time course mode of the spectrometer

¹⁰ Kamer, P. C. J.; Van Rooy, A.; Schoemaker, G. C.; Van Leeuwen, P. W. N. M. *Coord. Chem. Rev.* **2004**, *248*, 2409–2424.

were used to take “pictures” of the spectra with time. In those experiments in which substrate was used, after the catalyst was formed (preformation, 1 h), the autoclave was depressurized and the substrate was added. Next, the autoclave was pressurised again to 20 bar of syngas and monitoring of the reaction was performed as explained when substrate was not involved. Blank samples were performed by loading the reactor with solvent and syngas at 20 bar (if other pressures were explored, the blank was always performed at the pressure of the experiment). In the experiments involving deuterium, same procedure was followed replacing the syngas to 5 bar of D₂ and 5 bar of CO (experiments performed at 10 bar of D₂/CO mixture).

9.4. Computational calculations and simulations

9.4.1. Variable Temperature (VT) NMR

Exchange barrier in *o*-Miranphos (Chapter 3) was determined by means of VT-NMR experiments and the corresponding computational simulations.

Experimental: acquisition of the NMR spectra at different temperatures

The procedure used to perform the VT experiments differs only slightly from the common process to acquire regular NMR spectra, although a few indications should be mentioned: Shimming was only performed once the temperature of choice was reached. In order to ensure temperature equilibration of the sample, the spectra acquisition were performed at least two minutes after reaching the temperature of the experiment. Each spectrum was performed twice in different sets of experiments and the exact temperature of the experiment was used in the calculations. Experiments at temperature up to 323 K were performed in acetone-D₆. For higher temperatures DMSO-D₆ was used, however in order to minimise solvent effects, only values in acetone-D₆ were used for the calculations.

Calculations: NMR spectra simulations

The computational calculations consisted in the determination of the constant *k* for the exchange between the *P* (clockwise) and *M* (counter clockwise) helix conformations of *o*-Miranphos at each temperature. The calculations were performed using IvorySoft gNMR ver 5.0.6.0 software. Full-lineshape analysis was performed, and linewidths

were never included in the calculations. 1.4 % tris(2-trifluoromethylphenyl)phosphine (**9**), found experimentally as impurity in the *o*-Miranphos, was included in the simulations. In those experiments at lower temperatures, the value of concentration of **9** was set to be freely iterated showing the same values as found experimentally (1.33 %). Chemical shifts, coupling constants and concentrations for the simulations were determined using the experiments at low temperatures and checked with the experimental values. These values were kept fixed for the simulations at higher temperatures (with broader signals). Otherwise the calculations with broad signals did not converge.

Table 9.1 shows the values of rate constant (*k*) obtained at each temperature for the helix conformation exchange between the *P* and *M* enantiomeric forms of *o*-Miranphos.

Table 9.1. Values of the constant *k* for the for the helix conformation exchange between the *P* and *M* enantiomeric forms of *o*-Miranphos at different temperatures determined by NMR simulations

Temperature (K)	Rate constant, <i>k</i> (s⁻¹)
270.5	82.7
271.8	85.9
274.5	108.0
275.0	115.0
279.4	160.0
280.1	185.0
285.0	287.0
289.9	415.0
290.1	425.0
294.1	579.0
298.0	740.0
298.6	827.0
300.2	982.0
301.9	1120.0
305.0	1390.0
314.9	2590.0
315.1	2580.0
323.1	4450.0
323.2	4540.0

The energy parameters associated to the *P* and *M* enantiomeric exchange was graphically determined using the values of *k* at each temperature found in the simulations.

Eyring equation (9.1) was used to graphically determine the values of ΔH^\ddagger and ΔS^\ddagger by plotting $\ln(k/T)$ vs $1/T$, where k is the rate constant at each temperature (T). According to Eyring equation, slope is $-\Delta H^\ddagger/R$ and Y-intercept is $\Delta S^\ddagger/R + 23.7600$. Once ΔH^\ddagger and ΔS^\ddagger are known, ΔG^\ddagger at each temperature can be determined ($\Delta G^\ddagger = \Delta H^\ddagger - T\Delta S^\ddagger$).

$$\ln\left(\frac{k}{T}\right) = -\frac{\Delta H^\ddagger}{RT} + \frac{\Delta S^\ddagger}{R} + \ln\left(\frac{k_b}{h}\right) \quad (9.1)$$

where $R = 1.987$ cal and $\ln(k_b/h) = 23.7600$

Similarly, Arrhenius equation (9.2) was applied to calculate the energy of activation (E_a) by plotting $\ln(k)$ vs $1/T$. In this case, the slope is $-E_a/R$ and the Y-intercept is $\ln A$ (A is the Arrhenius frequency factor).¹¹ Knowing that $E_a = \Delta H^\ddagger + RT$, ΔH^\ddagger was also determined at each temperature.

$$\ln k = -\frac{E_a}{RT} + \ln A \quad (9.2)$$

9.4.2. Molecular Mechanics: determination of the chelating mode of P-bz and M-bz

Molecular mechanics calculations on the chelating mode of diphosphine ligands **P-bz** and **M-bz** were performed using the Tinker package (ver. 7.1)¹² with the MM3-2000 force field¹³ included in the software. The methodology used for the calculations has been previously reported in the literature.¹⁴ Parameters involving Rh (atom type, angles and distances) are not included in the original MM3-2000 force field and have been taken from the literature.^{14,15} In the same way, some parameters related to the benzamide moiety are not included in the force field and have been included in the

¹¹ Zimmer, K. D.; Shoemaker, R.; Ruminski, R. R. *Inorg. Chim. Acta* **2006**, 359 (5), 1478–1484.

¹² a) Kong, Y.; Ponder, J. W. *J. Chem. Phys.* 1997, 107 (2), 481–492. b) Tinker Molecular Modeling. Tinker - Software Tools for Molecular Design. **2018**. <https://dasher.wustl.edu/tinker/>

¹³ Schmitz, L. R.; Allinger, N. L. *J. Am. Chem. Soc.* **1990**, 112 (23), 8307–8315.

¹⁴ Freixa, Z.; Pereira, M. M.; Pais, A. A. C. C.; Bayón, J. C. *J. Chem. Soc. Dalton Trans.* **1999**, No. 18, 3245–3251.

¹⁵ a) Casey, C. P.; Whiteker, G. T. *Isr. J. Chem.* **1990**, 30 (4), 299–304. b) Casey, C. P.; Whiteker, G. T.; Melville, M. G.; Petrovich, L. M.; Gavney, J. A.; Powell, D. R. *J. Am. Chem. Soc.* **1992**, 114 (14), 5535–5543.

calculations from the values reported in the literature.¹⁶ Complete list of these parameters used is provided in **Table 9.2**.

Table 9.2. Additional parameters used in the molecular mechanics calculations

Descriptors for Rh atom	
Element symbol	Rh
Atomic weight	102.906
Atomic number	45
Valence	2
van der Waals	radius = 2.00 Å $\epsilon = 0.63$ kcal/mol $q = 0$ C
Stretching	
Rh-P(phosphine)	$k^{15} = 201$ kcal·mol ⁻¹ ·Å ⁻² ; $d = 2.315$ Å
C(sp ²)-C(sp ²)	$k = 6.560$ mdyn·Å ⁻¹ ; $d = 1.389$ Å
C(sp ²)-C(carbonyl)	$k = 6.560$ mdyn·Å ⁻¹ ; $d = 1.485$ Å
C(carbonyl)-O(carbonyl)	$k = 10.100$ mdyn·Å ⁻¹ ; $d = 1.223$ Å
C(carbonyl)-N(sp ²)	$k = 6.700$ mdyn·Å ⁻¹ ; $d = 1.331$ Å
O(carbonyl)-H(amide)	$k = 4.440$ mdyn·Å ⁻¹ ; $d = 2.070$ Å
Bending	
P(phosphine)-Rh-P(phosphine)	$k^a = 0$ kcal·mol ⁻¹ ·rad ⁻²
Rh-P(phosphine)-C(sp ²)	$k = 0.4685$ mdyn·Å·rad ⁻² ; $\theta_0 = 109.5^\circ$
C(sp ²)-C(carbonyl)-N(sp ²)	$k = 1.000$ mdyn·Å·rad ⁻² ; $\theta_0 = 114.0^\circ$
Torsion	
Rh-P(phosphine)-C(sp ²)-C(sp ²)	$k = 0$ kcal·mol ⁻¹
P(phosphine)-Rh-P(phosphine)-C(sp ²)	$k = 0$ kcal·mol ⁻¹
C(sp ²)-C(sp ²)-C(sp ²)-C(sp ²)	-0.670, 4.304, 0.000 ^b
C(sp ²)-C(sp ²)-C(carbonyl)-O(carbonyl)	0.000, 3.300, 0.000 ^b
C(sp ²)-C(sp ²)-C(carbonyl)-N(sp ²)	0.000, 0.700, 0.000 ^b
C(sp ²)-C(carbonyl)-N(sp ²)-H(amide)	0.000, 6.270, 0.000 ^b
H ^d -C(sp ²)-C(sp ²)-C(sp ²)	0.250, 5.534, -0.550 ^b
H ^d -C(sp ²)-C(sp ²)-H ^c	0.000, 7.072, 0.000 ^b
O(carbonyl)-C(carbonyl)-N(sp ²)-H ^c	1.000, 6.765, 0.000 ^b

^a No P-Rh-P bending constant is included in the calculation of the natural bite angle or the dynamic bite angle. This ensures that the bite angle will depend on the backbone and not to Metal-Ligand preferences. In the calculation of the flexibility range, the value of k is increased to 5000 kcal·mol⁻¹·rad⁻² thus fixing the P-Rh-P angle. ^b V_1, V_2, V_3 parameters, respectively (in kcal·mol⁻¹). ^c H atom except on N, O, S

¹⁶ Hay, B. P.; Dixon, D. A.; Vargas, R.; Garza, J.; Raymond, K. N. *Inorg. Chem.* **2001**, *40* (16), 3922–3935.

Natural bite angle

As the very first step in the molecular mechanics calculations of the chelating mode of the diphosphines, the coordinate files containing the position in the space of the atoms was generated. In this case, Chem3D¹⁷ was used to draw the three-dimensional structure of the ligands and thus generating the corresponding coordinate files which were exported as Tinker MM3 input files (.xyz format). Four different structures were drawn for each of the diphosphine ligands varying the conformation of the amide groups. Following, the coordinate files were edited to give proper format and to check the connectivity. Lone pairs should be removed and atom type should be defined as follows: 1 (sp³ carbon), 2 (sp² carbon), 3 (carbonyl carbon), 5 (hydrogen, except on N, O, S), 7 (carbonyl oxygen), 8 (sp³ nitrogen), 9 (sp² nitrogen, amide nitrogen), 11 (fluorine), 25 (phosphine phosphorus), 28 (hydrogen on amide nitrogen) and rhodium atom was defined as 170. The key file containing the additional parameters of **Table 9.2** was also created at this point. It is noteworthy that the strength constant defining the P-Rh-P angle should be set to zero to allow free movement only determined by the ligand backbone.

Once the files were ready, exploration on each structure was performed to find the most stable conformers. DYNAMIC module on Tinker was used to randomly generate different conformations (600 K, 10000 steps, 1.0 fs, dump = 0.5 ps). The simulation heats the structure at 600 K for 10000 steps, with a time step length of 1.0 fs, and records the output coordinates every 0.5 ps thus generating 20 different conformers. Each one of them was then subjected to energy minimisation (MINIMIZE module) until rms dropped below 0.01 kcal/mol.

With this procedure the energy surface is explored starting from randomly generated structures. The process can be visualised as depicted in **Figure 9.6**: by starting from different points we aim to distinguish between the local minima and to find the global minima. In total, between 80 and 100 different randomly generated starting conformers were evaluated for each ligand. As general trend, the most stable structures showed the amine group in *endo* conformation, meaning that the lone pair is pointing to the Rh atom. Additional stabilisation was observed in those conformers in which H-bonding

¹⁷ PerkinElmer Chem3D ver. 16.0.1.4 included in the ChemBiooffice 2016 package

interactions between either the amide proton and the amino group or between the amide proton and the carbonyl oxygen were possible. Also π - π staking between the aryl groups of the phosphines was observed as added stabilisation factor. In the case of the *para*-isomer, **P-bz**, two equally stable conformers with different orientation of the benzyl group were found as global minima. These conformers were referred as *ponytail*, when the benzyl group is orientated backwards with respect to the Rh atom, and *fringe* when this group orientates forward, **Figure 9.7**. Both conformers showed the same value of natural bite angle and the same range of flexibility. However, the *fringe*-conformation is less likely to happen in the experimental conditions where the disposition of the benzyl group would hamper the coordination of other ligands to the Rh atom.

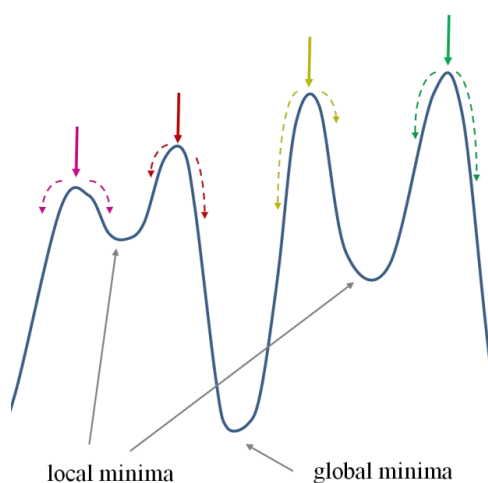


Figure 9.6. Exploration of the energy surface starting from different points (coloured arrows)

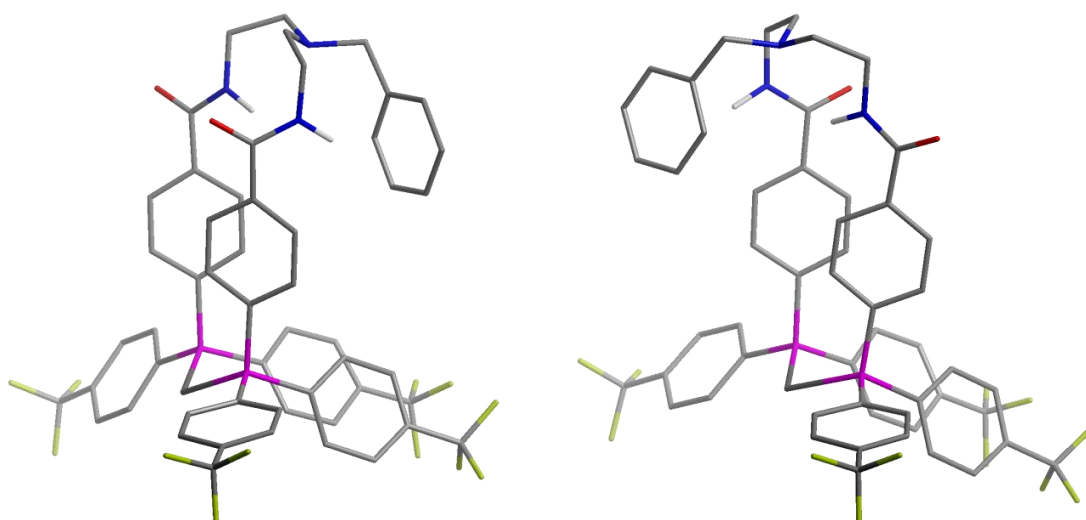


Figure 9.7. Stick representation of the most stable conformers of **P-bz**. Aromatic hydrogen omitted for clarity. **left-** *ponytail* conformer. **right-** *fringe* conformer

Flexibility range

Once the most stable conformers of **P-bz** and **M-bz** were determined, the flexibility of the chelates, defined as the range of angles that the ligand can adopt within 3 kcal/mol, was evaluated.^{15a} In a first instance, the force constant associated to the P-Rh-P angle was increased to $5000 \text{ kcal}\cdot\text{mol}^{-1}\cdot\text{rad}^{-2}$. By using this overly high constant, the bite angle will remain fixed at a given value during the energy minimisation. Therefore, the value of angle was modified in intervals of 5° followed by an energy minimisation (MINIMIZE module). Plotting the strain energy *versus* the angle gives the energy diagram of the chelate.

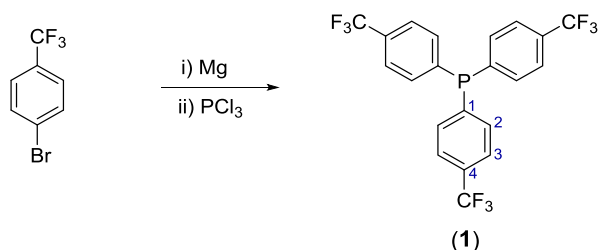
Dynamic bite angle

Another procedure to evaluate the flexibility of the ligands is the *dynamic bite angle*. This procedure was developed in our group¹⁴ and can be defined as the average value of bite angle adopted by the ligand when a determined amount of thermal energy is applied. While the natural bite angle is calculated at a temperature of 0 K, the dynamic bite angle is simulated at a temperature of 400 K. Consequently, the dynamic angle is thought to provide a more realistic view of the chelating mode of the ligand. Using the same parameters as described for the bite angle simulations, keeping the bending strength constant of the P-Rh-P angle equal to zero, the calculations were performed with the DYNAMIC module on Tinker (400 K, 10000 steps, 1.0 fs, dump = 0.1 ps) to generate 100 different coordinate files, each one of them corresponding to a different conformation of the ligand. The P-Rh-P bond of the 100 structures was then measured and the average value of them was defined as the dynamic bite angle.

9.5. Synthetic procedures

9.5.1. Trifluoromethylated homoleptic phosphines and oxides

Tris(4-trifluoromethylphenyl)phosphine (**1**)

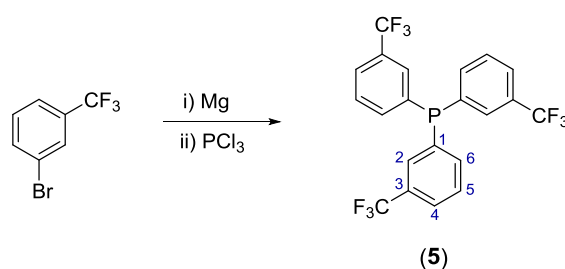


Magnesium chips (4.7 g, 0.19 mol) were suspended in 120 ml of anhydrous Et₂O in a two-necked round-bottom flask, equipped with an addition funnel and a Liebig condenser. The addition funnel was loaded with a solution of 18.1 ml of 4-(trifluoromethyl)bromobenzene (29.5 g, 0.13 mol) in 40 ml of dry Et₂O and *ca.* 10 % of the volume of the solution was added onto the suspension of Mg. After stirring vigorously for a few seconds, the suspension was gently warmed up until reflux started (either bear hands or a water bath can be used to increase the temperature gently). Following, the rest of the solution of the bromo-derivative was added dropwise while keeping the reflux and moderate stirring rate. At this point, an ice bath will be prepared in case in case the reaction temperature runs out of control. Quantitative addition was ensured with two portions of 20 ml of dry Et₂O. The reaction mixture was then refluxed for 2 more hours before cooling down to room temperature. Excess Mg was filtered off the reaction mixture through a cannula with glass wool. The dark orange solution containing the Grignard derivative was cooled down to 0 °C and a solution of 3.7 ml of PCl₃ (5.9 g, 42.9 mmol) in 30 ml of dry Et₂O was added dropwise via addition funnel. After complete addition, the mixture was refluxed for 1 h. After this time, the orange suspension obtained was cooled down in an ice bath before the addition of 150 ml of 10 % aqueous HCl. The orange organic phase was separated and the aqueous phase was extracted three times with 40 ml of Et₂O. The organic fractions were combined and dried over anhydrous MgSO₄. After filtration, the solvent was vacuum evaporated to obtain an orange solid which was purified through flash column in silica gel (CH₂Cl₂:hexanes, 6:1). 12.5 g (63 % yield) of tris(4-trifluoromethylphenyl)phosphine (**1**) as pale yellow solid was obtained.

$^{31}\text{P}\{^1\text{H}\}$ NMR (161.98 MHz, CDCl_3), δ (ppm): -5.74 (s). ^1H NMR (400.13 MHz, CDCl_3), δ (ppm): 7.63 (d, 6H, H_{C_3} , $^3\text{J}_{\text{HH}} = 7.9$ Hz); 7.41 (*pseudo-t*, 6H, H_{C_2} , $^3\text{J}_{\text{HH}} = ^3\text{J}_{\text{HP}} = 7.9$ Hz). $^{13}\text{C}\{^1\text{H}\}$ NMR (62.90 MHz, CDCl_3), δ (ppm): 140.5 (d, C_1 , $^1\text{J}_{\text{CP}} = 14.1$ Hz); 134.1 (d, C_2 , $^2\text{J}_{\text{CP}} = 20.1$ Hz); 131.8 (q, C_4 , $^2\text{J}_{\text{CF}} = 32.7$ Hz); 125.8 (dq, C_3 , $^3\text{J}_{\text{CP}} = 7.1$ Hz, $^3\text{J}_{\text{CF}} = 3.7$ Hz); 124.0 (q, $\text{C}\{\text{CF}_3\}$, $^2\text{J}_{\text{CF}} = 272.3$ Hz). $^{19}\text{F}\{^1\text{H}\}$ NMR (376.50 MHz, CDCl_3), δ (ppm): -62.28 (s, CF_3).

The NMR data are consistent with the reported values in the literature¹⁸

Tris(3-trifluoromethylphenyl)phosphine (**5**)



The synthesis of **5** was performed similar to the described procedure for **1**. A suspension of Mg chips (5.7 g, 0.24 mol) in 80 ml of anhydrous Et_2O was prepared in a two-necked round-bottom flask, equipped with an addition funnel and a Liebig condenser. Approximately 10 % volume of a solution of 23 ml of 3-(trifluoromethyl)bromobenzene (36.0 g, 0.16 mol) in 80 ml of dry Et_2O was added onto the suspension of Mg via addition funnel. After stirring vigorously for a few seconds, the suspension was gently warmed up until reflux started (either bear hands or a water bath can be used to increase the temperature gently). Following, complete addition of the solution of the bromo-derivative was carried out dropwise while keeping the reflux and moderate stirring rate. At this point, an ice bath will be prepared in case in case the reaction temperature gets out of control. The quantitative addition of the bromo-derivative was achieved with 2 portions of 20 ml of dry Et_2O . Then, the reaction mixture was refluxed for 2 more hours before cooling down to room temperature. Excess Mg was filtered off the reaction mixture through a cannula with glass wool. The dark solution containing the Grignard derivative was cooled down to 0 °C and a solution of 4.6 ml of PCl_3 (7.9 g, 52.7 mmol) in 40 ml of dry Et_2O was added dropwise via addition funnel. After complete addition, the mixture was refluxed for 1 h. After this

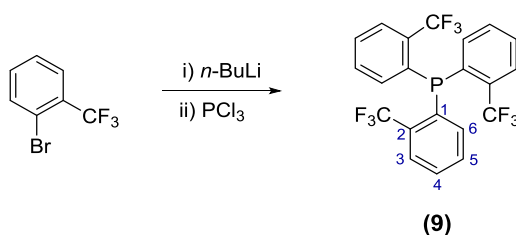
¹⁸ a) Eapen, K. C.; Tamborski, C. *J. Fluor. Chem.* **1980**, *15* (3), 239–243. b) Jeschke, J.; Korb, M.; Ruffer, T.; Gäbler, C.; Lang, H. *Adv. Synth. Catal.* **2015**, *357* (18), 4069–4081.

time, the orange-yellowish suspension obtained was cooled down in an ice bath before the addition of 120 ml of 10 % aqueous HCl. The orange organic phase was separated and the aqueous phase was extracted three times with 40 ml of Et₂O. The organic fractions were combined and dried with anhydrous MgSO₄. After filtration, the solvent was vacuum evaporated to obtain an orange oil which was purified through flash column (silica, CH₂Cl₂ : hexanes 6:1). 21.9 g 87 % yield) of tris(3-trifluoromethylphenyl)phosphine (**1**) as pale yellow oil.

³¹P{¹H} NMR (161.98 MHz, CDCl₃), δ (ppm): -4.54 (s). ¹H NMR (400.13 MHz, CDCl₃), δ (ppm): 7.68 (d, 3H, H_{C4}, ³J_{HH} = 7.6 Hz); 7.63 (d, 3H, H_{C2}, ³J_{HP} = 7.6 Hz); 7.53 (t, 3H, H_{C5}, ³J_{HH} = 7.6 Hz); 7.43 (*pseudo-t*, 3H, H_{C6}, ³J_{HH} = ³J_{HP} = 7.6 Hz). ¹³C{¹H} NMR (100.61 MHz, CDCl₃), δ (ppm): 137.4 (d, C₁, ¹J_{CP} = 14.1 Hz); 136.9 (d, C₆, ²J_{CP} = 16.4 Hz); 131.7 (qd, C₃, ²J_{CF} = 32.5 Hz, ³J_{CP} = 8.1 Hz); 130.6 (dq, C₂, ²J_{CP} = 24.9 Hz, ³J_{CF} = 3.7 Hz); 129.6 (d, C₅, ³J_{CP} = 5.8 Hz); 126.6 (q, C₄, ³J_{CF} = 3.8 Hz); 124.7 (q, C{CF₃}, ¹J_{CF} = 272.2 Hz). ¹⁹F{¹H} NMR (376.50 MHz, CDCl₃), δ (ppm): -62.60 (s, CF₃). HR-MS (ESI⁺ *m/z*) [M+H]⁺: calculated for [C₂₁H₁₃F₉P]⁺ 467.0606; found 467.0606.

The NMR data are consistent with the reported values in the literature.^{18a}

Tris(2-trifluoromethylphenyl)phosphine (**9**)



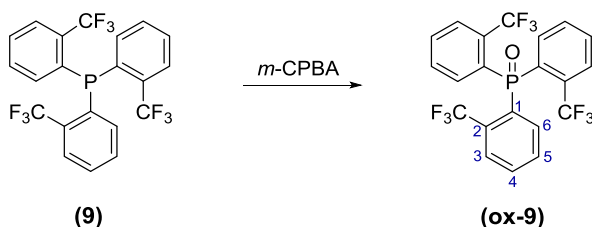
The synthesis of **9** was performed according to the reported procedure in the literature, with minor modifications.^{18a} 44 ml of *n*-buthyllithium (2.5 M in hexanes, 0.11 mol) were added dropwise (during 30 min) to a solution of 15 ml of 2-(trifluoromethyl)bromobenzene (24.8 g, 0.11 mol) in 150 ml of anhydrous Et₂O at 0 °C (ice bath). The addition of the first ml of *n*-BuLi causes the colourless solution of the bromo-derivative to turn to green, which changes to orange with the further addition of *n*-BuLi. After complete addition, the reaction mixture was stirred further 30 minutes, while maintaining the temperature at 0 °C. A solution of 3.2 ml of phosphorus trichloride (5.0 g, 37 mmol) in 40 ml of dry Et₂O was then added dropwise via addition

funnel during 25 min, resulting in the formation of a yellow suspension. The reaction mixture was then stirred at room temperature overnight. Afterwards 150 ml of 10 % aqueous HCl was added while keeping the reaction mixture at 0 °C. The organic phase was decanted and the aqueous phase was further extracted with two portions of 20 ml of Et₂O. The organic fractions were dried over MgSO₄. Filtration and evaporation of the solvent gave a yellow solid which was washed four times with 30 ml of hexanes to yield 14.5 g of tris(2-trifluoromethylphenyl)phosphine (**9**) as pale yellow solid (85.3 % yield).

³¹P{¹H} NMR (161.98 MHz, CDCl₃), δ (ppm): -17.5 (dec, ⁴T_SJ_{PF} = 55.5 Hz). ¹H NMR (400.13 MHz, CDCl₃), δ (ppm): 7.78 (ddd, 3H, H_{C3}, ³J_{HH} = 7.6 Hz, ⁴J_{HP} = 4.2 Hz, ⁴J_{HH} = 1.4 Hz); 7.49 (td, 3H, H_{C4}, ³J_{HH} = ³J_{HH} = 7.6 Hz, ⁴J_{HH} = 0.9 Hz); 7.43 (td, 3H, H_{C5}, ³J_{HH} = ³J_{HH} = 7.6 Hz, ⁴J_{HH} = 1.4 Hz); 6.94 (bdd, 3H, H_{C6}, ³J_{HH} = 7.6 Hz, ³J_{HP} = 3.6 Hz). ¹³C{¹H} NMR (100.61 MHz, CDCl₃), δ (ppm): 136.15 (s, C₆); 135.0 (d, C₁, ¹J_{CP} = 31.0 Hz); 134.5 (qd, C₂, ²J_{CP} = 30.5 Hz, ²J_{CF} = 26.9 Hz); 131.76 (s, C₅); 129.45 (s, C₄); 127.13 (quint, C₃, ³J_{CF} = 5.7 Hz); 124.2 (q, C{CF₃}, ¹J_{CF} = 275.5 Hz). ¹⁹F{¹H} NMR (376.50 MHz, CDCl₃), δ (ppm): -57.3 (d, ⁴T_SJ_{PF} = 55.5 Hz, CF₃)

The NMR data are consistent with the reported values in the literature.^{18a}

Tris(2-trifluoromethylphenyl)phosphine oxide (ox-9)



The synthesis of **ox-9** was performed following a modification of the reported procedures.^{18a,19} 0.20 g of phosphine **9** (0.4 mmol) were dissolved in 4 ml of toluene. To this solution, *m*-chloroperbenzoic acid (0.080 g, 0.47 mmol) in 4 ml of toluene was added and the mixture was stirred overnight at room temperature. After that time, complete conversion of **9** was checked by TLC (silica, CH₂Cl₂). The reaction mixture was then stirred with 10 ml of 10 % aqueous Na₂CO₃. The organic layer was separated and the aqueous phase was extracted four times with 5 ml of CH₂Cl₂. The organic

¹⁹ Howell, J. A. S.; Fey, N.; Lovatt, J. D.; Yates, P. C.; McArdle, P.; Cunningham, D.; Sadeh, E.; Gottlieb, H. E.; Goldschmidt, Z.; Hursthouse, M. B.; et al. *J. Chem. Soc. Dalton Trans.* **1999**, No. 17, 3015–3028.

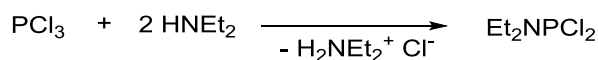
fractions were combined and dried over MgSO₄. A white powder was obtained after filtration and evaporation of the solvent. Recrystallisation in acetone/hexanes afforded **ox-9** as crystalline white solid (0.21 g, quantitative yield).

³¹P{¹H} NMR (161.98 MHz, CDCl₃), δ (ppm): 34.5 (s). ¹H NMR (400.13 MHz, CDCl₃), δ (ppm): 7.92 (ddd, 3H, H_{C3}, ³J_{HH} = 7.7 Hz, ⁴J_{HP} = 4.2 Hz, ⁴J_{HH} = 0.8 Hz); 7.70 (bt, 3H, H_{C4}, ³J_{HH} = ³J_{HH} = 7.7 Hz); 7.53 (bt, 3H, H_{C5}, ³J_{HH} = ³J_{HH} = 7.7 Hz); 7.33 (dd, 3H, H_{C6}, ³J_{HP} = 15.2 Hz, ³J_{HH} = 7.7 Hz). ¹³C{¹H} NMR (100.61 MHz, CDCl₃), δ (ppm): 135.25 (d, C₆, ²J_{CP} = 10.8 Hz); 133.7 (qd, C₂, ²J_{CF} = 32.6 Hz, ²J_{CP} = 5.17 Hz); 132.44 (d, C₄, ⁴J_{CP} = 2.36 Hz); 131.8 (d, C₁, ¹J_{CP} = 102.7 Hz); 131.13 (d, C₅, ³J_{CP} = 12.1 Hz); 128.45 (m, C₃, ³J_{CP} = 8.3 Hz, ³J_{CF} = 5.6 Hz); 123.4 (qd, C{CF₃}, ¹J_{CF} = 274.8 Hz, ³J_{CP} = 3.2 Hz). ¹⁹F{¹H} NMR (376.50 MHz, CDCl₃), δ (ppm): -56.36 (s, CF₃). **Elemental analysis:** calculated for C₂₁H₁₂F₉PO: C, 52.30; H, 2.51; found: C, 52.28; H, 2.39.

9.5.2. Trifluoromethylated heteroleptic phosphines and related compounds

The preparation of the heteroleptic trifluoromethylated phosphines implied the synthesis of the trifluoromethylated chlorophosphines **26** and **27**, which were performed following the reported methodologies in the literature with minor modifications.²⁰ The synthesis of these chlorophosphines required the preparation of the ethylphosphoramidous derivatives Et₂NPCl₂ and (Et₂N)₂PCl which were also performed following the reported methodologies with minor modifications.²¹

N,N-diethylphosphoramidous dichloride (Et₂NPCl₂)



Et₂NPCl₂ was prepared following a modification of the reported procedure in the literature.^{21a} 35 ml of PCl₃ (55 g, 0.40 mol) were dissolved in 190 ml of dry Et₂O and was cooled down in an ice bath (0 °C). Next, a solution of 77.5 ml of freshly distilled diethylamine (55 g, 0.75 mol) in 20 ml of dry Et₂O was added dropwise to the solution

²⁰ a) Casalnuovo, A. L.; RajanBaby, T. V.; Ayers, T. A.; Warren, T. H. *J. Am. Chem. Soc.* **1994**, *116* (22), 9869–9882. b) Klaehn, J. R.; Peterman, D. R.; Harrup, M. K.; Tillotson, R. D.; Luther, T. A.; Law, J. D.; Daniels, L. M. *Inorg. Chim. Acta* **2008**, *361* (8), 2522–2532. c) Holstein, P. M.; Vogler, M.; Larini, P.; Pilet, G.; Clot, E.; Baudoin, O. *ACS Catal.* **2015**, *5* (7), 4300–4308.

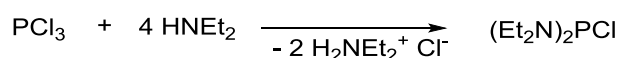
²¹ a) Whitaker, C. M.; Kott, K. L.; McMahon, R. J. *J. Org. Chem.* **1995**, *60* (11), 3499–3508. b) Sylvester, K. T.; Wu, K.; Doyle, A. G. *J. Am. Chem. Soc.* **2012**, *134* (41), 16967–16970.

of phosphorus trichloride during 30 min. Immediate formation of diethylammonium chloride as white bulky solid was observed. The reaction was allowed to warm at room temperature while stirring for 1.5 h. Following, it was brought to 35 °C and stirred for 1 more hour. The white precipitate was then filtered off and extracted three times with 20 ml of dry Et₂O. The organic fractions were combined and vacuum evaporated to eliminate the solvent. Finally, vacuum distillation afforded 35.3 g (54 % yield) of *N,N*-diethylphosphoramidous dichloride as a colourless liquid (boiling point 43-45°C, 3 mbar).

³¹P{¹H} NMR (101.27 MHz, CDCl₃), δ (ppm): 162.64 (s). ¹H NMR (250.16 MHz, CDCl₃), δ (ppm): 3.32 (dq, 2H -CH₂, ³J_{HP} = 14.4 Hz, ³J_{HH} = 7.1 Hz); 1.17 (t, 3H, -CH₃, ³J_{HH} = 7.1 Hz). ¹³C{¹H} NMR (62.90 MHz, CDCl₃), δ (ppm): 41.72 (d, -CH₂, ²J_{CP} = 22.8 Hz); 14.2 (d, -CH₃, ³J_{CP} = 4.8 Hz)

The NMR data are consistent with the reported values in the literature.^{21a}

***N,N,N',N'*-tetraethylphosphorodiamidous chloride ((Et₂N)₂PCl)**

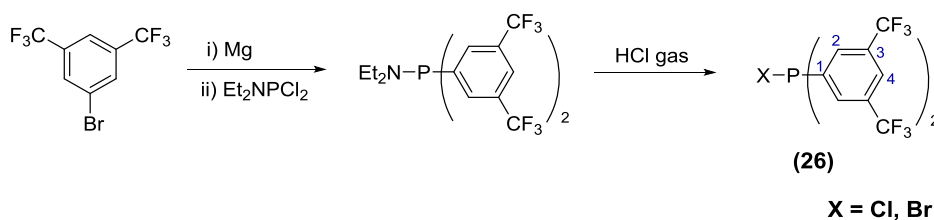


The synthesis of (Et₂N)₂PCl was performed following a modification of the reported procedure in the literature.^{21b} It is important to notice that relative large volumes of solvent are required in this preparation. Otherwise, manipulation of the high quantity of ammonium salts generated becomes extremely difficult. 10 ml of phosphorus trichloride (15.7 g, 0.11 mol) were dissolved in 100 ml of dry Et₂O and cooled down in an ice bath (0 °C). Next, 50 ml of diethylamine (35.5 g, 0.485 mol) dissolved in 120 ml of dry Et₂O were added dropwise to the solution of PCl₃ over a period of 1 hour. Formation of ammonium salts as bulky white solid is immediately observed. The reaction mixture is then allowed to warm to room temperature and is vigorously stirred for 30 minutes. The white precipitate is then filtered off and extracted three times with 20 ml of dry Et₂O. The organic solutions containing the (Et₂N)₂PCl were vacuum evaporated. Finally, vacuum distillation afforded 13.9 g of *N,N,N',N'*-tetraethylphosphorodiamidous chloride as colourless liquid (boiling point 80-83 °C, 5 mbar).

$^{31}\text{P}\{^1\text{H}\}$ NMR (101.27 MHz, CDCl_3), δ (ppm): 157.37 (s). ^1H NMR (250.16 MHz, CDCl_3), δ (ppm): 3.11 (m, 4H $-\text{CH}_2$); 1.09 (t, 6H, $-\text{CH}_3$, $^3J_{\text{HH}} = 7.1$ Hz). $^{13}\text{C}\{^1\text{H}\}$ NMR (62.90 MHz, CDCl_3), δ (ppm): 41.49 (d, $-\text{CH}_2$, $^2J_{\text{CP}} = 18.1$ Hz); 14.2 (d, $-\text{CH}_3$, $^3J_{\text{CP}} = 4.8$ Hz)

The NMR data are consistent with the reported values in the literature.^{21b}

Bis(3,5-bis(trifluoromethyl)phenyl)chlorophosphine (26)



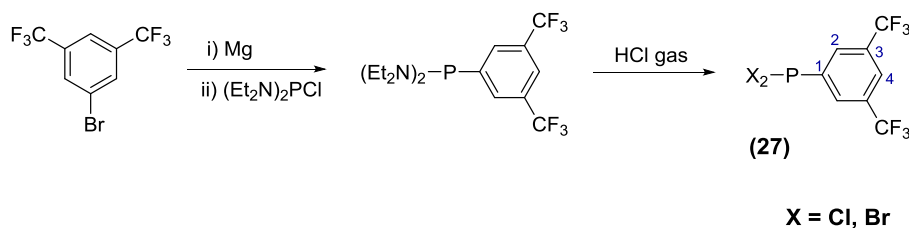
A two-necked round-bottom flask equipped with a reflux condenser and an addition funnel was filled with 50 ml of anhydrous Et_2O and 3.4 g of Mg (0.14 mol). Then, the addition funnel was filled with a solution of 18 ml of 3,5-bis(trifluoromethyl)bromobenzene (30.6 g, 0.10 mol) in 20 ml of dry Et_2O and *ca.* 10 % of the volume of the solution was added onto the suspension of Mg. After stirring vigorously for a few seconds, the suspension was gently warmed up until reflux started. Following, the rest of the solution of the bromo-derivative was added dropwise during 1 h while keeping the reflux and moderate stirring rate. At this point, an ice bath will be prepared in case in case the reaction temperature gets out of control. After complete addition, the reaction mixture was refluxed for 1.5 more hours before cooling down to room temperature. Excess Mg was filtered off the reaction mixture through a cannula with glass wool. The dark solution containing the Grignard derivative was cooled down to 0 °C. Next, a solution of 7.3 ml of Et_2NPCI_2 (8.7 g, 0.05 mol) in 15 ml of dry Et_2O was added dropwise during 5-10 minutes and was stirred overnight at room temperature. A pale brown precipitate was observed. Following, the reaction mixture was cooled down to 0 °C and, under vigorous stirring, 100 ml of a solution of HCl in dry Et_2O (2 M) was added dropwise. After 30 min, complete P-N cleavage was checked by $^{31}\text{P}\{^1\text{H}\}$ NMR. The precipitate was removed by filtration and washed three times with 20 ml of dry Et_2O . After evaporation of the solvent, vacuum distillation (116-118 °C, 4-5 mbar) yielded 17.4 g of **26** as colourless liquid (70.5 % yield). Both bromo- and

chloro-derivatives were obtained due to the ability of phosphorus to exchange halogens, as observed in the NMR spectra.

$^{31}\text{P}\{^1\text{H}\}$ NMR (161.98 MHz, CDCl_3), δ (ppm): 71.16 (s, X = Cl); 57.93 (s, X = Br). ^1H NMR (400.13 MHz, CDCl_3), δ (ppm): 8.07 (d, 4H, $\text{H}_{\text{C}2}$; $^3J_{\text{HP}} = 6.8$ Hz); 7.97 (s, 2H, $\text{H}_{\text{C}4}$). $^{19}\text{F}\{^1\text{H}\}$ NMR (376.50 MHz, CDCl_3), δ (ppm): -63.2 (m, CF_3)

The NMR data are consistent with the values reported in the literature.^{20a,b}

(3,5-bis(trifluoromethyl)phenyl)dichlorophosphine (27)



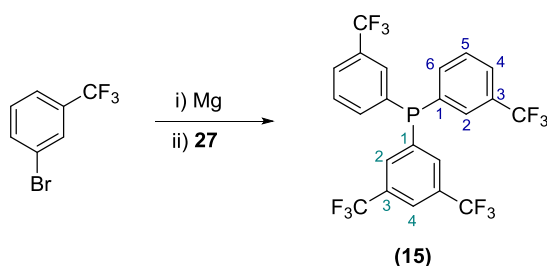
The reaction procedure was analogous to that reported for **26**. A two-necked round-bottom flask equipped with a reflux condenser and an addition funnel was filled with 15 ml of anhydrous Et_2O and 0.41 g of Mg (0.016 mol). Then, the addition funnel was filled with a solution of 2.4 ml of 3,5-bis(trifluoromethyl)bromobenzene (4.2 g, 0.14 mol) in 10 ml of dry Et_2O and *ca.* 10 % of the volume of the solution was added onto the suspension of Mg. After stirring vigorously for a few seconds, the suspension was gently warmed up until reflux started. Following, the rest of the solution of the bromo-derivative was added dropwise during 30 min while keeping the reflux and moderate stirring rate. At this point, an ice bath will be prepared in case in case the reaction temperature gets out of control. After complete addition, the reaction mixture was refluxed for 1.5 more hours before cooling down to room temperature. Excess Mg was filtered off the reaction mixture through a cannula with glass wool. The dark solution containing the Grignard derivative was cooled down to 0 °C. Next, a solution of 8.7 g of Et_2NPCl_2 (0.05 mol) in 30 ml of dry Et_2O was added dropwise during 10 minutes and was stirred overnight at room temperature. A pale brown precipitate was observed. Following, the reaction mixture was cooled down to 0 °C and, under vigorous stirring, 35.6 ml of a solution of HCl in dry Et_2O (2 M) was added dropwise. After 1 h, complete P-N cleavage was checked by $^{31}\text{P}\{^1\text{H}\}$ NMR. The precipitate was removed by filtration and washed three times with 10 ml of dry Et_2O . After evaporation of the solvent, vacuum distillation (65-67 °C, 4-5 mbar) yielded 2.4 g of **27** as colourless liquid (52 %

yield). Bromo-, chloro-, and bromochloro-derivatives were obtained due to the ability of phosphorus to exchange halogens, as observed in the NMR spectra.

$^{31}\text{P}\{^1\text{H}\}$ NMR (101.27 MHz, CDCl_3), δ (ppm): 148.35 (s, X = Cl); 142.65 (s, X = Cl, Br); 135.02 (s, X = Br). ^1H NMR (250.16 MHz, CDCl_3), δ (ppm): 8.38 (m, 2H, $\text{H}_{\text{C}2}$); 8.08 (m, 1H, $\text{H}_{\text{C}4}$)

The NMR data are consistent with the reported values in the literature.^{20c}

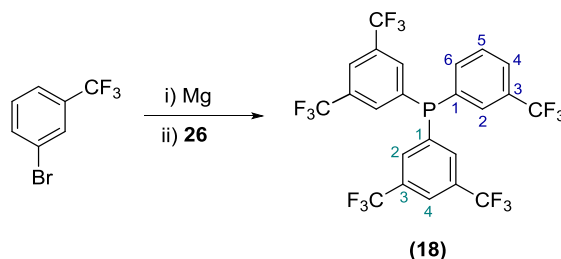
(3,5-bis(trifluoromethyl)phenyl)bis(3-(trifluoromethyl)phenyl)phosphine (**15**)



A solution of 3-(trifluoromethyl)phenyl magnesium bromide was prepared by addition of 5.2 ml of 3-(trifluoromethyl)bromobenzene (8.3 g, 37.0 mmol) dissolved in 10 ml of anhydrous Et_2O to a suspension of Mg chips (1.1 g, 44 mmol) in 50 ml of anhydrous Et_2O . (Detailed description of the preparation of this Grignard derivative can be found in the synthesis of **5**). Afterwards, 5.8 g (18.4 mmol) of the trifluoromethylated dichlorophosphine **27** were dissolved in 20 ml of dry Et_2O and cooled in an ice bath. The solution of the Grignard derivative was then added dropwise to the dichlorophosphine and the resulting orange suspension was stirred overnight at room temperature. After that time, the reaction mixture was cooled down to 0 °C (ice bath) and 130 ml of 10 % aqueous HCl were added. The organic layer was separated and the aqueous phase was extracted three times with 30 ml of Et_2O . The organic fractions were combined and dried over MgSO_4 . Filtration and evaporation of the solvent gave a brown oil which was further purified through flash silica column (CH_2Cl_2 :hexanes, 7:3) to yield 6.3 g of heteroleptic phosphine **15** as yellow oil (63 % yield).

$^{31}\text{P}\{^1\text{H}\}$ NMR (161.98 MHz, CDCl_3), δ (ppm): -3.92 (s). ^1H NMR (400.13 MHz, CDCl_3), δ (ppm): 7.90 (s, 1H, $\text{H}_{\text{C}_4}\{\text{C}_6\text{H}_3(\text{CF}_3)_2\}$); 7.71 (d, 4H, $\text{H}_{\text{C}_2}\{\text{C}_6\text{H}_3(\text{CF}_3)_2\}$ - $\text{H}_{\text{C}_4}\{\text{C}_6\text{H}_4\text{CF}_3\}$); 7.65 (d, 2H, $\text{H}_{\text{C}_2}\{\text{C}_6\text{H}_4\text{CF}_3\}$, $^3J_{\text{HP}} = 8.1$ Hz); 7.57 (t, 2H, $\text{H}_{\text{C}_5}\{\text{C}_6\text{H}_4\text{CF}_3\}$, $^3J_{\text{HH}} = 7.8$ Hz); 7.45 (*pseudo-t*, 2H, $\text{H}_{\text{C}_6}\{\text{C}_6\text{H}_4\text{CF}_3\}$, $^3J_{\text{HH}} = ^3J_{\text{HP}} = 7.8$ Hz). $^{13}\text{C}\{^1\text{H}\}$ NMR (100.61 MHz, CDCl_3), δ (ppm): 140.0 (d, $\text{C}_1\{\text{C}_6\text{H}_3(\text{CF}_3)_2\}$, $^1J_{\text{CP}} = 18.1$ Hz); 136.85 (*bd*, $\text{C}_6\{\text{C}_6\text{H}_4\text{CF}_3\}$, $^2J_{\text{CP}} = 16.0$ Hz); 136.06 (d, $\text{C}_1\{\text{C}_6\text{H}_4\text{CF}_3\}$, $^1J_{\text{CP}} = 13.7$ Hz); 133.25 (*bd*, $\text{C}_2\{\text{C}_6\text{H}_3(\text{CF}_3)_2\}$, $^2J_{\text{CP}} = 20.4$ Hz); 132.42 (*qd*, $\text{C}_3\{\text{C}_6\text{H}_3(\text{CF}_3)_2\}$, $^2J_{\text{CF}} = 34.3$ Hz, $^2J_{\text{CP}} = 6.4$ Hz); 131.89 (*qd*, $\text{C}_3\{\text{C}_6\text{H}_4\text{CF}_3\}$, $^2J_{\text{CF}} = 32.6$ Hz, $^3J_{\text{CP}} = 8.7$ Hz); 130.70 (*dq*, $\text{C}_2\{\text{C}_6\text{H}_4\text{CF}_3\}$, $^2J_{\text{CP}} = 26.4$ Hz, $^3J_{\text{CF}} = 3.7$ Hz); 129.93 (d, $\text{C}_5\{\text{C}_6\text{H}_4\text{CF}_3\}$, $^3J_{\text{CP}} = 5.8$ Hz); 127.10 (q, $\text{C}_4\{\text{C}_6\text{H}_4\text{CF}_3\}$, $^3J_{\text{CF}} = 3.7$ Hz); 123.83 (q, $\text{CF}_3\{\text{C}_6\text{H}_4\text{CF}_3\}$, $^1J_{\text{CF}} = 272.4$ Hz); 123.50 (*sept*, $\text{C}_4\{\text{C}_6\text{H}_3(\text{CF}_3)_2\}$, $^3J_{\text{CF}} = 3.8$ Hz); 123.17 (q, $\text{CF}_3\{\text{C}_6\text{H}_3(\text{CF}_3)_2\}$, $^1J_{\text{CF}} = 272.8$ Hz). $^{19}\text{F}\{^1\text{H}\}$ NMR (376.50 MHz, CDCl_3), δ (ppm): -62.21 (*bs*, 6F, CF_3); -62.33 (*bs*, 6F, CF_3). **HR-MS** (ESI $^+$ m/z) $[\text{M}+\text{H}]^+$: calculated for $[\text{C}_{22}\text{H}_{12}\text{F}_{12}\text{P}]^+$ 535.0480; found 535.0489. **Elemental analysis**: calculated for $\text{C}_{22}\text{H}_{11}\text{F}_{12}\text{P}$: C, 49.46; H, 2.08; found: C, 50.30; H, 2.11.

Bis(3,5-bis(trifluoromethyl)phenyl)(3-(trifluoromethyl)phenyl)phosphine (**18**)

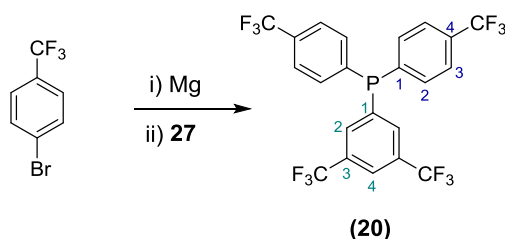


Phosphine **18** was prepared with the same procedure than **15**. A solution of 3-(trifluoromethyl)phenyl magnesium bromide was prepared by addition of 2.3 ml of 3-(trifluoromethyl)bromobenzene (3.7 g, 16.4 mmol) dissolved 10 ml of anhydrous Et_2O to a suspension of Mg chips (0.48 g, 19.8 mmol) in 20 ml of anhydrous Et_2O . (Detailed description of the preparation of this Grignard derivative can be found in the synthesis of **5**). Afterwards, 8.2 g (16.7 mmol) of the trifluoromethylated chlorophosphine **26** were dissolved in 30 ml of dry Et_2O and cooled in an ice bath. The solution of the Grignard derivative was then added dropwise to the chlorophosphine and the resulting orange suspension was stirred overnight at room temperature. After that time, the reaction mixture was cooled down to 0 °C (ice bath) and 70 ml of 10 % aqueous HCl were added. The organic layer was separated and the aqueous phase was extracted three

times with 30 ml of Et₂O. The organic fractions were combined and dried over MgSO₄. Filtration and evaporation of the solvent gave a brown oil which was further purified through flash silica column (CH₂Cl₂:hexanes, 7:3) to yield 7.6 g of heteroleptic phosphine **18** as yellow oil (76 % yield).

³¹P{¹H} NMR (161.98 MHz, CDCl₃), δ (ppm): -3.83 (s). ¹H NMR (400.13 MHz, CDCl₃), δ (ppm): 7.94 (s, 2H, H_{C4}{C₆H₃(CF₃)₂}); 7.76 (d, 4H, H_{C4}{C₆H₄CF₃}, ³J_{HH} = 7.8 Hz); 7.72 (d, 4H, H_{C2}{C₆H₃(CF₃)₂}, ³J_{HP} = 6.5 Hz); 7.68 (d, 1H, H_{C2}{C₆H₄CF₃}, ³J_{HP} = 6.5 Hz); 7.61 (t, 1H, H_{C5}{C₆H₄CF₃}, ³J_{HH} = 7.8 Hz); 7.45 (*pseudo-t*, 1H, H_{C6}{C₆H₄CF₃}, ³J_{HH} = ³J_{HP} = 7.8 Hz). ¹³C{¹H} NMR (100.61 MHz, CDCl₃), δ (ppm): 138.72 (d, C₁{C₆H₃(CF₃)₂}, ¹J_{CP} = 17.9 Hz); 136.79 (*bd*, C₆{C₆H₄CF₃}, ²J_{CP} = 15.4 Hz); 134.84 (d, C₁{C₆H₄CF₃}, ¹J_{CP} = 13.4 Hz); 133.30 (*bd*, C₂{C₆H₃(CF₃)₂}, ²J_{CP} = 21.3 Hz); 132.76 (*qd*, C₃{C₆H₃(CF₃)₂}, ²J_{CF} = 33.7 Hz, ²J_{CP} = 6.4 Hz); 132.20 (*qd*, C₃{C₆H₄CF₃}, ²J_{CF} = 32.6 Hz, ³J_{CP} = 9.1 Hz); 130.92 (*dq*, C₂{C₆H₄CF₃}, ²J_{CP} = 28.3 Hz, ³J_{CF} = 3.9 Hz); 130.29 (d, C₅{C₆H₄CF₃}, ³J_{CP} = 5.8 Hz); 127.68 (q, C₄{C₆H₄CF₃}, ³J_{CF} = 3.6 Hz); 124.01 (*sept*, C₄{C₆H₃(CF₃)₂}, ³J_{CF} = 3.8 Hz); 123.65 (q, CF₃{C₆H₄CF₃}, ¹J_{CF} = 272.5 Hz); 123.00 (q, CF₃{C₆H₃(CF₃)₂}, ¹J_{CF} = 273.1 Hz). ¹⁹F{¹H} NMR (376.50 MHz, CDCl₃), δ (ppm): -63.04 (*bs*, 3F, CF₃{C₆H₄CF₃}); -62.33 (*bs*, 12F, CF₃{C₆H₃(CF₃)₂}). **HR-MS** (ESI⁺ *m/z*) [M+H]⁺: calculated for [C₂₃H₁₁F₁₅P]⁺ 603.0353; found 603.0371. **Elemental analysis**: calculated for C₂₃H₁₀F₁₅P: C, 45.87; H, 1.67; found: C, 45.86; H, 1.66.

(3,5-bis(trifluoromethyl)phenyl)bis(4-(trifluoromethyl)phenyl)phosphine (**20**)



A solution of 4-(trifluoromethyl)phenyl magnesium bromide was prepared by addition of 2.0 ml of 4-(trifluoromethyl)bromobenzene (3.14 g, 13.9 mmol) dissolved 7.5 ml of anhydrous Et₂O to a suspension of Mg chips (0.41 g, 16.9 mmol) in 20 ml of anhydrous Et₂O. (Detailed description of the preparation of this Grignard derivative can be found in the synthesis of **1**). Afterwards, 2.2 g (7.0 mmol) of the trifluoromethylated dichlorophosphine **27** were dissolved in 7.5 ml of dry Et₂O and cooled in an ice bath.

The solution of the Grignard derivative was then added dropwise to the dichlorophosphine and the resulting orange suspension was stirred overnight at room temperature. After that time, the reaction mixture was cooled down to 0 °C (ice bath) and 10 ml of 10 % aqueous HCl were added. The organic layer was separated and the aqueous phase was extracted three times with 10 ml of Et₂O. The organic fractions were combined and dried over MgSO₄. Filtration and evaporation of the solvent gave an orange-brown solid which was further purified through flash silica column (CH₂Cl₂:hexanes, 9:1) to yield 1.9 g of heteroleptic phosphine **20** as an orange yellowish solid (51.2 % yield).

³¹P{¹H} NMR (161.98 MHz, CDCl₃), δ (ppm): -4.62 (s). ¹H NMR (400.13 MHz, CDCl₃), δ (ppm): 7.91 (s, 1H, H_{C4}{C₆H₃(CF₃)₂}); 7.73 (d, 2H, H_{C2}{C₆H₃(CF₃)₂}, ³J_{HP} = 6.2 Hz); 7.67 (d, 4H, H_{C3}{C₆H₃CF₃}, ³J_{HH} = 7.6 Hz); 7.42 (*pseudo-t*, 3H, H_{C2}{C₆H₄CF₃}, ³J_{HP} = ³J_{HH} = 7.6 Hz). ¹³C{¹H} NMR (100.61 MHz, CDCl₃), δ (ppm): 139.70 (d, C₁{C₆H₃(CF₃)₂}, ¹J_{CP} = 19.0 Hz); 139.33 (*bd*, C₁{C₆H₄CF₃}, ¹J_{CP} = 14.0 Hz); 134.13 (d, C₂{C₆H₄CF₃}, ²J_{CP} = 21.1 Hz); 133.5 (*bd*, C₂{C₆H₃(CF₃)₂}, ²J_{CP} = 21.0 Hz); 132.5 (qd, C₃{C₆H₃(CF₃)₂}, ²J_{CF} = 33.5 Hz, ²J_{CP} = 6.0 Hz); 132.24 (q, C₄{C₆H₄CF₃}, ²J_{CF} = 32.8 Hz); 126.12 (m, C₃{C₆H₄CF₃}, ³J_{CP} = 7.5 Hz, ³J_{CF} = 3.8 Hz); 123.89 (q, CF₃{C₆H₄CF₃}, ¹J_{CF} = 272.6 Hz); 123.64 (*sept*, C₄{C₆H₃(CF₃)₂}, ³J_{CF} = 3.6 Hz); 123.17 (q, CF₃{C₆H₃(CF₃)₂}, ¹J_{CF} = 272.6 Hz). ¹⁹F{¹H} NMR (376.50 MHz, CDCl₃), δ (ppm): -62.07 (s, 6F, CF₃{C₆H₃(CF₃)₂}); -62.17 (s, 6F, CF₃{C₆H₄CF₃}). **HR-MS** (ESI⁺ *m/z*) [M+H]⁺: calculated for [C₂₂H₁₂F₁₂P]⁺ 535.0480; found 535.0491. **Elemental analysis**: calculated for C₂₂H₁₁F₁₂P: C, 49.46; H, 2.08; found: C, 49.94; H, 2.19.

X-ray diffraction data for **20**

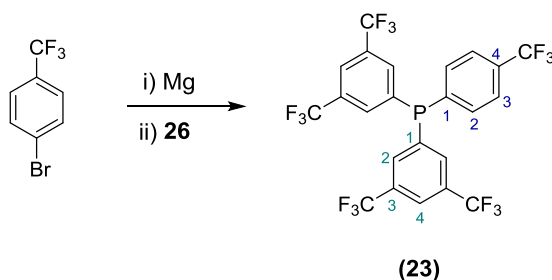
Crystals of suitable quality for X-ray diffraction were obtained by slow crystallisation of the phosphine in CH₂Cl₂. The structure was solved by direct methods. All non-hydrogen atoms were refined with anisotropic displacement thermal parameters. All hydrogen atoms were idealised and were positioned geometrically and refined using the riding model with U_{iso}(H) = 1.2 U_{eq}(C). The CF₃ group at C17 was disordered over three different orientations in approx 39.9, 43.3 and 16.7 % ratio. The geometry of the disordered CF₃ (distances and angles) was refined to conform a C_{3v} geometry according

to a modification of the procedure reported in literature.²² The following restraints were applied (with DFIX command): C(17)-F distances were allowed to refine as one free variable FVAR2; C(14)-F (ipso) distances were restrained to 1.746(11) times FVAR2. Moreover, F-F distances of the disordered F atoms were restrained to be equal within sd of 0.03 (with SADI command) and the Uij were restrained with SIMU instruction. All disordered atoms were refined anisotropically and the sum of the site occupation factors was restrained to 1.000.

Crystal data (20)

Chemical formula	C ₂₂ H ₁₁ F ₁₂ P	a	9.7822(6)
Molecular weight	534.3	b	11.2459(7)
Space group	Triclinic, P-1	c	11.3475(6)
wavelength	0.71073 (Mo K α)	α	61.3300(10)
Temperature	293(2) K	β	88.8990(10)
Volume	1090.54 (7) Å ³	γ	84.8900(10)
Z	2	R[I>2 σ (I)]	0.0773
		S	1.0490

Bis(3,5-bis(trifluoromethyl)phenyl)(4-(trifluoromethyl)phenyl)phosphine (23)



Phosphine **23** was prepared in analogy to **20**. A solution of 4-(trifluoromethyl)phenyl magnesium bromide was prepared by addition of 0.7 ml of 4-(trifluoromethyl)bromobenzene (1.05 g, 4.66 mmol) dissolved 5 ml of anhydrous Et₂O to a suspension of Mg chips (0.14 g, 5.56 mmol) in 7.5 ml of anhydrous Et₂O. (Detailed description of the preparation of this Grignard derivative can be found in the synthesis of **1**). Afterwards, 2.3 g (4.67 mmol) of the trifluoromethylated chlorophosphine **26**

²² Guzei, I. A.; Spencer, L. C.; Ojwach, S. O.; Darkwa, J. *Acta Crystallogr. Sect. C Cryst. Struct. Commun.* **2008**, *64* (3), m114–m116.

were dissolved in 7.5 ml of dry Et₂O and cooled in an ice bath. The solution of the Grignard derivative was then added dropwise to the chlorophosphine and the resulting dark orange suspension was stirred overnight at room temperature. After that time, the reaction mixture was cooled down to 0 °C (ice bath) and 10 ml of 10 % aqueous HCl were added. The organic layer was separated and the aqueous phase was extracted three times with 10 ml of Et₂O. The organic fractions were combined and dried over MgSO₄. Filtration and evaporation of the solvent gave an orange-brown oil which was further purified through flash silica column (CH₂Cl₂:hexanes, 9:1) to yield 1.79 g of heteroleptic phosphine **23** as an orange solid (63.7 % yield).

³¹P{¹H} NMR (161.98 MHz, CDCl₃), δ (ppm): -3.91 (s). ¹H NMR (400.13 MHz, CDCl₃), δ (ppm): 7.95 (s, 2H, H_{C4}{C₆H₃(CF₃)₂}); 7.73 (m, 6H, H_{C2}{C₆H₃(CF₃)₂}-H_{C3}{C₆H₃CF₃}); 7.43 (*pseudo-t*, 2H, H_{C2}{C₆H₄CF₃}), ³J_{HP} = ³J_{HH} = 7.9 Hz). ¹³C{¹H} NMR (100.61 MHz, CDCl₃), δ (ppm): 138.68 (d, C₁{C₆H₃(CF₃)₂}, ¹J_{CP} = 17.1 Hz); 138.22 (*bd*, C₁{C₆H₄CF₃}, ¹J_{CP} = 15.1 Hz); 134.24 (d, C₂{C₆H₄CF₃}, ²J_{CP} = 21.1 Hz); 133.5 (*bd*, C₂{C₆H₃(CF₃)₂}, ²J_{CP} = 22.1 Hz); 132.82 (qd, C₃{C₆H₃(CF₃)₂}, ²J_{CF} = 33.8 Hz, ²J_{CP} = 6.5 Hz); 132.82 (q, C₄{C₆H₄CF₃}, ²J_{CF} = 33.8 Hz); 126.46 (m, C₃{C₆H₄CF₃}, ³J_{CP} = 7.1 Hz, ³J_{CF} = 3.5 Hz); 124.09 (*sept*, C₄{C₆H₃(CF₃)₂}, ³J_{CF} = 3.6 Hz); 123.79 (q, CF₃{C₆H₄CF₃}, ¹J_{CF} = 272.1 Hz); 123.06 (q, CF₃{C₆H₃(CF₃)₂}, ¹J_{CF} = 272.7 Hz). ¹⁹F{¹H} NMR (376.50 MHz, CDCl₃), δ (ppm): -62.27 (s, 12F, CF₃{C₆H₃(CF₃)₂}); -62.35 (s, 3F, CF₃{C₆H₄CF₃}). **HR-MS** (ESI⁺ *m/z*) [M+H]⁺: calculated for [C₂₃H₁₁F₁₅P]⁺ 603.0353; found 603.0358. **Elemental analysis**: calculated for C₂₃H₁₀F₁₅P: C, 45.87; H, 1.67; found: C, 46.32; H, 1.77.

9.5.3. Iridium complexes

The iridium precursor $[\text{Ir}(\text{COD})\text{Cl}]_2$ was prepared according to the reported procedure in the literature with minor modifications.²³ 1.00 g of IrCl_3 hydrate (53.06 % Ir) and 1 ml of 1,5-cyclooctadiene (COD) were dissolved in 24 ml of 96 % EtOH and 12 ml of water. Following, 0.5 g of hydroquinone were added and the resulting brown slurry was brought to reflux for 5 h. (It is important to add the reactants in this order. COD prevents Ir^{3+} from being reduced to Ir^0 when in contact with EtOH. Also a plastic spatula should be used to manipulate IrCl_3 , instead of using the more common metallic spatulas). The colouration of reaction mixture evolved from the starting brown to dark orange to the final light orange colour. Approximately half of the volume of the solvent was vacuum evaporated and, as consequence, $[\text{Ir}(\text{COD})\text{Cl}]_2$ precipitated as orange-red solid. After filtration, the yellow solution was discarded and the orange-red solid was washed 4 times with 5 ml of MeOH and vacuum dried to yield 0.578 g of the iridium precursor $[\text{Ir}(\text{COD})\text{Cl}]_2$ (63 % yield).

Vaska-type compounds *trans*- $[\text{Ir}(\text{CO})\text{Cl}(\text{L})_2]$

Synthesis of Vaska-type compounds were performed as follows. 26.9 mg of the iridium precursor (0.04 mmol) and 2 equivalents of the corresponding ligand (0.16 mmol) were dissolved in CH_2Cl_2 to give an orange solution. A flow of CO was then bubbled into the solution for about 10-15 minutes. Rapid change in the colour of the solution to bright yellow was observed. Precipitation of the complex was achieved by reducing half of the volume of solvent and subsequent the addition of 1 ml of Et_2O . This procedure worked with triphenylphosphine. For the trifluoromethylated phosphines, precipitation of the complex was achieved using mixtures of Et_2O :*n*-hexanes (1:1). All the complexes were yellow solids. **Table 9.3** shows the characterisation of the Vaska-type complexes.

²³ Bezman, S. A.; Bird, P. H.; Frase, A. R.; Osborn, J. A. *Inorg. Chem.* **1980**, *19* (12), 3755.

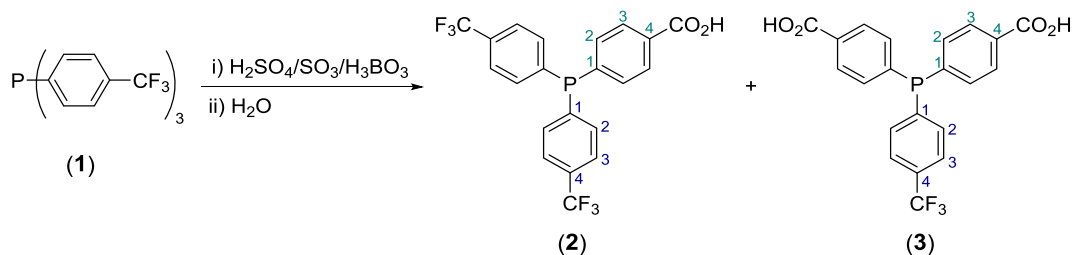
Table 9.3. Characterisation of the Vaska-type complexes, *trans*-[Ir(CO)Cl(L)₂]

Ligand (L)	IR ν_{CO} (cm ⁻¹)	ATR-FTIR	HR-MS (ESI ⁺ <i>m/z</i>)	³¹ P{ ¹ H} ^a	¹⁹ F{ ¹ H} ^b	NMR (acetone D-6)	¹ H ^c
PPh₃	1964	1949	calcd 745.198 found 745.1375	25.44 (s)	-		7.76 (m, 12H), 7.48 (m, 18H)
<i>m</i> -trisCF ₃ (5)	1976	1982	calcd 1153.0641 found 1153.0618	28.16 (s)	-62.60 (s)		8.20 (<i>bs</i> , 6H); 8.04 (<i>bd</i> , 6H, J = 7.7 Hz); 7.95 (d, 6H, J = 7.9 Hz); 7.81 (t, 6H, J = 7.7 Hz)
3,5-2 <i>m</i> -1 (18)	1983	1988	calcd 1425.0137 found 1425.0137	29.50 (s)	-62.43 (s, 6F) -62.50 (s, 24F)		8.49 (t, 8H, J = 5.2 Hz); 8.31 (s, 6H); 8.27 (q, 2H, J = 6.6); 8.02 (d, 2H, J = 7.9); 7.85 (t, 2H, J = 7.9)
3,5-1 <i>p</i> -2 (20)	1979	1972	calcd 1289.0389 found 1289.0352	27.72 (s)	-62.38 (s, 12F) -62.62 (s, 12F)		8.46 (<i>pseudo-t</i> , 4H, J _{HP} = 4.8 Hz); 8.30 (s, 2H); 8.10 (<i>pseudo-tq</i> 8H, J _{HH} = 8.0 Hz, J _{HP} = 5.8 Hz); 7.92 (d, 8H, J _{HH} = 8.2 Hz)
3,5-2 <i>p</i> -1 (23)	1983	1973	calcd 1425.0137 found 1425.0113	29.49 (s)	-62.80 (s, 24F) -63.03 (s, 6F)		8.53 (<i>pseudo-t</i> , 8H, J _{HP} = 4.9 Hz); 8.30 (s, 4H); 8.16 (<i>pseudo-q</i> , 4H, J _{HH} = 8.1 Hz, J _{HP} = 6.0 Hz); 7.93 (d, 4H, J _{HH} = 8.2 Hz)

^a 161.98 MHz. ^b 376.50 MHz. ^c 400.13 MHz

9.5.4. Carboxylic-trifluoromethylated phosphines and spirocyclic oxyphosphoranes

4-(bis(4-(trifluoromethyl)phenyl)phosphanyl)benzoic acid, *p*-Miranphos (2), and 4,4'-((4-(trifluoromethyl)phenyl)phosphanediyl)dibenzoic acid, *p*-Miran2phos (3)



In a typical reaction, 3.5 g of tris(4-trifluoromethylphenyl)phosphine (1) (7.5 mmol) were dissolved in 15 ml of a solution of boric acid (2.3 g, 37.2 mmol) in 98 % sulfuric acid at 0 °C. A strong red or orange solution was obtained once the phosphine was completely dissolved. At this point, the solution was kept at 0 °C and 32.5 ml of 65 % SO₃ fuming sulfuric acid (0.53 mol SO₃) was slowly added during 30 minutes with vigorous stirring. The dark brown mixture was then further stirred at room temperature for 18 h to give a mixture of *ca.* 42 % of monocarboxylic phosphine 2, 50 % of dicarboxylic 3 and 8 % of unreacted phosphine 1. It is advisable to monitor the evolution of the reaction by ³¹P{¹H} NMR since the rate of the reaction is fairly sensitive to the concentration of SO₃ in oleum and, at the same time, this concentration decreases with the number of times the bottle has been opened. The reaction mixture was then gently poured on 150 g of deoxygenated ice, which was prepared by freezing 150 ml of deoxygenated water. The resulting brown slurry was extracted 3 times with 100 ml of Et₂O. The organic phases were combined and washed 2 times with 50 ml of brine. The separation of the phosphine compounds was then carried out by means of extractions in water at different pH. Firstly the volume of organic solvent was reduced to *ca.* 100 ml and 100 ml of water was added. After vigorous stirring, biphasic mixture was allowed to separate and the aqueous phase was brought to pH 6.0 by addition of 5 % aqueous NaOH. The biphasic mixture was then vigorously stirred again for a few seconds and allowed to settle. At this point, the pH of the aqueous phase was measured and corrected if necessary. If so, the process was repeated (pH correction, stirring, phase separation and pH measuring) until reaching pH 6.0. At this pH both the oxide of phosphine 3 and the tricarboxylic phosphine 4, if present, are extracted as sodium salts in the aqueous phase which was therefore discarded. Next fresh water (100 ml) was

added to the organic phase and the pH of the aqueous solution was brought to 7.6, following the procedure described above. At this pH, phosphine **3** is extracted into the aqueous phase as sodium salt. After decantation, the organic phase was extracted again with 50 ml of water at pH 7.6. The organic layer was kept under nitrogen in a round-bottom flask for later treatment. The aqueous phases were combined and, after acidification to *ca.* pH 2 with 10 % aqueous H₂SO₄, phosphine **3** was extracted in the acidic form with 3 portions of 30 ml of Et₂O. The organic layers were dried over MgSO₄ and the solvent was vacuum evaporated to give 1.1 g (35 % yield) of the dicarboxylic phosphine, *p*-Miran2phos (**3**), in its hemihydrate form as a white solid in purity higher than 95 %. The organic phase separated at pH 7.6, which contained the monocarboxylic phosphine **2** and the starting phosphine **1**, was vacuum evaporated and treated with a solution of NaOH (5 %, in methanol) until complete neutralisation of the carboxylic group of **2**. This reaction can be monitored by TLC in silica. Then, the solvent was vacuum evaporated to dryness and the resulting solid residue was extracted with cyclohexane to remove phosphine **1**. Best results were obtained when the extraction was performed in a Soxhlet extractor overnight. After evaporation of the cyclohexane, 0.2 g of **1** were obtained (6 % recovered), which can be used again in a new reaction. The solid residue that remained after the extraction with cyclohexane, corresponding to the sodium salt of **2**, was suspended in a biphasic mixture of 30 ml of water and 30 ml of Et₂O. After acidification to *ca.* pH 2 with 10 % aqueous H₂SO₄, **2** was extracted to the organic phase in its acid form. After decantation, the aqueous phase was further extracted 2 times with 30 ml of Et₂O. The organic layers were dried over MgSO₄ and finally the solvent was vacuum evaporated to give 1.40 g (42 % yield) of the carboxylic phosphine, *p*-Miranphos (**2**), as white solid, in purity above 95 %.

In the case that only monocarboxylic phosphine **2** was the product of interest, the reaction with oleum was stopped after 4 h. With this a mixture of **1** and **2** in about 50-50 % was obtained which could be separated as described above: neutralisation with NaOH (5 %, in methanol), extraction with cyclohexane to remove **1** and re-acidification to extract **2** in biphasic water-ether.

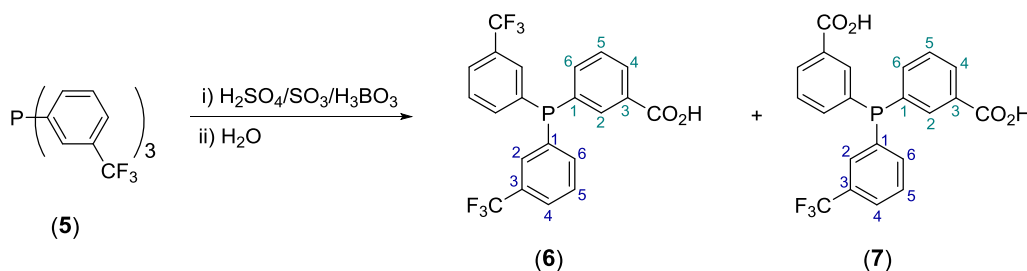
Data for *p*-Miranphos (2)

$^{31}\text{P}\{^1\text{H}\}$ NMR (101.27 MHz, CDCl_3), δ (ppm): -5.27 (s). ^1H NMR (400.13 MHz, CDCl_3), δ (ppm): 8.10 (dd, 2H, $\text{H}_{\text{C}_3}\{\text{C}_6\text{H}_4\text{CO}_2\text{H}\}$, $^3J_{\text{HH}} = 8.5$ Hz, $^4J_{\text{HP}} = 1.5$ Hz); 7.63 (d, 4H, $\text{H}_{\text{C}_3}\{\text{C}_6\text{H}_4\text{CF}_3\}$, $^3J_{\text{HH}} = 8.0$ Hz); 7.41 (m, 6H, $\text{H}_{\text{C}_2}\{\text{C}_6\text{H}_4\text{CO}_2\text{H}\}$ - $\text{H}_{\text{C}_2}\{\text{C}_6\text{H}_4\text{CF}_3\}$). $^{13}\text{C}\{^1\text{H}\}$ NMR (100.61 MHz, CDCl_3), δ (ppm): 171.7 (s, CO_2H); 142.77 (d, $\text{C}_1\{\text{C}_6\text{H}_4\text{CO}_2\text{H}\}$, $^1J_{\text{CP}} = 14.4$ Hz); 140.4 (d, $\text{C}_1\{\text{C}_6\text{H}_4\text{CF}_3\}$, $^1J_{\text{CP}} = 14.2$ Hz); 134.20 (d, $\text{C}_2\{\text{C}_6\text{H}_4\text{CF}_3\}$, $^2J_{\text{CP}} = 20.2$ Hz); 133.7 (d, $\text{C}_2\{\text{C}_6\text{H}_4\text{CO}_2\text{H}\}$, $^2J_{\text{CP}} = 19.6$ Hz); 131.7 (q, $\text{C}_4\{\text{C}_6\text{H}_4\text{CF}_3\}$, $^2J_{\text{CF}} = 32.6$ Hz); 130.5 (d, $\text{C}_3\{\text{C}_6\text{H}_4\text{CO}_2\text{H}\}$, $^3J_{\text{CP}} = 6.9$ Hz); 130.2 (s, $\text{C}_4\{\text{C}_6\text{H}_4\text{CO}_2\text{H}\}$); 125.8 (dq, $\text{C}_3\{\text{C}_6\text{H}_4\text{CF}_3\}$, $^3J_{\text{CP}} = 7.4$ Hz, $^3J_{\text{CF}} = 3.6$ Hz); 125.5 (q, CF_3 , $^1J_{\text{CF}} = 272.5$ Hz). $^{19}\text{F}\{^1\text{H}\}$ NMR (376.50 MHz, CDCl_3), δ (ppm): -62.27 (s). **HR-MS** (ESI m/z) $[\text{M}-\text{H}]^-$: calculated for $[\text{C}_{21}\text{H}_{12}\text{F}_6\text{O}_2\text{P}]^-$ 441.0485; found 441.0486. **Elemental analysis**: calculated for $\text{C}_{21}\text{H}_{13}\text{F}_6\text{O}_2\text{P}$: C, 57.03; H, 2.96; found: C, 57.40; H, 3.06.

Data for *p*-Miran2phos (3)

$^{31}\text{P}\{^1\text{H}\}$ NMR (101.27 MHz, CD_3OD), δ (ppm): -4.66 (s). ^1H NMR (400.13 MHz, CD_3OD), δ (ppm): 8.0 (*bd*, 4H, $\text{H}_{\text{C}_3}\{\text{C}_6\text{H}_4\text{CO}_2\text{H}\}$, $^3J_{\text{HH}} = 8.3$ Hz); 7.7 (d, 2H, $\text{H}_{\text{C}_3}\{\text{C}_6\text{H}_4\text{CF}_3\}$, $^3J_{\text{HH}} = 8.1$ Hz); 7.5 (*pseudo-t*, 2H, $\text{H}_{\text{C}_2}\{\text{C}_6\text{H}_4\text{CF}_3\}$, $^3J_{\text{HH}} = ^3J_{\text{HP}} = 7.7$ Hz); 7.4 (*bt*, 2H, $\text{H}_{\text{C}_2}\{\text{C}_6\text{H}_4\text{CO}_2\text{H}\}$, $^3J_{\text{HH}} = ^3J_{\text{HP}} = 7.7$ Hz). $^{13}\text{C}\{^1\text{H}\}$ NMR (100.61 MHz, CD_3OD), δ (ppm): 169.2 (s, CO_2H); 142.8 (d, $\text{C}_1\{\text{C}_6\text{H}_4\text{CO}_2\text{H}\}$, $^1J_{\text{CP}} = 13.7$ Hz); 142.7 (d, $\text{C}_1\{\text{C}_6\text{H}_4\text{CF}_3\}$, $^1J_{\text{CP}} = 14.2$ Hz); 135.3 (d, $\text{C}_2\{\text{C}_6\text{H}_4\text{CF}_3\}$, $^2J_{\text{CP}} = 20.0$ Hz); 134.7 (d, $\text{C}_2\{\text{C}_6\text{H}_4\text{CO}_2\text{H}\}$, $^2J_{\text{CP}} = 20.1$ Hz); 132.9 (s, $\text{C}_4\{\text{C}_6\text{H}_4\text{COOH}\}$); 132.2 (q, $\text{C}_4\{\text{C}_6\text{H}_4\text{CF}_3\}$, $^2J_{\text{CF}} = 32.7$ Hz); 131.0 (d, $\text{C}_3\{\text{C}_6\text{H}_4\text{CO}_2\text{H}\}$, $^3J_{\text{CP}} = 7.0$ Hz); 126.5 (dq, $\text{C}_3\{\text{C}_6\text{H}_4\text{CF}_3\}$, $^3J_{\text{CP}} = 7.0$ Hz, $^3J_{\text{CF}} = 3.7$ Hz); 125.4 (q, CF_3 , $^1J_{\text{CF}} = 271.2$ Hz). $^{19}\text{F}\{^1\text{H}\}$ NMR (235.39 MHz, CD_3OD), δ (ppm): -62.0 (s). **HR-MS** (ESI m/z) $[\text{M}-\text{H}]^-$: calculated for $[\text{C}_{21}\text{H}_{13}\text{F}_3\text{O}_4\text{P}]^-$ 417.0509; found 417.0503. **Elemental analysis**: calculated for $\text{C}_{21}\text{H}_{14}\text{F}_3\text{O}_4\text{P} \cdot 1/2\text{H}_2\text{O}$: C, 59.03; H, 3.54; found: C, 59.19; H, 3.36

3-(bis(3-(trifluoromethyl)phenyl)phosphanyl)benzoic acid, *m*-Miranphos (6), and 3,3'-((3-(trifluoromethyl)phenyl)phosphanediyl)dibenzoic acid, *m*-Miran2phos (7)



The same procedure and reaction conditions as described for the *para*-substituted phosphines were followed in the hydrolysis of the *meta*-substituted phosphine **5**. In this case, when the dicarboxylic phosphine **7** was the aimed product of the synthesis, the trifluoromethylated phosphine **5** was allowed to react with oleum for 20 h, yielding a mixture composed of 6 % of **6**, 60 % of **7** and 20 % of the tricarboxylic phosphine **8**. If, instead, the monocarboxylic phosphine **6** was aimed, the reaction with oleum was stopped after 0.5 h, yielding 48 % of unreacted phosphine **5**, 41 % of phosphine **6** and 6 % of **7**. Reaction times between 0.5 and 20 h gave intermediate results. In an example of reaction 5.5 g of **5** (11.8 mmol) and 3.6 g of boric acid (58.2 mmol) were dissolved in 22.8 ml of 98 % sulfuric acid. Following 51.0 ml of 65 % SO₃ fuming sulfuric acid (0.8 mol of SO₃) were added and allowed to react for 3 h. After quenching with water, NMR analysis of the mixture showed *ca.* 8 % of **5**, 35 % of **6**, 46 % of **7** and 5 % of **8**. Finally, after the process of separation, 1.8 g of *m*-Miranphos (34.6 % yield) and 2.1 g of *m*-Miran2phos (42.5 % yield) were isolated as white solids in purities above 95 %.

Data for *m*-Miranphos (6)

³¹P{¹H} NMR (101.27 MHz, CDCl₃), δ (ppm): -4.93 (s). ¹H NMR (400.13 MHz, CDCl₃), δ (ppm): 8.14l (m, 1H, H_{C4}{C₆H₄CO₂H}); 8.10 (d, 1H, H_{C2}{C₆H₄CO₂H}, ³J_{HP} = 8.7 Hz); 7.65 (d, 2H, H_{C4}{C₆H₄CF₃}, ³J_{HH} = 7.7 Hz); 7.60 (d, 2H, H_{C2}{C₆H₄CF₃}, ³J_{HP} = 7.9 Hz); 7.51 (m, 4H, H_{C5}{C₆H₄CF₃}-H_{C5}{C₆H₄CO₂H}- H_{C6}{C₆H₄CO₂H}); 7.44 (*pseudo-t*, 2H, H_{C6}{C₆H₄CF₃}, ³J_{HH} = ³J_{HP} = 7.1 Hz). ¹³C{¹H} NMR (100.61 MHz, CDCl₃), δ (ppm): 171.4 (s, CO₂H); 138.8 (d, C₆{C₆H₄CO₂H}, ²J_{CP} = 17.2 Hz); 137.4 (d, C₁{C₆H₄CF₃}, ¹J_{CP} = 14.0 Hz); 136.8 (d, C₆{C₆H₄CF₃}, ²J_{CP} = 16.1 Hz); 136.6 (d, C₁{C₆H₄CO₂H}, ¹J_{CP} = 13.3 Hz); 135.5 (d, C₂{C₆H₄CO₂H}, ²J_{CP} = 23.9 Hz); 131.5 (qd, C₃{C₆H₄CF₃}, ²J_{CF} = 32.5 Hz, ³J_{CP} = 8.1 Hz); 131.4 (s, C₄{C₆H₄CO₂H}); 130.4 (dq, C₂{C₆H₄CF₃}, ²J_{CP} = 25.0 Hz, ³J_{CF} = 3.8 Hz); 130.15 (d, C₃{C₆H₄CO₂H}, ³J_{CP}=7.7Hz);

129.5 (d, C₅{C₆H₄CF₃}, ³J_{CP} = 5.6 Hz); 129.4 (d, C₅{C₆H₄CO₂H}, ³J_{CP} = 6.1 Hz); 126.4 (q, C₄{C₆H₄CF₃}, ³J_{CF} = 3.6 Hz); 124.0 (q, CF₃, ¹J_{CF} = 272.2 Hz). ¹⁹F{¹H} NMR (235.39 MHz, CDCl₃), δ (ppm): -62.40 (s). **HR-MS** (ESI *m/z*) [M-H]⁻: calculated for [C₂₁H₁₂F₆O₂P]⁻ 441.0485; found 441.0489. **Elemental analysis**: calculated for C₂₁H₁₃F₆O₂P: C, 57.03; H, 2.96; found: C, 57.15; H, 3.02.

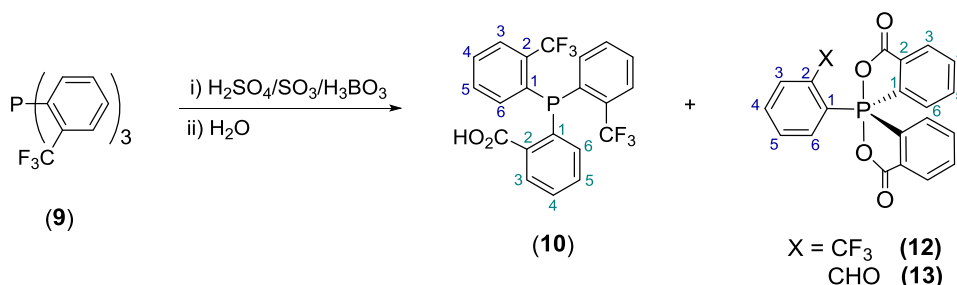
Data for *m*-Miran2phos (7)

³¹P{¹H} NMR (161.98 MHz, CD₃OD), δ (ppm): -4.61 (s). ¹H NMR (400.13 MHz, CD₃OD), δ (ppm): 8.07 (m, 2H, H_{C4}{C₆H₄CO₂H}); 7.98 (bd, 2H, H_{C2}{C₆H₄CO₂H}, ³J_{HP} = 8.0 Hz); 7.70 (bd, 1H, H_{C4}{C₆H₄CF₃}, ³J_{HH} = 7.9 Hz); 7.59 (bt, 1H, H_{C5}{C₆H₄CF₃}, ³J_{HP} = 7.7 Hz); 7.52 (m, 6H, H_{C2}{C₆H₄CF₃}-H_{C6}{C₆H₄CF₃}-H_{C5}{C₆H₄CO₂H}-H_{C6}{C₆H₄CO₂H}). ¹³C{¹H} NMR (100.61 MHz, CD₃OD), δ (ppm): 169.08 (s, CO₂H); 139.7 (d, C₆{C₆H₄CF₃}, ²J_{CP} = 14.7 Hz); 139.0 (d, C₆{C₆H₄CO₂H}, ²J_{CP} = 19.3 Hz); 138.2 (d, C₁{C₆H₄CF₃}, ¹J_{CP} = 17.9 Hz); 137.9 (d, C₁{C₆H₄CO₂H}, ¹J_{CP} = 12.9 Hz); 135.8 (d, C₂{C₆H₄CO₂H}, ²J_{CP} = 21.9 Hz); 132.7 (d, C₃{C₆H₄CO₂H}, ³J_{CP} = 7.0 Hz); 132.2 (qd, C₃{C₆H₄CF₃}, ²J_{CF} = 32.2 Hz, ³J_{CP} = 7.2 Hz); 131.8 (s, C₄{C₆H₄CO₂H}); 130.9 (dq, C₂{C₆H₄CF₃}, ²J_{CP} = 22.4 Hz, ³J_{CF} = 3.9 Hz); 130.7 (d, C₅{C₆H₄CF₃}, ³J_{CP} = 5.9 Hz); 130.2 (d, C₅{C₆H₄CO₂H}, ³J_{CP} = 6.7 Hz); 127.06 (q, C₄{C₆H₄CF₃}, ³J_{CP} = 3.7 Hz); 125.33 (q, CF₃, ¹J_{CF} = 272.2 Hz). ¹⁹F{¹H} NMR (376.50 MHz, CD₃OD), δ (ppm): -62.07(s). **HR-MS** (ESI *m/z*) [M-H]⁻: calculated for [C₂₁H₁₃F₃O₄P]⁻ 417.0509; found 417.0512. **Elemental analysis**: calculated for C₂₁H₁₄F₃O₄P: C, 60.30; H, 3.37; found: C, 59.58; H, 3.34.

Data for 3,3',3''-phosphanetriyltribenzoic acid (8)

³¹P{¹H} NMR (101.27 MHz, CD₃OD), δ (ppm): -5.07 (s). ¹H NMR (400.13 MHz, CD₃OD), δ (ppm): 8.06 (m, 3H, H_{C4}); 7.98 (bd, 3H, H_{C2}, ³J_{HP} = 8.1 Hz); 7.52 (m, 6H, H_{C5}+H_{C6}). ¹³C{¹H} NMR (100.61 MHz, CD₃OD), δ (ppm): 169.2 (s, CO₂H); 140.0 (d, C₆{C₆H₄CO₂H}, ²J_{CP} = 19.0 Hz); 138.4 (d, C₁{C₆H₄CO₂H}, ¹J_{CP} = 12.9 Hz); 135.8 (d, C₂{C₆H₄CO₂H}, ²J_{CP} = 21.9 Hz); 132.6 (d, C₃{C₆H₄CO₂H}, ³J_{CP} = 7.0 Hz); 131.6 (s, C₄{C₆H₄CO₂H}); 130.2 (d, C₅{C₆H₄CO₂H}, ³J_{CP} = 6.5 Hz). **HR-MS** (ESI *m/z*) [M-H]⁻: calculated for [C₂₁H₁₄O₆P]⁻ 393.0533; found 393.0509.

2-(bis(2-(trifluoromethyl)phenyl)phosphanyl) benzoic acid, *o*-Miranphos (10), and the spirocyclic oxyphosphoranes 1-(2-(trifluoromethyl)phenyl)-1λ⁵-1,1'-spirobi[benzo[*c*][1,2]oxaphosphole]-3,3'(1*H*)-dione (12) and 2-(3,3'-dioxo-1,3,3'-trihydro-1λ⁵-1,1'-spirobi[benzo[*c*][1,2]oxaphosphol]-1-yl)benzaldehyde (13)



In a reaction example, 2.0 g of phosphine **9** (4.3 mmol) and 7.54 g of boric acid (0.12 mol) were dissolved in 14 ml of 98 % sulfuric acid and the mixture was cooled down to 0 °C (ice bath). Under vigorous stirring, 55.5 ml of 65 % SO₃ fuming sulfuric acid (0.9 mol) were slowly added. The mixture was then stirred at room temperature for 96 h, time after which it was quenched over 300 g of deoxygenated ice (prepared by freezing 300 ml of deoxygenated water). The phosphorus compounds were then extracted with Et₂O (five times with 100 ml each). The ³¹P{¹H} NMR analysis showed a composition of *ca.* 17 % of **9**, 70 % of **10** and 5 % of each of the spirocyclic compounds **12** and **13**. The volume of organic solvent was reduced to 50 ml and the same volume of water was added to proceed to the separation of the products. The aqueous phase was brought to pH 7.2 under vigorous stirring to extract the spirocyclic oxyphosphorane **13** together with any phosphine oxides. Addition of fresh Et₂O and acidification of the aqueous phase to pH 2 allowed the extraction of **13** into the organic phase after repeated extractions with Et₂O, while most of the oxides remained as an insoluble white solid interphase. **13** was further purified by column chromatography in silica (ethyl acetate:CH₂Cl₂, 5:5) and was isolated as white solid (0.08 g, 4.9 % yield). Fresh water was added to the organic phase from the extraction at pH 7.2 containing phosphines **9** and **10** and the spirocyclic **12**. The aqueous phase was brought to pH 11.5 to extract the carboxylic phosphine **10** as sodium salt. Phase separation and re-acidification of the aqueous phase allowed the extraction of **10** into fresh Et₂O. The organic layer was separated and dried over MgSO₄. Solvent evaporation afforded 0.4 g of *o*-Miranphos **10** (21 % yield) as white solid. Finally, the organic phase extracted at pH 11.5, containing phosphine **9** and the spirocyclic oxyphosphorane **12**, was vacuum evaporated and the

compounds were separated by column chromatography in silica gel (Et₂O). 0.15 g of the trifluoromethylated phosphine **9** were recovered (7.5 % yield) together with 20 mg of the spirocycle **12** (1.1 % yield) as pale yellow solid.

Data for *o*-Miranphos (**10**)

³¹P{¹H} NMR (161.98 MHz, acetone-D₆), δ (ppm): -11.6 (sept, ⁴T_SJ_{PF} = 57.8 Hz). ¹H NMR (400.13 MHz, acetone-D₆), δ (ppm): 8.21 (m, 1H, H_{C3}{C₆H₄CO₂H}, ⁴J_{HP} = 4.3 Hz); 7.84 (dd, 2H, H_{C3}{C₆H₄CF₃}, ³J_{HH} = 7.6 Hz, ⁴J_{HP} = 4.0 Hz); 7.56 (m, 6H, H_{C4}+H_{C5}{C₆H₄CF₃}-H_{C4}+H_{C5}{C₆H₄CO₂H}); 7.06 (dd, 2H, H_{C6}{C₆H₄CF₃}, ³J_{HH} = 7.4 Hz, ⁴J_{HP} = 2.6 Hz); 6.80 (m, 1H, H_{C6}{C₆H₄CO₂H}, ³J_{HP} = 3.5 Hz). ¹³C{¹H} NMR (100.61 MHz, acetone-D₆), δ (ppm): 167.50 (d, CO₂H); 140.45 (bd, C₂{C₆H₄CO₂H}, ²J_{CP} = 29.5 Hz); 138.71 (bd, C₂{C₆H₄CF₃}, ²J_{CP} = 30.9 Hz); 136.59 (bs, C₆{C₆H₄CF₃}); 135.65 (s, C₆{C₆H₄CO₂H}), 134.50 (d, J_{CP} = 19.7 Hz); 133.31 (s); 132.87 (s); 132.16 (d, C₃{C₆H₄CO₂H}, ³J_{CP} = 2.0 Hz); 130.08 (s, C₅{C₆H₄CO₂H}); 129.76 (s, C₅{C₆H₄CF₃}); 127.39 (quint, C₃{C₆H₄CF₃}, ³J_{CP} = ³J_{CF} = 5.8 Hz); 125.47 (q, CF₃, ³J_{CF} = 274.5 Hz). ¹⁹F{¹H} NMR (376.50 MHz, acetone-D₆, 298 K), δ (ppm): -56.52 (bd). ¹⁹F{¹H} NMR (376.50 MHz, acetone-D₆, 275 K), δ (ppm): -56.06 (d, 3F, ⁴T_SJ_{PF} = 60.3 Hz); -57.00 (d, 3F, ⁴T_SJ_{PF} = 53.3 Hz). **HR-MS** (ESI⁺ *m/z*) [M+Na]⁺: calculated for [C₂₁H₁₃F₆O₂PNa]⁺ 465.0450; found 465.0450. **Elemental analysis**: calculated for C₂₁H₁₃F₆O₂P: C, 57.03; H, 2.96; found: C, 57.13; H, 3.04.

X-ray diffraction data for **10**

Crystals of suitable quality for XRD were obtained from slow precipitation in acetone. The structure was solved by direct methods. All non-hydrogen atoms were refined with anisotropic displacement thermal parameters. All hydrogen atoms attached to carbon atoms were idealised and were positioned geometrically and refined using the riding model with U_{iso}(H) = 1.2 U_{eq}(C). The hydrogen atom of the OH group was located from the difference-Fourier map and refined with isotropic displacement parameters. No disorder in the CF₃ groups was observed.

Crystal data (10)

Chemical formula	C ₂₁ H ₁₃ F ₆ O ₂ P	a	6.9841(3)
Molecular weight	442.3	b	18.9623(8)
Space group	Monoclinic, P 21/c	c	14.8050(6)
wavelength	0.71073 (Mo K α)	α	90
Temperature	293(2) K	β	98.0000(10)
Volume	1941.61(14) Å ³	γ	90
Z	4	R[I>2 σ (I)]	0.04765
		S	1.025

Data for spirocyclic oxyphosphorane 12:

³¹P{¹H} NMR (161.98 MHz, CDCl₃), δ (ppm): -54.40 (s). ¹H NMR (400.13 MHz, CDCl₃), δ (ppm): 8.39 (m, 2H, {spirocycle}, J_{HP} = 12.4 Hz); 8.19 (m, 2H, {spirocycle}); 7.86 (m, 4H, {spirocycle}); 7.75 (*pseudo-t*, 1H, H_{C3}{C₆H₄CF₃}, ³J_{HH} = ⁴J_{HP} = 7.8 Hz); 7.54 (t, 1H, H_{C4}{C₆H₄CF₃}, ³J_{HH} = ³J_{HH} = 7.8 Hz); 7.47 (td, 1H, H_{C5}{C₆H₄CF₃}, ³J_{HH} = ³J_{HH} = 7.7 Hz, ⁴J_{HH} = 3.2 Hz); 7.35 (dd, 1H, H_{C6}{C₆H₄CF₃}, ³J_{HP} = 21.8 Hz, ³J_{HH} = 7.7). ¹³C{¹H} NMR (100.61 MHz, CDCl₃), δ (ppm): 164.78 (d, CO₂P, ³J_{CP} = 3.0 Hz); 137.13 (d, C₂{spirocycle}, ²J_{CP} = 17.8 Hz); 135.80 (*bs*); 135.54 (d, C{spirocycle}, J_{CP} = 3.3 Hz); 134.68 (d, C{spirocycle}, J_{CP} = 15.2 Hz); 133.57 (*bd*, C₁{C₆H₄CF₃}, ¹J_{CP} = 180.4 Hz); 133.32 (d, C₁{spirocycle}, ¹J_{CP} = 155.9 Hz); 132.18 (d, C₅{C₆H₄CF₃}, ³J_{CP} = 18.5 Hz); 130.5 (d, C₄{C₆H₄CF₃}, ⁴J_{CP} = 3.6 Hz); 129.01 (d, C₆{C₆H₄CF₃}, ²J_{CP} = 11.9 Hz); 127.50 (*bd*, C{spirocycle}, J_{CP} = 15.1 Hz); 127.13 (m, C₃{C₆H₄CF₃}); 123.23 (qd, CF₃, ¹J_{CF} = 274.2 Hz, ³J_{CP} = 5.8 Hz). ¹⁹F{¹H} NMR (376.50 MHz, CDCl₃), δ (ppm): -57.81 (s). **HR-MS** (ESI⁺ *m/z*) [M+H]⁺: calculated for [C₂₁H₁₃F₃O₄P]⁺ 417.0498; found 417.0504.

Analysis data for spirocyclic oxyphosphorane 13:

³¹P{¹H} NMR (161.98 MHz, CDCl₃), δ (ppm): -57.94 (s). ¹H NMR (400.13 MHz, CDCl₃), δ (ppm): 10.20 (s, 1H, CHO); 8.43 (m, 2H, {spirocycle}); 8.18 (m, 2H, {spirocycle}); 7.95 (*pseudo-td*, 1H, {C₆H₄CHO}, J_{HP} = 7.8, J_{HH} = 6.8, J_{HH} = 1.4 Hz), 7.87 (m, 4H, {spirocycle}); 7.58 (m, 3H, {C₆H₄CHO}). ¹³C{¹H} NMR (100.61 MHz, CDCl₃), δ (ppm): 190.48 (d, CHO, ³J_{CP} = 5.9 Hz); 164.89 (d, CO₂P, ³J_{CP} = 3.2 Hz); 136.64-127.64 (m, C_{aryl}). **HR-MS** (ESI⁺ *m/z*) [M+H]⁺: calculated for [C₂₁H₁₄O₅P]⁺

377.0573; found 377.0577. **Elemental analysis:** calculated for $C_{21}H_{13}O_5P \cdot 1/2H_2O$: C, 65.46; H, 3.66; found: C, 65.53; H, 3.64.

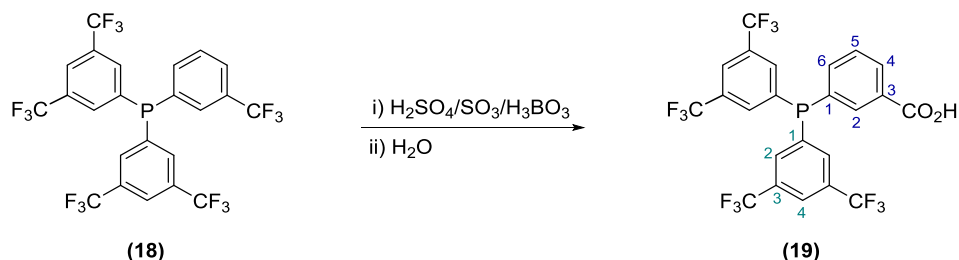
X-ray diffraction data for 13

Crystals of good quality for XRD were obtained by slow crystallization of the product dissolved in CH_2Cl_2 with slow diffusion of ethyl acetate. The structure was solved by Direct methods. All non-hydrogen atoms were refined with anisotropic displacement thermal parameters. The aldehyde hydrogen atom was located from the difference-Fourier map and refined with $U_{iso}(H) = 1.2 U_{eq}(C)$. All hydrogen atoms were idealised and were positioned geometrically and refined using the riding model with $U_{iso}(H) = 1.2 U_{eq}(C)$.

Crystal data (13)

Chemical formula	$C_{21}H_{13}O_5P$	a	9.5867(4)
Molecular weight	376.28	b	12.6989(5)
Space group	Monoclinic, P 21/c	c	14.6985(6)
wavelength	0.71073 (Mo $K\alpha$)	α	90
Temperature	296(2) K	β	104.4760(10)
Volume	1732.59(12) \AA^3	γ	90
Z	4	R[I>2 σ (I)]	0.0391
		S	1.020

**3-(bis(3,5-bis(trifluoromethyl)phenyl)phosphanyl)benzoic acid,
3,5-2 *m*-Miranphos (19)**

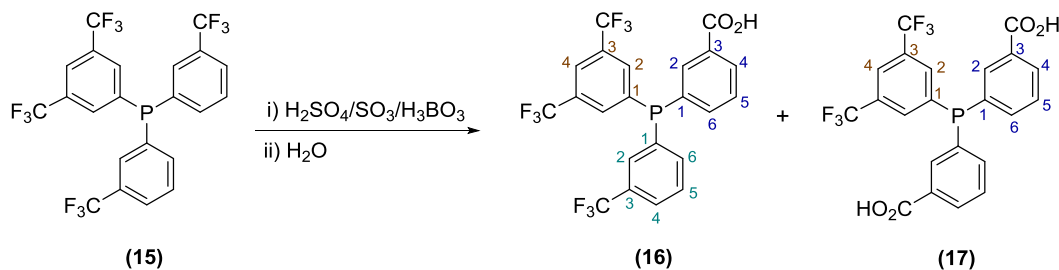


Carboxylic phosphine **19** was prepared in analogy to the Miranphos ligands (**2** and **6**). 2.6 g of the trifluoromethylated phosphine **18** (4.3 mmol) and 1.30 g of boric acid (21 mmol) were dissolved in 24 ml of sulfuric acid resulting in the formation of an orange solution. The mixture was cooled in an ice bath and 28 ml of 65 % SO_3 fuming sulfuric acid (0.46 mol of SO_3) were added dropwise. After the complete addition of oleum, the

dark mixture was stirred at room temperature for 62 h before being poured on 150 g of deoxygenated ice (prepared by freezing 150 ml of deoxygenated water). The resulting slurry was extracted 4 times with 50 ml of Et₂O. The organic solvent was evaporated and giving a white solid. At this point, ³¹P{¹H} NMR analysis showed a composition of *ca.* 65 % of **19** and 35 % of phosphine oxides. Small amount of the starting phosphine **18** were also detected by TLC in silica (CH₂Cl₂). Therefore, the solid was treated with NaOH (5 % in methanol) until neutralisation of the carboxylic groups. Following the solvent was vacuum evaporated and the solid was extracted with cyclohexane (Soxhlet extractor, overnight). The solid residue containing the carboxylic phosphine was mixed with 20 ml of water and 20 ml of diethyl ether and the pH was brought to 5-6. The two phases were then decanted and the aqueous phase was extracted with 2 portions of 20 ml of Et₂O. The organic layers were dried over MgSO₄ and the solvent was vacuum evaporated to afford 0.88 g of the carboxylic phosphine **19** (35 % yield) in purity above 95 %.

³¹P{¹H} NMR (161.98 MHz, CDCl₃, at 323 K), δ (ppm): -3.49 (s). ¹H NMR (400.13 MHz, CDCl₃, at 323 K), δ (ppm): 8.22 (d, 1H, H_{C4}{C₆H₄CO₂H}, ³J_{HH} = 7.3 Hz); 8.14 (d, 1H, H_{C2}{C₆H₄CO₂H}, ³J_{HP} = 8.5 Hz); 7.93 (s, 2H, H_{C4}{C₆H₃(CF₃)₂}); 7.73 (d, 4H, H_{C2}{C₆H₃(CF₃)₂}, ³J_{HP} = 6.6 Hz); 7.59 (*bt*, 1H, H_{C5}{C₆H₄CO₂H}, ³J_{HH} = 7.3 Hz); 7.52 (*bt*, 1H, H_{C6}{C₆H₄CO₂H}, ³J_{HH} = ³J_{HP} = 7.3 Hz). ¹³C{¹H} NMR (100.61 MHz, CDCl₃, at 323 K), δ (ppm): 170.31 (s, CO₂H); 139.17 (d, C₁{C₆H₃(CF₃)₂}, ¹J_{CP} = 18.3 Hz); 138.66 (d, C₆{C₆H₄CO₂H}, ²J_{CP} = 17.1 Hz); 135.83 (d, C₂{C₆H₄CO₂H}, ²J_{CP} = 26.0 Hz); 134.40 (d, C₁{C₆H₄CO₂H}, ¹J_{CP} = 13.1 Hz); 133.31 (*bd*, C₂{C₆H₃(CF₃)₂}, ²J_{CP} = 20.5 Hz); 132.86 (*qd*, C₃{C₆H₃(CF₃)₂}, ²J_{CF} = 33.6 Hz, ³J_{CP} = 6.3 Hz); 132.50 (s, C₄{C₆H₄CO₂H}); 130.85 (d, C₃{C₆H₄CO₂H}, ³J_{CP} = 8.7 Hz); 130.05 (d, C₅{C₆H₄CO₂H}, ³J_{CP} = 6.3 Hz); 123.91 (*sept*, C₄{C₆H₃(CF₃)₂}, ³J_{CF} = 3.7 Hz); 123.10 (*q*, CF₃, ¹J_{CF} = 273.8 Hz). ¹⁹F{¹H} NMR (376.50 MHz, CDCl₃, at 323 K), δ (ppm): -63.36 (s). **HR-MS** (ESI *m/z*) [M-H]⁻: calculated for [C₂₃H₁₀F₁₂O₂P]⁻ 577.0232; found 577.0251. **Elemental analysis**: calculated for C₂₃H₁₁F₁₂O₂P: C, 47.77; H, 1.96; found: C, 47.40; H, 1.97.

3-((3,5-bis(trifluoromethyl)phenyl)(3-(trifluoromethyl)phenyl)phosphanyl)benzoic acid, 3,5-1 *m*-Miranphos (16), and 3,3'-((3,5-bis(trifluoromethyl)phenyl)-phosphanediyl)dibenzoic acid, 3,5-1 *m*-Miranphos (17)



Carboxylic phosphines **16** and **17** were prepared in analogy to the Miranphos ligands (**2** and **6**) and Miran2phos ligands (**3** and **7**). A solution of 2.5 g of phosphine **15** (4.7 mmol) and 3.25 g of boric acid (52.6 mmol) in 30 ml of 98 % sulfuric acid was cooled down to 0 °C in an ice bath. Following, 37 ml of 65 % SO₃ fuming sulfuric acid (0.6 mol of SO₃) were added dropwise and the mixture was allowed to react for 18.5 h at room temperature. The mixture was then quenched on 180 g of deoxygenated ice and extracted three times with 100 ml of Et₂O. The aqueous phase was discarded and the volume of the organic phase was reduced to about 100 ml. At this point, the NMR analysis showed *ca.* 50 % of the monocarboxylic phosphine **16** and 50 % of the dicarboxylic phosphine **17**. Water (100 ml) was then added and the pH was brought to 6.7 with an aqueous solution of NaOH (5 %). The aqueous phase was discarded to eliminate any possible trace of the oxide of **17** and fresh water was added to the organic phase. The pH was now brought to 8.5 to extract **17** in the aqueous phase as sodium salt. After phase separation, the organic phase was saved for later and the aqueous one was acidified with 10 % aqueous H₂SO₄ until pH 6.6 and the dicarboxylic phosphine **17** was extracted twice with Et₂O in its acid form. After drying over MgSO₄, the organic solvent was vacuum evaporated to yield 0.63 g of **17** as white solid (26.4 % yield). The organic phase from the extraction at pH 8.5, containing mainly the monocarboxylic phosphine **16**, was vacuum evaporated. A solution of 5 % NaOH in methanol was used to neutralise the carboxylic groups of **16**. After evaporation of the solvent to complete dryness, the resulting solid was extracted with cyclohexane (Soxhlet extractor, overnight) to remove traces of unreacted phosphine **15** present in the mixture. Finally, the sodium salt of **16** was mixed with equal volume of water and diethylether (about 30 ml). Acidification with 10 % aqueous H₂SO₄ until pH 5-6 allowed the extraction of **16**

to the organic phase which, after decantation, was finally dried over MgSO_4 and vacuum evaporated to afford 0.70 g of **16** (31 % yield) as white solid.

Data for monocarboxylic phosphine, 3,5-1 *m*-Miranphos (**16**)

$^{31}\text{P}\{^1\text{H}\}$ NMR (161.98 MHz, CDCl_3), δ (ppm): -4.4 (s). ^1H NMR (400.13 MHz, CDCl_3), δ (ppm): 8.17 (d, 1H, $\text{H}_{\text{C}_4}\{\text{C}_6\text{H}_4\text{CO}_2\text{H}\}$, $^3\text{J}_{\text{HH}} = 7.4$ Hz); 8.12 (d, 1H, $\text{H}_{\text{C}_2}\{\text{C}_6\text{H}_4\text{CO}_2\text{H}\}$, $^3\text{J}_{\text{HP}} = 8.1$ Hz); 7.88 (s, 1H, $\text{H}_{\text{C}_4}\{\text{C}_6\text{H}_3(\text{CF}_3)_2\}$); 7.70 (m, 3H, $\text{H}_{\text{C}_2}\{\text{C}_6\text{H}_3(\text{CF}_3)_2\}$ - $\text{H}_{\text{C}_4}\{\text{C}_6\text{H}_4\text{CF}_3\}$); 7.63 (d, 1H, $\text{H}_{\text{C}_2}\{\text{C}_6\text{H}_4\text{CF}_3\}$, $^3\text{J}_{\text{HP}} = 8.3$ Hz); 7.55 (m, 2H, $\text{H}_{\text{C}_5}\{\text{C}_6\text{H}_4\text{CO}_2\text{H}\}$ - $\text{H}_{\text{C}_5}\{\text{C}_6\text{H}_4\text{CF}_3\}$); 7.50 (*pseudo-t*, 1H, $\text{H}_{\text{C}_6}\{\text{C}_6\text{H}_4\text{CO}_2\text{H}\}$, $^3\text{J}_{\text{HH}} = ^3\text{J}_{\text{HP}} = 7.5$ Hz); 7.44 (*pseudo-t*, 1H, $\text{H}_{\text{C}_6}\{\text{C}_6\text{H}_4\text{CF}_3\}$, $^3\text{J}_{\text{HH}} = ^3\text{J}_{\text{HP}} = 7.3$ Hz). $^{13}\text{C}\{^1\text{H}\}$ NMR (100.61 MHz, CDCl_3), δ (ppm): 170.95 (s, CO_2H); 140.22 (d, $\text{C}_1\{\text{C}_6\text{H}_3(\text{CF}_3)_2\}$, $^1\text{J}_{\text{CP}} = 18.2$ Hz); 138.72 (d, $\text{C}_6\{\text{C}_6\text{H}_4\text{CO}_2\text{H}\}$, $^2\text{J}_{\text{CP}} = 17.0$ Hz); 136.72 (bd, $\text{C}_1\{\text{C}_6\text{H}_4\text{CF}_3\}$, $^2\text{J}_{\text{CP}} = 15.9$ Hz); 136.25 (d, $\text{C}_1\{\text{C}_6\text{H}_4\text{CF}_3\}$, $^1\text{J}_{\text{CP}} = 13.8$ Hz); 135.68 (d, $\text{C}_2\{\text{C}_6\text{H}_4\text{CO}_2\text{H}\}$, $^2\text{J}_{\text{CP}} = 25.3$ Hz); 135.32 (d, $\text{C}_1\{\text{C}_6\text{H}_4\text{CO}_2\text{H}\}$, $^1\text{J}_{\text{CP}} = 12.9$ Hz); 133.20 (bdq, $\text{C}_2\{\text{C}_6\text{H}_3(\text{CF}_3)_2\}$, $^2\text{J}_{\text{CP}} = 19.8$ Hz, $^3\text{J}_{\text{CF}} = 3.3$ Hz); 132.29 (qd, $\text{C}_3\{\text{C}_6\text{H}_3(\text{CF}_3)_2\}$, $^2\text{J}_{\text{CF}} = 33.3$ Hz, $^3\text{J}_{\text{CP}} = 6.2$ Hz); 131.95 (s, $\text{C}_4\{\text{C}_6\text{H}_4\text{CO}_2\text{H}\}$); 131.71 (qd, $\text{C}_3\{\text{C}_6\text{H}_4\text{CF}_3\}$, $^2\text{J}_{\text{CF}} = 32.5$ Hz, $^3\text{J}_{\text{CP}} = 8.4$ Hz); 130.65 (dq, $\text{C}_2\{\text{C}_6\text{H}_4\text{CF}_3\}$, $^2\text{J}_{\text{CF}} = 26.6$ Hz); 130.45 (d, $\text{C}_3\{\text{C}_6\text{H}_4\text{CO}_2\text{H}\}$, $^3\text{J}_{\text{CP}} = 8.9$ Hz); 129.84 (d, $\text{C}_5\{\text{C}_6\text{H}_4\text{CF}_3\}$, $^3\text{J}_{\text{CP}} = 5.8$ Hz); 129.70 (d, $\text{C}_5\{\text{C}_6\text{H}_4\text{CO}_2\text{H}\}$, $^3\text{J}_{\text{CP}} = 6.1$ Hz); 126.97 (q, $\text{C}_4\{\text{C}_6\text{H}_4\text{CF}_3\}$, $^3\text{J}_{\text{CF}} = 3.7$ Hz); 123.80 (q, $\text{CF}_3\{\text{C}_6\text{H}_4\text{CF}_3\}$, $^1\text{J}_{\text{CF}} = 272.8$ Hz); 123.36 (sept, $\text{C}_4\{\text{C}_6\text{H}_3(\text{CF}_3)_2\}$, $^3\text{J}_{\text{CF}} = 3.6$ Hz); 123.15 (q, $\text{CF}_3\{\text{C}_6\text{H}_3(\text{CF}_3)_2\}$, $^1\text{J}_{\text{CF}} = 272.9$ Hz). $^{19}\text{F}\{^1\text{H}\}$ NMR (376.50 MHz, CDCl_3), δ (ppm): -62.88 (s, 3F, $\text{CF}_3\{\text{C}_6\text{H}_4\text{CF}_3\}$), -62.99 (s, 6F, $\text{CF}_3\{\text{C}_6\text{H}_3(\text{CF}_3)_2\}$). **HR-MS** (ESI m/z) [M-H]: calculated for $[\text{C}_{22}\text{H}_{11}\text{F}_9\text{O}_2\text{P}]^-$ 509.0358; found 509.0361. **Elemental analysis**: calculated for $\text{C}_{22}\text{H}_{12}\text{F}_9\text{O}_2\text{P}$: C, 51.78; H, 2.37; found: C, 51.45; H, 2.49.

Data for dicarboxylic phosphine, 3,5-1 *m*-Miran2phos (**17**)

$^{31}\text{P}\{^1\text{H}\}$ NMR (161.98 MHz, acetone- D_6), δ (ppm): -3.50 (s). ^1H NMR (400.13 MHz, acetone- D_6), δ (ppm): 8.14 (d, 2H, $\text{H}_{\text{C}_4}\{\text{C}_6\text{H}_4\text{CO}_2\text{H}\}$, $^3\text{J}_{\text{HH}} = 6.8$ Hz); 8.08 (m, 3H, $\text{H}_{\text{C}_4}\{\text{C}_6\text{H}_3(\text{CF}_3)_2\}$ - $\text{H}_{\text{C}_2}\{\text{C}_6\text{H}_4\text{CO}_2\text{H}\}$); 7.91 (d, 2H, $\text{H}_{\text{C}_2}\{\text{C}_6\text{H}_3(\text{CF}_3)_2\}$, $^3\text{J}_{\text{HP}} = 6.0$ Hz); 7.66 (m, 4H, $\text{H}_{\text{C}_5} + \text{H}_{\text{C}_6}\{\text{C}_6\text{H}_4\text{CO}_2\text{H}\}$). $^{13}\text{C}\{^1\text{H}\}$ NMR (100.61 MHz, acetone- D_6), δ (ppm): 166.90 (s, CO_2H); 142.34 (d, $\text{C}_1\{\text{C}_6\text{H}_3(\text{CF}_3)_2\}$, $^1\text{J}_{\text{CP}} = 19.2$ Hz); 138.91 (d, $\text{C}_6\{\text{C}_6\text{H}_4\text{CO}_2\text{H}\}$, $^2\text{J}_{\text{CP}} = 18.5$ Hz); 136.43 (d, $\text{C}_1\{\text{C}_6\text{H}_4\text{CO}_2\text{H}\}$, $^1\text{J}_{\text{CP}} = 12.8$ Hz); 135.68 (d, $\text{C}_2\{\text{C}_6\text{H}_4\text{CO}_2\text{H}\}$, $^2\text{J}_{\text{CP}} = 23.8$ Hz); 134.14 (bd, $\text{C}_2\{\text{C}_6\text{H}_3(\text{CF}_3)_2\}$, $^2\text{J}_{\text{CP}} = 20.5$ Hz);

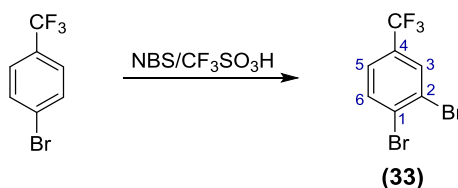
132.41 (qd, $C_3\{C_6H_3(CF_3)_2\}$, $^2J_{CF} = 33.4$ Hz, $^3J_{CP} = 5.8$ Hz); 132.33 (d, $C_3\{C_6H_4CO_2H\}$, $^3J_{CP} = 7.6$ Hz); 131.97 (s, $C_4\{C_6H_4CO_2H\}$); 130.46 (d, $C_5\{C_6H_4CO_2H\}$, $^3J_{CP} = 6.6$ Hz); 124.18 (q, CF_3 , $^1J_{CF} = 272.6$ Hz); 123.86 (sept, $C_4\{C_6H_3(CF_3)_2\}$, $^3J_{CF} = 3.9$ Hz). $^{19}F\{^1H\}$ NMR (376.50 MHz, acetone- D_6), δ (ppm): -62.38 (s). **HR-MS** (ESI m/z) $[M-H]^-$: calculated for $[C_{22}H_{12}F_6O_4P]^-$ 577.0232; found 577.0251. **Elemental analysis**: calculated for $C_{22}H_{13}F_6O_4P$: C, 47.77; H, 1.96; found: C, 47.40; H, 1.97.

9.5.5. Trifluoromethylated diphosphines and intermediate compounds

9.5.5.1. Diphosphine 30, diphosphine 31 and intermediate compounds

The synthesis of diphosphine **30** and **31** required the preparation of several intermediates, both phosphines and organic molecules, the synthesis of which will be also described in the following lines.

1,2-dibromo-4-(trifluoromethyl)benzene (**33**)



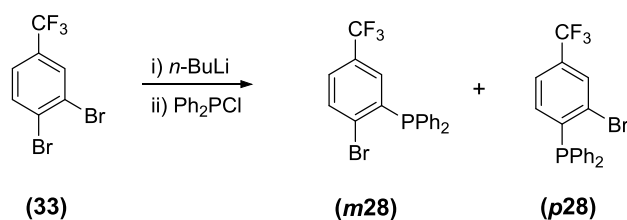
1,2-dibromo-4-(trifluoromethyl)benzene was prepared following a modification of the reported methodology for the iodination of deactivated aromatics.²⁴ No inert conditions were required in this procedure. In a round-bottom flask, 25 ml of 4-(trifluoromethyl)bromobenzene (40 g, 0.18 mol) and 41 ml of triflic acid (69.3 g, 0.46 mol) were mixed under vigorous stirring (both compounds are immiscible). *N*-bromosuccinimide (31.4 g, 0.18 mol) was added gradually during a period of 10-15 minutes. Afterwards, the mixture was allowed to react for 18 h. At this time, the analysis of the reaction mixture by GC showed *ca.* 81 % conversion. The mixture was then warmed up to 40 °C and allowed to react for 1 h. Following, the reaction mixture was poured on 200 g of ice and, after complete melting of the ice, it was extracted 4 times with 100 ml of Et_2O . The organic phase was first washed with 10 % aqueous $NaHCO_3$ (2x100 ml) and then with brine (100 ml) before being dried over $MgSO_4$.

²⁴ a) Olah, G. A.; Wang, Q.; Sandford, G.; Prakash, G. K. S. *J. Org. Chem.* **1993**, 58 (11), 3194–3195. b) Blurton, P.; Burkamp, F.; Churcher, I.; Harrison, T.; Joseph, N. *Arylacetic acids and related compounds for treatment of alzheimer's disease*. WO2006008558 (A1). **2006**.

Evaporation of the solvent gave orange oil with 87.5 % of 1,2-dibromo-4-(trifluoromethyl)benzene (**33**) according to GC analysis. Vacuum distillation (48-50 °C, 1-2 mbar) finally yielded 40.4 g of **33** (74 % yield) as colourless oil with purity above 99 % according to GC.

$^1\text{H NMR}$ (400.13 MHz, CDCl_3), δ (ppm): 7.87 (*bs*, 1H, H_{C_3}); 7.75 (*d*, 1H, H_{C_6} , $^3J_{\text{HH}} = 8.3$ Hz); 7.42 (*bdd*, 1H, H_{C_5} , $^3J_{\text{HH}} = 8.3$ Hz, $^4J_{\text{HH}} = 1.4$ Hz). $^{13}\text{C}\{^1\text{H}\}$ NMR (100.61 MHz, CDCl_3), δ (ppm): 134.31 (*s*, C_6); 131.14 (*q*, C_4 , $^2J_{\text{CF}} = 33.4$ Hz); 130.74 (*q*, C_3 , $^3J_{\text{CF}} = 4.0$ Hz); 129.30 (*bq*, C_1 , $^5J_{\text{CF}} = 1.4$ Hz); 125.65 (*s*, C_2); 125.31 (*q*, C_5 , $^3J_{\text{CF}} = 3.6$ Hz); 123.0 (*q*, CF_3 , $^1J_{\text{CF}} = 272.5$ Hz). $^{19}\text{F}\{^1\text{H}\}$ NMR (376.50 MHz, CDCl_3), δ (ppm): -62.78 (*s*). **GC-MS**: calculated for $\text{C}_7\text{H}_3\text{Br}_2\text{F}_3$ 301.86 (51.4 %, $^{79}\text{Br}_2$), 303.85 (100.0 %, $^{79}\text{Br}^{81}\text{Br}$), 305.85 (48.6 %, $^{81}\text{Br}_2$); found 303.85 (100.0 %), 301.80 (52.1%), 305.80 (48.1 %).

Bromophosphines 28. Mixture of isomers (2-bromo-5-(trifluoromethyl)phenyl)diphenylphosphine (*m*28) and (2-bromo-4-(trifluoromethyl)phenyl)diphenylphosphine (*p*28)



4 ml (6.4g, 28.4 mmol) of 1,2-dibromo-4-(trifluoromethyl)benzene (**33**) were dissolved in 240 ml of anhydrous THF:Et₂O (1:1). The mixture was cooled down to -95 °C (toluene/liq.N₂) and 9.9 ml of *n*-BuLi (2.5 M in hexanes, 24.8 mmol) were added dropwise during 20 minutes. Slow addition is important in order to prevent the rise of the temperature and thus the decomposition of the organolithium derivative of **33**. After the addition of *n*-BuLi the mixture was further stirred at -95 °C for 30 minutes. The colour of the mixture then turned from colourless to pale yellow. At this point, dark colouration of the solution would indicate decomposition of the organolithium derivative. Next, 4.2 ml of freshly distilled chlorodiphenylphosphine (5.0 g, 22.8 mmol) were added dropwise for 5-10 minutes, keeping the reaction temperature at -95 °C. The reaction mixture turned orange with the firsts droplets of the chlorophosphines and finally to dark brown after complete addition. The reaction was the allowed to warm up

to room temperature progressively for 1 h and further stirred for 45 minutes at room temperature. No change in the colour was observed. Evaporation of the solvent gave a brownish oily substance which was re-suspended in 20 ml of Et₂O. After cooling in an ice bath, 20 ml of aqueous NH₄Cl (10 %) were added and the resulting biphasic mixture was vigorously stirred for a few seconds. The organic phase was then separated and the aqueous one was extracted 3 times with 20 ml of Et₂O. The organic layers were combined and dried over MgSO₄. After solvent evaporation, a dark brown oil was obtained which was purified through column chromatography in silica gel (hexanes: CH₂Cl₂, 7:1) to yield 5.2 g of **28** (48.9 % yield) as white powder (mixture of isomers *m28* and *p28* in 1:0.25 ratio).

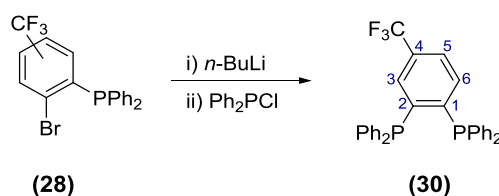
³¹P{¹H} NMR (161.98 MHz, CDCl₃), δ (ppm): -3.65 (s, 1P, *m28*); -3.89 (bq, 0.25P, *p28*, ⁶J_{PF} = 1.6 Hz). ¹H NMR (400.13 MHz, CDCl₃), δ (ppm): 7.72 (dd, 1.50H, H_{C(aryl)}, J = 7.9 Hz, J = 3.6 Hz); 7.47-7.35 (m, 11H, H_{C(aryl)}); 7.35-7.25 (m, 6.7H, H_{C(aryl)}); 6.99 (bs, 1H, H_{C(aryl)}); 6.88 (bd, 0.29H, H_{C(aryl)}, J = 8.2 Hz). ¹³C{¹H} NMR (100.61 MHz, CDCl₃), δ (ppm): 141.26-126.81 (m, C_{aryl}); 123.83 (q, CF₃, ¹J_{CF} = 273.0 Hz). ¹⁹F{¹H} NMR (376.50 MHz, CDCl₃), δ (ppm): -63.04 (s). HR-MS (ESI⁺ *m/z*) [M(O)+H]⁺: calculated for [C₁₉H₁₄BrF₃PO]⁺ 424.9912 (100.0 %, ⁷⁹Br), 426.9894 (97.3 %, ⁸¹Br); found 424.9919 (100.0 %), 426.9893 (97.8 %). **Elemental analysis**: calculated for C₁₉H₁₃BrF₃P: C, 55.7; H, 3.20; found: C, 54.68; H, 3.12.

X-ray diffraction data for *p28*

Suitable crystals for X-ray diffraction were obtained by slow crystallization in CH₂Cl₂/*n*-hexane. Data for a single-crystal of *p28* was collected in a Rigaku Spider with Cu Kα. The structure was solved by direct methods. All non-hydrogen atoms were refined with anisotropic displacement thermal parameters. All hydrogen atoms were idealised and were positioned geometrically and refined using the riding model with U_{iso}(H) = 1.2 U_{eq}(C). The CF₃ group was disordered over three different orientations in aprox 27.6, 39.7 and 32.7 % ratio. The following bond length and angle restrains (DFIX) were applied: C-F distance = 1.31(2); C_{ipso}-F distance = 2.35 (4). Moreover, F-F distances of the disordered F atoms were restrained to be equal within sd of 0.03 (with SADI command) and the U_{ij} were restrained with SIMU instruction. All disordered atoms were refined anisotropically and the sum of the site occupation factors was restrained to 1.000.

Crystal data (p28)

Chemical formula	C ₁₉ H ₁₃ BrF ₃ P	a	10.204(9)
Molecular weight	409.18	b	19.519(7)
Space group	Monoclinic, P 21/c	c	9.074(4)
wavelength	1.54187 (Cu K α)	α	90
Temperature	293(2) K	β	100.92(3)
Volume	1774.6 (19) Å ³	γ	90
Z	4	R[I>2 σ (I)]	0.0935
		S	0.9890

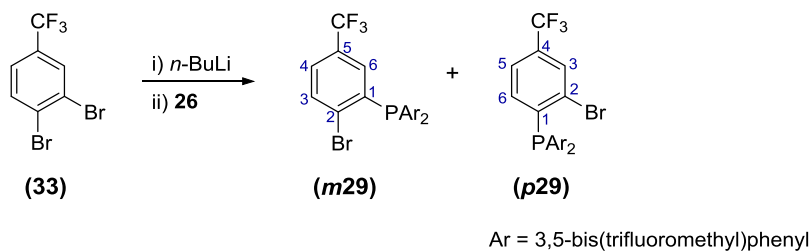
(4-(Trifluoromethyl)-1,2-phenylene)bis(diphenylphosphine) (30)

0.35 g (0.86 mmol) of **28** (mixture of isomers *m28* and *p28*) were dissolved in 2.5 ml of anhydrous Et₂O. The colourless solution was cooled down to 0 °C (ice bath) and 0.35 ml of *n*-BuLi (2.5M in hexanes, 0.88 mmol) were added dropwise for 15 min. Rapid change in colour to red was observed with the first droplets of *n*-BuLi with further evolves to dark reddish brown after complete addition. Light brown solid precipitate was also observed. The mixture was stirred at 0 °C for 20 more minutes and then was allowed to warm to room temperature and stirred for 30 minutes. The reaction mixture was cooled down again to 0 °C and 0.15 ml of chlorodiphenylphosphine (0.18 g, 0.84 mmol) were added dropwise for 5 minutes. The reaction mixture was stirred for 20 minutes and then was allowed to further react at room temperature for 2 h, giving an orange solution with light brown precipitate. 2 ml of water were added and, after phase separation, the aqueous phase was extracted two times with 2 ml of Et₂O. The organic layers were dried over MgSO₄ and the solvent was vacuum evaporated to give an orange sticky solid. Column chromatography purification on silica gel (CH₂Cl₂:hexanes, 9:1) afforded 0.21 g of diphosphine **30** (48 % yield) as a white solid.

³¹P{¹H} NMR (161.98 MHz, CDCl₃), δ (ppm): -13.52 (s). ¹H NMR (400.13 MHz, acetone-D₆), δ (ppm): 7.68 (d, 1H, H_(Caryl){C₆H₃CF₃}, J = 7.9 Hz); 7.36 (bs, 12H, H_{C3}+H_{C4}{C₆H₅}); 7.23 (m, 10H, H_{C2}{C₆H₅}-H_(Caryl){C₆H₃CF₃}). ¹³C{¹H} NMR (100.61

MHz, acetone-D₆), δ (ppm): [150-126.64] (m, C_{aryl}); 125.0 (q, CF₃, $^1J_{CF} = 271.95$ Hz). $^{19}\text{F}\{^1\text{H}\}$ NMR (376.50 MHz, CDCl₃), δ (ppm): -62.70 (s). HR-MS (ESI⁺ m/z) [M+Na]⁺: calculated for [C₃₁H₂₃F₃P₂Na]⁺ 537.1119; found 537.1120.

Bromophosphines 29. Mixture of isomers bis(3,5-bis(trifluoromethyl)phenyl)(2-bromo-5-(trifluoromethyl)phenyl)phosphine (m29) and bis(3,5-bis(trifluoromethyl)phenyl)(2-bromo-4-(trifluoromethyl)phenyl)phosphine (p29)

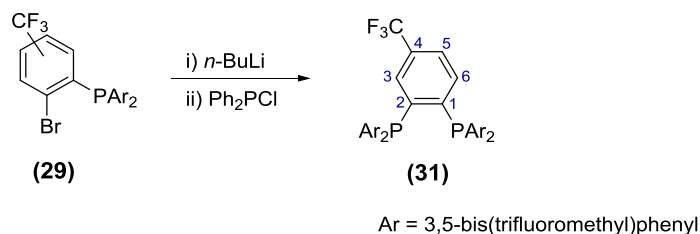


Bromophosphines **29** were prepared following the procedure above described for bromophosphines **28**. 2.5 ml of **33** (5 g, 16.5 mmol) were dissolved in 150 ml of anhydrous THF:Et₂O (1:1). The mixture was cooled down to -95 °C (toluene/liq.N₂) and 6.0 ml of *n*-BuLi (2.5 M in hexanes, 15 mmol) were added dropwise during 15 minutes. Slow addition is important in order to prevent the rise of the temperature and thus the decomposition of the organolithium derivative of **33**. After the complete addition of *n*-BuLi the mixture was further stirred at -95 °C for 40 minutes. The colour of the mixture then turned from colourless to pale yellow. At this point, dark colouration of the solution would indicate decomposition of the organolithium derivative. Next, 6.54 g of bis(3,5-bis(trifluoromethyl)phenyl)chlorophosphine (**26**) (13.3 mmol) were added dropwise for 15 minutes, keeping the reaction temperature at -95 °C. The reaction mixture turned to dark blue with the first droplets of the chlorophosphine and to dark green after complete addition. The reaction was then allowed to warm up to room temperature progressively for 1 h and further stirred for 1.5 h at room temperature. A dark brown solution was observed after this process. Evaporation of the solvent gave a dark brown oil, which was stirred in 40 ml of Et₂O. After cooling in an ice bath, 60 ml of aqueous NH₄Cl (10 %) were added and the resulting biphasic mixture was vigorously stirred for a few seconds. The organic phase was then separated and the aqueous one was extracted 3 times with 20 ml of Et₂O. The organic layers were combined and dried over MgSO₄. After solvent evaporation, an orange-brown oil was obtained which was

vacuum distilled via Kugelrohr (aprox 220-250 °C, 5-7 mbar) to yield 5.4 g of **29** (60 % yield) as colourless sticky oil (mixture of isomers *m29* and *p29* in 1:0.38 ratio).

$^{31}\text{P}\{^1\text{H}\}$ NMR (161.98 MHz, CDCl_3), δ (ppm): -3.46 (s, 1P, *m29*); -4.23 (bq, 0.38P, *p29*, $^6J_{\text{PF}} = 1.0$ Hz). ^1H NMR (400.13 MHz, CDCl_3), δ (ppm): 7.99 (s, 2.80H, $\text{H}_{\text{C4}}\{\text{C}_6\text{H}_3(\text{CF}_3)_2\}$, *m29+p29*); 7.85 (dd, 1H, $\text{H}_{\text{C3}}\{\text{C}_6\text{H}_3\text{BrCF}_3\}$, *m29*, $^3J_{\text{HH}} = 8.3$ Hz, $^4J_{\text{HP}} = 3.9$ Hz); 7.72 (m, 5.5H, $\text{H}_{(\text{Caryl})}\{\text{C}_6\text{H}_3(\text{CF}_3)_2\}$, *m29+p29*); 7.59 (m, 1.41H, $\text{H}_{(\text{Caryl})}\{\text{C}_6\text{H}_3(\text{CF}_3)_2\}$, *m29+p29*); 6.93 (bs, 1H, $\text{H}_{\text{C6}}\{\text{C}_6\text{H}_3\text{BrCF}_3\}$, *m29*); 6.82 (dd, 0.4H, $\text{H}_{\text{C5}}\{\text{C}_6\text{H}_3\text{BrCF}_3\}$, *p29*, $^3J_{\text{HH}} = 8.0$ Hz, $^4J_{\text{HP}} = 1.8$ Hz). $^{19}\text{F}\{^1\text{H}\}$ NMR (376.50 MHz, CDCl_3), δ (ppm): -63.02 (s, 5F, $\text{CF}_3\{\text{C}_6\text{H}_3(\text{CF}_3)_2\}$, *p29*); -63.10 (s, 12F, $\text{CF}_3\{\text{C}_6\text{H}_3(\text{CF}_3)_2\}$, *m29*); -63.15 (s, 1.2F, $\text{CF}_3\{\text{C}_6\text{H}_3\text{Br}\}$, *p29*); -63.17 (s, 3F, $\text{CF}_3\{\text{C}_6\text{H}_3\text{Br}\}$, *m29*). HR-MS (ESI⁺ m/z) $[\text{M}(\text{O})+\text{H}]^+$: calculated for $[\text{C}_{23}\text{H}_{10}\text{BrF}_{15}\text{PO}]^+$ 696.9408 (100.0 %, ^{79}Br), 698.9390 (97.3 %, ^{81}Br); found 696.9395 (100.0 %), 698.9386 (97.5 %). Elemental analysis: calculated for $\text{C}_{23}\text{H}_9\text{BrF}_{15}\text{P}$: C, 40.56; H, 1.33; found: C, 40.74; H, 1.30.

(4-(Trifluoromethyl)-1,2-phenylene)bis(bis(3,5-bis(trifluoromethyl)phenyl)-phosphine) (31)



Diphosphine **31** was prepared in analogy to the methodology applied for **30**. 2.86 g (4.19 mmol) of **29** (mixture of isomers *m29* and *p29*) were dissolved in 30 ml of anhydrous Et_2O . The colourless solution was cooled down to -84 °C (ethyl acetate/liquid N_2) and 1.6 ml of *n*-BuLi (2.5M in hexanes, 4.0 mmol) were added dropwise for 10 min with the formation of a dark mixture. Keeping the reaction temperature at -84 °C, 2.07 g of the trifluoromethylated chlorophosphine **26** (4.2 mmol) were added dropwise during 10 minutes. Change in the colour of the mixture to brown was observed. The reaction mixture was stirred for 10 minutes and then was allowed to further react at room temperature for 2.5 h, resulting in brown solution with white precipitate. 20 ml of saturated NH_4Cl aqueous solution were added and, after phase separation, the aqueous phase was extracted four times with 15 ml of Et_2O . For better

phase separation, NaCl was added. The organic layers were dried over MgSO₄ and the solvent was vacuum evaporated to give a yellow solid which was washed twice with cold acetonitrile to yield 1.71 g of diphosphine **31** (39 % yield) as a white solid.

³¹P{¹H} NMR (161.98 MHz, acetone-D₆), δ (ppm): second order spectra. ¹H NMR (500.13 MHz, CDCl₃), δ (ppm): 7.91 (s, 4H, H_{C4}+H_{C4'}{C₆H₃(CF₃)₂}); 7.79 (dd, 1H, H_{C5}{C₆H₃CF₃}, ³J_{HH} = 8.1 Hz, ⁴J_{HH} = 1.4 Hz); 7.56 (m, 8H, H_{C2}+H_{C2'}{C₆H₃(CF₃)₂}); 7.34 (*pseudo*-q, 1H, H_{C3}{C₆H₃CF₃}, ³J_{HP} = 3.5 Hz, ⁴J_{HH} = 1.4 Hz); 7.23 (dt, 1H, H_{C6}{C₆H₃CF₃}, ³J_{HH} = 8.1 Hz, ³J_{HP} = ⁴J_{HP} = 3.8 Hz). ¹³C{¹H} NMR (100.61 MHz, acetone-D₆), δ (ppm): 146.1 (d, C{C₆H₃CF₃}, J_{CP} = 25.0 Hz); 142.4 (dd, C₁{C₆H₃(CF₃)₂}, ¹J_{CP} = 25.0 Hz, ⁴J_{CP} = 3.1); 138.38 (m, C{C₆H₃CF₃}); 135.74 (d, C{C₆H₃CF₃}, J_{CP} = 5.5 Hz); 133.88 (*bd*, C₂{C₆H₃(CF₃)₂}, ²J_{CP} = 17.4 Hz); 132.39 (q, C₄{C₆H₃CF₃}, ³J_{CF} = 32.6 Hz); 131.75 (dq, C₃+C_{3'}{C₆H₃(CF₃)₂}, ²J_{CF} = 33.4 Hz); 131.0 (m, C{C₆H₃CF₃}); 127.91 (q, C₅{C₆H₃CF₃}, ³J_{CF} = 3.8 Hz); 123.72 (m, C₄{C₆H₃(CF₃)₂}); 123.49 (q, CF₃{C₆H₃CF₃}, ¹J_{CF} = 271.5 Hz); 123.02 (q, CF₃{C₆H₃(CF₃)₂}, ¹J_{CF} = 273.0 Hz). ¹⁹F{¹H} NMR (376.50 MHz, acetone-D₆), δ (ppm): -62.66 (s, 12F, CF₃{C₆H₃(CF₃)₂}); -62.70 (s, 12F, CF₃{C₆H₃(CF₃)₂}); -62.9 (s, 3F, CF₃{C₆H₃CF₃}). **HR-MS** (ESI⁺ *m/z*) [M(O)₂+Na]⁺: calculated for [C₃₉H₁₅F₂₇P₂O₂Na]⁺ 113.0008; found 1112.9994. **Elemental analysis**: calculated for C₃₉H₁₅F₂₇P₂: C, 44.26; H, 1.43; found: C, 44.10; H, 1.49.

X-ray diffraction data for **31**

Crystals of good quality for X-ray diffraction were obtained by slow crystallisation of the phosphine in CH₂Cl₂/n-hexane. The structure was solved by Patterson methods (SHELXS-86). All non-hydrogen atoms were refined with anisotropic displacement thermal parameters. All hydrogen atoms were idealised and were positioned geometrically and refined using the riding model with U_{iso}(H) = 1.2 U_{eq}(C). All the CF₃ groups were disordered over two different orientations in the following approximate ratios: C(17) 56.5 and 43.5 %; C(18) 73.2 and 26.8 %; C(27) 63.7 and 36.3 %; C(28) 53.3 and 46.7 %; C(37) 53.0 and 47.0 %; C(47) 53.7 and 46.3 %; C(48) 80.5 and 19.5 %; C(57) 53.5 and 46.5 %; C(58) 60.1 and 39.9 %. The following bond length and angle restraints (DFIX) were applied: C-F distance = 1.33(2); C_{ipso}-F distance = 2.35 (4). Moreover, F-F distances of the disordered F atoms were restrained to be equal within sd of 0.03 (with SADI command) and the U_{ij} were restrained with SIMU instruction. All

disordered atoms were refined anisotropically and the sum of the site occupation factors was restrained to 1.000.

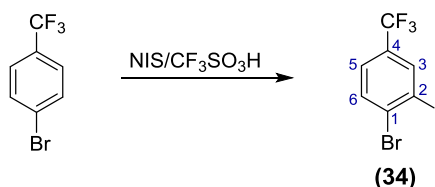
Crystal data

Chemical formula	C ₃₉ H ₁₅ F ₂₇ P ₂	a	12.2501(15)
Molecular weight	1058.44	b	16.1080(2)
Space group	Monoclinic, P 21/c	c	21.4020(3)
wavelength	0.71073 (Mo K α)	α	90
Temperature	293(2) K	β	94.836(2)
Volume	4208.1(5) Å ³	γ	90
Z	4	R[I>2 σ (I)]	0.1074
		S	0.9770

9.5.5.2. Diphosphine **32** and related compounds

The intermediates required for the synthesis of **32** will be described next together with the synthetic procedure for **32**. Also the biphenyl derivatives prepared in the failed synthesis of **32** will be described.

1-Bromo-2-iodo-4-(trifluoromethyl)benzene (**34**)

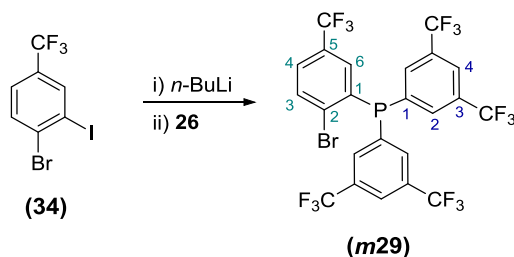


1-Bromo-2-iodo-4-(trifluoromethyl)benzene (**34**) was prepared following the reported procedures in the literature with minor modifications.²⁴ No inert conditions were required in this procedure. In a round-bottom flask, at 0 °C (ice bath), 15.8 ml of 4-(trifluoromethyl)bromobenzene (25.3 g, 0.11 mol) and 20 ml of triflic acid were vigorously stirred (they are immiscible). *N*-iodosuccinimide (25.4 g, 0.11 mol) were added gradually during 10 minutes and the resulting dark mixture was further stirred for 1.5 h at 0 °C before being allowed to react at room temperature for more 14 h. After this time, the mixture had turned into an orange suspension, and GC analysis showed *ca.* 80 % of conversion. The reaction was warmed up to 43 °C during 1 h. Afterwards it was quenched over 100 g of ice and, once the ice had melted, the reaction products (heavier than the aqueous phase) were extracted with three portions of 75 ml of CH₂Cl₂.

Following, the organic phase was washed with 10 % aqueous NaHCO₃ until pH 6-7 and with 50 ml of 10 % aqueous Na₂SO₃. After drying over MgSO₄, the organic solvent was vacuum evaporated to give an orange liquid. Vacuum distillation (65-69 °C, 2-3 mbar) yielded 35.3 g of 1-bromo-2-iodo-4-(trifluoromethyl)benzene (**34**) as colourless liquid (89.3 %, yield) in purity higher than 99 % according to GC.

¹H NMR (400.13 MHz, CDCl₃), δ (ppm): 8.09 (d, 1H, H_{C3}, ⁴J_{HH} = 1.4 Hz); 7.73 (bd, 1H, H_{C6}, ³J_{HH} = 8.3 Hz); 7.45 (bdd, 1H, H_{C5}, ³J_{HH} = 8.3 Hz, ⁴J_{HH} = 1.4 Hz). ¹³C{¹H} NMR (100.61 MHz, CDCl₃), δ (ppm): 137.19 (q, C₃, ³J_{CF} = 3.7 Hz); 134.23 (bq, C₁, ⁵J_{CF} = 1.5 Hz); 133.12 (s, C₆); 130.83 (q, C₄, ²J_{CF} = 33.3 Hz); 126.29 (q, C₅, ³J_{CF} = 3.6 Hz); 122.79 (q, CF₃, ¹J_{CF} = 273.3 Hz); 101.54 (s, C₂). ¹⁹F{¹H} NMR (376.50 MHz, CDCl₃), δ (ppm): -62.63 (s, CF₃). GC-MS: calculated for C₇H₃BrF₃I 349.84 (100 %, ⁷⁹Br), 351.84 (97.3 %, ⁸¹Br); found 349.80 (100.0), 351.80 (96.0)

Bis(3,5-bis(trifluoromethyl)phenyl)(2-bromo-5-(trifluoromethyl)phenyl)phosphine (*m29*)

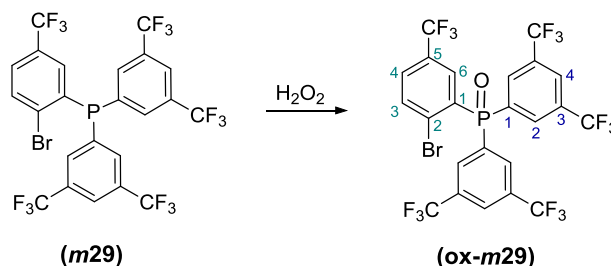


The phosphine *m29* was synthesised following the procedure as described for **29** (mixture of isomers *m29* and *p29*) with minor modifications. In an example reaction, 10 g of **34** (28.4 mmol) were dissolved in 300 ml of anhydrous THF:Et₂O (1:1). The mixture was cooled down to -95 °C (toluene/liq.N₂) and 11.5 ml of *n*-BuLi (2.5 M in hexanes, 28.8 mmol) were added dropwise during 10 minutes. Slow addition is important in order to prevent the rise of the temperature and thus the decomposition of the organolithium derivative of **34**. After the complete addition of *n*-BuLi the mixture was further stirred at -95 °C for 35 minutes. The colour of the mixture then turned from colourless to pale yellow. At this point, dark colouration of the solution would indicate decomposition of the organolithium derivative. Next, 13.9 g of bis(3,5-bis(trifluoromethyl)phenyl)chlorophosphine (**26**) (28.2 mmol) were added dropwise within an interval of time of 15 minutes, while keeping the reaction temperature at -95 °C. During the addition, the reaction mixture acquired a wide range of colours: first

orange, then pink, purple and finally dark violet after complete addition of the chlorophosphine. The reaction was then allowed to warm up to room temperature progressively for 30 min and further stirred at room temperature for 1.5 h. A dark blue solution was observed after this process. Next, 100 ml of water was added to the reaction mixture and, after phase separation, the aqueous phase was extracted 3 times with 40 ml of Et₂O. The organic layers were combined and dried over MgSO₄. After solvent evaporation the dark orange oil was purified by vacuum distillation via Kugelrohr (aprox 220-250 °C, 5-7 mbar) to yield 14.1 g of **29** (72 % yield) as colourless sticky oil.

³¹P{¹H} NMR (161.98 MHz, CDCl₃), δ (ppm): -3.46 (s). ¹H NMR (400.13 MHz, CDCl₃), δ (ppm): 7.91 (s, 2H, H_{C4}{C₆H₃(CF₃)₂}); 7.85 (dd, 1H, H_{C3}{C₆H₃BrCF₃}, ³J_{HH} = 8.2 Hz, ⁴J_{HP} = 3.5 Hz); 7.72 (d, 4H, H_{C2}{C₆H₃(CF₃)₂}, ³J_{HP} = 6.7 Hz); 7.59 (dd, 1H, H_{C4}{C₆H₃BrCF₃}, ³J_{HH} = 8.2 Hz, ⁴J_{HH} = 2.0 Hz); 6.94 (bs, 1H, H_{C6}{C₆H₃BrCF₃}). ¹³C{¹H} NMR (100.61 MHz, CDCl₃), δ (ppm): 137.25 (d, C₁{C₆H₃(CF₃)₂}, ¹J_{CP} = 17.8 Hz); 136.96 (d, C₁{C₆H₃BrCF₃}, ¹J_{CP} = 13.5 Hz); 134.59 (d, C₃{C₆H₃BrCF₃}, ³J_{CP} = 2.2 Hz); 133.7 (dq, C₂{C₆H₃(CF₃)₂}, ²J_{CP} = 21.4 Hz, ³J_{CF} = 2.6 Hz); 132.96 (qd, C₃{C₆H₃(CF₃)₂}, ²J_{CF} = 33.9 Hz, ³J_{CP} = 6.7 Hz); 131.9 (q, C₅{C₆H₃BrCF₃}, ²J_{CF} = 33.4 Hz); 130.4 (bs, C₆{C₆H₃BrCF₃}); 128.66 (q, C₄{C₆H₃BrCF₃}, ³J_{CF} = 3.2 Hz); 124.4 (m, C₄{C₆H₃(CF₃)₂}-C₂{C₆H₃BrCF₃}); 123.35 (q, CF₃{C₆H₃BrCF₃}, ¹J_{CF} = 272.3 Hz); 122.97 (q, CF₃{C₆H₃(CF₃)₂}, ¹J_{CF} = 273.4 Hz). ¹⁹F{¹H} NMR (376.50 MHz, CDCl₃), δ (ppm): -63.1 (s, 12F, CF₃{C₆H₃(CF₃)₂}); -63.2 (s, 3F, CF₃{C₆H₃BrCF₃}). **HR-MS** (ESI⁺ *m/z*) [M(O)+H]⁺: calculated for [C₂₃H₁₀BrF₁₅PO]⁺ 696.9408 (100.0 %, ⁷⁹Br), 698.9390 (97.3 %, ⁸¹Br); found 696.9414 (100.0 %), 698.9393 (97.7 %). **Elemental analysis**: calculated for C₂₃H₉BrF₁₅P: C, 40.56; H, 1.33; found: C, 40.45; H, 1.32.

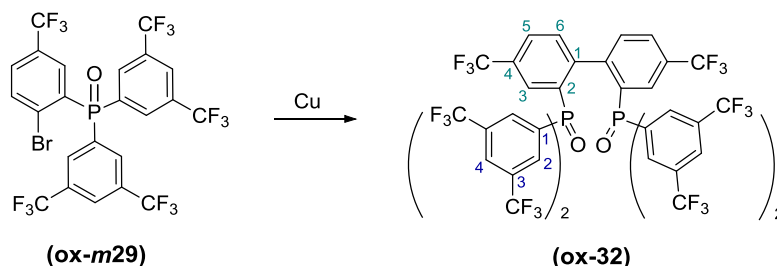
Bis(3,5-bis(trifluoromethyl)phenyl)(2-bromo-5-(trifluoromethyl)phenyl)phosphine oxide (ox-*m29*)



No inert conditions were required in this preparation. In a round-bottom flask, 10.0 g of *m29* (14.7) were dissolved in 15 ml of CH₂Cl₂. Following, 10 ml of water were introduced and, under vigorous stirring, 6.8 ml of 36 % (v/v) aqueous solution of hydrogen peroxide (73.4 mmol) were added. The resulting mixture was allowed to react for around 48 h (one weekend). After that time, the phases were separated and the aqueous one was extracted three times with 10 ml of CH₂Cl₂. The organic layers were combined and dried over MgSO₄. The organic solvent was finally evaporated to afford 9.19 g of *ox-m29* as white solid (89.8 % yield).

³¹P{¹H} NMR (161.98 MHz, CDCl₃), δ (ppm): 24.2 (s). ¹H NMR (400.13 MHz, CDCl₃), δ (ppm): 8.21 (s, 2H, H_{C4}{C₆H₃(CF₃)₂}); 8.17 (m, 5H, H_{C6}{C₆H₃BrCF₃}-H_{C2}{C₆H₃(CF₃)₂}); 7.91 (dd, 1H, H_{C3}{C₆H₃BrCF₃}, ³J_{HH} = 8.3 Hz, ⁴J_{HH} = 4.1 Hz); 7.81 (bd, 1H, H_{C4}{C₆H₃BrCF₃}, ³J_{HH} = 8.3 Hz). ¹³C{¹H} NMR (100.61 MHz, CDCl₃), δ (ppm): 136.22 (d, C₃{C₆H₃BrCF₃}, ³J_{CP} = 7.9 Hz); 133.47 (d, C₆{C₆H₃BrCF₃}, ²J_{CP} = 10.0 Hz, ³J_{CF} = 3.7 Hz); 133.11 (d, C₁{C₆H₃(CF₃)₂}, ¹J_{CP} = 108.5 Hz); 133.07 (qd, C₃{C₆H₃(CF₃)₂}, ²J_{CF} = 34.1 Hz, ³J_{CP} = 13.0 Hz); 132.22 (m, C₄{C₆H₃BrCF₃}-C₄{C₆H₃(CF₃)₂}); 131.32 (qd, C₅{C₆H₃BrCF₃}, ²J_{CF} = 34.0 Hz, ³J_{CP} = 11.2 Hz); 131.27 (d, C₁{C₆H₃BrCF₃}, ¹J_{CP} = 108.4 Hz); 129.65 (d, C₂₄{C₆H₃BrCF₃}, ²J_{CP} = 5.6 Hz); 127.07 (m, C₂{C₆H₃(CF₃)₂}, ³J_{CF} = 3.8 Hz); 123.12 (q, CF₃{C₆H₃BrCF₃}, ¹J_{CF} = 273.1 Hz); 122.66 (q, CF₃{C₆H₃(CF₃)₂}, ¹J_{CF} = 273.4 Hz). ¹⁹F{¹H} NMR (376.50 MHz, CDCl₃), δ (ppm): -62.96 (s, 3F, CF₃{C₆H₃BrCF₃}); -63.02 (s, 12F, CF₃{C₆H₃(CF₃)₂}). **HR-MS** (ESI⁺ *m/z*) [M+H]⁺: calculated for [C₂₃H₁₀BrF₁₅PO]⁺ 696.9408 (100.0 %, ⁷⁹Br), 698.9390 (97.3 %, ⁸¹Br); found 696.9411 (100.0 %), 698.9392 (97.4 %). **Elemental analysis**: calculated for C₂₃H₉BrF₁₅PO: C, 39.70; H, 1.30; found: C, 39.79; H, 1.29.

4,4'-bis(trifluoromethyl)-[1,1'-biphenyl]-2,2'-diylbis(bis(3,5-bis(trifluoromethyl)-phenyl)phosphine oxide (ox-32)



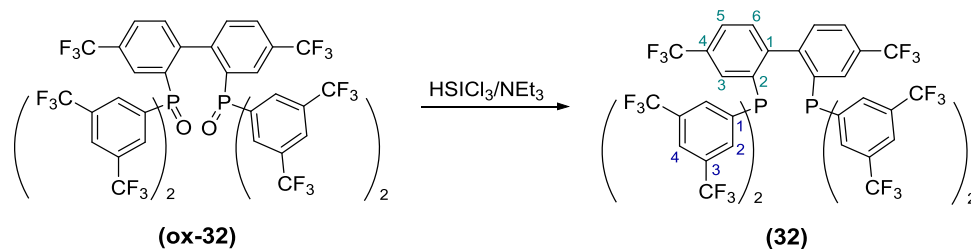
The synthesis of **ox-32** was performed following a modification of the reported procedures in the literature.²⁵ 7.25 g of the phosphine oxide **ox-*m*29** (10.8 mmol) were dissolved in 25 ml of anhydrous DMF. Freshly activated²⁶ Cu⁰ (2.69 g, 42.3 mmol) was added and the suspension was stirred at 150 °C for 20 h. The orange suspension was then filtered with a celite pad and washed four times with 10 ml of THF. The green solution was then vacuum evaporated to give a black-green oil which was stirred with 6 ml of Et₂O and 14 ml of *n*-hexane and cooled down in an ice bath with the formation of an orange solution and the precipitation **ox-32** as orange-yellowish solid. Filtration afforded the isolation of **ox-32** as yellow solid. A few more milligrams of the compound were obtained by evaporation of the solution and re-precipitation in Et₂O:*n*-hexanes. All the solids were combined and re-crystallised in Et₂O/*n*-hexanes to yield 3.55 g of **ox-32** as white solid (57 % yield).

³¹P{¹H} NMR (161.98 MHz, CDCl₃), δ (ppm): 23.55 (s). ¹H NMR (400.13 MHz, CDCl₃), δ (ppm): 8.19 (m, 10H, H_{C4}+ H_{C4}+H_{C2}{C₆H₃(CF₃)₂}); 8.02 (s, 2H, H_{C2}{C₆H₃(CF₃)₂}); 7.52 (m, 4H, C_(aryl){biphenyl}); 7.00 (m, 2H, C_(aryl){biphenyl}). ¹³C{¹H} NMR (100.61 MHz, CDCl₃), δ (ppm): [145.88-126.88] (m, C_(aryl)); 122.68 (q, CF₃{biphenyl}, ¹J_{CF} = 273.5 Hz); 122.60 (q, CF₃{C₆H₃(CF₃)₂}, ¹J_{CF} = 273.2 Hz); 122.5 (q, CF₃'{C₆H₃(CF₃)₂}, ¹J_{CF} = 273.6 Hz). ¹⁹F{¹H} NMR (376.50 MHz, CDCl₃), δ (ppm): -63.1 (s, 12F, CF₃{C₆H₃(CF₃)₂}); -63.3 (s, 12F, CF₃'{C₆H₃(CF₃)₂}); -63.5 (s, 6F; CF₃{biphenyl}). HR-MS (ESI⁺ *m/z*) [M+H]⁺: calculated for [C₄₆H₁₉F₃₀P₂O₂]⁺ 1235.0376; found 1235.038.

²⁵ a) Desponds, O.; Schlosser, M. *J. Organomet. Chem.* **1996**, 507 (1–2), 257–261. b) Xu, W.; Zou, J. P.; Zhang, W. *Tetrahedron Lett.* **2010**, 51 (19), 2639–2643.

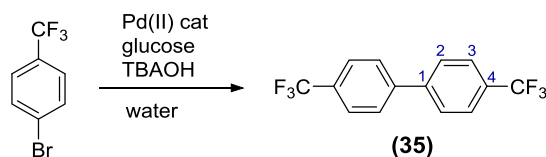
²⁶ Cu was activated as follows: Cu powder was suspended in acetone and stirred with a small crystal of I₂. After a few minutes the cloudiness of the solvent indicated the presence of small amounts of CuI, as grey powder. The suspension was then filtered and the red Cu was stirred with 10 % aqueous HCl. After filtration, Cu was washed three times with acetone and vacuum dried

4,4'-bis(trifluoromethyl)-[1,1'-biphenyl]-2,2'-diylbis(bis(3,5-bis(trifluoromethyl)-phenyl)phosphine (32)



The reaction of reduction of **ox-32** was performed in a stainless steel autoclave equipped with a glass vessel and a magnetic stirrer. The autoclave vacuum dried previous to being loaded with a solution of 2.0 g of **ox-32** (1.62 mmol) in 34 ml of anhydrous toluene, 1.65 ml of trichlorosilane (16.2 mmol) and 2.3 ml of freshly distilled triethylamine (16.2 mmol). Then it was charged with 3 bar of N₂ and heated up to 200 °C for 12 h. The autoclave was cooled down in an ice bath and the content was poured over a 5 % NaOH aqueous solution. High amount of grey precipitate was observed and was filtered of in a schlenk filter with a sintered glass disk and washed with 40 ml of CH₂Cl₂. The resulting biphasic solution was decanted and the aqueous phase was extracted with CH₂Cl₂ (3 x 40 ml). The organic layers were combined and dried over MgSO₄. After solvent evaporation, diphosphine **32** was further purified through flash column (silica, CH₂Cl₂:hexanes, 2:1) to yield 0.59 g of **32** (31 % yield) as white solid.

³¹P{¹H} NMR (161.98 MHz, CDCl₃), δ (ppm): -10.43 (s). ¹H NMR (400.13 MHz, CDCl₃), δ (ppm): 7.94 (s, 4H, H_{C4}{C₆H₃(CF₃)₂}), 7.68 (s, 4H, H_{C2}{C₆H₃(CF₃)₂}); 7.61 (d, 2H, H_{C5}{biphenyl}, ³J_{HH} = 8.1 Hz); 7.53 (s, 4H, H_{C2'}{C₆H₃(CF₃)₂}); 7.36 (s, 2H, H_{C3}{biphenyl}); 7.01 (bd, 2H, H_{C3}{biphenyl}, ³J_{HH} = 8.1 Hz). ¹³C{¹H} NMR (100.61 MHz, CDCl₃), δ (ppm): [148.72-124.06] (m, C_{aryl}); 123.17 (q, CF₃{biphenyl}, ¹J_{CF} = 272.8 Hz); 122.86 (q, CF₃{C₆H₃(CF₃)₂}, ¹J_{CF} = 273.6 Hz); 122.8 (q, CF₃'{C₆H₃(CF₃)₂}, ¹J_{CF} = 273.6 Hz). ¹⁹F{¹H} NMR (376.50 MHz, CDCl₃), δ (ppm): -63.09 (s, 12F, CF₃{C₆H₃(CF₃)₂}); -63.15 (s, 6F, CF₃{biphenyl}); -63.20 (s, 12F, CF₃'{C₆H₃(CF₃)₂}). **HR-MS** (ESI⁺ *m/z*) [M(O)₂+Na]⁺: calculated for [C₄₆H₁₈F₃₀P₂O₂Na]⁺ 1257.0195; found 1257.0194. **Elemental analysis**: calculated for C₄₆H₁₈F₃₀P₂: C, 45.94; H, 1.51; found: C, 46.04; H, 1.47.

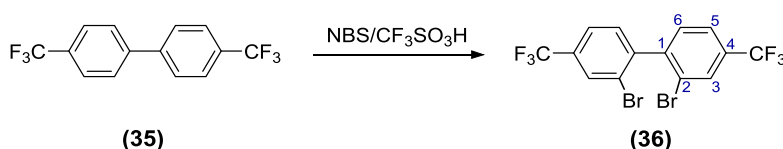
4,4'-bis(trifluoromethyl)-1,1'-biphenyl (**35**)

The synthesis of the trifluoromethylated biphenyl **35** was carried out following a reported methodology in the literature²⁷ with some modifications. No inert conditions were required in this preparation. A round-bottom flask was charged with 7.0 ml of 4-(trifluoromethyl)bromobenzene (11.2 g, 49.8 mmol), 4.5 g of glucose (25.0 mmol), 0.135 g of Pd(AcO)₂ (0.6 mmol) and 70 ml of a solution of TBAOH (1.5 M in water, 0.10 mol). The biphasic mixture was brought to reflux and, under vigorous stirring, was allowed to react for 40 h. After that time, 60 ml of 10 % aqueous HCl was added to the black mixture and the organic was extracted with CH₂Cl₂ (4 x 30 ml). The organic layers were combined and dried over MgSO₄ to give a black suspension. A sintered glass filter was loaded with about 0.5 mm of Celite and, on top of this, 5 cm of silica gel. The black suspension was filtered through the funnel. While silica retained the polar compounds (TBAOH, glucose and derivatives), the celite pad retained the particles of Pd, avoiding the clogging of the sintered glass. An orange solution was obtained. After solvent evaporation, an orange solid was obtained which was recrystallised in EtOH/H₂O to afford **35** as pale orange flakes (4.4 g, 61 % yield).

¹H NMR (400.13 MHz, CDCl₃), δ (ppm): 7.74 (*pseudo-q*, *second order spectrum*).

¹³C{¹H} NMR (100.61 MHz, CDCl₃), δ (ppm): 143.4 (s, C₁); 130.44 (q, C₄, ²J_{CF} = 33.1 Hz); 127.8 (s, C₂); 126.10 (q, C₃, ³J_{CF} = 3.6 Hz); 124.26 (q, CF₃, ¹J_{CF} = 272.2 Hz).

¹⁹F{¹H} NMR (376.50 MHz, CDCl₃), δ (ppm): -62.50 (s)

2,2'-dibromo-4,4'-bis(trifluoromethyl)-1,1'-biphenyl (**36**)

Bromination of **35** was performed in analogy to the reported procedure for the bromination and iodination of 4-(trifluoromethyl)bromobenzene. No inert conditions

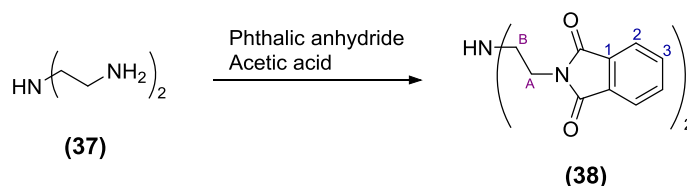
²⁷ Monopoli, A.; Calò, V.; Ciminale, F.; Cotugno, P.; Angelici, C.; Cioffi, N.; Nacci, A. *J. Org. Chem.* **2010**, 75 (11), 3908–3911.

were required in this synthetic procedure. 1.5 g (5.2 mmol) of 4,4'-bis(trifluoromethyl)-1,1'-biphenyl (**35**) were dissolved in 4.4 ml of triflic acid (49.7 mmol). The mixture was cooled down to 0 °C in an ice bath previous to the portion wise addition of 3.1 g of *N*-bromosuccinimide (17.2 mmol). For better control of the selectivity of the reaction (*ca.* avoid polybromination) the reaction mixture was monitored by GC after the addition of 75 and 90 % of the total amount of NBS and special care was required to avoid the rise of the reaction temperature. The orange mixture was then allowed to react at room temperature for 14 h before being poured over 20 ml of water. Afterwards, it was extracted with Et₂O (5 x 10 ml) and the organic layers were washed with aqueous NaHCO₃ until pH 7-8 and dried over MgSO₄. Distillation via Kugelrohr afforded 1.60 g 2,2'-dibromo-4,4'-bis(trifluoromethyl)-1,1'-biphenyl (**36**) as colourless oil (70 % yield).

¹H NMR (400.13 MHz, CDCl₃), δ (ppm): 7.97 (s, 2H, H_{C3}); 7.68 (bd, 2H, H_{C5}, ³J_{HH} = 7.9 Hz); 7.37 (d, 2H, H_{C6}, ³J_{HH} = 7.9 Hz). ¹³C{¹H} NMR (100.61 MHz, CDCl₃), δ (ppm): 144.54 (s, C₁); 132.37 (q, C₄, ²J_{CF} = 33.2 Hz); 131.24 (s, C₆); 130.04 (q, C₃, ³J_{CF} = 3.8 Hz); 124.46 (q, C₅, ³J_{CF} = 3.7 Hz); 123.62 (s, C₂); 123.15 (q, CF₃, ¹J_{CF} = 272.6 Hz). ¹⁹F{¹H} NMR (376.50 MHz, CDCl₃), δ (ppm): -62.88 (s). GC-MS calculated for C₁₄H₆Br₂F₆ molecular peak 447.9; found 448.1. The isotopic distribution agrees with 2 bromine atoms.

9.5.6. Miranphos derivatives: Chelating diphosphine-diamides and intermediate compounds

N,N-bis(2-phthalimidoethyl)amine (**38**)



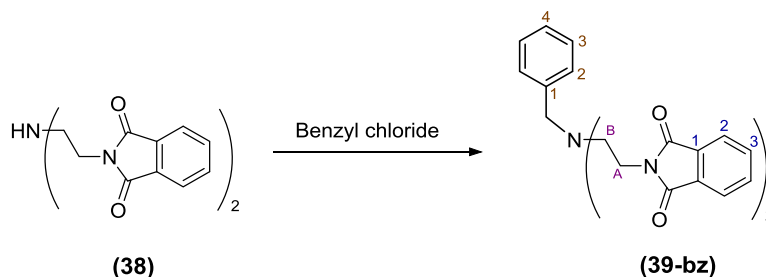
The protected amine **38** was prepared following the reported methodology in the literature with minor modifications.²⁸ 15.1 g of phthalic anhydride (0.10 mol) and 5.2 ml (5.0 g, 48.5 mmol) of diethylenetriamine (**37**) were refluxed in 80 ml of glacial acetic acid during 5 h. The solvent was then removed by distillation to yield a yellow sticky

²⁸ Miranda, C.; Escartí, F.; Lamarque, L.; Yunta, M. J. R.; Navarro, P.; García-España, E.; Jimeno, M. L. *J. Am. Chem. Soc.* **2004**, *126* (3), 823–833.

solid which stirred overnight with 50 ml of EtOH. A yellow suspension was formed which was further stirred at 70 °C for 15 min to achieve the complete suspension of the yellow sticky solid. Afterwards, the suspension was cooled down to room temperature and filtered. The white solid was washed three times with cold EtOH and other three times with 30 ml of Et₂O. Finally it was vacuum dried to afford 13.14 g of **38** as white solid (75 % yield).

¹H NMR (500.13 MHz, CDCl₃), δ (ppm): 7.69 (m, 8H, H_{C1}+ H_{C2}+H_{C3}); 3.77 (t, 4H, -CH₂-(A), ³J_{HH} = 6.1 Hz); 2.95 (t, 4H, -CH₂-(B), ³J_{HH} = 6.1 Hz); 1.59 (bs, 1H, NH). ¹³C{¹H} NMR (125.80 MHz, CDCl₃), δ (ppm): 168.56 (s, CON); 133.86 (s, C₃); 132.31 (s, C₁); 123.26 (s, C₂); 47.32 (s, -CH₂-(B)); 37.69 (s, -CH₂-(A)). HR-MS (ESI⁺ m/z) [M+H]⁺: calculated for [C₂₀H₁₈N₃O₄]⁺ 364.1292; found 364.1293. Elemental analysis: calculated for C₂₀H₁₇N₃O₄: C, 66.11; H, 4.72; N, 11.56; found: C, 65.20; H, 4.60; N, 10.98.

Benzyl-bis(2-phthalimidoethyl)amine (39-bz)



39-bz was synthesised following the reported methodologies in the literature with minor modifications.^{28,29} 16 g (44.0 mmol) of the protected amine **38**, 6.7 ml of benzyl chloride (7.4 g, 58.2 mmol) and 11.1 g of K₂CO₃ (0.11 mol) were refluxed in 150 ml of acetonitrile for 24 h. The solvent was then evaporated and the solid residue was suspended in 50 ml of CH₂Cl₂. After filtration, the white solid was extracted three more times with 50 ml of CH₂Cl₂. The organic layers were combined and evaporated to dryness to remove the solvent and the volatile organics yielding 18.5 g of **39-bz** (93 % yield) as pale yellow powder.

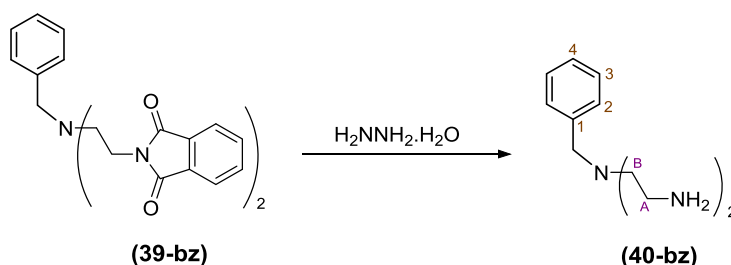
¹H NMR (500.13 MHz, CDCl₃), δ (ppm): 7.70 (m, 8H, H_{C1}+ H_{C2}+H_{C3}{phthalimide}); 7.06 (d, 2H, H_{C2}{C₆H₅}, ³J_{HH} = 7.4 Hz); 7.02 (t, 1H, H_{C4}{C₆H₅}, ³J_{HH} = ³J_{HH} = 7.4

²⁹ Lermontova, E. K.; Huan, M. M.; Churakov, A. V.; Howard, J. A. K.; Zabalov, M. V.; Karlov, S. S.; Zaitseva, G. S. *J. Chem. Soc. Dalton Trans.* **2009**, 2 (24), 4695–4702.

Hz); 6.93 (t, 2H, $\text{H}_{\text{C}_3}\{\text{C}_6\text{H}_5\}$, $^3J_{\text{HH}} = ^3J_{\text{HH}} = 7.4$ Hz); 3.77 (t, 4H, $-\text{CH}_2\text{-(A)}$, $^3J_{\text{HH}} = 6.3$ Hz); 3.67 (s, 2H, benzylic- $\text{CH}_2\text{-}$); 2.81 (t, 4H, $-\text{CH}_2\text{-(B)}$, $^3J_{\text{HH}} = 6.3$ Hz). $^{13}\text{C}\{^1\text{H}\}$ NMR (125.80 MHz, CDCl_3), δ (ppm): 168.29 (s, CON); 138.87 (s, $\text{C}_1\{\text{C}_6\text{H}_5\}$); 133.72 (s, $\text{C}_3\{\text{phthalimide}\}$); 132.54 (s, $\text{C}_1\{\text{phthalimide}\}$); 129.07 (s, $\text{C}_2\{\text{C}_6\text{H}_5\}$); 128.15 (s, $\text{C}_3\{\text{C}_6\text{H}_5\}$); 126.95 (s, $\text{C}_4\{\text{C}_6\text{H}_5\}$); 123.15 (s, $\text{C}_2\{\text{phthalimide}\}$); 58.36 (s, benzylic- $\text{CH}_2\text{-}$); 51.82 (s, $-\text{CH}_2\text{-(B)}$); 35.91 (s, $-\text{CH}_2\text{-(A)}$). **HR-MS** (ESI^+ m/z) $[\text{M}+\text{H}]^+$: calculated for $[\text{C}_{27}\text{H}_{24}\text{N}_3\text{O}_4]^+$ 454.1761; found 454.1756. **Elemental analysis**: calculated for $\text{C}_{27}\text{H}_{23}\text{N}_3\text{O}_4$: C, 71.51; H, 5.11; N, 9.27; found: C, 69.77; H, 4.98; N, 8.63.

The NMR data are consistent with the reported values in the literature.²⁸

4-benzyl-diethylenetriamine (40-bz)

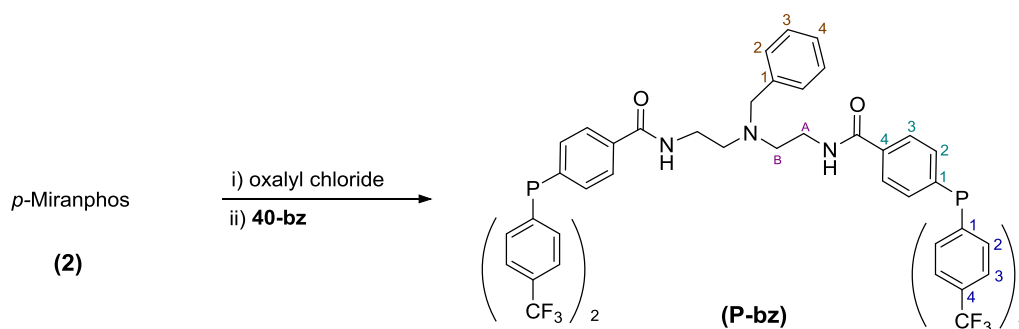


Deprotection of **39-bz** was performed following the reported methodology in the literature with minor modifications.^{28,30} 9 g of **39-bz** (19.8 mmol) were dissolved in a mixture of 300 ml of 96 % EtOH and 80 ml of CHCl_3 (the reaction have been essayed replacing, CHCl_3 to CH_2Cl_2 with no influence in the yield). Then 9.6 ml of hydrazine monohydrate (0.20 mol) were added and the mixture was stirred at reflux for 1.5 h. The reaction mixture was the cooled down to 0 °C (ice bath) and the white precipitate phthalhydrazide was filtered off and washed twice with 40 ml of CHCl_3 . The organic solution was vacuum evaporated to give turbid yellow oil. 35 ml of fresh CHCl_3 were added and the mixture was stirred for 24 h in order to precipitate any remaining phthalhydrazide. After filtration, the white solid was removed and the organic solution was evaporated to yield 2.77 g of **40-bz** as a yellow oil (72 % yield).

³⁰ Arbuse, A.; Font, M.; Martínez, M. A.; Fontrodona, X.; Prieto, M. J.; Moreno, V.; Sala, X.; Llobet, A. *Inorg. Chem.* **2009**, 48 (23), 11098–11107.

$^1\text{H NMR}$ (360.13 MHz, CD_2Cl_2), δ (ppm): 7.32 (m, 5H, $\{\text{C}_5\text{H}_6\}$); 3.58 (s, 2H, benzylic- CH_2 -); 2.72 (t, 4H, $-\text{CH}_2$ -(B), $^3J_{\text{HH}} = 6.0$ Hz); 2.50 (t, 4H, $-\text{CH}_2$ -(A), $^3J_{\text{HH}} = 6.0$ Hz); 2.13 (s, 4H, NH_2). $^{13}\text{C}\{^1\text{H}\}$ NMR (90.56 MHz, CD_2Cl_2), δ (ppm): 140.26 (s, $\text{C}_1\{\text{C}_6\text{H}_5\}$); 129.30 (s, $\text{C}_2\{\text{C}_6\text{H}_5\}$); 128.55 (s, $\text{C}_3\{\text{C}_6\text{H}_5\}$); 127.22 (s, $\text{C}_4\{\text{C}_6\text{H}_5\}$); 59.48 (s, benzylic- CH_2 -); 57.28 (s, $-\text{CH}_2$ -(A)); 39.98 (s, $-\text{CH}_2$ -(B)). **HR-MS** (ESI^+ m/z) $[\text{M}+\text{H}]^+$: calculated for $[\text{C}_{11}\text{H}_{20}\text{N}_3]^+$ 194.1652; found 194.1656.

Diphosphine-diamide P-bz

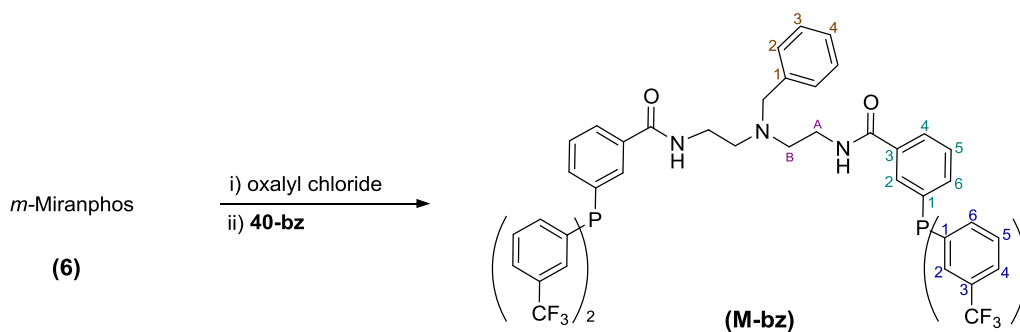


3.0 g (6.8 mmol) of *p*-Miranphos (**2**) were dissolved in 30 ml of anhydrous CH_2Cl_2 together with 0.105 ml of DMF (1.36 mmol). Following, 0.759 ml (8.8 mmol) of oxalyl chloride were added with the immediate evolution of bubbling from the solution. The mixture was stirred for 30 min before the addition of 1.23 ml (8.8 mmol) of freshly distilled triethylamine. Deep red solution was formed which was allowed to further react for 20 min with no apparent changes. Next, 0.64 g (3.3 mmol) of **40-bz** dissolved in 20 ml of anhydrous CH_2Cl_2 were added and the mixture was stirred for 5 h. After that time, the organic solution was washed twice with 15 ml of water, twice with 15 ml of 10 % aqueous NaHCO_3 and finally with 15 ml of additional water. The organic phase was dried over MgSO_4 and vacuum evaporated to give an orange solid which was purified by column chromatography in silica (ethyl acetate: hexanes, 8:4) to yield 1.5 g of diphosphine **P-bz** as pale yellow solid (42 % yield).

$^{31}\text{P}\{^1\text{H}\}$ NMR (161.98 MHz, CD_2Cl_2), δ (ppm): -5.62 (s). $^1\text{H NMR}$ (400.13 MHz, CD_2Cl_2), δ (ppm): 7.65 (d, 4H, $\text{H}_{\text{C}_3}\{\text{C}_6\text{H}_4\text{CON}\}$, $^3J_{\text{HH}} = 8.1$ Hz) 7.61 (d, 8H, $\text{H}_{\text{C}_3}\{\text{C}_6\text{H}_4\text{CF}_3\}$, $^3J_{\text{HH}} = 7.9$ Hz); 7.40 (*pseudo*-t, 8H, $\text{H}_{\text{C}_2}\{\text{C}_6\text{H}_4\text{CF}_3\}$, $^3J_{\text{HH}} = ^3J_{\text{HP}} = 7.9$ Hz); 7.24 (m, 6H, $\text{H}_{\text{C}_2}\{\text{C}_6\text{H}_4\text{CON}\}$ - $\text{H}_{\text{C}_2}\{\text{C}_6\text{H}_5\}$); 7.10 (m, 3H, $\text{H}_{\text{C}_3}+\text{H}_{\text{C}_4}\{\text{C}_6\text{H}_5\}$); 6.70 (*bs*, 2H, amide-NH); 3.60 (s, 2H, benzylic- CH_2 -); 3.53 (*pseudo*-q, 4H, $-\text{CH}_2$ -(A), $^3J_{\text{HH}} = 5.1$ Hz); 2.73 (*bs*, 4H, $-\text{CH}_2$ -(B)). $^{13}\text{C}\{^1\text{H}\}$ NMR (100.61 MHz, CD_2Cl_2), δ (ppm): 167.3

(s, CON); 141.43 (d, C₁{C₆H₄CON}, ¹J_{CP} = 14.7 Hz); 139.9 (s, C₁{C₆H₅}); 139.4 (d, C₁{C₆H₄CF₃}, ¹J_{CP} = 13.3 Hz); 136.1 (s, C₄{C₆H₄CON}); 134.4 (d, C₂{C₆H₄CF₃}, ²J_{CP} = 20.5 Hz); 134.1 (d, C₂{C₆H₄CON}, ²J_{CP} = 20.2 Hz); 131.4 (q, C₄{C₆H₄CF₃}, ²J_{CF} = 32.3 Hz); 129.43 (s, C₂{C₆H₅}); 128.68 (C₃{C₆H₅}); 127.82 (d, C₃{C₆H₄CON}, ³J_{CP} = 7.3 Hz); 127.39 (C₄{C₆H₅}); 125.85 (dq, C₃{C₆H₄CF₃}, ³J_{CP} = 7.4 Hz, ³J_{CF} = 3.5 Hz); 124.44 (q, CF₃, ¹J_{CF} = 272.0 Hz); 59.04 (s, benzylic-CH₂-); 54.04 (s, -CH₂-(B)); 38.37 (s, -CH₂-(A)). ¹⁹F{¹H} NMR (376.50 MHz, CD₂Cl₂), δ (ppm): -63.17 (s). **HR-MS** (ESI⁺ *m/z*) [M+H]⁺: calculated for [C₅₃H₄₂F₁₂N₃O₂P₂]⁺ 1042.2555; found 1042.2552. **Elemental analysis**: calculated for C₅₃H₄₁F₁₂N₃O₂P₂: C, 61.10; H, 3.97; N, 4.03; found: C, 61.22; H, 4.00; N, 3.96.

Diphosphine-diamide M-bz

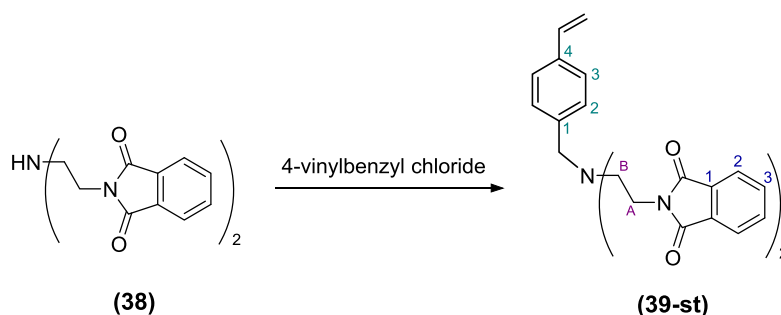


The very same procedure as described for **P-bz** was applied for the synthesis of **M-bz**, but using *m*-Miranphos (**6**), affording 1.94 g of diphosphine **M-bz** as pale yellow solid (54.8 % yield).

³¹P{¹H} NMR (161.98 MHz, CD₂Cl₂), δ (ppm): -4.62 (s). ¹H NMR (400.13 MHz, CD₂Cl₂), δ (ppm): 7.85 (d, 2H, H_{C2}{C₆H₄CON}, ³J_{HP} = 9.2 Hz); 7.67 (m, 2H, H_{C4}{C₆H₄CON}); 7.63 (d, 4H, H_{C4}{C₆H₄CF₃}, ³J_{HH} = 7.7 Hz); 7.60 (d, 4H, H_{C2}{C₆H₄CF₃}, ³J_{HP} = 7.9 Hz); 7.45 (m, 8H, H_{C5}+H_{C6}{C₆H₄CF₃}); 7.29 (m, 4H, H_{C5}+H_{C6}{C₆H₄CON}); 7.18 (m, 2H, H_{C2}{C₆H₅}); 7.05 (m, 3H, H_{C3}+H_{C4}{C₆H₅}); 6.70 (bt, 2H, amide-NH, ³J_{HH} = 5.3 Hz); 3.56 (s, 2H, benzylic-CH₂-); 3.49 (*pseudo*-q, 4H, -CH₂-(A), ³J_{HH} = 5.3 Hz); 2.69 (t, 4H, -CH₂-(B), ³J_{HH} = 5.3 Hz). ¹³C{¹H} NMR (100.61 MHz, CD₂Cl₂), δ (ppm): 167.23 (s, CON); 139.79 (s, C₁{C₆H₅}); 138.19 (d, C₆{C₆H₄CON}, ²J_{CP} = 14.6 Hz); 137.25 (d, C₆{C₆H₄CF₃}, ²J_{CP} = 16.0 Hz); 136.33 (d, C₁{C₆H₄CF₃}, ¹J_{CP} = 12.8 Hz); 135.72 (d, C₁{C₆H₄CON}, ¹J_{CP} = 8.8 Hz); 133.44 (d, C₂{C₆H₄CON}, ²J_{CP} = 28.8 Hz); 131.27 (qd, C₃{C₆H₄CF₃}, ²J_{CF} = 32.2 Hz, ³J_{CP} = 8.1

Hz); 130.62 (dq, $C_2\{C_6H_4CF_3\}$, $^2J_{CP} = 24.7$ Hz, $^3J_{CF} = 3.8$ Hz); 130.07 (d, $C_3\{C_6H_4CON\}$, $^3J_{CP} = 12.2$ Hz); 129.74 (d, $C_5\{C_6H_4CF_3\}$, $^3J_{CP} = 5.9$ Hz); 129.37 (d, $C_5\{C_6H_4CON\}$, $^3J_{CP} = 5.9$ Hz); 129.31 (s, $C_2\{C_6H_5\}$); 128.65 ($C_3\{C_6H_5\}$); 128.55 (s, $C_4\{C_6H_4CON\}$); 127.39 ($C_4\{C_6H_5\}$); 126.45 (q, $C_4\{C_6H_4CF_3\}$, $^3J_{CF} = 3.7$ Hz); 124.4 (q, CF_3 , $^1J_{CF} = 272.0$ Hz); 59.16 (s, benzylic- CH_2 -); 54.04 (s, $-CH_2$ -(B)); 38.38 (s, $-CH_2$ -(A)). $^{19}F\{^1H\}$ NMR (376.50 MHz, CD_2Cl_2), δ (ppm): -63.06 (s). **HR-MS** (ESI⁺ m/z) $[M+H]^+$: calculated for $[C_{53}H_{42}F_{12}N_3O_2P_2]^+$ 1042.2555; found 1042.2540. **Elemental analysis**: calculated for $C_{53}H_{41}F_{12}N_3O_2P_2$: C, 61.10; H, 3.97; N, 4.03; found: C, 61.18; H, 4.01; N, 3.79.

(4-Vinylbenzyl)-bis(2-phthalimidoethyl)amine (39-st)



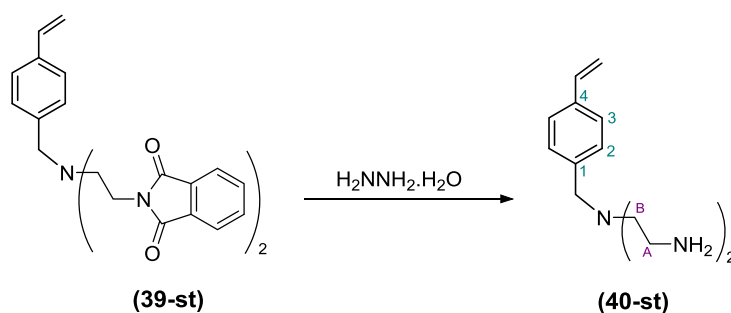
The vinylic derivative **39-st** was prepared in analogy to the methodology for the synthesis of **39-bz**. 10 g (27.5 mmol) of the protected amine **38**, 5.1 ml of 4-vinylbenzyl chloride (5.5 g, 36.2 mmol) and 9.5 g of K_2CO_3 (93.9 mmol) were refluxed in 80 ml of acetonitrile for 21 h. The solvent was then evaporated and the solid residue was suspended in 50 ml of CH_2Cl_2 . After filtration, the white solid was extracted three more times with 50 ml of CH_2Cl_2 . The organic layers were combined and evaporated to dryness to remove the solvent and the volatile organics, yielding 11.5 g of **39-st** (87 % yield) as white powder.

1H NMR (500.13 MHz, $CDCl_3$), δ (ppm): 7.70 (m, 8H, $H_{C1} + H_{C2} + H_{C3}$ {phthalimide}); 7.00 (d, 2H, $H_{C3}\{C_6H_4\}$, $^3J_{HH} = 8.0$ Hz); 6.92 (d, 2H, $H_{C2}\{C_6H_4\}$, $^3J_{HH} = 8.0$ Hz); 6.53 (dd, 1H, $-CH=CH_2$, $^3J_{HH(trans)} = 17.6$ Hz, $^3J_{HH(cis)} = 10.8$ Hz); 5.54 (dd, 1H, $-CH=CH_2$, $^3J_{HH(trans)} = 17.6$ Hz, $^2J_{HH(gem)} = 0.8$ Hz); 5.15 (dd, 1H, $-CH=CH_2$, $^3J_{HH(cis)} = 10.8$ Hz, $^2J_{HH(gem)} = 0.8$ Hz); 3.76 (t, 4H, $-CH_2$ -(A), $^3J_{HH} = 6.1$ Hz); 3.63 (s, 2H, benzylic- CH_2 -); 2.81 (t, 4H, $-CH_2$ -(B), $^3J_{HH} = 6.1$ Hz). $^{13}C\{^1H\}$ NMR (125.80 MHz, $CDCl_3$), δ (ppm): 168.3 (s, CON); 138.67 (s, $C_1\{C_6H_4\}$); 136.86 (s, $-CH=CH_2$); 136.20 (s, $C_4\{C_6H_4\}$); 133.70 (s, C_3 {phthalimide}); 132.55 (s, C_1 {phthalimide}); 129.30 (s, $C_3\{C_6H_4\}$);

126.04 (s, C₂{C₆H₄}); 123.15 (s, C₂{phthalimide}); 113.17 (s, -CH=CH₂); 58.02 (s, benzylic-CH₂-); 51.92 (s, -CH₂-(B)); 35.98 (s, -CH₂-(A)). **HR-MS** (ESI⁺ *m/z*) [M+H]⁺: calculated for [C₂₉H₂₆N₃O₄]⁺ 480.1918; found 480.1916. **Elemental analysis**: calculated for C₂₉H₂₅N₃O₄: C, 72.64; H, 5.26; N, 8.76; found: C, 72.56; H, 5.24; N, 8.60.

The NMR data are consistent with the reported values in the literature.³¹

4-(4-Vinylbenzyl)diethylenetriamine (40-st)



Deprotection of **39-st** was performed in analogy to the deprotection of **39-bz** with some modifications and with the precaution of minimising contact with light, especially during the process of purification. 0.5 g of **39-st** (1.0 mmol) were dissolved in a mixture of 24.2 ml of 96 % EtOH and 5 ml of CHCl₃. Then 0.5 ml of hydrazine monohydrate (5.0 mmol) were added and the mixture was stirred vigorously for 24 h. After this time a white suspension was formed. The white precipitate phthalhydrazide was filtered off and washed twice with 5 ml of CHCl₃. The organic solution was vacuum evaporated to give turbid yellow oil. 4 ml of fresh CHCl₃ were added and the mixture was stirred for 1.5 h in order to precipitate any remaining phthalhydrazide. After filtration, the white solid was removed and the organic solution was evaporated to yield 0.17 g of **40-st** as pale yellow oil (72 % yield), containing 7 % of the product of reduction of the vinyl group. **40-st** was immediately stored at -34 °C.

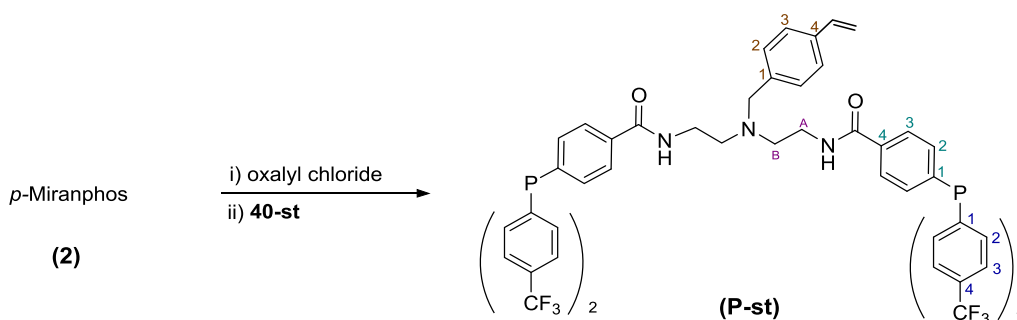
¹H NMR (400.13 MHz, CD₂Cl₂), δ (ppm): 7.37 (d, 2H, H_{C3}{C₆H₄}), ³J_{HH} = 8.2 Hz); 7.29 (d, 2H, H_{C2}{C₆H₄}), ³J_{HH} = 8.2 Hz); 6.72 (dd, 1H, -CH=CH₂, ³J_{HH(trans)} = 17.8 Hz, ³J_{HH(cis)} = 10.8 Hz); 5.74 (dd, 1H, -CH=CH₂, ³J_{HH(trans)} = 17.8 Hz, ²J_{HH(gem)} = 0.9 Hz); 5.22 (dd, 1H, -CH=CH₂, ³J_{HH(cis)} = 10.8 Hz, ²J_{HH(gem)} = 0.9 Hz); 3.56 (s, 2H, benzylic-CH₂-); 2.71 (t, 4H, -CH₂-(B), ³J_{HH} = 6.0 Hz); 2.47 (t, 4H, -CH₂-(A), ³J_{HH} = 6.0 Hz);

³¹ Striegler, S. *Tetrahedron* **2001**, 57 (12), 2349–2354.

1.30 (s, 4H, NH₂). ¹³C{¹H} NMR (100.61 MHz, CD₂Cl₂), δ (ppm): 140.29 (s, C₁{C₆H₄}); 136.99 (s, -CH=CH₂); 136.61 (s, C₄{C₆H₄}); 129.43 (s, C₃{C₆H₄}); 126.36 (s, C₂{C₆H₄}); 113.48 (s, -CH=CH₂); 59.30 (s, benzylic-CH₂-); 57.97 (s, -CH₂-(A)); 40.28 (s, -CH₂-(B))

The NMR data agree with the values reported in the literature.³¹

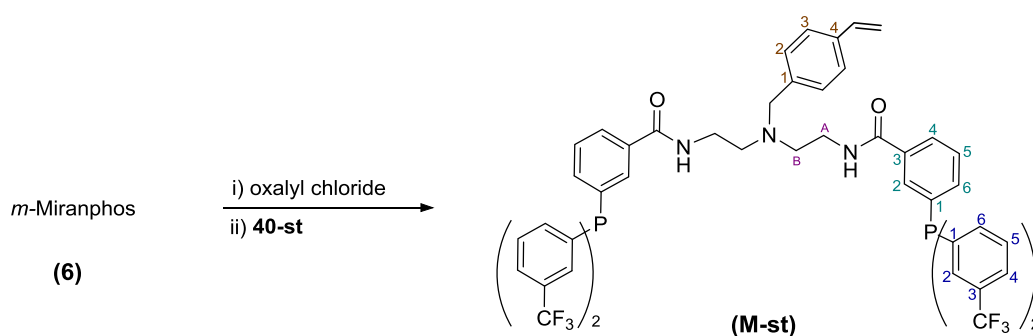
Diphosphine-diamide P-st



Diphosphine **P-st** was prepared analogously to **P-bz**. 0.8 g (1.8 mmol) of *p*-Miranphos (**2**) were dissolved in 10 ml of anhydrous CH₂Cl₂ together with 34.8 μl of DMF (0.45 mmol). Following, 217 μl (2.5 mmol) of oxalyl chloride were added with the immediate evolution of bubbling from the solution. The mixture was stirred for 25 min before the addition of 377 μl (2.5 mmol) of freshly distilled triethylamine. Deep red solution was formed which was allowed to further react for 3 min with no apparent changes. Next, 0.20 g (1.0 mmol) of **40-st** dissolved in 10 ml of anhydrous CH₂Cl₂ were added and the mixture was stirred for 2 h. After that time, the organic solution was washed twice with 10 ml of water and twice with 10 ml of 10 % aqueous NaHCO₃ and finally with 10 ml more of water. The organic phase was dried over MgSO₄ and vacuum evaporated to give an orange solid which was purified by column chromatography in silica (ethyl acetate: hexanes, 8:2) and vacuum dried to yield 0.14 g of diphosphine **P-st** as pale orange solid (14.7 % yield).

$^{31}\text{P}\{^1\text{H}\}$ NMR (161.98 MHz, CD_2Cl_2), δ (ppm): -5.64 (s). ^1H NMR (400.13 MHz, CD_2Cl_2), δ (ppm): 7.62 (m, 12H, $\text{H}_{\text{C}_3}\{\text{C}_6\text{H}_4\text{CON}\}-\text{H}_{\text{C}_3}\{\text{C}_6\text{H}_4\text{CF}_3\}$); 7.41 (*pseudo-t*, 8H, $\text{H}_{\text{C}_2}\{\text{C}_6\text{H}_4\text{CF}_3\}$, $^3J_{\text{HH}} = ^3J_{\text{HP}} = 7.5$ Hz); 7.24 (*pseudo-t*, 4H, $\text{H}_{\text{C}_2}\{\text{C}_6\text{H}_4\text{CON}\}$, $^3J_{\text{HH}} = ^3J_{\text{HP}} = 7.8$ Hz); 7.19 (d, 2H, $\text{H}_{\text{C}_3}\{\text{C}_6\text{H}_4\}$, $^3J_{\text{HH}} = 8.2$ Hz); 7.12 (d, 2H, $\text{H}_{\text{C}_2}\{\text{C}_6\text{H}_4\}$, $^3J_{\text{HH}} = 8.2$ Hz); 6.74 (*bt*, 2H, amide-NH, $^3J_{\text{HH}} = 5.2$ Hz); 6.52 (dd, 1H, $-\text{CH}=\text{CH}_2$, $^3J_{\text{HH}(\text{trans})} = 17.4$ Hz, $^3J_{\text{HH}(\text{cis})} = 11.0$ Hz); 5.52 (d, 1H, $-\text{CH}=\text{CH}_2$, $^3J_{\text{HH}(\text{trans})} = 17.4$ Hz); 5.09 (d, 1H, $-\text{CH}=\text{CH}_2$, $^3J_{\text{HH}(\text{cis})} = 11.0$ Hz); 3.57 (s, 2H, benzylic- CH_2 -); 3.53 (q, 4H, $-\text{CH}_2$ -(A), $^3J_{\text{HH}} = 5.2$ Hz); 2.72 (*bt*, 4H, $-\text{CH}_2$ -(B), $^3J_{\text{HH}} = 5.2$ Hz). $^{13}\text{C}\{^1\text{H}\}$ NMR (100.61 MHz, CD_2Cl_2), δ (ppm): 167.30 (s, CON); 141.40 (d, $\text{C}_1\{\text{C}_6\text{H}_4\text{CON}\}$, $^1J_{\text{CP}} = 14.1$ Hz); 139.64 (s, $\text{C}_1\{\text{C}_6\text{H}_4\}$); 139.42 (d, $\text{C}_1\{\text{C}_6\text{H}_4\text{CF}_3\}$, $^1J_{\text{CP}} = 12.9$ Hz); 136.82 (s, $\text{C}_4\{\text{C}_6\text{H}_4\}$); 136.68 (s, $-\text{CH}=\text{CH}_2$); 136.00 (s, $\text{C}_4\{\text{C}_6\text{H}_4\text{CON}\}$); 134.41 (d, $\text{C}_2\{\text{C}_6\text{H}_4\text{CF}_3\}$, $^2J_{\text{CP}} = 19.9$ Hz); 134.04 (d, $\text{C}_2\{\text{C}_6\text{H}_4\text{CON}\}$, $^2J_{\text{CP}} = 20.4$ Hz); 131.43 (q, $\text{C}_4\{\text{C}_6\text{H}_4\text{CF}_3\}$, $^2J_{\text{CF}} = 32.5$ Hz); 129.72 ($\text{C}_3\{\text{C}_6\text{H}_4\}$); 127.85 (d, $\text{C}_3\{\text{C}_6\text{H}_4\text{CON}\}$, $^3J_{\text{CP}} = 7.1$ Hz); 126.51 (s, $\text{C}_2\{\text{C}_6\text{H}_4\}$); 125.86 (dq, $\text{C}_3\{\text{C}_6\text{H}_4\text{CF}_3\}$, $^3J_{\text{CP}} = 7.0$ Hz, $^3J_{\text{CF}} = 3.6$ Hz); 124.43 (q, CF_3 , $^1J_{\text{CF}} = 272.1$ Hz); 113.77 (s, $-\text{CH}=\text{CH}_2$); 58.71 (s, benzylic- CH_2 -); 54.31 (s, $-\text{CH}_2$ -(B)); 38.40 (s, $-\text{CH}_2$ -(A)). $^{19}\text{F}\{^1\text{H}\}$ NMR (376.50 MHz, CD_2Cl_2), δ (ppm): -63.03 (s). **HR-MS** (ESI⁺ m/z) $[\text{M}+\text{H}]^+$: calculated for $[\text{C}_{55}\text{H}_{44}\text{F}_{12}\text{N}_3\text{O}_2\text{P}_2]^+$ 1068.2712; found 1068.2713. **Elemental analysis**: calculated for $\text{C}_{55}\text{H}_{43}\text{F}_{12}\text{N}_3\text{O}_2\text{P}_2$: C, 61.86; H, 4.06; N, 3.93; found: C, 61.95; H, 4.09; N, 3.65.

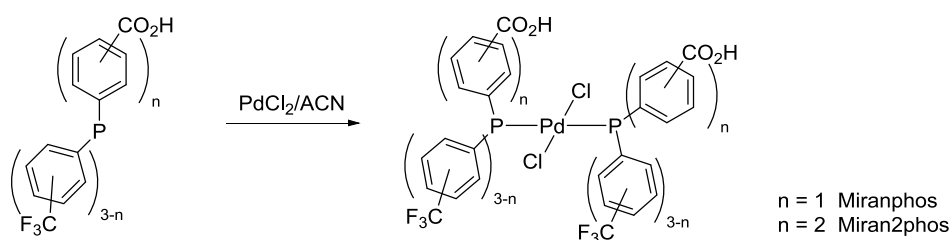
Diphosphine-diamide M-st



The same procedure as described for **P-st** was applied for the synthesis of **M-st**, but using *m*-Miranphos (**6**), affording 0.229 g of diphosphine **M-bz** as pale orange solid (23.5 % yield).

$^{31}\text{P}\{^1\text{H}\}$ NMR (161.98 MHz, CD_2Cl_2), δ (ppm): -4.65 (s). ^1H NMR (400.13 MHz, CD_2Cl_2), δ (ppm): 7.88 (d, 2H, $\text{H}_{\text{C}_2}\{\text{C}_6\text{H}_4\text{CON}\}$, $^3\text{J}_{\text{HP}} = 8.9$ Hz); 7.67 (m, 2H, $\text{H}_{\text{C}_4}\{\text{C}_6\text{H}_4\text{CON}\}$); 7.62 (m, 8H, $\text{H}_{\text{C}_2+\text{H}_{\text{C}_4}\{\text{C}_6\text{H}_4\text{CF}_3\}$); 7.45 (m, 8H, $\text{H}_{\text{C}_5+\text{H}_{\text{C}_6}\{\text{C}_6\text{H}_4\text{CF}_3\}$); 7.28 (m, 4H, $\text{H}_{\text{C}_5+\text{H}_{\text{C}_6}\{\text{C}_6\text{H}_4\text{CON}\}$); 7.16 (m, 4H, $\text{H}_{\text{C}_2+\text{H}_{\text{C}_3}\{\text{C}_6\text{H}_4\}$); 6.77 (bt, 2H, amide-NH, $^3\text{J}_{\text{HH}} = 5.2$ Hz); 6.58 (dd, 1H, $-\text{CH}=\text{CH}_2$, $^3\text{J}_{\text{HH}(\text{trans})} = 17.6$ Hz, $^3\text{J}_{\text{HH}(\text{cis})} = 10.9$ Hz); 5.61 (dd, 1H, $-\text{CH}=\text{CH}_2$, $^3\text{J}_{\text{HH}(\text{trans})} = 17.6$ Hz, $^2\text{J}_{\text{HH}(\text{gem})} = 0.9$ Hz); 5.17 (dd, 1H, $-\text{CH}=\text{CH}_2$, $^3\text{J}_{\text{HH}(\text{cis})} = 10.9$ Hz, $^2\text{J}_{\text{HH}(\text{gem})} = 0.9$ Hz); 3.56 (s, 2H, benzylic- CH_2 -); 3.48 (q, 4H, $-\text{CH}_2$ -(A), $^3\text{J}_{\text{HH}} = 5.2$ Hz); 2.69 (t, 4H, $-\text{CH}_2$ -(B), $^3\text{J}_{\text{HH}} = 5.2$ Hz). $^{13}\text{C}\{^1\text{H}\}$ NMR (100.61 MHz, CD_2Cl_2), δ (ppm): 167.22 (s, CON); 139.47 (s, $\text{C}_1\{\text{C}_6\text{H}_4\}$); 138.15 (d, $\text{C}_6\{\text{C}_6\text{H}_4\text{CON}\}$, $^2\text{J}_{\text{CP}} = 14.3$ Hz); 137.23 (bd, $\text{C}_6\{\text{C}_6\text{H}_4\text{CF}_3\}$, $^2\text{J}_{\text{CP}} = 15.8$ Hz); 136.83 (s, $\text{C}_4\{\text{C}_6\text{H}_4\}$); 136.36 (s, $-\text{CH}=\text{CH}_2$); 136.33 (d, $\text{C}_1\{\text{C}_6\text{H}_4\text{CF}_3\}$, $^1\text{J}_{\text{CP}} = 12.5$ Hz); 135.69 (d, $\text{C}_1\{\text{C}_6\text{H}_4\text{CON}\}$, $^1\text{J}_{\text{CP}} = 9.0$ Hz); 133.39 (d, $\text{C}_2\{\text{C}_6\text{H}_4\text{CON}\}$, $^2\text{J}_{\text{CP}} = 28.3$ Hz); 131.25 (qd, $\text{C}_3\{\text{C}_6\text{H}_4\text{CF}_3\}$, $^2\text{J}_{\text{CF}} = 32.1$ Hz, $^3\text{J}_{\text{CP}} = 7.9$ Hz); 130.62 (dq, $\text{C}_2\{\text{C}_6\text{H}_4\text{CF}_3\}$, $^2\text{J}_{\text{CP}} = 24.8$ Hz, $^3\text{J}_{\text{CF}} = 3.8$ Hz); 129.74 (d, $\text{C}_3\{\text{C}_6\text{H}_4\text{CON}\}$, $^3\text{J}_{\text{CP}} = 5.7$ Hz); 129.71 (d, $\text{C}_5\{\text{C}_6\text{H}_4\text{CF}_3\}$, $^3\text{J}_{\text{CP}} = 5.9$ Hz); 129.55 (s, $\text{C}_3\{\text{C}_6\text{H}_4\}$); 129.36 (d, $\text{C}_5\{\text{C}_6\text{H}_4\text{CON}\}$, $^3\text{J}_{\text{CP}} = 5.1$ Hz); 128.47 (s, $\text{C}_4\{\text{C}_6\text{H}_4\text{CON}\}$); 126.49 (s, $\text{C}_2\{\text{C}_6\text{H}_4\}$); 126.43 (q, $\text{C}_4\{\text{C}_6\text{H}_4\text{CF}_3\}$, $^3\text{J}_{\text{CF}} = 3.7$ Hz); 124.4 (q, CF_3 , $^1\text{J}_{\text{CF}} = 272.6$ Hz); 113.78 (s, $-\text{CH}=\text{CH}_2$); 58.86 (s, benzylic- CH_2 -); 54.04 (s, $-\text{CH}_2$ -(B)); 38.3 (s, $-\text{CH}_2$ -(A)). $^{19}\text{F}\{^1\text{H}\}$ NMR (376.50 MHz, CD_2Cl_2), δ (ppm): -63.07 (s). **HR-MS** (ESI⁺ m/z) [$\text{M}+\text{H}$]⁺: calculated for $[\text{C}_{55}\text{H}_{44}\text{F}_{12}\text{N}_3\text{O}_2\text{P}_2]^+$ 1068.2712; found 1068.2700.

9.5.7. Palladium complexes of Miranphos and Miran2phos ligands. *trans*-[PdCl₂L₂]



General procedure for the synthesis of *trans*-[PdCl₂L₂] of Miranphos and Miran2phos ligands: In an example reaction, 0.38 mmol of the corresponding carboxylic phosphine were dissolved in a mixture of 3 ml of acetonitrile and 1 ml of CH_2Cl_2 . A solution of 0.19 mmol of palladium (II) chloride in 1 ml of acetonitrile was added to the solution of the phosphine and the mixture was stirred at 40 °C for 1 h. After that time, the palladium complex precipitated as a yellow solid. The solution was cooled down to

room temperature and the complex was collected by filtration and washed 3 times with acetonitrile. This procedure worked as described for the *p*-Miranphos, *p*-Miran2phos and *m*-Miran2phos ligands. However the *m*-Miranphos complex showed high solubility in several solvents (CH₂Cl₂, Et₂O, acetone, CH₃CN and ethyl acetate) and could not be precipitated from the reaction mixture. Therefore, the solvent was vacuum evaporated and the yellow solid was recrystallised from CH₂Cl₂/cyclohexane.

Data for *trans*-[PdCl₂(*p*-Miranphos)₂]

³¹P{¹H} NMR (161.98 MHz, acetone-D₆), δ (ppm): 25.50 (s). ¹H NMR (400.13 MHz, acetone-D₆), δ (ppm): 8.16 (d, 4H, H_{C3}{C₆H₄CO₂H}, ³J_{HH} = 8.0 Hz); 7.99 (m, 12H, H_{C2}{C₆H₄CF₃}-H_{C2}{C₆H₄CO₂H}); 7.88 (d, 8H, H_{C3}{C₆H₄CF₃}, ³J_{HH} = 8.0 Hz).

¹⁹F{¹H} NMR (376.50 MHz, acetone-D₆), δ (ppm): -62.54 (s). **HR-MS** (ESI⁺ *m/z*) [M+Na]⁺: calculated for [C₄₂H₂₆Cl₂F₁₂O₄P₂PdNa]⁺ 1082.9419; found 1082.9386. **Elemental analysis**: calculated for C₄₂H₂₆Cl₂F₁₂O₄P₂Pd: C, 47.50; H, 2.47; found: C, 47.04; H, 2.41.

X-ray diffraction data for *trans*-[PdCl₂(*p*-Miranphos)₂]·acetone

Crystals of good quality for X-ray diffraction were obtained by slow evaporation of a saturated solution of the complex in a mixture of acetone/n-hexane. The structure was solved by Direct methods. All non-hydrogen atoms were refined with anisotropic displacement thermal parameters. All hydrogen atoms were idealised and were positioned geometrically and refined using the riding model with U_{iso}(H) = 1.2 U_{eq}(C) for those attached to carbon and with U_{iso}(H) = 1.2 U_{eq}(O) for those of the OH group. The hydrogen atoms of the acetone molecule were also idealised and positioned geometrically but refined using the riding model with U_{iso}(H) = 1.5 U_{eq}(C). All the CF₃ groups were disordered over two different orientations in the following approximate ratios: C(17) 62.0 and 38.0 %; C(27) 53.0 and 47.0 %; C(47) 53.7 and 46.3 %; C(57) 63.0 and 37.0 %. The following bond length and angle restraints (DFIX) were applied: C-F distance = 1.33(2); C_{ipso}-F distance = 2.35 (4). Moreover, F-F distances of the disordered F atoms were restrained to be equal within sd of 0.03 (with SADI command) and the U_{ij} were restrained with SIMU instruction. All disordered atoms were refined anisotropically and the sum of the site occupation factors was restrained to 1.000.

Crystal data trans-[PdCl₂(p-Miranphos)₂]·acetone

Chemical formula	C ₄₅ H ₃₂ F ₁₂ O ₅ P ₂ Pd	a	15.3938(7)
Molecular weight	1119.94	b	15.6175(8)
Space group	Monoclinic, P 21/c	c	20.4211(10)
wavelength	0.71073 (Mo K α)	α	90
Temperature	293(2) K	β	97.1070(10)
Volume	4871.8(4) Å ³	γ	90
Z	4	R[I>2 σ (I)]	0.0464
		S	1.0280

Data for *trans*-[PdCl₂(*m*-Miranphos)₂]

³¹P{¹H} NMR (161.98 MHz, acetone-D₆), δ (ppm): 26.37 (s). ¹H NMR (400.13 MHz, acetone-D₆), δ (ppm): 8.43 (m, 2H, H_{C2}{C₆H₄CF₃}); 8.25 (d, 2H, H_{C4}{C₆H₄CO₂H}, ³J_{HH} = 7.8 Hz); 8.15 (m, 6H, H_{C2}{C₆H₄CF₃}-H_{C6}{C₆H₄CO₂H}); 8.02 (*pseudo*-q, 4H, H_{C6}{C₆H₄CF₃}, ³J_{HH} = 7.7, ³J_{HP} = 6.0 Hz); 7.95 (d, 4H, H_{C4}{C₆H₄CF₃}, ³J_{HH} = 7.5 Hz); 7.79 (t, 4H, H_{C5}{C₆H₄CF₃}, ³J_{HH} = 7.5 Hz); 7.73 (t, 2H, H_{C5}{C₆H₄CO₂H}, ³J_{HH} = 7.8 Hz). ¹⁹F{¹H} NMR (376.50 MHz, acetone-D₆), δ (ppm): -62.26 (s). **HR-MS** (ESI⁺ *m/z*) [M+Na]⁺: calculated for [C₄₂H₂₆Cl₂F₁₂O₄P₂PdNa]⁺ 1082.9419; found 1082.9376. **Elemental analysis**: calculated for C₄₂H₂₆Cl₂F₁₂O₄P₂Pd: C, 47.50; H, 2.47; found: C, 47.32; H, 2.81.

X-ray diffraction data for *trans*-[PdCl₂(*m*-Miranphos)₂]

Crystals of good quality for X-ray diffraction were obtained by slow diffusion of *n*-hexane into a solution of the complex in CH₂Cl₂. The structure was solved by direct methods. All non-hydrogen atoms were refined with anisotropic displacement thermal parameters. All hydrogen atoms were idealised and were positioned geometrically and refined using the riding model with U_{iso}(H) = 1.2 U_{eq}(C) for those attached to carbon and with U_{iso}(H) = 1.2 U_{eq}(O) for those of the OH group. Two of the CF₃ groups were disordered, C(47) and C(57). C(47) was refined over two different orientations with the F atoms defined anisotropically in approximately 54.6 and 45.4 % ratios. C(57) was refined over 3 different orientations with the F atoms defined isotropically in approximately 40.4, 28.6 and 30.9 % ratio. In both cases the following bond length and angle restraints (DFIX) were applied: C-F distance = 1.33(2); C_{ipso}-F distance = 2.35 (4).

Moreover, F-F distances of the disordered F atoms were restrained to be equal within sd of 0.03 (with SADI command) and the sum of the site occupation factors was restrained to 1.000. No restraints were imposed in the non-disordered CF₃ groups.

Crystal data trans-[PdCl₂(m-Miranphos)₂]

Chemical formula	C ₄₂ H ₂₆ F ₁₂ O ₄ P ₂ Pd	a	10.1026(5)
Molecular weight	1061.87	b	27.1594(13)
Space group	Orthorhombic, P bca	c	36.7299(17)
wavelength	0.71073 (Mo K α)	α	90
Temperature	293(2) K	β	90
Volume	10078.0(8) Å ³	γ	90
Z	8	R[I>2 σ (I)]	0.0847
		S	1.0320

Data for *trans*-[PdCl₂(*p*-Miran2phos)₂]

³¹P{¹H} NMR (161.98 MHz, acetone-D6), δ (ppm): 25.61 (s). ¹H NMR (400.13 MHz, acetone-D6), δ (ppm): 8.16 (d, 8H, H_{C3}{C₆H₄CO₂H}, ³J_{HH} = 8.2 Hz); 7.95 (m, 12H, H_{C2}{C₆H₄CF₃}-H_{C2}{C₆H₄CO₂H}); 7.87 (d, 4H, H_{C3}{C₆H₄CF₃}, ³J_{HH} = 8.0 Hz). ¹⁹F{¹H} NMR (376.50 MHz, acetone-D6), δ (ppm): -62.49 (s). **HR-MS** (ESI⁺ *m/z*) [M+Na]⁺: calculated for [C₄₂H₂₈Cl₂F₆O₈P₂PdNa]⁺ 1034.9468; found 1034.9443. **Elemental analysis**: calculated for C₄₂H₂₈Cl₂F₆O₈P₂Pd: C, 49.75; H, 2.78; found: C, 49.19; H, 2.67.

Data for *trans*-[PdCl₂(*m*-Miran2phos)₂]

³¹P{¹H} NMR (161.98 MHz, acetone-D6), δ (ppm): 26.35 (s). ¹H NMR (400.13 MHz, acetone-D6), δ (ppm): 8.44 (*bt*, 4H, H_{C2}{C₆H₄CF₃}, ³J_{HH} = ³J_{HP} = 5.7 Hz); 8.24 (*bd*, 4H, H_{C4}{C₆H₄CO₂H}, ³J_{HH} = 7.6 Hz); 8.13 (m, 6H, H_{C2}{C₆H₄CF₃}-H_{C6}{C₆H₄CO₂H}); 8.03 (*pseudo-q*, 2H, H_{C6}{C₆H₄CF₃}, ³J_{HH} = 7.9 Hz, ³J_{HP} = ⁵J_{HP} = 5.9 Hz); 7.93 (d, 2H, H_{C4}{C₆H₄CF₃}, ³J_{HH} = 7.8 Hz); 7.79 (t, 2H, H_{C5}{C₆H₄CF₃}, ³J_{HH} = 7.8 Hz); 7.73 (t, 4H, H_{C5}{C₆H₄CO₂H}, ³J_{HH} = 7.8 Hz). ¹⁹F{¹H} NMR (376.50 MHz, acetone-D6), δ (ppm): -62.19 (s). **HR-MS** (ESI⁺ *m/z*) [M+Na]⁺: calculated for [C₄₂H₂₈Cl₂F₆O₈P₂PdNa]⁺ 1034.9468; found 1034.9425. **Elemental analysis**: calculated for C₄₂H₂₈Cl₂F₆O₈P₂Pd: C, 49.75; H, 2.78; found: C, 49.67; H, 2.70.

Supporting Information

Hydrolysis of the Trifluoromethyl Group in Triarylphosphines: Scope of the Reaction in the Preparation of Carboxylic-Trifluoromethylated Phosphines and their Applications

Daniel Herrera Miranda

Tesi Doctoral

Programa de Doctorat en Química

Prof. Joan Carles Bayón Rueda

Departament de Química

Facultat de Ciències

2018

Table of contents

1. Characterisation of trifluoromethylated phosphines, phosphine oxides and intermediates

1.1. Homoleptic phosphines

Tris(4-trifluoromethylphenyl)phosphine (1)	1
Tris(3-trifluoromethylphenyl)phosphine (5)	3
Tris(2-trifluoromethylphenyl)phosphine (9)	6
Tris(2-trifluoromethylphenyl)phosphine oxide (ox-9)	10

1.2. Heteroleptic phosphines

(3,5-bis(trifluoromethyl)phenyl)bis(3-(trifluoromethyl)phenyl)phosphine (15)	14
Bis(3,5-bis(trifluoromethyl)phenyl)(3-(trifluoromethyl)phenyl)phosphine (18)	18
(3,5-bis(trifluoromethyl)phenyl)bis(4-(trifluoromethyl)phenyl)phosphine (20)	21
Bis(3,5-bis(trifluoromethyl)phenyl)(4-(trifluoromethyl)phenyl)phosphine (23)	25

1.3. Chlorophosphines

<i>N,N</i> -diethylphosphoramidous dichloride (Et_2NPCl_2)	29
<i>N,N,N',N'</i> -tetraethylphosphorodiamidous chloride ($(\text{Et}_2\text{N})_2\text{PCl}$)	30
Bis(3,5-bis(trifluoromethyl)phenyl)chlorophosphine (26)	32
(3,5-bis(trifluoromethyl)phenyl)dichlorophosphine (27)	33

2. Characterisation of carboxylic-trifluoromethylated phosphines

2.1. Derived from homoleptic phosphines

4-(bis(4-(trifluoromethyl)phenyl)phosphanyl)benzoic acid, <i>p</i> -Miranphos (2)	34
4,4'-((4-(trifluoromethyl)phenyl)phosphanediyl)dibenzoic acid, <i>p</i> -Miran2phos (3)	39
3-(bis(3-(trifluoromethyl)phenyl)phosphanyl)benzoic acid, <i>m</i> -Miranphos (6)	42
3,3'-((3-(trifluoromethyl)phenyl)phosphanediyl)dibenzoic acid, <i>m</i> -Miran2phos (7)	46
3,3',3''-phosphanetriyltribenzoic acid (8)	50
2-(bis(2-(trifluoromethyl)phenyl)phosphanyl)benzoic acid, <i>o</i> -Miranphos (10)	54

2.2. Derived from heteroleptic phosphines

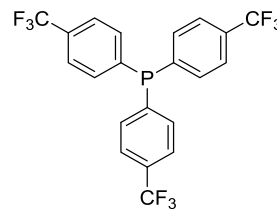
3-(bis(3,5-bis(trifluoromethyl)phenyl)phosphanyl)benzoic acid (19)	60
3-((3,5-bis(trifluoromethyl)phenyl)(3-(trifluoromethyl)phenyl)phosphanyl)benzoic acid (16)	64

3,3'-((3,5-bis(trifluoromethyl)phenyl)phosphanediyldibenzoic acid (17)	68
3. Characterisation of spirocyclic oxyphosphoranes	
1-(2-(trifluoromethyl)phenyl)-1 λ^5 -1,1'-spirobi[benzo[<i>c</i>][1,2]oxaphosphole]-3,3'(1 <i>H</i>)-dione (12)	73
(2-(3,3'-dioxo-1,3,3'-trihydro-1 λ^5 -1,1'-spirobi[benzo[<i>c</i>][1,2]oxaphosphol]-1-yl)benzaldehyde) (13)	79
4. Characterisation of trifluoromethylated diphosphines 30 and 31 and intermediate compounds	
1,2-dibromo-4-(trifluoromethyl)benzene (33)	85
Bromophosphines 28. Mixture of isomers	87
(4-(Trifluoromethyl)-1,2-phenylene)bis(diphenylphosphine) (30)	91
Bromophosphines 29. Mixture of isomers	95
(4-(Trifluoromethyl)-1,2-phenylene)bis(bis(3,5-bis(trifluoromethyl)phenyl)-phosphine) (31)	98
5. Characterisation of trifluoromethylated diphosphine 32 and intermediate compounds	
1-Bromo-2-iodo-4-(trifluoromethyl)benzene (34)	103
Bis(3,5-bis(trifluoromethyl)phenyl)(2-bromo-5-(trifluoromethyl)phenyl)-phosphine (<i>m</i> 29)	106
Bis(3,5-bis(trifluoromethyl)phenyl)(2-bromo-5-(trifluoromethyl)phenyl)-phosphine oxide (<i>ox-m</i> 29)	110
4,4'-bis(trifluoromethyl)-[1,1'-biphenyl]-2,2'-diylbis(bis(3,5-bis(trifluoromethyl)phenyl)phosphine oxide (<i>ox-32</i>)	114
4,4'-bis(trifluoromethyl)-[1,1'-biphenyl]-2,2'-diylbis(bis(3,5-bis(trifluoromethyl)-phenyl)phosphine (32)	119
4,4'-bis(trifluoromethyl)-1,1'-biphenyl (35)	124
2,2'-dibromo-4,4'-bis(trifluoromethyl)-1,1'-biphenyl (36)	127
6. Characterisation of diphosphines P-bz, M-bz, P-st, M-st and intermediate compounds	
<i>N,N</i> -bis(2-phthalimidoethyl)amine (38)	129
Benzyl-bis(2-phthalimidoethyl)amine (39-bz)	131
4-benzyl-diethylenetriamine (40-bz)	132

Diphosphine-diamide P-bz	134
Diphosphine-diamide M-bz	140
(4-Vinylbenzyl)-bis(2-phthalimidoethyl)amine (39-st)	146
4-(4-Vinylbenzyl)diethylenetriamine (40-st)	147
Diphosphine-diamide P-st	149
Diphosphine-diamide M-st	154
7. Characterisation of metal complexes	
7.1. Vaska-type compounds <i>trans</i>-[Ir(CO)Cl(L)₂]	
L = triphenylphosphine	160
L = tris(3-trifluoromethylphenyl)phosphine	163
L = Bis(3,5-bis(trifluoromethyl)phenyl)(3-(trifluoromethyl)phenyl)phosphine	166
L = (3,5-bis(trifluoromethyl)phenyl)bis(4-(trifluoromethyl)phenyl)phosphine	169
L = Bis(3,5-bis(trifluoromethyl)phenyl)(4-(trifluoromethyl)phenyl)phosphine	172
7.2. Pd complexes <i>trans</i>-[PdCl₂L₂]	
L = <i>p</i> -Miranphos	176
L = <i>m</i> -Miranphos	178
L = <i>p</i> -Miran2phos	181
L = <i>m</i> -Miran2phos	183
8. X-ray diffraction data. CIF files	
8.1. (3,5-bis(trifluoromethyl)phenyl)bis(4-(trifluoromethyl)phenyl)phosphine (20)	186
8.2. <i>o</i> -Miranphos (10)	194
8.3. Spirocyclic oxyphosphorane 13	201
8.4. Phosphine <i>p</i> 28	208
8.5. Diphosphine 31	215
8.6. <i>trans</i> -[PdCl ₂ (<i>p</i> -Miranphos) ₂]·acetone	228
8.7. <i>trans</i> -[PdCl ₂ (<i>m</i> -Miranphos) ₂]	241

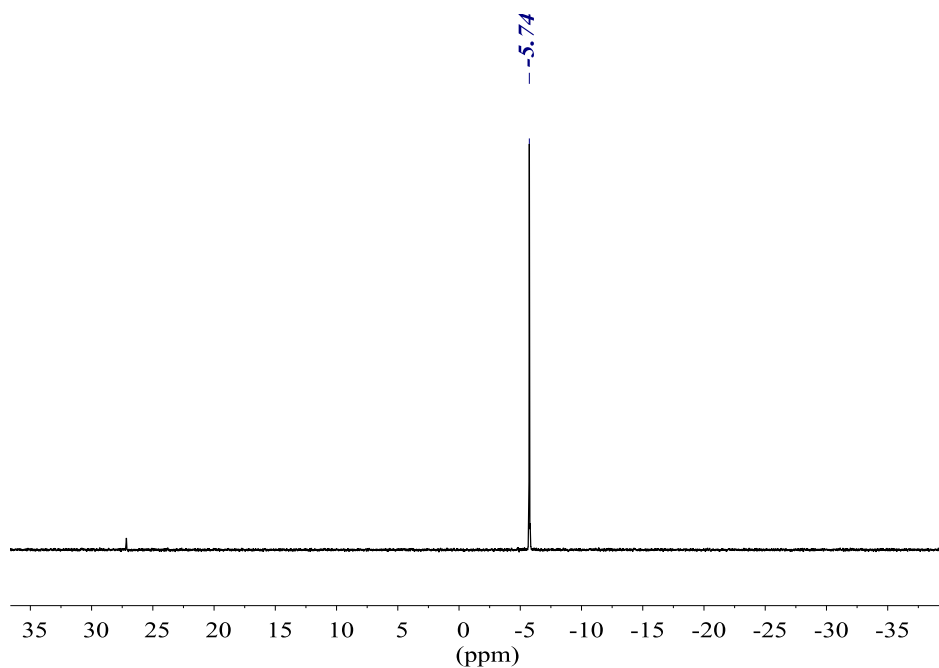
1. Characterisation of trifluoromethylated phosphines, phosphine oxides and intermediates

1.1. Homoleptic phosphines

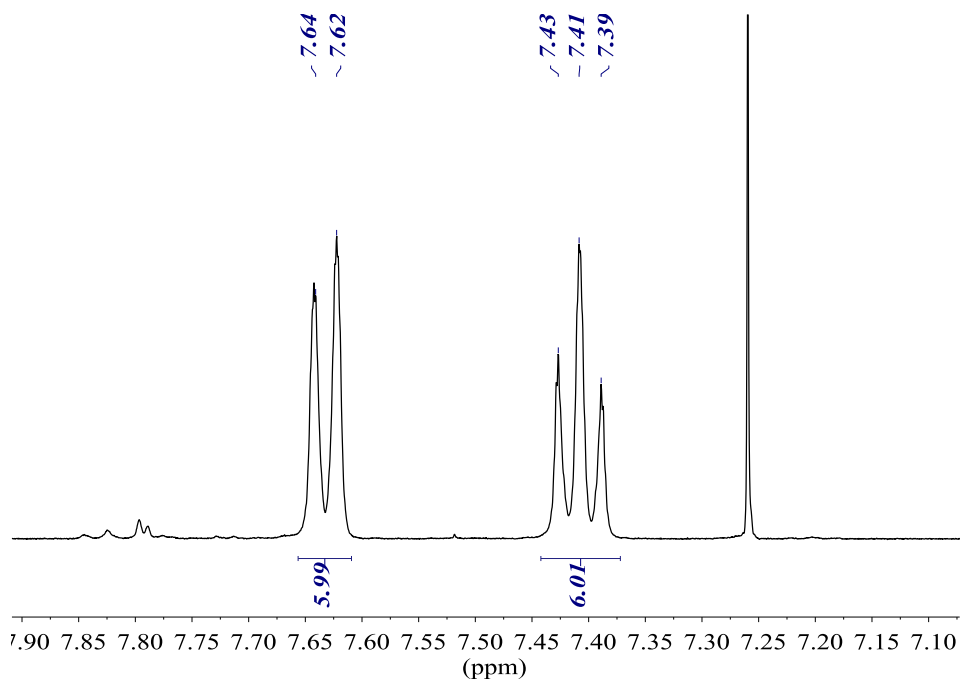


Tris(4-trifluoromethylphenyl)phosphine (1)

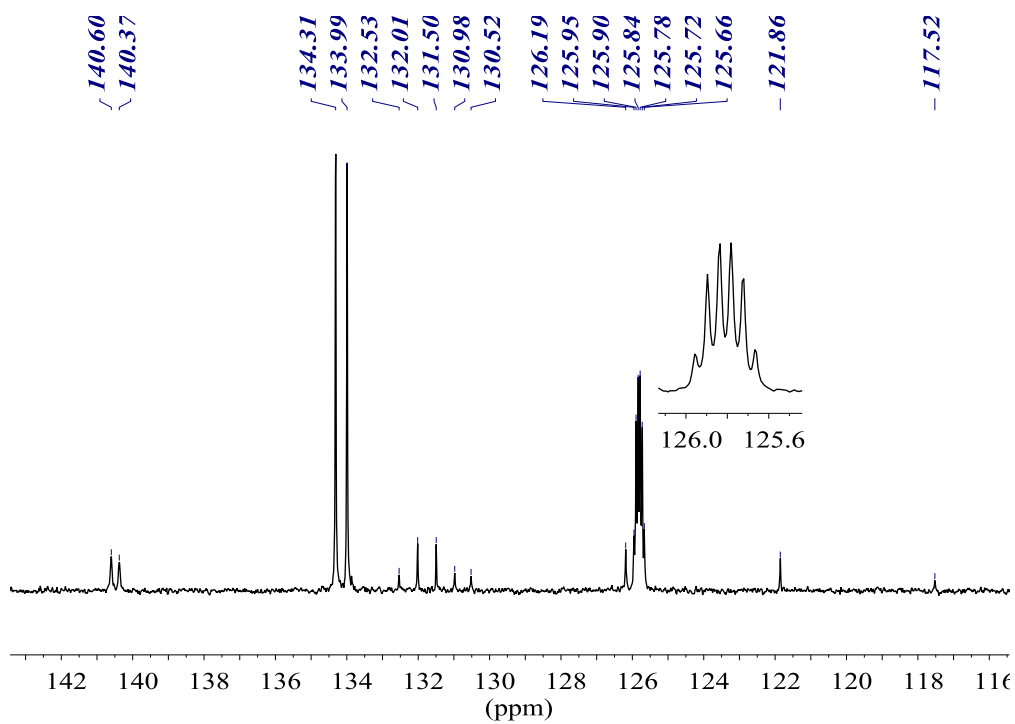
$^{31}\text{P}\{^1\text{H}\}$ NMR (161.98 MHz, CDCl_3)



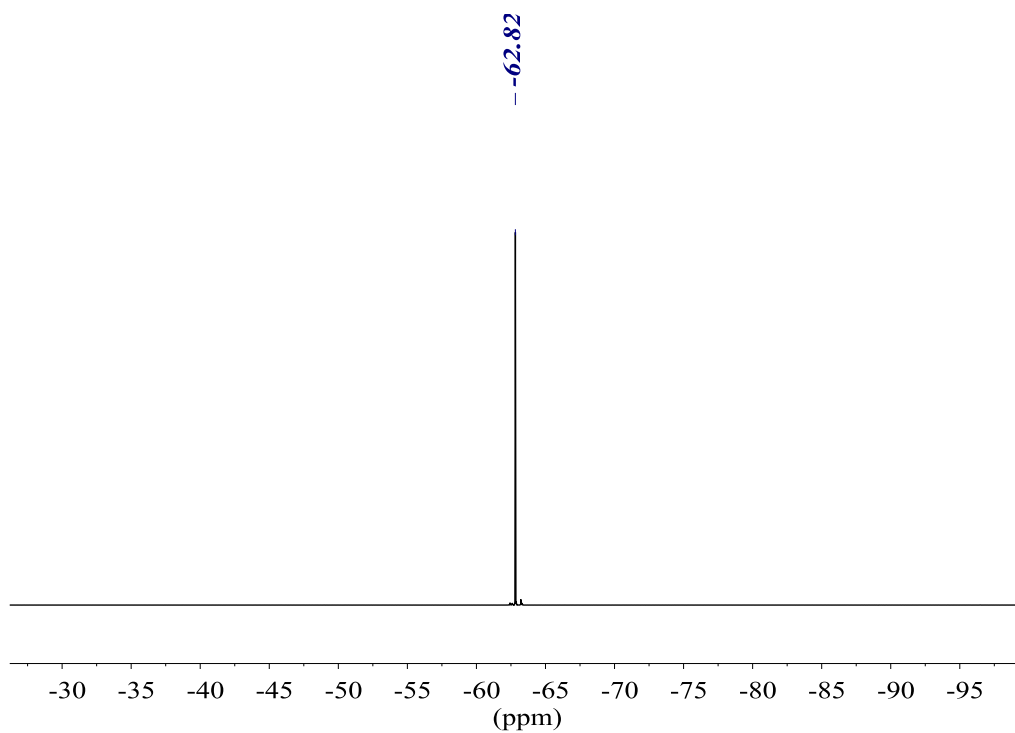
^1H NMR (400.13 MHz, CDCl_3)



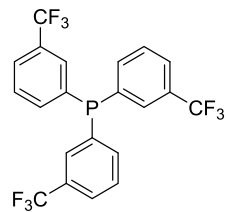
$^{13}\text{C}\{^1\text{H}\}$ NMR (62.90 MHz, CDCl_3)



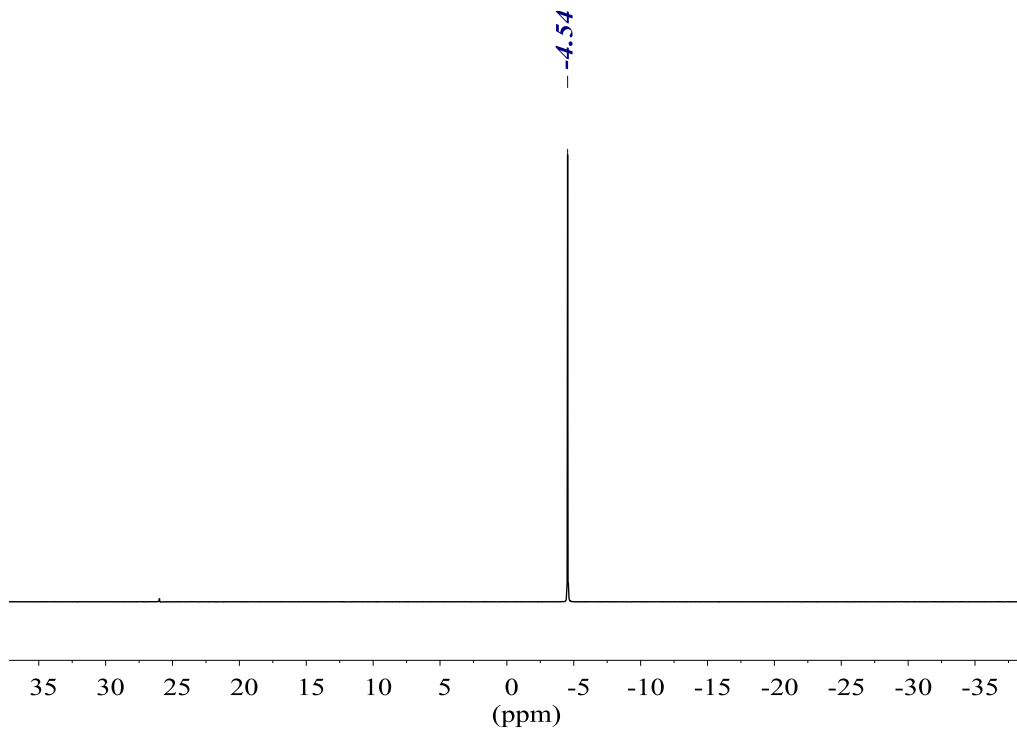
$^{19}\text{F}\{^1\text{H}\}$ NMR (376.50 MHz, CDCl_3)



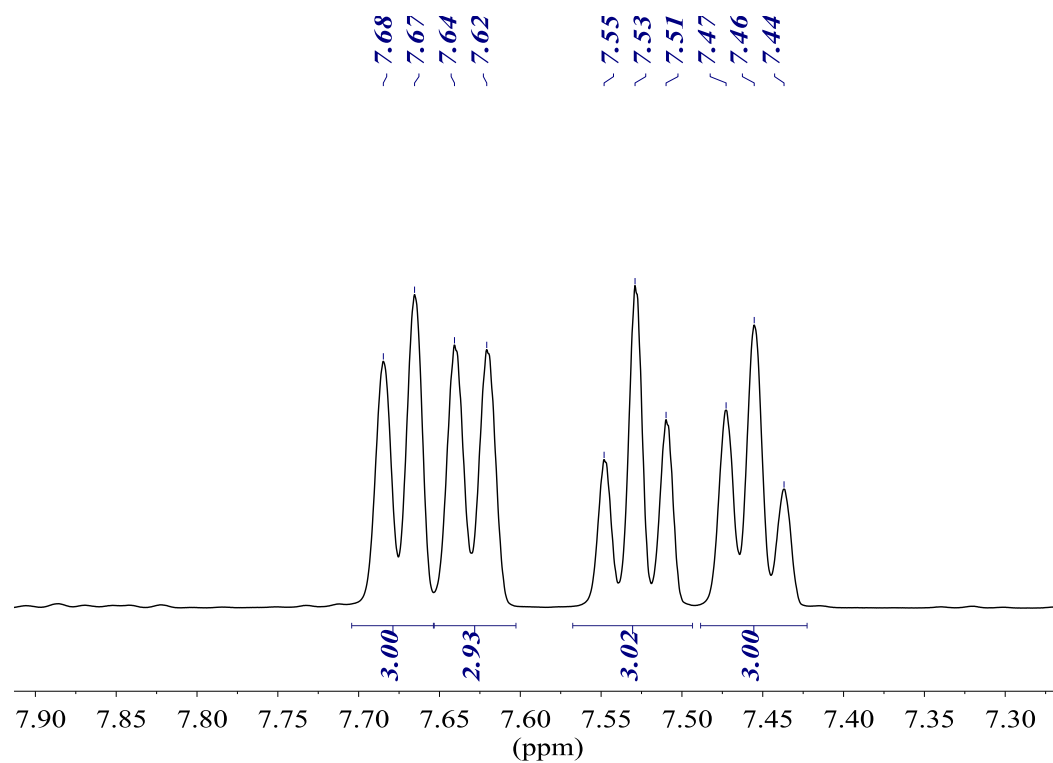
Tris(3-trifluoromethylphenyl)phosphine (5)



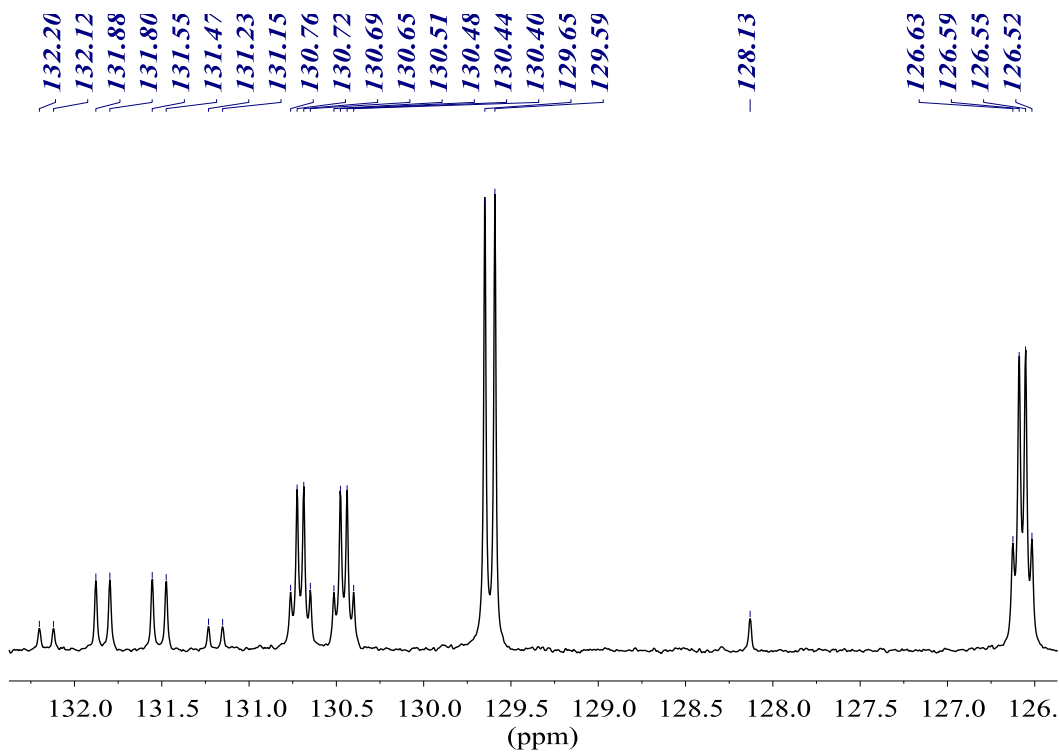
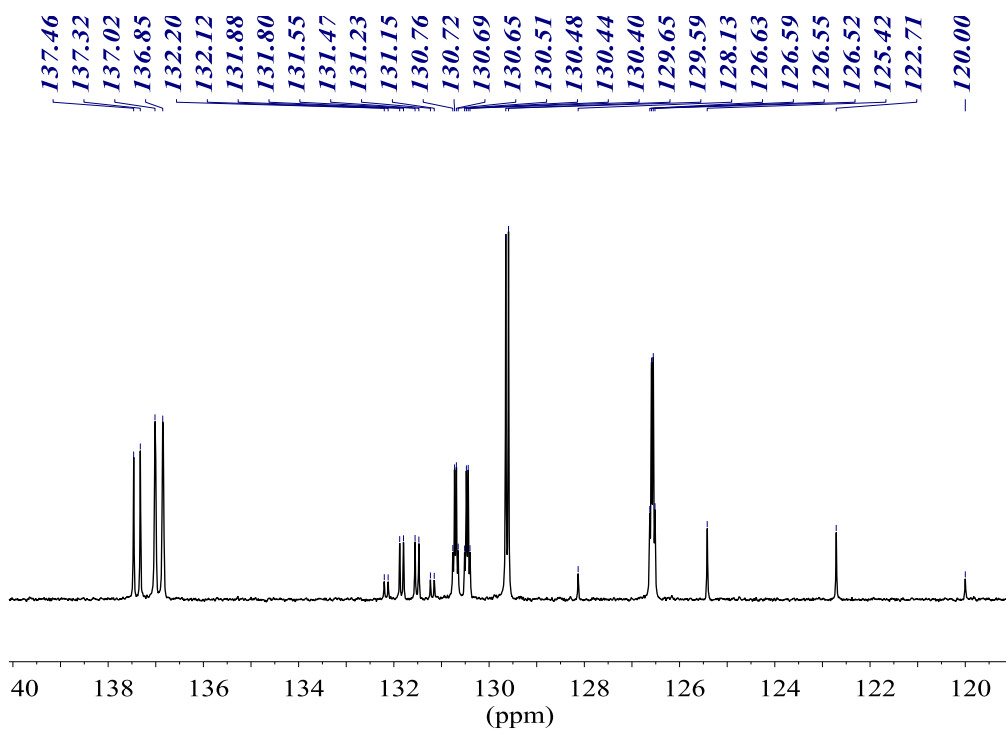
$^{31}\text{P}\{^1\text{H}\}$ NMR (161.98 MHz, CDCl_3)



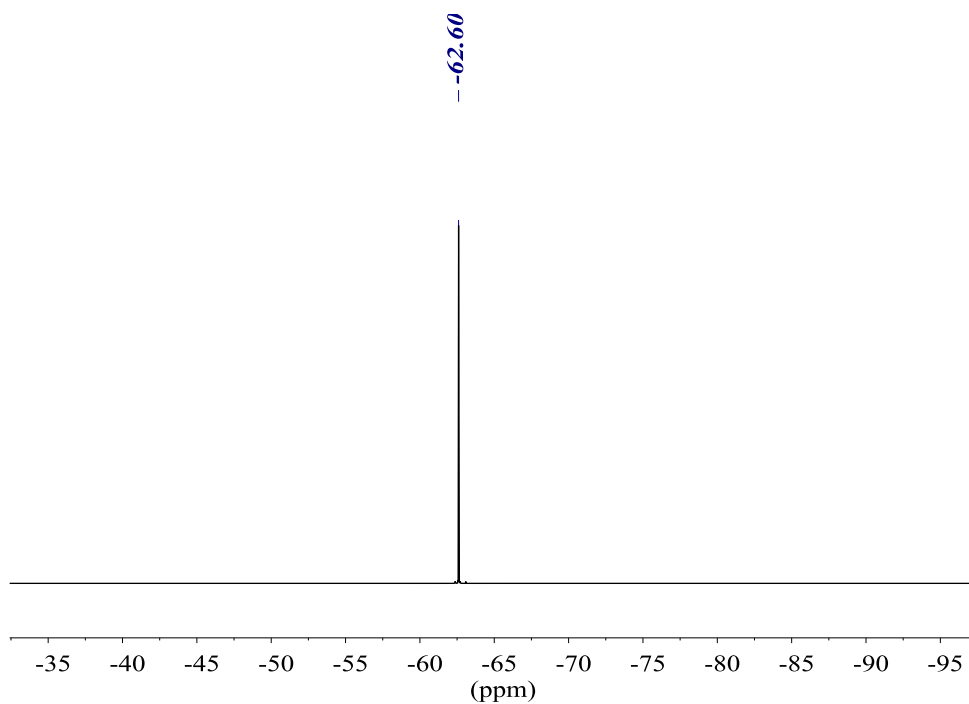
^1H NMR (400.13 MHz, CDCl_3)



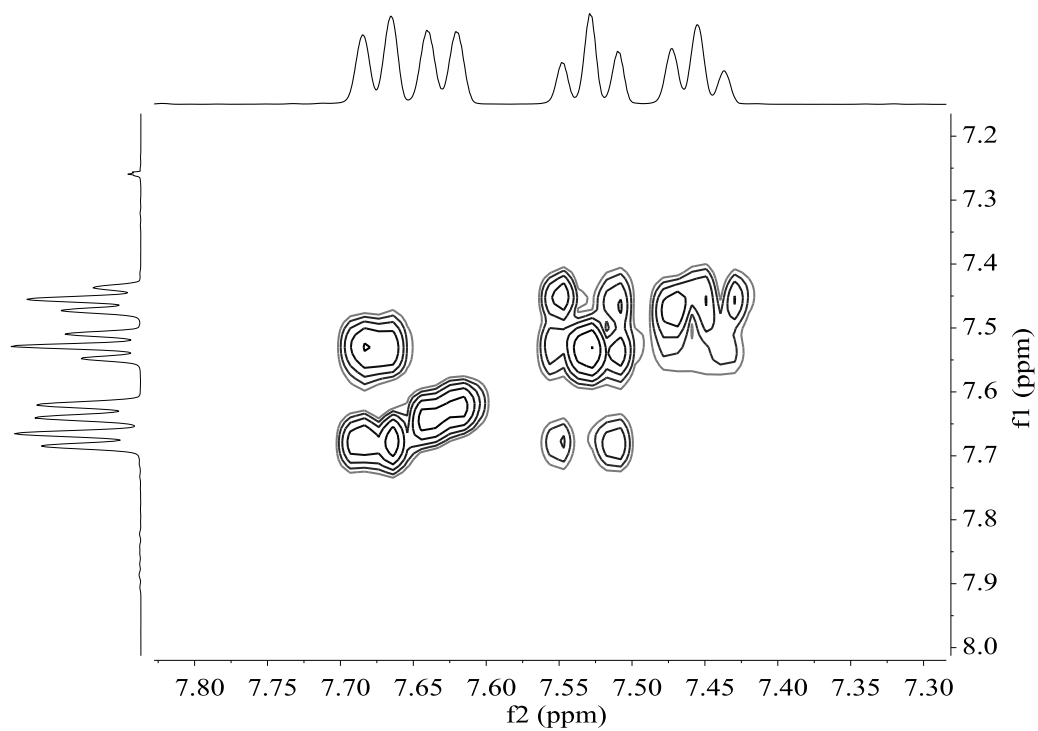
$^{13}\text{C}\{^1\text{H}\}$ NMR (100.61 MHz, CDCl_3)



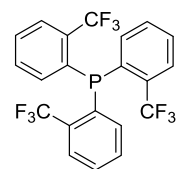
$^{19}\text{F}\{^1\text{H}\}$ NMR (376.50 MHz, CDCl_3)



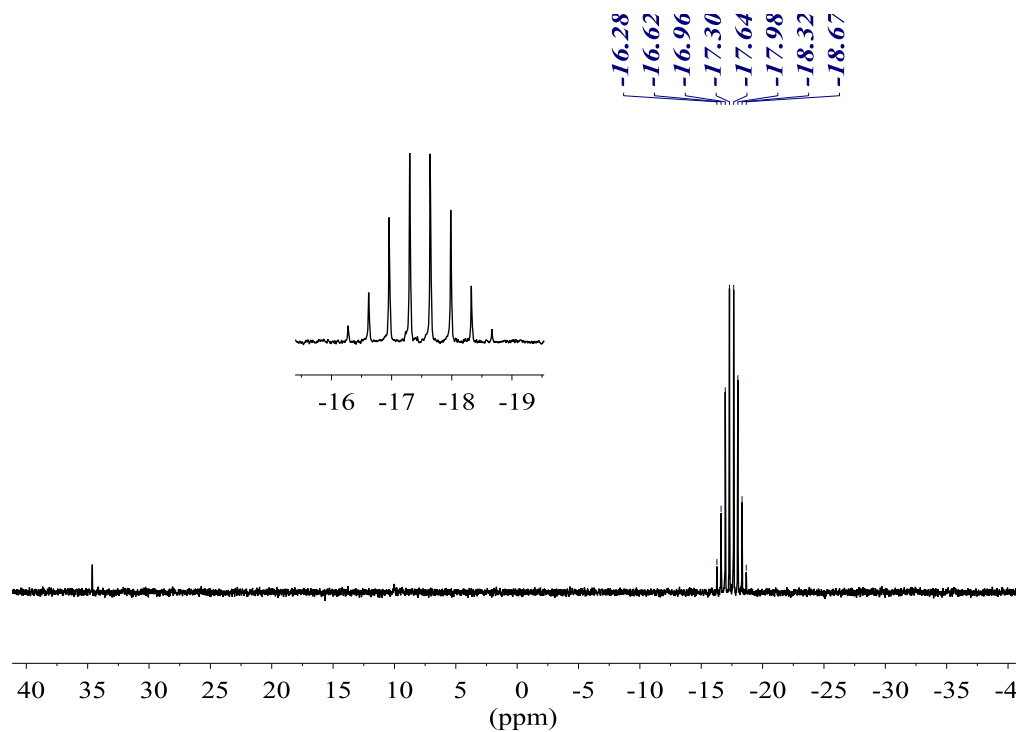
COSY NMR (400.13 MHz, CDCl_3)



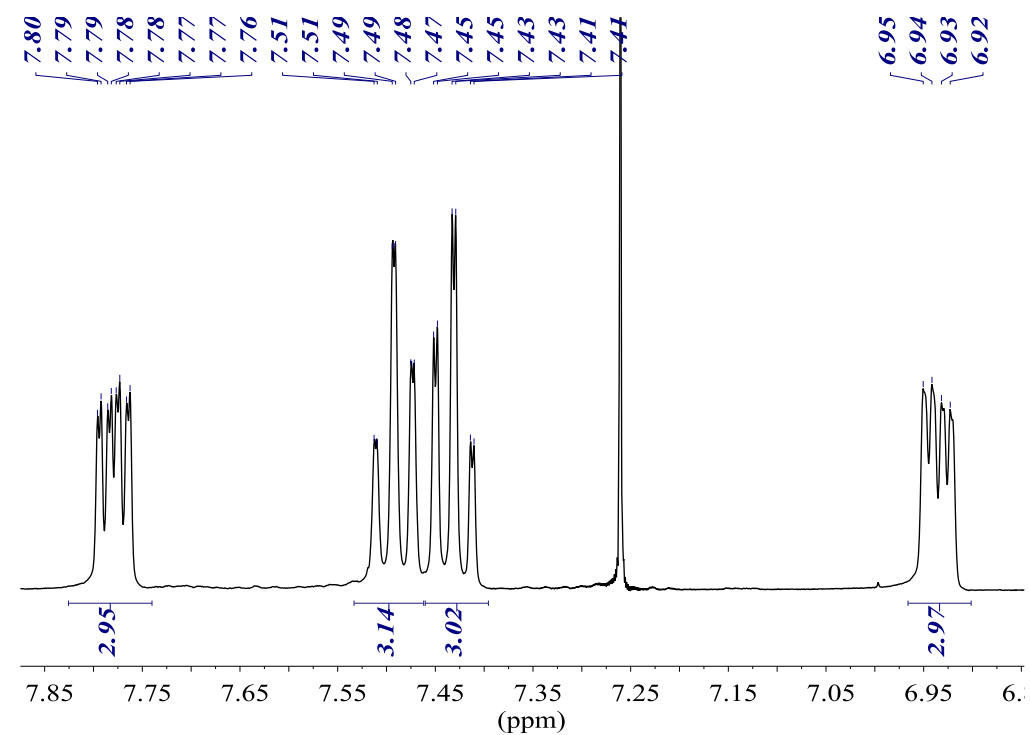
Tris(2-trifluoromethylphenyl)phosphine (9)

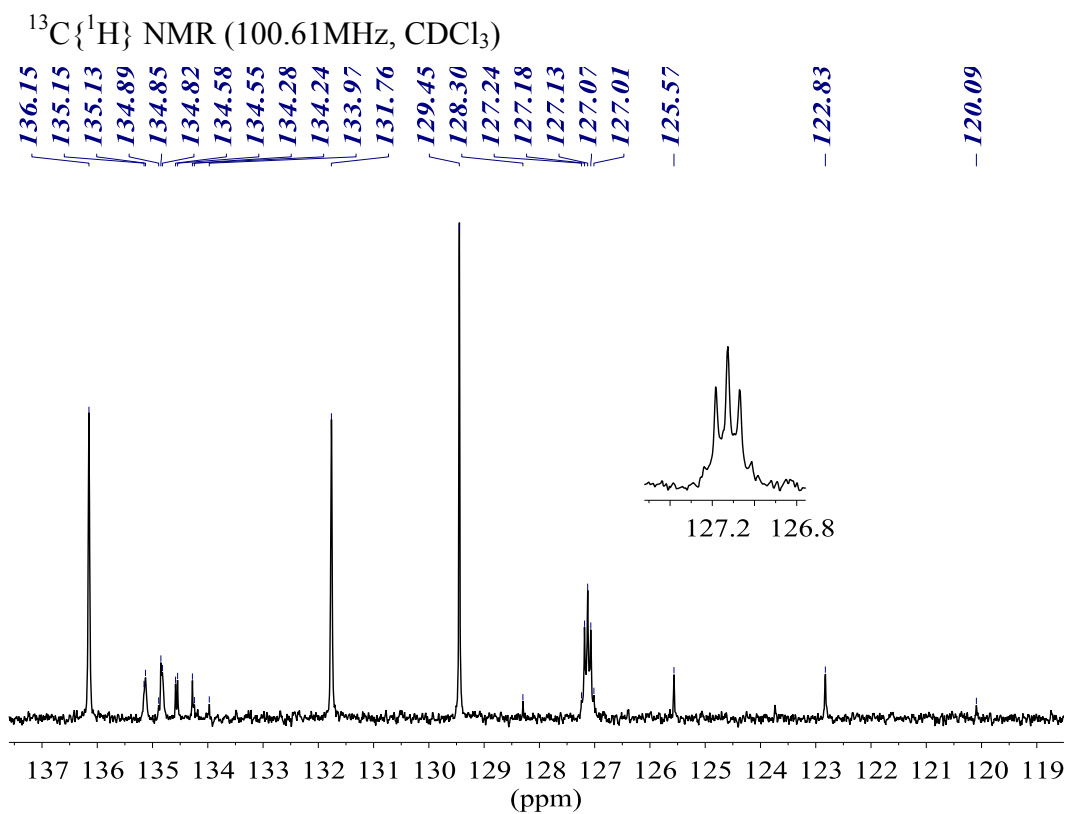
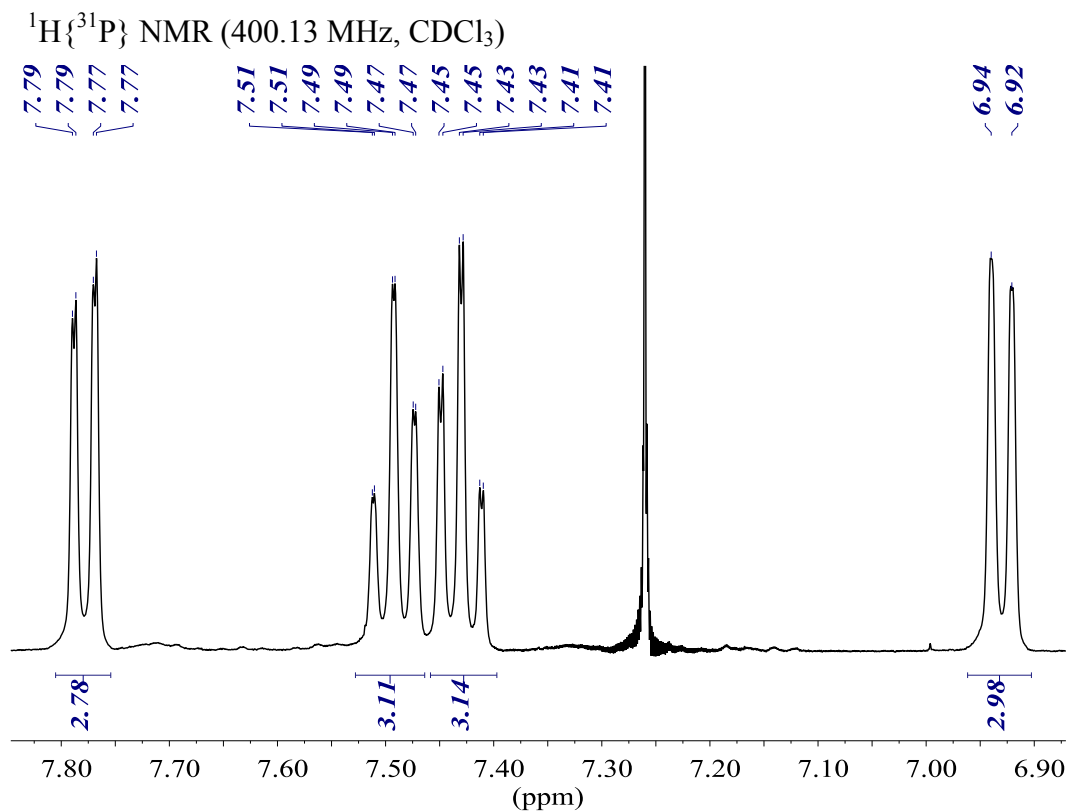


$^{31}\text{P}\{^1\text{H}\}$ NMR (161.98 MHz, CDCl_3)

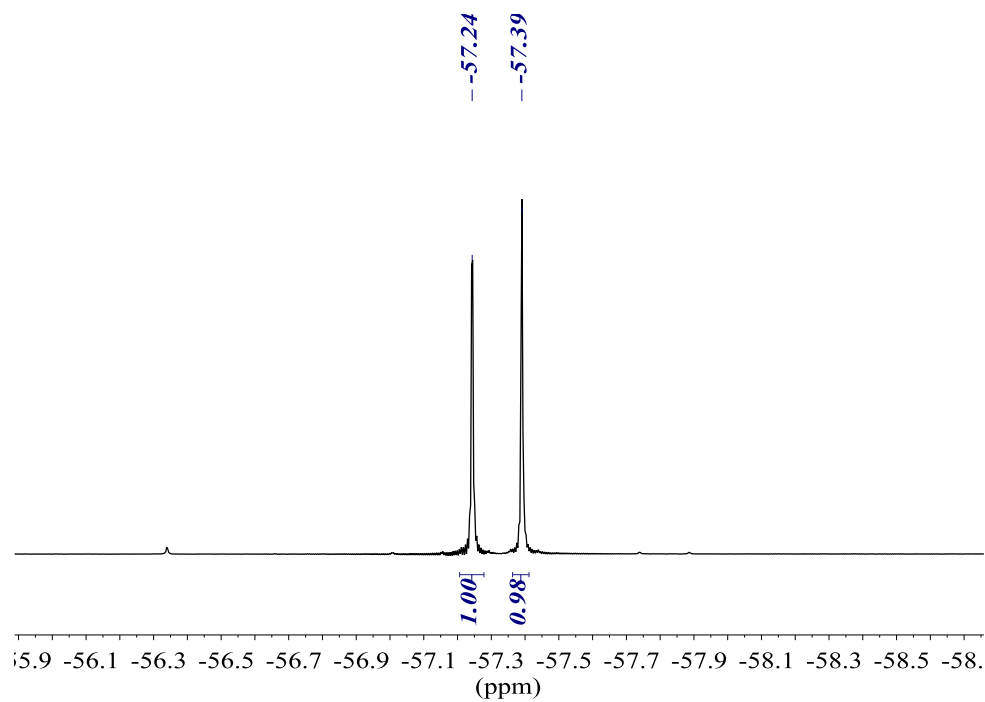


^1H NMR (400.13 MHz, CDCl_3)

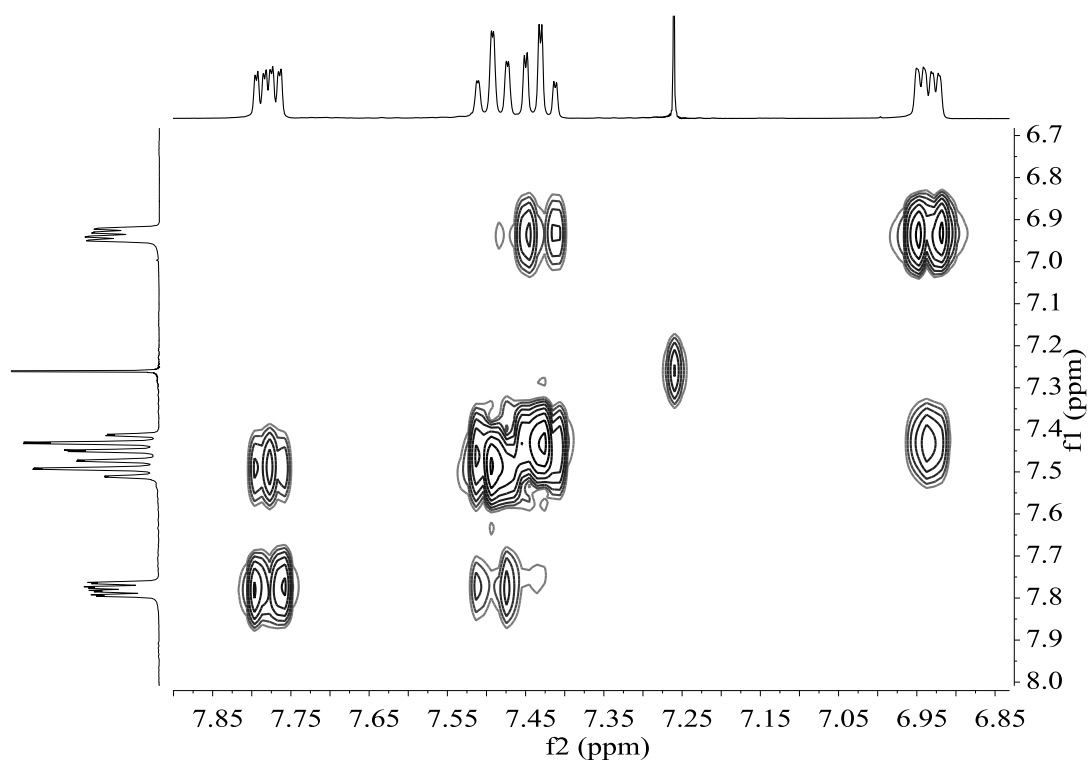




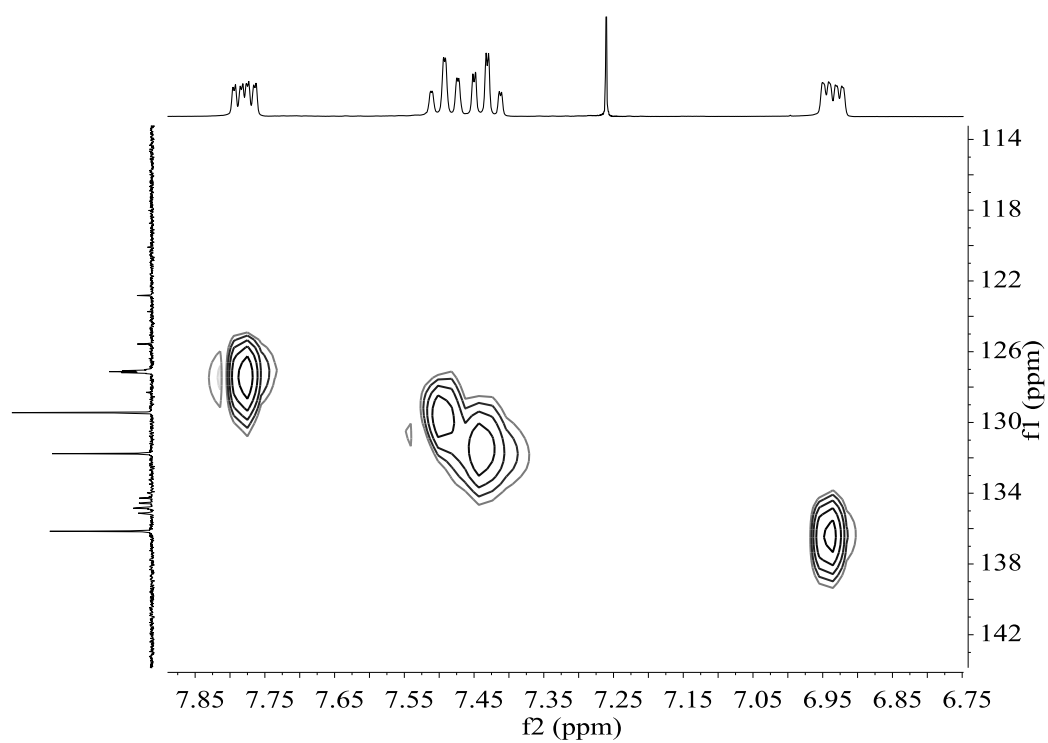
$^{19}\text{F}\{^1\text{H}\}$ NMR (376.50 MHz, CDCl_3)



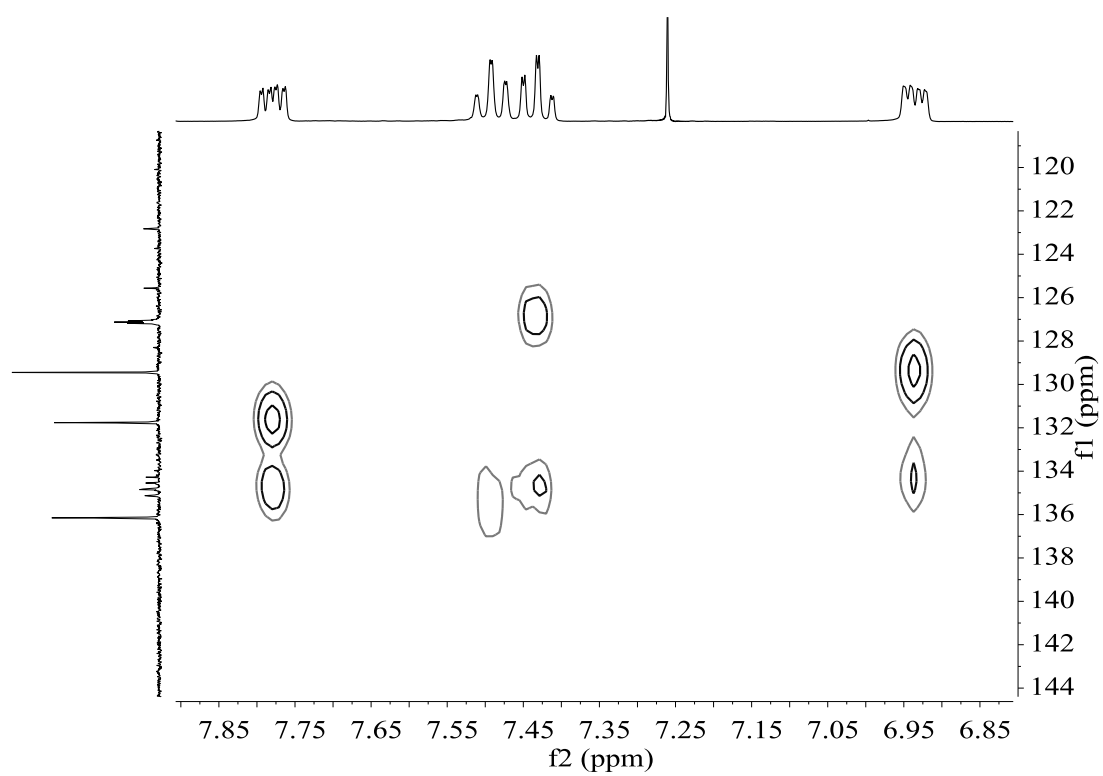
COSY NMR (400.13 MHz, CDCl_3)



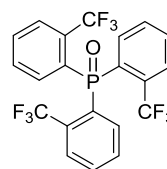
HSQC NMR (400.13 MHz, CDCl₃)



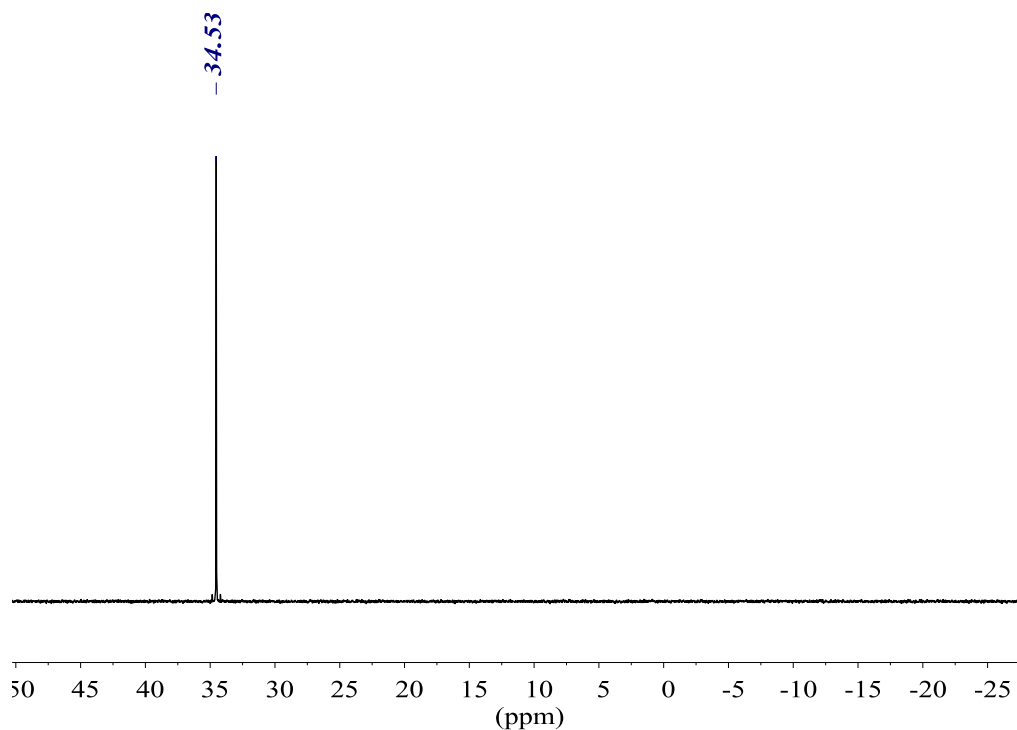
HMBC NMR (400.13 MHz, CDCl₃)



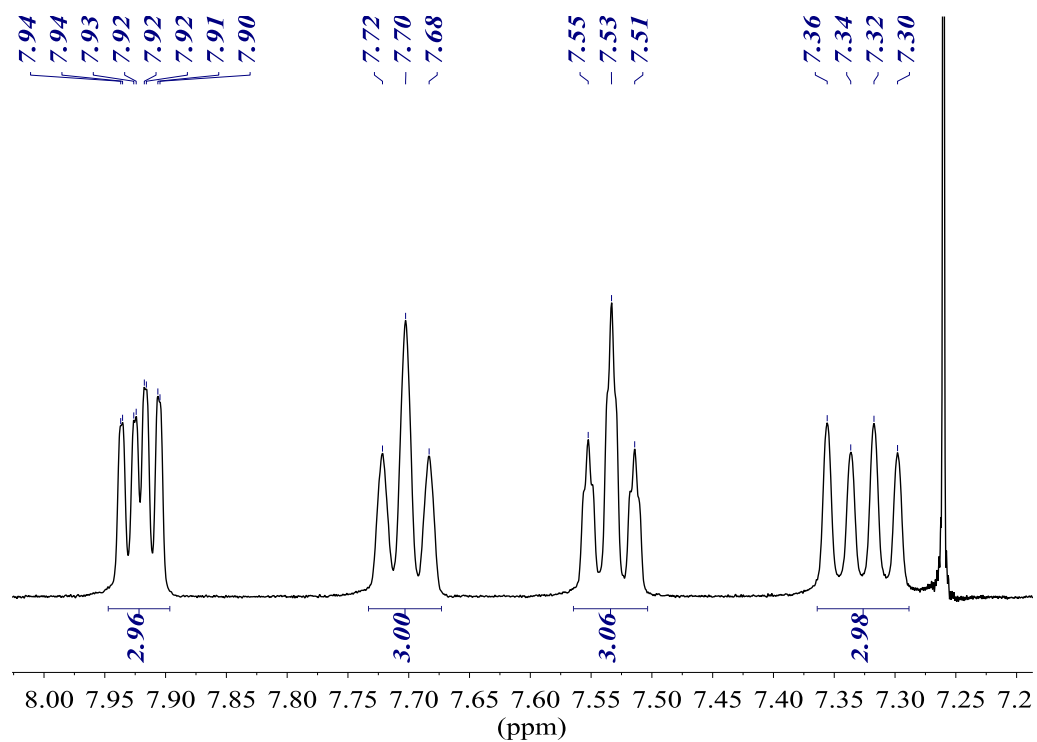
Tris(2-trifluoromethylphenyl)phosphine oxide (ox-9)



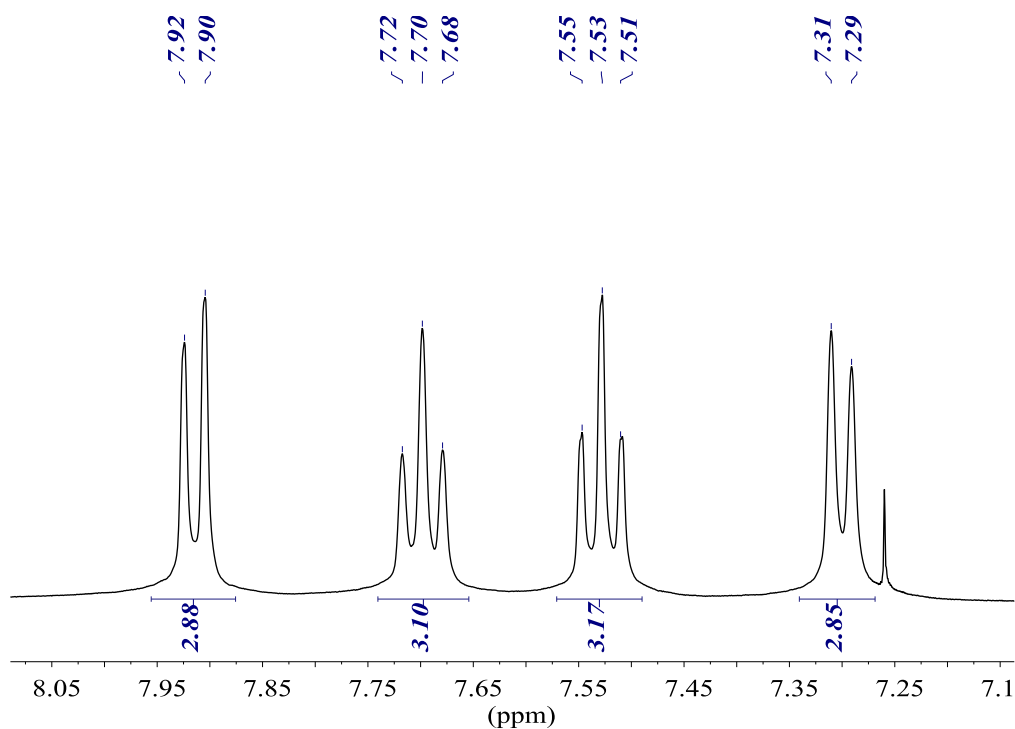
$^{31}\text{P}\{^1\text{H}\}$ NMR (161.98 MHz, CDCl_3)



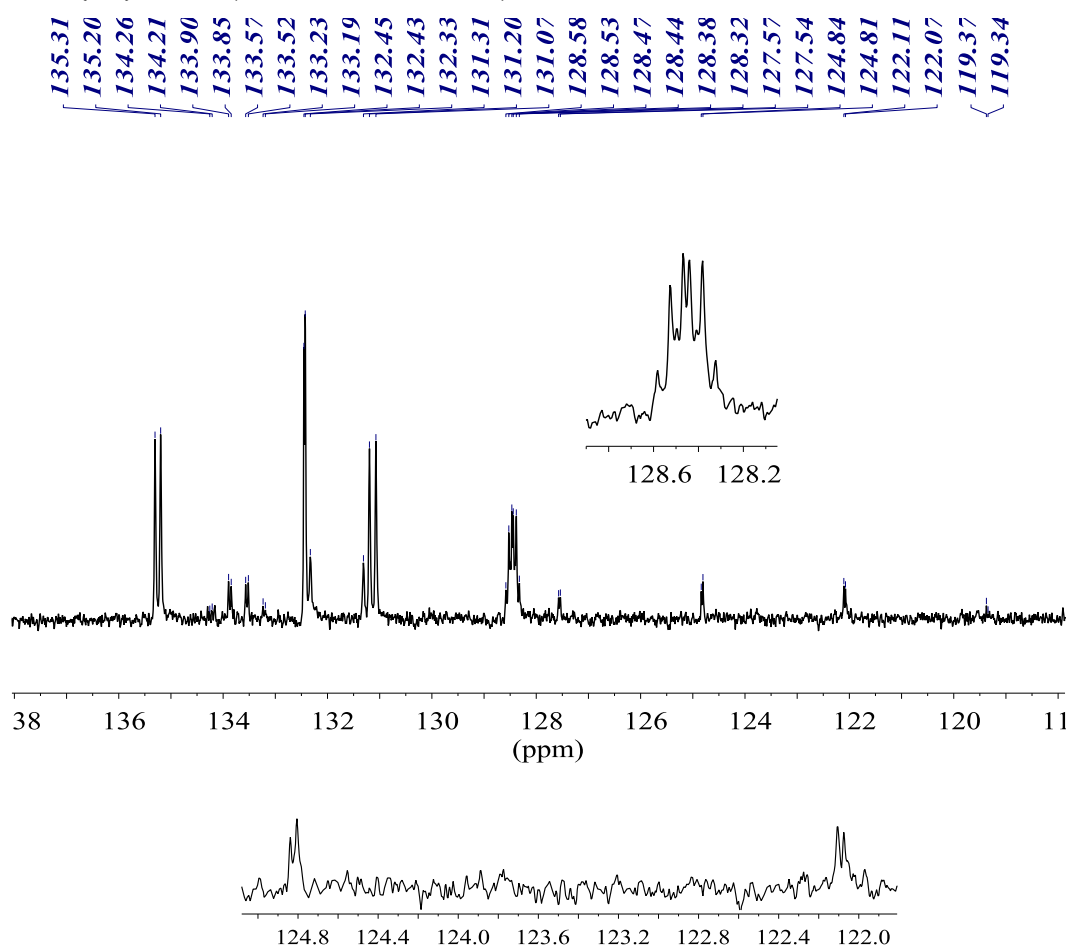
^1H NMR (400.13 MHz, CDCl_3)



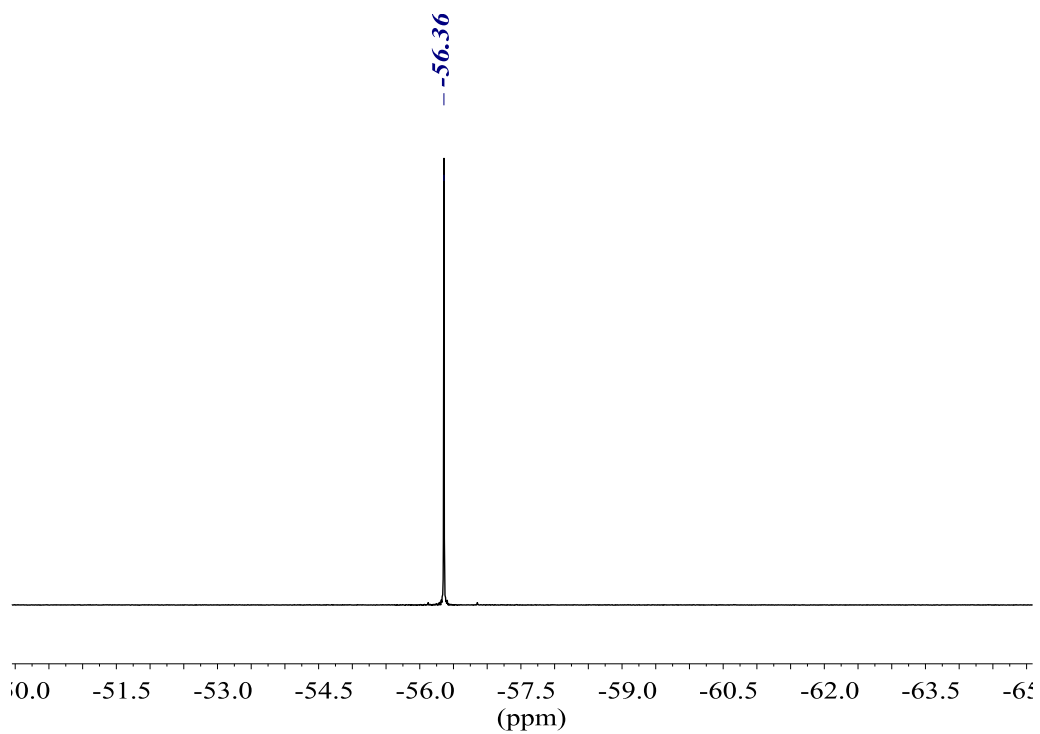
$^1\text{H}\{^{31}\text{P}\}$ NMR (400.13 MHz, CDCl_3)



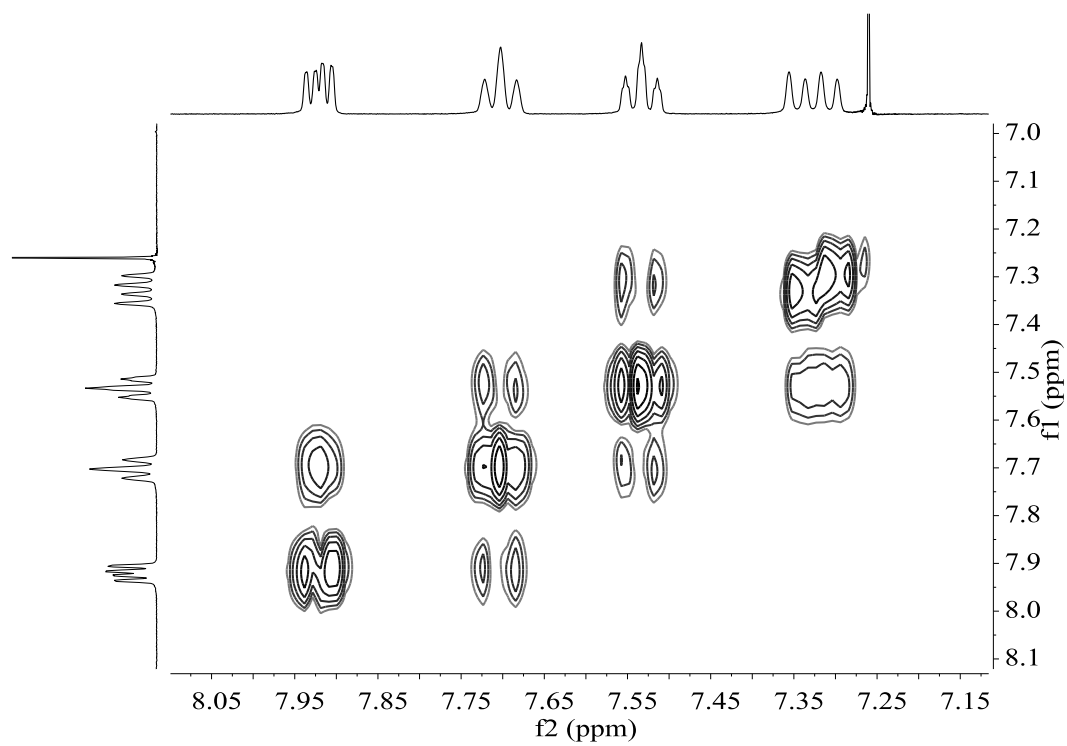
$^{13}\text{C}\{^1\text{H}\}$ NMR (100.61 MHz, CDCl_3)



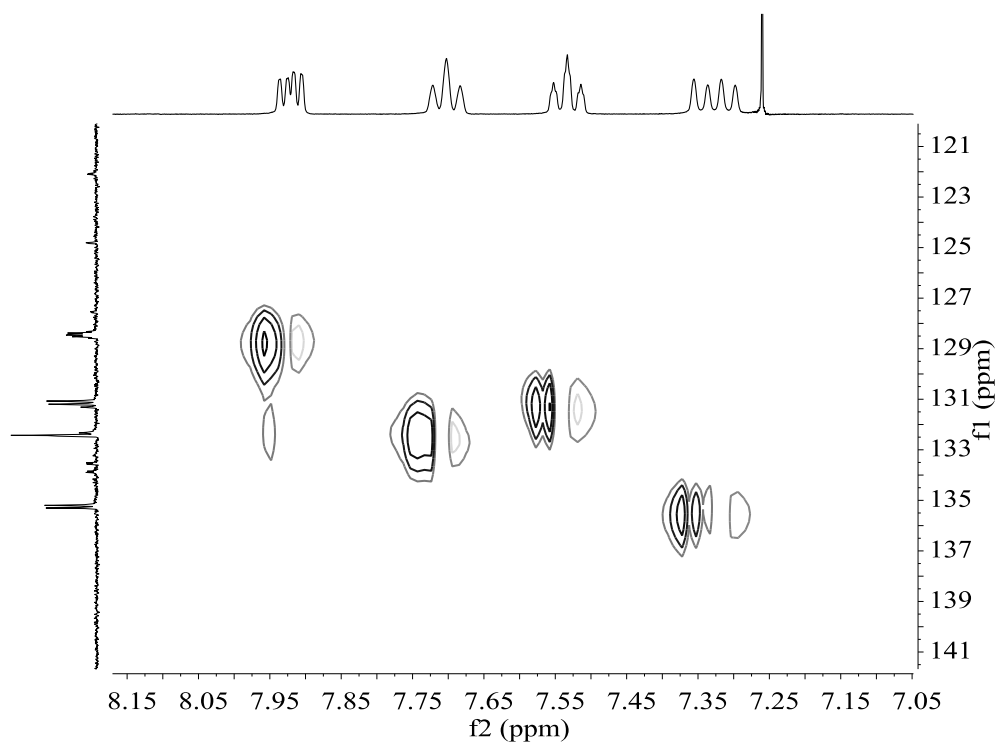
$^{19}\text{F}\{^1\text{H}\}$ NMR (376.50 MHz, CDCl_3)



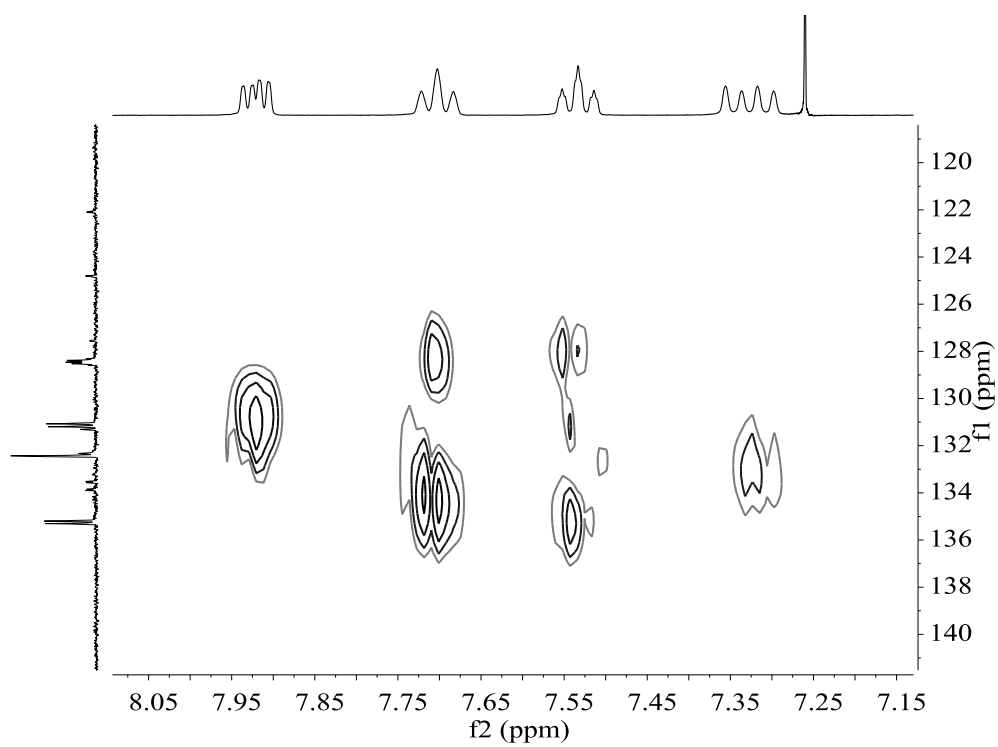
COSY NMR (400.13 MHz, CDCl_3)



HSQC NMR (400.13 MHz, CDCl₃)

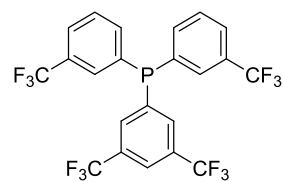


HMBC NMR (400.13 MHz, CDCl₃)

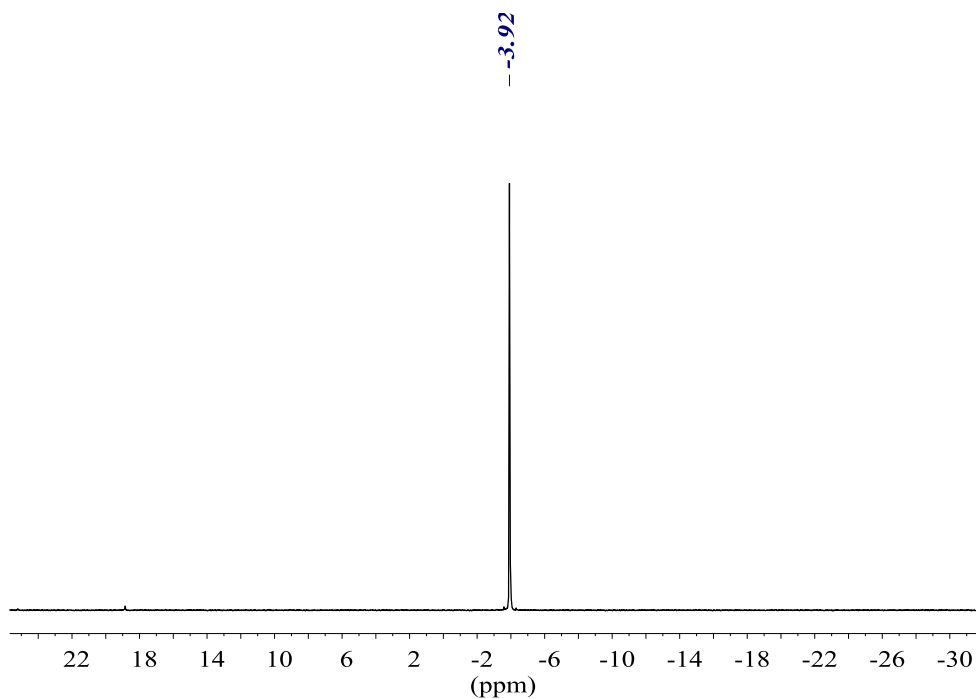


1.2. Heteroleptic phosphines

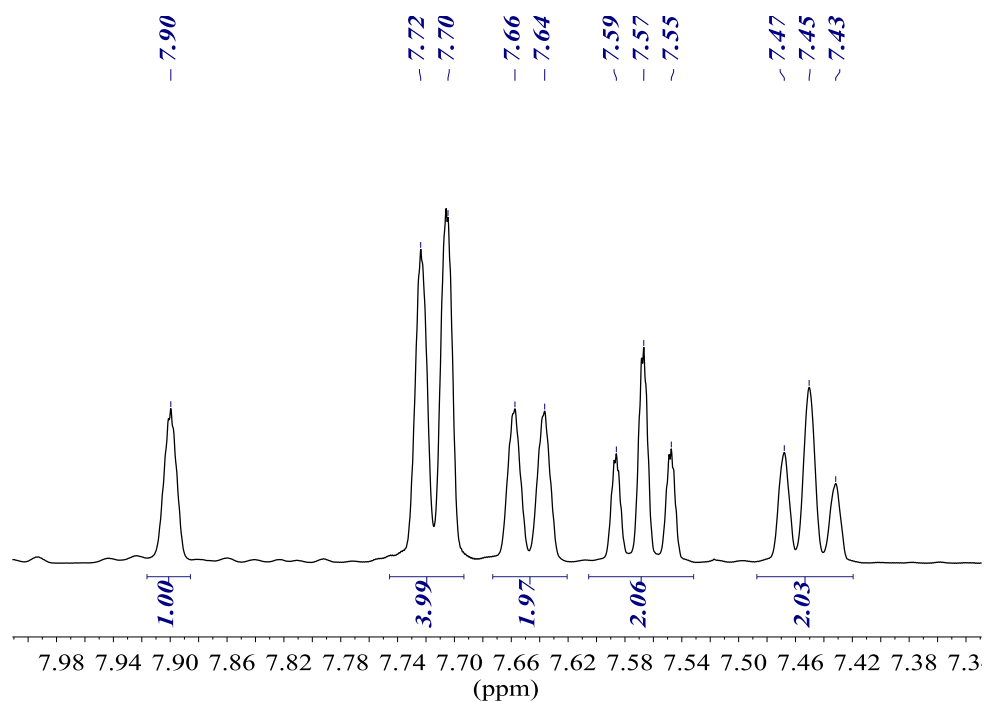
(3,5-bis(trifluoromethyl)phenyl)bis(3-(trifluoromethyl)phenyl)phosphine (15)



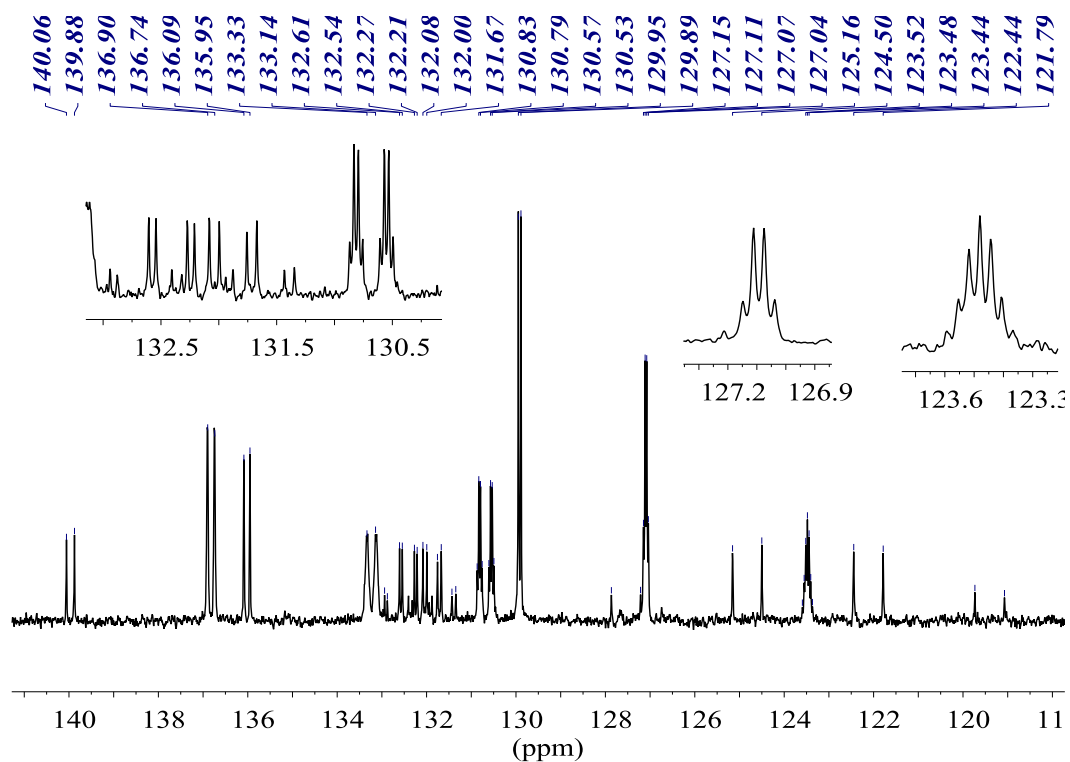
$^{31}\text{P}\{^1\text{H}\}$ NMR (161.98 MHz, CDCl_3)



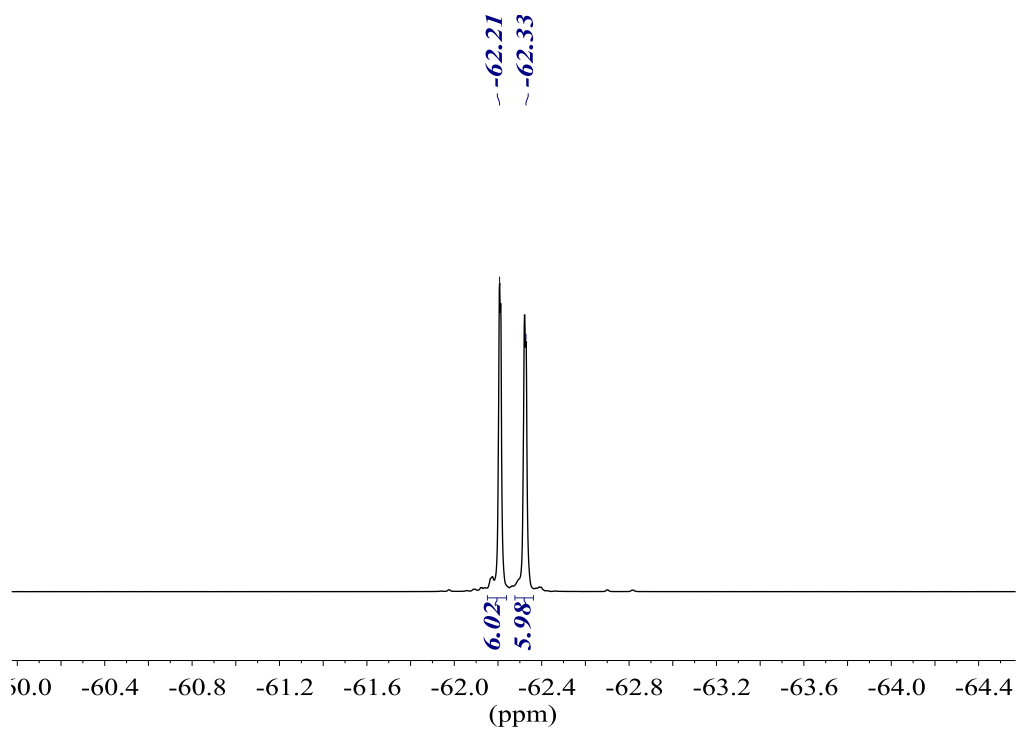
^1H NMR (400.13 MHz, CDCl_3)



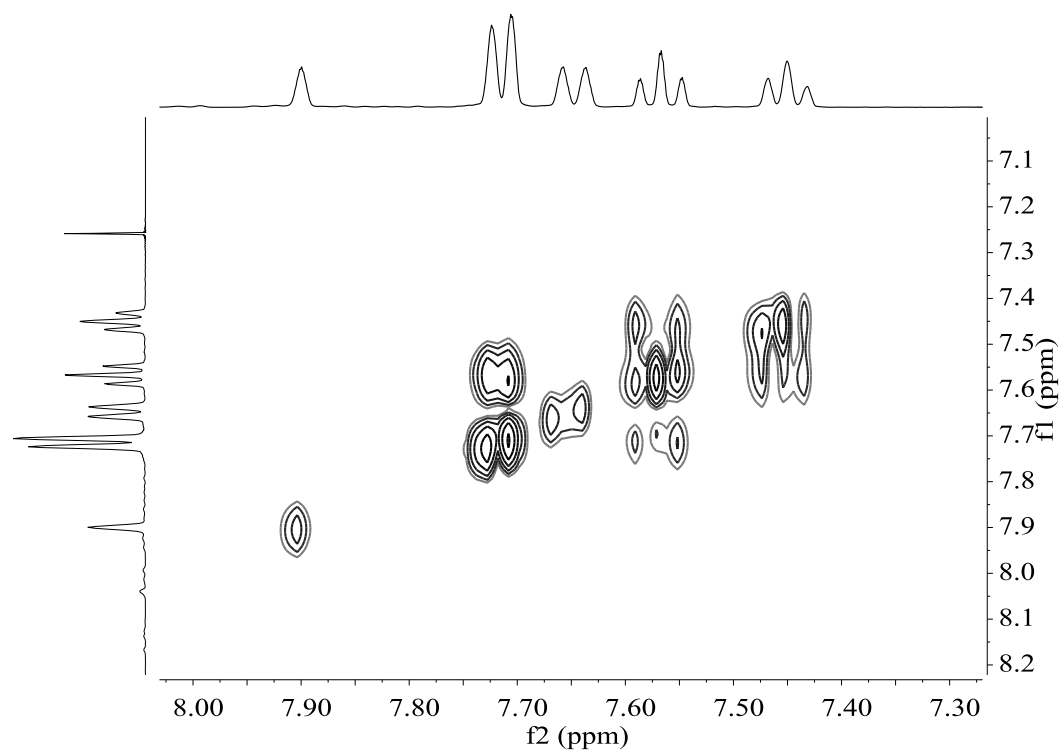
$^{13}\text{C}\{^1\text{H}\}$ NMR (100.61 MHz, CDCl_3)



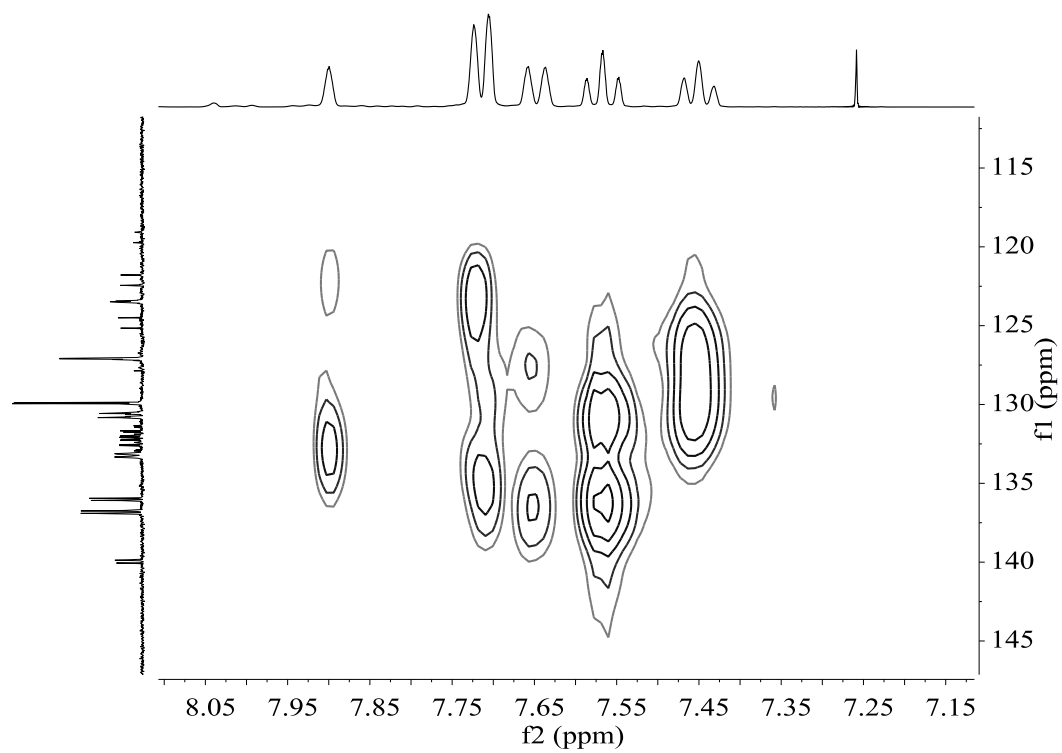
$^{19}\text{F}\{^1\text{H}\}$ NMR (376.50 MHz, CDCl_3)



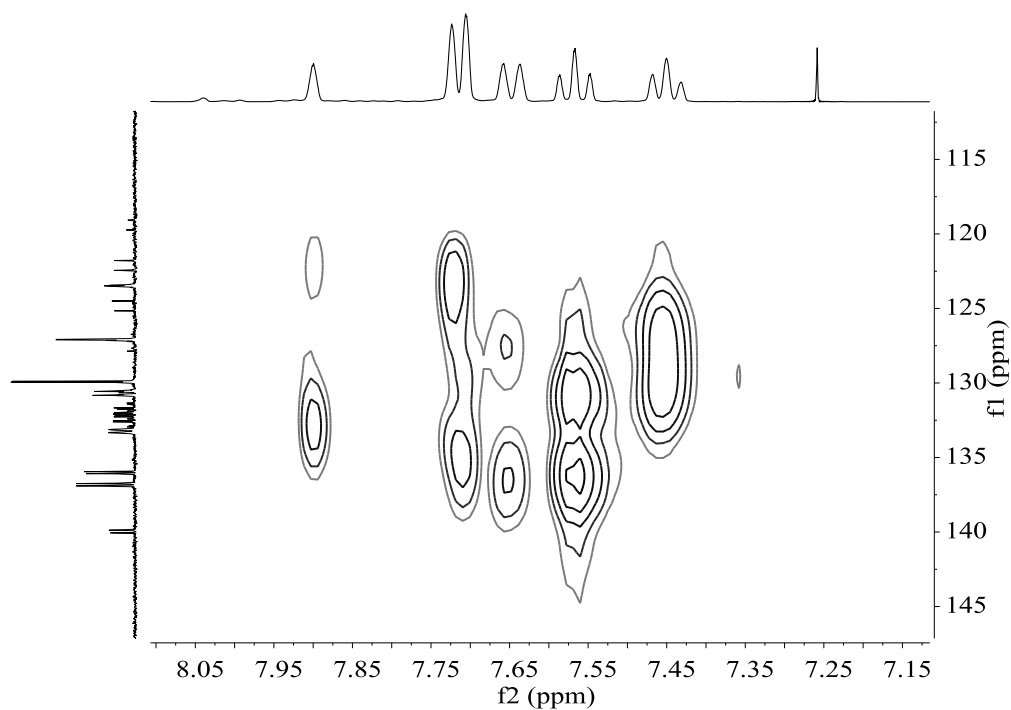
COSY NMR (400.13 MHz, CDCl₃)



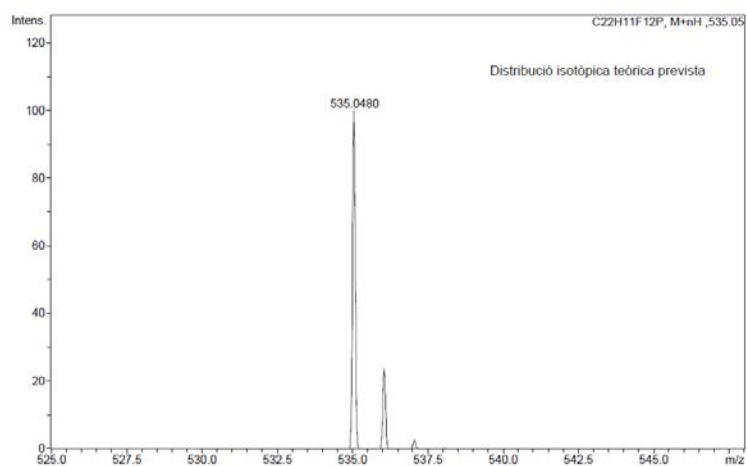
HSQC NMR (400.13 MHz, CDCl₃)



HMBC NMR (400.13 MHz, CDCl₃)

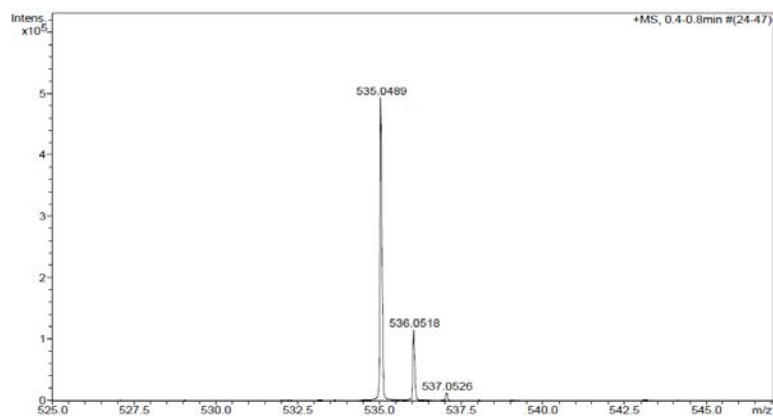


HR-MS (ESI⁺ *m/z*) [M+H]⁺
calculated for [C₂₂H₁₂F₁₂P]⁺



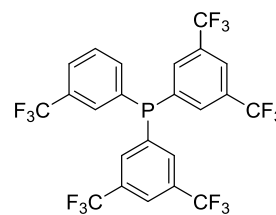
#	<i>m/z</i>	I	I %
1	535.0480	100	100.0
2	536.0513	24	23.9
3	537.0547	3	2.7

found

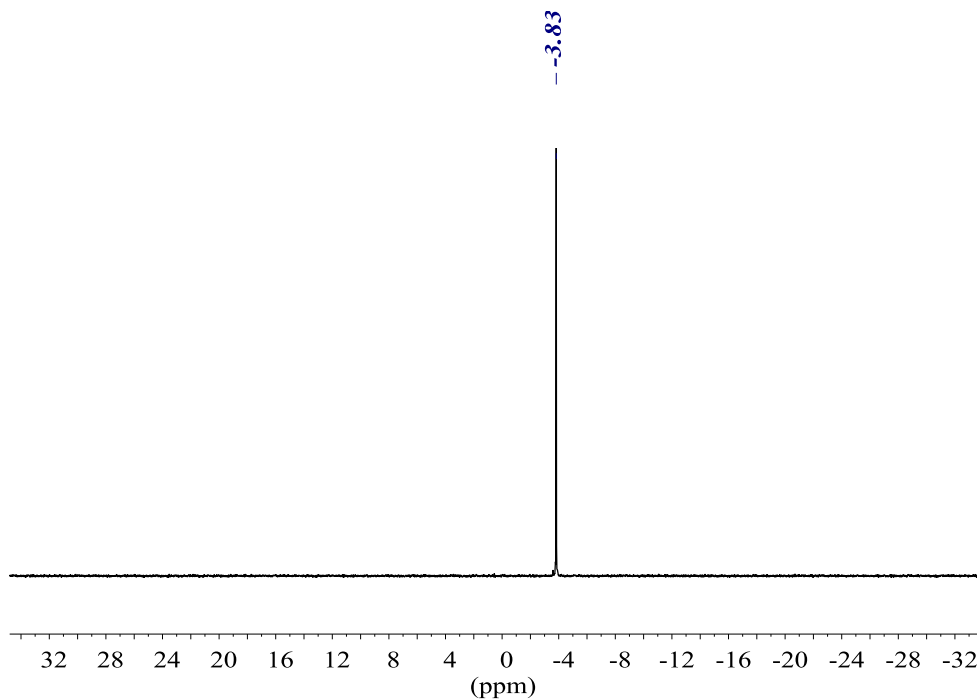


#	<i>m/z</i>	I	I %
1	535.0489	493418	100.0
2	536.0518	115356	23.4
3	537.0526	12934	2.6

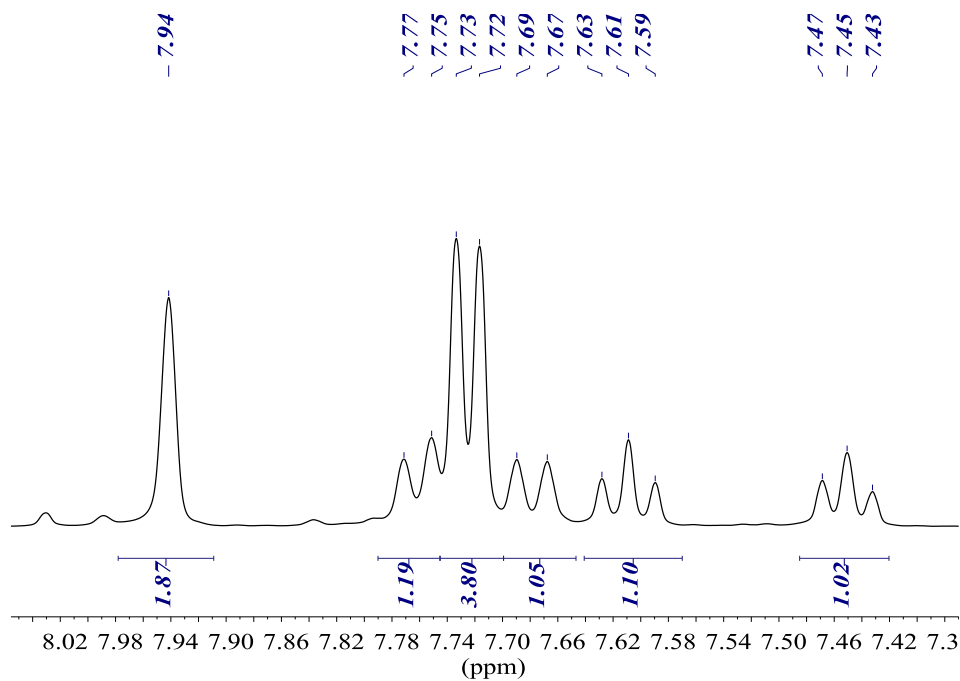
Bis(3,5-bis(trifluoromethyl)phenyl)(3-(trifluoromethyl)phenyl)phosphine (18)



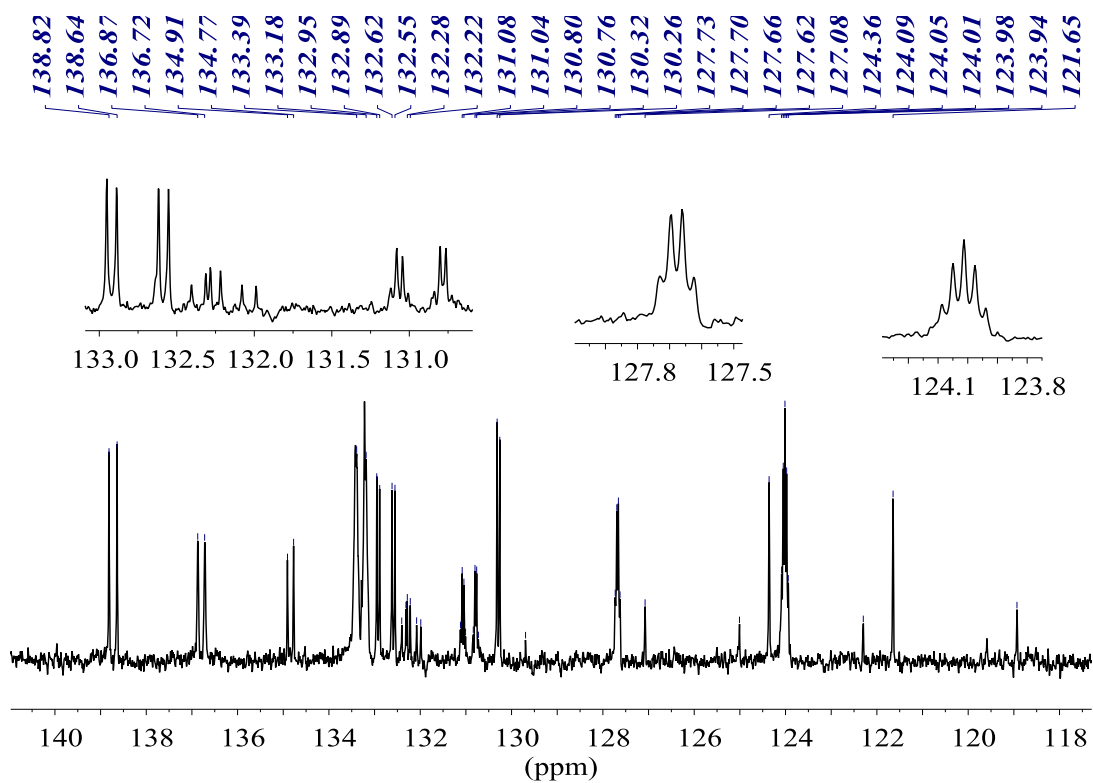
$^{31}\text{P}\{^1\text{H}\}$ NMR (161.98 MHz, CDCl_3)



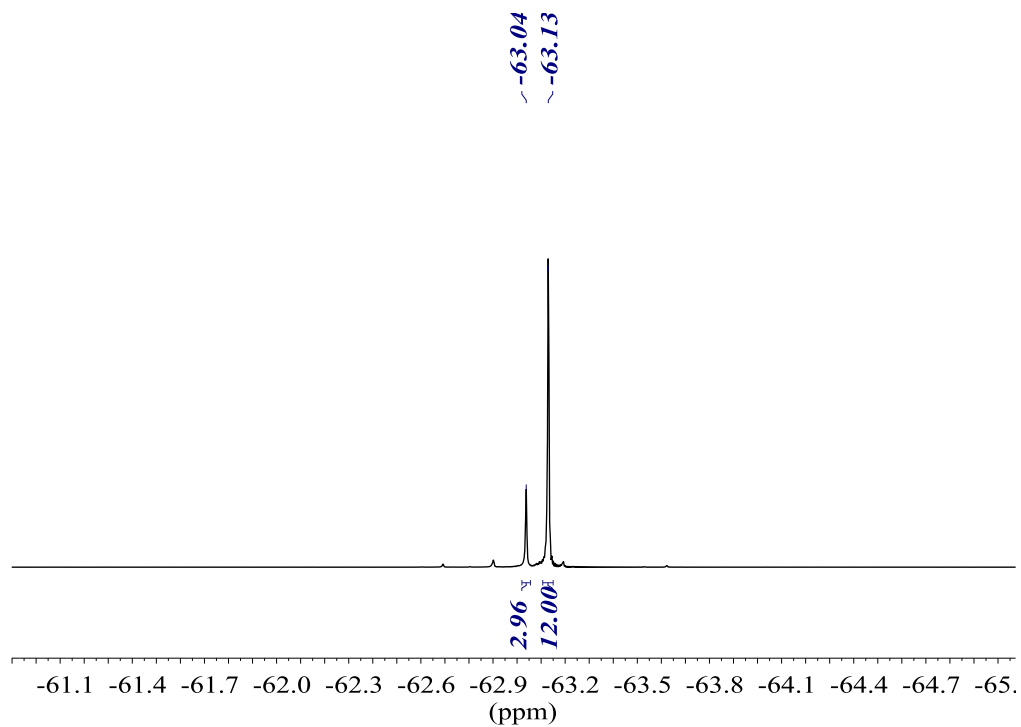
^1H NMR (400.13 MHz, CDCl_3)



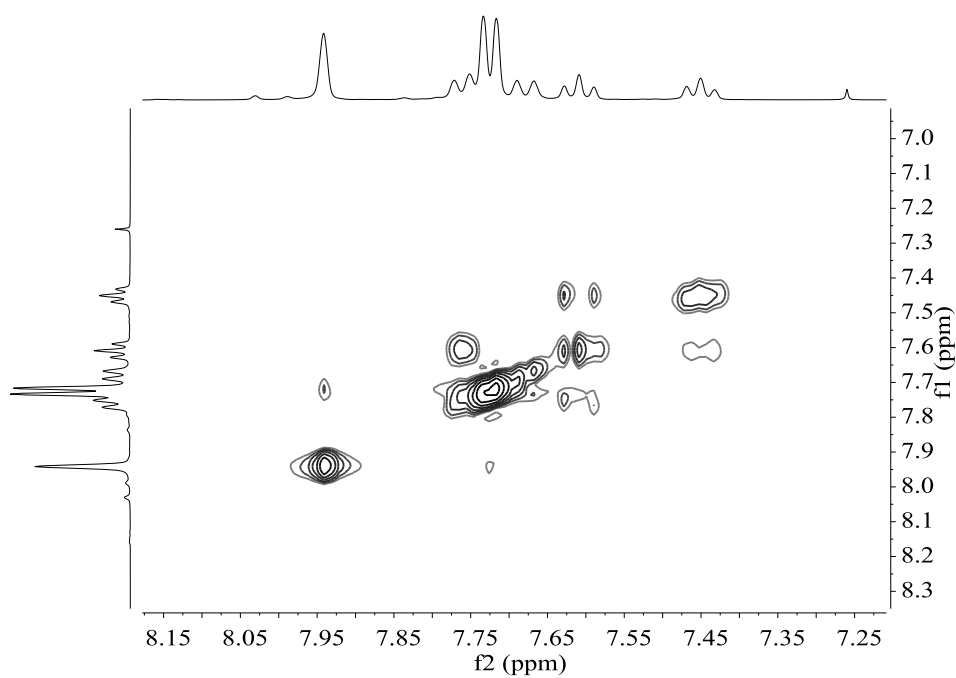
$^{13}\text{C}\{^1\text{H}\}$ NMR (100.61 MHz, CDCl_3)



$^{19}\text{F}\{^1\text{H}\}$ NMR (376.50 MHz, CDCl_3)

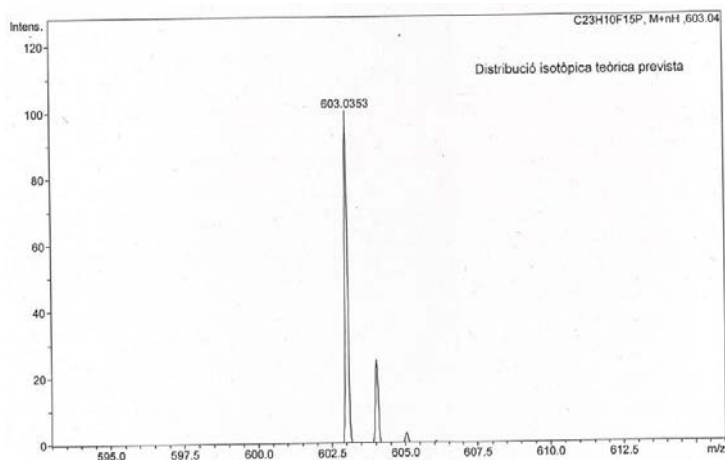


COSY NMR (400.13 MHz, CDCl₃)



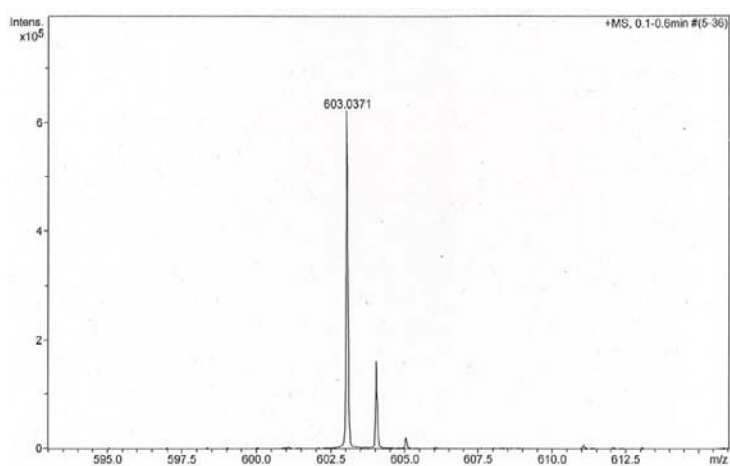
HR-MS (ESI⁺ *m/z*) [M+H]⁺

calculated for [C₂₃H₁₁F₁₅P]⁺



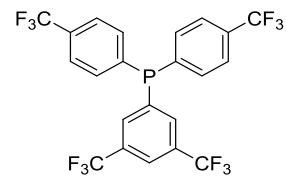
#	<i>m/z</i>	I	I %
1	603.0353	100	100.0
2	604.0387	25	25.0
3	605.0420	3	3.0

found

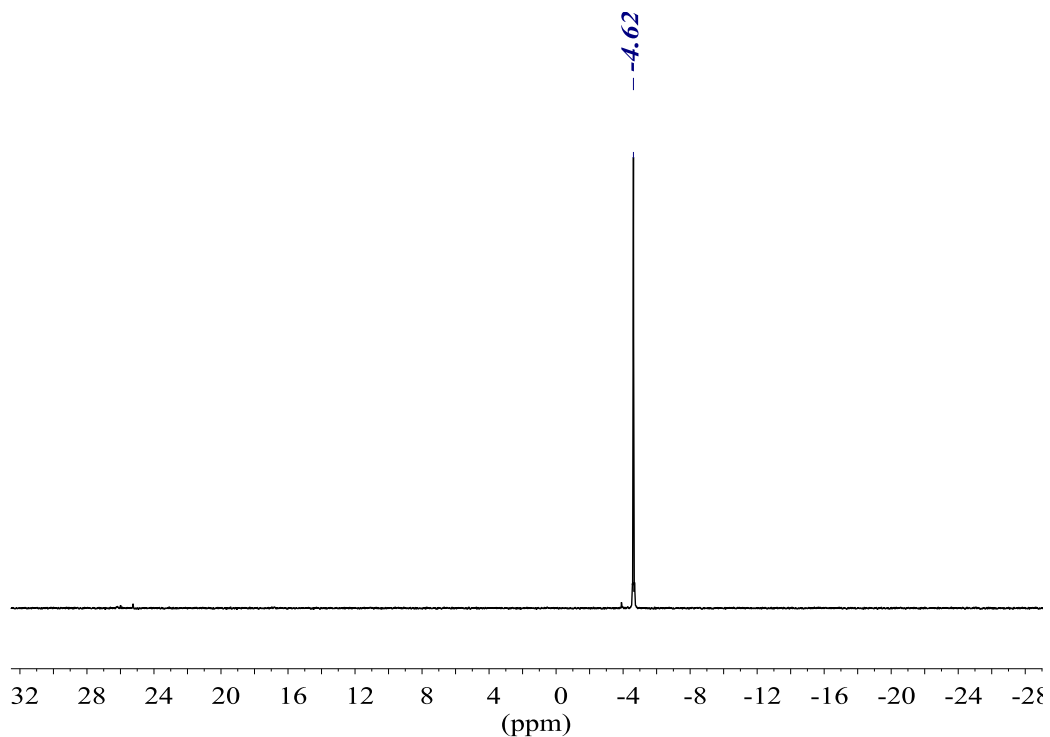


#	<i>m/z</i>	I	I %
1	603.0371	621428	100.0
2	604.0396	161410	26.0
3	605.0394	19803	3.2

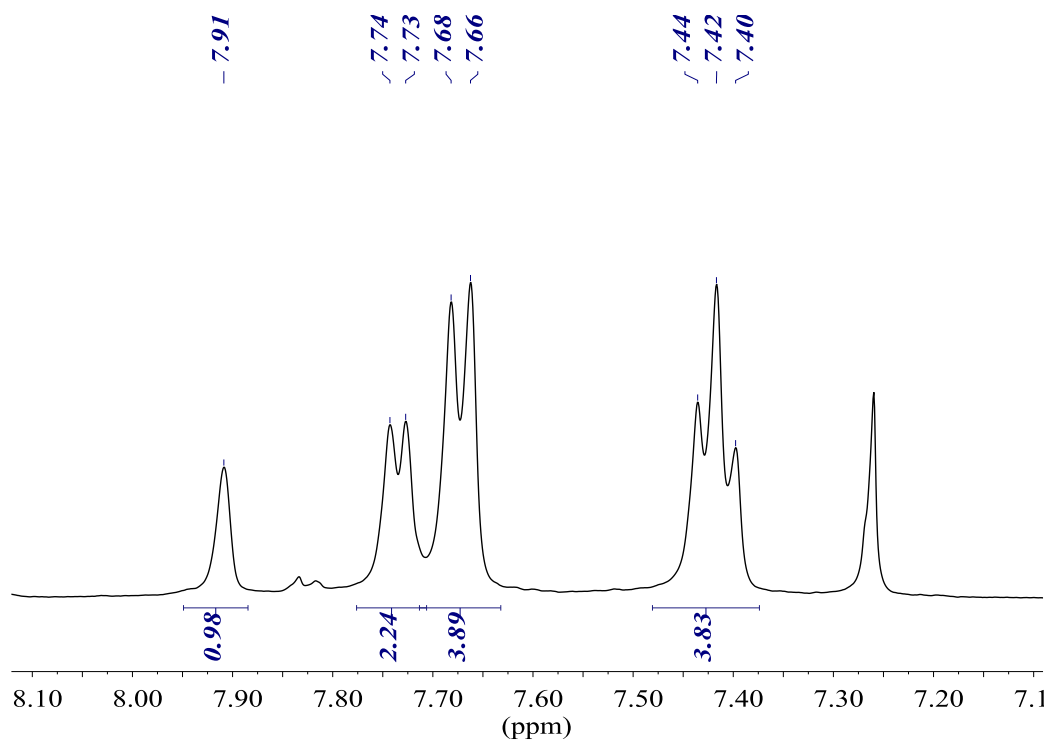
(3,5-bis(trifluoromethyl)phenyl)bis(4-(trifluoromethyl)phenyl)phosphine (20)

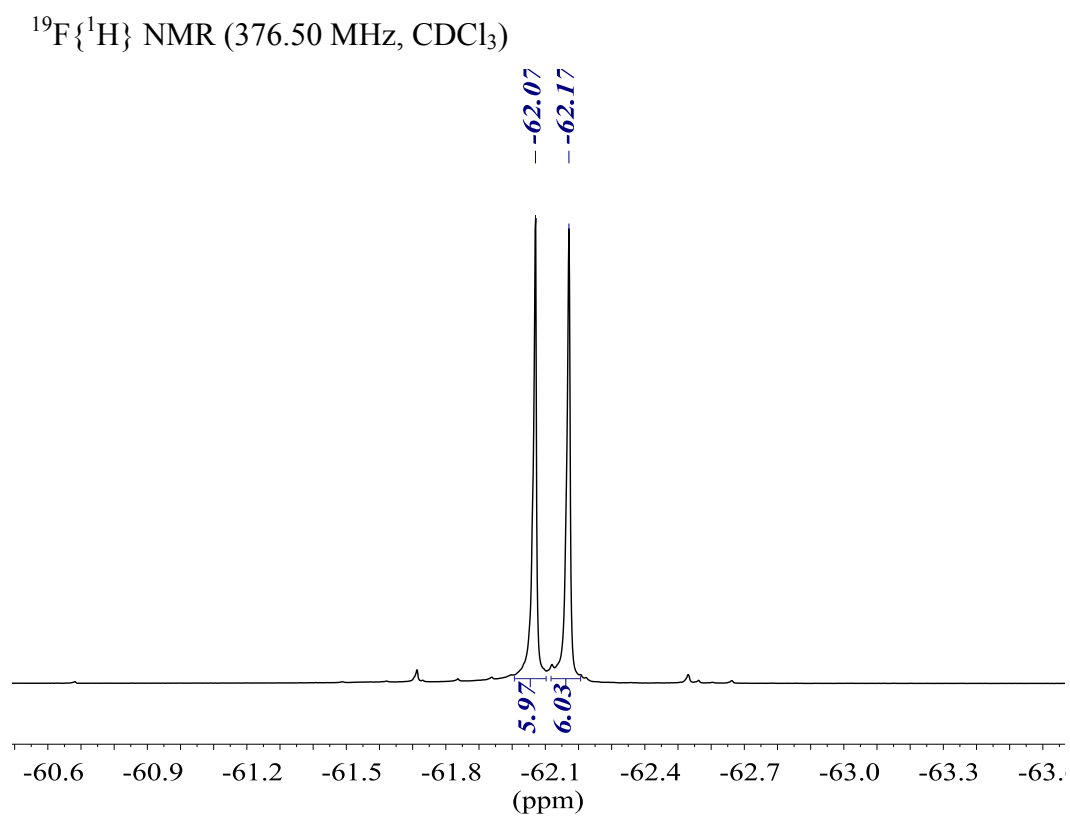
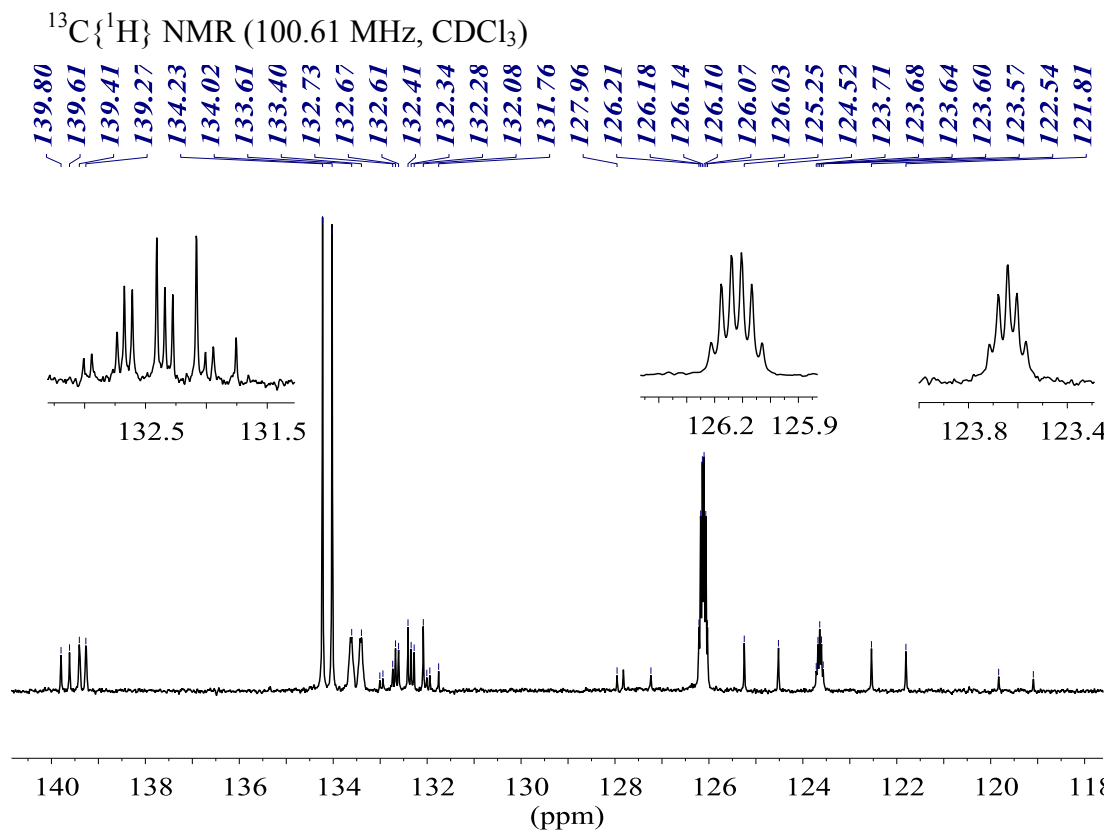


$^{31}\text{P}\{^1\text{H}\}$ NMR (161.98 MHz, CDCl_3)

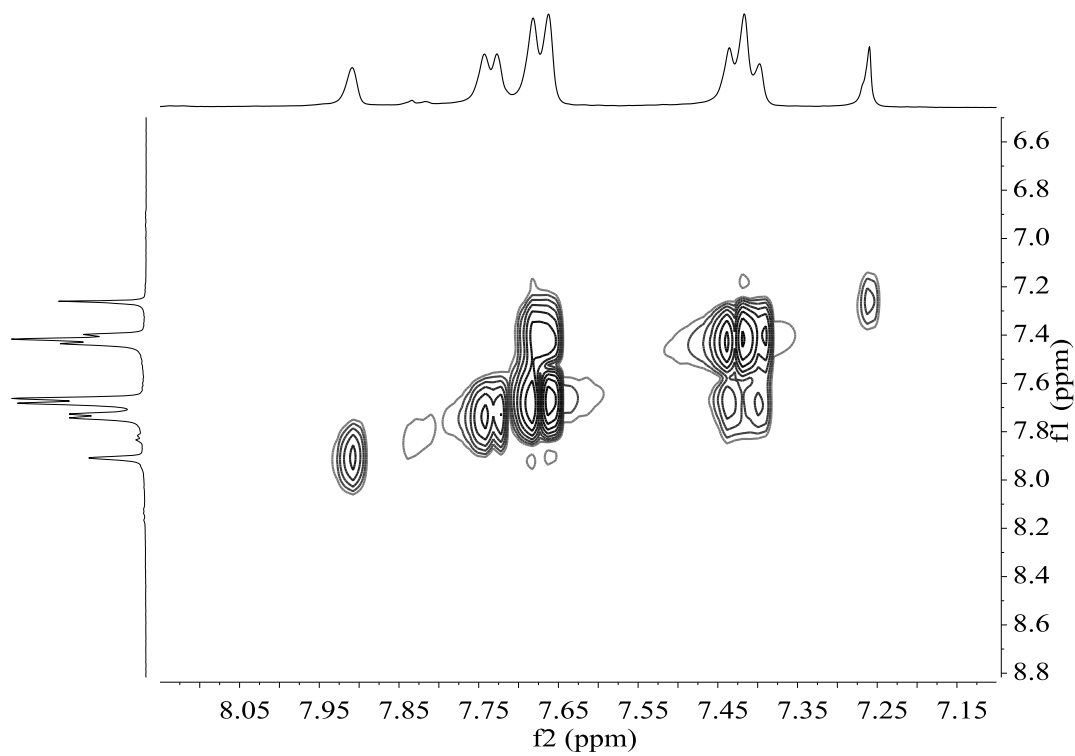


^1H NMR (400.13 MHz, CDCl_3)

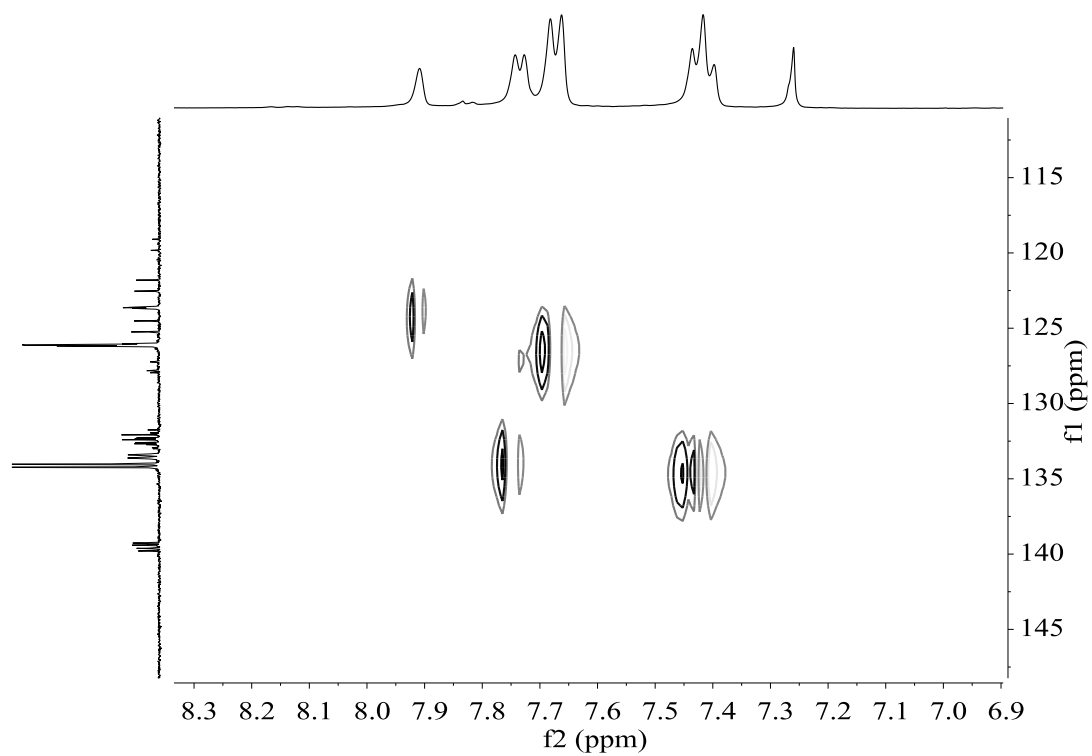




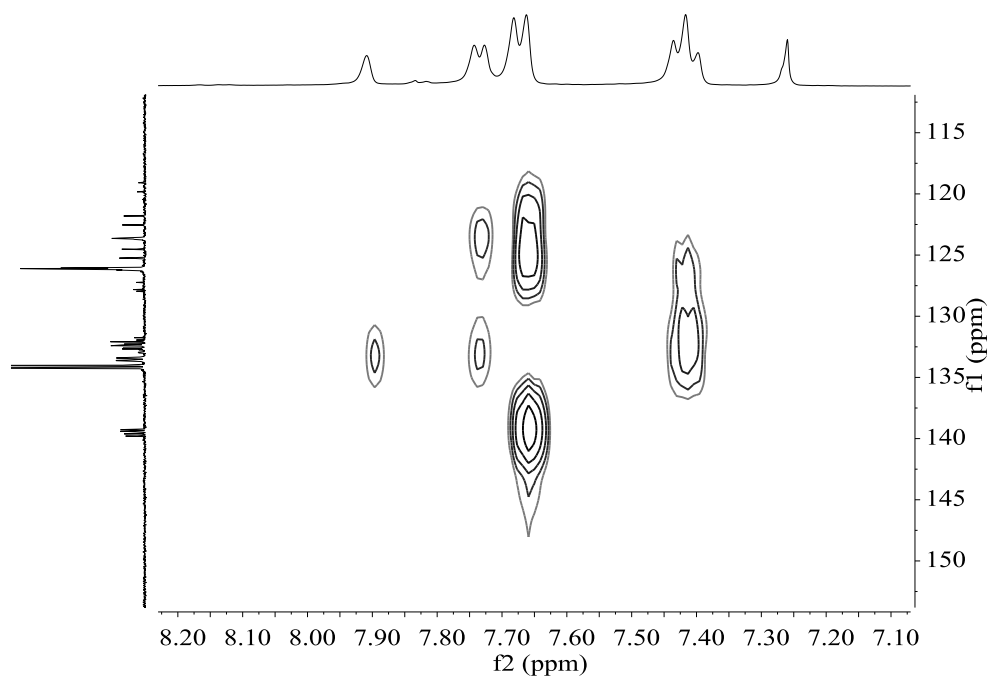
COSY NMR (400.13 MHz, CDCl₃)



HSQC NMR (400.13 MHz, CDCl₃)

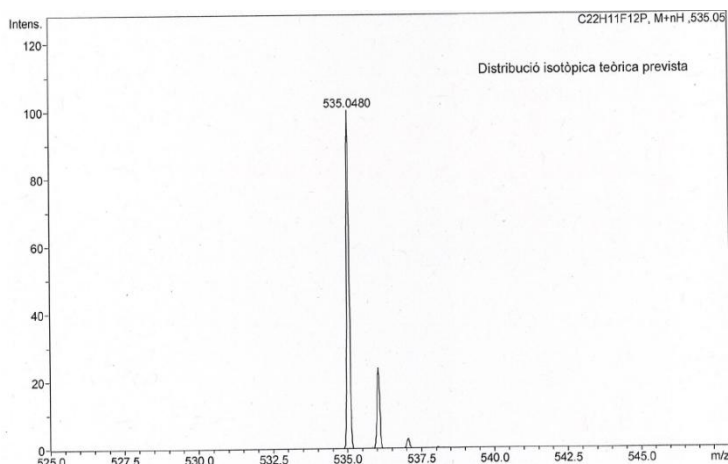


HMBC NMR (400.13 MHz, CDCl₃)



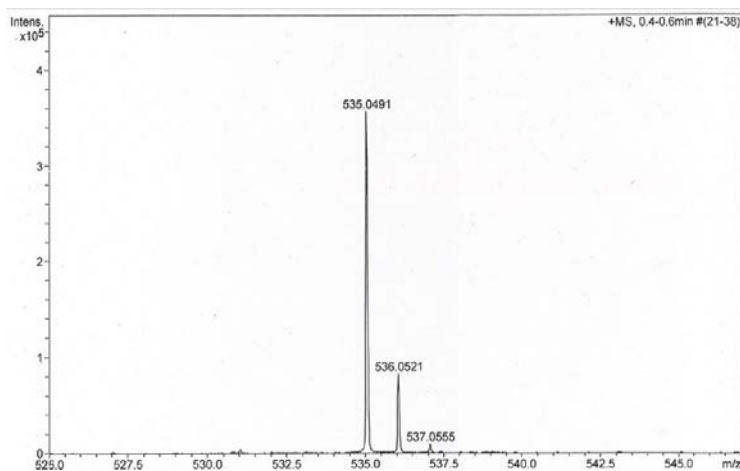
HR-MS (ESI⁺ *m/z*) [M+H]⁺

calculated for [C₂₂H₁₂F₁₂P]⁺



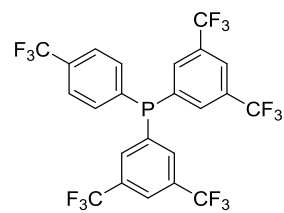
#	<i>m/z</i>	I	I%
1	535.0480	100	100.0
2	536.0513	24	23.9
3	537.0547	3	2.7

found

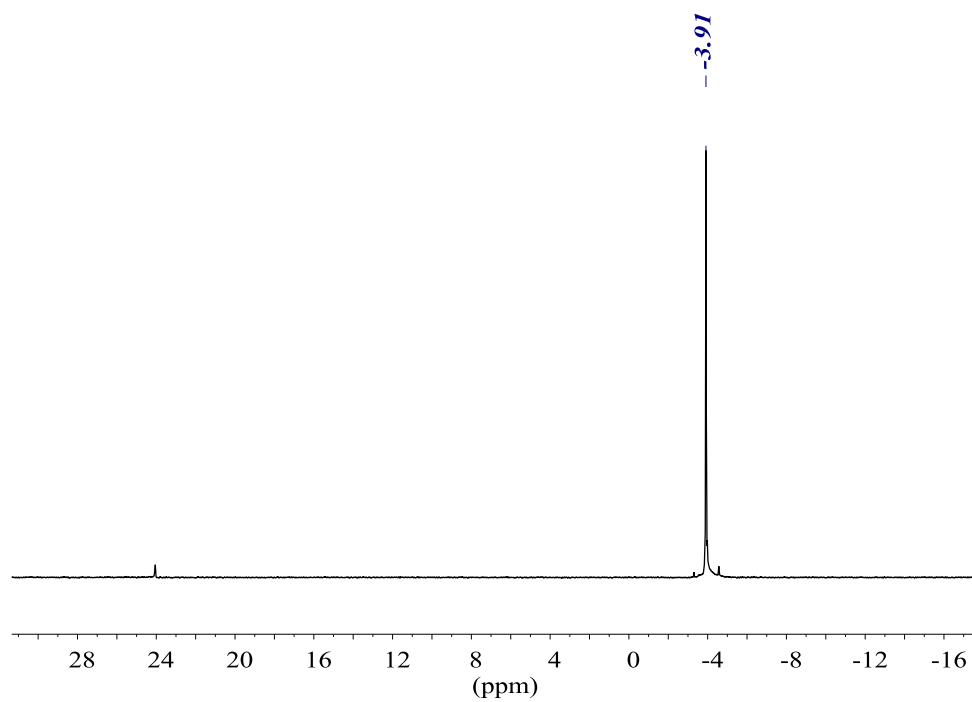


#	<i>m/z</i>	I	I%
1	535.0491	356924	100.0
2	536.0521	82665	23.2
3	537.0555	9366	2.6

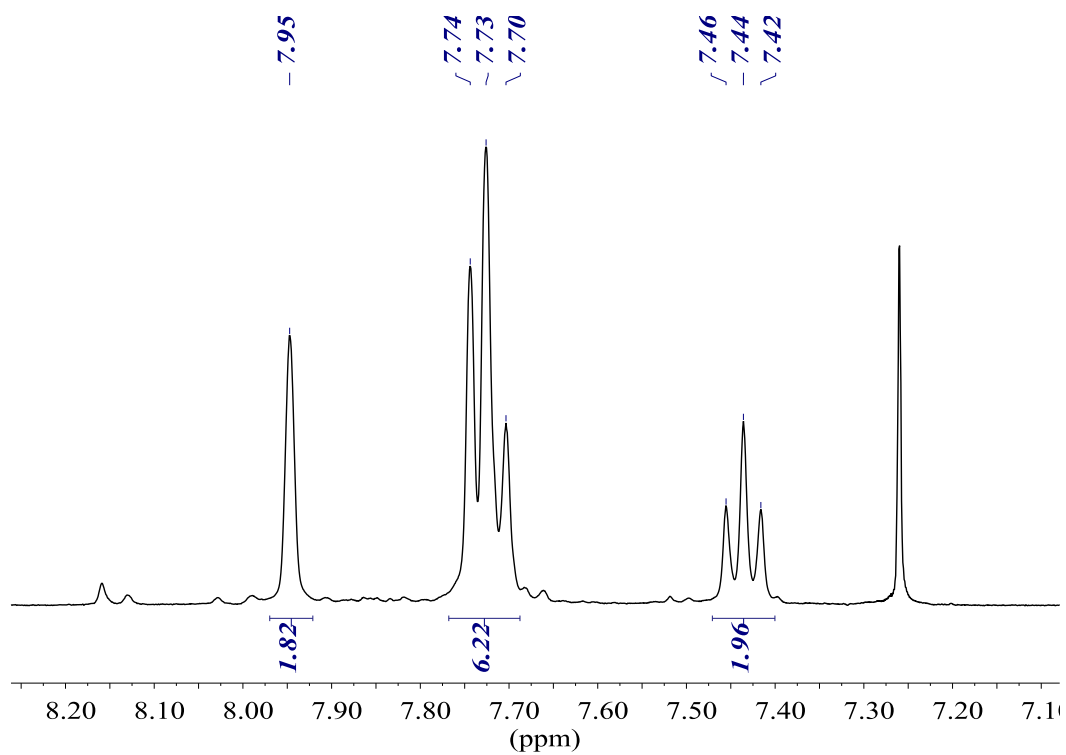
Bis(3,5-bis(trifluoromethyl)phenyl)(4-(trifluoromethyl)phenyl)phosphine (23)



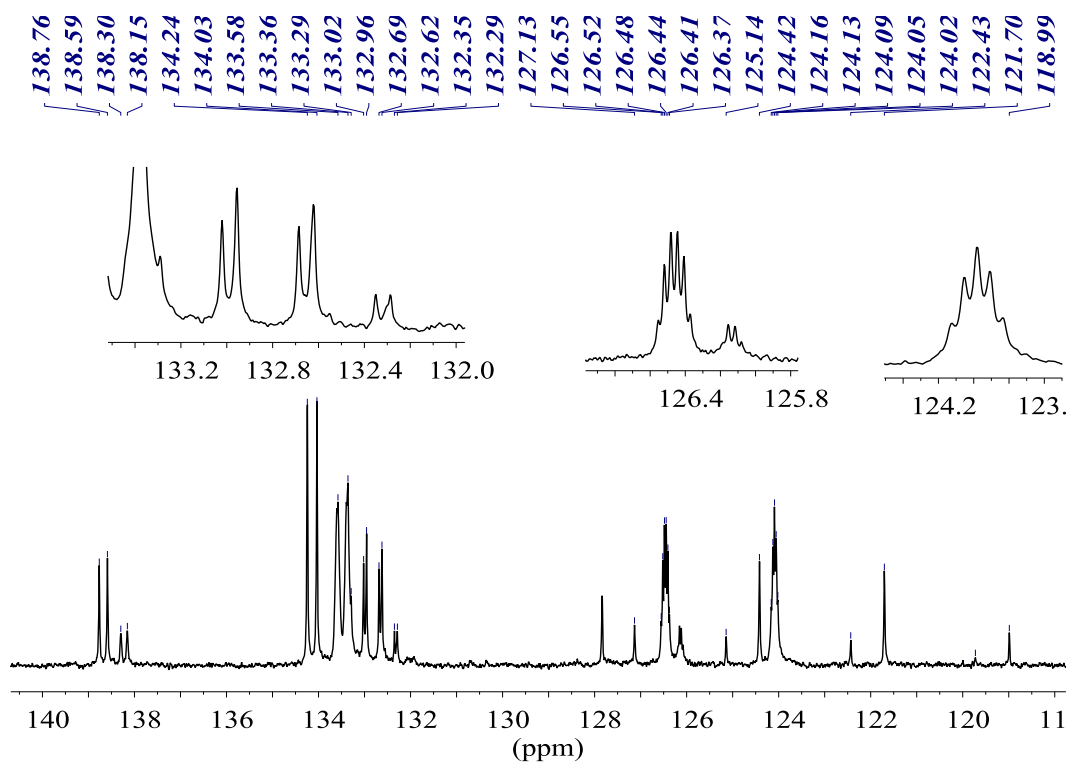
$^{31}\text{P}\{^1\text{H}\}$ NMR (161.98 MHz, CDCl_3)



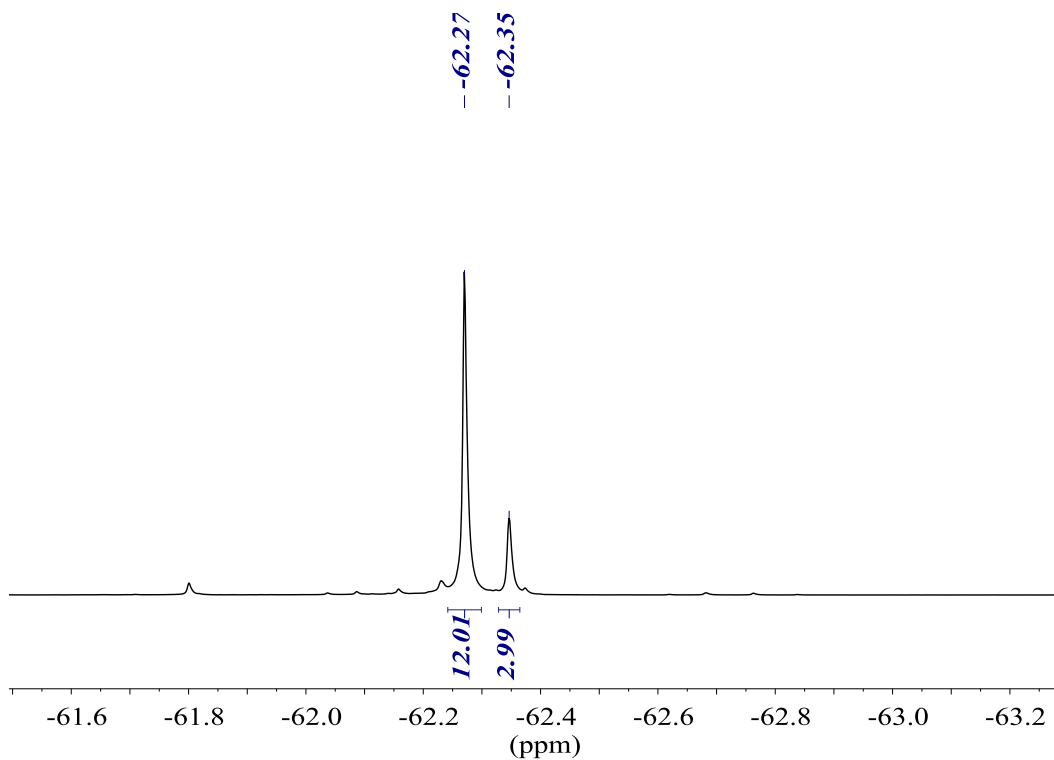
^1H NMR (400.13 MHz, CDCl_3)



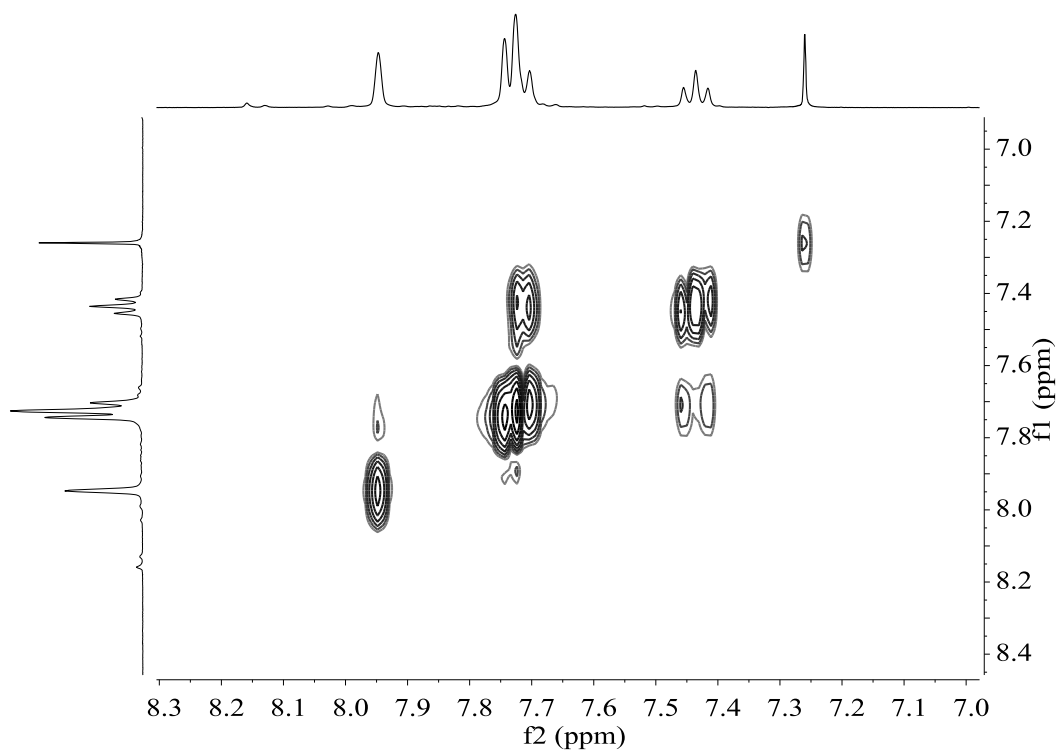
$^{13}\text{C}\{^1\text{H}\}$ NMR (100.61 MHz, CDCl_3)



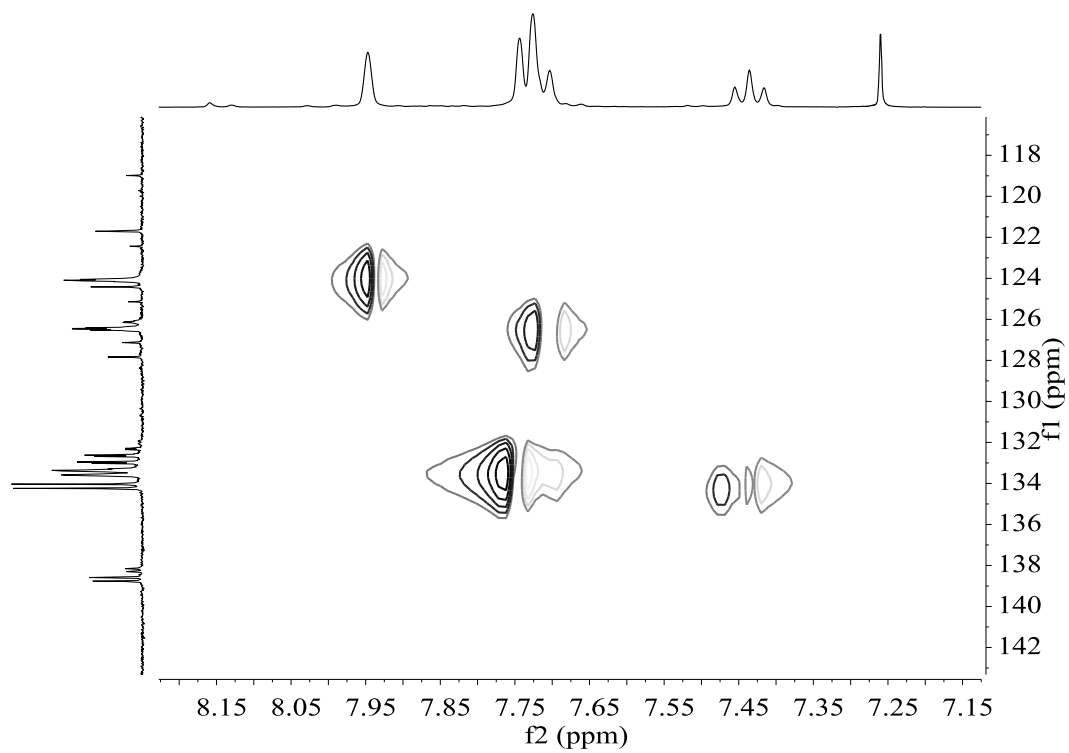
$^{19}\text{F}\{^1\text{H}\}$ NMR (376.50 MHz, CDCl_3)



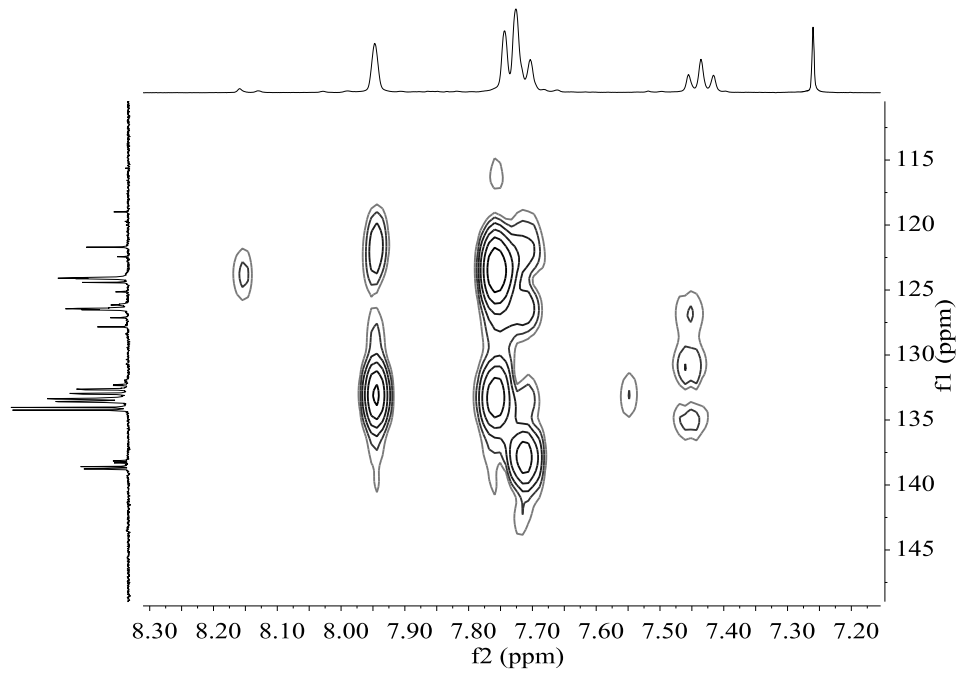
COSY NMR (400.13 MHz, CDCl₃)



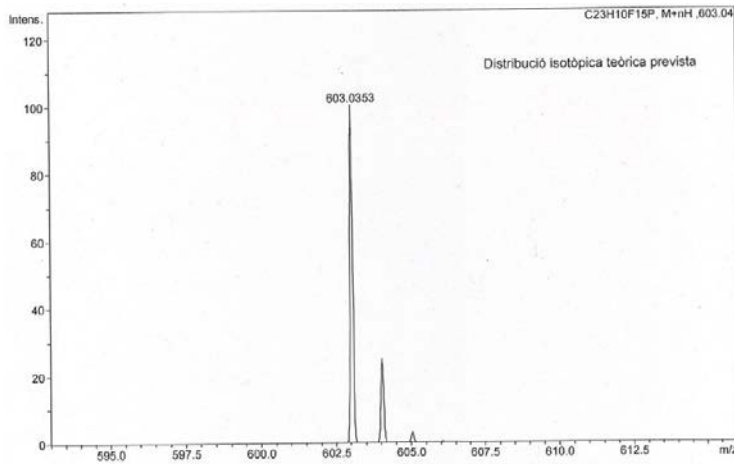
HSQC NMR (400.13 MHz, CDCl₃)



HMBC NMR (400.13 MHz, CDCl₃)

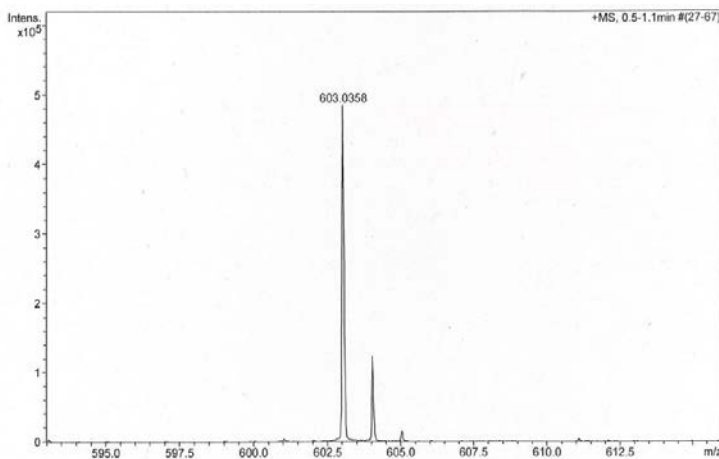


HR-MS (ESI⁺ *m/z*) [M+H]⁺
 calculated for [C₂₃H₁₁F₁₅P]⁺



#	<i>m/z</i>	I	I%
1	603.0353	100	100.0
2	604.0387	25	25.0
3	605.0420	3	3.0

found

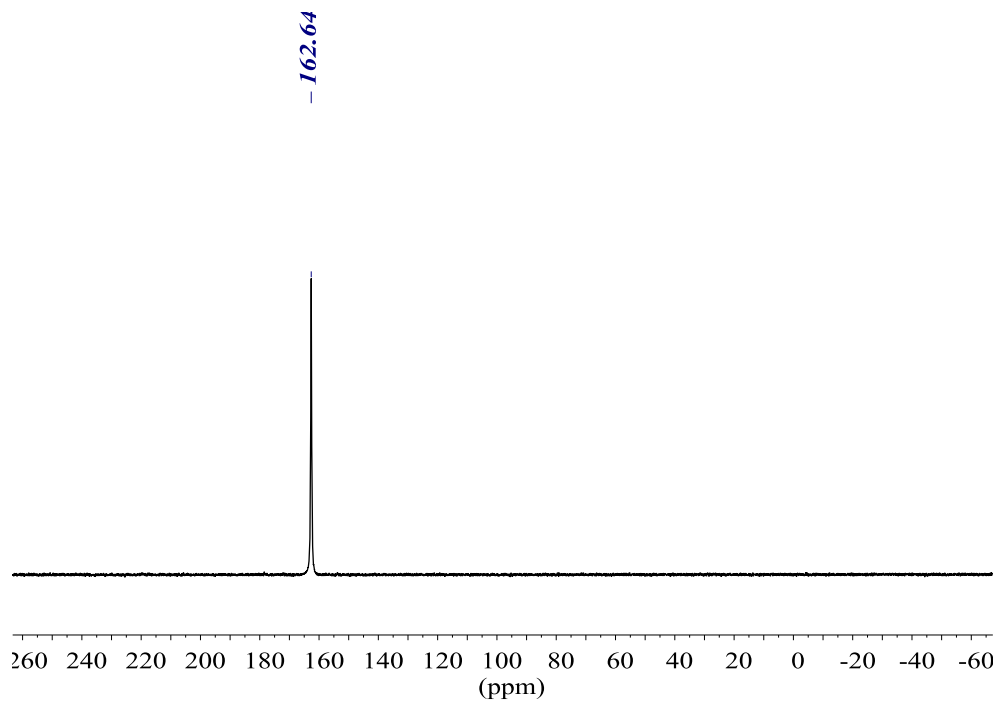


#	<i>m/z</i>	I	I%
1	603.0358	484202	100.0
2	604.0385	123322	25.5
3	605.0398	15780	3.3

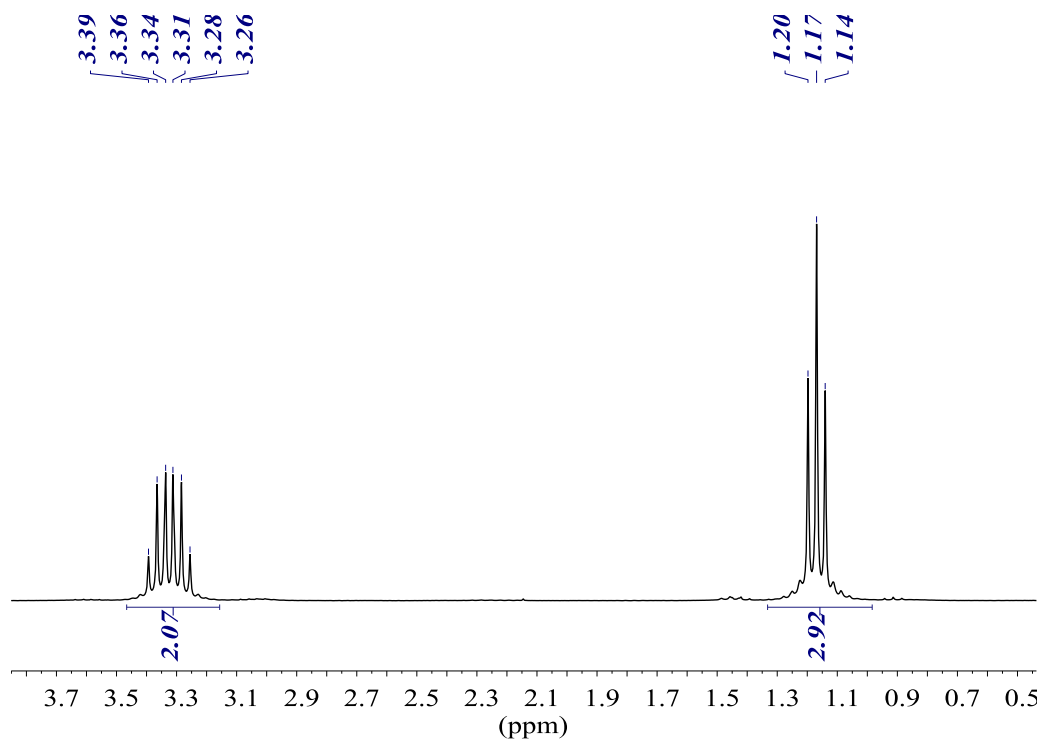
1.3. Chlorophosphines

N,N-diethylphosphoramidous dichloride (Et_2NPCl_2)

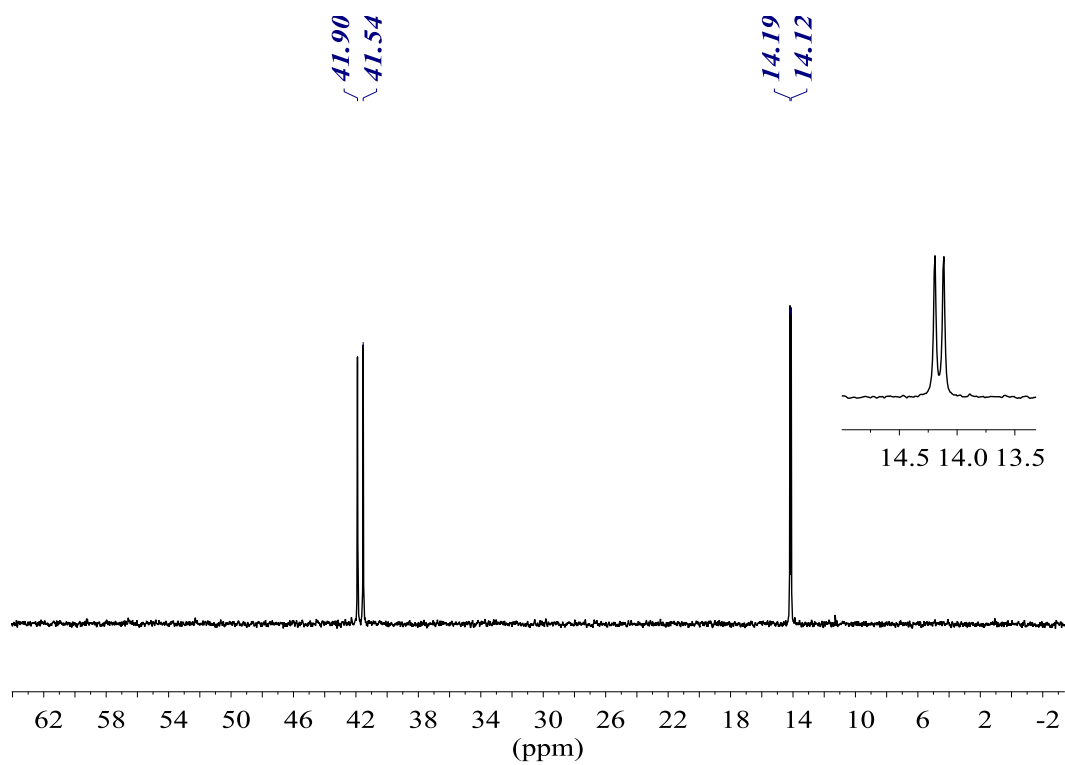
$^{31}\text{P}\{^1\text{H}\}$ NMR (101.2 MHz, CDCl_3)



^1H NMR (250.16 MHz, CDCl_3)

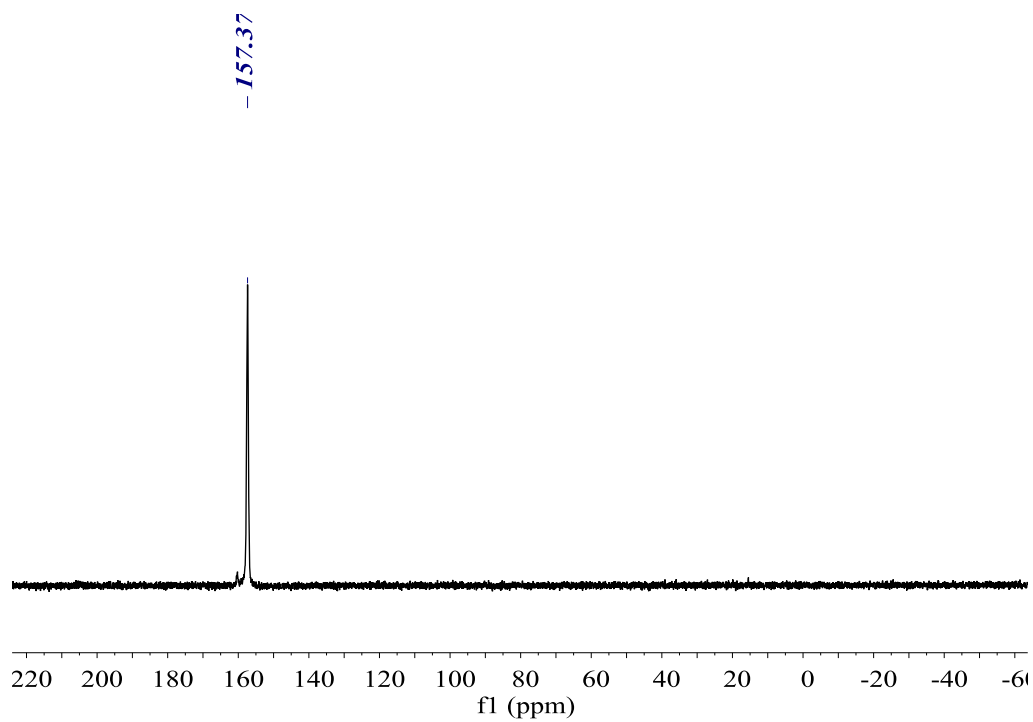


$^{13}\text{C}\{^1\text{H}\}$ NMR (62.90 MHz, CDCl_3)

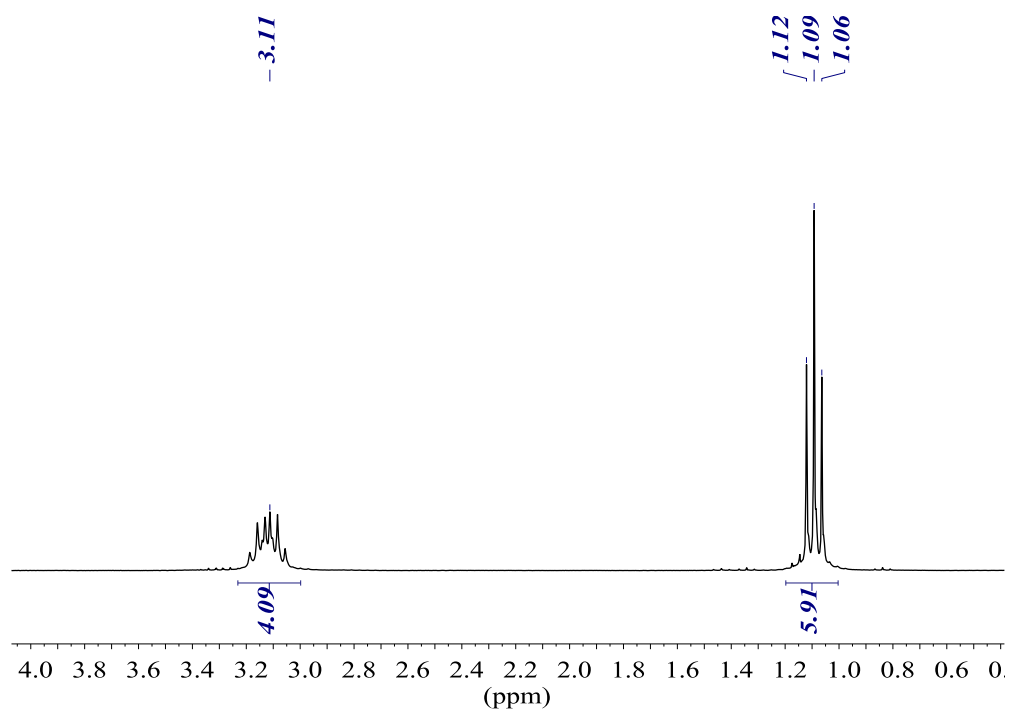


***N,N,N',N'*-tetraethylphosphorodiamidous chloride ($(\text{Et}_2\text{N})_2\text{PCl}$)**

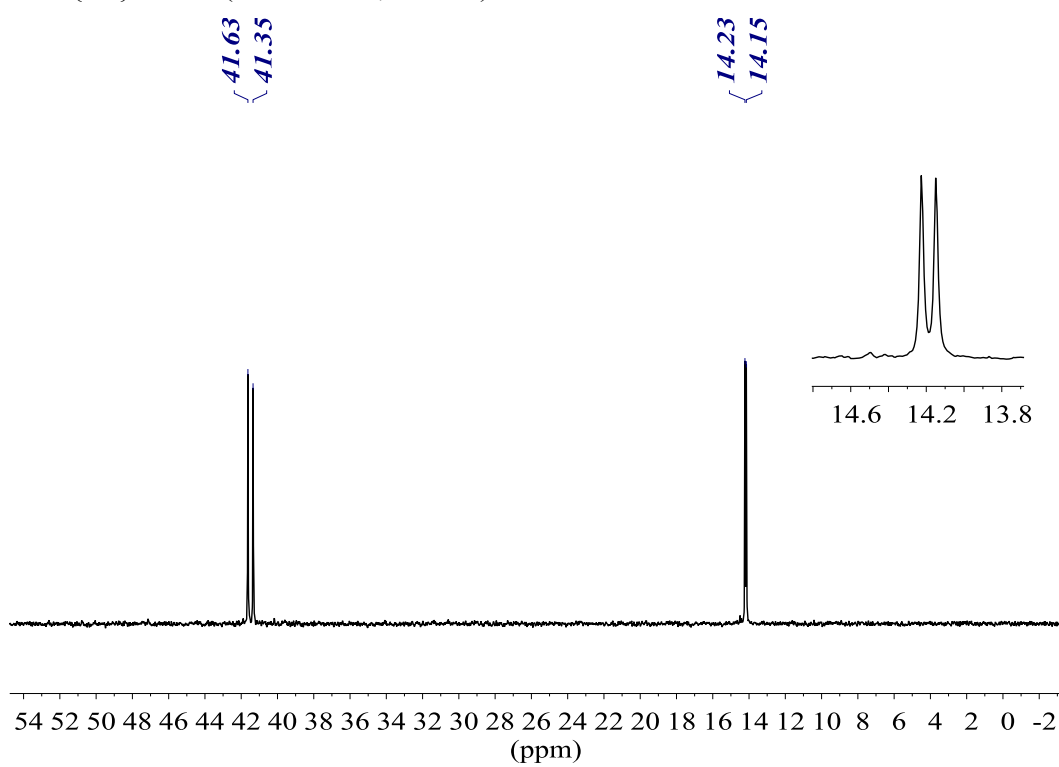
$^{31}\text{P}\{^1\text{H}\}$ NMR (101.2 MHz, CDCl_3)



^1H NMR (250.16 MHz, CDCl_3)

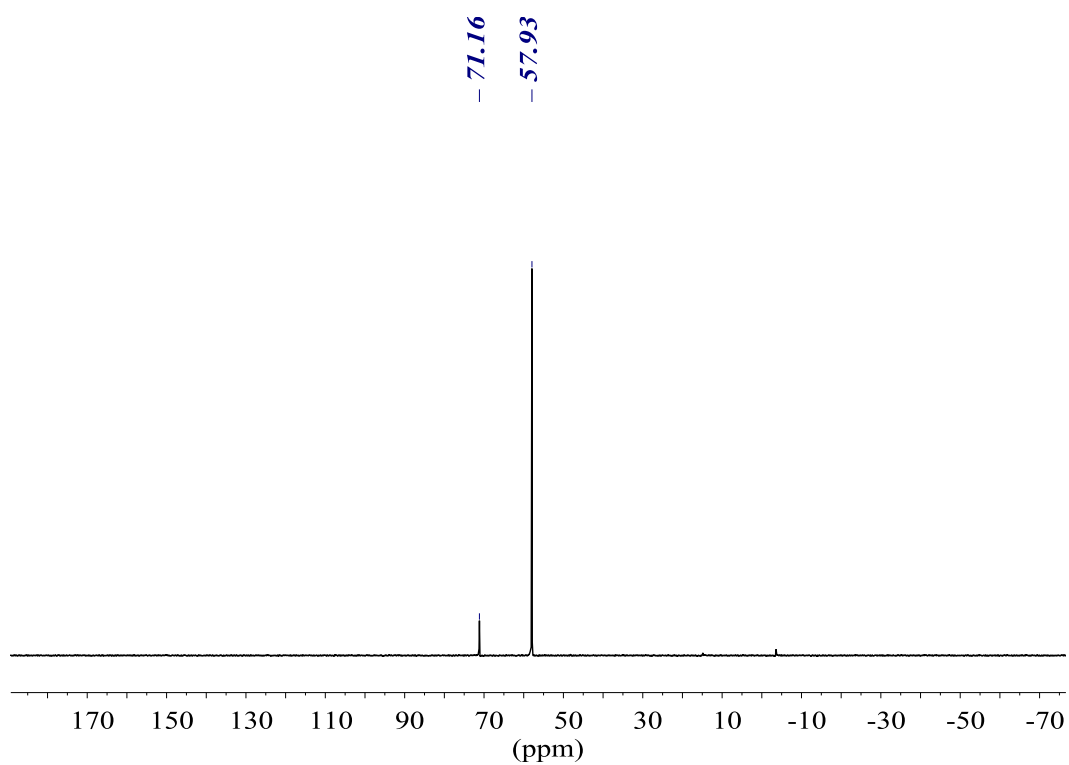
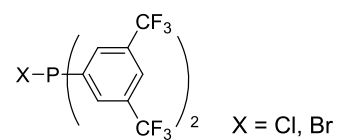


$^{13}\text{C}\{^1\text{H}\}$ NMR (62.90 MHz, CDCl_3)

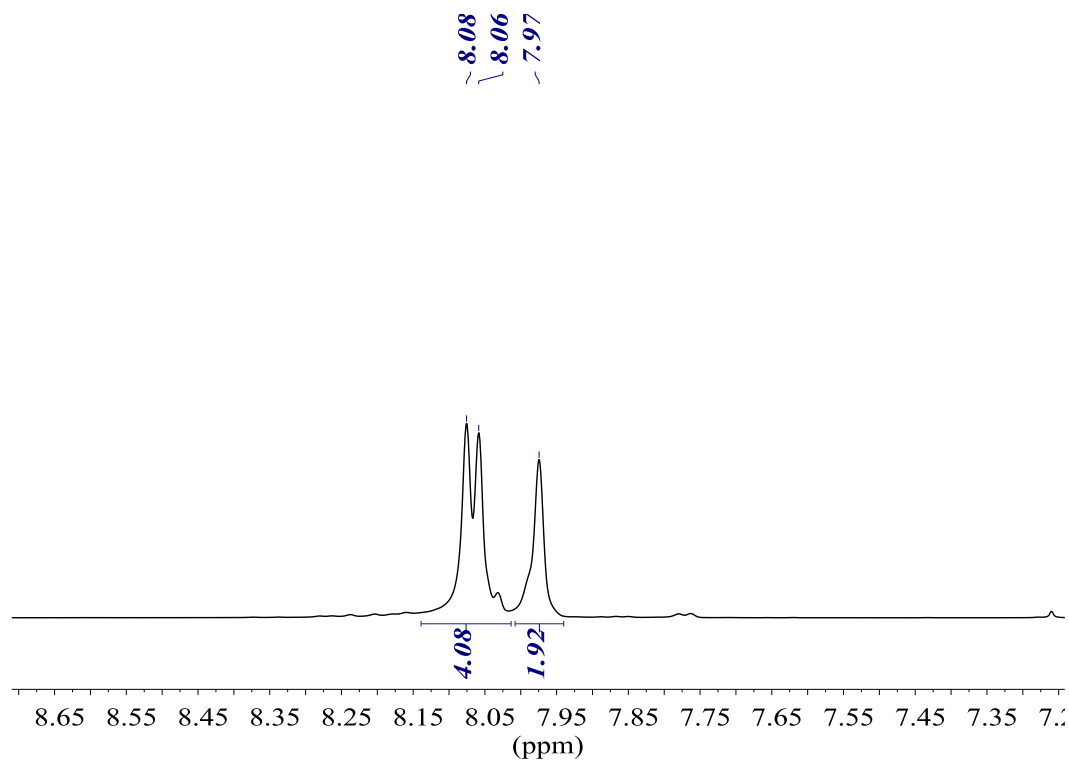


Bis(3,5-bis(trifluoromethyl)phenyl)chlorophosphine (26)

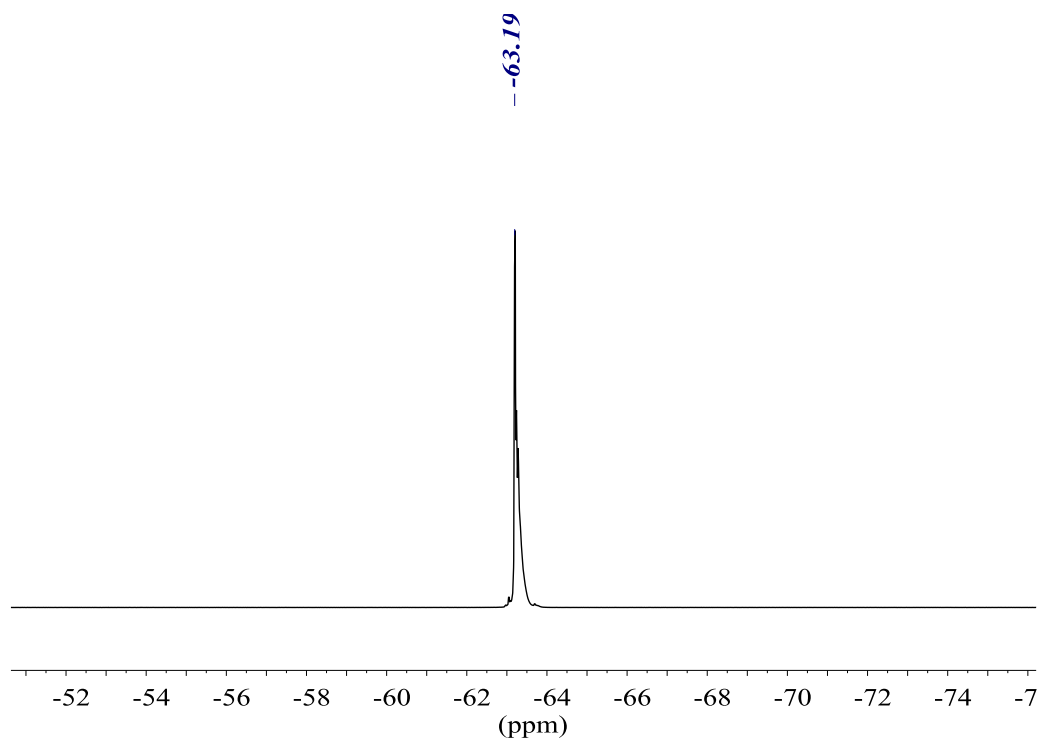
$^{31}\text{P}\{^1\text{H}\}$ NMR (161.98 MHz, CDCl_3)



^1H NMR (400.13 MHz, CDCl_3)

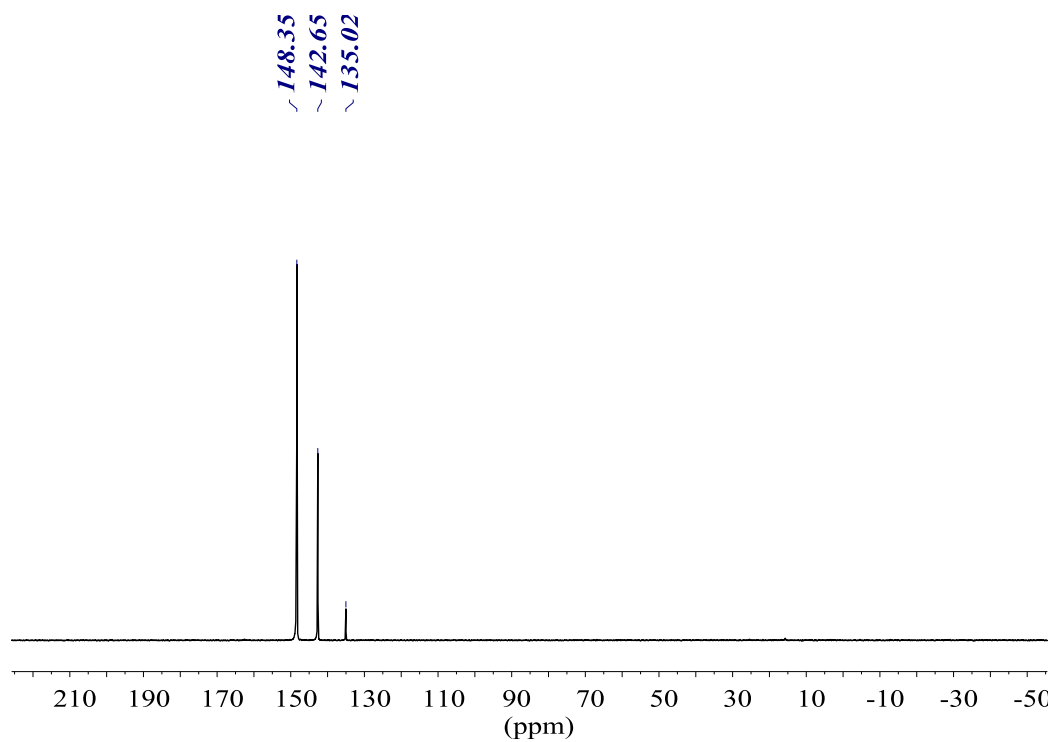
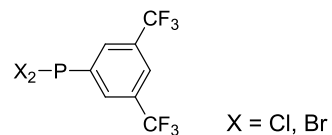


$^{19}\text{F}\{^1\text{H}\}$ NMR (376.50 MHz, CDCl_3)

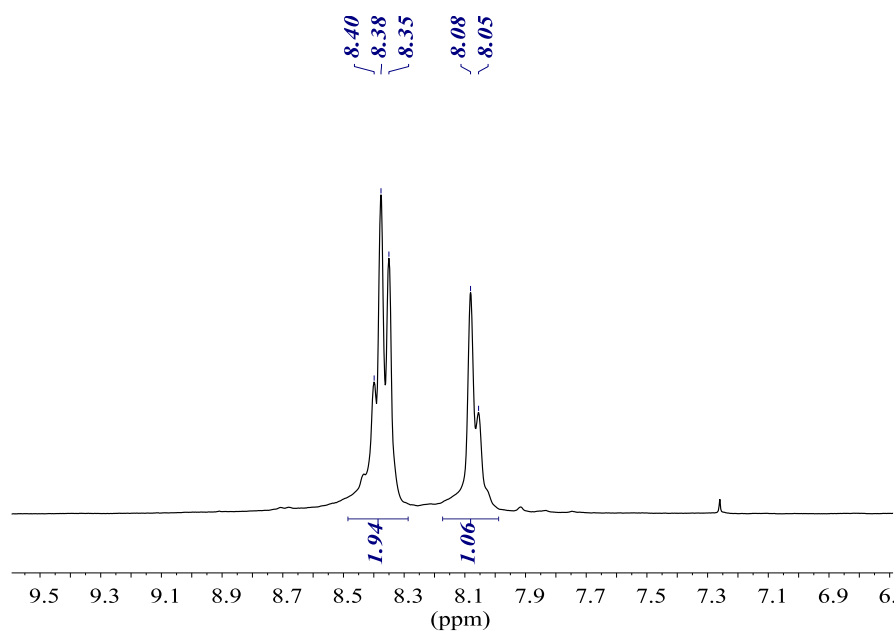


(3,5-bis(trifluoromethyl)phenyl)dichlorophosphine (27)

$^{31}\text{P}\{^1\text{H}\}$ NMR (101.2 MHz, CDCl_3)



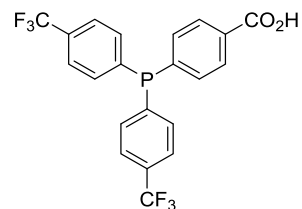
^1H NMR (250.16 MHz, CDCl_3)



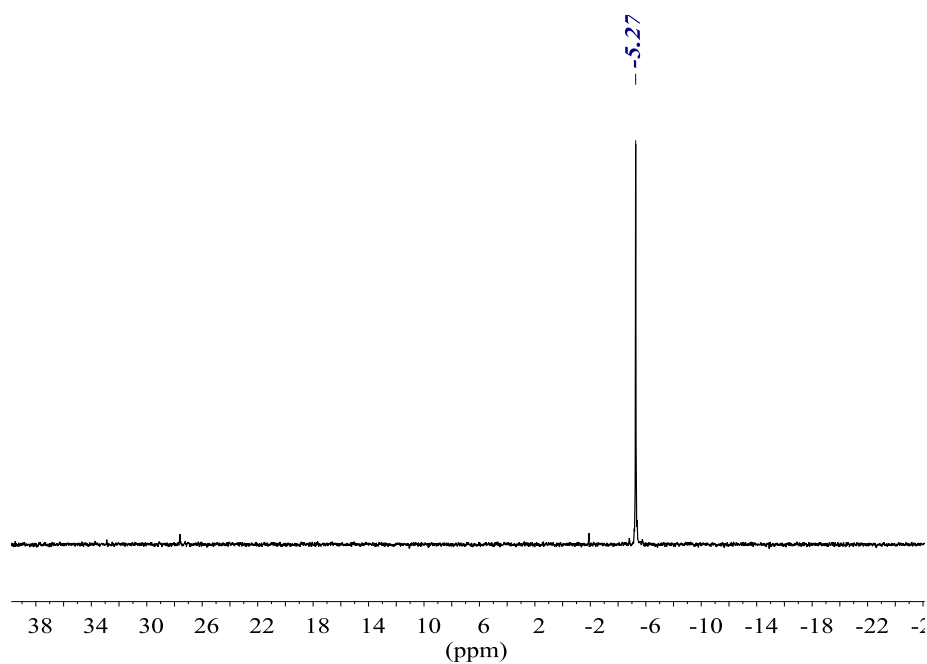
2. Characterisation of carboxylic-trifluoromethylated phosphines

2.1. Derived from homoleptic phosphines

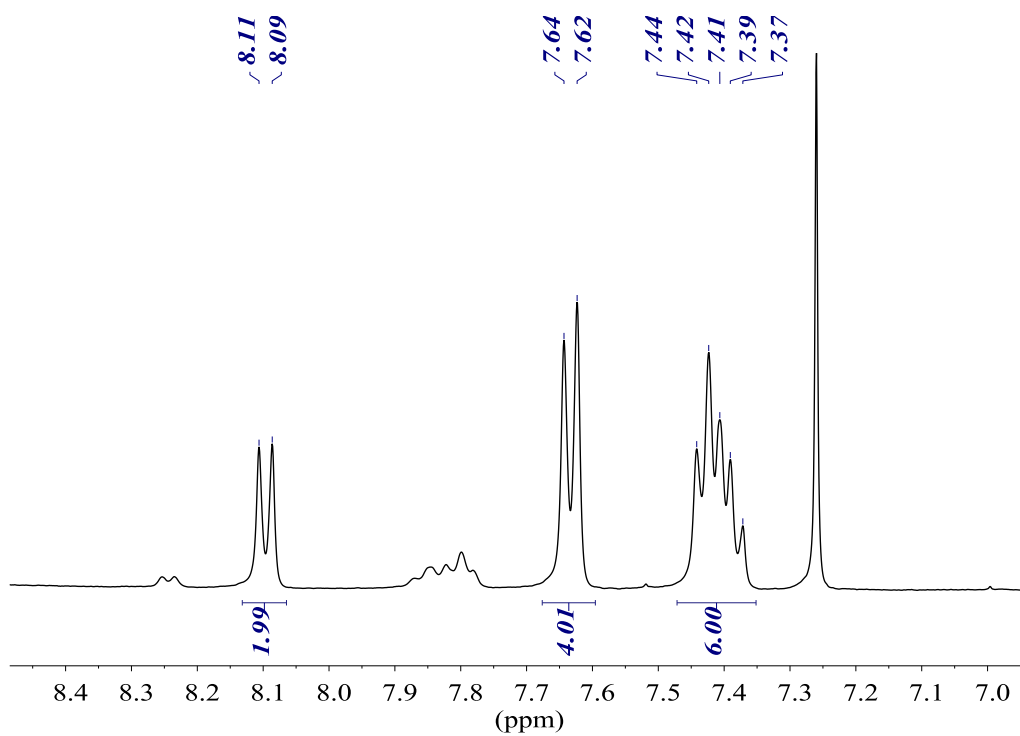
4-(bis(4-(trifluoromethyl)phenyl)phosphanyl)benzoic acid, *p*-Miranphos (2)



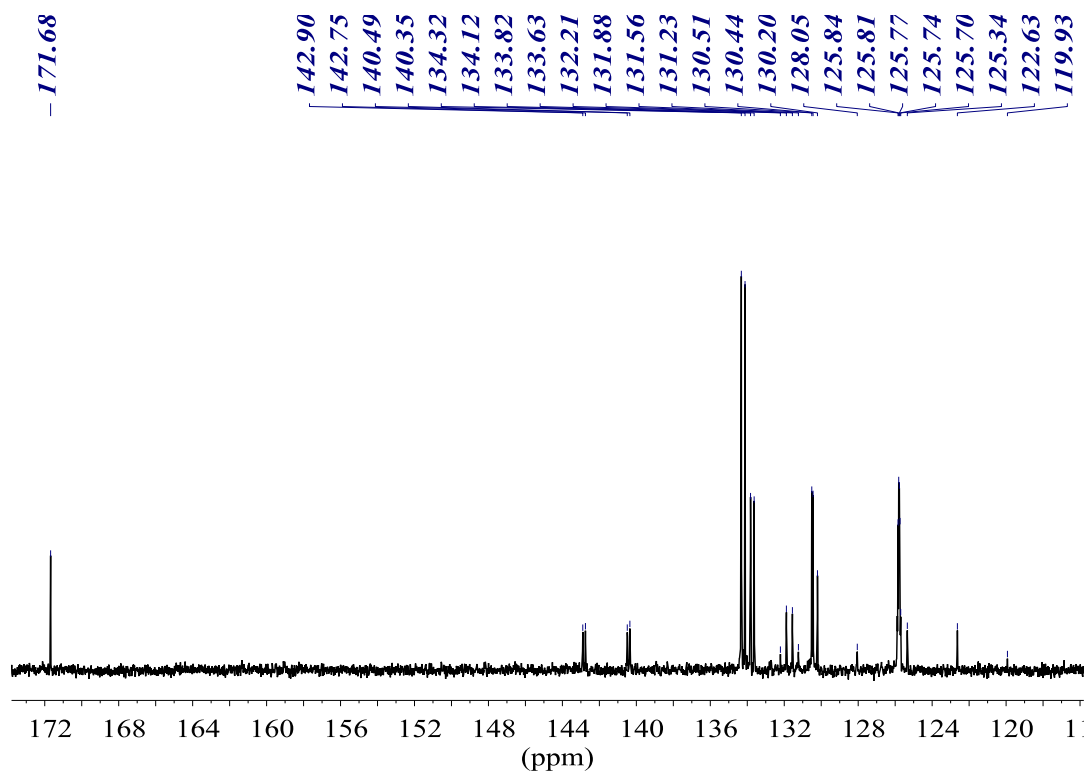
$^{31}\text{P}\{^1\text{H}\}$ NMR (101.27 MHz, CDCl_3)

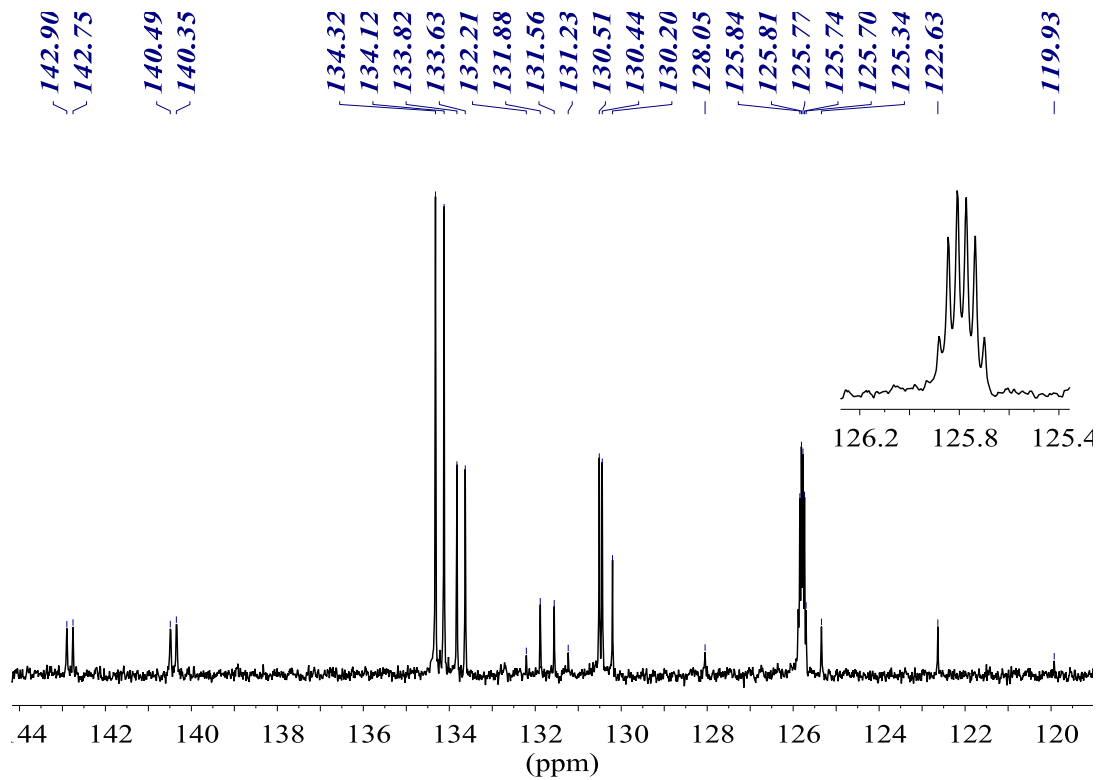


^1H NMR (400.13 MHz, CDCl_3)

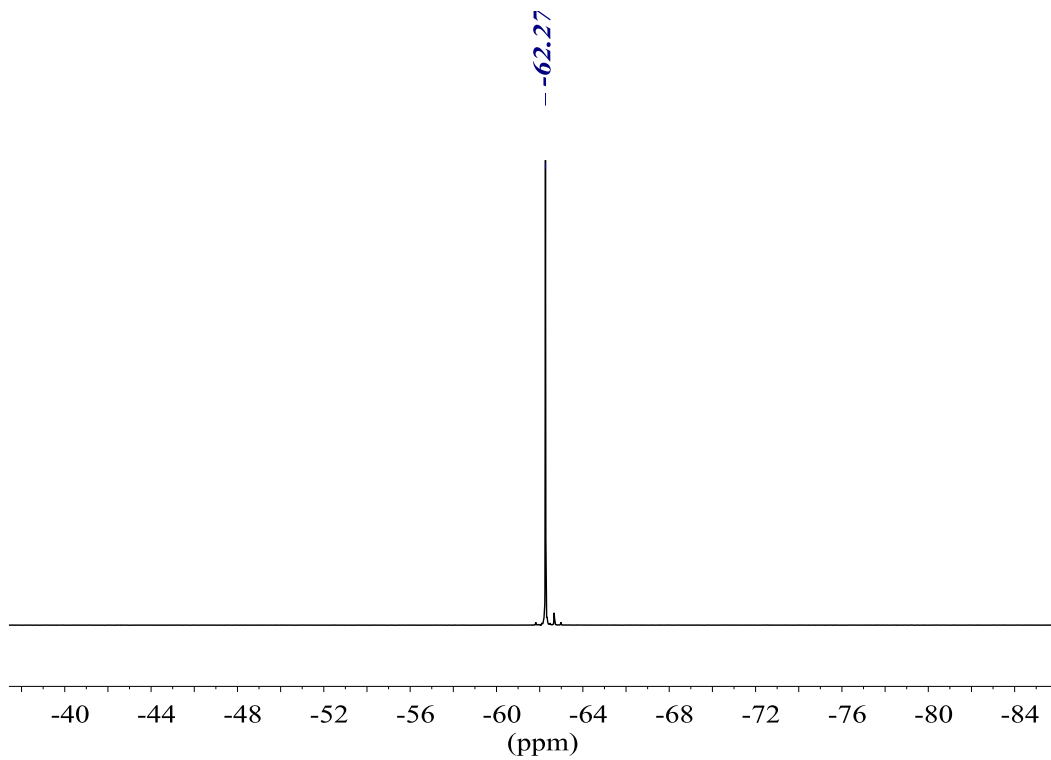


$^{13}\text{C}\{^1\text{H}\}$ NMR (100.61 MHz, CDCl_3)

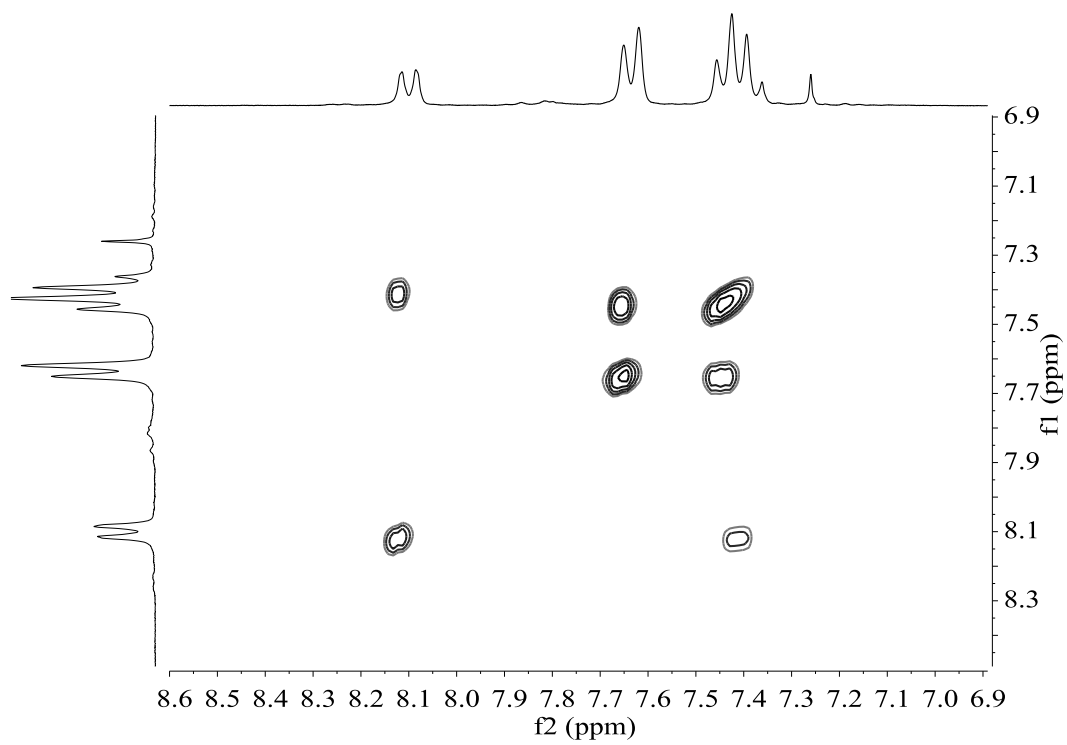




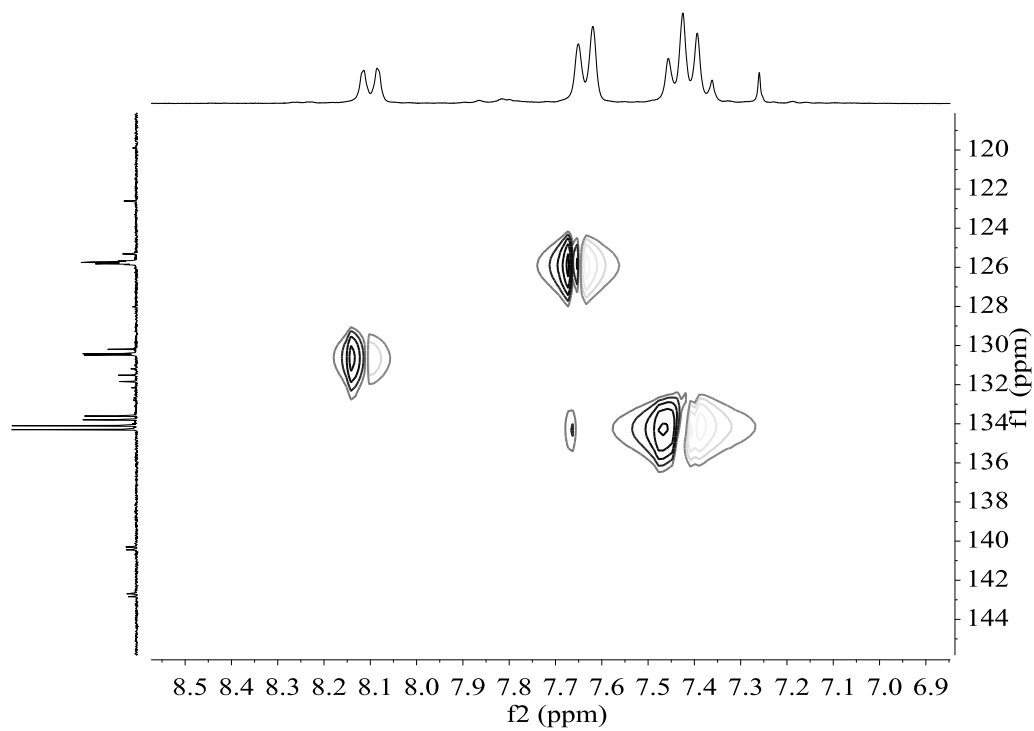
$^{19}\text{F}\{^1\text{H}\}$ NMR (376.50 MHz, CDCl_3)



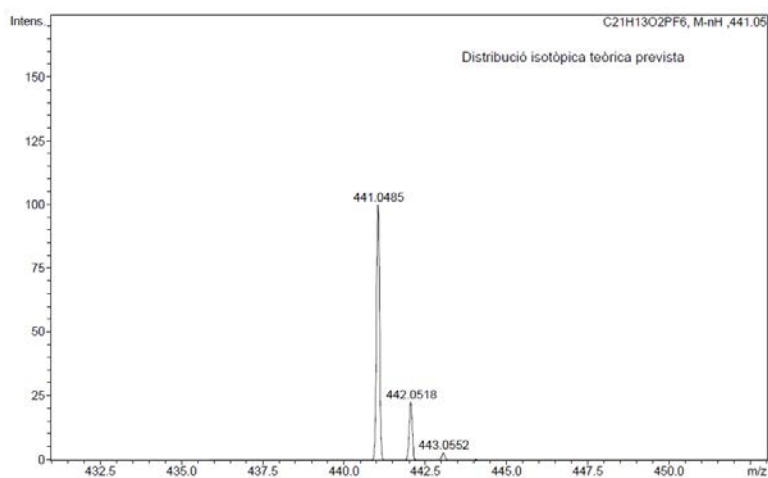
COSY NMR (400.13 MHz, CDCl₃)



HSQC NMR (400.13 MHz, CDCl₃)

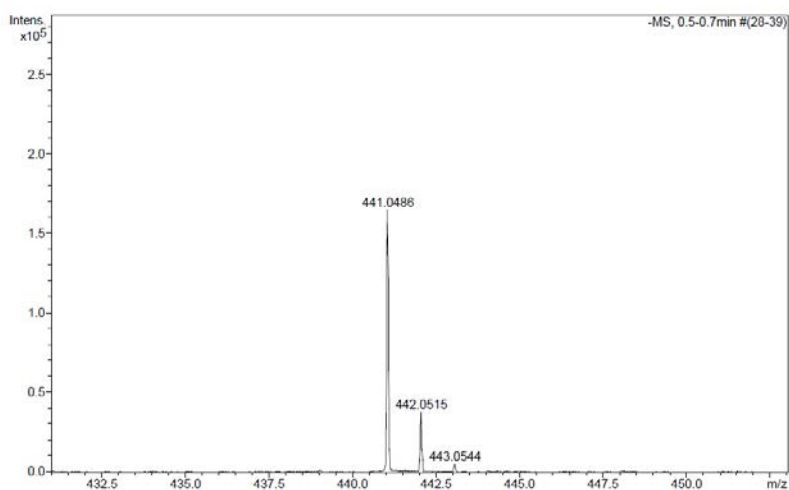


HR-MS (ESI m/z) [M-H]⁻
 calculated for [C₂₁H₁₂F₆O₂P]⁻



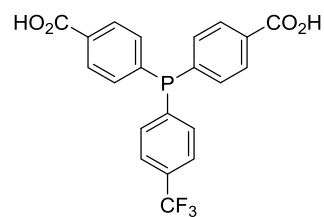
#	m/z	I	I%
1	441.0485	100	100.0
2	442.0518	23	22.9
3	443.0552	3	2.9

found

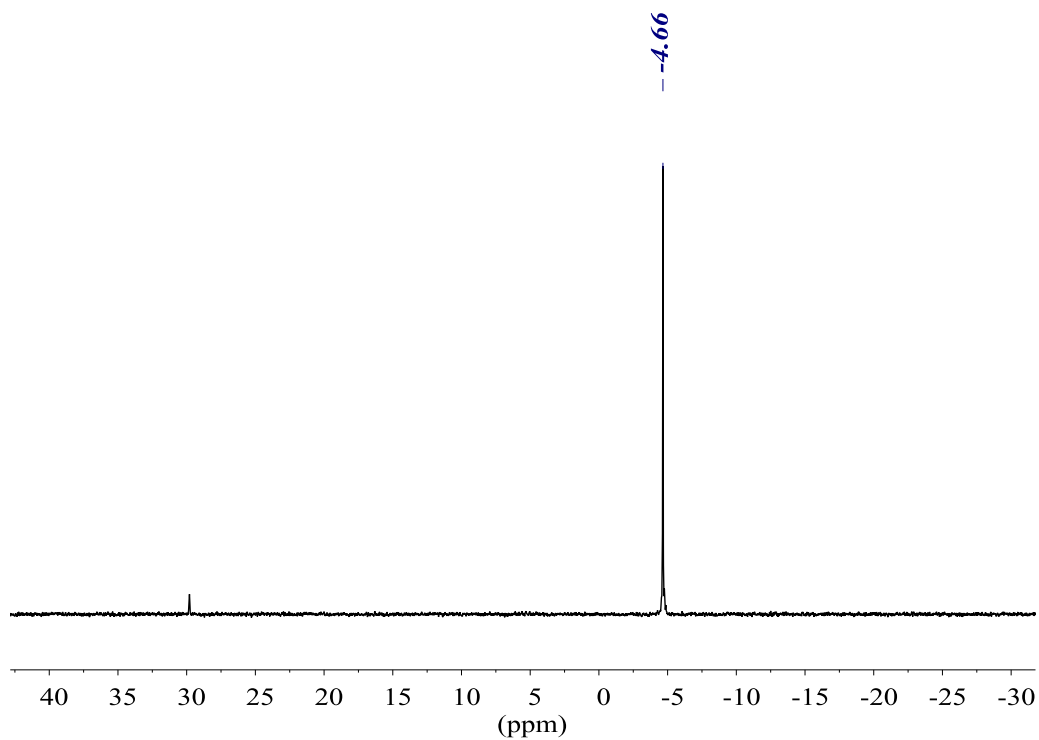


#	m/z	I	I%
1	441.0486	164644	100.0
2	442.0515	37951	23.1
3	443.0544	5198	3.2

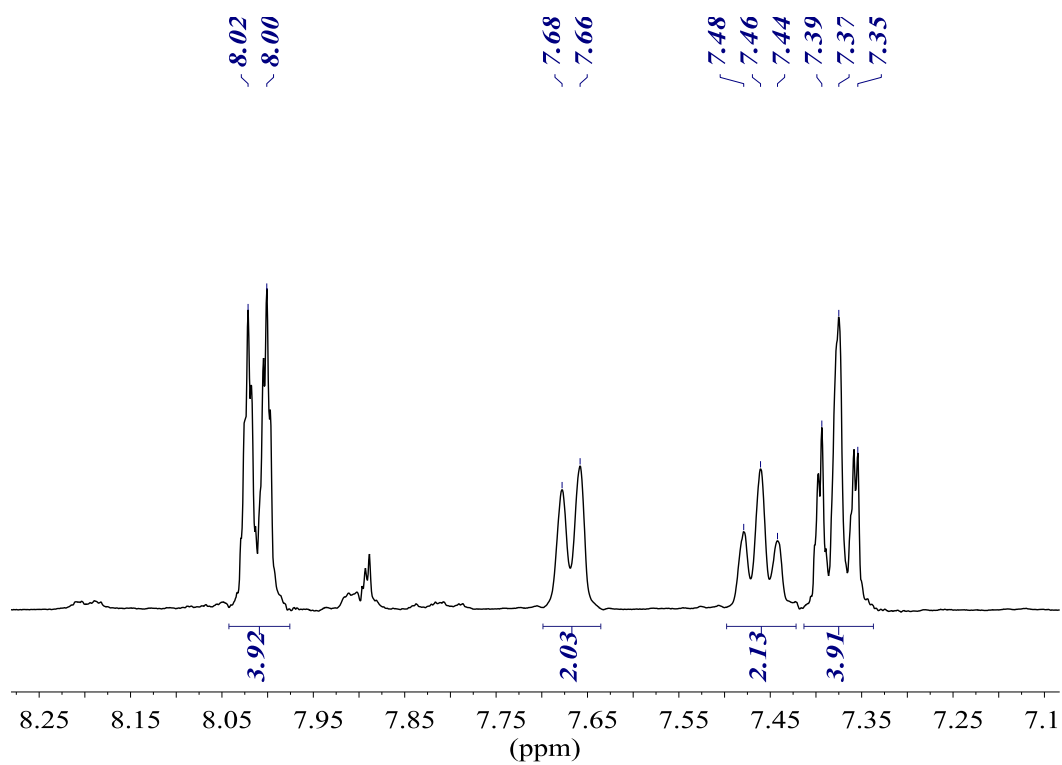
4,4'-((4-(trifluoromethyl)phenyl)phosphanediyl)dibenzoic acid, *p*-Miran2phos (3)



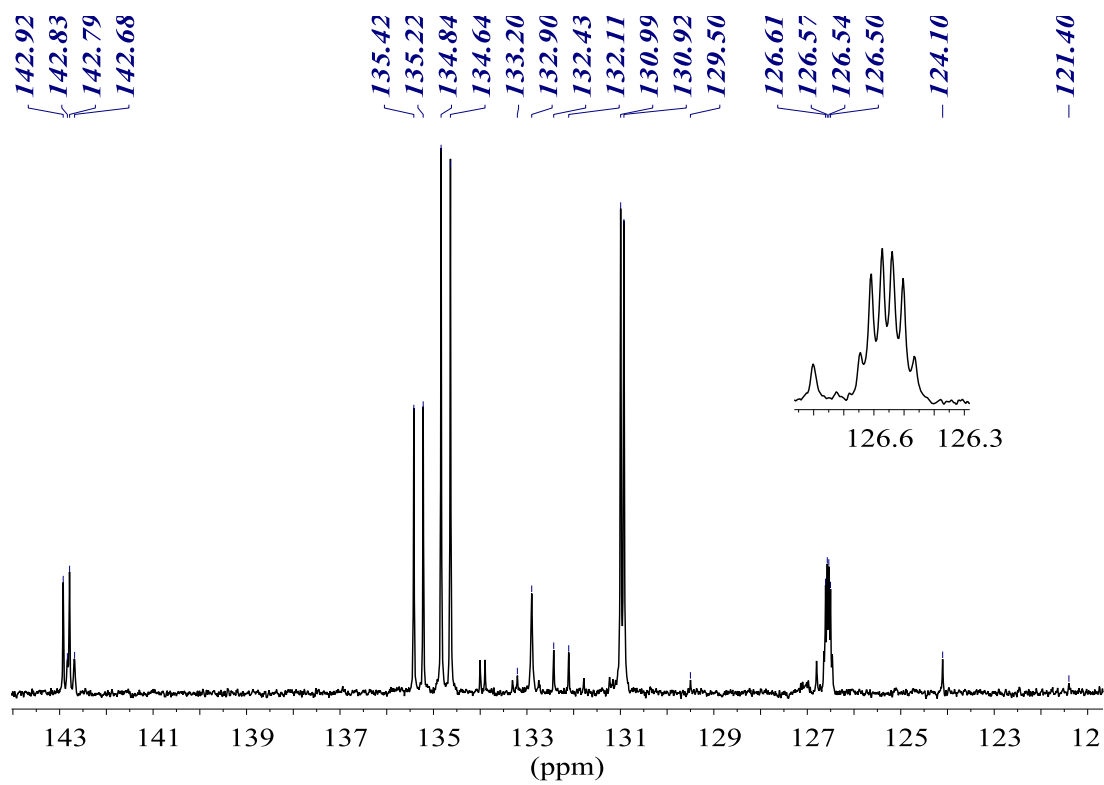
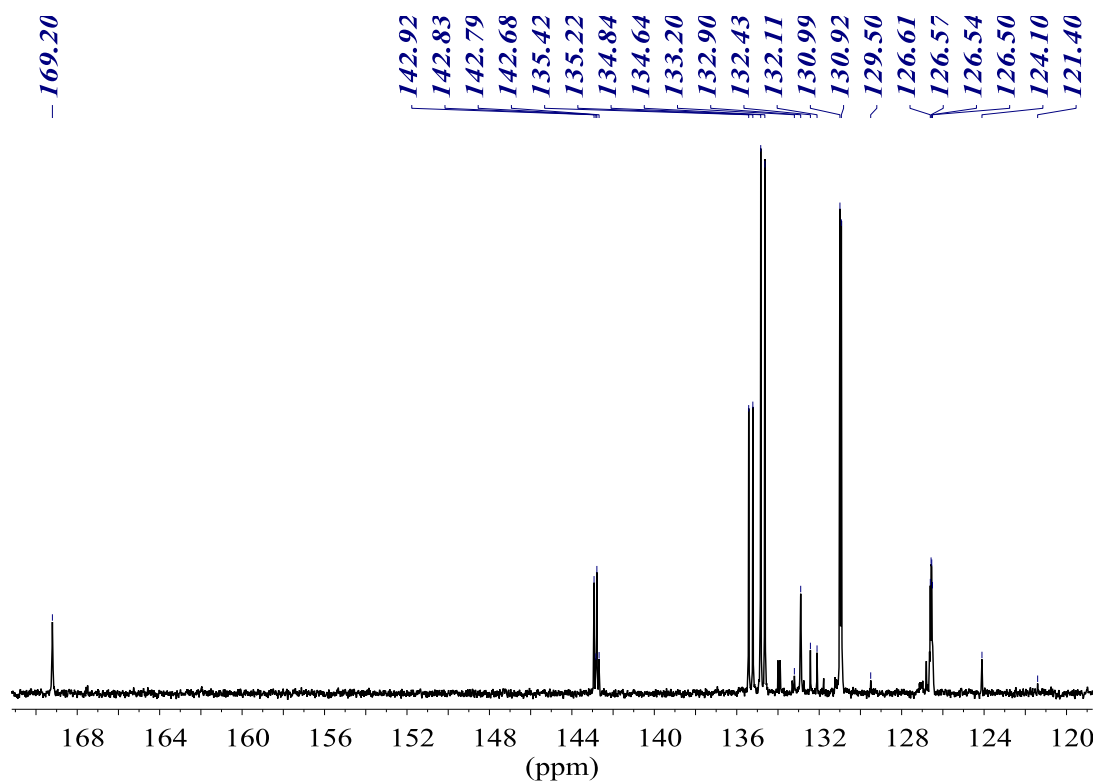
$^{31}\text{P}\{^1\text{H}\}$ NMR (101.27 MHz, CD_3OD)



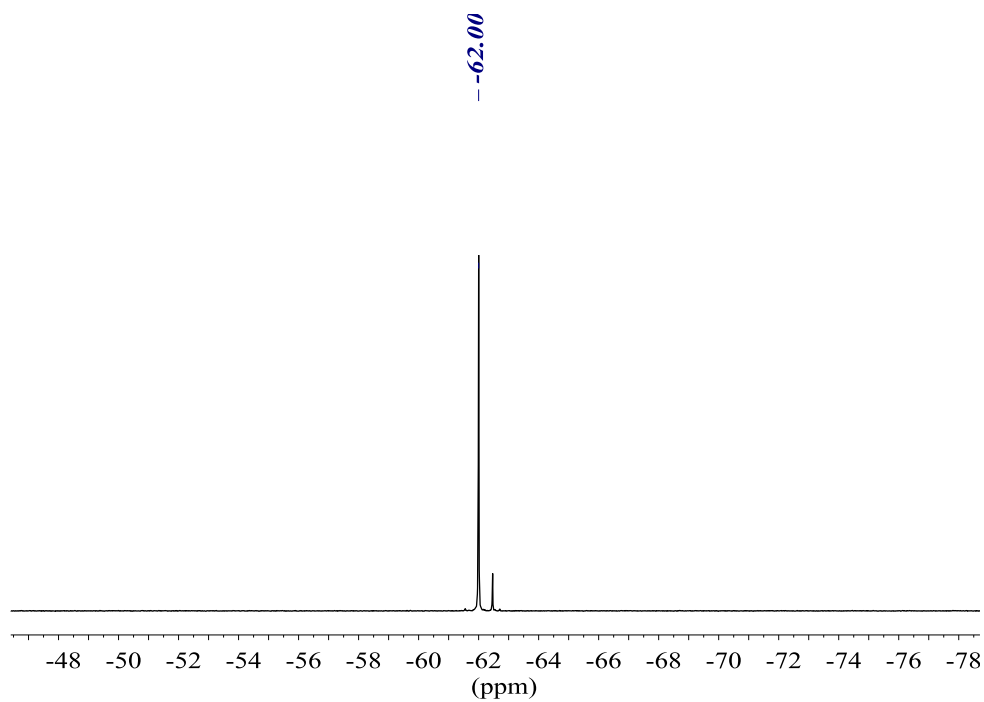
^1H NMR (400.13 MHz, CD_3OD)



$^{13}\text{C}\{^1\text{H}\}$ NMR (100.61 MHz, CD_3OD)

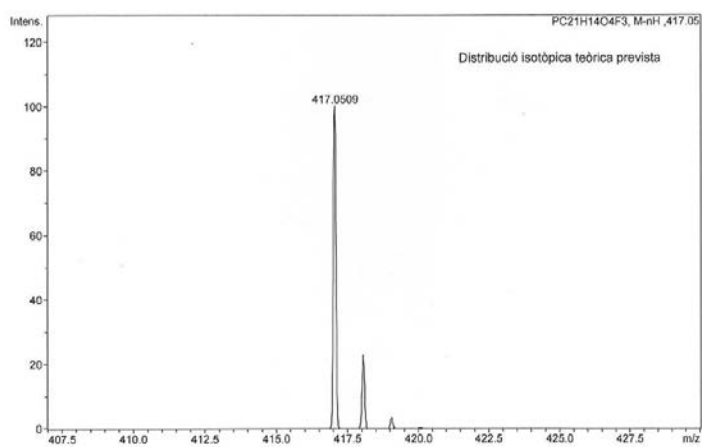


$^{19}\text{F}\{^1\text{H}\}$ NMR (235.39 MHz, CD_3OD)



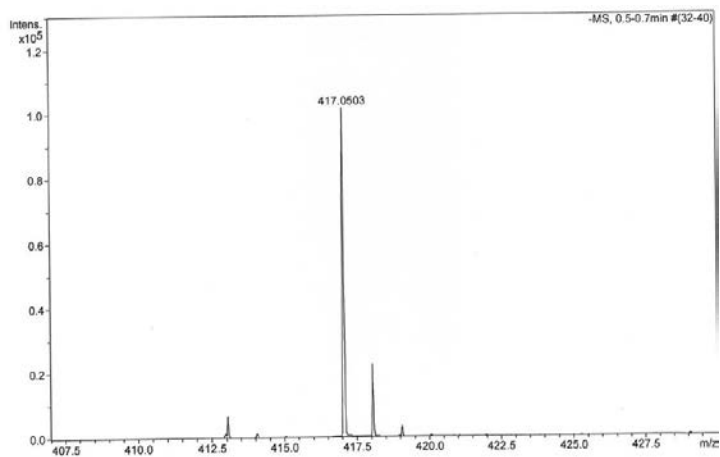
HR-MS (ESI m/z) $[\text{M-H}]^-$

calculated for $[\text{C}_{21}\text{H}_{13}\text{F}_3\text{O}_4\text{P}]^-$



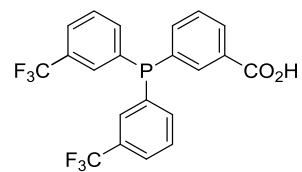
#	m/z	I	I %
1	417.0509	100	100.0
2	418.0543	23	23.0
3	419.0576	3	3.3

found

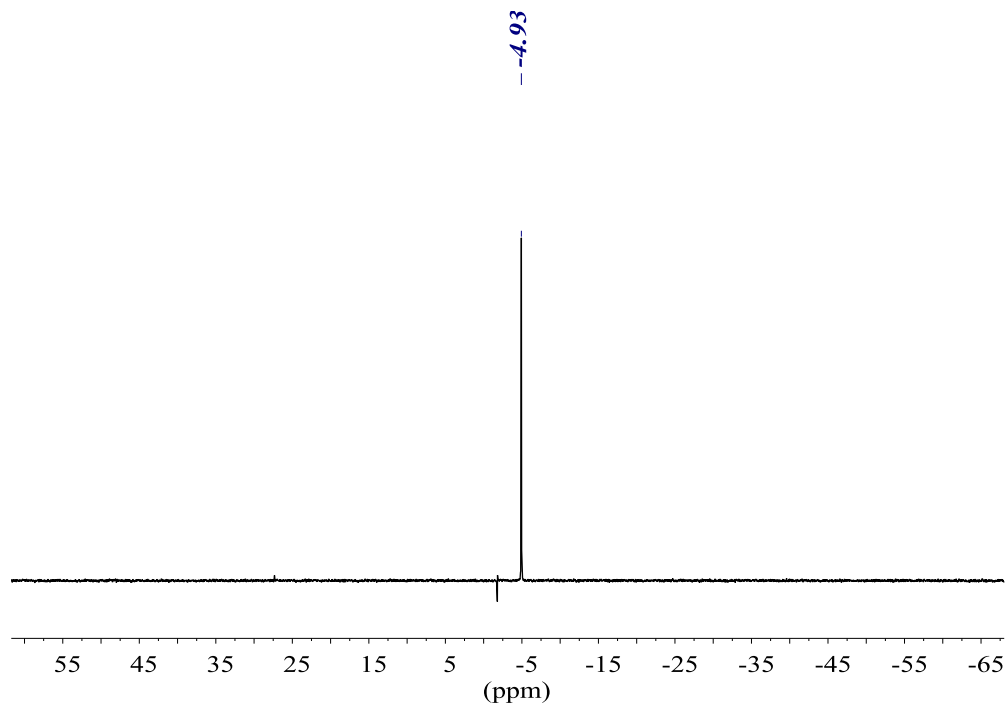


#	m/z	I	I %
1	417.0503	101686	100.0
2	418.0529	22379	22.0
3	419.0556	3231	3.2

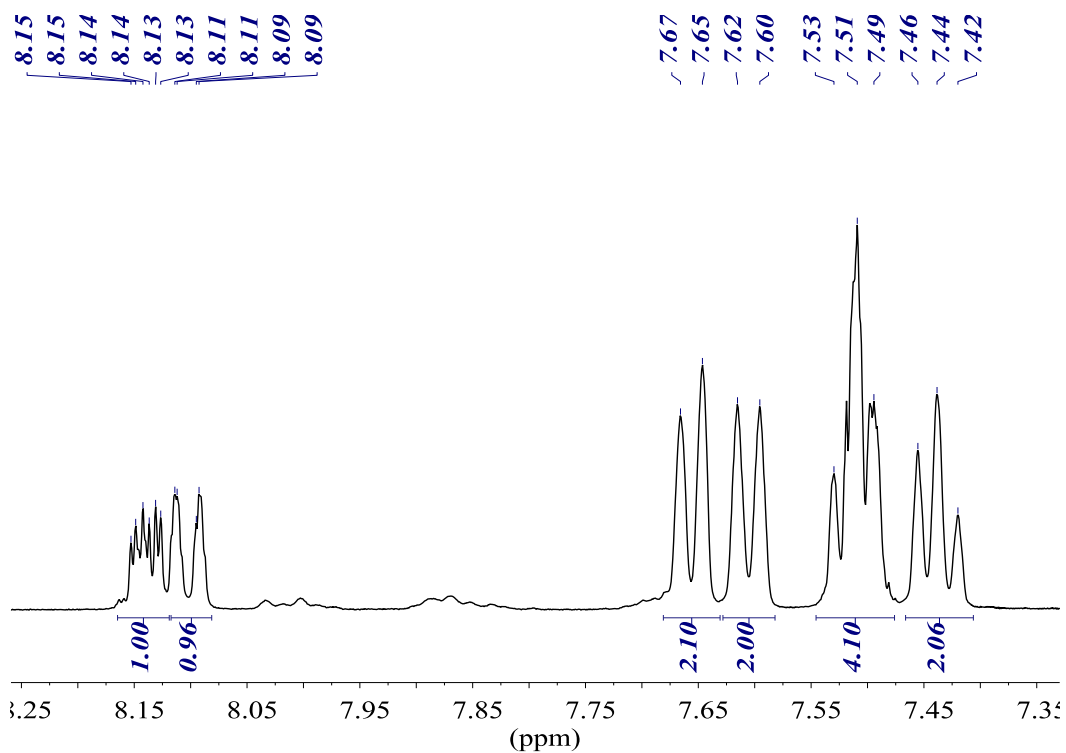
3-(bis(3-(trifluoromethyl)phenyl)phosphanyl)benzoic acid, *m*-Miranphos (6)



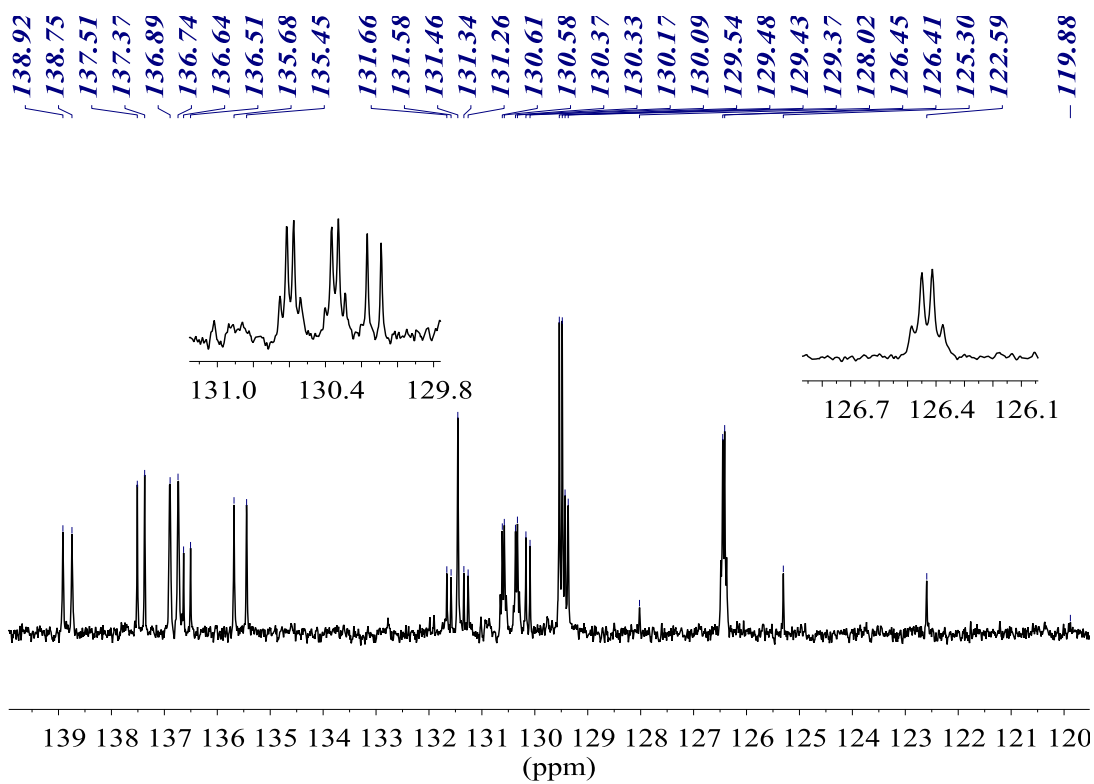
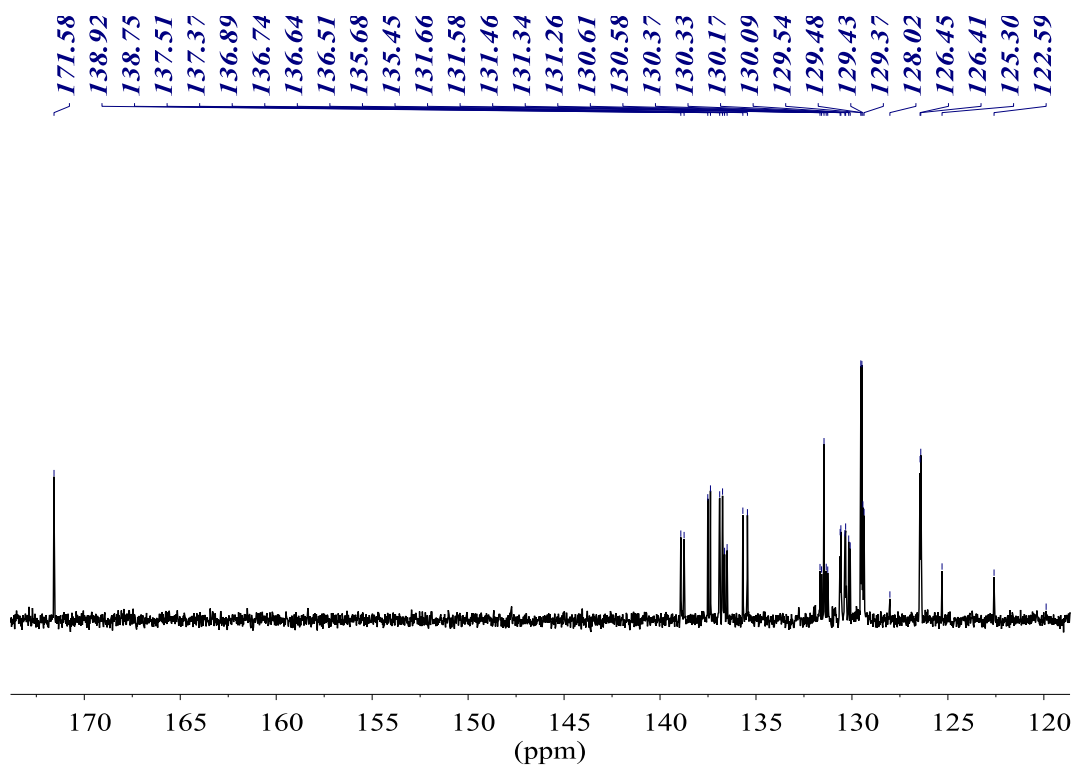
$^{31}\text{P}\{^1\text{H}\}$ NMR (161.98 MHz, CDCl_3)



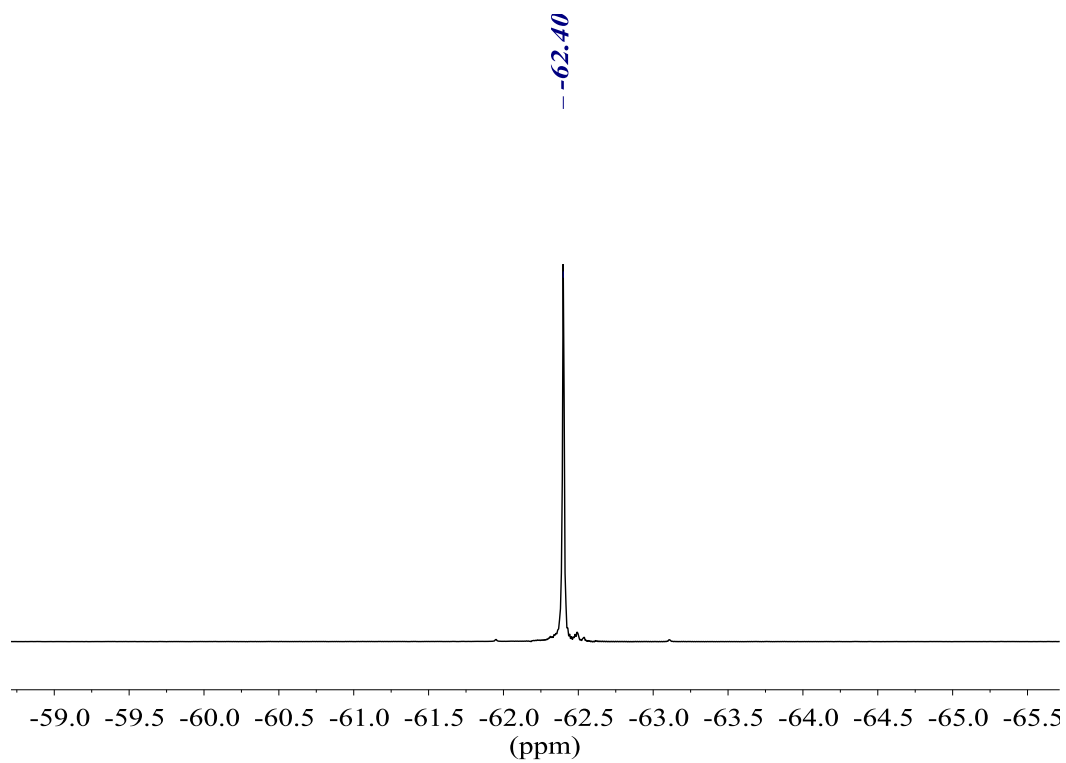
^1H NMR (400.13 MHz, CDCl_3)



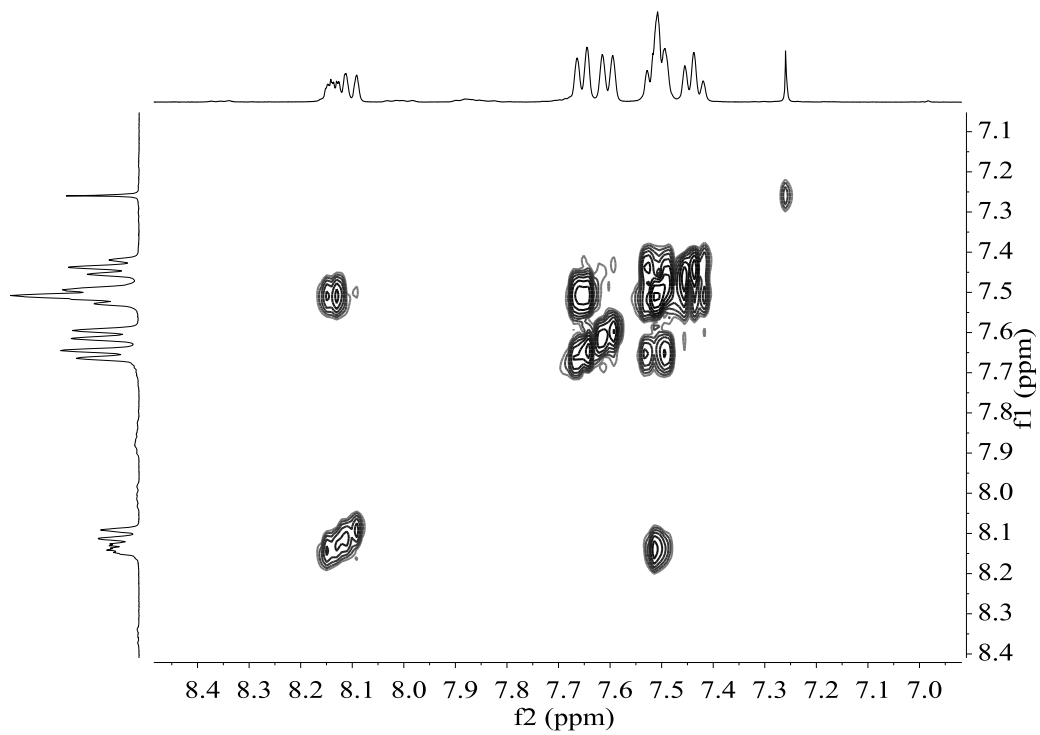
$^{13}\text{C}\{^1\text{H}\}$ NMR (100.61 MHz, CDCl_3)



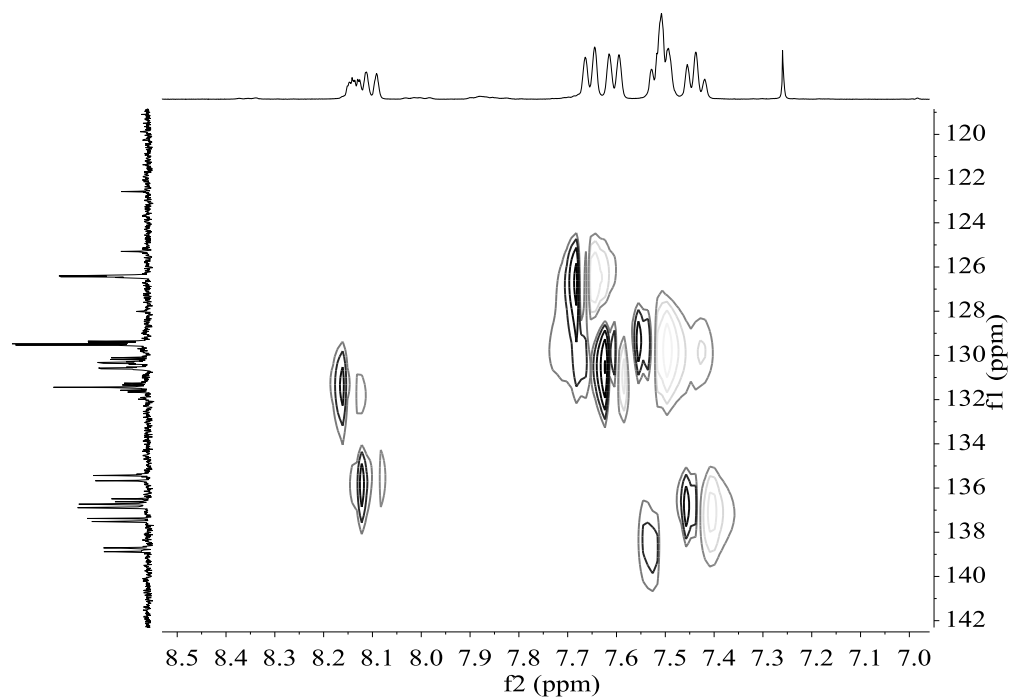
$^{19}\text{F}\{^1\text{H}\}$ NMR (376.50 MHz, CDCl_3)



COSY NMR (400.13 MHz, CDCl_3)

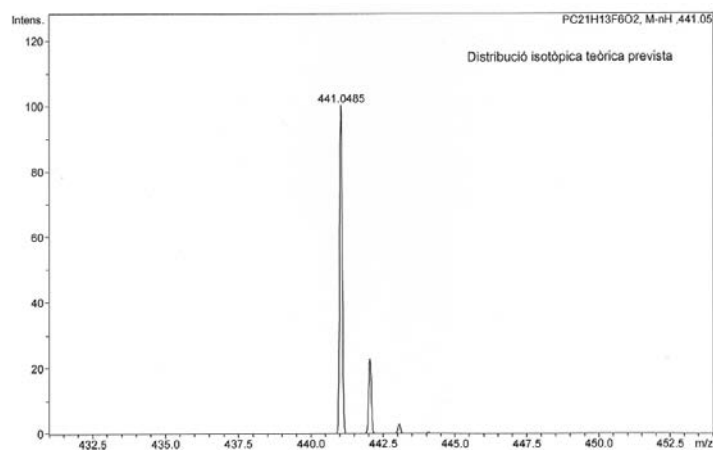


HSQC NMR (400.13 MHz, CDCl₃)



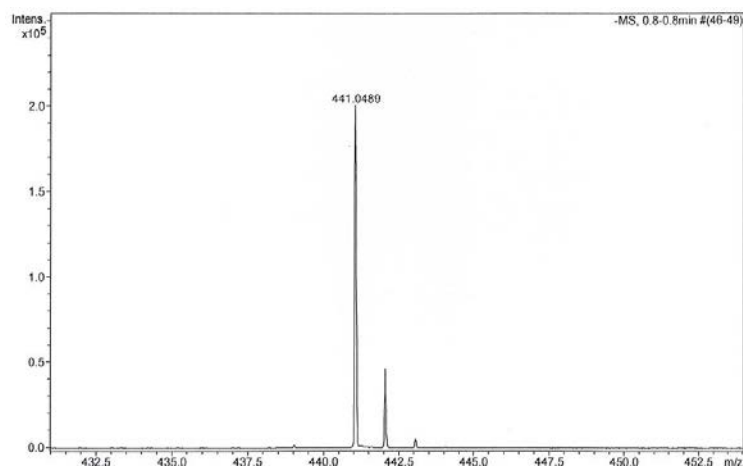
HR-MS (ESI⁻ *m/z*) [M-H]⁻

calculated for [C₂₁H₁₂F₆O₂P]⁻



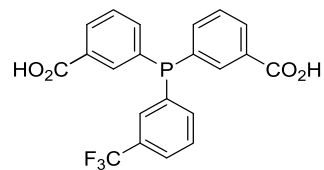
#	<i>m/z</i>	I	I%
1	441.0485	100	100.0
2	442.0518	23	22.9
3	443.0552	3	2.9

found

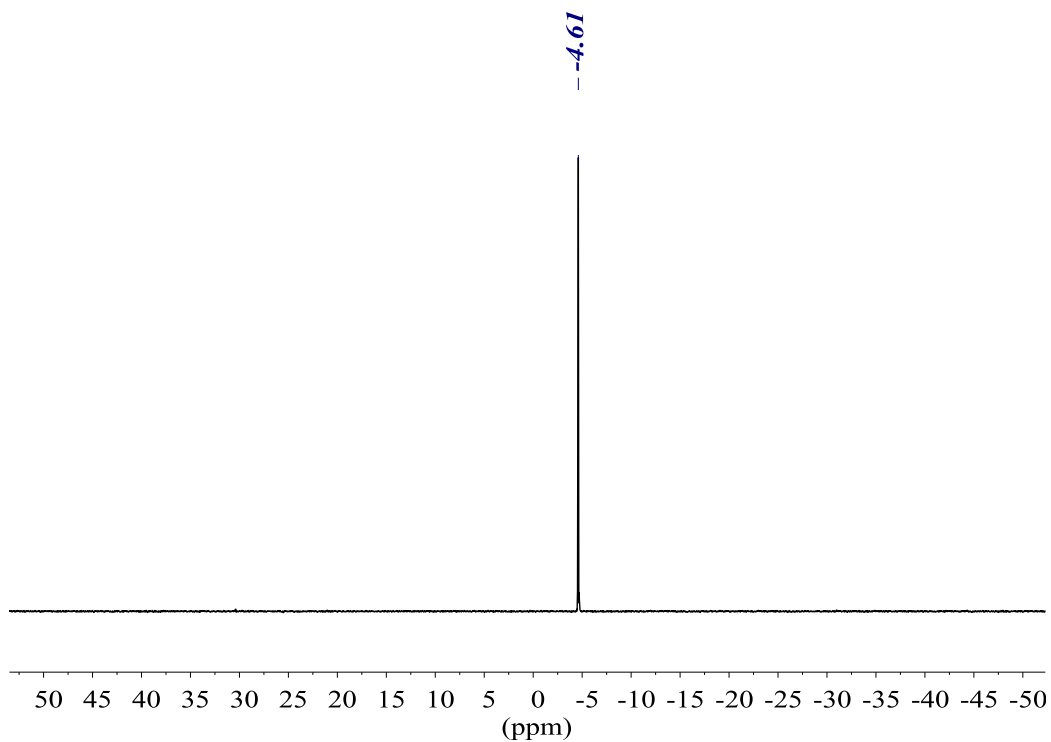


#	<i>m/z</i>	I	I%
1	441.0489	200125	100.0
2	442.0512	46380	23.2
3	443.0547	5585	2.8

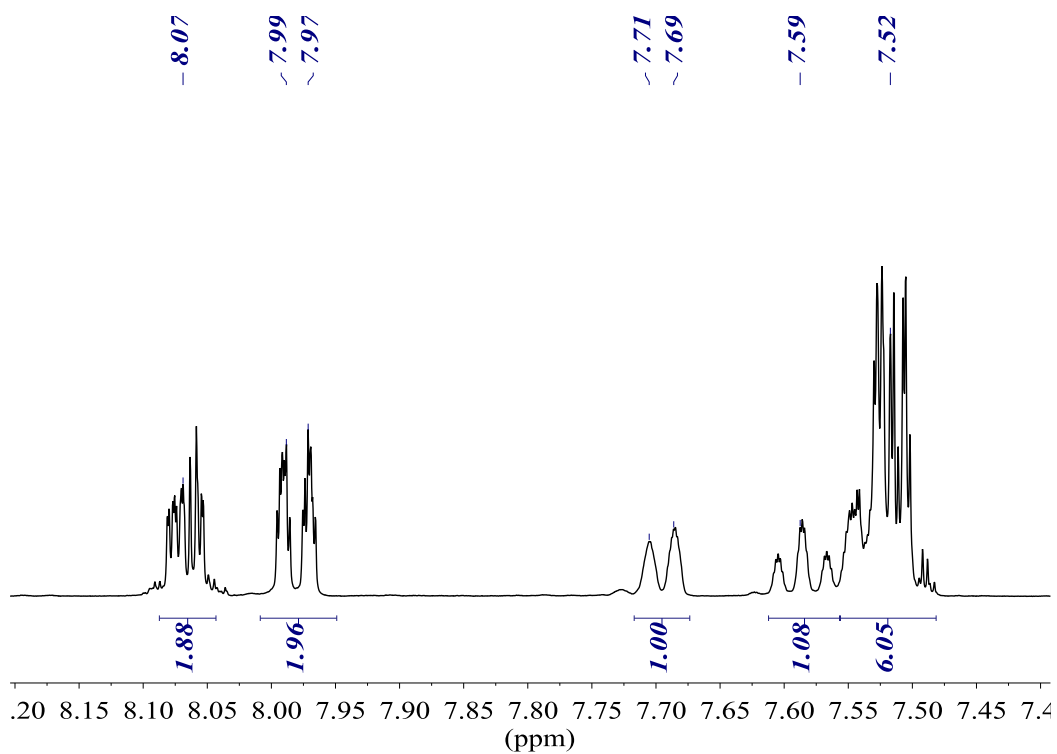
3,3'-((3-(trifluoromethyl)phenyl)phosphanediy)dibenzoic acid, *m*-Miran2phos (7)



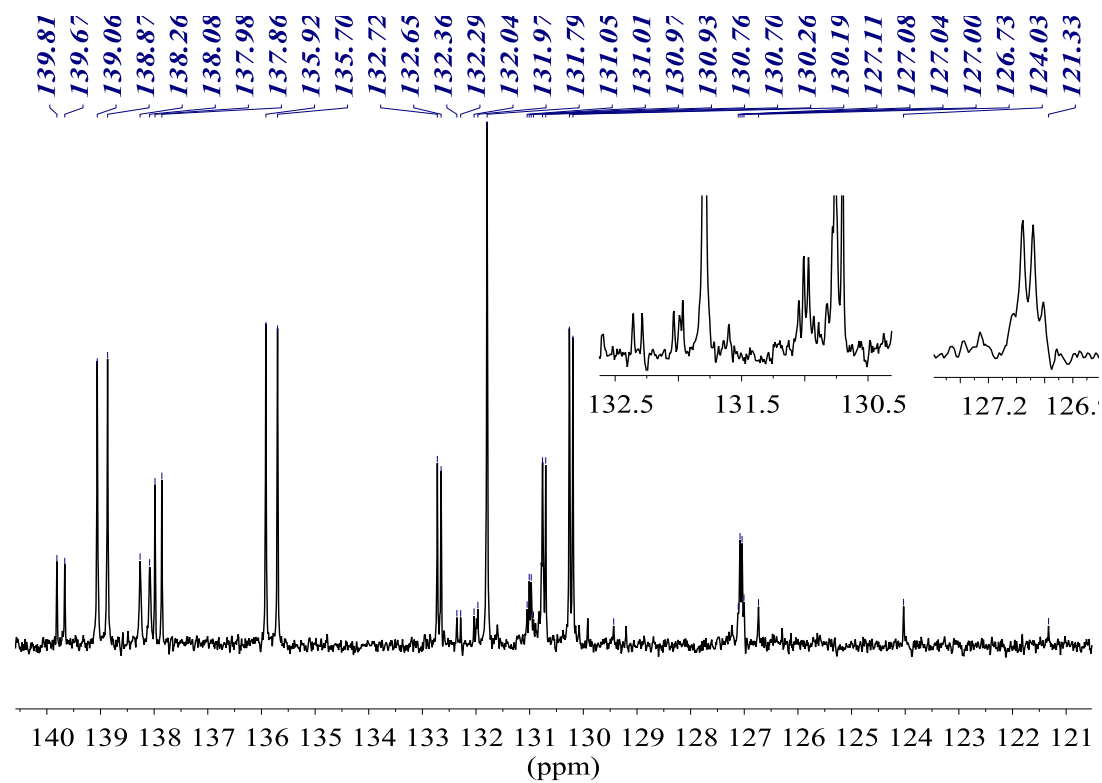
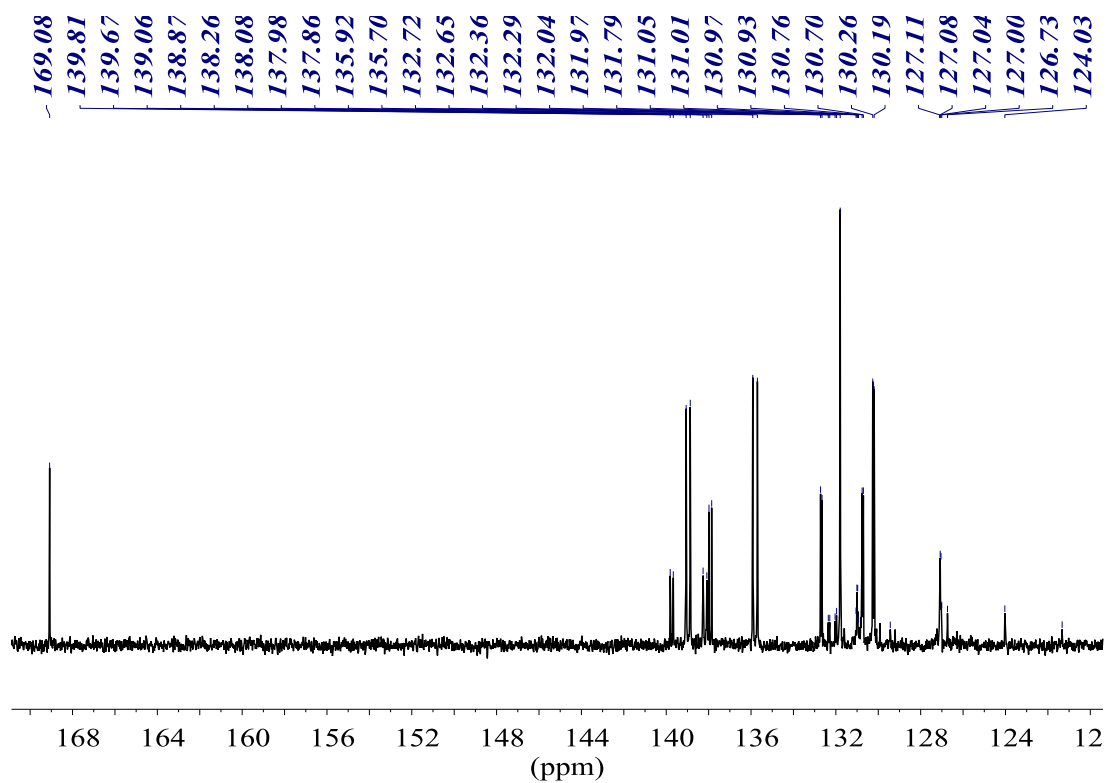
$^{31}\text{P}\{^1\text{H}\}$ NMR (161.98 MHz, CD_3OD)



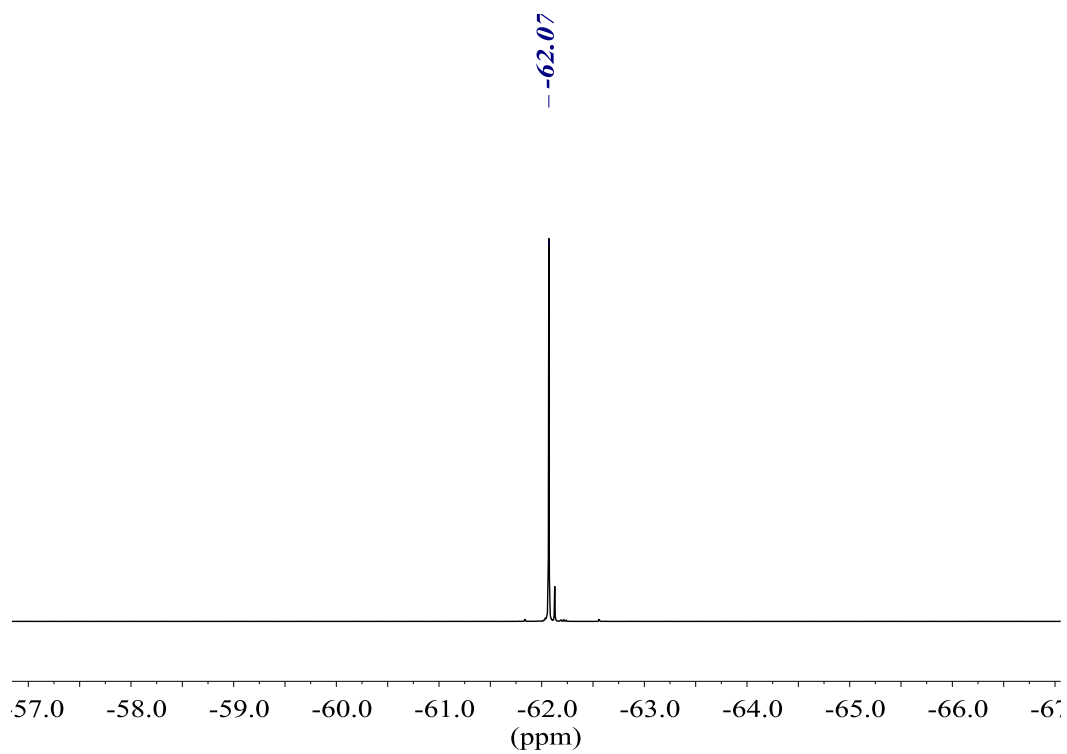
^1H NMR (400.13 MHz, CD_3OD)



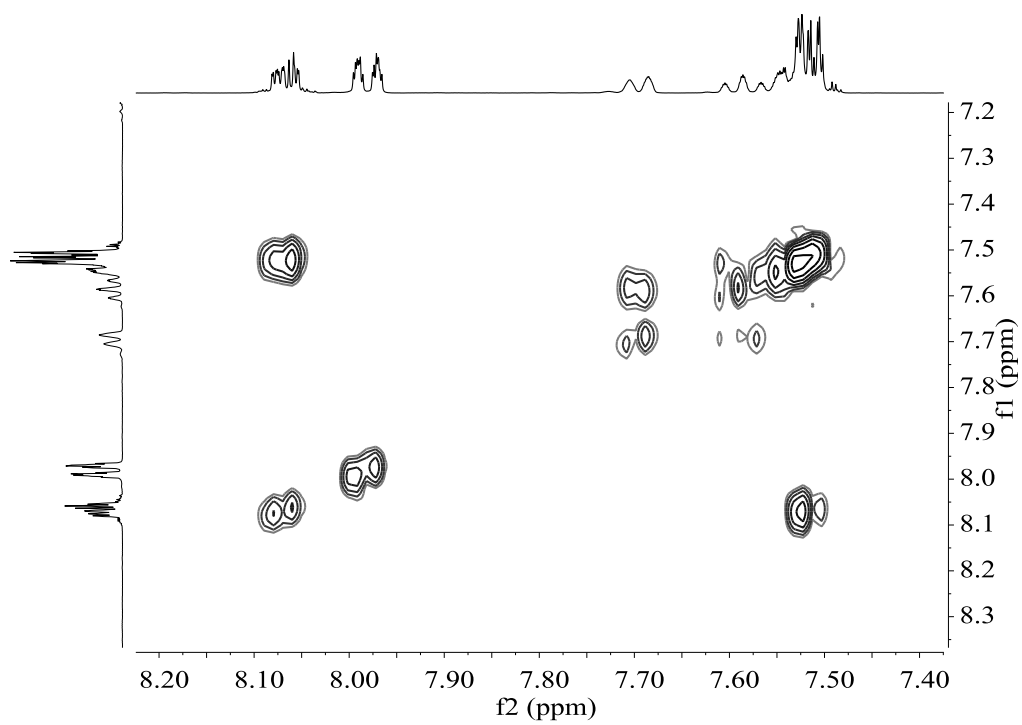
$^{13}\text{C}\{^1\text{H}\}$ NMR (100.61 MHz, CD_3OD)



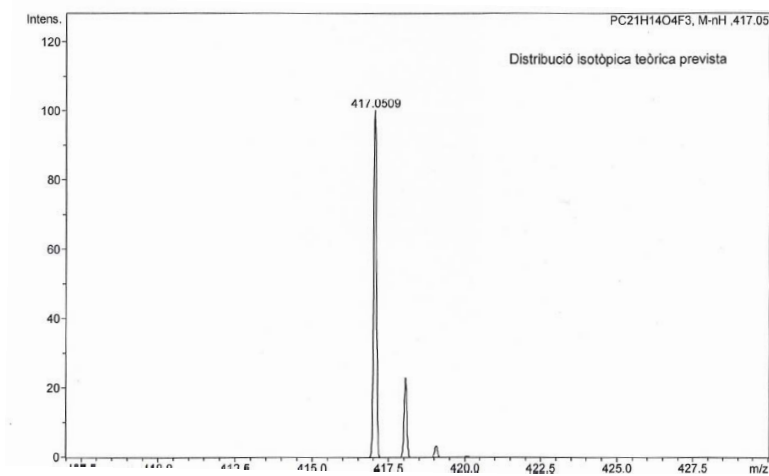
$^{19}\text{F}\{^1\text{H}\}$ NMR (376.50 MHz, CD_3OD)



COSY NMR (400.13 MHz, CD_3OD)

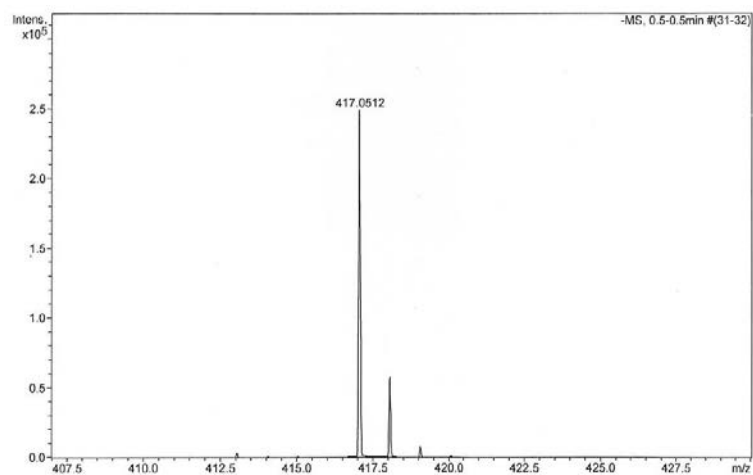


HR-MS (ESI m/z) [M-H]⁻
 calculated for [C₂₁H₁₃F₃O₄P]⁻



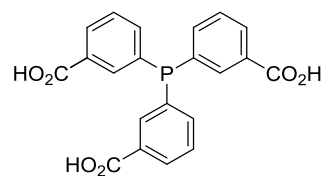
#	m/z	I	I %
1	417.0509	100	100.0
2	418.0543	23	23.0
3	419.0576	3	3.3

found

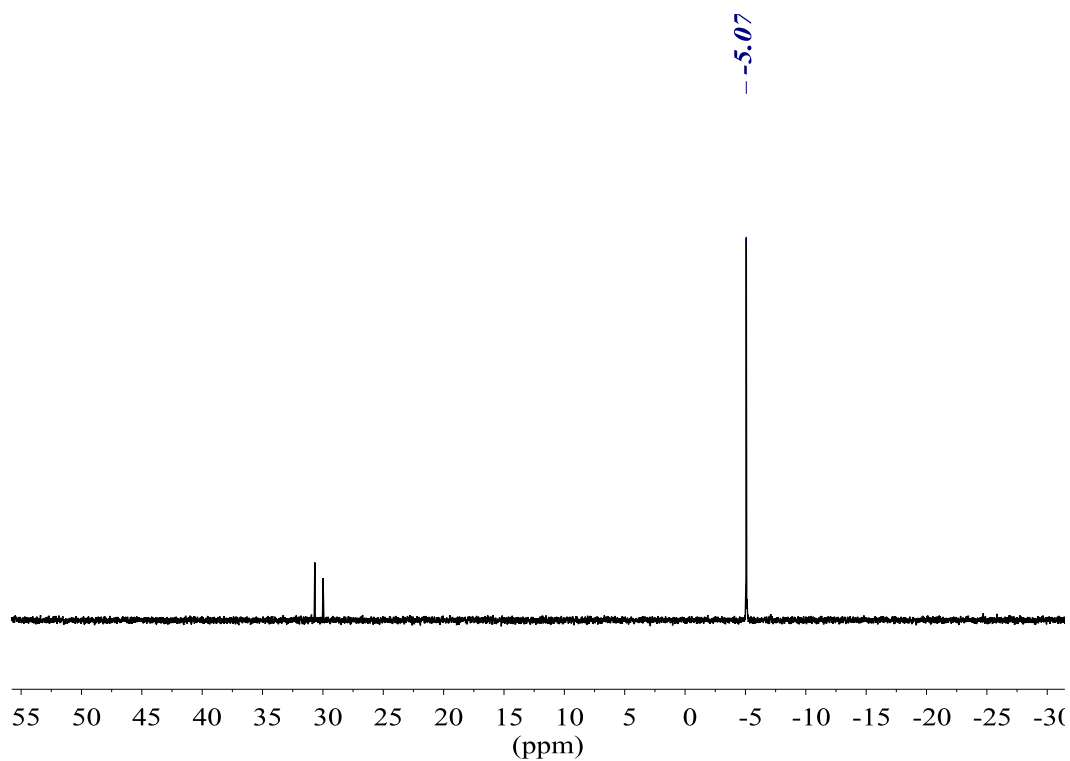


#	m/z	I	I %
1	417.0512	248910	100.0
2	418.0537	57557	23.1
3	419.0555	7600	3.1

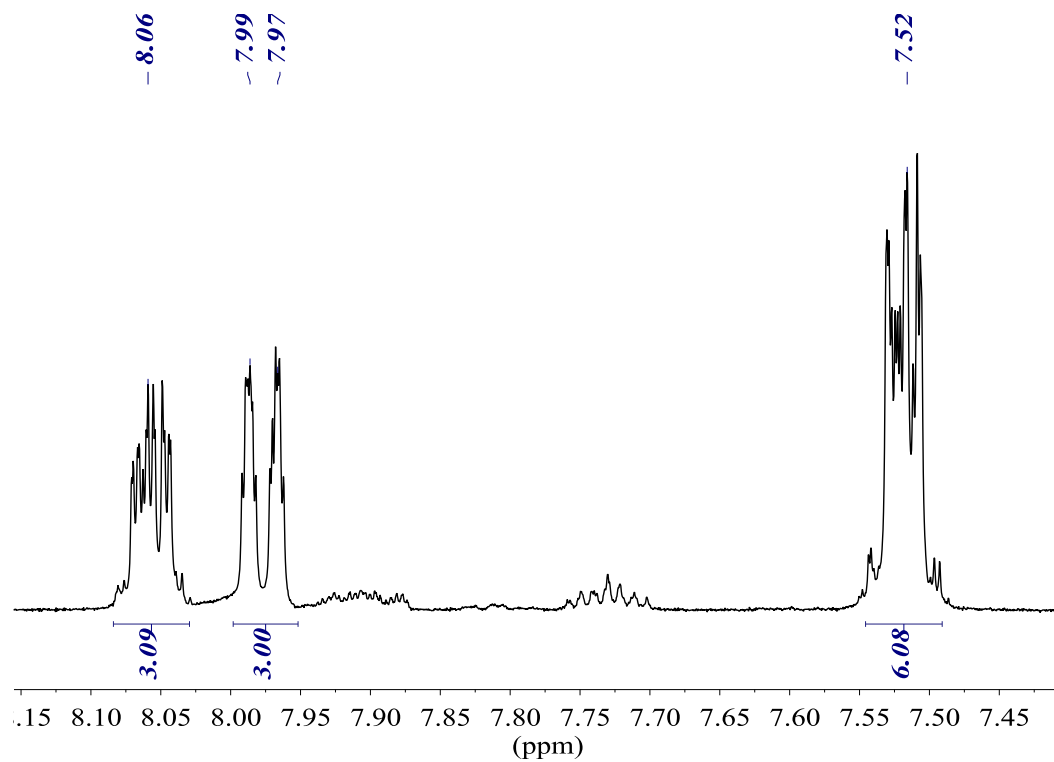
3,3',3''-phosphanetriyltribenzoic acid (8)



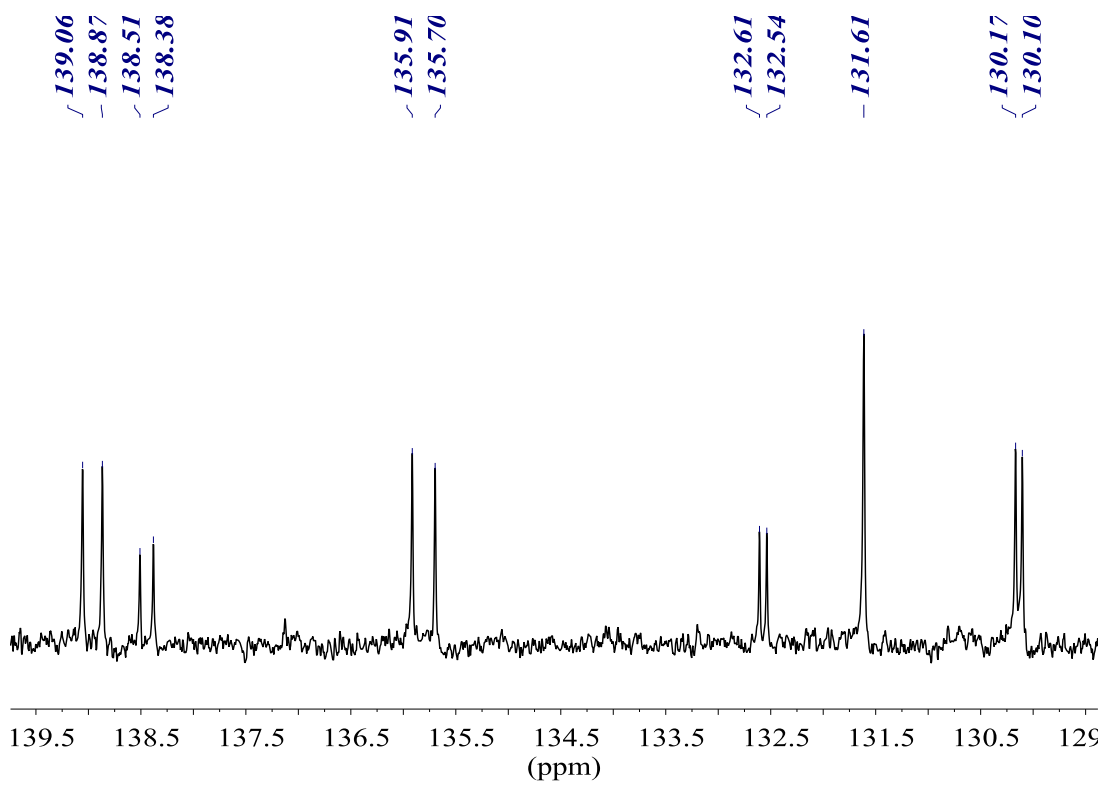
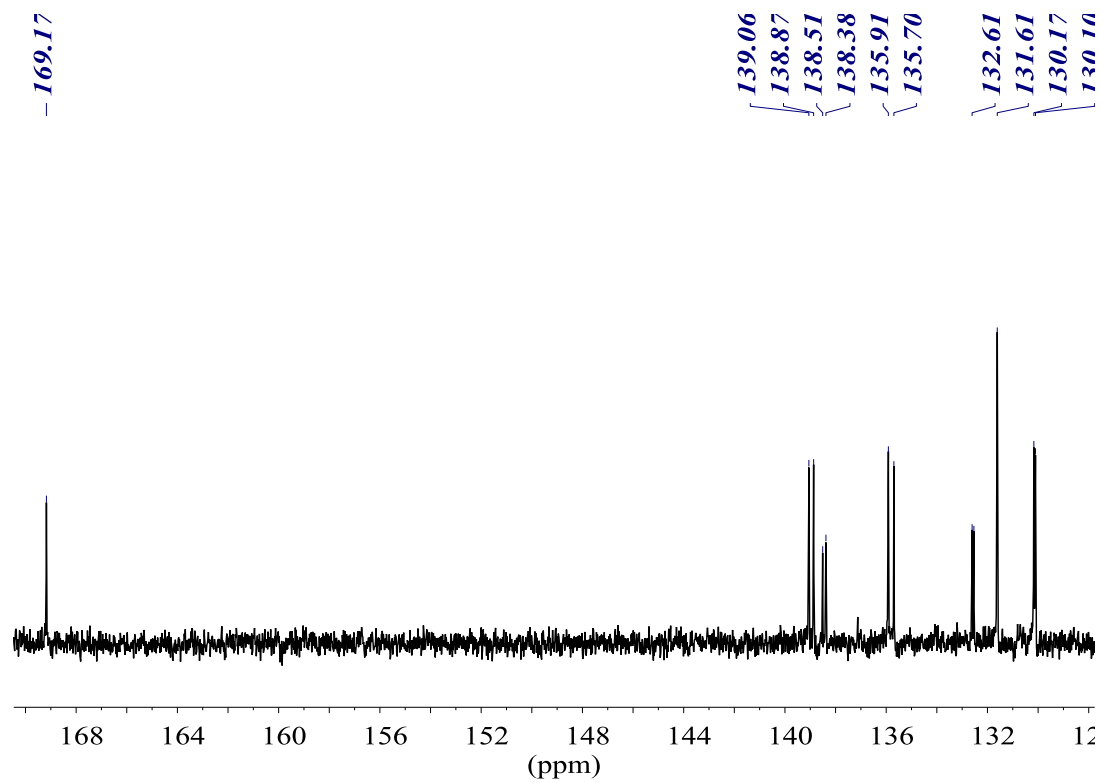
$^{31}\text{P}\{^1\text{H}\}$ NMR (161.98 MHz, CD_3OD)



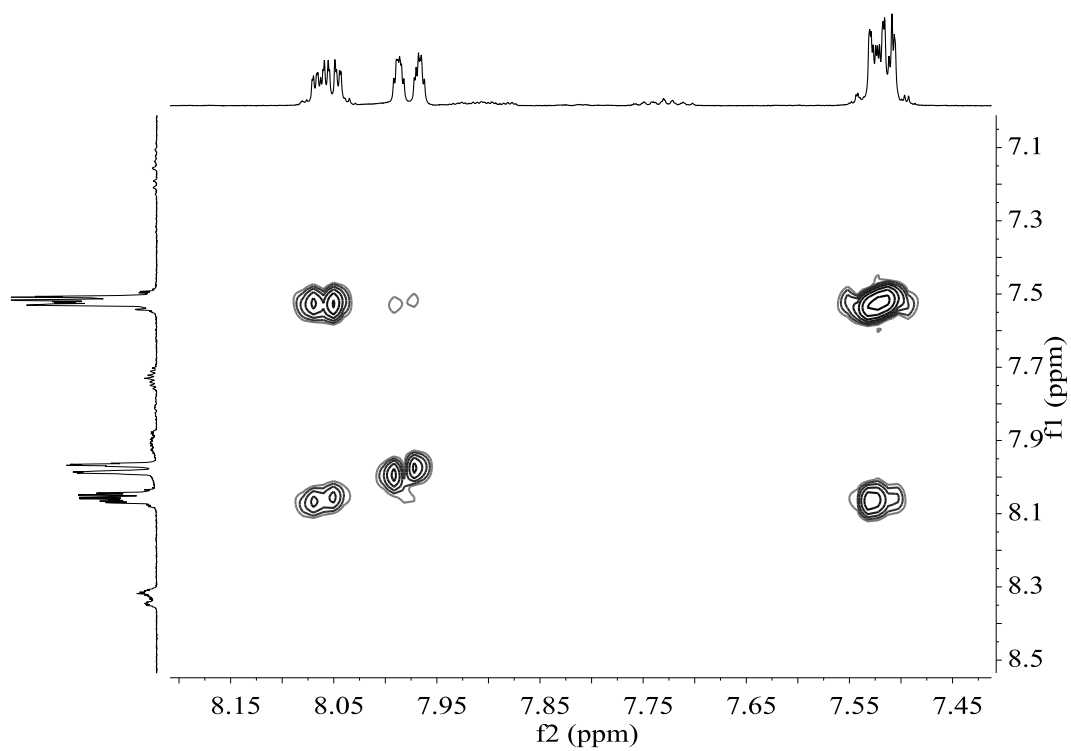
^1H NMR (400.13 MHz, CD_3OD)



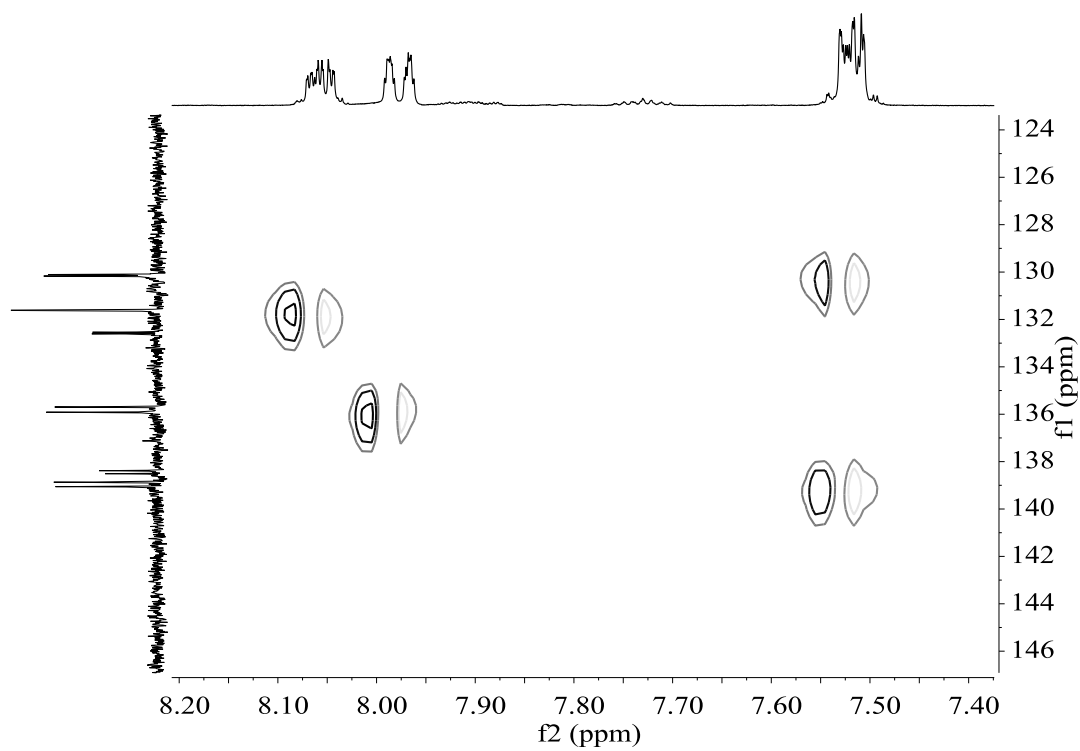
$^{13}\text{C}\{^1\text{H}\}$ NMR (100.61 MHz, CD_3OD)



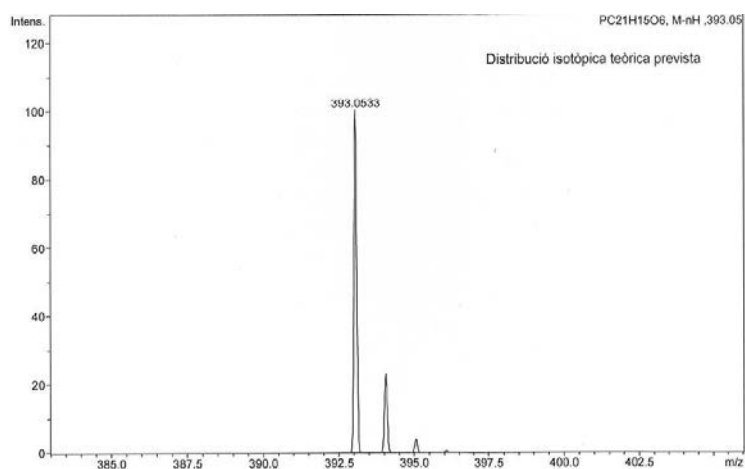
COSY NMR (400.13 MHz, CD₃OD)



HSQC NMR (400.13 MHz, CD₃OD)

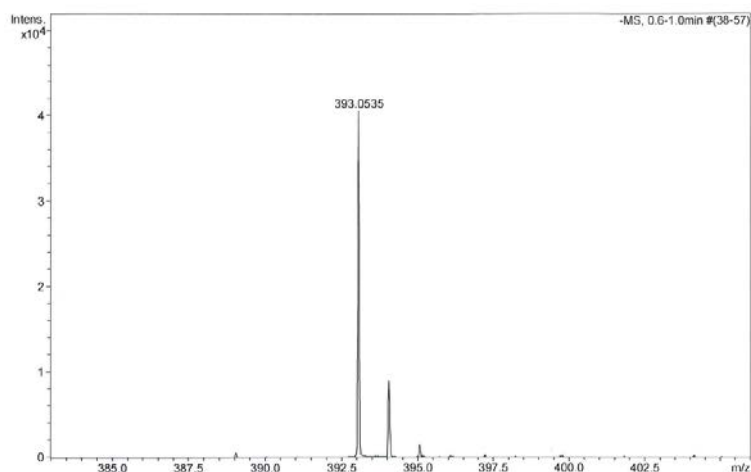


HR-MS (ESI m/z) [M-H]⁻
 calculated for [C₂₁H₁₄O₆P]⁻



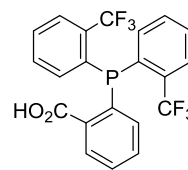
#	m/z	I	I %
1	393.0533	100	100.0
2	394.0567	23	23.1
3	395.0600	4	3.8

found

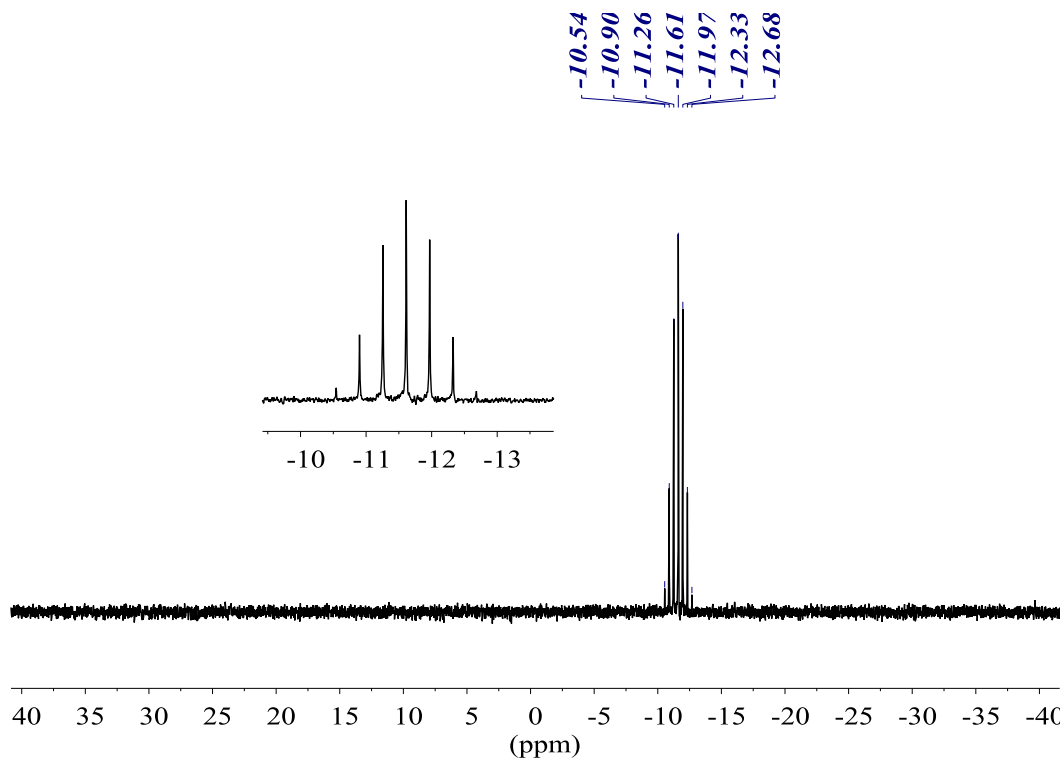


#	m/z	I	I %
1	393.0535	40578	100.0
2	394.0559	8988	22.2
3	395.0589	1474	3.6

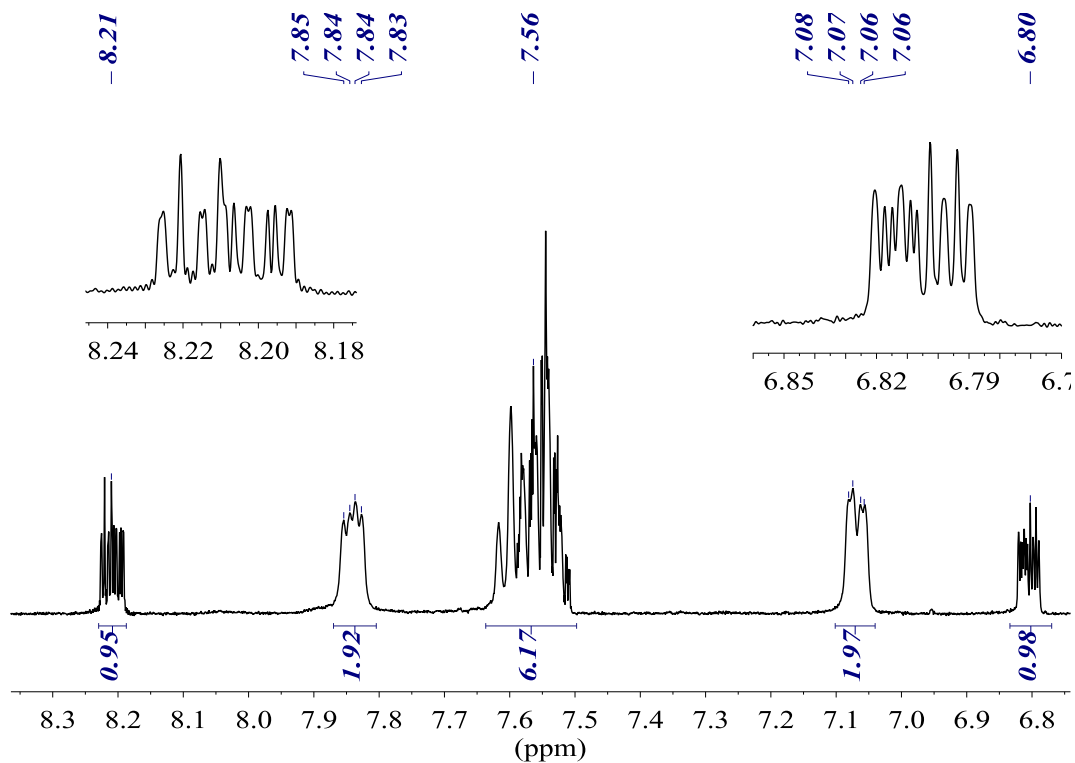
2-(bis(2-(trifluoromethyl)phenyl)phosphaneyl)benzoic acid, *o*-Miranphos (10)



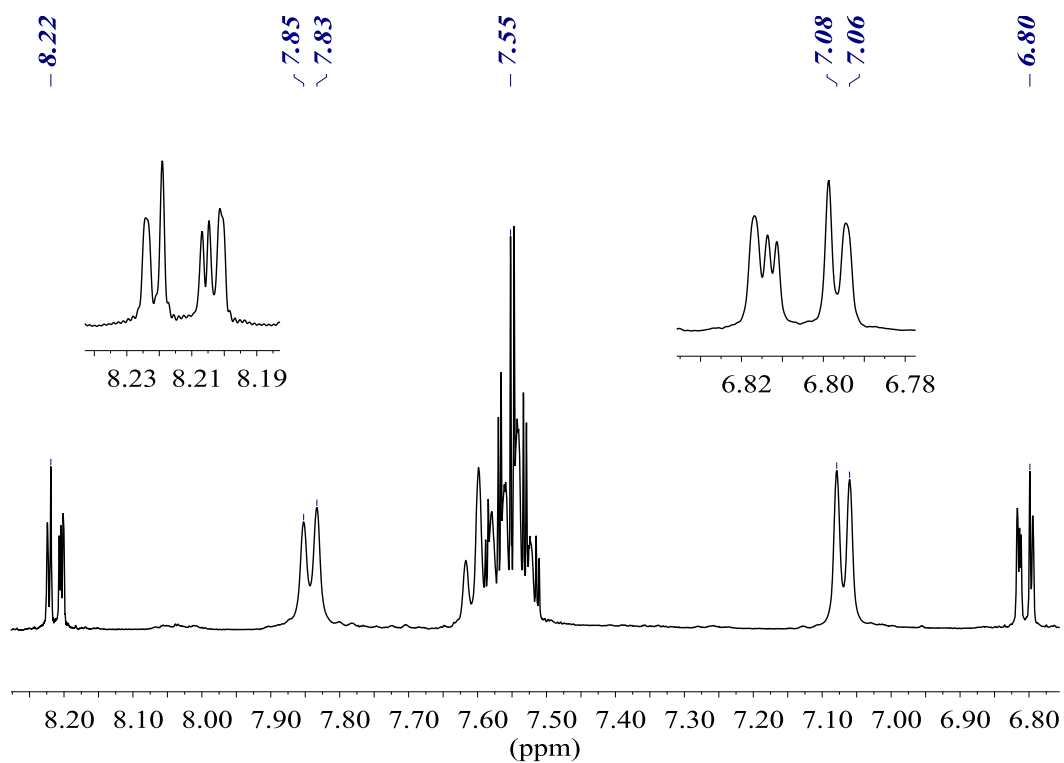
$^{31}\text{P}\{^1\text{H}\}$ NMR (161.98 MHz, acetone- D_6)



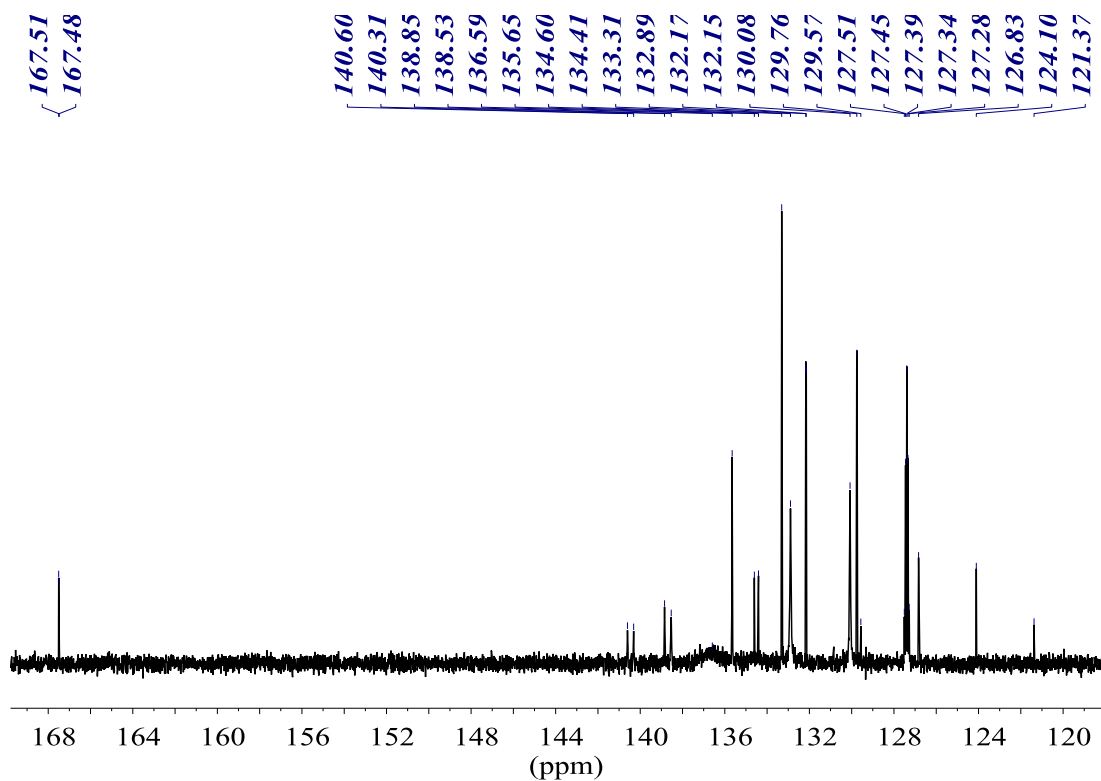
^1H NMR (400.13 MHz, acetone- D_6)

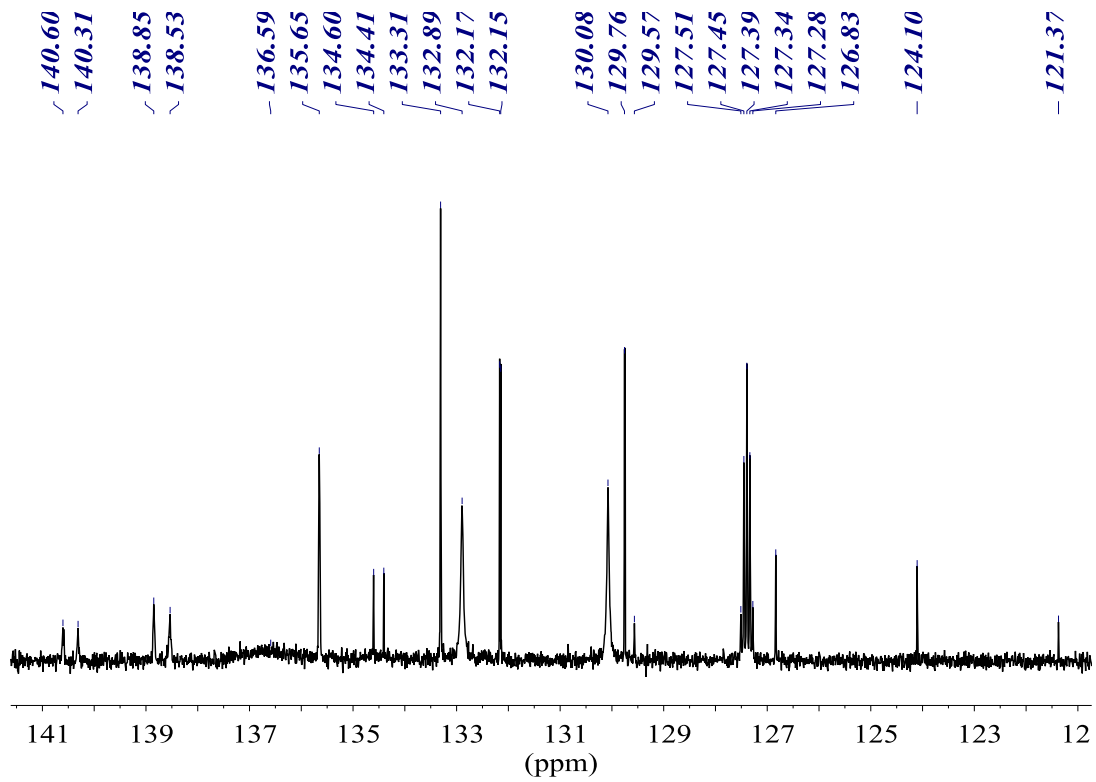


$^1\text{H}\{^{31}\text{P}\}$ NMR (400.13 MHz, acetone-D6)

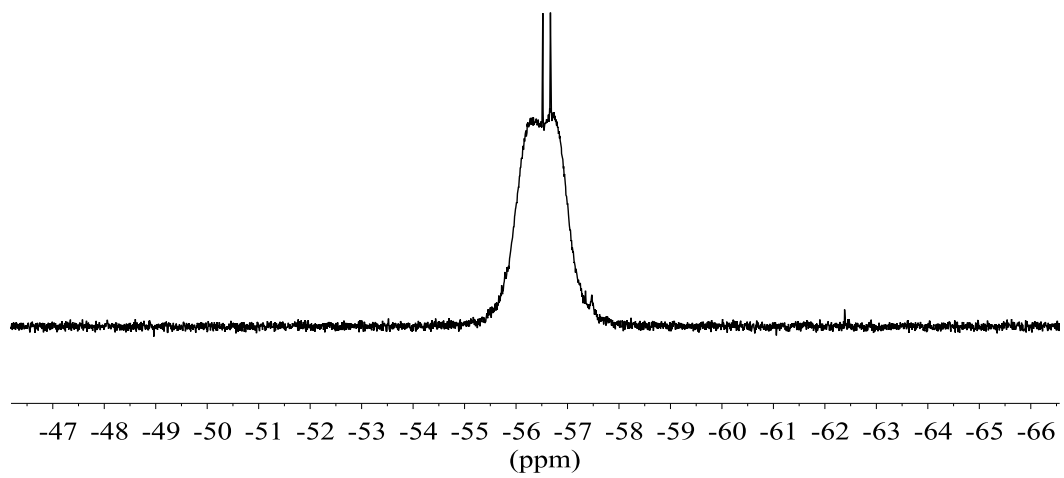


$^{13}\text{C}\{^1\text{H}\}$ NMR (100.61 MHz, acetone-D6)

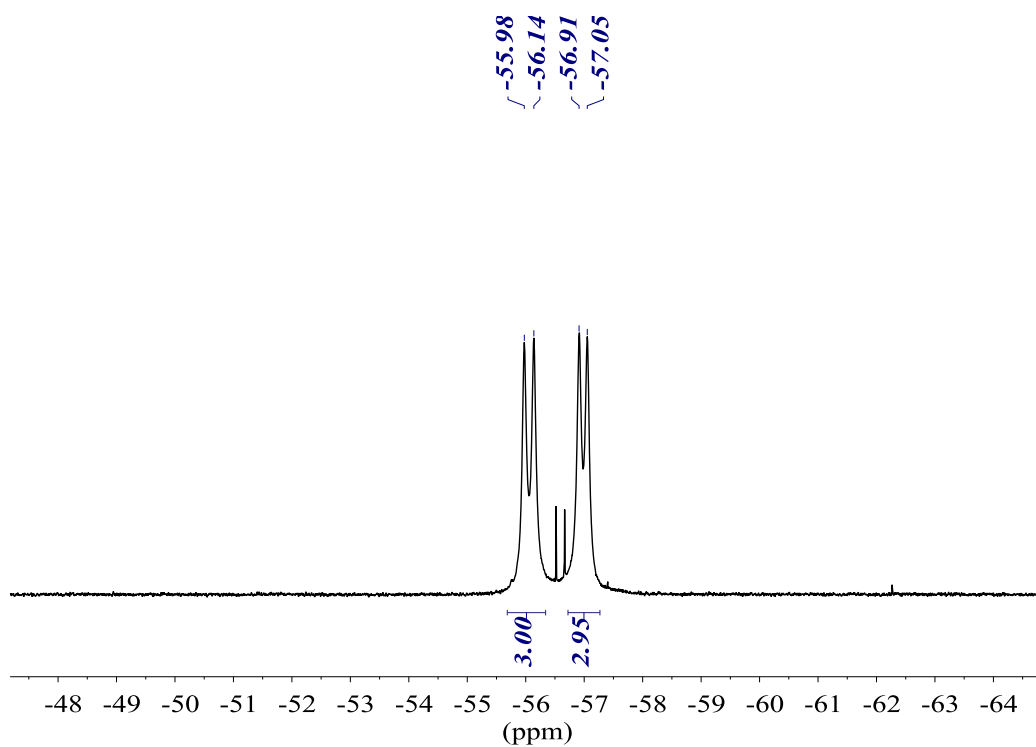




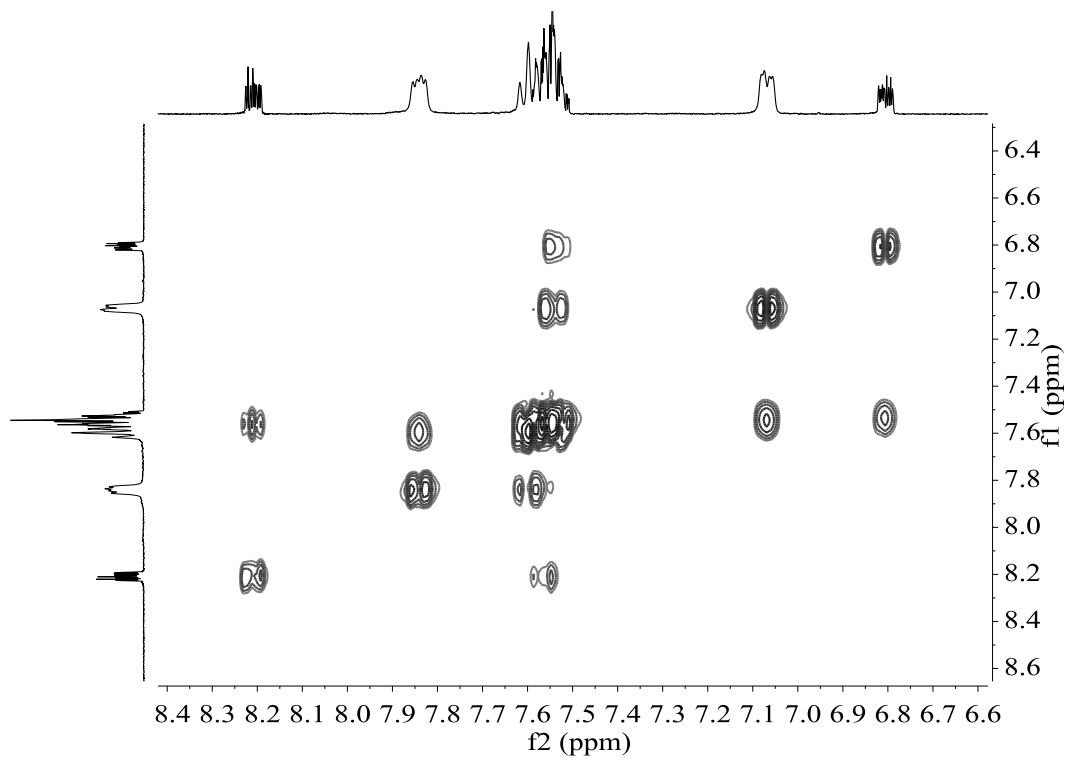
$^{19}\text{F}\{^1\text{H}\}$ NMR (376.50 MHz, acetone-D₆) 298 K



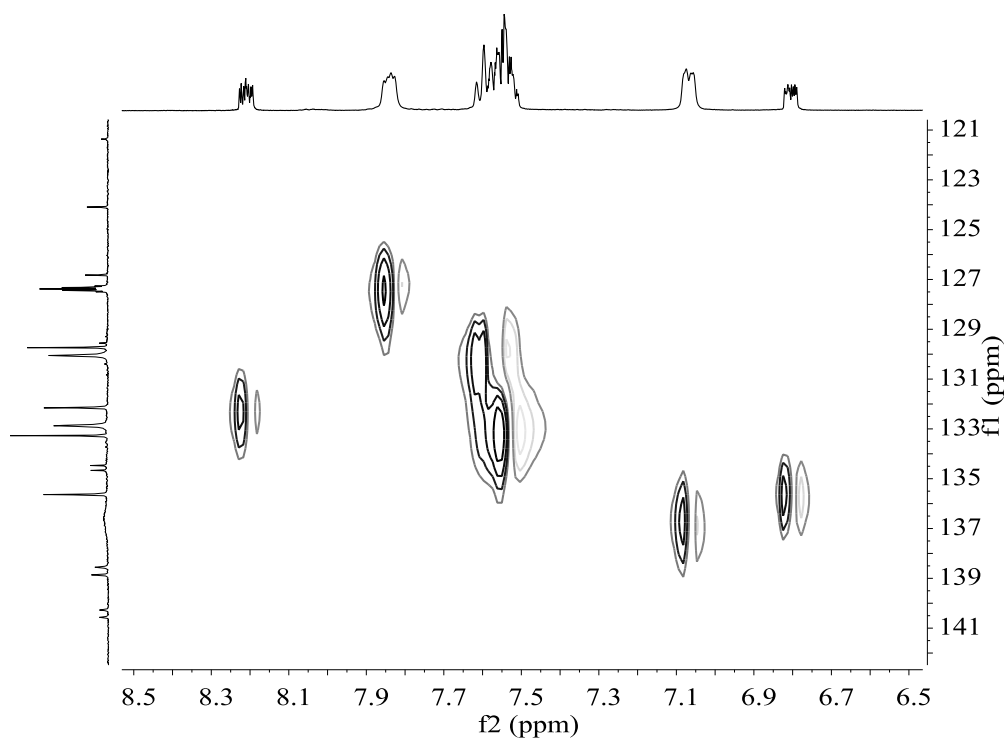
$^{19}\text{F}\{^1\text{H}\}$ NMR (376.50 MHz, acetone-D6) 274.8 K



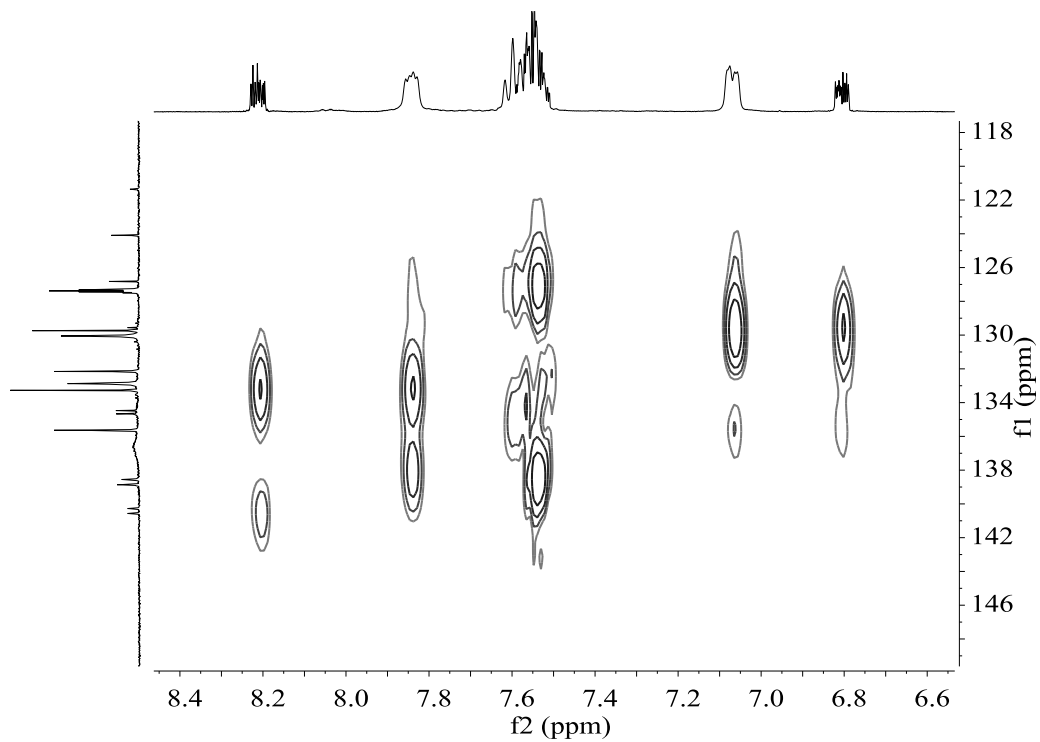
COSY NMR (400.13 MHz, acetone-D6)



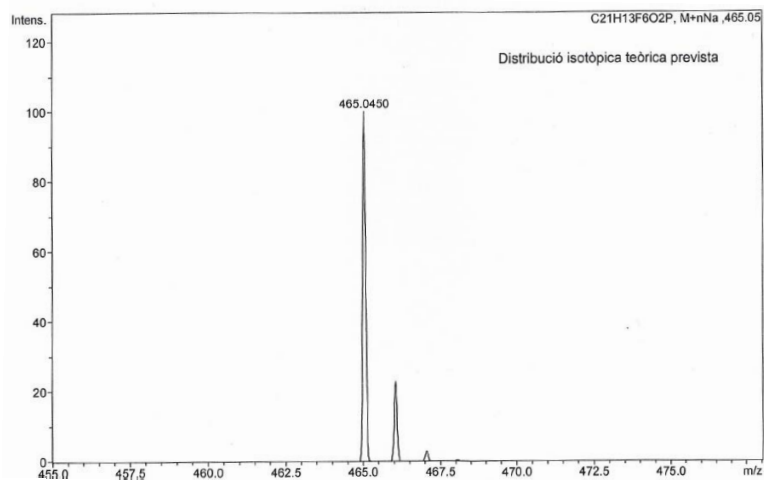
HSQC NMR (400.13 MHz, acetone-D6)



HMBC NMR (400.13 MHz, acetone-D6)

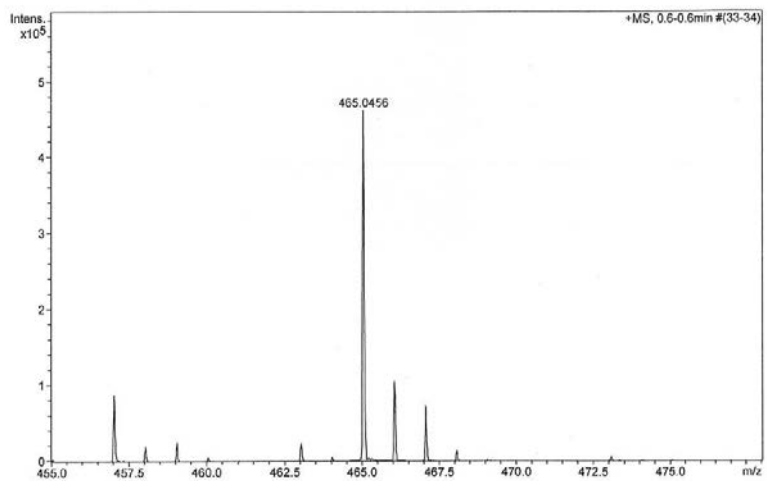


HR-MS (ESI⁺ *m/z*) [M+Na]⁺
 calculated for [C₂₁H₁₃F₆O₂PNa]⁺



#	<i>m/z</i>	I	I%
1	465.0450	100	100.0
2	466.0483	23	22.9
3	467.0517	3	2.9

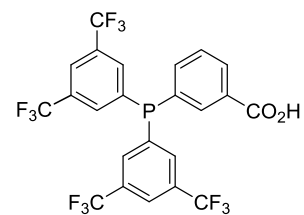
found



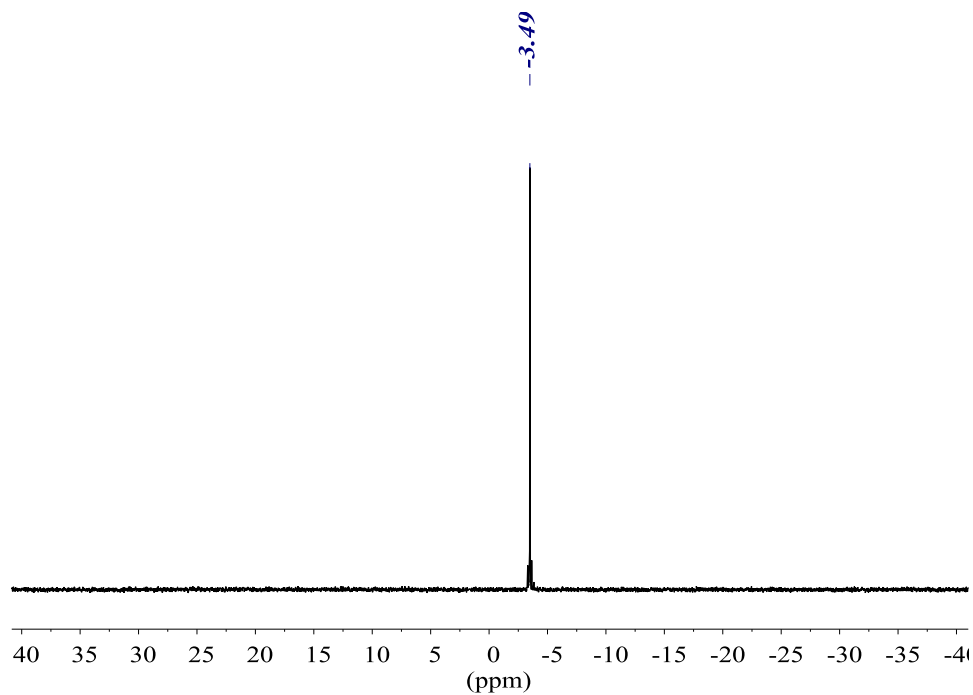
#	<i>m/z</i>	I	I%
1	465.0456	461435	100.0
2	466.0496	105075	22.8
3	467.0592	73255	15.9

2.2. Derived from heteroleptic phosphines

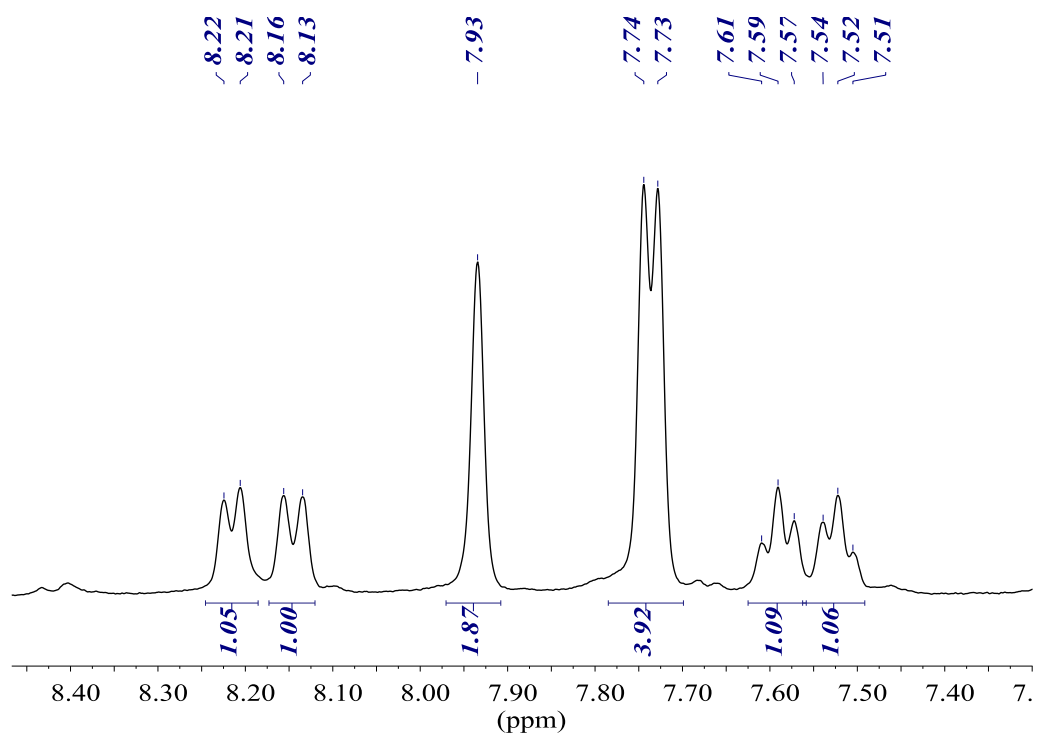
3-(bis(3,5-bis(trifluoromethyl)phenyl)phosphanyl) benzoic acid (19)



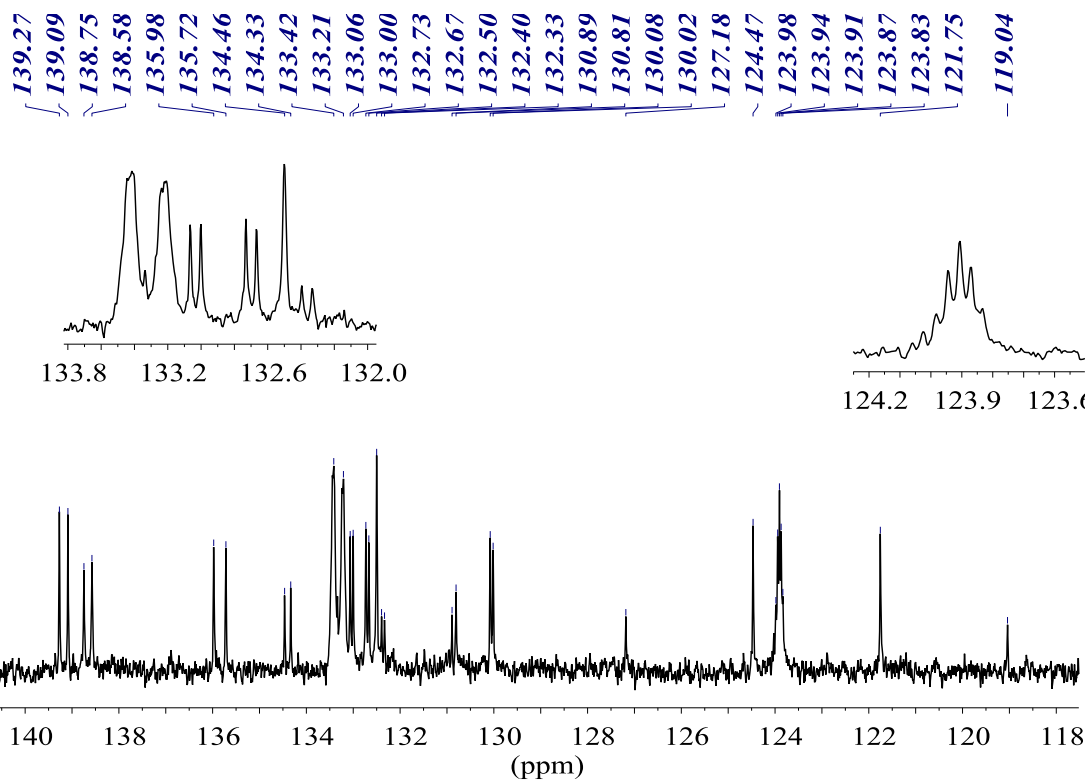
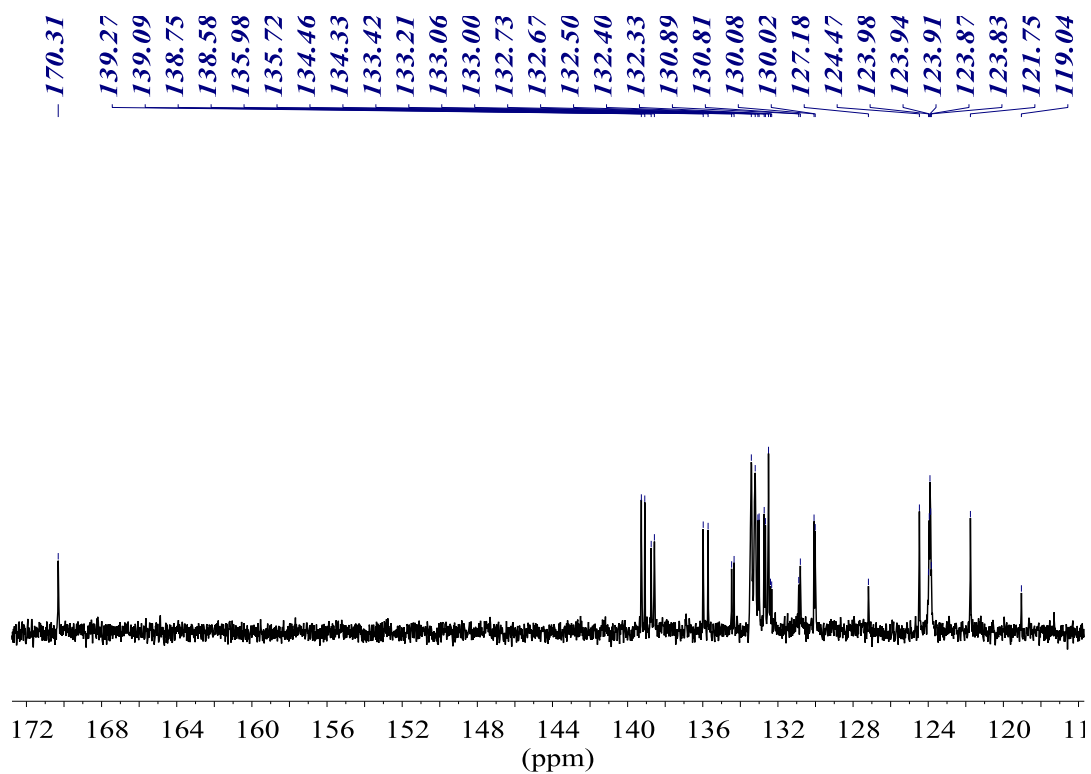
$^{31}\text{P}\{^1\text{H}\}$ NMR (161.98 MHz, CDCl_3) 323 K



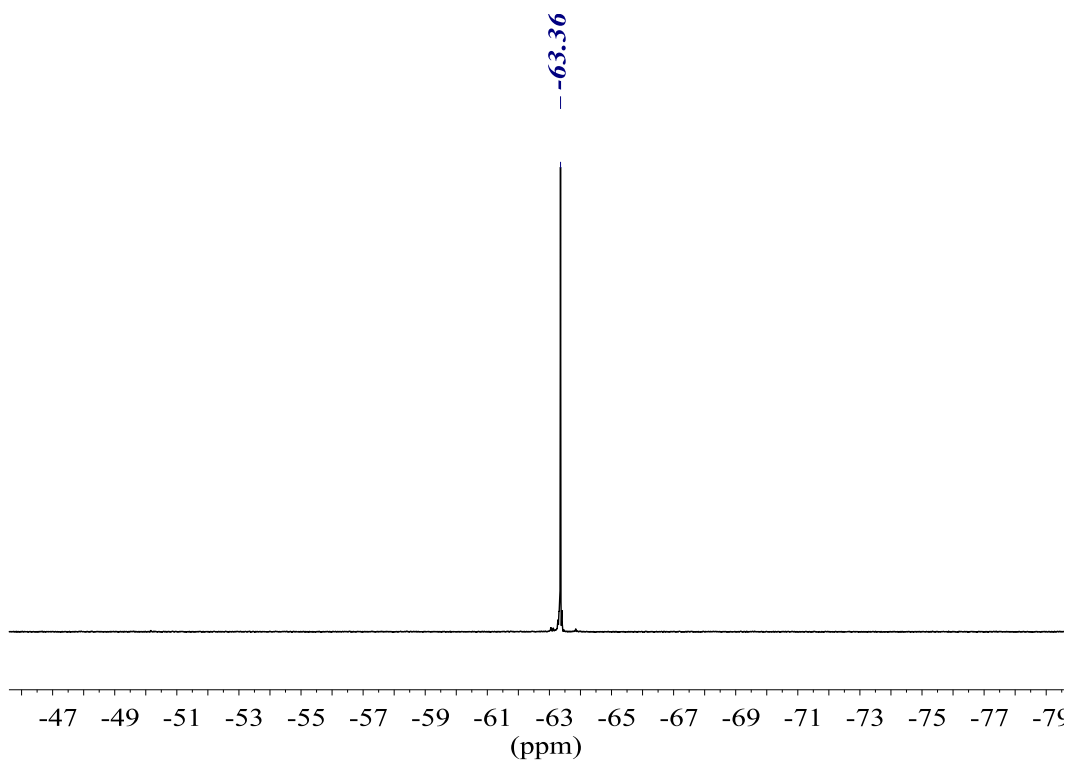
^1H NMR (400.13 MHz, CDCl_3) 323 K



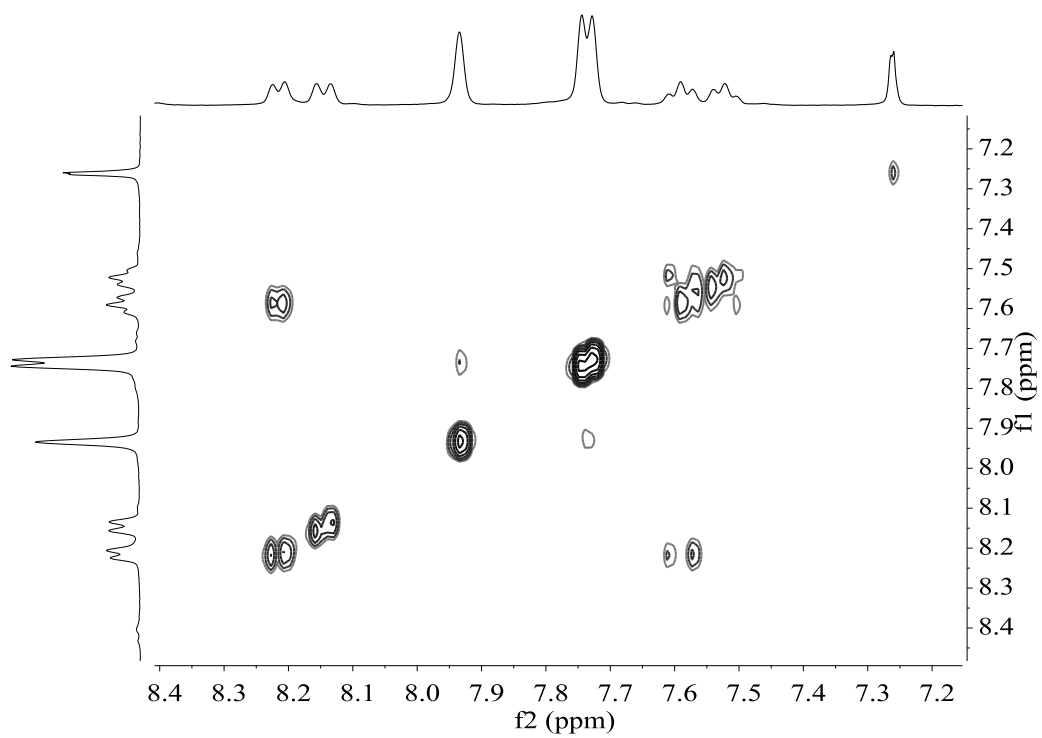
$^{13}\text{C}\{^1\text{H}\}$ NMR (100.61 MHz, CDCl_3) 323 K



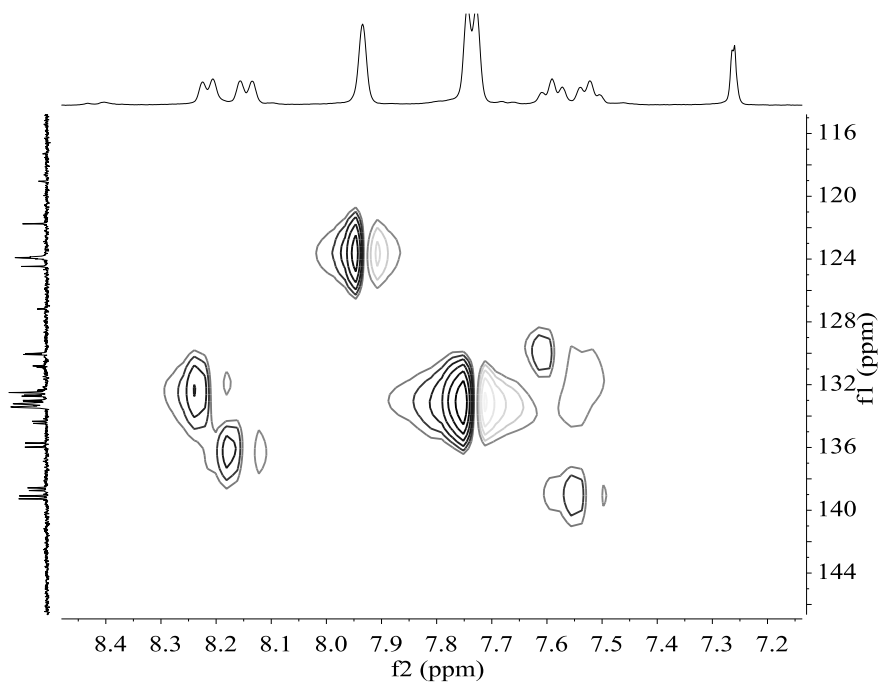
$^{19}\text{F}\{^1\text{H}\}$ NMR (376.50 MHz, CDCl_3) 323 K



COSY NMR (400.13 MHz, CDCl_3) 323 K

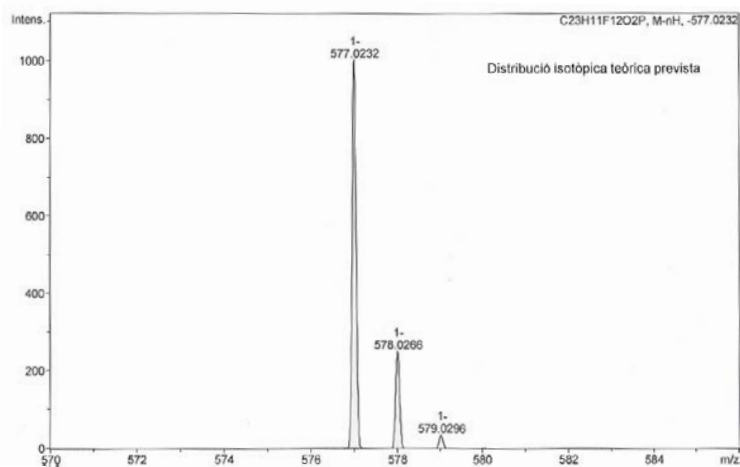


HSQC NMR (400.13 MHz, CDCl₃) 323 K



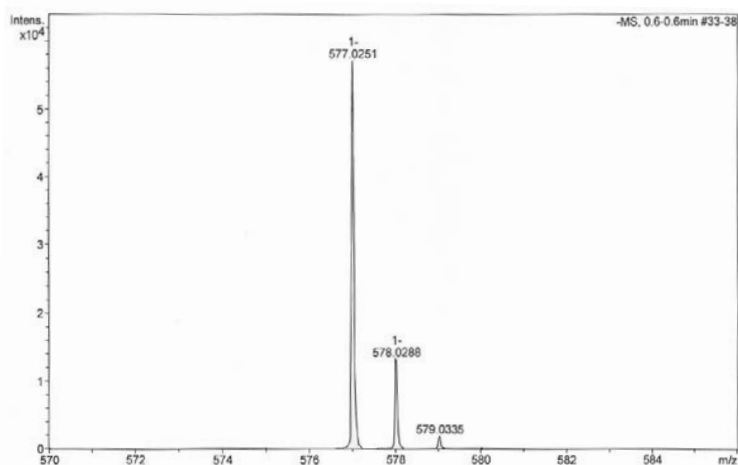
HR-MS (ESI m/z) [M-H]⁻

calculated for [C₂₃H₁₀F₁₂O₂P]⁻



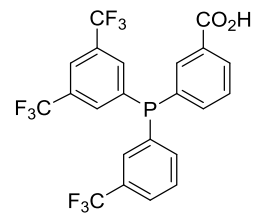
#	m/z	I	I%
1	577.0232	1000	100.0
2	578.0266	250	25.0
3	579.0296	34	3.4

found

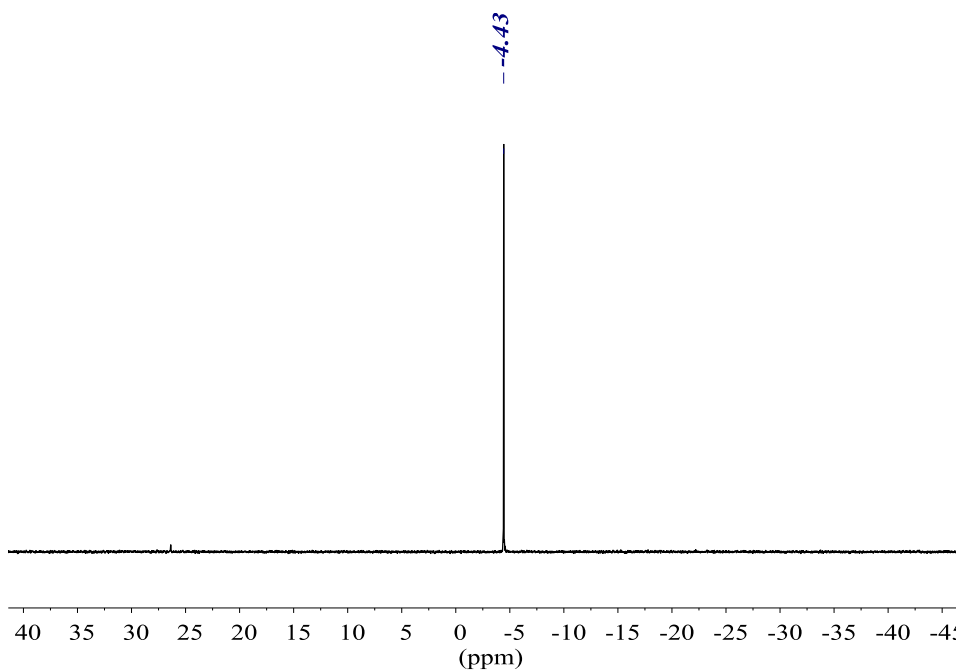


#	m/z	I	I%
1	577.0251	57043	100.0
2	578.0288	13250	23.2
3	579.0335	1891	3.3

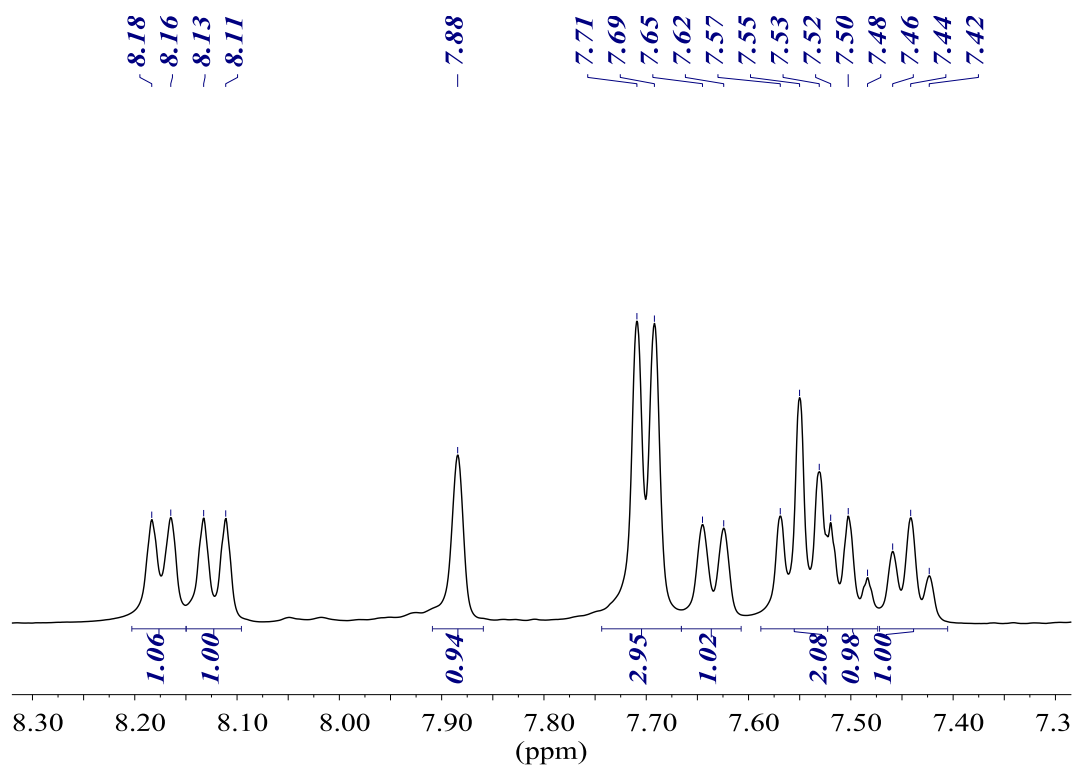
3-((3,5-bis(trifluoromethyl)phenyl)(3-(trifluoromethyl)phenyl)phosphanyl)benzoic acid (16)



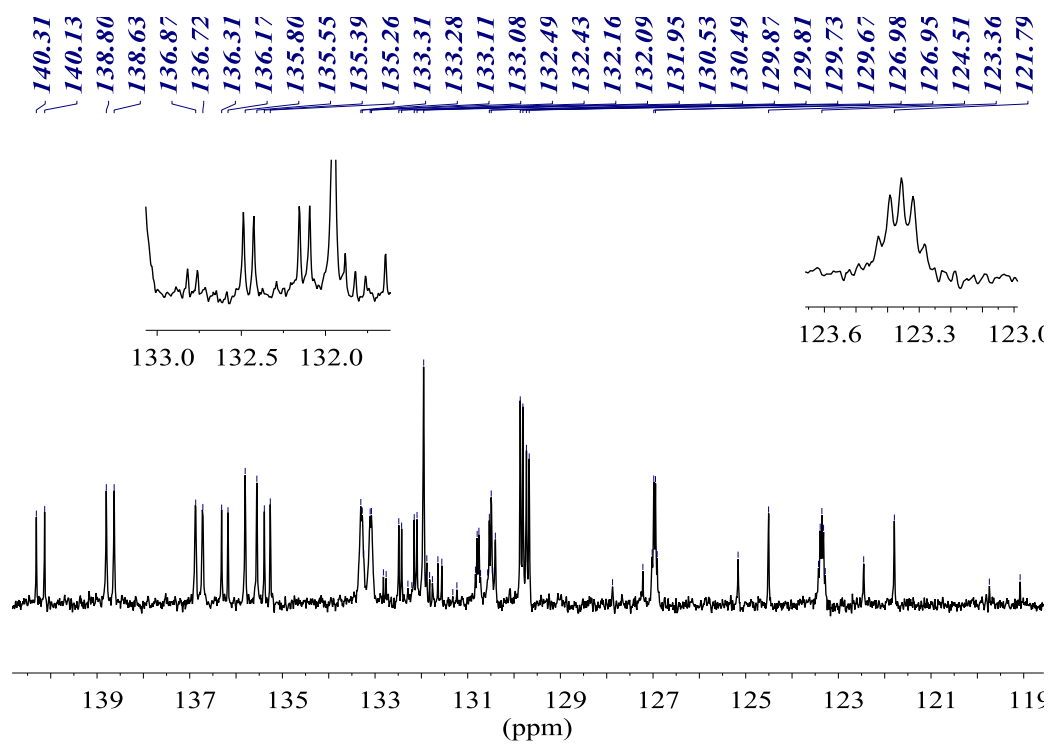
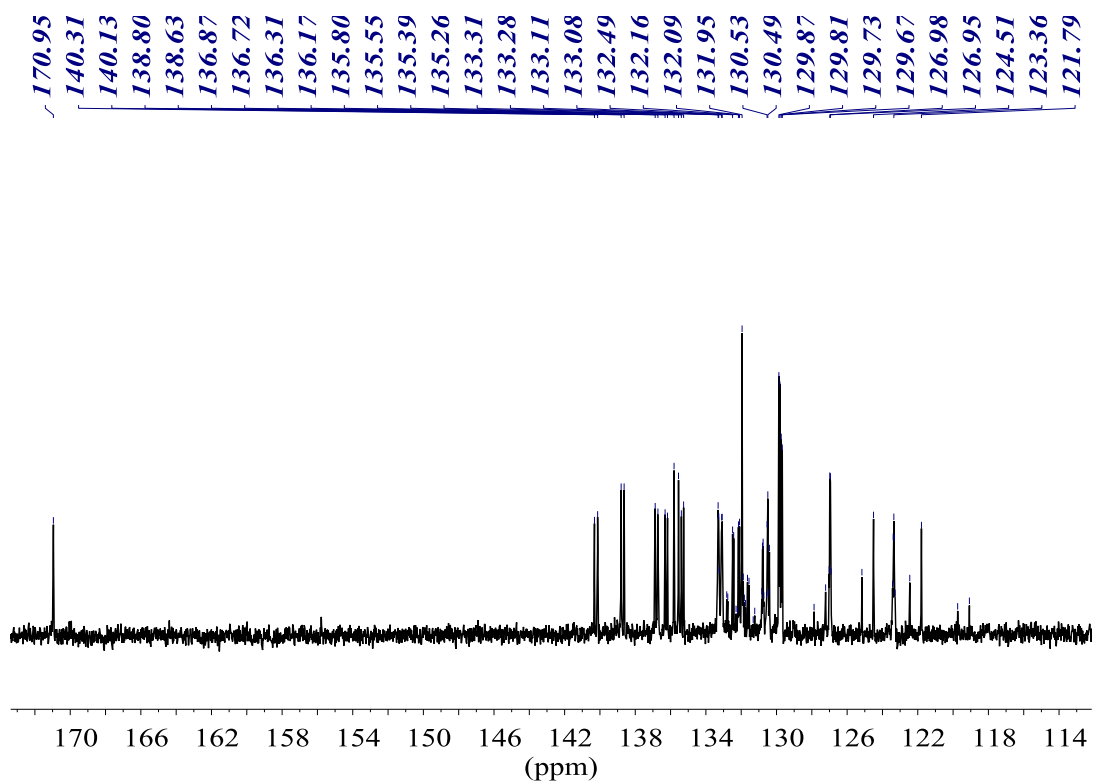
$^{31}\text{P}\{^1\text{H}\}$ NMR (161.98 MHz, CDCl_3)



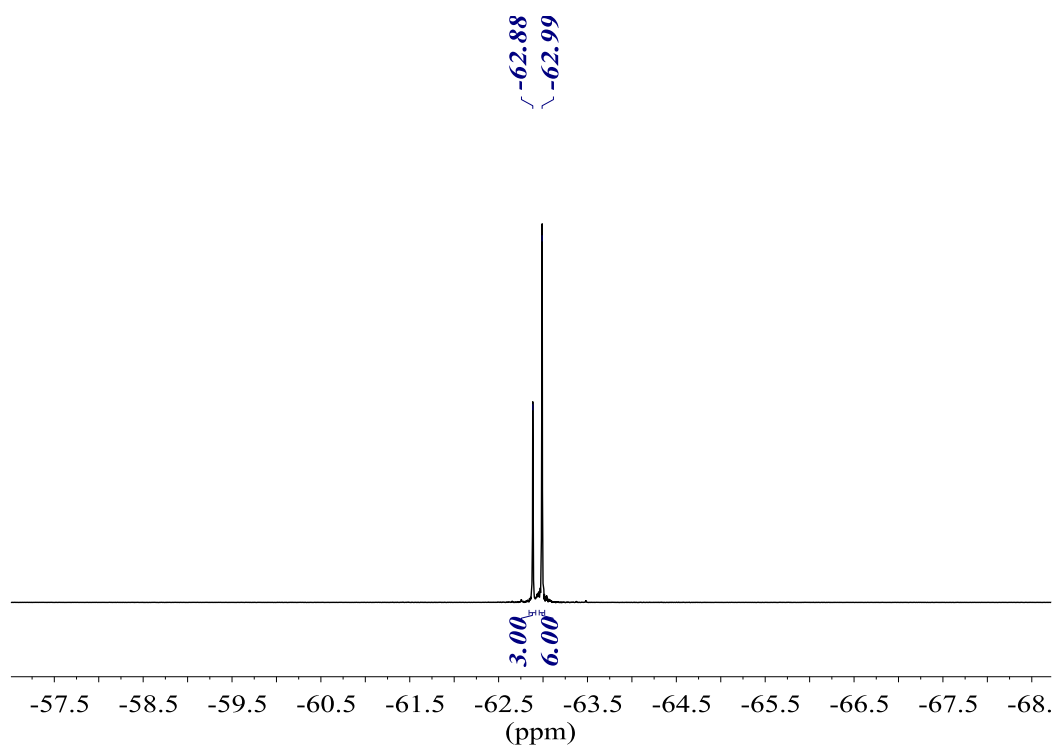
^1H NMR (400.13 MHz, CDCl_3)



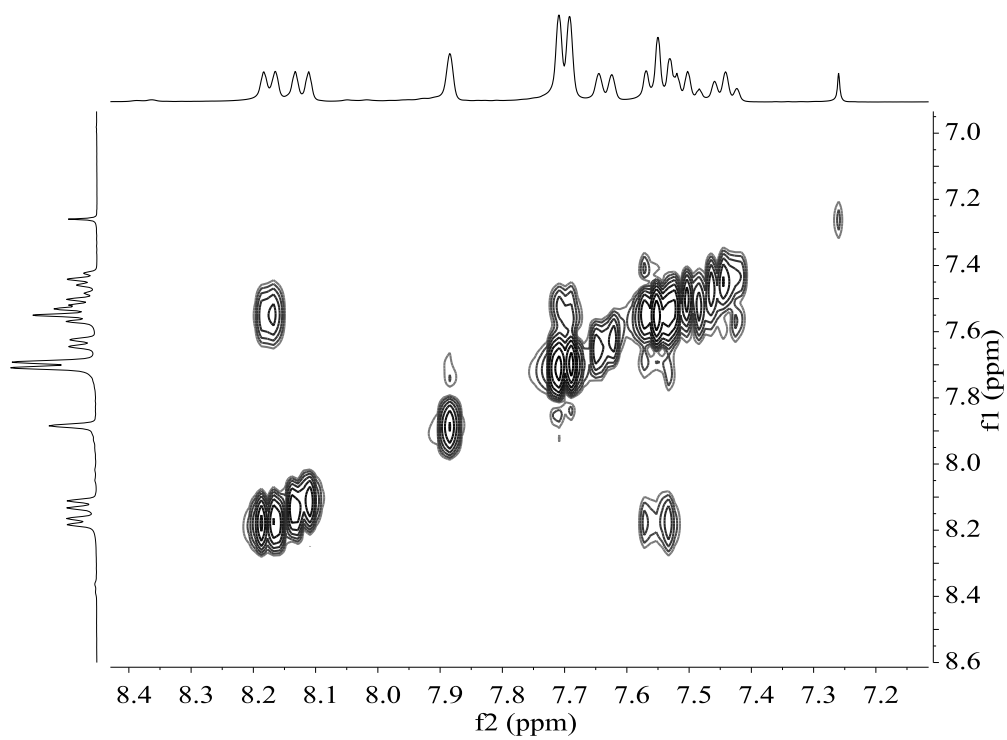
$^{13}\text{C}\{^1\text{H}\}$ NMR (100.61 MHz, CDCl_3)



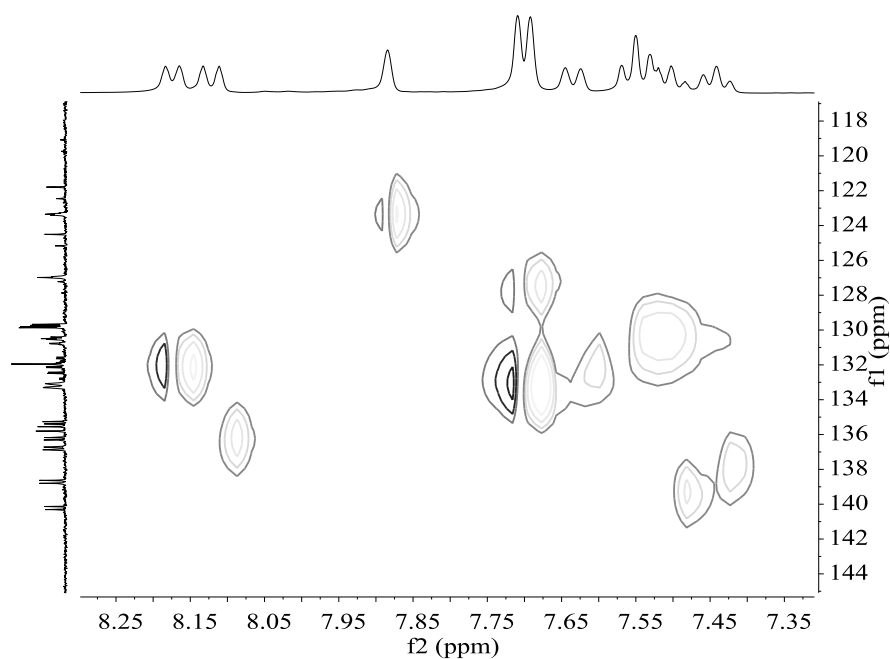
$^{19}\text{F}\{^1\text{H}\}$ NMR (376.50 MHz, CDCl_3)



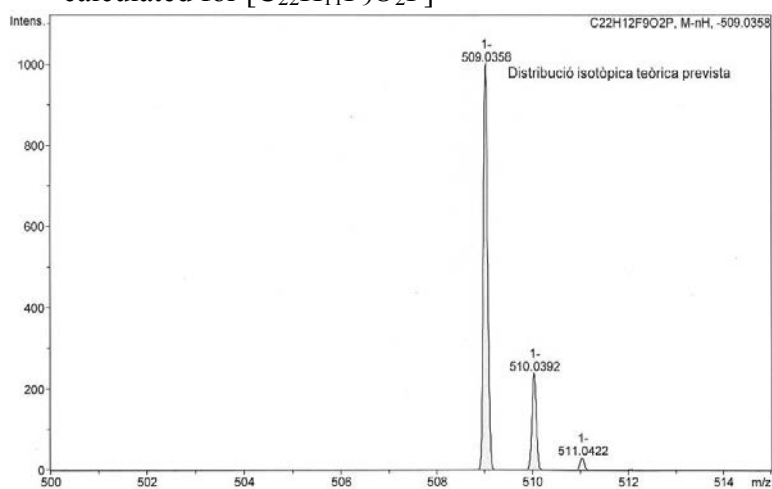
COSY NMR (400.13 MHz, CDCl_3)



HSQC NMR (400.13 MHz, CDCl₃)

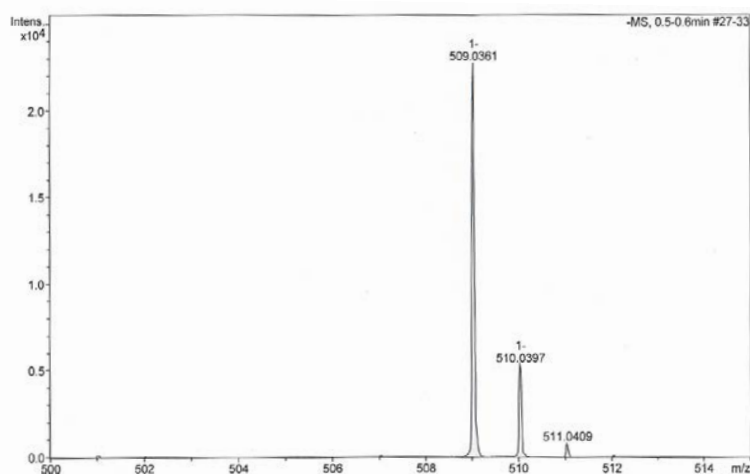


HR-MS (ESI⁻ *m/z*) [M-H]⁻
calculated for [C₂₂H₁₁F₉O₂P]⁻



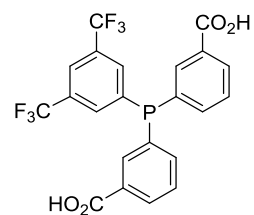
#	<i>m/z</i>	I	I%
1	509.0358	1000	100.0
2	510.0392	239	23.9
3	511.0422	31	3.1

found

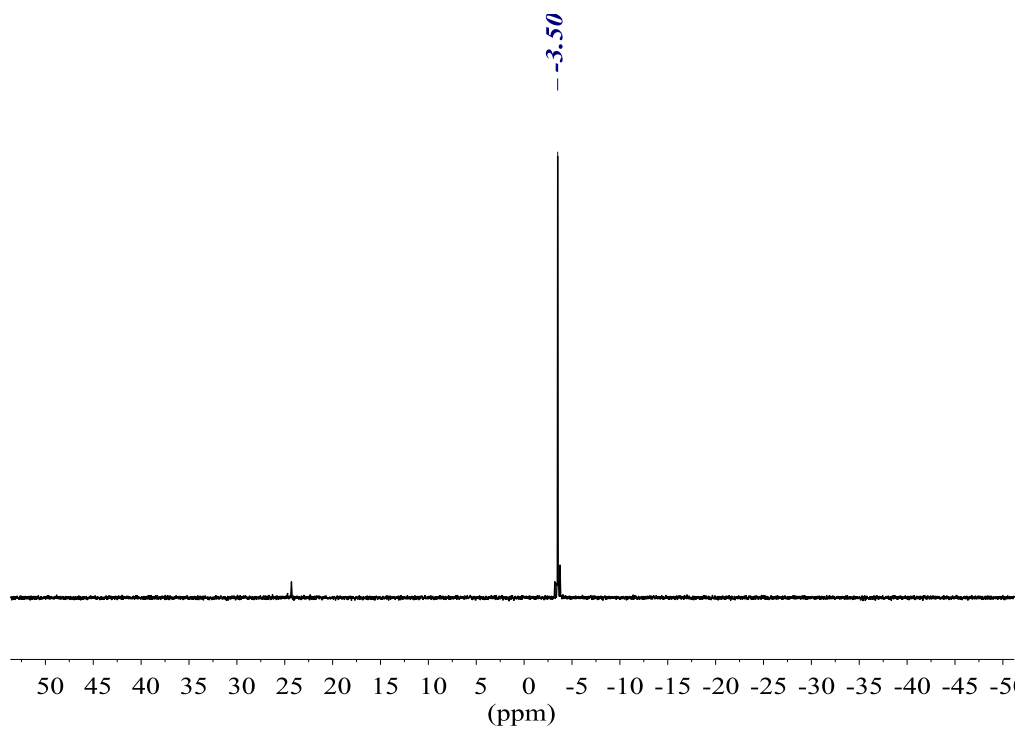


#	<i>m/z</i>	I	I%
1	509.0361	22740	100.0
2	510.0397	5340	23.5
3	511.0409	805	3.5

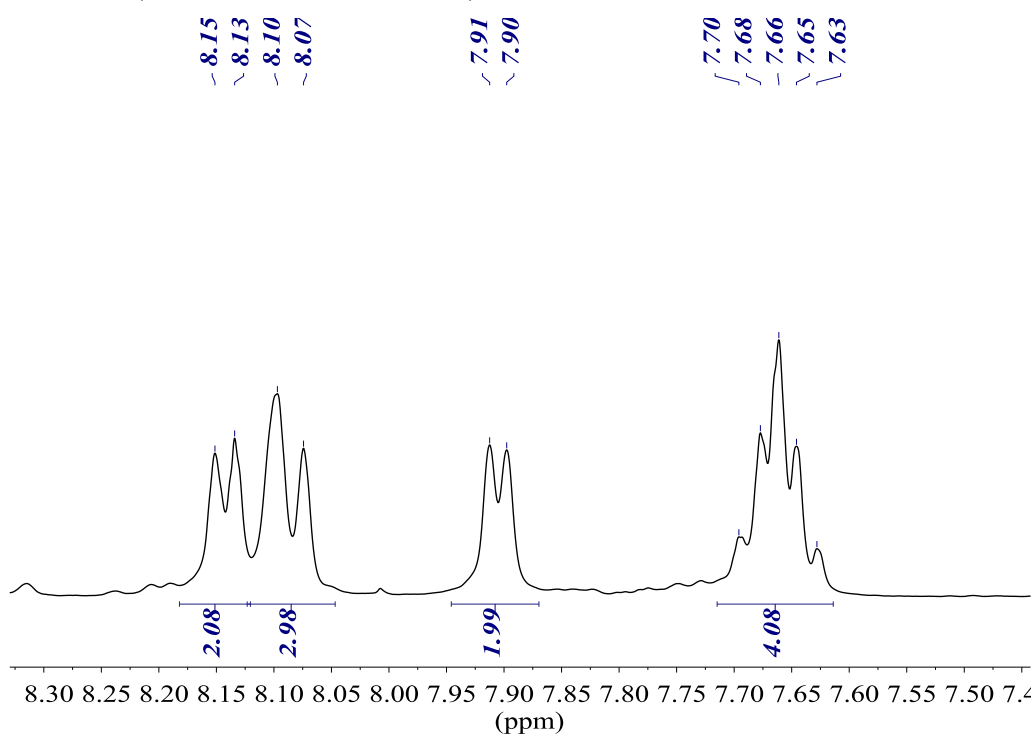
3,3'-((3,5-bis(trifluoromethyl)phenyl)phosphanediyl)dibenzoic acid (17)



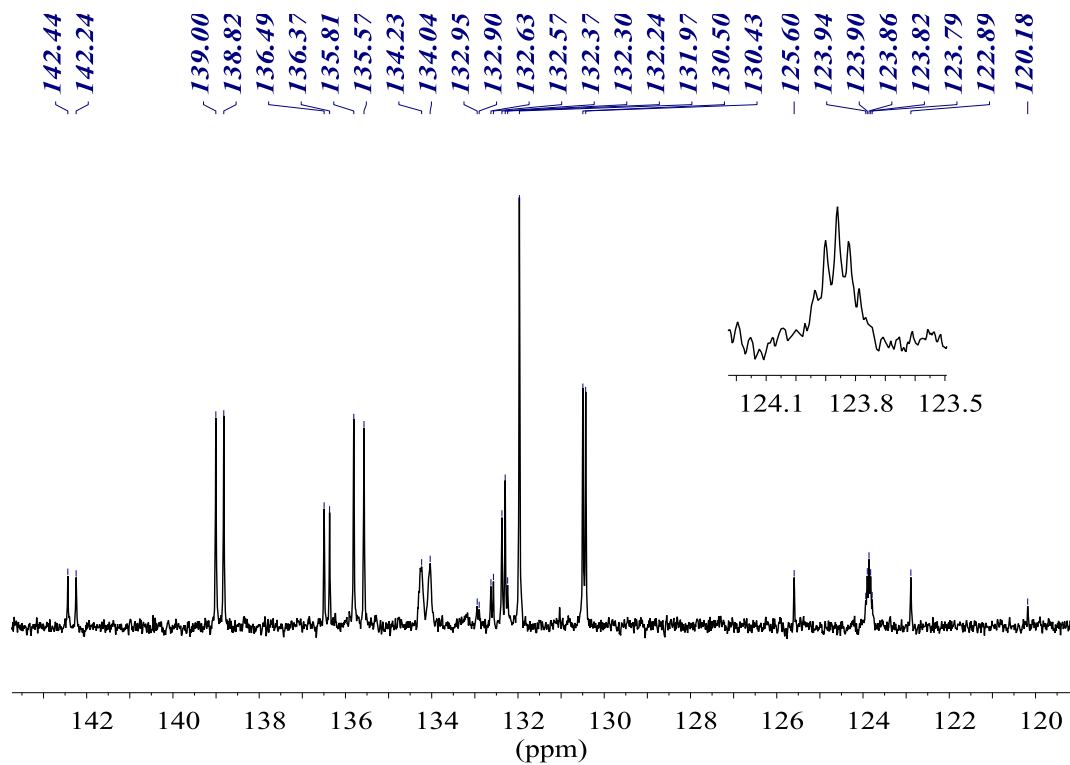
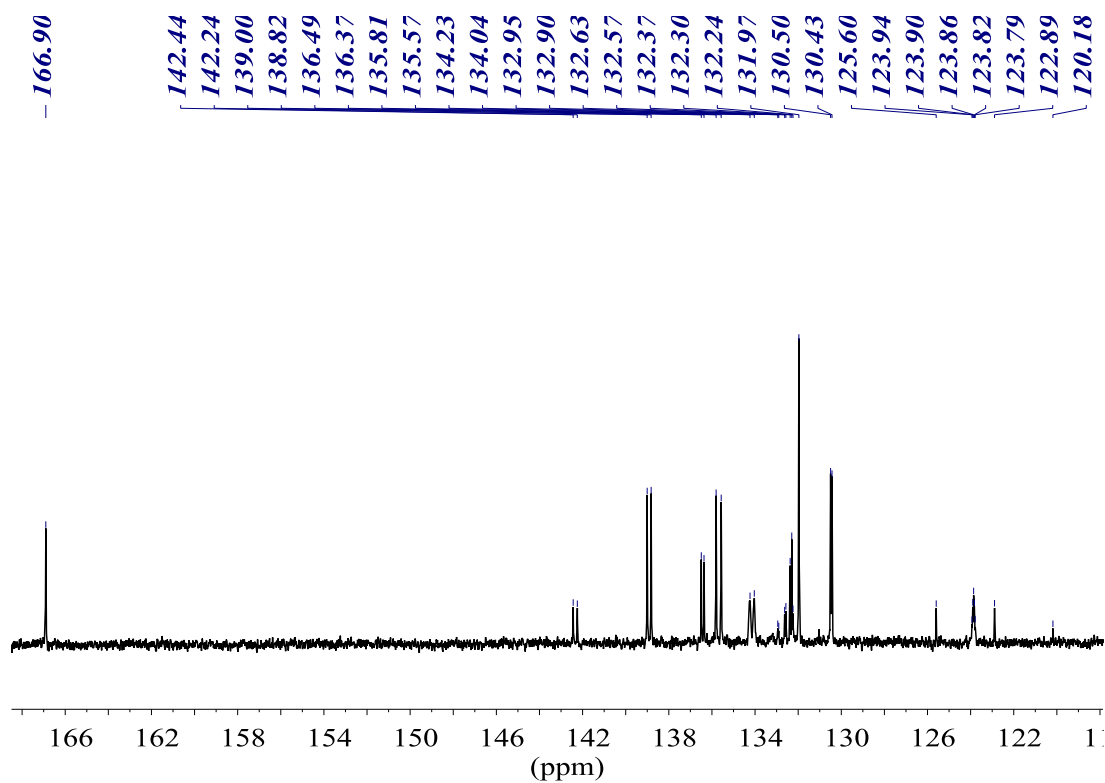
$^{31}\text{P}\{^1\text{H}\}$ NMR (161.98 MHz, acetone- D_6)



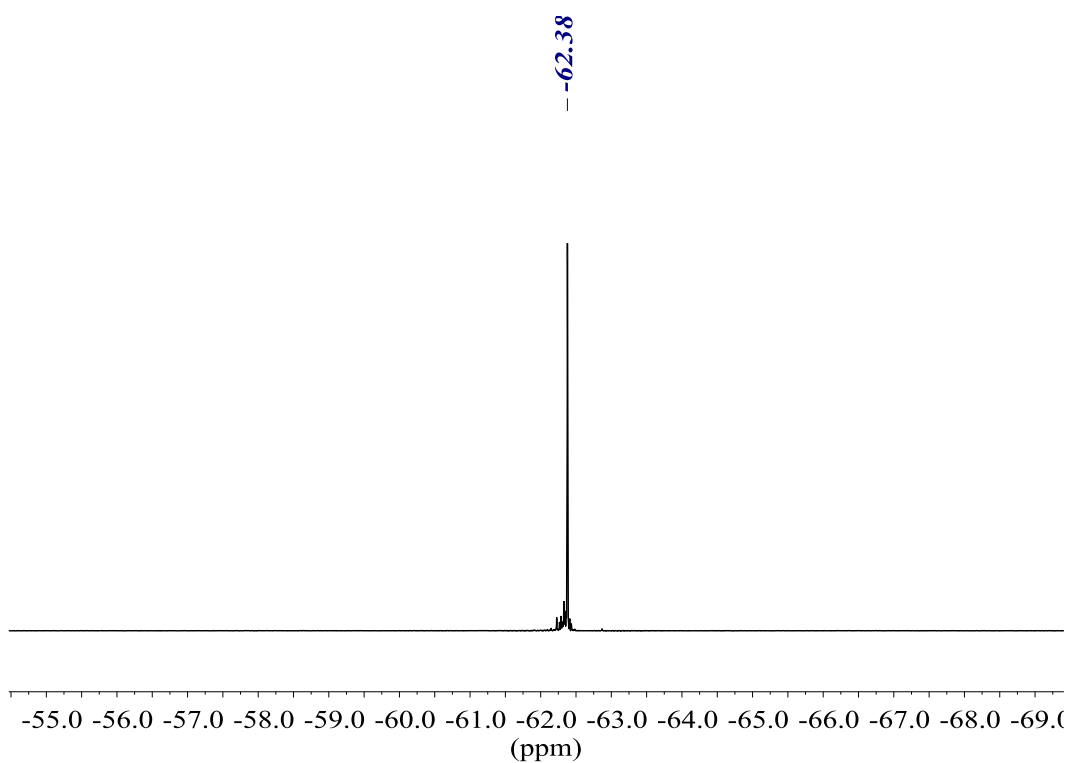
^1H NMR (400.13 MHz, acetone- D_6)



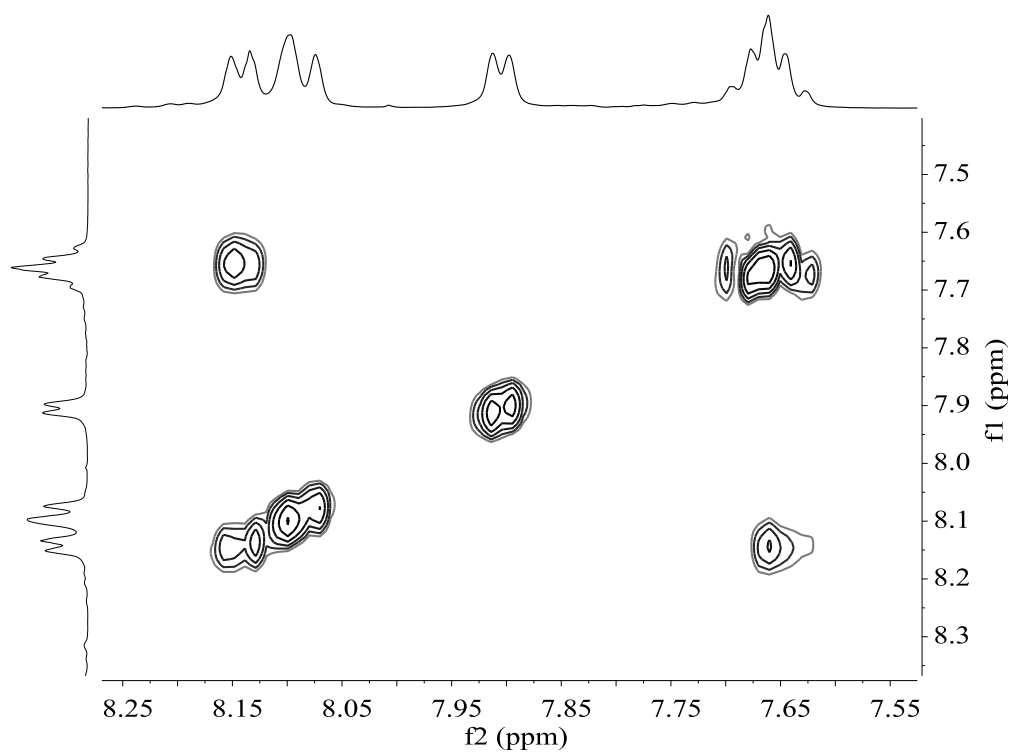
$^{13}\text{C}\{^1\text{H}\}$ NMR (100.61 MHz, acetone-D6)



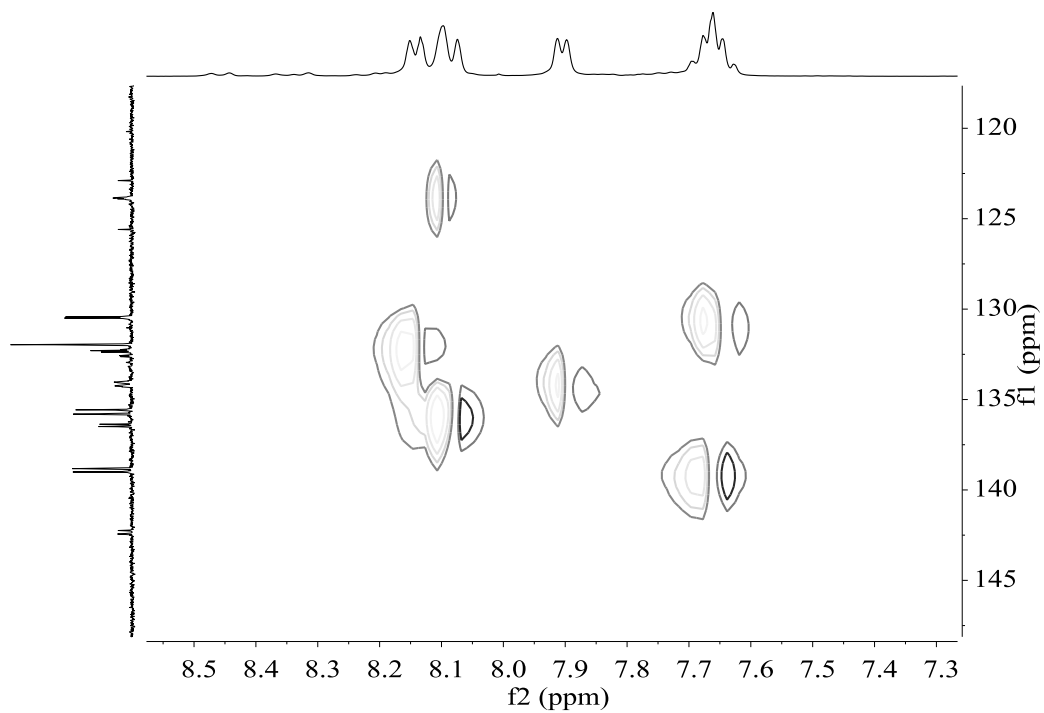
$^{19}\text{F}\{^1\text{H}\}$ NMR (376.50 MHz, acetone- D_6)



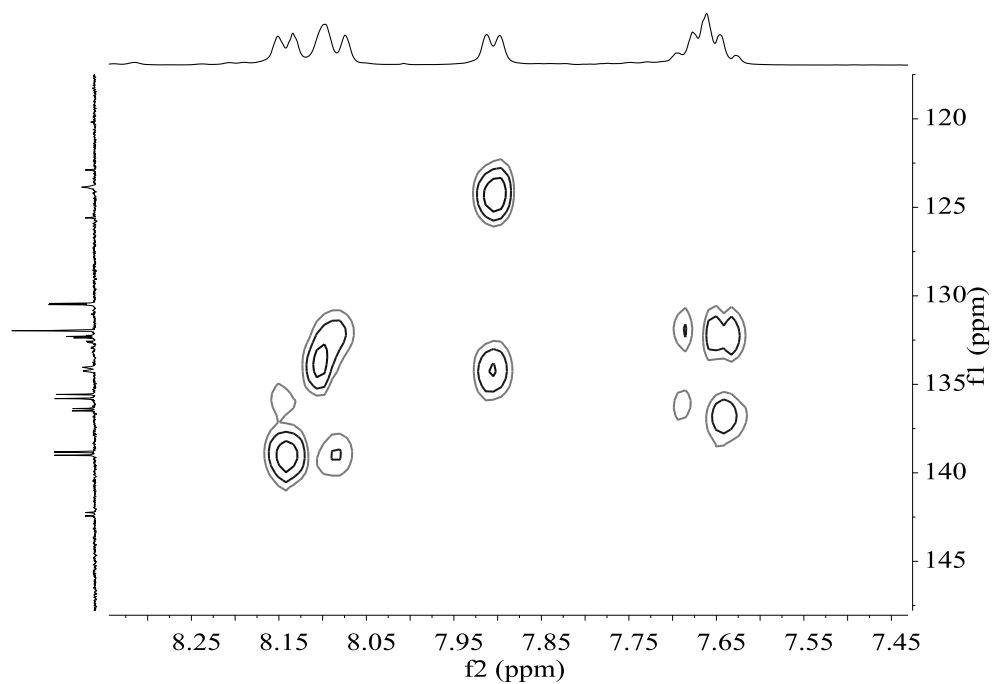
COSY NMR (400.13 MHz, acetone- D_6)



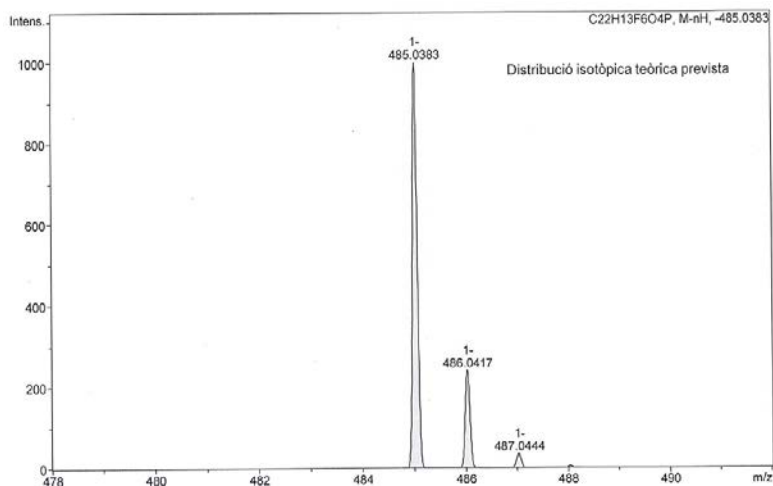
HSQC NMR (400.13 MHz, acetone-D6)



HMBC NMR (400.13 MHz, acetone-D6)

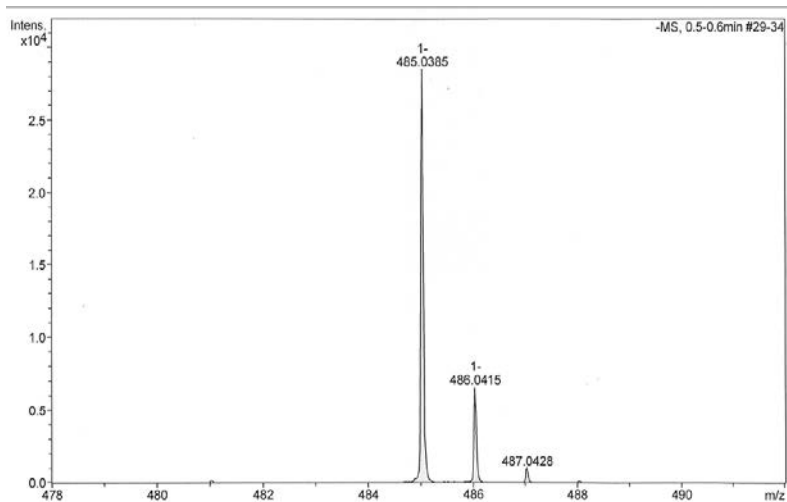


HR-MS (ESI⁻ m/z) [M-H]⁻
calculated for [C₂₂H₁₂F₆O₄P]⁻



#	m/z	I	I %
1	485.0383	1000	100.0
2	486.0417	241	24.1
3	487.0444	36	3.6

found

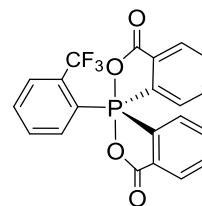


#	m/z	I	I %
1	485.0385	28499	100.0
2	486.0415	6598	23.2
3	487.0428	1028	3.6

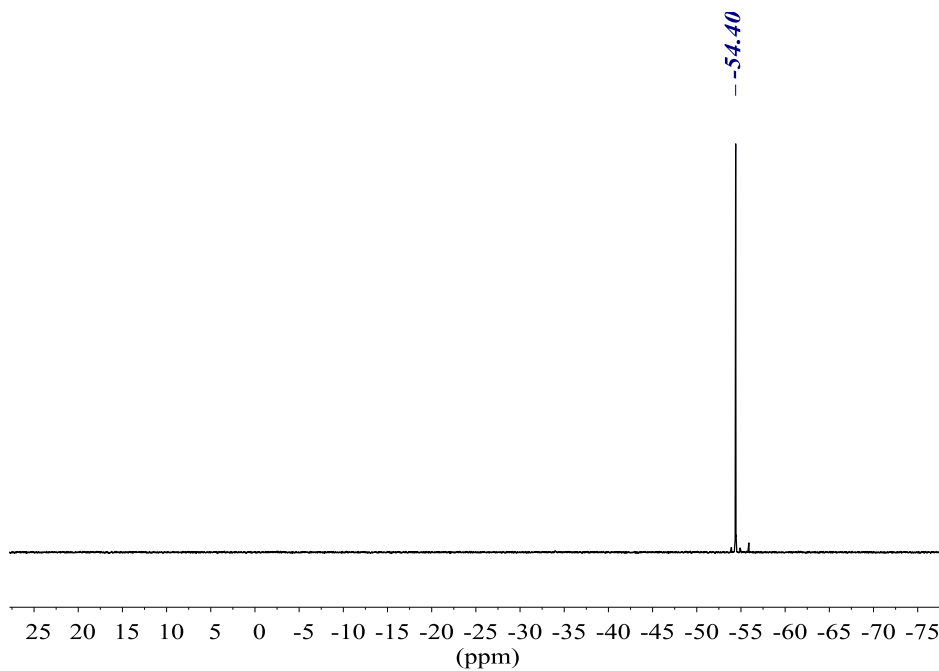
3. Characterisation of spirocyclic oxyphosphoranes

1-(2-(trifluoromethyl)phenyl)-1 λ^5 -1,1'-spirobi[benzo[*c*][1,2]oxaphosphole]-3,3'(1*H*)-dione

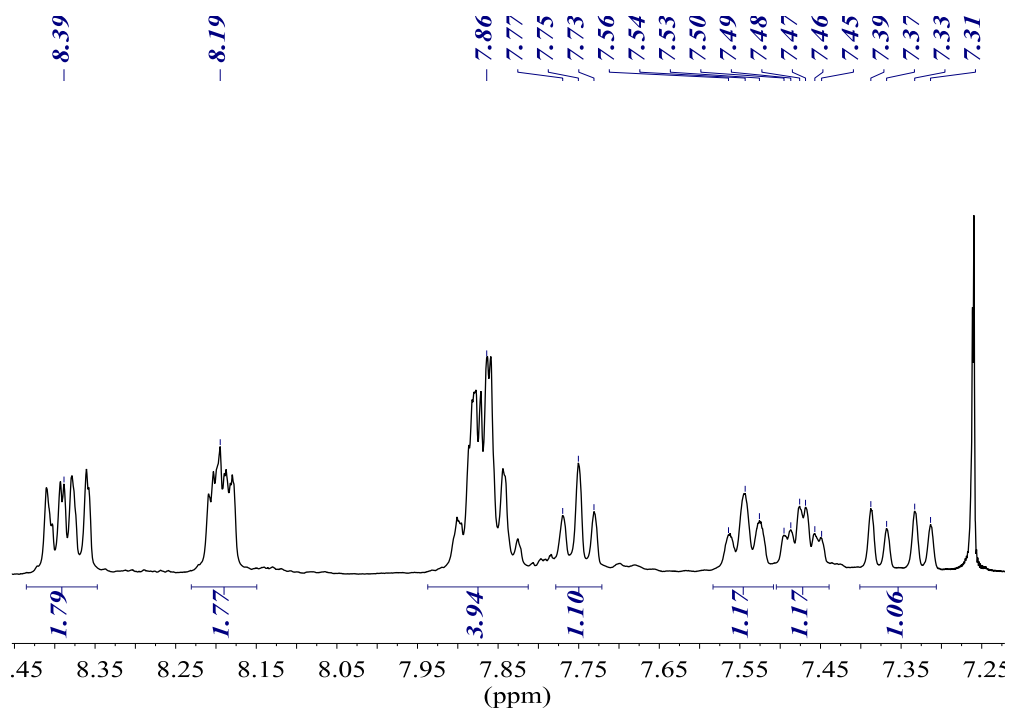
(spirocyclic oxyphosphorane 12)



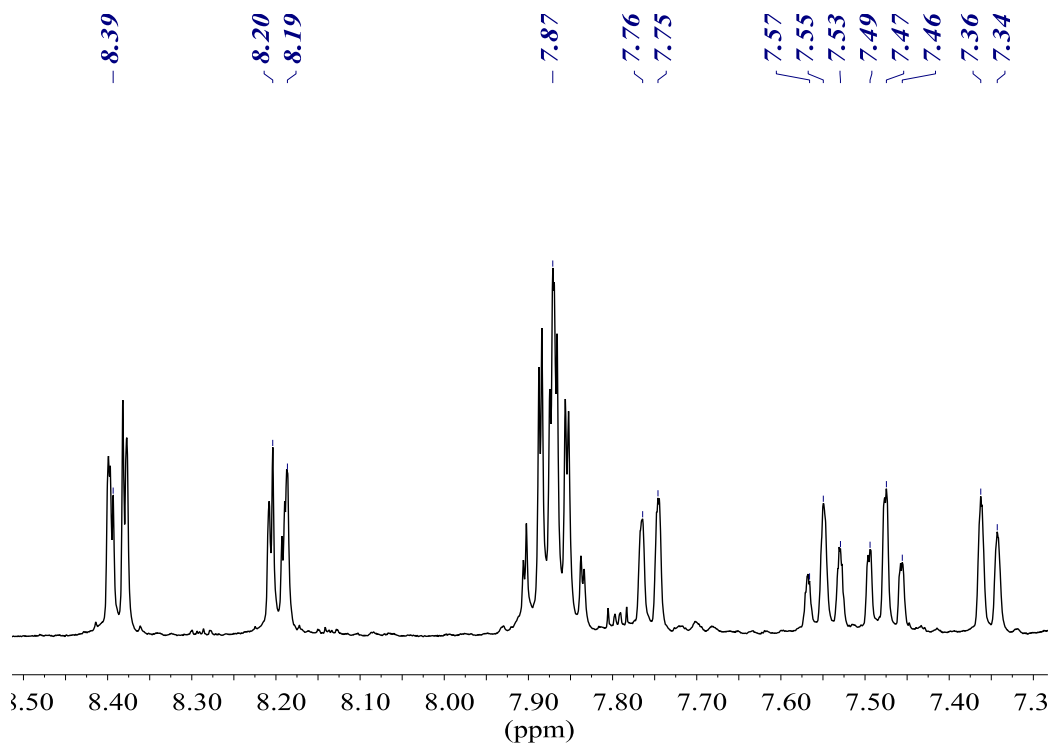
$^{31}\text{P}\{^1\text{H}\}$ NMR (161.98 MHz, CDCl_3)



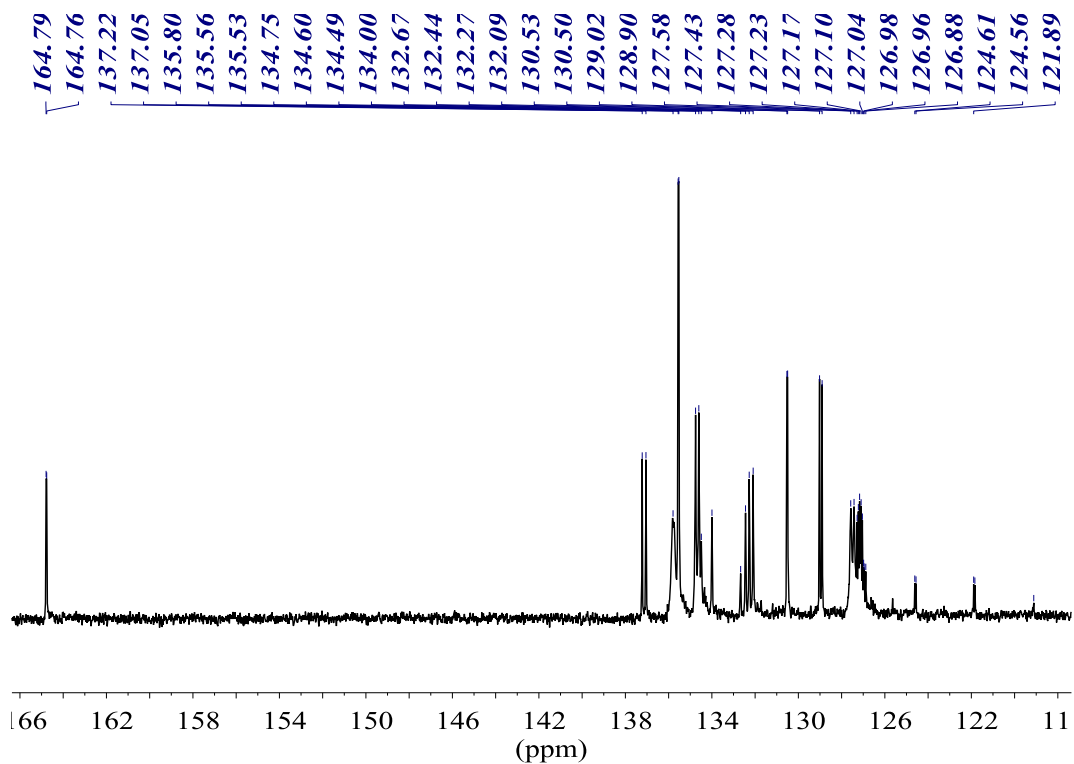
^1H NMR (400.13 MHz, CDCl_3)

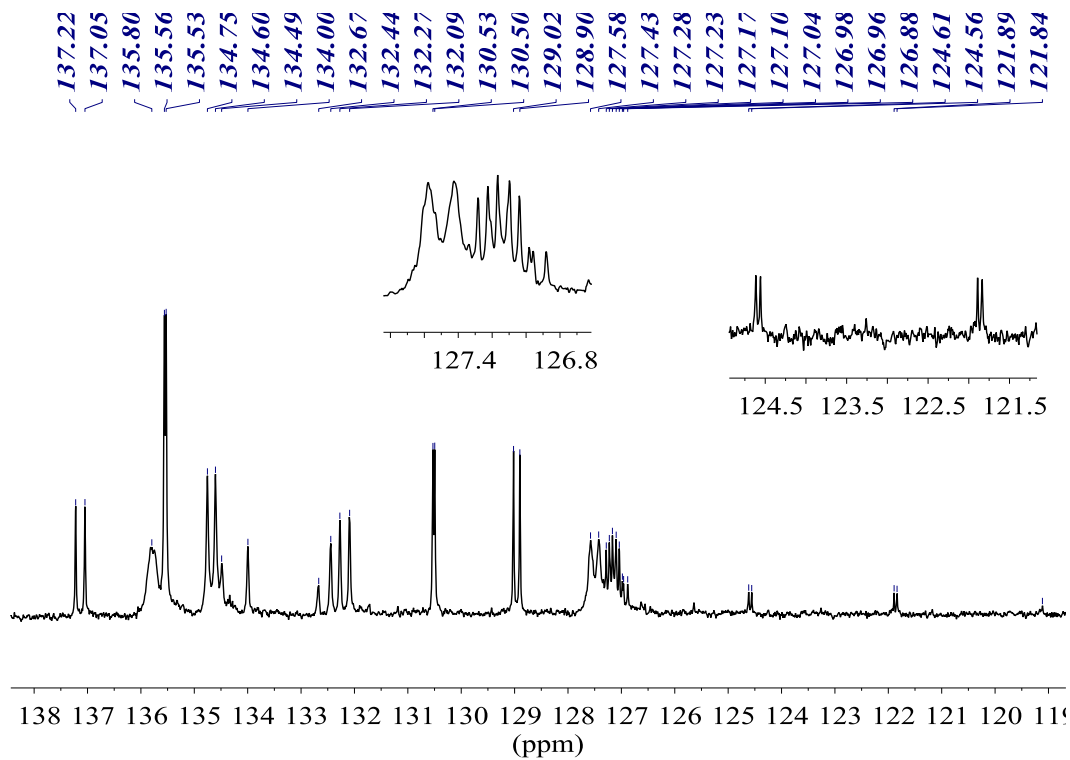


$^1\text{H}\{^{31}\text{P}\}$ NMR (400.13 MHz, CDCl_3)

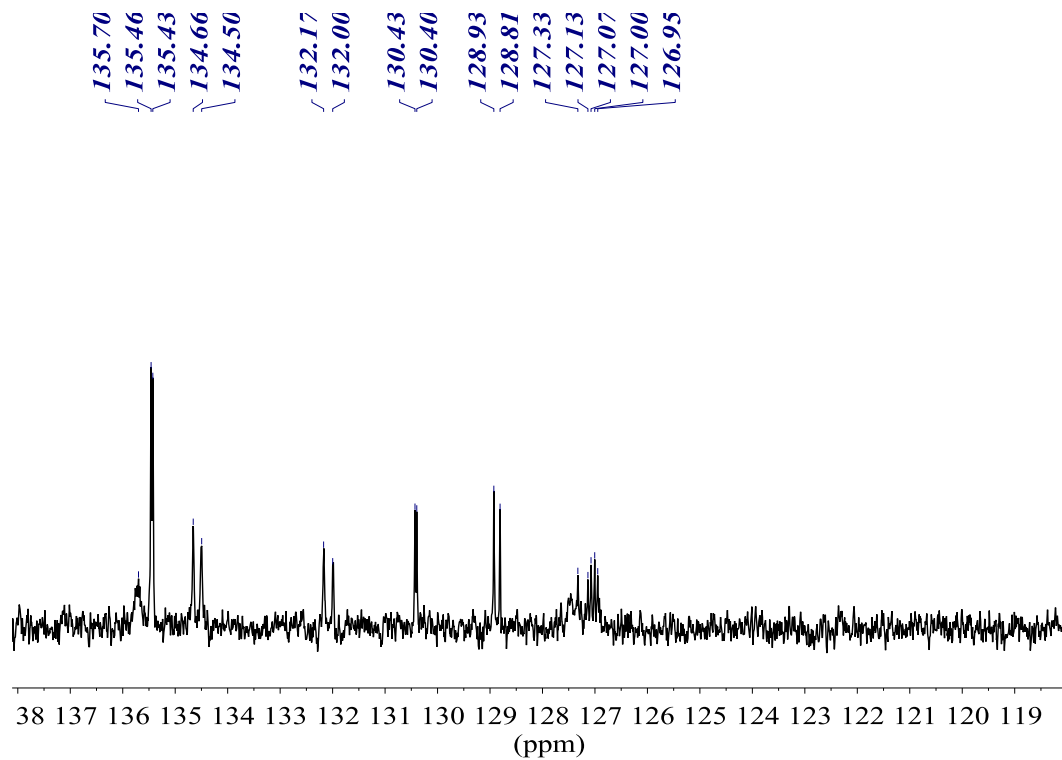


$^{13}\text{C}\{^1\text{H}\}$ NMR (100.61 MHz, CDCl_3)

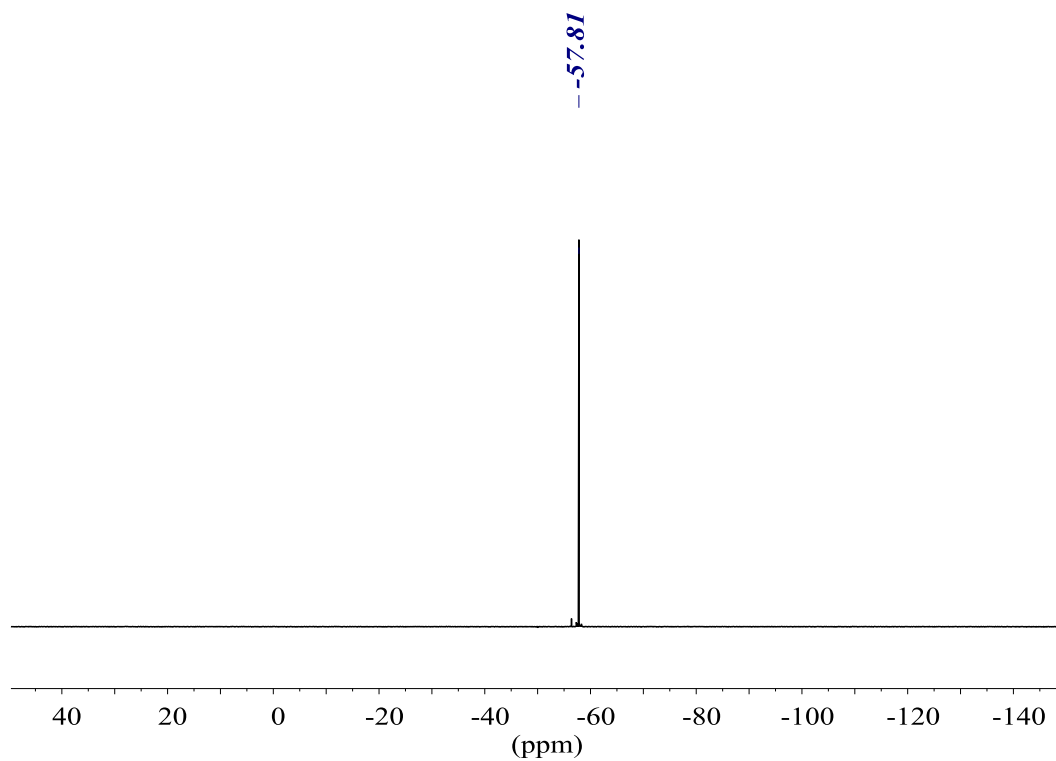




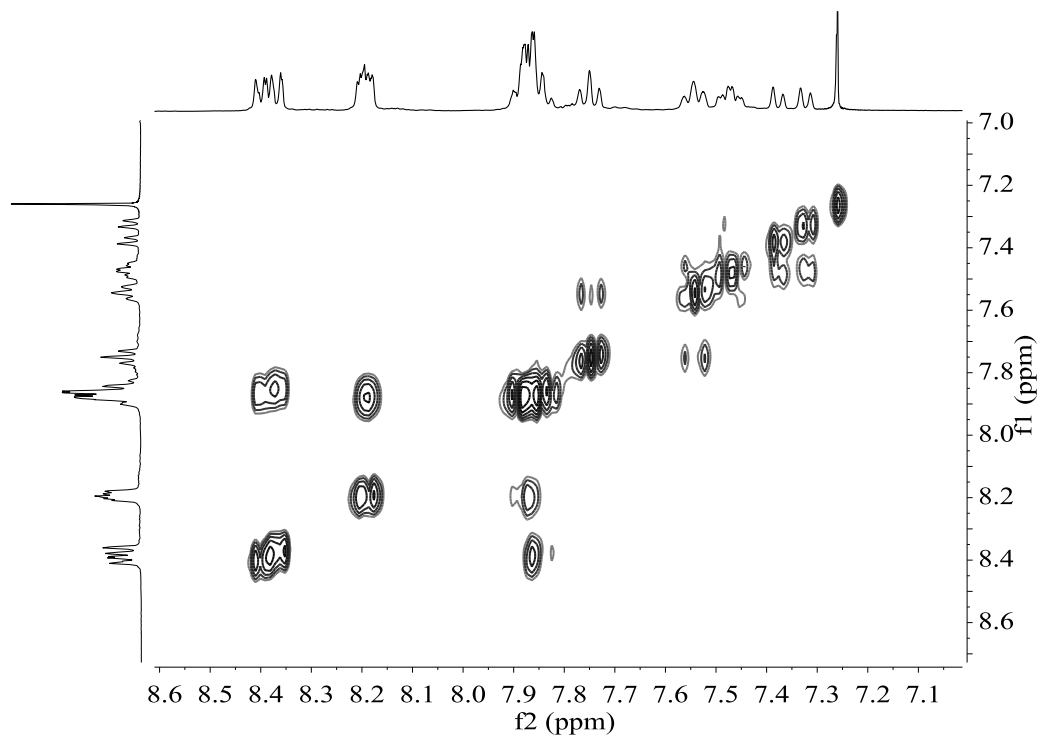
DEPT-45 NMR (100.61 MHz, CDCl₃)



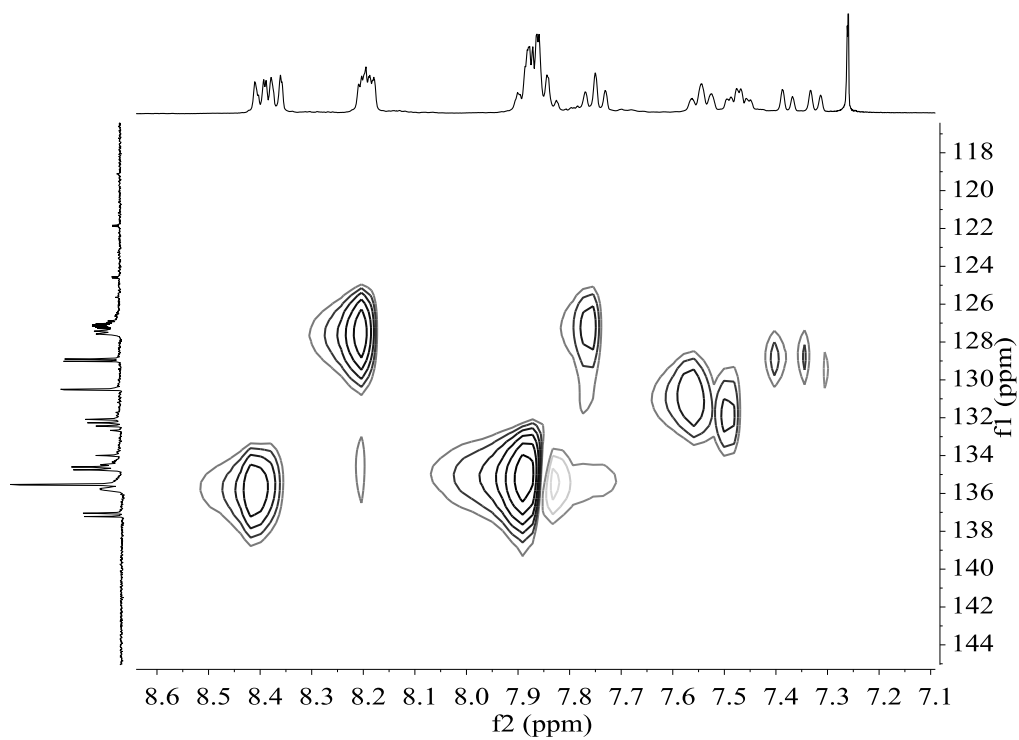
$^{19}\text{F}\{^1\text{H}\}$ NMR (376.50 MHz, CDCl_3)



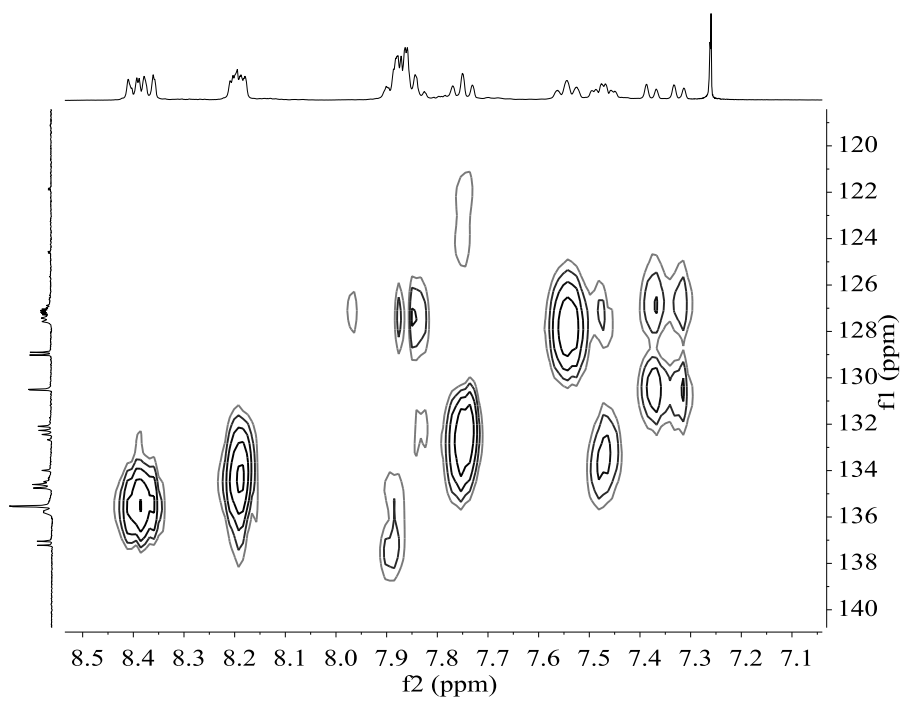
COSY NMR (400.13 MHz, CDCl_3)



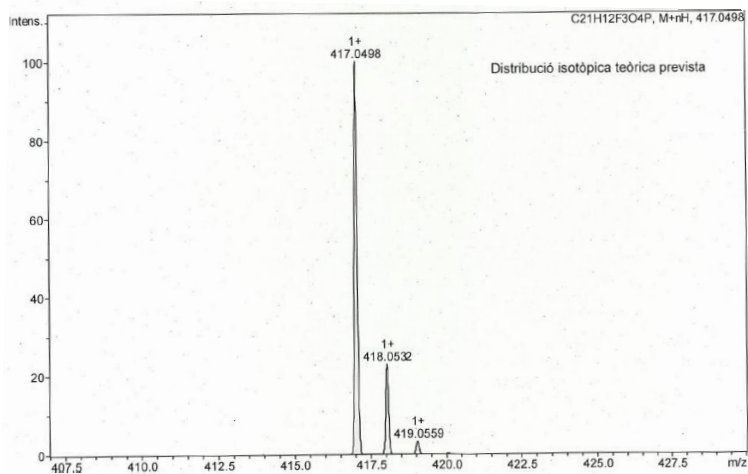
HSQC NMR (400.13 MHz, CDCl₃)



HMBC NMR (400.13 MHz, CDCl₃)

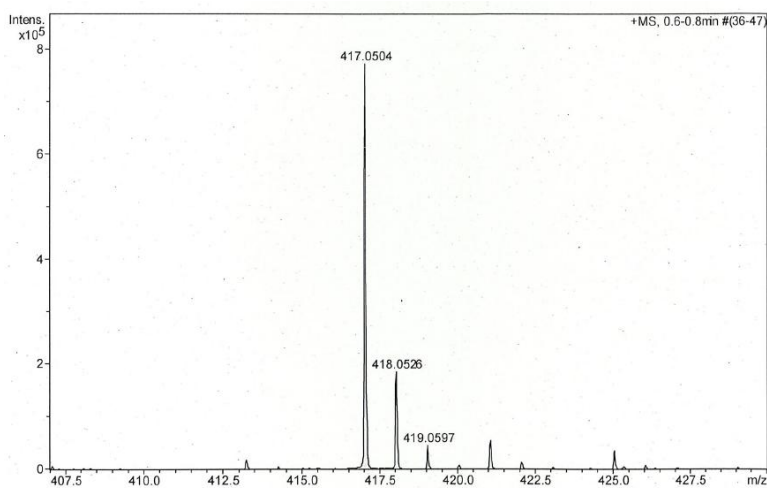


HR-MS (ESI⁺ m/z) [M+H]⁺
 calculated for [C₂₁H₁₃F₃O₄P]⁺



#	m/z	I	I %
1	417.0498	100	100.0
2	418.0532	23	23.0
3	419.0559	3	3.3

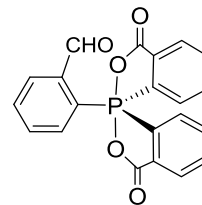
found



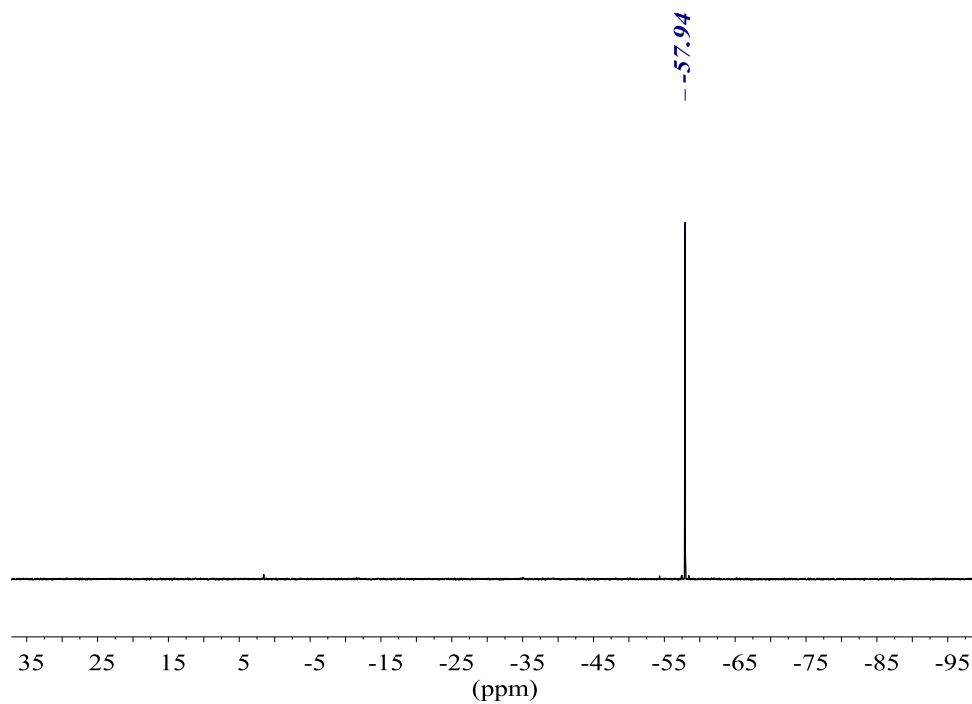
#	m/z	I	I %
1	417.0504	771355	100.0
2	418.0526	185157	24.0
3	419.0597	45199	5.9

1-(2-(trifluoromethyl)phenyl)-1 λ^5 -1,1'-spirobi[benzo[*c*][1,2]oxaphosphole]-3,3'(1*H*)-dione

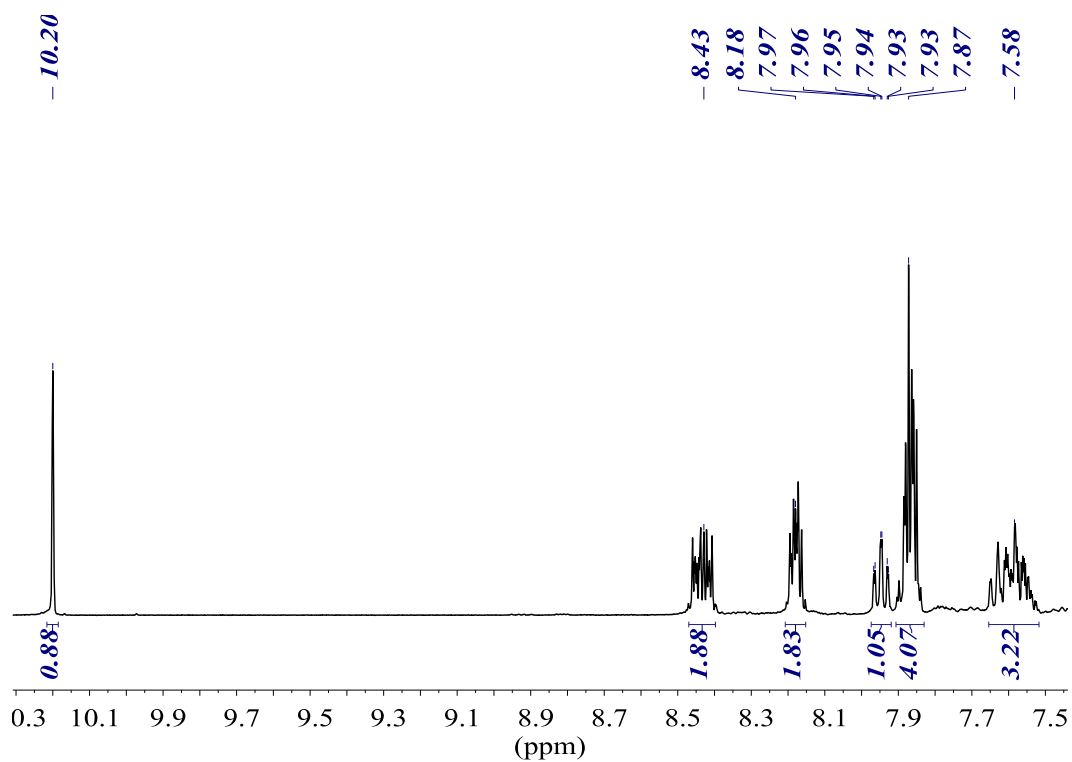
(spirocyclic oxyphosphorane 13)

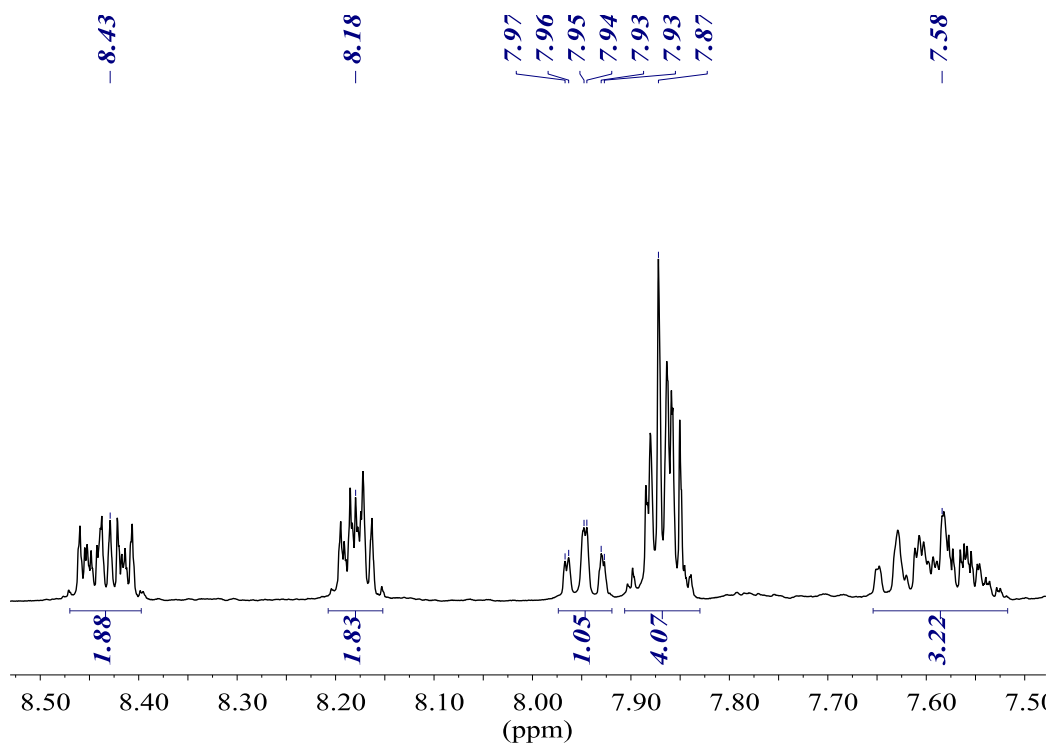


$^{31}\text{P}\{^1\text{H}\}$ NMR (161.98 MHz, CDCl_3)

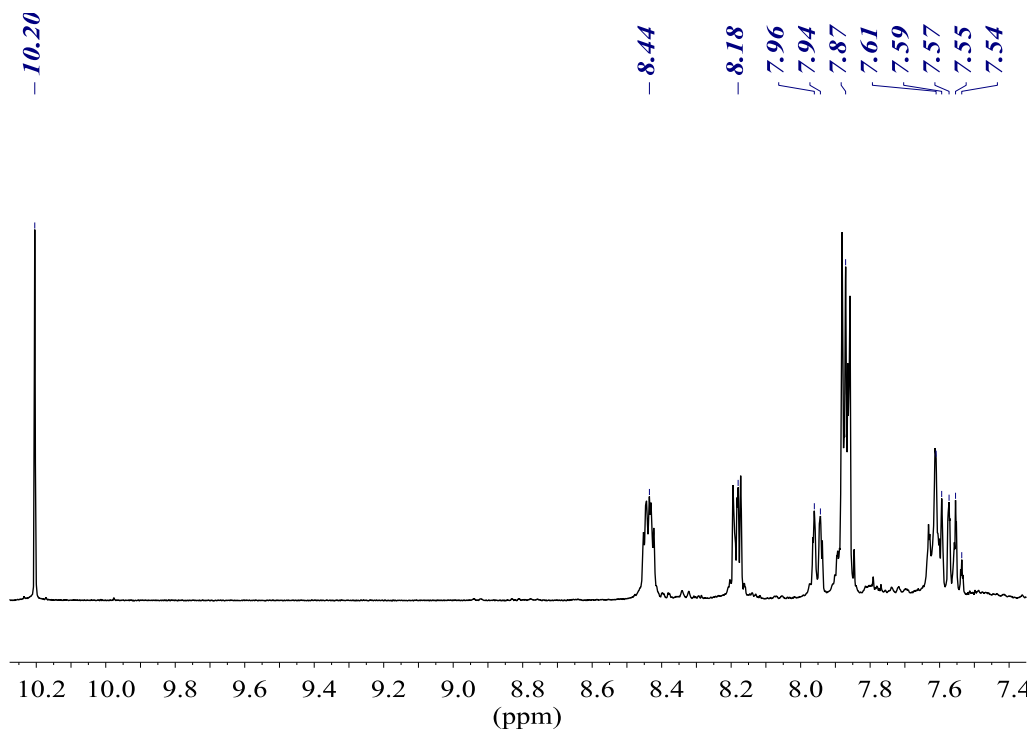


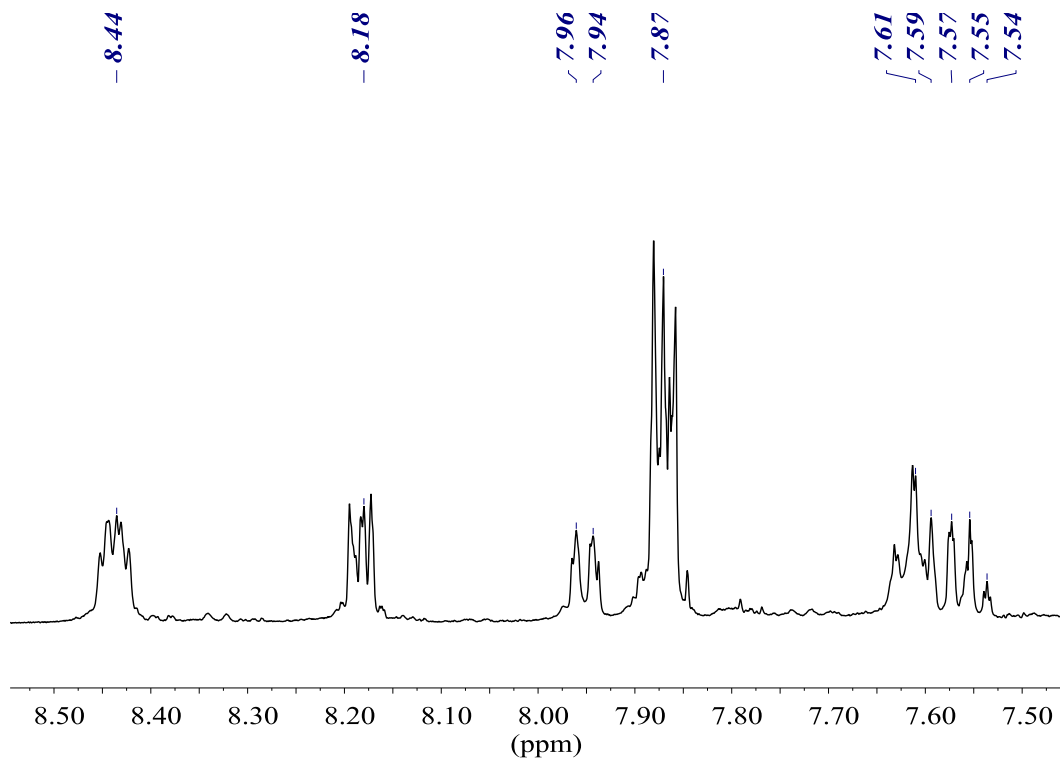
^1H NMR (400.13 MHz, CDCl_3)



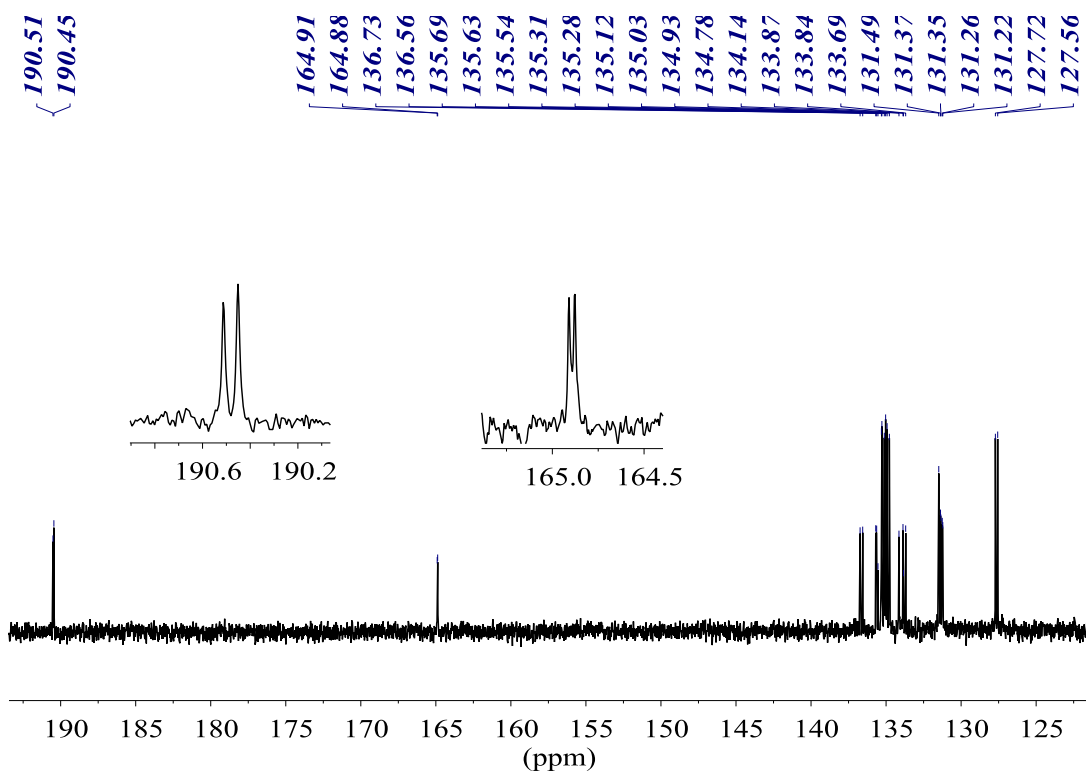


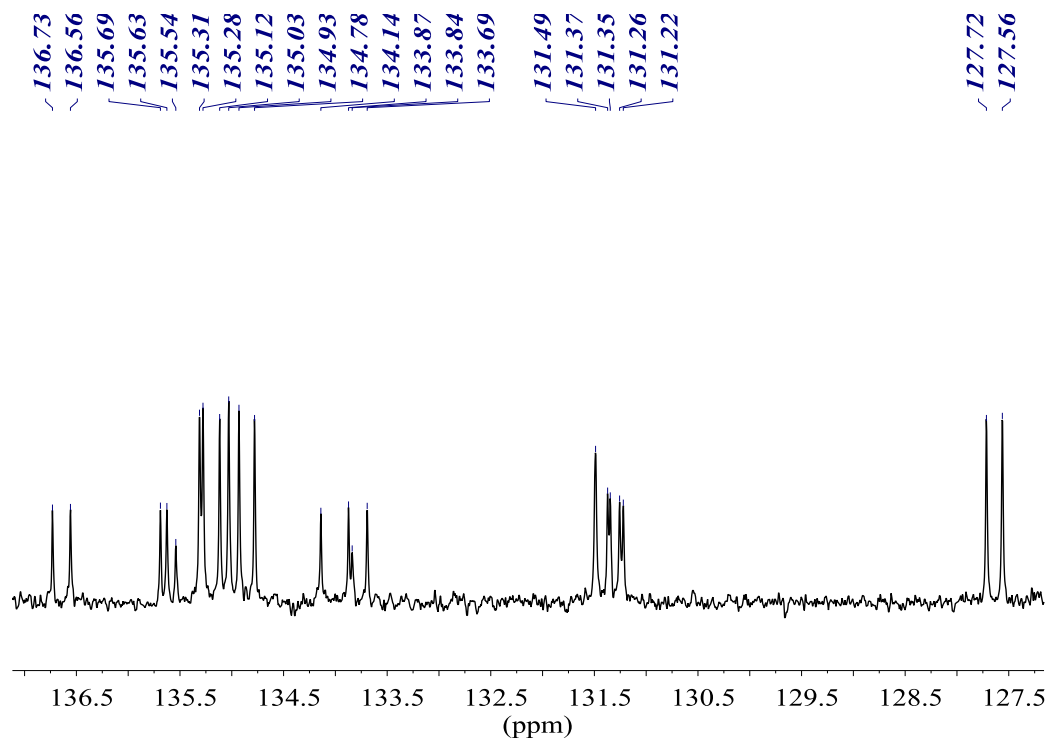
$^1\text{H}\{^{31}\text{P}\}$ NMR (400.13 MHz, CDCl_3)



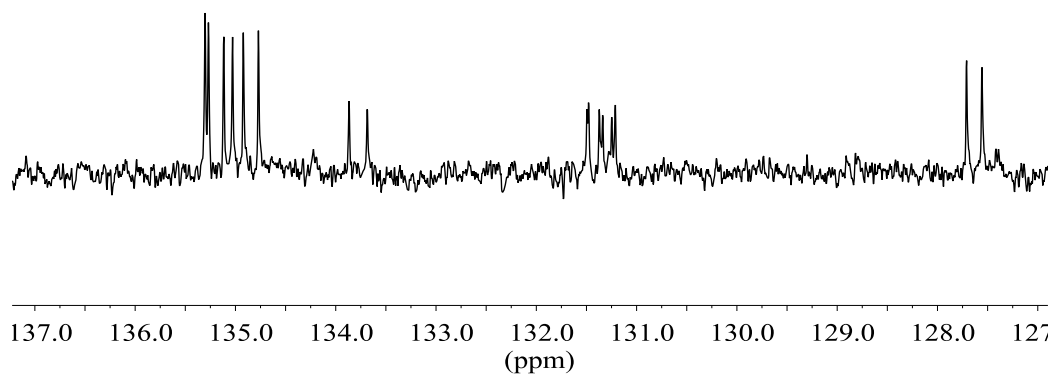


$^{13}\text{C}\{^1\text{H}\}$ NMR (100.61 MHz, CDCl_3)

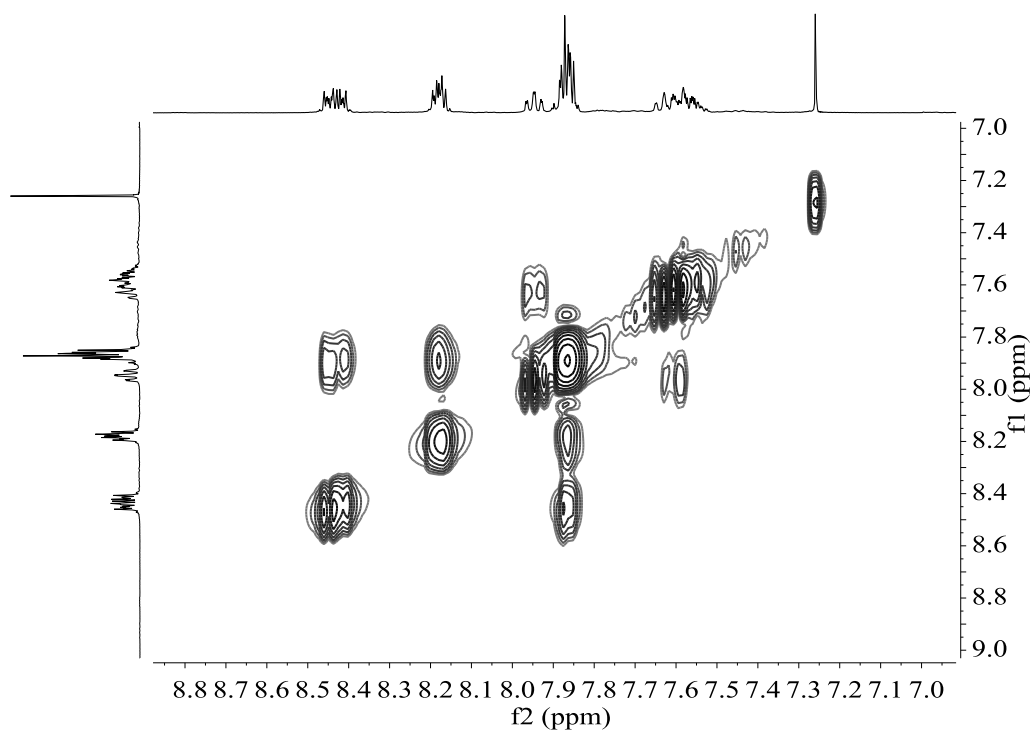




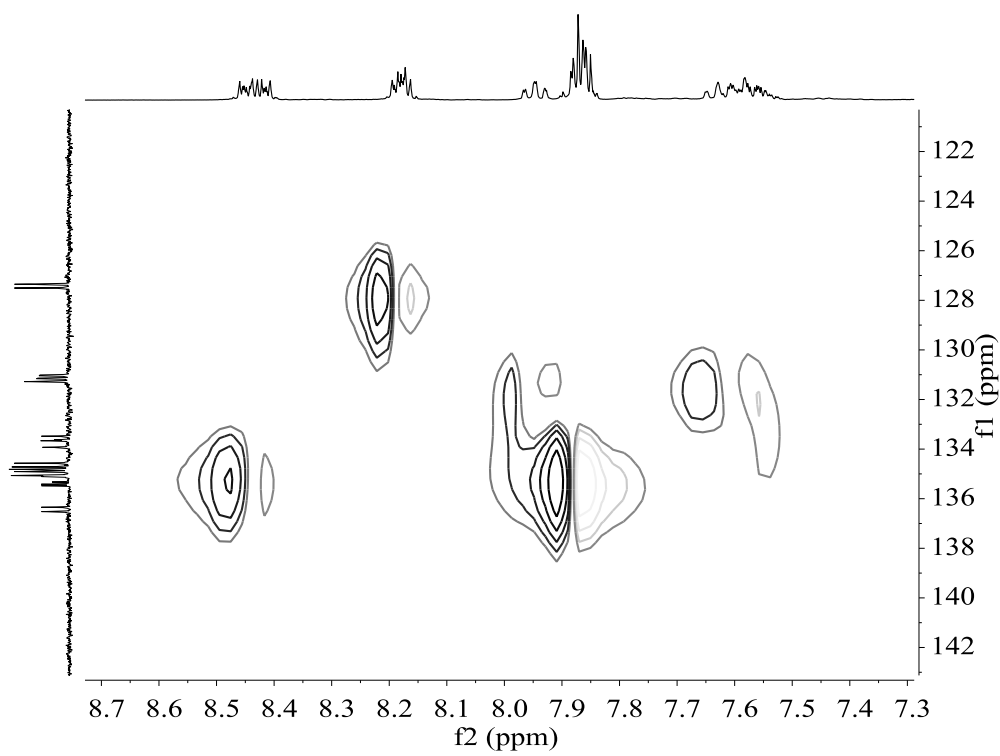
DEPT-45 NMR (100.61 MHz, CDCl3)



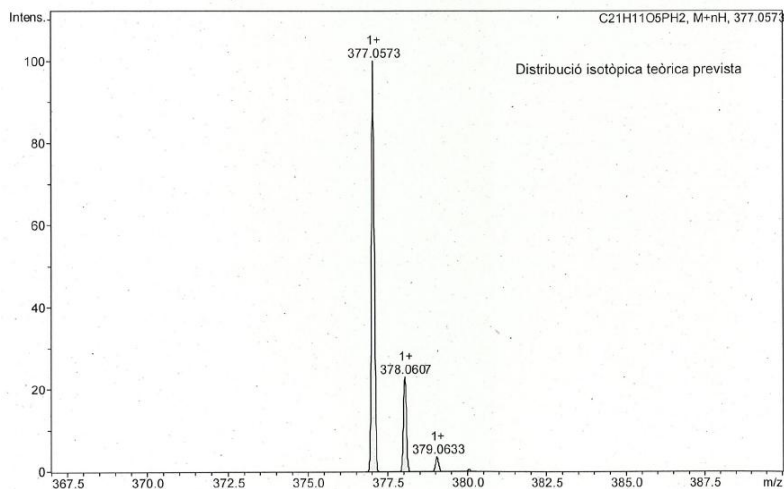
COSY NMR (400.13 MHz, CDCl₃)



HSQC NMR (400.13 MHz, CDCl₃)

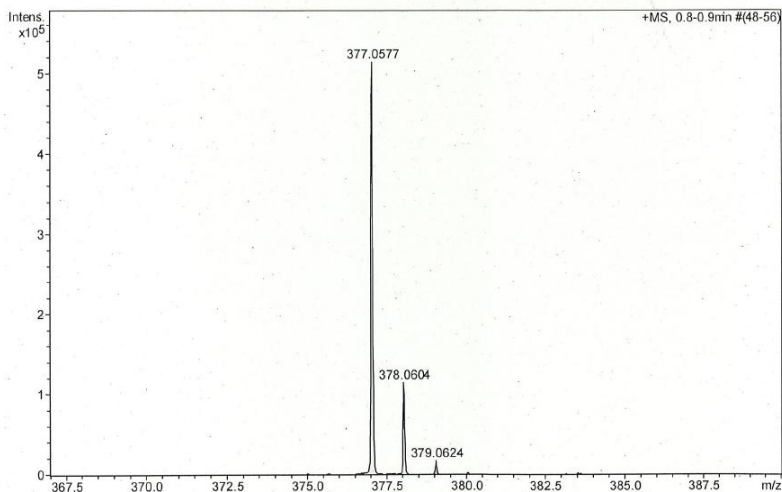


HR-MS (ESI⁺ *m/z*) [M+H]⁺
 calculated for [C₂₁H₁₄O₅P]⁺



#	<i>m/z</i>	I	I %
1	377.0573	100	100.0
2	378.0607	23	23.1
3	379.0633	4	3.6

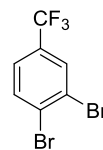
found



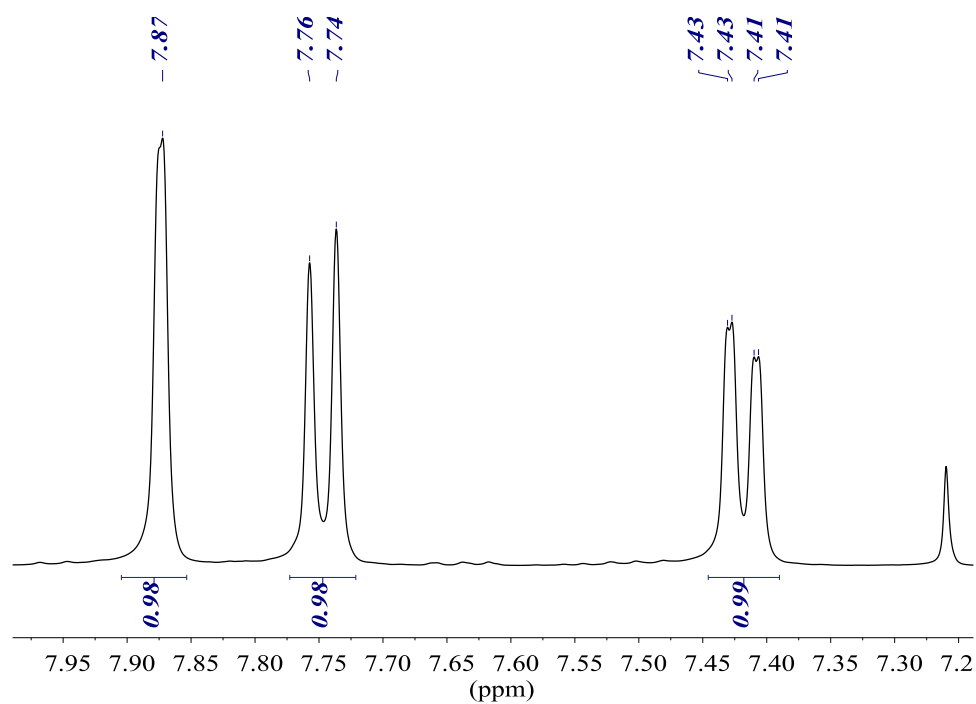
#	<i>m/z</i>	I	I %
1	377.0577	514078	100.0
2	378.0604	115012	22.4
3	379.0624	17545	3.4

4. Characterisation of trifluoromethylated diphosphines 30 and 31 and intermediate compounds

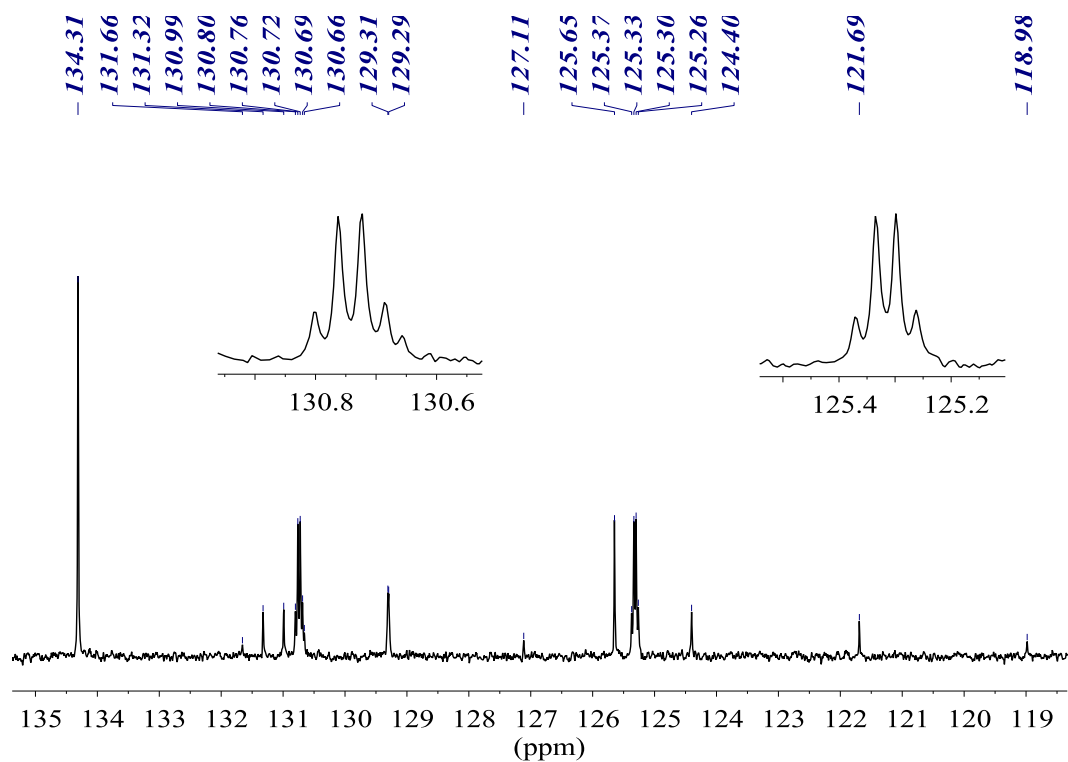
1,2-dibromo-4-(trifluoromethyl)benzene (33)



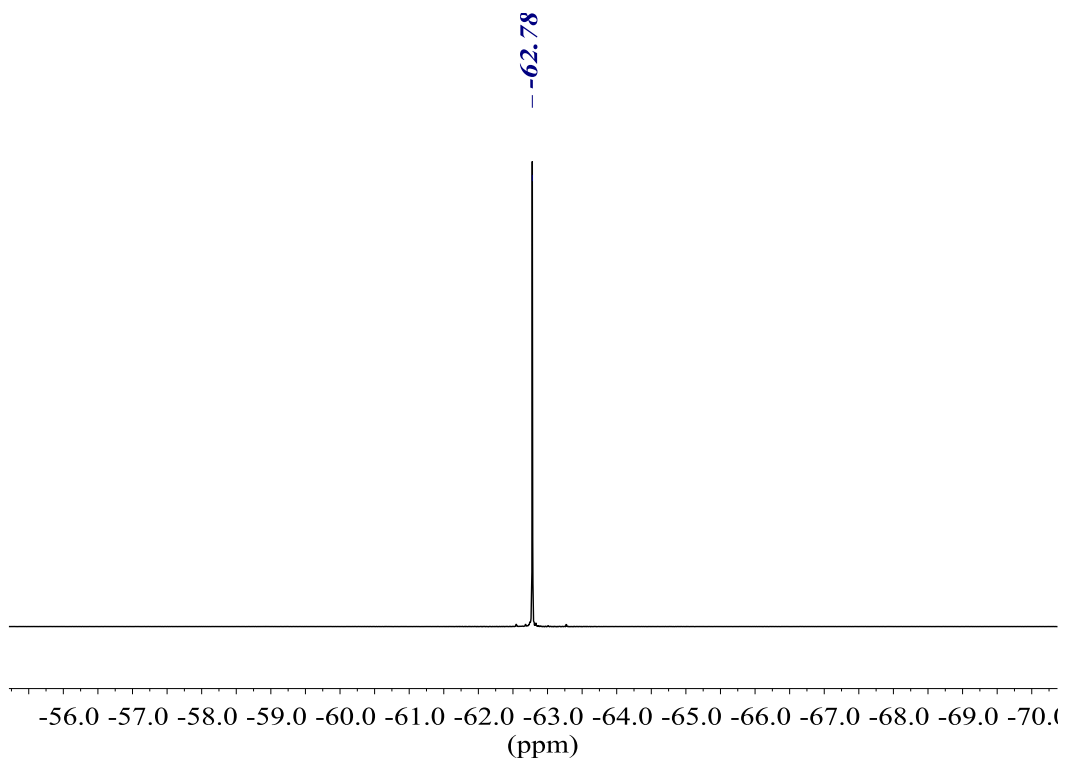
^1H NMR (400.13 MHz, CDCl_3)



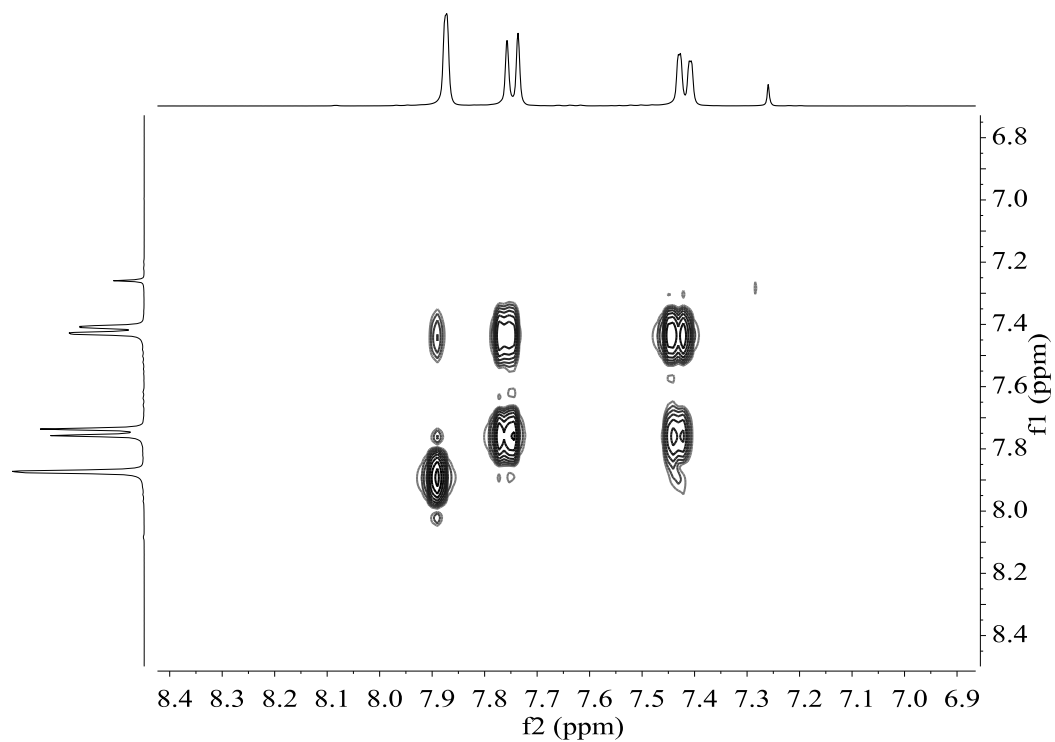
$^{13}\text{C}\{^1\text{H}\}$ NMR (100.61 MHz, CDCl_3)



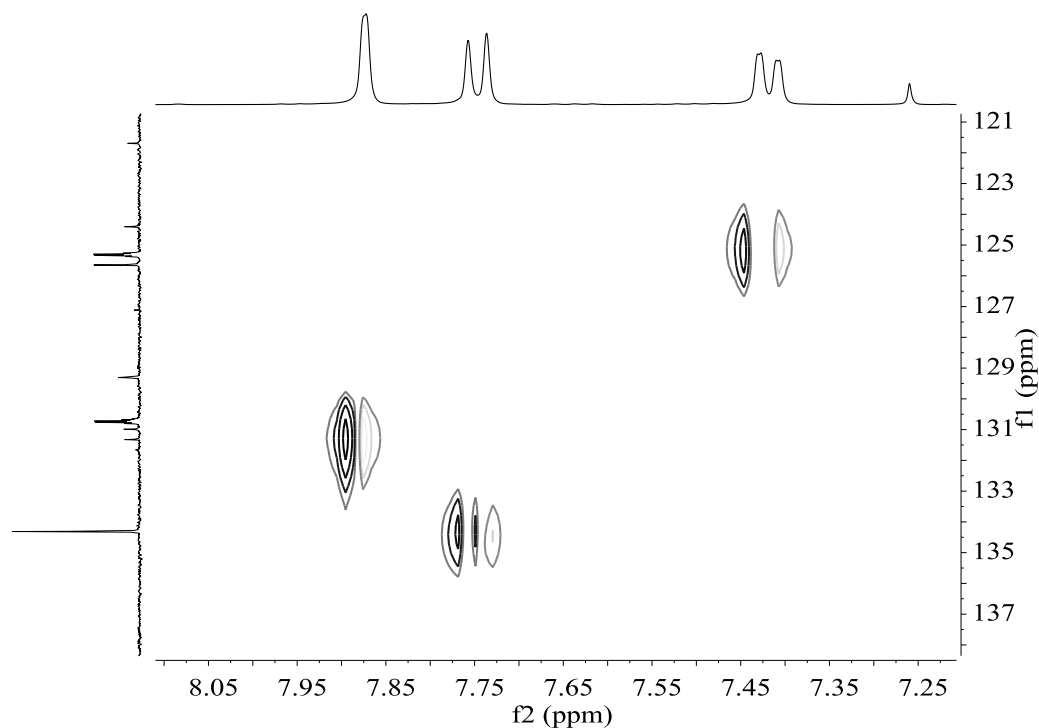
$^{19}\text{F}\{^1\text{H}\}$ NMR (376.50 MHz, CDCl_3)



COSY NMR (400.13 MHz, CDCl_3)

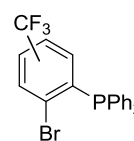


HSQC NMR (400.13 MHz, CDCl₃)

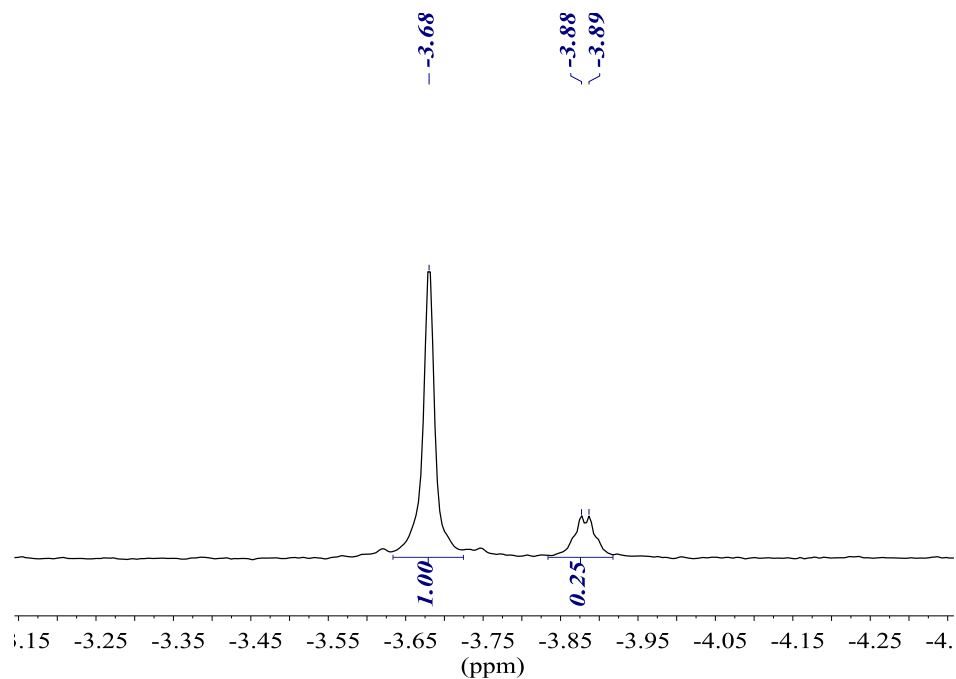


Bromophosphines 28. Mixture of isomers

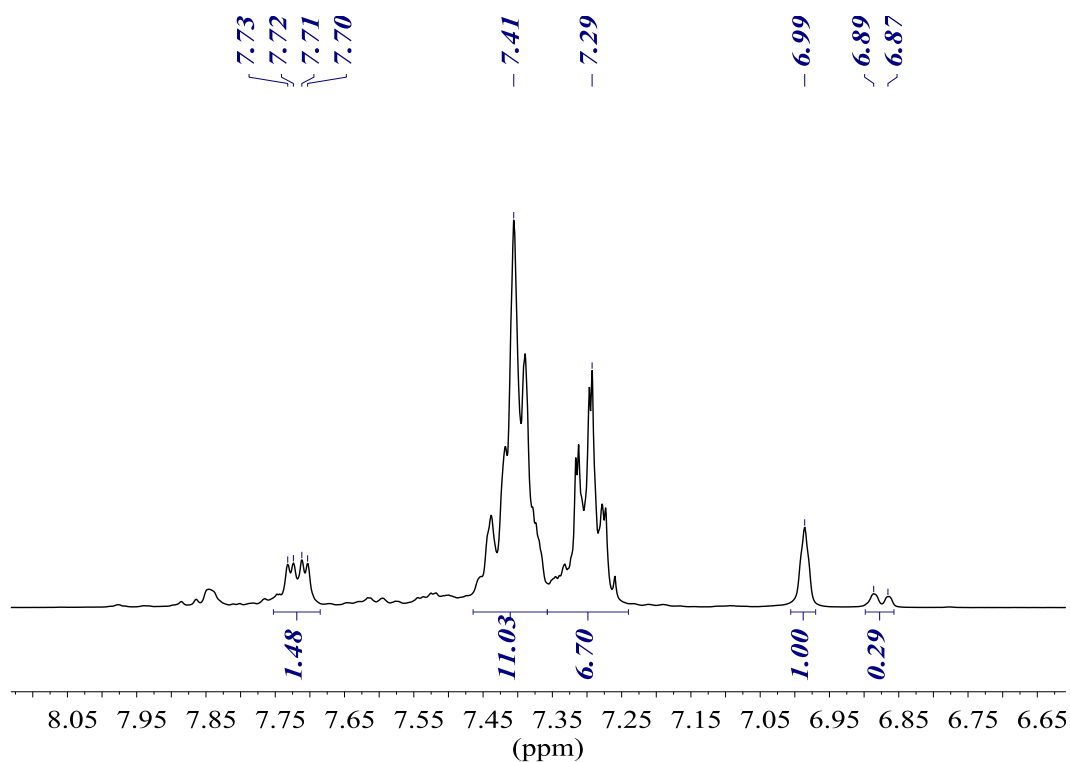
(2-bromo-5-(trifluoromethyl)phenyl)diphenylphosphine (*m*28) +
(2-bromo-4-(trifluoromethyl)phenyl)diphenylphosphine (*p*28)



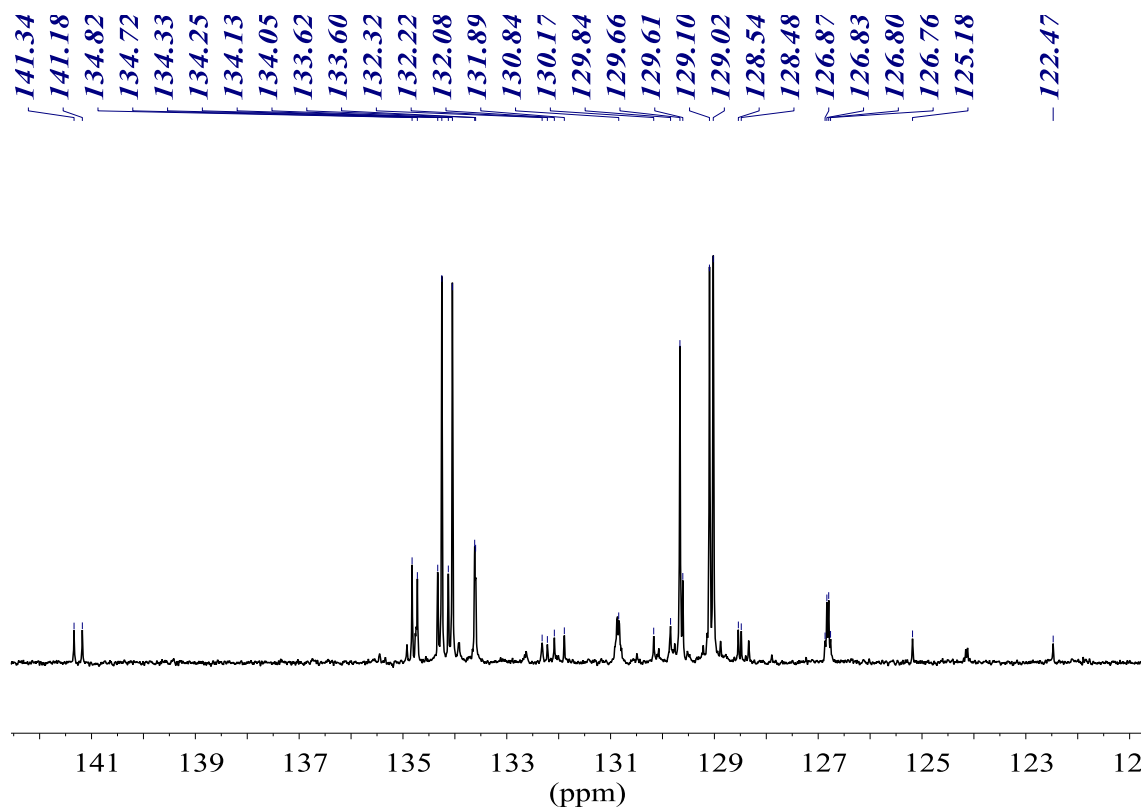
³¹P{¹H} NMR (161.98 MHz, CDCl₃)



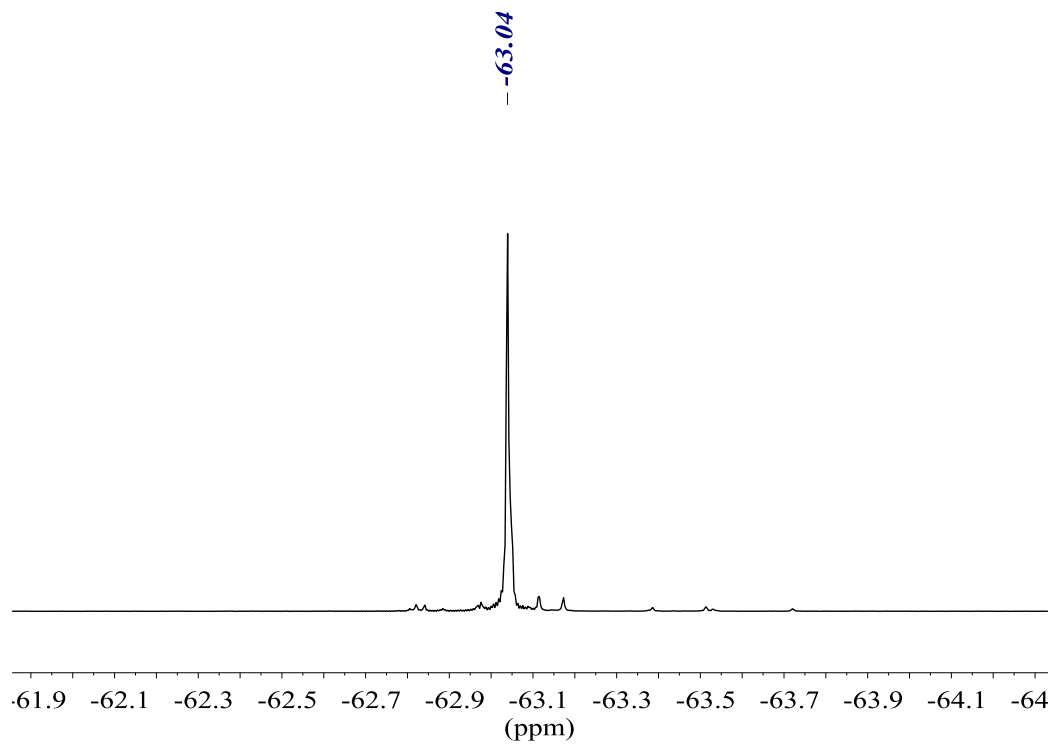
^1H NMR (400.13 MHz, CDCl_3)



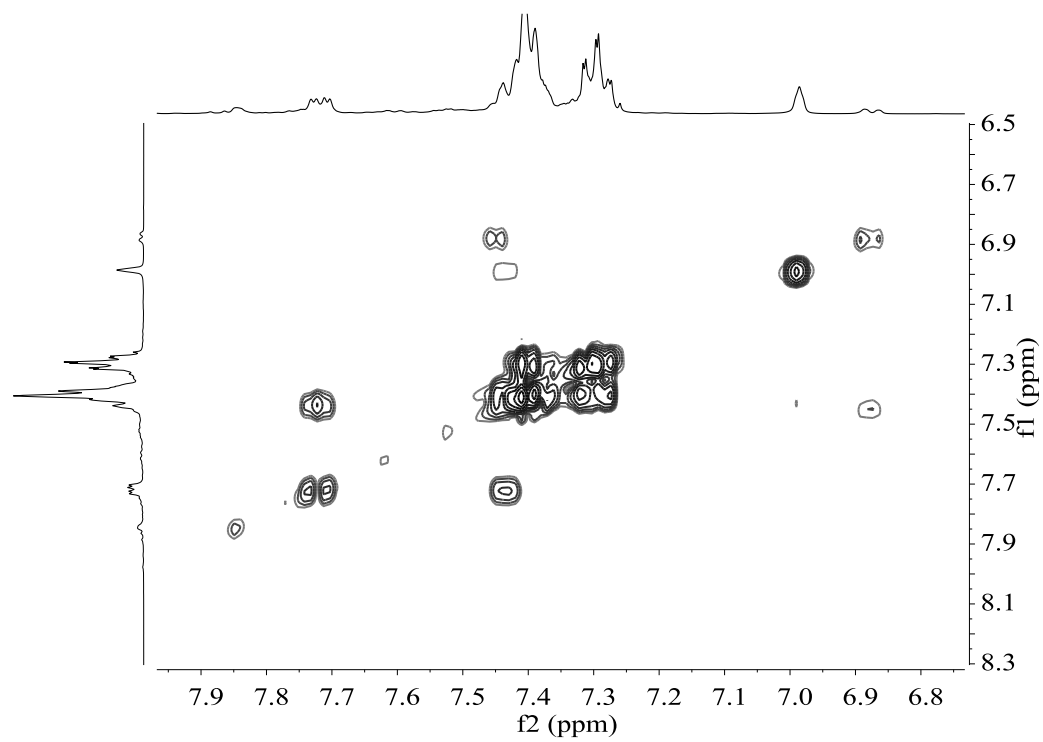
$^{13}\text{C}\{^1\text{H}\}$ NMR (100.61 MHz, CDCl_3)



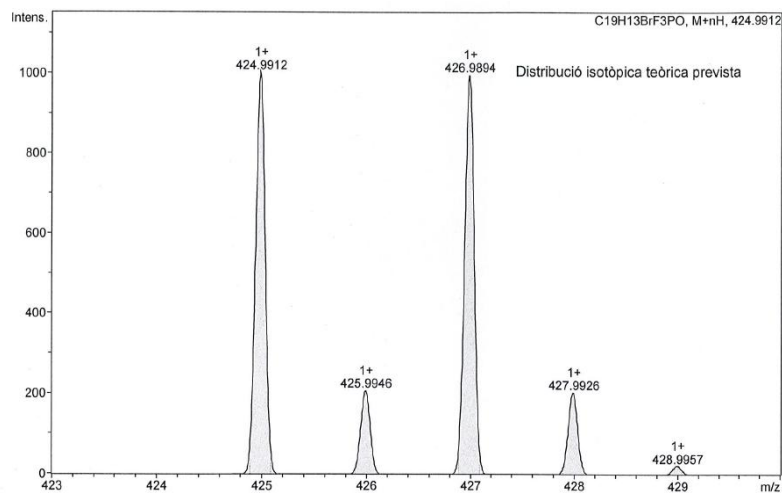
$^{19}\text{F}\{^1\text{H}\}$ NMR (376.50 MHz, CDCl_3)



COSY NMR (400.13 MHz, CDCl_3)

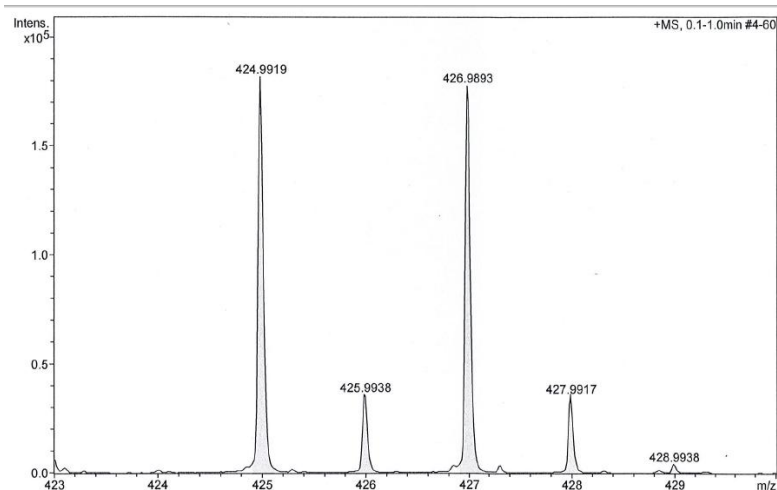


HR-MS (ESI⁺ m/z) [M(O)+H]⁺
 calculated for [C₁₉H₁₄BrF₃PO]⁺



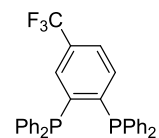
#	m/z	I	I %
1	424.9912	1000	100.0
2	425.9946	207	20.7
3	426.9894	995	99.5
4	427.9926	203	20.3
5	428.9957	22	2.2

found

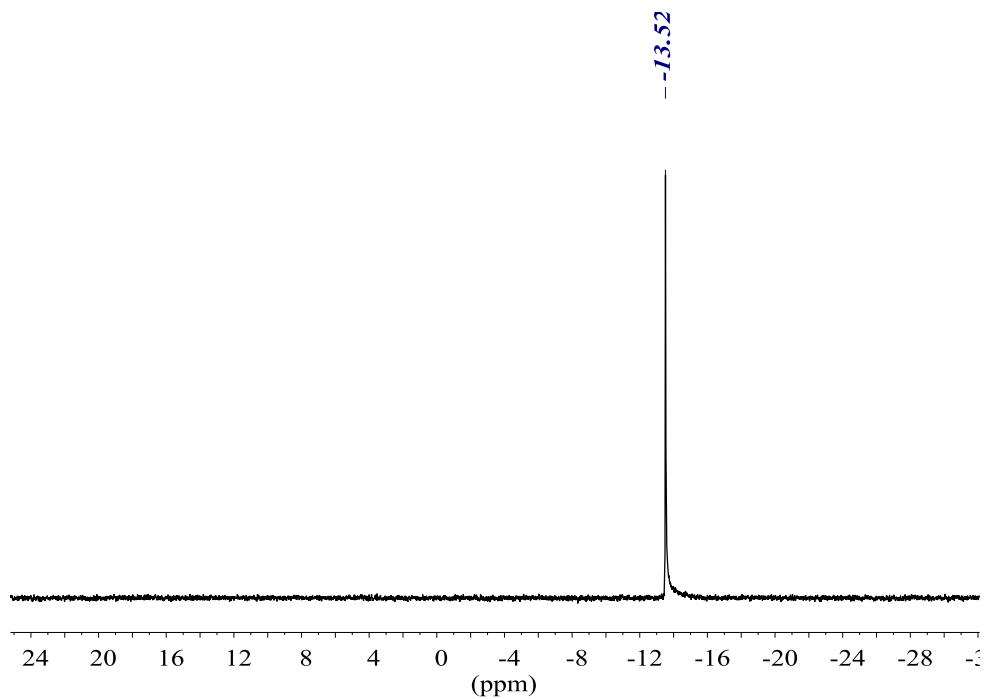


#	m/z	I	I %
1	424.9919	181767	100.0
2	425.9938	36034	19.8
3	426.9893	177723	97.8
4	427.9917	35384	19.5
5	428.9938	4325	2.4

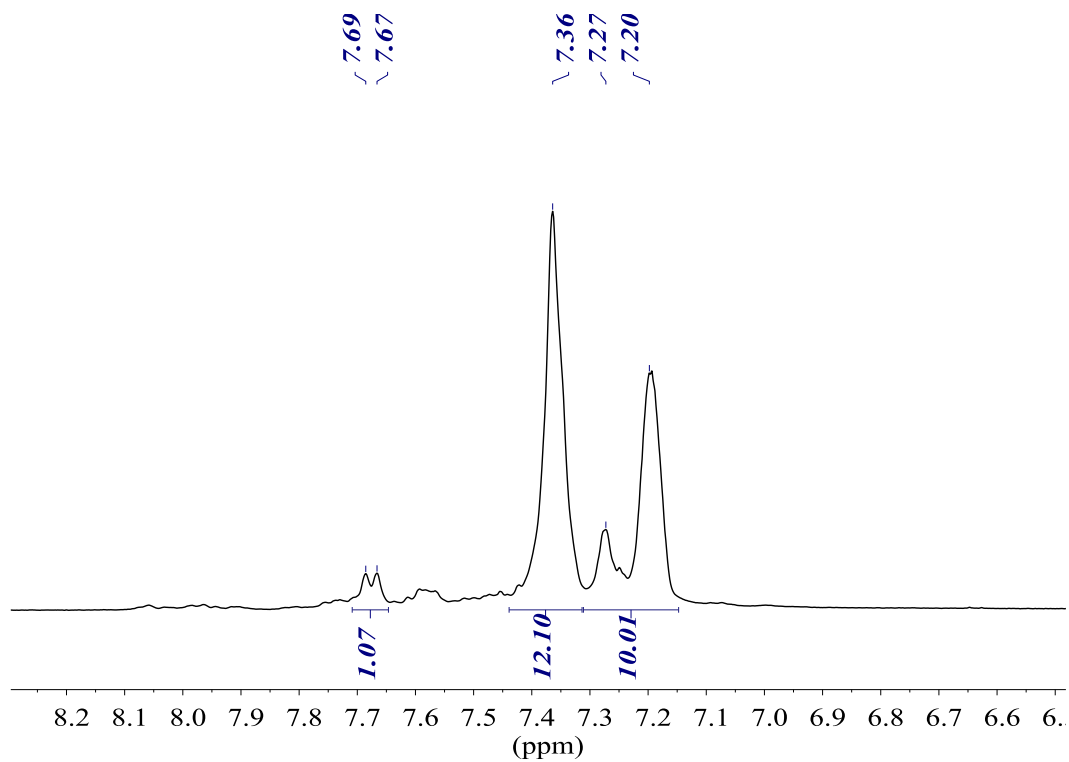
(4-(Trifluoromethyl)-1,2-phenylene)bis(diphenylphosphine) (30)



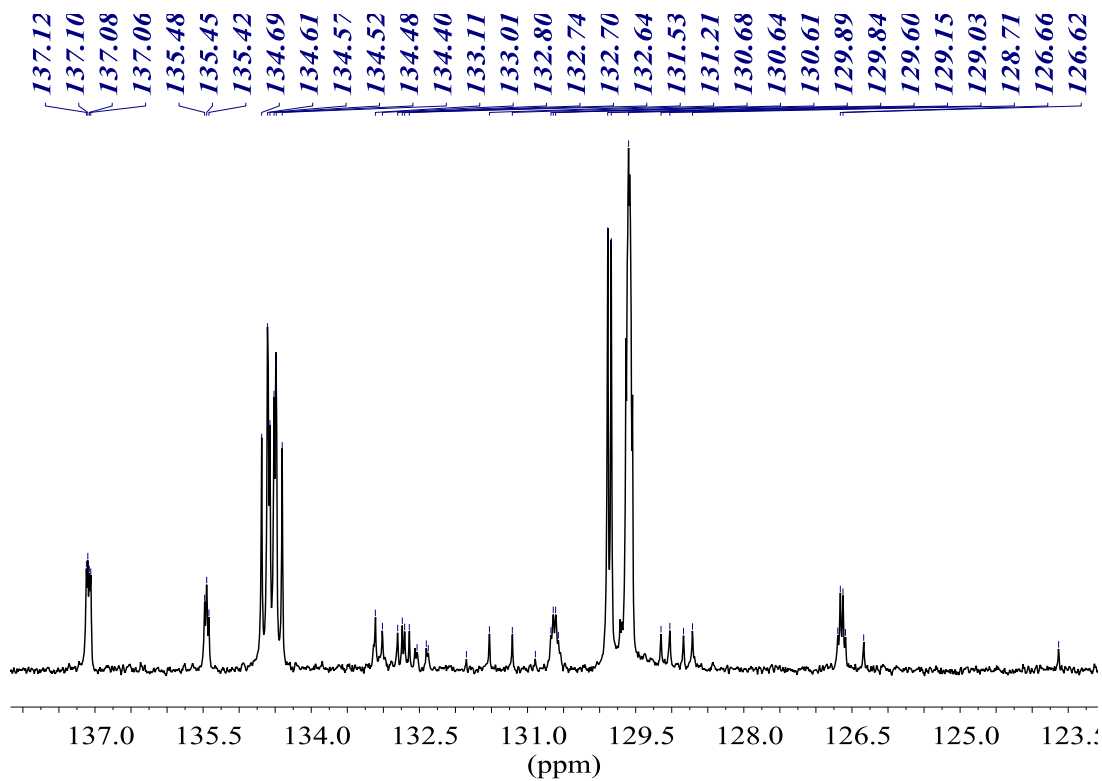
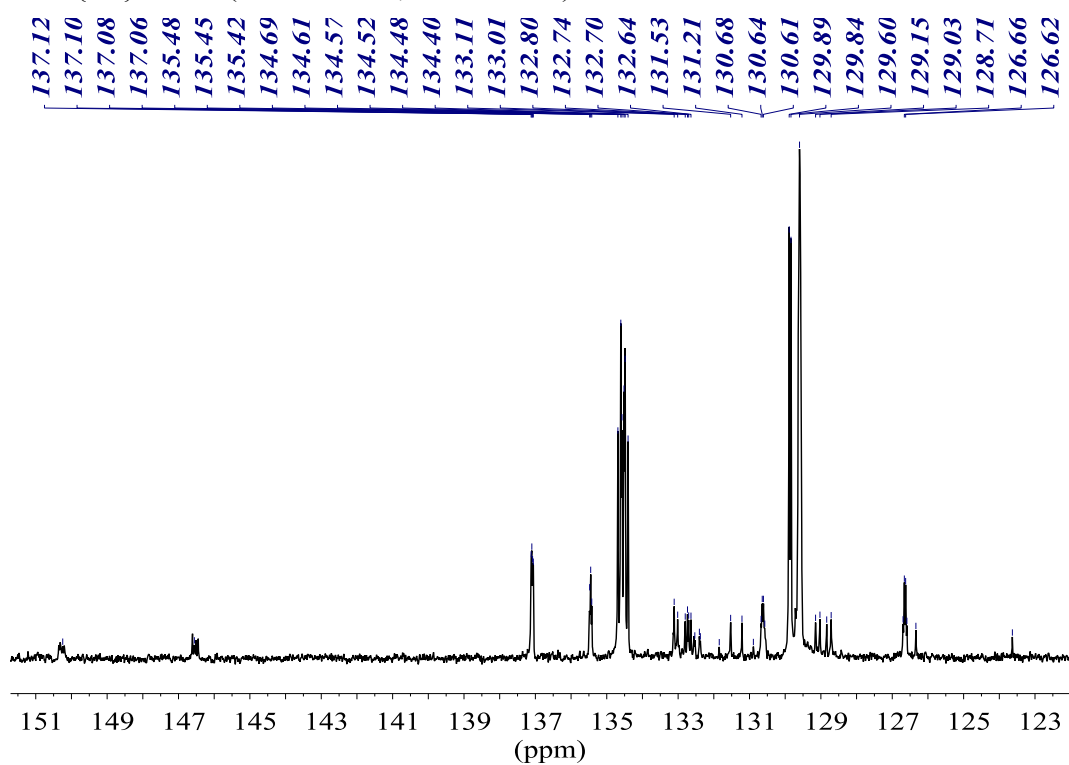
$^{31}\text{P}\{^1\text{H}\}$ NMR (161.98 MHz, CDCl_3)



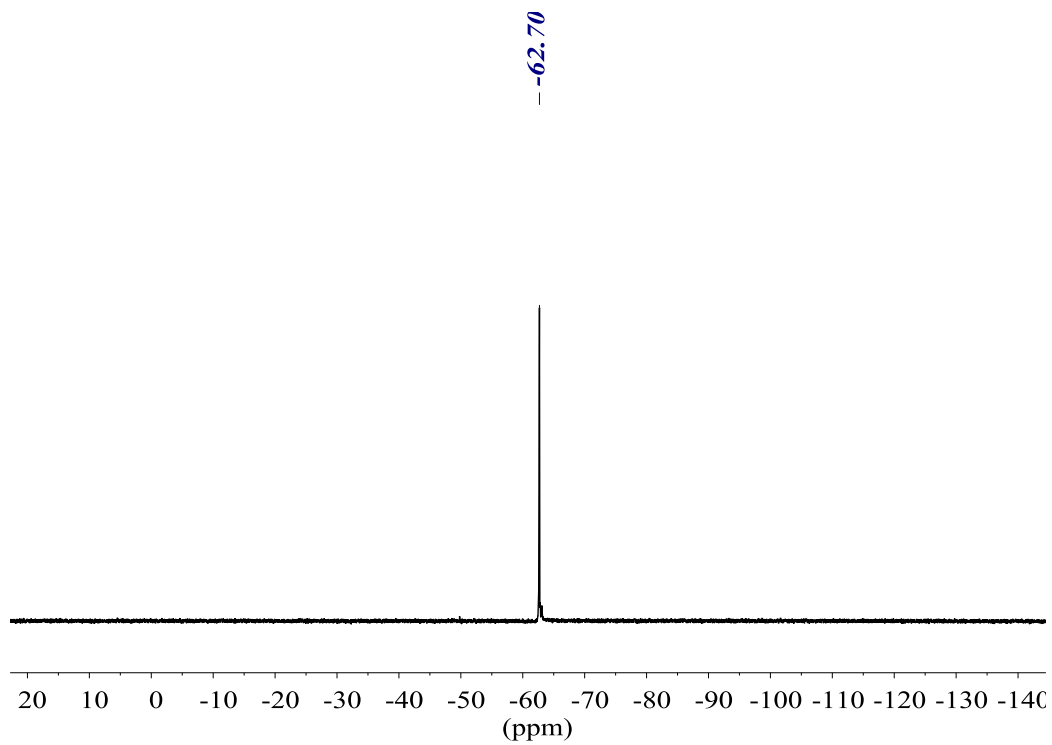
^1H NMR (400.13 MHz, acetone- D_6)



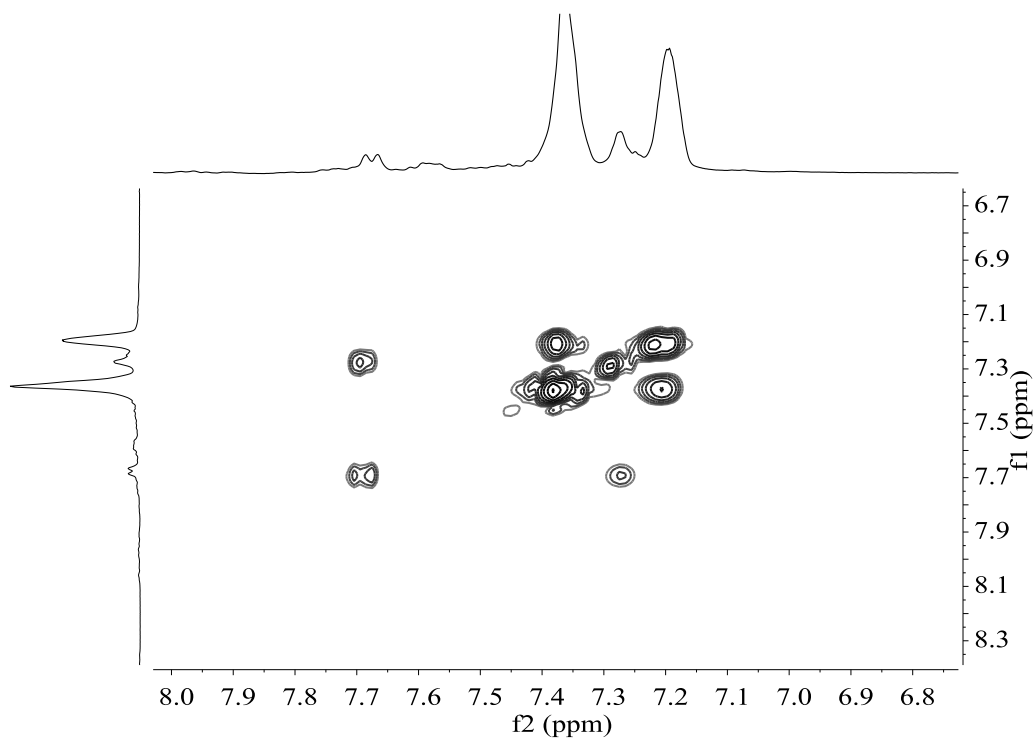
$^{13}\text{C}\{^1\text{H}\}$ NMR (100.61 MHz, acetone- D_6)



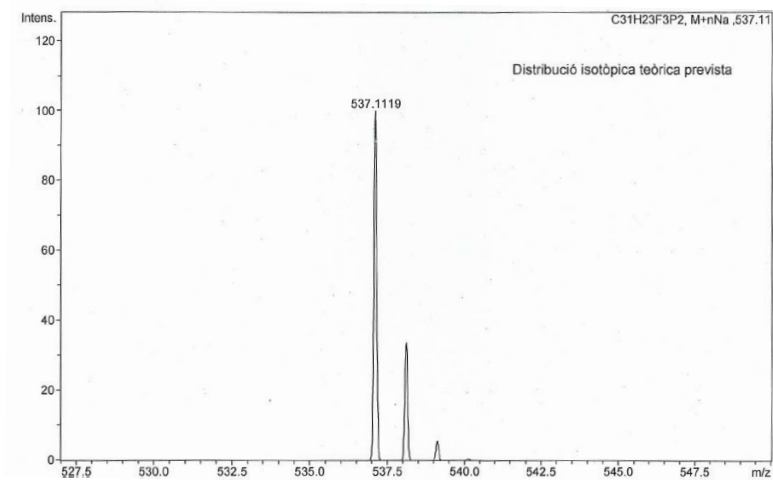
$^{19}\text{F}\{^1\text{H}\}$ NMR (376.50 MHz, CDCl_3)



COSY NMR (400.13 MHz, CDCl_3)

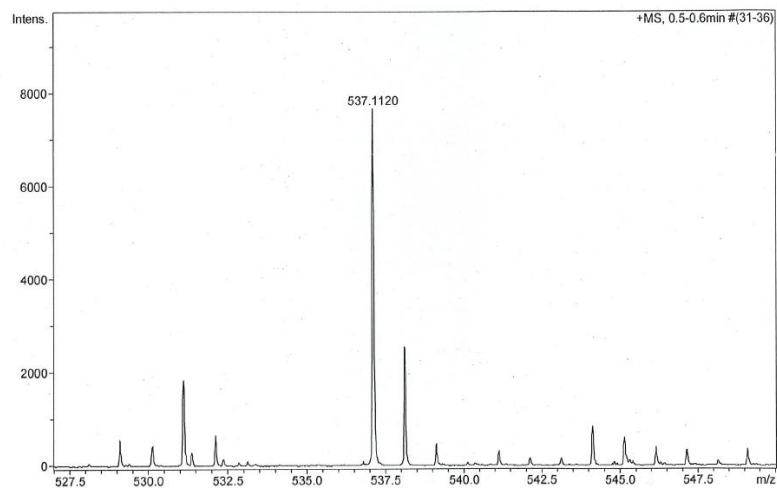


HR-MS (ESI⁺ m/z) [M+Na]⁺
 calculated for [C₃₁H₂₃F₃P₂Na]⁺



#	m/z	I	I %
1	537.1119	100	100.0
2	538.1153	34	33.8
3	539.1186	6	5.5

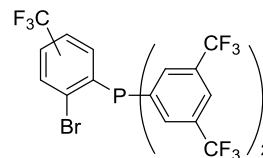
found



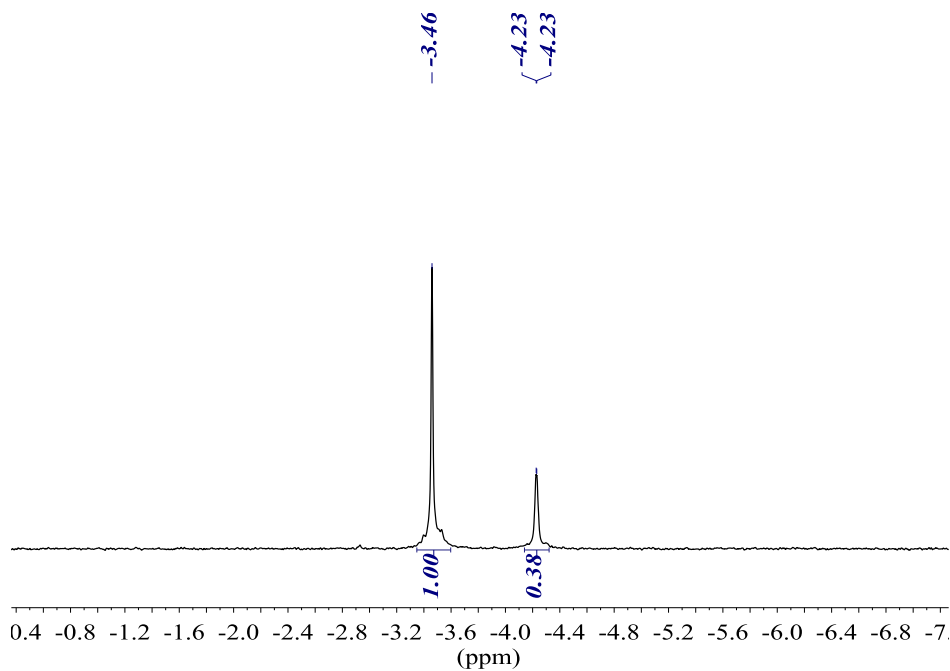
#	m/z	I	I %
1	537.1120	7670	100.0
2	538.1160	2554	33.3
3	539.1189	472	6.1

Bromophosphines 29. Mixture of isomers

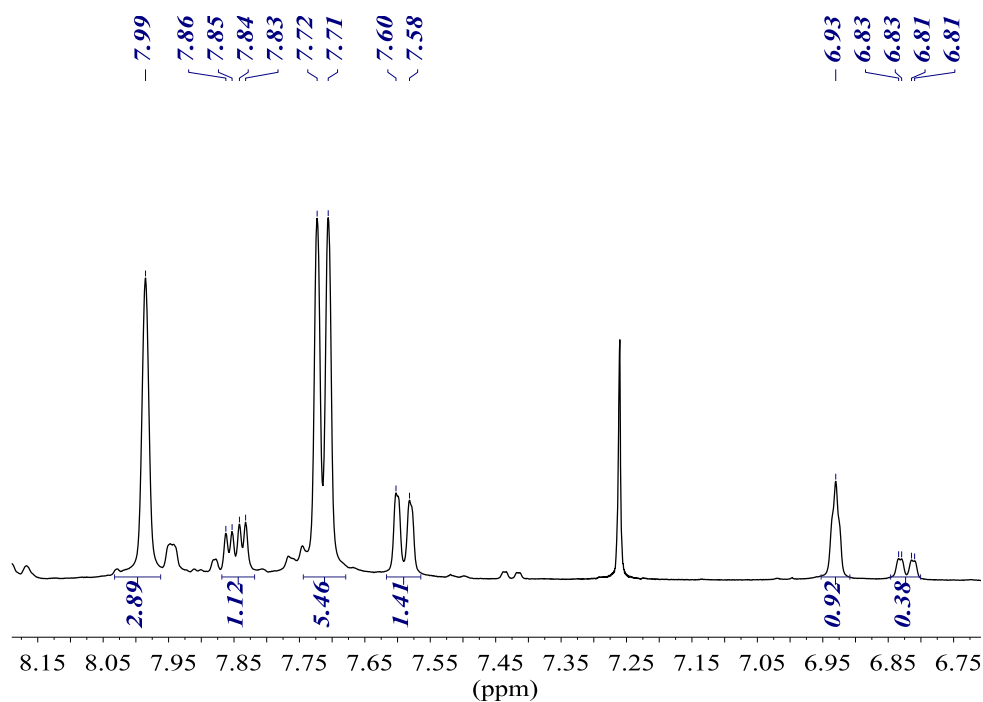
bis(3,5-bis(trifluoromethyl)phenyl)(2-bromo-5-(trifluoromethyl)phenyl)phosphine (*m*29) + bis(3,5-bis(trifluoromethyl)phenyl)(2-bromo-4-trifluoromethyl)phenyl phosphine (*p*29)



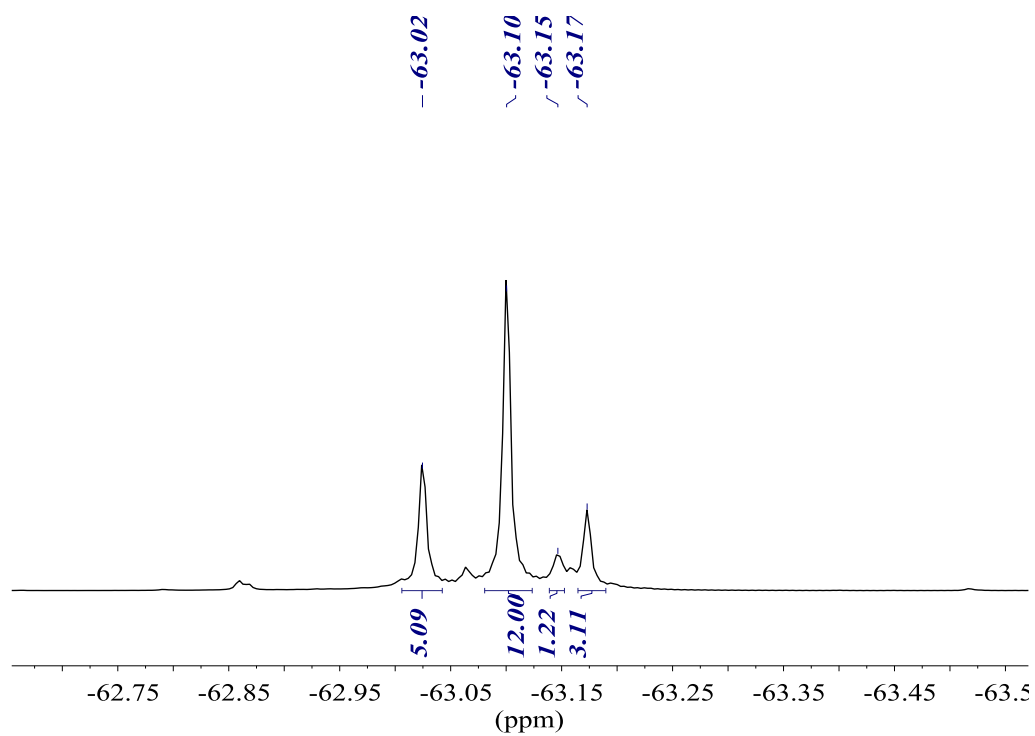
$^{31}\text{P}\{^1\text{H}\}$ NMR (161.98 MHz, CDCl_3)



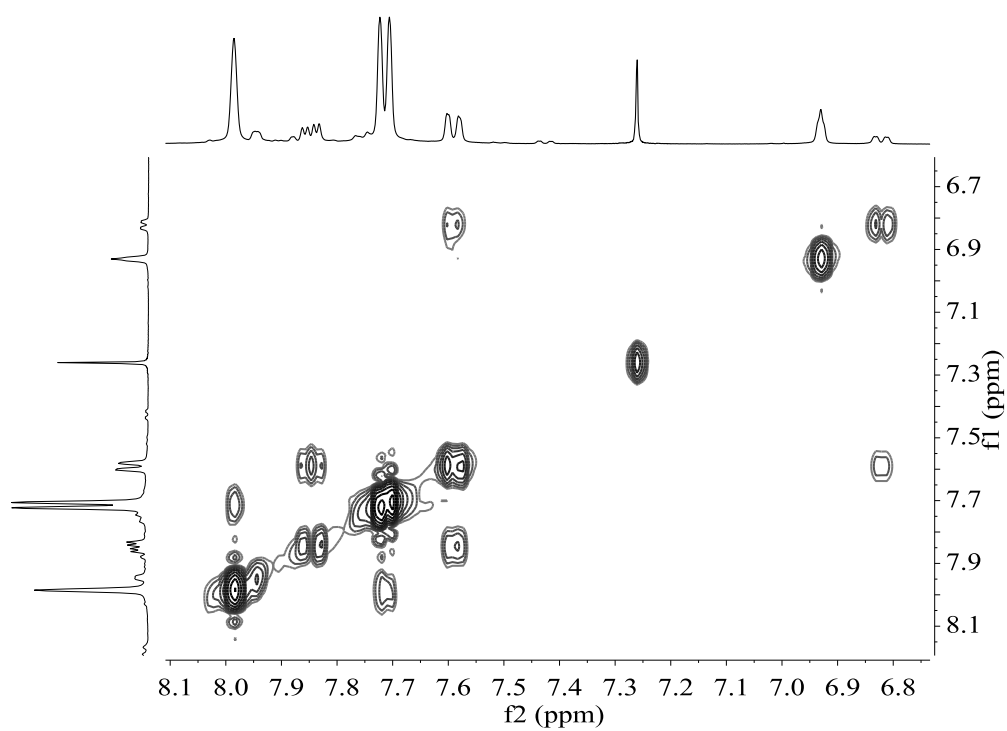
^1H NMR (400.13 MHz, CDCl_3)



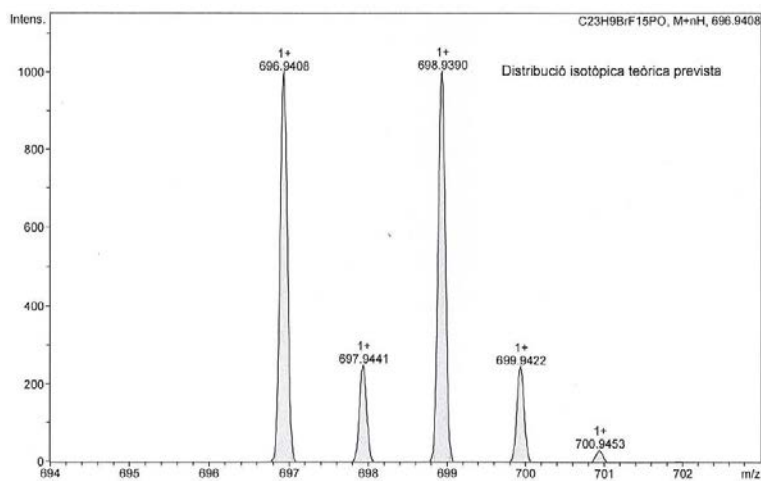
$^{19}\text{F}\{^1\text{H}\}$ NMR (376.50 MHz, CDCl_3)



COSY NMR (400.13 MHz, CDCl_3)

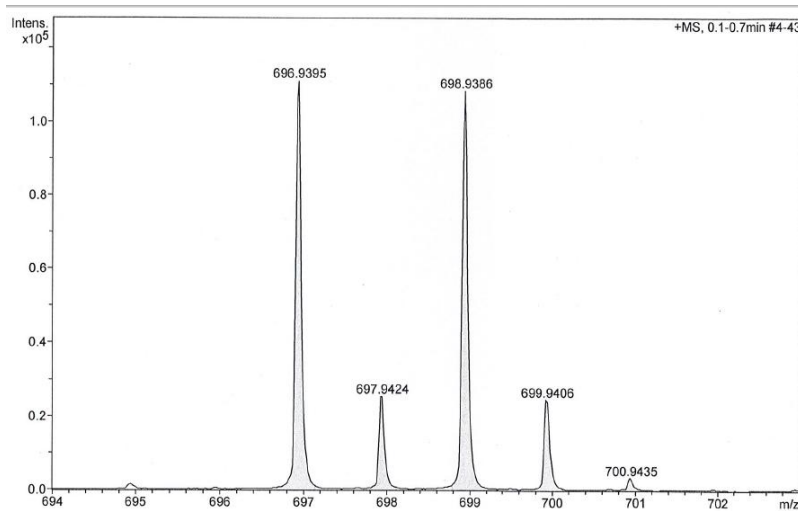


HR-MS (ESI⁺ m/z) [M(O)+H]⁺
 calculated for [C₂₃H₁₀BrF₁₅PO]⁺



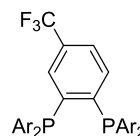
#	m/z	I	I %
1	696.9408	995	99.5
2	697.9441	249	24.9
3	698.9390	1000	100.0
4	699.9422	245	24.5
5	700.9453	31	3.1

found



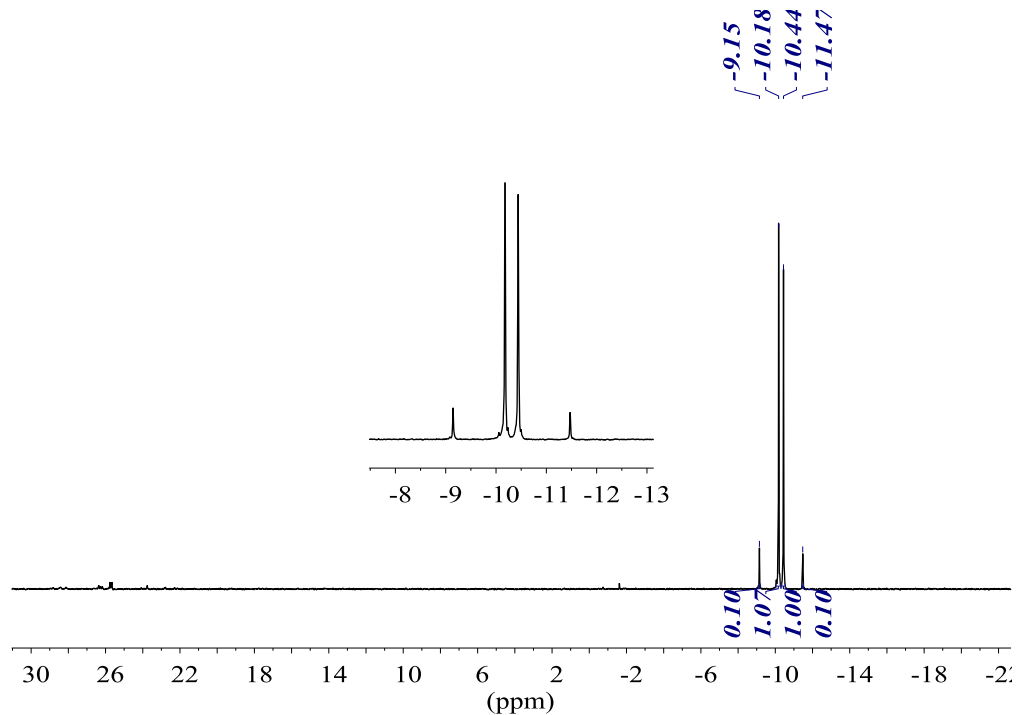
#	m/z	I	I %
1	696.9395	111083	100.0
2	697.9424	25660	23.1
3	698.9386	108328	97.5
4	699.9406	24790	22.3
5	700.9435	3508	3.2

(4-(Trifluoromethyl)-1,2-phenylene)bis(bis(3,5-bis(trifluoromethyl)phenyl)-phosphine) (31)

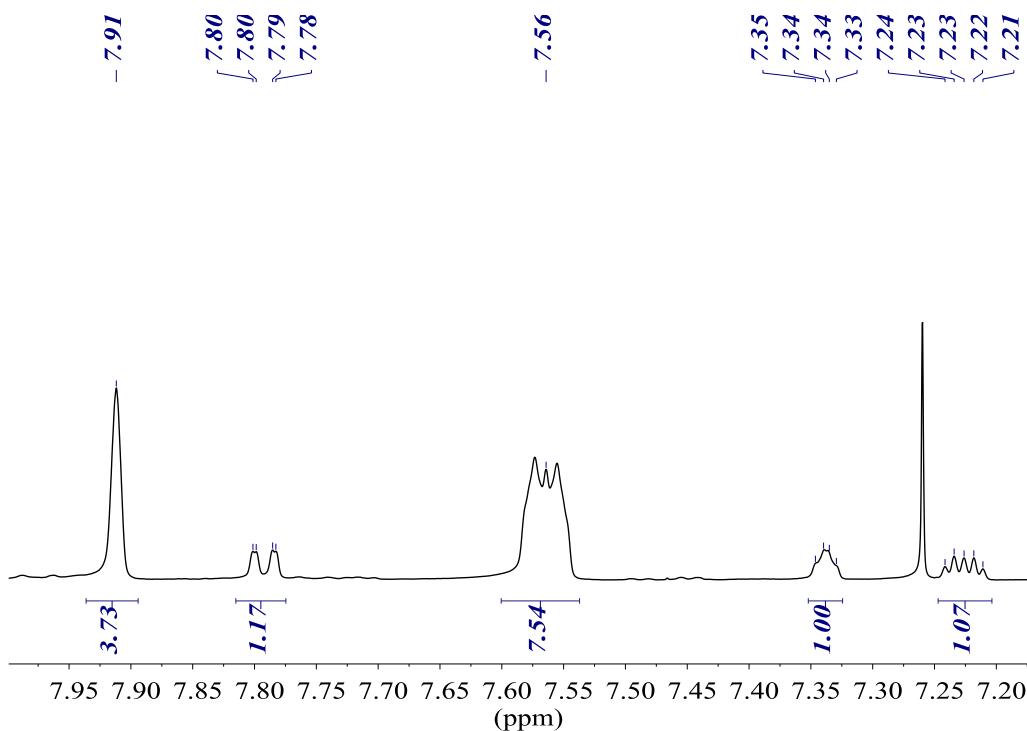


Ar = 3,5-bis(trifluoromethyl)phenyl

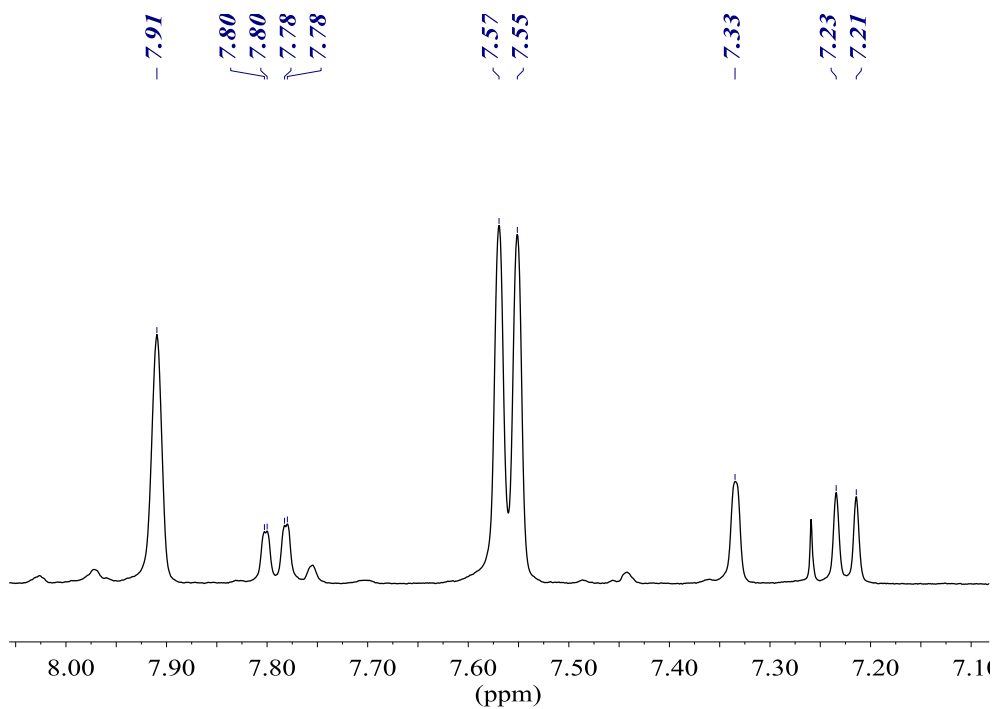
$^{31}\text{P}\{^1\text{H}\}$ NMR (161.98 MHz, acetone- D_6)



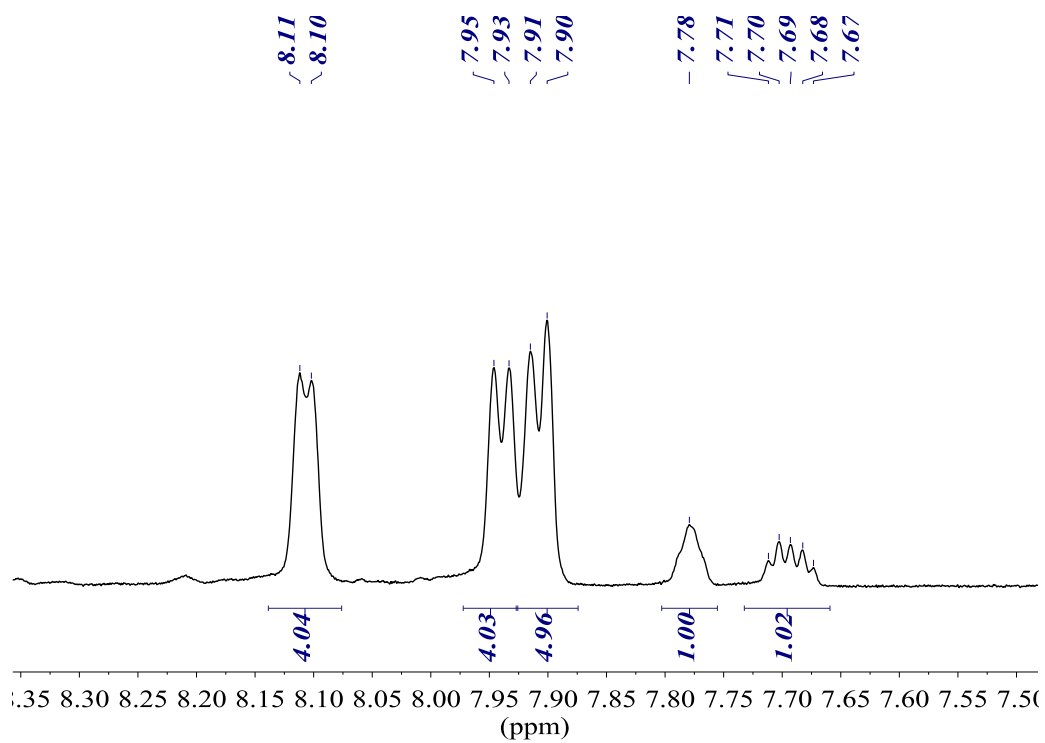
^1H NMR (500.13 MHz, CDCl_3)



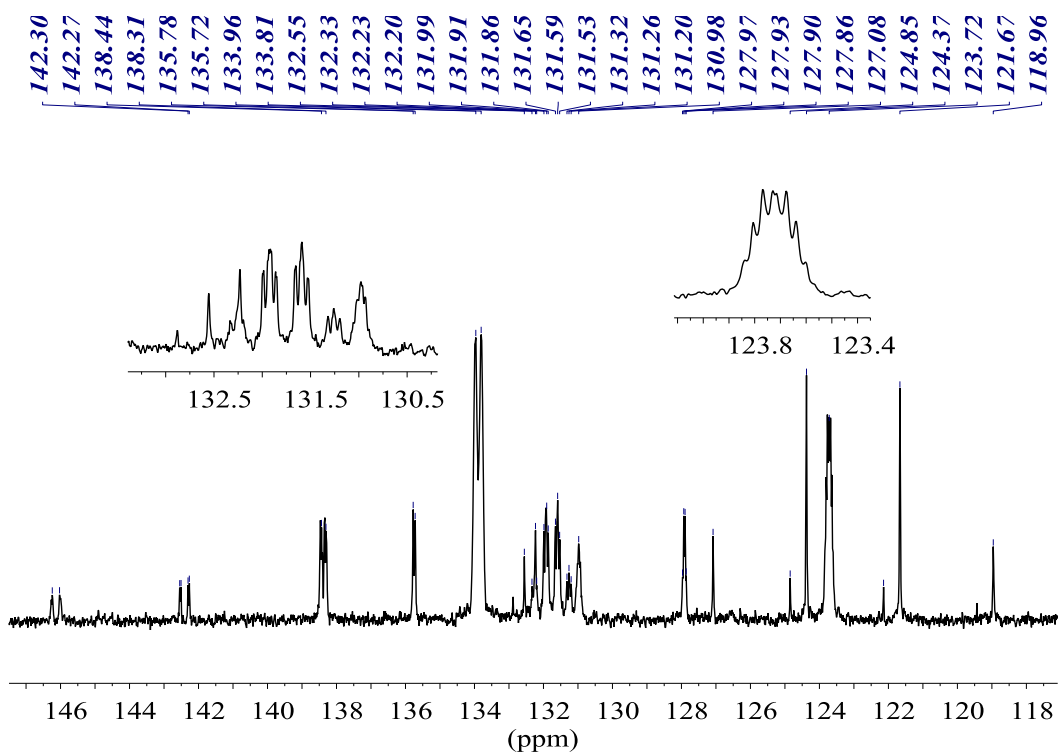
$^1\text{H}\{^{31}\text{P}\}$ NMR (400.13 MHz, CDCl_3)



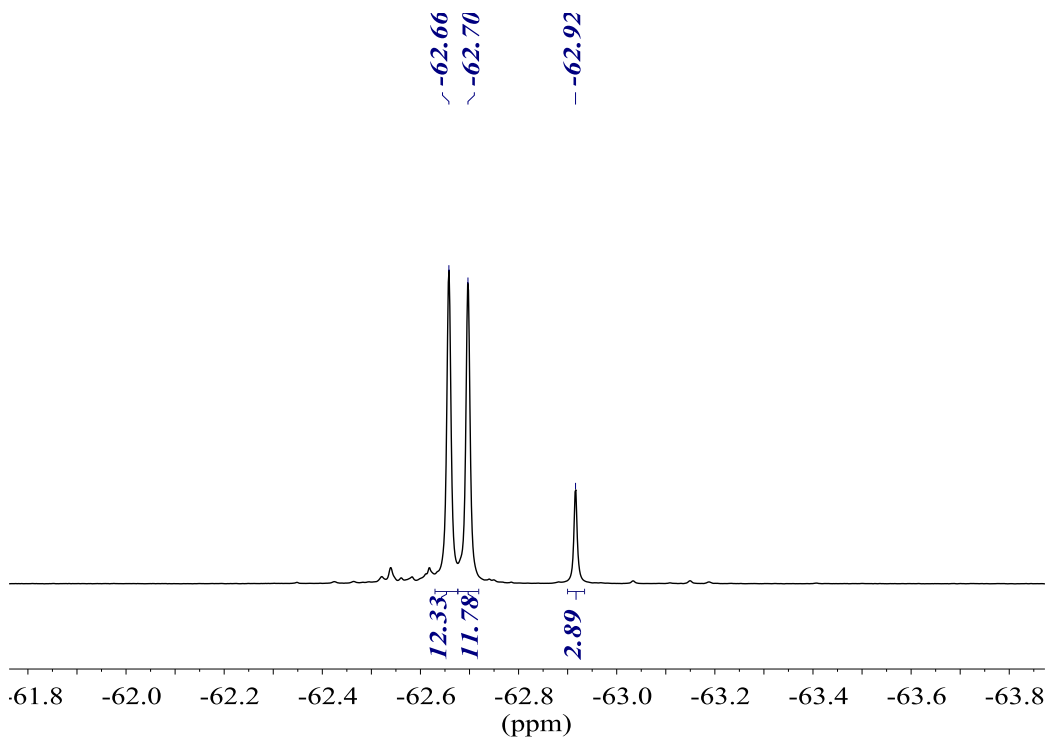
^1H NMR (400.13 MHz, acetone- D_6)



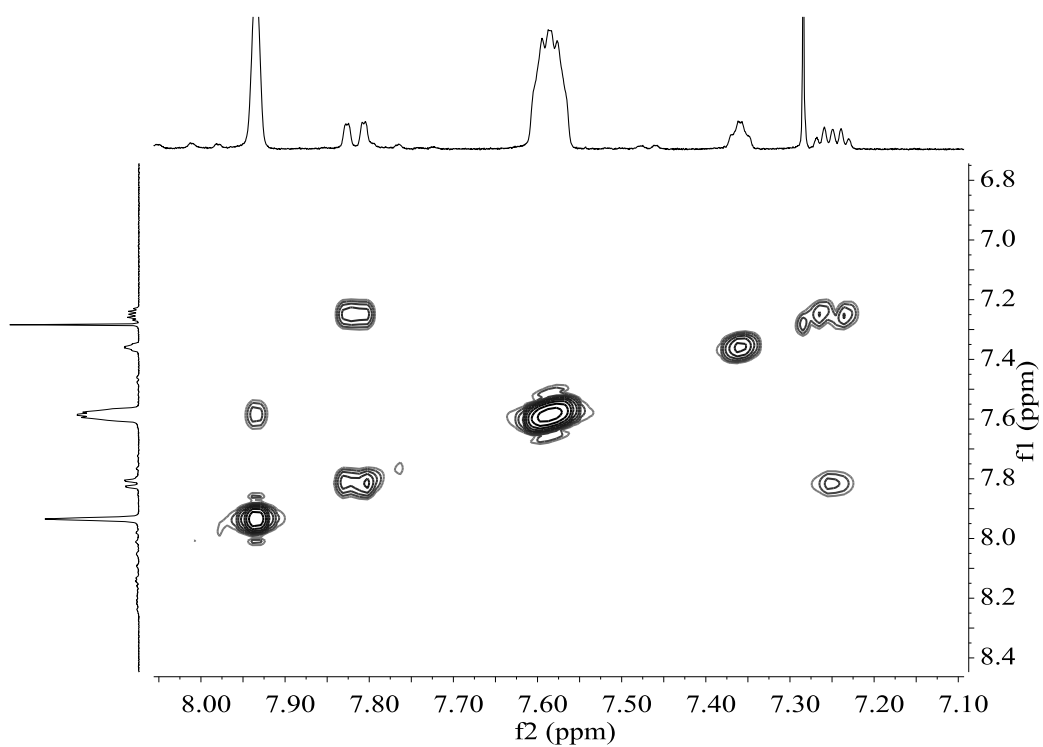
$^{13}\text{C}\{^1\text{H}\}$ NMR (100.61 MHz, acetone-D6)



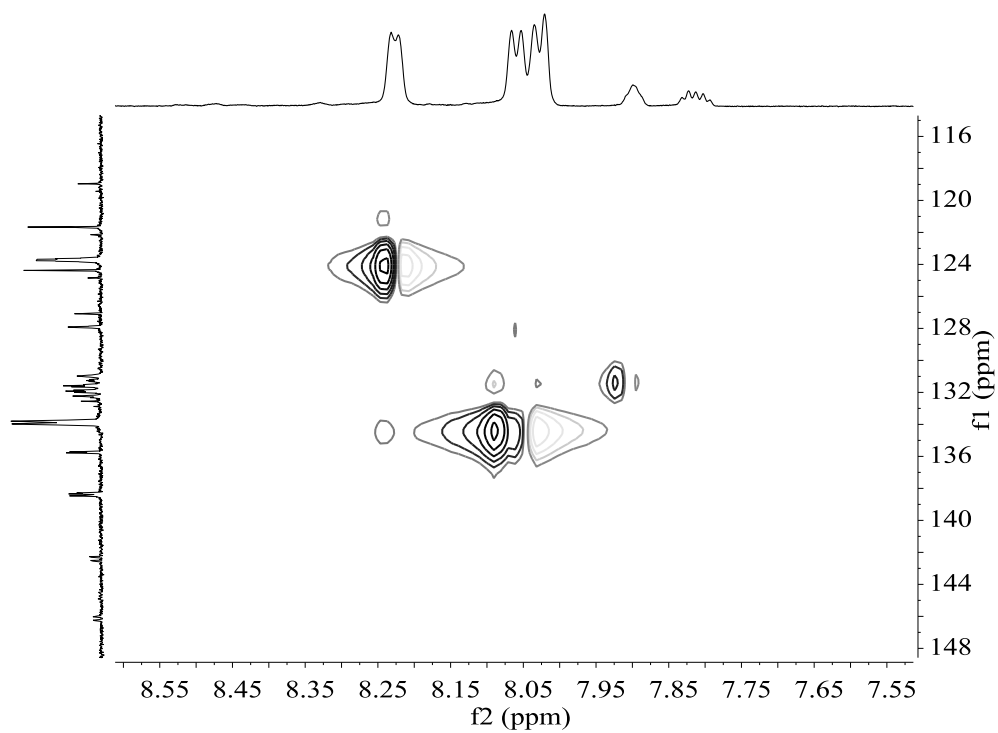
$^{19}\text{F}\{^1\text{H}\}$ NMR (376.50 MHz, acetone-D6)



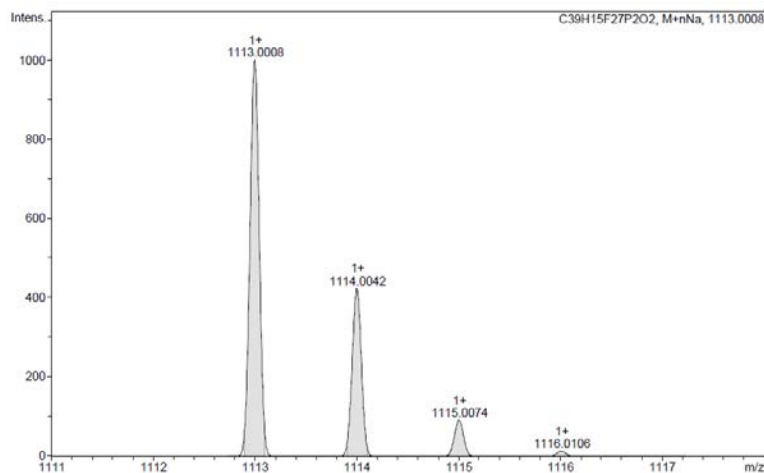
COSY NMR (400.13 MHz, CDCl₃)



HSQC NMR (400.13 MHz, acetone-D₆)

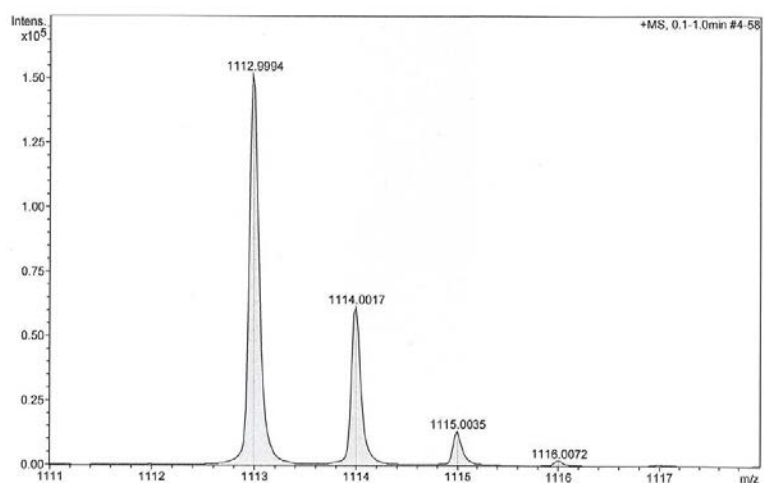


**HR-MS (ESI⁺ *m/z*) [M(O)₂+Na]⁺
 calculated for [C₃₉H₁₅F₂₇P₂O₂Na]⁺**



#	<i>m/z</i>	I	I %
1	1113.0008	1000	100.0
2	1114.0042	424	42.4
3	1115.0074	92	9.2
4	1116.0106	13	1.3

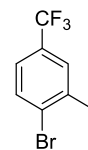
found



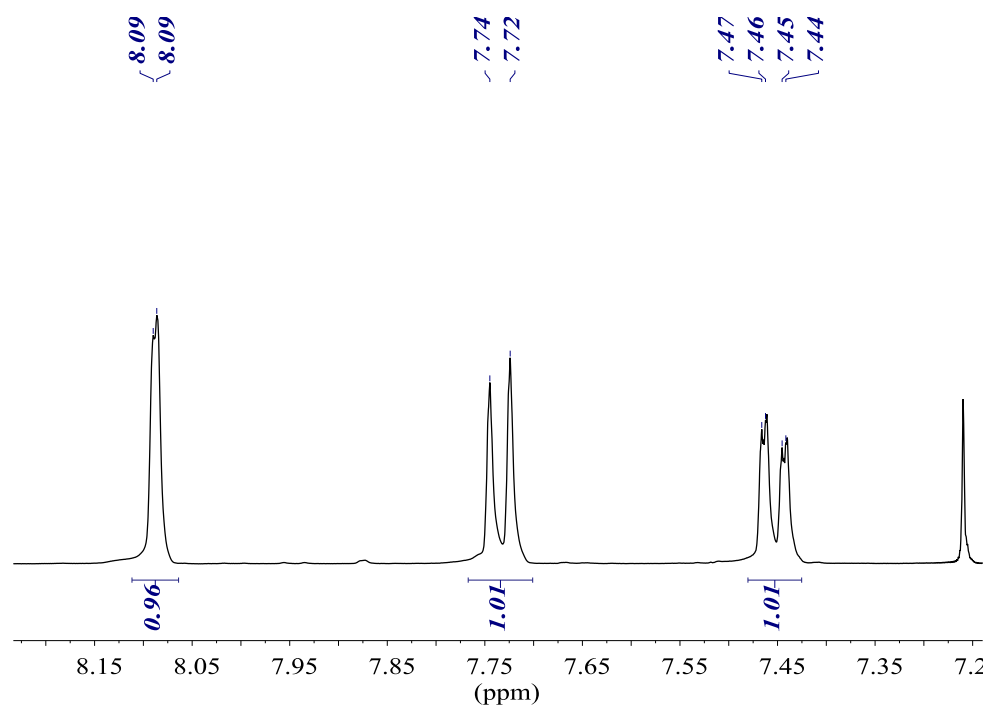
#	<i>m/z</i>	I	I %
1	1112.9994	151948	100.0
2	1114.0017	61671	40.6
3	1115.0035	13300	8.8
4	1116.0072	2131	1.4

5. Characterisation of trifluoromethylated diphosphine 32 and intermediate compounds

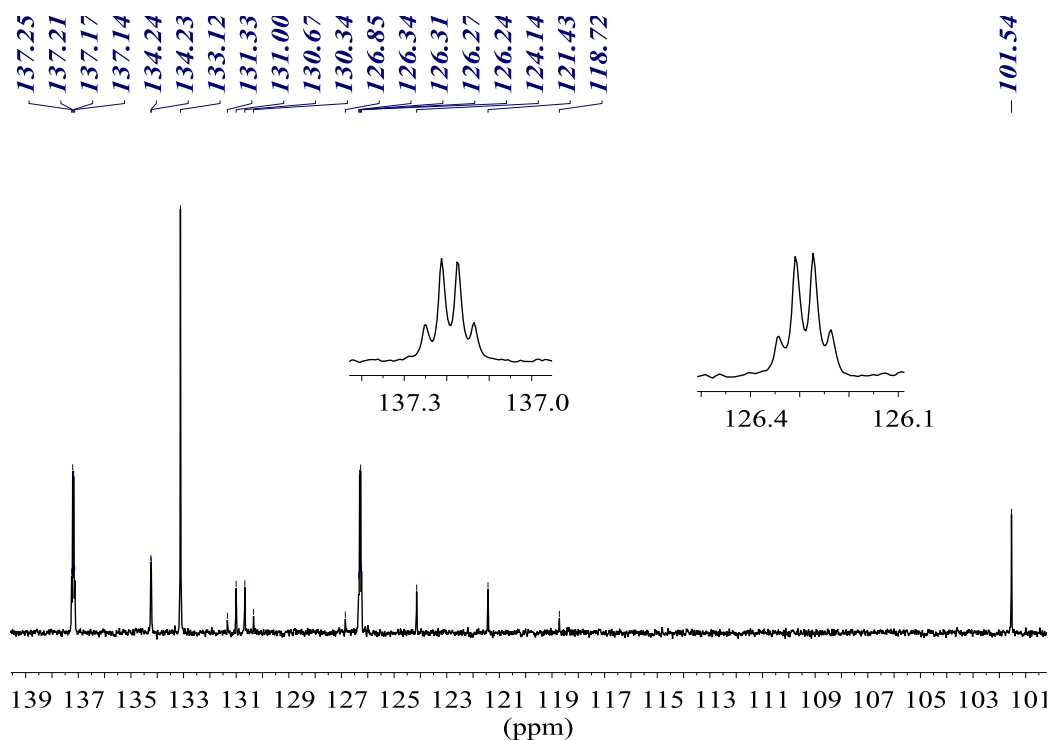
1-Bromo-2-iodo-4-(trifluoromethyl)benzene (34)



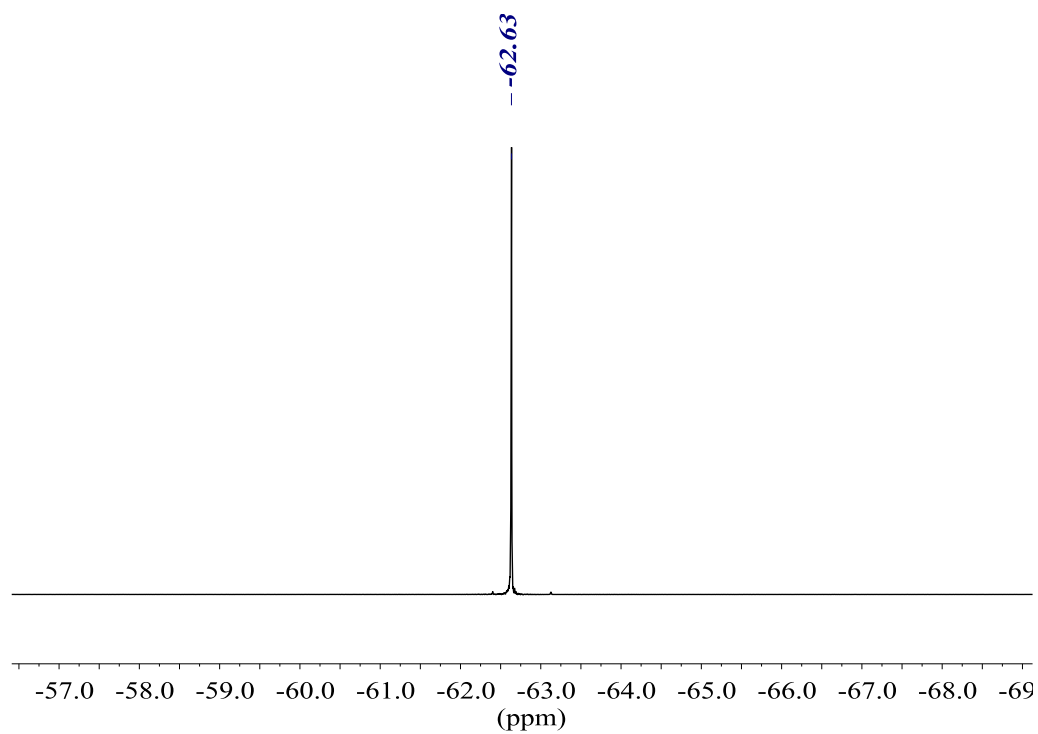
^1H NMR (400.13 MHz, CDCl_3)



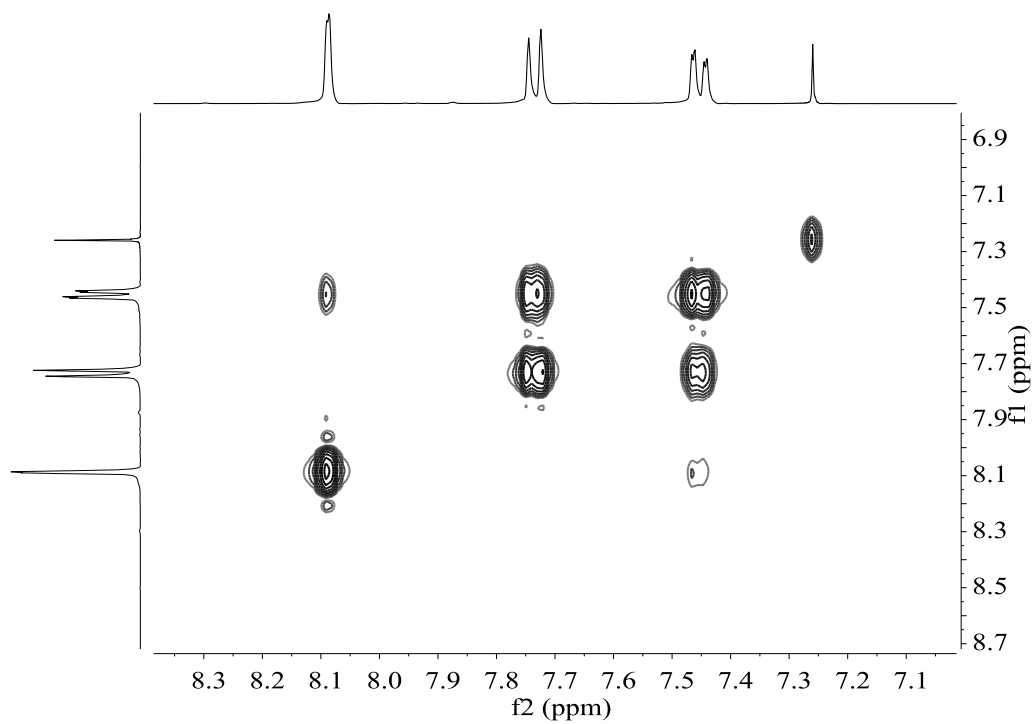
$^{13}\text{C}\{^1\text{H}\}$ NMR (100.61 MHz, CDCl_3)



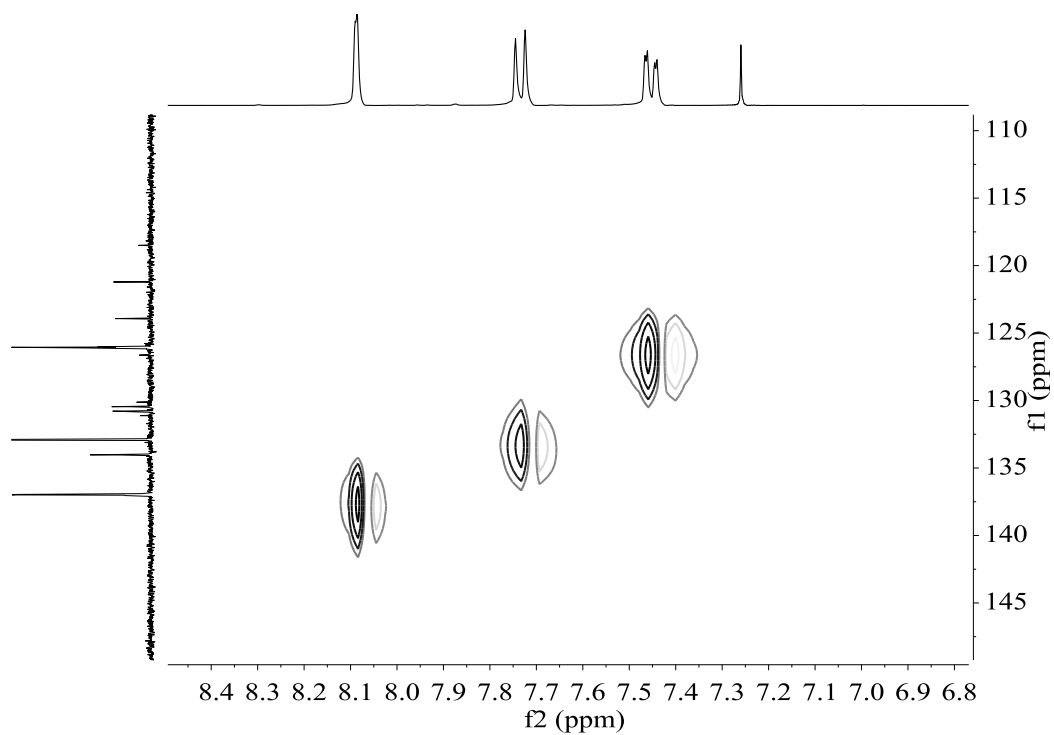
$^{19}\text{F}\{^1\text{H}\}$ NMR (376.50 MHz, CDCl_3)



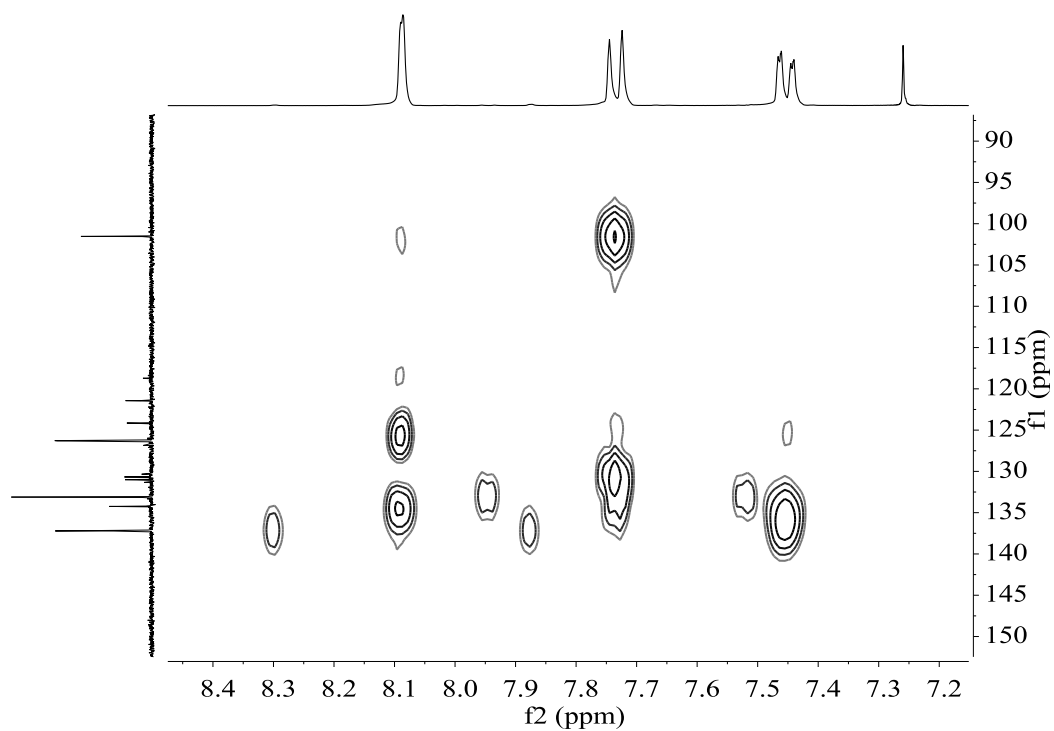
COSY NMR (400.13 MHz, CDCl_3)



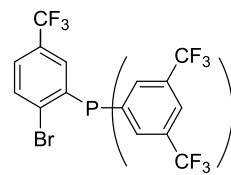
HSQC NMR (400.13 MHz, CDCl₃)



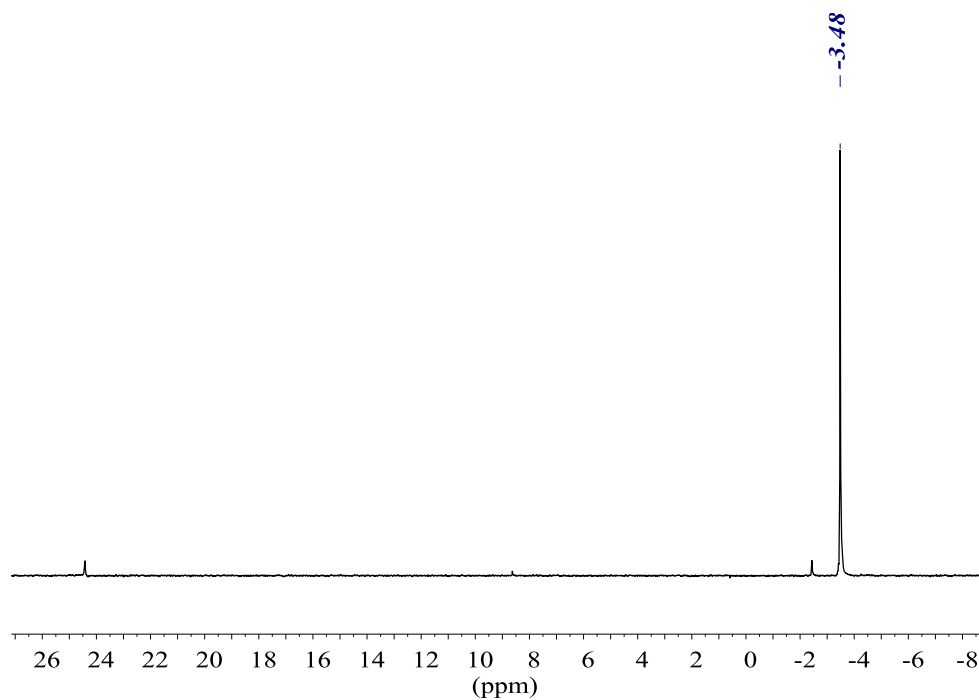
HMBC NMR (400.13 MHz, CDCl₃)



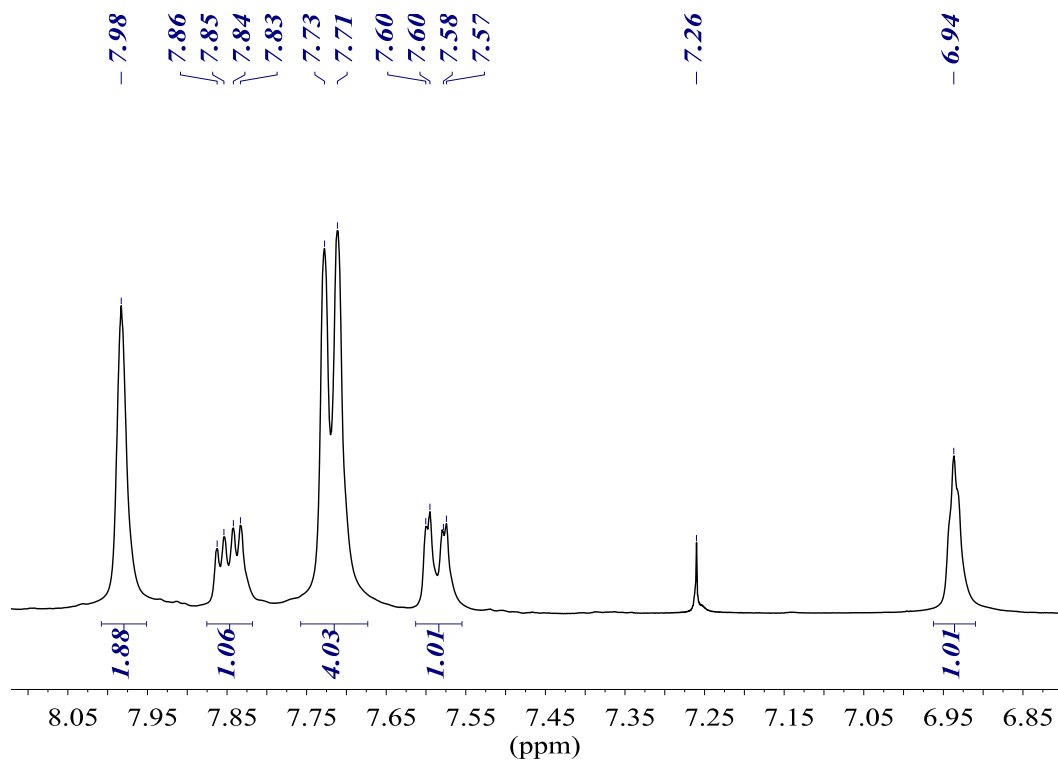
**Bis(3,5-bis(trifluoromethyl)phenyl)(2-bromo-5-(trifluoromethyl)phenyl)phosphine
(m29)**



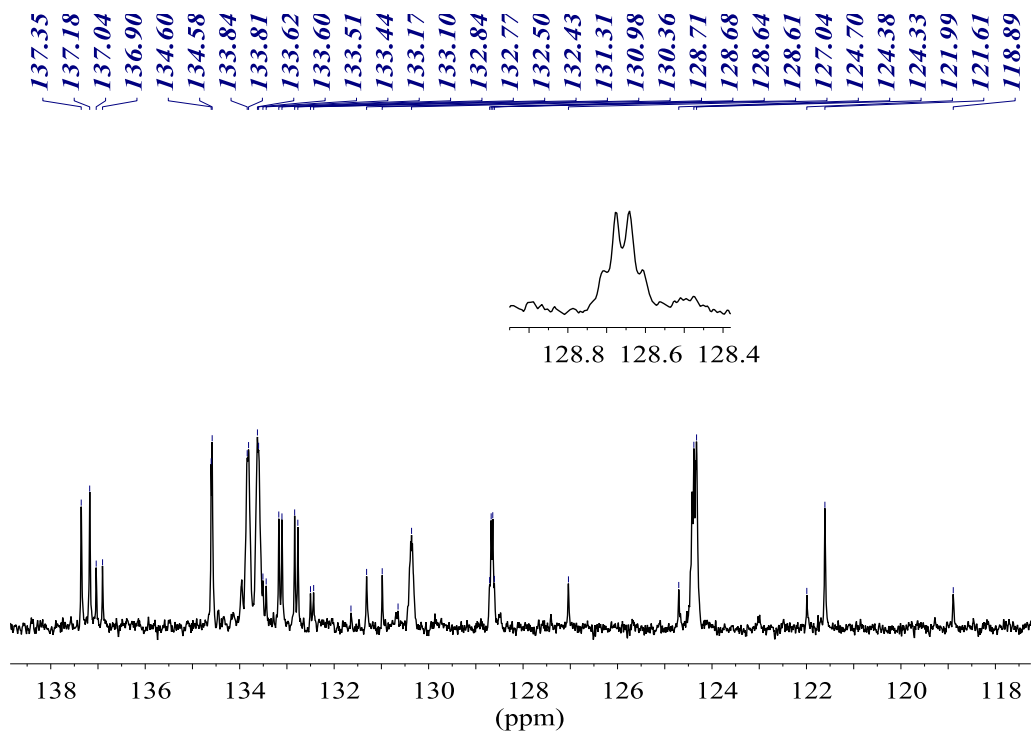
$^{31}\text{P}\{^1\text{H}\}$ NMR (161.98 MHz, CDCl_3)



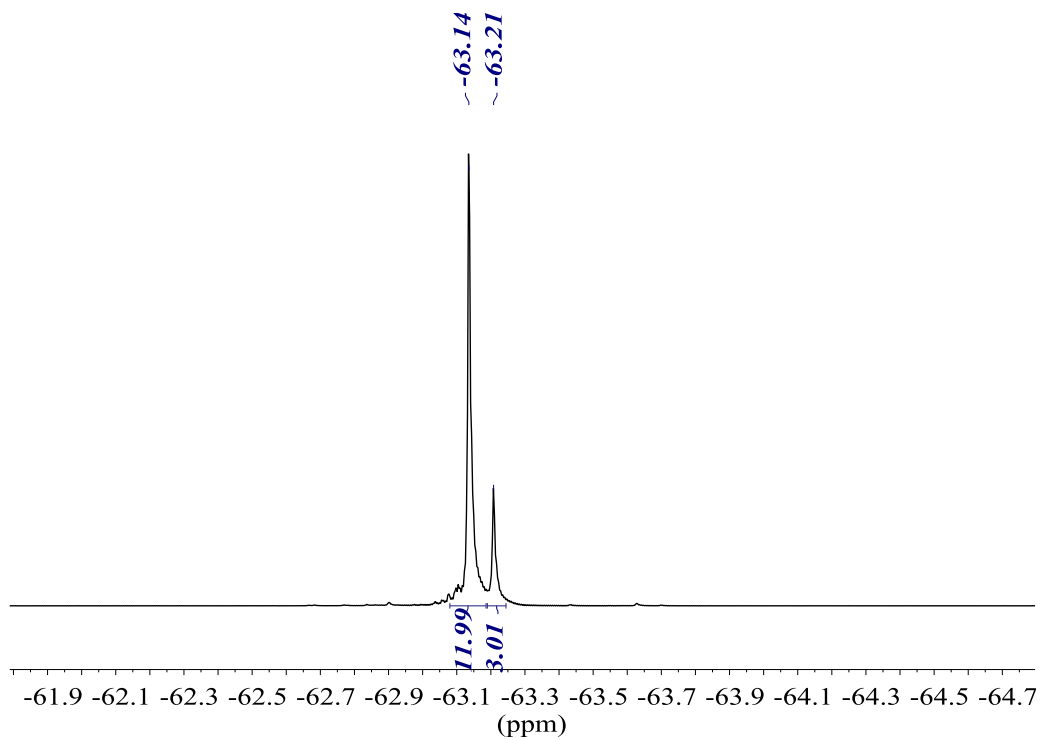
^1H NMR (400.13 MHz, CDCl_3)



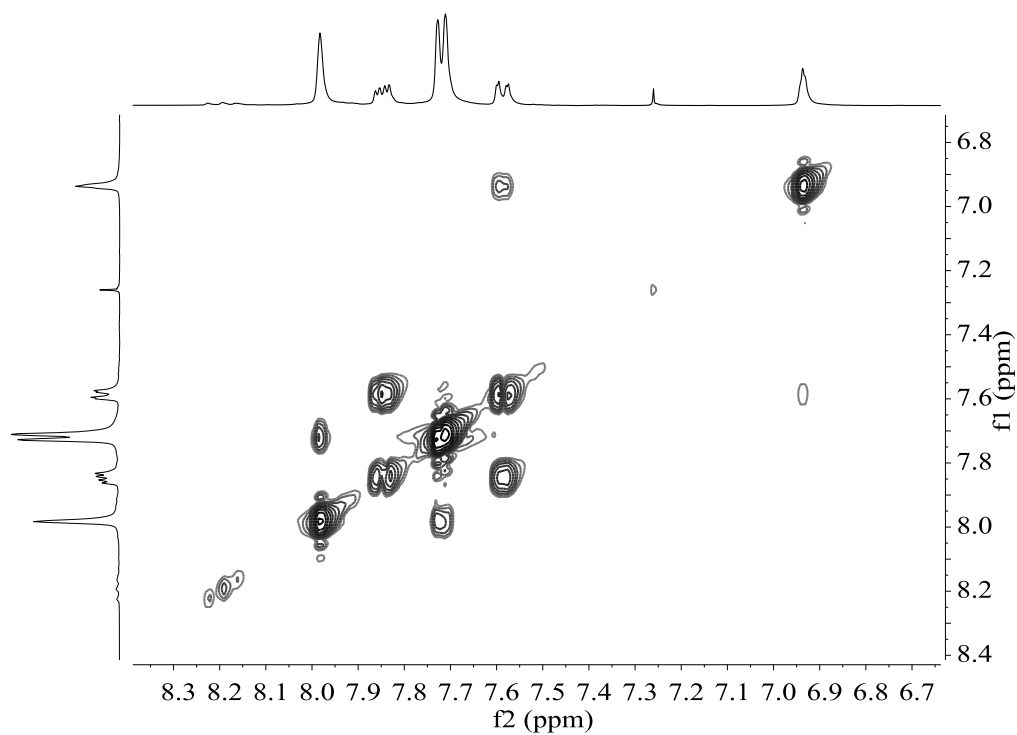
$^{13}\text{C}\{^1\text{H}\}$ NMR (100.61 MHz, CDCl_3)



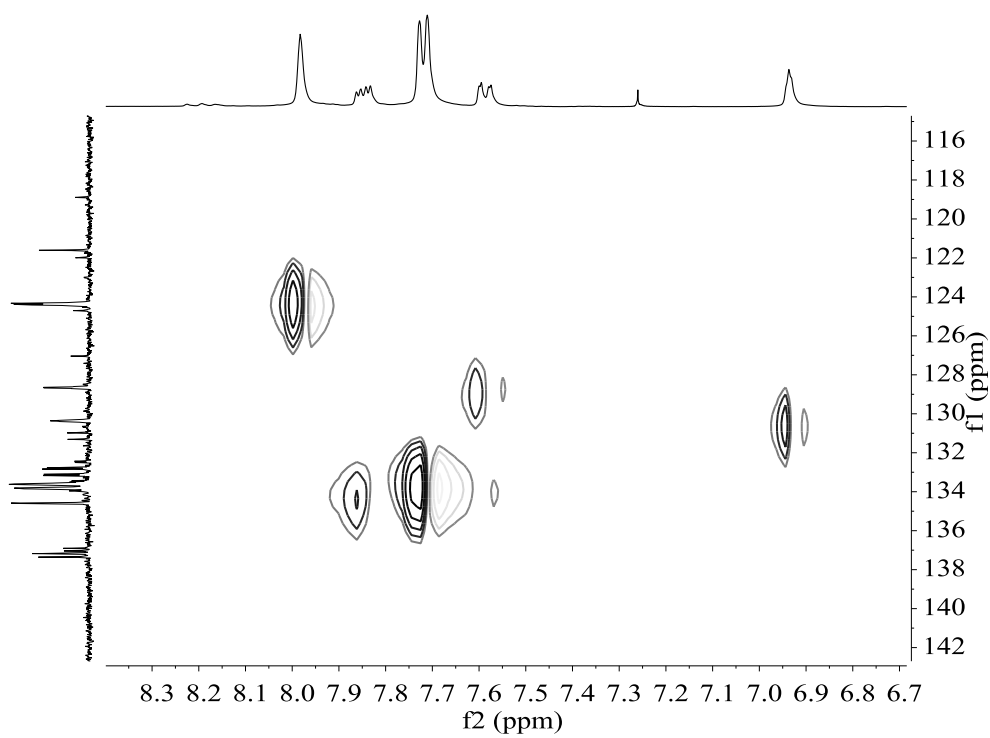
$^{19}\text{F}\{^1\text{H}\}$ NMR (376.50 MHz, CDCl_3)



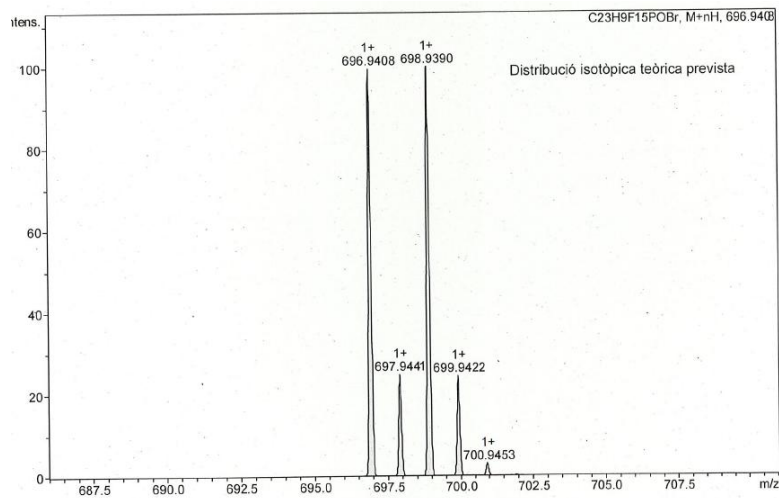
COSY NMR (400.13 MHz, CDCl₃)



HSQC NMR (400.13 MHz, CDCl₃)

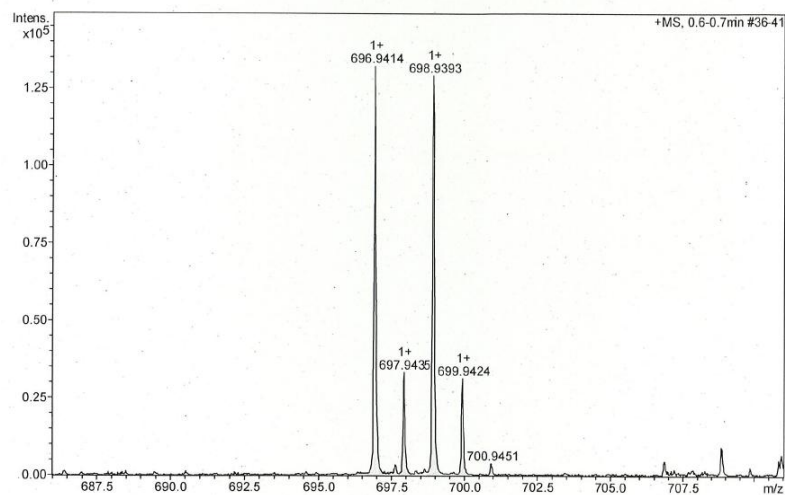


HR-MS (ESI⁺ *m/z*) [M(O)+H]⁺
calculated for [C₂₃H₁₀BrF₁₅PO]⁺



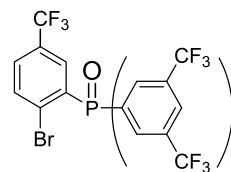
#	<i>m/z</i>	I	I %
1	696.9408	100	99.5
2	697.9441	25	24.9
3	698.9390	100	100.0
4	699.9422	24	24.5
5	700.9453	3	3.1

found

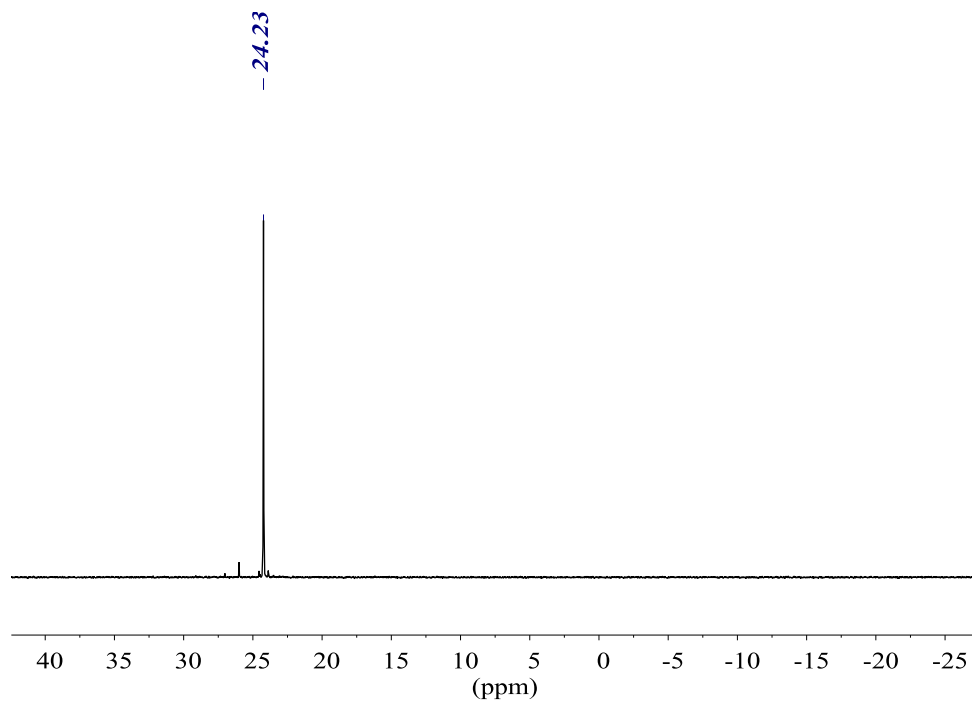


#	<i>m/z</i>	I	I %
1	696.9414	132228	100.0
2	697.9435	33470	25.3
3	698.9393	129175	97.7
4	699.9424	31446	23.8
5	700.9451	4040	3.1

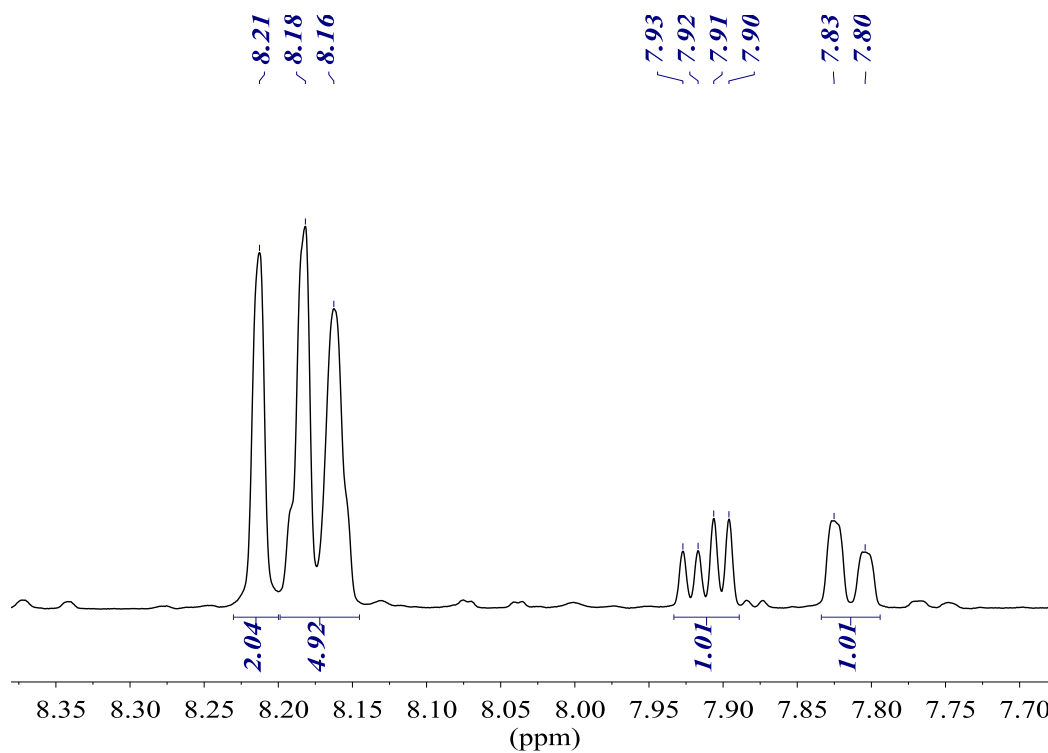
Bis(3,5-bis(trifluoromethyl)phenyl)(2-bromo-5-(trifluoromethyl)phenyl)phosphine oxide (ox-*m*29)



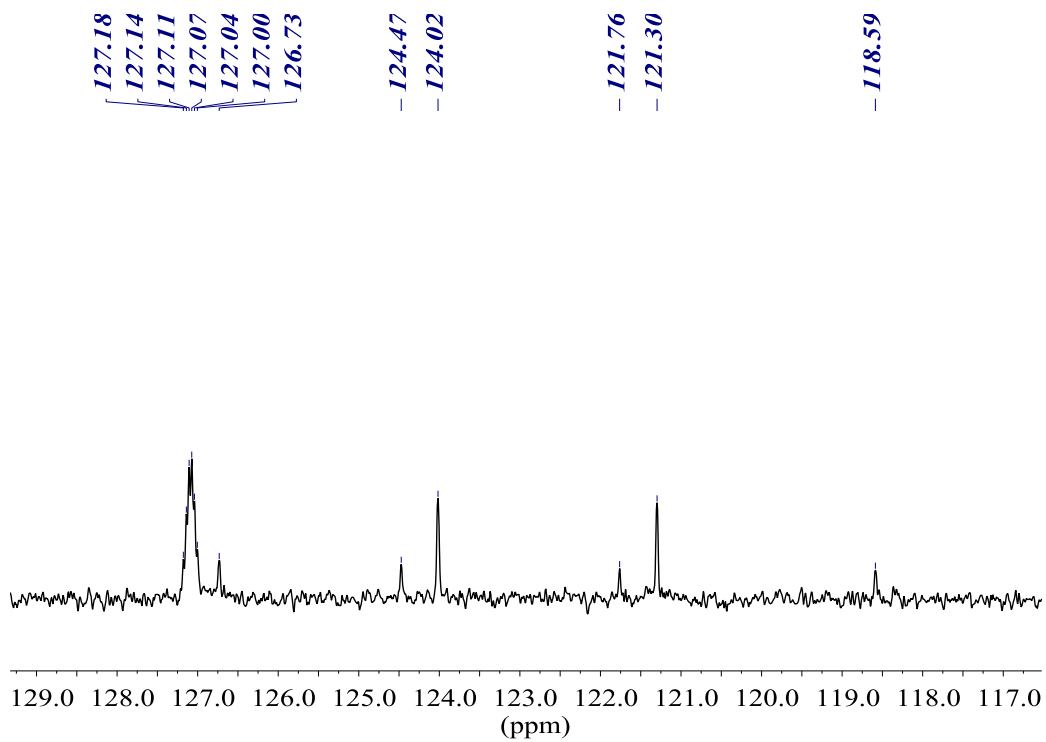
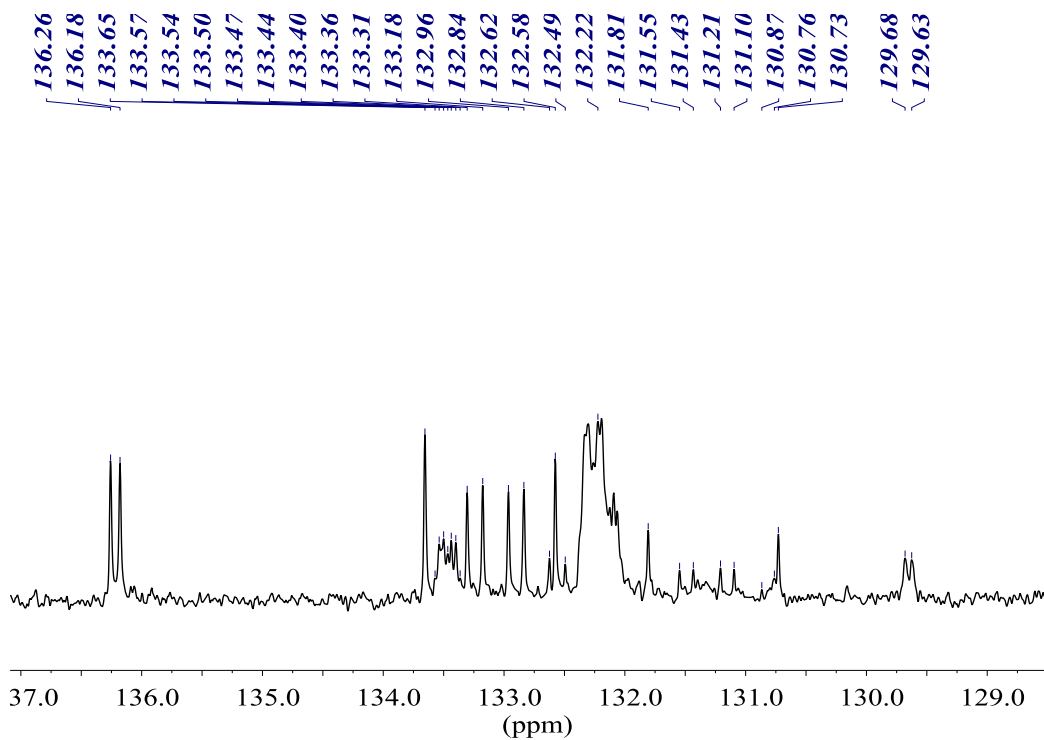
$^{31}\text{P}\{^1\text{H}\}$ NMR (161.98 MHz, CDCl_3)



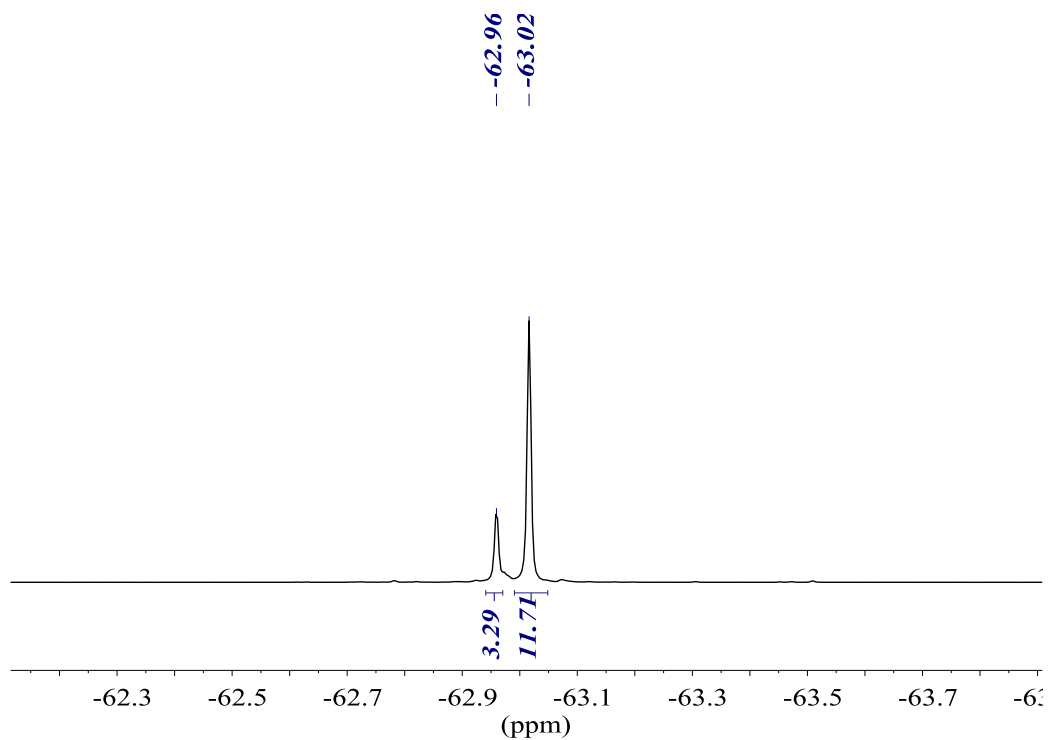
^1H NMR (400.13 MHz, CDCl_3)



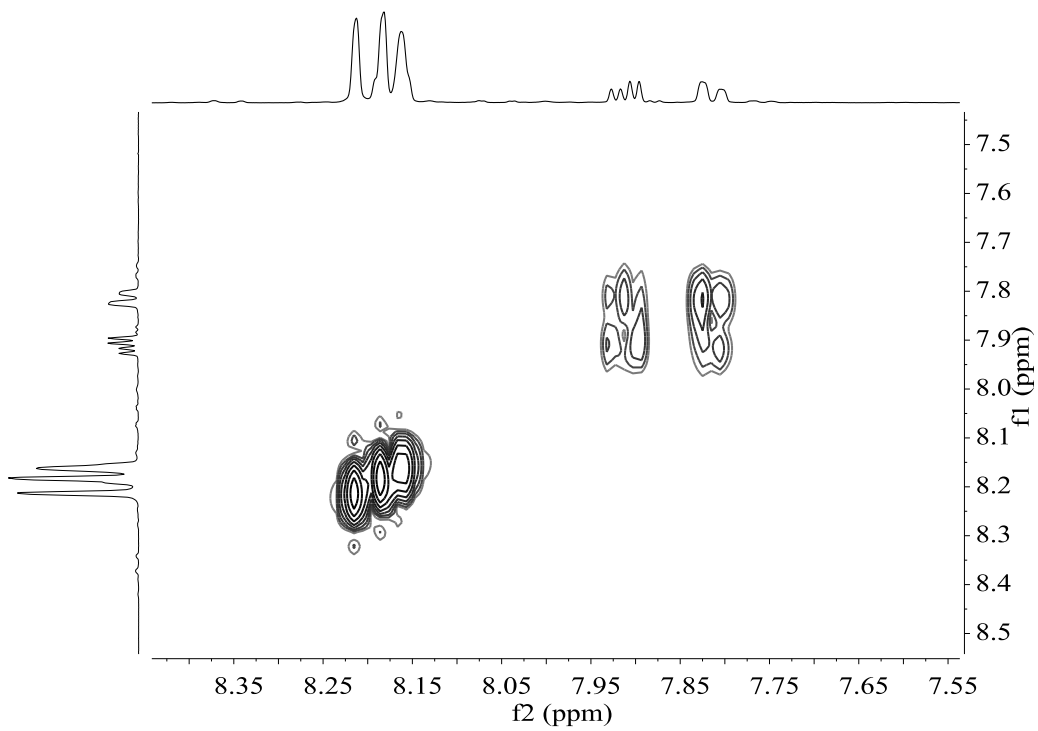
$^{13}\text{C}\{^1\text{H}\}$ NMR (100.61 MHz, CDCl_3)



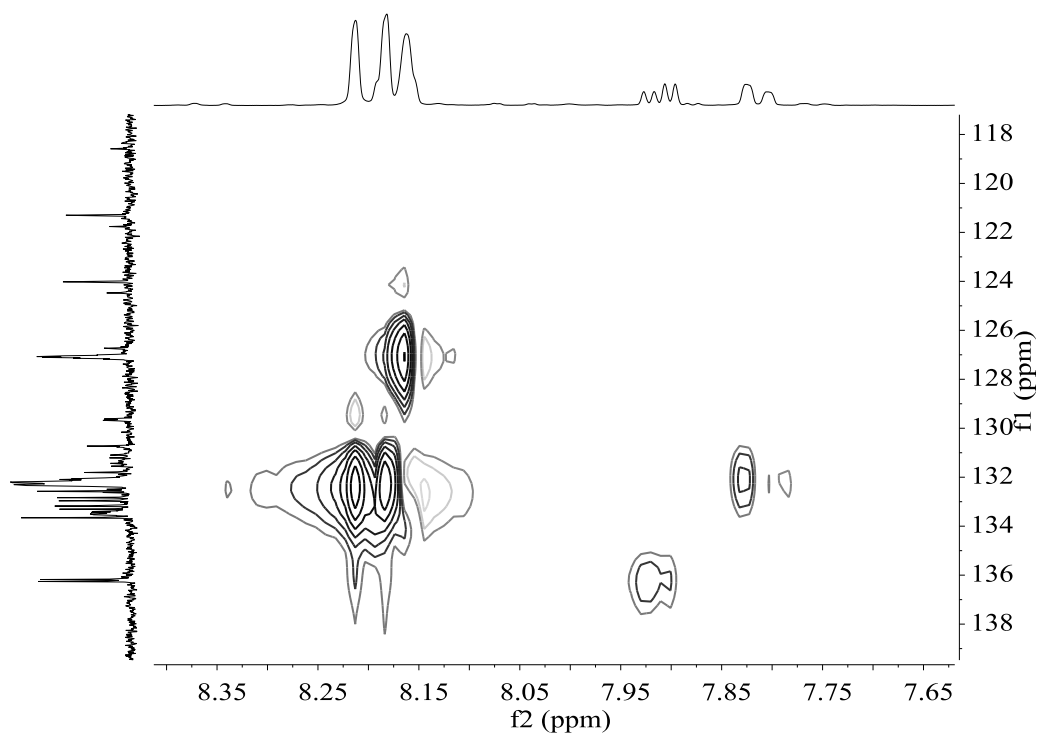
$^{19}\text{F}\{^1\text{H}\}$ NMR (376.50 MHz, CDCl_3)



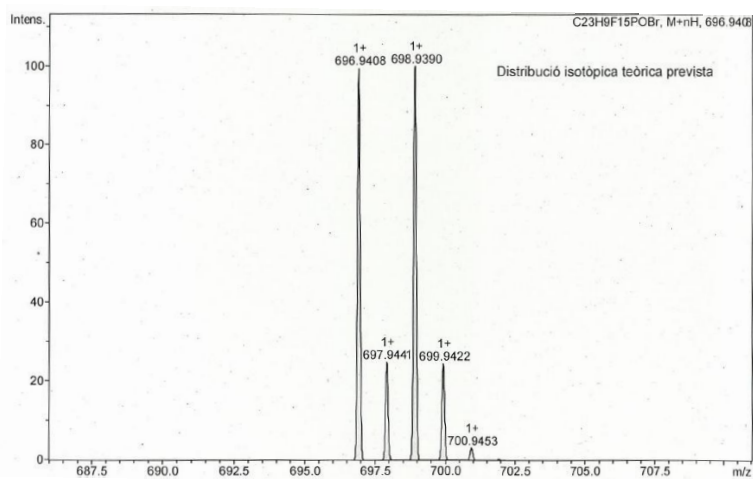
COSY NMR (400.13 MHz, CDCl_3)



HSQC NMR (400.13 MHz, CDCl₃)

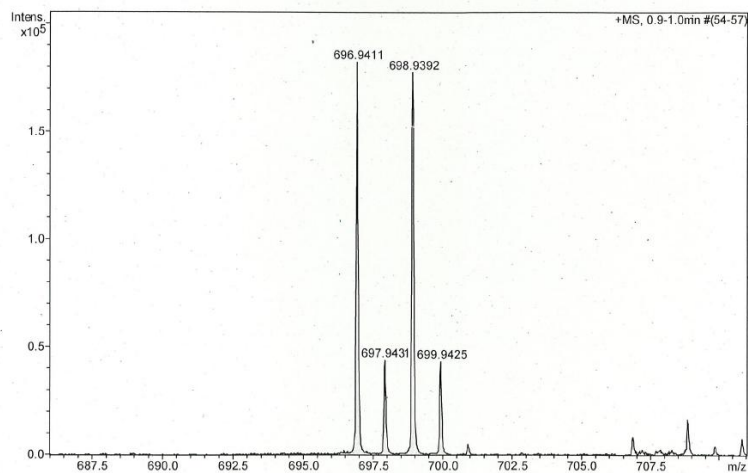


HR-MS (ESI⁺ *m/z*) [M+H]⁺
 calculated for [C₂₃H₁₀BrF₁₅PO]⁺



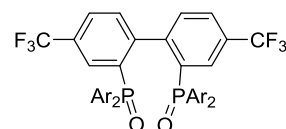
#	<i>m/z</i>	I	I %
1	696.9408	100	99.5
2	697.9441	25	24.9
3	698.9390	100	100.0
4	699.9422	24	24.5
5	700.9453	3	3.1

found



#	m/z	I	I%
1	696.9411	182163	100.0
2	697.9431	44029	24.2
3	698.9392	177366	97.4
4	699.9425	43278	23.8

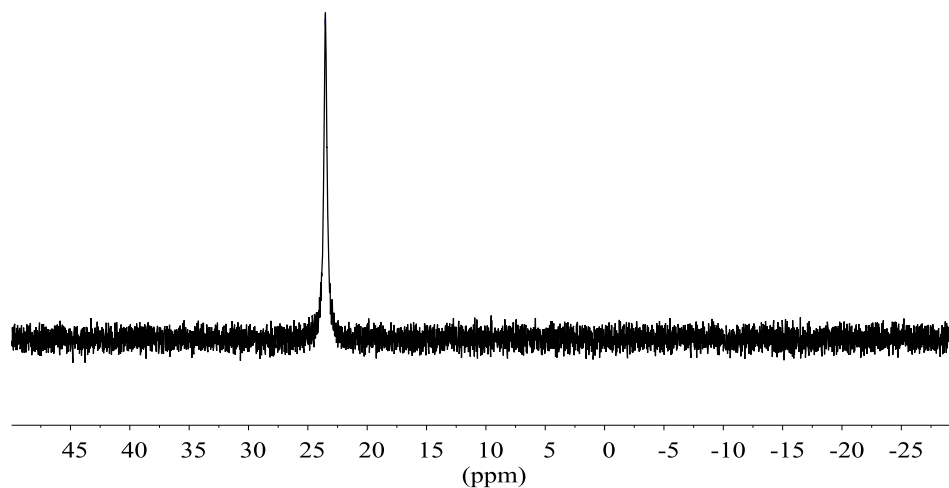
4,4'-bis(trifluoromethyl)-[1,1'-biphenyl]-2,2'-diylbis(bis(3,5-bis(trifluoromethyl)-phenyl)phosphine oxide (ox-32)



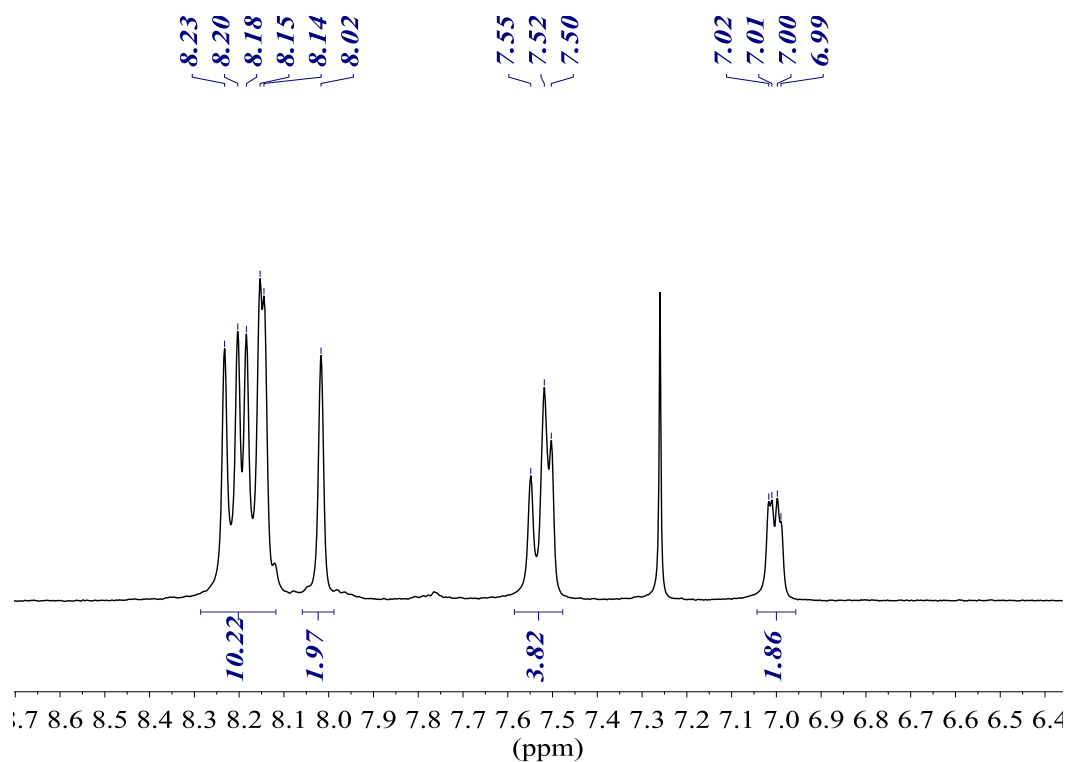
Ar = 3,5-bis(trifluoromethyl)phenyl

$^{31}\text{P}\{^1\text{H}\}$ NMR (161.98 MHz, CDCl_3)

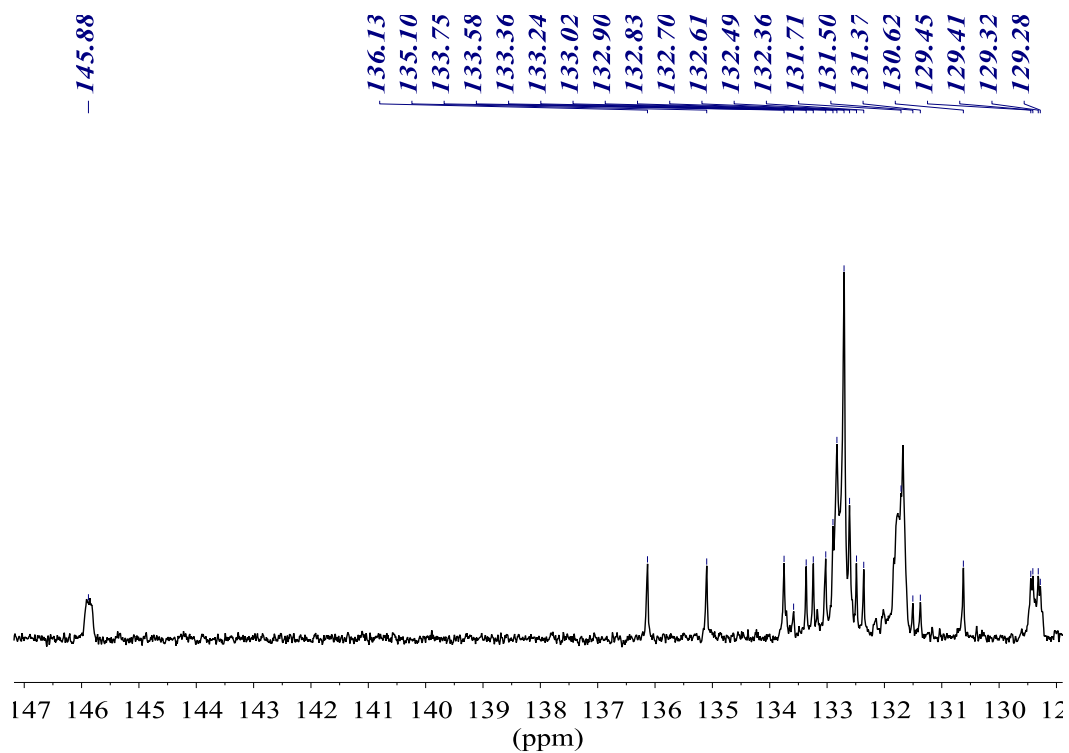
-23.55

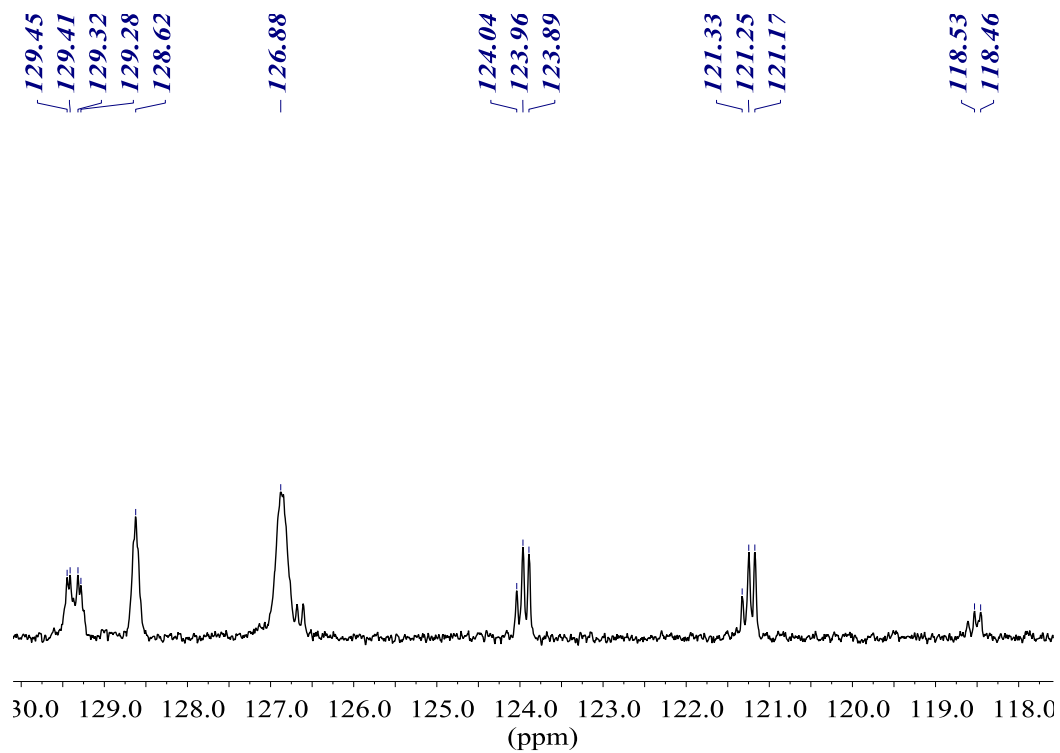


^1H NMR (400.13 MHz, CDCl_3)

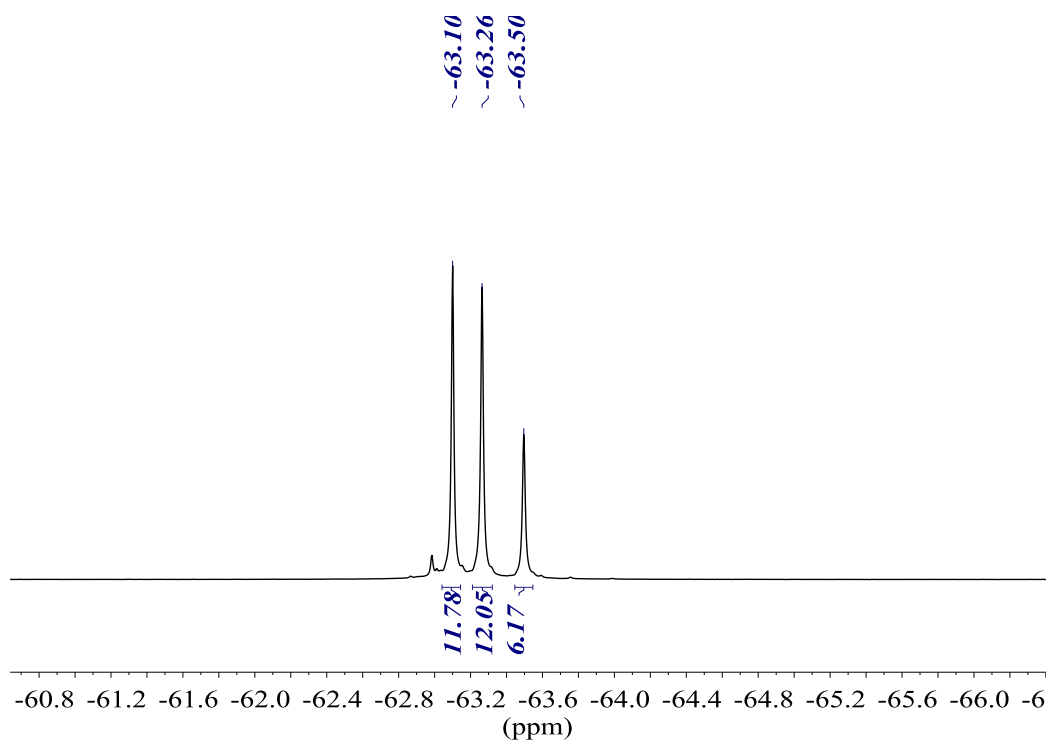


$^{13}\text{C}\{^1\text{H}\}$ NMR (100.61 MHz, CDCl_3)

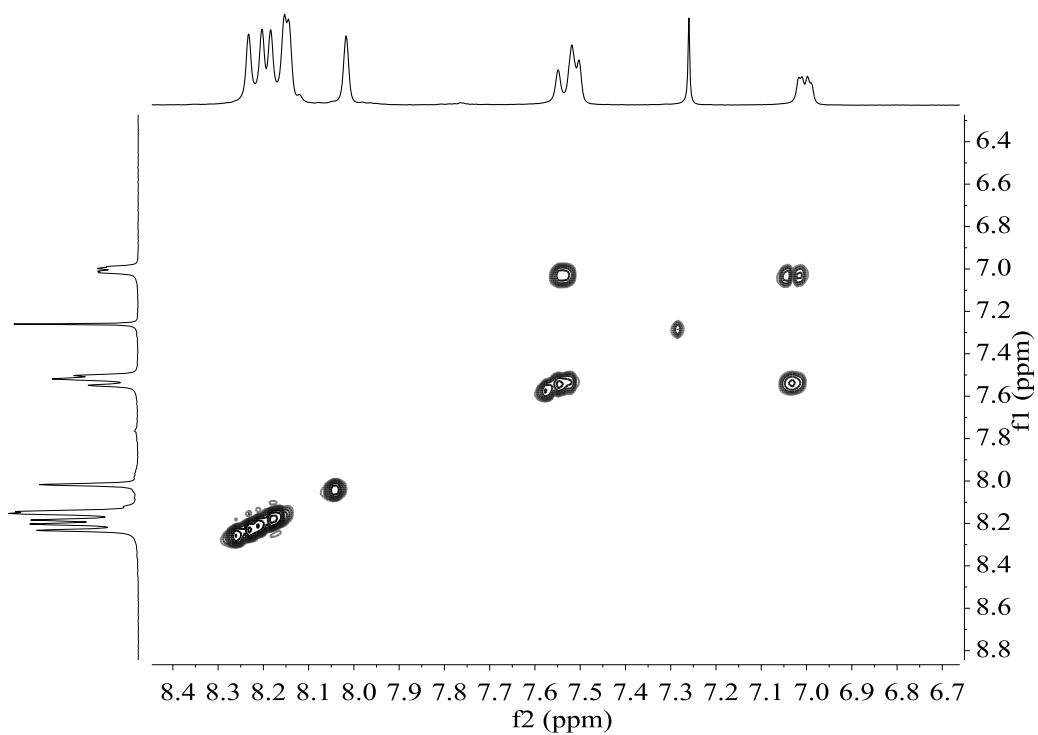




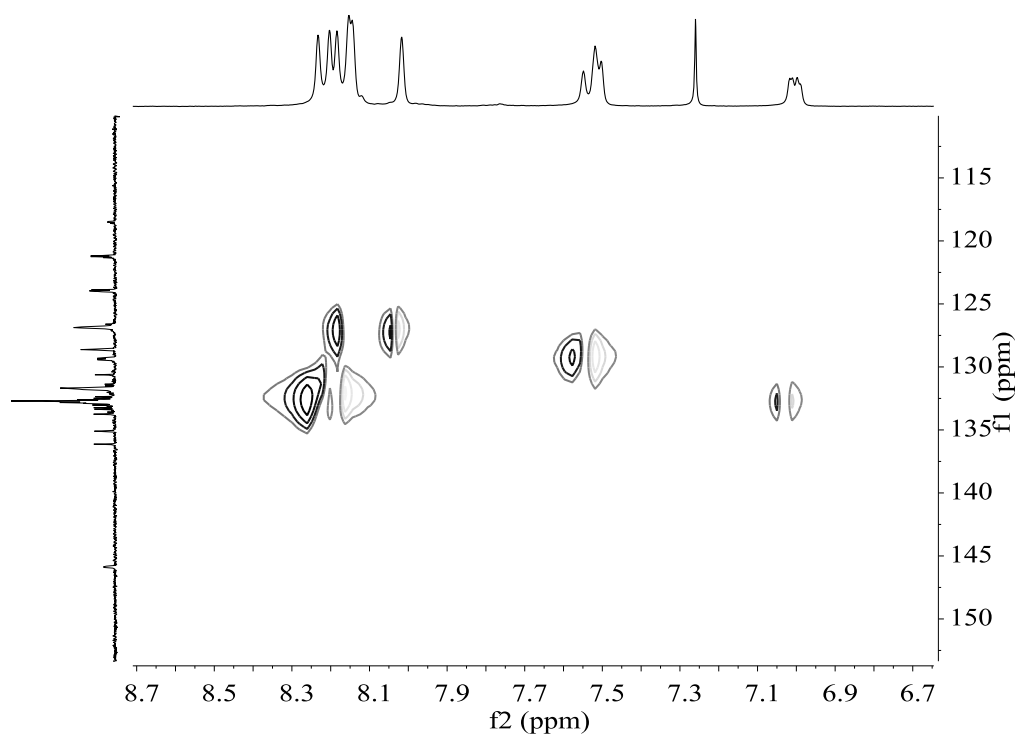
$^{19}\text{F}\{^1\text{H}\}$ NMR (376.50 MHz, CDCl_3)



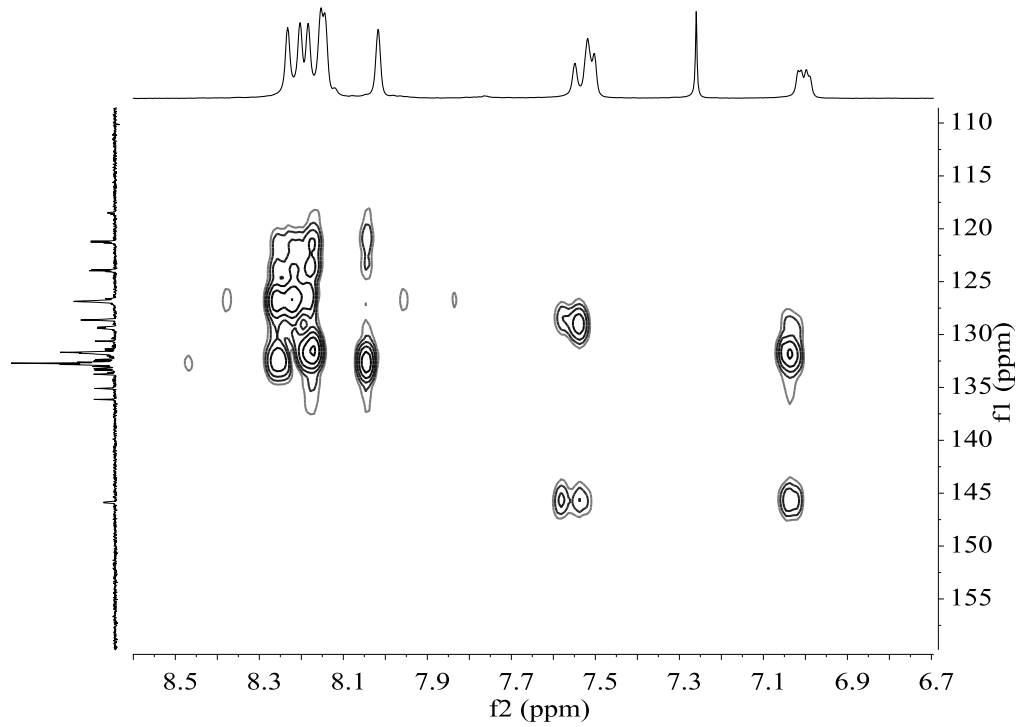
COSY NMR (400.13 MHz, CDCl₃)



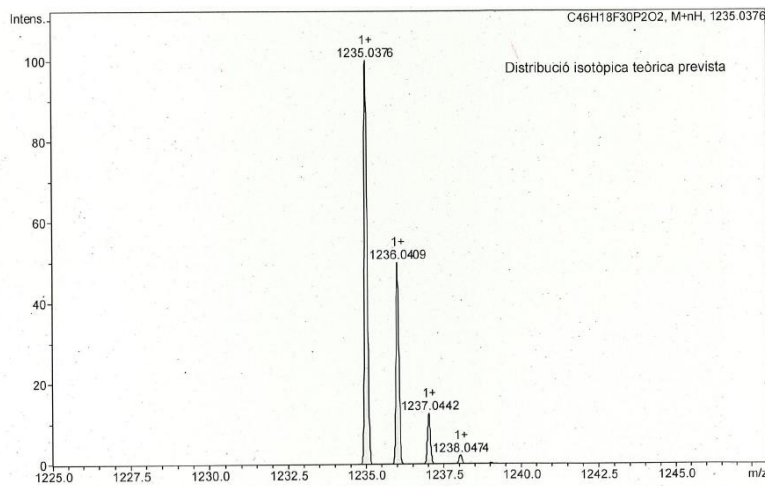
HSQC NMR (400.13 MHz, CDCl₃)



HMBC NMR (400.13 MHz, CDCl₃)

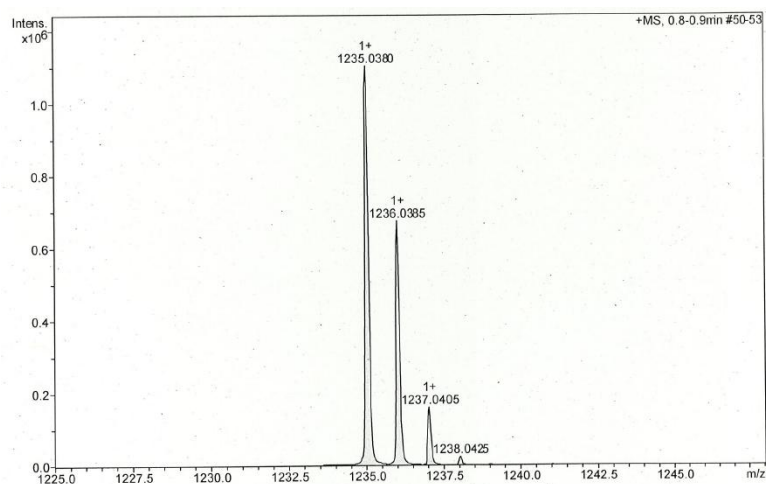


HR-MS (ESI⁺ *m/z*) [M+H]⁺
 calculated for [C₄₆H₁₉F₃₀P₂O₂]⁺



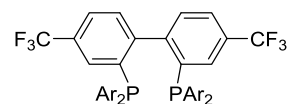
#	<i>m/z</i>	I	I%
1	1235.0376	100	100.0
2	1236.0409	50	50.0
3	1237.0442	13	12.6
4	1238.0474	2	2.2

found



#	m/z	I	I %
1	1235.0380	1102012	100.0
2	1236.0385	674226	61.2
3	1237.0405	161620	14.7
4	1238.0425	23898	2.2

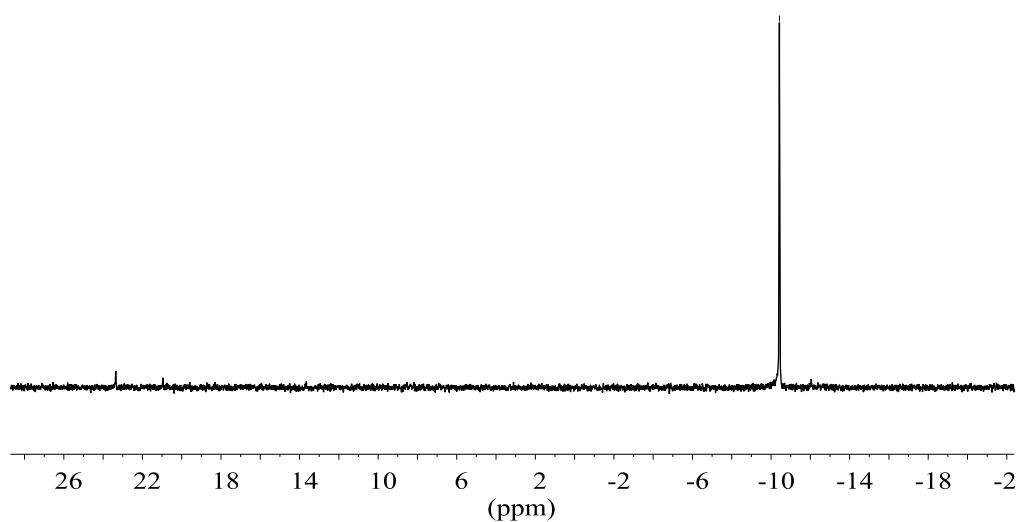
4,4'-bis(trifluoromethyl)-[1,1'-biphenyl]-2,2'-diylbis(bis(3,5-bis(trifluoromethyl)phenyl)phosphine (32)



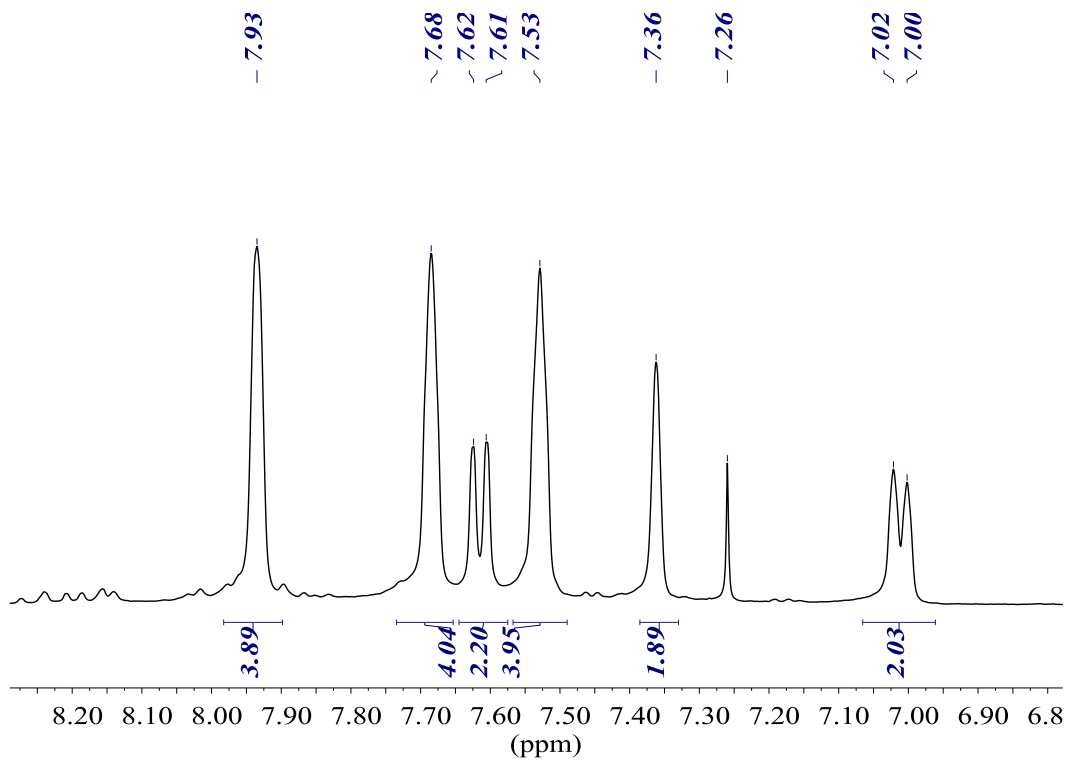
$^{31}\text{P}\{^1\text{H}\}$ NMR (161.98 MHz, CDCl_3)

Ar = 3,5-bis(trifluoromethyl)phenyl

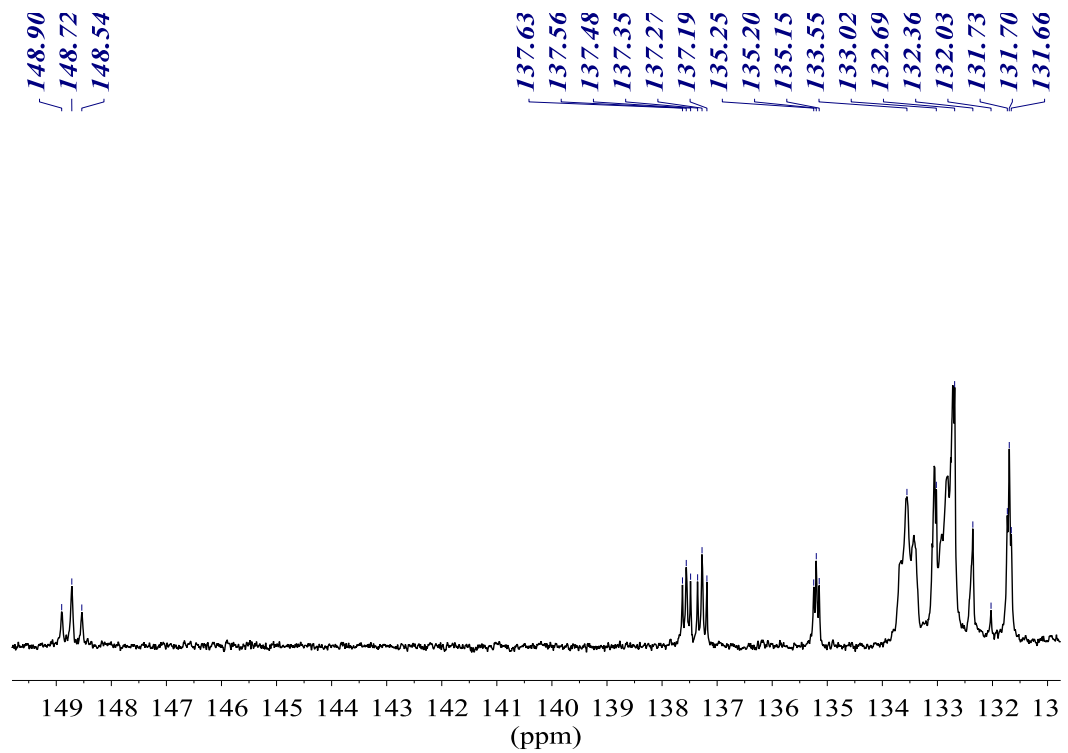
-10.43

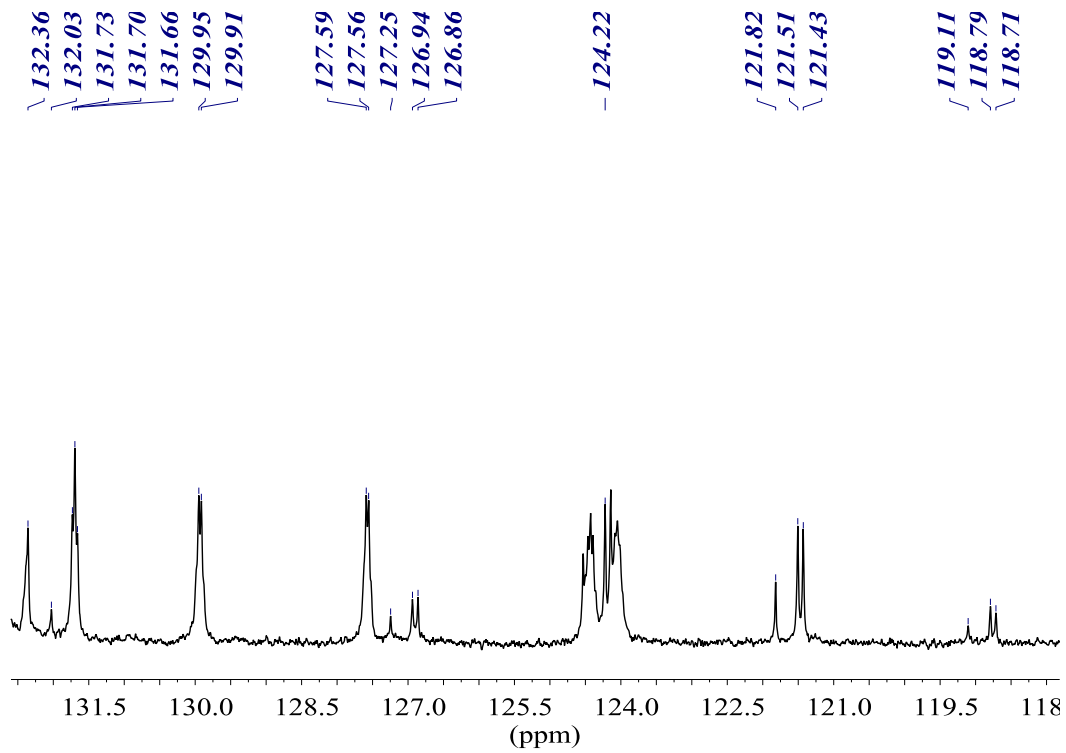


^1H NMR (400.13 MHz, CDCl_3)

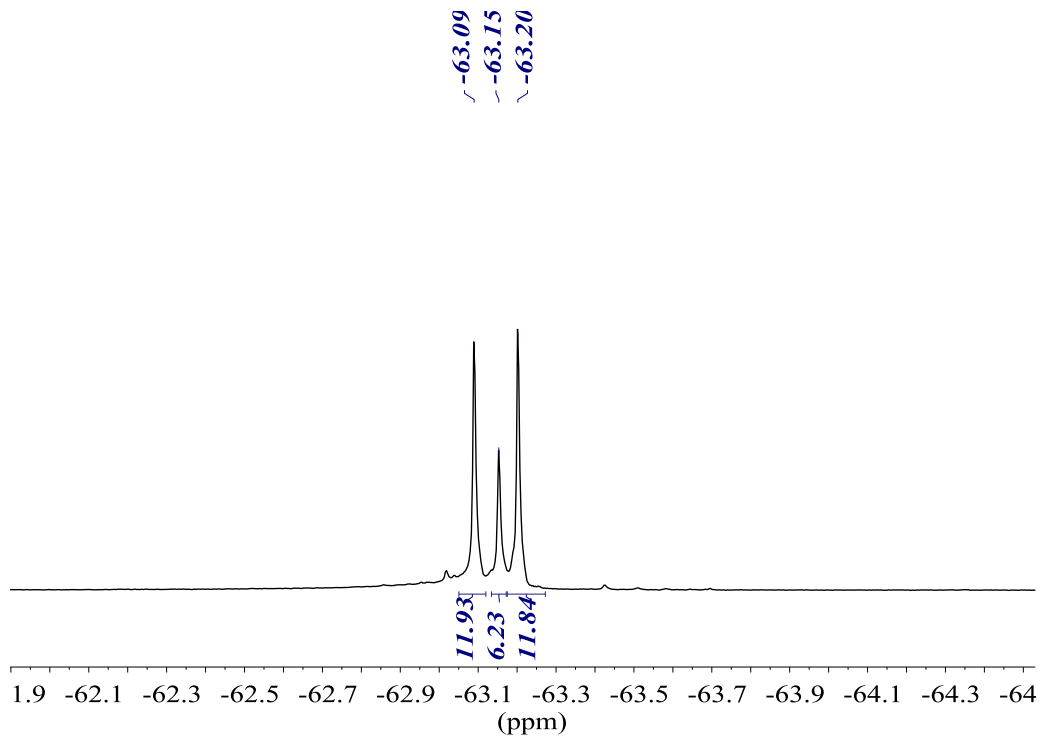


$^{13}\text{C}\{^1\text{H}\}$ NMR (100.61 MHz, CDCl_3)

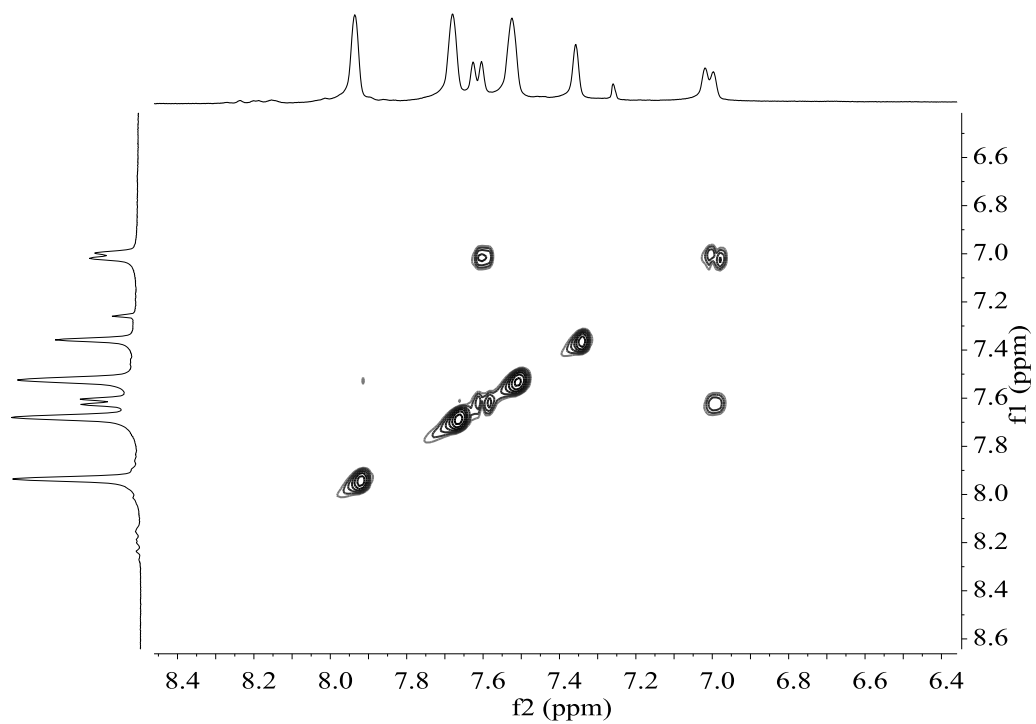




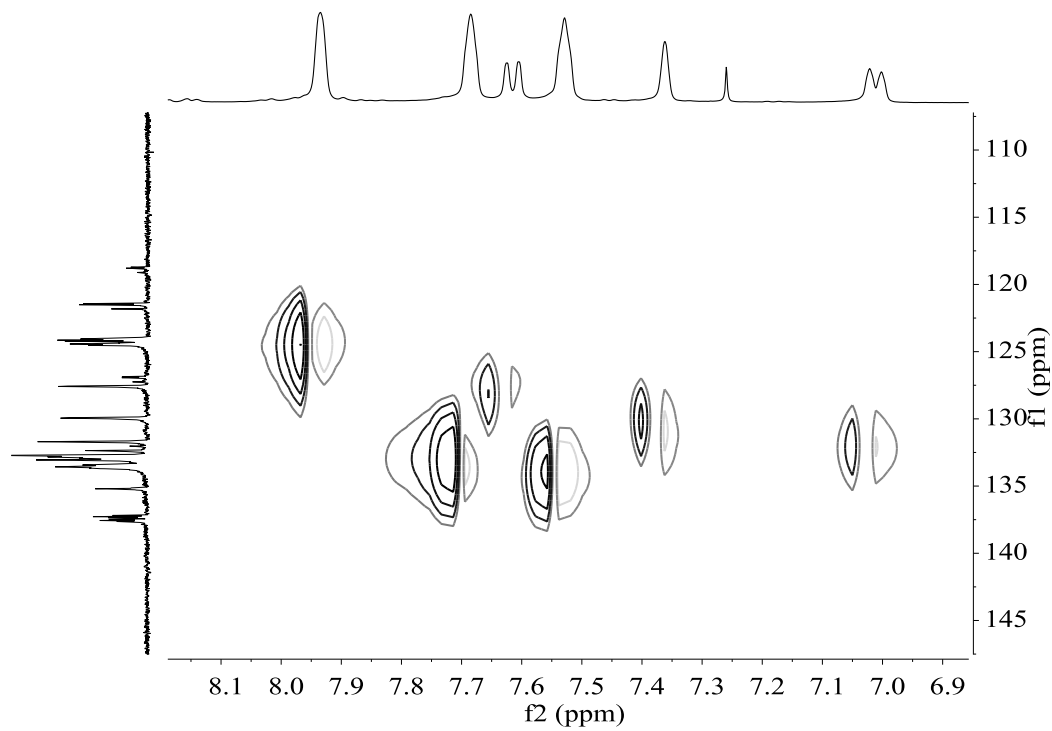
$^{19}\text{F}\{^1\text{H}\}$ NMR (376.50 MHz, CDCl_3)



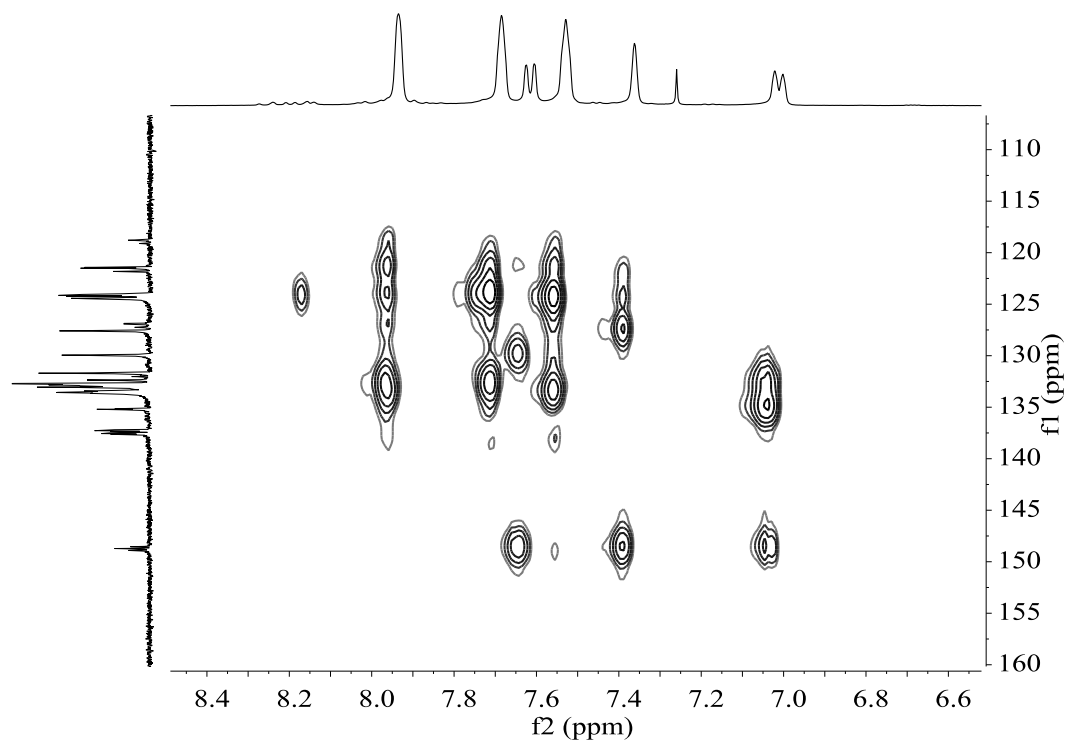
COSY NMR (400.13 MHz, CDCl₃)



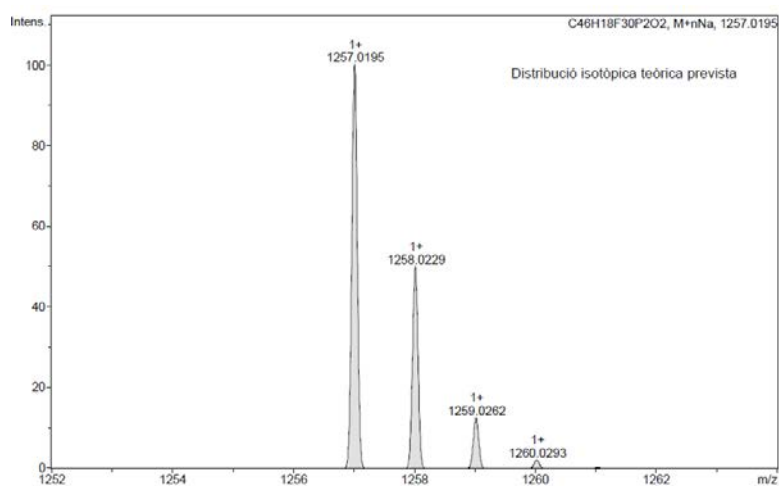
HSQC NMR (400.13 MHz, CDCl₃)



HMBC NMR (400.13 MHz, CDCl₃)

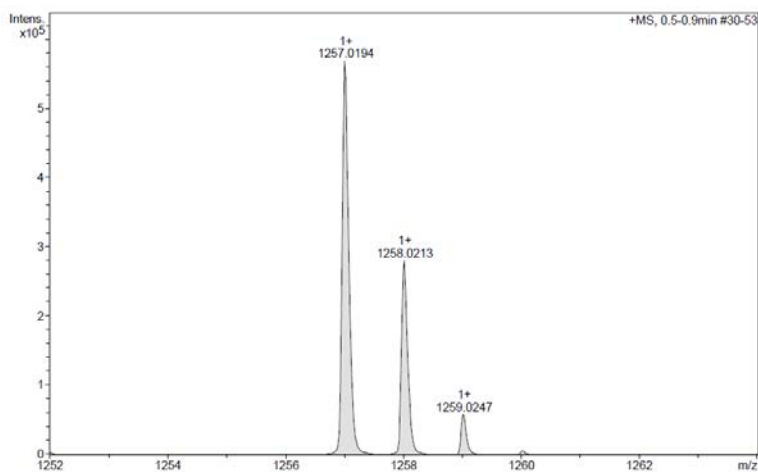


HR-MS (ESI⁺ *m/z*) [M(O)₂+Na]⁺
 calculated for [C₄₆H₁₈F₃₀P₂O₂Na]⁺



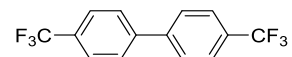
#	<i>m/z</i>	I	I %
1	1257.0195	100	100.0
2	1258.0229	50	50.0
3	1259.0262	13	12.6
4	1260.0293	2	2.2

found



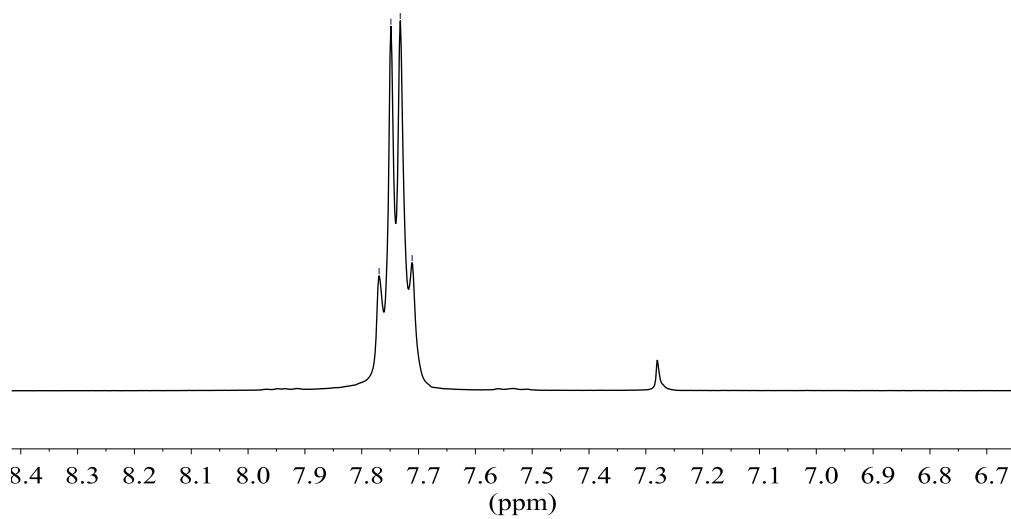
#	m/z	I	I %
1	1257.0194	568650	100.0
2	1258.0213	280619	49.3
3	1259.0247	58304	10.3
4	1260.0269	5733	1.0

4,4'-bis(trifluoromethyl)-1,1'-biphenyl (35)

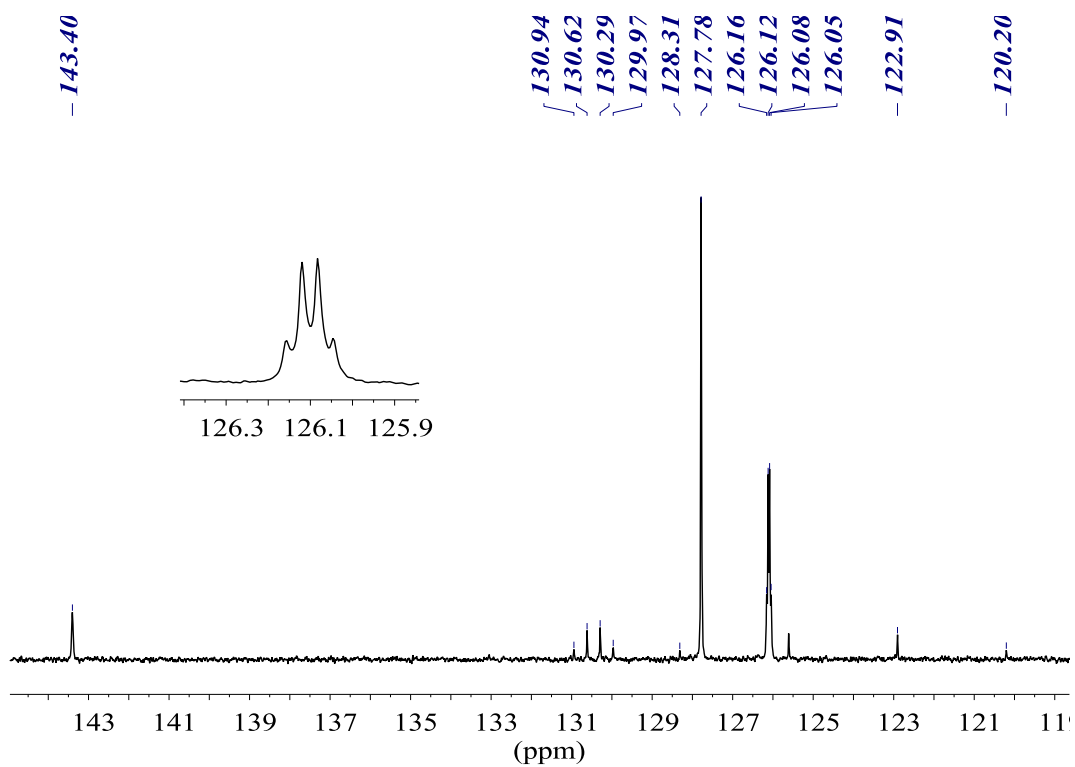


$^1\text{H NMR}$ (400.13 MHz, CDCl_3)

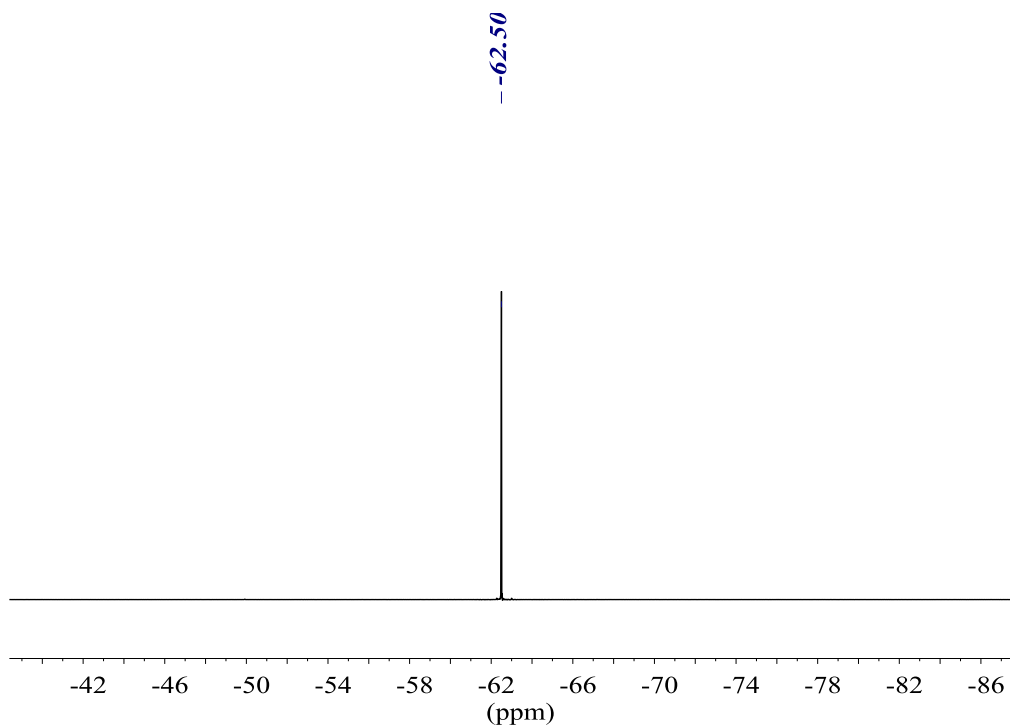
7.77
7.75
7.73
7.71



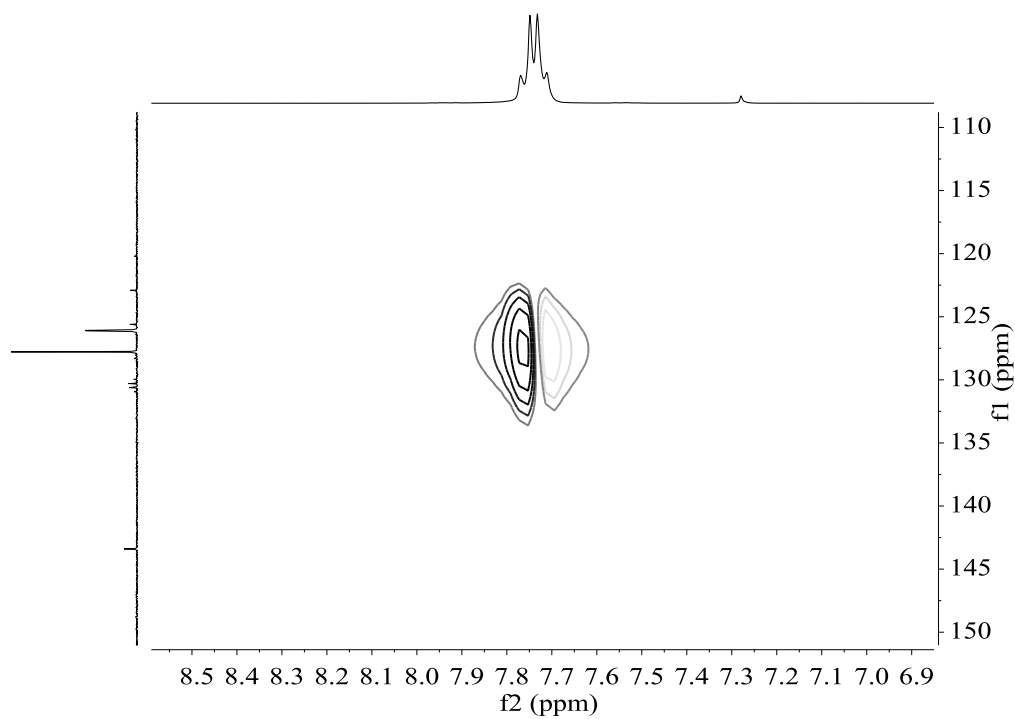
$^{13}\text{C}\{^1\text{H}\}$ NMR (100.61 MHz, CDCl_3)



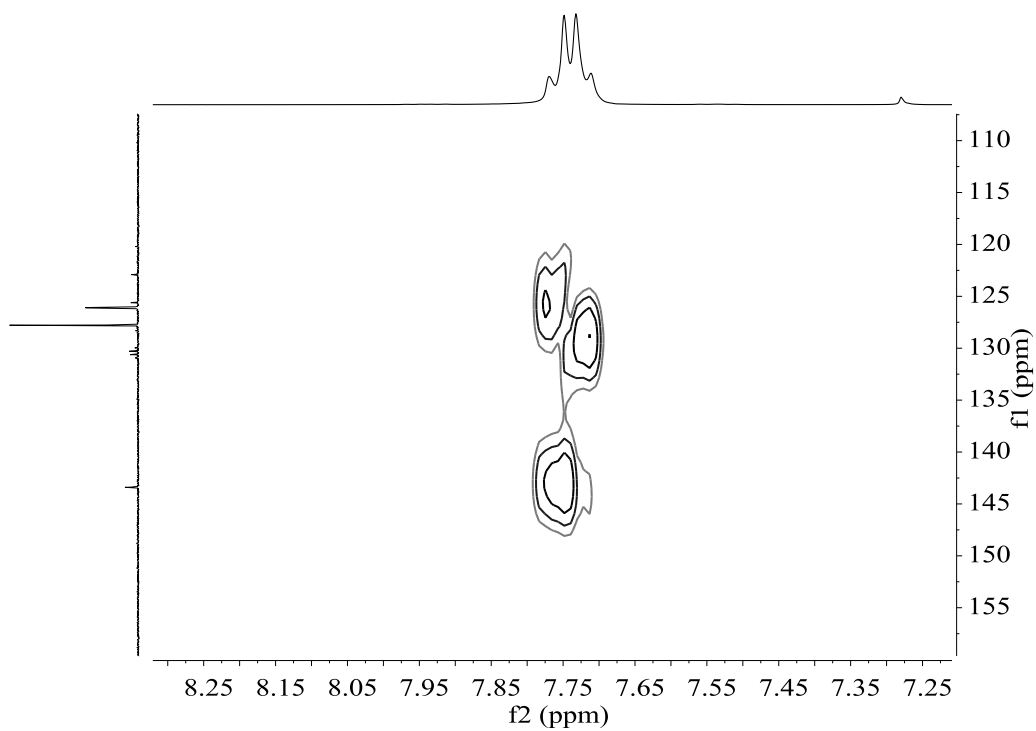
$^{19}\text{F}\{^1\text{H}\}$ NMR (376.50 MHz, CDCl_3)



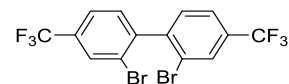
HSQC NMR (400.13 MHz, CDCl₃)



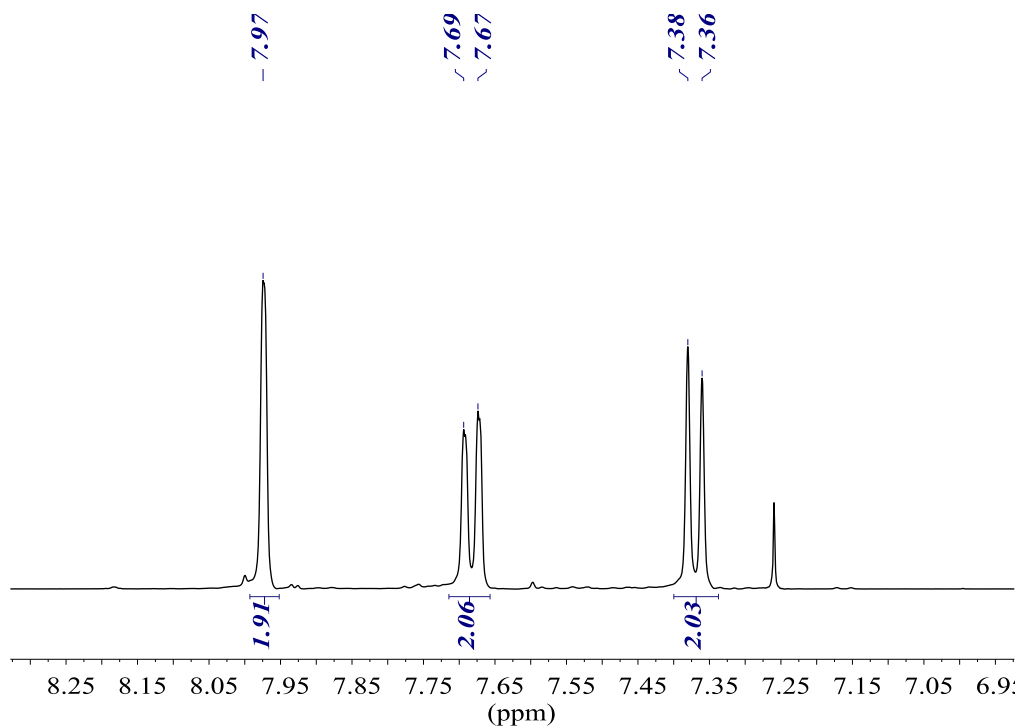
HMBC NMR (400.13 MHz, CDCl₃)



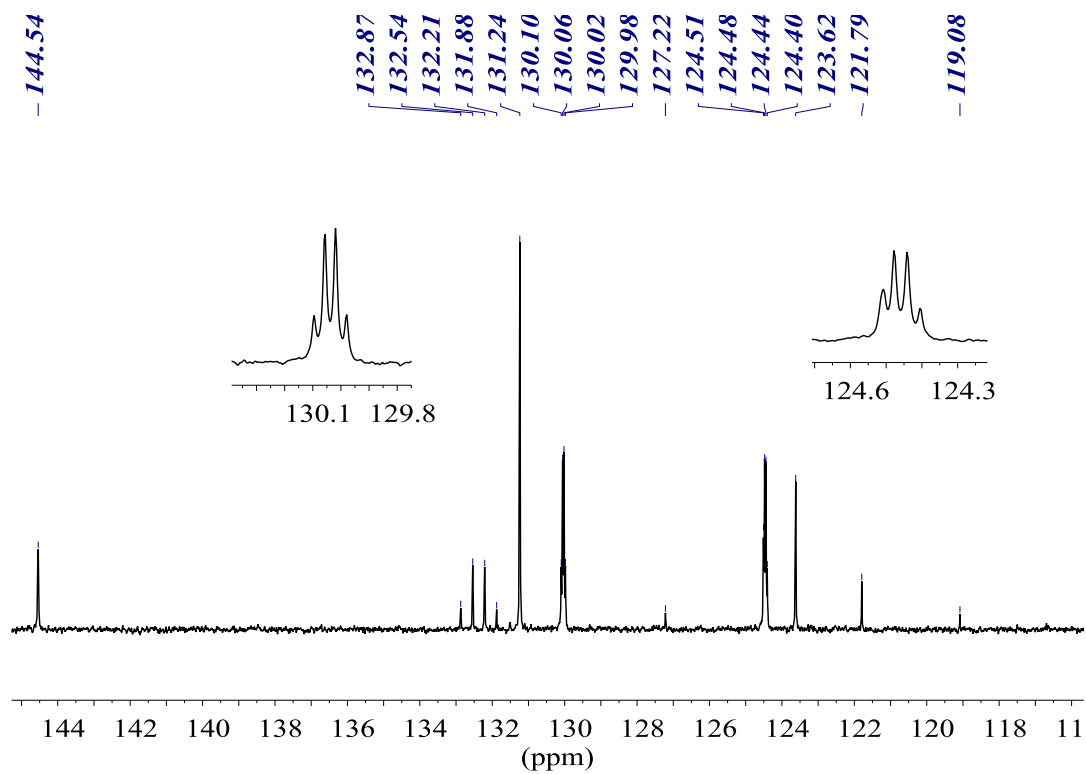
2,2'-dibromo-4,4'-bis(trifluoromethyl)-1,1'-biphenyl (36)



^1H NMR (400.13 MHz, CDCl_3)

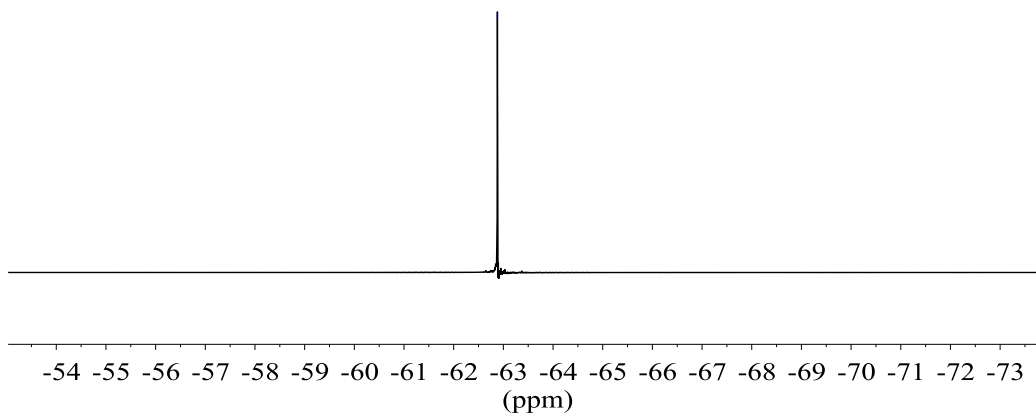


$^{13}\text{C}\{^1\text{H}\}$ NMR (100.61 MHz, CDCl_3)

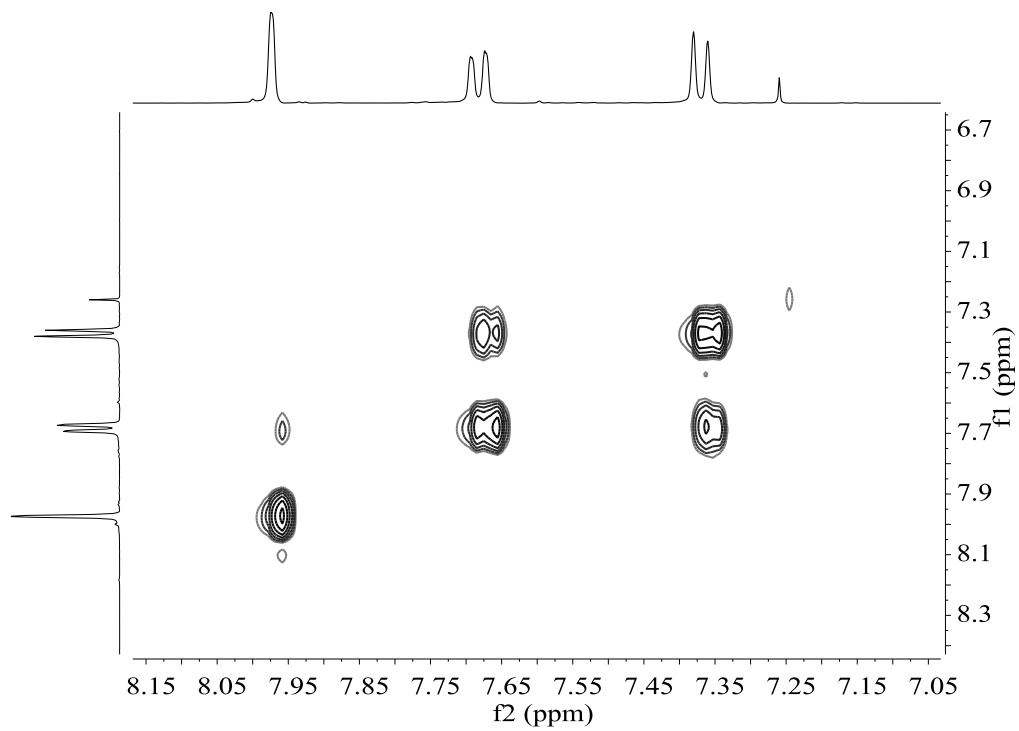


$^{19}\text{F}\{^1\text{H}\}$ NMR (376.50 MHz, CDCl_3)

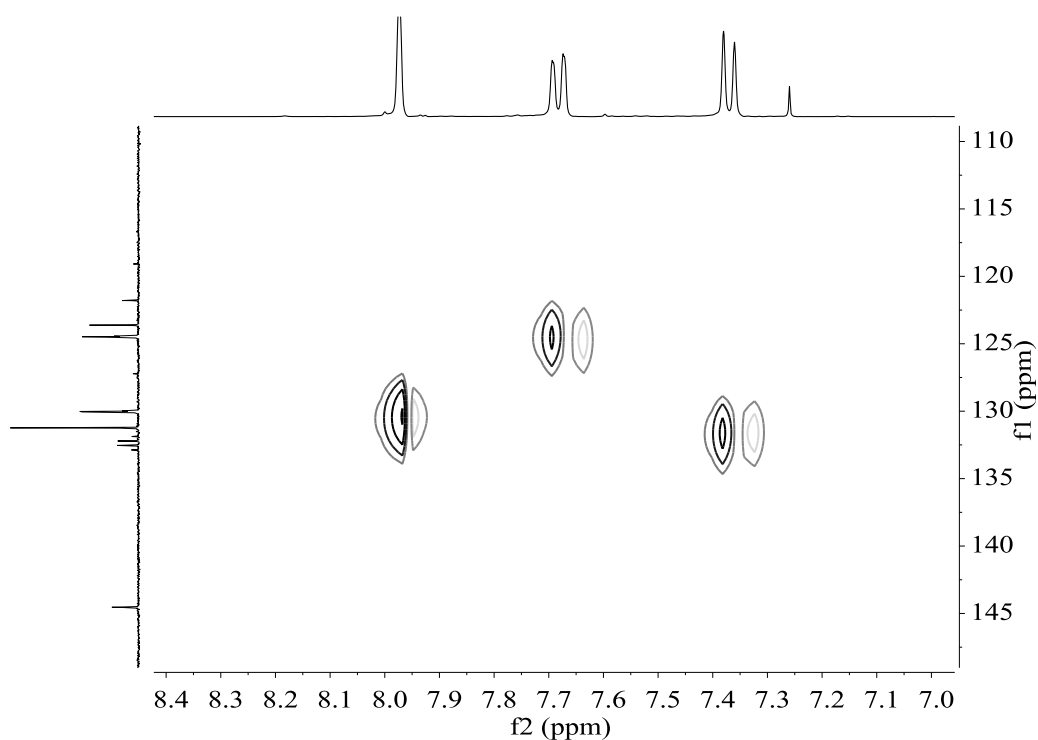
--62.88



COSY NMR (400.13 MHz, CDCl_3)

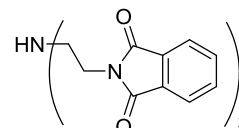


HSQC NMR (400.13 MHz, CDCl₃)

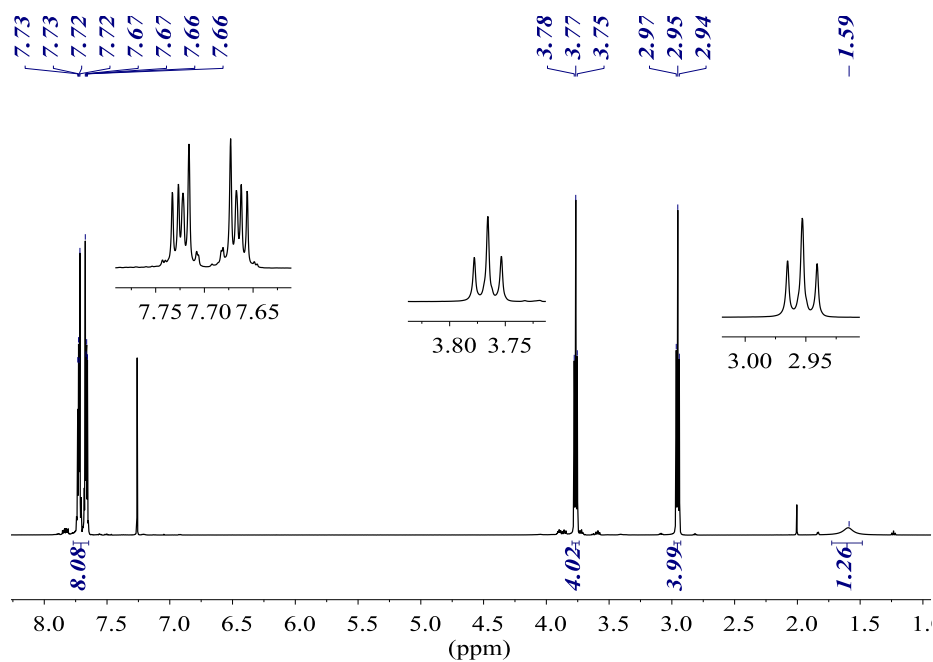


6. Characterisation of diphosphines P-bz, M-bz, P-st, M-st and intermediate compounds

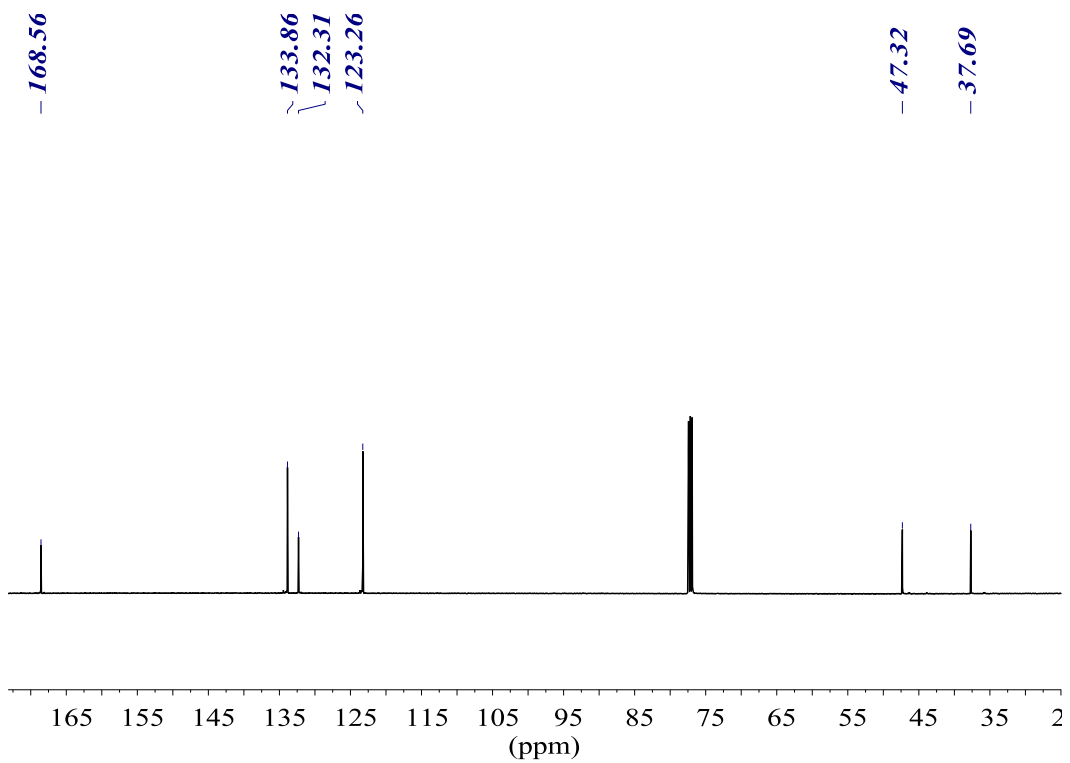
N,N-bis(2-phthalimidoethyl)amine (38)



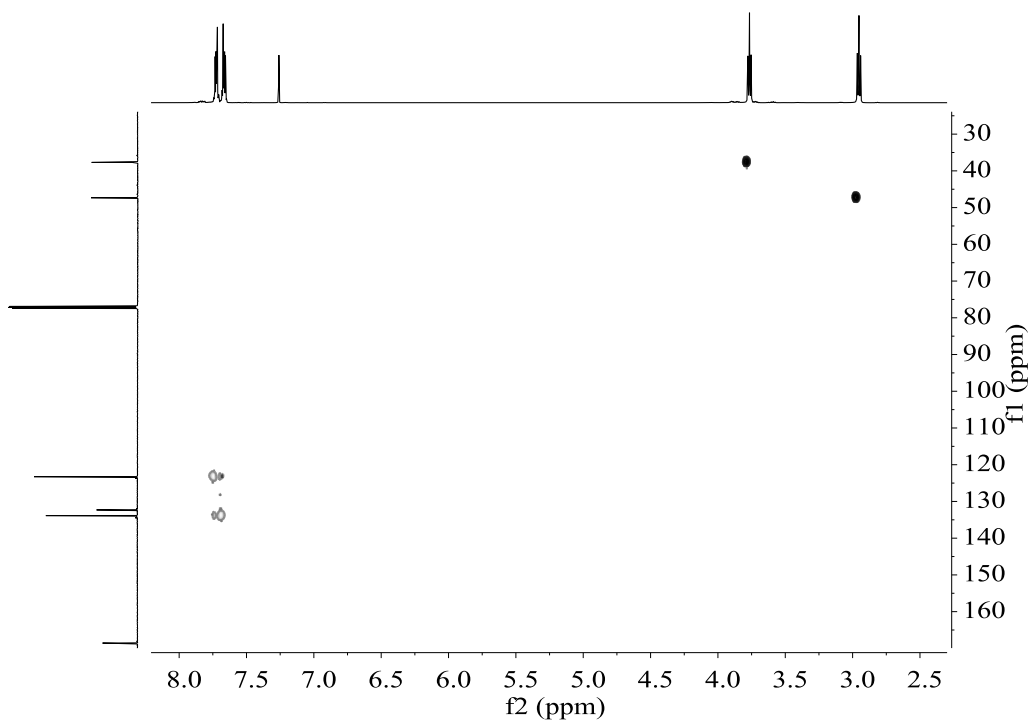
¹H NMR (500.13 MHz, CDCl₃)



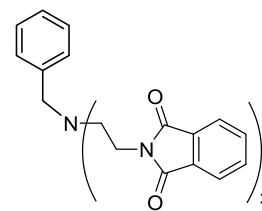
$^{13}\text{C}\{^1\text{H}\}$ NMR (125.80 MHz, CDCl_3)



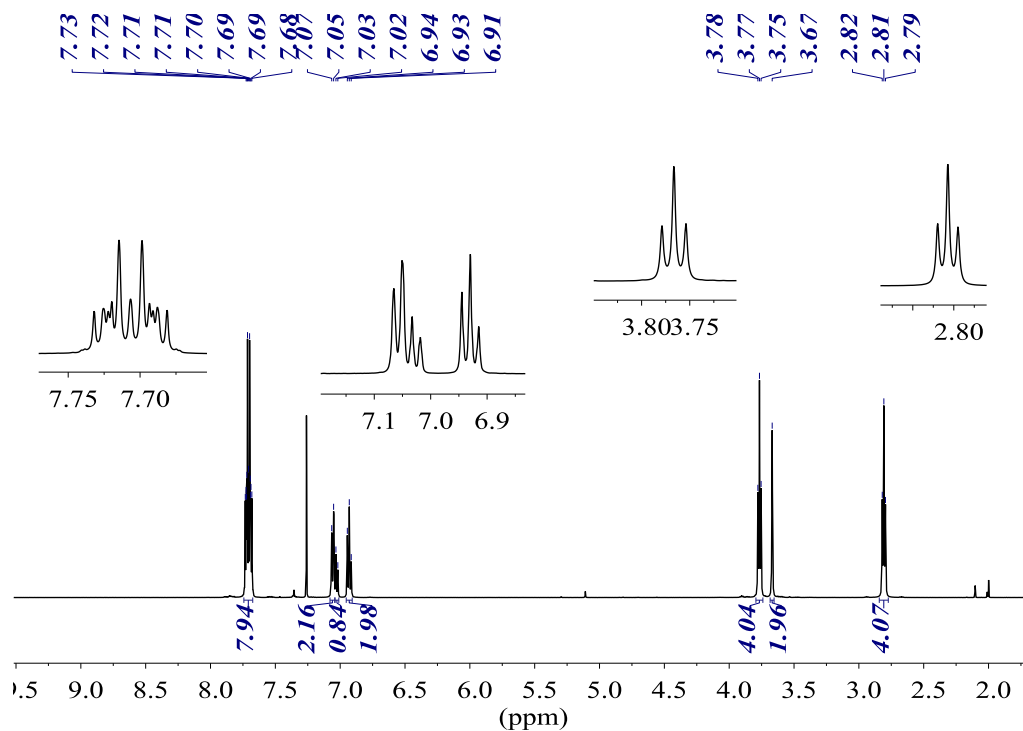
HSQC NMR (500.13 MHz, CDCl_3)



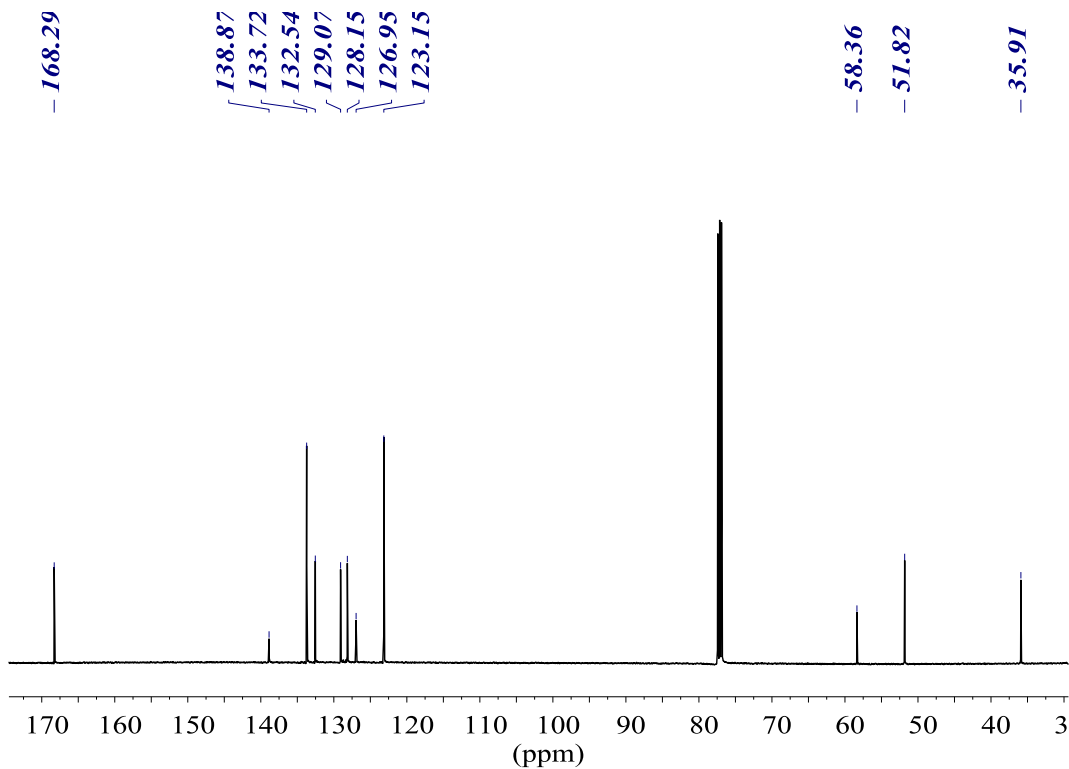
Benzyl-bis(2-phthalimidoethyl)amine (39-bz)



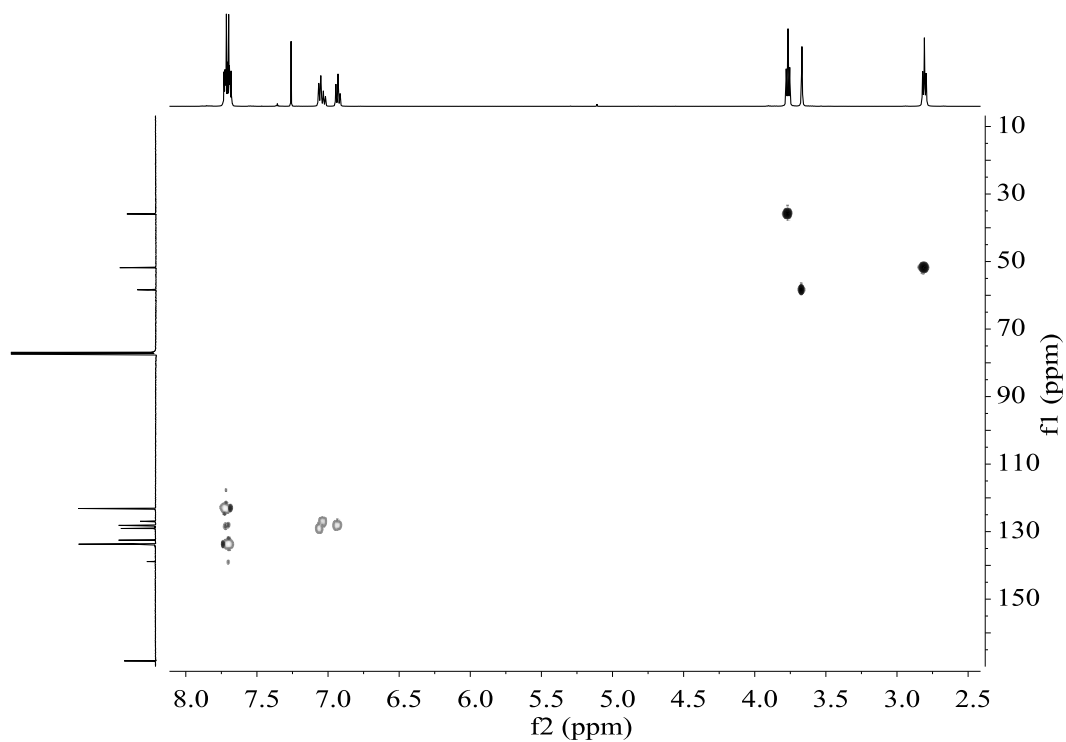
^1H NMR (500.13 MHz, CDCl_3)



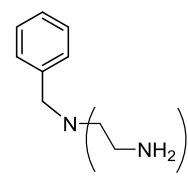
$^{13}\text{C}\{^1\text{H}\}$ NMR (125.80 MHz, CDCl_3)



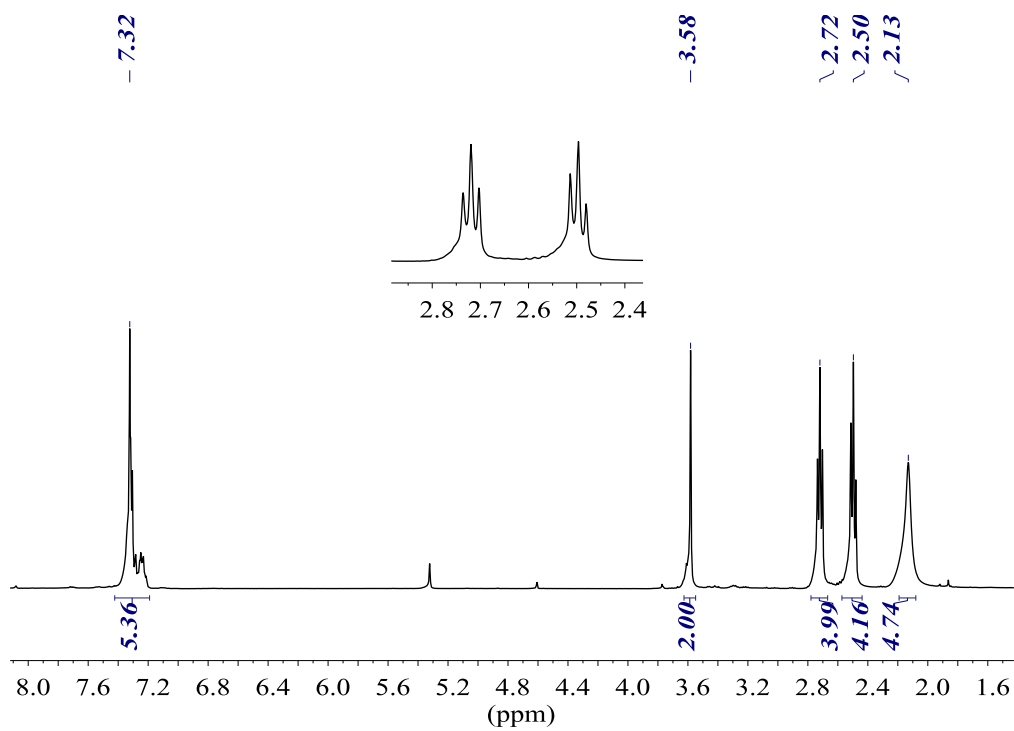
HSQC NMR (500.13 MHz, CDCl₃)



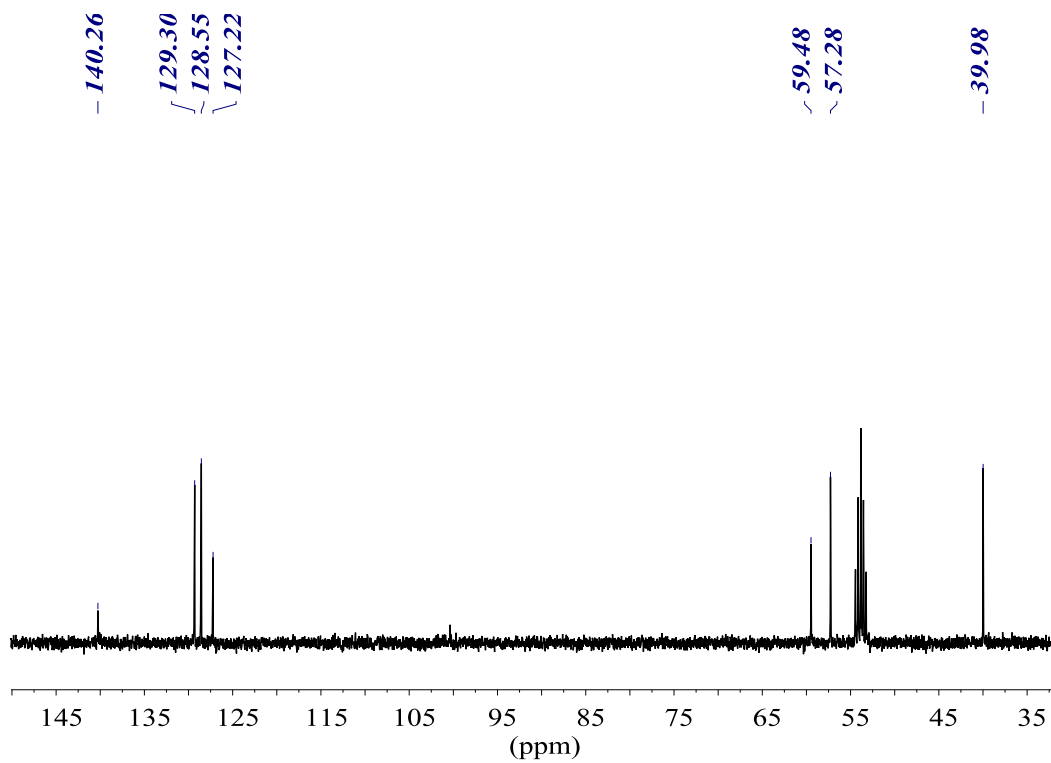
4-benzyl-diethylenetriamine (40-bz)



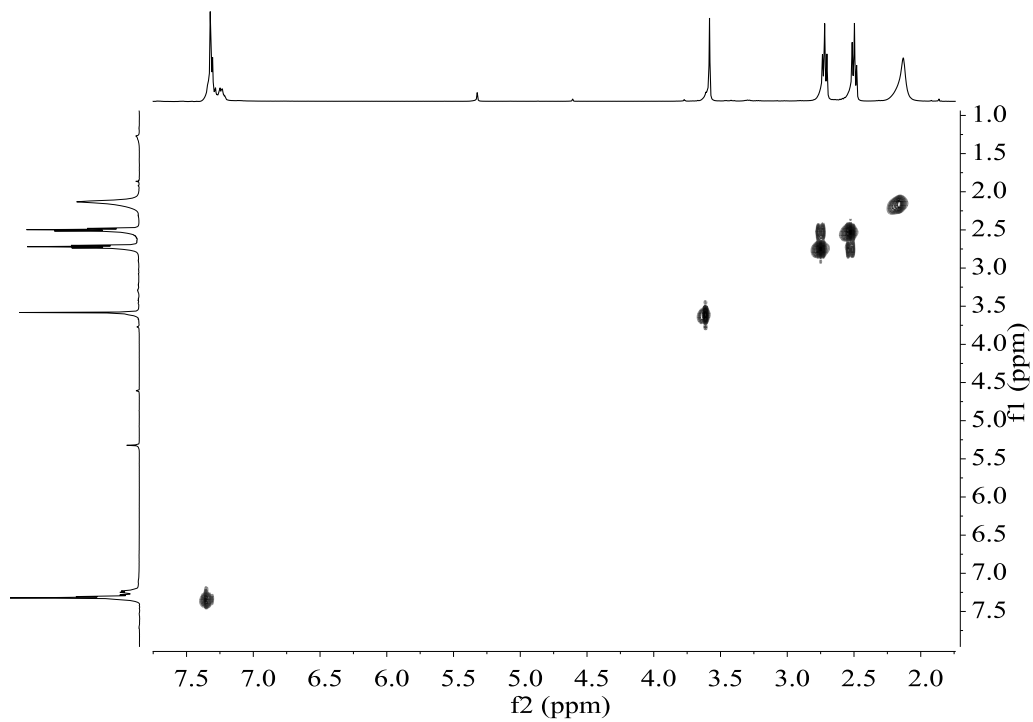
¹H NMR (360.13 MHz, CD₂Cl₂)



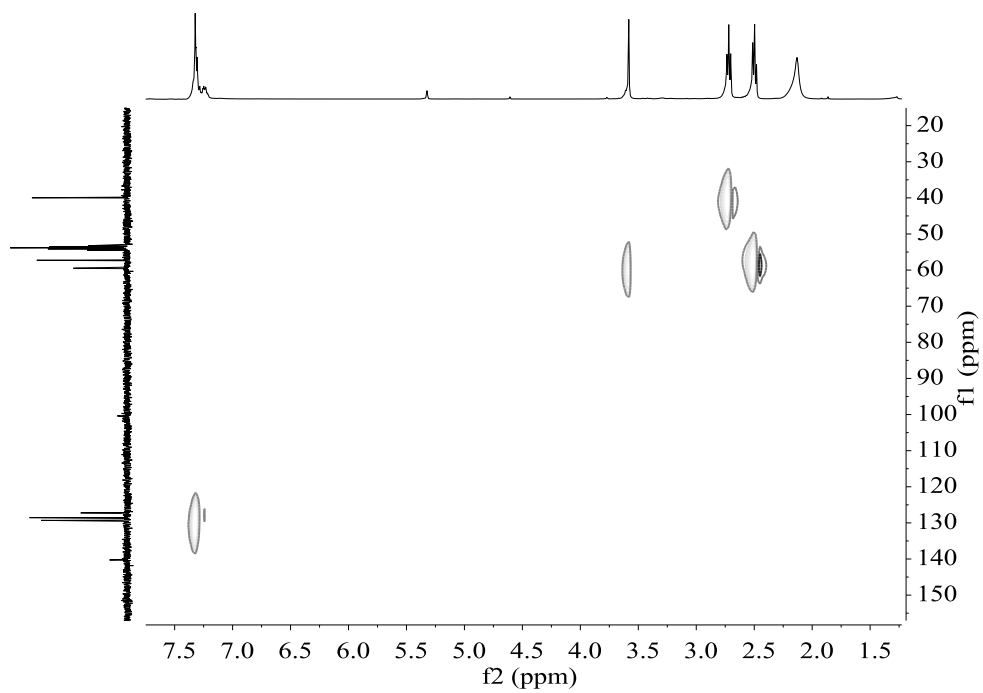
$^{13}\text{C}\{^1\text{H}\}$ NMR (90.56 MHz, CD_2Cl_2)



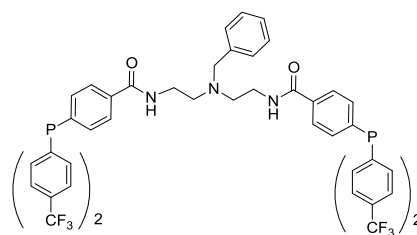
COSY NMR (360.13 MHz, CD_2Cl_2)



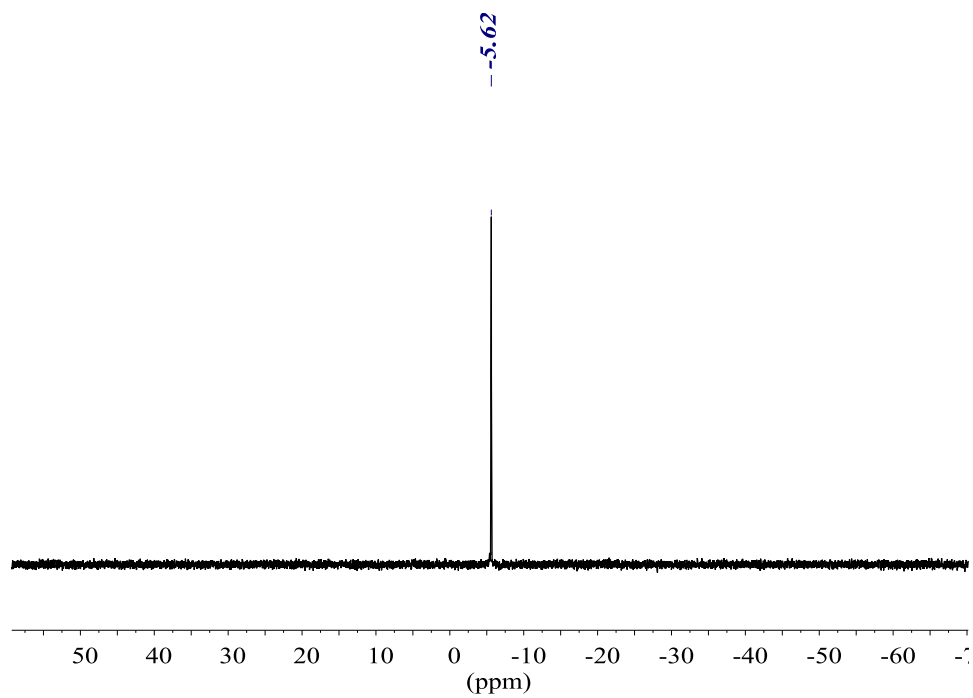
HSQC NMR (360.13 MHz, CD₂Cl₂)

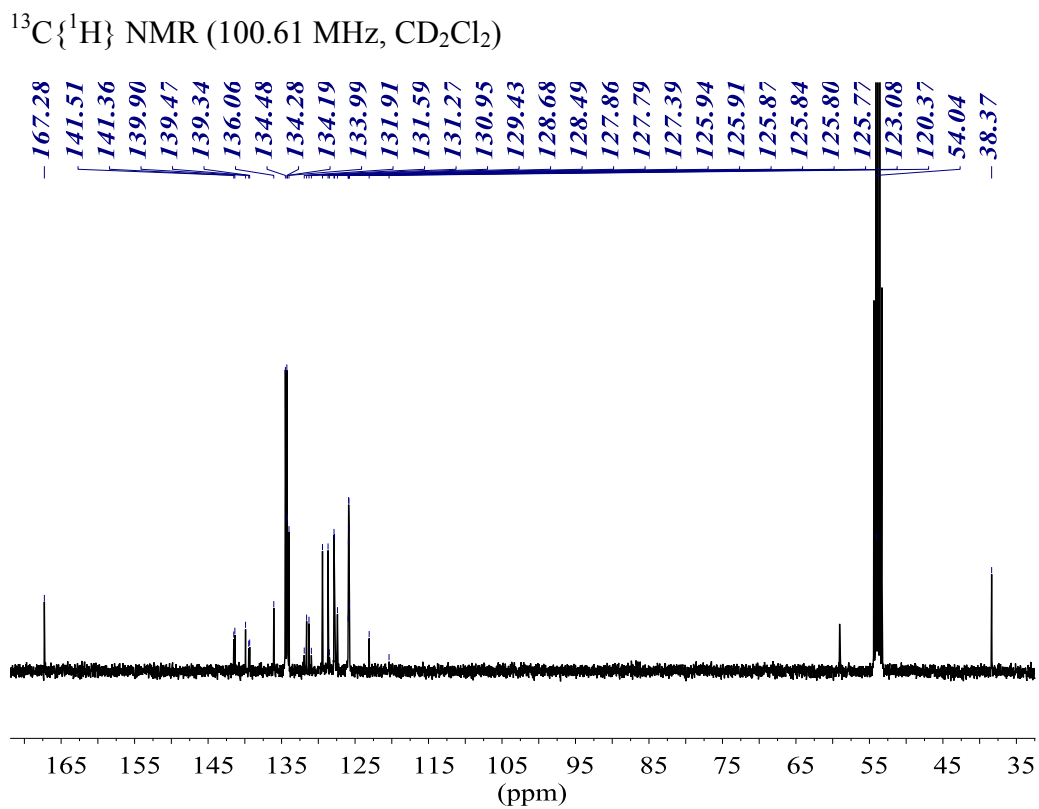
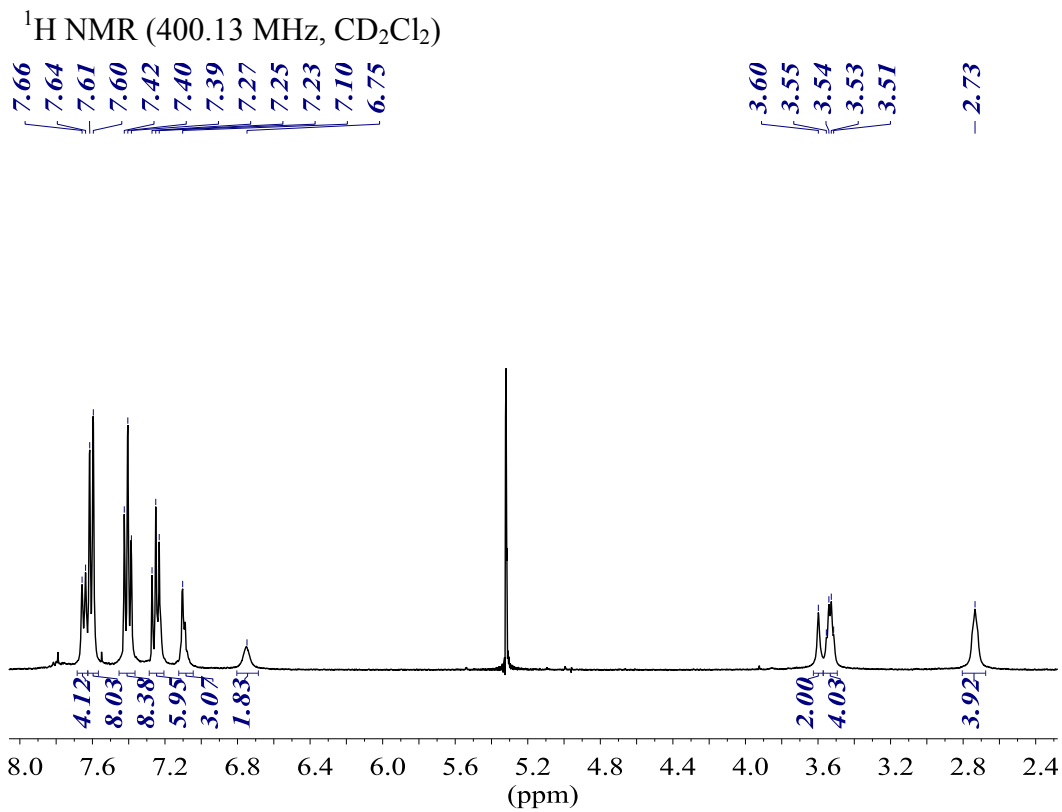


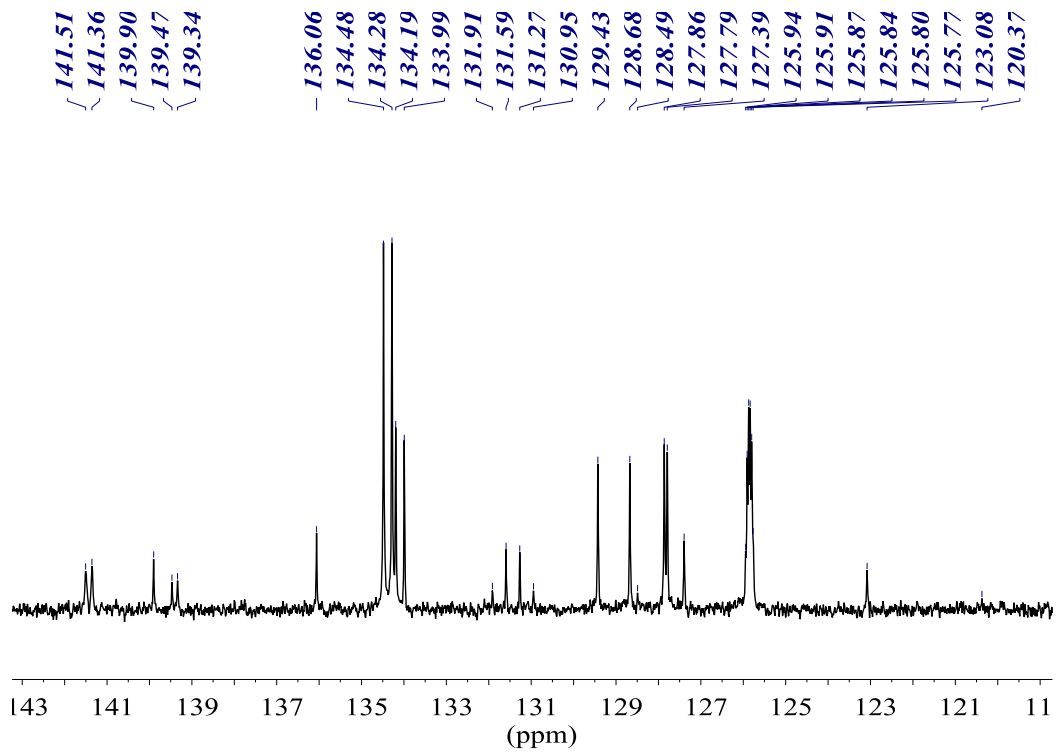
Diphosphine-diamide P-bz



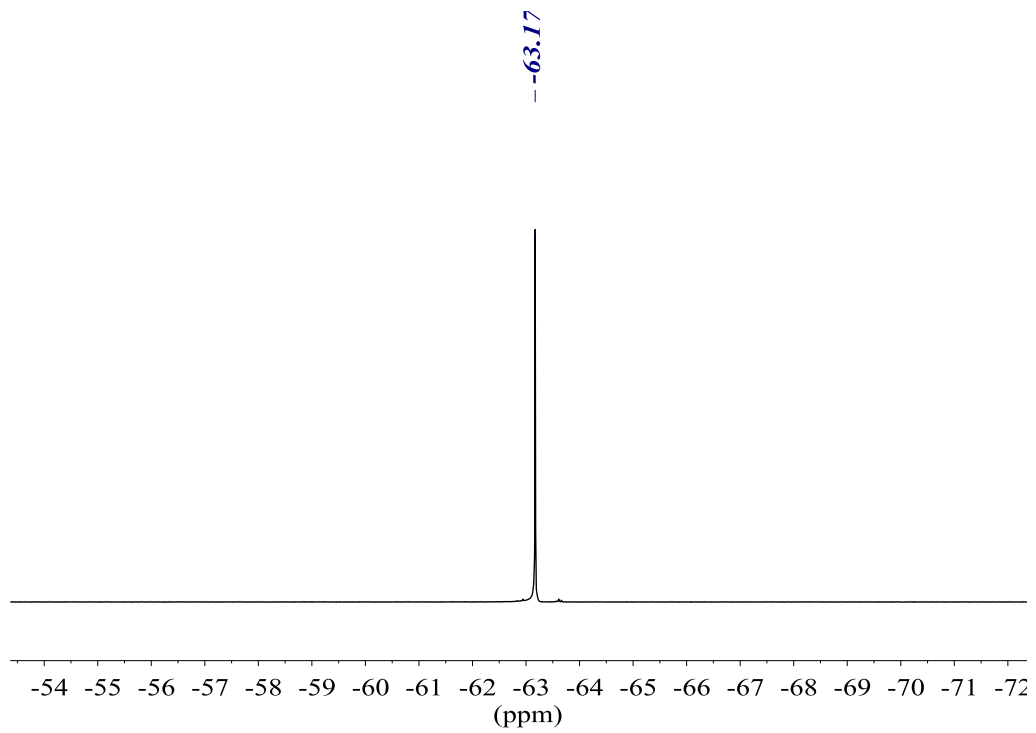
³¹P{¹H} NMR (161.98 MHz, CD₂Cl₂)



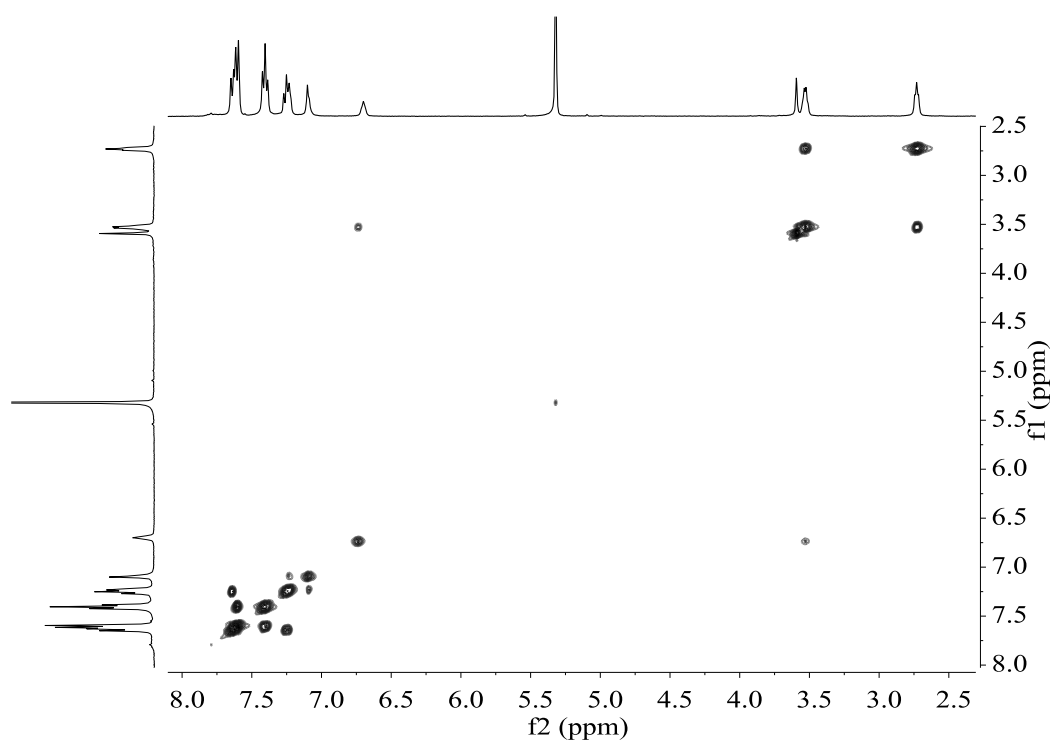




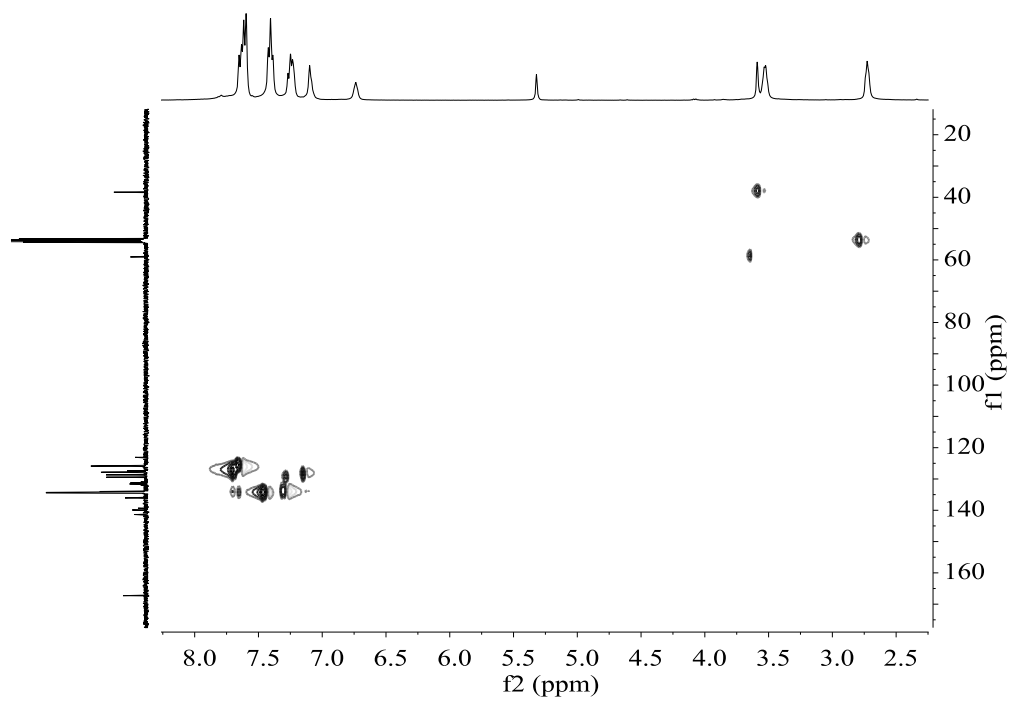
$^{19}\text{F}\{^1\text{H}\}$ NMR (376.50 MHz, CD_2Cl_2)

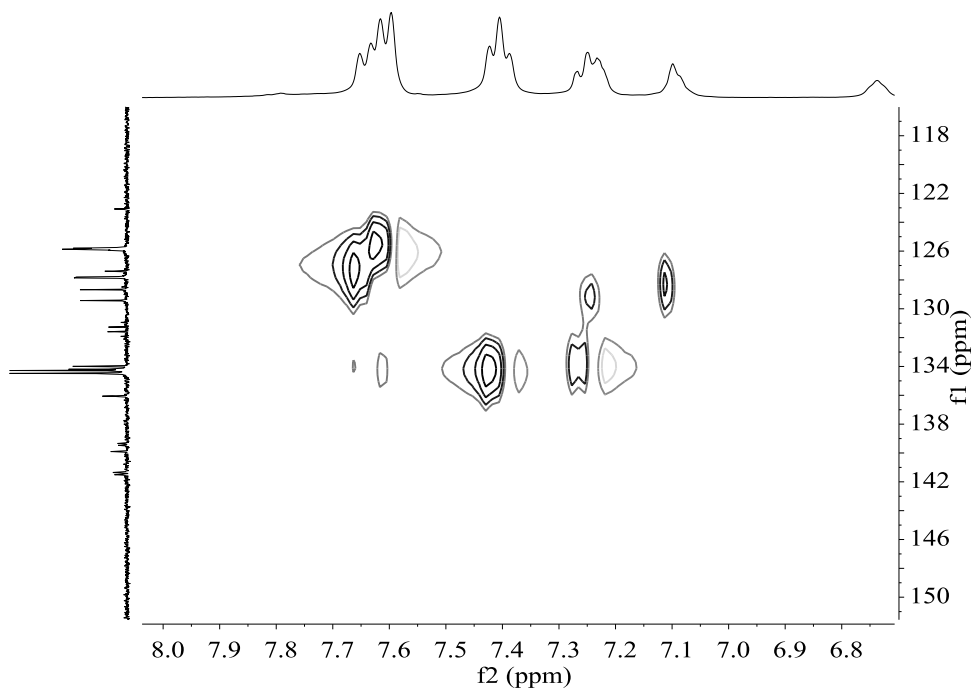


COSY NMR (400.13 MHz, CD₂Cl₂)

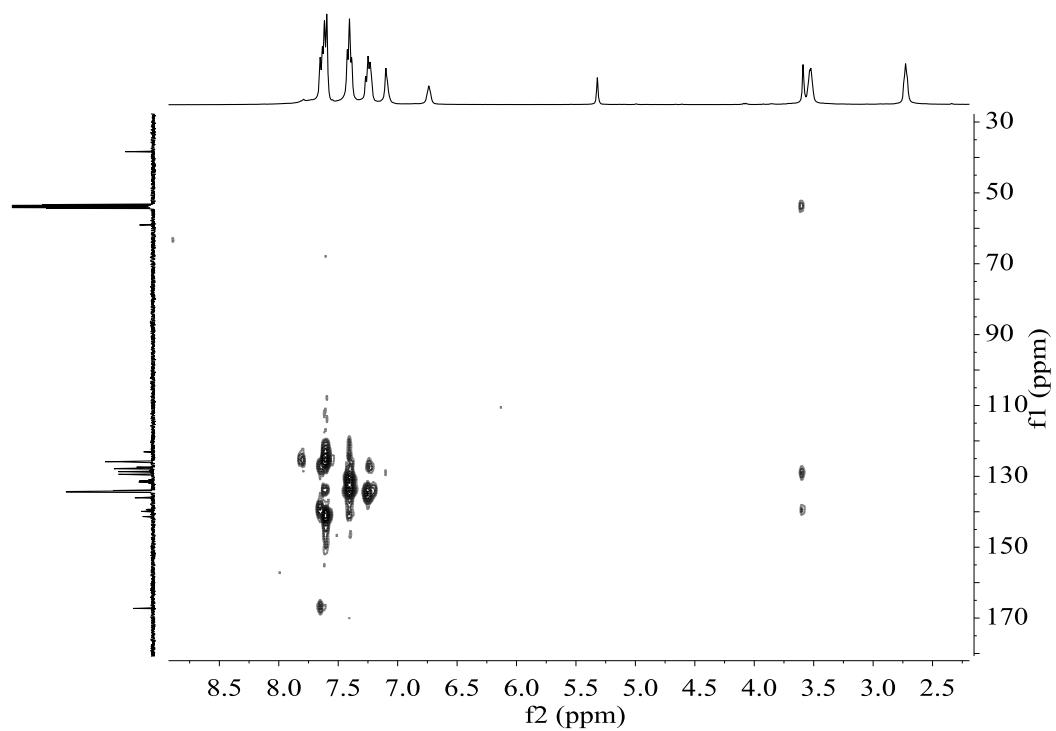


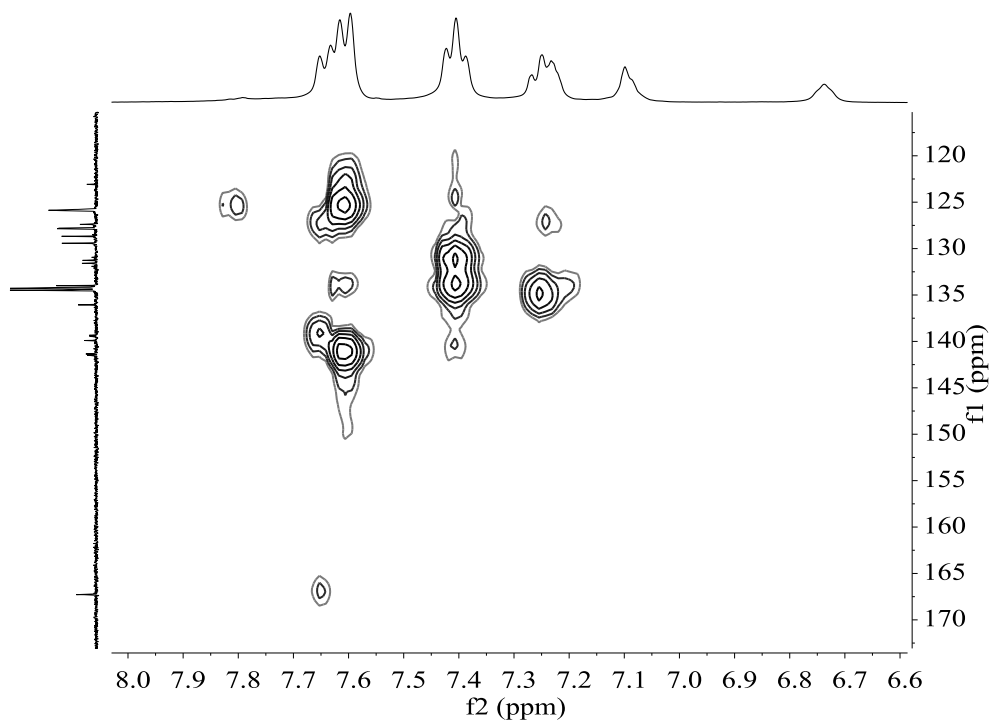
HSQC NMR (400.13 MHz, CD₂Cl₂)



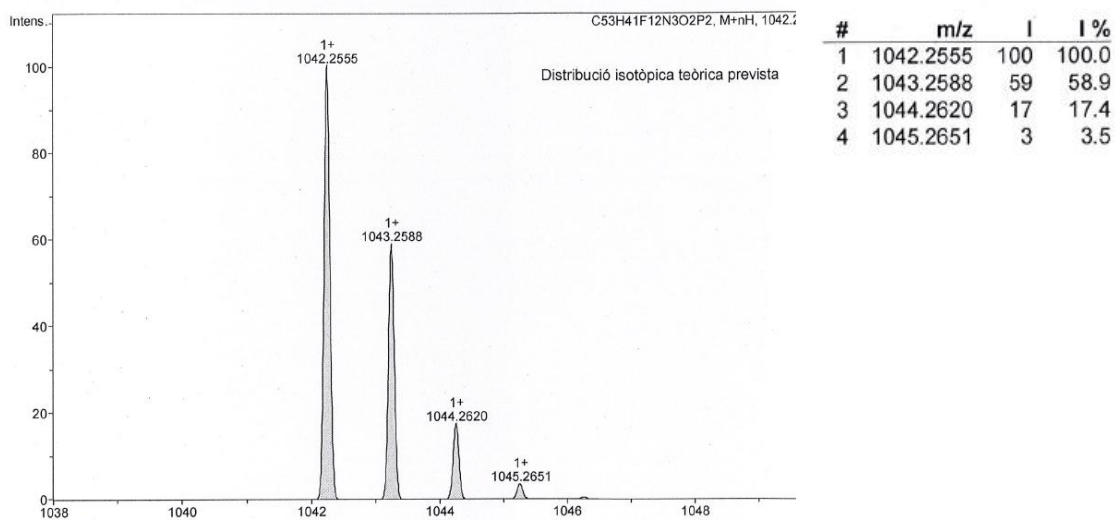


HMBC NMR (400.13 MHz, CD₂Cl₂)

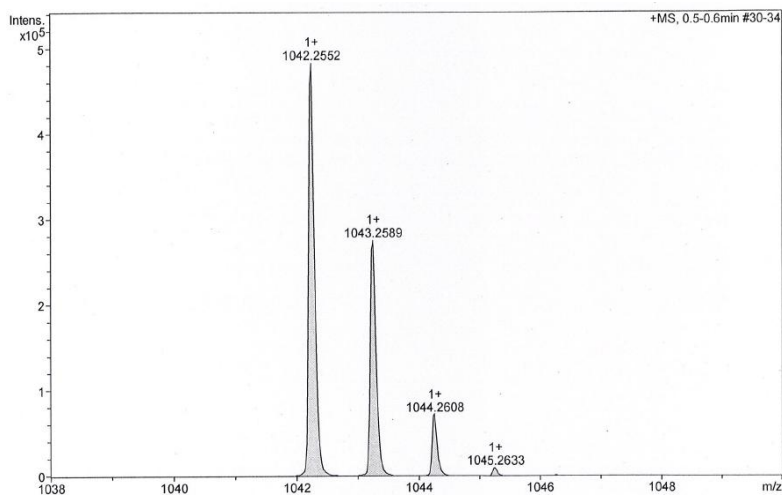




HR-MS (ESI⁺ *m/z*) [M+H]⁺
 calculated for [C₅₃H₄₂F₁₂N₃O₂P₂]⁺

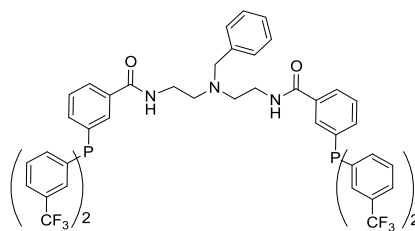


found



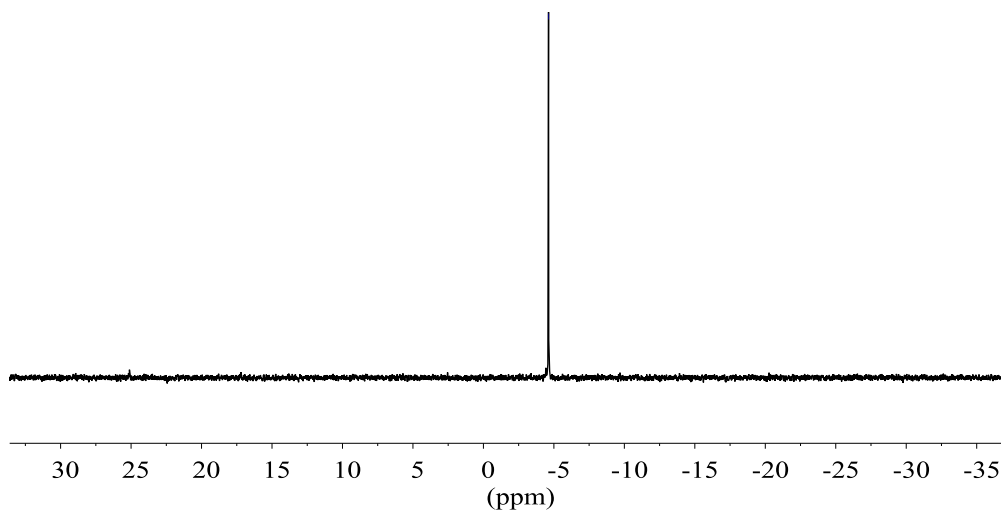
#	m/z	I	I %
1	1042.2552	482896	100.0
2	1043.2589	275441	57.0
3	1044.2608	71748	14.9
4	1045.2633	9779	2.0

Diphosphine-diamide M-bz

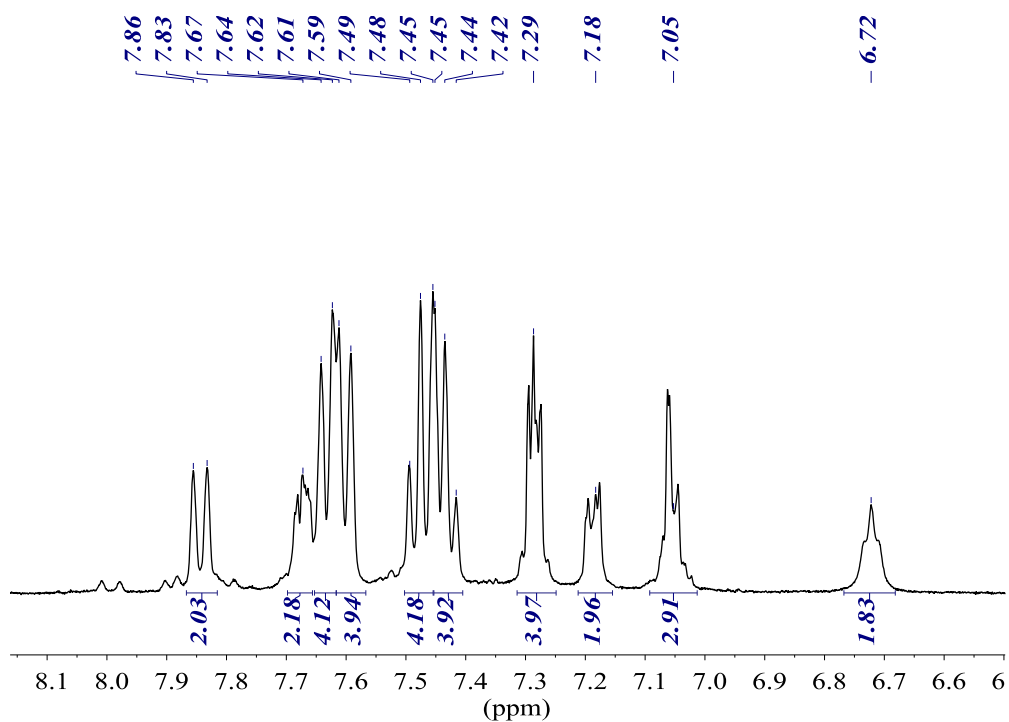
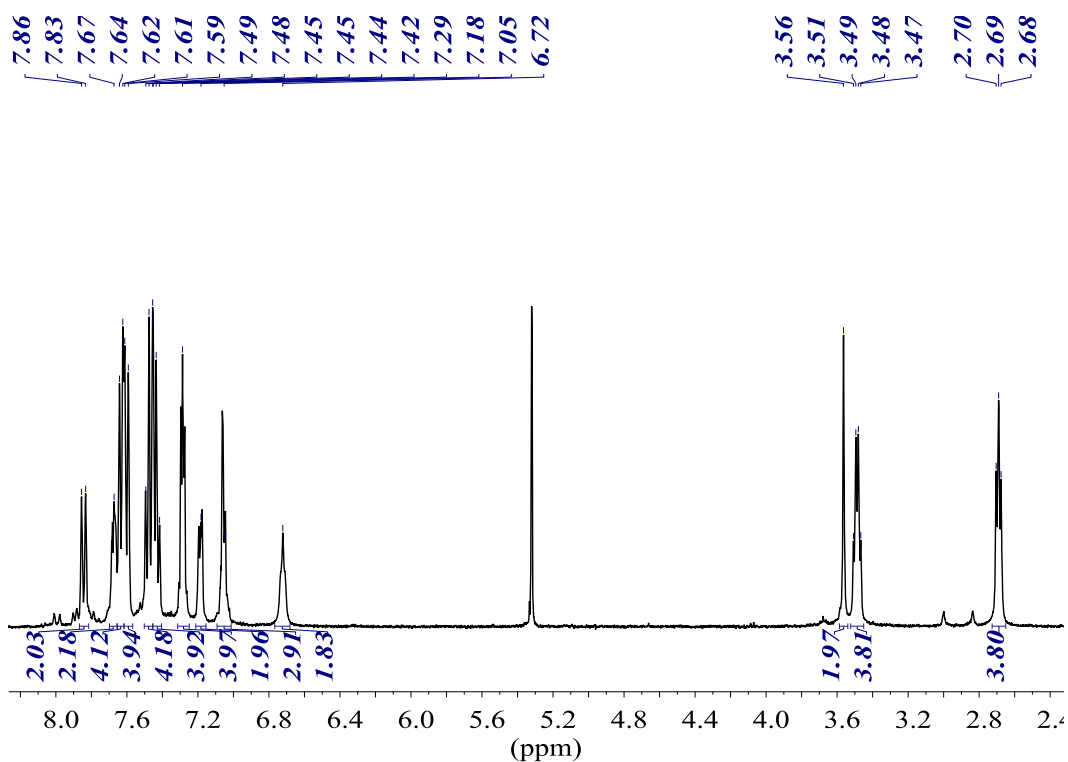


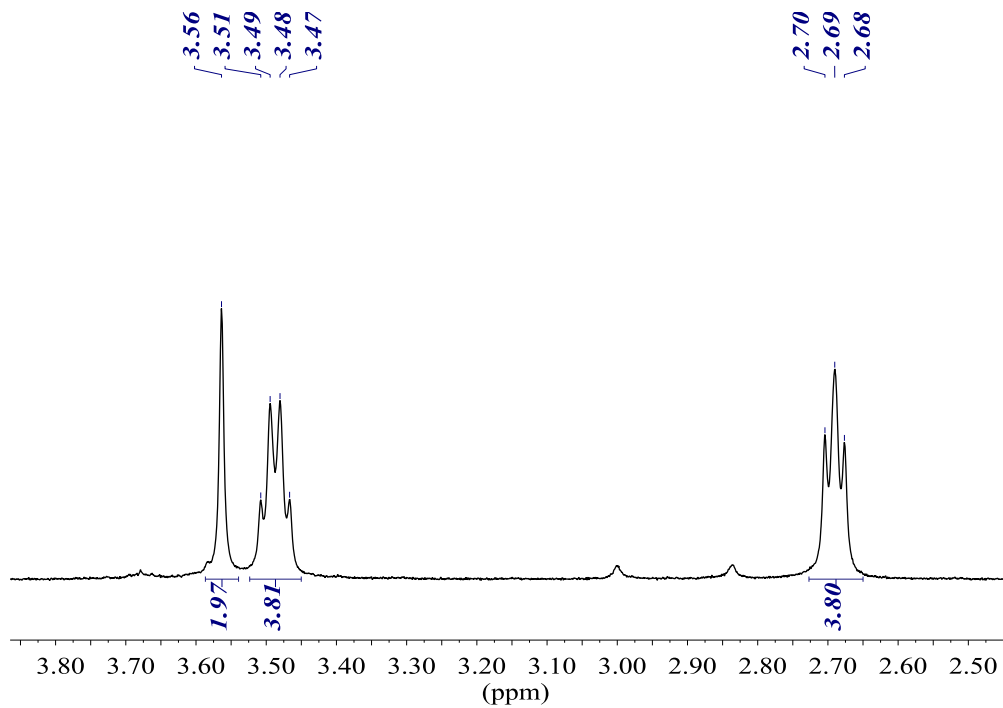
$^{31}\text{P}\{^1\text{H}\}$ NMR (161.98 MHz, CD_2Cl_2)

--4.62

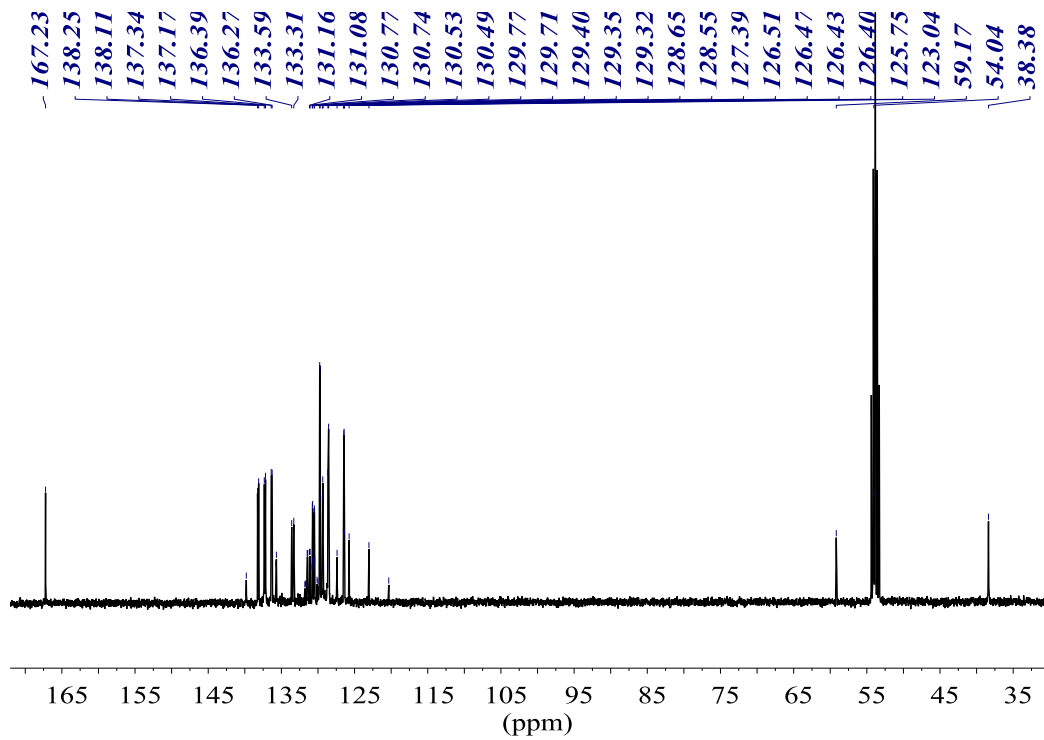


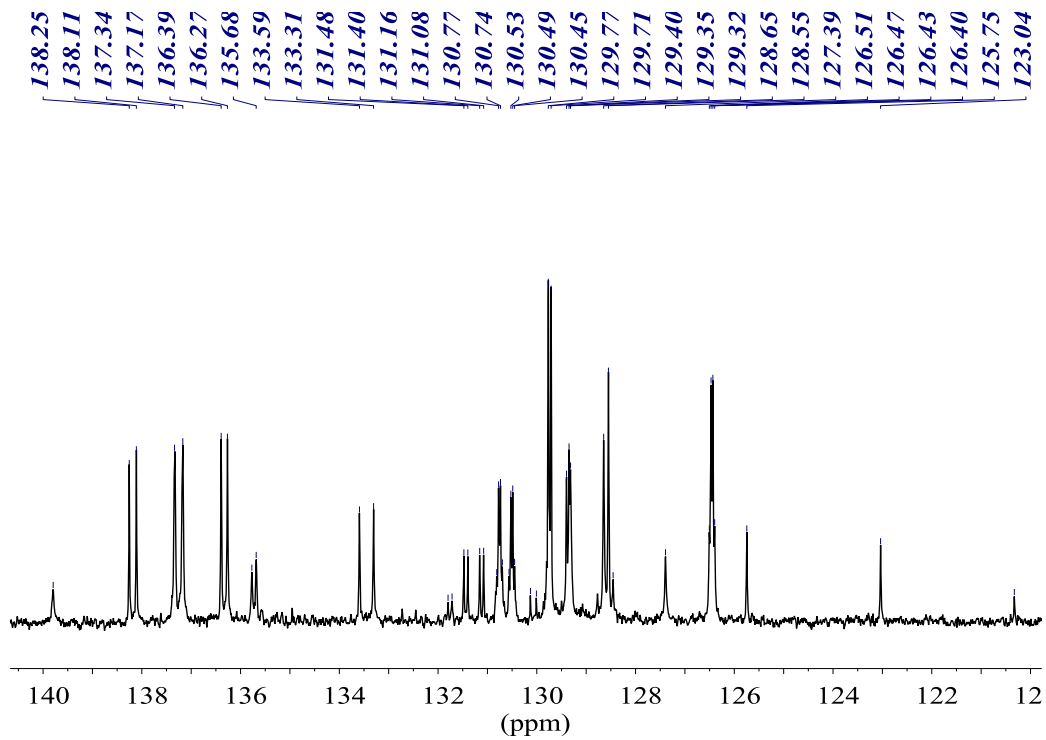
^1H NMR (400.13 MHz, CD_2Cl_2)



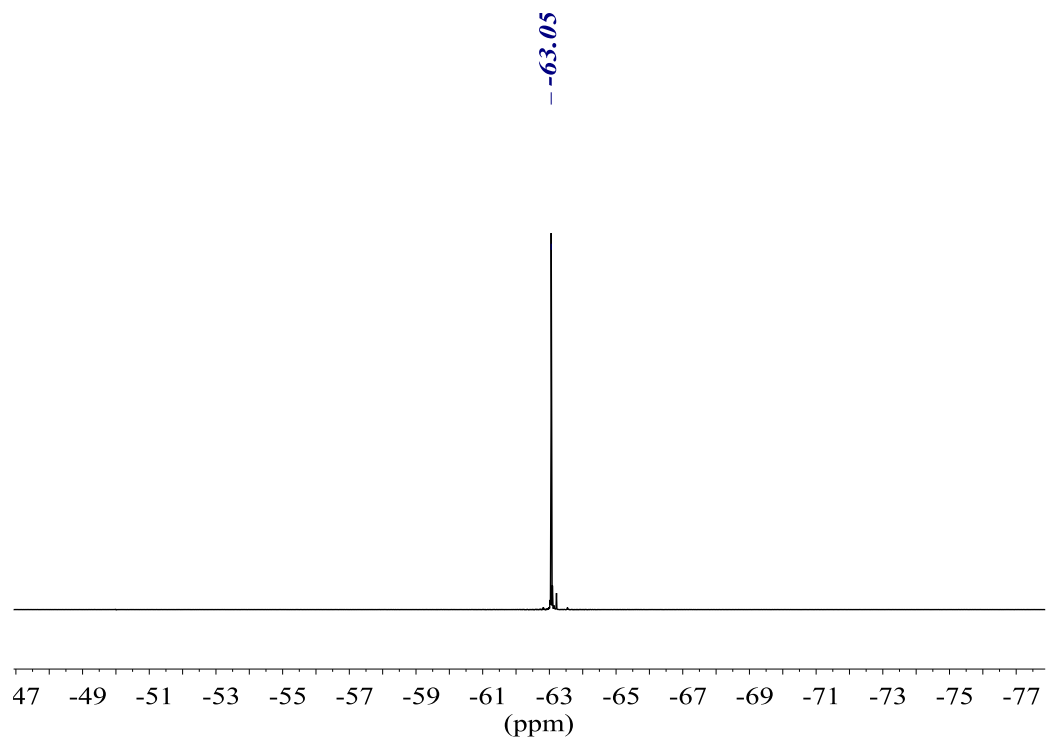


¹³C {¹H} NMR (100.61 MHz, CD₂Cl₂)

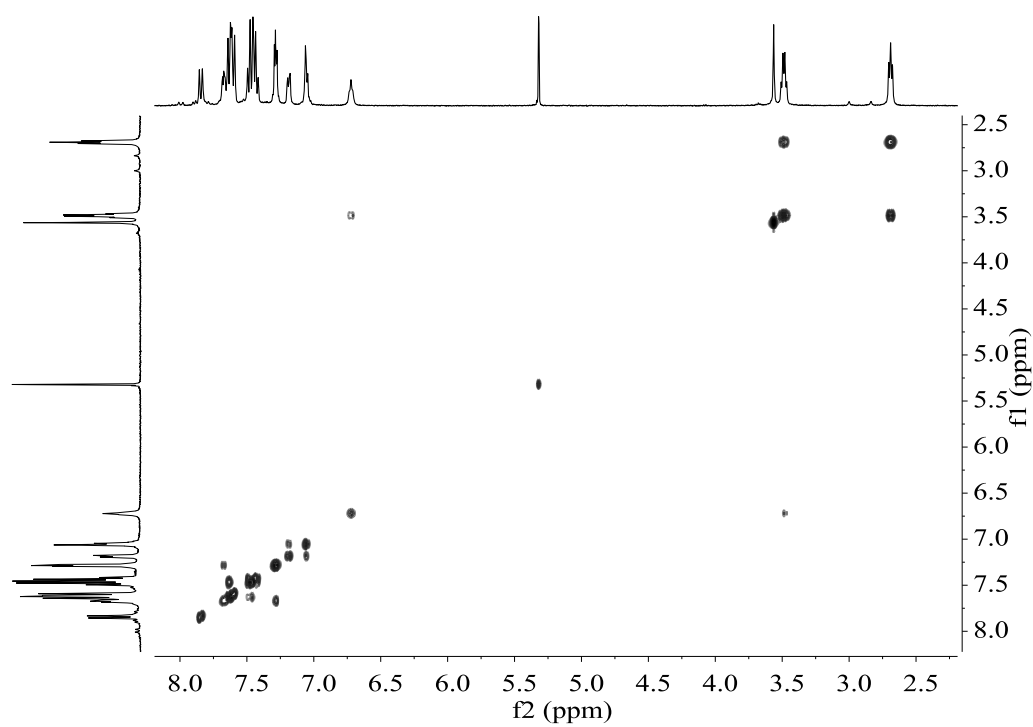




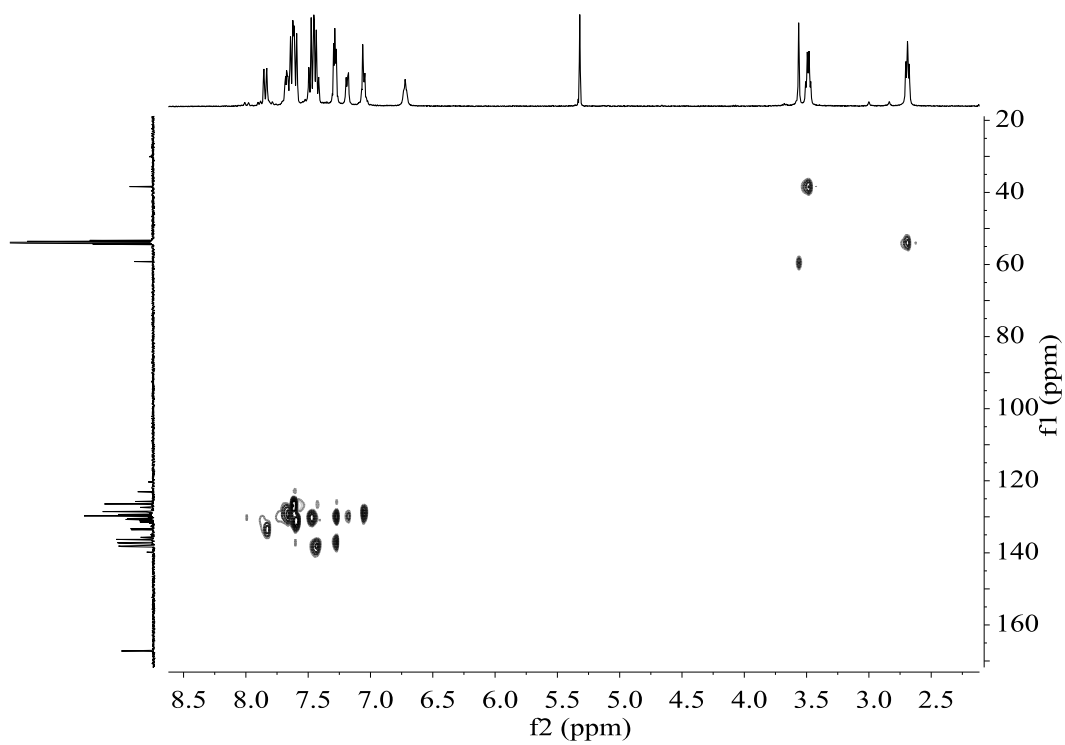
$^{19}\text{F}\{^1\text{H}\}$ NMR (376.50 MHz, CD_2Cl_2)

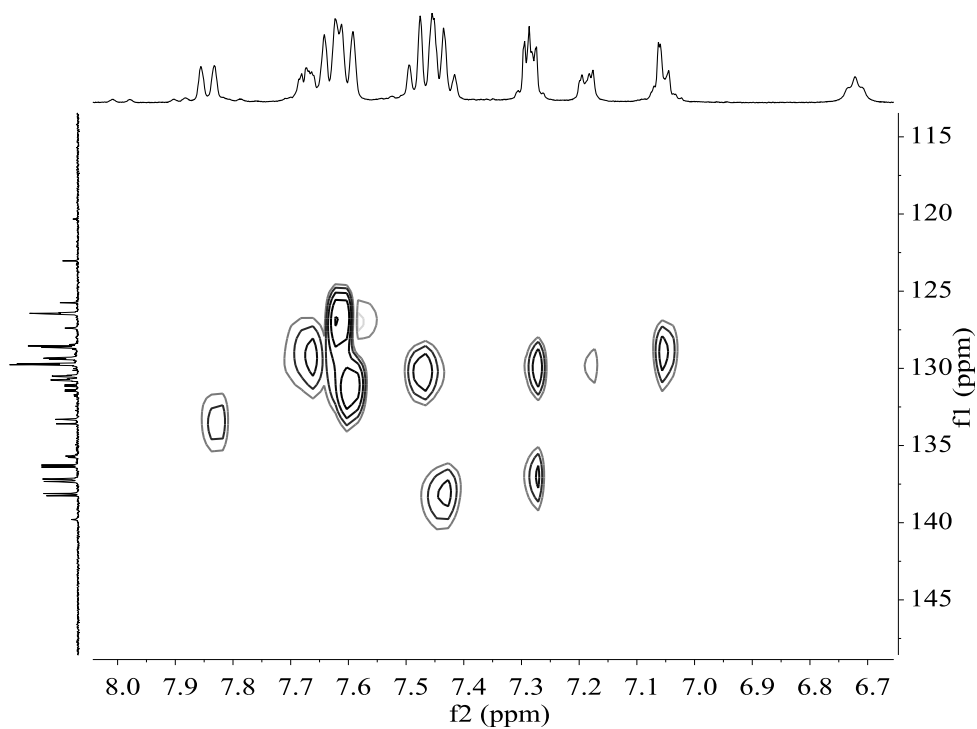


COSY NMR (400.13 MHz, CD₂Cl₂)

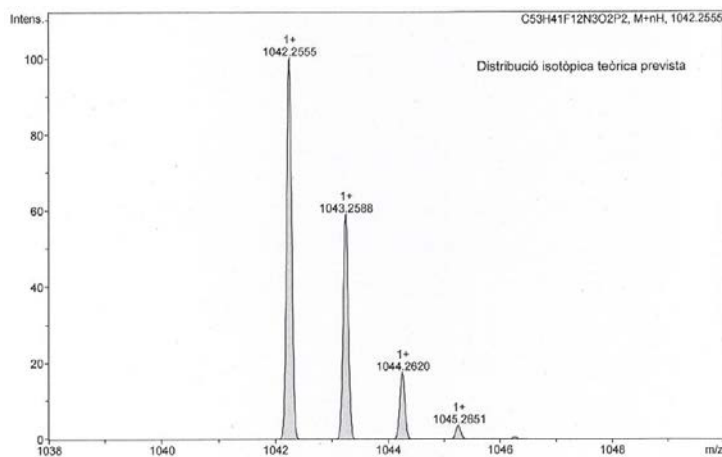


HSQC NMR (400.13 MHz, CD₂Cl₂)



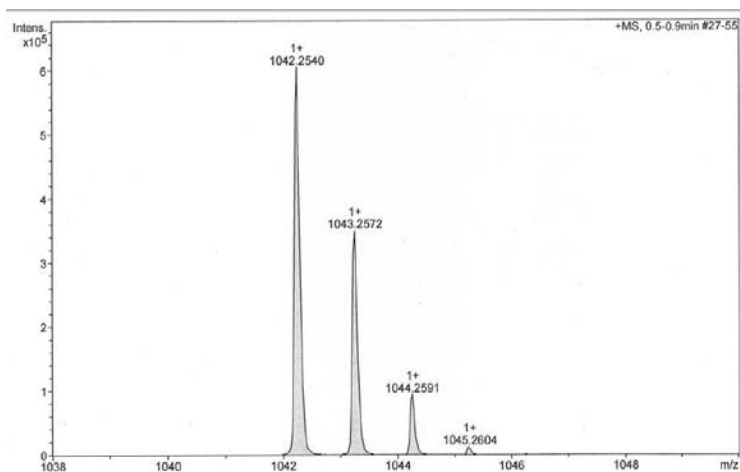


HR-MS (ESI⁺ *m/z*) [M+H]⁺
 calculated for [C₅₃H₄₂F₁₂N₃O₂P₂]⁺



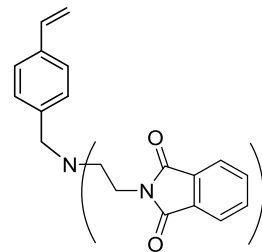
#	<i>m/z</i>	I	I %
1	1042.2555	100	100.0
2	1043.2588	59	58.9
3	1044.2620	17	17.4
4	1045.2651	3	3.5

found

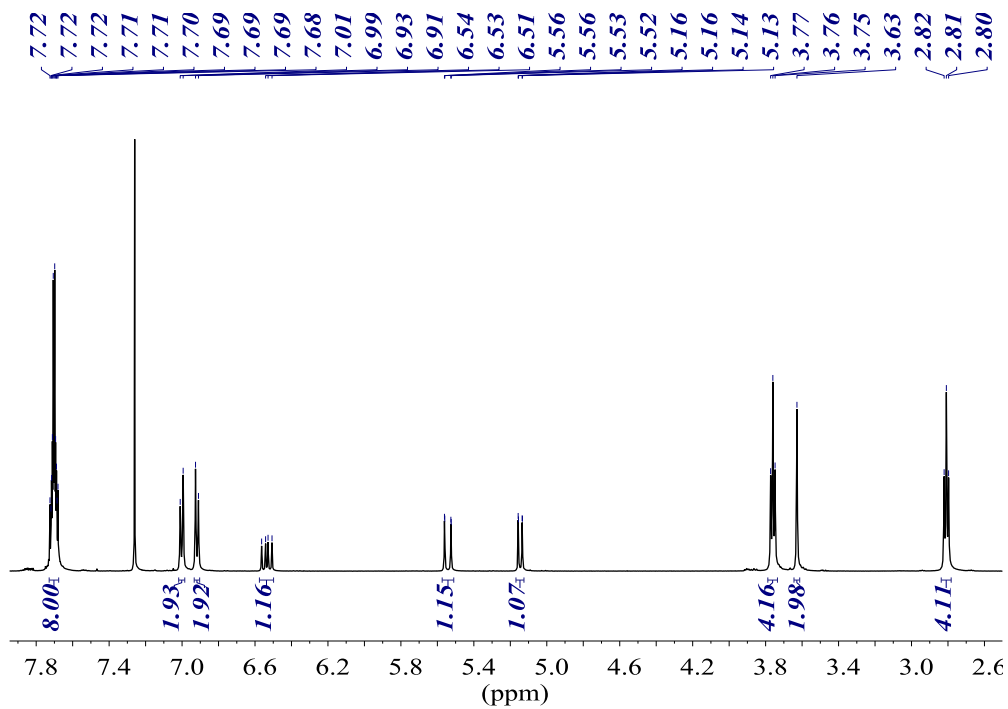


#	<i>m/z</i>	I	I %
1	1042.2540	603815	100.0
2	1043.2572	348870	57.8
3	1044.2591	93084	15.4
4	1045.2604	11904	2.0

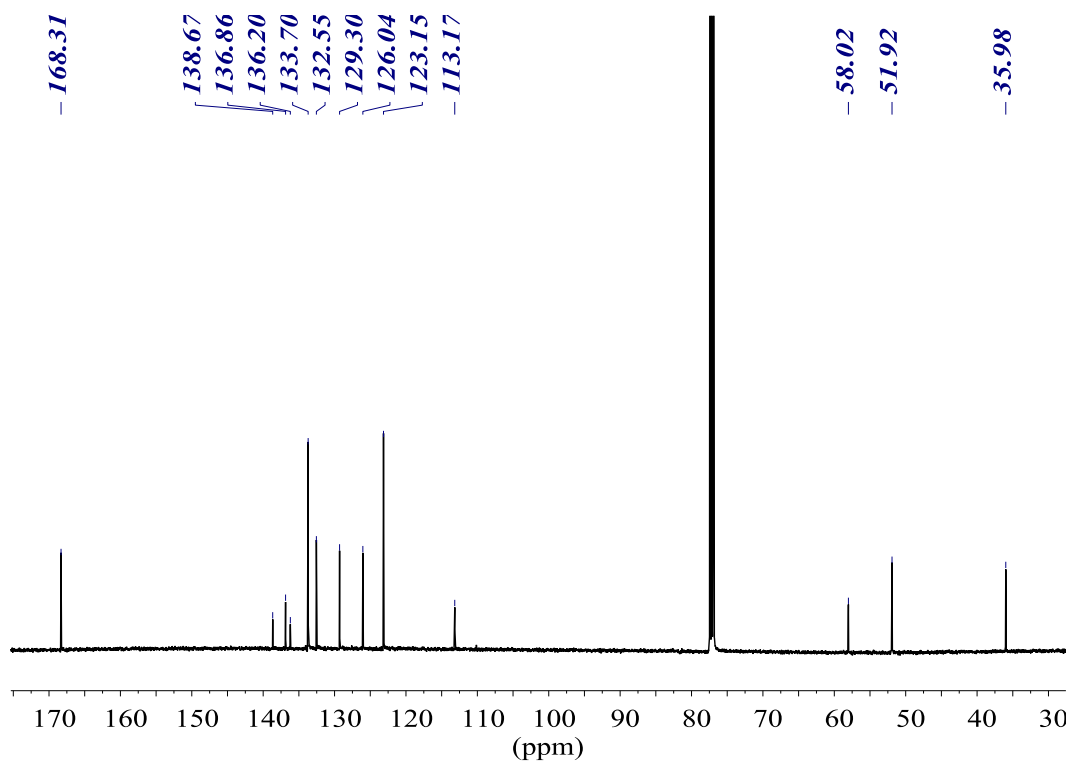
(4-Vinylbenzyl)-bis(2-phthalimidoethyl)amine (39-st)



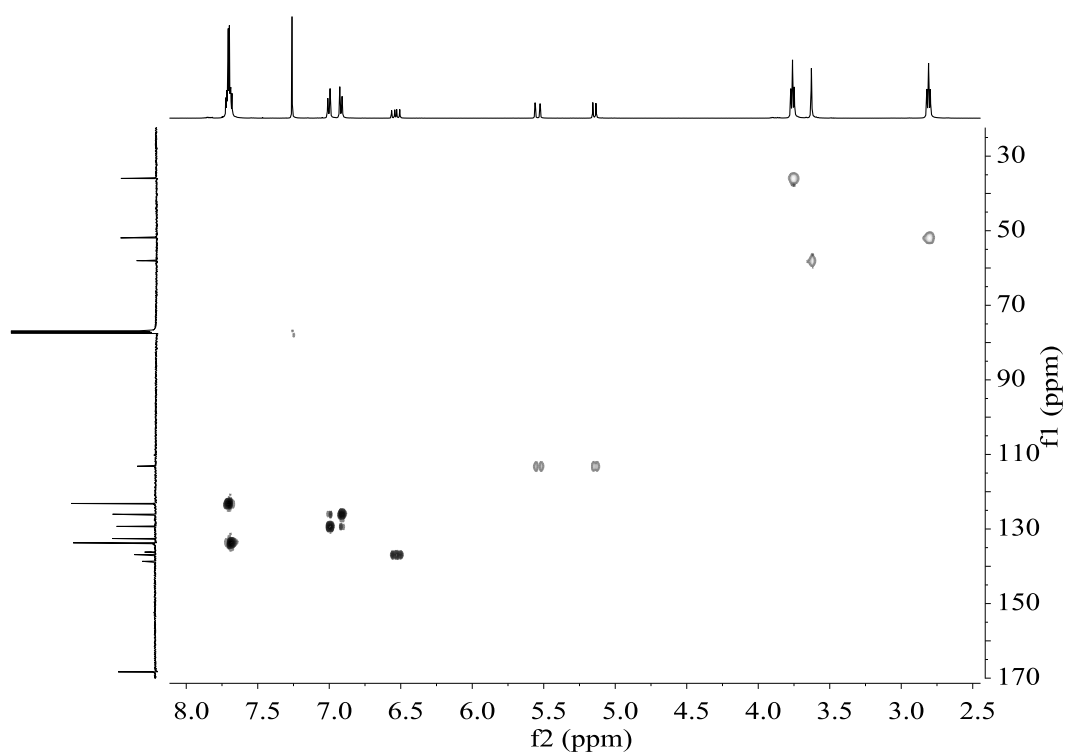
^1H NMR (500.13 MHz, CDCl_3)



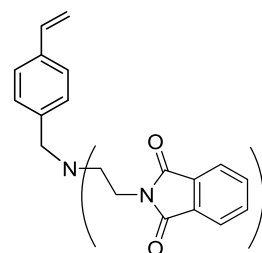
$^{13}\text{C}\{^1\text{H}\}$ NMR (125.80 MHz, CDCl_3)



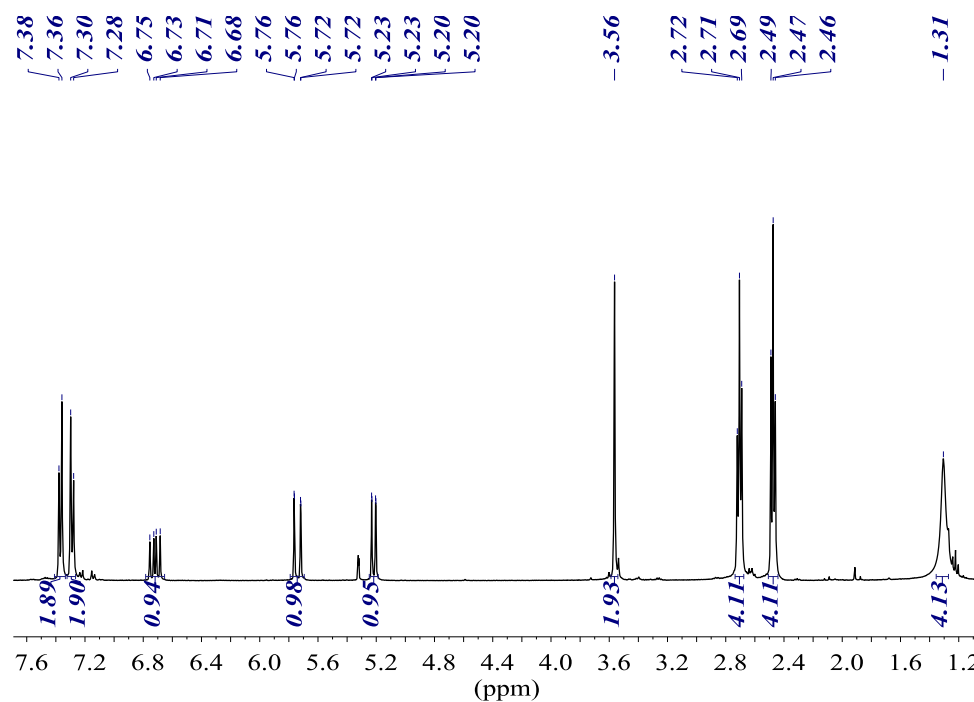
HSQC NMR (500.13 MHz, CDCl₃)



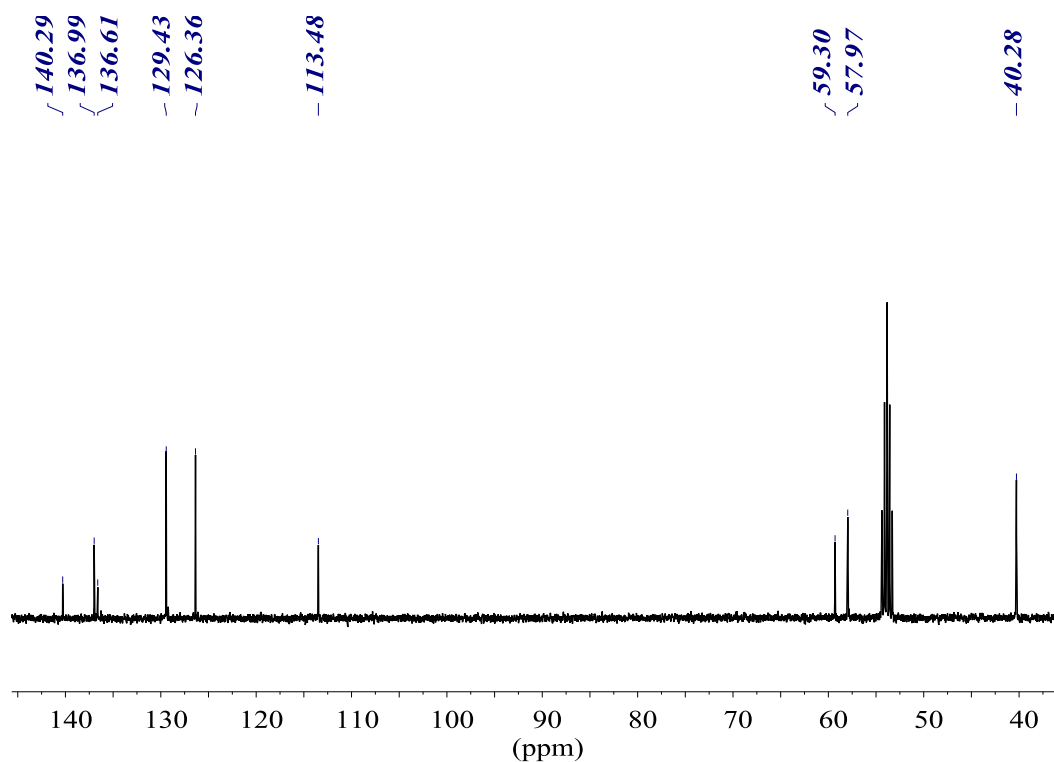
4-(4-Vinylbenzyl)diethylenetriamine (40-st)



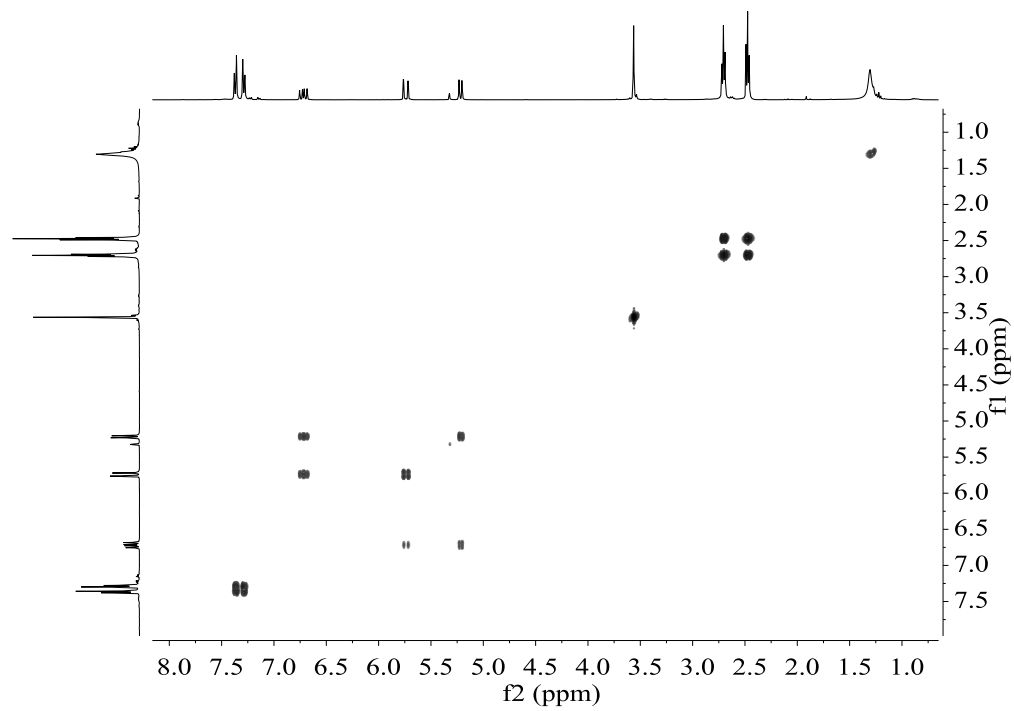
¹H NMR (400.13 MHz, CD₂Cl₂)



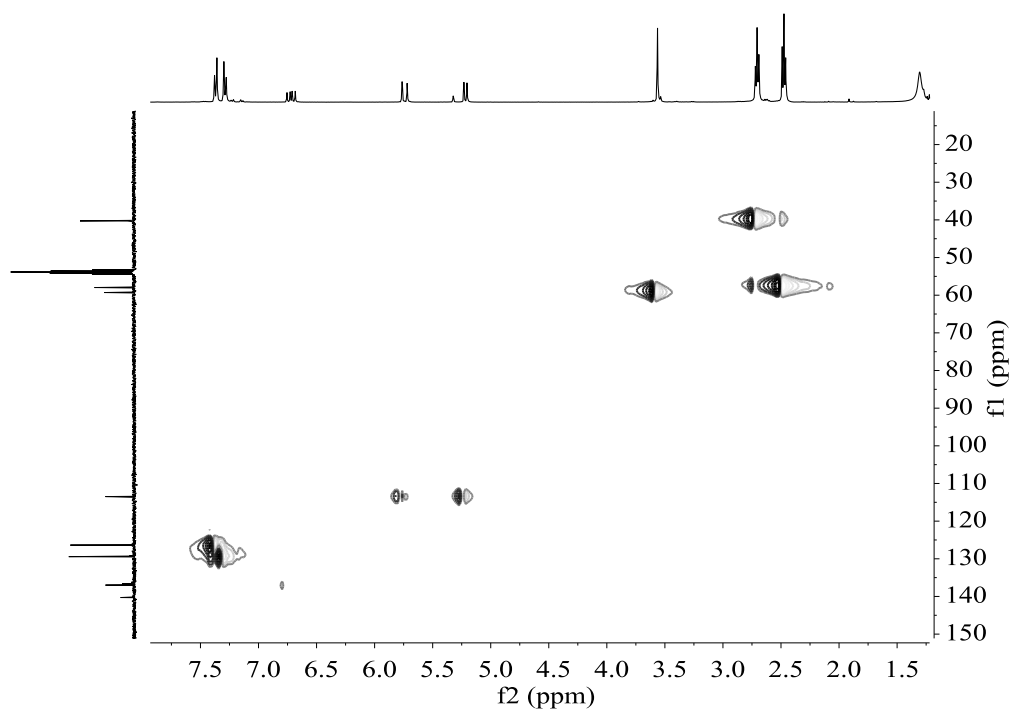
$^{13}\text{C}\{^1\text{H}\}$ NMR (100.61 MHz, CD_2Cl_2)



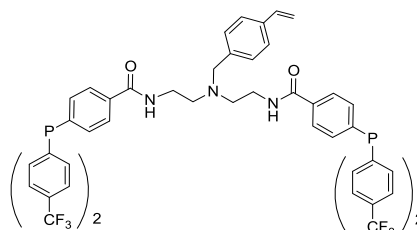
COSY NMR (400.13 MHz, CD_2Cl_2)



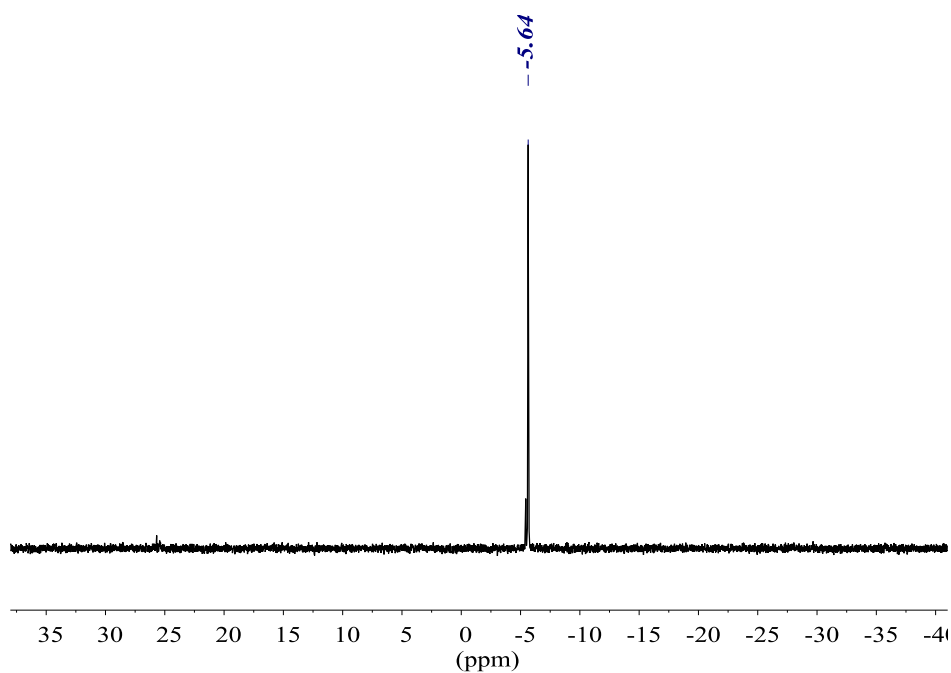
HSQC NMR (400.13 MHz, CD₂Cl₂)

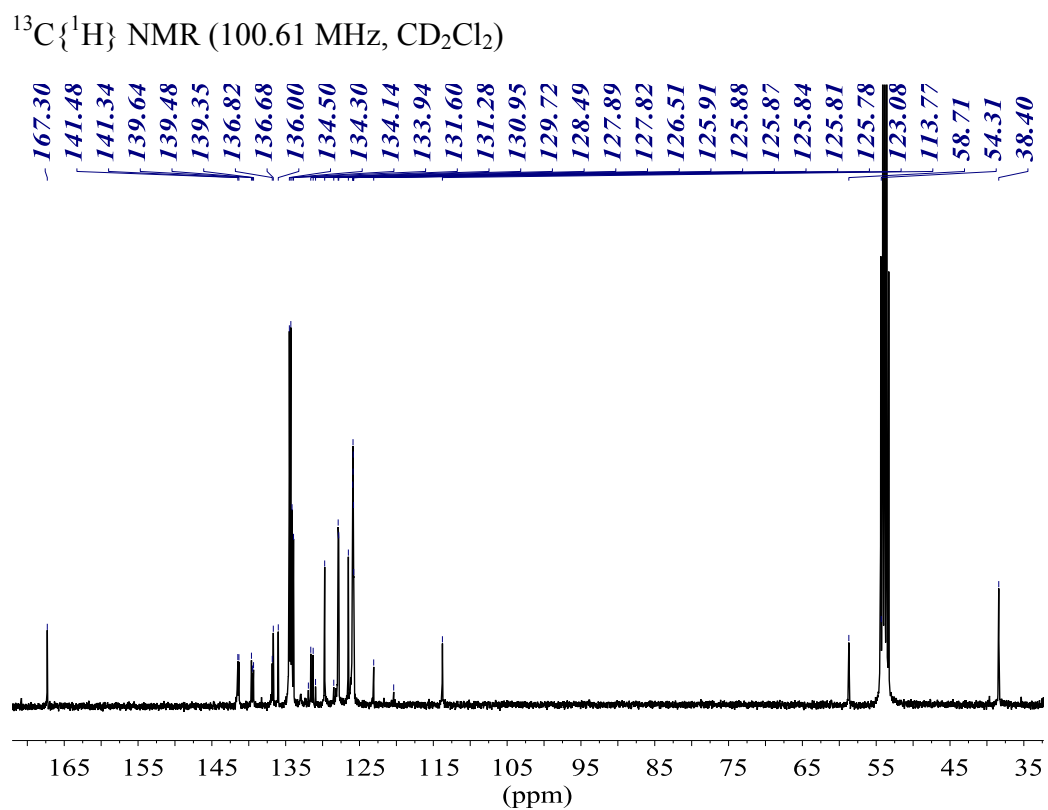
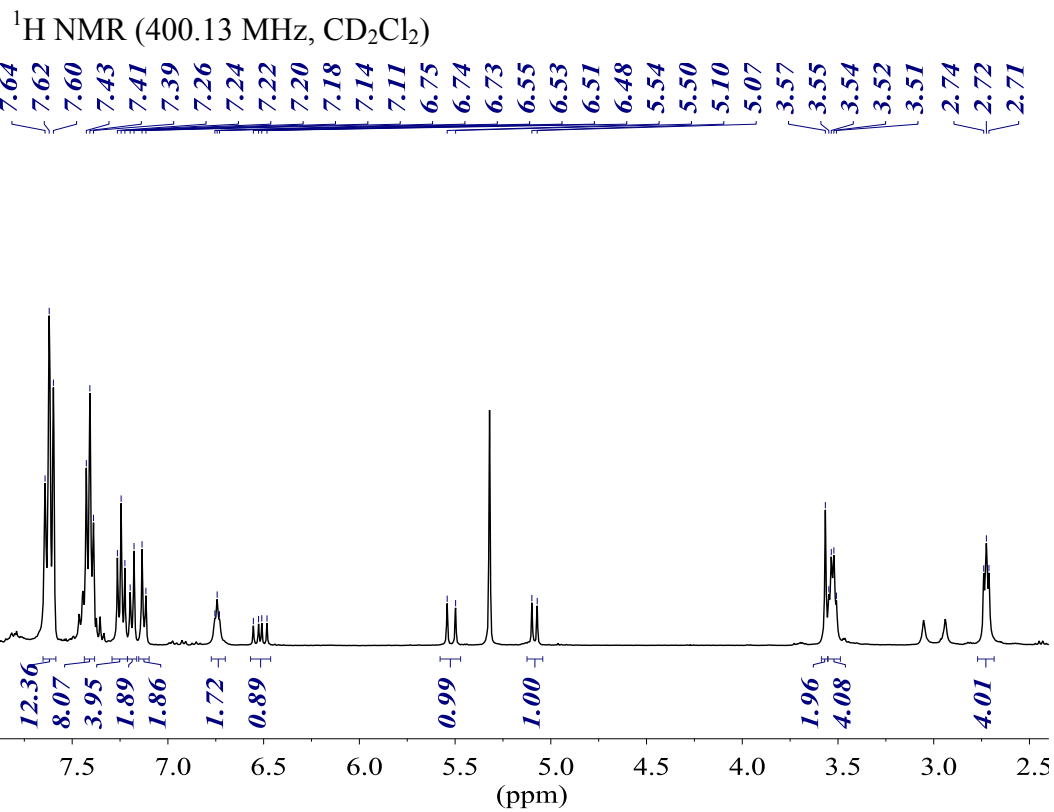


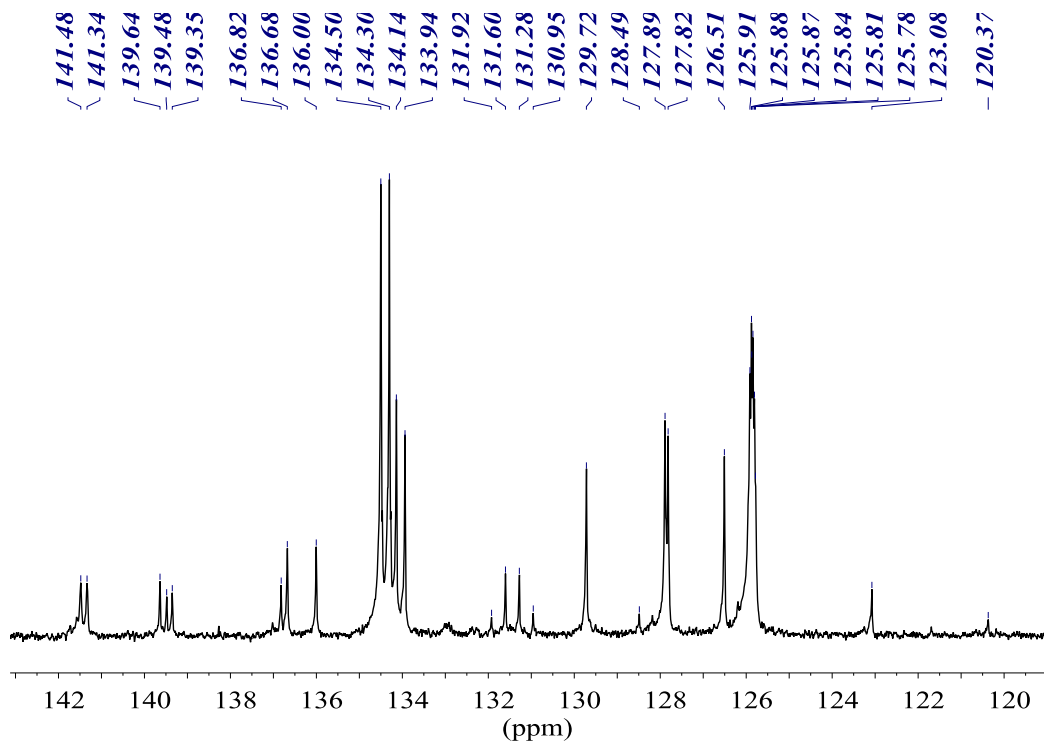
Diphosphine-diamide P-st



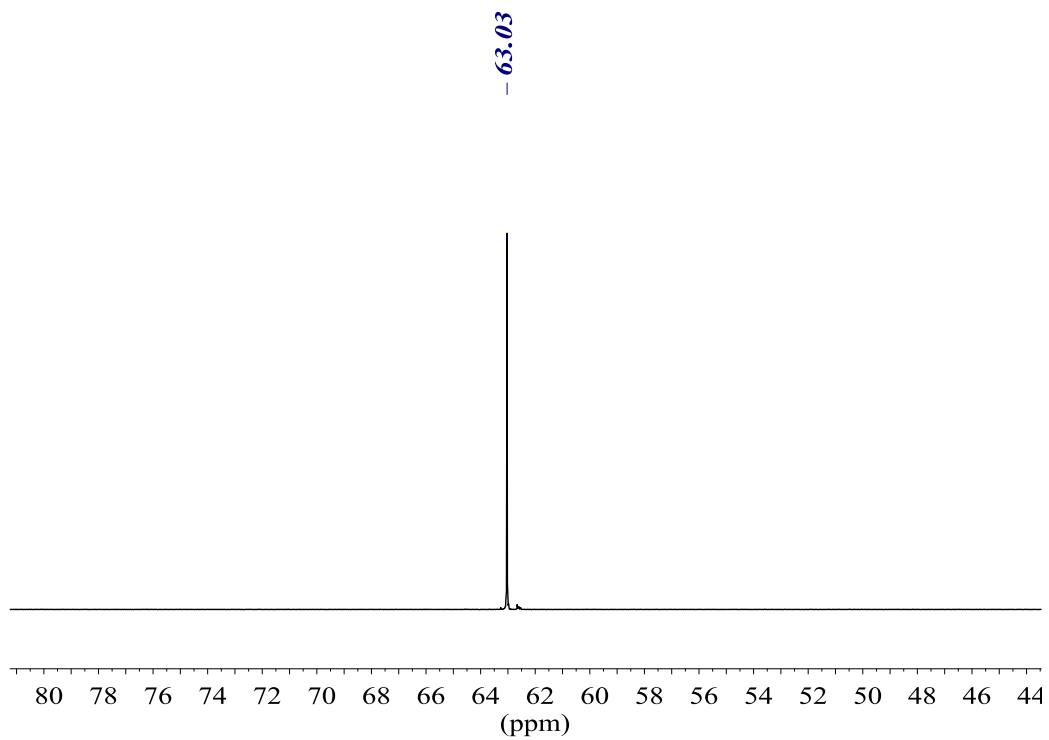
³¹P{¹H} NMR (161.98 MHz, CD₂Cl₂)



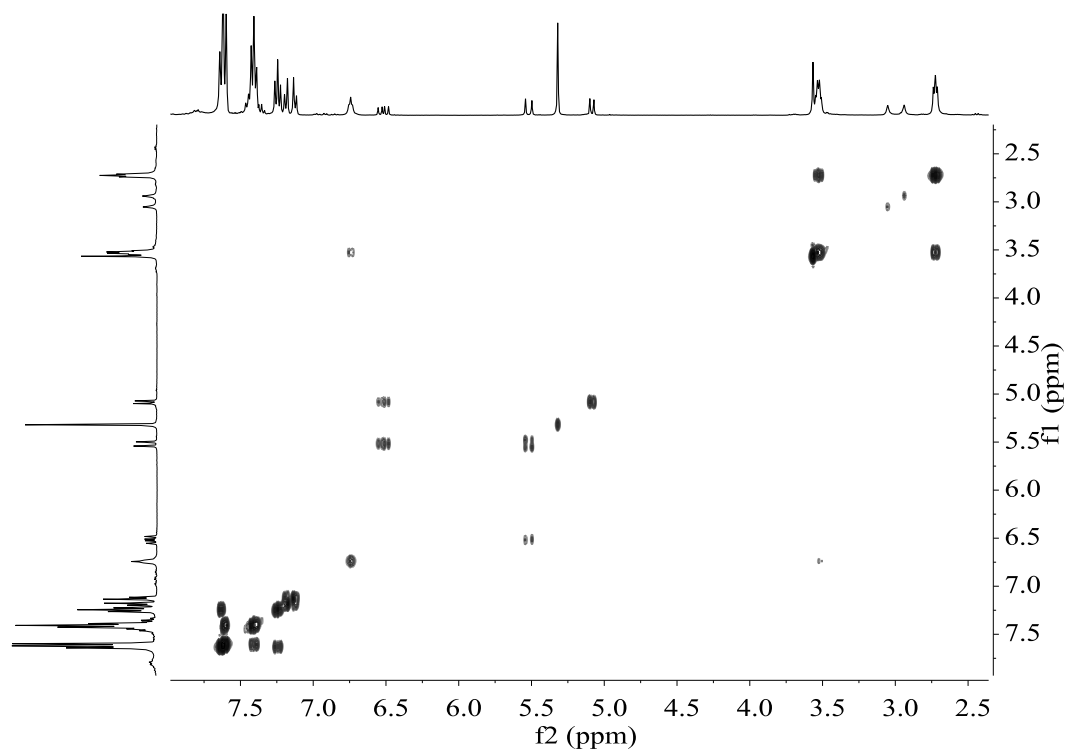




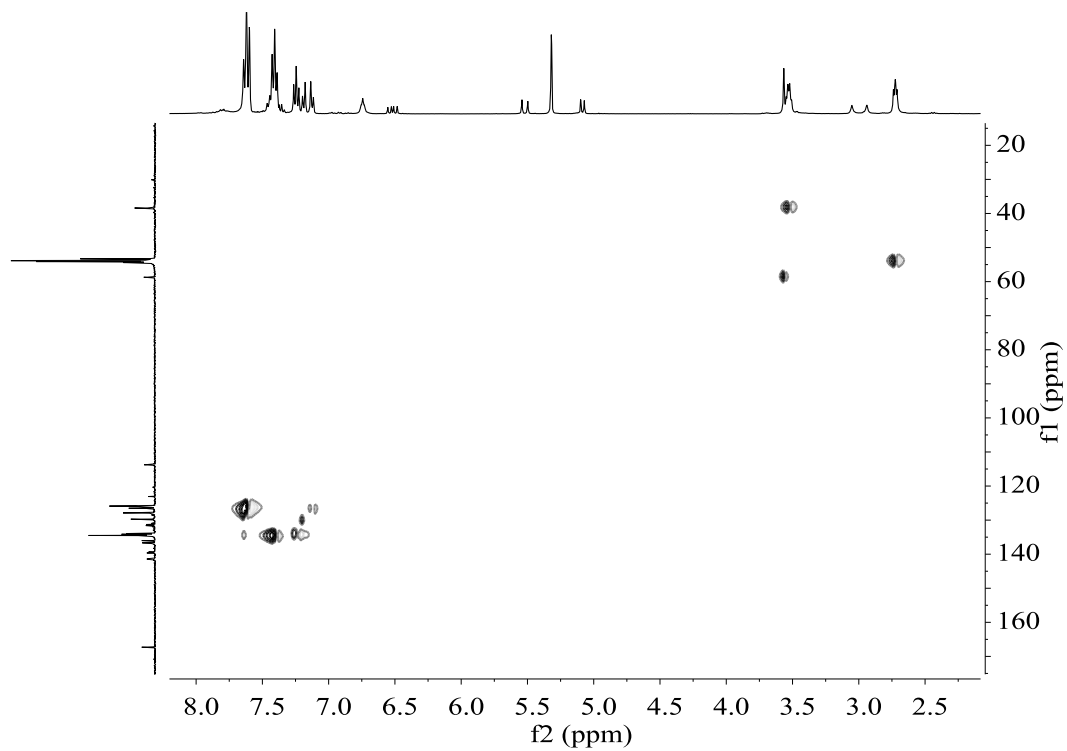
$^{19}\text{F}\{^1\text{H}\}$ NMR (376.50 MHz, CD_2Cl_2)

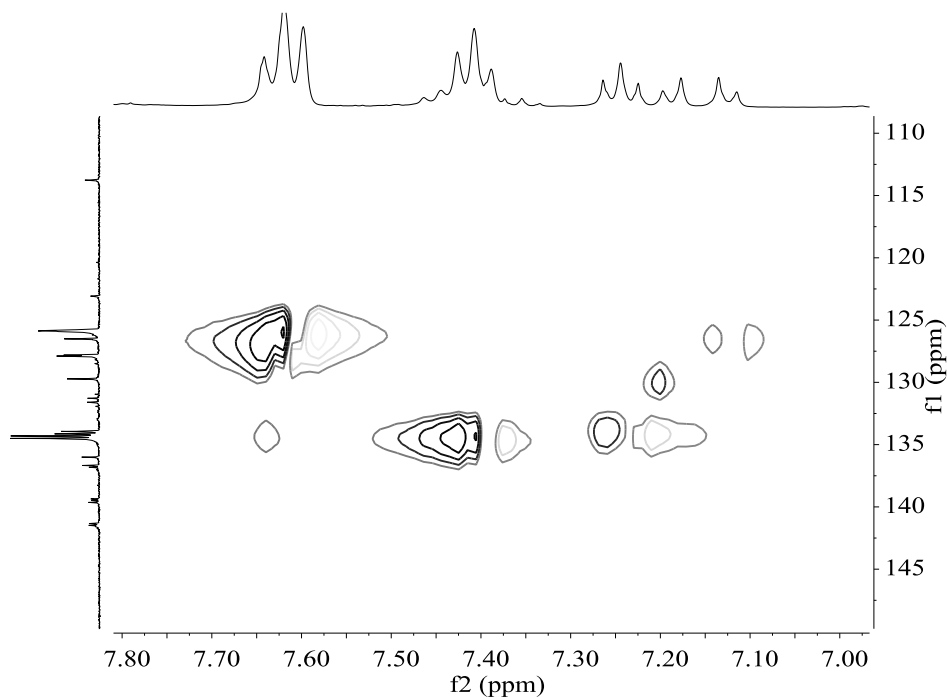


COSY NMR (400.13 MHz, CD₂Cl₂)



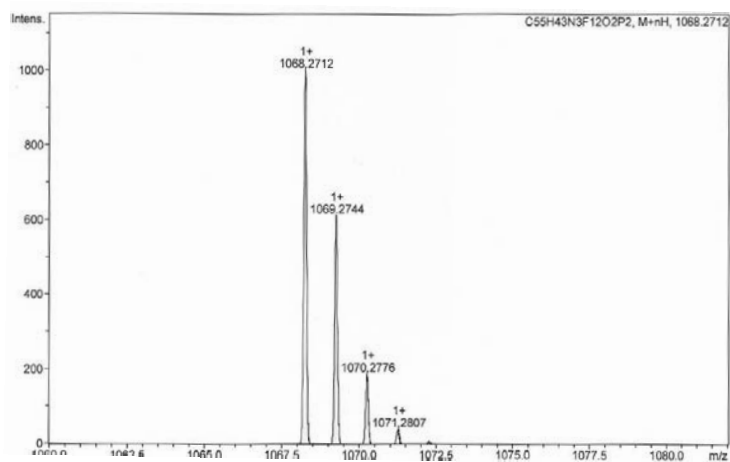
HSQC NMR (400.13 MHz, CD₂Cl₂)





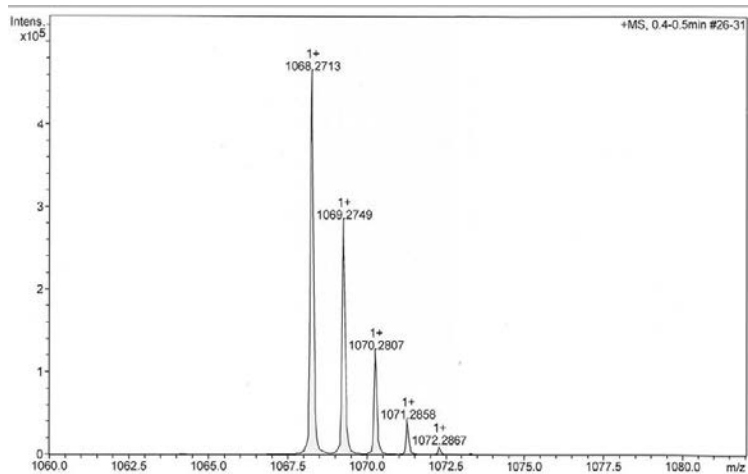
HR-MS (ESI⁺ *m/z*) [M+H]⁺

calculated for [C₅₅H₄₄F₁₂N₃O₂P₂]⁺



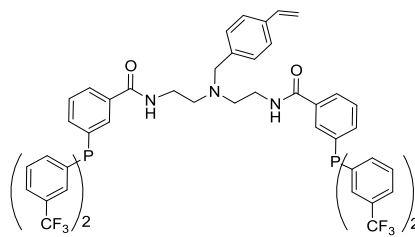
#	<i>m/z</i>	I	I %
1	1068.2712	1000	100.0
2	1069.2744	611	61.1
3	1070.2776	187	18.7
4	1071.2807	39	3.9

found

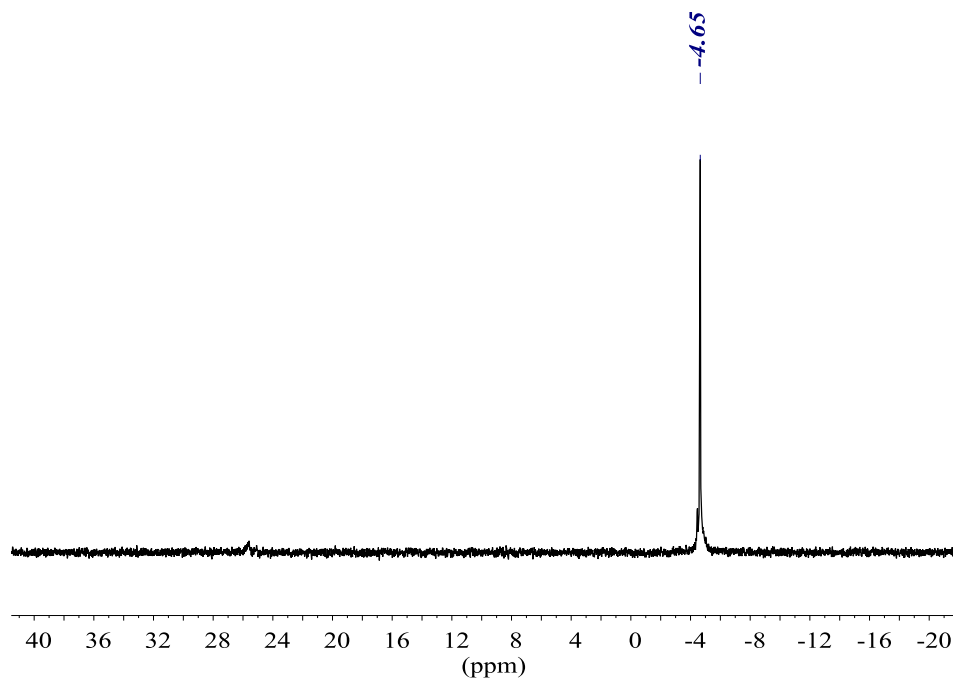


#	<i>m/z</i>	I	I %
1	1068.2713	462325	100.0
2	1069.2749	282504	61.1
3	1070.2807	124339	26.9
4	1071.2858	41207	8.9
5	1072.2867	9503	2.1

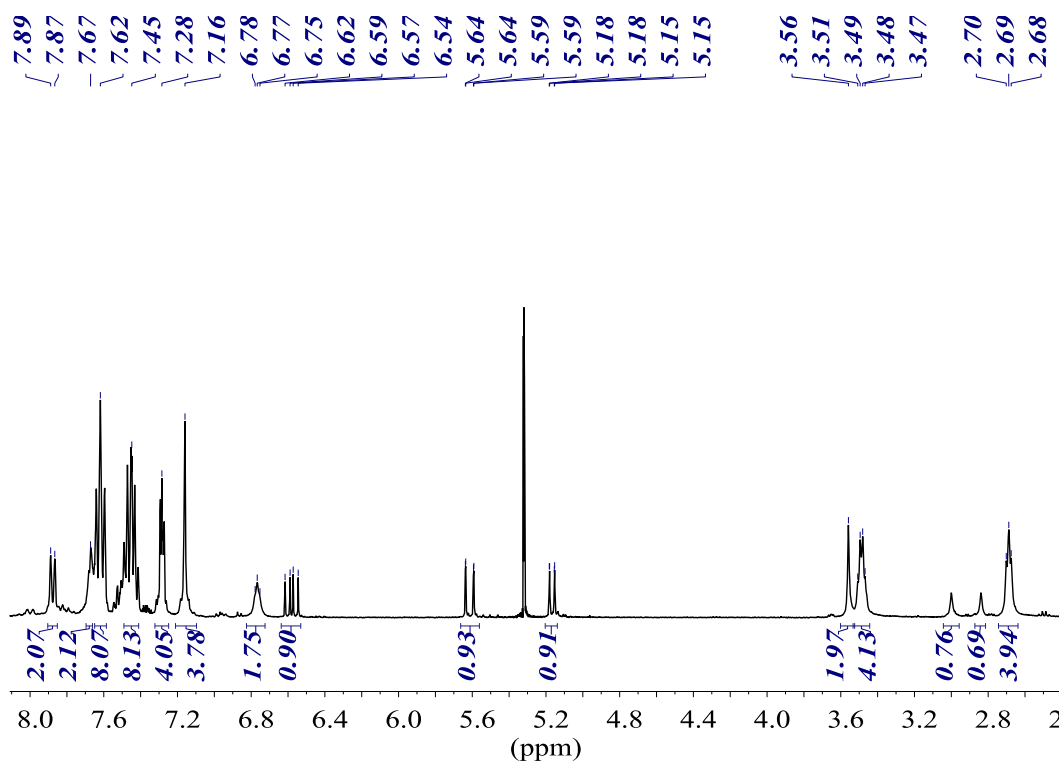
Diphosphine-diamide M-st



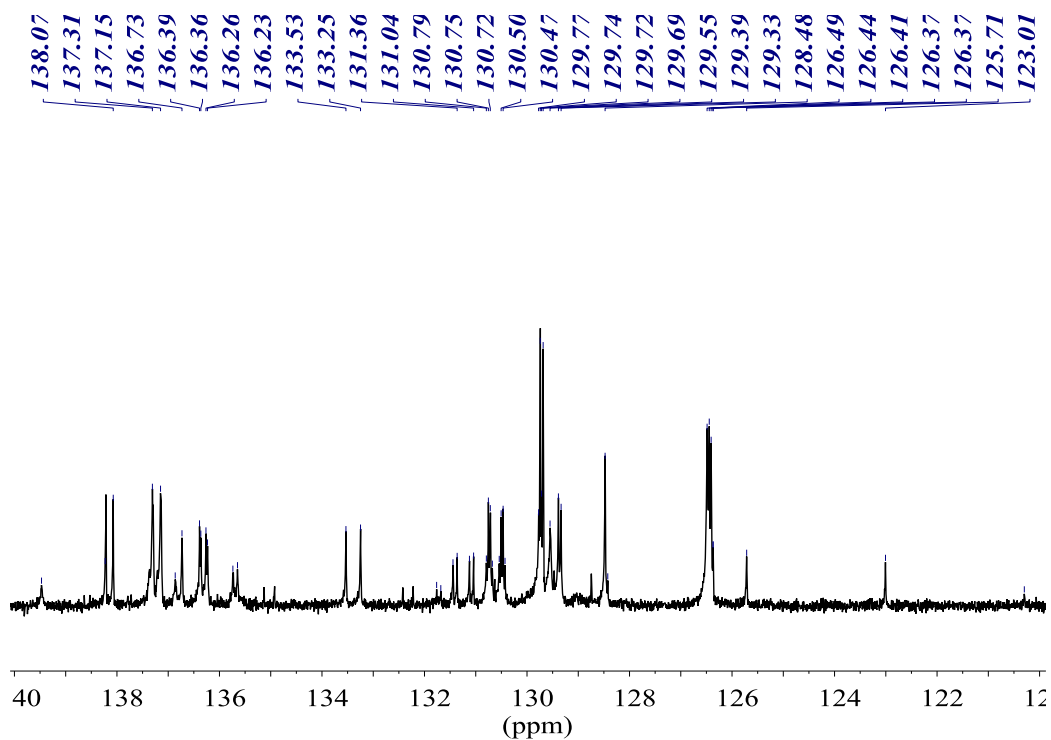
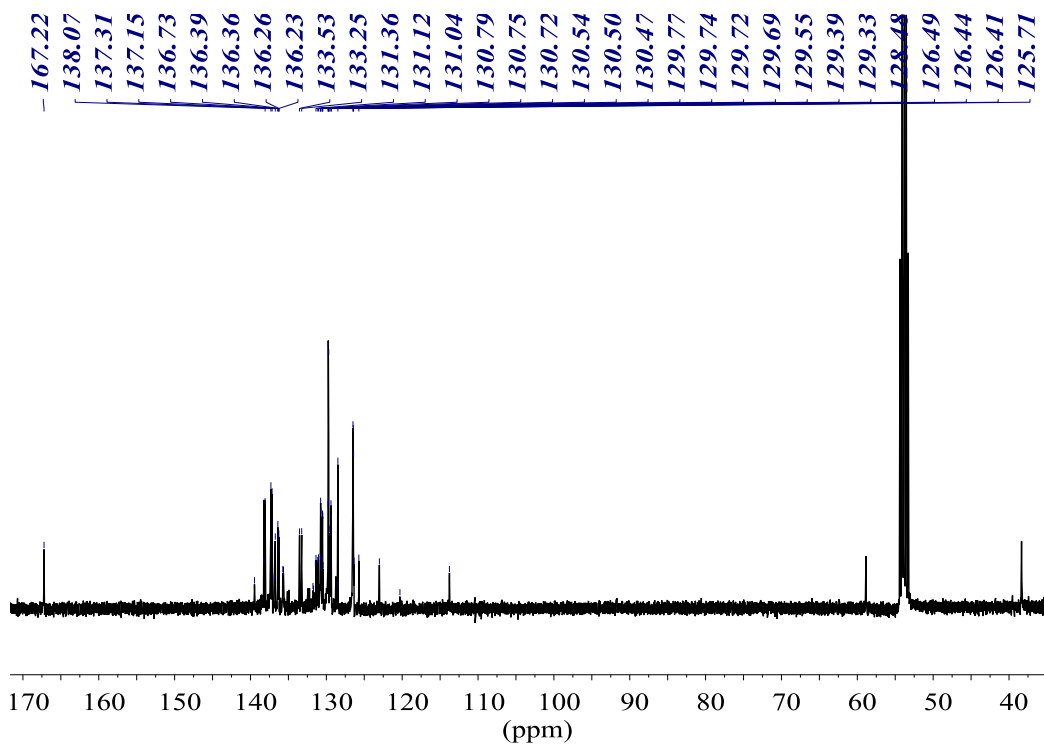
$^{31}\text{P}\{^1\text{H}\}$ NMR (161.98 MHz, CD_2Cl_2)



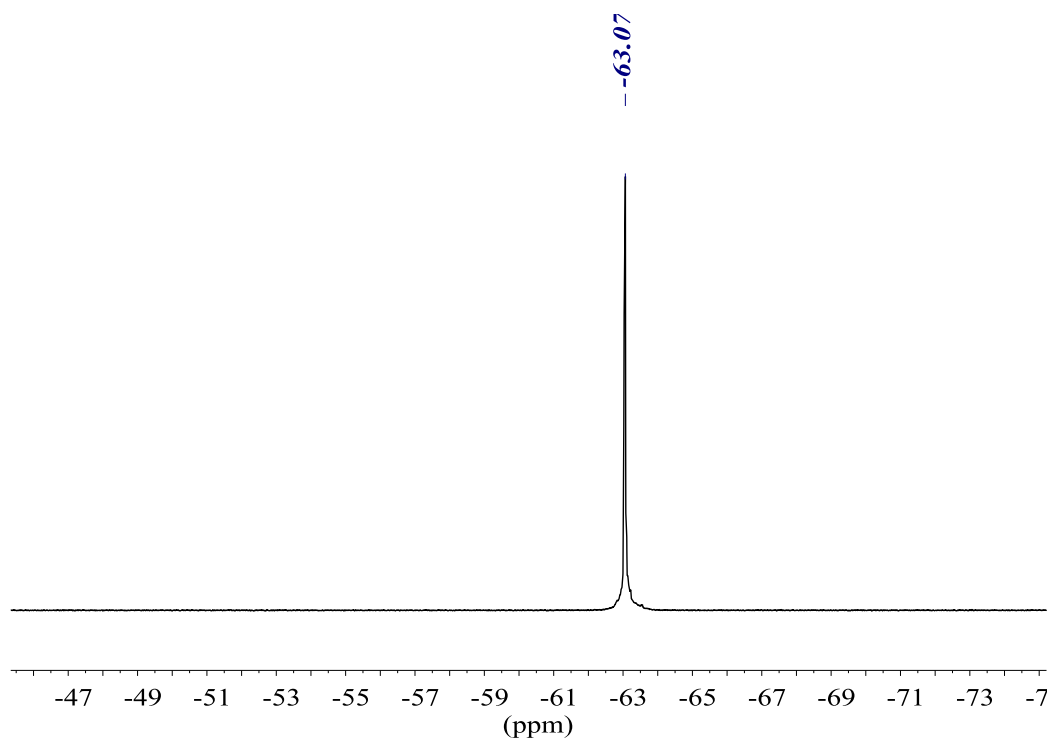
^1H NMR (400.13 MHz, CD_2Cl_2)



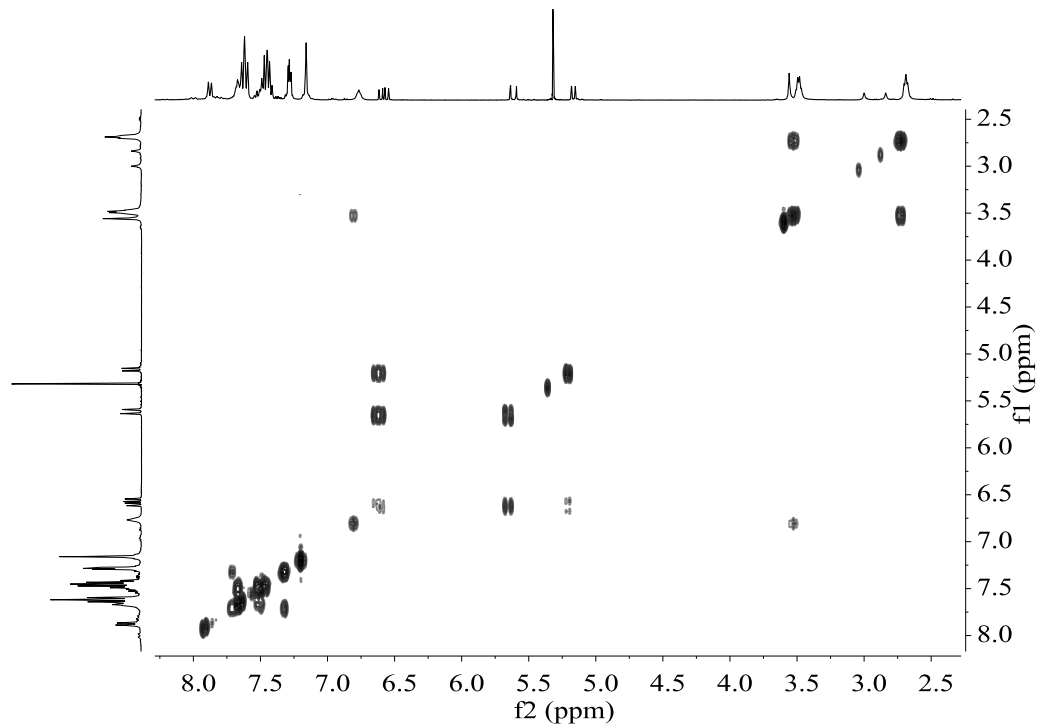
$^{13}\text{C}\{^1\text{H}\}$ NMR (100.61 MHz, CD_2Cl_2)



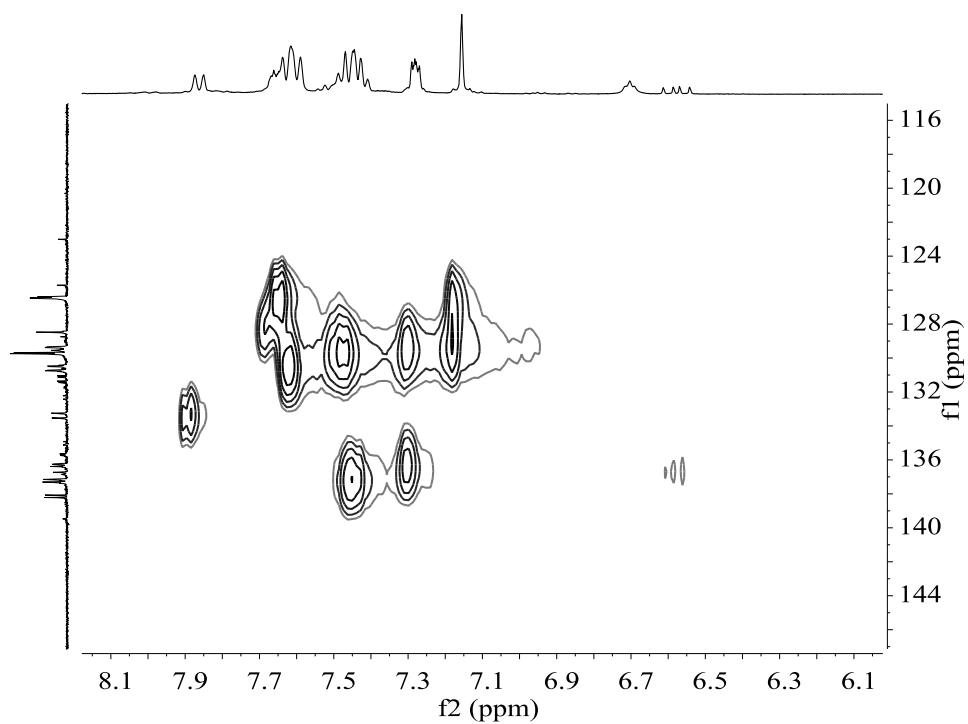
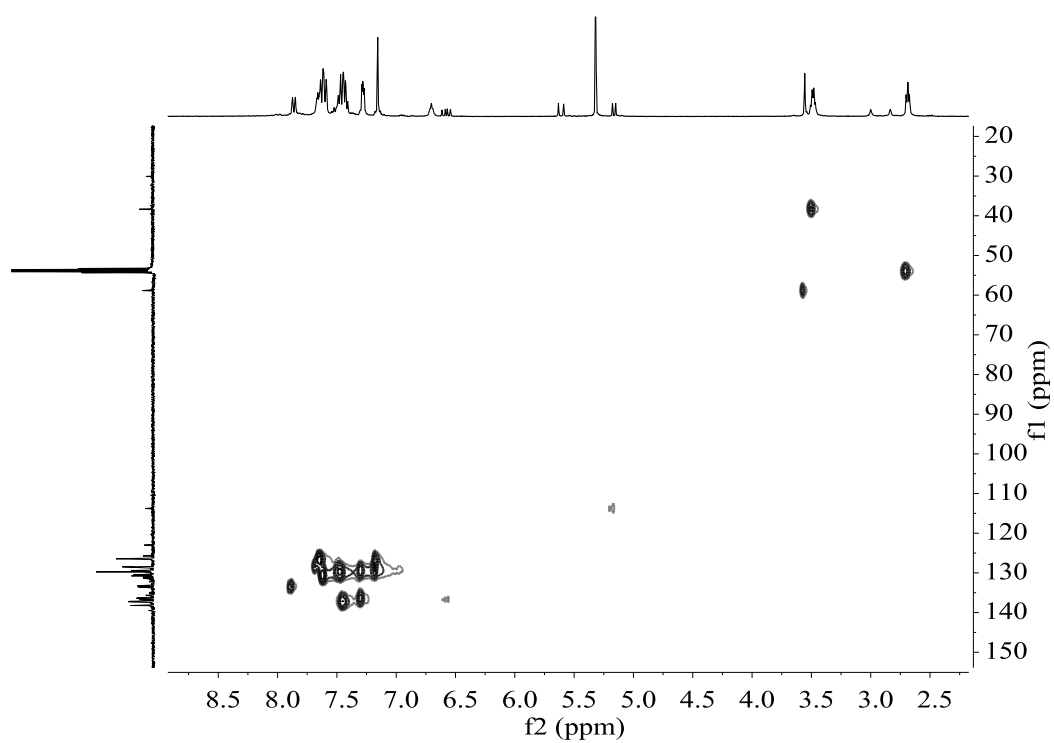
$^{19}\text{F}\{^1\text{H}\}$ NMR (376.50 MHz, CD_2Cl_2)



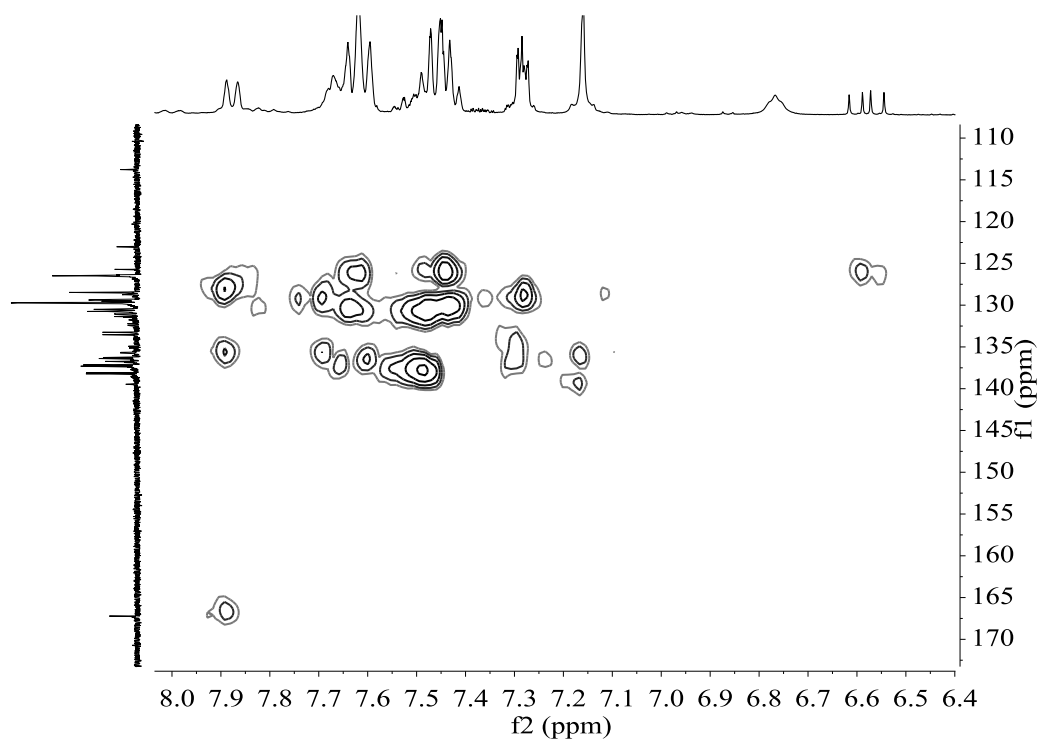
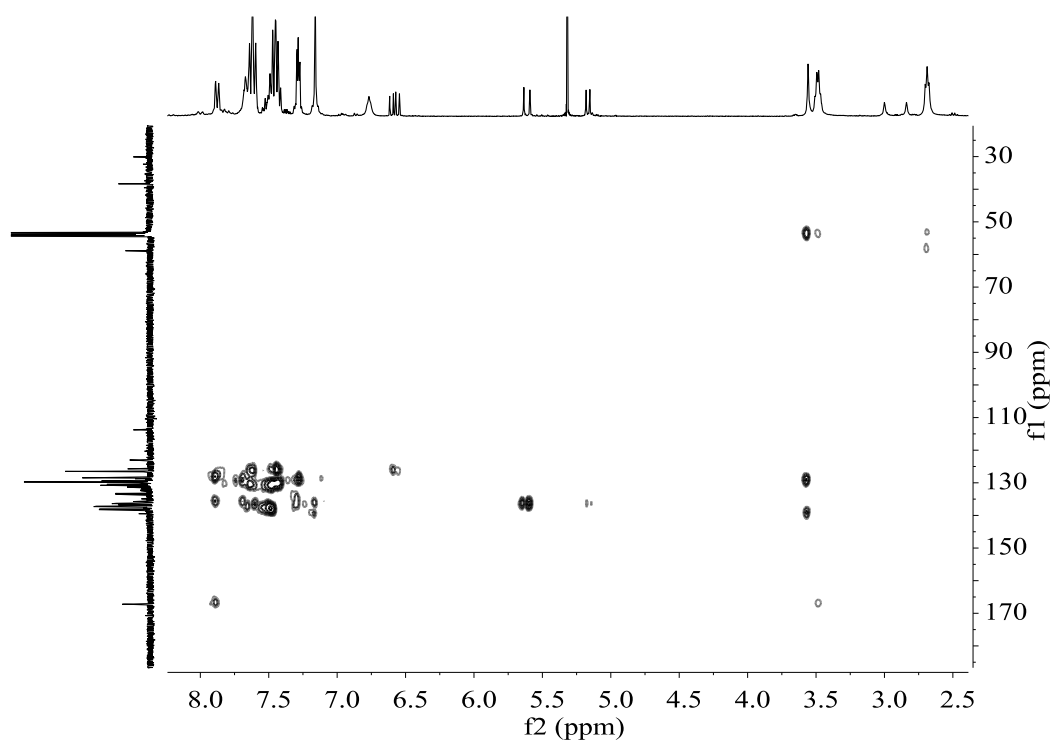
COSY NMR (400.13 MHz, CD_2Cl_2)



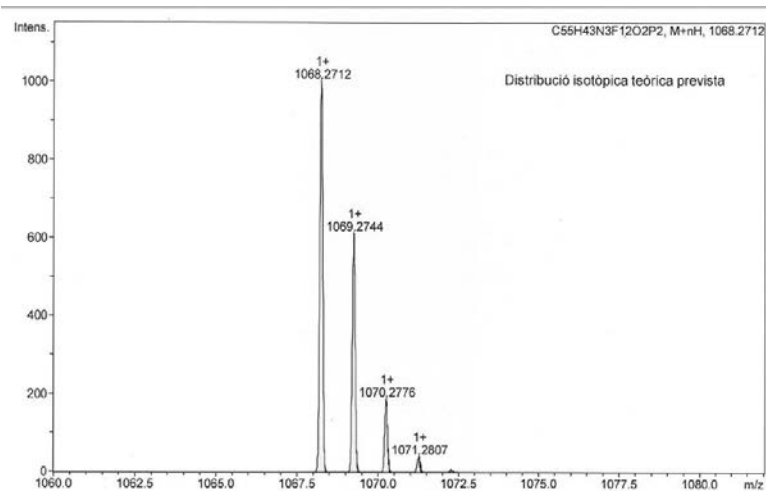
HSQC NMR (400.13 MHz, CD₂Cl₂)



HMBC NMR (400.13 MHz, CD₂Cl₂)

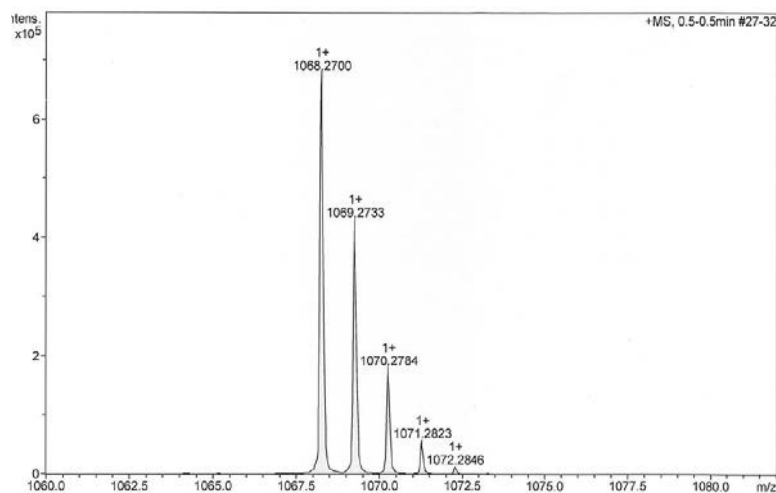


HR-MS (ESI⁺ m/z) [M+H]⁺
 calculated for [C₅₅H₄₄F₁₂N₃O₂P₂]⁺



#	m/z	I	I %
1	1068.2712	1000	100.0
2	1069.2744	611	61.1
3	1070.2776	187	18.7
4	1071.2807	39	3.9

found



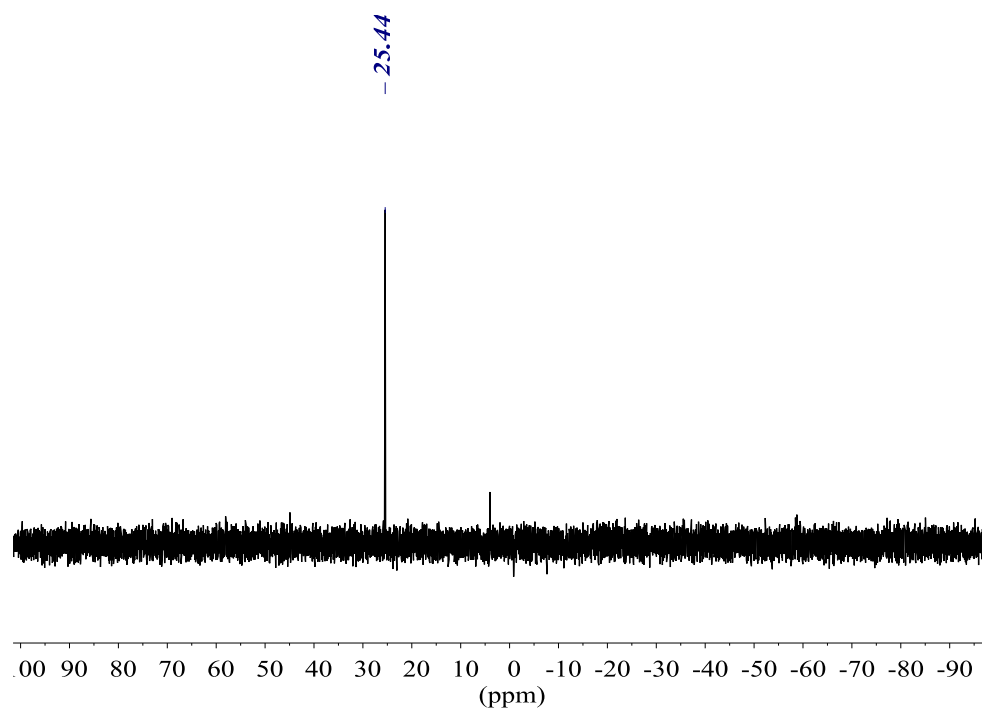
#	m/z	I	I %
1	1068.2700	678381	100.0
2	1069.2733	429354	63.3
3	1070.2784	179800	26.5
4	1071.2823	56764	8.4
5	1072.2846	12693	1.9

7. Characterisation of metal complexes

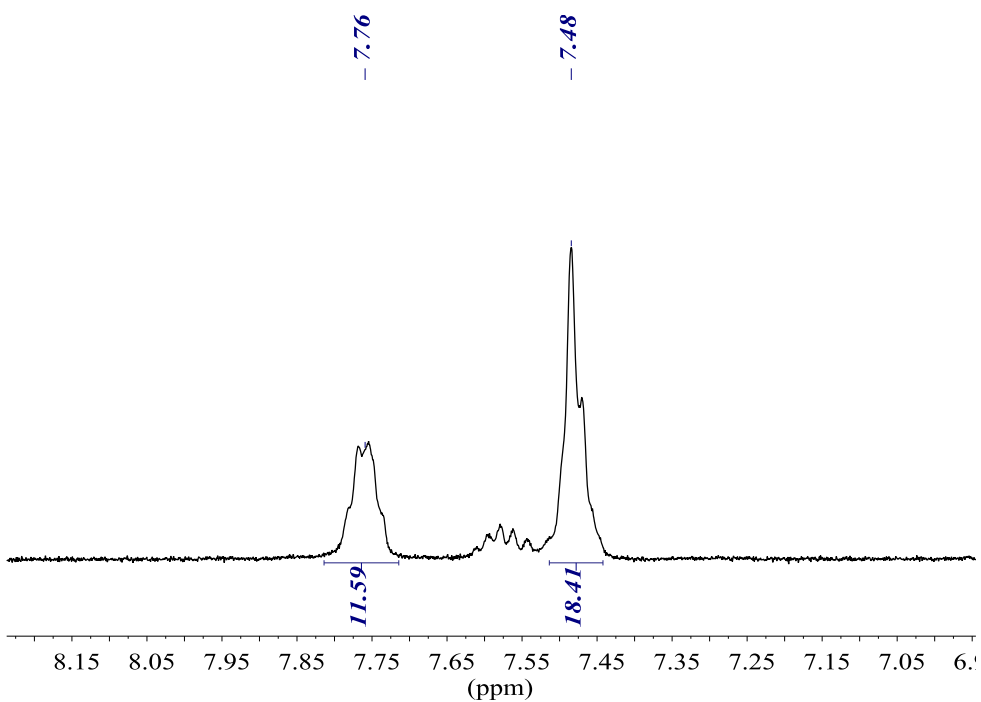
7.1. Vaska-type compounds *trans*-[Ir(CO)Cl(L)₂]

L = triphenylphosphine

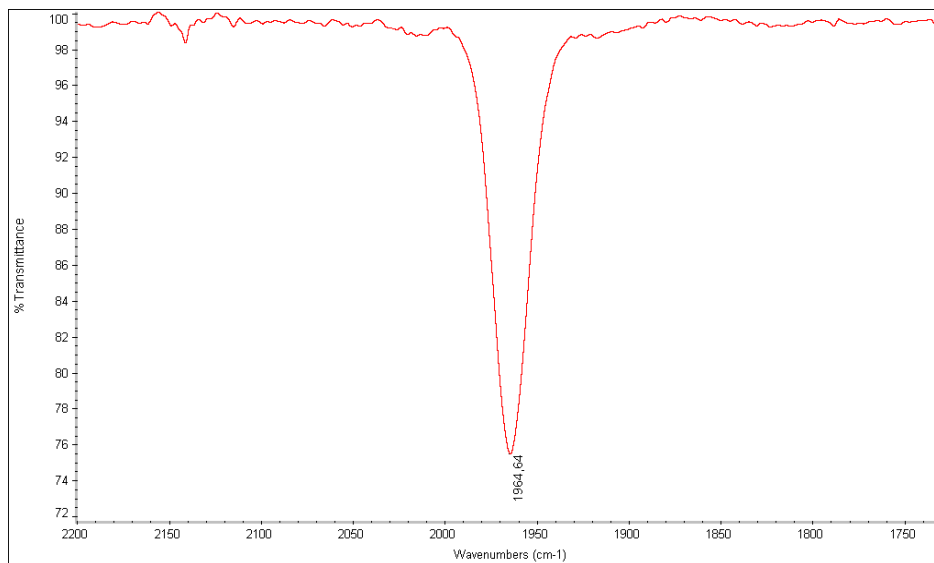
³¹P{¹H} NMR (161.98 MHz, acetone-D₆)



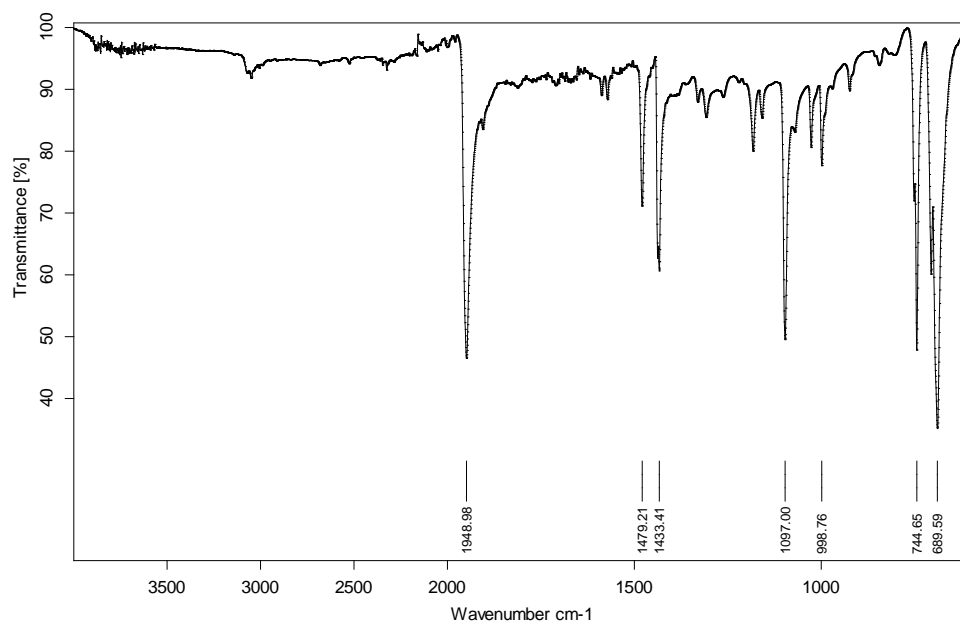
¹H NMR (400.13 MHz, acetone-D₆)



IR (CH₂Cl₂)

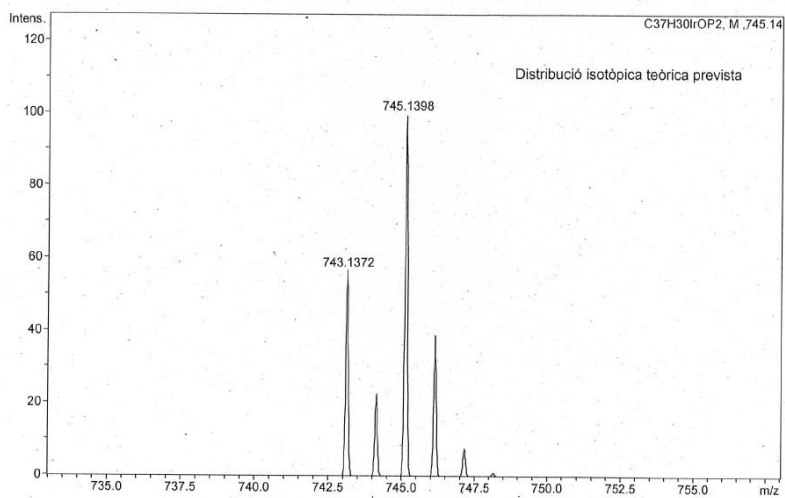


IR (ATR)



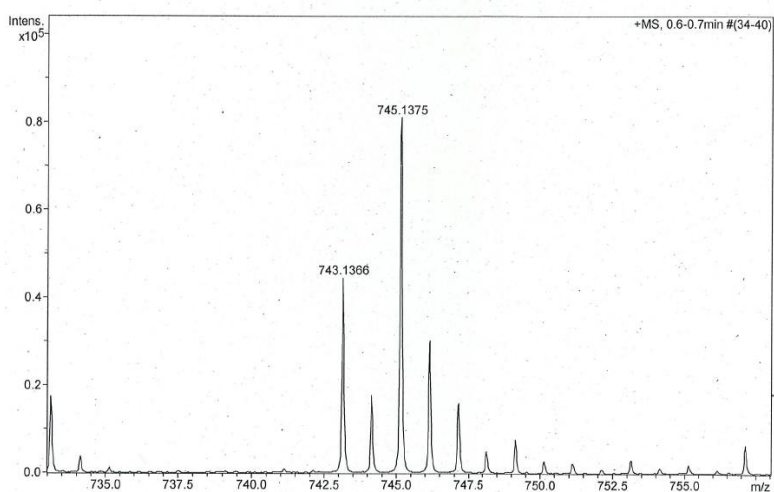
HR-MS (ESI⁺ m/z) [M-Cl]⁺

calculated



#	m/z	I	I%
1	743.1372	57	56.7
2	744.1406	23	22.9
3	745.1398	100	100.0
4	746.1429	39	39.1
5	747.1463	8	7.8
6	748.1496	1	1.0

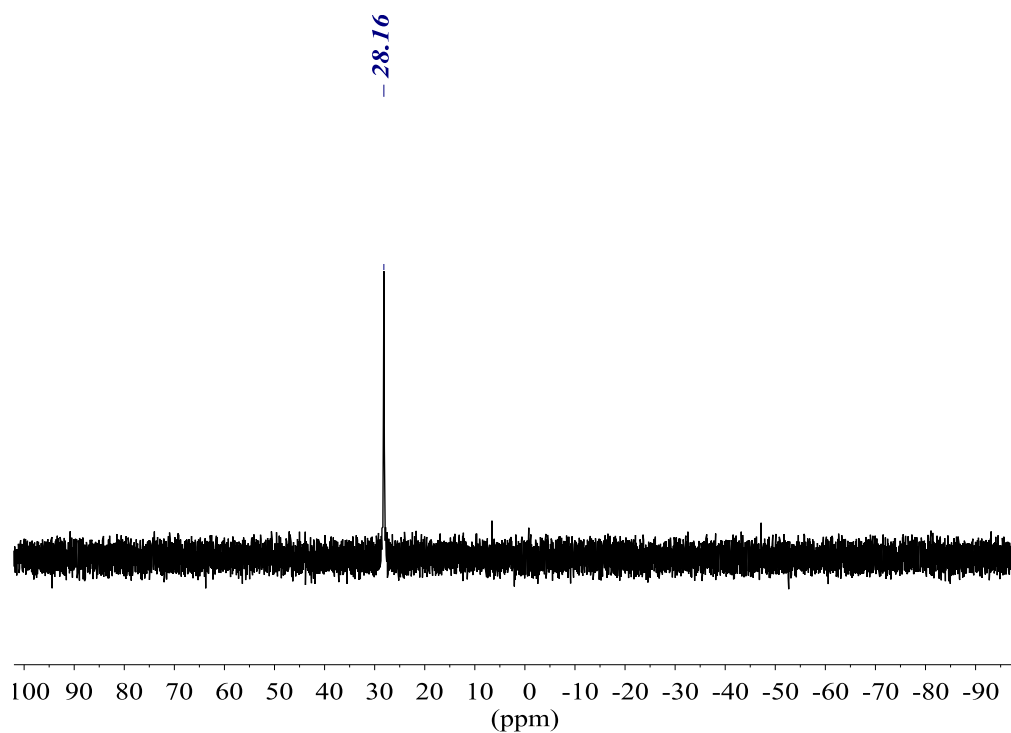
found



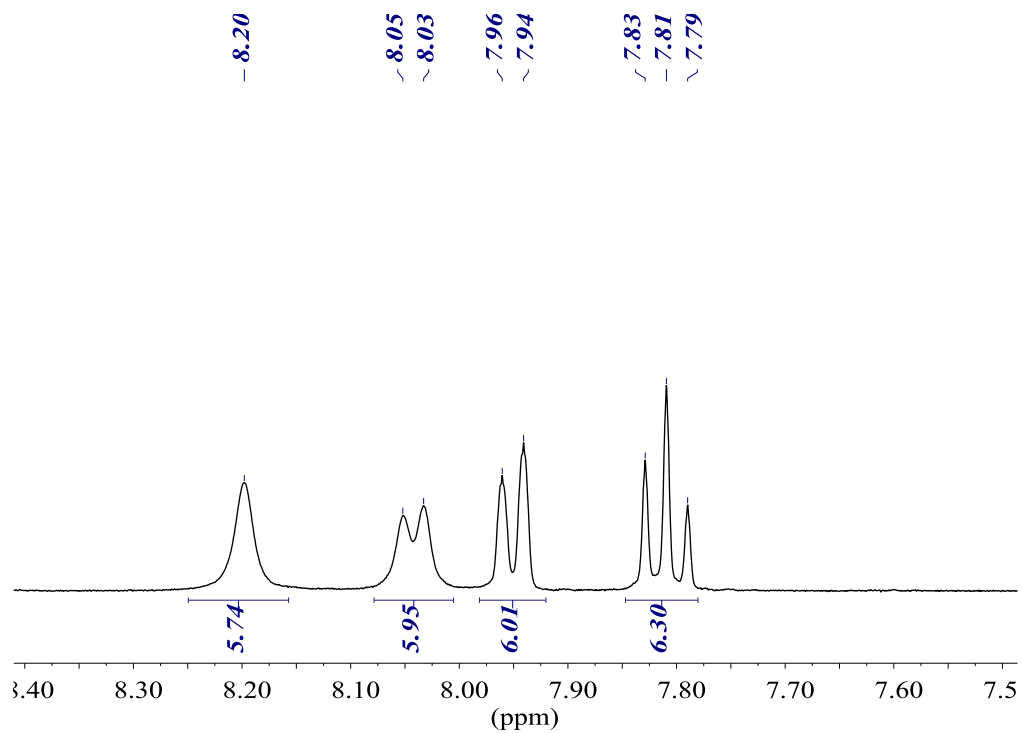
#	m/z	I	I%
1	743.1366	44613	55.0
2	744.1393	18013	22.2
3	745.1375	81096	100.0
4	746.1408	30398	37.5
5	747.1306	16001	19.7

L = tris(3-trifluoromethylphenyl)phosphine (5)

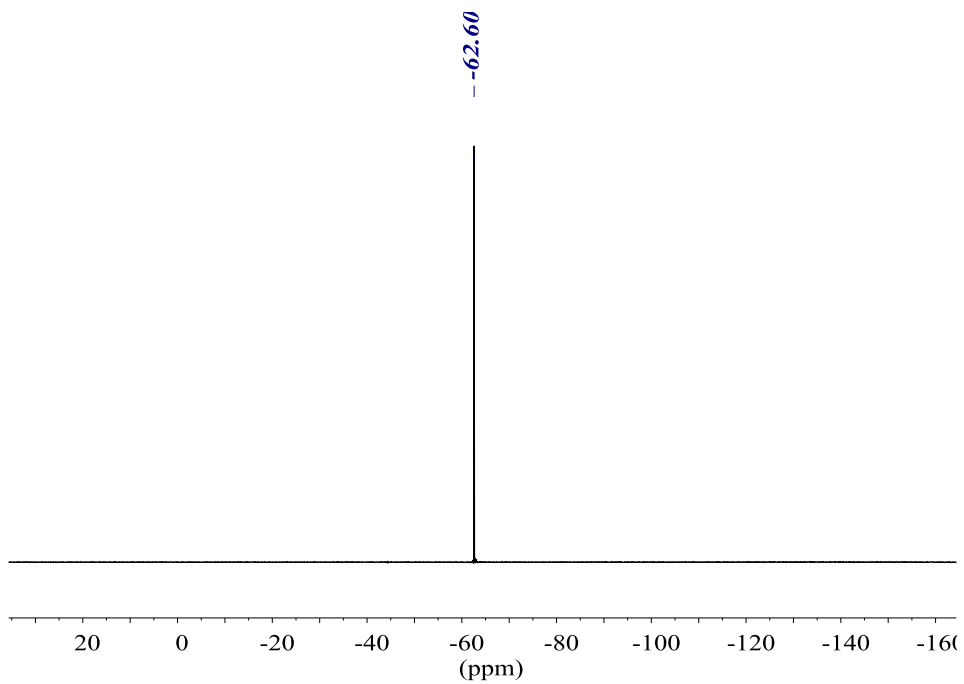
$^{31}\text{P}\{^1\text{H}\}$ NMR (161.98 MHz, acetone-D6)



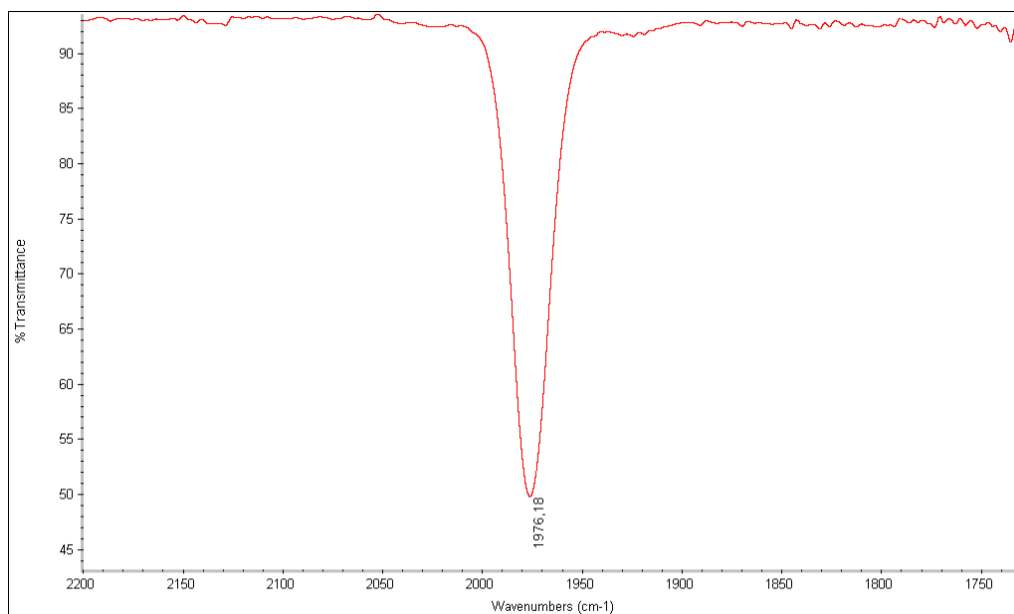
^1H NMR (400.13 MHz, acetone-D6)



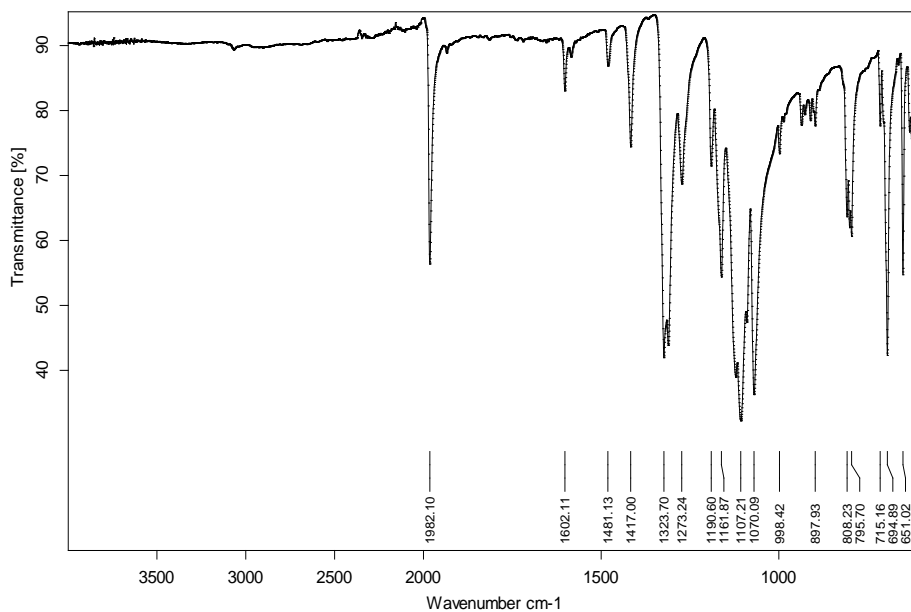
$^{19}\text{F}\{^1\text{H}\}$ NMR (376.50 MHz, acetone- D_6)



IR (CH_2Cl_2)

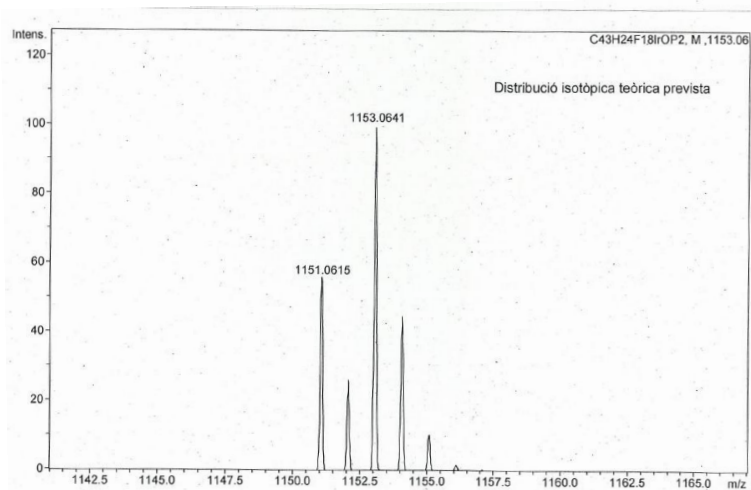


IR (ATR)



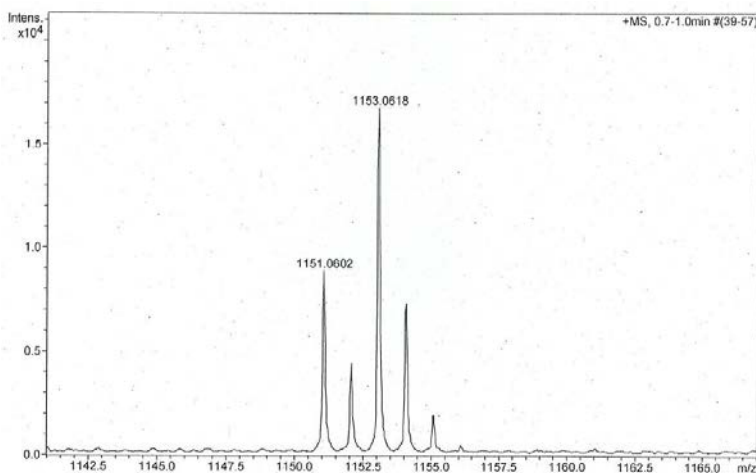
HR-MS (ESI⁺ *m/z*) [M-Cl]⁺

calculated



#	<i>m/z</i>	I	I %
1	1151.0615	56	55.9
2	1152.0649	26	26.1
3	1153.0641	100	100.0
4	1154.0672	45	44.9
5	1155.0706	10	10.3
6	1156.0739	2	1.6

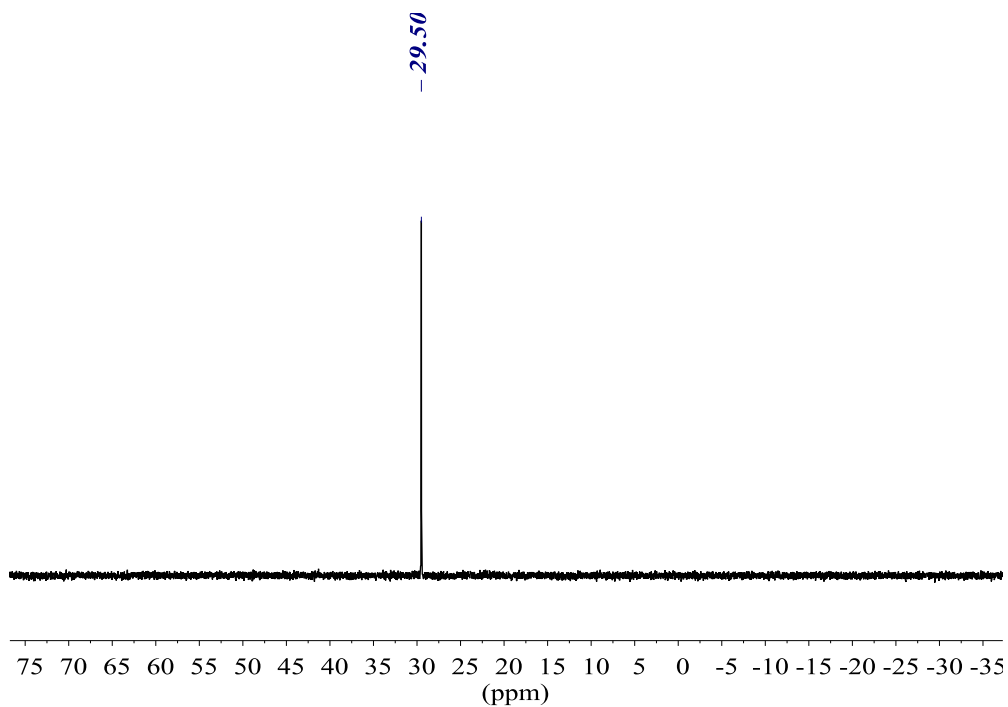
found



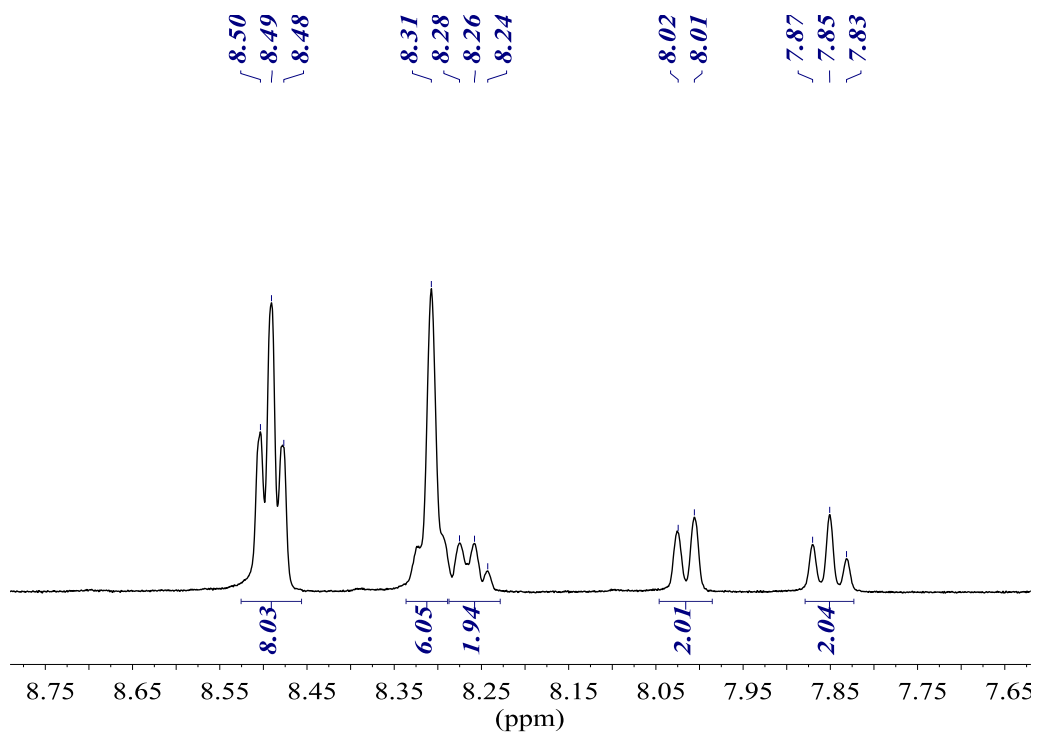
#	<i>m/z</i>	I	I %
1	1151.0602	8912	53.1
2	1152.0616	4513	26.9
3	1153.0618	16791	100.0
4	1154.0641	7367	43.9
5	1155.0693	1973	11.7
6	1156.0767	251	1.5

L = Bis(3,5-bis(trifluoromethyl)phenyl)(3-(trifluoromethyl)phenyl)phosphine (18)

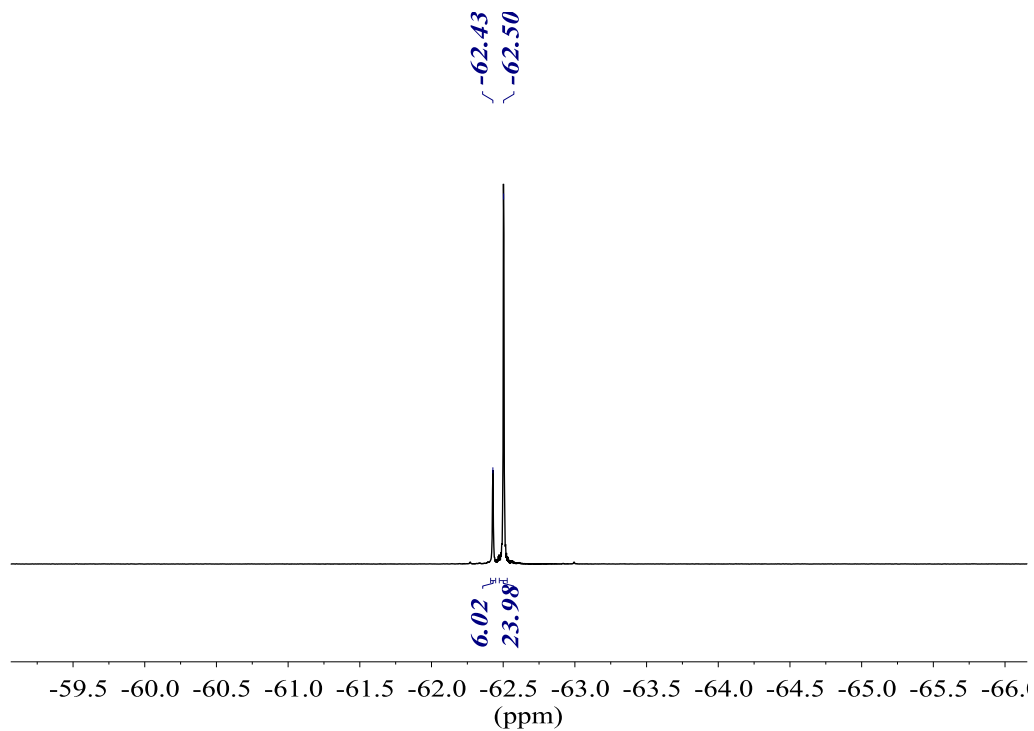
$^{31}\text{P}\{^1\text{H}\}$ NMR (161.98 MHz, acetone-D6)



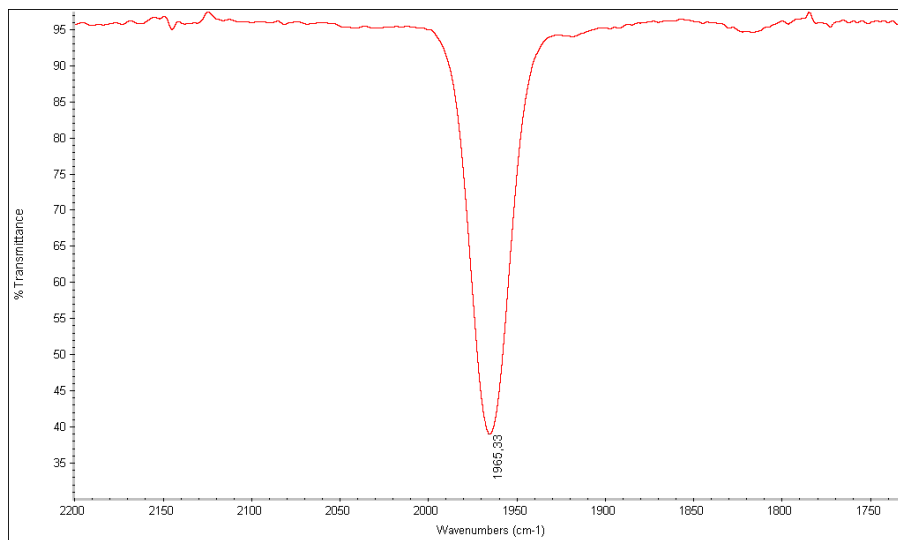
^1H NMR (400.13 MHz, acetone-D6)



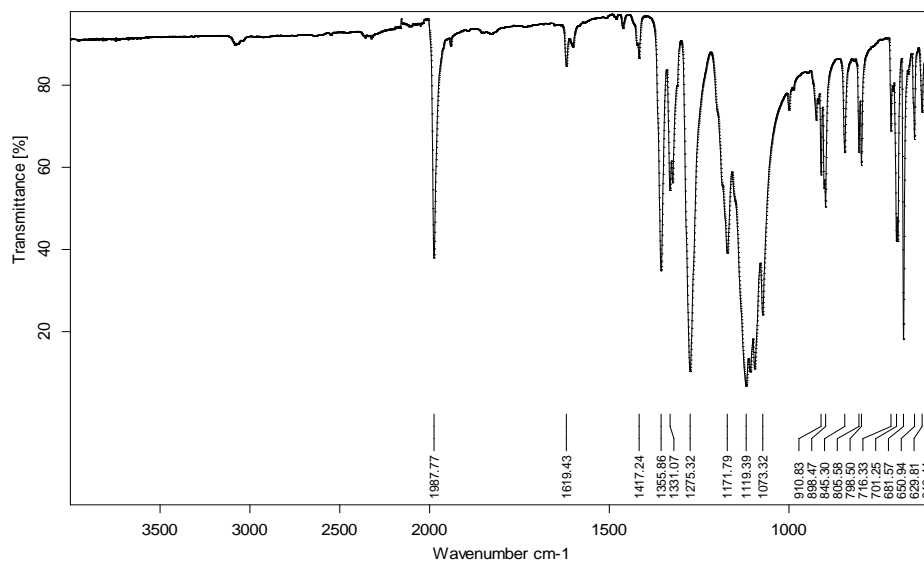
$^{19}\text{F}\{^1\text{H}\}$ NMR (376.50 MHz, acetone- D_6)



IR (CH_2Cl_2)

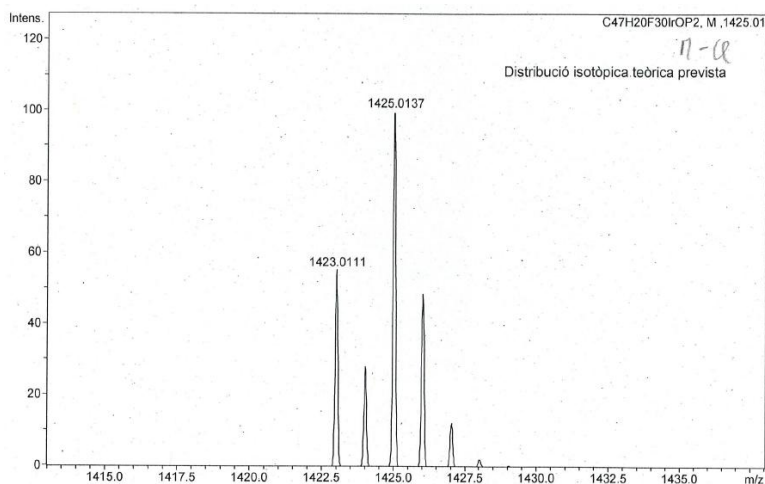


IR (ATR)



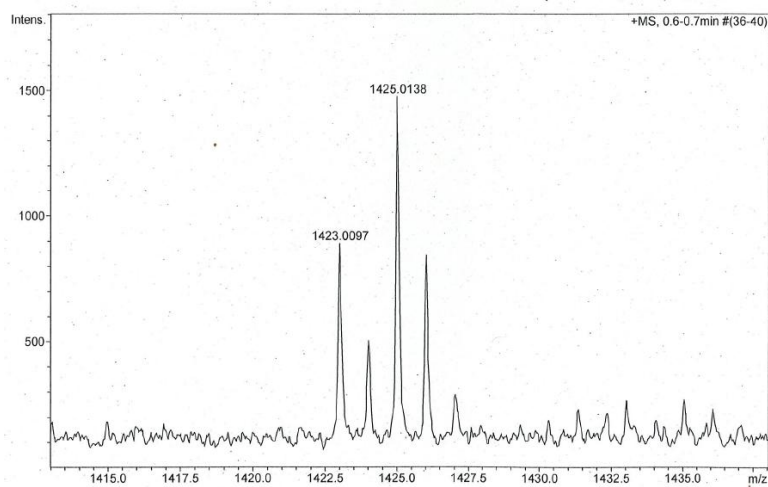
HR-MS (ESI⁺ m/z) [M-Cl]⁺

calculated



#	m/z	I	I%
1	1423.0111	55	55.2
2	1424.0144	28	28.2
3	1425.0137	100	100.0
4	1426.0168	49	48.6
5	1427.0201	12	12.2
6	1428.0235	2	2.0
7	1429.0268	0	0.3

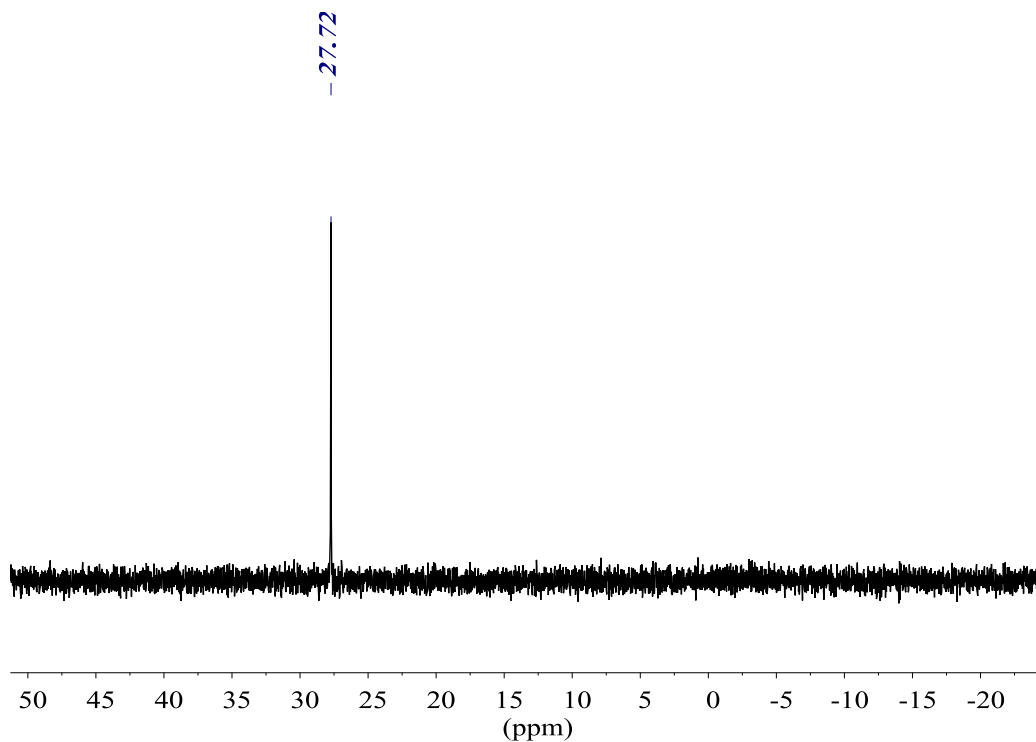
found



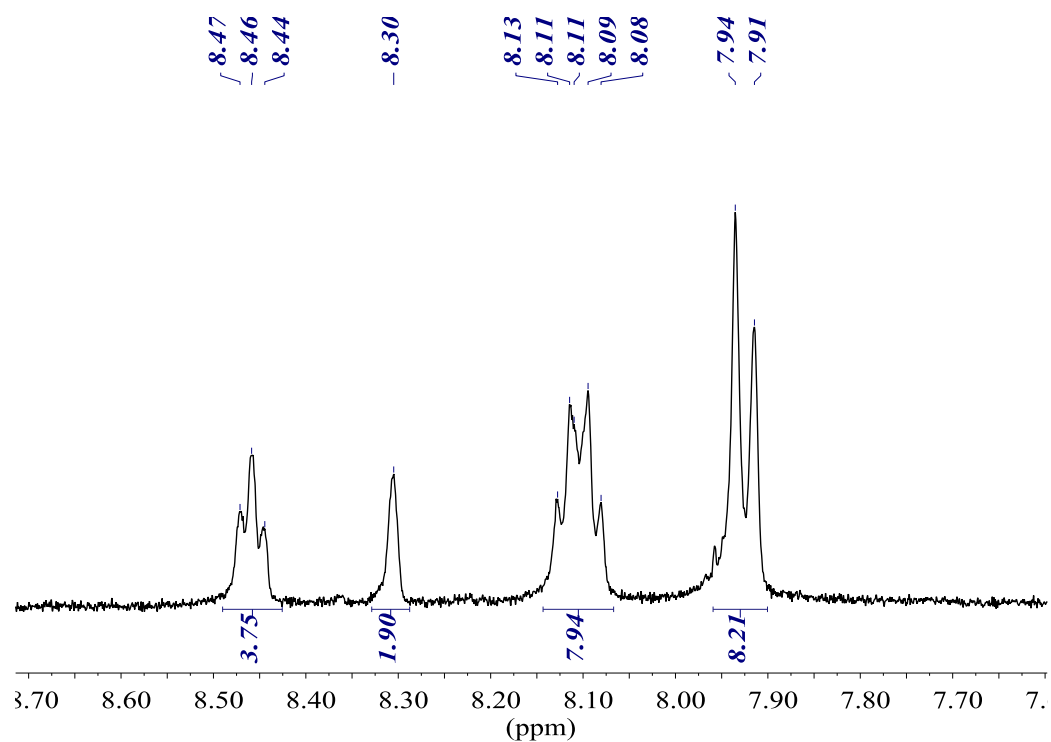
#	m/z	I	I%
1	1423.0097	892	60.4
2	1424.0207	373	25.3
3	1425.0138	1477	100.0
4	1426.0152	709	48.0
5	1427.0277	155	10.5
6	1427.9524	33	2.3

L = (3,5-bis(trifluoromethyl)phenyl)bis(4-(trifluoromethyl)phenyl)phosphine (20)

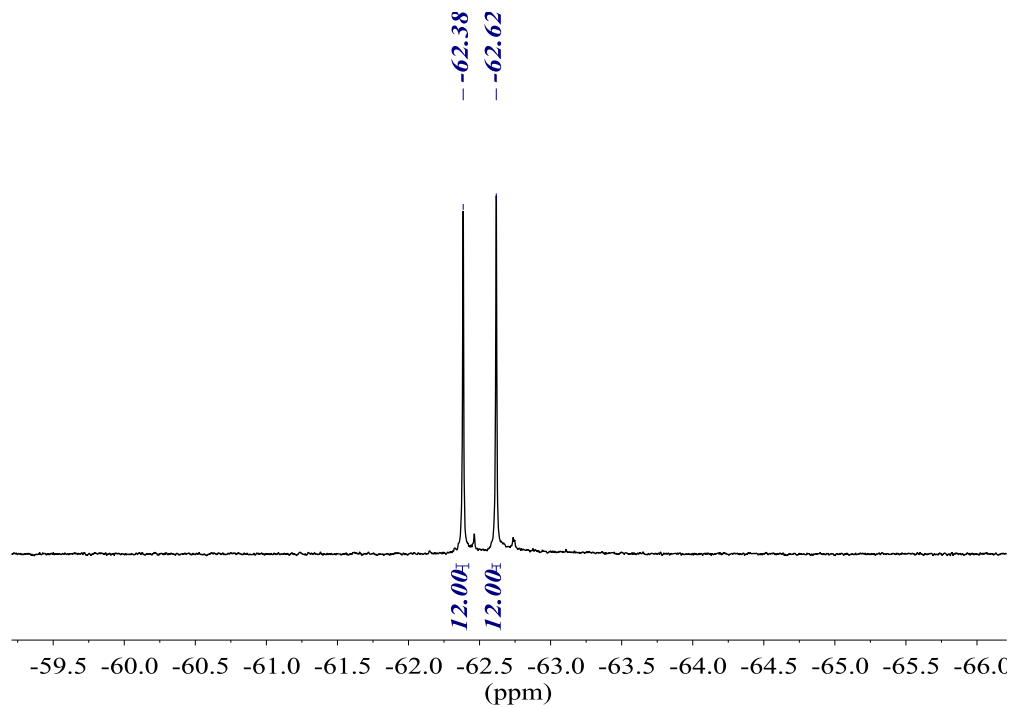
$^{31}\text{P}\{^1\text{H}\}$ NMR (161.98 MHz, acetone-D6)



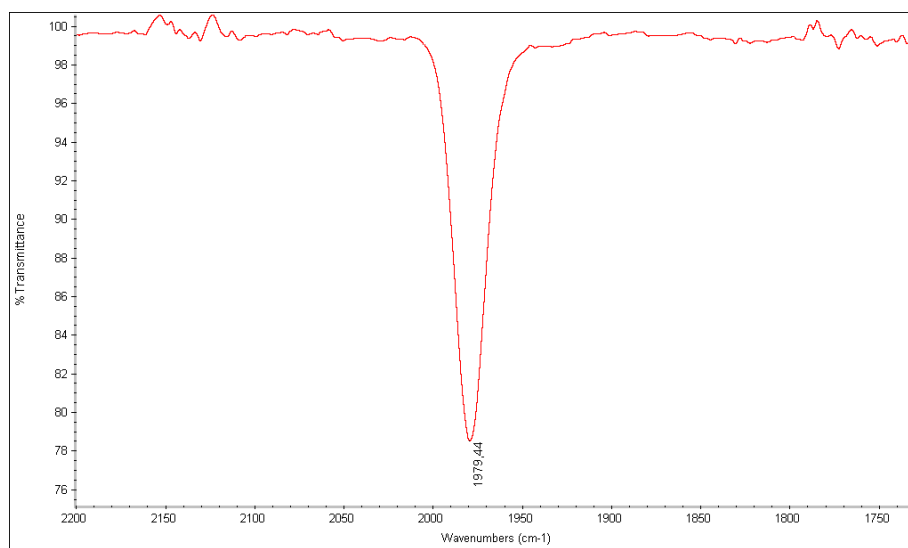
^1H NMR (400.13 MHz, acetone-D6)



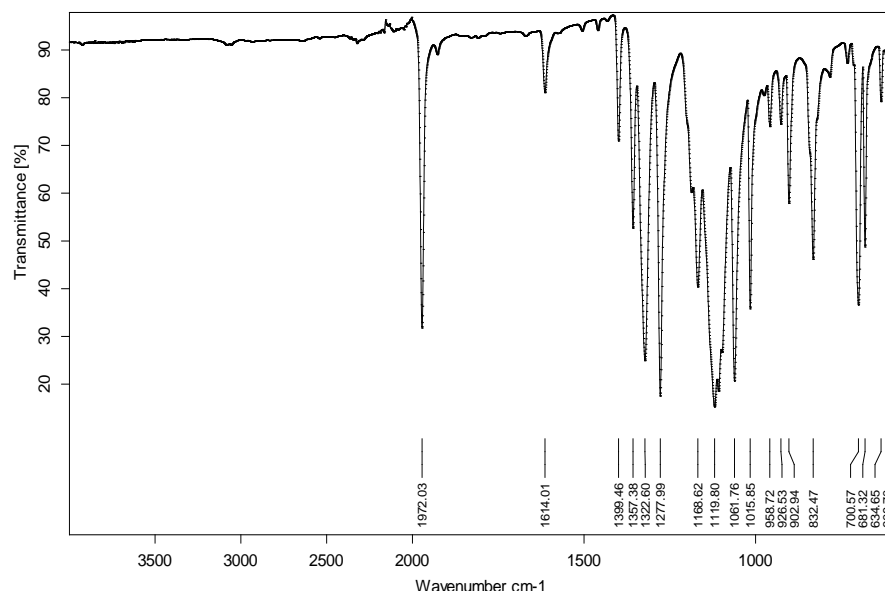
$^{19}\text{F}\{^1\text{H}\}$ NMR (376.50 MHz, acetone-D6)



IR (CH₂Cl₂)

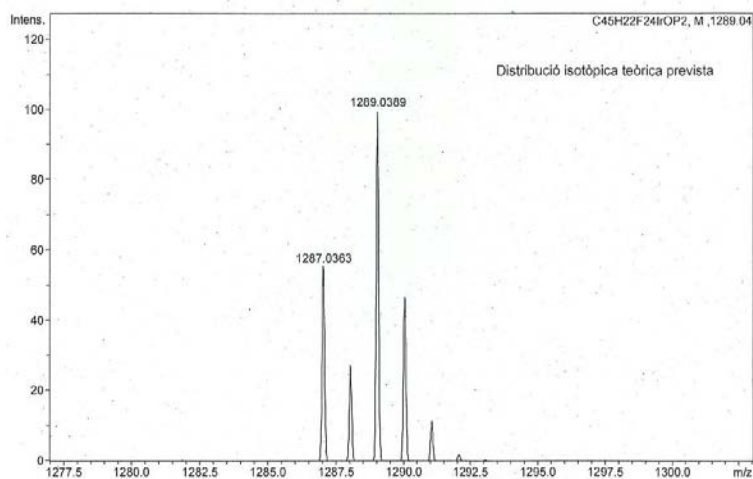


IR (ATR)



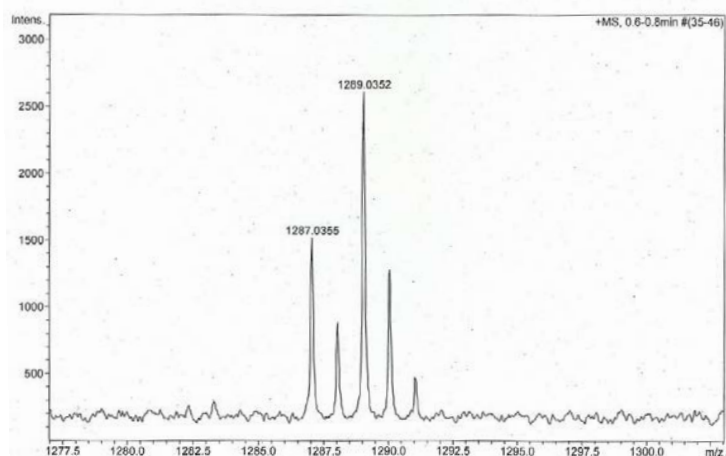
HR-MS (ESI⁺ *m/z*) [M-Cl]⁺

calculated



#	<i>m/z</i>	I	I%
1	1287.0363	56	55.6
2	1288.0397	27	27.2
3	1289.0389	100	100.0
4	1290.0420	47	46.8
5	1291.0454	11	11.3
6	1292.0487	2	1.8

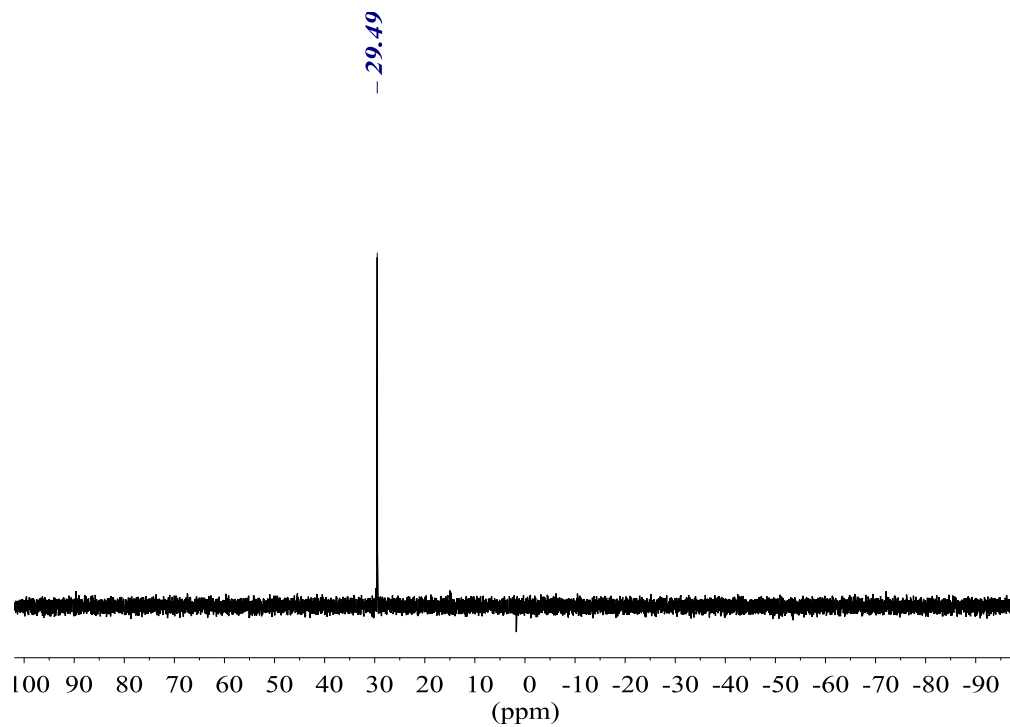
found



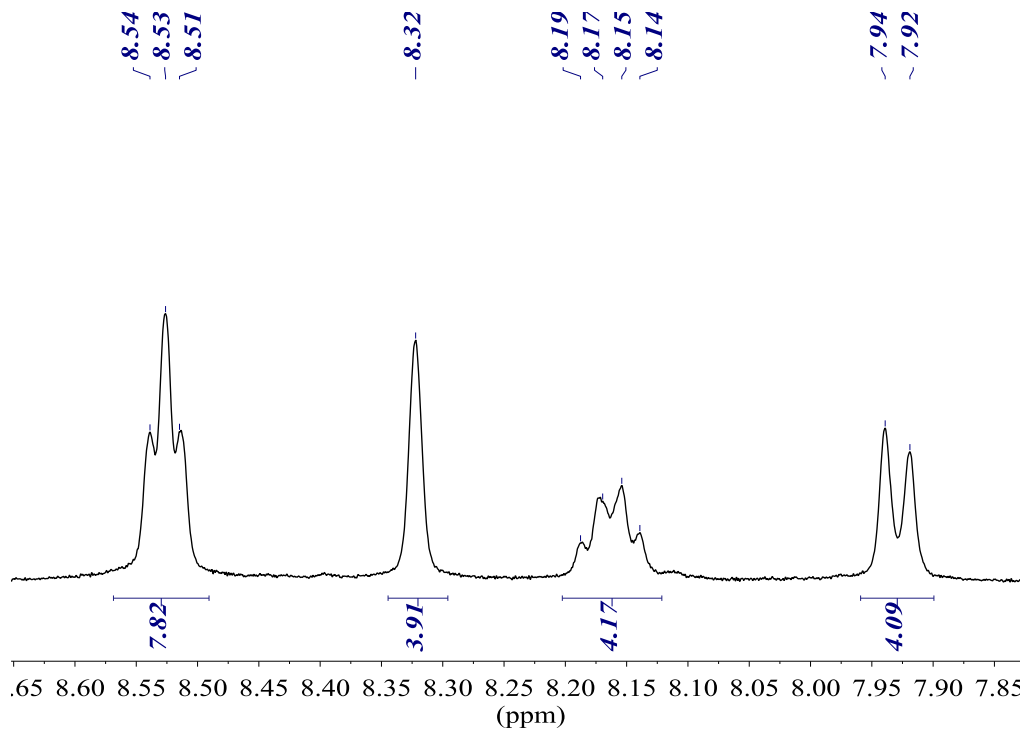
#	<i>m/z</i>	I	I%
1	1287.0355	1521	58.2
2	1288.0338	700	26.8
3	1289.0352	2611	100.0
4	1290.0382	1097	42.0
5	1291.0394	290	11.1
6	1292.0387	47	1.8

L = Bis(3,5-bis(trifluoromethyl)phenyl)(4-(trifluoromethyl)phenyl)phosphine (23)

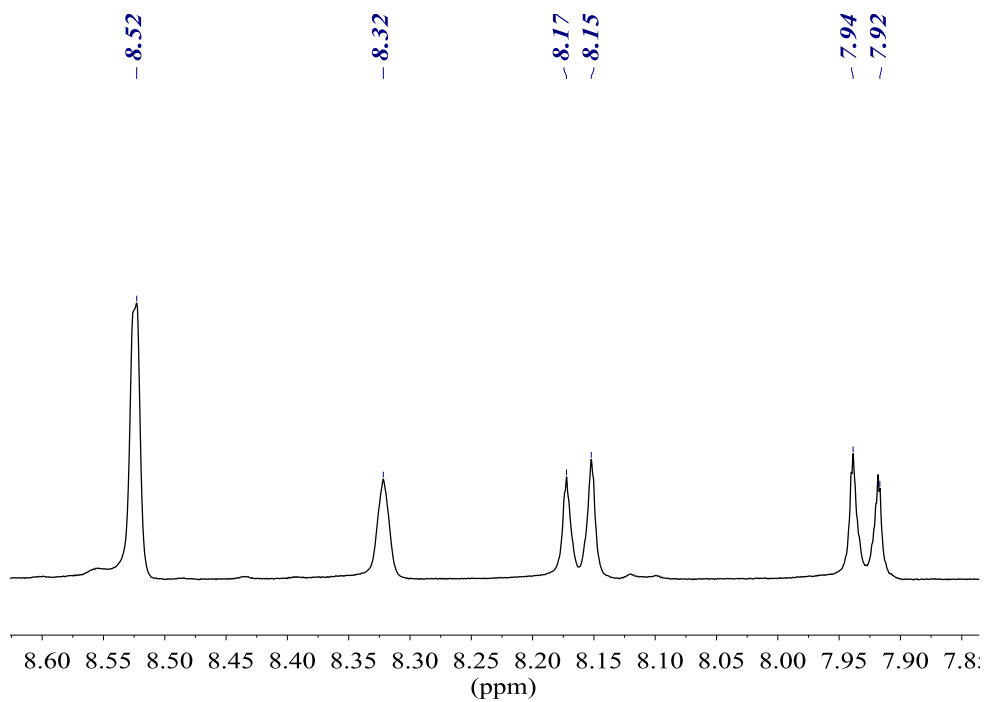
$^{31}\text{P}\{^1\text{H}\}$ NMR (161.98 MHz, acetone-D6)



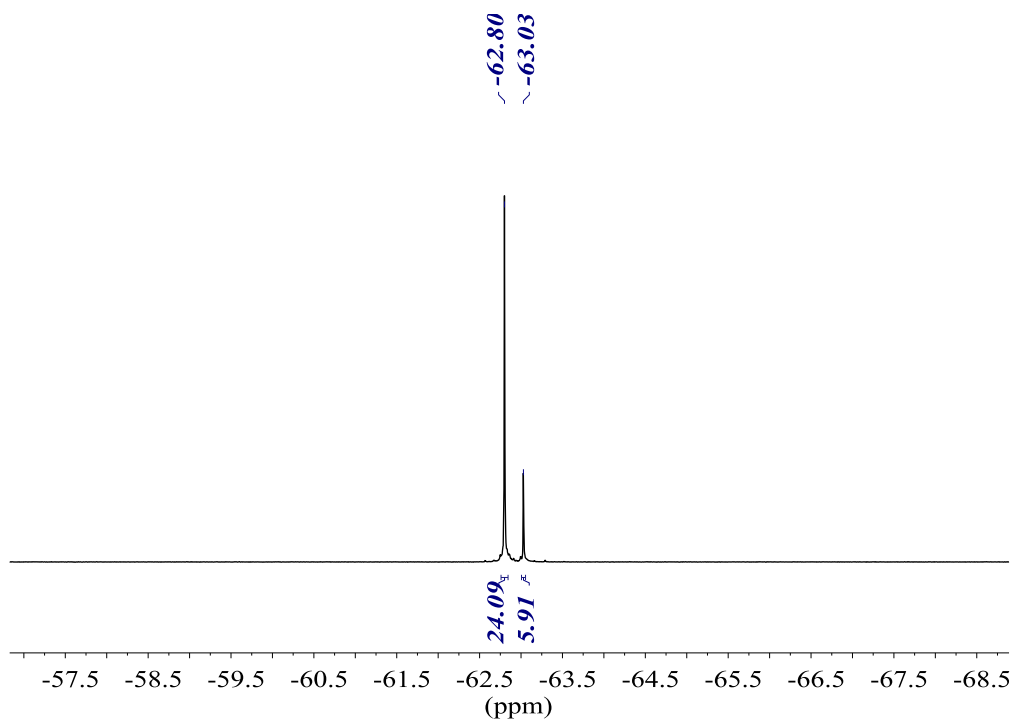
^1H NMR (400.13 MHz, acetone-D6)



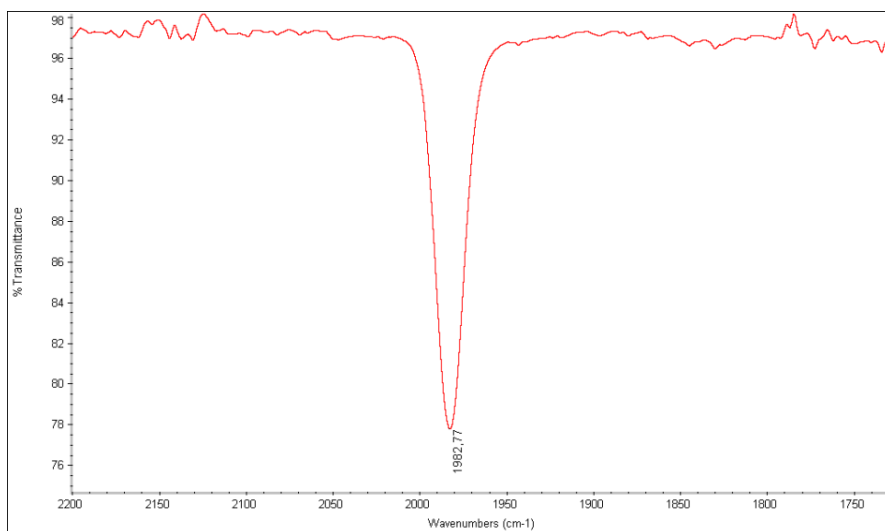
$^1\text{H}\{^{31}\text{P}\}$ NMR (400.13 MHz, acetone-D6)



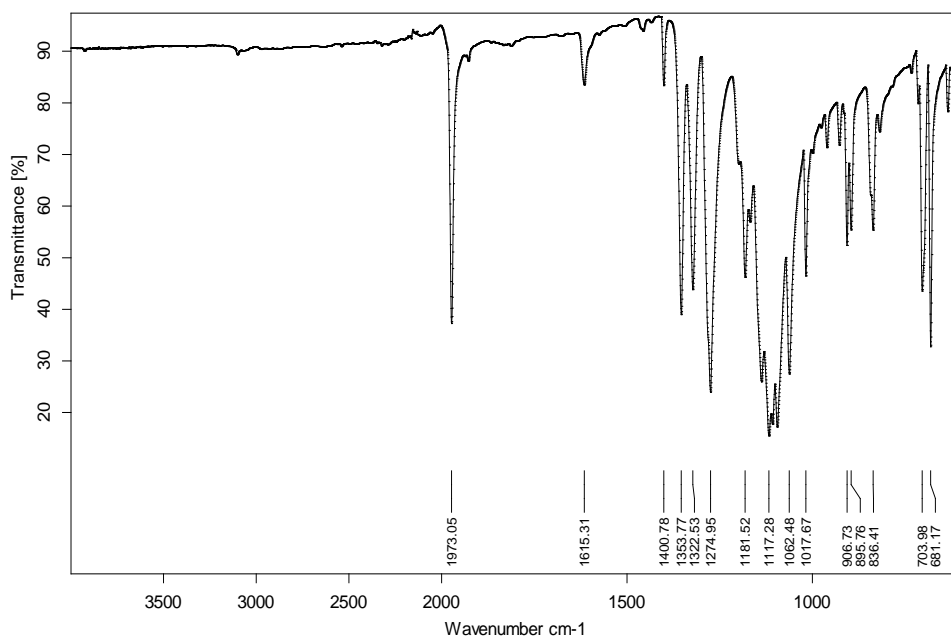
$^{19}\text{F}\{^1\text{H}\}$ NMR (376.50 MHz, acetone- D_6)



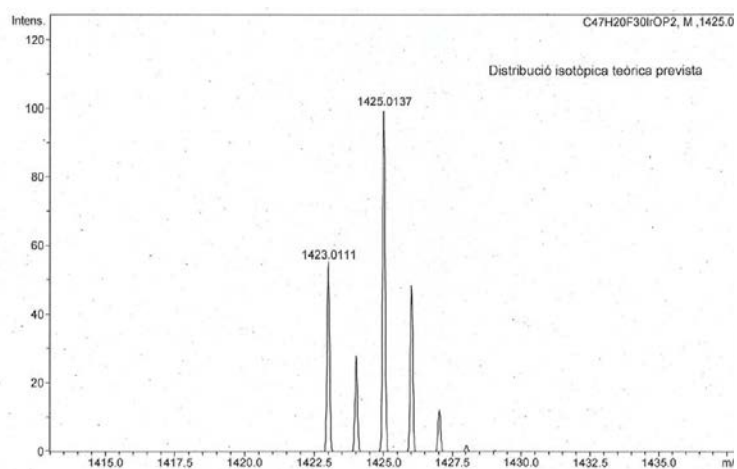
IR (CH_2Cl_2)



IR (ATR)

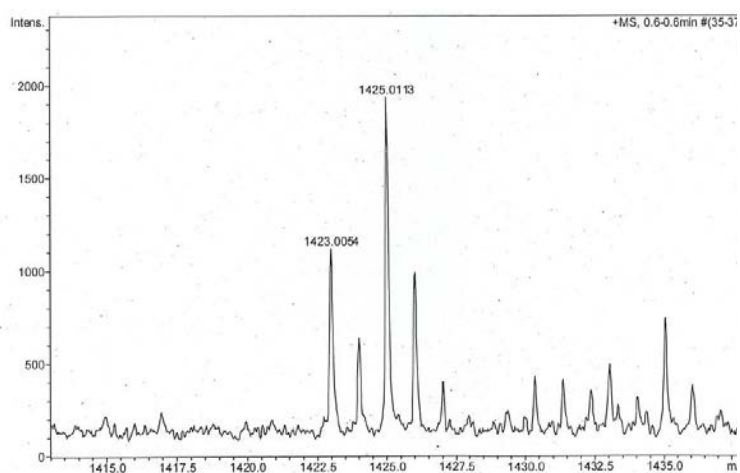


HR-MS (ESI⁺ *m/z*) [M-Cl]⁺
calculated



#	<i>m/z</i>	I	I%
1	1423.0111	55	55.2
2	1424.0144	28	28.2
3	1425.0137	100	100.0
4	1426.0168	49	48.6
5	1427.0201	12	12.2
6	1428.0235	2	2.0

found

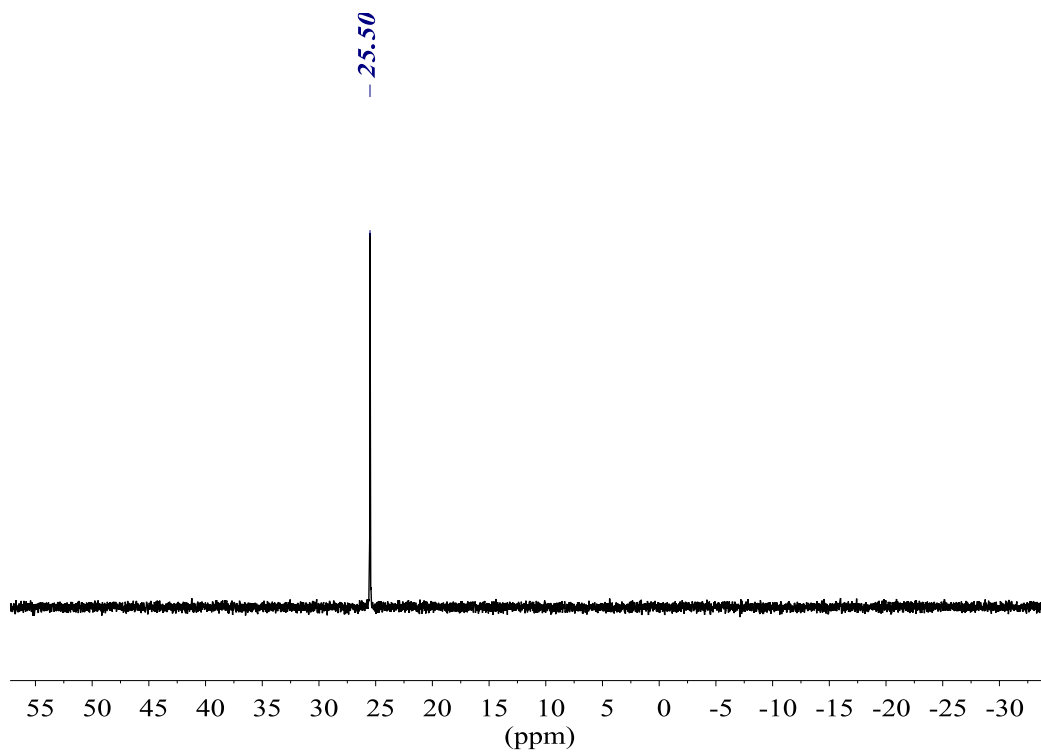


#	<i>m/z</i>	I	I%
1	1423.0054	1121	57.9
2	1424.0123	491	25.3
3	1425.0113	1937	100.0
4	1426.0122	841	43.4
5	1427.0073	251	13.0
6	1427.9557	68	3.5

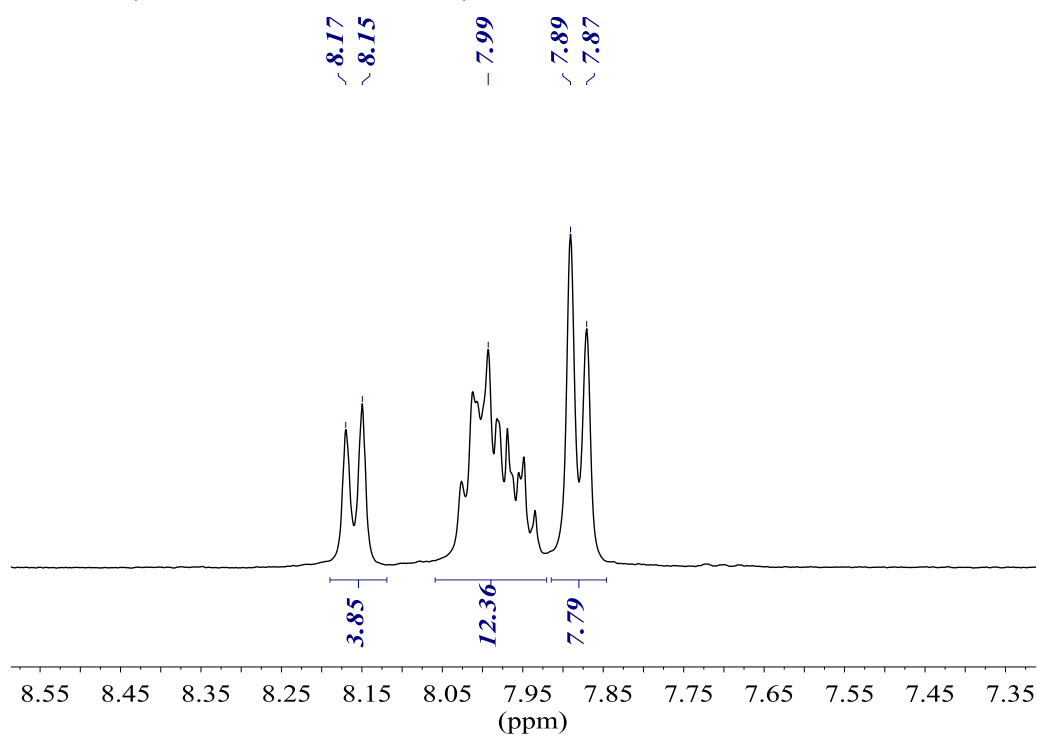
7.2. Pd complexes *trans*-[PdCl₂L₂]

L = *p*-Miranphos

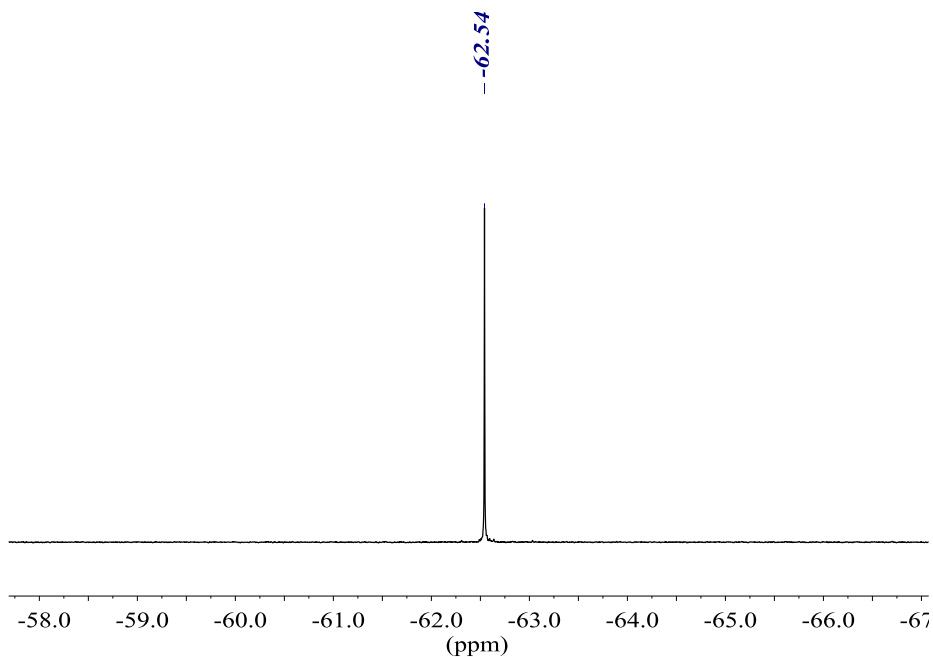
³¹P{¹H} NMR (161.98 MHz, acetone-D₆)



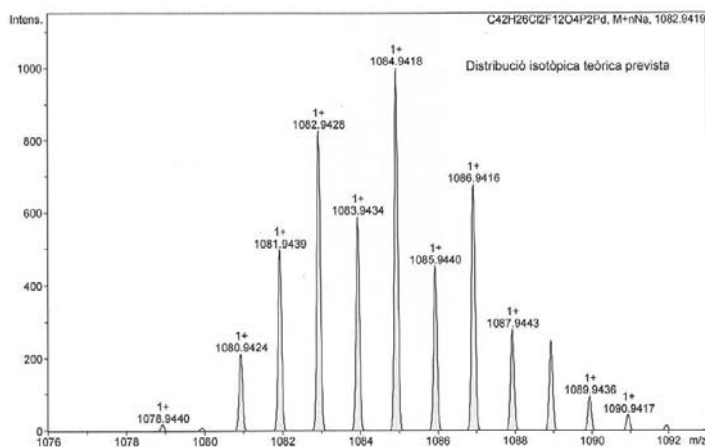
¹H NMR (400.13 MHz, acetone-D₆)



$^{19}\text{F}\{^1\text{H}\}$ NMR (376.50 MHz, acetone- D_6)

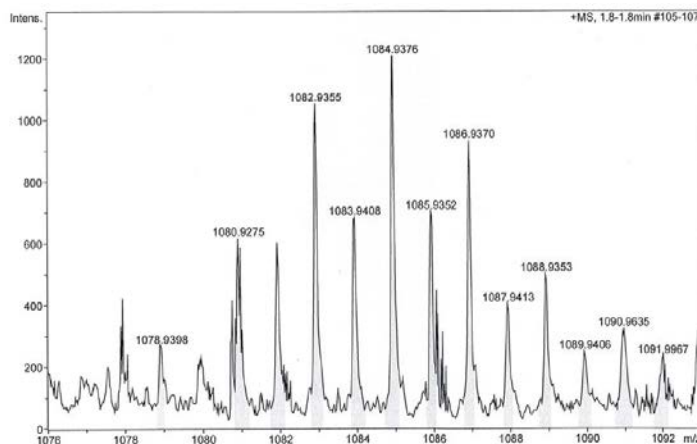


HR-MS (ESI⁺ m/z) [M+Na]⁺
 calculated for $[\text{C}_{42}\text{H}_{26}\text{Cl}_2\text{F}_{12}\text{O}_4\text{P}_2\text{PdNa}]^+$



#	m/z	I	I %
1	1078.9440	18	1.8
2	1080.9424	213	21.3
3	1081.9439	496	49.6
4	1082.9428	825	82.5
5	1083.9434	587	58.7
6	1084.9418	1000	100.0
7	1085.9440	452	45.2
8	1086.9416	677	67.7
9	1087.9443	278	27.8
10	1088.9415	248	24.8
11	1089.9436	94	9.4
12	1090.9417	43	4.3
13	1091.9430	13	1.3

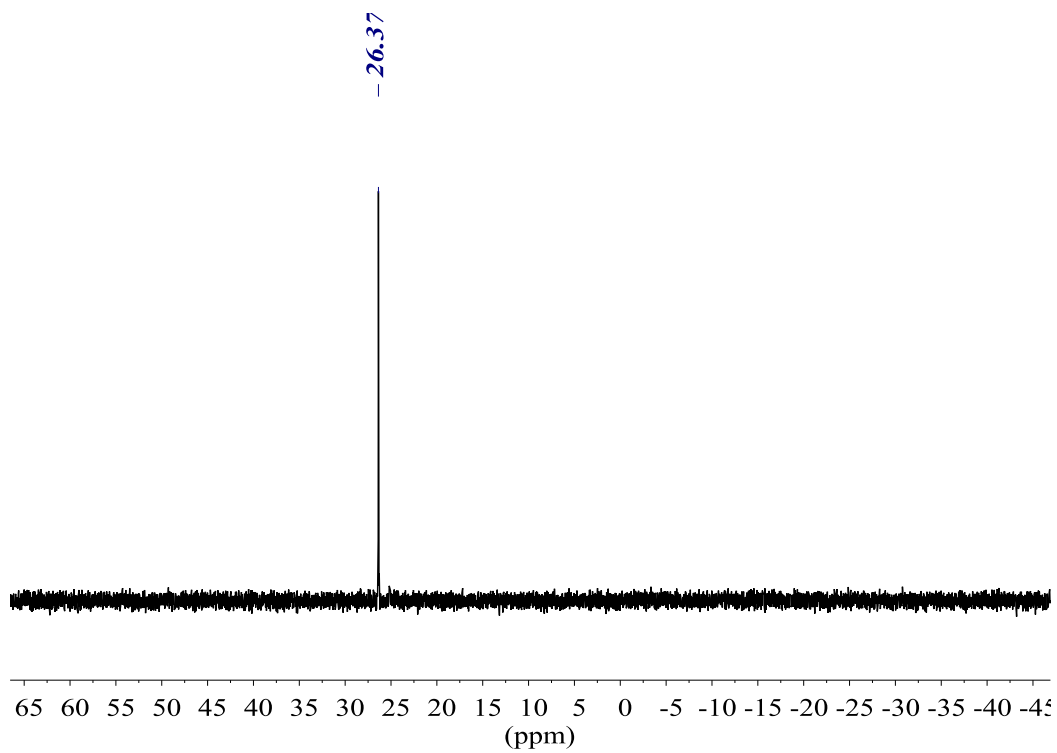
found



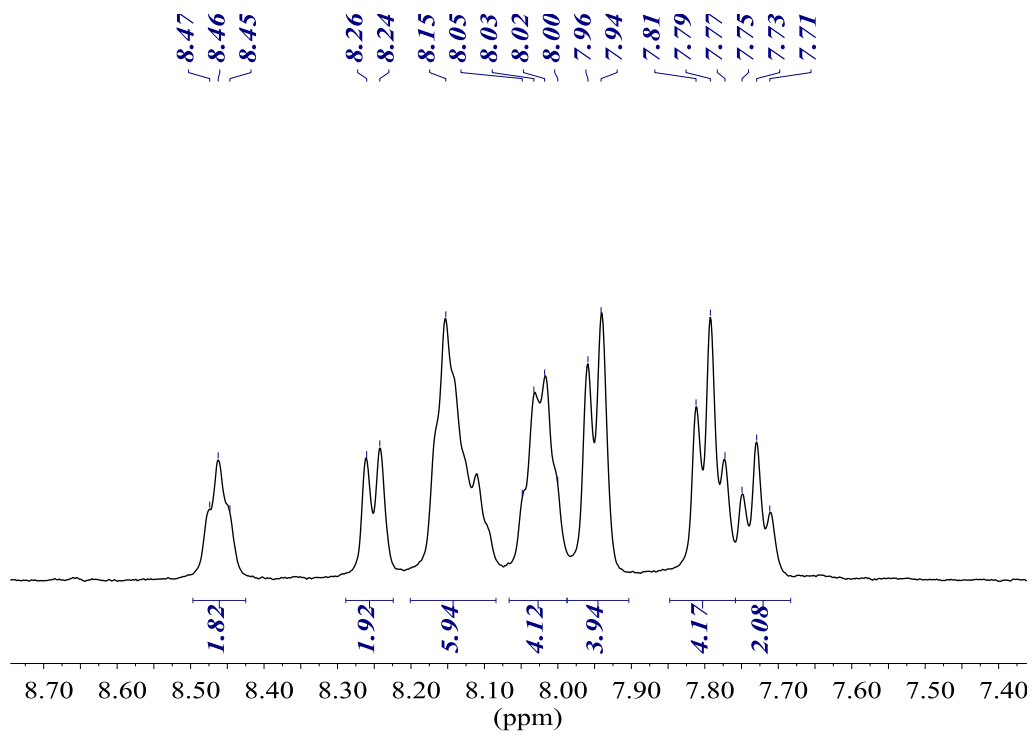
#	m/z	I	I %
1	1078.9398	269	22.3
2	1080.9275	617	51.1
3	1081.9453	604	50.0
4	1082.9355	1053	87.2
5	1083.9408	683	56.6
6	1084.9376	1207	100.0
7	1085.9352	702	58.2
8	1086.9370	932	77.2
9	1087.9413	403	33.4
10	1088.9353	501	41.5
11	1089.9406	249	20.6
12	1090.9635	324	26.8
13	1091.9967	235	19.4

L = *m*-Miranphos

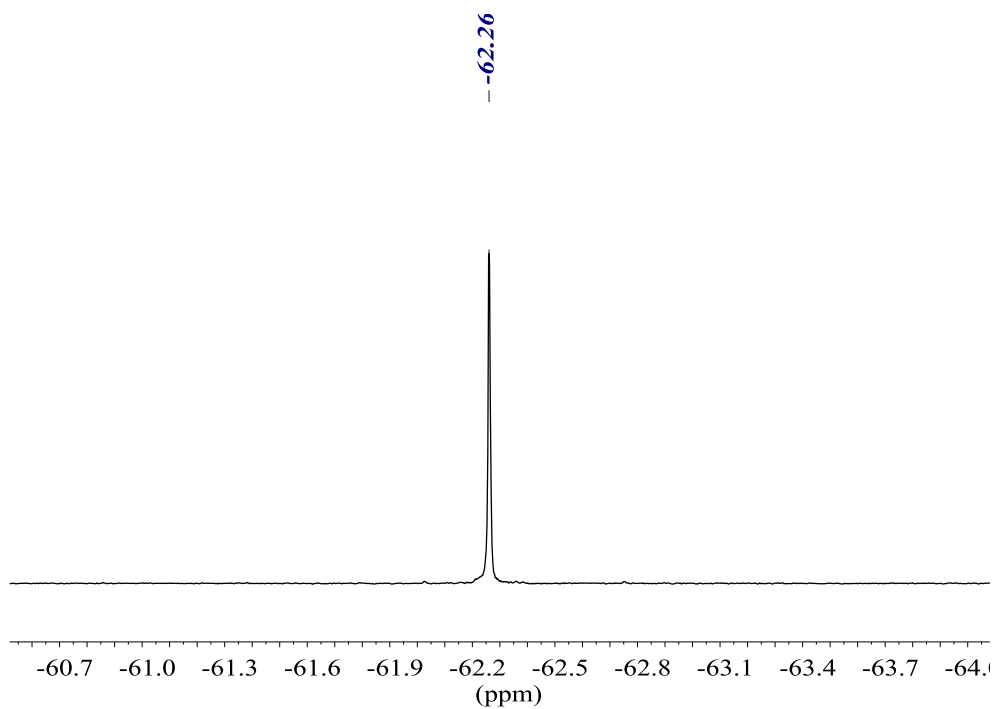
$^{31}\text{P}\{^1\text{H}\}$ NMR (161.98 MHz, acetone-D6)



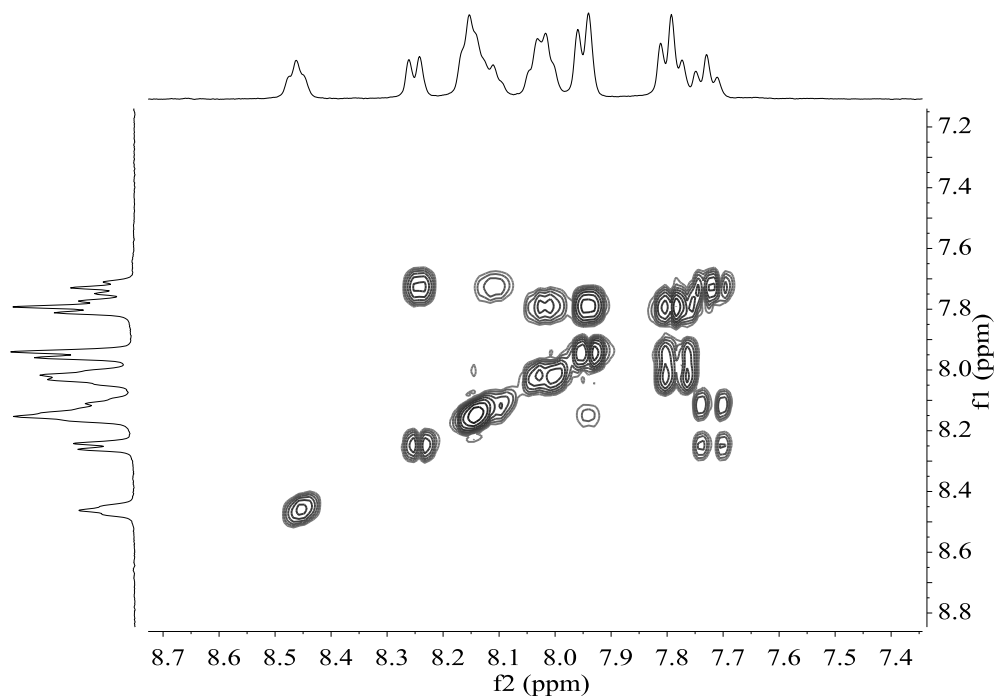
^1H NMR (400.13 MHz, acetone-D6)



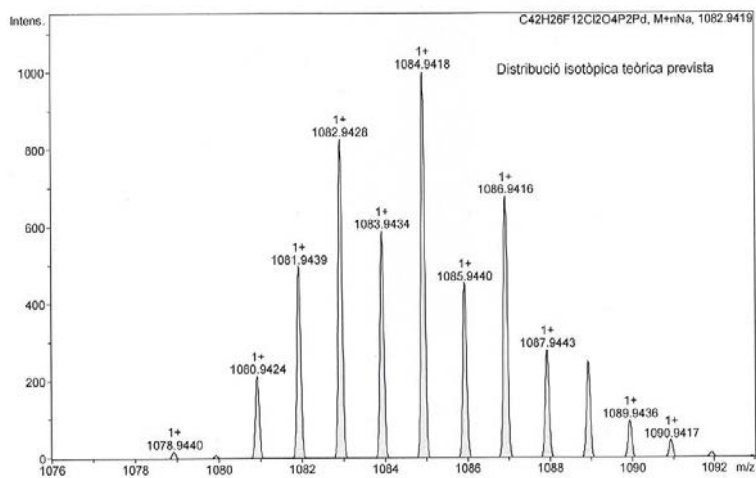
$^{19}\text{F}\{^1\text{H}\}$ NMR (376.50 MHz, acetone- D_6)



COSY NMR (400.13 MHz, acetone- D_6)

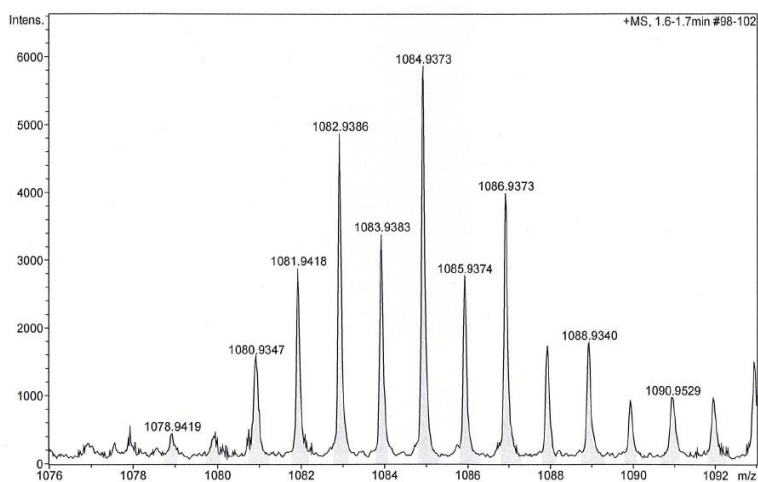


HR-MS (ESI⁺ *m/z*) [M+Na]⁺
 calculated for [C₄₂H₂₆Cl₂F₁₂O₄P₂PdNa]⁺



#	<i>m/z</i>	I	I %
1	1078.9440	18	1.8
2	1079.9474	8	0.8
3	1080.9424	213	21.3
4	1081.9439	496	49.6
5	1082.9428	825	82.5
6	1083.9434	587	58.7
7	1084.9418	1000	100.0
8	1085.9440	452	45.2
9	1086.9416	677	67.7
10	1087.9443	278	27.8
11	1088.9415	248	24.8
12	1089.9436	94	9.4
13	1090.9417	43	4.3
14	1091.9430	13	1.3

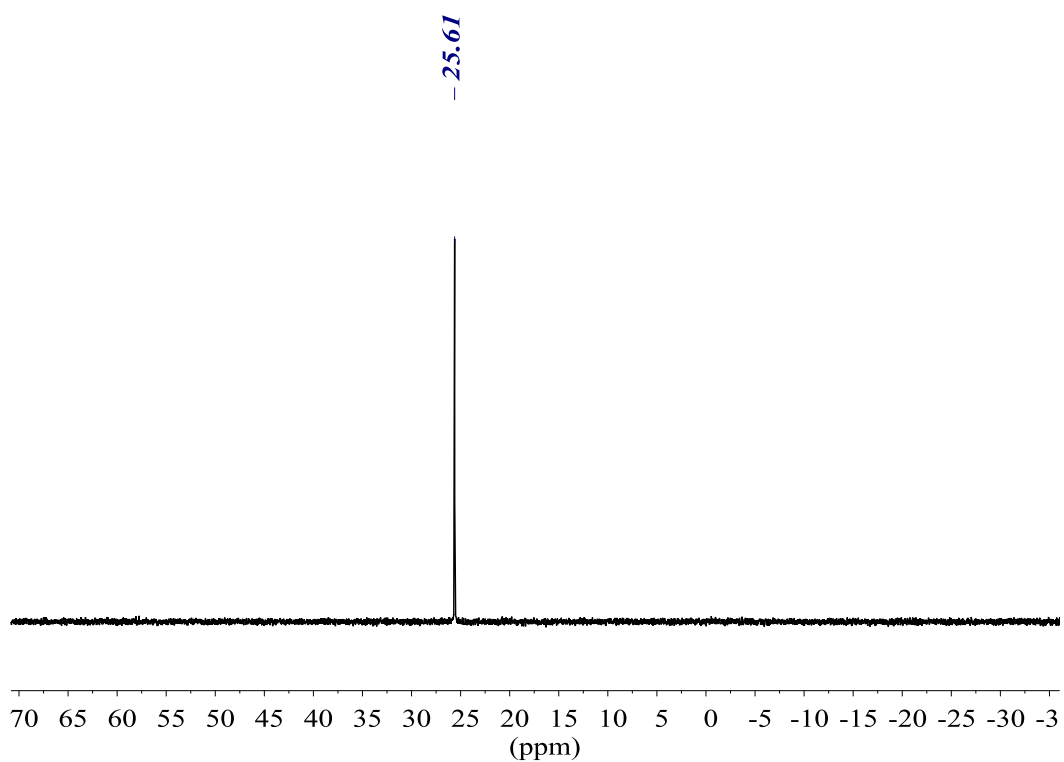
found



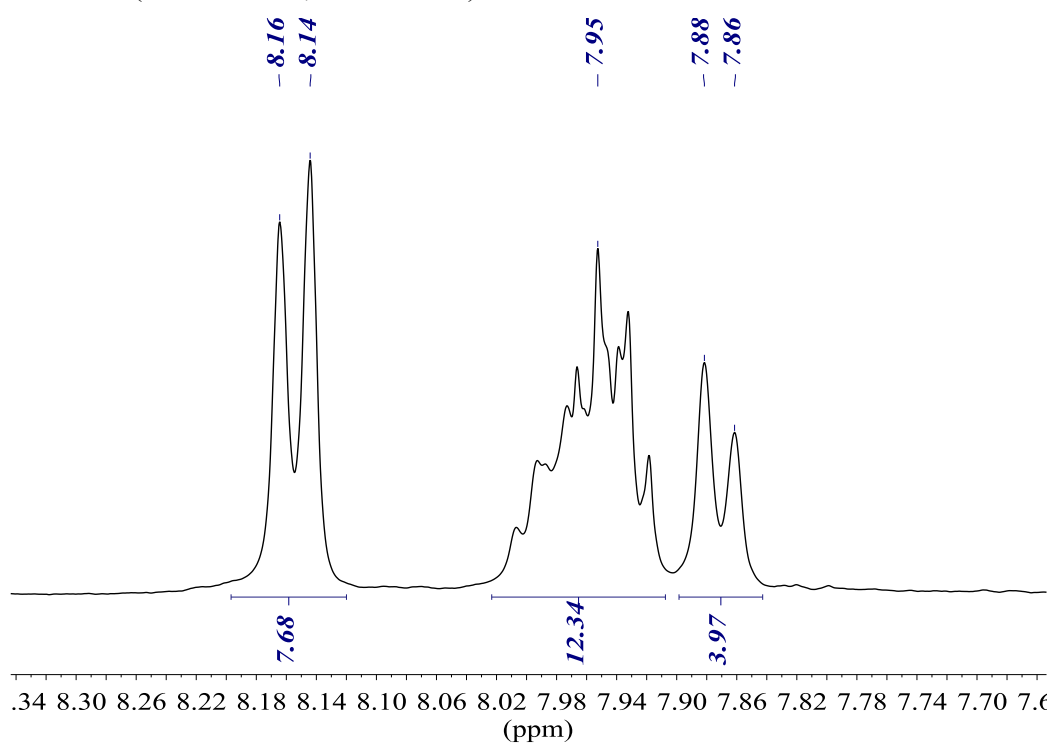
#	<i>m/z</i>	I	I %
1	1078.9419	451	7.7
2	1079.9383	418	7.1
3	1080.9347	1579	27.0
4	1081.9418	2887	49.3
5	1082.9386	4870	83.1
6	1083.9383	3384	57.8
7	1084.9373	5857	100.0
8	1085.9374	2776	47.4
9	1086.9373	3993	68.2
10	1087.9398	1739	29.7
11	1088.9340	1789	30.5
12	1089.9376	923	15.8
13	1090.9529	978	16.7

L = *p*-Miran2phos

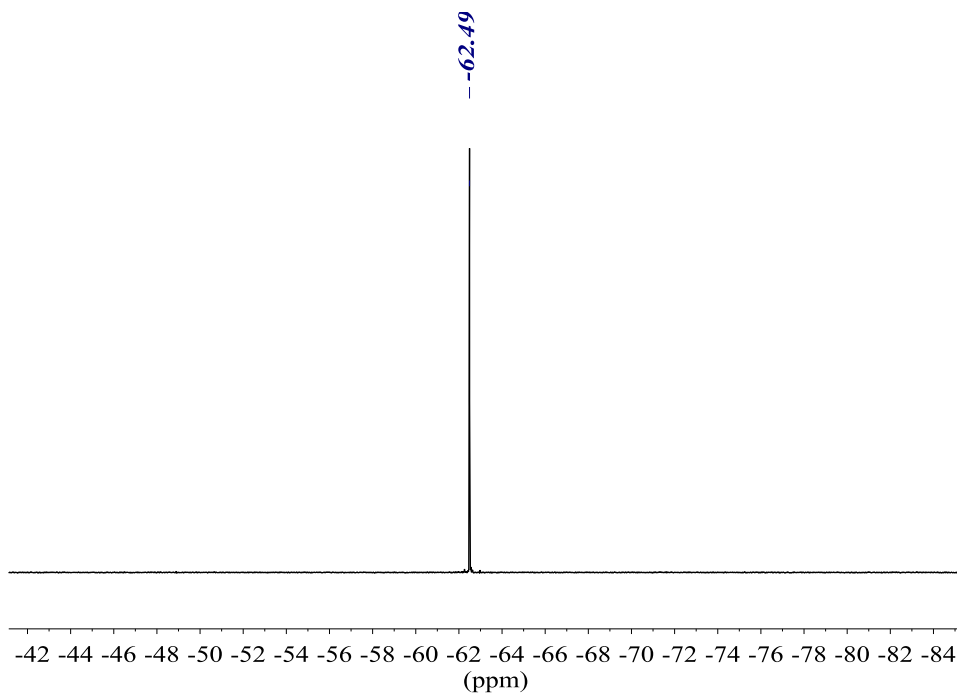
$^{31}\text{P}\{^1\text{H}\}$ NMR (161.98 MHz, acetone-D6)



^1H NMR (400.13 MHz, acetone-D6)

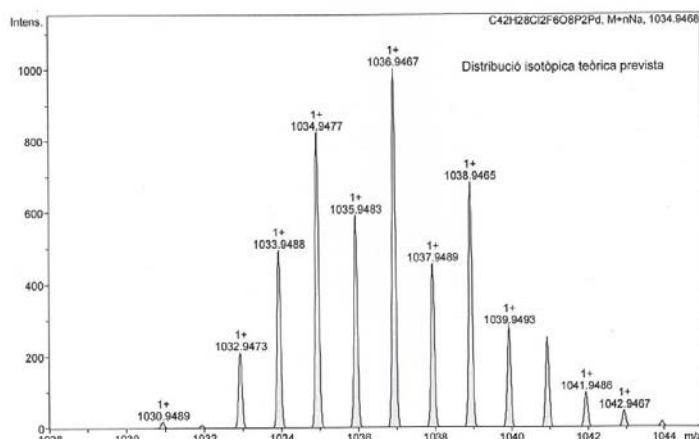


$^{19}\text{F}\{^1\text{H}\}$ NMR (376.50 MHz, acetone- D_6)



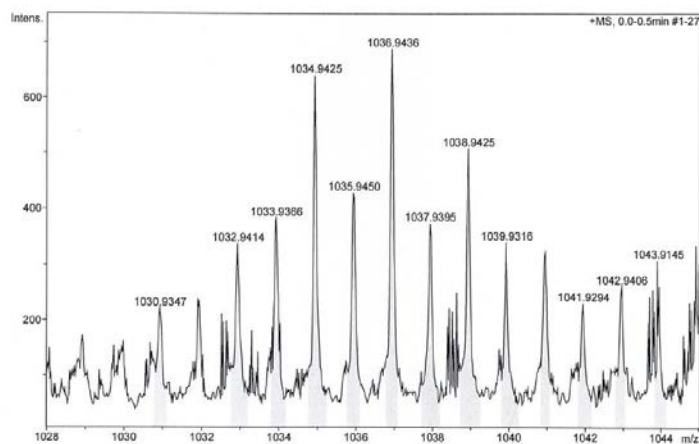
HR-MS (ESI⁺ m/z) $[\text{M}+\text{Na}]^+$

calculated for $[\text{C}_{42}\text{H}_{28}\text{Cl}_2\text{F}_6\text{O}_8\text{P}_2\text{PdNa}]^+$



#	m/z	I	I %
1	1030.9489	18	1.8
2	1032.9473	211	21.1
3	1033.9488	493	49.3
4	1034.9477	821	82.1
5	1035.9483	588	58.8
6	1036.9467	1000	100.0
7	1037.9489	455	45.5
8	1038.9465	681	68.1
9	1039.9493	281	28.1
10	1040.9465	252	25.2
11	1041.9486	96	9.6
12	1042.9467	45	4.5
13	1043.9481	14	1.4

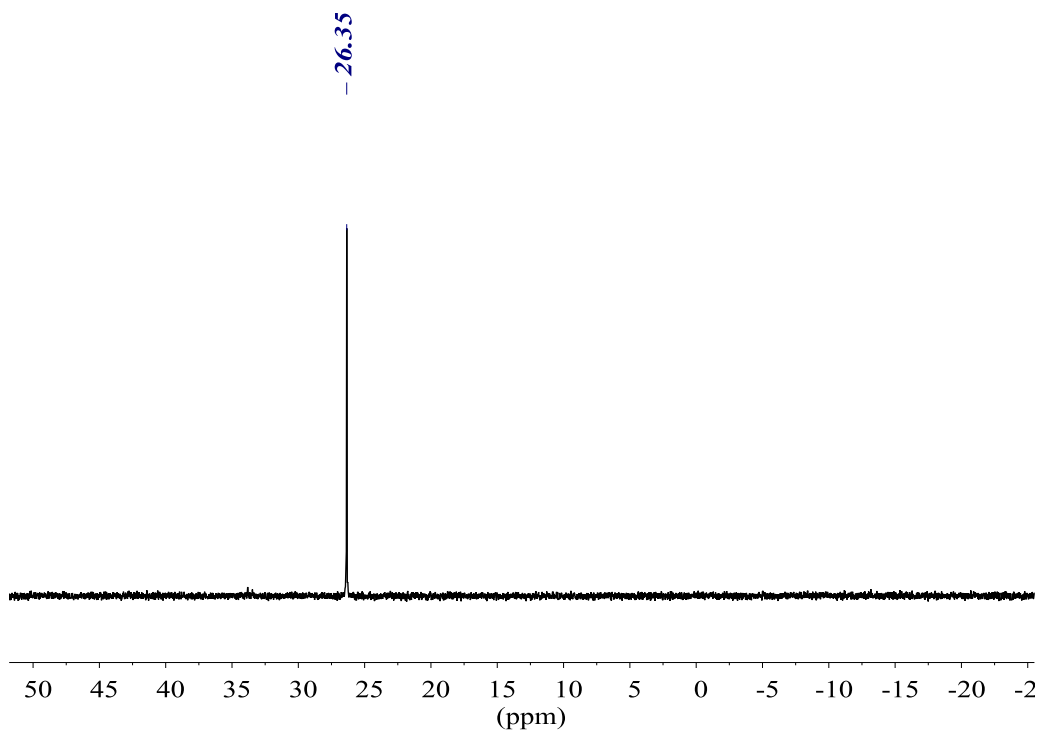
found



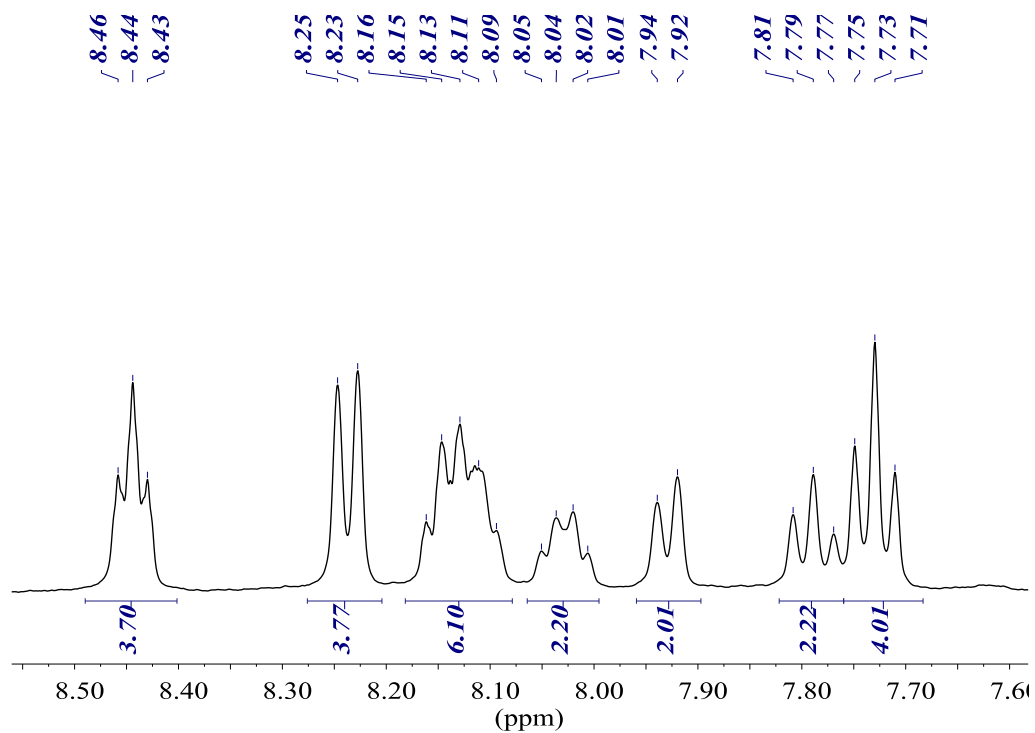
#	m/z	I	I %
1	1030.9347	222	32.2
2	1032.9414	338	49.1
3	1033.9366	383	55.7
4	1034.9425	640	93.0
5	1035.9450	428	62.3
6	1036.9436	688	100.0
7	1037.9395	375	54.5
8	1038.9425	508	73.8
9	1039.9316	340	49.4
10	1040.9405	325	47.2
11	1041.9294	232	33.7
12	1042.9406	263	38.2
13	1043.9145	309	44.9

L = *m*-Miran2phos

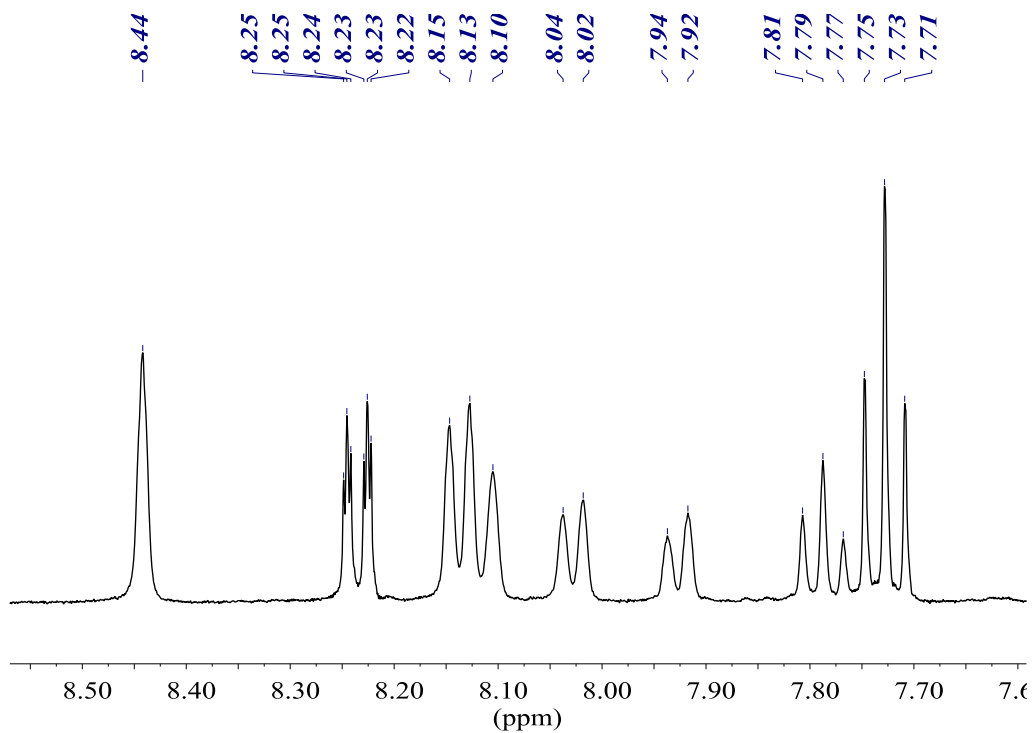
$^{31}\text{P}\{^1\text{H}\}$ NMR (161.98 MHz, acetone-D6)



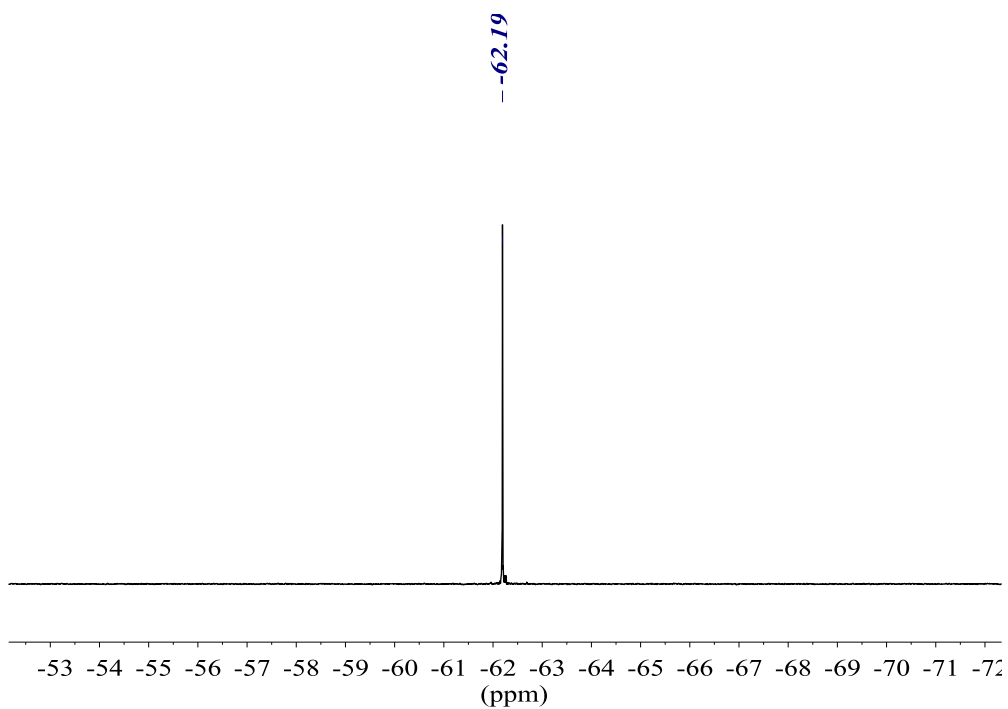
^1H NMR (400.13 MHz, acetone-D6)



$^1\text{H}\{^{31}\text{P}\}$ NMR (400.13 MHz, acetone-D6)

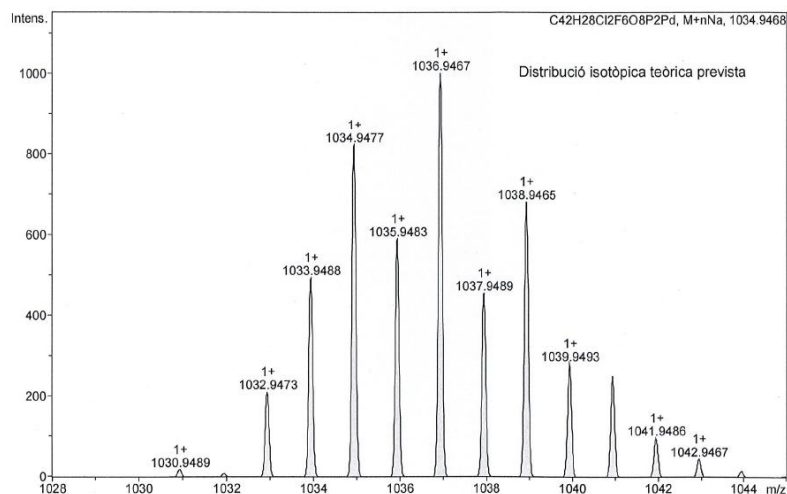


$^{19}\text{F}\{^1\text{H}\}$ NMR (376.50 MHz, acetone-D6)



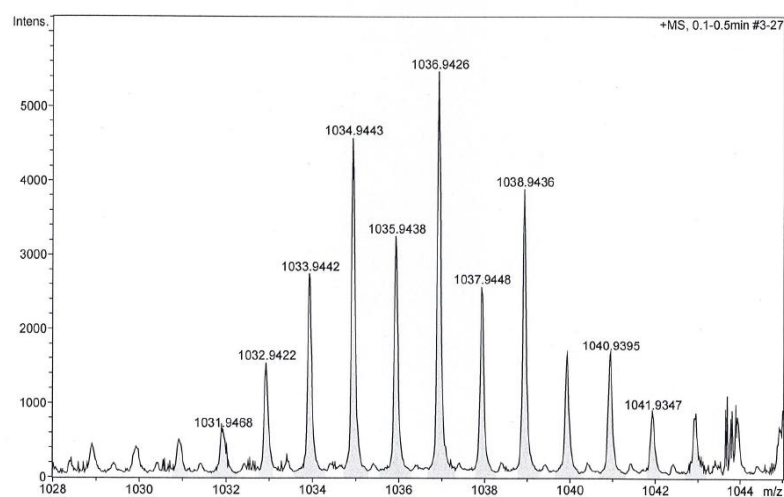
HR-MS (ESI⁺ *m/z*) [M+Na]⁺

calculated for [C₄₂H₂₈Cl₂F₆O₈P₂PdNa]⁺



#	<i>m/z</i>	I	I %
1	1030.9489	18	1.8
2	1031.9523	8	0.8
3	1032.9473	211	21.1
4	1033.9488	493	49.3
5	1034.9477	821	82.1
6	1035.9483	588	58.8
7	1036.9467	1000	100.0
8	1037.9489	455	45.5
9	1038.9465	681	68.1
10	1039.9493	281	28.1
11	1040.9465	252	25.2
12	1041.9486	96	9.6
13	1042.9467	45	4.5
14	1043.9481	14	1.4

found



#	<i>m/z</i>	I	I %
1	1030.9437	513	9.4
2	1031.9468	647	11.8
3	1032.9422	1554	28.4
4	1033.9442	2751	50.4
5	1034.9443	4578	83.8
6	1035.9438	3258	59.6
7	1036.9426	5464	100.0
8	1037.9448	2581	47.2
9	1038.9436	3889	71.2
10	1039.9399	1683	30.8
11	1040.9395	1694	31.0
12	1041.9347	901	16.5
13	1042.9369	885	16.2

8. X-ray diffraction data. CIF files

8.1. (3,5-bis(trifluoromethyl)phenyl)bis(4-(trifluoromethyl)phenyl)phosphine (20)

data_shelx

```
_audit_creation_method          SHELXL-2014
_chemical_name_systematic
;
?
;
_chemical_name_common           ?
_chemical_melting_point         ?
_chemical_formula_moiety        ?
_chemical_formula_sum           'C22 H11 F12 P'
_chemical_formula_weight        534.28
```

```
loop_
  _atom_type_symbol
  _atom_type_description
  _atom_type_scatter_dispersion_real
  _atom_type_scatter_dispersion_imag
  _atom_type_scatter_source
  'C'  'C'  0.0033  0.0016
  'International Tables Vol C Tables 4.2.6.8 and 6.1.1.4'
  'H'  'H'  0.0000  0.0000
  'International Tables Vol C Tables 4.2.6.8 and 6.1.1.4'
  'F'  'F'  0.0171  0.0103
  'International Tables Vol C Tables 4.2.6.8 and 6.1.1.4'
  'P'  'P'  0.1023  0.0942
  'International Tables Vol C Tables 4.2.6.8 and 6.1.1.4'
```

```
_space_group_crystal_system    triclinic
_space_group_IT_number         2
_space_group_name_H-M_alt      'P -1'
_space_group_name_Hall         '-P 1'
```

_shelx_space_group_comment

```
;
The symmetry employed for this shelxl refinement is uniquely
defined
by the following loop, which should always be used as a source of
symmetry information in preference to the above space-group names.
They are only intended as comments.
```

;

```
loop_
  _space_group_symop_operation_xyz
  'x, y, z'
  '-x, -y, -z'

_cell_length_a                 9.7822(6)
_cell_length_b                 11.2459(7)
_cell_length_c                 11.3475(6)
```

```

_cell_angle_alpha          61.3300(10)
_cell_angle_beta          88.8990(10)
_cell_angle_gamma        84.8900(10)
_cell_volume              1090.54(11)
_cell_formula_units_Z     2
_cell_measurement_temperature 293(2)
_cell_measurement_reflns_used 3673
_cell_measurement_theta_min 2.81
_cell_measurement_theta_max 27.68

_exptl_crystal_description prim
_exptl_crystal_colour     yellow
_exptl_crystal_density_meas ?
_exptl_crystal_density_method ?
_exptl_crystal_density_diffn 1.627
_exptl_crystal_F_000     532
_exptl_transmission_factor_min ?
_exptl_transmission_factor_max ?
_exptl_crystal_size_max   0.3
_exptl_crystal_size_mid   0.3
_exptl_crystal_size_min   0.3
_exptl_absorpt_coefficient_mu 0.236
_shelx_estimated_absorpt_T_min ?
_shelx_estimated_absorpt_T_max ?
_exptl_absorpt_correction_type ?
_exptl_absorpt_correction_T_min ?
_exptl_absorpt_correction_T_max ?
_exptl_absorpt_process_details ?

_exptl_special_details
;
?
;

_diffn_ambient_temperature 293(2)
_diffn_radiation_wavelength 0.71073
_diffn_radiation_type      MoK\alpha
_diffn_source              ?
_diffn_measurement_device_type 'Bruker SMART CCD area detector'
_diffn_measurement_method   ?
_diffn_detector_area_resol_mean ?
_diffn_reflns_number        8755
_diffn_reflns_av_unetI/netI 0.0268
_diffn_reflns_av_R_equivalents 0.0159
_diffn_reflns_limit_h_min   -12
_diffn_reflns_limit_h_max   12
_diffn_reflns_limit_k_min   -14
_diffn_reflns_limit_k_max   15
_diffn_reflns_limit_l_min   -15
_diffn_reflns_limit_l_max   15
_diffn_reflns_theta_min     2.046
_diffn_reflns_theta_max     28.746
_diffn_reflns_theta_full    25.242
_diffn_measured_fraction_theta_max 0.895
_diffn_measured_fraction_theta_full 0.990
_diffn_reflns_Laue_measured_fraction_max 0.895
_diffn_reflns_Laue_measured_fraction_full 0.990
_diffn_reflns_point_group_measured_fraction_max 0.895

```

```

_diffrn_reflms_point_group_measured_fraction_full  0.990
_reflms_number_total                               5064
_reflms_number_gt                                  3908
_reflms_threshold_expression                        'I > 2\s(I) '
_reflms_Friedel_coverage                           0.000
_reflms_Friedel_fraction_max                       .
_reflms_Friedel_fraction_full                     .

_reflms_special_details
;
Reflections were merged by SHELXL according to the crystal
class for the calculation of statistics and refinement.

_reflms_Friedel_fraction is defined as the number of unique
Friedel pairs measured divided by the number that would be
possible theoretically, ignoring centric projections and
systematic absences.
;

_computing_data_collection                         ?
_computing_cell_refinement                         ?
_computing_data_reduction                          ?
_computing_structure_solution                     ?
_computing_structure_refinement                   'SHELXL-2014 (Sheldrick, 2014) '
_computing_molecular_graphics                     ?
_computing_publication_material                   ?

_refine_special_details
;
?
;
_refine_ls_structure_factor_coef                   Fsqd
_refine_ls_matrix_type                             full
_refine_ls_weighting_scheme                        calc
_refine_ls_weighting_details
'w=1/[\s^2*(Fo^2)+(0.1174P)^2+0.6169P] where P=(Fo^2+2Fc^2)/3'
_atom_sites_solution_primary                       ?
_atom_sites_solution_secondary                     ?
_atom_sites_solution_hydrogens                     geom
_refine_ls_hydrogen_treatment                      constr
_refine_ls_extinction_method                       none
_refine_ls_extinction_coef                         .
_refine_ls_number_reflms                           5064
_refine_ls_number_parameters                       374
_refine_ls_number_restraints                       121
_refine_ls_R_factor_all                            0.0860
_refine_ls_R_factor_gt                             0.0708
_refine_ls_wR_factor_ref                           0.2180
_refine_ls_wR_factor_gt                            0.2017
_refine_ls_goodness_of_fit_ref                     1.049
_refine_ls_restrained_S_all                        1.186
_refine_ls_shift/su_max                            0.010
_refine_ls_shift/su_mean                           0.000

loop_
_atom_site_label
_atom_site_type_symbol
_atom_site_fract_x

```

```

_atom_site_fract_y
_atom_site_fract_z
_atom_site_U_iso_or_equiv
_atom_site_adp_type
_atom_site_occupancy
_atom_site_site_symmetry_order
_atom_site_calc_flag
_atom_site_refinement_flags_posn
_atom_site_refinement_flags_adp
_atom_site_refinement_flags_occupancy
_atom_site_disorder_assembly
_atom_site_disorder_group
P1 P 0.12334(7) 0.83571(7) 0.45417(7) 0.0486(2) Uani 1 1 d . . . .
.
C11 C 0.0944(3) 0.8065(3) 0.3111(3) 0.0480(6) Uani 1 1 d . . . .
C12 C 0.1474(3) 0.8796(3) 0.1854(3) 0.0569(7) Uani 1 1 d . . . .
H12 H 0.2041 0.9475 0.1698 0.068 Uiso 1 1 calc R U . . .
C13 C 0.1170(3) 0.8529(3) 0.0824(3) 0.0637(8) Uani 1 1 d . . . .
H13 H 0.1530 0.9039 -0.0019 0.076 Uiso 1 1 calc R U . . .
C14 C 0.0346(3) 0.7524(3) 0.1024(3) 0.0584(7) Uani 1 1 d D . . . .
C15 C -0.0208(4) 0.6797(4) 0.2277(4) 0.0736(9) Uani 1 1 d . . . .
H15 H -0.0774 0.6118 0.2429 0.088 Uiso 1 1 calc R U . . .
C16 C 0.0076(4) 0.7076(4) 0.3300(3) 0.0691(9) Uani 1 1 d . . . .
H16 H -0.0320 0.6595 0.4130 0.083 Uiso 1 1 calc R U . . .
C17 C 0.0074(3) 0.7209(3) -0.0069(3) 0.0830(11) Uani 1 1 d D . . .
.
F1A F -0.0273(13) 0.8328(5) -0.1238(5) 0.145(6) Uani 0.399(3) 1 d D
U P A 1
F2A F -0.0792(11) 0.6239(10) 0.0290(8) 0.116(4) Uani 0.399(3) 1 d D
U P A 1
F3A F 0.1209(5) 0.6653(8) -0.0366(7) 0.091(2) Uani 0.399(3) 1 d D U
P A 1
F1B F 0.0374(7) 0.8201(5) -0.1285(3) 0.0769(18) Uani 0.436(3) 1 d D
U P A 2
F2B F -0.1274(4) 0.7234(11) -0.0289(7) 0.111(4) Uani 0.436(3) 1 d D
U P A 2
F3B F 0.0799(12) 0.6069(8) 0.0094(9) 0.166(7) Uani 0.436(3) 1 d D U
P A 2
F1C F 0.1090(9) 0.7528(16) -0.0951(10) 0.115(6) Uani 0.165(3) 1 d D
U P A 3
F2C F -0.1062(10) 0.7922(13) -0.0796(11) 0.111(8) Uani 0.165(3) 1 d
D U P A 3
F3C F -0.0102(16) 0.5889(5) 0.0402(7) 0.093(6) Uani 0.165(3) 1 d D
U P A 3
C21 C 0.2563(3) 0.9554(3) 0.3922(3) 0.0472(6) Uani 1 1 d . . . .
C22 C 0.3886(3) 0.9238(3) 0.3633(3) 0.0511(6) Uani 1 1 d . . . .
H22 H 0.4149 0.8364 0.3773 0.061 Uiso 1 1 calc R U . . .
C23 C 0.4822(3) 1.0214(3) 0.3138(3) 0.0530(6) Uani 1 1 d . . . .
C24 C 0.4450(3) 1.1510(3) 0.2937(3) 0.0586(7) Uani 1 1 d . . . .
H24 H 0.5078 1.2163 0.2605 0.070 Uiso 1 1 calc R U . . .
C25 C 0.3145(3) 1.1832(3) 0.3231(3) 0.0561(7) Uani 1 1 d . . . .
C26 C 0.2200(3) 1.0859(3) 0.3726(3) 0.0515(6) Uani 1 1 d . . . .
H26 H 0.1321 1.1085 0.3927 0.062 Uiso 1 1 calc R U . . .
C27 C 0.6219(3) 0.9870(4) 0.2761(4) 0.0664(8) Uani 1 1 d . . . .
F4 F 0.6651(3) 0.8589(3) 0.3433(3) 0.1267(12) Uani 1 1 d . . . .
F5 F 0.6242(3) 1.0158(4) 0.1495(3) 0.1235(11) Uani 1 1 d . . . .
F6 F 0.7172(3) 1.0521(4) 0.2928(5) 0.1449(14) Uani 1 1 d . . . .
C28 C 0.2750(5) 1.3243(3) 0.2996(4) 0.0784(10) Uani 1 1 d . . . .

```


F7 F 0.1510(4) 1.3458(3) 0.3245(6) 0.202(3) Uani 1 1 d
 F8 F 0.3526(4) 1.3577(3) 0.3722(4) 0.1443(14) Uani 1 1 d
 F9 F 0.2992(4) 1.4169(2) 0.1786(3) 0.1383(12) Uani 1 1 d
 C31 C 0.2250(3) 0.6782(3) 0.5707(3) 0.0479(6) Uani 1 1 d
 C32 C 0.2899(3) 0.5830(3) 0.5377(3) 0.0564(7) Uani 1 1 d
 H32 H 0.2825 0.5968 0.4503 0.068 Uiso 1 1 calc R U . . .
 C33 C 0.3654(3) 0.4679(3) 0.6344(3) 0.0626(7) Uani 1 1 d
 H33 H 0.4072 0.4042 0.6118 0.075 Uiso 1 1 calc R U . . .
 C34 C 0.3787(3) 0.4473(3) 0.7638(3) 0.0599(7) Uani 1 1 d
 C35 C 0.3129(3) 0.5391(3) 0.7986(3) 0.0630(8) Uani 1 1 d
 H35 H 0.3199 0.5244 0.8863 0.076 Uiso 1 1 calc R U . . .
 C36 C 0.2364(3) 0.6533(3) 0.7026(3) 0.0576(7) Uani 1 1 d
 H36 H 0.1918 0.7146 0.7268 0.069 Uiso 1 1 calc R U . . .
 C37 C 0.4590(5) 0.3231(4) 0.8673(4) 0.0826(10) Uani 1 1 d
 F10 F 0.5534(4) 0.2739(5) 0.8188(3) 0.189(2) Uani 1 1 d
 F11 F 0.5166(4) 0.3419(3) 0.9600(3) 0.1439(13) Uani 1 1 d
 F12 F 0.3824(4) 0.2247(3) 0.9369(4) 0.1586(16) Uani 1 1 d

loop_

_atom_site_aniso_label
 _atom_site_aniso_U_11
 _atom_site_aniso_U_22
 _atom_site_aniso_U_33
 _atom_site_aniso_U_23
 _atom_site_aniso_U_13
 _atom_site_aniso_U_12
 P1 0.0494(4) 0.0486(4) 0.0548(4) -0.0300(3) 0.0112(3) -0.0089(3)
 C11 0.0460(13) 0.0495(13) 0.0533(14) -0.0286(11) 0.0035(10) -
 0.0050(10)
 C12 0.0586(16) 0.0586(16) 0.0569(15) -0.0288(13) 0.0058(12) -
 0.0165(13)
 C13 0.0680(18) 0.0731(19) 0.0560(16) -0.0347(15) 0.0104(14) -
 0.0149(15)
 C14 0.0550(16) 0.0653(18) 0.0659(17) -0.0407(15) -0.0015(13) -
 0.0021(13)
 C15 0.081(2) 0.078(2) 0.077(2) -0.0455(18) 0.0084(17) -0.0358(18)
 C16 0.074(2) 0.081(2) 0.0609(17) -0.0362(16) 0.0145(15) -0.0353(17)
 C17 0.098(3) 0.089(3) 0.080(2) -0.055(2) -0.003(2) -0.011(2)
 F1A 0.190(13) 0.115(7) 0.144(9) -0.080(6) -0.125(8) 0.058(8)
 F2A 0.136(9) 0.148(9) 0.136(8) -0.118(8) 0.048(7) -0.071(7)
 F3A 0.135(5) 0.086(6) 0.057(4) -0.043(4) 0.011(4) 0.025(5)
 F1B 0.081(4) 0.103(5) 0.058(3) -0.049(3) -0.003(3) 0.003(3)
 F2B 0.106(5) 0.170(10) 0.075(5) -0.064(6) 0.004(4) -0.070(6)
 F3B 0.300(17) 0.101(8) 0.111(8) -0.073(7) -0.057(9) 0.066(9)
 F1C 0.146(15) 0.122(14) 0.111(13) -0.086(11) 0.016(12) 0.003(13)
 F2C 0.153(18) 0.085(11) 0.105(14) -0.049(10) -0.050(13) -0.028(11)
 F3C 0.094(13) 0.108(10) 0.143(13) -0.115(10) -0.006(11) 0.007(10)
 C21 0.0528(14) 0.0475(13) 0.0463(13) -0.0258(11) 0.0036(10) -
 0.0101(11)
 C22 0.0553(15) 0.0483(14) 0.0534(14) -0.0272(12) 0.0058(11) -
 0.0074(11)
 C23 0.0548(15) 0.0582(16) 0.0462(13) -0.0242(12) 0.0049(11) -
 0.0119(12)
 C24 0.0675(18) 0.0541(16) 0.0519(15) -0.0215(12) 0.0056(13) -
 0.0199(13)
 C25 0.0722(18) 0.0442(14) 0.0515(14) -0.0219(12) 0.0023(13) -
 0.0096(12)

```

C26  0.0581(15)  0.0497(14)  0.0505(14)  -0.0273(12)  0.0024(11)  -
0.0042(11)
C27  0.0589(17)  0.069(2)  0.072(2)  -0.0334(16)  0.0107(15)  -0.0133(15)
F4  0.0801(16)  0.0921(18)  0.159(3)  -0.0249(18)  0.0390(16)  0.0095(13)
F5  0.1012(19)  0.179(3)  0.0791(16)  -0.0579(17)  0.0265(13)  0.0097(19)
F6  0.0665(15)  0.187(3)  0.254(4)  -0.160(3)  0.0377(19)  -0.0462(18)
C28  0.098(3)  0.0488(17)  0.088(2)  -0.0321(17)  0.012(2)  -0.0135(17)
F7  0.135(3)  0.0717(18)  0.401(7)  -0.115(3)  0.116(4)  -0.0239(17)
F8  0.226(4)  0.0854(18)  0.151(3)  -0.0792(19)  -0.031(3)  -0.012(2)
F9  0.222(4)  0.0516(13)  0.106(2)  -0.0110(13)  0.014(2)  -0.0046(17)
C31  0.0517(14)  0.0490(13)  0.0473(13)  -0.0255(11)  0.0131(11)  -
0.0136(11)
C32  0.0673(17)  0.0579(16)  0.0505(14)  -0.0316(13)  0.0092(12)  -
0.0052(13)
C33  0.0722(19)  0.0558(17)  0.0631(17)  -0.0326(14)  0.0093(14)
0.0009(14)
C34  0.0620(17)  0.0565(16)  0.0554(15)  -0.0217(13)  0.0050(13)  -
0.0085(13)
C35  0.076(2)  0.0684(19)  0.0482(15)  -0.0306(14)  0.0024(13)  -
0.0102(15)
C36  0.0698(18)  0.0585(16)  0.0570(15)  -0.0374(13)  0.0098(13)  -
0.0093(13)
C37  0.088(3)  0.073(2)  0.071(2)  -0.0239(18)  -0.0029(19)  0.0066(19)
F10  0.178(4)  0.211(4)  0.104(2)  -0.040(2)  -0.016(2)  0.130(3)
F11  0.190(3)  0.115(2)  0.106(2)  -0.0398(18)  -0.074(2)  0.024(2)
F12  0.145(3)  0.0744(17)  0.170(3)  0.0106(19)  -0.015(2)  -0.0049(18)

```

```
_geom_special_details
```

```
;
```

```

All esds (except the esd in the dihedral angle between two l.s.
planes)
are estimated using the full covariance matrix. The cell esds are
taken
into account individually in the estimation of esds in distances,
angles
and torsion angles; correlations between esds in cell parameters
are only
used when they are defined by crystal symmetry. An approximate
(isotropic)
treatment of cell esds is used for estimating esds involving l.s.
planes.

```

```
;
```

```
loop_
```

```

_geom_bond_atom_site_label_1
_geom_bond_atom_site_label_2
_geom_bond_distance
_geom_bond_site_symmetry_2
_geom_bond_publ_flag
P1 C31 1.834(3) . ?
P1 C21 1.835(3) . ?
P1 C11 1.836(3) . ?
C11 C12 1.379(4) . ?
C11 C16 1.391(4) . ?
C12 C13 1.382(4) . ?
C13 C14 1.374(4) . ?
C14 C15 1.385(5) . ?
C14 C17 1.480(3) . ?

```

C15 C16 1.378(5) . ?
 C17 F3B 1.340(2) . ?
 C17 F1A 1.340(2) . ?
 C17 F2A 1.341(2) . ?
 C17 F1C 1.341(2) . ?
 C17 F3C 1.341(2) . ?
 C17 F1B 1.341(2) . ?
 C17 F2C 1.341(2) . ?
 C17 F2B 1.341(2) . ?
 C17 F3A 1.342(2) . ?
 C21 C22 1.387(4) . ?
 C21 C26 1.388(4) . ?
 C22 C23 1.388(4) . ?
 C23 C24 1.378(4) . ?
 C23 C27 1.497(4) . ?
 C24 C25 1.374(5) . ?
 C25 C26 1.392(4) . ?
 C25 C28 1.493(4) . ?
 C27 F4 1.298(4) . ?
 C27 F6 1.306(4) . ?
 C27 F5 1.312(4) . ?
 C28 F7 1.268(5) . ?
 C28 F9 1.298(5) . ?
 C28 F8 1.329(5) . ?
 C31 C36 1.389(4) . ?
 C31 C32 1.394(4) . ?
 C32 C33 1.387(4) . ?
 C33 C34 1.379(4) . ?
 C34 C35 1.379(5) . ?
 C34 C37 1.488(5) . ?
 C35 C36 1.383(4) . ?
 C37 F10 1.282(5) . ?
 C37 F12 1.302(5) . ?
 C37 F11 1.314(5) . ?

loop_
 _geom_angle_atom_site_label_1
 _geom_angle_atom_site_label_2
 _geom_angle_atom_site_label_3
 _geom_angle
 _geom_angle_site_symmetry_1
 _geom_angle_site_symmetry_3
 _geom_angle_publ_flag
 C31 P1 C21 100.90(12) . . ?
 C31 P1 C11 101.94(12) . . ?
 C21 P1 C11 102.27(12) . . ?
 C12 C11 C16 118.0(3) . . ?
 C12 C11 P1 124.7(2) . . ?
 C16 C11 P1 117.3(2) . . ?
 C11 C12 C13 120.7(3) . . ?
 C14 C13 C12 121.1(3) . . ?
 C13 C14 C15 118.7(3) . . ?
 C13 C14 C17 120.7(2) . . ?
 C15 C14 C17 120.6(2) . . ?
 C16 C15 C14 120.3(3) . . ?
 C15 C16 C11 121.2(3) . . ?
 F1A C17 F2A 113.9(6) . . ?
 F1C C17 F3C 108.1(8) . . ?

F3B C17 F1B 106.5(6) . . ?
 F1C C17 F2C 105.4(8) . . ?
 F3C C17 F2C 106.9(8) . . ?
 F3B C17 F2B 113.5(6) . . ?
 F1B C17 F2B 98.3(5) . . ?
 F1A C17 F3A 103.0(6) . . ?
 F2A C17 F3A 102.5(6) . . ?
 F3B C17 C14 112.5(3) . . ?
 F1A C17 C14 112.6(3) . . ?
 F2A C17 C14 112.5(3) . . ?
 F1C C17 C14 112.1(3) . . ?
 F3C C17 C14 112.0(3) . . ?
 F1B C17 C14 112.9(2) . . ?
 F2C C17 C14 112.0(3) . . ?
 F2B C17 C14 112.2(3) . . ?
 F3A C17 C14 111.5(3) . . ?
 C22 C21 C26 118.7(2) . . ?
 C22 C21 P1 124.2(2) . . ?
 C26 C21 P1 117.1(2) . . ?
 C21 C22 C23 120.7(3) . . ?
 C24 C23 C22 120.3(3) . . ?
 C24 C23 C27 120.1(3) . . ?
 C22 C23 C27 119.6(3) . . ?
 C25 C24 C23 119.6(3) . . ?
 C24 C25 C26 120.5(3) . . ?
 C24 C25 C28 119.1(3) . . ?
 C26 C25 C28 120.4(3) . . ?
 C21 C26 C25 120.3(3) . . ?
 F4 C27 F6 105.6(3) . . ?
 F4 C27 F5 105.1(3) . . ?
 F6 C27 F5 106.5(3) . . ?
 F4 C27 C23 114.0(3) . . ?
 F6 C27 C23 113.5(3) . . ?
 F5 C27 C23 111.5(3) . . ?
 F7 C28 F9 108.3(4) . . ?
 F7 C28 F8 106.9(4) . . ?
 F9 C28 F8 101.2(3) . . ?
 F7 C28 C25 114.5(3) . . ?
 F9 C28 C25 113.0(3) . . ?
 F8 C28 C25 112.1(3) . . ?
 C36 C31 C32 118.3(3) . . ?
 C36 C31 P1 116.2(2) . . ?
 C32 C31 P1 125.5(2) . . ?
 C33 C32 C31 120.4(3) . . ?
 C34 C33 C32 120.4(3) . . ?
 C35 C34 C33 120.0(3) . . ?
 C35 C34 C37 119.9(3) . . ?
 C33 C34 C37 120.1(3) . . ?
 C34 C35 C36 119.7(3) . . ?
 C35 C36 C31 121.3(3) . . ?
 F10 C37 F12 106.1(5) . . ?
 F10 C37 F11 107.6(4) . . ?
 F12 C37 F11 102.8(4) . . ?
 F10 C37 C34 113.7(3) . . ?
 F12 C37 C34 112.6(4) . . ?
 F11 C37 C34 113.2(4) . . ?

_refine_diff_density_max 0.606

```
_refine_diff_density_min    -0.405
_refine_diff_density_rms    0.063
```

8.2. *o*-Miranphos (10)

```
data_shelx
```

```
_audit_creation_method      SHELXL-2014
_chemical_name_systematic
;
?
;
_chemical_name_common        ?
_chemical_melting_point      ?
_chemical_formula_moiety     ?
_chemical_formula_sum        'C21 H13 F6 O2 P'
_chemical_formula_weight     442.28
```

```
loop_
  _atom_type_symbol
  _atom_type_description
  _atom_type_scatter_dispersion_real
  _atom_type_scatter_dispersion_imag
  _atom_type_scatter_source
  'C' 'C' 0.0033 0.0016
  'International Tables Vol C Tables 4.2.6.8 and 6.1.1.4'
  'H' 'H' 0.0000 0.0000
  'International Tables Vol C Tables 4.2.6.8 and 6.1.1.4'
  'F' 'F' 0.0171 0.0103
  'International Tables Vol C Tables 4.2.6.8 and 6.1.1.4'
  'O' 'O' 0.0106 0.0060
  'International Tables Vol C Tables 4.2.6.8 and 6.1.1.4'
  'P' 'P' 0.1023 0.0942
  'International Tables Vol C Tables 4.2.6.8 and 6.1.1.4'
```

```
_space_group_crystal_system monoclinic
_space_group_IT_number       14
_space_group_name_H-M_alt    'P 21/c'
_space_group_name_Hall       '-P 2ybc'
```

```
_shelx_space_group_comment
```

```
;
```

The symmetry employed for this shelxl refinement is uniquely defined

by the following loop, which should always be used as a source of symmetry information in preference to the above space-group names. They are only intended as comments.

```
;
```

```
loop_
  _space_group_symop_operation_xyz
  'x, y, z'
  '-x, y+1/2, -z+1/2'
  '-x, -y, -z'
  'x, -y-1/2, z-1/2'
```

_cell_length_a	6.9841(3)
_cell_length_b	18.9623(8)
_cell_length_c	14.8050(6)
_cell_angle_alpha	90
_cell_angle_beta	98.0000(10)
_cell_angle_gamma	90
_cell_volume	1941.61(14)
_cell_formula_units_Z	4
_cell_measurement_temperature	296(2)
_cell_measurement_reflns_used	7127
_cell_measurement_theta_min	2.56
_cell_measurement_theta_max	28.1
_exptl_crystal_description	prism
_exptl_crystal_colour	colourless
_exptl_crystal_density_meas	?
_exptl_crystal_density_method	?
_exptl_crystal_density_diffn	1.513
_exptl_crystal_F_000	896
_exptl_transmission_factor_min	?
_exptl_transmission_factor_max	?
_exptl_crystal_size_max	0.67
_exptl_crystal_size_mid	0.18
_exptl_crystal_size_min	0.14
_exptl_absorpt_coefficient_mu	0.213
_shelx_estimated_absorpt_T_min	?
_shelx_estimated_absorpt_T_max	?
_exptl_absorpt_correction_type	?
_exptl_absorpt_correction_T_min	?
_exptl_absorpt_correction_T_max	?
_exptl_absorpt_process_details	?
_exptl_special_details	
;	
?	
;	
_diffn_ambient_temperature	296(2)
_diffn_radiation_wavelength	0.71073
_diffn_radiation_type	MoK\alpha
_diffn_source	?
_diffn_measurement_device_type	'Bruker SMART CDD area detector'
_diffn_measurement_method	?
_diffn_detector_area_resol_mean	?
_diffn_reflns_number	15198
_diffn_reflns_av_unetI/netI	0.0180
_diffn_reflns_av_R_equivalents	0.0177
_diffn_reflns_limit_h_min	-9
_diffn_reflns_limit_h_max	9
_diffn_reflns_limit_k_min	-24
_diffn_reflns_limit_k_max	25
_diffn_reflns_limit_l_min	-18
_diffn_reflns_limit_l_max	19
_diffn_reflns_theta_min	1.756
_diffn_reflns_theta_max	28.673
_diffn_reflns_theta_full	25.242
_diffn_measured_fraction_theta_max	0.935

```

_diffn_measured_fraction_theta_full 1.000
_diffn_reflns_Laue_measured_fraction_max 0.935
_diffn_reflns_Laue_measured_fraction_full 1.000
_diffn_reflns_point_group_measured_fraction_max 0.935
_diffn_reflns_point_group_measured_fraction_full 1.000
_reflns_number_total 4686
_reflns_number_gt 3852
_reflns_threshold_expression 'I > 2\s(I)'
_reflns_Friedel_coverage 0.000
_reflns_Friedel_fraction_max .
_reflns_Friedel_fraction_full .

_reflns_special_details
;
Reflections were merged by SHELXL according to the crystal
class for the calculation of statistics and refinement.

_reflns_Friedel_fraction is defined as the number of unique
Friedel pairs measured divided by the number that would be
possible theoretically, ignoring centric projections and
systematic absences.
;

_computing_data_collection ?
_computing_cell_refinement ?
_computing_data_reduction ?
_computing_structure_solution ?
_computing_structure_refinement 'SHELXL-2014 (Sheldrick, 2014)'
_computing_molecular_graphics ?
_computing_publication_material ?

_refine_special_details
;
?
;
_refine_ls_structure_factor_coef Fsqd
_refine_ls_matrix_type full
_refine_ls_weighting_scheme calc
_refine_ls_weighting_details
'w=1/[\s^2^(Fo^2^)+(0.0739P)^2^+0.6152P] where P=(Fo^2^+2Fc^2^)/3'
_atom_sites_solution_primary ?
_atom_sites_solution_secondary ?
_atom_sites_solution_hydrogens mixed
_refine_ls_hydrogen_treatment mixed
_refine_ls_extinction_method none
_refine_ls_extinction_coef .
_refine_ls_number_reflns 4686
_refine_ls_number_parameters 275
_refine_ls_number_restraints 0
_refine_ls_R_factor_all 0.0564
_refine_ls_R_factor_gt 0.0465
_refine_ls_wR_factor_ref 0.1335
_refine_ls_wR_factor_gt 0.1259
_refine_ls_goodness_of_fit_ref 1.025
_refine_ls_restrained_S_all 1.025
_refine_ls_shift/su_max 0.001
_refine_ls_shift/su_mean 0.000

```

```

loop_
  _atom_site_label
  _atom_site_type_symbol
  _atom_site_fract_x
  _atom_site_fract_y
  _atom_site_fract_z
  _atom_site_U_iso_or_equiv
  _atom_site_adp_type
  _atom_site_occupancy
  _atom_site_site_symmetry_order
  _atom_site_calc_flag
  _atom_site_refinement_flags_posn
  _atom_site_refinement_flags_adp
  _atom_site_refinement_flags_occupancy
  _atom_site_disorder_assembly
  _atom_site_disorder_group
P1 P 0.30890(6) 0.59752(2) 0.73757(3) 0.03647(13) Uani 1 1 d . . .
. .
C11 C 0.2807(3) 0.50633(9) 0.77741(11) 0.0417(4) Uani 1 1 d . . .
.
C12 C 0.1143(3) 0.46777(10) 0.75020(13) 0.0515(4) Uani 1 1 d . . .
. .
H12 H 0.0131 0.4885 0.7118 0.062 Uiso 1 1 calc R U . . .
C13 C 0.0952(4) 0.39853(12) 0.77906(18) 0.0729(7) Uani 1 1 d . . .
. .
H13 H -0.0170 0.3732 0.7597 0.087 Uiso 1 1 calc R U . . .
C14 C 0.2444(5) 0.36786(13) 0.8367(2) 0.0855(9) Uani 1 1 d . . .
.
H14 H 0.2319 0.3219 0.8569 0.103 Uiso 1 1 calc R U . . .
C15 C 0.4102(5) 0.40457(14) 0.86418(19) 0.0777(8) Uani 1 1 d . . .
. .
H15 H 0.5099 0.3834 0.9029 0.093 Uiso 1 1 calc R U . . .
C16 C 0.4315(3) 0.47306(12) 0.83496(14) 0.0577(5) Uani 1 1 d . . .
. .
C17 C 0.6186(4) 0.51051(18) 0.8651(2) 0.0827(8) Uani 1 1 d . . .
.
F11 F 0.7411(3) 0.47395(15) 0.92235(19) 0.1506(10) Uani 1 1 d . . .
. .
F12 F 0.5998(3) 0.57247(12) 0.90137(14) 0.1069(6) Uani 1 1 d . . .
. .
F13 F 0.7131(2) 0.52286(14) 0.79275(16) 0.1244(8) Uani 1 1 d . . .
. .
C21 C 0.0960(2) 0.60728(8) 0.64914(10) 0.0356(3) Uani 1 1 d . . .
.
C22 C -0.0737(3) 0.64018(10) 0.66718(12) 0.0454(4) Uani 1 1 d . . .
. .
H22 H -0.0837 0.6543 0.7265 0.054 Uiso 1 1 calc R U . . .
C23 C -0.2268(3) 0.65222(11) 0.59946(14) 0.0509(4) Uani 1 1 d . . .
. .
H23 H -0.3391 0.6731 0.6139 0.061 Uiso 1 1 calc R U . . .
C24 C -0.2146(3) 0.63345(11) 0.51015(14) 0.0511(4) Uani 1 1 d . . .
. .
H24 H -0.3174 0.6420 0.4644 0.061 Uiso 1 1 calc R U . . .
C25 C -0.0479(3) 0.60181(9) 0.48980(12) 0.0434(4) Uani 1 1 d . . .
. .
H25 H -0.0383 0.5896 0.4297 0.052 Uiso 1 1 calc R U . . .
C26 C 0.1058(2) 0.58785(8) 0.55760(10) 0.0355(3) Uani 1 1 d . . .
.

```


C27 C 0.2787(2) 0.55063(8) 0.53260(10) 0.0364(3) Uani 1 1 d
 .
 F21 F 0.3429(3) 0.75179(8) 0.70397(9) 0.0813(4) Uani 1 1 d
 .
 F22 F 0.4254(3) 0.82434(7) 0.81230(12) 0.0927(5) Uani 1 1 d
 .
 F23 F 0.5901(2) 0.73080(9) 0.80093(13) 0.0894(5) Uani 1 1 d
 .
 C31 C 0.2271(2) 0.64707(9) 0.83342(11) 0.0390(3) Uani 1 1 d
 .
 C32 C 0.1154(3) 0.61569(11) 0.89283(12) 0.0491(4) Uani 1 1 d
 . .
 H32 H 0.0757 0.5692 0.8828 0.059 Uiso 1 1 calc R U
 C33 C 0.0614(3) 0.65199(12) 0.96688(14) 0.0590(5) Uani 1 1 d
 . .
 H33 H -0.0151 0.6301 1.0052 0.071 Uiso 1 1 calc R U
 C34 C 0.1214(4) 0.72039(12) 0.98316(14) 0.0654(6) Uani 1 1 d
 . .
 H34 H 0.0866 0.7447 1.0329 0.078 Uiso 1 1 calc R U
 C35 C 0.2330(4) 0.75285(12) 0.92577(15) 0.0625(6) Uani 1 1 d
 . .
 H35 H 0.2733 0.7992 0.9370 0.075 Uiso 1 1 calc R U
 C36 C 0.2860(3) 0.71700(10) 0.85122(12) 0.0463(4) Uani 1 1 d
 . .
 C37 C 0.4097(3) 0.75567(11) 0.79266(16) 0.0608(5) Uani 1 1 d
 . .
 O1 O 0.2906(2) 0.55134(8) 0.44444(8) 0.0522(3) Uani 1 1 d
 O2 O 0.39661(18) 0.52145(7) 0.58871(8) 0.0451(3) Uani 1 1 d
 .
 H1 H 0.380(4) 0.5283(13) 0.4386(16) 0.058(7) Uiso 1 1 d

loop_

_atom_site_aniso_label
 _atom_site_aniso_U_11
 _atom_site_aniso_U_22
 _atom_site_aniso_U_33
 _atom_site_aniso_U_23
 _atom_site_aniso_U_13
 _atom_site_aniso_U_12
 P1 0.0380(2) 0.0406(2) 0.0324(2) -0.00504(15) 0.01035(16)
 0.00089(16)
 C11 0.0508(10) 0.0409(8) 0.0367(8) -0.0024(6) 0.0180(7) 0.0070(7)
 C12 0.0646(12) 0.0450(9) 0.0480(10) -0.0043(8) 0.0190(9) -0.0027(8)
 C13 0.1010(19) 0.0508(12) 0.0749(15) -0.0078(11) 0.0408(14) -
 0.0150(12)
 C14 0.136(3) 0.0478(12) 0.0852(18) 0.0163(12) 0.0579(18) 0.0190(15)
 C15 0.0959(19) 0.0662(15) 0.0768(16) 0.0243(12) 0.0322(15)
 0.0320(14)
 C16 0.0630(12) 0.0618(12) 0.0518(11) 0.0099(9) 0.0205(9) 0.0214(10)
 C17 0.0544(13) 0.105(2) 0.0868(18) 0.0288(16) 0.0018(12) 0.0232(14)
 F11 0.0933(14) 0.170(2) 0.172(2) 0.0707(18) -0.0398(14) 0.0305(14)
 F12 0.0766(11) 0.1148(15) 0.1193(15) -0.0118(12) -0.0222(10) -
 0.0006(10)
 F13 0.0597(10) 0.186(2) 0.1323(16) 0.0299(16) 0.0315(10) 0.0065(11)
 C21 0.0395(8) 0.0350(7) 0.0339(7) -0.0017(6) 0.0105(6) 0.0001(6)
 C22 0.0456(9) 0.0504(10) 0.0420(9) -0.0048(7) 0.0128(7) 0.0056(7)
 C23 0.0406(9) 0.0550(11) 0.0584(11) -0.0018(8) 0.0113(8) 0.0088(8)
 C24 0.0458(10) 0.0538(11) 0.0515(10) 0.0018(8) -0.0006(8) 0.0028(8)

C25 0.0511(10) 0.0426(9) 0.0365(8) -0.0014(6) 0.0064(7) -0.0030(7)
 C26 0.0428(8) 0.0309(7) 0.0346(7) -0.0012(6) 0.0116(6) -0.0011(6)
 C27 0.0456(9) 0.0331(7) 0.0327(7) -0.0036(6) 0.0130(6) -0.0025(6)
 F21 0.1191(12) 0.0746(9) 0.0517(7) 0.0046(6) 0.0177(8) -0.0262(8)
 F22 0.1339(14) 0.0519(8) 0.0994(11) -0.0185(7) 0.0411(11) -
 0.0286(8)
 F23 0.0668(9) 0.0968(12) 0.1098(13) -0.0020(9) 0.0303(8) -0.0136(8)
 C31 0.0421(8) 0.0445(8) 0.0313(7) -0.0054(6) 0.0077(6) 0.0050(7)
 C32 0.0586(11) 0.0488(10) 0.0433(9) -0.0041(8) 0.0194(8) 0.0035(8)
 C33 0.0722(13) 0.0666(13) 0.0437(10) 0.0004(9) 0.0271(9) 0.0136(10)
 C34 0.0885(16) 0.0641(13) 0.0471(11) -0.0148(9) 0.0217(11)
 0.0182(11)
 C35 0.0828(15) 0.0520(11) 0.0544(11) -0.0194(9) 0.0152(10)
 0.0043(10)
 C36 0.0521(10) 0.0473(10) 0.0397(9) -0.0075(7) 0.0074(7) 0.0021(8)
 C37 0.0739(14) 0.0507(11) 0.0595(12) -0.0106(9) 0.0159(10) -
 0.0134(10)
 O1 0.0646(9) 0.0614(8) 0.0343(6) 0.0037(5) 0.0197(6) 0.0191(7)
 O2 0.0495(7) 0.0530(7) 0.0349(6) -0.0025(5) 0.0130(5) 0.0101(6)

_geom_special_details

;

All esds (except the esd in the dihedral angle between two l.s. planes)

are estimated using the full covariance matrix. The cell esds are taken

into account individually in the estimation of esds in distances, angles

and torsion angles; correlations between esds in cell parameters are only

used when they are defined by crystal symmetry. An approximate (isotropic)

treatment of cell esds is used for estimating esds involving l.s. planes.

;

loop_

_geom_bond_atom_site_label_1

_geom_bond_atom_site_label_2

_geom_bond_distance

_geom_bond_site_symmetry_2

_geom_bond_publ_flag

P1 C11 1.8464(18) . ?

P1 C21 1.8487(17) . ?

P1 C31 1.8568(16) . ?

C11 C12 1.385(3) . ?

C11 C16 1.408(3) . ?

C12 C13 1.393(3) . ?

C13 C14 1.380(4) . ?

C14 C15 1.363(4) . ?

C15 C16 1.383(3) . ?

C16 C17 1.500(4) . ?

C17 F12 1.306(4) . ?

C17 F11 1.315(3) . ?

C17 F13 1.355(3) . ?

C21 C22 1.398(2) . ?

C21 C26 1.415(2) . ?

C22 C23 1.379(3) . ?

C23 C24 1.383(3) . ?
 C24 C25 1.380(3) . ?
 C25 C26 1.389(2) . ?
 C26 C27 1.489(2) . ?
 C27 O2 1.218(2) . ?
 C27 O1 1.3194(19) . ?
 F21 C37 1.333(3) . ?
 F22 C37 1.335(2) . ?
 F23 C37 1.335(3) . ?
 C31 C32 1.388(2) . ?
 C31 C36 1.402(2) . ?
 C32 C33 1.390(2) . ?
 C33 C34 1.374(3) . ?
 C34 C35 1.376(3) . ?
 C35 C36 1.390(3) . ?
 C36 C37 1.498(3) . ?

loop_
 _geom_angle_atom_site_label_1
 _geom_angle_atom_site_label_2
 _geom_angle_atom_site_label_3
 _geom_angle
 _geom_angle_site_symmetry_1
 _geom_angle_site_symmetry_3
 _geom_angle_publ_flag
 C11 P1 C21 102.06(8) . . ?
 C11 P1 C31 99.90(7) . . ?
 C21 P1 C31 100.84(7) . . ?
 C12 C11 C16 117.79(18) . . ?
 C12 C11 P1 121.61(14) . . ?
 C16 C11 P1 120.58(15) . . ?
 C11 C12 C13 121.4(2) . . ?
 C14 C13 C12 119.4(3) . . ?
 C15 C14 C13 120.4(2) . . ?
 C14 C15 C16 120.7(3) . . ?
 C15 C16 C11 120.4(2) . . ?
 C15 C16 C17 118.6(2) . . ?
 C11 C16 C17 121.0(2) . . ?
 F12 C17 F11 107.7(3) . . ?
 F12 C17 F13 104.9(3) . . ?
 F11 C17 F13 104.8(2) . . ?
 F12 C17 C16 114.5(2) . . ?
 F11 C17 C16 113.9(3) . . ?
 F13 C17 C16 110.3(3) . . ?
 C22 C21 C26 117.04(15) . . ?
 C22 C21 P1 121.96(12) . . ?
 C26 C21 P1 120.71(12) . . ?
 C23 C22 C21 121.81(16) . . ?
 C22 C23 C24 120.51(17) . . ?
 C25 C24 C23 119.12(17) . . ?
 C24 C25 C26 121.05(16) . . ?
 C25 C26 C21 120.43(15) . . ?
 C25 C26 C27 118.86(14) . . ?
 C21 C26 C27 120.70(15) . . ?
 O2 C27 O1 123.35(15) . . ?
 O2 C27 C26 122.70(14) . . ?
 O1 C27 C26 113.94(15) . . ?
 C32 C31 C36 117.51(15) . . ?

C32 C31 P1 121.81(13) . . ?
 C36 C31 P1 120.59(13) . . ?
 C31 C32 C33 121.70(19) . . ?
 C34 C33 C32 119.7(2) . . ?
 C33 C34 C35 119.95(18) . . ?
 C34 C35 C36 120.5(2) . . ?
 C35 C36 C31 120.56(18) . . ?
 C35 C36 C37 117.33(18) . . ?
 C31 C36 C37 122.11(16) . . ?
 F21 C37 F23 105.50(19) . . ?
 F21 C37 F22 105.97(19) . . ?
 F23 C37 F22 106.05(19) . . ?
 F21 C37 C36 113.09(18) . . ?
 F23 C37 C36 112.77(19) . . ?
 F22 C37 C36 112.81(18) . . ?

_refine_diff_density_max 0.373
 _refine_diff_density_min -0.277
 _refine_diff_density_rms 0.048

8.3. Spirocyclic oxyphosphorane 13

data_shelx

_audit_creation_method SHELXL-2014
 _chemical_name_systematic
 ;
 ?
 ;
 _chemical_name_common ?
 _chemical_melting_point ?
 _chemical_formula_moiety ?
 _chemical_formula_sum
 'C21 H13 O5 P'
 _chemical_formula_weight 376.28

 loop_
 _atom_type_symbol
 _atom_type_description
 _atom_type_scatter_dispersion_real
 _atom_type_scatter_dispersion_imag
 _atom_type_scatter_source
 'C' 'C' 0.0033 0.0016
 'International Tables Vol C Tables 4.2.6.8 and 6.1.1.4'
 'H' 'H' 0.0000 0.0000
 'International Tables Vol C Tables 4.2.6.8 and 6.1.1.4'
 'O' 'O' 0.0106 0.0060
 'International Tables Vol C Tables 4.2.6.8 and 6.1.1.4'
 'P' 'P' 0.1023 0.0942
 'International Tables Vol C Tables 4.2.6.8 and 6.1.1.4'

 _space_group_crystal_system monoclinic
 _space_group_IT_number 14
 _space_group_name_H-M_alt 'P 21/c'
 _space_group_name_Hall '-P 2ybc'

 _shelx_space_group_comment

```

;
The symmetry employed for this shelxl refinement is uniquely
defined
by the following loop, which should always be used as a source of
symmetry information in preference to the above space-group names.
They are only intended as comments.
;

```

```

loop_
  _space_group_symop_operation_xyz
    'x, y, z'
    '-x, y+1/2, -z+1/2'
    '-x, -y, -z'
    'x, -y-1/2, z-1/2'

  _cell_length_a          9.5867(4)
  _cell_length_b         12.6989(5)
  _cell_length_c         14.6985(6)
  _cell_angle_alpha      90
  _cell_angle_beta       104.4760(10)
  _cell_angle_gamma      90
  _cell_volume           1732.59(12)
  _cell_formula_units_Z  4
  _cell_measurement_temperature 296(2)
  _cell_measurement_reflns_used 7741
  _cell_measurement_theta_min 2.72
  _cell_measurement_theta_max 28.5

  _exptl_crystal_description prism
  _exptl_crystal_colour colourless
  _exptl_crystal_density_meas ?
  _exptl_crystal_density_method ?
  _exptl_crystal_density_diffn 1.443
  _exptl_crystal_F_000 776
  _exptl_transmission_factor_min ?
  _exptl_transmission_factor_max ?
  _exptl_crystal_size_max 0.82
  _exptl_crystal_size_mid 0.28
  _exptl_crystal_size_min 0.20
  _exptl_absorpt_coefficient_mu 0.190
  _shelx_estimated_absorpt_T_min ?
  _shelx_estimated_absorpt_T_max ?
  _exptl_absorpt_correction_type ?
  _exptl_absorpt_correction_T_min ?
  _exptl_absorpt_correction_T_max ?
  _exptl_absorpt_process_details ?

  _exptl_special_details
;
?
;

  _diffn_ambient_temperature 296(2)
  _diffn_radiation_wavelength 0.71073
  _diffn_radiation_type MoK\alpha
  _diffn_source ?
  _diffn_measurement_device_type 'Bruker SMART CCD area detector'
  _diffn_measurement_method ?

```

```

_diffrn_detector_area_resol_mean ?
_diffrn_reflns_number 13514
_diffrn_reflns_av_unetI/netI 0.0162
_diffrn_reflns_av_R_equivalents 0.0160
_diffrn_reflns_limit_h_min -12
_diffrn_reflns_limit_h_max 12
_diffrn_reflns_limit_k_min -16
_diffrn_reflns_limit_k_max 16
_diffrn_reflns_limit_l_min -19
_diffrn_reflns_limit_l_max 19
_diffrn_reflns_theta_min 2.149
_diffrn_reflns_theta_max 28.672
_diffrn_reflns_theta_full 25.242
_diffrn_measured_fraction_theta_max 0.934
_diffrn_measured_fraction_theta_full 0.999
_diffrn_reflns_Laue_measured_fraction_max 0.934
_diffrn_reflns_Laue_measured_fraction_full 0.999
_diffrn_reflns_point_group_measured_fraction_max 0.934
_diffrn_reflns_point_group_measured_fraction_full 0.999
_reflns_number_total 4163
_reflns_number_gt 3615
_reflns_threshold_expression 'I > 2\s(I) '
_reflns_Friedel_coverage 0.000
_reflns_Friedel_fraction_max .
_reflns_Friedel_fraction_full .

_reflns_special_details
;
Reflections were merged by SHELXL according to the crystal
class for the calculation of statistics and refinement.

_reflns_Friedel_fraction is defined as the number of unique
Friedel pairs measured divided by the number that would be
possible theoretically, ignoring centric projections and
systematic absences.
;

_computing_data_collection ?
_computing_cell_refinement ?
_computing_data_reduction ?
_computing_structure_solution ?
_computing_structure_refinement 'SHELXL-2014 (Sheldrick, 2014) '
_computing_molecular_graphics ?
_computing_publication_material ?

_refine_special_details
;
?
;
_refine_ls_structure_factor_coef Fsqd
_refine_ls_matrix_type full
_refine_ls_weighting_scheme calc
_refine_ls_weighting_details
'w=1/[\s^2^(Fo^2^)+(0.0642P)^2^+0.4443P] where P=(Fo^2^+2Fc^2^)/3'
_atom_sites_solution_primary ?
_atom_sites_solution_secondary ?
_atom_sites_solution_hydrogens mixed
_refine_ls_hydrogen_treatment mixed

```

```

_refine_ls_extinction_method      none
_refine_ls_extinction_coef        .
_refine_ls_number_reflns          4163
_refine_ls_number_parameters      247
_refine_ls_number_restraints      0
_refine_ls_R_factor_all           0.0449
_refine_ls_R_factor_gt            0.0391
_refine_ls_wR_factor_ref          0.1117
_refine_ls_wR_factor_gt          0.1069
_refine_ls_goodness_of_fit_ref    1.020
_refine_ls_restrained_S_all       1.020
_refine_ls_shift/su_max           0.001
_refine_ls_shift/su_mean          0.000

loop_
  _atom_site_label
  _atom_site_type_symbol
  _atom_site_fract_x
  _atom_site_fract_y
  _atom_site_fract_z
  _atom_site_U_iso_or_equiv
  _atom_site_adp_type
  _atom_site_occupancy
  _atom_site_site_symmetry_order
  _atom_site_calc_flag
  _atom_site_refinement_flags_posn
  _atom_site_refinement_flags_adp
  _atom_site_refinement_flags_occupancy
  _atom_site_disorder_assembly
  _atom_site_disorder_group
P1 P 0.77033(4) 0.67413(3) 0.09043(2) 0.03507(11) Uani 1 1 d . . .
. . .
C11 C 0.78506(14) 0.59269(11) -0.00770(9) 0.0366(3) Uani 1 1 d . .
. . .
C12 C 0.71838(14) 0.49612(11) -0.00656(9) 0.0366(3) Uani 1 1 d . .
. . .
C13 C 0.70925(17) 0.42316(13) -0.07773(12) 0.0489(4) Uani 1 1 d . .
. . .
H13 H 0.6633 0.3589 -0.0764 0.059 Uiso 1 1 calc R U . . .
C14 C 0.7700(2) 0.44821(15) -0.15074(13) 0.0581(4) Uani 1 1 d . . .
. . .
H14 H 0.7631 0.4012 -0.2002 0.070 Uiso 1 1 calc R U . . .
C15 C 0.8411(2) 0.54300(15) -0.15073(13) 0.0586(4) Uani 1 1 d . . .
. . .
H15 H 0.8841 0.5578 -0.1994 0.070 Uiso 1 1 calc R U . . .
C16 C 0.84977(18) 0.61613(13) -0.07988(12) 0.0485(4) Uani 1 1 d . .
. . .
H16 H 0.8979 0.6796 -0.0805 0.058 Uiso 1 1 calc R U . . .
C17 C 0.65736(14) 0.48243(11) 0.07570(10) 0.0369(3) Uani 1 1 d . .
. . .
O1 O 0.68195(11) 0.56725(8) 0.13045(7) 0.0430(2) Uani 1 1 d . . . .
.
O2 O 0.59424(12) 0.40587(8) 0.09313(8) 0.0493(3) Uani 1 1 d . . . .
.
C21 C 0.90953(15) 0.67879(11) 0.19904(10) 0.0382(3) Uani 1 1 d . .
. . .
C22 C 1.00551(15) 0.76031(11) 0.19836(10) 0.0403(3) Uani 1 1 d . .
. . .

```

C23 C 1.11829(17) 0.78141(14) 0.27567(12) 0.0503(4) Uani 1 1 d . .
 . . .
 H23 H 1.1822 0.8361 0.2744 0.060 Uiso 1 1 calc R U . . .
 C24 C 1.13352(19) 0.71996(15) 0.35399(12) 0.0562(4) Uani 1 1 d . .
 . . .
 H24 H 1.2080 0.7337 0.4068 0.067 Uiso 1 1 calc R U . . .
 C25 C 1.0394(2) 0.63741(15) 0.35579(11) 0.0552(4) Uani 1 1 d . . .
 . . .
 H25 H 1.0523 0.5960 0.4095 0.066 Uiso 1 1 calc R U . . .
 C26 C 0.92560(18) 0.61576(13) 0.27811(10) 0.0471(3) Uani 1 1 d . .
 . . .
 H26 H 0.8623 0.5606 0.2793 0.057 Uiso 1 1 calc R U . . .
 C27 C 0.97418(16) 0.81985(11) 0.10913(11) 0.0420(3) Uani 1 1 d . .
 . . .
 O3 O 0.85830(11) 0.78017(8) 0.04867(7) 0.0415(2) Uani 1 1 d
 .
 O4 O 1.04107(14) 0.89379(10) 0.09092(9) 0.0619(3) Uani 1 1 d . . .
 . . .
 C31 C 0.61790(15) 0.75943(11) 0.09208(10) 0.0383(3) Uani 1 1 d . .
 . . .
 C32 C 0.53748(16) 0.81758(11) 0.01620(11) 0.0418(3) Uani 1 1 d . .
 . . .
 C33 C 0.42998(18) 0.88530(13) 0.02984(13) 0.0523(4) Uani 1 1 d . .
 . . .
 H33 H 0.3759 0.9236 -0.0207 0.063 Uiso 1 1 calc R U . . .
 C34 C 0.4027(2) 0.89635(15) 0.11705(15) 0.0612(5) Uani 1 1 d . . .
 . . .
 H34 H 0.3314 0.9424 0.1253 0.073 Uiso 1 1 calc R U . . .
 C35 C 0.4813(2) 0.83892(16) 0.19192(14) 0.0622(5) Uani 1 1 d . . .
 . . .
 H35 H 0.4634 0.8465 0.2509 0.075 Uiso 1 1 calc R U . . .
 C36 C 0.58721(18) 0.76986(14) 0.17962(11) 0.0512(4) Uani 1 1 d . .
 . . .
 H36 H 0.6383 0.7301 0.2302 0.061 Uiso 1 1 calc R U . . .
 C37 C 0.5578(2) 0.80817(14) -0.08021(11) 0.0523(4) Uani 1 1 d . . .
 . . .
 O5 O 0.4878(2) 0.85633(12) -0.14613(10) 0.0810(5) Uani 1 1 d . . .
 . . .
 H1 H 0.635(3) 0.762(2) -0.0941(18) 0.097 Uiso 1 1 d . U . . .

loop_
 _atom_site_aniso_label
 _atom_site_aniso_U_11
 _atom_site_aniso_U_22
 _atom_site_aniso_U_33
 _atom_site_aniso_U_23
 _atom_site_aniso_U_13
 _atom_site_aniso_U_12
 P1 0.03790(19) 0.0388(2) 0.02911(18) -0.00345(13) 0.00952(13) -
 0.00842(13)
 C11 0.0359(7) 0.0406(7) 0.0337(6) -0.0037(5) 0.0092(5) -0.0025(5)
 C12 0.0310(6) 0.0385(7) 0.0386(7) -0.0011(5) 0.0054(5) 0.0003(5)
 C13 0.0471(8) 0.0428(8) 0.0562(9) -0.0113(7) 0.0120(7) -0.0022(6)
 C14 0.0663(11) 0.0574(10) 0.0537(9) -0.0189(8) 0.0211(8) 0.0038(8)
 C15 0.0711(11) 0.0632(10) 0.0512(9) -0.0066(8) 0.0334(8) 0.0026(9)
 C16 0.0548(9) 0.0490(8) 0.0484(8) -0.0027(7) 0.0251(7) -0.0058(7)
 C17 0.0310(6) 0.0384(7) 0.0386(7) 0.0022(5) 0.0036(5) -0.0017(5)
 O1 0.0503(6) 0.0452(5) 0.0358(5) -0.0025(4) 0.0154(4) -0.0136(4)


```

O2 0.0497(6) 0.0422(6) 0.0565(7) 0.0049(5) 0.0142(5) -0.0098(5)
C21 0.0388(7) 0.0416(7) 0.0333(6) -0.0060(5) 0.0071(5) -0.0010(5)
C22 0.0371(7) 0.0414(7) 0.0421(7) -0.0110(6) 0.0090(6) -0.0008(5)
C23 0.0399(8) 0.0536(9) 0.0527(9) -0.0151(7) 0.0028(7) -0.0016(6)
C24 0.0478(9) 0.0627(11) 0.0492(9) -0.0138(8) -0.0045(7) 0.0079(8)
C25 0.0628(10) 0.0603(10) 0.0374(8) -0.0001(7) 0.0028(7) 0.0132(8)
C26 0.0530(9) 0.0487(8) 0.0380(7) -0.0004(6) 0.0085(6) -0.0005(7)
C27 0.0420(7) 0.0400(7) 0.0463(8) -0.0099(6) 0.0152(6) -0.0076(6)
O3 0.0450(5) 0.0432(5) 0.0367(5) -0.0011(4) 0.0110(4) -0.0123(4)
O4 0.0666(8) 0.0553(7) 0.0637(8) -0.0035(6) 0.0161(6) -0.0273(6)
C31 0.0383(7) 0.0426(7) 0.0348(6) -0.0063(5) 0.0106(5) -0.0081(5)
C32 0.0446(8) 0.0385(7) 0.0411(7) -0.0037(6) 0.0086(6) -0.0081(6)
C33 0.0486(9) 0.0446(8) 0.0611(10) -0.0018(7) 0.0089(7) -0.0027(7)
C34 0.0523(10) 0.0571(10) 0.0801(13) -0.0127(9) 0.0276(9) 0.0009(8)
C35 0.0624(11) 0.0767(12) 0.0563(10) -0.0136(9) 0.0312(9) -
0.0020(9)
C36 0.0524(9) 0.0653(10) 0.0390(8) -0.0039(7) 0.0173(7) -0.0012(8)
C37 0.0661(10) 0.0493(9) 0.0390(8) 0.0012(7) 0.0084(7) -0.0015(8)
O5 0.1141(13) 0.0758(9) 0.0484(7) 0.0141(7) 0.0112(8) 0.0235(9)

```

```
_geom_special_details
```

```
;
```

```
All esds (except the esd in the dihedral angle between two l.s.
planes)
```

```
are estimated using the full covariance matrix. The cell esds are
taken
```

```
into account individually in the estimation of esds in distances,
angles
```

```
and torsion angles; correlations between esds in cell parameters
are only
```

```
used when they are defined by crystal symmetry. An approximate
(isotropic)
```

```
treatment of cell esds is used for estimating esds involving l.s.
planes.
```

```
;
```

```
loop_
```

```
_geom_bond_atom_site_label_1
```

```
_geom_bond_atom_site_label_2
```

```
_geom_bond_distance
```

```
_geom_bond_site_symmetry_2
```

```
_geom_bond_publ_flag
```

```
P1 O1 1.7763(10) . ?
```

```
P1 O3 1.7776(10) . ?
```

```
P1 C21 1.8077(14) . ?
```

```
P1 C11 1.8088(14) . ?
```

```
P1 C31 1.8240(15) . ?
```

```
C11 C12 1.3850(19) . ?
```

```
C11 C16 1.3886(19) . ?
```

```
C12 C13 1.384(2) . ?
```

```
C12 C17 1.4792(19) . ?
```

```
C13 C14 1.380(2) . ?
```

```
C14 C15 1.383(3) . ?
```

```
C15 C16 1.382(2) . ?
```

```
C17 O2 1.2060(17) . ?
```

```
C17 O1 1.3298(17) . ?
```

```
C21 C22 1.387(2) . ?
```

```
C21 C26 1.388(2) . ?
```

C22 C23 1.385(2) . ?
C22 C27 1.478(2) . ?
C23 C24 1.368(3) . ?
C24 C25 1.388(3) . ?
C25 C26 1.395(2) . ?
C27 O4 1.2043(18) . ?
C27 O3 1.3357(17) . ?
C31 C36 1.396(2) . ?
C31 C32 1.398(2) . ?
C32 C33 1.395(2) . ?
C32 C37 1.482(2) . ?
C33 C34 1.378(3) . ?
C34 C35 1.377(3) . ?
C35 C36 1.387(2) . ?
C37 O5 1.199(2) . ?

loop_
_geom_angle_atom_site_label_1
_geom_angle_atom_site_label_2
_geom_angle_atom_site_label_3
_geom_angle
_geom_angle_site_symmetry_1
_geom_angle_site_symmetry_3
_geom_angle_publ_flag
O1 P1 O3 179.12(5) . . ?
O1 P1 C21 92.32(6) . . ?
O3 P1 C21 88.34(6) . . ?
O1 P1 C11 88.05(6) . . ?
O3 P1 C11 91.11(6) . . ?
C21 P1 C11 122.37(6) . . ?
O1 P1 C31 89.96(6) . . ?
O3 P1 C31 90.32(6) . . ?
C21 P1 C31 112.70(6) . . ?
C11 P1 C31 124.94(6) . . ?
C12 C11 C16 119.65(13) . . ?
C12 C11 P1 111.62(10) . . ?
C16 C11 P1 128.72(11) . . ?
C13 C12 C11 121.73(14) . . ?
C13 C12 C17 125.17(13) . . ?
C11 C12 C17 113.08(12) . . ?
C14 C13 C12 118.31(15) . . ?
C13 C14 C15 120.29(15) . . ?
C16 C15 C14 121.41(16) . . ?
C15 C16 C11 118.53(15) . . ?
O2 C17 O1 123.15(13) . . ?
O2 C17 C12 126.18(13) . . ?
O1 C17 C12 110.67(11) . . ?
C17 O1 P1 116.46(8) . . ?
C22 C21 C26 120.12(14) . . ?
C22 C21 P1 111.27(11) . . ?
C26 C21 P1 128.58(12) . . ?
C23 C22 C21 121.45(15) . . ?
C23 C22 C27 124.96(14) . . ?
C21 C22 C27 113.59(12) . . ?
C24 C23 C22 118.51(16) . . ?
C23 C24 C25 120.92(15) . . ?
C24 C25 C26 120.82(16) . . ?
C21 C26 C25 118.17(16) . . ?

O4 C27 O3 123.15(15) . . ?
 O4 C27 C22 126.48(14) . . ?
 O3 C27 C22 110.37(12) . . ?
 C27 O3 P1 116.33(9) . . ?
 C36 C31 C32 118.95(14) . . ?
 C36 C31 P1 115.01(12) . . ?
 C32 C31 P1 125.94(11) . . ?
 C33 C32 C31 119.40(14) . . ?
 C33 C32 C37 117.73(15) . . ?
 C31 C32 C37 122.83(14) . . ?
 C34 C33 C32 121.03(17) . . ?
 C35 C34 C33 119.74(16) . . ?
 C34 C35 C36 120.20(16) . . ?
 C35 C36 C31 120.65(16) . . ?
 O5 C37 C32 123.43(18) . . ?

_refine_diff_density_max 0.328
 _refine_diff_density_min -0.223
 _refine_diff_density_rms 0.046

8.4. Phosphine *p28*

data_shelx

_audit_creation_method SHELXL-2014
 _chemical_name_systematic
 ;
 ?
 ;
 _chemical_name_common ?
 _chemical_melting_point ?
 _chemical_formula_moiety ?
 _chemical_formula_sum
 'C19 H13 Br F3 P'
 _chemical_formula_weight 409.18

loop_
 _atom_type_symbol
 _atom_type_description
 _atom_type_scatter_dispersion_real
 _atom_type_scatter_dispersion_imag
 _atom_type_scatter_source
 'C' 'C' 0.0180 0.0090
 'International Tables Vol C Tables 4.2.6.8 and 6.1.1.4'
 'H' 'H' 0.0000 0.0000
 'International Tables Vol C Tables 4.2.6.8 and 6.1.1.4'
 'Br' 'Br' -0.6760 1.2810
 'International Tables Vol C Tables 4.2.6.8 and 6.1.1.4'
 'F' 'F' 0.0730 0.0530
 'International Tables Vol C Tables 4.2.6.8 and 6.1.1.4'
 'P' 'P' 0.2960 0.4330
 'International Tables Vol C Tables 4.2.6.8 and 6.1.1.4'

_space_group_crystal_system monoclinic
 _space_group_IT_number 14
 _space_group_name_H-M_alt 'P 21/c'
 _space_group_name_Hall '-P 2ybc'

```

_shelx_space_group_comment
;
The symmetry employed for this shelxl refinement is uniquely
defined
by the following loop, which should always be used as a source of
symmetry information in preference to the above space-group names.
They are only intended as comments.
;

loop_
_space_group_symop_operation_xyz
'x, y, z'
'-x, y+1/2, -z+1/2'
'-x, -y, -z'
'x, -y-1/2, z-1/2'

_cell_length_a          10.204(9)
_cell_length_b          19.519(7)
_cell_length_c          9.074(4)
_cell_angle_alpha       90
_cell_angle_beta        100.92(3)
_cell_angle_gamma       90
_cell_volume            1774.6(19)
_cell_formula_units_Z   4
_cell_measurement_temperature 293(2)
_cell_measurement_reflns_used 5364
_cell_measurement_theta_min ?
_cell_measurement_theta_max ?

_exptl_crystal_description prism
_exptl_crystal_colour    colourless
_exptl_crystal_density_meas ?
_exptl_crystal_density_method ?
_exptl_crystal_density_diffn 1.532
_exptl_crystal_F_000     816
_exptl_transmission_factor_min ?
_exptl_transmission_factor_max ?
_exptl_crystal_size_max  0.3
_exptl_crystal_size_mid  0.3
_exptl_crystal_size_min  0.3
_exptl_absorpt_coefficient_mu 4.258
_shelx_estimated_absorpt_T_min ?
_shelx_estimated_absorpt_T_max ?
_exptl_absorpt_correction_type ?
_exptl_absorpt_correction_T_min ?
_exptl_absorpt_correction_T_max ?
_exptl_absorpt_process_details ?

_exptl_special_details
;
?
;

_diffn_ambient_temperature 293(2)
_diffn_radiation_wavelength 1.54187
_diffn_radiation_type      CuK\alpha
_diffn_source               ?

```

```

_diffrn_measurement_device_type    'Rigaku Spider'
_diffrn_measurement_method         ?
_diffrn_detector_area_resol_mean   ?
_diffrn_reflns_number              7341
_diffrn_reflns_av_unetI/netI       0.1052
_diffrn_reflns_av_R_equivalents    0.1107
_diffrn_reflns_limit_h_min         -11
_diffrn_reflns_limit_h_max         11
_diffrn_reflns_limit_k_min         -22
_diffrn_reflns_limit_k_max         23
_diffrn_reflns_limit_l_min         -10
_diffrn_reflns_limit_l_max         10
_diffrn_reflns_theta_min           4.413
_diffrn_reflns_theta_max           67.679
_diffrn_reflns_theta_full          67.687
_diffrn_measured_fraction_theta_max 0.968
_diffrn_measured_fraction_theta_full 0.968
_diffrn_reflns_Laue_measured_fraction_max 0.968
_diffrn_reflns_Laue_measured_fraction_full 0.968
_diffrn_reflns_point_group_measured_fraction_max 0.968
_diffrn_reflns_point_group_measured_fraction_full 0.968
_reflns_number_total               3106
_reflns_number_gt                   1660
_reflns_threshold_expression        'I > 2\s(I)'
_reflns_Friedel_coverage            0.000
_reflns_Friedel_fraction_max       .
_reflns_Friedel_fraction_full      .

_reflns_special_details
;
Reflections were merged by SHELXL according to the crystal
class for the calculation of statistics and refinement.

_reflns_Friedel_fraction is defined as the number of unique
Friedel pairs measured divided by the number that would be
possible theoretically, ignoring centric projections and
systematic absences.
;

_computing_data_collection          ?
_computing_cell_refinement          ?
_computing_data_reduction           ?
_computing_structure_solution       ?
_computing_structure_refinement     'SHELXL-2014 (Sheldrick, 2014)'
_computing_molecular_graphics       ?
_computing_publication_material     ?

_refine_special_details
;
?
;
_refine_ls_structure_factor_coef    Fsqd
_refine_ls_matrix_type              full
_refine_ls_weighting_scheme         calc
_refine_ls_weighting_details
'w=1/[\s^2^(Fo^2^)+(0.1328P)^2^] where P=(Fo^2^+2Fc^2^)/3'
_atom_sites_solution_primary        ?
_atom_sites_solution_secondary      ?

```

```

_atom_sites_solution_hydrogens      geom
_refine_ls_hydrogen_treatment      constr
_refine_ls_extinction_method        SHELXL
_refine_ls_extinction_coef          0.0035(6)
_refine_ls_extinction_expression    'Fc^*^=kFc[1+0.001xFc^2^\l^3^\sin(2\q)]^-1/4^'
_refine_ls_number_reflns            3106
_refine_ls_number_parameters        275
_refine_ls_number_restraints        145
_refine_ls_R_factor_all              0.1382
_refine_ls_R_factor_gt               0.0935
_refine_ls_wR_factor_ref             0.2674
_refine_ls_wR_factor_gt             0.2293
_refine_ls_goodness_of_fit_ref       0.989
_refine_ls_restrained_S_all          0.973
_refine_ls_shift/su_max              0.003
_refine_ls_shift/su_mean             0.000

loop_
  _atom_site_label
  _atom_site_type_symbol
  _atom_site_fract_x
  _atom_site_fract_y
  _atom_site_fract_z
  _atom_site_U_iso_or_equiv
  _atom_site_adp_type
  _atom_site_occupancy
  _atom_site_site_symmetry_order
  _atom_site_calc_flag
  _atom_site_refinement_flags_posn
  _atom_site_refinement_flags_adp
  _atom_site_refinement_flags_occupancy
  _atom_site_disorder_assembly
  _atom_site_disorder_group
P1 P 0.2232(2) 0.12699(11) 0.4120(2) 0.0700(7) Uani 1 1 d . . . . .
Br1 Br 0.07168(10) 0.18960(5) 0.08888(9) 0.0880(5) Uani 1 1 d . . .
. .
C11 C 0.0420(7) 0.1440(4) 0.3823(8) 0.0657(18) Uani 1 1 d . . . . .
C12 C -0.0237(8) 0.1730(4) 0.2466(8) 0.0662(19) Uani 1 1 d . . . .
.
C13 C -0.1689(8) 0.1477(4) 0.4652(8) 0.074(2) Uani 1 1 d . . . . .
H13 H -0.2182 0.1380 0.5390 0.089 Uiso 1 1 calc R U . . .
C14 C -0.2306(7) 0.1776(4) 0.3321(10) 0.076(2) Uani 1 1 d D . . . .
C15 C -0.1586(9) 0.1898(4) 0.2224(9) 0.076(2) Uani 1 1 d . . . . .
H15 H -0.1996 0.2094 0.1319 0.091 Uiso 1 1 calc R U . . .
C16 C -0.0347(8) 0.1321(4) 0.4894(9) 0.074(2) Uani 1 1 d . . . . .
H16 H 0.0053 0.1130 0.5808 0.089 Uiso 1 1 calc R U . . .
C17 C -0.3777(11) 0.1937(5) 0.3029(11) 0.106(3) Uani 1 1 d D . . .
.
F1A F -0.410(3) 0.232(2) 0.413(3) 0.124(9) Uani 0.276(3) 1 d D U P
A 1
F2A F -0.415(3) 0.233(2) 0.180(3) 0.109(8) Uani 0.276(3) 1 d D U P
A 1
F3A F -0.454(3) 0.1393(12) 0.283(6) 0.128(9) Uani 0.276(3) 1 d D U
P A 1
F1B F -0.431(2) 0.1876(18) 0.425(2) 0.121(7) Uani 0.397(3) 1 d D U
P A 2

```

F2B F -0.402(2) 0.2557(9) 0.248(4) 0.119(7) Uani 0.397(3) 1 d D U P
 A 2
 F3B F -0.446(2) 0.1497(13) 0.204(3) 0.123(8) Uani 0.397(3) 1 d D U
 P A 2
 F1C F -0.437(3) 0.1546(17) 0.394(4) 0.126(8) Uani 0.327(3) 1 d D U
 P A 3
 F2C F -0.394(3) 0.2588(10) 0.340(5) 0.112(7) Uani 0.327(3) 1 d D U
 P A 3
 F3C F -0.438(3) 0.182(2) 0.164(2) 0.124(9) Uani 0.327(3) 1 d D U P
 A 3
 C21 C 0.2252(8) 0.0433(4) 0.3198(8) 0.0692(19) Uani 1 1 d
 C22 C 0.3488(9) 0.0122(5) 0.3260(9) 0.082(2) Uani 1 1 d
 H22 H 0.4251 0.0333 0.3791 0.099 Uiso 1 1 calc R U . . .
 C23 C 0.3604(11) -0.0491(5) 0.2547(10) 0.095(3) Uani 1 1 d
 .
 H23 H 0.4436 -0.0698 0.2628 0.113 Uiso 1 1 calc R U . . .
 C24 C 0.2486(13) -0.0802(5) 0.1711(10) 0.102(3) Uani 1 1 d
 .
 H24 H 0.2569 -0.1207 0.1194 0.122 Uiso 1 1 calc R U . . .
 C25 C 0.1283(11) -0.0516(5) 0.1654(10) 0.092(3) Uani 1 1 d
 .
 H25 H 0.0529 -0.0735 0.1126 0.110 Uiso 1 1 calc R U . . .
 C26 C 0.1137(9) 0.0111(4) 0.2376(9) 0.081(2) Uani 1 1 d
 H26 H 0.0297 0.0307 0.2302 0.097 Uiso 1 1 calc R U . . .
 C31 C 0.2566(7) 0.1037(4) 0.6105(8) 0.0657(19) Uani 1 1 d
 C32 C 0.3025(8) 0.1558(5) 0.7120(9) 0.078(2) Uani 1 1 d
 H32 H 0.3140 0.1999 0.6775 0.094 Uiso 1 1 calc R U . . .
 C33 C 0.3313(9) 0.1418(6) 0.8652(10) 0.092(3) Uani 1 1 d
 H33 H 0.3604 0.1768 0.9331 0.111 Uiso 1 1 calc R U . . .
 C34 C 0.3167(10) 0.0757(7) 0.9173(10) 0.102(3) Uani 1 1 d
 H34 H 0.3350 0.0668 1.0198 0.123 Uiso 1 1 calc R U . . .
 C35 C 0.2750(10) 0.0229(5) 0.8169(10) 0.092(3) Uani 1 1 d
 H35 H 0.2661 -0.0215 0.8504 0.110 Uiso 1 1 calc R U . . .
 C36 C 0.2473(8) 0.0383(5) 0.6661(9) 0.079(2) Uani 1 1 d
 H36 H 0.2209 0.0030 0.5983 0.095 Uiso 1 1 calc R U . . .

loop_
 _atom_site_aniso_label
 _atom_site_aniso_U_11
 _atom_site_aniso_U_22
 _atom_site_aniso_U_33
 _atom_site_aniso_U_23
 _atom_site_aniso_U_13
 _atom_site_aniso_U_12
 P1 0.0652(13) 0.0691(15) 0.0705(12) 0.0054(9) -0.0007(9) -
 0.0055(10)
 Br1 0.0982(9) 0.0867(9) 0.0751(7) 0.0136(4) 0.0062(5) -0.0043(5)
 C11 0.069(5) 0.059(5) 0.066(4) -0.003(3) 0.003(4) -0.004(4)
 C12 0.071(5) 0.057(5) 0.064(4) -0.002(3) -0.003(3) -0.013(4)
 C13 0.077(6) 0.074(6) 0.071(5) -0.006(4) 0.012(4) -0.005(4)
 C14 0.061(5) 0.076(6) 0.085(5) -0.009(4) -0.004(4) -0.004(4)
 C15 0.075(6) 0.063(6) 0.080(5) -0.003(4) -0.008(4) 0.002(4)
 C16 0.069(5) 0.073(6) 0.074(5) 0.006(4) -0.004(4) 0.000(4)
 C17 0.089(8) 0.096(10) 0.124(10) 0.006(7) -0.002(7) 0.008(7)
 F1A 0.095(15) 0.13(2) 0.140(17) -0.030(16) 0.007(14) 0.025(16)
 F2A 0.087(13) 0.115(18) 0.118(16) -0.001(15) 0.000(13) 0.008(15)
 F3A 0.064(11) 0.145(17) 0.16(2) -0.022(17) -0.019(17) -0.029(12)
 F1B 0.060(10) 0.148(19) 0.157(13) -0.038(14) 0.024(9) 0.013(13)

F2B 0.102(11) 0.095(12) 0.150(18) -0.011(12) 0.001(16) 0.022(10)
 F3B 0.082(11) 0.138(16) 0.133(15) -0.017(13) -0.019(13) -0.012(12)
 F1C 0.073(11) 0.148(18) 0.150(17) -0.013(16) -0.002(13) -0.019(14)
 F2C 0.083(11) 0.104(14) 0.145(18) -0.005(14) 0.009(15) 0.034(10)
 F3C 0.072(11) 0.14(2) 0.136(15) 0.001(15) -0.042(10) -0.002(15)
 C21 0.064(5) 0.079(6) 0.061(4) 0.002(4) 0.004(3) 0.002(4)
 C22 0.073(6) 0.090(7) 0.079(5) 0.000(4) 0.003(4) 0.006(5)
 C23 0.090(7) 0.095(8) 0.097(6) 0.013(6) 0.014(5) 0.033(6)
 C24 0.144(10) 0.077(7) 0.082(6) -0.002(5) 0.017(6) 0.033(7)
 C25 0.121(8) 0.064(6) 0.082(5) -0.009(4) -0.004(5) -0.002(6)
 C26 0.077(6) 0.073(6) 0.090(5) 0.001(4) 0.007(4) 0.002(4)
 C31 0.046(4) 0.076(6) 0.071(4) -0.006(4) 0.001(3) -0.004(4)
 C32 0.076(5) 0.070(6) 0.082(5) -0.006(4) -0.003(4) 0.002(4)
 C33 0.082(6) 0.112(9) 0.072(5) -0.028(5) -0.012(4) 0.007(5)
 C34 0.086(7) 0.152(11) 0.065(5) 0.009(6) 0.003(4) 0.018(6)
 C35 0.113(8) 0.086(7) 0.074(5) 0.016(5) 0.012(5) -0.008(5)
 C36 0.072(5) 0.073(6) 0.087(5) 0.003(4) 0.004(4) -0.005(4)

geom_special_details

;

All esds (except the esd in the dihedral angle between two l.s. planes)

are estimated using the full covariance matrix. The cell esds are taken

into account individually in the estimation of esds in distances, angles

and torsion angles; correlations between esds in cell parameters are only

used when they are defined by crystal symmetry. An approximate (isotropic)

treatment of cell esds is used for estimating esds involving l.s. planes.

;

loop_

geom_bond_atom_site_label_1

geom_bond_atom_site_label_2

geom_bond_distance

geom_bond_site_symmetry_2

geom_bond_publ_flag

P1 C31 1.826(7) . ?

P1 C21 1.838(9) . ?

P1 C11 1.847(8) . ?

Br1 C12 1.905(8) . ?

C11 C16 1.378(10) . ?

C11 C12 1.405(10) . ?

C12 C15 1.392(11) . ?

C13 C16 1.379(11) . ?

C13 C14 1.381(11) . ?

C14 C15 1.365(12) . ?

C14 C17 1.507(13) . ?

C17 F3A 1.308(16) . ?

C17 F3C 1.309(17) . ?

C17 F2B 1.313(15) . ?

C17 F2C 1.335(16) . ?

C17 F1B 1.335(15) . ?

C17 F1A 1.335(16) . ?

C17 F3B 1.337(15) . ?

C17 F1C 1.351(17) . ?
 C17 F2A 1.352(16) . ?
 C21 C26 1.388(11) . ?
 C21 C22 1.391(11) . ?
 C22 C23 1.377(13) . ?
 C23 C24 1.385(14) . ?
 C24 C25 1.341(14) . ?
 C25 C26 1.408(12) . ?
 C31 C36 1.383(11) . ?
 C31 C32 1.392(10) . ?
 C32 C33 1.393(12) . ?
 C33 C34 1.393(14) . ?
 C34 C35 1.387(13) . ?
 C35 C36 1.377(11) . ?

loop_
 _geom_angle_atom_site_label_1
 _geom_angle_atom_site_label_2
 _geom_angle_atom_site_label_3
 _geom_angle
 _geom_angle_site_symmetry_1
 _geom_angle_site_symmetry_3
 _geom_angle_publ_flag
 C31 P1 C21 102.2(4) . . ?
 C31 P1 C11 100.6(3) . . ?
 C21 P1 C11 101.0(4) . . ?
 C16 C11 C12 116.5(7) . . ?
 C16 C11 P1 123.6(6) . . ?
 C12 C11 P1 119.9(6) . . ?
 C15 C12 C11 121.8(7) . . ?
 C15 C12 Br1 118.2(6) . . ?
 C11 C12 Br1 120.0(6) . . ?
 C16 C13 C14 120.4(7) . . ?
 C15 C14 C13 119.5(7) . . ?
 C15 C14 C17 119.4(8) . . ?
 C13 C14 C17 121.0(8) . . ?
 C14 C15 C12 119.7(8) . . ?
 C11 C16 C13 122.0(7) . . ?
 F3C C17 F2C 110.4(15) . . ?
 F2B C17 F1B 108.5(13) . . ?
 F3A C17 F1A 109.3(16) . . ?
 F2B C17 F3B 107.5(14) . . ?
 F1B C17 F3B 105.1(14) . . ?
 F3C C17 F1C 107.8(16) . . ?
 F2C C17 F1C 106.7(15) . . ?
 F3A C17 F2A 106.2(15) . . ?
 F1A C17 F2A 103.3(15) . . ?
 F3A C17 C14 113.5(16) . . ?
 F3C C17 C14 113.6(16) . . ?
 F2B C17 C14 111.8(13) . . ?
 F2C C17 C14 109.0(13) . . ?
 F1B C17 C14 112.8(12) . . ?
 F1A C17 C14 111.5(16) . . ?
 F3B C17 C14 110.8(14) . . ?
 F1C C17 C14 108.9(15) . . ?
 F2A C17 C14 112.5(15) . . ?
 C26 C21 C22 118.0(8) . . ?
 C26 C21 P1 124.7(6) . . ?

```

C22 C21 P1 117.2(6) . . ?
C23 C22 C21 121.2(9) . . ?
C22 C23 C24 120.2(9) . . ?
C25 C24 C23 119.4(9) . . ?
C24 C25 C26 121.4(9) . . ?
C21 C26 C25 119.7(9) . . ?
C36 C31 C32 118.1(7) . . ?
C36 C31 P1 125.2(6) . . ?
C32 C31 P1 116.6(6) . . ?
C31 C32 C33 119.9(9) . . ?
C32 C33 C34 120.3(9) . . ?
C35 C34 C33 120.3(8) . . ?
C36 C35 C34 118.1(9) . . ?
C35 C36 C31 123.3(8) . . ?

_refine_diff_density_max      1.242
_refine_diff_density_min     -0.800
_refine_diff_density_rms     0.122

```

8.5. Diphosphine 31

```

data_shelx

_audit_creation_method          SHELXL-2014
_chemical_name_systematic
;
?
;
_chemical_name_common           ?
_chemical_melting_point         ?
_chemical_formula_moiety        ?
_chemical_formula_sum
'C39 H15 F27 P2'
_chemical_formula_weight        1058.44

loop_
_atom_type_symbol
_atom_type_description
_atom_type_scatter_dispersion_real
_atom_type_scatter_dispersion_imag
_atom_type_scatter_source
'C' 'C' 0.0030 0.0020
'International Tables Vol C Tables 4.2.6.8 and 6.1.1.4'
'H' 'H' 0.0000 0.0000
'International Tables Vol C Tables 4.2.6.8 and 6.1.1.4'
'F' 'F' 0.0170 0.0100
'International Tables Vol C Tables 4.2.6.8 and 6.1.1.4'
'P' 'P' 0.1020 0.0940
'International Tables Vol C Tables 4.2.6.8 and 6.1.1.4'

_space_group_crystal_system     monoclinic
_space_group_IT_number          14
_space_group_name_H-M_alt       'P 21/n'
_space_group_name_Hall          '-P 2yn'

_shelx_space_group_comment
;

```

The symmetry employed for this shelxl refinement is uniquely defined by the following loop, which should always be used as a source of symmetry information in preference to the above space-group names. They are only intended as comments.

```

;

loop_
  _space_group_symop_operation_xyz
    'x, y, z'
    '-x+1/2, y+1/2, -z+1/2'
    '-x, -y, -z'
    'x-1/2, -y-1/2, z-1/2'

  _cell_length_a          12.2501(15)
  _cell_length_b          16.1080(2)
  _cell_length_c          21.4020(3)
  _cell_angle_alpha       90
  _cell_angle_beta        94.836(2)
  _cell_angle_gamma       90
  _cell_volume            4208.1(5)
  _cell_formula_units_Z   4
  _cell_measurement_temperature 293(2)
  _cell_measurement_reflns_used 957
  _cell_measurement_theta_min 2.53
  _cell_measurement_theta_max 12.885

  _exptl_crystal_description prism
  _exptl_crystal_colour colourless
  _exptl_crystal_density_meas ?
  _exptl_crystal_density_method ?
  _exptl_crystal_density_diffrn 1.671
  _exptl_crystal_F_000 2088
  _exptl_transmission_factor_min ?
  _exptl_transmission_factor_max ?
  _exptl_crystal_size_max 0.2
  _exptl_crystal_size_mid 0.2
  _exptl_crystal_size_min 0.2
  _exptl_absorpt_coefficient_mu 0.254
  _shelx_estimated_absorpt_T_min ?
  _shelx_estimated_absorpt_T_max ?
  _exptl_absorpt_correction_type ?
  _exptl_absorpt_correction_T_min ?
  _exptl_absorpt_correction_T_max ?
  _exptl_absorpt_process_details ?

  _exptl_special_details
;
?
;

  _diffrn_ambient_temperature 293(2)
  _diffrn_radiation_wavelength 0.71073
  _diffrn_radiation_type MoK\alpha
  _diffrn_source ?
  _diffrn_measurement_device_type 'Bruker SMART CCD area detector'
  _diffrn_measurement_method ?
  _diffrn_detector_area_resol_mean ?

```

```

_diffrn_reflns_number          33335
_diffrn_reflns_av_unetI/netI   0.2702
_diffrn_reflns_av_R_equivalents 0.2313
_diffrn_reflns_limit_h_min     -16
_diffrn_reflns_limit_h_max     16
_diffrn_reflns_limit_k_min     -20
_diffrn_reflns_limit_k_max     21
_diffrn_reflns_limit_l_min     -28
_diffrn_reflns_limit_l_max     28
_diffrn_reflns_theta_min       1.584
_diffrn_reflns_theta_max       28.741
_diffrn_reflns_theta_full      25.242
_diffrn_measured_fraction_theta_max 0.936
_diffrn_measured_fraction_theta_full 1.000
_diffrn_reflns_Laue_measured_fraction_max 0.936
_diffrn_reflns_Laue_measured_fraction_full 1.000
_diffrn_reflns_point_group_measured_fraction_max 0.936
_diffrn_reflns_point_group_measured_fraction_full 1.000
_reflns_number_total          10235
_reflns_number_gt             2987
_reflns_threshold_expression   'I > 2\s(I) '
_reflns_Friedel_coverage      0.000
_reflns_Friedel_fraction_max  .
_reflns_Friedel_fraction_full .

_reflns_special_details
;
Reflections were merged by SHELXL according to the crystal
class for the calculation of statistics and refinement.

_reflns_Friedel_fraction is defined as the number of unique
Friedel pairs measured divided by the number that would be
possible theoretically, ignoring centric projections and
systematic absences.
;

_computing_data_collection    ?
_computing_cell_refinement    ?
_computing_data_reduction     ?
_computing_structure_solution ?
_computing_structure_refinement 'SHELXL-2014 (Sheldrick, 2014) '
_computing_molecular_graphics ?
_computing_publication_material ?

_refine_special_details
;
?
;
_refine_ls_structure_factor_coef Fsqd
_refine_ls_matrix_type          full
_refine_ls_weighting_scheme     calc
_refine_ls_weighting_details
'w=1/[\s^2^(Fo^2)+(0.0724P)^2] where P=(Fo^2+2Fc^2)/3'
_atom_sites_solution_primary   ?
_atom_sites_solution_secondary ?
_atom_sites_solution_hydrogens geom
_refine_ls_hydrogen_treatment  constr
_refine_ls_extinction_method    none

```

```

_refine_ls_extinction_coef      .
_refine_ls_number_reflns      10235
_refine_ls_number_parameters    865
_refine_ls_number_restraints   418
_refine_ls_R_factor_all        0.3393
_refine_ls_R_factor_gt         0.1074
_refine_ls_wR_factor_ref       0.2414
_refine_ls_wR_factor_gt        0.1659
_refine_ls_goodness_of_fit_ref  0.977
_refine_ls_restrained_S_all    0.974
_refine_ls_shift/su_max        0.837
_refine_ls_shift/su_mean       0.032

loop_
  _atom_site_label
  _atom_site_type_symbol
  _atom_site_fract_x
  _atom_site_fract_y
  _atom_site_fract_z
  _atom_site_U_iso_or_equiv
  _atom_site_adp_type
  _atom_site_occupancy
  _atom_site_site_symmetry_order
  _atom_site_calc_flag
  _atom_site_refinement_flags_posn
  _atom_site_refinement_flags_adp
  _atom_site_refinement_flags_occupancy
  _atom_site_disorder_assembly
  _atom_site_disorder_group
P1 P 0.16938(13) 0.10426(11) 0.06548(7) 0.0499(5) Uani 1 1 d . . .
. .
C11 C 0.1006(5) 0.1795(4) 0.1139(3) 0.0490(16) Uani 1 1 d . . . . .
C12 C 0.0653(5) 0.1520(4) 0.1701(3) 0.0642(19) Uani 1 1 d . . . . .
H12 H 0.0822 0.0984 0.1839 0.077 Uiso 1 1 calc R U . . .
C13 C 0.0050(6) 0.2036(5) 0.2060(3) 0.070(2) Uani 1 1 d D . . . . .
C14 C -0.0209(5) 0.2822(5) 0.1853(4) 0.071(2) Uani 1 1 d . . . . .
H14 H -0.0607 0.3172 0.2094 0.085 Uiso 1 1 calc R U . . .
C15 C 0.0117(5) 0.3095(4) 0.1289(4) 0.0588(18) Uani 1 1 d D . . . . .
C16 C 0.0722(5) 0.2582(4) 0.0937(3) 0.0544(17) Uani 1 1 d . . . . .
H16 H 0.0942 0.2771 0.0557 0.065 Uiso 1 1 calc R U . . .
C17 C -0.0316(9) 0.1738(7) 0.2670(5) 0.110(3) Uani 1 1 d D . . . . .
F1A F -0.1274(13) 0.2071(17) 0.2746(9) 0.130(9) Uani 0.38(2) 1 d D
U P A 1
F2A F 0.0358(19) 0.2099(19) 0.3131(10) 0.165(12) Uani 0.38(2) 1 d D
U P A 1
F3A F -0.030(3) 0.0970(9) 0.2767(14) 0.197(18) Uani 0.38(2) 1 d D U
P A 1
F1B F -0.1303(10) 0.1312(16) 0.2551(7) 0.184(10) Uani 0.62(2) 1 d D
U P A 2
F2B F 0.0305(11) 0.1153(10) 0.2929(7) 0.121(7) Uani 0.62(2) 1 d D U
P A 2
F3B F -0.045(3) 0.2289(9) 0.3078(8) 0.215(13) Uani 0.62(2) 1 d D U
P A 2
C18 C -0.0191(7) 0.3947(6) 0.1077(4) 0.085(2) Uani 1 1 d D . . . . .
F4A F -0.042(7) 0.445(2) 0.1537(18) 0.20(3) Uani 0.27(5) 1 d D . P
B 1
F5A F 0.059(4) 0.432(3) 0.078(3) 0.126(18) Uani 0.27(5) 1 d D . P B
1

```

F6A F -0.107(4) 0.396(3) 0.067(4) 0.17(3) Uani 0.27(5) 1 d D . P B
1
F5B F 0.0260(18) 0.4168(10) 0.0560(9) 0.134(7) Uani 0.73(5) 1 d D .
P B 2
F4B F 0.0063(15) 0.4520(7) 0.1507(6) 0.121(6) Uani 0.73(5) 1 d D .
P B 2
F6B F -0.1256(7) 0.4026(10) 0.0940(9) 0.104(6) Uani 0.73(5) 1 d D .
P B 2
C21 C 0.2988(5) 0.0823(4) 0.1122(3) 0.0461(16) Uani 1 1 d
C22 C 0.3460(5) 0.1275(4) 0.1622(3) 0.0561(18) Uani 1 1 d
H22 H 0.3115 0.1756 0.1742 0.067 Uiso 1 1 calc R U . . .
C25 C 0.4427(5) 0.1035(4) 0.1948(3) 0.0555(17) Uani 1 1 d D
C24 C 0.4980(5) 0.0343(4) 0.1756(3) 0.0615(19) Uani 1 1 d
H24 H 0.5647 0.0192 0.1965 0.074 Uiso 1 1 calc R U . . .
C23 C 0.4540(5) -0.0120(4) 0.1256(3) 0.0576(18) Uani 1 1 d D . . .
.
C26 C 0.3542(5) 0.0125(4) 0.0948(3) 0.0541(17) Uani 1 1 d
H26 H 0.3240 -0.0193 0.0615 0.065 Uiso 1 1 calc R U . . .
C27 C 0.5114(7) -0.0875(5) 0.1046(5) 0.085(3) Uani 1 1 d D
F7A F 0.514(4) -0.094(3) 0.0439(8) 0.170(19) Uani 0.37(5) 1 d D U P
C 1
F8A F 0.456(3) -0.1542(16) 0.122(3) 0.187(17) Uani 0.37(5) 1 d D U
P C 1
F9A F 0.6118(19) -0.101(2) 0.1296(18) 0.147(14) Uani 0.37(5) 1 d D
U P C 1
F7B F 0.557(2) -0.0710(12) 0.0520(9) 0.142(8) Uani 0.63(5) 1 d D U
P C 2
F8B F 0.4441(12) -0.1500(8) 0.0904(10) 0.102(6) Uani 0.63(5) 1 d D
U P C 2
F9B F 0.5867(18) -0.1124(9) 0.1460(10) 0.136(7) Uani 0.63(5) 1 d D
U P C 2
C28 C 0.4921(7) 0.1551(6) 0.2476(4) 0.081(2) Uani 1 1 d D
F10A F 0.522(3) 0.1114(9) 0.2986(7) 0.112(8) Uani 0.54(4) 1 d D U P
D 1
F11A F 0.4261(16) 0.2121(13) 0.2670(10) 0.099(7) Uani 0.54(4) 1 d D
U P D 1
F12A F 0.580(2) 0.195(2) 0.2338(10) 0.151(11) Uani 0.54(4) 1 d D U
P D 1
F10B F 0.584(2) 0.1204(15) 0.2746(17) 0.148(11) Uani 0.46(4) 1 d D
U P D 2
F11B F 0.4272(19) 0.167(3) 0.2904(12) 0.144(12) Uani 0.46(4) 1 d D
U P D 2
F12B F 0.526(3) 0.2274(11) 0.2296(11) 0.134(10) Uani 0.46(4) 1 d D
U P D 2
C31 C 0.2140(4) 0.1742(4) 0.0044(3) 0.0449(15) Uani 1 1 d
C32 C 0.1549(4) 0.1748(4) -0.0542(3) 0.0462(16) Uani 1 1 d
.
C33 C 0.1806(5) 0.2351(4) -0.0980(3) 0.0595(18) Uani 1 1 d
.
H33 H 0.1419 0.2363 -0.1372 0.071 Uiso 1 1 calc R U . . .
C34 C 0.2633(6) 0.2934(4) -0.0835(3) 0.067(2) Uani 1 1 d
H34 H 0.2787 0.3338 -0.1126 0.081 Uiso 1 1 calc R U . . .
C35 C 0.3212(5) 0.2902(4) -0.0263(3) 0.0575(18) Uani 1 1 d D . . .
.
C36 C 0.2980(5) 0.2320(4) 0.0175(3) 0.0551(18) Uani 1 1 d
H36 H 0.3385 0.2309 0.0562 0.066 Uiso 1 1 calc R U . . .
C37 C 0.4096(8) 0.3533(6) -0.0113(5) 0.097(3) Uani 1 1 d D

F13A F 0.3793(18) 0.4019(17) 0.0348(12) 0.159(10) Uani 0.53(3) 1 d
D . P E 1
F14A F 0.4262(19) 0.4022(14) -0.0578(8) 0.141(9) Uani 0.53(3) 1 d D
. P E 1
F15A F 0.5019(11) 0.3188(10) 0.0102(16) 0.139(10) Uani 0.53(3) 1 d
D U P E 1
F13B F 0.3719(17) 0.4302(9) -0.019(2) 0.207(16) Uani 0.47(3) 1 d D
. P E 2
F14B F 0.4875(18) 0.348(2) -0.0507(11) 0.167(13) Uani 0.47(3) 1 d D
U P E 2
F15B F 0.460(2) 0.3456(19) 0.0444(8) 0.144(12) Uani 0.47(3) 1 d D U
P E 2
P2 P 0.04431(13) 0.09761(11) -0.06927(8) 0.0524(5) Uani 1 1 d . . .
F 2
C41 C -0.0706(5) 0.1578(4) -0.0433(3) 0.0496(16) Uani 1 1 d . . . F
2
C42 C -0.1285(5) 0.1265(4) 0.0043(3) 0.0584(18) Uani 1 1 d . . . F
2
H42 H -0.1103 0.0746 0.0211 0.070 Uiso 1 1 calc R U . F 2
C43 C -0.2138(5) 0.1714(5) 0.0272(3) 0.0606(19) Uani 1 1 d D . . F
2
C44 C -0.2411(5) 0.2477(5) 0.0027(4) 0.073(2) Uani 1 1 d . . . F 2
H44 H -0.2977 0.2780 0.0181 0.088 Uiso 1 1 calc R U . F 2
C45 C -0.1836(6) 0.2804(4) -0.0457(3) 0.068(2) Uani 1 1 d D . . F 2
C46 C -0.1003(5) 0.2357(4) -0.0680(3) 0.0605(19) Uani 1 1 d . . . F
2
H46 H -0.0627 0.2575 -0.1002 0.073 Uiso 1 1 calc R U . F 2
C47 C -0.2727(7) 0.1372(6) 0.0787(4) 0.086(3) Uani 1 1 d D . . F 2
F16A F -0.236(2) 0.0667(15) 0.1017(14) 0.141(12) Uani 0.54(3) 1 d D
U P G 1
F17A F -0.269(3) 0.1872(14) 0.1268(9) 0.134(10) Uani 0.54(3) 1 d D
U P G 1
F18A F -0.3757(11) 0.128(3) 0.0612(10) 0.155(14) Uani 0.54(3) 1 d D
. P G 1
F16B F -0.2138(19) 0.126(3) 0.1313(10) 0.144(12) Uani 0.46(3) 1 d D
U P F 2
F17B F -0.360(3) 0.1758(19) 0.0917(16) 0.159(16) Uani 0.46(3) 1 d D
. P F 2
F18B F -0.307(3) 0.0588(13) 0.0660(11) 0.125(11) Uani 0.46(3) 1 d D
. P F 2
C48 C -0.2167(8) 0.3622(6) -0.0748(5) 0.109(3) Uani 1 1 d D
F19A F -0.2810(13) 0.4055(6) -0.0400(8) 0.166(6) Uani 0.804(18) 1 d
D U P F 1
F20A F -0.1316(7) 0.4095(6) -0.0814(8) 0.138(5) Uani 0.804(18) 1 d
D U P F 1
F21A F -0.2669(15) 0.3523(6) -0.1307(6) 0.170(6) Uani 0.804(18) 1 d
D U P F 1
F19B F -0.190(5) 0.4278(15) -0.039(2) 0.162(19) Uani 0.196(18) 1 d
D U P F 2
F20B F -0.175(5) 0.377(3) -0.128(2) 0.162(19) Uani 0.196(18) 1 d D
U P F 2
F21B F -0.3261(15) 0.368(3) -0.088(3) 0.136(15) Uani 0.196(18) 1 d
D U P F 2
C51 C 0.0180(5) 0.0997(4) -0.1547(3) 0.0484(16) Uani 1 1 d
.
C52 C -0.0893(5) 0.1002(4) -0.1832(3) 0.0544(17) Uani 1 1 d
.
H222 H -0.1480 0.1071 -0.1588 0.065 Uiso 1 1 calc R U . . .

C53 C -0.1083(5) 0.0905(4) -0.2479(3) 0.0575(18) Uani 1 1 d D . . .
 .
 C54 C -0.0216(6) 0.0830(4) -0.2835(3) 0.0652(19) Uani 1 1 d
 .
 H54 H -0.0347 0.0786 -0.3268 0.078 Uiso 1 1 calc R U . . .
 C55 C 0.0848(5) 0.0819(4) -0.2570(3) 0.0604(19) Uani 1 1 d D . . .
 .
 C56 C 0.1024(5) 0.0886(4) -0.1937(3) 0.0601(18) Uani 1 1 d
 .
 H56 H 0.1740 0.0858 -0.1755 0.072 Uiso 1 1 calc R U . . .
 C57 C -0.2226(6) 0.0934(6) -0.2762(4) 0.082(2) Uani 1 1 d D
 F22A F -0.2575(13) 0.0171(8) -0.2891(18) 0.157(10) Uani 0.54(3) 1 d
 D U P H 1
 F23A F -0.2337(13) 0.136(2) -0.3282(11) 0.136(9) Uani 0.54(3) 1 d D
 U P H 1
 F24A F -0.2955(10) 0.122(2) -0.2401(8) 0.123(9) Uani 0.54(3) 1 d D
 U P H 1
 F22B F -0.2295(15) 0.073(2) -0.3369(7) 0.129(9) Uani 0.46(3) 1 d D
 U P H 2
 F23B F -0.2614(17) 0.1708(9) -0.2764(19) 0.135(9) Uani 0.46(3) 1 d
 D U P H 2
 F24B F -0.2901(15) 0.047(2) -0.2514(12) 0.142(12) Uani 0.46(3) 1 d
 D U P H 2
 C58 C 0.1784(7) 0.0762(6) -0.2964(4) 0.086(3) Uani 1 1 d D
 F25A F 0.1601(16) 0.0245(17) -0.3437(11) 0.124(9) Uani 0.61(4) 1 d
 D . P I 1
 F26A F 0.2709(12) 0.053(2) -0.2668(6) 0.134(11) Uani 0.61(4) 1 d D
 . P I 1
 F27A F 0.199(2) 0.1476(8) -0.3214(15) 0.141(10) Uani 0.61(4) 1 d D
 U P I 1
 F25B F 0.152(2) 0.080(4) -0.3560(7) 0.160(17) Uani 0.39(4) 1 d D U
 P I 2
 F26B F 0.233(3) 0.0055(19) -0.287(2) 0.162(16) Uani 0.39(4) 1 d D .
 P I 2
 F27B F 0.249(2) 0.134(2) -0.281(2) 0.143(14) Uani 0.39(4) 1 d D U P
 I 2

loop_

_atom_site_aniso_label
 _atom_site_aniso_U_11
 _atom_site_aniso_U_22
 _atom_site_aniso_U_33
 _atom_site_aniso_U_23
 _atom_site_aniso_U_13
 _atom_site_aniso_U_12
 P1 0.0470(10) 0.0563(12) 0.0461(10) -0.0022(9) 0.0013(8) 0.0047(9)
 C11 0.040(4) 0.051(5) 0.057(4) -0.003(4) 0.007(3) 0.005(3)
 C12 0.058(5) 0.061(5) 0.074(5) 0.001(4) 0.005(4) -0.001(4)
 C13 0.070(5) 0.076(6) 0.065(5) -0.010(5) 0.019(4) 0.006(4)
 C14 0.046(4) 0.084(6) 0.084(6) -0.025(5) 0.016(4) 0.004(4)
 C15 0.044(4) 0.052(5) 0.080(5) -0.006(4) 0.003(4) -0.001(4)
 C16 0.041(4) 0.061(5) 0.062(5) -0.006(4) 0.010(3) -0.006(4)
 C17 0.135(11) 0.116(11) 0.085(9) -0.007(8) 0.045(8) 0.008(9)
 F1A 0.155(16) 0.13(2) 0.123(18) -0.007(14) 0.115(13) -0.015(14)
 F2A 0.26(3) 0.17(3) 0.064(13) 0.006(13) 0.015(15) 0.056(19)
 F3A 0.35(4) 0.066(13) 0.21(3) -0.018(16) 0.21(3) -0.02(2)
 F1B 0.117(10) 0.28(3) 0.157(11) 0.091(14) 0.048(8) -0.026(12)
 F2B 0.148(10) 0.145(17) 0.070(7) 0.040(8) 0.014(7) -0.004(9)

F3B 0.42(4) 0.133(12) 0.115(16) -0.041(11) 0.14(2) 0.01(2)
 C18 0.076(7) 0.077(7) 0.104(8) -0.002(6) 0.015(6) 0.005(6)
 F4A 0.29(6) 0.08(2) 0.27(6) -0.09(3) 0.13(5) 0.02(3)
 F5A 0.12(2) 0.11(2) 0.16(3) 0.03(2) 0.06(2) -0.036(19)
 F6A 0.19(5) 0.10(2) 0.20(4) -0.02(3) -0.11(4) 0.05(3)
 F5B 0.163(15) 0.064(7) 0.186(12) 0.036(8) 0.076(11) 0.043(9)
 F4B 0.128(10) 0.066(7) 0.162(13) -0.023(7) -0.028(8) 0.014(5)
 F6B 0.070(8) 0.095(10) 0.145(10) 0.012(8) 0.005(6) 0.029(6)
 C21 0.047(4) 0.051(4) 0.039(4) -0.002(3) -0.002(3) 0.006(3)
 C22 0.067(5) 0.050(5) 0.053(4) 0.005(3) 0.010(4) 0.018(4)
 C25 0.064(4) 0.051(4) 0.050(4) -0.002(4) -0.004(3) 0.007(4)
 C24 0.045(4) 0.074(5) 0.064(5) 0.016(4) -0.003(4) -0.001(4)
 C23 0.059(5) 0.050(5) 0.063(5) -0.002(4) 0.004(4) 0.003(4)
 C26 0.054(4) 0.058(5) 0.050(4) 0.000(3) 0.002(3) 0.000(4)
 C27 0.082(8) 0.062(7) 0.111(9) -0.004(6) 0.008(7) 0.020(6)
 F7A 0.22(3) 0.16(3) 0.12(2) -0.07(2) -0.05(2) 0.14(3)
 F8A 0.11(2) 0.11(2) 0.33(5) -0.02(2) -0.02(3) 0.043(16)
 F9A 0.039(11) 0.22(3) 0.18(3) -0.08(2) -0.006(13) 0.059(12)
 F7B 0.158(13) 0.122(10) 0.158(17) -0.027(10) 0.084(14) 0.025(10)
 F8B 0.104(8) 0.045(7) 0.151(14) -0.026(6) -0.035(7) -0.001(6)
 F9B 0.120(12) 0.078(9) 0.196(14) -0.034(8) -0.064(11) 0.071(8)
 C28 0.079(7) 0.090(8) 0.072(7) -0.025(6) -0.011(6) 0.011(6)
 F10A 0.168(19) 0.093(8) 0.064(8) 0.003(6) -0.058(10) 0.031(11)
 F11A 0.131(14) 0.097(12) 0.063(10) -0.034(7) -0.032(9) 0.031(9)
 F12A 0.144(16) 0.17(2) 0.144(17) -0.064(16) 0.051(13) -0.078(16)
 F10B 0.127(17) 0.144(18) 0.16(2) -0.069(16) -0.073(15) 0.028(14)
 F11B 0.145(18) 0.23(3) 0.060(13) -0.053(16) 0.012(12) -0.029(19)
 F12B 0.17(2) 0.062(10) 0.162(17) -0.050(9) -0.033(18) -0.019(12)
 C31 0.032(3) 0.046(4) 0.058(4) -0.004(3) 0.006(3) 0.000(3)
 C32 0.043(4) 0.051(4) 0.044(4) 0.004(3) -0.003(3) 0.004(3)
 C33 0.058(4) 0.068(5) 0.051(4) 0.007(4) -0.003(4) 0.006(4)
 C34 0.060(5) 0.076(5) 0.068(5) 0.004(4) 0.012(4) 0.000(4)
 C35 0.041(4) 0.067(5) 0.065(5) -0.003(4) 0.006(4) -0.008(4)
 C36 0.050(4) 0.068(5) 0.047(4) -0.006(4) 0.001(3) 0.003(4)
 C37 0.092(8) 0.106(9) 0.090(8) -0.008(7) 0.000(7) -0.027(7)
 F13A 0.160(17) 0.123(18) 0.20(2) -0.066(15) 0.035(15) -0.075(15)
 F14A 0.089(14) 0.153(17) 0.180(16) 0.090(13) -0.003(10) -0.047(12)
 F15A 0.051(8) 0.158(12) 0.20(3) 0.009(16) -0.038(12) -0.021(7)
 F13B 0.159(19) 0.085(12) 0.38(5) -0.01(2) 0.06(3) -0.046(11)
 F14B 0.083(14) 0.32(3) 0.103(16) -0.043(17) 0.031(11) -0.094(17)
 F15B 0.16(2) 0.18(3) 0.082(11) -0.015(12) 0.005(12) -0.106(19)
 P2 0.0463(10) 0.0564(12) 0.0534(11) 0.0052(9) -0.0033(8) 0.0035(9)
 C41 0.041(4) 0.047(4) 0.060(4) 0.001(3) -0.002(3) 0.005(3)
 C42 0.063(5) 0.057(5) 0.055(4) 0.004(4) 0.005(4) -0.010(4)
 C43 0.040(4) 0.073(6) 0.069(5) -0.009(4) 0.008(4) -0.016(4)
 C44 0.050(5) 0.069(6) 0.099(6) -0.014(5) 0.000(4) 0.002(4)
 C45 0.057(5) 0.063(5) 0.084(6) 0.015(4) 0.010(4) -0.008(4)
 C46 0.040(4) 0.072(5) 0.070(5) -0.007(4) 0.005(3) -0.004(4)
 C47 0.087(8) 0.098(8) 0.077(7) -0.001(6) 0.032(6) -0.002(7)
 F16A 0.15(2) 0.106(18) 0.18(2) 0.063(16) 0.094(18) 0.032(14)
 F17A 0.22(2) 0.122(14) 0.069(11) -0.010(9) 0.056(12) -0.023(15)
 F18A 0.055(11) 0.29(4) 0.123(14) 0.046(16) 0.032(8) -0.051(17)
 F16B 0.171(18) 0.16(3) 0.099(13) 0.064(16) -0.002(11) -0.069(18)
 F17B 0.17(3) 0.19(2) 0.13(3) 0.020(18) 0.10(2) 0.05(2)
 F18B 0.13(2) 0.116(17) 0.131(15) -0.026(12) 0.044(14) -0.074(17)
 C48 0.089(9) 0.098(9) 0.142(11) 0.036(8) 0.017(8) 0.024(7)
 F19A 0.157(11) 0.094(8) 0.261(15) 0.049(8) 0.103(11) 0.072(8)
 F20A 0.112(6) 0.074(7) 0.234(13) 0.041(7) 0.056(7) 0.007(5)

F21A 0.174(13) 0.139(9) 0.187(10) 0.073(8) -0.051(10) 0.026(9)
 F19B 0.21(4) 0.10(3) 0.17(4) 0.01(2) -0.02(3) 0.05(3)
 F20B 0.20(4) 0.07(3) 0.22(4) 0.10(3) 0.07(4) 0.04(3)
 F21B 0.13(3) 0.13(3) 0.13(3) 0.02(3) -0.03(3) 0.06(2)
 C51 0.043(4) 0.055(4) 0.046(4) 0.004(3) -0.003(3) 0.004(3)
 C52 0.049(4) 0.060(5) 0.055(4) 0.002(4) 0.006(3) 0.002(3)
 C53 0.050(4) 0.063(5) 0.058(5) 0.007(4) -0.004(4) -0.006(4)
 C54 0.075(5) 0.067(5) 0.052(4) -0.003(4) -0.002(4) -0.001(4)
 C55 0.044(4) 0.083(6) 0.054(5) 0.000(4) -0.002(4) 0.002(4)
 C56 0.040(4) 0.069(5) 0.070(5) 0.001(4) -0.001(4) 0.005(4)
 C57 0.061(6) 0.117(9) 0.065(6) -0.003(7) -0.014(5) -0.007(6)
 F22A 0.065(10) 0.148(12) 0.25(3) -0.079(17) -0.029(13) -0.041(8)
 F23A 0.087(9) 0.22(2) 0.091(13) 0.046(14) -0.033(10) 0.020(14)
 F24A 0.039(7) 0.22(2) 0.109(11) -0.027(14) -0.021(6) 0.026(12)
 F22B 0.081(10) 0.22(3) 0.084(12) -0.022(14) -0.014(7) -0.032(16)
 F23B 0.061(11) 0.158(15) 0.18(2) 0.019(16) -0.045(13) 0.025(10)
 F24B 0.063(12) 0.25(3) 0.111(17) 0.064(17) -0.004(10) -0.041(18)
 C58 0.078(7) 0.094(8) 0.087(8) -0.022(7) 0.019(6) -0.011(6)
 F25A 0.093(11) 0.190(18) 0.095(13) -0.058(11) 0.041(10) -0.017(10)
 F26A 0.062(8) 0.26(3) 0.083(8) -0.017(12) 0.005(5) 0.074(12)
 F27A 0.126(16) 0.138(12) 0.17(2) 0.030(12) 0.073(15) -0.003(10)
 F25B 0.112(15) 0.30(5) 0.066(12) -0.02(2) 0.025(10) 0.00(3)
 F26B 0.12(2) 0.19(2) 0.18(4) -0.03(2) 0.04(2) 0.06(2)
 F27B 0.052(16) 0.23(3) 0.15(3) -0.04(2) 0.050(15) -0.047(17)

_geom_special_details

;

All esds (except the esd in the dihedral angle between two l.s.
 planes)
 are estimated using the full covariance matrix. The cell esds are
 taken
 into account individually in the estimation of esds in distances,
 angles
 and torsion angles; correlations between esds in cell parameters
 are only
 used when they are defined by crystal symmetry. An approximate
 (isotropic)
 treatment of cell esds is used for estimating esds involving l.s.
 planes.

;

loop_

_geom_bond_atom_site_label_1
_geom_bond_atom_site_label_2
_geom_bond_distance
_geom_bond_site_symmetry_2
_geom_bond_publ_flag
 P1 C21 1.836(6) . ?
 P1 C31 1.843(6) . ?
 P1 C11 1.844(6) . ?
 C11 C16 1.376(8) . ?
 C11 C12 1.385(8) . ?
 C12 C13 1.387(8) . ?
 C13 C14 1.370(9) . ?
 C13 C17 1.494(11) . ?
 C14 C15 1.374(9) . ?
 C15 C16 1.376(8) . ?
 C15 C18 1.485(10) . ?

C17 F3B 1.267(13) . ?
C17 F3A 1.255(15) . ?
C17 F1A 1.314(15) . ?
C17 F2B 1.305(13) . ?
C17 F2A 1.362(16) . ?
C17 F1B 1.396(15) . ?
C18 F4B 1.322(12) . ?
C18 F6B 1.319(12) . ?
C18 F4A 1.323(17) . ?
C18 F5B 1.326(12) . ?
C18 F5A 1.329(17) . ?
C18 F6A 1.332(18) . ?
C21 C22 1.379(8) . ?
C21 C26 1.381(8) . ?
C22 C25 1.378(8) . ?
C25 C24 1.385(8) . ?
C25 C28 1.489(9) . ?
C24 C23 1.378(8) . ?
C23 C26 1.395(8) . ?
C23 C27 1.493(9) . ?
C27 F9B 1.288(12) . ?
C27 F7A 1.304(16) . ?
C27 F9A 1.318(16) . ?
C27 F8B 1.321(12) . ?
C27 F7B 1.326(14) . ?
C27 F8A 1.341(17) . ?
C28 F11B 1.278(14) . ?
C28 F12A 1.305(14) . ?
C28 F12B 1.305(15) . ?
C28 F11A 1.315(13) . ?
C28 F10A 1.323(12) . ?
C28 F10B 1.339(14) . ?
C31 C32 1.395(7) . ?
C31 C36 1.398(8) . ?
C32 C33 1.403(8) . ?
C32 P2 1.847(6) . ?
C33 C34 1.396(8) . ?
C34 C35 1.364(8) . ?
C35 C36 1.373(8) . ?
C35 C37 1.500(10) . ?
C37 F14A 1.298(13) . ?
C37 F15B 1.302(14) . ?
C37 F15A 1.309(12) . ?
C37 F13B 1.326(14) . ?
C37 F14B 1.329(13) . ?
C37 F13A 1.337(14) . ?
P2 C51 1.830(6) . ?
P2 C41 1.834(6) . ?
C41 C42 1.384(8) . ?
C41 C46 1.397(8) . ?
C42 C43 1.394(8) . ?
C43 C44 1.367(9) . ?
C43 C47 1.474(10) . ?
C44 C45 1.402(9) . ?
C45 C46 1.368(8) . ?
C45 C48 1.499(11) . ?
C47 F17B 1.286(14) . ?
C47 F16B 1.296(13) . ?

C47 F18B 1.352(13) . ?
 C48 F21A 1.309(12) . ?
 C48 F20A 1.309(10) . ?
 C48 F20B 1.316(17) . ?
 C48 F19B 1.326(17) . ?
 C48 F19A 1.327(11) . ?
 C48 F21B 1.351(17) . ?
 C51 C56 1.393(7) . ?
 C51 C52 1.401(7) . ?
 C52 C53 1.393(8) . ?
 C53 C54 1.364(8) . ?
 C53 C57 1.479(9) . ?
 C54 C55 1.378(8) . ?
 C55 C56 1.358(8) . ?
 C55 C58 1.483(9) . ?
 C57 F24B 1.267(14) . ?
 C57 F23A 1.302(13) . ?
 C57 F24A 1.310(12) . ?
 C57 F22A 1.323(13) . ?
 C57 F23B 1.333(13) . ?
 C57 F22B 1.337(13) . ?
 C58 F25B 1.292(15) . ?
 C58 F27B 1.292(14) . ?
 C58 F27A 1.301(12) . ?
 C58 F26A 1.306(12) . ?
 C58 F25A 1.315(13) . ?
 C58 F26B 1.328(15) . ?

loop_
 _geom_angle_atom_site_label_1
 _geom_angle_atom_site_label_2
 _geom_angle_atom_site_label_3
 _geom_angle
 _geom_angle_site_symmetry_1
 _geom_angle_site_symmetry_3
 _geom_angle_publ_flag
 C21 P1 C31 102.1(3) . . ?
 C21 P1 C11 103.6(3) . . ?
 C31 P1 C11 100.0(3) . . ?
 C16 C11 C12 118.6(6) . . ?
 C16 C11 P1 123.0(5) . . ?
 C12 C11 P1 118.0(5) . . ?
 C11 C12 C13 120.6(7) . . ?
 C14 C13 C12 119.7(7) . . ?
 C14 C13 C17 120.1(7) . . ?
 C12 C13 C17 120.2(8) . . ?
 C13 C14 C15 120.2(7) . . ?
 C14 C15 C16 119.9(7) . . ?
 C14 C15 C18 118.6(7) . . ?
 C16 C15 C18 121.4(7) . . ?
 C15 C16 C11 121.0(6) . . ?
 F3A C17 F1A 112.6(15) . . ?
 F3B C17 F2B 108.6(14) . . ?
 F3A C17 F2A 107.4(16) . . ?
 F1A C17 F2A 103.2(13) . . ?
 F3B C17 F1B 107.7(13) . . ?
 F2B C17 F1B 100.7(12) . . ?
 F3B C17 C13 116.4(12) . . ?

F3A C17 C13 117.4(13) . . ?
 F1A C17 C13 108.3(12) . . ?
 F2B C17 C13 113.4(10) . . ?
 F2A C17 C13 106.7(14) . . ?
 F1B C17 C13 108.6(10) . . ?
 F4B C18 F6B 105.0(10) . . ?
 F4B C18 F5B 107.7(11) . . ?
 F6B C18 F5B 105.2(11) . . ?
 F4A C18 F5A 106.2(18) . . ?
 F4A C18 F6A 105.8(17) . . ?
 F5A C18 F6A 104.6(18) . . ?
 F4B C18 C15 113.2(9) . . ?
 F6B C18 C15 112.2(10) . . ?
 F4A C18 C15 114(2) . . ?
 F5B C18 C15 113.0(9) . . ?
 F5A C18 C15 112.8(19) . . ?
 F6A C18 C15 113(2) . . ?
 C22 C21 C26 117.0(5) . . ?
 C22 C21 P1 127.4(5) . . ?
 C26 C21 P1 115.6(5) . . ?
 C25 C22 C21 122.1(6) . . ?
 C22 C25 C24 119.8(6) . . ?
 C22 C25 C28 120.4(7) . . ?
 C24 C25 C28 119.7(6) . . ?
 C23 C24 C25 119.8(6) . . ?
 C24 C23 C26 118.9(6) . . ?
 C24 C23 C27 120.8(7) . . ?
 C26 C23 C27 120.3(7) . . ?
 C21 C26 C23 122.3(6) . . ?
 F7A C27 F9A 107.0(15) . . ?
 F9B C27 F8B 108.5(11) . . ?
 F9B C27 F7B 108.4(13) . . ?
 F8B C27 F7B 105.0(12) . . ?
 F7A C27 F8A 105.5(16) . . ?
 F9A C27 F8A 103.5(16) . . ?
 F9B C27 C23 112.1(11) . . ?
 F7A C27 C23 114.3(14) . . ?
 F9A C27 C23 117.5(15) . . ?
 F8B C27 C23 112.9(10) . . ?
 F7B C27 C23 109.6(10) . . ?
 F8A C27 C23 107.8(18) . . ?
 F11B C28 F12B 107.6(14) . . ?
 F12A C28 F11A 105.4(12) . . ?
 F12A C28 F10A 106.0(12) . . ?
 F11A C28 F10A 104.1(10) . . ?
 F11B C28 F10B 107.7(12) . . ?
 F12B C28 F10B 103.2(13) . . ?
 F11B C28 C25 113.1(12) . . ?
 F12A C28 C25 113.1(11) . . ?
 F12B C28 C25 113.0(12) . . ?
 F11A C28 C25 114.0(9) . . ?
 F10A C28 C25 113.3(10) . . ?
 F10B C28 C25 111.6(12) . . ?
 C32 C31 C36 119.5(6) . . ?
 C32 C31 P1 118.7(4) . . ?
 C36 C31 P1 121.5(5) . . ?
 C31 C32 C33 118.4(6) . . ?
 C31 C32 P2 118.0(5) . . ?

C33 C32 P2 123.6(5) . . ?
C34 C33 C32 121.2(6) . . ?
C35 C34 C33 119.0(7) . . ?
C34 C35 C36 121.2(6) . . ?
C34 C35 C37 118.5(7) . . ?
C36 C35 C37 120.3(7) . . ?
C35 C36 C31 120.6(6) . . ?
F14A C37 F15A 109.9(11) . . ?
F15B C37 F13B 109.4(14) . . ?
F15B C37 F14B 105.4(12) . . ?
F13B C37 F14B 104.0(13) . . ?
F14A C37 F13A 106.4(13) . . ?
F15A C37 F13A 105.9(12) . . ?
F14A C37 C35 113.8(10) . . ?
F15B C37 C35 114.1(11) . . ?
F15A C37 C35 112.0(10) . . ?
F13B C37 C35 111.7(11) . . ?
F14B C37 C35 111.5(11) . . ?
F13A C37 C35 108.3(10) . . ?
C51 P2 C41 102.6(3) . . ?
C51 P2 C32 103.1(3) . . ?
C41 P2 C32 99.3(3) . . ?
C42 C41 C46 118.2(6) . . ?
C42 C41 P2 118.9(5) . . ?
C46 C41 P2 122.9(5) . . ?
C41 C42 C43 121.0(6) . . ?
C44 C43 C42 119.9(6) . . ?
C44 C43 C47 120.3(7) . . ?
C42 C43 C47 119.9(7) . . ?
C43 C44 C45 119.9(7) . . ?
C46 C45 C44 119.7(7) . . ?
C46 C45 C48 120.1(7) . . ?
C44 C45 C48 120.1(7) . . ?
C45 C46 C41 121.3(7) . . ?
F17B C47 F16B 106.7(13) . . ?
F17B C47 F18B 104.2(13) . . ?
F16B C47 F18B 101.0(12) . . ?
F17B C47 C43 116.6(12) . . ?
F16B C47 C43 115.3(11) . . ?
F18B C47 C43 111.3(10) . . ?
F21A C48 F20A 106.8(11) . . ?
F20B C48 F19B 105.5(17) . . ?
F21A C48 F19A 108.8(10) . . ?
F20A C48 F19A 105.7(10) . . ?
F20B C48 F21B 104.4(17) . . ?
F19B C48 F21B 105.1(17) . . ?
F20B C48 C45 114.1(15) . . ?
F19B C48 C45 114.7(17) . . ?
F21B C48 C45 112.1(16) . . ?
C56 C51 C52 117.1(5) . . ?
C56 C51 P2 121.3(4) . . ?
C52 C51 P2 121.0(5) . . ?
C53 C52 C51 120.3(6) . . ?
C54 C53 C52 119.5(6) . . ?
C54 C53 C57 121.9(6) . . ?
C52 C53 C57 118.5(6) . . ?
C53 C54 C55 121.7(6) . . ?
C56 C55 C54 118.3(6) . . ?

C56 C55 C58 120.5(6) . . ?
 C54 C55 C58 121.1(7) . . ?
 C55 C56 C51 123.0(6) . . ?
 F23A C57 F24A 107.1(12) . . ?
 F23A C57 F22A 107.5(11) . . ?
 F24A C57 F22A 102.8(13) . . ?
 F24B C57 F23B 108.2(13) . . ?
 F24B C57 F22B 105.6(12) . . ?
 F23B C57 F22B 103.6(12) . . ?
 F24B C57 C53 116.0(11) . . ?
 F23A C57 C53 113.2(10) . . ?
 F24A C57 C53 116.0(8) . . ?
 F22A C57 C53 109.5(10) . . ?
 F23B C57 C53 110.8(9) . . ?
 F22B C57 C53 111.8(11) . . ?
 F25B C58 F27B 108.4(15) . . ?
 F27A C58 F26A 105.4(11) . . ?
 F27A C58 F25A 105.6(12) . . ?
 F26A C58 F25A 106.1(11) . . ?
 F25B C58 F26B 106.4(15) . . ?
 F27B C58 F26B 105.5(14) . . ?
 F25B C58 C55 114.6(14) . . ?
 F27B C58 C55 110.0(11) . . ?
 F27A C58 C55 111.3(10) . . ?
 F26A C58 C55 115.0(9) . . ?
 F25A C58 C55 112.7(10) . . ?
 F26B C58 C55 111.5(14) . . ?

_refine_diff_density_max 0.231
 _refine_diff_density_min -0.267
 _refine_diff_density_rms 0.053

8.6. *trans*-[PdCl₂(*p*-Miranphos)₂]·acetone

data_shelx

_audit_creation_method SHELXL-2014
 _chemical_name_systematic
 ;
 ?
 ;
 _chemical_name_common ?
 _chemical_melting_point ?
 _chemical_formula_moiety ?
 _chemical_formula_sum
 'C45 H32 Cl2 F12 O5 P2 Pd'
 _chemical_formula_weight 1119.94

 loop_
 _atom_type_symbol
 _atom_type_description
 _atom_type_scatter_dispersion_real
 _atom_type_scatter_dispersion_imag
 _atom_type_scatter_source
 'C' 'C' 0.0033 0.0016
 'International Tables Vol C Tables 4.2.6.8 and 6.1.1.4'
 'H' 'H' 0.0000 0.0000

```
'International Tables Vol C Tables 4.2.6.8 and 6.1.1.4'
'Cl' 'Cl' 0.1484 0.1585
'International Tables Vol C Tables 4.2.6.8 and 6.1.1.4'
'F' 'F' 0.0171 0.0103
'International Tables Vol C Tables 4.2.6.8 and 6.1.1.4'
'O' 'O' 0.0106 0.0060
'International Tables Vol C Tables 4.2.6.8 and 6.1.1.4'
'P' 'P' 0.1023 0.0942
'International Tables Vol C Tables 4.2.6.8 and 6.1.1.4'
'Pd' 'Pd' -0.9988 1.0072
'International Tables Vol C Tables 4.2.6.8 and 6.1.1.4'
```

```
_space_group_crystal_system    monoclinic
_space_group_IT_number         14
_space_group_name_H-M_alt      'P 21/c'
_space_group_name_Hall         '-P 2ybc'
```

```
_shelx_space_group_comment
```

```
;
```

The symmetry employed for this shelxl refinement is uniquely defined

by the following loop, which should always be used as a source of symmetry information in preference to the above space-group names. They are only intended as comments.

```
;
```

```
loop_
```

```
_space_group_symop_operation_xyz
'x, y, z'
'-x, y+1/2, -z+1/2'
'-x, -y, -z'
'x, -y-1/2, z-1/2'
```

```
_cell_length_a                15.3938(7)
_cell_length_b                 15.6175(8)
_cell_length_c                 20.4211(10)
_cell_angle_alpha              90
_cell_angle_beta               97.1070(10)
_cell_angle_gamma              90
_cell_volume                   4871.8(4)
_cell_formula_units_Z          4
_cell_measurement_temperature  293(2)
_cell_measurement_reflns_used  5981
_cell_measurement_theta_min    2.195
_cell_measurement_theta_max    26.185
```

```
_exptl_crystal_description    prism
_exptl_crystal_colour         yellow
_exptl_crystal_density_meas   ?
_exptl_crystal_density_method ?
_exptl_crystal_density_diffrn 1.527
_exptl_crystal_F_000          2240
_exptl_transmission_factor_min ?
_exptl_transmission_factor_max ?
_exptl_crystal_size_max       0.46
_exptl_crystal_size_mid       0.42
_exptl_crystal_size_min       0.39
_exptl_absorpt_coefficient_mu 0.645
```



```

_shelx_estimated_absorpt_T_min      ?
_shelx_estimated_absorpt_T_max      ?
_exptl_absorpt_correction_type       ?
_exptl_absorpt_correction_T_min      ?
_exptl_absorpt_correction_T_max      ?
_exptl_absorpt_process_details       ?

_exptl_special_details
;
?
;

_diffrn_ambient_temperature          293(2)
_diffrn_radiation_wavelength          0.71073
_diffrn_radiation_type                MoK\alpha
_diffrn_source                        ?
_diffrn_measurement_device_type       'Bruker SMART CCD area detector'
_diffrn_measurement_method            ?
_diffrn_detector_area_resol_mean      ?
_diffrn_reflns_number                 38513
_diffrn_reflns_av_unetI/netI          0.0330
_diffrn_reflns_av_R_equivalents       0.0313
_diffrn_reflns_limit_h_min            -19
_diffrn_reflns_limit_h_max            20
_diffrn_reflns_limit_k_min            -20
_diffrn_reflns_limit_k_max            20
_diffrn_reflns_limit_l_min            -26
_diffrn_reflns_limit_l_max            26
_diffrn_reflns_theta_min               1.333
_diffrn_reflns_theta_max               28.804
_diffrn_reflns_theta_full              25.242
_diffrn_measured_fraction_theta_max    0.934
_diffrn_measured_fraction_theta_full   1.000
_diffrn_reflns_Laue_measured_fraction_max 0.934
_diffrn_reflns_Laue_measured_fraction_full 1.000
_diffrn_reflns_point_group_measured_fraction_max 0.934
_diffrn_reflns_point_group_measured_fraction_full 1.000
_reflns_number_total                   11872
_reflns_number_gt                       8672
_reflns_threshold_expression            'I > 2\sigma(I)'
_reflns_Friedel_coverage                0.000
_reflns_Friedel_fraction_max           .
_reflns_Friedel_fraction_full          .

_reflns_special_details
;
Reflections were merged by SHELXL according to the crystal
class for the calculation of statistics and refinement.

_reflns_Friedel_fraction is defined as the number of unique
Friedel pairs measured divided by the number that would be
possible theoretically, ignoring centric projections and
systematic absences.
;

_computing_data_collection              ?
_computing_cell_refinement              ?
_computing_data_reduction               ?

```

```

_computing_structure_solution      ?
_computing_structure_refinement    'SHELXL-2014 (Sheldrick, 2014)'
_computing_molecular_graphics      ?
_computing_publication_material    ?

_refine_special_details
;
?
;
_refine_ls_structure_factor_coef   Fsqd
_refine_ls_matrix_type             full
_refine_ls_weighting_scheme        calc
_refine_ls_weighting_details
'w=1/[\s^2^(Fo^2)+(0.0605P)^2+2.2860P] where P=(Fo^2+2Fc^2)/3'
_atom_sites_solution_primary       ?
_atom_sites_solution_secondary     ?
_atom_sites_solution_hydrogens     geom
_refine_ls_hydrogen_treatment      constr
_refine_ls_extinction_method       none
_refine_ls_extinction_coef         .
_refine_ls_number_reflns           11872
_refine_ls_number_parameters       711
_refine_ls_number_restraints       213
_refine_ls_R_factor_all             0.0696
_refine_ls_R_factor_gt             0.0464
_refine_ls_wR_factor_ref           0.1241
_refine_ls_wR_factor_gt           0.1116
_refine_ls_goodness_of_fit_ref     1.028
_refine_ls_restrained_S_all        1.032
_refine_ls_shift/su_max            0.007
_refine_ls_shift/su_mean           0.000

loop_
_atom_site_label
_atom_site_type_symbol
_atom_site_fract_x
_atom_site_fract_y
_atom_site_fract_z
_atom_site_U_iso_or_equiv
_atom_site_adp_type
_atom_site_occupancy
_atom_site_site_symmetry_order
_atom_site_calc_flag
_atom_site_refinement_flags_posn
_atom_site_refinement_flags_adp
_atom_site_refinement_flags_occupancy
_atom_site_disorder_assembly
_atom_site_disorder_group
O1S O -0.1142(3) 1.1021(2) 0.2180(2) 0.1481(17) Uani 1 1 d . . . .
.
C1S C -0.1112(4) 1.1630(4) 0.2577(3) 0.1063(15) Uiso 1 1 d . . . .
.
C3S C -0.1621(6) 1.1594(4) 0.3098(3) 0.187(4) Uani 1 1 d . . . .
H1S H -0.1530 1.2104 0.3360 0.281 Uiso 1 1 calc R U . . .
H2S H -0.2228 1.1551 0.2924 0.281 Uiso 1 1 calc R U . . .
H3S H -0.1456 1.1103 0.3368 0.281 Uiso 1 1 calc R U . . .
C2S C -0.0712(4) 1.2443(4) 0.2425(5) 0.184(4) Uani 1 1 d . . . .
H4S H -0.0744 1.2838 0.2781 0.276 Uiso 1 1 calc R U . . .

```

H5S H -0.0110 1.2349 0.2366 0.276 Uiso 1 1 calc R U . . .
H6S H -0.1018 1.2675 0.2026 0.276 Uiso 1 1 calc R U . . .
Pd1 Pd 0.35490(2) 0.96954(2) 0.22292(2) 0.04573(8) Uani 1 1 d . . .
. .
C11 Cl 0.38089(6) 1.09697(5) 0.17528(5) 0.0703(2) Uani 1 1 d . . .
. .
C12 Cl 0.31582(6) 0.83554(5) 0.25639(6) 0.0824(3) Uani 1 1 d . . .
. .
P1 P 0.49721(5) 0.91842(5) 0.21911(4) 0.04943(18) Uani 1 1 d . . .
. .
C11 C 0.5708(2) 0.98320(19) 0.17656(16) 0.0561(7) Uani 1 1 d . . .
. .
C12 C 0.6079(3) 0.9520(3) 0.1228(2) 0.0783(11) Uani 1 1 d
H12 H 0.5975 0.8957 0.1092 0.094 Uiso 1 1 calc R U . . .
C13 C 0.6606(3) 1.0039(3) 0.0890(2) 0.0910(12) Uani 1 1 d
H13 H 0.6848 0.9824 0.0529 0.109 Uiso 1 1 calc R U . . .
C14 C 0.6767(3) 1.0867(3) 0.1087(2) 0.0793(10) Uani 1 1 d D
C15 C 0.6416(2) 1.1185(2) 0.1617(2) 0.0769(10) Uani 1 1 d
H15 H 0.6533 1.1747 0.1752 0.092 Uiso 1 1 calc R U . . .
C16 C 0.5884(2) 1.0673(2) 0.19544(19) 0.0662(9) Uani 1 1 d
. .
H16 H 0.5642 1.0897 0.2313 0.079 Uiso 1 1 calc R U . . .
C17 C 0.7329(4) 1.1411(4) 0.0704(3) 0.1083(16) Uani 1 1 d D
F1A F 0.7017(8) 1.1468(10) 0.0093(5) 0.173(7) Uani 0.620(19) 1 d D
U P A 1
F2A F 0.8131(5) 1.1063(7) 0.0671(6) 0.129(4) Uani 0.620(19) 1 d D U
P A 1
F3A F 0.7487(11) 1.2171(6) 0.0952(9) 0.182(7) Uani 0.620(19) 1 d D
U P A 1
F1B F 0.7340(17) 1.1223(15) 0.0112(9) 0.185(11) Uani 0.380(19) 1 d
D U P A 2
F2B F 0.8051(12) 1.157(2) 0.1015(10) 0.200(11) Uani 0.380(19) 1 d D
U P A 2
F3B F 0.6917(16) 1.2215(10) 0.0667(10) 0.175(8) Uani 0.380(19) 1 d
D U P A 2
C21 C 0.5572(2) 0.89483(19) 0.30030(15) 0.0542(7) Uani 1 1 d . . .
. .
C22 C 0.5242(3) 0.8342(3) 0.33957(19) 0.0838(11) Uani 1 1 d
. .
H22 H 0.4700 0.8097 0.3257 0.101 Uiso 1 1 calc R U . . .
C23 C 0.5692(3) 0.8090(3) 0.3987(2) 0.0918(13) Uani 1 1 d
H23 H 0.5458 0.7673 0.4238 0.110 Uiso 1 1 calc R U . . .
C24 C 0.6472(3) 0.8446(3) 0.42022(18) 0.0790(11) Uani 1 1 d D
. .
C25 C 0.6806(3) 0.9066(3) 0.3834(2) 0.0924(13) Uani 1 1 d
H25 H 0.7339 0.9321 0.3985 0.111 Uiso 1 1 calc R U . . .
C26 C 0.6353(2) 0.9317(3) 0.32311(19) 0.0761(10) Uani 1 1 d
. .
H26 H 0.6585 0.9740 0.2983 0.091 Uiso 1 1 calc R U . . .
C27 C 0.6998(4) 0.8150(5) 0.4835(3) 0.1128(18) Uani 1 1 d D
F4A F 0.685(2) 0.7374(9) 0.5005(11) 0.210(11) Uani 0.53(2) 1 d D U
P B 1
F5A F 0.7837(7) 0.8276(18) 0.4847(8) 0.182(10) Uani 0.53(2) 1 d D U
P B 1
F6A F 0.6804(10) 0.8633(11) 0.5328(4) 0.136(5) Uani 0.53(2) 1 d D U
P B 1
F4B F 0.7445(13) 0.7484(13) 0.4705(6) 0.143(6) Uani 0.47(2) 1 d D U
P B 2

F5B F 0.760(2) 0.8691(14) 0.5080(12) 0.211(13) Uani 0.47(2) 1 d D U
P B 2
F6B F 0.6515(11) 0.789(2) 0.5266(8) 0.196(12) Uani 0.47(2) 1 d D U
P B 2
C31 C 0.49380(19) 0.81648(18) 0.17583(15) 0.0515(7) Uani 1 1 d . .
. . .
C32 C 0.5511(2) 0.7498(2) 0.19483(16) 0.0587(8) Uani 1 1 d
.
H32 H 0.5918 0.7553 0.2322 0.070 Uiso 1 1 calc R U . . .
C33 C 0.5475(2) 0.67547(19) 0.15826(16) 0.0607(8) Uani 1 1 d . . .
. . .
H33 H 0.5858 0.6308 0.1712 0.073 Uiso 1 1 calc R U . . .
C34 C 0.4877(2) 0.66697(19) 0.10280(15) 0.0553(7) Uani 1 1 d . . .
. . .
C35 C 0.4297(2) 0.7325(2) 0.08410(19) 0.0749(10) Uani 1 1 d
.
H35 H 0.3892 0.7268 0.0466 0.090 Uiso 1 1 calc R U . . .
C36 C 0.4321(2) 0.8066(2) 0.12135(17) 0.0721(10) Uani 1 1 d
.
H36 H 0.3918 0.8500 0.1096 0.087 Uiso 1 1 calc R U . . .
C37 C 0.4881(2) 0.5901(2) 0.06002(17) 0.0632(8) Uani 1 1 d
.
O2 O 0.44110(19) 0.58818(17) 0.00650(13) 0.0896(9) Uani 1 1 d . . .
. . .
O1 O 0.54055(19) 0.53010(15) 0.08137(14) 0.0860(9) Uani 1 1 d . . .
. . .
H1 H 0.5364 0.4905 0.0548 0.129 Uiso 1 1 calc R U . . .
P2 P 0.21422(5) 1.01444(4) 0.23521(4) 0.04427(16) Uani 1 1 d . . .
. . .
C41 C 0.1828(2) 0.97912(18) 0.31412(14) 0.0506(7) Uani 1 1 d . . .
. . .
C42 C 0.0971(3) 0.9658(3) 0.32458(18) 0.0737(10) Uani 1 1 d
.
H42 H 0.0523 0.9740 0.2902 0.088 Uiso 1 1 calc R U . . .
C43 C 0.0775(3) 0.9405(3) 0.3857(2) 0.0885(12) Uani 1 1 d
H43 H 0.0195 0.9315 0.3925 0.106 Uiso 1 1 calc R U . . .
C44 C 0.1434(3) 0.9286(3) 0.43672(18) 0.0803(11) Uani 1 1 d D . . .
.
C45 C 0.2278(3) 0.9426(3) 0.42714(19) 0.0857(12) Uani 1 1 d
.
H45 H 0.2723 0.9354 0.4618 0.103 Uiso 1 1 calc R U . . .
C46 C 0.2476(3) 0.9675(2) 0.36593(17) 0.0719(10) Uani 1 1 d
.
H46 H 0.3057 0.9767 0.3596 0.086 Uiso 1 1 calc R U . . .
C47 C 0.1227(5) 0.8990(4) 0.5025(3) 0.1169(18) Uani 1 1 d D
F7A F 0.0522(15) 0.8543(18) 0.5009(8) 0.215(11) Uani 0.54(3) 1 d D
U P C 1
F8A F 0.1096(16) 0.9616(8) 0.5408(8) 0.164(7) Uani 0.54(3) 1 d D U
P C 1
F9A F 0.1876(13) 0.8551(17) 0.5339(7) 0.189(9) Uani 0.54(3) 1 d D U
P C 1
F7B F 0.138(2) 0.8196(8) 0.5117(13) 0.198(11) Uani 0.46(3) 1 d D U
P C 2
F8B F 0.0381(9) 0.907(2) 0.5105(10) 0.169(8) Uani 0.46(3) 1 d D U P
C 2
F9B F 0.165(2) 0.9403(18) 0.5509(6) 0.199(12) Uani 0.46(3) 1 d D U
P C 2

C51 C 0.13279(19) 0.97285(17) 0.17060(14) 0.0483(6) Uani 1 1 d . .
. . .
C52 C 0.1551(2) 0.9084(2) 0.12981(16) 0.0612(8) Uani 1 1 d
.
H52 H 0.2122 0.8877 0.1343 0.073 Uiso 1 1 calc R U . . .
C53 C 0.0931(3) 0.8743(2) 0.08231(18) 0.0747(10) Uani 1 1 d
.
H53 H 0.1086 0.8309 0.0547 0.090 Uiso 1 1 calc R U . . .
C54 C 0.0090(3) 0.9041(2) 0.07570(17) 0.0717(10) Uani 1 1 d D . . .
.
C55 C -0.0138(2) 0.9694(3) 0.11483(19) 0.0766(10) Uani 1 1 d . . .
. . .
H55 H -0.0710 0.9900 0.1098 0.092 Uiso 1 1 calc R U . . .
C56 C 0.0483(2) 1.0049(2) 0.16193(17) 0.0665(9) Uani 1 1 d
.
H56 H 0.0332 1.0503 0.1878 0.080 Uiso 1 1 calc R U . . .
C57 C -0.0597(4) 0.8636(4) 0.0268(3) 0.1066(16) Uani 1 1 d D . . .
.
F10A F -0.0285(10) 0.8449(10) -0.0287(4) 0.162(6) Uani 0.63(2) 1 d
D U P D 1
F11A F -0.1290(9) 0.9041(11) 0.0134(10) 0.184(8) Uani 0.63(2) 1 d D
U P D 1
F12A F -0.0784(10) 0.7854(7) 0.0481(6) 0.149(4) Uani 0.63(2) 1 d D
U P D 1
F10B F -0.0367(16) 0.812(2) -0.0124(15) 0.193(14) Uani 0.37(2) 1 d
D U P D 2
F11B F -0.1256(19) 0.832(3) 0.0578(7) 0.180(12) Uani 0.37(2) 1 d D
U P D 2
F12B F -0.1066(17) 0.9244(13) -0.0083(10) 0.133(7) Uani 0.37(2) 1 d
D U P D 2
C61 C 0.19499(18) 1.12954(17) 0.23540(14) 0.0473(6) Uani 1 1 d . .
. . .
C62 C 0.1759(2) 1.1734(2) 0.17659(15) 0.0589(8) Uani 1 1 d
.
H62 H 0.1718 1.1437 0.1369 0.071 Uiso 1 1 calc R U . . .
C63 C 0.1628(2) 1.2602(2) 0.17624(17) 0.0624(8) Uani 1 1 d
.
H63 H 0.1485 1.2886 0.1364 0.075 Uiso 1 1 calc R U . . .
C64 C 0.1708(2) 1.30555(19) 0.23429(17) 0.0571(7) Uani 1 1 d . . .
. . .
C65 C 0.1927(2) 1.2636(2) 0.29303(17) 0.0635(8) Uani 1 1 d
.
H65 H 0.2002 1.2944 0.3323 0.076 Uiso 1 1 calc R U . . .
C66 C 0.2037(2) 1.1754(2) 0.29409(16) 0.0586(8) Uani 1 1 d
.
H66 H 0.2170 1.1470 0.3341 0.070 Uiso 1 1 calc R U . . .
C67 C 0.1550(2) 1.4004(2) 0.2317(2) 0.0685(9) Uani 1 1 d
O4 O 0.1293(2) 1.43632(17) 0.18084(17) 0.1003(10) Uani 1 1 d
. . .
O3 O 0.1747(3) 1.43979(18) 0.28724(16) 0.1093(11) Uani 1 1 d . . .
. . .
H3 H 0.1644 1.4910 0.2822 0.164 Uiso 1 1 calc R U . . .

loop_
 _atom_site_aniso_label
 _atom_site_aniso_U_11
 _atom_site_aniso_U_22
 _atom_site_aniso_U_33

_atom_site_aniso_U_23
 _atom_site_aniso_U_13
 _atom_site_aniso_U_12
 O1S 0.221(5) 0.066(2) 0.175(4) -0.016(2) 0.092(3) -0.017(2)
 C3S 0.370(12) 0.088(4) 0.113(5) 0.016(3) 0.063(6) 0.019(6)
 C2S 0.140(6) 0.079(4) 0.351(11) -0.026(5) 0.100(7) -0.031(4)
 Pd1 0.04436(13) 0.03288(11) 0.05901(14) -0.00448(9) 0.00273(9)
 0.00256(8)
 C11 0.0607(5) 0.0502(4) 0.1019(6) 0.0183(4) 0.0176(4) 0.0049(4)
 C12 0.0701(6) 0.0423(4) 0.1364(9) 0.0173(5) 0.0192(6) 0.0037(4)
 P1 0.0479(4) 0.0394(4) 0.0597(4) -0.0111(3) 0.0017(3) 0.0054(3)
 C11 0.0488(17) 0.0522(17) 0.0662(19) -0.0054(14) 0.0031(14)
 0.0044(13)
 C12 0.091(3) 0.066(2) 0.081(2) -0.0112(19) 0.026(2) 0.001(2)
 C13 0.101(3) 0.093(3) 0.085(3) 0.001(2) 0.036(2) 0.000(3)
 C14 0.069(2) 0.078(3) 0.091(3) 0.017(2) 0.010(2) 0.000(2)
 C15 0.064(2) 0.056(2) 0.108(3) 0.002(2) 0.002(2) -0.0026(17)
 C16 0.057(2) 0.0561(19) 0.086(2) -0.0118(17) 0.0098(17) -0.0002(15)
 C17 0.101(4) 0.110(5) 0.113(4) 0.036(4) 0.011(4) -0.010(3)
 F1A 0.140(7) 0.237(13) 0.131(9) 0.118(10) -0.020(6) -0.016(7)
 F2A 0.077(4) 0.167(7) 0.148(7) 0.070(5) 0.038(4) 0.018(4)
 F3A 0.200(14) 0.092(5) 0.285(15) -0.021(7) 0.147(12) -0.055(6)
 F1B 0.20(2) 0.214(18) 0.169(19) -0.010(14) 0.115(17) -0.073(15)
 F2B 0.135(14) 0.30(3) 0.170(15) 0.056(18) 0.022(11) -0.091(16)
 F3B 0.23(2) 0.147(12) 0.157(12) 0.061(10) 0.041(12) -0.047(12)
 C21 0.0510(17) 0.0496(16) 0.0606(17) -0.0166(14) 0.0011(13)
 0.0100(13)
 C22 0.089(3) 0.085(3) 0.073(2) 0.007(2) -0.011(2) -0.017(2)
 C23 0.110(4) 0.089(3) 0.072(2) 0.005(2) -0.006(2) -0.001(3)
 C24 0.084(3) 0.088(3) 0.062(2) -0.014(2) -0.0048(19) 0.032(2)
 C25 0.061(2) 0.126(4) 0.084(3) -0.010(3) -0.015(2) 0.005(2)
 C26 0.058(2) 0.092(3) 0.075(2) 0.000(2) -0.0035(17) -0.0024(19)
 C27 0.113(5) 0.142(5) 0.077(3) -0.010(3) -0.013(3) 0.049(4)
 F4A 0.30(3) 0.130(9) 0.168(16) 0.049(9) -0.088(15) 0.024(11)
 F5A 0.100(7) 0.32(3) 0.117(9) 0.022(12) -0.023(6) 0.080(12)
 F6A 0.149(9) 0.183(10) 0.067(4) -0.024(5) -0.018(5) 0.037(8)
 F4B 0.148(11) 0.175(12) 0.097(6) 0.008(7) -0.021(6) 0.095(10)
 F5B 0.25(3) 0.196(14) 0.152(17) 0.002(11) -0.129(18) -0.031(16)
 F6B 0.164(11) 0.33(3) 0.093(8) 0.092(13) 0.034(8) 0.117(17)
 C31 0.0529(17) 0.0404(14) 0.0597(17) -0.0124(12) 0.0006(13)
 0.0078(12)
 C32 0.0578(18) 0.0523(17) 0.0621(18) -0.0130(14) -0.0081(14)
 0.0127(14)
 C33 0.067(2) 0.0464(16) 0.0652(19) -0.0106(14) -0.0065(15)
 0.0191(14)
 C34 0.0560(18) 0.0436(15) 0.0643(18) -0.0122(13) -0.0005(14)
 0.0069(13)
 C35 0.072(2) 0.066(2) 0.078(2) -0.0257(18) -0.0220(18) 0.0193(17)
 C36 0.072(2) 0.0557(19) 0.081(2) -0.0207(17) -0.0209(18) 0.0261(16)
 C37 0.063(2) 0.0490(17) 0.074(2) -0.0174(15) -0.0048(16) 0.0078(15)
 O2 0.102(2) 0.0704(16) 0.0868(18) -0.0366(14) -0.0266(15)
 0.0284(14)
 O1 0.102(2) 0.0530(14) 0.0945(18) -0.0317(13) -0.0217(15)
 0.0264(13)
 P2 0.0443(4) 0.0373(3) 0.0503(4) -0.0041(3) 0.0020(3) 0.0018(3)
 C41 0.0537(17) 0.0429(15) 0.0543(16) -0.0034(12) 0.0033(13) -
 0.0013(12)
 C42 0.062(2) 0.095(3) 0.064(2) 0.0015(19) 0.0093(16) -0.0062(19)

C43 0.080(3) 0.112(3) 0.077(3) 0.003(2) 0.025(2) -0.019(2)
C44 0.110(3) 0.070(2) 0.063(2) 0.0017(18) 0.021(2) -0.012(2)
C45 0.095(3) 0.100(3) 0.058(2) 0.013(2) -0.004(2) -0.005(2)
C46 0.065(2) 0.087(3) 0.061(2) 0.0090(18) -0.0028(16) -0.0081(18)
C47 0.151(6) 0.123(5) 0.080(3) 0.022(4) 0.028(4) -0.020(5)
F7A 0.32(2) 0.201(18) 0.147(9) 0.018(13) 0.098(13) -0.131(16)
F8A 0.256(17) 0.161(9) 0.093(8) -0.001(6) 0.093(10) 0.034(11)
F9A 0.250(14) 0.222(19) 0.102(9) 0.082(12) 0.055(8) 0.069(14)
F7B 0.37(3) 0.085(7) 0.165(16) 0.054(7) 0.139(19) 0.000(11)
F8B 0.204(13) 0.198(19) 0.120(10) 0.028(12) 0.082(9) -0.024(12)
F9B 0.33(3) 0.20(2) 0.068(5) -0.016(10) 0.035(12) -0.129(18)
C51 0.0503(16) 0.0445(15) 0.0494(15) -0.0023(12) 0.0028(12) -
0.0009(12)
C52 0.065(2) 0.0540(18) 0.0637(19) -0.0118(15) 0.0026(15)
0.0023(15)
C53 0.095(3) 0.061(2) 0.066(2) -0.0177(17) 0.0007(19) -0.009(2)
C54 0.080(3) 0.068(2) 0.062(2) -0.0033(17) -0.0115(17) -0.0174(19)
C55 0.055(2) 0.089(3) 0.081(2) -0.004(2) -0.0111(17) 0.0014(18)
C56 0.0567(19) 0.072(2) 0.068(2) -0.0134(17) -0.0035(15) 0.0075(16)
C57 0.115(4) 0.107(4) 0.087(4) -0.009(3) -0.030(3) -0.032(4)
F10A 0.209(10) 0.196(12) 0.069(4) -0.025(5) -0.035(4) -0.059(9)
F11A 0.116(7) 0.169(11) 0.237(18) -0.058(10) -0.099(10) 0.005(8)
F12A 0.143(8) 0.129(7) 0.161(8) -0.011(5) -0.031(6) -0.074(6)
F10B 0.169(18) 0.168(19) 0.22(3) -0.137(18) -0.078(17) 0.023(14)
F11B 0.170(17) 0.27(3) 0.096(8) 0.011(12) -0.021(9) -0.152(17)
F12B 0.146(15) 0.141(10) 0.093(8) 0.018(7) -0.063(7) -0.033(10)
C61 0.0440(15) 0.0386(13) 0.0589(16) -0.0048(12) 0.0054(12)
0.0038(11)
C62 0.072(2) 0.0483(16) 0.0551(17) -0.0031(13) 0.0039(15)
0.0060(15)
C63 0.071(2) 0.0473(17) 0.068(2) 0.0042(15) 0.0055(16) 0.0074(15)
C64 0.0463(16) 0.0438(15) 0.082(2) -0.0039(15) 0.0109(15)
0.0010(13)
C65 0.068(2) 0.0508(17) 0.071(2) -0.0183(16) 0.0055(16) 0.0012(15)
C66 0.069(2) 0.0484(16) 0.0571(17) -0.0070(14) 0.0007(15)
0.0025(14)
C67 0.0527(19) 0.0489(18) 0.104(3) -0.007(2) 0.0115(18) 0.0025(15)
O4 0.130(3) 0.0492(14) 0.117(2) 0.0072(15) -0.005(2) 0.0193(16)
O3 0.166(3) 0.0460(14) 0.113(2) -0.0153(15) 0.005(2) 0.0120(18)

_geom_special_details

;

All esds (except the esd in the dihedral angle between two l.s.
planes)
are estimated using the full covariance matrix. The cell esds are
taken
into account individually in the estimation of esds in distances,
angles
and torsion angles; correlations between esds in cell parameters
are only
used when they are defined by crystal symmetry. An approximate
(isotropic)
treatment of cell esds is used for estimating esds involving l.s.
planes.

;

loop_
_geom_bond_atom_site_label_1

```

    _geom_bond_atom_site_label_2
    _geom_bond_distance
    _geom_bond_site_symmetry_2
    _geom_bond_publ_flag
O1S C1S 1.248(6) . ?
C1S C3S 1.398(8) . ?
C1S C2S 1.461(7) . ?
Pd1 C11 2.2723(8) . ?
Pd1 C12 2.3044(8) . ?
Pd1 P2 2.3194(8) . ?
Pd1 P1 2.3419(8) . ?
P1 C11 1.819(3) . ?
P1 C31 1.819(3) . ?
P1 C21 1.833(3) . ?
C11 C16 1.386(4) . ?
C11 C12 1.387(5) . ?
C12 C13 1.389(6) . ?
C13 C14 1.368(6) . ?
C14 C15 1.362(6) . ?
C14 C17 1.499(6) . ?
C15 C16 1.388(5) . ?
C17 F2B 1.235(13) . ?
C17 F1B 1.247(16) . ?
C17 F1A 1.284(11) . ?
C17 F3A 1.301(10) . ?
C17 F2A 1.358(9) . ?
C17 F3B 1.405(15) . ?
C21 C26 1.362(5) . ?
C21 C22 1.378(5) . ?
C22 C23 1.373(5) . ?
C23 C24 1.347(6) . ?
C24 C25 1.365(6) . ?
C24 C27 1.511(6) . ?
C25 C26 1.394(5) . ?
C27 F6B 1.285(15) . ?
C27 F4A 1.290(13) . ?
C27 F4B 1.292(12) . ?
C27 F5B 1.303(15) . ?
C27 F5A 1.304(15) . ?
C27 F6A 1.322(10) . ?
C31 C36 1.379(4) . ?
C31 C32 1.388(4) . ?
C32 C33 1.378(4) . ?
C33 C34 1.374(4) . ?
C34 C35 1.381(4) . ?
C34 C37 1.486(4) . ?
C35 C36 1.383(4) . ?
C37 O2 1.234(4) . ?
C37 O1 1.277(4) . ?
P2 C61 1.822(3) . ?
P2 C51 1.823(3) . ?
P2 C41 1.824(3) . ?
C41 C46 1.374(4) . ?
C41 C42 1.377(5) . ?
C42 C43 1.379(5) . ?
C43 C44 1.374(6) . ?
C44 C45 1.355(6) . ?
C44 C47 1.491(6) . ?

```


C45 C46 1.379(5) . ?
 C47 F7B 1.271(11) . ?
 C47 F8A 1.282(12) . ?
 C47 F7A 1.287(12) . ?
 C47 F9B 1.290(12) . ?
 C47 F9A 1.313(11) . ?
 C47 F8B 1.338(13) . ?
 C51 C52 1.377(4) . ?
 C51 C56 1.384(4) . ?
 C52 C53 1.380(5) . ?
 C53 C54 1.367(6) . ?
 C54 C55 1.369(5) . ?
 C54 C57 1.501(5) . ?
 C55 C56 1.385(5) . ?
 C57 F10B 1.218(16) . ?
 C57 F11A 1.241(11) . ?
 C57 F10A 1.317(12) . ?
 C57 F12A 1.340(10) . ?
 C57 F12B 1.344(16) . ?
 C57 F11B 1.356(16) . ?
 C61 C62 1.382(4) . ?
 C61 C66 1.388(4) . ?
 C62 C63 1.369(4) . ?
 C63 C64 1.374(5) . ?
 C64 C65 1.372(5) . ?
 C64 C67 1.502(4) . ?
 C65 C66 1.388(4) . ?
 C67 O4 1.204(5) . ?
 C67 O3 1.292(5) . ?

loop_
 _geom_angle_atom_site_label_1
 _geom_angle_atom_site_label_2
 _geom_angle_atom_site_label_3
 _geom_angle
 _geom_angle_site_symmetry_1
 _geom_angle_site_symmetry_3
 _geom_angle_publ_flag
 O1S C1S C3S 119.0(6) . . ?
 O1S C1S C2S 120.4(6) . . ?
 C3S C1S C2S 119.2(6) . . ?
 C11 Pd1 C12 171.34(4) . . ?
 C11 Pd1 P2 89.87(3) . . ?
 C12 Pd1 P2 87.76(3) . . ?
 C11 Pd1 P1 93.98(3) . . ?
 C12 Pd1 P1 88.85(3) . . ?
 P2 Pd1 P1 175.18(3) . . ?
 C11 P1 C31 103.72(14) . . ?
 C11 P1 C21 105.68(15) . . ?
 C31 P1 C21 104.16(13) . . ?
 C11 P1 Pd1 117.85(10) . . ?
 C31 P1 Pd1 110.10(10) . . ?
 C21 P1 Pd1 114.01(10) . . ?
 C16 C11 C12 117.9(3) . . ?
 C16 C11 P1 120.4(3) . . ?
 C12 C11 P1 121.6(3) . . ?
 C11 C12 C13 120.7(4) . . ?
 C14 C13 C12 120.1(4) . . ?

C15 C14 C13 120.2(4) . . ?
C15 C14 C17 121.2(5) . . ?
C13 C14 C17 118.5(5) . . ?
C14 C15 C16 120.0(4) . . ?
C11 C16 C15 121.0(3) . . ?
F2B C17 F1B 115.3(13) . . ?
F1A C17 F3A 110.1(10) . . ?
F1A C17 F2A 102.2(8) . . ?
F3A C17 F2A 104.9(8) . . ?
F2B C17 F3B 102.5(13) . . ?
F1B C17 F3B 102.5(11) . . ?
F2B C17 C14 112.8(8) . . ?
F1B C17 C14 116.8(11) . . ?
F1A C17 C14 112.1(8) . . ?
F3A C17 C14 114.0(7) . . ?
F2A C17 C14 112.7(5) . . ?
F3B C17 C14 104.4(9) . . ?
C26 C21 C22 117.7(3) . . ?
C26 C21 P1 123.3(3) . . ?
C22 C21 P1 118.9(3) . . ?
C23 C22 C21 121.7(4) . . ?
C24 C23 C22 120.1(4) . . ?
C23 C24 C25 119.6(4) . . ?
C23 C24 C27 121.0(5) . . ?
C25 C24 C27 119.3(5) . . ?
C24 C25 C26 120.3(4) . . ?
C21 C26 C25 120.5(4) . . ?
F6B C27 F4B 104.9(12) . . ?
F6B C27 F5B 112.5(13) . . ?
F4B C27 F5B 103.3(13) . . ?
F4A C27 F5A 110.4(12) . . ?
F4A C27 F6A 105.5(12) . . ?
F5A C27 F6A 102.5(10) . . ?
F6B C27 C24 112.8(8) . . ?
F4A C27 C24 115.0(7) . . ?
F4B C27 C24 108.3(6) . . ?
F5B C27 C24 114.1(9) . . ?
F5A C27 C24 113.3(8) . . ?
F6A C27 C24 109.2(6) . . ?
C36 C31 C32 119.5(3) . . ?
C36 C31 P1 117.7(2) . . ?
C32 C31 P1 122.8(2) . . ?
C33 C32 C31 120.0(3) . . ?
C34 C33 C32 120.4(3) . . ?
C33 C34 C35 120.0(3) . . ?
C33 C34 C37 120.8(3) . . ?
C35 C34 C37 119.1(3) . . ?
C34 C35 C36 119.7(3) . . ?
C31 C36 C35 120.4(3) . . ?
O2 C37 O1 124.2(3) . . ?
O2 C37 C34 119.7(3) . . ?
O1 C37 C34 116.1(3) . . ?
C61 P2 C51 104.81(13) . . ?
C61 P2 C41 103.62(13) . . ?
C51 P2 C41 107.32(13) . . ?
C61 P2 Pd1 116.92(10) . . ?
C51 P2 Pd1 112.42(10) . . ?
C41 P2 Pd1 110.95(10) . . ?

C46 C41 C42 118.6(3) . . ?
 C46 C41 P2 118.2(3) . . ?
 C42 C41 P2 123.1(3) . . ?
 C41 C42 C43 120.4(4) . . ?
 C44 C43 C42 120.0(4) . . ?
 C45 C44 C43 120.0(4) . . ?
 C45 C44 C47 119.7(5) . . ?
 C43 C44 C47 120.2(5) . . ?
 C44 C45 C46 120.0(4) . . ?
 C41 C46 C45 120.9(4) . . ?
 F8A C47 F7A 103.5(11) . . ?
 F7B C47 F9B 107.9(12) . . ?
 F8A C47 F9A 105.5(10) . . ?
 F7A C47 F9A 108.5(10) . . ?
 F7B C47 F8B 103.6(10) . . ?
 F9B C47 F8B 105.7(12) . . ?
 F7B C47 C44 112.3(9) . . ?
 F8A C47 C44 112.4(8) . . ?
 F7A C47 C44 114.8(8) . . ?
 F9B C47 C44 113.0(8) . . ?
 F9A C47 C44 111.5(8) . . ?
 F8B C47 C44 113.7(9) . . ?
 C52 C51 C56 119.2(3) . . ?
 C52 C51 P2 119.8(2) . . ?
 C56 C51 P2 121.0(2) . . ?
 C51 C52 C53 120.3(3) . . ?
 C54 C53 C52 120.1(3) . . ?
 C53 C54 C55 120.3(3) . . ?
 C53 C54 C57 120.2(4) . . ?
 C55 C54 C57 119.4(4) . . ?
 C54 C55 C56 119.9(4) . . ?
 C51 C56 C55 120.1(3) . . ?
 F11A C57 F10A 108.5(10) . . ?
 F11A C57 F12A 108.8(10) . . ?
 F10A C57 F12A 101.1(8) . . ?
 F10B C57 F12B 107.2(14) . . ?
 F10B C57 F11B 111.1(13) . . ?
 F12B C57 F11B 97.2(14) . . ?
 F10B C57 C54 118.5(12) . . ?
 F11A C57 C54 116.7(8) . . ?
 F10A C57 C54 111.3(8) . . ?
 F12A C57 C54 109.2(6) . . ?
 F12B C57 C54 110.2(11) . . ?
 F11B C57 C54 110.5(7) . . ?
 C62 C61 C66 118.8(3) . . ?
 C62 C61 P2 120.3(2) . . ?
 C66 C61 P2 120.8(2) . . ?
 C63 C62 C61 120.7(3) . . ?
 C62 C63 C64 120.6(3) . . ?
 C65 C64 C63 119.6(3) . . ?
 C65 C64 C67 121.5(3) . . ?
 C63 C64 C67 118.9(3) . . ?
 C64 C65 C66 120.3(3) . . ?
 C65 C66 C61 120.0(3) . . ?
 O4 C67 O3 123.5(3) . . ?
 O4 C67 C64 121.6(4) . . ?
 O3 C67 C64 114.8(4) . . ?

```

loop_
  _geom_hbond_atom_site_label_D
  _geom_hbond_atom_site_label_H
  _geom_hbond_atom_site_label_A
  _geom_hbond_distance_DH
  _geom_hbond_distance_HA
  _geom_hbond_distance_DA
  _geom_hbond_angle_DHA
  _geom_hbond_site_symmetry_A
O1 H1 O2  0.82 1.82 2.615(3) 163.6 3_665
O3 H3 O1S  0.82 1.90 2.697(5) 164.6 2

_refine_diff_density_max    0.820
_refine_diff_density_min   -0.586
_refine_diff_density_rms   0.068

```

8.7. *trans*-[PdCl₂(*m*-Miranphos)₂]

```

data_shelx

_audit_creation_method      SHELXL-2014
_chemical_name_systematic
;
?
;
_chemical_name_common       ?
_chemical_melting_point     ?
_chemical_formula_moiety    ?
_chemical_formula_sum
'C42 H26 Cl2 F12 O4 P2 Pd'
_chemical_formula_weight    1061.87

loop_
  _atom_type_symbol
  _atom_type_description
  _atom_type_scatter_dispersion_real
  _atom_type_scatter_dispersion_imag
  _atom_type_scatter_source
'C' 'C'  0.0033  0.0016
'International Tables Vol C Tables 4.2.6.8 and 6.1.1.4'
'H' 'H'  0.0000  0.0000
'International Tables Vol C Tables 4.2.6.8 and 6.1.1.4'
'Cl' 'Cl'  0.1484  0.1585
'International Tables Vol C Tables 4.2.6.8 and 6.1.1.4'
'F' 'F'  0.0171  0.0103
'International Tables Vol C Tables 4.2.6.8 and 6.1.1.4'
'O' 'O'  0.0106  0.0060
'International Tables Vol C Tables 4.2.6.8 and 6.1.1.4'
'P' 'P'  0.1023  0.0942
'International Tables Vol C Tables 4.2.6.8 and 6.1.1.4'
'Pd' 'Pd' -0.9988  1.0072
'International Tables Vol C Tables 4.2.6.8 and 6.1.1.4'

_space_group_crystal_system orthorhombic
_space_group_IT_number      61
_space_group_name_H-M_alt   'P b c a'

```

```

_space_group_name_Hall          '-P 2ac 2ab'

_shelx_space_group_comment
;
The symmetry employed for this shelxl refinement is uniquely
defined
by the following loop, which should always be used as a source of
symmetry information in preference to the above space-group names.
They are only intended as comments.
;

loop_
_space_group_symop_operation_xyz
'x, y, z'
'-x+1/2, -y, z+1/2'
'x+1/2, -y+1/2, -z'
'-x, y+1/2, -z+1/2'
'-x, -y, -z'
'x-1/2, y, -z-1/2'
'-x-1/2, y-1/2, z'
'x, -y-1/2, z-1/2'

_cell_length_a                 10.1026(5)
_cell_length_b                 27.1594(13)
_cell_length_c                 36.7299(17)
_cell_angle_alpha              90
_cell_angle_beta               90
_cell_angle_gamma              90
_cell_volume                   10078.0(8)
_cell_formula_units_Z          8
_cell_measurement_temperature  293(2)
_cell_measurement_reflns_used  4969
_cell_measurement_theta_min    2.22
_cell_measurement_theta_max    20.355

_exptl_crystal_description     prim
_exptl_crystal_colour          yellow
_exptl_crystal_density_meas    ?
_exptl_crystal_density_method  ?
_exptl_crystal_density_diffn   1.400
_exptl_crystal_F_000           4224
_exptl_transmission_factor_min  ?
_exptl_transmission_factor_max  ?
_exptl_crystal_size_max        0.3
_exptl_crystal_size_mid        0.3
_exptl_crystal_size_min        0.3
_exptl_absorpt_coefficient_mu   0.618
_shelx_estimated_absorpt_T_min  ?
_shelx_estimated_absorpt_T_max  ?
_exptl_absorpt_correction_type  ?
_exptl_absorpt_correction_T_min ?
_exptl_absorpt_correction_T_max ?
_exptl_absorpt_process_details ?

_exptl_special_details
;
?
;

```

```

_diffrn_ambient_temperature      293(2)
_diffrn_radiation_wavelength     0.71073
_diffrn_radiation_type           MoK\alpha
_diffrn_source                   ?
_diffrn_measurement_device_type   'Bruker SMART CCD area detector'
_diffrn_measurement_method       ?
_diffrn_detector_area_resol_mean ?
_diffrn_reflns_number            77618
_diffrn_reflns_av_unetI/netI     0.1036
_diffrn_reflns_av_R_equivalents  0.1485
_diffrn_reflns_limit_h_min       -13
_diffrn_reflns_limit_h_max       13
_diffrn_reflns_limit_k_min       -35
_diffrn_reflns_limit_k_max       36
_diffrn_reflns_limit_l_min       -49
_diffrn_reflns_limit_l_max       48
_diffrn_reflns_theta_min         1.109
_diffrn_reflns_theta_max         28.875
_diffrn_reflns_theta_full        25.242
_diffrn_measured_fraction_theta_max 0.955
_diffrn_measured_fraction_theta_full 1.000
_diffrn_reflns_Laue_measured_fraction_max 0.955
_diffrn_reflns_Laue_measured_fraction_full 1.000
_diffrn_reflns_point_group_measured_fraction_max 0.955
_diffrn_reflns_point_group_measured_fraction_full 1.000
_reflns_number_total             12642
_reflns_number_gt                5851
_reflns_threshold_expression      'I > 2\s(I) '
_reflns_Friedel_coverage         0.000
_reflns_Friedel_fraction_max     .
_reflns_Friedel_fraction_full    .

_reflns_special_details
;
Reflections were merged by SHELXL according to the crystal
class for the calculation of statistics and refinement.

_reflns_Friedel_fraction is defined as the number of unique
Friedel pairs measured divided by the number that would be
possible theoretically, ignoring centric projections and
systematic absences.
;

_computing_data_collection       ?
_computing_cell_refinement       ?
_computing_data_reduction        ?
_computing_structure_solution    ?
_computing_structure_refinement  'SHELXL-2014 (Sheldrick, 2014) '
_computing_molecular_graphics    ?
_computing_publication_material ?

_refine_special_details
;
?
;
_refine_ls_structure_factor_coef  Fsqd
_refine_ls_matrix_type           full

```

```

_refine_ls_weighting_scheme      calc
_refine_ls_weighting_details
'w=1/[\s^2^(Fo^2^)+(0.1469P)^2^+5.6341P] where P=(Fo^2^+2Fc^2^)/3'
_atom_sites_solution_primary    ?
_atom_sites_solution_secondary  ?
_atom_sites_solution_hydrogens  geom
_refine_ls_hydrogen_treatment  constr
_refine_ls_extinction_method    none
_refine_ls_extinction_coef      .
_refine_ls_number_reflns       12642
_refine_ls_number_parameters    599
_refine_ls_number_restraints   100
_refine_ls_R_factor_all        0.1903
_refine_ls_R_factor_gt         0.0847
_refine_ls_wR_factor_ref       0.2926
_refine_ls_wR_factor_gt       0.2319
_refine_ls_goodness_of_fit_ref 1.032
_refine_ls_restrained_S_all    1.035
_refine_ls_shift/su_max        0.006
_refine_ls_shift/su_mean       0.000

loop_
_atom_site_label
_atom_site_type_symbol
_atom_site_fract_x
_atom_site_fract_y
_atom_site_fract_z
_atom_site_U_iso_or_equiv
_atom_site_adp_type
_atom_site_occupancy
_atom_site_site_symmetry_order
_atom_site_calc_flag
_atom_site_refinement_flags_posn
_atom_site_refinement_flags_adp
_atom_site_refinement_flags_occupancy
_atom_site_disorder_assembly
_atom_site_disorder_group
Pd1 Pd 0.99104(5) 0.36786(2) 0.13961(2) 0.04328(19) Uani 1 1 d . . .
. . .
P1 P 0.89418(18) 0.44505(7) 0.14265(5) 0.0458(4) Uani 1 1 d . . . .
.
C11 C 0.8550(8) 0.4656(3) 0.1883(2) 0.0551(19) Uani 1 1 d . . . . .
C12 C 0.7724(9) 0.5055(3) 0.1942(2) 0.065(2) Uani 1 1 d . . . . .
H12 H 0.7422 0.5237 0.1744 0.078 Uiso 1 1 calc R U . . .
C13 C 0.7341(10) 0.5186(3) 0.2289(3) 0.075(3) Uani 1 1 d . . . . .
C14 C 0.7751(12) 0.4915(5) 0.2584(3) 0.098(4) Uani 1 1 d . . . . .
H14 H 0.7469 0.4999 0.2817 0.118 Uiso 1 1 calc R U . . .
C15 C 0.8566(13) 0.4528(5) 0.2534(3) 0.107(4) Uani 1 1 d . . . . .
H15 H 0.8857 0.4351 0.2735 0.129 Uiso 1 1 calc R U . . .
C16 C 0.8991(10) 0.4383(4) 0.2182(2) 0.081(3) Uani 1 1 d . . . . .
H16 H 0.9547 0.4113 0.2151 0.098 Uiso 1 1 calc R U . . .
C17 C 0.6469(15) 0.5611(5) 0.2345(4) 0.109(4) Uani 1 1 d . . . . .
F1 F 0.5780(10) 0.5608(4) 0.2643(2) 0.182(4) Uani 1 1 d . . . . .
F2 F 0.7072(9) 0.6023(3) 0.2339(3) 0.185(4) Uani 1 1 d . . . . .
F3 F 0.5546(10) 0.5655(3) 0.2091(3) 0.170(4) Uani 1 1 d . . . . .
C21 C 1.0066(6) 0.4888(3) 0.1217(2) 0.0466(16) Uani 1 1 d . . . . .
C22 C 1.0490(8) 0.5318(3) 0.1387(2) 0.059(2) Uani 1 1 d . . . . .
H22 H 1.0194 0.5394 0.1620 0.071 Uiso 1 1 calc R U . . .

```

C23 C 1.1347(9) 0.5633(3) 0.1210(3) 0.069(2) Uani 1 1 d
C24 C 1.1783(9) 0.5520(4) 0.0863(3) 0.080(3) Uani 1 1 d
H24 H 1.2350 0.5735 0.0743 0.096 Uiso 1 1 calc R U
C25 C 1.1383(8) 0.5091(4) 0.0693(3) 0.073(2) Uani 1 1 d
H25 H 1.1677 0.5019 0.0459 0.088 Uiso 1 1 calc R U
C26 C 1.0550(8) 0.4771(3) 0.0871(2) 0.059(2) Uani 1 1 d
H26 H 1.0308 0.4476 0.0762 0.071 Uiso 1 1 calc R U
C27 C 1.1785(16) 0.6085(5) 0.1404(4) 0.118(5) Uani 1 1 d
F4 F 1.1877(13) 0.6467(3) 0.1190(3) 0.211(5) Uani 1 1 d
F5 F 1.2901(12) 0.6011(4) 0.1569(4) 0.251(7) Uani 1 1 d
F6 F 1.1003(11) 0.6261(3) 0.1650(3) 0.157(4) Uani 1 1 d
C31 C 0.7376(7) 0.4564(2) 0.1195(2) 0.0477(17) Uani 1 1 d
C32 C 0.7271(7) 0.4872(3) 0.08963(19) 0.0465(16) Uani 1 1 d
.
H32 H 0.8032 0.5015 0.0800 0.056 Uiso 1 1 calc R U
C33 C 0.6078(7) 0.4970(3) 0.0740(2) 0.0523(18) Uani 1 1 d
C34 C 0.4932(8) 0.4757(3) 0.0881(3) 0.066(2) Uani 1 1 d
H34 H 0.4113 0.4824 0.0776 0.079 Uiso 1 1 calc R U
C35 C 0.5020(8) 0.4444(3) 0.1178(3) 0.071(2) Uani 1 1 d
H35 H 0.4257 0.4305 0.1275 0.085 Uiso 1 1 calc R U
C36 C 0.6228(8) 0.4340(3) 0.1329(2) 0.060(2) Uani 1 1 d
H36 H 0.6285 0.4120 0.1522 0.072 Uiso 1 1 calc R U
C37 C 0.6024(8) 0.5303(3) 0.0424(2) 0.059(2) Uani 1 1 d
O2 O 0.7101(6) 0.5434(3) 0.02777(17) 0.0848(19) Uani 1 1 d
.
O1 O 0.4893(5) 0.5460(2) 0.03076(17) 0.0740(17) Uani 1 1 d
.
H1 H 0.5007 0.5641 0.0132 0.111 Uiso 1 1 calc R U
P2 P 1.1018(2) 0.29301(7) 0.13799(5) 0.0503(5) Uani 1 1 d
C41 C 1.0264(8) 0.2414(3) 0.1141(2) 0.059(2) Uani 1 1 d
C42 C 0.9108(9) 0.2211(3) 0.1286(3) 0.071(2) Uani 1 1 d
H42 H 0.8724 0.2344 0.1494 0.086 Uiso 1 1 calc R U
C43 C 0.8542(10) 0.1806(3) 0.1114(3) 0.088(3) Uani 1 1 d D
C44 C 0.9114(14) 0.1623(4) 0.0794(3) 0.108(4) Uani 1 1 d
H44 H 0.8713 0.1362 0.0672 0.130 Uiso 1 1 calc R U
C45 C 1.0207(13) 0.1814(4) 0.0662(4) 0.108(4) Uani 1 1 d
H45 H 1.0584 0.1683 0.0452 0.129 Uiso 1 1 calc R U
C46 C 1.0803(10) 0.2210(4) 0.0833(3) 0.081(3) Uani 1 1 d
H46 H 1.1583 0.2339 0.0739 0.097 Uiso 1 1 calc R U
C47 C 0.7350(15) 0.1577(4) 0.1265(4) 0.127(5) Uani 1 1 d D
F7A F 0.734(4) 0.1608(14) 0.1630(5) 0.189(13) Uani 0.45(3) 1 d D U
P A 1
F8A F 0.623(2) 0.1759(13) 0.1154(11) 0.181(13) Uani 0.45(3) 1 d D U
P A 1
F9A F 0.732(3) 0.1100(7) 0.1204(11) 0.182(13) Uani 0.45(3) 1 d D U
P A 1
F7B F 0.666(2) 0.1858(7) 0.1493(7) 0.133(8) Uani 0.55(3) 1 d D U P
A 2
F8B F 0.644(2) 0.1480(14) 0.1006(5) 0.199(12) Uani 0.55(3) 1 d D U
P A 2
F9B F 0.756(3) 0.1148(7) 0.1419(9) 0.204(12) Uani 0.55(3) 1 d D U P
A 2
C51 C 1.1317(9) 0.2669(3) 0.1834(2) 0.065(2) Uani 1 1 d
C52 C 1.1299(9) 0.2960(3) 0.2135(2) 0.065(2) Uani 1 1 d
H52 H 1.1146 0.3296 0.2113 0.078 Uiso 1 1 calc R U
C53 C 1.1505(11) 0.2760(4) 0.2469(2) 0.088(3) Uani 1 1 d D
C54 C 1.1755(17) 0.2273(5) 0.2509(3) 0.145(6) Uani 1 1 d
H54 H 1.1883 0.2138 0.2739 0.174 Uiso 1 1 calc R U

C55 C 1.182(2) 0.1975(5) 0.2195(3) 0.185(9) Uani 1 1 d
H55 H 1.2034 0.1644 0.2215 0.222 Uiso 1 1 calc R U . . .
C56 C 1.1565(15) 0.2169(4) 0.1872(3) 0.126(5) Uani 1 1 d
H56 H 1.1555 0.1968 0.1667 0.151 Uiso 1 1 calc R U . . .
C57 C 1.1449(11) 0.3102(5) 0.2813(4) 0.143(6) Uani 1 1 d D
F10A F 1.1018(18) 0.3546(5) 0.2750(5) 0.110 Uiso 0.404(3) 1 d D U P
B 1
F11A F 1.0930(18) 0.2890(6) 0.3096(4) 0.110 Uiso 0.404(3) 1 d D U P
B 1
F12A F 1.2870(13) 0.3139(7) 0.2897(5) 0.110 Uiso 0.404(3) 1 d D U P
B 1
F10B F 1.0218(19) 0.3324(9) 0.2781(6) 0.110 Uiso 0.286(3) 1 d D U P
B 2
F11B F 1.241(2) 0.3432(8) 0.2797(6) 0.110 Uiso 0.286(3) 1 d D U P B
2
F12B F 1.151(2) 0.2807(8) 0.3099(5) 0.110 Uiso 0.286(3) 1 d D U P B
2
F10C F 1.162(2) 0.3565(6) 0.2733(6) 0.110 Uiso 0.309(3) 1 d D U P B
3
F11C F 1.0140(17) 0.3038(9) 0.2937(6) 0.110 Uiso 0.309(3) 1 d D U P
B 3
F12C F 1.223(2) 0.2958(8) 0.3078(5) 0.110 Uiso 0.309(3) 1 d D U P B
3
C61 C 1.2596(8) 0.3019(3) 0.1159(2) 0.0558(19) Uani 1 1 d
C62 C 1.2660(8) 0.3340(3) 0.0864(2) 0.059(2) Uani 1 1 d
H62 H 1.1894 0.3500 0.0788 0.071 Uiso 1 1 calc R U . . .
C63 C 1.3836(8) 0.3428(3) 0.06794(19) 0.0559(19) Uani 1 1 d
.
C64 C 1.4959(8) 0.3192(3) 0.0793(3) 0.071(2) Uani 1 1 d
H64 H 1.5754 0.3245 0.0672 0.086 Uiso 1 1 calc R U . . .
C65 C 1.4919(9) 0.2881(4) 0.1083(3) 0.089(3) Uani 1 1 d
H65 H 1.5696 0.2728 0.1157 0.106 Uiso 1 1 calc R U . . .
C66 C 1.3761(9) 0.2786(4) 0.1271(3) 0.074(2) Uani 1 1 d
H66 H 1.3758 0.2571 0.1468 0.089 Uiso 1 1 calc R U . . .
C67 C 1.3887(8) 0.3778(3) 0.0379(2) 0.062(2) Uani 1 1 d
O4 O 1.4928(6) 0.3846(3) 0.02060(18) 0.0801(18) Uani 1 1 d
.
O3 O 1.2808(6) 0.4006(2) 0.02994(17) 0.0857(19) Uani 1 1 d
.
H3 H 1.2941 0.4193 0.0128 0.129 Uiso 1 1 calc R U . . .
C11 Cl 1.1765(2) 0.40322(7) 0.16576(6) 0.0626(5) Uani 1 1 d
.
C12 Cl 0.8142(2) 0.33577(8) 0.11027(7) 0.0756(7) Uani 1 1 d
.
loop_
 _atom_site_aniso_label
 _atom_site_aniso_U_11
 _atom_site_aniso_U_22
 _atom_site_aniso_U_33
 _atom_site_aniso_U_23
 _atom_site_aniso_U_13
 _atom_site_aniso_U_12
Pd1 0.0483(3) 0.0390(3) 0.0426(3) -0.0002(2) -0.0026(2) 0.0004(2)
P1 0.0494(11) 0.0396(10) 0.0485(11) 0.0001(8) 0.0043(9) -0.0008(8)
C11 0.067(5) 0.051(4) 0.047(4) -0.005(4) 0.010(4) -0.010(4)
C12 0.079(6) 0.053(5) 0.063(5) -0.009(4) 0.016(4) -0.009(4)
C13 0.088(7) 0.062(5) 0.076(7) -0.023(5) 0.028(5) -0.008(5)

C14 0.111(9) 0.110(9) 0.074(8) -0.019(7) 0.032(6) -0.010(7)
C15 0.139(11) 0.125(10) 0.057(6) 0.024(6) 0.024(7) 0.003(8)
C16 0.108(8) 0.077(6) 0.059(6) 0.003(5) 0.008(5) 0.005(6)
C17 0.136(11) 0.098(9) 0.092(9) -0.048(7) 0.020(8) 0.000(8)
F1 0.212(9) 0.191(9) 0.144(7) -0.029(6) 0.092(7) 0.062(7)
F2 0.163(7) 0.084(5) 0.310(13) -0.073(7) 0.014(8) -0.003(5)
F3 0.171(8) 0.163(8) 0.177(9) -0.073(7) -0.001(7) 0.079(7)
C21 0.041(4) 0.044(4) 0.054(4) 0.011(3) -0.004(3) 0.001(3)
C22 0.067(5) 0.053(5) 0.056(5) 0.005(4) -0.005(4) -0.012(4)
C23 0.066(5) 0.059(5) 0.082(6) 0.013(5) -0.006(5) -0.015(4)
C24 0.067(6) 0.071(6) 0.103(8) 0.032(6) 0.015(5) -0.010(5)
C25 0.061(5) 0.080(7) 0.078(6) 0.016(5) 0.020(5) 0.007(5)
C26 0.051(4) 0.058(5) 0.068(5) 0.003(4) 0.011(4) 0.005(4)
C27 0.115(11) 0.088(9) 0.151(13) -0.011(9) 0.009(10) -0.061(8)
F4 0.335(15) 0.090(5) 0.208(10) 0.015(6) -0.007(10) -0.108(8)
F5 0.176(10) 0.154(9) 0.42(2) -0.105(11) -0.157(12) -0.003(7)
F6 0.196(10) 0.101(6) 0.173(8) -0.043(5) 0.021(8) -0.051(6)
C31 0.045(4) 0.043(4) 0.055(4) -0.004(3) 0.004(3) 0.001(3)
C32 0.045(4) 0.045(4) 0.049(4) 0.001(3) 0.004(3) 0.005(3)
C33 0.047(4) 0.049(4) 0.061(5) -0.004(4) 0.002(4) 0.008(3)
C34 0.044(5) 0.063(5) 0.091(7) -0.011(5) 0.000(4) 0.004(4)
C35 0.052(5) 0.067(5) 0.093(7) 0.001(5) 0.013(5) -0.008(4)
C36 0.050(5) 0.053(5) 0.077(6) 0.005(4) 0.005(4) -0.004(4)
C37 0.055(5) 0.062(5) 0.061(5) 0.000(4) 0.001(4) 0.011(4)
O2 0.061(4) 0.111(5) 0.083(4) 0.037(4) -0.001(3) 0.007(3)
O1 0.058(4) 0.089(4) 0.076(4) 0.011(3) -0.008(3) 0.010(3)
P2 0.0640(12) 0.0454(10) 0.0414(10) -0.0009(8) -0.0038(9) 0.0097(9)
C41 0.074(6) 0.048(4) 0.054(5) -0.004(4) -0.008(4) 0.012(4)
C42 0.089(7) 0.048(5) 0.076(6) -0.001(4) 0.010(5) 0.001(5)
C43 0.108(8) 0.048(5) 0.107(8) 0.001(5) -0.007(7) -0.016(5)
C44 0.138(11) 0.073(7) 0.113(10) -0.037(7) -0.010(9) -0.012(7)
C45 0.126(10) 0.091(8) 0.105(9) -0.045(7) 0.013(7) -0.019(7)
C46 0.094(7) 0.075(6) 0.073(6) -0.020(5) 0.000(5) -0.003(5)
C47 0.162(15) 0.080(10) 0.138(13) -0.007(9) 0.023(12) -0.029(10)
F7A 0.24(3) 0.16(3) 0.17(2) -0.014(18) 0.072(19) -0.12(2)
F8A 0.132(18) 0.17(3) 0.24(3) 0.05(2) 0.04(2) 0.014(17)
F9A 0.22(3) 0.118(18) 0.21(3) -0.040(18) 0.06(2) -0.098(17)
F7B 0.125(14) 0.128(14) 0.145(16) 0.008(13) 0.024(12) -0.061(11)
F8B 0.16(2) 0.25(3) 0.181(19) -0.049(19) 0.012(15) -0.11(2)
F9B 0.32(3) 0.086(13) 0.20(3) 0.052(14) 0.06(2) -0.049(17)
C51 0.082(6) 0.064(5) 0.048(5) 0.007(4) -0.010(4) 0.019(4)
C52 0.088(6) 0.060(5) 0.046(4) 0.004(4) -0.004(4) -0.005(4)
C53 0.139(10) 0.083(7) 0.040(5) -0.004(5) -0.007(5) -0.004(6)
C54 0.249(18) 0.113(10) 0.073(8) 0.040(8) -0.035(9) 0.055(11)
C55 0.39(3) 0.096(9) 0.068(8) 0.006(7) -0.043(12) 0.101(13)
C56 0.238(16) 0.081(7) 0.058(6) 0.007(5) -0.017(8) 0.078(9)
C57 0.139(13) 0.181(15) 0.108(10) 0.072(11) -0.023(9) -0.014(11)
C61 0.057(5) 0.060(5) 0.050(4) -0.013(4) -0.011(4) 0.012(4)
C62 0.060(5) 0.071(5) 0.046(4) -0.002(4) -0.007(4) 0.019(4)
C63 0.054(5) 0.071(5) 0.042(4) -0.004(4) -0.007(3) 0.009(4)
C64 0.054(5) 0.082(6) 0.078(6) 0.002(5) 0.001(4) 0.015(4)
C65 0.068(6) 0.109(8) 0.089(7) 0.015(7) -0.019(5) 0.023(6)
C66 0.062(6) 0.088(7) 0.073(6) 0.013(5) -0.009(5) 0.014(5)
C67 0.052(5) 0.082(6) 0.050(5) -0.004(4) 0.004(4) 0.009(4)
O4 0.067(4) 0.098(5) 0.075(4) 0.008(4) 0.011(3) 0.012(3)
O3 0.071(4) 0.107(5) 0.079(4) 0.032(4) 0.010(3) 0.027(4)
C11 0.0584(12) 0.0555(11) 0.0738(13) -0.0030(10) -0.0135(10) -
0.0064(9)

C12 0.0678(13) 0.0556(12) 0.1034(18) -0.0164(12) -0.0317(12)
0.0017(10)

_geom_special_details

;

All esds (except the esd in the dihedral angle between two l.s. planes)

are estimated using the full covariance matrix. The cell esds are taken

into account individually in the estimation of esds in distances, angles

and torsion angles; correlations between esds in cell parameters are only

used when they are defined by crystal symmetry. An approximate (isotropic)

treatment of cell esds is used for estimating esds involving l.s. planes.

;

loop_

_geom_bond_atom_site_label_1

_geom_bond_atom_site_label_2

_geom_bond_distance

_geom_bond_site_symmetry_2

_geom_bond_publ_flag

Pd1 C12 2.261(2) . ?

Pd1 C11 2.3140(19) . ?

Pd1 P1 2.3163(19) . ?

Pd1 P2 2.3212(19) . ?

P1 C11 1.812(7) . ?

P1 C21 1.814(7) . ?

P1 C31 1.821(7) . ?

C11 C12 1.383(11) . ?

C11 C16 1.397(12) . ?

C12 C13 1.381(11) . ?

C13 C14 1.374(15) . ?

C13 C17 1.466(15) . ?

C14 C15 1.349(15) . ?

C15 C16 1.417(13) . ?

C17 F2 1.276(15) . ?

C17 F1 1.298(13) . ?

C17 F3 1.325(15) . ?

C21 C22 1.391(10) . ?

C21 C26 1.397(10) . ?

C22 C23 1.379(11) . ?

C23 C24 1.382(13) . ?

C23 C27 1.489(15) . ?

C24 C25 1.383(13) . ?

C25 C26 1.376(11) . ?

C27 F6 1.290(16) . ?

C27 F5 1.296(17) . ?

C27 F4 1.304(16) . ?

C31 C32 1.385(10) . ?

C31 C36 1.399(10) . ?

C32 C33 1.362(10) . ?

C33 C34 1.395(11) . ?

C33 C37 1.473(11) . ?

C34 C35 1.385(13) . ?

C35 C36 1.371(11) . ?
 C37 O2 1.264(9) . ?
 C37 O1 1.291(9) . ?
 P2 C61 1.804(8) . ?
 P2 C41 1.821(8) . ?
 P2 C51 1.837(8) . ?
 C41 C46 1.370(11) . ?
 C41 C42 1.397(12) . ?
 C42 C43 1.392(12) . ?
 C43 C44 1.401(15) . ?
 C43 C47 1.464(16) . ?
 C44 C45 1.313(15) . ?
 C45 C46 1.382(14) . ?
 C47 F8A 1.303(16) . ?
 C47 F9B 1.313(15) . ?
 C47 F9A 1.317(16) . ?
 C47 F7B 1.329(15) . ?
 C47 F7A 1.341(16) . ?
 C47 F8B 1.352(16) . ?
 C51 C52 1.360(11) . ?
 C51 C56 1.387(12) . ?
 C52 C53 1.358(11) . ?
 C53 C54 1.354(15) . ?
 C53 C57 1.568(16) . ?
 C54 C55 1.408(17) . ?
 C55 C56 1.325(14) . ?
 C57 F11A 1.298(13) . ?
 C57 F10A 1.302(14) . ?
 C57 F10C 1.302(16) . ?
 C57 F12C 1.311(15) . ?
 C57 F12B 1.323(15) . ?
 C57 F11B 1.324(15) . ?
 C57 F10B 1.386(15) . ?
 C57 F11C 1.410(15) . ?
 C57 F12A 1.472(13) . ?
 C61 C62 1.394(11) . ?
 C61 C66 1.398(11) . ?
 C62 C63 1.388(11) . ?
 C63 C64 1.368(10) . ?
 C63 C67 1.458(11) . ?
 C64 C65 1.358(13) . ?
 C65 C66 1.383(12) . ?
 C67 O4 1.242(9) . ?
 C67 O3 1.288(9) . ?

loop_
 _geom_angle_atom_site_label_1
 _geom_angle_atom_site_label_2
 _geom_angle_atom_site_label_3
 _geom_angle
 _geom_angle_site_symmetry_1
 _geom_angle_site_symmetry_3
 _geom_angle_publ_flag
 Cl2 Pd1 Cl1 175.92(9) . . ?
 Cl2 Pd1 P1 92.18(7) . . ?
 Cl1 Pd1 P1 86.92(7) . . ?
 Cl2 Pd1 P2 91.78(7) . . ?
 Cl1 Pd1 P2 89.07(7) . . ?

P1 Pd1 P2 175.98(7) . . ?
C11 P1 C21 109.1(4) . . ?
C11 P1 C31 101.0(4) . . ?
C21 P1 C31 103.6(3) . . ?
C11 P1 Pd1 114.6(3) . . ?
C21 P1 Pd1 107.9(2) . . ?
C31 P1 Pd1 119.8(2) . . ?
C12 C11 C16 119.1(7) . . ?
C12 C11 P1 121.1(6) . . ?
C16 C11 P1 119.6(7) . . ?
C13 C12 C11 120.9(9) . . ?
C14 C13 C12 120.5(9) . . ?
C14 C13 C17 119.5(10) . . ?
C12 C13 C17 120.0(11) . . ?
C15 C14 C13 119.5(9) . . ?
C14 C15 C16 121.9(11) . . ?
C11 C16 C15 118.1(9) . . ?
F2 C17 F1 106.0(10) . . ?
F2 C17 F3 104.1(13) . . ?
F1 C17 F3 102.5(13) . . ?
F2 C17 C13 113.8(12) . . ?
F1 C17 C13 115.8(12) . . ?
F3 C17 C13 113.4(9) . . ?
C22 C21 C26 119.3(7) . . ?
C22 C21 P1 123.6(6) . . ?
C26 C21 P1 117.1(6) . . ?
C23 C22 C21 120.2(8) . . ?
C22 C23 C24 119.8(8) . . ?
C22 C23 C27 118.2(10) . . ?
C24 C23 C27 122.0(9) . . ?
C23 C24 C25 120.7(8) . . ?
C26 C25 C24 119.7(9) . . ?
C25 C26 C21 120.3(8) . . ?
F6 C27 F5 105.3(15) . . ?
F6 C27 F4 99.9(14) . . ?
F5 C27 F4 110.0(12) . . ?
F6 C27 C23 117.3(10) . . ?
F5 C27 C23 110.7(14) . . ?
F4 C27 C23 112.8(13) . . ?
C32 C31 C36 118.6(7) . . ?
C32 C31 P1 122.5(5) . . ?
C36 C31 P1 118.9(6) . . ?
C33 C32 C31 121.4(7) . . ?
C32 C33 C34 119.7(7) . . ?
C32 C33 C37 119.1(7) . . ?
C34 C33 C37 121.2(7) . . ?
C35 C34 C33 119.6(8) . . ?
C36 C35 C34 120.2(8) . . ?
C35 C36 C31 120.4(8) . . ?
O2 C37 O1 121.9(8) . . ?
O2 C37 C33 118.4(7) . . ?
O1 C37 C33 119.7(7) . . ?
C61 P2 C41 104.8(4) . . ?
C61 P2 C51 108.3(4) . . ?
C41 P2 C51 102.1(4) . . ?
C61 P2 Pd1 108.7(3) . . ?
C41 P2 Pd1 119.0(3) . . ?
C51 P2 Pd1 113.2(3) . . ?

C46 C41 C42 119.1(8) . . ?
C46 C41 P2 122.9(7) . . ?
C42 C41 P2 118.0(6) . . ?
C43 C42 C41 118.8(9) . . ?
C42 C43 C44 119.5(10) . . ?
C42 C43 C47 120.1(10) . . ?
C44 C43 C47 120.5(10) . . ?
C45 C44 C43 121.0(10) . . ?
C44 C45 C46 120.4(11) . . ?
C41 C46 C45 121.1(10) . . ?
F8A C47 F9A 107.3(17) . . ?
F9B C47 F7B 108.7(15) . . ?
F8A C47 F7A 106.5(17) . . ?
F9A C47 F7A 103.5(15) . . ?
F9B C47 F8B 103.9(15) . . ?
F7B C47 F8B 101.4(15) . . ?
F8A C47 C43 115.9(16) . . ?
F9B C47 C43 114.1(16) . . ?
F9A C47 C43 112.0(16) . . ?
F7B C47 C43 115.2(12) . . ?
F7A C47 C43 110.9(15) . . ?
F8B C47 C43 112.2(15) . . ?
C52 C51 C56 119.3(8) . . ?
C52 C51 P2 120.8(6) . . ?
C56 C51 P2 119.9(7) . . ?
C53 C52 C51 120.1(8) . . ?
C54 C53 C52 121.1(9) . . ?
C54 C53 C57 120.0(9) . . ?
C52 C53 C57 119.0(8) . . ?
C53 C54 C55 118.8(10) . . ?
C56 C55 C54 119.7(11) . . ?
C55 C56 C51 121.0(11) . . ?
F11A C57 F10A 114.7(14) . . ?
F10C C57 F12C 112.1(15) . . ?
F12B C57 F11B 114.3(14) . . ?
F12B C57 F10B 111.8(14) . . ?
F11B C57 F10B 111.1(14) . . ?
F10C C57 F11C 108.4(14) . . ?
F12C C57 F11C 106.7(13) . . ?
F11A C57 F12A 104.8(11) . . ?
F10A C57 F12A 107.4(12) . . ?
F11A C57 C53 113.3(13) . . ?
F10A C57 C53 114.7(12) . . ?
F10C C57 C53 112.6(13) . . ?
F12C C57 C53 113.5(13) . . ?
F12B C57 C53 106.2(14) . . ?
F11B C57 C53 109.9(13) . . ?
F10B C57 C53 102.9(13) . . ?
F11C C57 C53 102.8(12) . . ?
F12A C57 C53 100.1(11) . . ?
C62 C61 C66 118.2(8) . . ?
C62 C61 P2 118.4(6) . . ?
C66 C61 P2 123.5(7) . . ?
C63 C62 C61 121.9(7) . . ?
C64 C63 C62 118.7(8) . . ?
C64 C63 C67 120.5(8) . . ?
C62 C63 C67 120.8(7) . . ?
C65 C64 C63 120.3(8) . . ?

C64 C65 C66 122.2(8) . . ?
C65 C66 C61 118.7(9) . . ?
O4 C67 O3 122.0(8) . . ?
O4 C67 C63 120.9(8) . . ?
O3 C67 C63 117.1(7) . . ?

loop_
_geom_hbond_atom_site_label_D
_geom_hbond_atom_site_label_H
_geom_hbond_atom_site_label_A
_geom_hbond_distance_DH
_geom_hbond_distance_HA
_geom_hbond_distance_DA
_geom_hbond_angle_DHA
_geom_hbond_site_symmetry_A
O1 H1 O4 0.82 1.87 2.674(9) 167.3 5_765
O3 H3 O2 0.82 1.80 2.610(8) 168.2 5_765

_refine_diff_density_max 1.345
_refine_diff_density_min -0.791
_refine_diff_density_rms 0.225